

User guide for the **SASfit** software package

Joachim Kohlbrecher

June 28, 2025

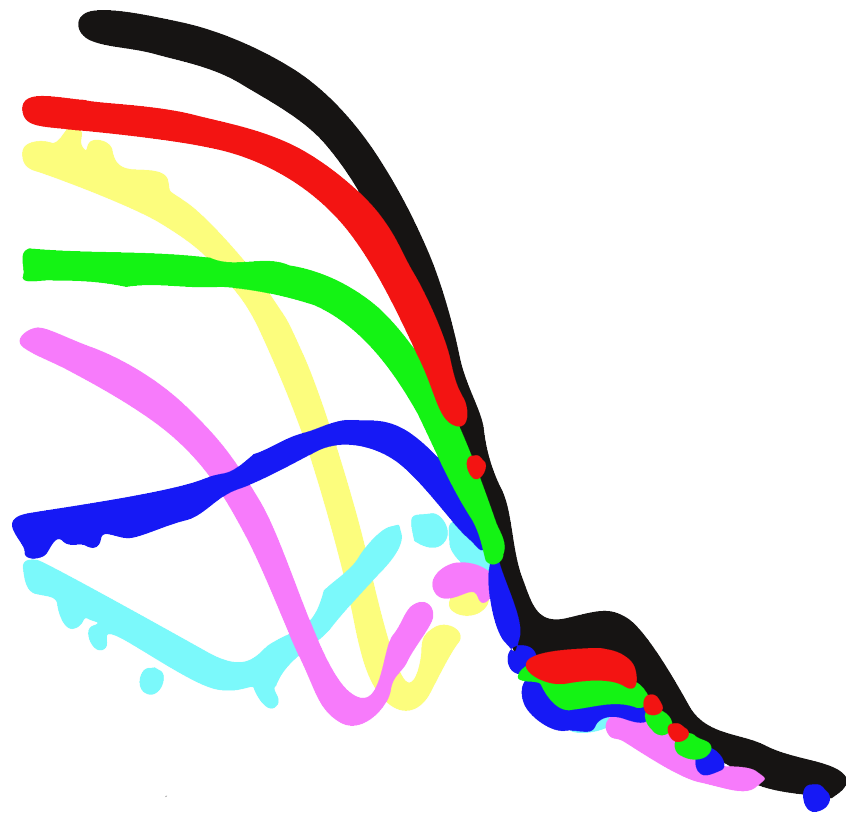


SASfit: A program for fitting simple structural models to small angle scattering data

Joachim Kohlbrecher

PAUL SCHERRER INSTITUTE
LABORATORY FOR NEUTRON SCATTERING AND IMAGING (LNS)
CH-5232 VILLIGEN PSI
JOACHIM.KOHLBRECHER@PSI.CH

JUNE 28, 2025



ABSTRACT. **SASfit** has been written for analyzing and plotting small angle scattering data. It can calculate integral structural parameters like radius of gyration, scattering invariant, Porod constant. Furthermore it can fit size distributions together with several form factors including different structure factors. Additionally an algorithm has been implemented, which allows to simultaneously fit several scattering curves with a common set of (global) parameters. This last option is especially important in contrast variation experiments or measurements with polarised neutrons. The global fit helps to determine fit parameters unambiguously which by analyzing a single curve would be otherwise strongly correlated. The program has been written to fulfill the needs at the small angle neutron scattering facility at PSI (<http://www.psi.ch>). The numerical routines have been written in C whereas the menu interface has been written in tcl/tk and the plotting routine with the extension blt. The newest **SASfit** version can be downloaded from <http://github.com/SASfit/SASfit/>.

Contents

Chapter 1. Introduction to the data analysis program SASfit	17
1.1. Overview	17
Chapter 2. Quick Start Tour	21
2.1. User Interface Window	21
2.2. Importing data files for a single data set	22
2.3. Importing data files for multiple data sets	24
2.4. Reducing the number of data points	24
2.5. Simulating scattering curves	26
2.6. Fitting	26
2.6.1. Model Independent Fitting (Integral parameters)	27
2.6.2. Model dependent analysis	28
2.6.2.1. Modeling a single data set	28
2.6.2.2. Modeling multiple data sets	30
2.7. Criteria for goodness-of-fit	33
2.7.1. chi square test	33
2.7.2. R-factor	34
2.7.3. other methods to compare similarity or distance between theory and data	35
2.7.4. Confidence interval of the fitting parameter	36
2.8. references to numerical strategies SASfit make use of	38
2.8.1. Integrals for Form Factors	38
2.8.2. Orientational and Size Distribution	39
2.8.3. SESANS - MSAS - resolution function	41
2.8.3.1. SESANS	41
2.8.3.2. Multiple Small Angle Scattering (MSAS)	41
2.8.3.3. Resolution Function	42
2.8.4. Summary	42
2.8.5. Integration algorithms in SASfit for normal one- or multi-dimensional integration	43
2.9. orientation average	45
2.9.1. Hankel transform	45
2.10. Fitting strategies	47
2.11. Data I/O Formats	48
2.11.1. ASCII Input Format	48
2.11.2. ASCII data without error bar	50
2.11.3. BerSANS Input Format	50
2.11.4. SESANS Input Format	51
2.11.5. Export Format	52

2.12. Scattering length density calculator	53
2.13. Resolution Function	55
 Chapter 3. Form Factors	57
3.1. Spheres & Shells	57
3.1.1. Sphere	57
3.1.2. Spherical Shell i	59
3.1.3. Spherical Shell ii	61
3.1.4. Spherical Shell iii	63
3.1.5. Bilayered Vesicle	65
3.1.6. Multi Lamellar Vesicle	67
3.1.7. RNDMultiLamellarVesicle	69
3.1.8. Vesicle with aligned flat capped ends [255, 256]	71
3.2. Polymers and Micelles	74
3.2.1. Unified Exponential Power Law according to Beaucage	75
3.2.1.1. Beaucage	75
3.2.1.2. Beaucage2	78
3.2.2. WormLikeChainEXV	80
3.2.3. KholodenkoWorm	82
3.2.4. Diblock copolymer micelles	85
3.2.4.1. Micelles with a homogeneous core and Gaussian chains on the surface	85
3.2.4.1.1. spherical core:	86
3.2.4.1.2. ellipsoidal core with semi-axis ($R, R, \epsilon R$):	89
3.2.4.1.3. cylindrical core with radius R_{core} and height H :	92
3.2.4.1.4. wormlike micelles with circular cross-section:	95
3.2.4.1.5. micelles with rod-like core:	98
3.2.4.2. Micelles with a homogeneous core and a corona with decaying density profile of the form $\varphi(r) \propto r^{-\alpha}$	100
3.2.4.2.1. spherical core:	101
3.2.4.2.2. rodlike core:	104
3.2.4.3. Sphere with Gaussian chains attached	107
3.2.4.4. Sphere with Gaussian chains attached (block copolymer micelle)	109
3.2.5. spherical Micelles with a corona of semi-flexible interacting self-avoiding chains	110
3.3. Local Planar Objects	111
3.3.1. Shape factors $P'(Q)$	111
3.3.1.1. Polydisperse infinitesimal thin discs	111
3.3.1.2. Infinitesimal thin spherical shell	111
3.3.1.3. Infinitesimal thin elliptical shell	112
3.3.1.4. Infinitesimal thin cylindrical shell	112
3.3.2. Cross-section form factors $P_{\text{cs}}(Q)$	113
3.3.2.1. homogeneousXS	113
3.3.3. TwoInfinitelyThinPlates	114
3.3.4. LayeredCentroSymmetricXS	115
3.3.5. BiLayerGauss	116
3.4. Magnetic Scattering	117

3.4.1. Magnetic Saturation	119
3.4.1.1. MagneticShellAniso	119
3.4.1.2. MagneticShellCrossTerm	120
3.4.1.3. MagneticShellPsi	121
3.4.2. Superparamagnetic Particles (like ferrofluids)	122
3.4.2.1. SuperparamagneticFFpsi	122
3.4.2.2. SuperparamagneticFFAniso	122
3.4.2.3. SuperparamagneticFFIso	122
3.4.2.4. SuperparamagneticFFCrossTerm	122
3.5. Other functions	123
3.5.1. DLS_Sphere_RDG	123
3.5.2. Langevin	124
3.5.3. SuperParStroboPsi	125
3.5.4. SuperParStroboPsiSQ	132
3.5.5. SuperParStroboPsiSQBt	133
3.5.6. SuperParStroboPsiSQLx	133
3.5.7. SuperParStroboPsiSQL2x	133
 Chapter 4. Analytical Solutions for Structure factors	 135
4.1. Methods to include structure factors	135
4.1.1. Monodisperse approach	135
4.1.2. Decoupling approximation	135
4.1.3. Local monodisperse approximation	136
4.1.4. partial structure factors	136
4.1.5. Scaling approximation	137
4.1.6. van der Waals one-fluid approximation	137
4.2. Hard & Sticky Hard Sphere	139
4.2.1. Hard Sphere	139
4.3. Other Structure Factors	141
4.3.1. Hayter-Penfold RMSA	141
4.3.2. MacroIon	142
4.3.3. Critical Scattering	143
4.3.4. Cylinder(PRISM)	143
4.3.5. Voigt Peak	144
 Chapter 5. Numerical solution of Fredholm integrals using regularization	 145
5.1. Problem description	145
5.1.1. Size distribution $N(R)$	146
5.1.2. Orientation distribution $p_{ODF}()$	147
5.1.3. Pair distance distribution function $p(r)$	148
5.1.4. Size distribution $N_h(R_h)$ from dynamic light scattering	149
5.2. Expectation Maximization (EM)	152
5.2.1. EM with linear and non-linear smoothing operator	155
5.2.2. EM with maximum entropy regularization	156
5.2.3. Acceleration of EM iteration scheme	160
5.3. Linear least square regularization (LLS)	162

5.4. Non-negative linear least square regularization (NNLLS)	165
5.5. Chahine inversion scheme	165
 Chapter 6. Numerical solutions of the Ornstein Zernike equations	167
6.1. Background	167
6.2. Numerical implementation of the iterative algorithm in SASFIT	169
6.3. Thermodynamic Parameters and Consistency Tests	172
6.4. Closures	175
6.4.1. Hypernetted-chain(HNC) approximation	175
6.4.2. Reference hypernetted chain closure (RHNC)	175
6.4.3. modified hypernetted chain closure (MHNC)	175
6.4.4. Kovalenko-Hirata or partially linearized HNC closure (PLHNC)	176
6.4.5. Percus-Yevick (PY) approximation	176
6.4.6. Mean Spherical Approximation (MSA)	176
6.4.7. Rescaled Mean Spherical Approximation (RMSA)	177
6.4.8. "Soft core" MSA (SMSA) Approximation	177
6.4.9. modified MSA (mMSA) Approximation	177
6.4.10. Verlet Approximation	178
6.4.11. Choudhury-Gosh (CG) Approximation	178
6.4.12. Duh-Haymet (DH) Approximation	178
6.4.13. Martynov-Sarkisov (MS) Approximation	178
6.4.14. Ballone, Pastore, Galli, and Gazzillo (BPGG) approximations	179
6.4.15. Vompe-Martynov (VM) Approximation	179
6.4.16. Bomont-Bretonnet (BB) Approximation	179
6.4.17. Charpentier-Jakse' semi-empirical extension of VM approximation (CJ-VM)	179
6.4.18. HNC-SMSA (HMSA) Approximation	180
6.4.19. Roger-Young (RY) closure	180
6.4.20. Zero separation theorem based closure (ZSEP)	180
6.5. Interaction Potentials	181
6.5.1. Hard Sphere Potential	182
6.5.2. Sticky Hard Sphere Potential (SHS)	183
6.5.3. Soft Sphere Potential	185
6.5.4. Penetrable Sphere Model	186
6.5.5. Generalized Gaussian Core Model Potential - GGCM-n Potential	187
6.5.6. Fermi Distribution Model	188
6.5.7. Star Polymer Potential	189
6.5.8. Lennard-Jones Potential	190
6.5.9. Depletion Potential	191
6.5.10. Ionic Microgel Potential	196
6.5.11. DLVO Potential	197
6.5.12. Hard Core 3Yukawa Potential	199
6.6. GUI interface for the Ornstein Zernike solver	200
 Chapter 7. Size Distributions	203
7.1. Delta	205

7.2. Uniform distribution	205
7.3. Triangular distribution	206
7.4. Log-Normal distribution	207
7.5. Schulz-Zimm (Flory) distribution	209
7.6. Gamma distribution	211
7.7. PearsonIII distribution	213
7.8. Gauss distribution	214
7.9. Generalized exponential distribution (GEX)	215
7.10. Generalized extreme value distribution (GEV)	216
7.11. Maxwell distribution	218
7.12. Weibull distribution	219
7.13. fractal size distribution	220
 Chapter 8. Peak functions	 221
8.1. Beta	222
8.1.1. Beta (Amplitude)	222
8.1.2. Beta (Area)	222
8.2. Chi-Squared	224
8.2.1. Chi-Squared (Amplitude)	224
8.2.2. Chi-Squared (Area)	225
8.3. Erfc peak	227
8.3.1. Erfc (Amplitude)	227
8.3.2. Erfc (Area)	228
8.4. Error peak	229
8.4.1. Error (Amplitude)	229
8.4.2. Error (Area)	230
8.5. Exponentially Modified Gaussian	231
8.5.1. Exponentially Modified Gaussian (Amplitude)	231
8.5.2. Exponentially Modified Gaussian (Area)	233
8.6. Extreme Value	234
8.6.1. Extreme Value (Amplitude)	234
8.6.2. Extreme Value (Area)	235
8.7. F-Variance	236
8.7.1. F-Variance (Amplitude)	236
8.7.2. F-Variance (Area)	237
8.8. Gamma	239
8.8.1. Gamma (Amplitude)	239
8.8.2. Gamma (Area)	240
8.9. Gaussian or Normal distribution	242
8.9.1. Gaussian (Amplitude)	242
8.9.2. Gaussian (Area)	243
8.10. Gaussian-Lorentzian cross product	244
8.10.1. Gaussian-Lorentzian cross product (Amplitude)	245
8.10.2. Gaussian-Lorentzian cross product (Area)	246
8.11. Gaussian-Lorentzian sum	247
8.11.1. Gaussian-Lorentzian sum (Amplitude)	248

8.11.2. Gaussian-Lorentzian sum (Area)	249
8.12. generalized Gaussian 1	250
8.12.1. generalized Gaussian 1 (Amplitude)	251
8.12.2. generalized Gaussian 1 (Area)	252
8.13. generalized Gaussian 2	253
8.13.1. generalized Gaussian 2 (Amplitude)	254
8.13.2. generalized Gaussian 2 (Area)	256
8.14. Giddings	257
8.14.1. Giddings (Amplitude)	258
8.14.2. Giddings (Area)	259
8.15. Haarhoff - Van der Linde (Area)	260
8.16. Half Gaussian Modified Gaussian (Area)	261
8.17. Inverted Gamma	262
8.17.1. Inverted Gamma (Amplitude)	263
8.17.2. Inverted Gamma (Area)	264
8.18. Kumaraswamy	265
8.18.1. Kumaraswamy (Amplitude)	265
8.19. Kumaraswamy (Area)	267
8.20. Laplace	268
8.20.1. Laplace (Amplitude)	268
8.20.2. Laplace (Area)	270
8.21. Logistic	271
8.21.1. Logistic (Amplitude)	271
8.21.2. Logistic (Area)	273
8.22. LogNormal	274
8.22.1. LogNormal (Amplitude)	274
8.22.2. LogNormal (Area)	276
8.23. LogLogistic	277
8.23.1. LogLogistic (Amplitude)	277
8.23.2. LogLogistic (Area)	279
8.24. Lognormal 4-Parameter	280
8.24.1. Lognormal 4-Parameter (Amplitude)	280
8.24.2. Lognormal 4-Parameter (Area)	281
8.25. LogNormal	282
8.25.1. LogNormal (Amplitude)	283
8.25.2. LogNormal (Area)	284
8.26. Lorentzian or Cauchy distribution	285
8.26.1. Lorentzian (Amplitude)	285
8.26.2. Lorentzian (Area)	286
8.27. Maxwell-Boltzmann distribution	287
8.27.1. Maxwell (Amplitude)	288
8.27.2. Maxwell (Area)	289
8.27.3. generalized Maxwell (Amplitude)	290
8.27.4. generalized Maxwell (Area)	291
8.28. Pearson-IV	292
8.28.1. Pearson-IV (Amplitude)	292

8.28.2. Pearson-IV (Area)	293
8.29. Pearson-VII	294
8.29.1. Pearson-VII (Amplitude)	296
8.29.2. Pearson-VII (Area)	297
8.30. Pulse Peak	298
8.30.1. Pulse Peak (Amplitude)	298
8.30.2. Pulse Peak (Area)	299
8.31. Pulse Peak with 2nd Width Term	300
8.31.1. Pulse Peak with 2nd Width Term (Amplitude)	300
8.31.2. Pulse Peak with 2nd Width Term (Area)	301
8.32. Pulse Peak with Power Term	302
8.32.1. Pulse Peak with Power Term (Amplitude)	302
8.32.2. Pulse Peak with Power Term (Area)	303
8.33. Student-t	304
8.33.1. Student-t (Amplitude)	304
8.33.2. Student-t (Area)	305
8.34. Trapezoidal peak	306
8.34.1. Trapezoidal peak (Area)	306
8.34.2. Trapezoidal peak (Ampl)	307
8.35. Generalized trapezoidal peak	308
8.35.1. Generalized trapezoidal peak (Area)	308
8.35.2. Generalized trapezoidal peak (Ampl)	309
8.36. smoothed symmetric trapezoidal peak	310
8.36.1. smoothed symmetric trapezoidal peak (Area)	310
8.36.2. smoothed symmetric trapezoidal peak (Ampl)	311
8.37. Voigt	312
8.37.1. Voigt (Amplitude)	313
8.37.2. Voigt (Area)	314
8.37.3. Weibull	315
8.37.4. Weibull (Amplitude)	315
8.37.5. Weibull (Area)	317
 Chapter 9. Plugin functions for form factors	319
9.1. Non spherical-symmetric randomly oriented particles	319
9.1.1. Rectangular parallelepiped	319
9.1.2. Ribbon	321
9.2. Very thin particles (local planar & local cylindrical objects)	325
9.2.1. Pcs(Q) for planar obj.	326
9.2.1.1. Pcs(Q) for a homogeneous cross-section	327
9.2.1.2. Pcs(Q) for two infinitely thin parallel layers	329
9.2.1.3. Pcs(Q) for a layered centro symmetric cross-section structure	331
9.2.1.4. Pcs(Q) for a bilayer with a Gaussian electron density profile	333
9.2.2. Pcs(Q) for cylindrical obj.	335
9.2.2.1. Pcs(Q) for homogeneous cross-section of a cylinder	336
9.2.2.2. Pcs(Q) for cross-section of a cylindrical shell with elliptical cross section	338
9.2.2.3. $P_{cs}(q)$ for cross-section of circular core and shell with linear contrast	340

9.2.2.4.	$P_{\text{cs}}(q)$ for circular cross-section folded with a Gaussian	343
9.2.2.5.	$P_{\text{cs}}(q)$ for circular cross-section with a Boucher contrast profile	345
9.2.3.	$P'(Q)$ for local planar obj.	348
9.2.3.1.	$P'(Q)$: thin discs	349
9.2.3.2.	$P'(Q)$: thin spherical shell	351
9.2.3.3.	$P'(Q)$: thin ellipsoidal shell	353
9.2.3.4.	$P'(Q)$: thin-walled hollow cylinder	355
9.2.4.	$P'(Q)$ for local cylindrical obj.	357
9.2.4.1.	$P'(Q)$: Rod	358
9.2.4.2.	$P'(Q)$: freely joined chain of rods	360
9.2.4.3.	$P'(Q)$: Koyama worm	362
9.2.4.4.	$P'(Q)$: Kholodenko's worm	364
9.2.4.5.	$P'(Q)$: wormlike PS1	367
	Without Excluded Volume Effects.	367
	With Excluded Volume Effects.	369
9.2.4.6.	$P'(Q)$: wormlike PS2	371
9.2.4.7.	$P'(Q)$: wormlike PS3	373
9.2.4.8.	$P'(Q)$: semi-dilute wormlike PS3	376
9.2.5.	local planar obj.	378
9.2.5.1.	Disc+SD+BiLayerGauss	378
9.2.5.2.	Disc+SD+homoXS	378
9.2.5.3.	EllSh+SD+BiLayerGauss	378
9.2.5.4.	EllSh+SD+homoXS	379
9.2.5.5.	CylSh+SD+BiLayerGauss	379
9.2.5.6.	CylSh+SD+homoXS	380
9.2.6.	local cylindrical obj.	381
9.2.6.1.	Rod+SD+EllCylSh	381
9.2.7.	Liposomal structures	382
9.2.7.1.	PEGylated liposome with piecewise constant bilayer scattering length density profile	383
9.2.7.2.	PEGylated liposome with smeared scattering length density profile	386
9.3.	Spherical core-shell structures with smooth or fuzzy interfaces	390
9.3.1.	JuelichCoreShell	391
9.3.2.	Fuzzy Sphere	394
9.3.3.	CoreShellMicrogel	397
9.3.4.	Spherical shell with linear varying contrast profile (LinShell)	400
9.3.5.	LinShell2	403
9.3.6.	ExpShell	405
9.3.7.	BoucherSphere, radial profile for a sphere resulting in a Porod law both below and above q^{-4}	408
9.3.8.	Power law scattering profile (fuzzy sphere model)	411
9.3.9.	Generalized Exponential scattering profile (fuzzy sphere model)	412
9.3.10.	Generalized Gaussian scattering profile (fuzzy sphere model)	414
9.4.	Polymers and Micelles	415
9.4.1.	Gaussian chain	415
9.4.1.1.	Gauss	418

9.4.1.2. Gauss2	418
9.4.1.3. Gauss3	418
9.4.1.4. Polydisperse flexible polymers with Gaussian statistics	419
9.4.1.5. generalized Gaussian coil	420
9.4.1.6. generalized Gaussian coil 2	421
9.4.1.7. generalized Gaussian coil 3	422
9.4.2. Star-shaped polymers	423
9.4.2.1. Star polymer with Gaussian statistic according to Benoit	423
9.4.2.2. Star polymer with arms of rigid rods	425
9.4.2.3. Star polymer with semi-flexible arms	427
9.4.2.4. Star of gaussian polymer with excluded volume	430
9.4.2.5. Polydisperse star polymer with Gaussian statistics [62]	432
9.4.2.6. Star polymer according to Dozier	434
9.4.2.7. Dozier	434
9.4.2.8. Dozier2	436
9.4.3. Ring Polymers	438
9.4.3.1. Flexible Ring Polymer	438
9.4.3.2. m -membered twisted ring	441
9.4.3.3. Daisy-like Ring	443
9.4.4. Semi-flexible or worm-like polymers	445
9.4.4.1. wormlike polymer (PS1)	445
9.4.4.2. wormlike polymer (PS2)	445
9.4.4.3. wormlike polymer (PS3)	446
9.4.4.4. Kholodenko worm	446
9.4.4.5. Koyama worm	446
9.4.4.6. Freely joined chain of rigid rods	447
9.4.5. branched polymer	448
9.4.5.1. random f -functional polycondensates	448
9.4.5.2. hyperbranched polymer: fractal approach	448
9.4.5.3. Hyper-branched AB_2 polymers perturbed by excluded volume interaction	448
9.4.5.4. comb	449
9.4.5.5. bottle-brush polymer	451
9.4.5.6. soft sphere model	452
9.5. Lorenz-Mie Form Factors for Static Light Scattering	453
9.5.1. MieSphere	453
9.5.2. MieShell	455
9.6. Ellipsoidal Objects	457
9.6.1. Ellipsoid of revolution or spheroid	457
9.6.2. Spheroid with a Gamma size distribution	461
9.6.3. Ellipsoid with two equal equatorial semi-axis R and volume V	463
9.6.4. Ellipsoidal core shell structure	464
9.6.5. triaxial ellipsoidal core shell structure	467
9.7. Cylindrical objects	470
9.7.1. Disc	470
9.7.2. Rod	471

9.7.3.	Porod's approximation for a long cylinder	472
9.7.4.	Porod's approximation for a flat cylinder	474
9.7.5.	Porod's approximations for cylinder	476
9.7.6.	Cylinder of length L , radius R and scattering contrast $\Delta\eta$	478
9.7.7.	Random oriented cylindrical shell with circular cross-section	479
9.7.8.	Random oriented cylindrical shell with elliptical cross-section	482
9.7.9.	Random oriented solid cylinder with circular cross-section and globular end caps	486
9.7.10.	Cylinders packed in a hexagonal lattice with paracrystalline distortion	488
9.7.10.1.	Scattering perpendicular to paracrystalline hexagonal packed cylinders	489
9.7.10.2.	Scattering of randomly oriented bundles of paracrystalline hexagonal packed cylinders	490
9.7.11.	Torus with elliptical shell cross-section	493
9.7.12.	Helical structures	495
9.7.12.1.	Fanlike helix	495
9.7.12.2.	Helix with round cross-section	497
9.7.12.3.	Beads model of a single helical strand	499
9.7.12.4.	straight superhelix	502
9.7.12.5.	coiled superhelix	504
9.8.	Generalized form factor compliant for Titchmarsh transform	507
9.9.	Sheared and deformed objects	510
9.9.1.	Non-equilibrium static form factor of a reptating chain	510
9.9.2.	step-deformed polymer networks	512
9.9.3.	polymer under shear flow	515
9.9.4.	linear polymer under shear flow	517
9.9.5.	Ring polymer under shear flow	521
9.9.6.	Sheared Cylinder according to Hayter and Penfold	523
9.9.7.	partly aligned anisotropic objects	526
9.9.7.1.	Maier-Saupe orientation distribution	531
9.9.7.2.	Onsager orientation distribution	533
9.9.7.3.	Boltzmann orientation distribution	535
9.9.7.4.	Gaussian orientation distribution	537
9.9.7.5.	Boxed orientation distribution (HeavisidePi)	539
9.10.	Functions for analysing azimuthal averaged data	541
9.10.1.	\sin^2 - \sin^4 azimuthal analysis	541
9.10.2.	Ellipsoidal azimuthal analysis	542
9.10.3.	affine shrinkage	543
9.10.4.	Maier-Saupe azimuthal analysis	544
9.10.5.	azimuthal analysis of very long oriented structures with Maier-Saupe or Onsager orientation distribution	545
9.10.6.	azimuthal analysis of sheared or deformed structures	547
9.11.	anisotropic form factors of oriented primitive objects	549
9.11.1.	perfect and random oriented ellipsoid	551
9.11.2.	perfect and random oriented parallelepiped	553
9.11.3.	perfect and random oriented cylinder	556
9.11.4.	oriented and random oriented cone	559

9.11.5. oriented and random oriented cone with 6-fold symmetry	562
9.11.6. oriented and random oriented tetrahedron	564
9.11.7. oriented and random oriented square basis pyramid	565
9.11.8. oriented and random oriented octahedron	567
9.11.9. oriented and random oriented rhombic dodecahedron	569
9.11.10. oriented superellipsoid	571
9.11.11. oriented super-egg	575
9.11.12. oriented super-shapes and rational super-shaped	578
9.12. oriented super-toroid and super-helix	581
9.13. Form factors of magnetic objects	583
9.13.1. Magnetic spin misalignment	583
9.13.2. Ferrofluids	585
9.13.3. Langevin statistics for averages of the form factor and averages of the squared form factor	588
9.14. Bi-continuous and non-particulate structures	592
9.14.1. Stochastic models of disordered porous materials	592
9.14.1.1. dead-leaves model	593
9.14.1.2. boolean (union model)	595
9.14.1.3. boolean (intersection model)	597
9.14.1.4. clipped random fields	598
Single threshold:	598
Two-cut model:	599
Two-cut intersection model:	599
9.14.2. Teubner-Strey	603
9.14.3. Debye-Anderson-Brumberger(DAB)	606
9.14.4. Generalization of the Debye-Anderson-Brumberger model	607
9.14.5. deformed random oriented Debye-Anderson-Brumberger model	609
9.14.6. Blob	611
9.14.6.1. blob (beaucage)	611
9.14.6.2. blob (star)	611
9.14.6.3. blob (dendrimer)	612
9.14.7. Spinodal	614
9.14.8. Phase separation	616
9.14.9. OrnsteinZernike	618
9.14.10. Broad-Peak	619
9.14.11. generalized Guinier approximation	621
9.14.12. generalized Guinier-Porod law	623
9.15. Clustered Objects	625
9.15.1. Mass Fractal	625
9.15.2. Stacked Discs	627
9.15.3. DumbbellShell	629
9.15.4. DoubleShellChain	630
9.15.5. fractal size distribution of particles	633
9.16. Plugin functions for SESANS	637
9.16.1. $G(\delta)$ of a sphere	639

9.16.2. $G(\delta)$ of a randomly distributed, two-phase system (DAB) and its generalisation (gDAB)	641
9.16.3. $G(\delta)$ for a generalized Gaussian coil (gGc)	642
9.17. Plugin functions for multiple scattering models	645
9.17.1. Multiple scattering of Spheres	646
9.17.2. Multiple scattering of polydisperse Spheres	647
9.17.3. Multiple scattering of Gaussian coils	648
9.17.4. Multiple scattering of a self-affine random distribution model	649
 Chapter 10. Plugin functions for size distributions	651
10.1. LogNorm	651
10.1.1. LogNorm_fp	651
10.1.2. bi-LogNorm	654
10.1.3. shifted LogNorm	654
10.2. metalog distribution	654
10.2.1. unbounded metalog distribution	654
10.2.2. semi-bounded metalog distribution	655
10.2.3. bounded metalog distribution	655
10.3. Johnson's distribution	655
10.3.1. Johnson S_B	655
10.3.2. Johnson S_L	655
10.3.3. Johnson S_U	655
10.3.4. Johnson S_N	655
10.4. generalized Johnson's distribution	655
 Chapter 11. Plugin functions for structure factors	657
11.1. Three dimensional structure factors for hard sphere systems	657
11.1.1. Carnahan and Starling	658
11.1.2. Padé(4,3) of van Rensburg and Sánchez	659
11.1.3. Malijevský and Veverka	660
11.1.4. López de Haro and Robles	661
11.1.5. Grundke and Henderson	662
11.1.6. Hard Sphere (PY)	664
11.2. Structure factor for a two dimensional hard spheres/disks fluid	666
11.2.1. Two dimensional hard sphere/disks fluid according to Rosenfeld	666
11.2.2. Two dimensional hard sphere/disks fluid according to Guo	667
11.3. One dimensional structure factors	669
11.3.1. Structure factor for a hard spheres potential in one dimension	669
11.3.2. One dimensional paracrystal	670
11.4. three dimensional structure factor for sticky hard sphere systems	671
11.4.1. Sticky Hard Sphere	671
11.4.2. Sticky Hard Sphere (2 nd version)	672
11.4.3. Square Well Potential	674
11.4.4. Square Well Potential 2	675
11.4.5. Structure factor of fluids interacting via piece-wise constant potentials and a hard core	676

11.5. ordered particle systems	678
11.5.1. Domains of ordered particle systems isotropically oriented	679
11.5.2. Domains of ordered particle systems with preferred orientation	682
11.6. Multi Lamellar Structures	684
11.6.1. Multi-Lamellar Structures, perfect finite stack	684
11.6.2. Multi-Lamellar Structures, Thermal Disorder	686
11.6.3. Multi-Lamellar Structures, Paracrystalline Theory	688
11.6.4. Multi-Lamellar Structures, Modified Caillé Theory	691
11.7. Mass Fractal	694
11.7.1. Mass Fractal (Exp Cut-Off)	696
11.7.2. Mass Fractal (Exp(-x ^a) Cut-Off)	697
11.7.3. Mass Fractal (Gaussian Cut-Off)	698
11.7.4. Mass Fractal (OverlapSph Cut-Off)	699
11.7.5. Structure factor of a random flight model	700
11.7.6. Structure factor of a random flight model with a paracrystalline like disorder parameter	701
11.7.7. Extended cluster structure factor with local hardsphere interactions	701
11.7.8. Mass fractal with nearest neighbor perturbations	702
11.7.9. aggregate with nearest neighbor perturbations	703
11.7.9.1. DLC aggregate with nearest neighbor perturbations	705
11.7.9.2. RLC aggregate with nearest neighbor perturbations	705
11.8. Structure factors for Yukawa like potentials	707
11.8.1. Hard core double Yukawa interaction	707
11.8.2. Hayter-Penfold structure factor for a screened coulomb interaction (single Yukawa, RMSA)	708
Chapter 12. Special topics	709
12.1. Fitting absolute intensities	709
12.2. Forward Scattering - Volume Fraction - Absolute Scale	711
12.3. Moments of scattering curves and size distribution	713
12.4. Volume fractions	715
12.5. How to use quantile distribution function in SAS	718
12.5.1. List of some selected quantile distribution function to describe size distributions	719
12.5.2. MetaLog distribution	721
12.5.3. use of quantile distribution function to describe size distributions	722
12.5.4. highly flexible quantile distribution function used as scattering length distribution profiles	724
12.5.5. Test of some quantile distribution function describing SLD profiles	726
Chapter 13. Basic Analysis of Dynamic Light Scattering Data	727
13.1. Cumulant Analysis	728
13.2. Double Decay Cumulant Analysis	729
13.3. Fit of Double Stretched Exponentials	730
13.3.1. The least squares minimiser and the robust least squares procedure	731
Chapter 14. Scattering Theory	733

14.1. Scattering Cross-Section	733
14.1.1. Scattering of neutrons on atoms	734
14.1.1.1. Nuclear scattering	735
14.1.1.2. Magnetic Scattering	736
14.1.2. Scattering of x-ray at atoms	738
14.1.2.1. Anomalous scattering of x-rays	739
14.2. Small angle scattering	740
14.2.1. Autocorrelation function $\Gamma(\mathbf{r})$ and $\gamma(\mathbf{r})$	741
14.2.1.1. Isotropic averages	741
14.2.1.2. Absence of long range order	741
14.2.1.3. Limits $r = 0$ and $r = \infty$	742
14.2.2. Volume fraction	743
14.2.3. Interparticle interferences	743
14.2.3.1. Isotropic ensemble of particles	744
14.2.4. Influence of the relative arrangement of scatterers on interparticle interferences	745
14.2.4.1. Formula from Prins and Zernicke	746
14.2.4.2. Isolate particles	747
14.2.4.3. Polydisperse System of isolated particles	747
14.2.5. Influence of $N(R)$ and $F(Q, R)$ on interparticle interferences	747
14.2.6. Scattering laws and structural parameter	748
14.2.6.1. Porod volume	748
14.2.6.2. Radius of gyration and Guinier approximation	749
14.2.6.3. Correlation length	750
14.2.6.4. Porod law and specific surfaces	750
Chapter 15. Experimental Setup of a Small Angle Scattering Instrument	753
15.1. SANS-Camera	753
15.2. SAXS-Camera	753
Chapter 16. Data Reduction in SAS	755
16.1. Correction and Normalization of SANS-Raw data	755
16.1.1. Contribution of the isolated sample	755
16.1.2. Correction for sample holder and background noise	756
16.2. Correction and normalization of SAXS raw data	757
Appendix. Bibliography	773

CHAPTER 1

Introduction to the data analysis program **SASfit**

Small-angle scattering (SAS) is one of the powerful techniques to investigate the structure of materials on a mesoscopic length scale (10 - 10000 Å). It is used to study the shapes and sizes of the particles dispersed in a homogenous medium. The materials could be a macromolecule (biological molecule, polymer, micelle, etc) in a solvent, a precipitate of material A in a matrix of another material B, a microvoid in certain metal or a magnetic inhomogeneity in a non-magnetic material. This technique is also used to study the spatial distribution of particles in a medium, thus providing the information about the inter-particle interactions. The small angle scattering methods includes small angle neutron, x-ray or light scattering. The type of samples that can be studied by scattering techniques, the sample environment that can be applied, the actual length scale probed and the information that can be obtained, all depend on the nature of the radiation employed. The advantage of small-angle neutron scattering (SANS) over other SAS methods is the deuteration method. This consists in using deuterium labeled components in the sample in order to enhance their contrast. Whereas the disadvantage of SANS over small-angle x-ray scattering (SAXS) is the intrinsically low flux of neutron sources compared to the orders of magnitude higher flux at x-ray sources. Neutron scattering in general is sensitive to fluctuations in the density of nuclei in the sample. X-ray scattering is sensitive to inhomogeneities in electron densities whereas light scattering is sensitive to fluctuations in polarizability (refractive index). In general, irrespective of the type of radiation, they also share several similarities. Perhaps the most important of these is the fact that, with minor adjustments to account for the different types of radiation, the same basic equations and laws can be used to analyze data from these techniques. The small-angle scattering data can contain information concerning both the structure and interaction within the system. This information can be obtained by either performing model-independent analysis or detailed model dependent analysis. **SASfit** is such a software package built originally for analysis of small-angle scattering data in the field of soft matter. The main emphasis of the software is to provide easy to use graphical user interface. The software package contains most of the tools to treat the basic scientific problems for data produced on a SAS instrument. It allows users to derive useful information from the SAS scattering data.

1.1. Overview

SASfit is designed for analysing small angle scattering data and also supplies some simple analysis for dynamic light scattering data. At the moment it performs the following analysis routines to both single 1D data sets as well as multiple 1D data sets, where one like to simultaneously fit several data sets, like from concentration series or contrast

variation experiments. In principle by this way also 2D data sets can be analysed by loading segmentationally averaged 2D data.

- determining integral structural parameters by simple Guinier and Porod analysis
- fitting and simulating single or multiple data sets in terms of size distribution, form factor and structure factors
- analysing DLS data in terms of stretched exponentials or cumulants.
- calculating scattering length densities for x-rays and neutrons
- solving numerically the Ornstein-Zernike equations for any combination of supplied pair interaction potential and closure relation
- allows to read, transforms, merge, clip and scale data files. The number of formats is limited.

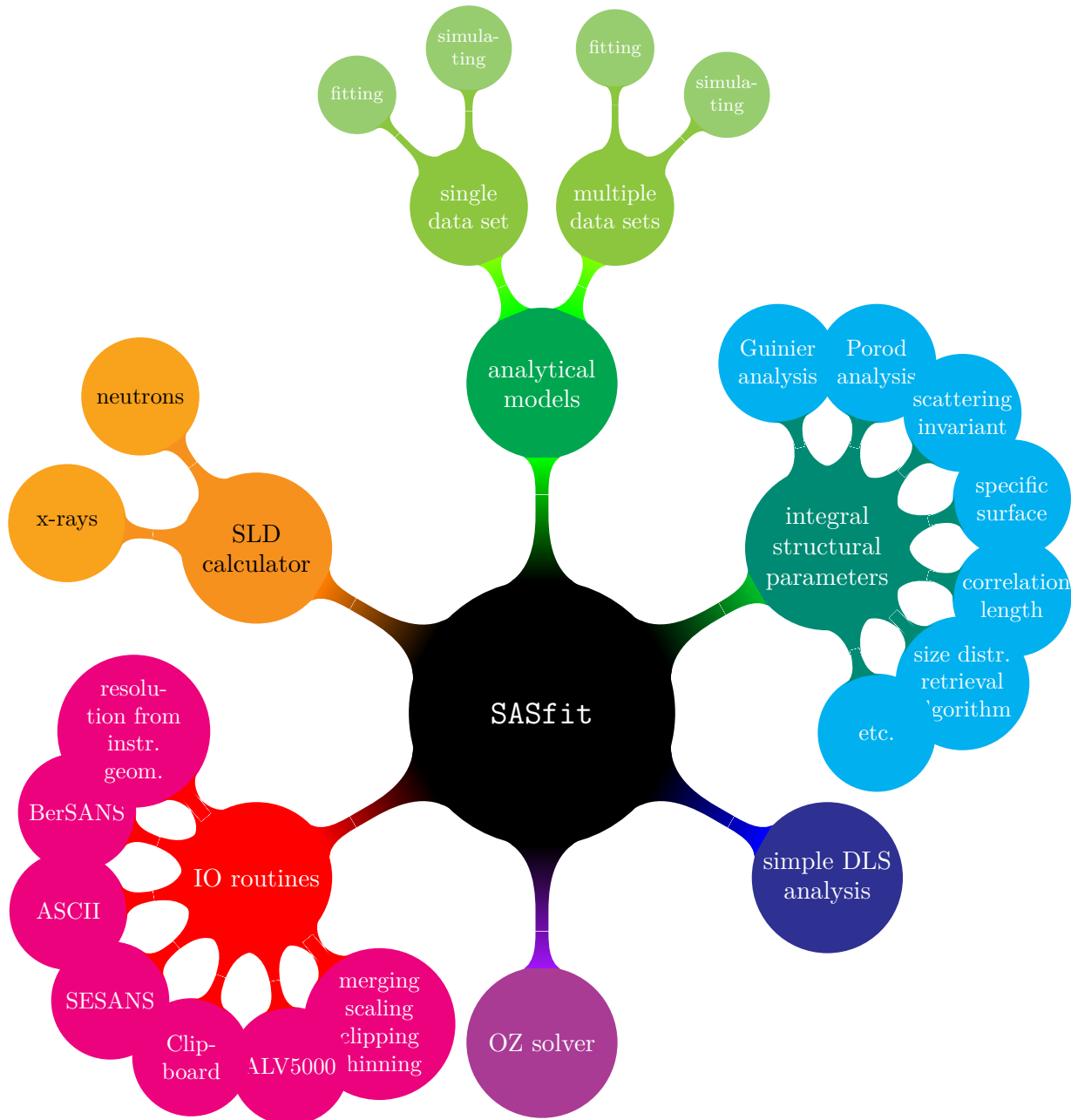
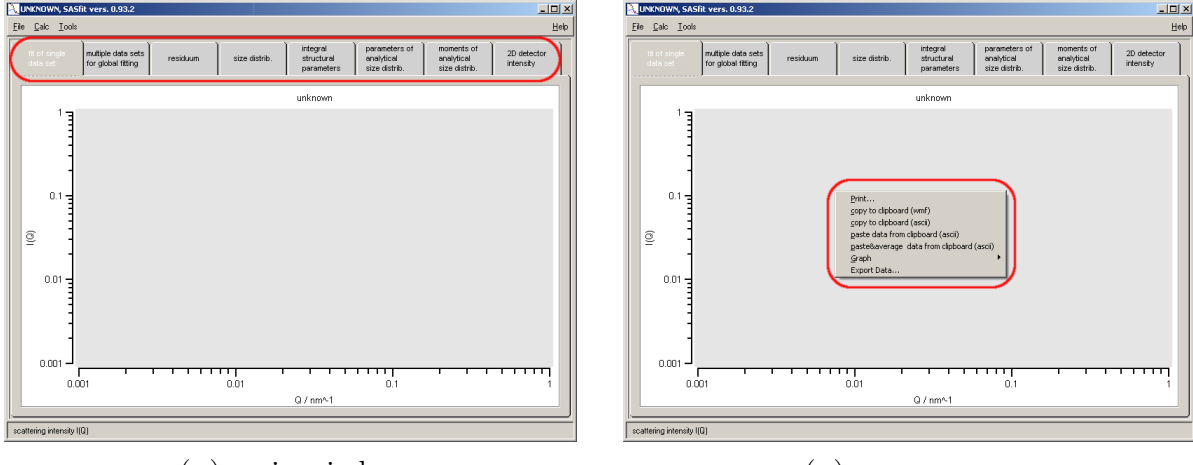


FIGURE 1.1. Mind map about the tools in SASfit

CHAPTER 2

Quick Start Tour

2.1. User Interface Window



(A) main window

(B) popup menu

FIGURE 2.1. Main SASfit graphical user interface window

The core **SASfit** window consists of various tabs (shown in the oval marking in the figure 2.1a, they are "fit of single data set", "multiple data sets for global fitting", "residuum", "size distrib.", "integral structural parameters", "parameters of analytical size distrib.", "moments of analytical size distrib.", and "2D detector intensity" as shown in the red oval selection. The tabs for single data set and multiple data sets are used to plot single or multiple data files and view the plotted graphs along with the operations to perform during fitting. Residuum shows the difference between the experimental and theoretical fits. Size distributions give the plotted view of the number density versus radius of the particle, whereas number density times cubed radius versus radius $R \rightarrow N(R)R^3$ is the default plotting configuration. Integral structural parameters are obtained using model independent fitting, such as Guinier approximation, Porod law etc. Parameters of analytical size distributions provides with details of size distributions used and the numbers obtained, whereas moments of analytical size distribution shows the contribution of scattering from different size distribution. The final tab 2D detector intensity is used in case of anisotropic scattering data. The window where the graphs are generated has options of printing the graph plotted view, copying the data in the ASCII format or as an image (wmf) format for further processing or presenting (figure 2.1b). **SASfit** accepts the isotropic data in the ASCII format. The data can be imported as a single data set or for multiple data sets (several scattering curves).

2.2. Importing data files for a single data set

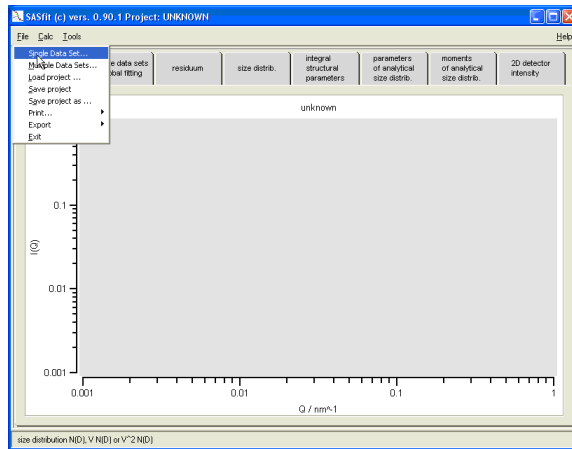


FIGURE 2.2. Menu interface for input single data set

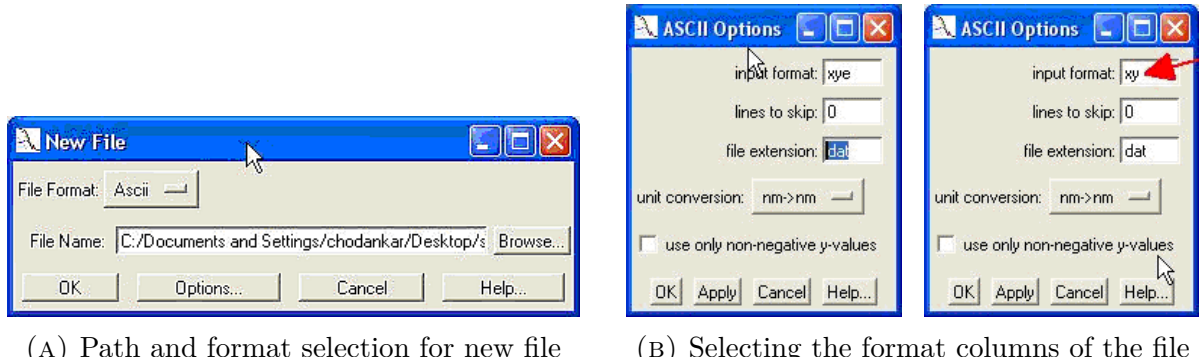


FIGURE 2.3. Importing single data sets

The single data set option allows the user to perform operation on a single data file only. The file is imported via, [File|Single Data Set...] (Figure 2.2). This will open a new file window as shown in figure 2.3a. The location of the file could be browsed and respectively selected. The options buttons is supplied to select the input format, which is performed by supplying a string such as xye . Where x , y and e stands for the scattering vector Q , scattering intensity $I(Q)$, e signifies the error bar $\Delta I(Q)$ on the measured scattering intensity. The error bars are required during the fitting operation and for files which do not contain the error bar column it would be calculated by default from the smoothing of the curve. There is an option to skip lines at the beginning of the data, which is intended to be used to skip header information in a data file , which could be misinterpreted as data. The number n specified in the menu defines the number of lines skipped at the beginning of the data file. Furthermore a file extension can be provided, unit conversions can be performed as well as only non-negative y -values could be selected for plotting and performing further analysis. On pressing ok the data is loaded and the graph is plotted, with a new window labeled merge files being opened.

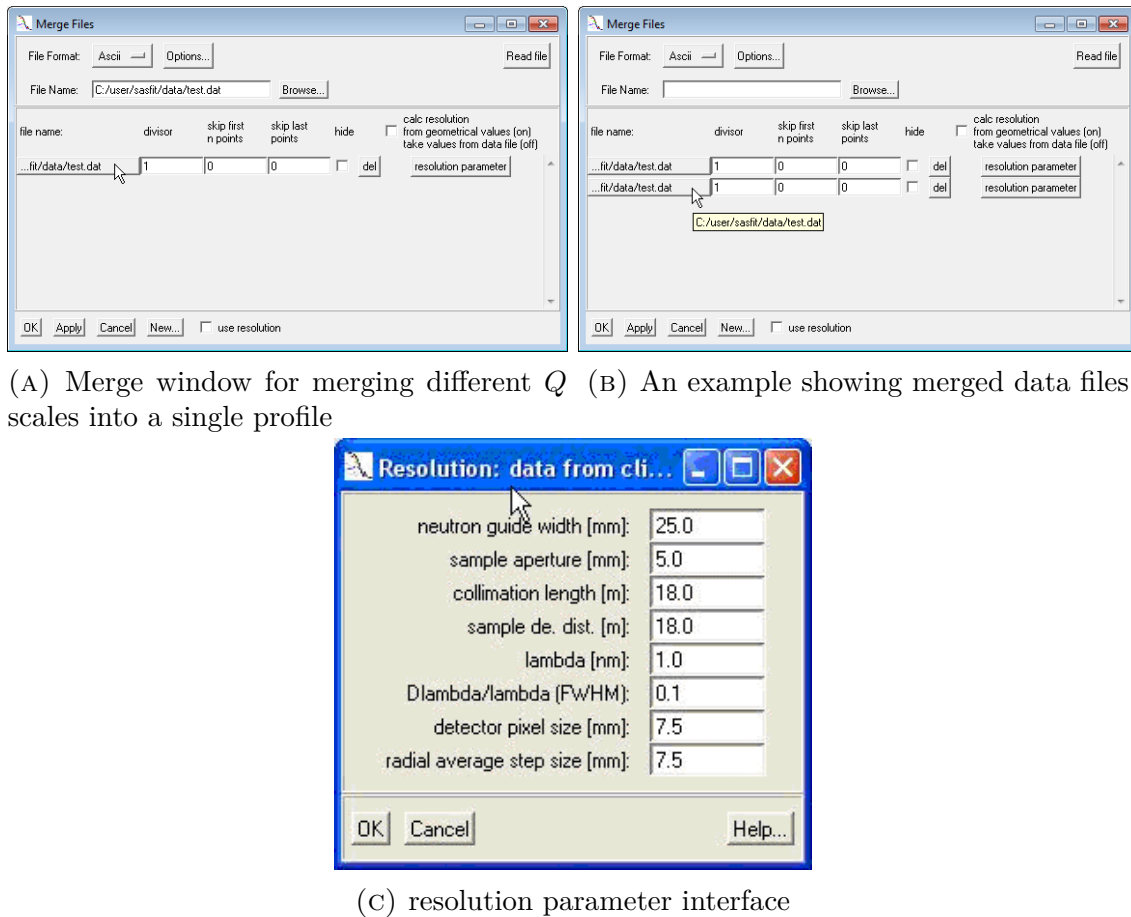


FIGURE 2.4. Merging many data files to one data set

In SAS, data can be collected at different collimator and sample to detector distances to correspond for a wide Q scale. Thus for a single sample at a given condition there can be more than one data files, to merge all of them together for completing the scattering profile, the above shown window comes into play. As shown in the merge files window, the new file could be browsed and selected; it has to be read using the read file button. The newly read file is listed below the first file, if it's a wrong selection it could be deleted back, also one can scale the different files measured at different Q windows, using the divisor column to have a continuous scattering profile. After scaling all the data profiles into one single profile, the statistically bad and unwanted data points can be removed by skipping the points at the beginning and at the end of the data files. The resolution parameters can be provided by pressing the resolution button and the required information such as sample to detector distance, collimation distance, cross section of the guide etc as shown in figure 2.4c has to be entered to use resolution smearing during the fitting. The new button is use to discard all the current selections and plotted data files and starts a new session. The file could also be imported by pasting the clipboard data on the graph view as shown in the figure below. The conditions for columns are same as that for reading the file via browse method.

2.3. Importing data files for multiple data sets

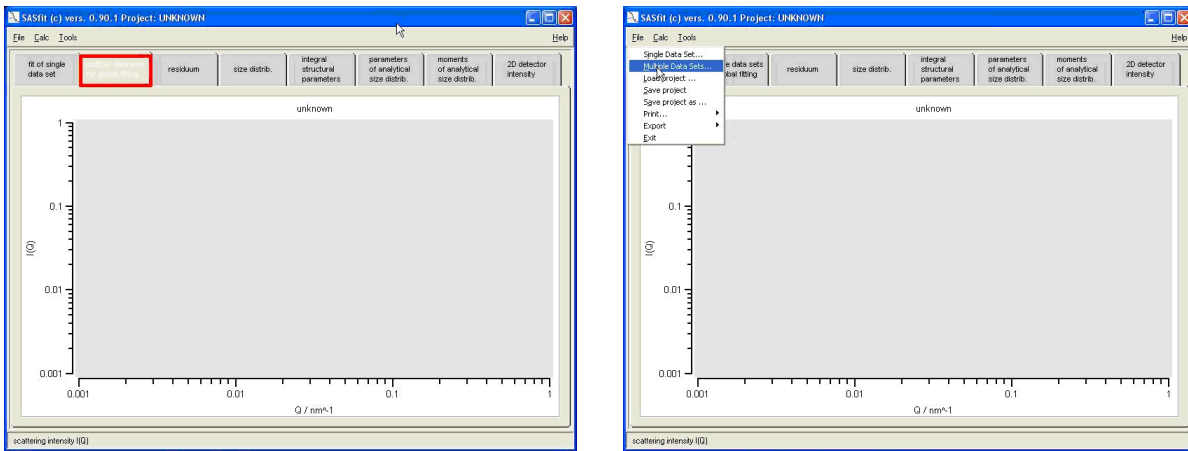


FIGURE 2.5. Procedure for importing data files for multiple data sets

The multiple data set option allows the user to perform operation on multiple data files by using common set of (global) parameters. This option is especially important in contrast variation experiments or measurements with polarized neutrons. The global fit helps to determine the fit parameters unambiguously which by analyzing a single curve would be otherwise strongly correlated. The file is imported by first going to multiple data sets for global fitting (red box in Figure 2.5) and then via, [File|Multiple Data Set...]. This will open a new window as was the case for importing single data set as shown below. The procedure for importing the first file is same as was the case for single file. On reading the first file the merge file window opens, which has additional buttons as compared to the merge file window in single data set (shown in the red rectangular box in figure 2.6(c)). In multiple data fitting, almost any number of data files could be loaded. The present active number of data is shown next to the data set in the merge file window. One can switch over from one data file to another by clicking previous or next. Add and remove buttons are used to add or remove another file. The addition of curves for different Q scales is performed similar to as mentioned in the Input single data set

2.4. Reducing the number of data points

SASfit is calculating the intensity for each data point. To make the minimization faster it can be useful to reduce the number of data points. A reduction of data points make sense if they are oversampled, i.e. within the distance of neighbouring q -values the intensity is only changing little. SASfit supplies two algorithms for reducing the number of data points and one algorithm which is averaging data points. After reading a data file a new entry is generated in the GUI, see e. g. 2.6(c). The filename button activates the GUI (see fig. 2.7) for choosing an algorithm to reduce optionally the number of data points. Three procedures are supplied at the moment:

- (1) averaging neighbouring data points depending on error bar and q difference
- (2) skipping equally data points to reduce their numbers to a certain percentage

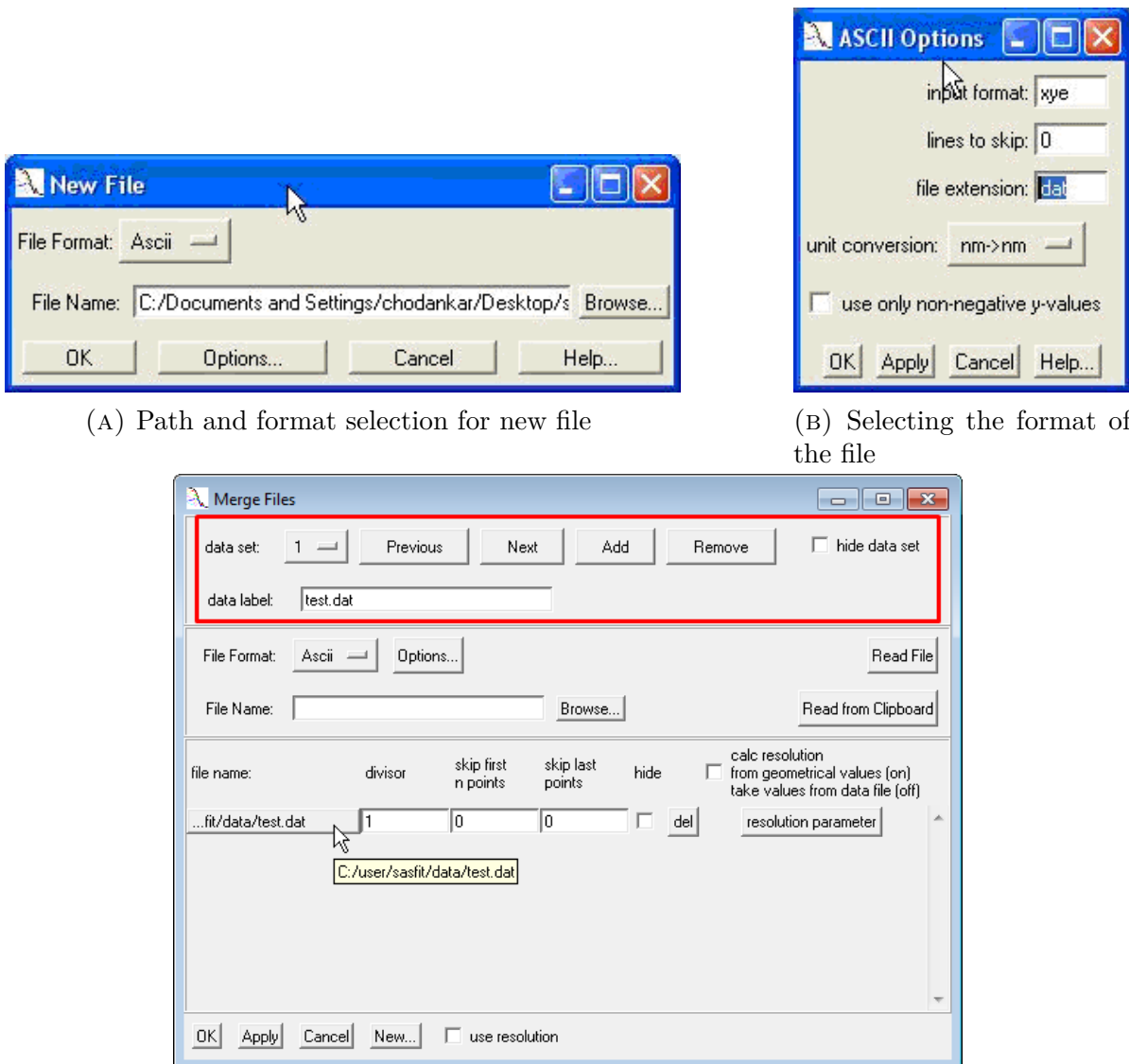


FIGURE 2.6. Procedure for importing data files for multiple data sets

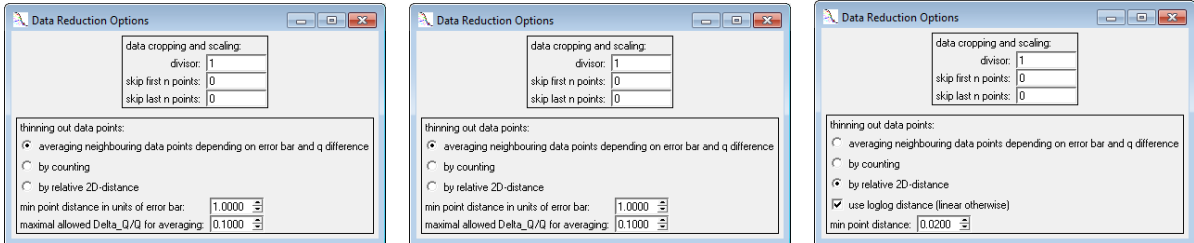
(3) skipping nearby data points

By using the first option an averaging of data points $I_k(q_k) \dots I_l(q_l)$ is done as long as they fulfill the conditions that

$$\forall n \in (k, l] : |I_k - I_n| < D_{\min}(\Delta I_k + \Delta I_n) \quad \wedge \quad |q_k - q_n|/\bar{q} < \Delta q_{\max} \quad (2.1)$$

where D_{\min} and Δq_{\max} are user supplied values. The averaging of data points therefore depends on a user-defined maximum allowed q -smearing Δq_{\max} and a user-defined maximum distance in intensity in units of the error bar (D_{\min}), so that an averaging is

only performed, if the intensities look similar with D_{\min} -times the intensity error bars and are not too far away from each other on the q-axes. The second option simply skips data points equally to reduce the amount data. The parameter "percentage/100 to load" defines the amount of data to be kept. A value of 1 means all data are kept and a value of 0.5 means every second data point will be kept. In the third option one can define a distance in the $q : I(q)$ -plot or $\log q : \log I(q)$ plot. The next data point, which will be plotted must have either in the linear or logarithmic plot a distance exceeding a user defined value.



- (A) Averaging data points depending on the error bar and resulting resolution
- (B) skipping data points to reduce the number of points to a certain amount
- (C) reducing the number of data points by defining a minimum distance between them to be plotted

FIGURE 2.7. GUI for input values of the two algorithms for reducing the number of data points and for one algorithm which is averaging data points.

2.5. Simulating scattering curves

In addition to reading and loading data set, one can also have a realistic view of the experimental scattering data for a known structure by simulating the scattering profile beforehand to get a feel of the actual experiment scattering profile. The simulation can be performed either for a single data set or for multiple data sets using global parameters. To generate theoretical scattering profile, follow [Calc|Single Data Set...|simulate] or [Calc|Multiple Data Sets...|simulate], either of them to generate a single data set or multiple data sets varied by changing the global parameter. The data can be generated for vast number of form factors and structure factor included in the software. The simulation is calculated using physically relevant parameters, this is useful to plan the experiment and to know whether a given concentration and contrast would produce a measurable signal.

2.6. Fitting

SASfit can analyse the data using both model-independent analysis and using a non-linear least square method to fit models. The model-independent analysis is a preliminary process of analyzing SAS data and does not require any advanced knowledge of the system to extract structural information this includes fittings (Guinier, Kratky, Porod, power-laws, etc.). On the other hand in case of non-linear least square methods



(A) simulation of a single curve

(B) simulation of multiple curves

FIGURE 2.8. Procedure for simulating data profiles for single as well as multiple data files

a detailed fitting to the experimental data is performed using a wide variety of form factors and structure factors. The **SASfit** model library consists of large number of such functions, which can be readily used for the analysis. Moreover it can also fit different size distributions.

2.6.1. Model Independent Fitting (Integral parameters).

Model independent analysis requires no advanced knowledge about the sample and most importantly no experimental bias of assumed structure. It includes linearized fitting (Guinier, Porod and Zimm plot) to extract structural information. Model independent analysis are performed via [Cals|integral parameters]. In **SASfit** there are basically three functions available to do the analysis; they are Guinier, Zimm and Porod approximations (shown in the blue box in Figure 2.9(b)). The number of data points to be included in the analysis can be accordingly varied and the resulting fit and the available parameters can be viewed instantaneously. For a large number of data a small script can be return to automate the process. This is performed by using the lower section of the integral structural parameters window (shown in red box). Plename indicates a character or string of characters with which all the data file names to be analysed starts with followed by certain numbers. The number of digits/characters in the filename could be given in the digits submission box, whereas the start number and the last file number are provided in their respective submission boxes. The step box indicates the incremental step of the file names which has to be analysed. The fitted parameters can be saved in the custom file to be viewed later. Load next file does step by step analysis of different files, whereas Do all would perform calculations on the entire file list, to be saved in the custom file for later viewing.

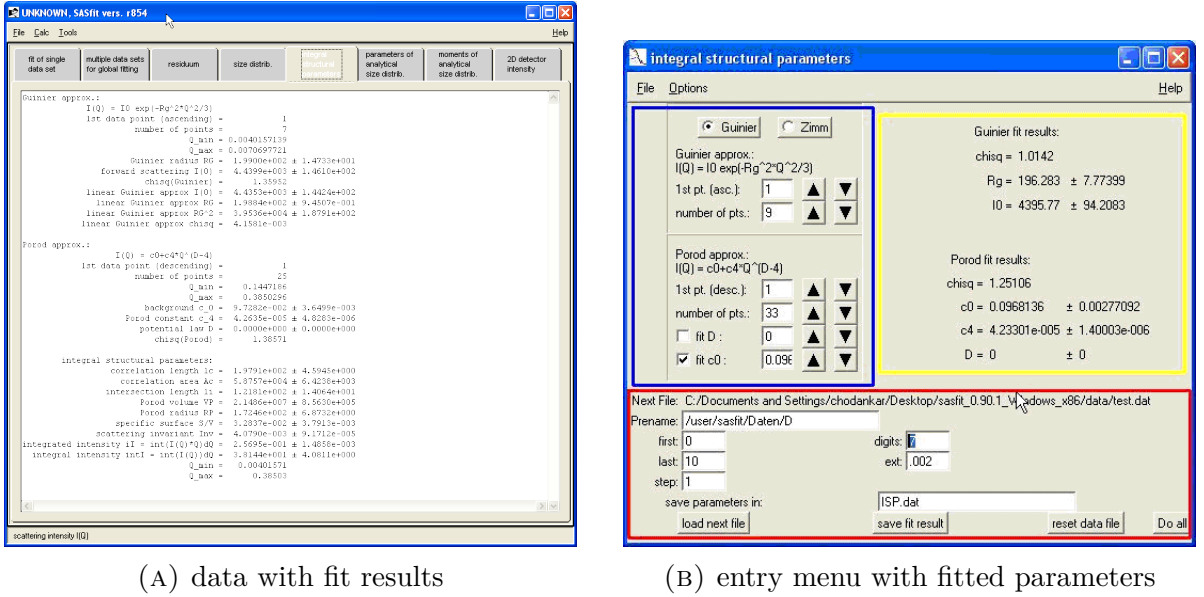


FIGURE 2.9. Integral fit parameters

A set of valuable size and integrated parameters that can be calculated directly from the scattering curves $I(Q)$ [94, 454, 93, 516, 342, 177] consists of

$$\tilde{Q}_{\text{inv}} = \int_0^{\infty} Q^2 I(Q) dQ \quad (\text{scattering invariant}) \quad (2.2a)$$

$$\frac{S}{V} = \frac{\pi}{\tilde{Q}_{\text{inv}}} \lim_{Q \rightarrow \infty} \left\{ Q^4 I(Q) \right\} \quad (\text{specific surface}) \quad (2.2b)$$

$$\langle R_G \rangle^2 = 3 \left(- \lim_{Q \rightarrow 0} \left\{ \frac{d[\ln I(Q)]}{d(Q^2)} \right\} \right) \quad (\text{squared Guinier radius}) \quad (2.2c)$$

$$\langle d \rangle = \frac{4}{\pi} \lim_{Q \rightarrow \infty} \left\{ Q^4 I(Q) \right\} \quad (\text{average intersection length}) \quad (2.2d)$$

$$\langle l \rangle = \frac{\pi}{\tilde{Q}_{\text{inv}}} \int_0^{\infty} Q I(Q) dQ \quad (\text{correlation length}) \quad (2.2e)$$

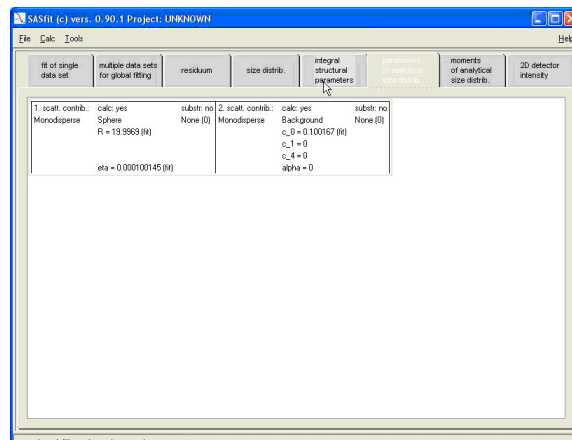
$$\langle A \rangle = \frac{2\pi}{\tilde{Q}_{\text{inv}}} \int_0^{\infty} I(Q) dQ \quad (\text{correlation surface}) \quad (2.2f)$$

$$\langle V \rangle = \frac{2\pi^2}{\tilde{Q}_{\text{inv}}} I(0) \quad (\text{correlation volume, Porod volume}) \quad (2.2g)$$

2.6.2. Model dependent analysis.

2.6.2.1. Modeling a single data set.

For Modeling a SANS data set the **SASfit** -programm allows to describe experimental data with an arbitrary number of scattering objects types. Each of them can have a size distribution, whereby the user can choose over which parameter a_i of the form factor



(c) Tab summarizing the analyzed parameters

FIGURE 2.10. Menus for fitting a single data set

the integration will be performed. For example in case of a spherical shell with a core radius of R and a shell thickness of ΔR **SASfit** allows to integrate either over the core radius $x = R$ or the shell thickness $x = \Delta R$ by marking the corresponding parameter (see option **distr** in Fig. 2.10b). Furthermore an additional structure factor can be included for each scattering object. Several ways to account for the structure factor have been implemented like the monodisperse approximation (4.1.1), decoupling approach (4.1.2), local monodisperse approximation (4.1.3), partial structure factor (4.1.4) and scaling approximation of partial structure factors (4.1.5). The details are described in chapter 4.

Implemented size distributions, form factors and structure factors are described in chapters 3, 4 and 7. Optional an additional smearing of this function with the instrument

resolution function $R_{av}(Q, \langle Q \rangle)$ can be activated so that

$$I(\langle Q \rangle) = \int_0^{\infty} R_{av}(Q, \langle Q \rangle) \frac{d\sigma}{d\Omega}(Q) dQ \quad (2.3)$$

A user interface shown in Fig. 2.10 is supplied to choose between the number of scattering objects and to define parameter for each of them. Next to varying the different parameters one can mark those to be fixed or fitted (see option **fit** in Fig. 2.10b). Model dependent analysis for single files are performed via [Calc|Single Data Set|Fit...].

2.6.2.2. Modeling multiple data sets.

The multiple data set option allows the user to perform operation on multiple data

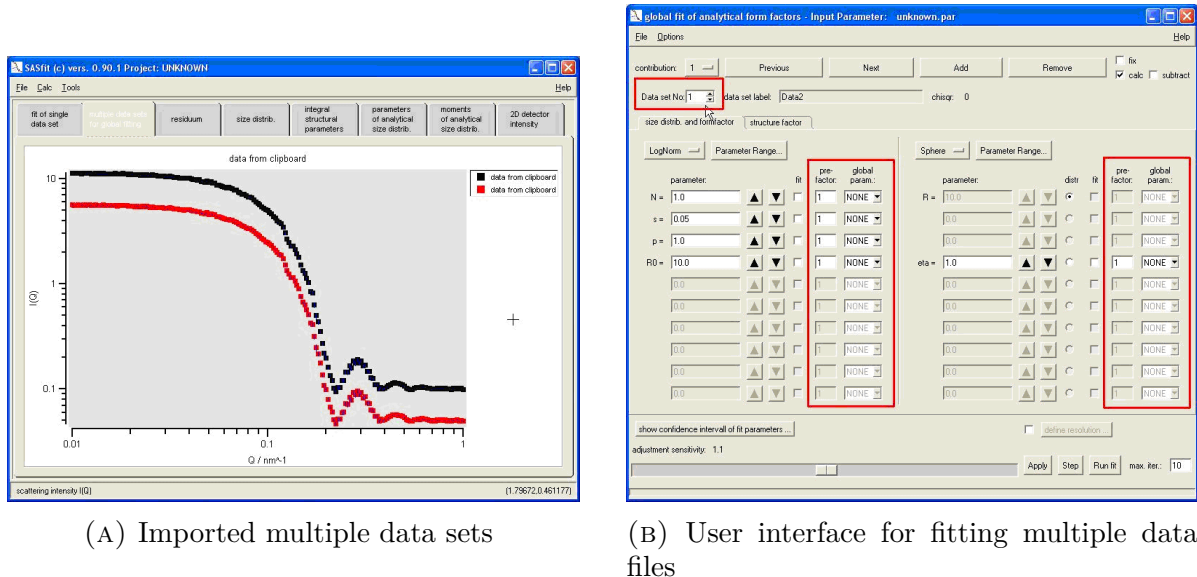


FIGURE 2.11. Menus for fitting a simultaneously multiple data sets

file by using common set (global) parameters. This option is especially important in contrast variation experiments or measurements with polarized neutrons. The global fitting helps the user to analyse large number of data which has a similar form or structure factor however different scaling constant. The data shown in the figure below is for a spherical monodispersed system both the data profile has identical features, except that the scaling factor between the two is of a factor of two. The data are called by the procedure explained in the input multiple data file section. The fitting of the data is performed by calling the fitting function via [Calc|Multiple Data Sets|Fit...]. The user interface for multiple data fitting has additional feature than to that for single data fitting, they are pre-factor and global parameters as shown in figure 2.11 red markings.

The procedure for fitting the data set is similar to that mentioned in the earlier section. The only difference is to include the global parameters for each function included. The scattering profile shown in the figure 2.11a is for a spherical monodispersed particle, both the profiles have identical features with a scaling factor of two. The user interface for fitting shows the following window in figures 2.12. The data set number shows the active data file, whereas contribution indicates the number of scattering objects. We



FIGURE 2.12. Different windows showing different controlling parameters during multiple data fitting.

have selected the form factor for a spherical particle. In the global parameter a new variable is produced for both radius and *eta* (scattering contrast). The pre-factor is kept constant at 1. A second contribution is added to the data set one by pressing add. In this case it is a background contribution, a new global parameter is introduced for it (P3). A similar procedure is done for second data set where the global parameter for the radius is kept same to that for data set one, whereas new global parameters are defined for scattering contrast and background. The fitting procedure can then be started by pressing Run fit. The figures 2.13 show the graphs during the fitting process. The parameters of fitting for all the contribution can be viewed by pressing parameters of analytical size distributions (figure ??).

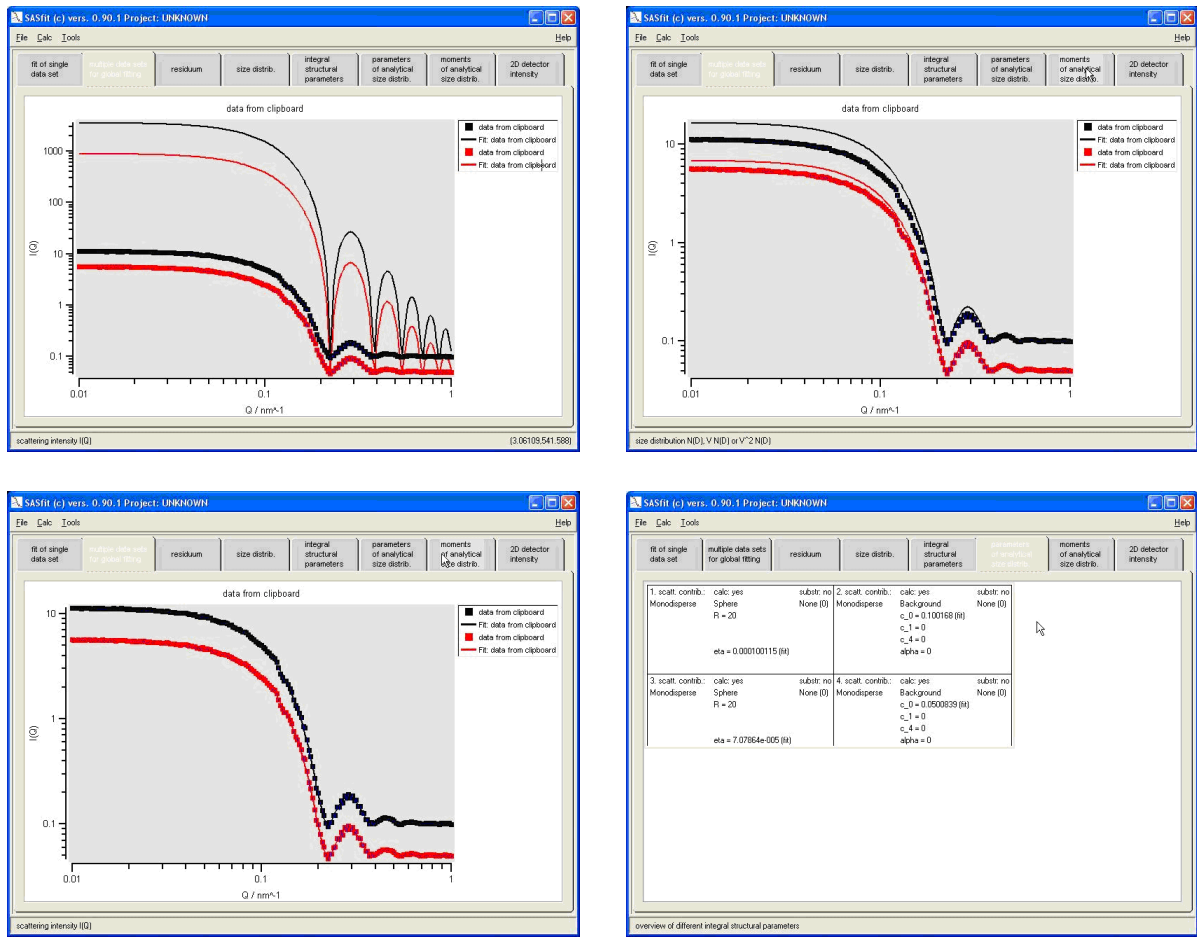


FIGURE 2.13. The scattering data profile and the analytical parameters obtained during the fitting process.

2.7. Criteria for goodness-of-fit

All criteria shown below for testing the goodness of a fit should be considered with caution [33, 397]. When you get data on a SAS instrument the measured intensities are measured with some statistical uncertainties. Normally one assumes Poisson statistics to determine the uncertainty in the counting statistics. The data reduction software should then perform a proper error propagation analysis for all succeeding data treatment operations. However, by this procedure only statistical uncertainties are taken into account. All systematic uncertainties are then hopefully covered during the data treatment, as for example background correction, transmission correction etc 16.

2.7.1. chi square test.

The method of least squares is built on the hypothesis that the optimum description of a set of data is one which minimizes the weighted sum of squares of deviations, between the data, $I_{\text{exp}}(q_i)$, and the fitting function $I_{\text{th}}(q_i)$:

$$\chi^2 = \sum_{i=1}^N \left(\frac{I_{\text{exp}}(q_i) - I_{\text{th}}(q_i)}{\Delta I(q_i)} \right)^2 \quad (2.4)$$

As a rule of thumb for chi-square fitting is the statement that a good fit is achieved when the reduced chi-square equals one. The reduced chi-square value, which equals the residual sum of square divided by the degree of freedom can be computed by

$$\chi_\nu^2 = \frac{1}{N-m} \sum_{i=1}^N \left(\frac{I_{\text{exp}}(q_i) - I_{\text{th}}(q_i)}{\Delta I(q_i)} \right)^2 = \frac{\chi^2}{N-m} \quad (2.5)$$

where N is the number of data points and m the number of fit parameters. $\nu = N - m$ is called the "number of degree of freedom". The reduced chi-square is closely related to the variance of the fit s^2 by

$$s^2 = \chi_\nu^2 \left(\frac{1}{N} \sum_{i=1}^N \frac{1}{(\Delta I_i^{\text{exp}})^2} \right)^{-1} \quad (2.6)$$

In the theory of hypothesis testing χ^2 can be used to test for goodness of a fit. The probability that a random set of N data points would yield a value of χ^2 equal or greater than the measured one is given by

$$Q_{\text{factor}} = Q \left(\frac{N-m}{2}, \frac{\chi^2}{2} \right) = \frac{\Gamma \left(\frac{N-m}{2}, \frac{\chi^2}{2} \right)}{\Gamma \left(\frac{N-m}{2} \right)} \quad \text{with } \Gamma(a, x) = \int_x^\infty t^{a-1} e^{-t} dt \quad (2.7)$$

For a fitting function being a good approximation to the data the experimental value of χ_ν^2 should be close to one and the probability Q_{factor} somewhere between 0.01 and 0.5. For probability values close to one the fit seems to be too good to be true.

The interpretation of the parameter Q_{factor} can be summarized as:

goodness-of-fit parameter: Q_{factor}

$Q_{\text{factor}} > 0.99$: too good

$Q_{\text{factor}} > 0.1$: believable

$Q_{\text{factor}} > 0.001$: may be acceptable

$Q_{\text{factor}} < 0.001$: questionable

The Q_{factor} -parameter is calculated after each calculation of the scattering curve together with χ^2_ν and s^2 . They are displayed and updated in the red marked area of the screen shot shown in fig. 2.14.

2.7.2. R-factor.

The crystallographers have introduced another parameter for the goodness of a fit. They use the R factor [361, 181] as a measure of model quality which is defined as

$$R = \frac{\sum_{i=1}^N ||I_{\text{exp}}(q_i)| - |I_{\text{th}}(q_i)||}{\sum_{i=1}^N |I_{\text{exp}}(q_i)|} \quad (2.8)$$

Theoretical values of R range from zero (perfect agreement of calculated and observed intensities) to infinity. R factors greater than 0.5 indicate in crystallography very poor agreement between observed and calculated intensities. Models refining to $R < 0.05$ are often considered to be good. However, the R factor must always be treated with caution, only as an indicator of precision and not accuracy. In Crystallography partially incorrect structures have been reported with R values below 0.1; many imprecise but essentially correct structures have been reported with higher R values.

In practice, weighted R factors R_w are more often used to track least-squares refinement, since the functions minimized are weighted according to estimates of the precision of the measured quantity. The weighted residuals are defined as:

$$R_w = \sqrt{\frac{\sum_{i=1}^N \left(\frac{|I_{\text{exp}}(q_i)| - |I_{\text{th}}(q_i)|}{\Delta I(q_i)} \right)^2}{\sum_{i=1}^N \frac{I_{\text{exp}}^2(q_i)}{\Delta I^2(q_i)}}} \quad (2.9)$$

The interpretation of the parameters R and R_w can be summarized as:

goodness-of-fit parameters: R, R_w

$R, R_w > 0.3$: questionable

$0.1 > R, R_w > 0.3$: may be acceptable

$R, R_w < 0.1$: believable

The parameters R and R_w are calculated like the Q_{factor} -parameter after each calculation of the scattering curve. They are displayed and updated together with other goodness-of-fit parameters in the red marked area of the screen shot shown in fig. 2.14. The goodness-of-fit parameters are not minimized. The parameter which is minimized

is the χ^2 -value, defined in eq. 2.4. The other goodness-of-fit parameters are than calculated after each fitting step or after evaluating the theoretical scattering curve via the "Apply"-button.

2.7.3. other methods to compare similarity or distance between theory and data.

- Kullback–Leibler divergency and Jensen–Shannon divergence

$$D_{\text{KL}}(P\|Q) = \sum_{i=1}^n p_i \log \frac{p_i}{q_i} - p_i + q_i \quad (2.10)$$

$$\begin{aligned} D_{\text{JS}}(P\|Q) &= \frac{1}{2} D_{\text{KL}}(P\|Q) + \frac{1}{2} D_{\text{KL}}(Q\|P) \\ &= \frac{1}{2} \sum_{i=1}^n (p_i - q_i) (\log p_i - \log q_i) \end{aligned} \quad (2.11)$$

- chi-squared divergence

$$D_{\chi^2} = \sum_{i=1}^n \frac{(p_i - q_i)^2}{q_i} \quad (2.12)$$

- Hellinger distance

$$H(P, Q) = \frac{1}{\sqrt{2}} \sqrt{\sum_{i=1}^k (\sqrt{p_i} - \sqrt{q_i})^2} \quad (2.13)$$

- squared Hellinger distance

$$H^2(P, Q) = 1 - \sum_{i=1}^k \sqrt{p_i q_i} \quad (2.14)$$

- Rényi divergence of order α :

$$D_\alpha(P\|Q) = \frac{1}{\alpha - 1} \log \left(\sum_{i=1}^n \frac{p_i^\alpha}{q_i^{\alpha-1}} \right) \quad (2.15)$$

$\alpha = 0$: $D_0(P\|Q) = -\log Q(\{i : p_i > 0\})$: minus the log probability under Q that $p_i > 0$

$\alpha = 1/2$: $D_{1/2}(P\|Q) = -2 \log \sum_{i=1}^n \sqrt{p_i q_i}$: minus twice the logarithm of the Bhattacharyya coefficient; (Nielsen & Boltz (2010))

$\alpha = 1$: $D_1(P\|Q) = \sum_{i=1}^n p_i \log \frac{p_i}{q_i}$: the Kullback–Leibler divergence;

$\alpha = 2$: $D_2(P\|Q) = \log \left\langle \frac{p_i}{q_i} \right\rangle$: the log of the expected ratio of the probabilities

$\alpha = \infty$: $D_\infty(P\|Q) = \log \sup_i \frac{p_i}{q_i}$: the log of the maximum ratio of the probabilities

- Wasserstein distance

- Canberra distance:

$$D_{CD} = \sum_{i=1}^n \frac{|p_i - q_i|}{|p_i| + |q_i|} \quad (2.16)$$

- Cosine distance

$$D_{\cos} = 1 - \frac{\sum_{i=1}^n p_i q_i}{\sqrt{\sum_{i=1}^n p_i^2} \sqrt{\sum_{i=1}^n q_i^2}} \quad (2.17)$$



FIGURE 2.14. The parameters Q, R, R_w , describing the goodness of the fit, are displayed in the marked area of the GUI

2.7.4. Confidence interval of the fitting parameter.

The confidence intervals of the fitting parameters are calculated at the minimum of the χ^2 . At the minimum first the partial derivatives according to the fit parameters a_i are calculated to get the matrix elements A_{kl} via

$$A_{kl} = \sum_{i=1}^N \frac{1}{(\Delta I_i^{\text{th}})^2} \frac{\partial I_i^{\text{th}}(q_i, \mathbf{a})}{\partial a_k} \frac{\partial I_i^{\text{th}}(q_i, \mathbf{a})}{\partial a_l} \quad (2.18)$$

The inversion of this matrix yield the covariance matrix

$$\mathbf{C} = \mathbf{A}^{-1} \quad (2.19)$$

The standard deviations Δa_i of the best-fit parameters are given by the square root of the corresponding diagonal elements of the covariance matrix

$$\Delta a_i = \sqrt{C_{ii}} \quad (2.20)$$

The correlation coefficient of the fit parameters a_k and a_l are given by

$$r_{kl} = \frac{C_{kl}}{\sqrt{C_{kk} C_{ll}}} = \frac{C_{kl}}{\Delta a_k \Delta a_l} \quad (2.21)$$

Both the non-diagonal elements of the correlation matrix $r_{k>l}$ and the confidence intervals of the fitting parameters Δa_k are calculated when the fit converges and displayed in a GUI (fig. 2.15b) which can be opened via a menu button as shown in fig. 2.15a.

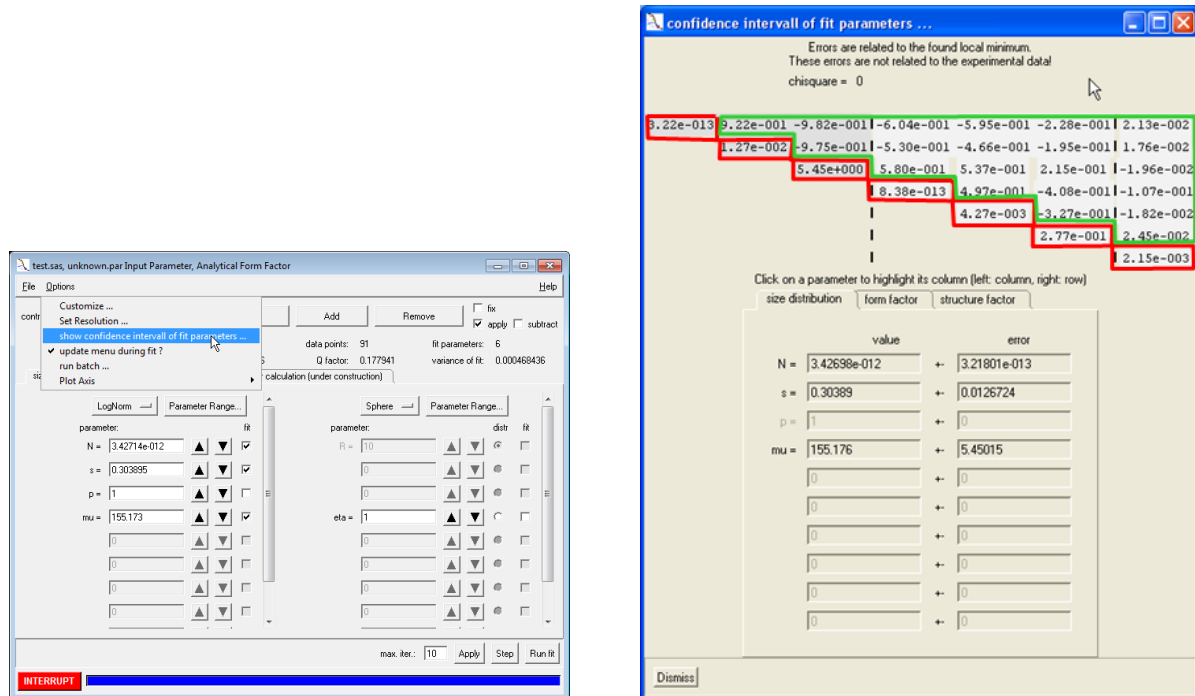


FIGURE 2.15. The confidence intervals are calculated at the end of the minimization procedure.

The routine can give nonphysical confidence intervals if

- no proper error bar for the experimental data are supplied
- a wrong physical model for describing the data is used
- the physical model has strongly correlated parameters

$$r_{kl} \approx 0, a_k \text{ and } a_l \text{ are uncorrelated parameters} \quad (2.22a)$$

$$r_{kl} \approx \pm 1, a_k \text{ and } a_l \text{ are strongly correlated parameters} \quad (2.22b)$$

The given value for the confidence interval of the fit parameters should not be used in the cases

- where the error is not normal distributed
- where the data is given without error bar
- where parameters are strongly correlated

2.8. references to numerical strategies SASfit make use of

In small angle scattering analysis numerical integrations tools are used regularly. To get the scattering amplitude a 3D Fourier transform needs to be calculated, which simplifies to lower dimensional integrals in case of point symmetric, spherical symmetric, cylindrical symmetric or planar objects. For non-spherical symmetric shapes typically an average over the orientation distribution needs to be performed. Furthermore for systems with a size distribution an additional smearing over those distributions are essential. For SESANS data a Hankel transformation is required. In case of multiple scattering both a forward and as well as inverse Hankel transform are necessary. It has turned out, that each of these tasks might require a specialized integration routine to be efficient. Efficiency or parallelization becomes in the end essential if several of these integrations have to be solved numerically.

2.8.1. Integrals for Form Factors.

To calculate the general case of a form factor of an object a 3D Fourier transform needs to be performed. When $\eta(\mathbf{r})$ is the scattering length density distribution of the scatterer the scattering amplitude $F(\mathbf{Q})$ is

$$F(\mathbf{Q}) = \iiint \eta(\mathbf{r}) e^{i\mathbf{Q}\mathbf{r}} d\mathbf{r} \quad (2.23)$$

For objects with a point symmetric shape the integral simplifies to cos transform, which is real valued and not anymore complex and for which specialized algorithms are available [70, 364, 84, 365, 172, 171]

$$F(\mathbf{Q}) = \iiint \eta(\mathbf{r}) \cos(\mathbf{Q}\mathbf{r}) d\mathbf{r} \quad (2.24)$$

For higher symmetric shapes the 3D Fourier transform simplifies further to lower dimensional integrals.

For spherical symmetric shapes one just needs to calculate

$$F(Q) = \int_0^\infty 4\pi r^2 \eta(r) \frac{\sin(Qr)}{Qr} dr \quad (2.25)$$

which now only depend on the modulus of Q and r . In this case a sin transform needs to be calculated. In all cases the integral has to be performed over an oscillating cos or sin function, which in the above two cases also have a constant oscillation frequency. Efficient algorithms can be found e.g. at [70, 364, 84, 365, 172, 171]

For cylindrical and point symmetric objects the Fourier transform reads as

$$F(\mathbf{Q}) = 2\pi \int_{-\infty}^{\infty} \cos(Q_z z) \int_0^\infty \Delta\eta_{cyl}(r, z) J_0(Q_r r) r dr dz \quad (2.26)$$

The integration over z is still a cos transform, whereas the integration over the other two direction turn into a Hankel transform. The Bessel function also oscillates around zero but not with a fixed frequency. The roots are not analytically known which means some additional efforts for numerically evaluating them. The form factor of a homogeneous

cylinder of length L and radius R oriented with the cylinder axis in z -direction therefore reads as

$$F_{\text{cyl}}(\mathbf{Q}) = 2\pi \int_{-L/2}^{L/2} \cos(Q_z z) \int_0^R J_0(Q_r r) r dr dz \quad (2.27a)$$

$$= \frac{\sin(Q_z L/2)}{Q_z L/2} \pi R^2 L \frac{2J_1(Q_r R)}{Q_r R} \quad (2.27b)$$

with

$$\mathbf{Q} = \begin{pmatrix} Q_r \cos(\phi) \\ Q_r \sin(\phi) \\ Q_z \end{pmatrix} \quad (2.27c)$$

In case of a homogeneous cylinder the cos and Hankel transform can be calculated analytically. For other more realistic models the integrations needs to be performed numerically. Algorithms for the cos transform already have been mentioned. For the Hankel transform several strategies have been discussed and used [85, 5, 365, 179, 362, 270, 263, 251] From these algorithms especially the one from [365] and [85] are those which both are fast as well as able to perform the transform with a given precision. The integral in eq. 2.27a likely would gain using different quadrature strategies for $\int dr$ (optimized Hankel transform quadrature [85]) and $\int dz$ (e.g. double exponential quadrature [346, 345]), i.e. a quadrature rule from a product of distinct optimum 1D quadrature rules needs to be investigated.

2.8.2. Orientational and Size Distribution.

To calculate scattering pattern of particles with orientational (o) and size distribution (s) the scattering intensity $I = \langle |F|^2 \rangle_{o,s}$ has to averaged in case of non interacting particles. $\langle \rangle_{o,s}$ denotes a multiple quadrature over the orientation and size probability function. In case of interacting particles both the averages of scattering intensities $I = \langle |F|^2 \rangle_{o,s}$ of a single particle as well as the averages of the scattering amplitude $|\langle F \rangle_{o,s}|^2$ of them are typically required.

In case of an averaged amplitude $\langle F \rangle_{o,s}$ the integrals over a 3D hyper cube can be extended to the required n -dimensional hypercube including orientational as well size distribution. The orientational distribution increases the dimension of the hyper cube by maximal 3 dimensions namely the three Euler angles. Distributions of the size can in principle have any number of dimensions depending on the parametrization. A three dimensional rectangular cuboidal multi shell can have many size parameters in its form factor, each having a distribution.

In contrast to the calculation of the average amplitude the calculating of the averaged intensity first needs a $|F(\mathbf{Q})|^2$ operation which avoids extending directly the strategies for quadrature algorithms over a hyper cube to higher dimensions. Size distribution and orientation distributions over m parameters a_i (with $\mathbf{a} = (a_1, \dots, a_m)^T$) and over the Euler angles (α, β, γ) with a common distribution $p(\mathbf{a}, \alpha, \beta, \gamma)$ of the form factor are

simply calculated by

$$\frac{d\sigma(\mathbf{Q})}{d\Omega} = I(Q) = \left\langle |F(\mathbf{Q}, \mathbf{a}, \alpha, \beta, \gamma)|^2 \right\rangle_{\text{o,s}} = \int \cdots \int p(\mathbf{a}, \alpha, \beta, \gamma) |F(\mathbf{Q}, \mathbf{a}, \alpha, \beta, \gamma)|^2 d\mathbf{a} d\alpha d\beta d\gamma \quad (2.28)$$

The determination of the distribution function $p(\mathbf{a}, \alpha, \beta, \gamma)$ is one of the core tasks in small angle scattering analysis. The integral in eq. 5.3 is a multidimensional Fredholm integral. The SASview as well SASfit packages try to solve this (ill-posed) integral equation by assuming analytical parametrized distribution functions to obtain the orientation and size distribution information. In many typical cases discussed in literature a size and orientation distributions are assumed to be factorizable as

$$p(\mathbf{a}, \alpha, \beta, \gamma) = p_o(\alpha, \beta, \gamma) \prod_{i=1}^m p_{s,i}(a_i) \quad (2.29)$$

where the size distribution $p_{s,i}(a_i)$ is described in first approximation by a simple distribution function like a normal, lognorm, gamma, ... distribution and $p_o(\alpha, \beta, \gamma)$ is describing the orientation distribution function in terms of Euler angles.

For cylindrical symmetric objects due to symmetry one integration around the symmetry axis can be done analytically, whereas the other two over the polar angles still might need to be performed numerically. For integration over polar angles, i.e. over the surface of a unit sphere special algorithms are available like Lebedev quadrature [291, 292, 293, 290], spherical designs [169, 202], or spherical Fibonacci point sets [329, 477]. However, these methods have the disadvantage of having no error estimate of the integral, but on the other side they might be easily adapted for parallelization due to the known grid points.

A special case of orientation distribution is the fully random orientation distribution. For this case all direction between the scattering object and the vector \mathbf{Q} are equal probable and an average over all direction of \mathbf{Q} is equivalent to averaging over all 3 Euler angles. This means, that a random orientational average requires again an integration over a unit sphere. A symmetry constrain like a cylindrical symmetry of the particles would reduce the orientation average to a single integral. In case of a random oriented cylinder like in eq. 2.27b the average reads as

$$|\langle F_{\text{cyl}}(\mathbf{Q})|^2 \rangle_{\text{rnd-o}} = \int_0^{\pi/2} \left| \pi R^2 L \frac{\sin(QL/2 \cos(\theta))}{QL/2 \cos(\theta)} \frac{2J_1(QR \sin(\theta))}{QR \sin(\theta)} \right|^2 \sin(\theta) d\theta \quad (2.30)$$

The kernel of this integral is an oscillating function, but it does not oscillate around zero as the kernel is strictly positive. Therefore certain integration strategies for oscillating functions can not be applied directly. We also have two oscillations, one depending on the length $QL/2$ and the other on QR . If the cylinder has additional size distributions

in L and R the final multidimensional integral to be solved is

$$\frac{d\sigma_{\text{cyl},\text{rnd-o,s}}(Q)}{d\Omega} = \left\langle |F_{\text{cyl}}(\mathbf{Q})|^2 \right\rangle_{\text{rnd-o,s}} = \int_0^\infty \int_0^\infty \int_0^{\pi/2} p_s(L, R) \times \\ \left| \pi R^2 L \frac{\sin(QL/2 \cos(\theta))}{QL/2 \cos(\theta)} \frac{2J_1(QR \sin(\theta))}{QR \sin(\theta)} \right|^2 \sin(\theta) d\theta dR dL \quad (2.31)$$

The integral kernel behaves well enough so that the order of the integrals can be changed. If the orientational average is done first, the resulting function in this case for $2R \approx L$ does not have anymore many oscillations and the outer integrations over L and R might be done easily with standard strategies for quadratures over hypercubes. However, for extreme aspect ratios this is not anymore valid.

2.8.3. SESANS - MSAS - resolution function.

2.8.3.1. SESANS.

In case of an isotropic scatterer the SESANS signal $\tilde{G}(\delta)$ is directly related to the SANS differential cross-section $\frac{d\sigma(Q)}{d\Omega}$ via a zero order Hankel transform [282, 6, 268] which reads as

$$\tilde{G}(\delta) = \frac{1}{2\pi} \mathcal{H}_0 \left[\frac{d\sigma(Q)}{d\Omega} \right] (\delta) = \frac{1}{2\pi} \int_0^\infty Q J_0(Q\delta) \frac{d\sigma(Q)}{d\Omega} dQ \quad (2.32)$$

Coming back to the example of random oriented cylinders with size distributions for the length and radius we finally end up with

$$\tilde{G}_{\text{cyl},\text{rnd-o,s}}(\delta) = \frac{1}{2\pi} \int_0^{q_{\max}} \int_0^\infty \int_0^\infty \int_0^{\pi/2} Q J_0(Q\delta) p_s(L, R) \times \\ \left| \pi R^2 L \frac{\sin(QL/2 \cos(\theta))}{QL/2 \cos(\theta)} \frac{2J_1(QR \sin(\theta))}{QR \sin(\theta)} \right|^2 \sin(\theta) d\theta dR dL dQ \quad (2.33)$$

As experimentally SESANS signals are only measured with a detector probing the polarization to a maximum value of q_{\max} , the Hankel transform might be significantly truncated. If in this case $\int_0^{q_{\max}} dQ$ can be replaced by $\int_0^\infty dQ - \int_{q_{\max}}^\infty dQ$ or if another routine preferable directly evaluates the integral $\int_0^{q_{\max}} dQ$ might depend on how many roots of the Bessel function are within the domain $[0, q_{\max}]$.

2.8.3.2. Multiple Small Angle Scattering (MSAS).

According to [438, 240] multiple small angle scattering can be computed from the single scattering approximation via the intermediate function $i_1(r)$.

$$i_1(r) = 2\pi t \int_0^\infty J_0(qr) \frac{d\sigma_1}{d\Omega}(q) q dq \quad (2.34)$$

$$= 2\pi t \mathcal{H}_0 \left[\frac{d\sigma_1}{d\Omega}(q) \right] (r) = 4\pi^2 t \tilde{G}(r) \quad (2.35)$$

$$i_m(r) = e^{-i_1(0)/k_0^2} k_0^2 \left(\exp \left(i_1(r)/k_0^2 \right) - 1 \right) \quad (2.36)$$

$$= k_0^2 \left[\exp \left(\frac{t}{k_0^2} (\tilde{G}(r) - \tilde{G}(0)) \right) - \exp \left(-\frac{t}{k_0^2} \tilde{G}(0) \right) \right] \quad (2.37)$$

$$\frac{d\sigma_m}{d\Omega}(q) = \frac{1}{2\pi t} \int_0^\infty J_0(qr) i_m(r) r dr = \frac{1}{2\pi t} \mathcal{H}_0 [i_m(r)] (q) \quad (2.38)$$

$$k_0 = \frac{2\pi}{\lambda} \quad (2.39)$$

where $\frac{d\sigma_m}{d\Omega}(q)$ is the measured scattering cross-section including multiple scattering contributions normalized on the sample volume and corrected for absorption and incoherent scattering, i.e. corrected for all beam attenuation effects except coherent small angle scattering. $\frac{d\sigma_1}{d\Omega}(q)$ is the corresponding single scattering cross-section per volume. It can be seen, that the intermediate function $i_1(r)$ is except a pre-factor identical to the projected correlation function $\tilde{G}(r)$ used in the theory of SESANS analysis, $i_1(r) = \tilde{G}(r) (2\pi)^2 t$.

What does this mean for the case of random oriented cylinders with a size distribution for the length and radius? Here we consider a system which would scatter that strong, that multiple scattering has to be considered. In this case first the correlation function in eq. 2.33 and afterwards the intermediate function including multiple scattering $i_m(r)$ is calculated. This functions then needs to be Hankel transformed again according to eq. 2.38. In total 5 nested numerical integration are required for the example of polydisperse random oriented cylinders.

2.8.3.3. Resolution Function.

If the resolution function needs to be included in the analysis eq. 2.38 or eq. 2.31 would need to be convoluted by a resolution function which would add another integral to the formula.

2.8.4. Summary.

Already for a simple model of a polydisperse random oriented cylinder several nested integrals needs to be solved numerically. A part of the integrals, like over a combined orientation and size distribution are calculated over a hyper cube. Adaptive algorithms have been discussed and supplied in [245, 150, 32, 58]. However, in the present case integrals in certain dimensions might profit if they would be treated with different strategies, like Hankel transforms, integrals over oscillating but positive functions, or orientational averages over a unit sphere. The question would be, if quadrature rules with mixed strategies for the different dimensions can be developed. Ideally they should

also be vectorizable for optional parallelization. For the given example of polydisperse random oriented cylinder performance test at the beginning using optimized one dimensional quadrature rules like for the Hankel transform or over strictly positive but oscillating functions might be useful, as those could immediately improve existing codes in SASview and SASfit.

To access in SASfit the specialized integration routines the functions `sasfit_integrate()`, `sasfit_cubature()`, `sasfit_orient_avg()`, and `sasfit_hankel()` are supplied. `sasfit_integrate()` performs one-dimensional integrations and `sasfit_cubature()` multidimensional integrations over multi-dimensional cubes. `sasfit_orient_avg()` performs efficient integrations over the surface of a sphere to perform orientational averages. `sasfit_hankel()` supplies highly optimized routines for Bessel or Hankel transforms containing oscillatory Bessel functions in the integrand. The window for fitting or simulating data (fig. 2.16) has a menu option under [Options|Customize...] opening a window to configure the internal integration routines.

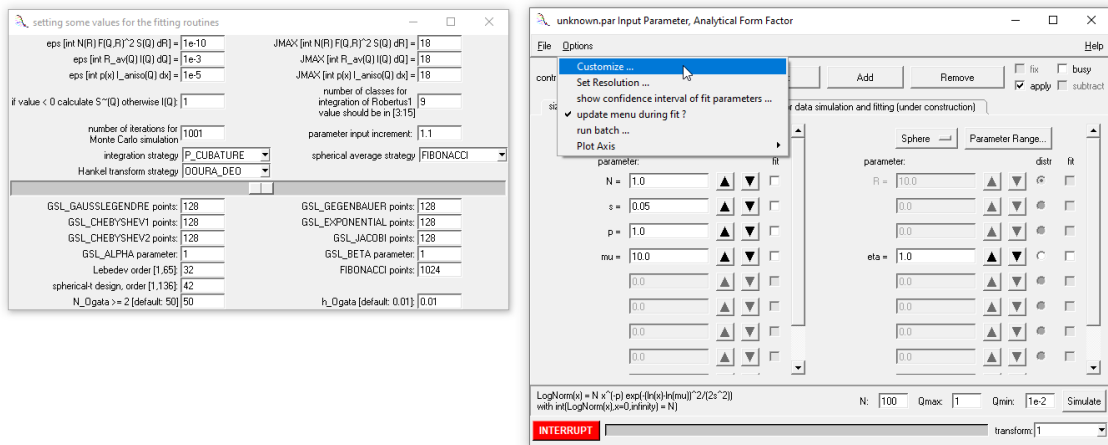


FIGURE 2.16. Menu for configuring internal integration routines in SASfit

2.8.5. Integration algorithms in SASfit for normal one- or multidimensional integration.

Within SASfit a configurable one dimensional integration routine as well as a multidimensional one with a common interface for the different algorithms is supplied. Depending on the mathematical behaviour of the integrant it has turned out that the different algorithms might differ a lot in terms of efficiency. For multidimensional quadrature algorithm so far the same strategy is used for all dimensions. The routines `sasfit_integrate()` and `sasfit_cubature()` have the same configuration options. For multidimensional integrations either by itself specialized multidimensional algorithms or nested calls of one-dimensional integration routines are used.

Possible options for them are:

- OOURA_DE:** double-exponential quadrature algorithm from [345, 346]
- OOURA_CC:** Clenshaw-Curtis-quadrature using Chebyshev series expansion (<https://www.kurims.kyoto-u.ac.jp/~ooura/intcc.html>)
- TANHSINH_1:**
TanhSinh quadrature [498, 499]
- TANHSINH_2:**
TanhSinh quadrature [498, 500]
- GSL_QUAD:** quad integration routine from gsl [144]
- GSL_QAG:** QAG integration routine from gsl [144]
- GSL_QNQ:** QNQ integration routine from gsl [144]
- H_CUBATURE:**
multidimensional integration routine hcubature from [245]
- P_CUBATURE:**
multidimensional integration routine pcubature from [245]
- GSL_LEGENDRE:**
Gauss-Legendre quadrature using gsl library [144]
- MC_MISER:** Monte-Carlo integration algorithm Miser using gsl library [144]
- MC_VEGAS:** Monte-Carlo integration algorithm Vegas using gsl library [144]
- MC_PLAIN:** plain Monte-Carlo integration algorithm using gsl library [144]
- QMC_HOLTON:**
quasi Monte Carlo integration [539] using the `gsl_qrng_halton` quasi random number generator from gsl [144].
- QMC_REVERSEHALTON:**
quasi Monte Carlo integration [539] using the `gsl_qrng_reversehalton` quasi random number generator from gsl [144].
- QMC_SOBOLE:** quasi Monte Carlo integration [539] using the `gsl_qrng_sobol` quasi random number generator from gsl [144].
- QMC_NIEDERREITER_2:**
quasi Monte Carlo integration [539] using the reverse `gsl_qrng_niederreiter_2` quasi random number generator from gsl [144].
- RQMC_SOBOLE_RDS:**
randomized quasi Monte Carlo integration using the quasi random Sobol sequence with additional random digit scrambling [72]
- RQMC_SOBOLE_OWEN:**
randomized quasi Monte Carlo integration using the quasi random using Owen-scrambled Sobol sequence [72, 368]
- RQMC_FAURE05:**
randomized quasi Monte Carlo integration using Owen-scrambled Faure (0,5) sequence [72, 368].
- RQMC_LAINE_KARRAS:**
randomized quasi Monte Carlo integration using Laine-Karras hash method mentioned in [72] and given as C source code in its supplement information.

SG_SMOLYAK:

A sparse grid is used, based on a "delayed" Clenshaw Curtis quadrature rule, using the Smolyak method [387, 71].

SG_CC_SMOLYAK:

A sparse grid is used, based on a Clenshaw Curtis quadrature rule, using the Smolyak method [387, 71].

SG_SMOLYAK_CLENSHAW_CURTIS:

The quadrature rule is associated with a sparse grid derived from a Smolyak construction using a closed 1D quadrature rule [358, 71].

SG_CLENSHAW_CURTIS_LINEAR:

sparse grid based on Clenshaw Curtis quadrature rule [208, 209, 69]

SG_CLENSHAW_CURTIS_SLOW:

sparse grid based on "slow growth" Clenshaw Curtis quadrature rule [208, 209, 69]

SG_CLENSHAW_CURTIS_EXP:

sparse grid based on Clenshaw-Curtis Exponential quadrature rule [208, 209, 69]

SG_GAUSS_LEGENDRE:

sparse grids based on Gauss-Legendre rules[208, 209, 69]

SG_KONROD_PATTERSON:

sparse grids based on Gauss-Patterson rules[208, 209, 69]

SG_FROLOV: sparse grids using optimized Frolov lattices [249, 232]

2.9. orientation average

Orientational averaging is a two dimensional integration over a unit sphere (`sasfit_orient_avg()`). In **SASfit** a specialized function for this is supplied. As the problem in principle can be handles with `sasfit_cubature` it include all strategies from that function plus a few specialized one especially efficient for quadrature over a the surface of unit sphere. These are

Lebedev: Lebedev quadrature [529, 291, 292, 293, 290] is an approximation to the surface integral of a function over a three-dimensional sphere. The number and location of the grid points together with a corresponding set of integration weights are determined by enforcing the exact integration of polynomials (or equivalently, spherical harmonics) up to a given order.

FIBONACCI: Almost equally spaced points can be easily generated by a Fibonacci on different surfaces, like square, disk, cylinder surface, spherical surface [329, 477].

spherical_t_design: The spherical t-design [530, 169, 202] has been used to generate equally spaced points on a spherical surface leading to a quadrature formula with equal weights.

2.9.1. Hankel transform.

The Hankel transform calculated by `sasfit_hankel()` is defined by

$$F(q) = \mathcal{H}_n [f(q)](r) = \int_0^\infty J_n(qr) f(r) r dr \quad (2.40)$$

This means an upper unbounded integral over the oscillating Bessel function $J_n()$ has to be solved numerically. Thos strategies already available for functions with an strictly periodic $\cos()$ or $\sin()$ term (Fourier type) can not be directly been used as only for large arguments of the bessel function in behaves as $J_n(x) \approx \sqrt{\frac{2}{\pi x}} \cos\left(x - \frac{\pi}{2}n - \frac{\pi}{4}\right)$.

QWE: Quadrature With Extrapolation computes an infinite integral using the partial sum of quadrature terms accelerated by sequence extrapolation using the Shanks transformation implemented with Wynn's epsilon algorithm [263].

CHAVE: This algorithm performs the integration of the product of the kernel and Bessel functions between the asymptotic zero crossings of the latter and sums the series of partial integrations using a continued fraction expansion, equivalent to an analytic continuation of the series [85].

OOURA_DEO: As for large arguments x the Bessel function asymptotically behaves as $J_n \approx \sqrt{\frac{2}{\pi x}} \cos\left(x - \frac{\pi}{2}n - \frac{\pi}{4}\right)$ the double exponential formula of [365] for oscillatory functions over the half infinite interval is used directly.

GSL_QAWF: This options tries to make use of the adaptive integration of Fourier integrals available in the gsl library (`gsl_integration_qawf()`). This function attempts to compute a Fourier integral of the function g over the semi-infinite interval $[a, +\infty)$ as $I = \int_a^{+\infty} dx g(x) \begin{Bmatrix} \sin(\omega x) \\ \cos(\omega x) \end{Bmatrix}$. By defining $g(r) = f(r) \frac{J_n(qr)}{\cos(qr - \frac{\pi}{2}n - \frac{\pi}{4})}$ we convert the Hankel transform in 2.40 into a cos-Fourier type transform after an additional substitutions of $r' = r - \frac{\pi n}{2q} - \frac{1}{q^4}\pi$.

Next to the quadrature algorithms above also fast digital filters for Hankel transform have been developed. A few of these have been supplied in SASfit for testing [5, 179, 362, 270, 263, 251]:

OGATA_2005, FBT0, FBT1, FBT2, GUPTASARMA_97, GUPTASARMA_97_FAST, KEY_51, KEY_101, KEY_201, ANDERSON_801

2.10. Fitting strategies

2.11. Data I/O Formats

2.11.1. ASCII Input Format.

SASfit supports a simple ASCII format. Options for reading ASCII data can be set in the corresponding menu, where one can set an input format and the number of lines to be skipped at the beginning of the data file. To set an input format one has to supply a string like "xyer". Each line which does not contain valid float numbers are skipped automatically. Each line further should at least contain as many valid numbers as the supplied format string characters. That means if the line contains only three numbers but the format string is 4 or more characters long the line will be ignored. Separators between numbers can be "white space", "tabulator", or ",". For identifying the columns the characters and their position in the string are interpreted. x, y and e stands for the scattering vector Q , scattering intensity $I(Q)$ and its error $\Delta I(Q)$, respectively. r defines the column for a resolution parameter σ . The position of the character in the string defines which data column is assigned to Q , $I(Q)$, $\Delta I(Q)$, and σ . In case of double occurrence of a character the position of the last one is the significant position. Any characters not belonging to {x,y,e,r} can be used to skip a column. A definition string need to contain at least the two characters x and y.

Example 1 (BerSANS format):

```
%File
FileName=D0002831.200 FileDate=28-Jun-99 FileTime=11:57:16
Type=SANSIso Title=IMF
%Counts
 2.651E-02, 2.372E+02, 4.650E+00
 3.240E-02, 2.170E+02, 2.291E+00
 3.829E-02, 1.898E+02, 1.713E+00
 4.418E-02, 1.743E+02, 1.479E+00
 5.007E-02, 1.528E+02, 1.318E+00
 5.596E-02, 1.361E+02, 1.153E+00
:
```

As the first lines start with a string, they will be automatically ignored. To interpret the three columns as Q , $I(Q)$, $\Delta I(Q)$ the format string should be simply xyz. The BerSANS format can also be read in by explicitly selecting the "BerSANS"-format button in the menu instead of the "ASCII"-format.

Example 2:

[19 0 0 0 0 0 0 6 0.100000E+01 0.100000E+04 0.000000E+00 0.100000E+01 0.120000E+01 0.000000E+00 0.000000E+00 0.000000E+00 0.000000E+00 0.000000E+00]
teflon instrument tests 1 2.617993E-04 3.700000E+01 4.301163E+00 2 1.062462E-03 6.412500E+01 1.634587E+00 3 2.107973E-03 1.410135E+03 5.207492E+00 4 3.167636E-03 1.752197E+03 4.801586E+00 5 4.189463E-03 7.581771E+02 2.810281E+00 :

```

45  1.255376E-02   1.486688E+01   2.197023E-01
46  1.360724E-02   1.204012E+01   1.927716E-01
47  1.466810E-02   1.026648E+01   1.679423E-01

```

A definition string `ixye` would ignore the leading line number at the beginning of each data line, but in the present example also the first 3 lines would also be interpreted as data points. To skip them one has to use the option for skipping leading lines in a data file. In the above case the number should be set to 3 or 4. As the 4th line is anyway ignore a value of 3 is sufficient to skip non data points.

Example 3: ILL data files from regrouped treatment (`gnnnnnn.eee`).

```

[ 37      0      0      0      0      0      0      0      6
  0.100000E+01  0.250000E+03  0.000000E+00  0.100000E+01  0.105400E+01
  0.000000E+00  0.000000E+00  0.000000E+00  0.000000E+00  0.000000E+00
  0.000000E+00  0.000000E+00  0.000000E+00 ]
```

$$\begin{array}{lll} 2.194656E-03 & 3.442688E-01 & 8.329221E-02 \\ 5.466116E-03 & 3.000000E-01 & 5.008947E-02 \\ 8.480323E-03 & 3.877941E-01 & 4.232426E-02 \\ 1.189216E-02 & 6.498784E-01 & 1.519078E-02 \\ 1.497785E-02 & 7.493181E-01 & 1.173622E-02 \end{array}$$

⋮

To read in a regrouped ILL data file one has to use the definition string `xye` and secondly one has to skip the first 44 lines in the data file to ignore also the lines marked with `[]`. If one does not skip the first 44 lines the marked lines are interpreted erroneously also as data points. The other lines at the beginning of the data file are ignored as they do not fulfill the condition that they have 3 columns containing only valid numbers.

2.11.2. ASCII data without error bar.

In case no error bar is supplied **SASfit** will try to guess one. To do this an polynomial $y_p(Q)$ of degree p

$$y_p(Q) = \sum_{k=0}^p c_k Q^k \quad (2.41)$$

is fitted to the data point i and its n^{th} neighbors to the left and right, i.e. is fitted to $2n + 1$ points from $I_{i-n}(Q_{i-n})$ to $I_{i+n}(Q_{i+n})$. After the fit χ_i^2 is calculated

$$\chi_i^2 = \sum_{j=i-n}^{i+n} (I_j(Q_j) - y_p(Q_j))^2 \quad (2.42)$$

The error bar ΔI_i for Q_i is than defined as

$$\Delta I_i = \sqrt{\frac{\chi_i^2}{2n - p}} \quad (2.43)$$

SASfit is using two nearest neighbors $n = 2$ and fitting a polynomial of degree $p = 2$ to it to guess an error bar. This procedure gives reasonable error bars as long as the data are oversampled and do not show sharp features within the data points $i - n$ and $i + n$. A diffraction peak or a minimum in a form factor like for monodisperse particle might not reasonable well described by the polynomial and consequently the resulting error bar will get large. Furthermore systematic errors in the absolute intensity like an overall scaling factor will not be recognized. The procedure to guess the error bar is basing on the assumption that the scattering curve behaves locally approximately like a polynomial function of degree $p = 2$.

2.11.3. BerSANS Input Format.

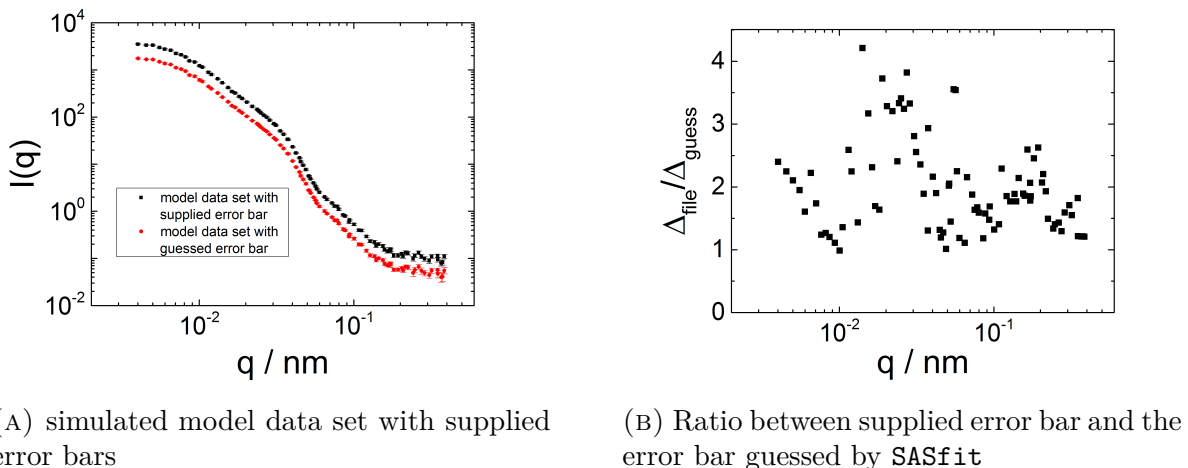


FIGURE 2.17. Comparison of a simulated model data set with supplied error bar and an error bar guessed by **SASfit**.

2.11.4. SESANS Input Format.

For SESANS data several data formats are available. However, the different sources supplying SESANS instruments have started to find a common ASCII format. At the moment **SASfit** supports some old file formats used by the University of Delft and the common format up to file format version 1.0.

Example of a data file in SESANS format:

```

FileFormatVersion      1.0
DataFileDialog        GNS_phi0p10_2mm_theta79_SESANS
Sample                GNS_phi0p10_2mm_theta79_SESANS
Thickness             2.000000
Thickness_unit         mm
Theta_zmax            0.050000000000000003
Theta_zmax_unit        radians
Theta_ymax             0.050000000000000003
Theta_ymax_unit        radians
Orientation           Z
SpinEchoLength_unit   A
Depolarisation_unit   A-2 cm-1
Wavelength_unit       A
Echo_constant          11.021360490530208

BEGIN_DATA
SpinEchoLength Depolarisation Depolarisation_error Wavelength
116.413 -0.00423856 0.00205263 3.25
154.988 -0.00334393 0.00123783 3.75
199.073 -0.00286365 0.00078342 4.25
248.669 -0.00369609 0.000621162 4.75

```

For the analysis of SESANS data **SASfit** [268] supplies a transformation of a scattering model into a projected correlation function 9.16 but also supplies some plug-in functions which directly calculate this quantity in 9.16.1 and the following sub-sections. Internally **SASfit** generates a 4-column structure. The first two columns are the x and y axes. The third column represents the error bar of the y -axis. The fourth column in the **SASfit** data represents for the differential cross-section the resolution parameter for the

x -axis. However, for SESANS data the fourth represents the maximum detectable scattering vector q_{rmmax} and limits the Hankel transform for the converting the scattering differential cross-section into a projected correlation function. For fitting the projected correlation function directly with the corresponding plug-in functions the fourth column is not used. Experimentally the differential cross-section is only measured up to a maximum scattering angle Θ_{\max} . The SESANS data files supply the maximum detected scattering angle and the used wavelength for each spin echo length from which **SASfit** calculates Q_{\max} as $Q_{\max} = \frac{4\pi}{\lambda} \sin \Theta_{\max}/2$.

2.11.5. Export Format.

Example for an exported data file:

0.00401571,	3497.47,	90.7282,	0,	0.00401571,	260294,	-1,	0,
0.00454087,	3340,	84.9531,	0,	0.00454087,	254548,	-1,	0,
0.0050096,	3322.47,	79.6313,	0,	0.0050096,	248833,	-1,	0,
0.00552335,	2983.23,	73.7254,	0,	0.00552335,	241949,	-1,	0,
0.00598495,	2737.17,	68.4395,	0,	0.00598495,	235226,	-1,	0,
0.0065309,	2598.76,	62.3109,	0,	0.0065309,	226647,	-1,	0,
0.00706977,	2233.9,	56.4829,	0,	0.00706977,	217551,	-1,	0,
0.00764207,	2080.96,	50.6186,	0,	0.00764207,	207264,	-1,	0,
0.00815988,	1882.88,	45.6557,	0,	0.00815988,	197459,	-1,	0,
:				:			
,	,	,	,	0.0445634,	1535.14,	-1,	0,
,	,	,	,	0.0453557,	1473.71,	-1,	0,
,	,	,	,	0.0470219,	1340.34,	-1,	0,
,	,	,	,	0.0490017,	1192.64,	-1,	0,
,	,	,	,	0.0510837,	1055.44,	-1,	0,

If one like to export the data of an xy -plot all curves are stored in a single data file. Each curve will occupy four columns (Q , $I(Q)$, $\Delta I(Q)$, σ). If an error $\Delta I(Q)$ is not available, e.g. for theoretical data curves, the corresponding column will be filled with -1. Similar is valid for the resolution parameter σ which will be set to 0 in case it is not available. The individual columns are separated by ",". If the curve have different amount of data points the column will be filled with empty space for the missing data. This comma separated data format has been chosen as it can be imported easily by many commercial plotting softwares. The drawback of this format is, however, that **SASfit** cannot read it correctly, if the individual curves are of different length.

2.12. Scattering length density calculator

The SLD calculator is using thermal neutron cross-sections only to calculate neutron scattering length density. For x-rays the energy dependent scattering coefficients f' and f'' are derived using the theoretical approximation developed by Cromer and Liberman. This theory gives accurate values far from an absorption edge but does not account for the effects of neighboring atoms, which can be very substantial near an absorption edge. Before conducting an anomalous scattering experiment close to an absorption edge it is therefore advisable to determine the actual scattering behavior of the sample. The x-ray data have been taken from http://skuld.bmsc.washington.edu/scatter/AS_periodic.html and those for neutrons from <http://www.ncnr.nist.gov/resources/n-lengths/list.html>. The menu in-

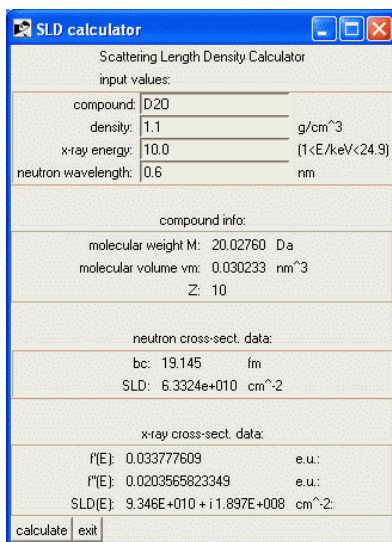


FIGURE 2.18. Input menu for the scattering length density calculator

terface in Fig. 2.18 has for input parameters, the sum formulae of the compound, its mass density in g/cm^3 , the x-ray energy in keV and the neutron wave length in nm. In the compound name non-integer stoichiometry is supported, e.g. H_{0.2}O_{0.1} and H₂O will calculate the same scattering length density. However, the molecular volume v_m and the molecular weight M of cause depend on such differences. The elements in the compound name are case sensitive. Therefore you have to use SiO₂ instead of SI02. Also isotopes are handled like C(13) (Carbon-13), H(2) (Deuterium), or O(18) (Oxygen-18). For Deuterium next to H(2) also D can be used.

Examples of how to format the compound name:

- Magnetite: Fe₃O₄, 5.15 g/cm^3
- Eucryptite: LiAlSiO₄, 2.67 g/cm^3
- protonated toluene, C₇H₈, 0.865 g/cm^3
- deuterated toluene, C₇D₈ or C₇H(2)₈, 0.94 g/cm^3
- mixture of 65/35 heavy water/light water, (D₂O)0.65(H₂O)0.35, 1.065 g/cm^3

From the compound name and the density first the molecular weight M , molecular volume v_m , and total number of electrons Z are calculated. Together with

the tabulated neutron scattering length and tabulated energy dependent scattering coefficient $f'(E)$ and $f''(E)$ the corresponding coherent neutron scattering length $b_c = \sum_i b_i$, coherent neutron scattering length density $\eta_{n,SLD} = b_c/v_m$ and for x-rays the complex energy dependent scattering scattering length density $\eta_{x,SLD} = (Z - (Z/82.5)^{2.37} + f'(E) + i f''(E)) / v_m$ of the compound are calculated.

2.13. Resolution Function

The resolution function is taken from [379].

$$\langle k \rangle = 2\pi/\lambda \quad (2.44)$$

$$\langle \theta \rangle = \arcsin(\langle Q_{av} / (2\langle k \rangle) \rangle) \quad (2.45)$$

$$a_1 = \frac{r_1}{L + l/\cos^2(2\langle \theta \rangle)} \quad (2.46)$$

$$a_2 = r_2 \cos^2(2\langle \theta \rangle)/l \quad (2.47)$$

$$\Delta\beta_1 = \begin{cases} a_1 \geq a_2 : & \frac{2r_1}{L} - \frac{r_2^2}{2r_1} \frac{\cos^4(2\langle \theta \rangle)}{l^2 L} \left(L + \frac{l}{\cos^2(2\langle \theta \rangle)} \right)^2 \\ a_1 < a_2 : & 2r_2 \left(\frac{1}{L} + \frac{\cos^2(2\langle \theta \rangle)}{l} \right) - \frac{r_1^2}{2r_2} \frac{l}{\cos^2(2\langle \theta \rangle)} \\ & \times \frac{1}{\left(L + \frac{l}{\cos^2(2\langle \theta \rangle)} \right)} \end{cases} \quad (2.48)$$

$$\sigma_W = \langle Q \rangle \frac{\Delta\lambda}{\lambda} \frac{1}{2\sqrt{2\ln(2)}} \quad (2.49)$$

$$\sigma_{C1} = \langle k \rangle \cos(\langle \theta \rangle) \frac{\Delta\beta_1}{2\sqrt{2\ln(2)}} \quad (2.50)$$

$$\sigma_{D1} = \langle k \rangle \cos(\langle \theta \rangle) \cos^2(2\langle \theta \rangle) \frac{D}{l 2\sqrt{2\ln(2)}} \quad (2.51)$$

$$\sigma_{av} = \langle k \rangle \cos(\langle \theta \rangle) \cos^2(2\langle \theta \rangle) \frac{\Delta D}{l 2\sqrt{2\ln(2)}} \quad (2.52)$$

$$\sigma = \sqrt{\sigma_W^2 + \sigma_{C1}^2 + \sigma_{D1}^2 + \sigma_{av}^2} \quad (2.53)$$

$$R_{av}(Q, \langle Q \rangle) = \frac{Q}{\sigma^2} \exp\left(-\frac{1}{2} (Q^2 + \langle Q \rangle^2) / \sigma^2\right) I_0(Q\langle Q \rangle / \sigma^2) \quad (2.54)$$

$$I(\langle Q \rangle) = \int_0^\infty R_{av}(Q, \langle Q \rangle) \frac{d\sigma}{d\Omega}(Q) dQ \quad (2.55)$$

$$\frac{d\sigma}{d\Omega}(Q) = \int_0^\infty N(R) F^2(Q, R) dR \quad (2.56)$$

CHAPTER 3

Form Factors

3.1. Spheres & Shells

3.1.1. Sphere.

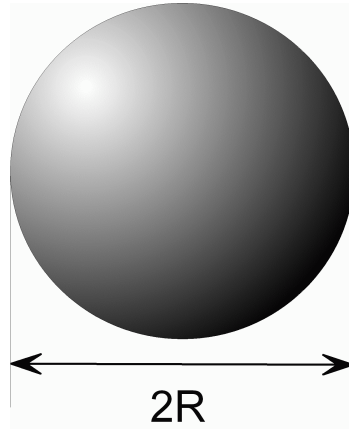


FIGURE 3.1. Sphere with diameter $2R$

The scattering intensity and scattering amplitude of a homogeneous sphere with a small relative refraction index is given by [409]

$$I_{\text{Sphere}}(Q, R) = K^2(Q, R, \Delta\eta) \quad (3.1a)$$

with

$$K(Q, R, \Delta\eta) = \frac{4}{3}\pi R^3 \Delta\eta 3 \frac{\sin QR - QR \cos QR}{(QR)^3} \quad (3.1b)$$

The forward scattering for $Q = 0$ is given by

$$\lim_{Q=0} I_{\text{Sphere}}(Q, R) = \left(\frac{4}{3}\pi R^3 \Delta\eta\right)^2$$

Input Parameters for model Sphere:

R: radius of sphere R

- - -: not used

- - -: not used

eta: scattering length density difference between particle and matrix $\Delta\eta$

Note:

- The parameters `param.p[1]` and `param.p[2]` are not used.

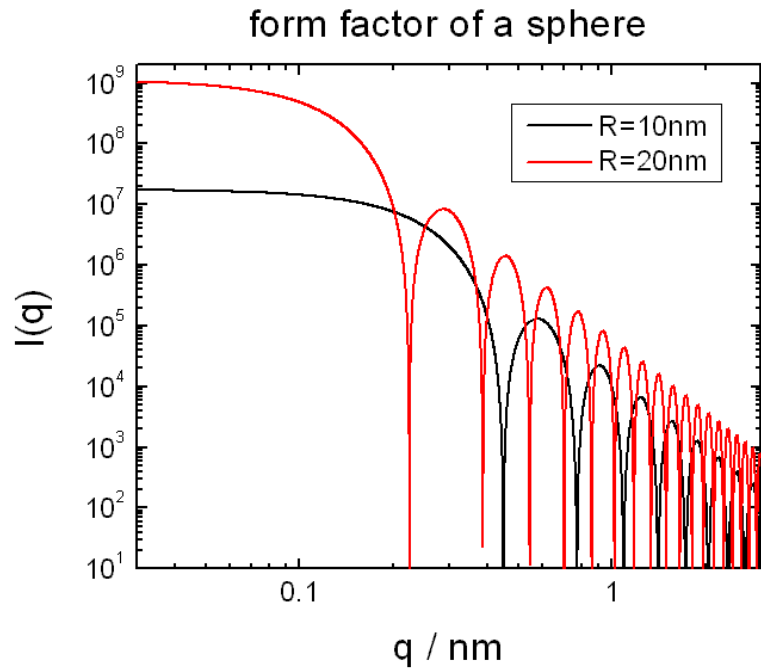


FIGURE 3.2. Scattering intensity of spheres with radii $R = 10\text{nm}$ and $R = 20\text{nm}$. The scattering length density contrast is set to 1.

3.1.2. Spherical Shell i.

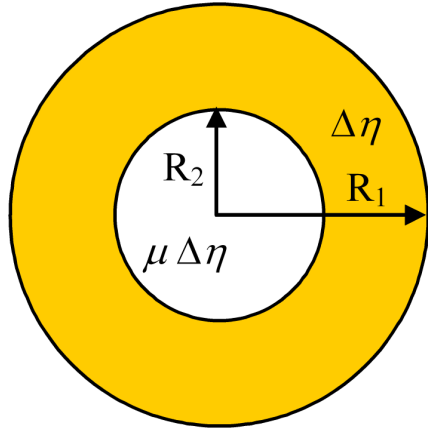


FIGURE 3.3. Spherical Shell i

This implementation of a spherical shell is parametrised with an inner radius R_2 and outer radius R_1 . The scattering contrast relative to the matrix of the core is $\mu\Delta\eta$ and the one of the shell $\Delta\eta$.

$$I_{\text{Shell1}}(Q, R_1, R_2, \Delta\eta, \mu) = [K(Q, R_1, \Delta\eta) - K(Q, R_2, \Delta\eta(1 - \mu))]^2 \quad (3.2)$$

with

$$K(Q, R, \Delta\eta) = \frac{4}{3}\pi R^3 \Delta\eta 3 \frac{\sin QR - QR \cos QR}{(QR)^3} \quad (3.3)$$

The forward scattering for $Q = 0$ is given by

$$\lim_{Q=0} I_{\text{Shell1}}(Q, R_1, R_2, \Delta\eta, \mu) = \left(\frac{4}{3}\pi \Delta\eta [R_1^3 - R_2^3(1 - \mu)] \right)^2$$

Input Parameters for model Spherical Shell i:

R1: overall radius of spherical shell R_1

R2: radius of core R_2

eta: scattering length density difference between shell and matrix $\Delta\eta$

mu: scattering length density difference between core and matrix relative to the shell contrast μ

Note:

None

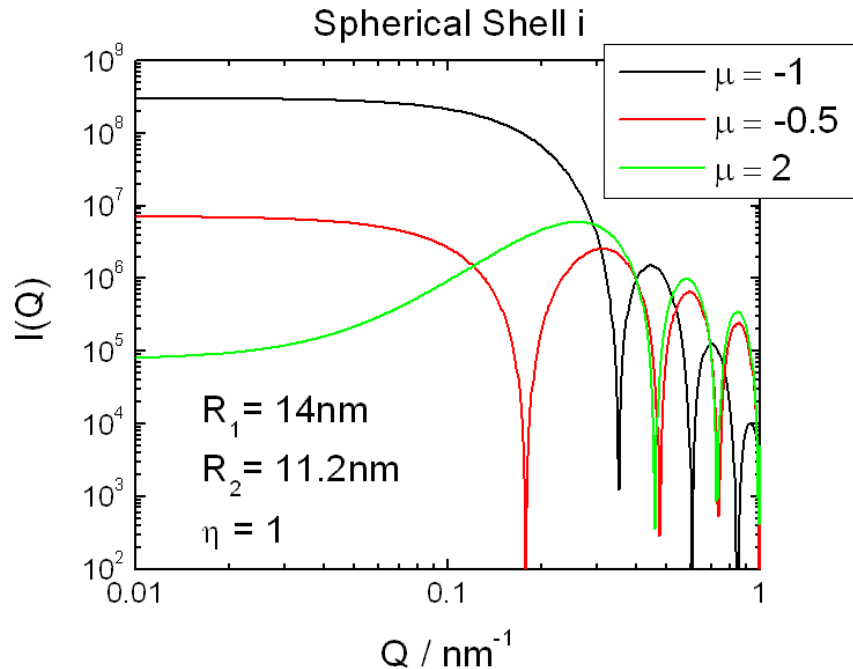


FIGURE 3.4. Scattering intensity of spherical shell with outer radius of $R_1 = 14\text{nm}$ and inner radius of $R_2 = 11.2\text{nm}$. The scattering length density contrast the shell is set to 1 and the one of the core to -1, -0.5, and 2.

3.1.3. Spherical Shell ii.

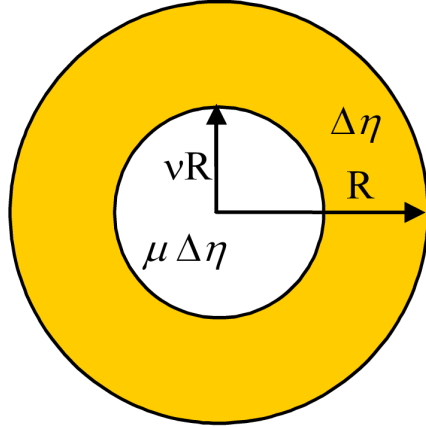


FIGURE 3.5. Spherical Shell ii

This implementation of a spherical shell is parametrised with an outer radius R and an inner radius νR . The scattering contrast relative to the matrix of the core is $\mu\Delta\eta$ and the one of the shell $\Delta\eta$.

$$I_{\text{Shell2}}(Q, R, \nu, \Delta\eta, \mu) = (K(Q, R, \Delta\eta) - K(Q, \nu R, \Delta\eta(1 - \mu)))^2 \quad (3.4)$$

with

$$K(Q, R, \Delta\eta) = \frac{4}{3}\pi R^3 \Delta\eta 3 \frac{\sin QR - QR \cos QR}{(QR)^3} \quad (3.5)$$

The forward scattering for $Q = 0$ is given by

$$\lim_{Q=0} I_{\text{Shell2}}(Q, R, R, \Delta\eta, \mu) = \left(\frac{4}{3}\pi \Delta\eta [R^3 - \nu^3 R^3 (1 - \mu)] \right)^2$$

Input Parameters for model Spherical Shell ii:

R: overall radius of spherical shell R

nu: the radius of the core is only the fraction ν of the overall radius R

eta: scattering length density difference between shell and matrix $\Delta\eta$

mu: scattering length density difference between core and matrix relative to the shell contrast μ

Note:

None

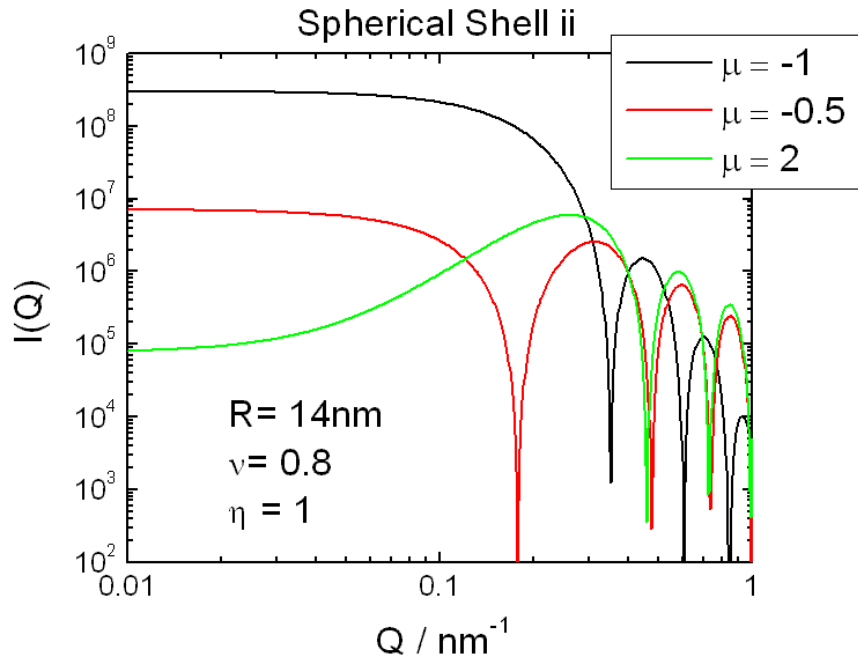


FIGURE 3.6. Scattering intensity of spherical shell with outer radius of $R = 14\text{nm}$ and inner radius of $\nu R = 11.2\text{nm}$. The scattering length density contrast the shell is set to 1 and the one of the core to -1, -0.5, and 2.

3.1.4. Spherical Shell iii.

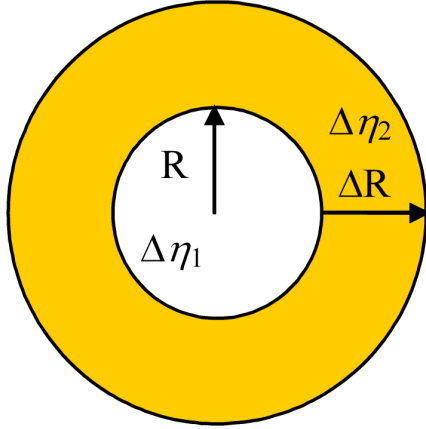


FIGURE 3.7. Spherical Shell iii

This implementation of a spherical shell is parametrised with an inner radius R and a shell thickness ΔR . The scattering contrast relative to the matrix of the core is $\Delta\eta_1$ and the one of the shell $\Delta\eta_2$.

$$I_{\text{Shell3}}(Q, R, \Delta R, \Delta\eta_1, \Delta\eta_2) = [K(Q, R + \Delta R, \Delta\eta_2) - K(Q, R, \Delta\eta_2 - \Delta\eta_1)]^2 \quad (3.6)$$

with

$$K(Q, R, \Delta\eta) = \frac{4}{3}\pi R^3 \Delta\eta 3 \frac{\sin QR - QR \cos QR}{(QR)^3} \quad (3.7)$$

The forward scattering for $Q = 0$ is given by

$$\lim_{Q=0} I_{\text{Shell3}}(Q, R, \Delta R, \Delta\eta_1, \Delta\eta_2) = \left(\frac{4}{3}\pi \left[(R + \Delta R)^3 \Delta\eta_2 - R^3 (\Delta\eta_2 - \Delta\eta_1) \right] \right)^2$$

Input Parameters for model Spherical Shell iii:

R: radius of core R

dR: thickness of the shell ΔR

eta1: scattering length density difference between core and matrix $\Delta\eta_1$

eta2: scattering length density difference between shell and matrix $\Delta\eta_2$

Note:

None

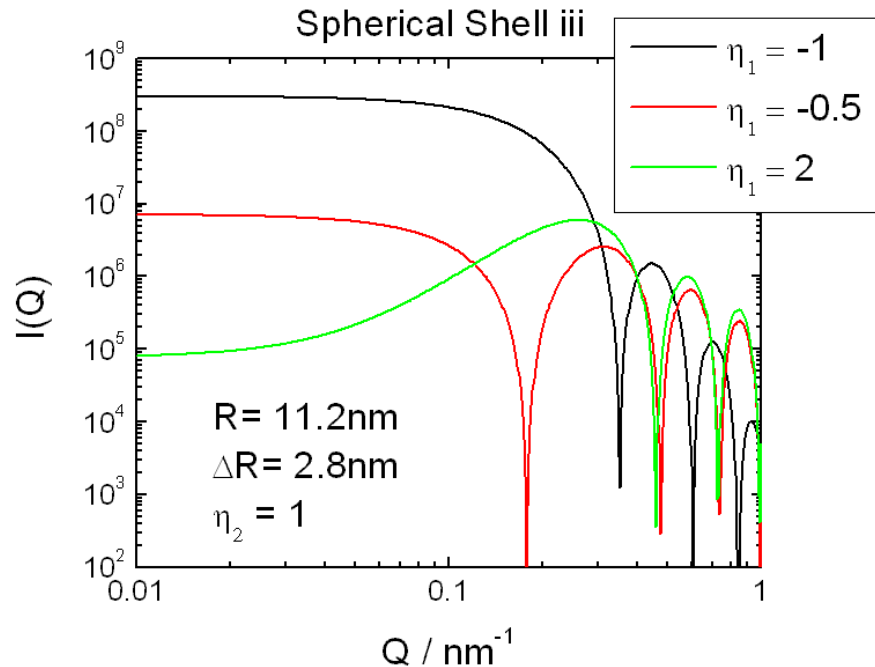


FIGURE 3.8. Scattering intensity of spherical shell with core radius of $R = 11.2\text{nm}$ and shell thickness of $\Delta R = 2.8\text{nm}$. The scattering length density contrast the shell is set to 1 and the one of the core to -1, -0.5, and 2.

3.1.5. Bilayered Vesicle.

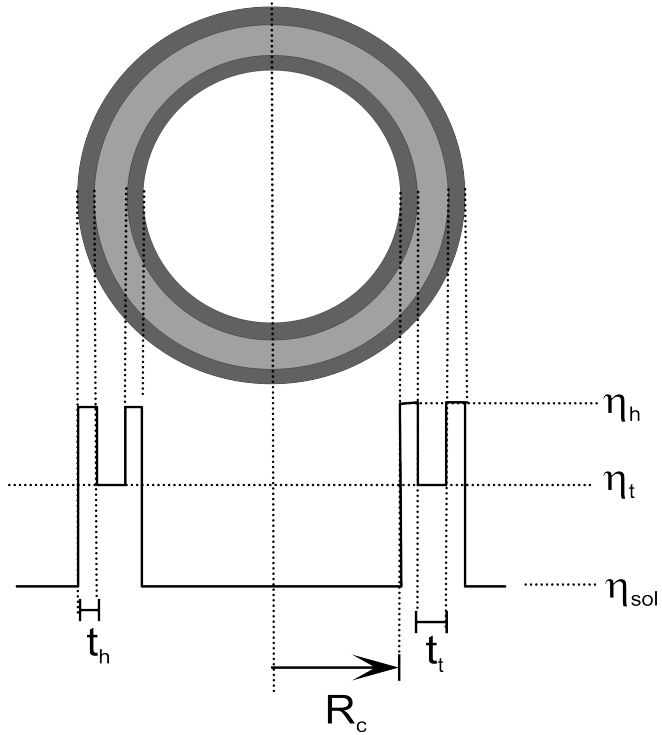


FIGURE 3.9. BiLayeredVesicle

$$I_{BLV}(Q) = \left(+ K(Q, R_c, \eta_{sol} - \eta_h) + K(Q, R_c + t_h, \eta_h - \eta_t) + K(Q, R_c + t_h + t_t, \eta_t - \eta_h) + K(Q, R_c + 2t_h + t_t, \eta_h - \eta_{sol}) \right)^2 \quad (3.8)$$

with

$$K(Q, R, \Delta\eta) = \frac{4}{3}\pi R^3 \Delta\eta 3 \frac{\sin QR - QR \cos QR}{(QR)^3} \quad (3.9)$$

Input Parameters for model BilayeredVesicle:

R_c: radius of core R_c which consists of solvent

t_h: thickness of outer part of bilayer (in contact with solvent, head group) t_h

t_t: thickness of inner part of bilayer (tail group) t_t

eta_sol: scattering length density of solvent η_{sol}

eta_h: scattering length density of outer part of bilayer η_h

eta_t: scattering length density of inner part of bilayer η_t

Note:

None

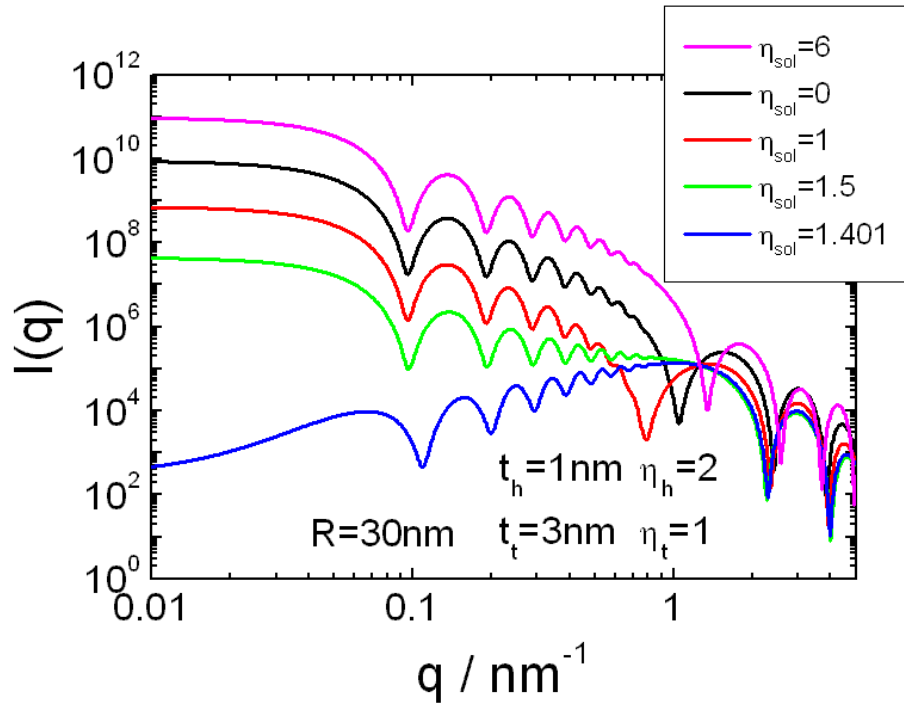


FIGURE 3.10. Scattering intensity of a bilayered vesicle. The scattering intensity has been calculated with a lognormal [LogNorm($N = 1, \sigma = 0.05, p = 1, R = 30$)] size distribution for the vesicle radius R_c .

3.1.6. Multi Lamellar Vesicle.

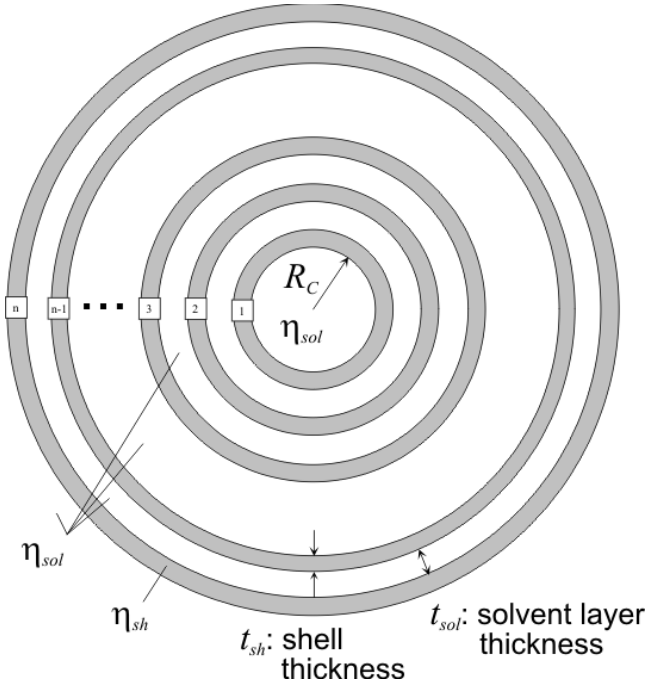


FIGURE 3.11. MultiLamellarVesicle

$$I_{MLV}(Q) = \left(\sum_{i=0}^{n-1} \left[K(Q, R_c + it_{sh} + it_{sol}, \eta_{sol} - \eta_{sh}) \right. \right. \\ \left. \left. + K(Q, R_c + (i+1)t_{sh} + it_{sol}, \eta_{sh} - \eta_{sol}) \right] \right)^2 \quad (3.10)$$

with

$$K(Q, R, \Delta\eta) = \frac{4}{3}\pi R^3 \Delta\eta 3 \frac{\sin QR - QR \cos QR}{(QR)^3} \quad (3.11)$$

Input Parameters for model MultiLamellarVesicle:

R_c: radius of core R_c which consists of solvent

t_sh: surfactant layer thickness t_{sh}

t_sol: thickness of solvent layer t_{sol}

eta_sh: scattering length density of surfactant layer η_{sh}

eta_sol: scattering length density of solvent η_{sol}

n: total number of surfactant layers n

Note:

None

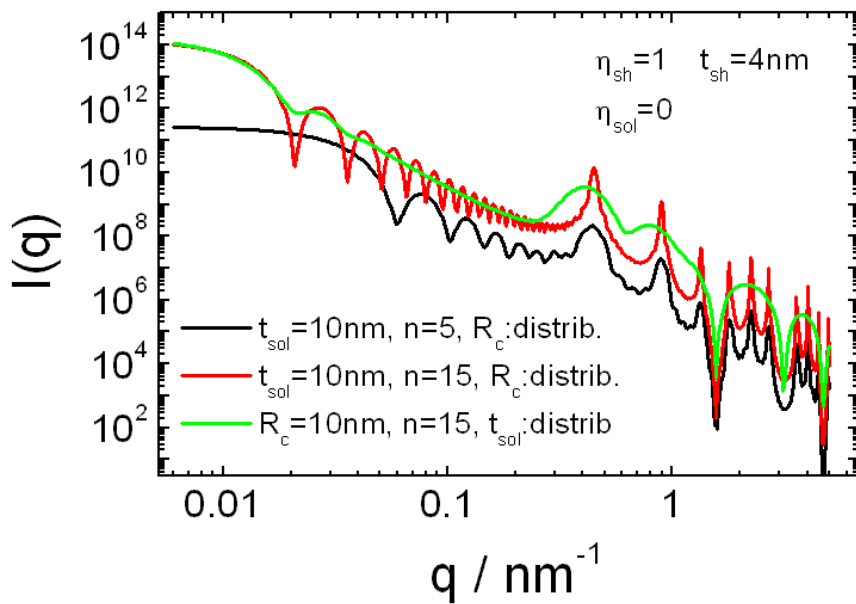


FIGURE 3.12. Scattering intensity of a multilamellar vesicle. The scattering intensities has been calculated for a&b) a distribution of the core radius R_c by $\int \text{LogNorm}(R_c; N = 1, \sigma = 0.3, p = 1, R = 10) I(q, R_c) dR_c$ and c) for a distribution of the distances between the lamellars $\int \text{LogNorm}(t_{\text{sol}}; N = 1, \sigma = 0.3, p = 1, R = 10) I(q, t_{\text{sol}}) dt_{\text{sol}}$.

3.1.7. RNDMultiLamellarVesicle.

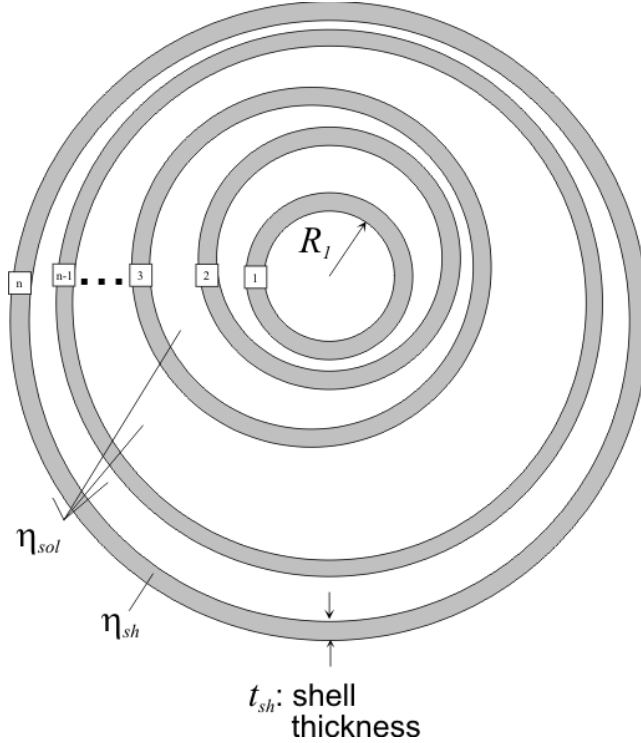


FIGURE 3.13. randomMultiLamellarVesicle

$$\begin{aligned} I_{\text{RndMLV}}(Q) = & \Delta\eta^2 \sum_{i=1}^N F_i^2(q, R_i, t_{sh,i}) \\ & + \Delta\eta^2 \sum_{i < j}^N 2F_i(q, R_i, t_{sh,i})F_j(q, R_j, t_{sh,j}) \frac{\sin qr_{ij}}{qr_{ij}} \end{aligned} \quad (3.12)$$

with

$$r_{ij} = |\mathbf{R}_i - \mathbf{R}_j| \quad (3.13a)$$

$$F_i(q, R_i, t_{sol,i}) = K(q, R_i + t_{sol,i}, \Delta\eta) - K(q, R_i, \Delta\eta) \quad (3.13b)$$

$$K(q, R, \Delta\eta) = \frac{4}{3}\pi R^3 \Delta\eta 3 \frac{\sin qR - qR \cos qR}{(qR)^3} \quad (3.13c)$$

$$R_1 = \text{ran}_{lognormal}(\log(R_c), \sigma_{R_c}) \quad (3.14a)$$

$$\Delta R_i = \text{ran}_{gaussian}(\sigma_{t_{sol}}) \quad (3.14b)$$

$$R_i = R_{i-1} + t_{sh,i-1} + \Delta R_i \quad (3.14c)$$

$$\mathbf{R}_i = R_i \text{ ran}_{dir,3D} \text{ ran}_{uniform} \Delta t_{sol} \quad (3.14d)$$

Input Parameters for model RNDMultiLamellarVesicle:

- t_sh:** average surfactant layer thickness t_{sh}
s_sh: Gaussian thickness distribution of surfactant layer with a width of σ_{sh}
R_c: average radius of core R_c which consists of solvent
s_c: lognormal size distribution of core radius R_c with a width of σ_c
n: average number of surfactant layers n
s_n: lognormal distribution of the number of surfactant layers with a width of σ_n
t_sol: average thickness of solvent layer t_{sol}
s_sol: lognormal thickness distribution of solvent layer with a width of σ_{sol}
Data_sh: scattering length density contrast $\Delta\eta$ between surfactant layer and solvent

Note:

The number of Monte Carlo iterations can be set via the menu [Options|Customize...]

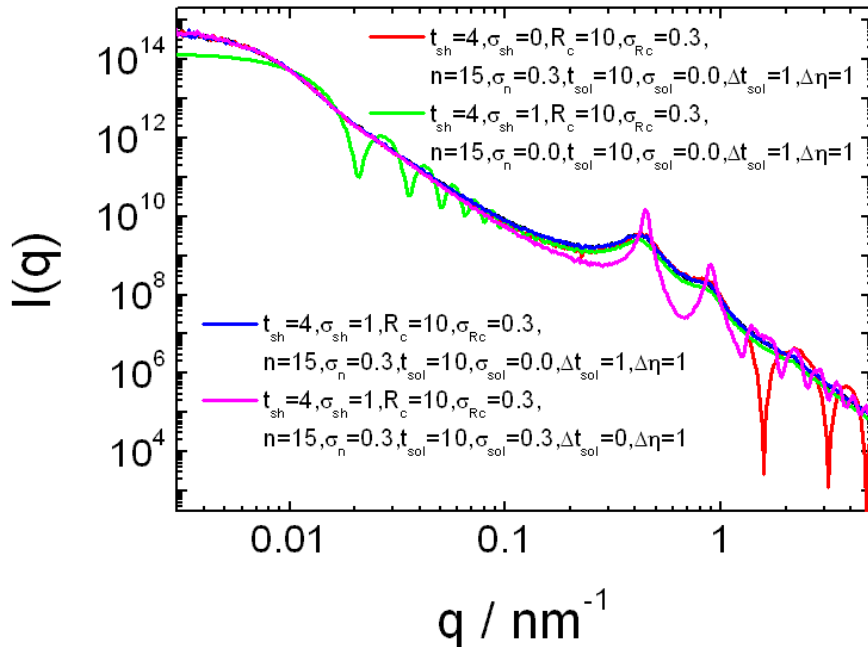


FIGURE 3.14. Scattering intensity of a multilamellar vesicle where several distribution of parameters within a single vesicle are calculated via a Monte Carlo algorithm. .

3.1.8. Vesicle with aligned flat capped ends [255, 256].

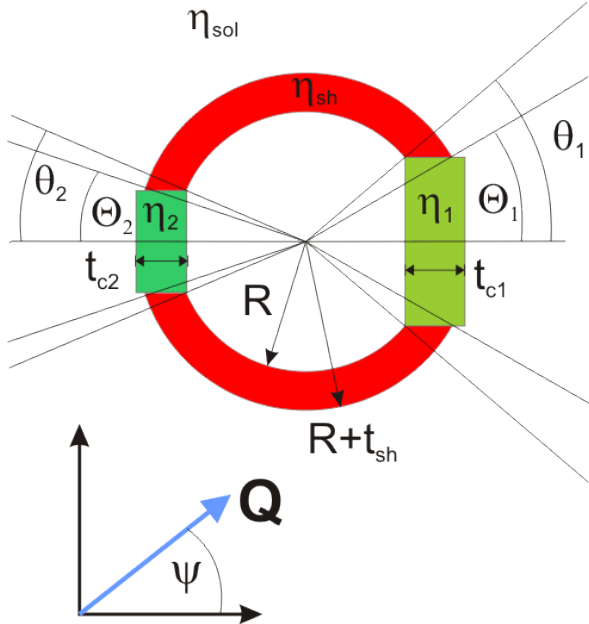


FIGURE 3.15. Sketch of a vesicle with horizontally aligned flat capped ends perpendicular to the incoming neutron beam

The shape of this form factor consist of spherical vesicle containing to flat domains. The flat thought to be aligned in a horizontal magnetic field perpendicular to the incoming neutron beam. The size of the domains are characterized by the angles θ_1 and θ_2 . The thicknesses t_{c1} and t_{c2} can be different than the thickness t_{sh} of the spherical part of the vesicles. The same hold for the scattering length densities η_{c1} , η_{c2} and η_{sh} . The form factor $F_{cv}(Q)$ of this object can be calculated by performing the Fourier transformation of the scattering length density in separate steps. First one calculates the Fourier transformation of a sphere F_{cSph} with flat capped ends on each side in cylinder coordinates.

$$F_{cSph}(Q, R, \psi, \theta_1, \theta_2, \Delta\eta) = \Delta\eta \int_{-R\cos\theta_2}^{R\cos\theta_1} dz \int_0^{\sqrt{R^2-z^2}} d\rho \int_0^{2\pi} d\phi e^{i\mathbf{Q}\cdot\mathbf{r}} \rho \quad (3.15a)$$

$$\text{with } \mathbf{Q} = Q \begin{pmatrix} 0 \\ \sin\psi \\ \cos\psi \end{pmatrix} \quad \text{and} \quad \mathbf{r} = \begin{pmatrix} \rho \cos\phi \\ \rho \sin\phi \\ z \end{pmatrix} \quad (3.15b)$$

The form factor of vesicle $F_{cv}(Q)$ with a layer thickness of t_{sh} can than be calculated by

$$F_{cv}(Q, R, t_{sh}, \theta_1, \theta_2, \Delta\eta_{sh}) = + F_{cSph}(Q, R + t_{sh}, \Theta_1, \Theta_2, \Delta\eta_{sh}) - F_{cSph}(Q, R, \theta_1, \theta_2, \Delta\eta_{sh}) \quad (3.16a)$$

with

$$\Theta_1 = \arcsin\left(\frac{R_{c1}}{R + t_{sh}}\right), \quad R_{c1} = R \sin(\theta_1), \quad (3.16b)$$

$$\Theta_2 = \arcsin\left(\frac{R_{c2}}{R + t_{sh}}\right), \quad R_{c2} = R \sin(\theta_2). \quad (3.16c)$$

As the flat capped ends are allowed to have independent thicknesses t_{c1}, t_{c2} and scattering length densities η_1, η_2 the scattering amplitude contribution of the flat capped ends, which have the shape of a disc, need to be corrected. Their contribution can be calculated by

$$\begin{aligned} F_c(Q, R, \theta_1, \theta_2, \dots) &= F_{c1}(Q, R, \theta_1, \Delta\eta_{c1}) - F_{d1}(Q, R, t_{d1}, \Delta\eta_{sh}) \\ &\quad + F_{c2}(Q, R, \theta_2, \Delta\eta_{c2}) - F_{d2}(Q, R, t_{d2}, \Delta\eta_{sh}) \\ &= \Delta\eta_{c1} \int_{l_{c1}}^{l_{c1}+t_{c1}} dz \int_0^{R_{c1}} d\rho \int_0^{2\pi} d\phi e^{i\mathbf{Q}\cdot\mathbf{r}} \rho - \Delta\eta_{sh} \int_{l_{c1}}^{l_{c1}+t_{d1}} dz \int_0^{R_{c1}} d\rho \int_0^{2\pi} d\phi e^{i\mathbf{Q}\cdot\mathbf{r}} \rho \\ &\quad + \Delta\eta_{c2} \int_{-(l_{c2}+t_{c2})}^{-l_{c2}} dz \int_0^{R_{c2}} d\rho \int_0^{2\pi} d\phi e^{i\mathbf{Q}\cdot\mathbf{r}} \rho - \Delta\eta_{sh} \int_{-(l_{c2}+t_{d2})}^{-l_{c2}} dz \int_0^{R_{c2}} d\rho \int_0^{2\pi} d\phi e^{i\mathbf{Q}\cdot\mathbf{r}} \rho \end{aligned} \quad (3.17)$$

with

$$\Delta\eta_{sh} = \eta_{sh} - \eta_{sol}, \quad \Delta\eta_{c1} = \eta_1 - \eta_{sol}, \quad \Delta\eta_{c2} = \eta_2 - \eta_{sol} \quad (3.18a)$$

$$l_{c1} = R \cos \theta_1, \quad l_{c2} = R \cos \theta_2 \quad (3.18b)$$

$$R_{c1} = R \sin \theta_1, \quad R_{c2} = R \sin \theta_2 \quad (3.18c)$$

$$t_{d1} = \sqrt{(R + t_{sh})^2 - R_{c1}^2} - \sqrt{R^2 - R_{c1}^2} \quad (3.18d)$$

$$t_{d2} = \sqrt{(R + t_{sh})^2 - R_{c2}^2} - \sqrt{R^2 - R_{c2}^2} \quad (3.18e)$$

$$(3.18f)$$

The solution of the integrals in eq. 3.15a and 3.17 are

$$\begin{aligned} F_{cSph}(Q, R, \psi, \theta_1, \theta_2, \Delta\eta) &= \Delta\eta \int_{-R \cos \theta_2}^{R \cos \theta_1} dz \int_0^{\sqrt{R^2 - z^2}} d\rho \int_0^{2\pi} d\phi e^{i\mathbf{Q}\cdot\mathbf{r}} \rho \\ &\quad \Delta\eta \int_{-R \cos \theta_2}^{R \cos \theta_1} dz \exp(iQz \cos \psi) 2\pi (R^2 - z^2) \frac{J_1(Q\sqrt{R^2 - z^2} \sin \psi)}{Q\sqrt{R^2 - z^2} \sin \psi} \end{aligned} \quad (3.19a)$$

and

$$\begin{aligned} F_{c_i, d_i}(Q, R_{c_i, d_i}, \psi, \Delta\eta) &= \Delta\eta \int_a^b dz \int_0^{R_{c_i}} d\rho \int_0^{2\pi} d\phi e^{i\mathbf{Q}\cdot\mathbf{r}} \rho \\ &= 4\pi R \frac{i(\exp(iaQ \cos \psi) - \exp(ibQ \cos \psi)) J_1(QR \sin \psi)}{\sin(2\psi) Q^2} \end{aligned} \quad (3.19b)$$

whereby J_1 the regular cylindrical Bessel function of first order. The overall scattering intensity $I_{\text{alignedVes}}(Q, \psi, \dots)$ is finally given by

$$I_{\text{alignedVes}}(Q, \psi, \dots) = |F_{\text{cv}}(Q, R, \psi, t_{\text{sh}}, \theta_1, \theta_2, \Delta\eta_{\text{sh}}) + F_{\text{c}}(Q, R, \psi, \theta_1, \theta_2, \dots)|^2 \quad (3.20)$$

Input Parameters for the models of `MagneticFieldAlignedVesicle`:

Rsh: radius of spherical vesicle shell

theta1: angle to describe size of first capped side

theta2: angle to describe size of second capped side

t_sh: thickness of spherical vesicle shell

t_c1: thickness of first flat capped side

t_c2: thickness of second flat capped side

eta_sh: scattering length density of spherical vesicle shell

eta_1: scattering length density of first capped side

eta_2: scattering length density of second capped side

eta_sol: scattering length density of solvent

Note:

None

3.2. Polymers and Micelles

3.2.1. Unified Exponential Power Law according to Beaucage.
The model is described in [19, 20].

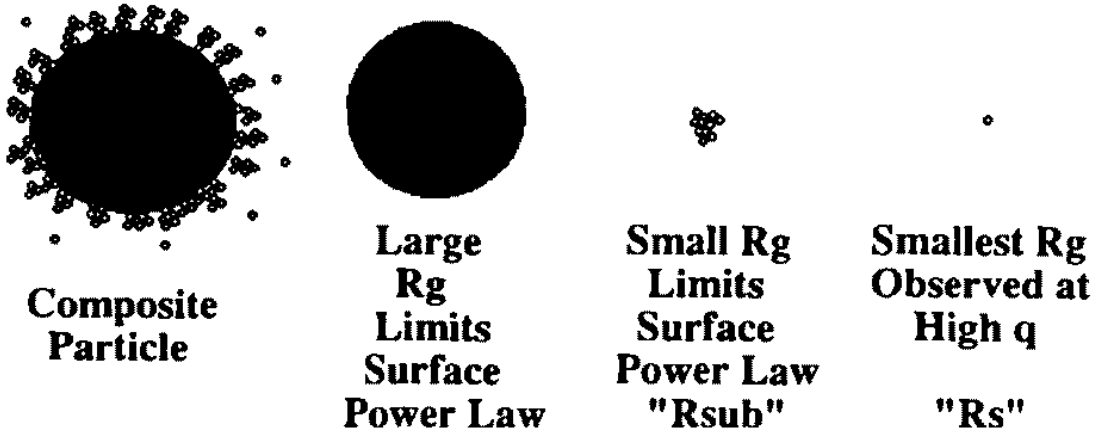


FIGURE 3.16. A typical case in which two R_g 's are observed. Particles composed of sub-particles where a radius of gyration for the entire particle, R_g , and a radius of gyration for the sub-particles, R_s , are observed. The surface-fractal cut-off radius of gyration, R_{sub} , differs from the high- Q radius of gyration, R_s , in this case. Generally, $R_s = R_{sub}$

3.2.1.1. Beaucage.

$$\begin{aligned}
 I_{\text{Beaucage}}(Q) \simeq & G \exp \left(-\frac{Q^2 R_g^2}{3} \right) \\
 & + B \exp \left(-\frac{Q^2 R_{sub}^2}{3} \right) \left(\frac{\left[\operatorname{erf} \left(Q k R_g / \sqrt{6} \right) \right]^3}{Q} \right)^P \\
 & + G_s \exp \left(-\frac{Q^2 R_s^2}{3} \right) \\
 & + B_s \left(\frac{\left[\operatorname{erf} \left(Q k_s R_s / \sqrt{6} \right) \right]^3}{Q} \right)^{P_s}
 \end{aligned} \tag{3.21}$$

The first term in eq. 3.21 describes the large-scale structure of size R_g composed of small subunits of size R_s , captured in the third term. The second term describes the mass-fractal regime with two structural limits. The low- Q limit is at R_g and is described by the error function. The high- Q limit is at R_{sub} and is described by the exponential pre-factor [19]. The final two terms are for the sub-structural mer unit. Using eq. 3.21, scattering from a system with multiple-size-scale features is parameterized. Generally, the high- Q cutoff for the intermediate power law, R_{sub} , is identical to the sub-structural radius of gyration, R_s . The assumption that $R_{sub} = R_s$ should always be true for typical

mass fractals. It should be noted that, although eq. 3.21 appears cumbersome, no new parameters have been introduced over local fits using exponentials and power laws.

G is the Guinier pre-factor defined above and B is a pre-factor specific to the type of power-law scattering: B is defined according to the regime in which the exponent P falls. Generally, for surface fractals $4 > P > 3$, for mass fractals $P < 3$ and for diffuse interfaces $P > 4$. For Porod's law, $P = 4$ and $B = N_p 2\pi \rho_c^2 p S_p$, where S_p , is the particulate surface area. For a Gaussian polymer, $P = 2$, and B is given by $2G/R_g^2$, through a comparison with the Debye form factor 9.4.1 at the high- Q limit as discussed below. The constant, k in 3.21, accounts for an approximation involved in the description of the low- Q power-law limit [19]. This is an emical constant that has a value of 1 for steep power-law decays, $P > 3$. For weak power-law decays, k deviates slightly from 1. For polymeric mass fractals of fractal dimension d_f close to 2 (1.5 to 3), k is emically found to be close to 1.06. Weak deviations are observed between the scattered intensity as calculated using 3.21 and exact calculations for values of Q between $2\pi/R_g$ and π/R_g in these cases when $k = 1$. These deviations are reduced to less than 3% of the calculated intensity using $k = 1.06$.

Input Parameters for model Beaucage:

G: G is the Guinier pre-factor of the larger structure

B: B is a pre-factor specific to the type of power-law scattering: B is defined according to the regime in which the exponent P falls.

Gs: G_s is the Guinier pre-factor of the smaller structure

Bs: B_s is a pre-factor specific to the type of power-law scattering: B_s is defined according to the regime in which the exponent P_s falls.

Rg: large-scale structure

Rsub: surface-fractal cut-off radius of gyration, R_{sub} defines the high- Q cutoff for the intermediate power law

Rs: size R_s of small subunits

P: scaling exponent of the power law assigned to the larger structure R_g

Ps: scaling exponent of the power law assigned to the smaller structure R_s

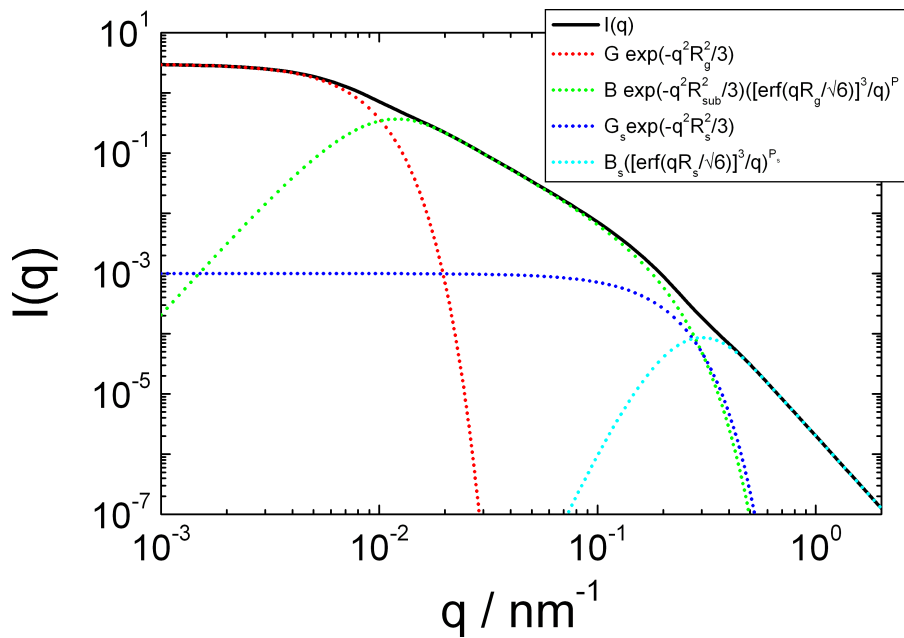


FIGURE 3.17

3.2.1.2. *Beaucage2.*

Equation 3.21 can be extended to describe an arbitrary number of interrelated structural levels under the generally applicable assumption that $R_{\text{sub}} = R_s$,

$$I_{\text{Beaucage}}(Q) \simeq \sum_{i=1}^n G_i \exp\left(-\frac{Q^2 R_{g,i}^2}{3}\right) + B_i \exp\left(-\frac{Q^2 R_{g,i+1}^2}{3}\right) \left(\frac{\left[\operatorname{erf}\left(Qk_i R_{g,i}/\sqrt{6}\right)\right]^3}{Q}\right)^{P_i} \quad (3.22)$$

In 3.22, $i = 1$ refers to the largest-size structural level. Extensions, such as eq. 3.22, can only be justified when data extend over many decades in Q . Eq. 3.22 introduces no new parameters over local Guinier and power-law fits.

Input Parameters for model **Beaucage2:**

G: Guinier pre-factor G_i

B: pre-factor B_i , specific to the type of power-law scattering: B_i is defined according to the regime in which the exponent P_i falls.

R_i: large-scale structure $R_{g,i}$

R_i+1: size $R_{g,i+1}$ of smaller subunits

k: This is an emical constant that has a value of 1 for steep power-law decays, $P > 3$.
For weak power-law decays, k deviates slightly from 1

P: scaling exponent of the power law assigned to the larger structure $R_{g,i}$

Note: For calculating a summation over n interrelated structural levels one has to use global fitting. For **R_i** and **R_i+1** one has to define global parameters, let say P1 and P2 in the first scattering contribution. In the second scattering contribution one has to use for **R_i** the same global parameter P2 as for **R_i+1** in the previous scattering contribution. The global parameters for **R_i** in one scattering contribution and the global parameter for **R_i+1** in the previous scattering contribution have to be the same. By this an arbitrary number of interrelated structural levels can be calculated.

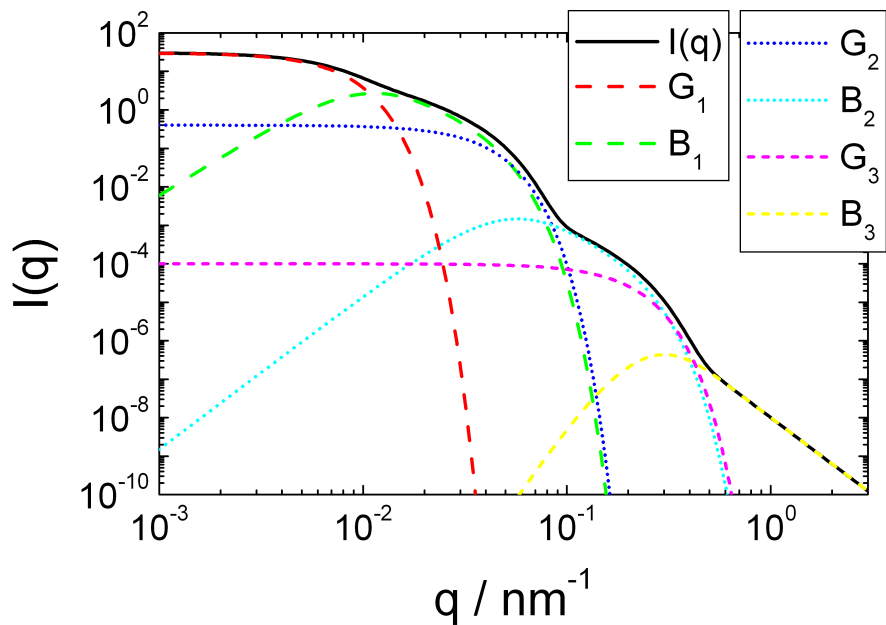


FIGURE 3.18

3.2.2. WormLikeChainEXV. [380]

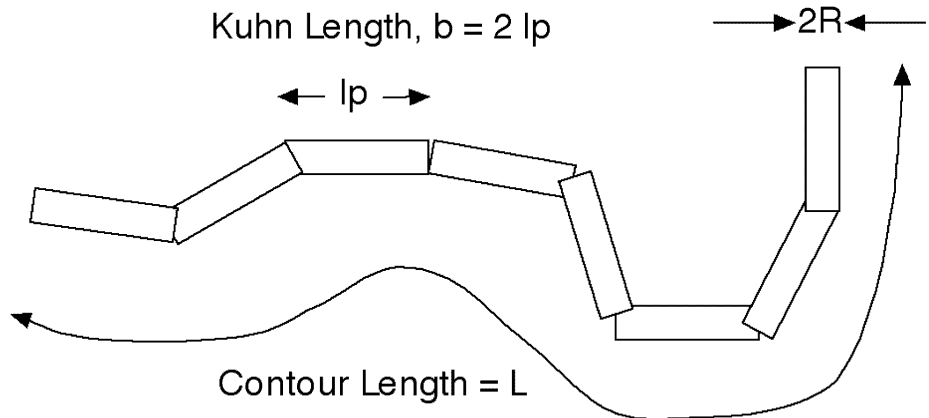


FIGURE 3.19. The chain of contour length, L , (the total length) can be described a chain of some number of locally stiff segments of length l_p . The persistence length, l_p , is the length along the cylinder over which the flexible cylinder can be considered a rigid rod. The Kuhn length (b) used in the model is also used to describe the stiffness of a chain, and is simply $b = 2l_p$.

This form factor calculates the form factor for a flexible cylinder with a circular cross section and a uniform scattering length density. The non-negligible diameter of the cylinder is included by accounting for excluded volume interactions within the walk of a single cylinder. Inter-cylinder interactions are NOT included. The function calculated has been given by Pedersen et al. [380]. The model "Method 3 With Excluded Volume" is used, which is a parametrization of simulations of a discrete representation of the worm-like chain model of Kratky and Porod applied in the pseudo-continuous limit.

Input Parameters for model WormLikeChainEXV:

R: radius R of cylindrical core with uniform scattering length density

1: Kuhn length¹ l of semi-flexible worm-like structure

L: contour length L of semi-flexible worm-like structure

¹The Kuhn length l is related to the length a of locally stiff segment simply via $l = 2a$

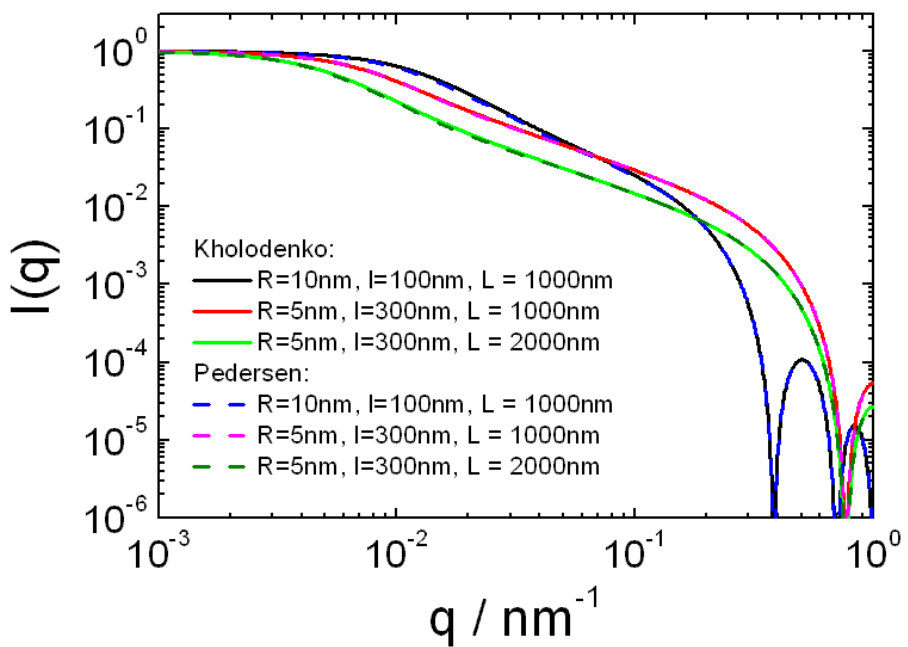


FIGURE 3.20. Comparison of wormlike micelles according to Pedersen [380] and Kholodenko [265]

3.2.3. KholodenkoWorm.

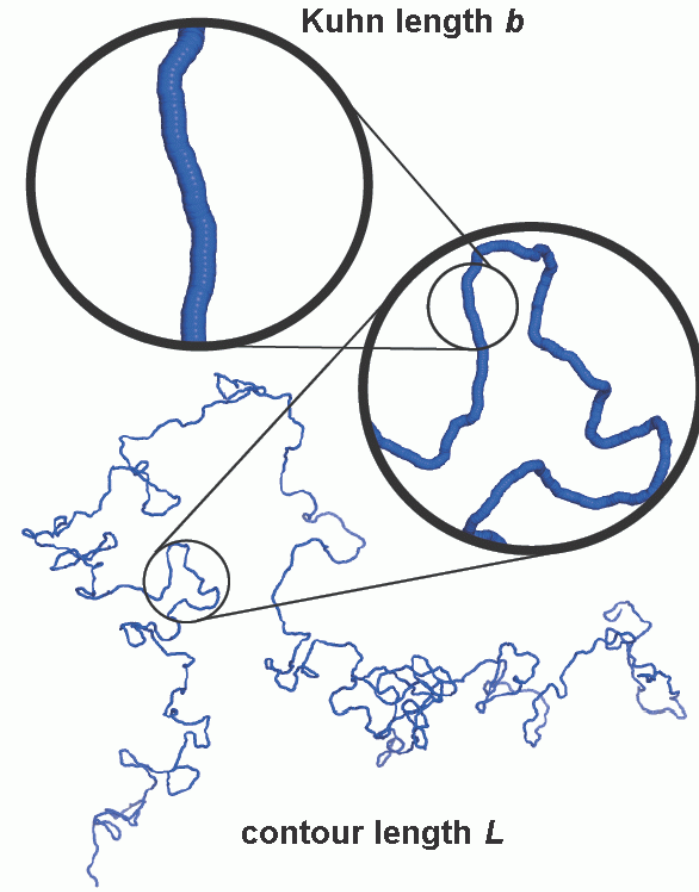


FIGURE 3.21

Kholodenko [265] presented a new approach using the analogy between Dirac's fermions and semi-flexible polymers. The form factor $P_0(Q)$ resulting from Kholodenko's approach is designed to reproduce correctly the rigid-rod limit and the random-coil limit. Defining $x = 3L/l$ (L : contour length, l : Kuhn length), it is given by

$$P_0(Q, L, l) = \frac{2}{x} \left[I_{(1)} - \frac{1}{x} I_{(2)} \right] \quad (3.23)$$

where

$$I_{(n)}(x) = \int_0^x f(z) z^{n-1} dz \quad (3.24)$$

together with

$$f(z) = \begin{cases} \frac{1}{E} \frac{\sinh(Ez)}{\sinh(z)} & \text{for } Q \leq \frac{3}{l} \\ \frac{1}{F} \frac{\sin(Fz)}{\sinh(z)} & \text{for } Q > \frac{3}{l} \end{cases} \quad (3.25)$$

and

$$E = \sqrt{1 - \left(\frac{lQ}{3}\right)^2} \quad \text{and} \quad F = \sqrt{\left(\frac{lQ}{3}\right)^2 - 1} \quad (3.26)$$

For flexible cylinders with a circular cross section and a uniform scattering length density the cross section form factor is given by

$$P_{cs} = \left(2 \frac{J_1(QR)}{QR}\right)^2 \quad (3.27)$$

so that the overall form factor is given by

$$P(Q, L, l, R) = P_0(Q, L, l) P_{cs}(Q, R) \quad (3.28)$$

Input Parameters for model KholodenkoWorm:

R: radius R of cylindrical core with uniform scattering length density

1: Kuhn length² l of semi-flexible worm-like structure

L: contour length L of semi-flexible worm-like structure

²The Kuhn length l is related to the length a of locally stiff segment simply via $l = 2a$

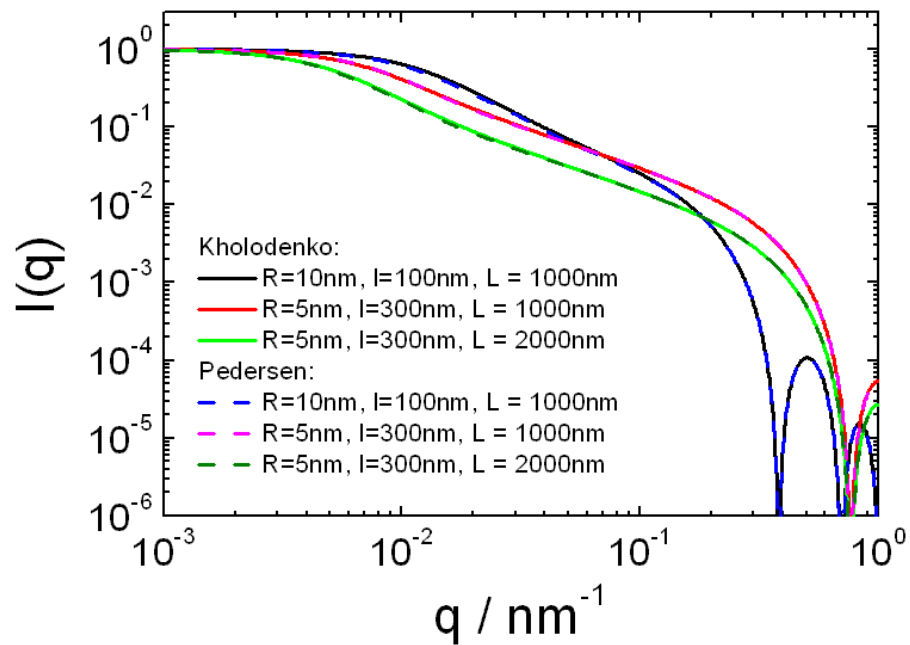


FIGURE 3.22. Comparison of wormlike micelles according to Pedersen [380] and Kholodenko [265].

3.2.4. Diblock copolymer micelles.

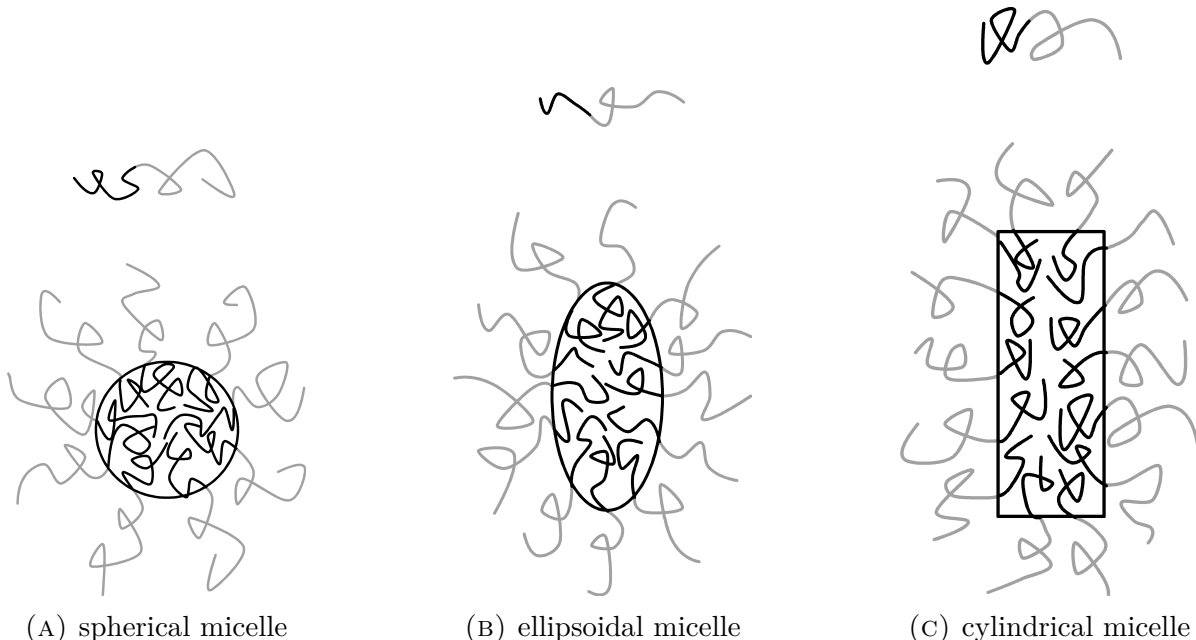


FIGURE 3.23. Block copolymer forming micelles of different shapes

For block copolymers, which form micelles, several form factor have been implemented [378, 375, 470] for spherical, ellipsoidal, and cylindrical shapes. It has been assumed that one unit is forming the core of the micelles and the other the corona. The core is assumed to have a homogeneous scattering length density, but may contain some amount of solvent. For the polymer chains in the corona either a model where Gaussian chains are attached to the core or a corona model of semi-flexible interacting self-avoiding chains (only for spherical core) or a continuous model, where a radial profile of the form $\Phi(r) \propto r^{-\alpha}$ has been assumed. The form factors have been parameterized such, that the excess scattering of the corona and the core are consistent with the composition and density of the two separate block units of the copolymer.

3.2.4.1. Micelles with a homogeneous core and Gaussian chains on the surface.

It is assumed that the diblock copolymer consist of a block unit for which the solvent is poor and a block unit with is good. The insoluble blocks form a relatively compact core whereas the soluble blocks form a diffuse corona surrounding the core. The form factor of a micelle contains four different terms: the self-correlation term of the core $N_{\text{agg}}^2 \beta_{\text{core}}^2 P_{\text{core}}(q)$, the self-correlation term of the chains $N_{\text{agg}} \beta_{\text{brush}}^2 P_{\text{brush}}(q)$, the cross-term between the core and chains $2N_{\text{agg}}^2 \beta_{\text{core}} \beta_{\text{brush}} S_{\text{brush-core}}(q)$, and the cross term between different chains $N_{\text{agg}}(N_{\text{agg}} - 1) \beta_{\text{brush}}^2 S_{\text{brush-brush}}(q)$. It can be written (Pedersen & Gerstenberg, 1996)

$$\begin{aligned} I_{\text{mic}} = & N_{\text{agg}}^2 \beta_{\text{core}}^2 P_{\text{core}}(q) + N_{\text{agg}} \beta_{\text{brush}}^2 P_{\text{brush}}(q) \\ & + 2N_{\text{agg}}^2 \beta_{\text{core}} \beta_{\text{brush}} S_{\text{brush-core}}(q) + N_{\text{agg}}(N_{\text{agg}} - 1) \beta_{\text{brush}}^2 S_{\text{brush-brush}}(q) \end{aligned} \quad (3.29)$$

N_{agg} is the aggregation number of diblock polymers forming the micelle and $\beta_{\text{brush}} = V_{\text{brush}}(\eta_{\text{brush}} - \eta_{\text{solv}})$ and $\beta_{\text{core}} = V_{\text{core}}(\eta_{\text{core}} - \eta_{\text{solv}})$ the excess scattering length of a block in the corona and in the core, respectively. V_{brush} and V_{core} are the total volume of a block in the corona and in the core. η_{brush} and η_{core} are the corresponding scattering length densities and η_{solv} is the scattering length density of the surrounding solvent. The functions $P_{\text{core}}(q)$, $P_{\text{brush}}(q)$, $S_{\text{brush-core}}(q)$, and $S_{\text{brush-brush}}(q)$ are all 1 for $q = 0$. The definitions of these four functions depend on the shape of the core and are given below.

3.2.4.1.1. spherical core:

$$P_{\text{core}}(q, R_{\text{core}}) = \Phi^2(qR_{\text{core}}) \quad (3.30)$$

$$\Phi(qR) = 3 \frac{\sin(qR) - qR \cos(qR)}{(qR)^3} \quad (3.31)$$

$$P_{\text{brush}}(q, R_g) = 2 \frac{\exp(-x) - 1 + x}{x^2} \text{ with } x = R_g^2 q^2 \quad (3.32)$$

$$S_{\text{brush-core}}(q, R_{\text{core}}, Rg, d) = \Phi(qR_{\text{core}})\psi(qR_g) \frac{\sin(q[R_{\text{core}} + dR_g])}{q[R_{\text{core}} + dR_g]} \quad (3.33)$$

$$\psi(qRg) = \frac{1 - \exp(-x)}{x} \text{ (form factor amplitude of the chain)}$$

$$S_{\text{brush-brush}}(q, R_{\text{core}}, d, R_g) = \psi^2(qR_g) \left[\frac{\sin(q[R_{\text{core}} + dR_g])}{q[R_{\text{core}} + dR_g]} \right]^2 \quad (3.34)$$

For micelles with a spherical core a few different parameterizations have been implemented **SPHERE+Chains(RW)**, **SPHERE+Chains(RW)_Rc** and **SPHERE+Chains(RW)_Nagg**. The parameters they all have in common are:

- V_{brush} : molecular volume the diblock copolymer part forming the corona
- η_{core} : scattering length density of the diblock copolymer part forming the core
- η_{brush} : scattering length density of the diblock copolymer part forming the corona
- η_{solv} : scattering length density of the solvent
- $x_{\text{solv,core}}$: volume fraction of solvent in the micellar core
- R_g : radius of gyration of the block unit in the corona
- d : non-penetration of the chains into the core is mimicked by $d \sim 1$ for $R_{\text{core}} \gg R_g$

For the model **SPHERE+Chains(RW)** the other parameters are

R_{core} : radius of the micellar core

n_{agg} : grafting density (number of copolymer molecules N_{agg} per surface are S , $n_{\text{agg}} = N_{\text{agg}}/S$)

In contrast to the form factor SPHERE+Chains(RW)_{Rc} and SPHERE+Chains(RW)_{Nagg} this one does not necessarily consist of copolymers. The excess scattering lengths and aggregation number needed in eq. 3.29 are then given by

$$N_{\text{agg}} = n_{\text{agg}} S \quad (3.35)$$

where the surface of the core is given by $S = 4\pi R_{\text{core}}^2$. Together with the core volume $V = \frac{4}{3}\pi R_{\text{core}}^3$ one gets for the excess scattering lengths

$$\beta_{\text{core}} = \frac{V(1 - x_{\text{solv,core}})}{N_{\text{agg}}}(\eta_{\text{core}} - \eta_{\text{solv}}) \quad (3.36)$$

$$\beta_{\text{brush}} = V_{\text{brush}}(\eta_{\text{brush}} - \eta_{\text{solv}}) \quad (3.37)$$

Input Parameters for model SPHERE+Chains(RW):

R_core: core radius

n_agg: specific aggregation number (number of chains per surface area)

V_brush: molecular volume of a block unit in the micellar corona

eta_core: scattering length density of spherical core

eta_brush: scattering length density of the block unit in the corona

eta_solv: scattering length density of solvent

xsolv_core: amount of solvent in core

Rg: gyration radius of polymer chains in the corona

d: This value should be around 1. Non-penetration of the chains into the core is mimicked by $d \sim 1$ for $R_{\text{core}} \gg R_g$

For the model SPHERE+Chains(RW)_{Rc} the other parameters are

R_core: core radius

V_core: molecular volume of single block unit in the micellar core

The excess scattering lengths and aggregation number in eq. 3.29 are given by

$$\beta_{\text{core}} = V_{\text{core}}(\eta_{\text{core}} - \eta_{\text{solv}}) \quad (3.38)$$

$$\beta_{\text{brush}} = V_{\text{brush}}(\eta_{\text{brush}} - \eta_{\text{solv}}) \quad (3.39)$$

$$N_{\text{agg}} = (1 - x_{\text{solv,core}})\frac{4}{3}\pi R_{\text{core}}^3/V_{\text{core}} \quad (3.40)$$

Input Parameters for model SPHERE+Chains(RW)_{Rc}:

R_core: core radius

V_core: molecular volume of single block unit in the micellar core

V_brush: molecular volume of single block unit in the micellar corona

eta_core: scattering length density of spherical core

eta_brush: scattering length density of the block unit in the corona

eta_solv: scattering length density of solvent

xsolv_core: amount of solvent in core

Rg: gyration radius of polymer chains in the corona

d: This value should be around 1. Non-penetration of the chains into the core is mimicked by $d \sim 1$ for $R_{\text{core}} \gg R_g$

For the model **SPHERE+Chains(RW)_Nagg** the other parameters are

Nagg: aggregation number

Vcore: molecular volume of single block unit in the micellar core

The excess scattering lengths and the core radius R_{core} needed in eq. 3.29 are given by

$$\beta_{\text{core}} = V_{\text{core}}(\eta_{\text{core}} - \eta_{\text{solv}}) \quad (3.41)$$

$$\beta_{\text{brush}} = V_{\text{brush}}(\eta_{\text{brush}} - \eta_{\text{solv}}) \quad (3.42)$$

$$R_{\text{core}} = \left(\frac{N_{\text{agg}} V_{\text{core}}}{1 - x_{\text{solv,core}}} \frac{3}{4\pi} \right)^{1/3} \quad (3.43)$$

Input Parameters for model SPHERE+Chains(RW)_Nagg:

N_agg: aggregation number

V_core: molecular volume of single block unit in the micellar core

V_brush: molecular volume of single block unit in the micellar corona

eta_core: scattering length density of spherical core

eta_brush: scattering length density of the block unit in the corona

eta_solv: scattering length density of solvent

xsolv_core: amount of solvent in core

Rg: gyration radius of polymer chains in the corona

d: This value should be around 1. Non-penetration of the chains into the core is mimicked by $d \sim 1$ for $R_{\text{core}} \gg R_g$

3.2.4.1.2. *ellipsoidal core with semi-axis ($R, R, \epsilon R$):*

$$P_{\text{core}}(q, R_{\text{core}}, \epsilon) = \int_0^{\pi/2} \Phi^2[qr(R_{\text{core}}, \epsilon, \alpha)] \sin \alpha d\alpha \quad (3.44)$$

with $r(R_{\text{core}}, \epsilon, \alpha) = R_{\text{core}} \sqrt{\sin^2 \alpha + \epsilon^2 \cos^2 \alpha}$

$$P_{\text{brush}}(q, R_g) = 2 \frac{\exp(-x) - 1 + x}{x^2} \text{ with } x = R_g^2 q^2 \quad (3.45)$$

$$S_{\text{brush-core}}(q, R_{\text{core}}, \epsilon, Rg, d) = \psi(qR_g) \int_0^{\pi/2} \Phi(qr(\dots)) \frac{\sin(q[r(\dots) + dR_g])}{q[r(\dots) + dR_g]} \sin \alpha d\alpha \quad (3.46)$$

$$S_{\text{brush-brush}}(q, R_{\text{core}}, d, R_g) = \psi^2(qR_g) \int_0^{\pi/2} \left[\frac{\sin(q[r(\dots) + dR_g])}{q[r(\dots) + dR_g]} \right]^2 \sin \alpha d\alpha \quad (3.47)$$

As for micelles with spherical core also for those with an ellipsoidal core several parameterizations have been implemented **ELL+Chains(RW)**, **ELL+Chains(RW)_Rc** and **ELL+Chains(RW)_Nagg**. The parameters they all have in common are:

V_{brush} : molecular volume the diblock copolymer part forming the corona

η_{core} : scattering length density of the diblock copolymer part forming the core

η_{brush} : scattering length density of the diblock copolymer part forming the corona

η_{solv} : scattering length density of the solvent

$x_{\text{solv,core}}$: volume fraction of solvent in the micellar core

R_g : radius of gyration of the block unit in the corona

d : non-penetration of the chains into the core is mimicked by $d \sim 1$ for $R_{\text{core}} \gg R_g$

ϵ : stretching factor of the ellipsoidal micelle ($R_{\text{core}}, R_{\text{core}}, \epsilon R_{\text{core}}$)

For the model **ELL+Chains(RW)** the other parameters are

R_{core} : radius of the micellar core ($R_{\text{core}}, R_{\text{core}}, \epsilon R_{\text{core}}$)

n_{agg} : grafting density (number of copolymer molecules N_{agg} per surface area S , $n_{\text{agg}} = N_{\text{agg}}/S$)

In contrast to the form factor **ELL+Chains(RW)_Rc** and **ELL+Chains(RW)_Nagg** this one does not necessarily consist of copolymers. The excess scattering lengths and aggregation number needed in eq. 3.29 are given by

$$N_{\text{agg}} = n_{\text{agg}} S \quad (3.48)$$

where the surface of the core is given by

$$S = \begin{cases} 2\pi R_{\text{core}}^2 \left(1 + \frac{\operatorname{arctanh}(\sin(\alpha))}{\sin(\alpha)} \right) & \text{for } \epsilon < 1 \\ 2\pi R_{\text{core}}^2 \left(1 + \frac{\alpha}{\tan(\alpha)} \right) & \text{for } \epsilon \geq 1 \end{cases} \quad (3.49)$$

$$\alpha = \begin{cases} \arccos(\epsilon) & \text{for } \epsilon < 1 \\ \arccos(1/\epsilon) & \text{for } \epsilon \geq 1 \end{cases}$$

Together with the core volume $V = \frac{4}{3}\pi\epsilon R_{\text{core}}^3$ one gets for the excess scattering lengths

$$\beta_{\text{core}} = \frac{V(1 - x_{\text{solv,core}})}{N_{\text{agg}}} (\eta_{\text{core}} - \eta_{\text{solv}}) \quad (3.50)$$

$$\beta_{\text{brush}} = V_{\text{brush}} (\eta_{\text{brush}} - \eta_{\text{solv}}) \quad (3.51)$$

Input Parameters for model ELL+Chains(RW):

R_core: core radius

n_agg: specific aggregation number (number of chains per surface area)

V_brush: molecular volume of a block unit in the micellar corona

eta_core: scattering length density of spherical core

eta_brush: scattering length density of the block unit in the corona

eta_solv: scattering length density of solvent

xsolv_core: amount of solvent in core

Rg: gyration radius of polymer chains in the corona

d: This value should be around 1. Non-penetration of the chains into the core is mimicked by $d \sim 1$ for $R_{\text{core}} \gg R_g$

epsilon: stretching factor of the ellipsoidal micelle ($R_{\text{core}}, R_{\text{core}}, \epsilon R_{\text{core}}$)

For the model ELL+Chains(RW)_Rc the other parameters are

Rcore: core radius

Vcore: molecular volume of single block unit in the micellar core

The excess scattering lengths and aggregation number in eq. 3.29 are given by

$$\beta_{\text{core}} = V_{\text{core}} (\eta_{\text{core}} - \eta_{\text{solv}}) \quad (3.52)$$

$$\beta_{\text{brush}} = V_{\text{brush}} (\eta_{\text{brush}} - \eta_{\text{solv}}) \quad (3.53)$$

$$N_{\text{agg}} = (1 - x_{\text{solv,core}}) \frac{4}{3}\pi\epsilon R_{\text{core}}^3 / V_{\text{core}} \quad (3.54)$$

Input Parameters for model ELL+Chains(RW)_Rc:

R_core: core radius

V_core: molecular volume of single block unit in the micellar core

V_brush: molecular volume of single block unit in the micellar corona

eta_core: scattering length density of spherical core

eta_brush: scattering length density of the block unit in the corona

eta_solv: scattering length density of solvent

xsolv_core: amount of solvent in core

Rg: gyration radius of polymer chains in the corona

d: This value should be around 1. Non-penetration of the chains into the core is mimicked by $d \sim 1$ for $R_{\text{core}} \gg R_g$

epsilon: stretching factor of the ellipsoidal micelle ($R_{\text{core}}, R_{\text{core}}, \epsilon R_{\text{core}}$)

For the model **ELL+Chains(RW)_Nagg** the other parameters are

Nagg: aggregation number

Vcore: molecular volume of single block unit in the micellar core

The excess scattering lengths and the core radius R_{core} needed in eq. 3.29 are given by

$$\beta_{\text{core}} = V_{\text{core}}(\eta_{\text{core}} - \eta_{\text{solv}}) \quad (3.55)$$

$$\beta_{\text{brush}} = V_{\text{brush}}(\eta_{\text{brush}} - \eta_{\text{solv}}) \quad (3.56)$$

$$R_{\text{core}} = \left(\frac{N_{\text{agg}} V_{\text{core}}}{1 - x_{\text{solv,core}}} \frac{3}{4\pi\epsilon} \right)^{1/3} \quad (3.57)$$

Input Parameters for model **ELL+Chains(RW)_Nagg**:

N_agg: aggregation number

V_core: molecular volume of single block unit in the micellar core

V_brush: molecular volume of single block unit in the micellar corona

eta_core: scattering length density of spherical core

eta_brush: scattering length density of the block unit in the corona

eta_solv: scattering length density of solvent

xsolv_core: amount of solvent in core

Rg: gyration radius of polymer chains in the corona

d: This value should be around 1. Non-penetration of the chains into the core is mimicked by $d \sim 1$ for $R_{\text{core}} \gg R_g$

epsilon: stretching factor of the ellipsoidal micelle ($R_{\text{core}}, R_{\text{core}}, \epsilon R_{\text{core}}$)

3.2.4.1.3. cylindrical core with radius R_{core} and height H :

$$P_{\text{core}}(q, R_{\text{core}}, H) = \int_0^{\pi/2} \Psi^2(q, R_{\text{core}}, H, \alpha) \sin \alpha d\alpha \quad (3.58)$$

$$\text{with } \Psi(q, R_{\text{core}}, H, \alpha) = \frac{2J_1(qR_{\text{core}} \sin \alpha)}{qR_{\text{core}} \sin \alpha} \frac{\sin(qH/2 \cos \alpha)}{qH/2 \cos \alpha} \quad (3.59)$$

and $J_1(x)$ is the first order Bessel function of the first kind.

$$P_{\text{brush}}(q, R_g) = 2 \frac{\exp(-x) - 1 + x}{x^2} \text{ with } x = R_g^2 q^2 \quad (3.60)$$

$$S_{\text{brush-core}}(q, R_{\text{core}}, H, Rg, d) = \psi(qR_g) \times \int_0^{\pi/2} \Psi(q, R_{\text{core}}, H, \alpha) \Xi(q, R + dR_g, H + 2dR_g, \alpha) \sin \alpha d\alpha \quad (3.61)$$

where $\Xi(q, R_{\text{core}}, H, \alpha)$ is the form factor amplitude of the shell:

$$\Xi(q, R_{\text{core}}, H, \alpha) = \left[\frac{R}{R_{\text{core}} + H} \frac{2J_1(qR_{\text{core}} \sin \alpha)}{qR_{\text{core}} \sin \alpha} \cos(qH/2 \cos \alpha) + \frac{H}{R_{\text{core}} + H} J_0(qR_{\text{core}} \sin \alpha) \frac{\sin(qH/2 \cos \alpha)}{qH/2 \cos \alpha} \right] \quad (3.62)$$

where $J_0(x)$ is the zeroth order Bessel function of the first kind.

$$S_{\text{brush-brush}}(q, R_{\text{core}}, H, d, R_g) = \psi^2(qR_g) \times \int_0^{\pi/2} \Xi^2(q, R_{\text{core}} + dR_g, H + 2dR_g, \alpha) \sin \alpha d\alpha \quad (3.63)$$

As for micelles with spherical core also for those with a cylindrical core several parameterizations have been implemented `CYL+Chains(RW)`, `CYL+Chains(RW)_Rc` and `CYL+Chains(RW)_Nagg`. The parameters they all have in common are:

- V_{brush} : molecular volume the diblock copolymer part forming the corona
- η_{core} : scattering length density of the diblock copolymer part forming the core
- η_{brush} : scattering length density of the diblock copolymer part forming the corona
- η_{solv} : scattering length density of the solvent
- $x_{\text{solv,core}}$: volume fraction of solvent in the micellar core
- R_g : radius of gyration of the block unit in the corona
- d : non-penetration of the chains into the core is mimicked by $d \sim 1$ for $R_{\text{core}} \gg R_g$
- H : height of the cylindrical core of the micelle

For the model `CYL+Chains(RW)` the other parameters are

- R_{core} : radius of the micellar core ($R_{\text{core}}, R_{\text{core}}, \epsilon R_{\text{core}}$)

n_{agg} : grafting density (number of copolymer molecules N_{agg} per surface area S , $n_{\text{agg}} = N_{\text{agg}}/S$)

In contrast to the form factor CYL+Chains(RW)_Rc and CYL+Chains(RW)_Nagg this one does not necessarily consist of copolymers. The excess scattering lengths and aggregation number needed in eq. 3.29 are then given by

$$N_{\text{agg}} = n_{\text{agg}} S \quad (3.64)$$

where the surface of the core is given by

$$S = 2\pi R_{\text{core}} H \quad (3.65)$$

Together with the core volume $V = \pi R_{\text{core}}^2 H$ one can calculate the excess scattering lengths by

$$\beta_{\text{core}} = \frac{V(1 - x_{\text{solv,core}})}{N_{\text{agg}}} (\eta_{\text{core}} - \eta_{\text{solv}}) \quad (3.66)$$

$$\beta_{\text{brush}} = V_{\text{brush}} (\eta_{\text{brush}} - \eta_{\text{solv}}) \quad (3.67)$$

Input Parameters for model CYL+Chains(RW):

R_core: core radius

n_agg: specific aggregation number (number of chains per surface area)

V_brush: molecular volume of a block unit in the micellar corona

eta_core: scattering length density of spherical core

eta_brush: scattering length density of the block unit in the corona

eta_solv: scattering length density of solvent

x_solv_core: amount of solvent in core

Rg: gyration radius of polymer chains in the corona

d: This value should be around 1. Non-penetration of the chains into the core is mimicked by $d \sim 1$ for $R_{\text{core}} \gg R_g$

H: height of the cylindrical core of the micelle

For the model CYL+Chains(RW)_Rc the other parameters are

R_core: core radius

V_core: molecular volume of single block unit in the micellar core

The excess scattering lengths and aggregation number in eq. 3.29 are then given by

$$\beta_{\text{core}} = V_{\text{core}} (\eta_{\text{core}} - \eta_{\text{solv}}) \quad (3.68)$$

$$\beta_{\text{brush}} = V_{\text{brush}} (\eta_{\text{brush}} - \eta_{\text{solv}}) \quad (3.69)$$

$$N_{\text{agg}} = (1 - x_{\text{solv,core}}) \pi R_{\text{core}}^2 H / V_{\text{core}} \quad (3.70)$$

Input Parameters for model CYL+Chains(RW)_Rc:

R_core: core radius

V_core: molecular volume of single block unit in the micellar core

V_brush: molecular volume of single block unit in the micellar corona

eta_core: scattering length density of spherical core

eta_brush: scattering length density of the block unit in the corona

eta_solv: scattering length density of solvent

xsolv_core: amount of solvent in core

Rg: gyration radius of polymer chains in the corona

d: This value should be around 1. Non-penetration of the chains into the core is mimicked by $d \sim 1$ for $R_{\text{core}} \gg R_g$

H: height of the cylindrical core of the micelle

For the model CYL+Chains(RW)_Nagg the other parameters are

Nagg: aggregation number

Vcore: molecular volume of single block unit in the micellar core

The excess scattering lengths and the core radius R_{core} are given by

$$\beta_{\text{core}} = V_{\text{core}}(\eta_{\text{core}} - \eta_{\text{solv}}) \quad (3.71)$$

$$\beta_{\text{brush}} = V_{\text{brush}}(\eta_{\text{brush}} - \eta_{\text{solv}}) \quad (3.72)$$

$$R_{\text{core}} = \sqrt{\frac{N_{\text{agg}} V_{\text{core}}}{1 - x_{\text{solv,core}}} \frac{1}{\pi H}} \quad (3.73)$$

Input Parameters for model CYL+Chains(RW)_Nagg:

N_agg: aggregation number

V_core: molecular volume of single block unit in the micellar core

V_brush: molecular volume of single block unit in the micellar corona

eta_core: scattering length density of spherical core

eta_brush: scattering length density of the block unit in the corona

eta_solv: scattering length density of solvent

xsolv_core: amount of solvent in core

Rg: gyration radius of polymer chains in the corona

d: This value should be around 1. Non-penetration of the chains into the core is mimicked by $d \sim 1$ for $R_{\text{core}} \gg R_g$

H: height of the cylindrical core of the micelle

3.2.4.1.4. wormlike micelles with circular cross-section:

The form factors for a worm-like micelles are approximated by the form factor of the Kholodenko-worm according to section 3.2.3 where the scattering length density profile across the worm segments are described by those of a rod-like micelle ???. The corresponding function in eq. 3.29 are given by

$$P_{\text{core}}(q, R_{\text{core}}, l, L) = P_{\text{worm}}(q, l, L)P_{\text{cs}}(q, R_{\text{core}}, d, R_g) \quad (3.74)$$

the contribution of the worm-like conformation of the micelle $P_{\text{worm}}(q, l, L)$ is described by the formula of Kholodenko for worm-like structures given in eq. 3.23. The contribution of the cross-section P_{cs} is the same as for rod-like micelles and given by

$$P_{\text{cs}}(q, R_{\text{core}}, d, R_g) = \left[\frac{2J_1(qR_{\text{core}})}{qR_{\text{core}}} \right]^2 \quad (3.75)$$

$$\text{Si}(x) = \int_0^x t^{-1} \sin t dt \quad (3.76)$$

$$P_{\text{brush}}(q, R_g) = 2 \frac{\exp(-x) - 1 + x}{x^2} \text{ with } x = R_g^2 q^2 \quad (3.77)$$

$$S_{\text{brush-core}}(q, R_{\text{core}}, l, L, R_g, d) = \psi(qR_g) \times \frac{2J_1(qR_{\text{core}})}{qR_{\text{core}}} J_0[q(r_{\text{core}} + dR_g)] P_{\text{worm}}(q, l, L) \quad (3.78)$$

$$S_{\text{brush-brush}}(q, R_{\text{core}}, l, L, d, R_g) = \psi^2(qR_g) J_0^2[q(r_{\text{core}} + dR_g)] P_{\text{worm}}(q, l, L) \quad (3.79)$$

As for micelles with spherical core also for those worm-like micelles several parameterizations have been implemented **WORM+Chains(RW)**, **WORM+Chains(RW)_Rc** and **WORM+Chains(RW)_nagg**. The parameters they all have in common are:

V_{brush} : molecular volume the diblock copolymer part forming the corona

η_{core} : scattering length density of the diblock copolymer part forming the core

η_{brush} : scattering length density of the diblock copolymer part forming the corona

η_{solv} : scattering length density of the solvent

$x_{\text{solv,core}}$: volume fraction of solvent in the micellar core

R_g : radius of gyration of the block unit in the corona

l : contour length of the worm-like of the micelle

L : contour length of the worm-like of the micelle

For the model **WORM+Chains(RW)** the other parameters are

R_{core} : radius of the micellar core

n_{agg} : grafting density (number of copolymer molecules N_{agg} per surface area S , $n_{\text{agg}} = N_{\text{agg}}/S$)

In contrast to the form factor `WORM+Chains(RW)_Rc` and `WORM+Chains(RW)_nagg` this one does not necessarily consist of copolymers. The excess scattering lengths and aggregation number needed in eq. 3.29 are then given by

$$N_{\text{agg}} = n_{\text{agg}} S \quad (3.80)$$

where the surface of the core is given by

$$S = 2\pi R_{\text{core}} L \quad (3.81)$$

Together with the core volume $V = \pi R_{\text{core}}^2 L$ one can calculate the excess scattering lengths by

$$\beta_{\text{core}} = \frac{V(1 - x_{\text{solv,core}})}{N_{\text{agg}}} (\eta_{\text{core}} - \eta_{\text{solv}}) \quad (3.82)$$

$$\beta_{\text{brush}} = V_{\text{brush}} (\eta_{\text{brush}} - \eta_{\text{solv}}) \quad (3.83)$$

Input Parameters for model `WORM+Chains(RW)`:

R_core: core radius

n_agg: specific aggregation number (number of chains per surface area)

V_brush: molecular volume of a block unit in the micellar corona

eta_core: scattering length density of spherical core

eta_brush: scattering length density of the block unit in the corona

eta_solv: scattering length density of solvent

xsolv_core: amount of solvent in core

Rg: gyration radius of polymer chains in the corona

l: contour length of the worm-like of the micelle

L: contour length of the worm-like of the micelle

For the model `WORM+Chains(RW)_Rc` the other parameters are

R_core: core radius

V_core: molecular volume of single block unit in the micellar core

The excess scattering lengths and aggregation number in eq. 3.29 are then given by

$$\beta_{\text{core}} = V_{\text{core}} (\eta_{\text{core}} - \eta_{\text{solv}}) \quad (3.84)$$

$$\beta_{\text{brush}} = V_{\text{brush}} (\eta_{\text{brush}} - \eta_{\text{solv}}) \quad (3.85)$$

$$N_{\text{agg}} = (1 - x_{\text{solv,core}}) \pi R_{\text{core}}^2 L / V_{\text{core}} \quad (3.86)$$

Input Parameters for model `CYL+Chains(RW)_Rc`:

R_core: core radius

V_core: molecular volume of single block unit in the micellar core

V_brush: molecular volume of single block unit in the micellar corona

eta_core: scattering length density of spherical core

eta_brush: scattering length density of the block unit in the corona

eta_solv: scattering length density of solvent

xsolv_core: amount of solvent in core

Rg: gyration radius of polymer chains in the corona
l: contour length of the worm-like of the micelle
L: contour length of the worm-like of the micelle

For the model **WORM+Chains(RW)_Nagg** the other parameters are

N_{agg}: aggregation number

V_{core}: molecular volume of single block unit in the micellar core

The excess scattering lengths and the core radius R_{core} are given by

$$\beta_{\text{core}} = V_{\text{core}}(\eta_{\text{core}} - \eta_{\text{solv}}) \quad (3.87)$$

$$\beta_{\text{brush}} = V_{\text{brush}}(\eta_{\text{brush}} - \eta_{\text{solv}}) \quad (3.88)$$

$$R_{\text{core}} = \sqrt{\frac{N_{\text{agg}}V_{\text{core}}}{1 - x_{\text{solv,core}}} \frac{1}{\pi L}} \quad (3.89)$$

Input Parameters for model **CYL+Chains(RW)_Nagg**:

N_agg: aggregation number

V_core: molecular volume of single block unit in the micellar core

V_brush: molecular volume of single block unit in the micellar corona

eta_core: scattering length density of spherical core

eta_brush: scattering length density of the block unit in the corona

eta_solv: scattering length density of solvent

xsolv_core: amount of solvent in core

Rg: gyration radius of polymer chains in the corona

l: contour length of the worm-like of the micelle

L: contour length of the worm-like of the micelle

3.2.4.1.5. micelles with rod-like core:

The form factors for micelles with a rod-like core are approximations of the form factors of micelles with a cylindrical core where $H \gg R_{\text{core}} + dR_g$. The corresponding function in eq. 3.29 are given by

$$P_{\text{core}}(q, R_{\text{core}}, H) = P_H(q, H)P_{\text{cs}}(q, R_{\text{core}}, d, R_g) \quad (3.90)$$

with

$$P_H(q, H) = 2\text{Si}(qH)/(qH) - 4\sin^2(qH/2)/(q^2H^2) \quad (3.91)$$

$$P_{\text{cs}}(q, R_{\text{core}}, d, R_g) = \left[\frac{2J_1(qR_{\text{core}})}{qR_{\text{core}}} \right]^2 \quad (3.92)$$

$$\text{Si}(x) = \int_0^x t^{-1} \sin t dt \quad (3.93)$$

$$P_{\text{brush}}(q, R_g) = 2 \frac{\exp(-x) - 1 + x}{x^2} \text{ with } x = R_g^2 q^2 \quad (3.94)$$

$$S_{\text{brush-core}}(q, R_{\text{core}}, H, Rg, d) = \psi(qR_g) \times \frac{2J_1(qR_{\text{core}})}{qR_{\text{core}}} J_0[q(r_{\text{core}} + dR_g)] P_H(q, H) \quad (3.95)$$

$$S_{\text{brush-brush}}(q, R_{\text{core}}, H, d, R_g) = \psi^2(qR_g) J_0^2[q(r_{\text{core}} + dR_g)] P_H(q, H) \quad (3.96)$$

As otherwise the definitions of the geometry for rod-like micelles are mainly the same than for cylindrical micelles only the list of input parameters are given here. There is only one difference in the model `ROD+Chains(RW)_Nagg` compared to the model `CYL+Chains(RW)_Nagg` and that is that for rod-like structures always the grafting density of polymer chains on the surface of the core is used, i.e. $n_{\text{agg}} = N_{\text{agg}}/S$ instead of N_{agg} . For the model `ROD+Chains(RW)_nagg` this means that the core radius has to be calculated by $R_{\text{core}} = 2n_{\text{agg}}V_{\text{core}}/(1 - x_{\text{solv,core}})$

Input Parameters for model `ROD+Chains(RW)`:

R_core: core radius

n_agg: specific aggregation number (number of chains per surface area)

V_brush: molecular volume of a block unit in the micellar corona

eta_core: scattering length density of spherical core

eta_brush: scattering length density of the block unit in the corona

eta_solv: scattering length density of solvent

xsolv_core: amount of solvent in core

Rg: gyration radius of polymer chains in the corona

d: This value should be around 1. Non-penetration of the chains into the core is mimicked by $d \sim 1$ for $R_{\text{core}} \gg R_g$

H: height of the rod-like core of the micelle

Input Parameters for model ROD+Chains(RW)_Rc:

R_core: core radius

V_core: molecular volume of single block unit in the micellar core

V_brush: molecular volume of single block unit in the micellar corona

eta_core: scattering length density of spherical core

eta_brush: scattering length density of the block unit in the corona

eta_solv: scattering length density of solvent

xsolv_core: amount of solvent in core

Rg: gyration radius of polymer chains in the corona

d: This value should be around 1. Non-penetration of the chains into the core is mim-

icked by $d \sim 1$ for $R_{\text{core}} \gg R_g$

H: height of the rod-like core of the micelle

Input Parameters for model ROD+Chains(RW)_nagg:

n_agg: specific aggregation number (number of chains per surface area)

V_core: molecular volume of single block unit in the micellar core

V_brush: molecular volume of single block unit in the micellar corona

eta_core: scattering length density of spherical core

eta_brush: scattering length density of the block unit in the corona

eta_solv: scattering length density of solvent

xsolv_core: amount of solvent in core

Rg: gyration radius of polymer chains in the corona

d: This value should be around 1. Non-penetration of the chains into the core is mim-

icked by $d \sim 1$ for $R_{\text{core}} \gg R_g$

H: height of the rod-like core of the micelle

3.2.4.2. *Micelles with a homogeneous core and a corona with decaying density profile of the form $\phi(r) \propto r^{-\alpha}$.*

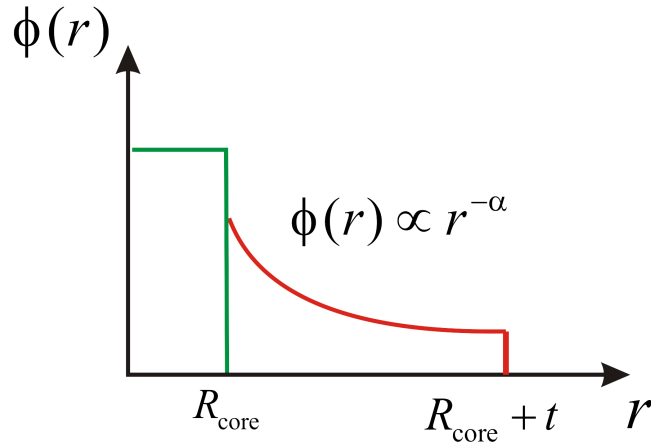


FIGURE 3.24. radial profile.

The structure of block copolymer micelles may be described in terms of the model of starlike polymer as proposed by Daoud and Cotton [96]. Starlike polymers consist of a homogeneous, dense polymer core surrounded by a polymer layer. As a consequence of the spherical or cylindrical geometry, the density profile $\phi(r)$ in the polymer layer decreases according to Wijmans & Zhulina [528] as

$$\phi(r) \begin{cases} \phi_{\text{core}} & \text{for } r < R_{\text{core}} \\ \phi_{\text{brush}} \left(\frac{r}{R_{\text{core}}} \right)^{-\alpha} & \text{for } R_{\text{core}} \leq r \leq R_{\text{core}} + t \\ 0 & \text{for } r > R_{\text{core}} + t \end{cases} \quad (3.97)$$

with $\alpha = (D - 1)(3\nu - 1)/(2\nu)$. D is determined by the dimension of the curvature of the grafted surface (spherical $D = 3$, cylindrical $D = 2$, planar $D = 1$). ν is the Flory exponent, which has characteristic values as given in Table 1. The corresponding density profile is schematically shown in Figure 3.24. Micelles consist of a well-defined micellar core with a radius R_{core} and a micellar shell or corona extending to the outer micellar radius $R_m = R_{\text{core}} + t$, where t is the thickness of the corona.

TABLE 1. Flory exponent ν and exponent α of the radial density profile for different thermodynamic states of the polymer chains

ν	α_{sphere}	α_{cylinder}	α_{planar}	remarks
$D = 3$	$D = 2$	$D = 1$		
1/3	0	0	0	collapsed polymer
1/2	1	1/2	0	polymer in Θ -solvent, semi-dilute solution
3/5	4/3	2/3	0	polymer in good solvent
1	2	1	0	polymer in stretched conformation, e.g. polyelectrolyte

For a given radial profile according to eq. 3.97 the form factor of spherical micelle can be calculated by

$$F_{\text{SPHERE}} = \int_0^\infty 2\pi r^2 \phi(r) \frac{\sin(qr)}{qr} dr \quad (3.98)$$

In case of a rod-like micelle the form factor can be separated in two terms $I(q) = P_H(q)P_{\text{cs}}(q)$ as already shown in eq. 3.90. The cross-term contribution to the scattering intensity is given by

$$\begin{aligned} P_{\text{cs}}(q) &= F_{\text{cs}}^2(q) \\ F_{\text{cs}}(q) &= \int_0^\infty 2\pi r \phi(r) J_0(q) dr \end{aligned} \quad (3.99)$$

However, as it is more convenient here to formulate the scattering intensity in terms of excess scattering length of the block units in the core β_{core} and the corona β_{brush} like in eq. 3.29 the form factor is split into two parts, the form factor of the homogeneous core $F_{\text{core}}(q)$ and the form factor of the corona $F_{\text{brush}}(q)$. The overall scattering intensity $I(q)$ is than given by

$$\begin{aligned} I(q) &= N_{\text{agg}}^2 \beta_{\text{core}}^2 F_{\text{core}}^2(q) + 2N_{\text{agg}}^2 \beta_{\text{core}} \beta_{\text{corona}} F_{\text{core}}(q) F_{\text{corona}}(q) \\ &\quad + N_{\text{agg}}(N_{\text{agg}} - 1) \beta_{\text{corona}}^2 F_{\text{corona}}^2(q) + N_{\text{agg}} P_{\text{brush}}(q) \end{aligned} \quad (3.100)$$

The excess scattering length of a block in the corona and in the core, respectively, $\beta_{\text{brush}} = V_{\text{brush}}(\eta_{\text{brush}} - \eta_{\text{solv}})$ and $\beta_{\text{core}} = V_{\text{core}}(\eta_{\text{core}} - \eta_{\text{solv}})$ are defined in the same way than in eq. 3.29. V_{brush} and V_{core} are the total volume of a block in the corona and in the core. η_{brush} and η_{core} are the corresponding scattering length densities and η_{solv} is the scattering length density of the surrounding solvent. $F_{\text{core}}(q)$ is the form factor of the core and normalized to 1 for $q = 0$. Also the form factor of the corona $F_{\text{corona}}(q)$ and the form factor of the local fluctuations in the corona originating from the individual chains $P_{\text{brush}}(q)$ are normalized to 1 for $q = 0$. Similar to section 3.2.4.1 models for spherical and rod-like shapes have been implemented which are described in the following paragraphs.

3.2.4.2.1. spherical core:

$$F_{\text{core}}(q, R) = 3 \frac{\sin(qR) - qR \cos(qR)}{(qR)^3} \quad (3.101)$$

$$F_{\text{brush}}(q, R, t) = \frac{1}{C_{\text{norm}}} \int_{R_{\text{core}}}^{R_{\text{core}}+t} 2\pi r^2 r^{-\alpha} \frac{\sin(qr)}{qr} dr \quad (3.102)$$

with

$$C_{\text{norm}} = \begin{cases} \frac{4}{3-\alpha} \pi \left((R_{\text{core}} + t)^{3-\alpha} - R_{\text{core}}^{3-\alpha} \right) & \text{for } \alpha \neq 2 \\ 4\pi \ln \left(\frac{R_{\text{core}}+t}{R_{\text{core}}} \right) & \text{for } \alpha = 2 \end{cases}$$

For the scattering contribution of the individual chains in the corona P_{brush} the scattering function for worm-like chains with excluded volume and negligible cross-section, contour length L and Kuhn-length b according to section 3.2.2 has been implemented.

For micelles with a spherical core a few different parameterizations have been implemented **SPHERE+R[^]-a**, **SPHERE+R[^]-a_Rc** and **SPHERE+R[^]-a_Nagg**.

The parameters they all have in common are:

V_{brush} : molecular volume the diblock copolymer part forming the corona

η_{core} : scattering length density of the diblock copolymer part forming the core

η_{brush} : scattering length density of the diblock copolymer part forming the corona

η_{solv} : scattering length density of the solvent

α : exponent of the radial scattering length density profile ($r^{-\alpha}$)

t : corona thickness

L : contour length of the chain in the corona

b : Kuhn-length of the chain in the corona

For the model **SPHERE+R[^]-a** the other parameters are

R_{core} : radius of the micellar core

n_{agg} : grafting density (number of copolymer molecules N_{agg} per surface area S , $n_{\text{agg}} = N_{\text{agg}}/S$)

In contrast to the form factor **SPHERE+R[^]-a_Rc** and **SPHERE+R[^]-a_Nagg** this one does not necessarily consist of copolymers. The excess scattering lengths and aggregation number are given by

$$N_{\text{agg}} = n_{\text{agg}} S \quad (3.103)$$

where the surface of the core is given by $S = 4\pi R_{\text{core}}^2$. Together with the core volume $V = \frac{4}{3}\pi R_{\text{core}}^3$ one gets for the excess scattering lengths

$$\beta_{\text{core}} = \frac{V(1 - x_{\text{solv,core}})}{N_{\text{agg}}}(\eta_{\text{core}} - \eta_{\text{solv}}) \quad (3.104)$$

$$\beta_{\text{brush}} = V_{\text{brush}}(\eta_{\text{brush}} - \eta_{\text{solv}}) \quad (3.105)$$

Input Parameters for model SPHERE+R[^]-a:

R_core: core radius

n_agg: specific aggregation number (number of chains per surface area)

V_brush: molecular volume of a block unit in the micellar corona

eta_core: scattering length density of spherical core

eta_brush: scattering length density of the block unit in the corona

eta_solv: scattering length density of solvent

alpha: exponent of the radial scattering length density profile ($r^{-\alpha}$)

t: corona thickness

L: contour length of the chain in the corona

b: Kuhn-length of the chain in the corona

For the model SPHERE+R[^]-a_Rc the other parameters are

R_{core}: core radius

V_{core}: molecular volume of single block unit in the micellar core

The excess scattering lengths and aggregation number for eq. 3.29 are given by

$$\beta_{\text{core}} = V_{\text{core}}(\eta_{\text{core}} - \eta_{\text{solv}}) \quad (3.106)$$

$$\beta_{\text{brush}} = V_{\text{brush}}(\eta_{\text{brush}} - \eta_{\text{solv}}) \quad (3.107)$$

$$N_{\text{agg}} = (1 - x_{\text{solv},\text{core}}) \frac{4}{3} \pi R_{\text{core}}^3 / V_{\text{core}} \quad (3.108)$$

Input Parameters for model SPHERE+R[^]-a_Rc:

R_core: core radius

V_core: molecular volume of single block unit in the micellar core

V_brush: molecular volume of single block unit in the micellar corona

eta_core: scattering length density of spherical core

eta_brush: scattering length density of the block unit in the corona

eta_solv: scattering length density of solvent

alpha: exponent of the radial scattering length density profile ($r^{-\alpha}$)

t: corona thickness

L: contour length of the chain in the corona

b: Kuhn-length of the chain in the corona

For the model SPHERE+R[^]-a_Nagg the other parameters are

N_{agg}: aggregation number

V_{core}: molecular volume of single block unit in the micellar core

The excess scattering lengths and the core radius R_{core} needed for eq. 3.29 are given by

$$\beta_{\text{core}} = V_{\text{core}}(\eta_{\text{core}} - \eta_{\text{solv}}) \quad (3.109)$$

$$\beta_{\text{brush}} = V_{\text{brush}}(\eta_{\text{brush}} - \eta_{\text{solv}}) \quad (3.110)$$

$$R_{\text{core}} = \left(\frac{N_{\text{agg}} V_{\text{core}}}{1 - x_{\text{solv},\text{core}}} \frac{3}{4\pi} \right)^{1/3} \quad (3.111)$$

Input Parameters for model SPHERE+R[^]-a_Nagg:

N_agg: aggregation number

V_core: molecular volume of single block unit in the micellar core

V_brush: molecular volume of single block unit in the micellar corona

eta_core: scattering length density of spherical core

eta_brush: scattering length density of the block unit in the corona

eta_solv: scattering length density of solvent

alpha: exponent of the radial scattering length density profile ($r^{-\alpha}$)

t: corona thickness

L: contour length of the chain in the corona

b: Kuhn-length of the chain in the corona

3.2.4.2.2. rodlike core:

In case of a rod-like micelle the form factor can be separated in two terms $I(q) = P_H(q)P_{\text{cs}}(q)$ as already shown in eq. 3.90. The cross-term contribution to the scattering intensity is given by

$$\begin{aligned} P_{\text{cs}}(q) &= F_{\text{cs}}^2(q) \\ F_{\text{cs}}(q) &= \int_0^\infty 2\pi r \phi(r) J_0(qr) dr = F_{\text{cs,core}}(q) + F_{\text{cs,brush}}(q) \end{aligned} \quad (3.112)$$

The contribution of the homogeneous core is given by

$$F_{\text{cs,core}}(q) = \frac{2J_1(qR_c)}{qR_c} \quad (3.113)$$

and for the corona by

$$F_{\text{cs,brush}}(q) = \frac{1}{c_\alpha} \int_{R_c}^{R_c+t} 2\pi r r^{-\alpha} J_0(qr) dr \quad (3.114)$$

$$\begin{aligned} c_\alpha &= \int_{R_c}^{R_c+t} 2\pi r r^{-\alpha} dr \\ &= \begin{cases} 2\pi \ln\left(\frac{R_c+t}{R_c}\right) & \text{for } \alpha = 2 \\ \frac{2}{2-\alpha}\pi((R_c+t)^{2-\alpha} - R_c^{2-\alpha}) & \text{for } \alpha \neq 2 \end{cases} \end{aligned} \quad (3.115)$$

For the scattering contribution of the individual chains in the corona P_{local} normally can be neglected for rod-like micelles in contrast to spherical structures as for structures with a lower dimension than spheres, this contribution becomes more and more negligible. To account for the scattering of the individual chains at least in first approximation and without introducing new parameters a form factor similar to the one of star polymers has been implemented.

$$\begin{aligned} P_{\text{local}}(q) &= \frac{\Gamma(\mu)}{qt} \frac{\sin(\mu \arctan(qt))}{(1+q^2t^2)^{\mu/2}} \\ \mu &= \frac{1}{\nu} - 1, \quad \alpha = \frac{3\nu - 1}{2\nu} \quad \Leftrightarrow \quad \mu = 2(1 - \alpha) \end{aligned} \quad (3.116)$$

The form factor to describe the scattering of the individual chains is identical to the blob scattering contribution in star-like polymers according to Dozier (9.4.2.6). The exponential damping length ξ in the definition of the star polymer has been set to the shell thickness t . In the original paper of Pedersen the P_{local} was described by the scattering of a semi-flexible chain with excluded volume according to section 3.2.2, which however would require to define two more parameters.

For micelles with a rod-like core a few different parameterizations have been implemented `ROD+R^-a`, `ROD+R^-a_Rc` and `ROD+R^-a_Nagg`.

The parameters they all have in common are:

V_{brush} : molecular volume the diblock copolymer part forming the corona

η_{core} : scattering length density of the diblock copolymer part forming the core
 η_{brush} : scattering length density of the diblock copolymer part forming the corona
 η_{solv} : scattering length density of the solvent
 $x_{\text{solv,core}}$: amount of solvent in the core
 α : exponent of the radial scattering length density profile ($r^{-\alpha}$)
 t : corona thickness
 H : height of the cylinder

For the model ROD+R^-a the other parameters are

R_{core} : radius of the micellar core

n_{agg} : grafting density (number of copolymer molecules N_{agg} per surface area S , $n_{\text{agg}} = N_{\text{agg}}/S$)

In contrast to the form factor ROD+R^-a_Rc and ROD+R^-a_Nagg this one does not necessarily consist of copolymers. The excess scattering lengths and aggregation number are given by

$$N_{\text{agg}} = n_{\text{agg}} S \quad (3.117)$$

where the surface of the core is given by $S = 2\pi R_{\text{core}} H$. Together with the core volume $V = \pi R_{\text{core}}^2 H$ one gets for the excess scattering lengths

$$\beta_{\text{core}} = \frac{V_{\text{core}}(1 - x_{\text{solv,core}})}{N_{\text{agg}}} (\eta_{\text{core}} - \eta_{\text{solv}}) \quad (3.118)$$

$$\beta_{\text{brush}} = V_{\text{brush}} (\eta_{\text{brush}} - \eta_{\text{solv}}) \quad (3.119)$$

Input Parameters for model ROD+R^-a:

R_{core} : core radius

n_{agg} : specific aggregation number (number of chains per surface area)

V_{brush} : molecular volume of a block unit in the micellar corona

η_{core} : scattering length density of spherical core

η_{brush} : scattering length density of the block unit in the corona

η_{solv} : scattering length density of solvent

$x_{\text{solv,core}}$: amount of solvent in the core

α : exponent of the radial scattering length density profile ($r^{-\alpha}$)

t : corona thickness

H : rod height

For the model ROD+R^-a_Rc the other parameters are

R_{core} : core radius

V_{core} : molecular volume of single block unit in the micellar core

The excess scattering lengths and aggregation number for eq. 3.29 are given by

$$\beta_{\text{core}} = V_{\text{core}} (\eta_{\text{core}} - \eta_{\text{solv}}) \quad (3.120)$$

$$\beta_{\text{brush}} = V_{\text{brush}} (\eta_{\text{brush}} - \eta_{\text{solv}}) \quad (3.121)$$

$$N_{\text{agg}} = 2\pi R_{\text{core}}^2 H \frac{1 - x_{\text{solv,core}}}{V_{\text{core}}} \quad (3.122)$$

Input Parameters for model ROD+R^{-a}_Rc:**R_core:** core radius**V_core:** molecular volume of single block unit in the micellar core**V_brush:** molecular volume of single block unit in the micellar corona**eta_core:** scattering length density of spherical core**eta_brush:** scattering length density of the block unit in the corona**eta_solv:** scattering length density of solvent**xsolv_core:** amount of solvent in the core**alpha:** exponent of the radial scattering length density profile ($r^{-\alpha}$)**t:** corona thickness**H:** rod heightFor the model ROD+R^{-a}_Nagg the other parameters are**n_{agg}:** specific aggregation number, aggregation number per surface area**V_{core}:** molecular volume of single block unit in the micellar coreThe excess scattering lengths and the core radius R_{core} needed for eq. 3.29 are given by

$$\beta_{\text{core}} = V_{\text{core}}(\eta_{\text{core}} - \eta_{\text{solv}}) \quad (3.123)$$

$$\beta_{\text{brush}} = V_{\text{brush}}(\eta_{\text{brush}} - \eta_{\text{solv}}) \quad (3.124)$$

$$R_{\text{core}} = \frac{2n_{\text{agg}} V_{\text{core}}}{1 - x_{\text{solv,core}}} \quad (3.125)$$

Input Parameters for model ROD+R^{-a}_nagg:**n_{agg}:** specific aggregation number (number of chains per surface area)**V_{core}:** molecular volume of single block unit in the micellar core**V_{brush}:** molecular volume of single block unit in the micellar corona**eta_{core}:** scattering length density of spherical core**eta_{brush}:** scattering length density of the block unit in the corona**eta_{solv}:** scattering length density of solvent**xsolv_{core}:** amount of solvent in the core**alpha:** exponent of the radial scattering length density profile ($r^{-\alpha}$)**t:** corona thickness**H:** rod height

REFERENCES:

[96, 126, 352, 528]

3.2.4.3. Sphere with Gaussian chains attached.

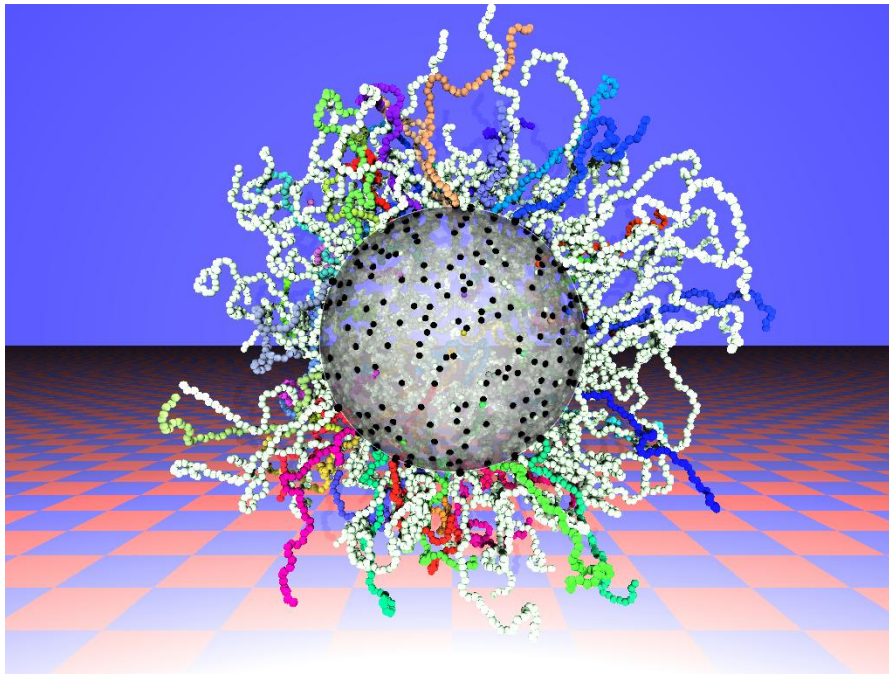


FIGURE 3.25. Block copolymer micelles.

The expressions have been derived by Pedersen and Gerstenberg [378, 375]. For a sphere with radius R and total excess scattering length ρ_s with N_{agg} attached chains

$$P_{\text{mic}}(Q) = N_{\text{agg}}^2 \rho_s^2 P_s(Q, R) + N_{\text{agg}} \rho_c^2 P_c(Q, R_g) + N_{\text{agg}}(N_{\text{agg}} - 1) \rho_c^2 S_{cc}(Q) + 2N_{\text{agg}}^2 \rho_s \rho_c S_{sc}(Q) \quad (3.126)$$

with:

$$P_s = \Phi^2(Q, R) \quad (3.127)$$

$$\Phi(Q, R) = 3 \frac{\sin(QR) - QR \cos(QR)}{(QR)^3} \quad (3.128)$$

$$P_c(Q, R_g) = 2 \frac{\exp(-x) - 1 + x}{x^2} \quad (3.129)$$

$$x = R_g^2 Q^2 \quad (3.130)$$

$$\Psi(Q, R_g) = \frac{1 - \exp(-x)}{x} \quad (3.131)$$

$$S_{cc}(Q) = \Psi^2(Q, R_g) \left(\frac{\sin(Q(R + d R_g))}{Q(R + d R_g)} \right)^2 \quad (3.132)$$

$$S_{sc}(Q) = \Psi(Q, R_g) \Phi(QR_g) \frac{\sin(Q(R + d R_g))}{Q(R + d R_g)} \quad (3.133)$$

where R_g is the root-mean-square radius of gyration of a chain. ρ_c is the total excess scattering length of a single chain. Non-penetrating of the chains into the core region is mimicked by $d \approx 1$ for $R \gg R_g$.

Input Parameters for model `SphereWithGaussChains`:

R: radius of core R

Rg: gyration radius of chain R_g

d: for non-penetration of the chains into the core region $d \approx 1$.

Nagg: aggregation number N_{agg}

rc: excess scattering length of a block in the chains ρ_c

rs: excess scattering length of a block in the core ρ_s

3.2.4.4. Sphere with Gaussian chains attached (block copolymer micelle).

This form factor is the same than for **SphereWithGaussChains**. It has only been slightly re-parametrised. Instead of the core radius R and excess scattering lengths ρ_s and ρ_c the volumes $V_{\text{polym,c}}$ and $V_{\text{polym,sh}}$ of the block units building the core and the shell are required together with the corresponding scattering length densities $\eta_{\text{poly,c}}$, $\eta_{\text{poly,sh}}$ and that one of the solvent η_{solv} . Furthermore $x_{\text{solv,c}}$ is the amount of solvent in the core which takes account for a possible swelling of the core. These parameters allow one to calculate the core radius and excess scattering lengths by

$$R = \left(\frac{N_{\text{agg}} V_{\text{polym,c}}}{1 - x_{\text{solv,c}}} \left| \frac{3}{4\pi} \right|^{1/3} \right) \quad (3.134)$$

$$\rho_s = V_{\text{polym,c}} (\eta_{\text{poly,c}} - \eta_{\text{solv}}) \quad (3.135)$$

$$\rho_c = V_{\text{polym,sh}} (\eta_{\text{poly,sh}} - \eta_{\text{solv}}) \quad (3.136)$$

The volumes $V_{\text{polym,c}}$ and $V_{\text{polym,sh}}$ can be calculated by knowing the molecular weights³ of the block units of the polymer in the core $M_{\text{polym,c}}$ and in the shell $M_{\text{polym,sh}}$ together with their bulk mass densities $\rho_{\text{polym,c}}$ and $\rho_{\text{polym,sh}}$. The volumes are then given by

$$V_{\text{polym,c}} = \frac{M_{\text{polym,c}}}{N_a \rho_{\text{polym,c}}} \quad \text{and} \quad V_{\text{polym,sh}} = \frac{M_{\text{polym,sh}}}{N_a \rho_{\text{polym,sh}}} \quad (3.137)$$

whereby N_a is Avogadro's constant⁴. The units of the block units has to be supplied in units corresponding to the scattering vector Q , i.e. in nm³ in case Q is given in nm⁻¹ or in Å³ in case Q is given in Å⁻¹.

Input Parameters for model BlockCopolymerMicelle:

Vpolym_c: volume of a single block unit of the chains in the core $V_{\text{polym,c}}$, it should be given in units of nm³ in case Q is given in nm⁻¹ and in units of Å³ in case Q is given in Å⁻¹.

xsolv_c: amount of solvent in the core ($x_{\text{solv,c}} \neq 1$)

Vpolym_sh: volume of a single block unit of the chains in the shell $V_{\text{polym,sh}}$, it should be given in units of nm³ in case Q is given in nm⁻¹ and in units of Å³ in case Q is given in Å⁻¹.

eta_poly_c: scattering length density of the block units in the core η_c

eta_poly_sh: scattering length density of the block units in the chains η_{sh}

eta_solv: scattering length density of the solvent η_{solv}

Nagg: aggregation number N_{agg}

Rg: gyration radius of chain R_g

d: for non-penetration of the chains into the core region $d \approx 1$.

³ $u = 1.66053886 \times 10^{-27}$ kg

⁴ $N_a = 6.0221415 \times 10^{23}$ mol⁻¹

3.2.5. spherical Micelles with a corona of semi-flexible interacting self-avoiding chains.

3.3. Local Planar Objects

The form factor of very anisotropic particles with local planar geometry can be shown to factorize (see, e.g. [393]) into a cross-section form factor $P_{\text{cs}}(Q)$ for the shorter dimensions and a shape factor $P'(Q)$ for the larger dimension:

$$P_{\text{planar}}(Q) = P'(Q)P_{\text{cs}}(Q) \quad (3.138)$$

The factorization in the cross-section factor $P_{\text{cs}}(Q)$, which only depends on parameters describing the inner structure of the layer with short dimensions and the shape factor $P'(Q)$, describing the overall shape in the larger dimension has the big advantage when both the shorter dimension as well as the larger dimensions have a polydispersity. In this case we do not end up with a double integral but rather a product of two integrals when both a short and a large dimension have a polydispersity. This speeds up the numerical computation significantly. Therefore the following form factors already have a polydispersity parameter included.

3.3.1. Shape factors $P'(Q)$.

The shape form factor $P'(Q)$ are normalized for $Q \rightarrow 0$ on the squared surface area S ($\lim_{Q \rightarrow 0} P'(Q) = S^2$) and can be that of an infinitely thin disc, spherical shell, elliptical shell, or cylindrical shell: The shape factors are accessible as a structure factor under [anisotropic obj.| $P'(Q)$:local planar geometry| $P'(Q)$ xxx] and using the monodisperse approximation. Actually these shape factors are foreseen to be used with the cross-section factors available as form factors under [anisotropic obj.| $P_{\text{cs}}(Q)$ for planar obj.| $P_{\text{cs}}(Q)$ xxx]. The shape factors are also available in combination with some cross-section factors as form factors under [planar obj.].

3.3.1.1. Polydisperse infinitesimal thin discs.

$$P'_{\text{disc}}(Q, R) = \frac{2\pi^2 R^4}{(QR)^2} \left(1 - \frac{J_1(2QR)}{QR} \right) \quad (3.139)$$

The polydispersity is included as a LogNormal-distribution from section 7.4 by

$$P'_{\text{ThinDiscs}}(Q, R, \sigma) = \int_0^\infty \text{LogNorm}(R', R, \sigma, 1) P'_{\text{disc}}(Q, R') dR' \quad (3.140)$$

3.3.1.2. Infinitesimal thin spherical shell.

$$P'_{\text{sph. shell}}(Q, R) = \left(4\pi R^2 \frac{\sin QR}{QR} \right)^2 \quad (3.141)$$

$$(3.142)$$

3.3.1.3. *Infinitesimal thin elliptical shell.*

$$P'_{\text{ell. shell}}(Q, R, \epsilon) = S^2 \int_0^{\pi/2} \left(\frac{\sin(QR\sqrt{\sin^2 \alpha + \epsilon^2 \cos^2 \alpha})}{QR\sqrt{\sin^2 \alpha + \epsilon^2 \cos^2 \alpha}} \right)^2 \sin(\alpha) d\alpha \quad (3.143)$$

$$\text{with } S = \begin{cases} 4\pi R^2 & \text{for } \epsilon = 1 \\ 2\pi R^2 \left(1 + \epsilon \frac{\arccos(1/\epsilon)}{\tan(\arccos(1/\epsilon))}\right) & \text{for } \epsilon > 1 \\ 2\pi R^2 \left(1 + \epsilon \frac{\operatorname{arctanh}(\sin(\arccos(\epsilon)))}{\sin(\arccos(\epsilon))}\right) & \text{for } \epsilon < 1 \end{cases} \quad (3.144)$$

3.3.1.4. *Infinitesimal thin cylindrical shell.*

$$P'_{\text{closed cyl. sh.}}(Q, R, H) = \int_0^{\pi/2} \left(2\pi R^2 + 2\pi RH \right)^2 \left(\frac{R}{R+H} \frac{2J_1(QR \sin(\alpha))}{QR \sin(\alpha)} \cos(QH \cos(\alpha)/2) + \frac{H}{R+H} J_0(QR \sin \alpha) \frac{\sin(QH \cos(\alpha)/2)}{QH \cos(\alpha)/2} \right)^2 \sin(\alpha) d\alpha \quad (3.145)$$

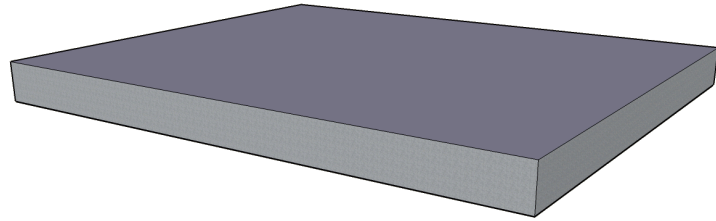
3.3.2. Cross-section form factors $P_{\text{cs}}(Q)$.3.3.2.1. *homogeneousXS*.

FIGURE 3.26. Planar object with homogeneous cross-section.

$$P_{\text{cs}}(Q, \eta, L) = \left(\eta L \frac{\sin(QL/2)}{QL/2} \right)^2 \quad (3.146)$$

3.3.3. TwoInfinitelyThinPlates.

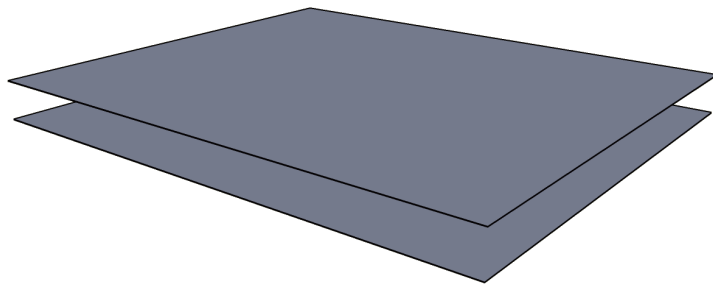


FIGURE 3.27. planar2thin.

$$P_{\text{cs}}(Q, \eta, L) = \eta^2 \cos^2(QL/2) \quad (3.147)$$

3.3.4. LayeredCentroSymmetricXS.

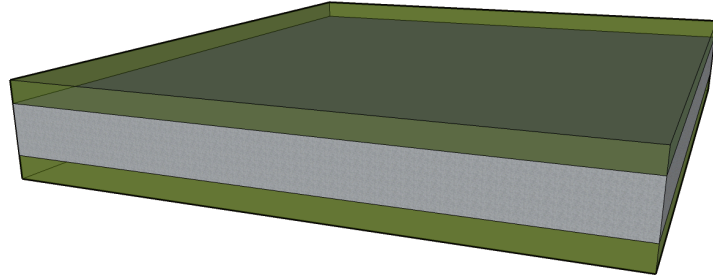


FIGURE 3.28. planar2centrosymHomo.

A layered centro symmetric cross-section structure with outer thickness L_{out} and a core of thickness L_c , where the core and the outer part have the scattering lengths density η_{out} and η_c , respectively, has

$$P_{\text{cs}}(Q, \eta_{\text{out}}, L_{\text{out}}, \eta_c, L_c) = \left(\frac{\eta_{\text{out}} L_{\text{out}} \sin\left(\frac{QL_{\text{out}}}{2}\right)}{QL_{\text{out}}/2} - \frac{(\eta_{\text{out}} - \eta_c)L_c \sin\left(\frac{QL_c}{2}\right)}{QL_c/2} \right)^2 \quad (3.148)$$

3.3.5. BiLayerGauss.

This model has been described in detail in [371].

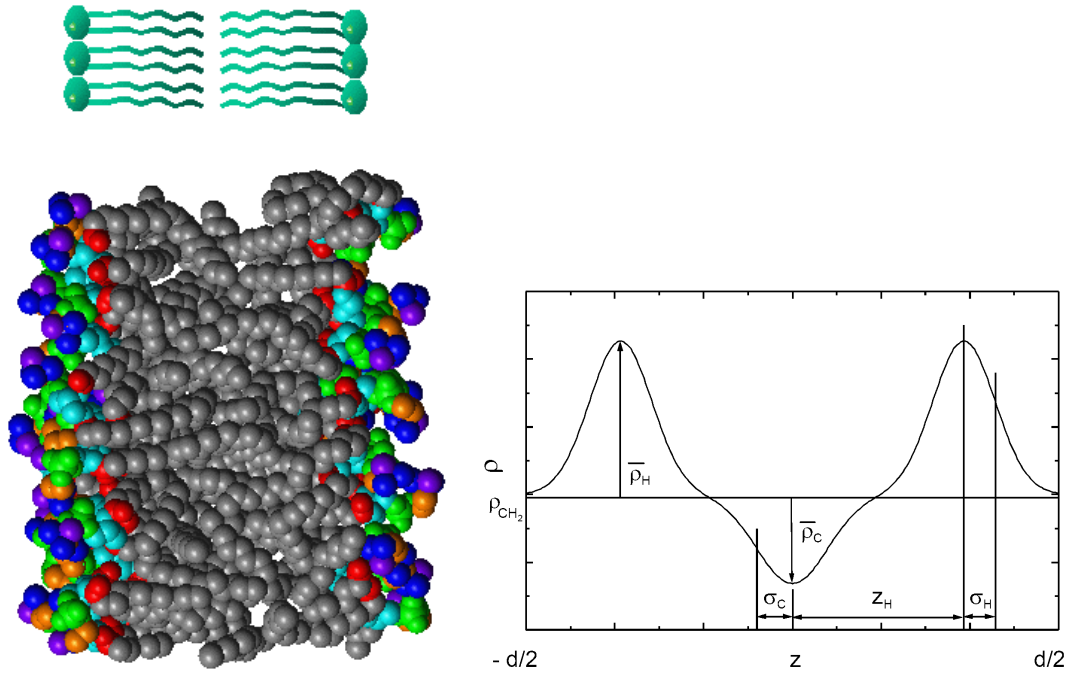


FIGURE 3.29. bilayerprof.

$$u_{\text{out}} = Q\sigma_{\text{out}} \quad (3.149)$$

$$u_{\text{core}} = Q\sigma_{\text{core}} \quad (3.150)$$

$$F_{\text{out}} = \sqrt{2\pi} \sigma_{\text{out}} b_{\text{out}} \exp(-u_{\text{out}}^2/2) \cos(Qt/2) \quad (3.151)$$

$$F_{\text{core}} = \sqrt{2\pi} \sigma_{\text{core}} b_{\text{core}} \exp(-u_{\text{core}}^2/2) \quad (3.152)$$

$$P_{\text{cs}} = (F_{\text{core}} + 2F_{\text{out}})^2 \quad (3.153)$$

3.4. Magnetic Scattering

In the case of magnetic moments in the sample, the neutron undergoes a magnetic interaction in addition to the nuclear interaction. The corresponding interaction potential is given by

$$V(\mathbf{r}) = -\boldsymbol{\mu}_N \cdot \mathbf{B}(\mathbf{r}) \quad \text{with} \quad \boldsymbol{\mu}_N = \gamma \frac{e\hbar}{2m_N c} \boldsymbol{\sigma}$$

where $\boldsymbol{\mu}_N = \gamma \frac{e\hbar}{2m_N c} \boldsymbol{\sigma}$ is the magnetic dipole moment of the neutron, $\boldsymbol{\sigma}$ the Pauli spin operator, $\gamma = -1.913$ the gyromagnetic ratio and $\mathbf{B}(\mathbf{r})$ the magnetic field induced by an atom at the position of the neutron. The latter has two components, one induced by the magnetic dipole moment $\boldsymbol{\mu}_S$ of the electrons, denoted $\mathbf{B}_S(\mathbf{r})$, and one by their orbital moment $\boldsymbol{\mu}_L$, denoted $\mathbf{B}_L(\mathbf{r})$. The (weak) magnetic interaction $V(\mathbf{r}) = -\boldsymbol{\mu}_N \cdot (\mathbf{B}_S(\mathbf{r}) + \mathbf{B}_L(\mathbf{r}))$ can as well be treated in first Born approximation, resulting in the magnetic scattering amplitude, in analogy to the nuclear scattering amplitude, given by the Fourier transform of the magnetic interaction potential $\mathcal{F}[V(\mathbf{r})]$:

$$b_M = -\frac{m_N}{2\pi\hbar^2} \boldsymbol{\mu}_N \cdot \int d^3r e^{i\mathbf{Q}\cdot\mathbf{r}} (\mathbf{B}_S(\mathbf{r}) + \mathbf{B}_L(\mathbf{r})). \quad (3.154)$$

An additional static magnetic field $\mathbf{H}(\mathbf{r})$ at the point of local magnetization $\mathbf{H}(\mathbf{r})$ (stemming from $\mathbf{B}_S(\mathbf{r}) + \mathbf{B}_L(\mathbf{r})$) induces a total local magnetic induction of

$$\mathbf{B}(\mathbf{r}) = \mu_0(\mathbf{H}(\mathbf{r}) + \mathbf{M}(\mathbf{r}))$$

and the Fourier transform of yields

$$\mathbf{B}(\mathbf{Q}) = \mu_0 \frac{\mathbf{Q} \times [\mathbf{M}(\mathbf{Q}) \times \mathbf{Q}]}{Q^2} = \mu_0 \mathbf{M}_\perp(\mathbf{Q}) = \mu_0 \mathbf{M}(\mathbf{Q}) \sin(\angle(\mathbf{Q}, \mathbf{M})) \quad (3.155)$$

where $\mathbf{M}(\mathbf{Q}) = \int d^3r \exp(i\mathbf{Q} \cdot \mathbf{r}) \mathbf{M}(\mathbf{r})$, with $\mathbf{M}(\mathbf{r})$ given in units of A/m. $\mathbf{M}_\perp(\mathbf{Q}) = \mathbf{Q} \times [\mathbf{M}(\mathbf{Q}) \times \mathbf{Q}]/Q^2$ is the magnetization component perpendicular to the scattering vector \mathbf{Q} . The magnetic scattering length then is

$$b_M = D_M \mu_0 \boldsymbol{\sigma} \cdot \mathbf{M}_\perp(\mathbf{Q}) \quad \text{with} \quad D_M = \frac{m_N}{2\pi\hbar^2} \mu_N = 2.3161 \times 10^{14} \frac{1}{\text{Vs}}. \quad (3.156)$$

For the differential scattering cross section one finally obtains

$$\frac{d\sigma_M}{d\Omega}(\mathbf{Q}) = \frac{D_M^2}{N} |\mu_0 \mathbf{M}_\perp(\mathbf{Q})|^2 \quad (3.157)$$

In the presence of a preferred direction, for example induced by an external magnetic field, the magnetic scattering depends on the spin state of the neutrons. Let the z-axis be the preferred direction, and let (+) and (-) denote the neutron spin polarizations parallel and antiparallel to the z-axis, then the scattering is described by four scattering processes: two processes where the incident states (+) and (-) remain unchanged (++) and (--), the so-called 'non-spin-flip' processes, and two processes where the spin is flipped (+- and -+), the 'spin-flip' processes. Keeping in mind that the nuclear scattering does not flip the neutron spin, the four related scattering lengths are

$$b_{\pm\pm} = b_N \mp D_M \mu_0 M_{\perp x} \quad (3.158)$$

$$b_{\pm\mp} = -D_M \mu_0 (M_{\perp z} \pm i M_{\perp y}). \quad (3.159)$$

Hereby b_N is the nuclear scattering length. For an unpolarized neutron beam (which may be taken as composed of 50% (+) and 50% (-) polarization) the square of the modulus of the scattering length is

$$(b_{++}^2 + b_{--}^2 + b_{+-}^2 + b_{-+}^2)/2 = b_N^2 + D_M^2 \mu_0^2 M_{\perp}^2. \quad (3.160)$$

The differential cross section of the unpolarized neutron beam can therefore be described by the sum of the nuclear and the magnetic cross section, without any cross terms.

3.4.1. Magnetic Saturation.

3.4.1.1. *MagneticShellAniso.*

$$K(Q, R, \Delta\eta) = \frac{4}{3}\pi R^3 \Delta\eta 3 \frac{\sin QR - QR \cos QR}{(QR)^3} \quad (3.161)$$

$$K_{\text{sh}}(Q, R, \Delta R, \Delta\eta_{\text{sh}}, \Delta\eta_c) = K(Q, R + \Delta R, \Delta\eta_{\text{sh}}) - K(Q, R, \Delta\eta_c) \quad (3.162)$$

$$K_{\text{NUC}}(Q) = K_{\text{sh}}(Q, R, \Delta R, \eta_{\text{sh NUC}} - \eta_{\text{m NUC}}, \eta_{\text{c NUC}} - \eta_{\text{m NUC}}) \quad (3.163)$$

$$K_{\text{MAG}}(Q) = K_{\text{sh}}(Q, R, \Delta R, \eta_{\text{sh MAG}} - \eta_{\text{m MAG}}, \eta_{\text{c MAG}} - \eta_{\text{m MAG}}) \quad (3.164)$$

$$\begin{aligned} I(Q) &= \frac{1-p}{2} (K_{\text{MAG}}^2(Q) + 2K_{\text{NUC}}(Q)K_{\text{MAG}}(Q)) \\ &\quad + \frac{1+p}{2} (K_{\text{MAG}}^2(Q) - 2K_{\text{NUC}}(Q)K_{\text{MAG}}(Q)) \end{aligned} \quad (3.165)$$

$$= K_{\text{MAG}}^2(Q) - 2pK_{\text{NUC}}(Q)K_{\text{MAG}}(Q) \quad (3.166)$$

p : neutron polarization, $p \in [-1 : 1]$

R : radius of particle core

ΔR : thickness of particle shell

$\eta_{\text{sh NUC}}$: nuclear scattering length density of particle shell

$\eta_{\text{m NUC}}$: nuclear scattering length density of matrix

$\eta_{\text{c NUC}}$: nuclear scattering length density of particle core

$\eta_{\text{sh MAG}}$: magnetic scattering length density of particle shell

$\eta_{\text{m MAG}}$: magnetic scattering length density of matrix

$\eta_{\text{c MAG}}$: magnetic scattering length density of particle core

3.4.1.2. MagneticShellCrossTerm.

$$K(Q, R, \Delta\eta) = \frac{4}{3}\pi R^3 \Delta\eta 3 \frac{\sin QR - QR \cos QR}{(QR)^3} \quad (3.167)$$

$$K_{\text{sh}}(Q, R, \Delta R, \Delta\eta_{\text{sh}}, \Delta\eta_c) = K(Q, R + \Delta R, \Delta\eta_{\text{sh}}) - K(Q, R, \Delta\eta_c) \quad (3.168)$$

$$K_{\text{NUC}}(Q) = K_{\text{sh}}(Q, R, \Delta R, \eta_{\text{sh NUC}} - \eta_{\text{m NUC}}, \eta_{\text{c NUC}} - \eta_{\text{m NUC}}) \quad (3.169)$$

$$K_{\text{MAG}}(Q) = K_{\text{sh}}(Q, R, \Delta R, \eta_{\text{sh MAG}} - \eta_{\text{m MAG}}, \eta_{\text{c MAG}} - \eta_{\text{m MAG}}) \quad (3.170)$$

$$I(Q) = 4p K_{\text{NUC}}(Q) K_{\text{MAG}}(Q) \quad (3.171)$$

p : neutron polarization, $p \in [-1 : 1]$

R : radius of particle core

ΔR : thickness of particle shell

$\eta_{\text{sh NUC}}$: nuclear scattering length density of particle shell

$\eta_{\text{m NUC}}$: nuclear scattering length density of matrix

$\eta_{\text{c NUC}}$: nuclear scattering length density of particle core

$\eta_{\text{sh MAG}}$: magnetic scattering length density of particle shell

$\eta_{\text{m MAG}}$: magnetic scattering length density of matrix

$\eta_{\text{c MAG}}$: magnetic scattering length density of particle core

3.4.1.3. MagneticShellPsi.

$$K(Q, R, \Delta\eta) = \frac{4}{3}\pi R^3 \Delta\eta 3 \frac{\sin QR - QR \cos QR}{(QR)^3} \quad (3.172)$$

$$K_{\text{sh}}(Q, R, \Delta R, \Delta\eta_{\text{sh}}, \Delta\eta_c) = K(Q, R + \Delta R, \Delta\eta_{\text{sh}}) - K(Q, R, \Delta\eta_c) \quad (3.173)$$

$$K_{\text{NUC}}(Q) = K_{\text{sh}}(Q, R, \Delta R, \eta_{\text{sh NUC}} - \eta_{\text{m NUC}}, \eta_{\text{c NUC}} - \eta_{\text{m NUC}}) \quad (3.174)$$

$$K_{\text{MAG}}(Q) = K_{\text{sh}}(Q, R, \Delta R, \eta_{\text{sh MAG}} - \eta_{\text{m MAG}}, \eta_{\text{c MAG}} - \eta_{\text{m MAG}}) \quad (3.175)$$

$$I(Q) = K_{\text{NUC}}^2(Q) + (K_{\text{MAG}}^2(Q) - 2pK_{\text{NUC}}(Q)K_{\text{MAG}}(Q)) \sin^2 \Psi \quad (3.176)$$

p : neutron polarization, $p \in [-1 : 1]$

R : radius of particle core

Ψ : angle between \mathbf{Q} and \mathbf{H}

ΔR : thickness of particle shell

$\eta_{\text{sh NUC}}$: nuclear scattering length density of particle shell

$\eta_{\text{m NUC}}$: nuclear scattering length density of matrix

$\eta_{\text{c NUC}}$: nuclear scattering length density of particle core

$\eta_{\text{sh MAG}}$: magnetic scattering length density of particle shell

$\eta_{\text{m MAG}}$: magnetic scattering length density of matrix

$\eta_{\text{c MAG}}$: magnetic scattering length density of particle core

3.4.2. Superparamagnetic Particles (like ferrofluids).

$$\frac{I_{\pm\pm}(\mathbf{Q})}{N} = \left| F_N(\mathbf{Q}) \mp \tilde{F}_M(\mathbf{Q}) [L(\alpha) - \gamma] \sin^2 \epsilon \right|^2 + \left| \tilde{F}_M(\mathbf{Q}) \right|^2 \left(\frac{L(\alpha)}{\alpha} \sin^2 \epsilon - \mathcal{L}(\alpha) \sin^4 \epsilon \right) \quad (3.177)$$

$$\frac{I_{\mp\pm}(\mathbf{Q})}{N} = (\sin^2 \epsilon - \sin^4 \epsilon) [L(\alpha) - \gamma]^2 \left| \tilde{F}_M(\mathbf{Q}) \right|^2 + \left| \tilde{F}_M(\mathbf{Q}) \right|^2 \left((\sin^4 \epsilon - \sin^2 \epsilon) \mathcal{L}(\alpha) + (2 - \sin^2 \epsilon) \frac{L(\alpha)}{\alpha} \right) \quad (3.178)$$

$$\begin{aligned} I_{\text{unp}}(\mathbf{Q}) &= \frac{1}{2} (I_{++}(\mathbf{Q}) + I_{+-}(\mathbf{Q}) + I_{--}(\mathbf{Q}) + I_{-+}(\mathbf{Q})) \\ &= N \left(\left| \tilde{F}_M(\mathbf{Q}) \right|^2 [L(\alpha) - \gamma]^2 \sin^2 \epsilon + |F_N(\mathbf{Q})|^2 \right) \\ &\quad + N \left| \tilde{F}_M(\mathbf{Q}) \right|^2 \left(2 \frac{L(\alpha)}{\alpha} - \mathcal{L}(\alpha) \sin^2 \epsilon \right) \end{aligned} \quad (3.179)$$

Hereby $L(\alpha) = \coth \alpha - \frac{1}{\alpha}$ is the classical Langevin function with $\alpha = \mu_0(H + M_{\text{eff}})M_s^{cr}V_P/kT$.

Furthermore the following functions are defined as:

$$\begin{aligned} \mathcal{L}(\alpha) &= L^2(\alpha) - 1 + 3 \frac{L(\alpha)}{\alpha}, \\ F_N(\mathbf{Q}) &= \Delta \eta V_N f_N(\mathbf{Q}), \\ \tilde{F}_M(\mathbf{Q}) &= D_M M_s^{cr} V_M f_M(\mathbf{Q}) \text{ and} \\ \gamma &= M_s^{am}/M_s^{cr}. \end{aligned}$$

ϵ describes the angle between \mathbf{Q} and the applied magnetic field \mathbf{B} . If the magnetic field lies in the plane of the detector, i.e. perpendicular to the incoming beam direction, ϵ is in practice identical to Ψ so that $\cos \epsilon = \sin \delta \cos \Psi \simeq \cos \Psi$ for $\delta \simeq \pi/2$ (\mathbf{Q} in plane of detector for SANS, only for large scattering angle this will change).

3.4.2.1. *SuperparamagneticFFpsi*.

3.4.2.2. *SuperparamagneticFFAniso*.

3.4.2.3. *SuperparamagneticFFIso*.

3.4.2.4. *SuperparamagneticFFCrossTerm*.

3.5. Other functions

3.5.1. DLS_Sphere_RDG.

This function has been implemented to simulate the relaxation signal $g_2(t) - 1 = g_1^2(t)$ of a DLS (dynamic light scattering) measurement. The Q dependent contribution to the relaxation signal by particles of different radius R is considered by weighting $g_2(t) - 1$ with the form factor of spherical particles in Rayleigh-Debye-Gans approximation:

$$I_{\text{DLS_Sphere_RDG}}(t, \eta, T, Q) = \int_0^\infty N(R) K_{\text{sp}}^2(Q, R) e^{-DQ^2 t} dR \quad (3.180)$$

with

$$D = \frac{k_B T}{6\pi\eta R}$$

$$K_{\text{sp}}(Q, R) = \frac{4}{3}\pi R^3 3 \frac{\sin QR - QR \cos QR}{(QR)^3}$$

R : radius

T : temperature

η : viscosity

Q : scattering vector

3.5.2. Langevin.

This function has been implemented to simulate the magnetisation curve $M(B)$ of superparamagnetic particles following the Langevin statistics with a size distribution $N(R)$: Magnetization curve of superparamagnetic particles with magnetization a M_s at temperature T

$$M(B) = \frac{\int_0^\infty N(R) \frac{4}{3}\pi R^3 M_p(B, R) dR}{\int_0^\infty N(R) \frac{4}{3}\pi R^3 dR} \quad (3.181)$$

$$M_p(B, R) = M_\infty \left(\coth(\alpha) - \frac{1}{\alpha} \right)$$

$$\alpha = \frac{BM_s \frac{4}{3}\pi R^3}{k_B T}$$

3.5.3. SuperParStroboPsi.

In the following the scattering of polarized incident neutrons with polarization analysis (POLARIS) is described. Experimental measured scattering signal are always a mixture of the spin dependent scattering cross-sections $I^{\pm\pm}(\mathbf{Q})$ and $I^{\pm\mp}(\mathbf{Q})$. The relative contribution of these cross-sections to the measured cross-section depend on the polarisation of the polarizer P_{pol} the efficiency of the spin flipper ϵ and the transmission values T_{\pm} of the polarization analyzer, which is assumed to be an opaque He-filter. If the neutron polarization of the polarizer is $P_{pol} \in [-1; 1]$ and the spin flipper is off the incident polarisation on the sample P_{in} is given by

$$P_{in} = P_{pol} = \frac{N_+ - N_-}{N_+ + N_-} = n_+ - n_- \quad (3.182a)$$

with

$$n_+ = \frac{N_+}{N_+ + N_-} \text{ and } n_- = \frac{N_-}{N_+ + N_-} \quad (3.182b)$$

$$\Rightarrow n_+ = \frac{1 + P_{pol}}{2} \text{ and } n_- = \frac{1 - P_{pol}}{2} \quad (3.182c)$$

N_{\pm} are the number of incident neutrons with spin polarizations up (+) and down (-). After switching on the spin flipper, which works with an efficiency of $\epsilon \in [0; 1]$ ($\epsilon = 0$: flipper off, $\epsilon \gtrapprox 1$: flipper on), one gets

$$\begin{aligned} n_+(P_{pol}, \epsilon) &= \epsilon \frac{1 - P_{pol}}{2} + (1 - \epsilon) \frac{1 + P_{pol}}{2} \\ &= \frac{1 - \epsilon P_{pol}}{2} \quad \text{and} \\ n_-(P_{pol}, \epsilon) &= \epsilon \frac{1 + P_{pol}}{2} + (1 - \epsilon) \frac{1 - P_{pol}}{2} \\ &= \frac{1 + \epsilon P_{pol}}{2} \end{aligned}$$

The efficiency of the analyzer to filter spin up (+) or spin down (-) neutrons is given in case of an opaque spin filter by its transmission $T_{\pm}(t) \in [0; 1]$, which can be a function of time, so that the measured scattering cross section $I_m(\mathbf{Q})$ is given by

$$\begin{aligned} I_m(\mathbf{Q}) &= n_+(P_{pol}, \epsilon) T_+(t) I_{++}(\mathbf{Q}) + n_+(P_{pol}, \epsilon) T_-(t) I_{+-}(\mathbf{Q}) \\ &\quad + n_-(P_{pol}, \epsilon) T_-(t) I_{--}(\mathbf{Q}) + n_-(P_{pol}, \epsilon) T_+(t) I_{-+}(\mathbf{Q}) \end{aligned} \quad (3.183)$$

The spin dependent scattering intensities of magnetic particles with an orientation distribution $f(\theta, \phi)$ of its magnetic moment can easily be calculated in terms of order parameters S_l if one assumes that the particle are spherical symmetric or the orientation of the magnetic moment of a particle is not correlated to the particle orientation. Furthermore it will be assumed that an external magnetic field is applied perpendicular to the incident neutron beam and that all orientations ϕ for a given angle θ , which is defined as the angle between the magnetisation vector of the particle and the direction of the external field \mathbf{B} have the same probability, i.e. the orientation distribution only depends on θ so that $f(\theta, \phi) = f(\theta)$. The orientation probability distribution function

can be expanded in terms of a complete set of orthogonal functions. Expanding it in terms of Legendre polynomials $P_l(\cos \theta)$ gives

$$f(\theta) = \sum_l c_l P_l(\cos \theta) = \sum_l \frac{2l+1}{2} S_l P_l(\cos \theta) \quad (3.184)$$

The expansion coefficients can be calculated by

$$c_l = \frac{2l+1}{2} \int_0^\pi f(\theta) P_l(\cos \theta) \sin \theta \, d\theta \quad (3.185)$$

or

$$S_l = \int_0^\pi f(\theta) P_l(\cos \theta) \sin \theta \, d\theta$$

The first three Legendre polynomials are defined by

$$P_0(\cos \theta) = 1 \quad (3.186a)$$

$$P_1(\cos \theta) = \cos \theta \quad (3.186b)$$

$$P_2(\cos \theta) = \frac{1}{2} (3 \cos^2 \theta - 1) \quad (3.186c)$$

For superparamagnetic particle the orientation probability distribution is given by

$$f(\theta) = \frac{\alpha}{4\pi \sinh \alpha} \exp(\alpha \cos \theta) \quad (3.187)$$

with $\alpha = BM_p V_p / (k_B T)$ being the Langevin parameter. For this orientation probability distribution the first order parameters can be calculated as

$$S_0 = 1 \quad (3.188a)$$

$$S_1 = L(\alpha) = \coth \alpha - \frac{1}{\alpha} \quad (3.188b)$$

$$S_2 = 1 - 3 \frac{L(\alpha)}{\alpha} \quad (3.188c)$$

The scattering from a system of many particles is obtained by summing up the scattering amplitudes of all precipitates weighted by the phase shift at each particle position. In the decoupling approach scattering intensity is given by

$$\frac{d\sigma_{\pm\pm}}{d\Omega}(\mathbf{Q}) = N \left\{ \left\langle \left| F_{\pm\pm}(\mathbf{Q}) \right|^2 \right\rangle + \left| \left\langle F_{\pm\pm}(\mathbf{Q}) \right\rangle \right|^2 (S(\mathbf{Q}) - 1) \right\} \quad (3.189)$$

which consists of two terms. The first one depends only on the particle structure and corresponds to the independent scattering of N particles, while the second one is also a function of their statistical distribution and reflects the interparticle interference, which is described by $S(\mathbf{Q})$. The $\langle \rangle$ indicates an average over all possible configurations, sizes and orientations of the magnetic moments of the particles. The spin dependent scattering amplitudes $F_{\pm\pm}(\mathbf{Q})$ can be calculated from the nuclear and magnetic amplitudes

$$F_{\pm\pm}(\mathbf{Q}) = F_N(\mathbf{Q}) \mp F_{M_{\perp x}}(\mathbf{Q}) \quad (3.190)$$

$$F_{\pm\mp}(\mathbf{Q}) = - (F_{M_{\perp y}}(\mathbf{Q}) \pm i F_{M_{\perp z}}(\mathbf{Q})) \quad (3.191)$$

The nuclear scattering amplitude is proportional to the nuclear excess scattering $\beta_N = F_N(Q = 0)$ and the nuclear form factor $f_N(\mathbf{Q})$

$$F_N(\mathbf{Q}) = \beta_N f_N(\mathbf{Q}) \quad (3.192)$$

The magnetic scattering amplitude $\mathbf{F}_{M_\perp}(\mathbf{Q})$ can be described as a vector, with

$$\mathbf{F}_{M_\perp}(\mathbf{Q}) = \hat{\boldsymbol{\mu}}_\perp D_M \mu f_M(\mathbf{Q}) = \hat{\boldsymbol{\mu}}_\perp F_M(\mathbf{Q}) \quad (3.193)$$

where $f_M(Q)$ is the magnetic form factor, $\boldsymbol{\mu} = \mathbf{M}_p V_p$ the magnetic moment of the particle, $D_M = \frac{\gamma e}{2\pi\hbar}$, and $\hat{\boldsymbol{\mu}}_\perp$ the Halpern-Johnson vector defined as

$$\hat{\boldsymbol{\mu}}_\perp = \frac{\mathbf{Q}}{Q} \times \left(\frac{\boldsymbol{\mu}}{\mu} \times \frac{\mathbf{Q}}{Q} \right) \quad (3.194)$$

It is assumed here that the neutron spin polarization is parallel or antiparallel to the axes \mathbf{e}_x which is the direction perpendicular to the incoming neutron beam. If only the Halpern-Johnson vector $\hat{\boldsymbol{\mu}}_\perp$ depends on the orientation distribution $f(\theta)$ of the magnetic moments $\boldsymbol{\mu}$ of the particles but not the form factor $f_M(\mathbf{Q})$, which is valid for spherical symmetric particles or anisotropic shaped particles where the particle shape is not correlated to the direction of the magnetic moment, the averages in 3.189 can be written in terms of the order parameters S_1 and S_2

$$\langle F_{\pm\pm}(\mathbf{Q}) \rangle = F_N(\mathbf{Q}) + F_M(\mathbf{Q}) S_1 \sin^2 \psi \quad (3.195a)$$

$$\langle F_{\pm\mp}(\mathbf{Q}) \rangle = F_M(\mathbf{Q}) S_1 \sin \psi \cos \psi \quad (3.195b)$$

$$\begin{aligned} \langle |F_{\pm\pm}(\mathbf{Q})|^2 \rangle &= |F_N(\mathbf{Q})|^2 + |F_M(\mathbf{Q})|^2 \left[S_2 \sin^4 \psi + \frac{1 - S_2}{3} \sin^2 \psi \right] \\ &\quad \mp [F_M(\mathbf{Q}) F_N^*(\mathbf{Q}) + F_N^*(\mathbf{Q}) F_M(\mathbf{Q})] S_1 \sin^2 \psi \end{aligned} \quad (3.195c)$$

$$\langle |F_{\pm\mp}(\mathbf{Q})|^2 \rangle = |F_M(\mathbf{Q})|^2 \left[2 \frac{1 - S_2}{3} - S_2 \sin^4 \psi + \frac{4S_2 - 1}{3} \sin^2 \psi \right] \quad (3.195d)$$

The spin-flip and spin-nonflip cross-section $\frac{d\sigma_{\pm\pm}}{d\Omega}(\mathbf{Q})$ can be obtained by combining 3.189 and 3.195. The cross-sections without polarization analysis $I_\pm(\mathbf{Q})$ and for unpolarized

neutrons $I_{unp}(\mathbf{Q})$ are given by

$$\begin{aligned} I_{\pm}(\mathbf{Q}) &= I_{\pm\pm}(\mathbf{Q}) + I_{\pm\mp}(\mathbf{Q}) \\ &= \left[|F_N(\mathbf{Q})|^2 + |F_M(\mathbf{Q})|^2 S_1^2 \sin^2 \psi \right. \\ &\quad \left. \mp [F_M(\mathbf{Q})F_N^*(\mathbf{Q}) + F_M^*(\mathbf{Q})F_N(\mathbf{Q})] S_1 \sin^2 \psi \right] S(\mathbf{Q}) \\ &\quad |F_M(\mathbf{Q})|^2 \left(\frac{2}{3} (1 - S_2) + (S_2 - S_1^2) \sin^2 \psi \right) \end{aligned} \quad (3.196a)$$

$$\begin{aligned} I_{unp}(\mathbf{Q}) &= \frac{1}{2} (I_+(\mathbf{Q}) + I_-(\mathbf{Q})) \\ &= \left(|F_N(\mathbf{Q})|^2 + |F_M(\mathbf{Q})|^2 S_1^2 \sin^2 \psi \right) S(\mathbf{Q}) \\ &\quad + |F_M(\mathbf{Q})|^2 \left(\frac{2}{3} (1 - S_2) + (S_2 - S_1^2) \sin^2 \psi \right) \end{aligned} \quad (3.196b)$$

In the case of a Boltzmann orientation distribution $f(\theta) = \exp\left(\frac{\mathbf{B}\mu}{k_B T}\right) = \exp\left(\frac{B\mu \cos \theta}{k_B T}\right)$ the order parameter S_l already have been given in eq. 3.188 and the spin dependent intensities can be written as

$$\begin{aligned} \frac{I_{\pm\pm}(\mathbf{Q})}{N} &= \left| F_M(\mathbf{Q})L(\alpha) \sin^2 \psi \pm F_N(\mathbf{Q}) \right|^2 S(\mathbf{Q}) \\ &\quad + |F_M(\mathbf{Q})|^2 \left(\frac{L(\alpha)}{\alpha} \sin^2 \psi - \left(L^2(\alpha) - 1 + 3 \frac{L(\alpha)}{\alpha} \right) \sin^4 \psi \right) \end{aligned} \quad (3.197a)$$

$$\begin{aligned} \frac{I_{\mp\pm}(\mathbf{Q})}{N} &= (\sin^2 \psi - \sin^4 \psi) L^2(\alpha) |F_M(\mathbf{Q})|^2 S(\mathbf{Q}) \\ &\quad + |F_M(\mathbf{Q})|^2 \left((\sin^4 \psi - \sin^2 \psi) \left(L^2(\alpha) - 1 + 3 \frac{L(\alpha)}{\alpha} \right) + (2 - \sin^2 \psi) \frac{L(\alpha)}{\alpha} \right) \end{aligned} \quad (3.197b)$$

ψ is the angle between \mathbf{Q} and the horizontal axis in the plane of the detector. $L(\alpha) = \coth(\alpha) - \frac{1}{\alpha}$ is the Langevin function. In the case of a static field the superparamagnetic particle are thermodynamic equilibrium and α is given by

$$\alpha = \frac{BM_P V_P}{k_B T}, \quad (3.198)$$

with M_P being the particle magnetization, V_P the particle volume, T the temperature in Kelvin and k_B the Boltzmann constant.

In our experiments we applied an oscillating magnetic field to the sample described by:

$$B(t, \nu; d_{SD}, \lambda, \rho_0) = B_1 - B_0 \cos(\phi(t, \nu); \dots) \quad (3.199a)$$

$$\phi(t, \nu; d_{SD}, \lambda, \rho_0) = 2\pi\nu(t - d_{SD}\lambda/3956) + \rho_0 \quad (3.199b)$$

where t in [s] is the time between neutron detection and the trigger signal from the frequency generator, d_{SD} in [m] is the sample detector distance, λ in [\AA] the neutron

wavelength, and ν in [Hz] the frequency of the oscillating magnetic field. As t is defined here as the time of the neutron detection one has therefore to correct the phase in the argument for the magnetic field with an additional phase term. The term $t_{SD} = d_{SD}\lambda/3956$ takes into account the flight time t_{SD} of the neutrons between the sample and the detector. The term ρ_0 accounts for any other additional constant phase shift between trigger signal and the magnetic field due to phase shifts in the amplifier. If the neutron polarization can follow adiabatically the varying magnetic field needs to be verified experimentally. Therefore we introduce here a parameter $a_{ad} \in [0; 1]$ which takes into account whether ($a_{ad} = 1$) or not ($a_{ad} = 0$) the neutron spin adiabatically follows the change of magnetic field direction ($\text{sgn}(B(t))$).

$$\mathbf{r}_{ad} = \begin{pmatrix} a_{ad} \\ (1 - a_{ad}) \end{pmatrix} \text{ and } \mathbf{s}_{ad} = \begin{pmatrix} \text{sgn}(B(t)) \\ 1 \end{pmatrix} \quad (3.200)$$

The measured intensity than reads as

$$I_m(\mathbf{Q}, t) = \sum_{i=1,2} r_{ad,i} \left[n_+ (s_{ad,i} P_{pol}, \epsilon) A_+ I_{++}(\mathbf{Q}, t) + n_+ (s_{ad,i} P_{pol}, \epsilon) A_- I_{+-}(\mathbf{Q}, t) + n_- (s_{ad,i} P_{pol}, \epsilon) A_- I_{--}(\mathbf{Q}, t) + n_- (s_{ad,i} P_{pol}, \epsilon) A_+ I_{-+}(\mathbf{Q}, t) \right] \quad (3.201a)$$

$$= \sum_{i=1,2} \sum_{k,l=+,-} r_{ad,i} n_k (s_{ad,i} P_{pol}, \epsilon) A_l I_{kl}(\mathbf{Q}, t) \quad (3.201b)$$

with

$$A_{\pm} = \left(\frac{1 + s_{ad,2}}{2} r_{ad,1} + \frac{1 + s_{ad,1}}{2} r_{ad,2} \right) T_{\pm}(t) + \left(\frac{1 - s_{ad,2}}{2} r_{ad,1} + \frac{1 - s_{ad,1}}{2} r_{ad,2} \right) T_{\mp}(t) \quad (3.201c)$$

To calculate the time dependent scattering cross section a model for the time evolution of the orientation distribution of the magnetic moments $f(\theta, t)$ is needed, from which the time dependent order parameter $S_1(t)$ and $S_2(t)$ can be obtained, as well as a model

for the time evolution of the structure factor $S(\mathbf{Q}, t)$.

$$\frac{dM}{dt} = -\frac{M(t) - M_\infty L(\alpha'(t))}{\tau} \quad (3.202a)$$

$$M(t = 0) = M_0 \quad (3.202b)$$

$$\alpha'(t) = \alpha_0 \cos(\omega t + \phi_0) + \alpha_1 \quad (3.202c)$$

$$\alpha_0 = \frac{-B_0 \mu}{k_B T} \quad (3.202d)$$

$$\alpha_1 = \frac{B_1 \mu}{k_B T} \quad (3.202e)$$

$$\omega = 2\pi\nu \quad (3.202f)$$

$$\phi_0 = \varphi_0 - \frac{\omega d_{SD} \lambda}{3956} \quad (3.202g)$$

In the limit of small values for the Langevin parameter α the Langevin function can be approximated by

$$L(\alpha) \rightarrow \frac{\alpha}{3} \quad (3.203)$$

for which the differential equation has an analytical solution

$$M(t) = e^{-\frac{t}{\tau}} \left[M_0 - M_\infty \left(\frac{\alpha_0}{3} \frac{\cos(\phi_0) + \omega\tau \sin(\phi_0)}{1 + \omega^2\tau^2} + \frac{\alpha_1}{3} \right) \right] \\ + M_\infty \left(\frac{\alpha_0}{3} \frac{\cos(\omega t + \phi_0) + \omega\tau \sin(\omega t + \phi_0)}{1 + \omega^2\tau^2} + \frac{\alpha_1}{3} \right) \quad (3.204)$$

$$\underset{t \gg \tau}{\simeq} M_\infty \left(\frac{\alpha_0}{3} \frac{\cos(\omega t + \phi_0 - \frac{\pi}{2} + \arcsin(\frac{1}{\sqrt{1+\omega^2\tau^2}}))}{\sqrt{1+\omega^2\tau^2}} + \frac{\alpha_1}{3} \right) \quad (3.205)$$

Assuming that the system is at any time in thermodynamic equilibrium with the actual magnetic field $B(t)$ than the time dependent oscillating SANS signal can be described by simply introducing a time dependent value for $\alpha(t)$:

$$\alpha(t, \lambda, d_{SD}, \rho_0, \mu_{kT}) = B(t, \lambda, d_{SD}, \rho_0) \frac{M_P V_P}{k_B T} = B(\dots) \mu_{kT} \quad (3.206)$$

with

$$\mu_{kT} = \frac{M_P V_P}{k_B T} \quad (3.207)$$

In case that the magnetic moments can not follow the external magnetic field this could be described by an additional phase $\Delta\phi_\alpha$ between α and B and a damping factor d_α so that

$$\alpha(t, \lambda, d_{SD}, \rho_0 - \Delta\phi_\alpha, \mu_{kT}) = d_\alpha B(t, \lambda, d_{SD}, \rho_0 - \Delta\phi_\alpha) \frac{M_P V_P}{k_B T}. \quad (3.208)$$

In such a case of such

$$\mathbf{r}_{ad} = \begin{pmatrix} (1 - a_{ad}) \operatorname{sgn}(B(t)) \\ a_{ad} \operatorname{sign}(B(t)\alpha(t)) \end{pmatrix} \quad (3.209)$$

Furthermore we assume here that the size of the form factors of the magnetic and nuclear scattering are the same except the scattering contrast that means the ratio of magnetic to nuclear form factor is Q -independent and equal to the squared ratio of magnetic to nuclear scattering length density

$$\frac{F_N^2(Q)}{\tilde{F}_M^2(Q)} = \text{const} = \left(\frac{\Delta b_{\text{nuc}}}{\Delta b_{\text{mag}}} \right)^2 \quad (3.210)$$

Therefore the time dependent signal on the detector for a given direction ψ is given by

$$y(t, \dots) = \int_{\lambda_0 - \Delta\lambda}^{\lambda_0 + \Delta\lambda} p_{\Delta}(\lambda) I_m(t, \lambda, \psi, \dots) d\lambda \quad (3.211)$$

whereby $p_{\Delta}(\lambda)$ describes the triangular shaped wave length distribution of the neutron beam.

3.5.4. SuperParStroboPsiSQ.

The external applied field is given by:

$$B(t, d_{\text{SD}}, \lambda, \rho_0) = B_1 - B_0 \cos(2\pi\nu(t - d_{\text{SD}}\lambda/3956) + \rho_0) \quad (3.212)$$

where t in [s] is the time between neutron detection and the trigger signal from the frequency generator, d_{SD} in [m] is the sample detector distance, λ in [\AA] the neutron wavelength, and ν in [Hz] the frequency of the oscillating magnetic field. As t is defined here as the time of the neutron detection one has therefore to correct the phase in the argument for the magnetic field with an addition phase term. The term $t_{\text{SD}} = d_{\text{SD}}\lambda/3956$ takes account for the flight time t_{SD} of the neutrons between the sample and the detector. The term ρ_0 takes account for any other additional constant phase shift between trigger signal and the magnetic field due to phase shifts in the amplifier.

The scattering intensity of superparamagnetic particles including a structure factor $S(Q)$ is given by

$$I(Q) = \underbrace{\tilde{F}_M^2(Q) 2 \frac{L(\alpha)}{\alpha} + F_N^2(Q) S(Q)}_{A(Q)} + \underbrace{\tilde{F}_M^2(Q) \left[\left(1 - 3 \frac{L(\alpha)}{\alpha} - L^2(\alpha) \right) + L^2(\alpha) S(Q) \right]}_{B(Q)} \sin^2 \Psi \quad (3.213)$$

Assuming that the system is in equilibrium faster than $1/\nu$ than the above equation can be used to describe the time dependent oscillating SANS signal simply by introducing a time dependent value for α :

$$\alpha(t, \lambda, d_{\text{SD}}, \rho_0, \mu_{\text{kT}}) = B(t, \lambda, d_{\text{SD}}, \rho_0) \frac{M_P V_P}{k_B T} = B(\dots) \mu_{\text{kT}} \quad (3.214)$$

with

$$\mu_{\text{kT}} = \frac{M_P V_P}{k_B T} \quad (3.215)$$

Furthermore we assume here that the size of the form factors of the magnetic and nuclear scattering are the same except the scattering contrast that means the ratio of magnetic to nuclear form factor is Q -independent and equal to the squared ratio of magnetic to nuclear scattering length density

$$\frac{F_N^2(Q)}{\tilde{F}_M^2(Q)} = \text{const} = \left(\frac{\Delta b_{\text{nuc}}}{\Delta b_{\text{mag}}} \right)^2 \quad (3.216)$$

Therefore the time dependent signal on the detector for a given direction Ψ and integrated over Q in this direction is given by

$$\begin{aligned} i(t, \dots) &= \int_{Q_{\min}}^{Q_{\max}} I(Q, t, \lambda, \Psi, d_{\text{SD}}, \rho_0) dQ \\ &= c \left[2 \frac{L(\alpha)}{\alpha} + \frac{F_N^2(Q)}{F_M^2(Q)} S(Q) + \left[\left(1 - 3 \frac{L(\alpha)}{\alpha} - L^2(\alpha) \right) + L^2(\alpha) S(Q) \right] \sin^2 \Psi \right] \\ &= c \left[2 \frac{L(\alpha)}{\alpha} + \left(\frac{\Delta b_{\text{nuc}}}{\Delta b_{\text{mag}}} \right)^2 S(Q) + \left[\left(1 - 3 \frac{L(\alpha)}{\alpha} - L^2(\alpha) \right) + L^2(\alpha) S(Q) \right] \sin^2 \Psi \right] \end{aligned} \quad (3.217)$$

$$y(t, \dots) = \int_{\lambda_0 - \Delta \lambda}^{\lambda_0 + \Delta \lambda} p_{\Delta}(\lambda) i(t, \lambda, \Psi, d_{\text{SD}}, \rho_0) d\lambda \quad (3.218)$$

whereby $p_{\Delta}(\lambda)$ describes the triangular shaped wave length distribution of the neutron beam.

3.5.5. SuperParStroboPsiSQBt.

The same as SuperParStroboPsiSQ except that the structure factor $S(Q, t)$ becomes field dependent:

$$S(Q, t) = 1 + [S(Q) - 1] \left| \frac{B(t, d_{\text{SD}}, \lambda, \rho_0)}{|B_1| + \frac{2}{\pi} |B_0|} \right| \quad (3.219)$$

3.5.6. SuperParStroboPsiSQLx.

The same as SuperParStroboPsiSQ except that the structure factor $S(Q, t)$ becomes field dependent:

$$S(Q, t) = 1 + [S(Q) - 1] |L(\alpha)| \quad (3.220)$$

3.5.7. SuperParStroboPsiSQL2x.

The same as SuperParStroboPsiSQ except that the structure factor $S(Q, t)$ becomes field dependent:

$$S(Q, t) = 1 + [S(Q) - 1] L^2(\alpha) \quad (3.221)$$

CHAPTER 4

Analytical Solutions for Structure factors

The different types of structure factors can be selected in the different submenus. Next top traditional structure factors also some functions, which are not structure factors at all have been implemented for some other purposes.

4.1. Methods to include structure factors

For each scattering object i next to a size distribution $N_i(x; \mathbf{l}_i)$ also a structure factor $S_i(Q; \mathbf{s}_i)$ can be included. When a structure factor is included several theoretical ways to account for it have been implemented like the monodisperse approximation (4.1.1), decoupling approach (4.1.2), local monodisperse approximation (4.1.3), partial structure factor (4.1.4) and scaling approximation of partial structure factors (4.1.5). At the moment it is assumed that there are no interactions between different species of scatterers so that the total scattering is given by the sum of the scattering of the individual species

$$\frac{d\sigma}{d\Omega}(Q) = \sum_{i=1}^N \frac{d\sigma_i}{d\Omega}(Q) \quad (4.1)$$

whereby different approaches to include structure factor effects in the differential scattering cross-sections $\frac{d\sigma_i}{d\Omega}(Q)$ of the species i of scatterer are defined below.

4.1.1. Monodisperse approach.

The monodisperse approach is the simplest way to include a structure factor in the analysis. This approach simply multiplies the size averaged form factor with the structure factor. Here it is assumed that the interaction potential between particles are spherical symmetric and independent of the particle size.

$$\frac{d\sigma_i}{d\Omega}(Q) = \left[\int_0^\infty N_i(x; \mathbf{l}_i) F_i^2(Q; \mathbf{a}_i, x) dx \right] S_i(Q; \mathbf{s}_i) \quad (4.2)$$

4.1.2. Decoupling approximation.

For systems with small polydispersities and small anisotropies leads to a decoupling approach of Kotlarchyk and Chen [273]. It is assumed that interactions are independent

of particle size and orientation.

$$\frac{d\sigma_i}{d\Omega}(Q) = \int_0^\infty N_i(x; \mathbf{l}_i) F_i^2(Q; \mathbf{a}_i, x) dx + \frac{1}{n_i} \left[\int_0^\infty N_i(x; \mathbf{l}_i) F_i(Q; \mathbf{a}_i, x) dx \right]^2 \times [S_i(Q; \mathbf{s}_i) - 1] \quad (4.3)$$

with

$$n_i = \int_0^\infty N_i(x; \mathbf{l}_i) dx. \quad (4.4)$$

The decoupling approximation can only be combined with those form factor, for which the scattering amplitude $F_i(Q; \mathbf{a}_i, x)$ has been implemented. However, for many form factors only the scattering intensity $F_i^2(Q; \mathbf{a}_i, x)$ is available. The combination of those form factors with the decoupling approach produces an error message in **SASfit**.

4.1.3. Local monodisperse approximation.

The opposite limit of the approximations as used for the decoupling approximation is used in the local monodisperse approximation [373]. In this approach it is assumed that a particle of a certain size is always surrounded by particles with the same size. Following this the scattering is approximated by that of monodisperse sub-systems weighted by the size distribution:

$$\frac{d\sigma_i}{d\Omega}(Q) = \int_0^\infty N_i(x; \mathbf{l}_i) F_i^2(Q; \mathbf{a}_i, x) S_i(Q; \mathbf{s}_i, R_i(\mathbf{a}_i, x)) dx \quad (4.5)$$

in which it has been indicated that the structure factor is for particles of size $R_i(\mathbf{a}_i, x)$. As the distribution $N_i(x; \mathbf{l}_i)$ does not necessarily describe the distribution of the overall size. **SASfit** assumes, that the radius of a particle with the form factor $F_i(Q; \mathbf{a}_i, x)$ used in the structure factor is given by the radius of a sphere with the same volume $V_i(\mathbf{a}_i, x)$

$$R_i(\mathbf{a}_i, x) = \sqrt[3]{\frac{3}{4\pi} V_i(\mathbf{a}_i, x)}. \quad (4.6)$$

This local monodisperse approximation works better than the decoupling approximation for systems with larger polydispersities and higher concentrations. As compared to the decoupling approximation and the scaling approximation described below, it has the advantage that the cross section is linear in the size distribution.

4.1.4. partial structure factors.

For polydisperse systems it is also not possible to write the scattering cross section as a product of a form factor and a structure factor. The scattering cross section has

the form

$$\begin{aligned} \frac{d\sigma_i}{d\Omega}(Q) = & \int_0^\infty N_i(x; \mathbf{l}_i) F_i^2(Q; \mathbf{a}_i, x) dx \\ & + \frac{1}{n_i} \int_0^\infty \int_0^\infty N_i(x; \mathbf{l}_i) N_i(x'; \mathbf{l}_i) F_i(Q; \mathbf{a}_i, x) F_i(Q; \mathbf{a}_i, x') \\ & \times [S_i(Q; \mathbf{s}_i, R_i(\mathbf{a}_i, x), R_i(\mathbf{a}_i, x')) - 1] dx dx' \end{aligned} \quad (4.7)$$

where monodisperse structure factor $S_i(Q; \mathbf{s}_i, \dots)$ is evaluated for the radius $(R_i(\mathbf{a}_i, x) + R_i(\mathbf{a}_i, x'))/2$. n_i and $R_i(\mathbf{a}_i, x)$ have the same definition as those in eq. 4.4 and 4.6.

4.1.5. Scaling approximation.

A scaling approximation has recently been introduced by Gazzillo et al. [148]. It is assumed that the pair correlation functions are identical except for a scaling constant. This leads to the following expression:

$$\begin{aligned} \frac{d\sigma_i}{d\Omega}(Q) = & \int_0^\infty N_i(x; \mathbf{l}_i) F_i^2(Q; \mathbf{a}_i, x) dx \\ & + \frac{1}{n_i} \int_0^\infty \int_0^\infty N_i(x; \mathbf{l}_i) N_i(x'; \mathbf{l}_i) F_i(Q; \mathbf{a}_i, x) F_i(Q; \mathbf{a}_i, x') \\ & \times \frac{\bar{V}_i(\mathbf{a}_i, x, x')}{V_{i,av}} [S_i(Q; \mathbf{s}_i, R_i(\mathbf{a}_i, x), R_i(\mathbf{a}_i, x')) - 1] dx dx' \end{aligned} \quad (4.8)$$

where $V_{i,av}$ is given by

$$V_{i,av} = \frac{\int_0^\infty N_i(x; \mathbf{l}_i) V_i(\mathbf{a}_i, x) dx}{\int_0^\infty N_i(x; \mathbf{l}_i) dx} \quad (4.9)$$

and $V_i(\mathbf{a}_i, x, x')$ by

$$\bar{V}_i(\mathbf{a}_i, x, x') = \frac{4}{3}\pi \left(\frac{1}{2} \left(\sqrt[3]{\frac{3}{4\pi} V_i(\mathbf{a}_i, x)} + \sqrt[3]{\frac{3}{4\pi} V_i(\mathbf{a}_i, x')} \right) \right)^3 \quad (4.10)$$

and the monodisperse structure factor is evaluated for the radius $(R_i(\mathbf{a}_i, x) + R_i(\mathbf{a}_i, x'))/2$. n_i and $R_i(\mathbf{a}_i, x)$ have the same definition as those in eq. 4.4 and 4.6.

Note that the expression is not linear in the size distribution and that it involves double integrations, which makes least-square fitting with this expression relatively slow.

4.1.6. van der Waals one-fluid approximation.

This approximation is similar to the scaling approximation introduced by Gazzillo et al.

[148]. The exact formula is given by

$$\begin{aligned} \frac{d\sigma_i}{d\Omega}(Q) = & \int_0^\infty N_i(x; \mathbf{l}_i) F_i^2(Q; \mathbf{a}_i, x) dx \\ & + \frac{1}{n_i} \int_0^\infty \int_0^\infty N_i(x; \mathbf{l}_i) N_i(x'; \mathbf{l}_i) F_i(Q; \mathbf{a}_i, x) F_i(Q; \mathbf{a}_i, x') \\ & \times \frac{\bar{V}_i(\mathbf{a}_i, x, x')}{V_{i,x}} [S_i(Q; \mathbf{s}_i, R_i(\mathbf{a}_i, x), R_i(\mathbf{a}_i, x')) - 1] dx dx' \end{aligned} \quad (4.11)$$

where $V_{i,x}$ is given by

$$V_{i,x} = \frac{\int_0^\infty \int_0^\infty N_i(x; \mathbf{l}_i) N_i(x'; \mathbf{l}_i) V_i(\mathbf{a}_i, x, x') dx dx'}{(\int_0^\infty N_i(x; \mathbf{l}_i) dx)^2} \quad (4.12)$$

and $V_i(\mathbf{a}_i, x, x')$ by

$$\bar{V}_i(\mathbf{a}_i, x, x') = \frac{4}{3}\pi \left(\frac{1}{2} \left(\sqrt[3]{\frac{3}{4\pi} V_i(\mathbf{a}_i, x)} + \sqrt[3]{\frac{3}{4\pi} V_i(\mathbf{a}_i, x')} \right) \right)^3 \quad (4.13)$$

Furthermore the structure factor is calculated for a slightly different volume fraction namely $\eta_{i,x} = \eta_i \frac{V_{i,x}}{V_{i,av}}$. The monodisperse structure factor is evaluated for the radius $(R_i(\mathbf{a}_i, x) + R_i(\mathbf{a}_i, x'))/2$. n_i and $R_i(\mathbf{a}_i, x)$ have the same definition as those in eq. 4.4 and 4.6.

Note that the expression is not linear in the size distribution and that it involves double integrations, which makes least-square fitting with this expression relatively slow.

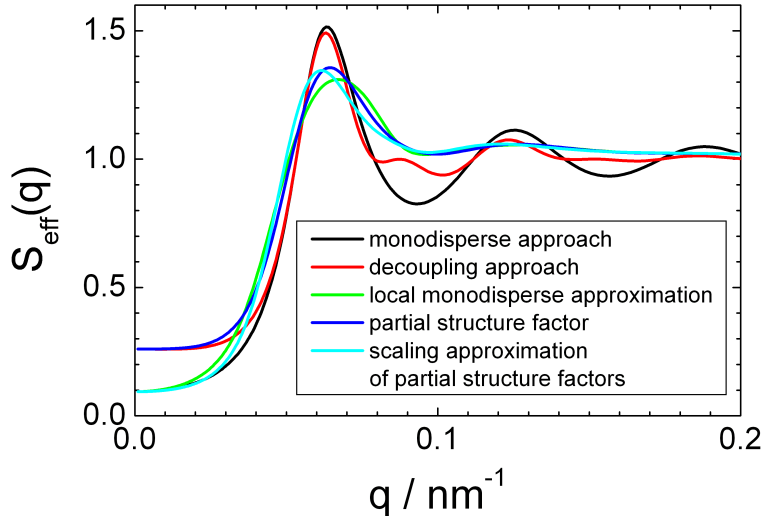


FIGURE 4.1. Effective structure factor $S_{\text{eff}}(q)$ for Spheres with Hard Sphere interaction potential. The fraction is assumed to be $\eta = 0.3$. A LogNormal distribution with $\sigma = 0.15$ and $R_0 = 50\text{nm}$ is assumed.

4.2. Hard & Sticky Hard Sphere

4.2.1. Hard Sphere. [385, 512]

$$U(r) = \begin{cases} \infty & \text{for } 0 < r < \sigma \\ 0 & \text{for } r > \sigma \end{cases} \quad (4.14)$$

$$\alpha = \frac{(1 + 2f_p)^2}{(1 - f_p)^4} \quad (4.15a)$$

$$\beta = -6f_p \frac{(1 + f_p/2)^2}{(1 - f_p)^4} \quad (4.15b)$$

$$\gamma = \frac{f_p \alpha}{2} \quad (4.15c)$$

$$A = 2R_{\text{HS}}q \quad (4.15d)$$

$$G(f_p, A) = \alpha \frac{\sin A - A \cos A}{A^2} + \beta \frac{2A \sin A + (2 - A^2) \cos A - 2}{A^3} + \gamma \frac{-A^4 \cos A + 4[(3A^2 - 6) \cos A + (A^3 - 6A) \sin A + 6]}{A^5} \quad (4.15e)$$

$$S_{\text{HS}}(q, R_{\text{HS}}, f_p) = \frac{1}{1 + 24f_p \frac{G(f_p, A)}{A}} \quad (4.15f)$$

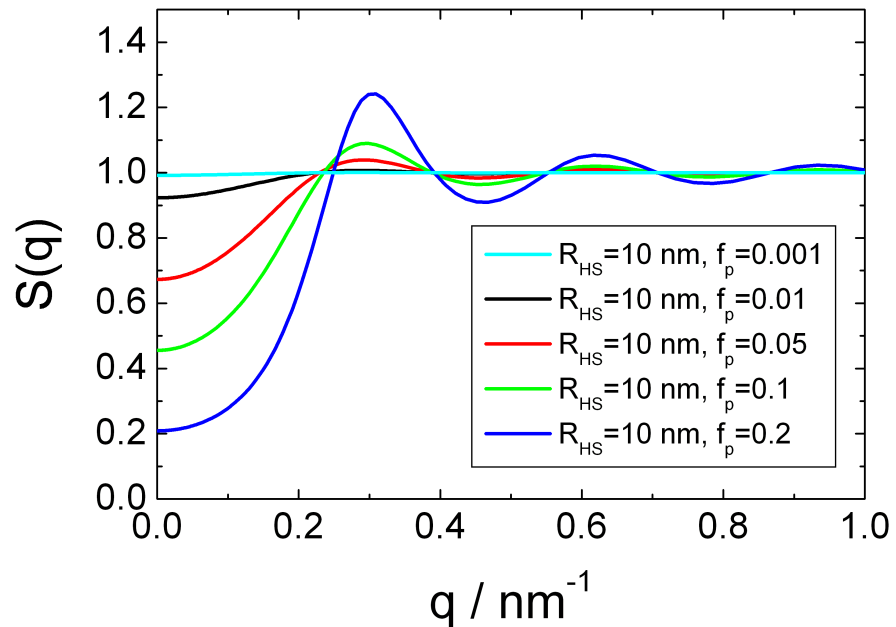


FIGURE 4.2. Structure factor $S(q)$ for a hard sphere interaction potential for the different volume fractions f_p .

4.3. Other Structure Factors

4.3.1. Hayter-Penfold RMSA. This is the structure factor for a system of charged, spheroidal objects in a dielectric medium [204, 191]. When combined with an appropriate form factor (such as sphere, core+shell, ellipsoid etc.), this allows for inclusion of the interparticle interference effects due to screened coulomb repulsion between charged particles. The salt concentration, is used to compute the ionic strength of the solution which in turn is used to compute the Debye screening length. At present there is no provision for entering the ionic strength directly nor for use of any multivalent salts. The counterions are also assumed to be monovalent.

Input Parameters for model Hayter Penfold RMSA:

RHS: hard sphere radius R_{HS} of particles in [nm].

Z: charge of particle in units of the charge of an electron $e = -1.6021766208 \times 10^{-19} \text{ C}$

eta: volume fraction η of particles

T: sample temperature T in Kelvin

salt: monovalent salt concentration in [M]

eps_r: dielectric constant ϵ_r of solvent (vacuum:1, water at 25°: 78.2, water at 20°: 80.4, ethanol at 20°: 25.16, toluene at 23°: 2.38)

4.3.2. MacroIon.

$$ETA = \text{volume fraction} \quad (4.16a)$$

$$AK = \kappa\sigma = \text{inv. screening length times diameter} \quad (4.16b)$$

$$\kappa = \sqrt{e^2/(\epsilon\epsilon_0 k_B T) * (\rho_c + 2\rho_s)} \quad (4.16c)$$

$$\rho_c = \text{density of counterions} = \rho_{\text{colloids}} Z \quad (4.16d)$$

$$\rho_s = \text{density of salt cations or anions} \quad (4.16e)$$

$$GEK = \text{charge}^2/(\pi k_B T \epsilon \epsilon_0 \sigma (2 + AK)^2) \quad (4.16f)$$

$$\text{charge} = \text{Ladung eines Kolloids} = eZ \quad (4.16g)$$

$$S = ETA^{1/3} = \text{scaling factor for rescaled MSA (RMSA)} \quad (4.16h)$$

$$GAMK = 2 * S * GEK * \exp(AK - AK/S). \quad (4.16i)$$

4.3.3. Critical Scattering.

$$S_{\text{crit}}(Q) = 1 + \frac{\kappa}{1 + \zeta^2 Q^2} \quad (4.17)$$

ζ : correlation length, κ : scaling factor

4.3.4. Cylinder(PRISM).

$$S_{\text{Cyl,PRISM}} = \frac{1}{1 + \nu C_q P_{15}} \quad (4.18)$$

$$x = 2QR$$

$$x_{P15} = Q(L - 2R)$$

$$P_{15} = 2 \frac{\text{Si}(x_{P15})}{x_{P15}} - 4 \frac{\sin^2(x_{P15}/2)}{x_{P15}^2}$$

$$C_q = 3 \frac{\sin(x) - x \cos(x)}{x^3}$$

4.3.5. Voigt Peak.

In spectroscopy, the Voigt profile is a spectral line profile named after Woldemar Voigt and found in all branches of spectroscopy in which a spectral line is broadened by two types of mechanisms, one of which alone would produce a Doppler profile, and the other of which would produce a Lorentzian profile. All normalized line profiles can be considered to be probability distributions. The Doppler profile is essentially a normal distribution and a Lorentzian profile is essentially a Cauchy distribution. Without loss of generality, we can consider only centered profiles which peak at zero. The Voigt profile is then the convolution of a Lorentzian profile and a Doppler profile:

$$V(x|\sigma, \gamma) = \int_{-\infty}^{\infty} D(x'|\sigma) L(x - x'|\gamma) dx' \quad (4.19a)$$

where x is frequency from line center, $D(x|\sigma)$ is the centered Doppler profile:

$$D(x|\sigma) = \frac{e^{-x^2/2\sigma^2}}{\sigma\sqrt{2\pi}} \quad (4.19b)$$

and $L(x|\gamma)$ is the centered Lorentzian profile:

$$L(x|\gamma) = \frac{\gamma}{\pi(x^2 + \gamma^2)}. \quad (4.19c)$$

The defining integral can be evaluated as:

$$V(x) = \frac{\Re[w(z)]}{\sigma\sqrt{2\pi}} \quad (4.19d)$$

where $\Re[w(z)]$ is the real part of the complex error function of z and

$$z = \frac{x + i\gamma}{\sigma\sqrt{2}} \quad (4.19e)$$

$$S_{\text{Voigt}}(Q, Q_m, A, \sigma, \gamma, c_0) = A V(Q - Q_m|\sigma, \gamma) + c_0 \quad (4.19f)$$

CHAPTER 5

Numerical solution of Fredholm integrals using regularization

In physics, many experimental data can be described theoretical by a Fredholm integral. To extract a physical interesting quantity the integral equation often has to be solved numerically. In many cases, this problem becomes ill-posed and an additional regularization technique has to be included in the analysis to obtain a stable solution. A general overview about regularization techniques can be found e.g. in [194, 193, 149, 440, 262].

5.1. Problem description

Also scattering techniques often measure a quantity which can be written in form of a Fredholm integral. The Fredholm equation of the first kind is defined as

$$g(t) = \int_a^b K(t, s) f(s) ds \quad (5.1)$$

and the problem is, given the continuous kernel function $K(t, s)$ and the function $g(t)$, which is often an experimental measurable quantity with an error bar, to find the function $f(s)$. Sometimes the values of the Kernel scale somehow with a power law s^α . In such a case a more stable solution can be obtained by rewriting the problem as

$$g(t) = \int_a^b s^{-\alpha} K(t, s) s^\alpha f(s) ds \quad (5.2)$$

where now the continuous kernel function is defined as $s^{-\alpha} K(t, s)$ and the function to be determined $s^\alpha f(s)$.

The above Fredholm equation is one dimensional. There are several cases where the physical problem to solve is described by a multi-dimensional Fredholm integral of the form

$$g(\mathbf{t}) = \iint_{\mathbb{R}^n} \cdots \int K(\mathbf{t}, \mathbf{s}) f(\mathbf{s}) ds_1 ds_2 \cdots ds_n \quad (5.3)$$

where $\mathbf{s} \in \mathbb{R}^n$ and $\mathbf{t} \in \mathbb{R}^{3m}$

One simple example is the smearing of the signal by a known resolution function. These folding integrals can in principle be solved in Fourier space. However, also the signal without any smearing are often described by a known or assumed function with one parameter having a distribution. The resulting signal is than an integral of the product of the known function and the probability distribution which one likes to determine. In both cases these integrals belongs to Fredholm integrals of first kind.

In small angle scattering the measured intensity I_m is given as a function of the scattering vector $q = 4\pi \sin(\theta)/\lambda$, with θ being the scattering vector and λ the wavelength of the probing radiation. The smearing by limited resolution resolution for a pinhole came can be written as

$$I_m(\langle Q \rangle) = \int_0^\infty R_{av}(Q, \langle Q \rangle, \sigma) I(Q) dQ \quad (5.4)$$

where $R_{av}(Q, \langle Q \rangle, \sigma)$ describes the known resolution function and σ the resolution parameter, which is known for each measured $\langle Q \rangle$ -value [379]. A desmearing of the data could help to accelerate the analysis as the model does not need to be folded anymore with the resolution function.

Typical tasks in the analysis of desmeared data are to determine size distribution $N(s)$, pair distribution functions $p(r)$ or scattering length density profiles ρ .

5.1.1. Size distribution $N(R)$.

The size distribution can be determined, if the particle shape is known. For many particle shapes the scattering intensity or form factor can be calculated via an analytical expression. The scattering intensity are than describes by integrating the squared form factor $F^2(Q, s)$ over a distribution function $N(s)$, where s describes the size of the scattering objects [374]. The intensity is than given by

$$I(Q) = \int_0^\infty N(s) |F(Q, s)|^2 ds \quad (5.5)$$

To solve equation 5.5 one often parameterize the size distribution by assuming an analytical distribution function like LogNormal, Gaussian, Weibull or Schulz-Zimm distribution, with a few input parameter and is fitting these parameters by performing the numerical integration and applying a Levenberg-Marquardt strategy to solve a non-linear least square problem [52]. This however assume a priori knowledge about the distribution function. More desirable would be a discretization of the size distribution N_i at the positions s_i and determine all N_i without any further assumption. This however is normally an ill posed problem and requires some additional regularization to determine a unique solution for the vector N_i . By discretization of the problem one also can easily include the resolution function. As the resolution function only depends on the scattering vector Q and not on the particle size s the order of integrations over the size distribution and the resolution function can be changed as all functions are continuous and integrable. Combining eq. 5.4 and 5.5 yields

$$I_m(\langle Q \rangle) = \int_0^\infty R_{av}(Q, \langle Q \rangle, \sigma) \int_0^\infty N(s) |F(Q, s)|^2 ds dQ \quad (5.6)$$

$$= \int_0^\infty N(s) \int_0^\infty R_{av}(Q, \langle Q \rangle, \sigma) |F(Q, s)|^2 dQ ds \quad (5.7)$$

As already mentioned in eq. 5.2 also here the squared form factor is scaling with the squared sample volume, which is in the case of spheres proportional to R^6 . Therefore the

distribution function to be determined often is chosen to be the intensity distribution $N(R)R^\alpha$ with $\alpha = 6$ so that eq. 5.7 is slightly modified to

$$I_m(\langle Q \rangle) = \int_0^\infty N(s)s^\alpha \int_0^\infty R_{av}(Q, \langle Q \rangle, \sigma) s^{-\alpha} |F(Q, s)|^2 dQ ds \quad (5.8)$$

which can be written as a linear matrix equation by discretization

$$b_i = \sum_{j=0}^{N-1} A_{i,j} x_j \quad (5.9)$$

$$\mathbf{b} = \hat{\mathbf{A}} \mathbf{x} \quad (5.10)$$

with $\hat{\mathbf{A}}$ being a $M \times N$ matrix, \mathbf{b} a vector of length M and \mathbf{x} a solution vector of length N where their elements are given by

$$x_j = N(s_j)s_j^\alpha \quad (5.11)$$

$$b_i = I(\langle Q \rangle_i) \quad (5.12)$$

$$A_{i,j} = \Delta s_j \int_0^\infty R_{av}(Q, \langle Q \rangle_i, \sigma_i) s_j^{-\alpha} |F(Q, s_j)|^2 dQ \quad (5.13)$$

$R_{av}(Q, \langle Q \rangle_i, \sigma_i)$ and $s_j^{-\alpha} |F(Q, s_j)|^2$ are known functions, so that the integral only has to be calculated once for each pair of $(\langle Q \rangle_i, s_j)$.

5.1.2. Orientation distribution $p_{ODF}()$.

Another case described by Fredholm integrals of first kind are scattering patterns from anisotropic objects with an orientation distribution. As the orientation distribution in its most general case depends on three angles, e.g. defined by Euler angles, the problem is described by a three dimensional Fredholm integral equation (see e.g. eq. 9.506 and 9.507)

$$I(\mathbf{Q}) = \iiint_{\mathbf{R}(\alpha, \beta, \gamma)} p_{ODF}(\alpha, \beta, \gamma) |F(\mathbf{Q}, \alpha, \beta, \gamma)|^2 d\alpha d\beta d\gamma \quad (5.14)$$

Often the studied samples are model systems with at least a cylindrical symmetry. In those cases two angles like spherical polar angles φ and θ are needed

$$I(\mathbf{Q}) = \iint_{\mathbf{R}(\varphi, \theta)} p_{ODF}(\varphi, \theta) |F(\mathbf{Q}, \varphi, \theta)|^2 d\varphi d\theta \quad (5.15)$$

If the most probable orientation is known experimentally this direction is often chosen to be perpendicular to the beam (section 9.9.7). For many practical applications only the angle between the direction of the particle symmetry axis (cylindrical symmetry) to the most probable direction matters. As this direction has been chosen to be parallel to one of the coordinate system axis the scattering intensity further simplifies to a single dimensional Fredholm integral (e.g. [21])

$$I(\mathbf{Q}) = \int p_{ODF}(\theta) |F(\mathbf{Q}, \theta)|^2 d\theta \quad (5.16)$$

5.1.3. Pair distance distribution function $p(r)$.

The above formalism is often applied if a priori knowledge about the shape of the scattering objects is available but not about their size distribution. If the shape of the scattering objects is also not known one often like to convert the intensity data from Q -space into r -space by calculating the pair distance distribution function. The scattering intensity is the square of the Fourier transformation of the scattering length density $\rho(\mathbf{r})$

$$I(\mathbf{Q}) = \left| \int_0^\infty \rho(\mathbf{r}) \exp(-i\mathbf{Q}\mathbf{r}) d\mathbf{r} \right|^2 \quad (5.17)$$

$$= \int_0^\infty d\mathbf{r} \exp(-i\mathbf{Q}\mathbf{r}) \int_0^\infty d\mathbf{r}_1 \rho(\mathbf{r}_1) \bar{\rho}(\mathbf{r}_1 - \mathbf{r}) \quad (5.18)$$

$$\int_0^\infty d\mathbf{r} \exp(-i\mathbf{Q}\mathbf{r}) \gamma(\mathbf{r}) \quad (5.19)$$

where $\gamma(\mathbf{r})$ is the autocorrelation function of the scattering length density. For isotropic media without texture the autocorrelation only depends on the modulus of r so that one obtains

$$I(Q) = \int_0^\infty 4\pi r^2 \gamma(r) \frac{\sin(Qr)}{Qr} dr \quad (5.20)$$

$$= 4\pi \int_0^\infty p(r) \frac{\sin(Qr)}{Qr} dr \quad (5.21)$$

with $p(r) = r^2 \gamma(r)$ being the pair distance distribution function. This function is calculated first by many people analysing SAS data and afterwards interpreted further. For the scattering intensity of objects with cylindrical symmetry and planar symmetry but random orientation one finds corresponding expressions:

$$I_{\text{cyl}}(Q) = 2\pi^2 L \int_0^\infty p(r) \frac{J_0(Qr)}{Q} dr \quad (5.22)$$

$$I_{\text{plan}}(Q) = 4\pi A \int_0^\infty p(r) \frac{\cos(Qr)}{Q^2} dr \quad (5.23)$$

where J_0 is the Bessel function of zero order, L the length of the cylindrical object and for planar structures A is the area of the object. The pair distance distribution function $p(r)$ is related to the correlation function $\gamma(r)$ through

$$p(r) = r^{\dim-1} \gamma(r) \quad (5.24)$$

Here \dim denotes the symmetry of the scatterer (1: planar, 2: cylindrical, 3: spherical) and

$$\gamma(r) = \int_{-\infty}^{\infty} \rho(x) \rho(x - r) dx \quad (5.25)$$

where $\rho(r)$ is the scattering length density distribution. For one-dimensional symmetry r is the normal distance from the plane, for two-dimensional symmetry the normal distance to the cylinder axis and for three-dimensional symmetry the distance from the center of the sphere. The integrals (5.21), (5.22) and (5.23) can be discretized on the grid r_i so that one obtains the matrix equation

$$b_i = A_{i,j}x_j \quad (5.26)$$

$$A_{i,j}^{\text{sp}} = \Delta r_j \frac{\sin(Q_i r_j)}{Q_i r_j} \quad (5.27)$$

$$x_j = p(r_j)r_j^\alpha \quad (5.28)$$

$$b_i = I(\langle Q \rangle_i) \quad (5.29)$$

$$(5.30)$$

Also here the resolution function can be easily include likewise as in 5.13. In this case normally no rescaling is done and $\alpha = 0$ is chosen.

5.1.4. Size distribution $N_h(R_h)$ from dynamic light scattering.

In dynamic light scattering (DLS) the scattering intensity is measured as a function of time. With a coherent laser beam one obtains a speckle pattern from the sample which is fluctuating due to Brownian motions. The intensity autocorrelation function $g_{(2)}(q, \tau) = \int I(q, t)I(q, t + \tau) dt / (\int I^2(q, t) dt)$. The Siegert equation relates the second-order autocorrelation function $g_{(2)}(q, \tau)$ (intensity autocorrelation) with the first-order autocorrelation function $g_{(1)}(q, \tau)$ (amplitude autocorrelation) as follows:

$$g_{(2)}(q, \tau) = A + \beta [g_{(1)}(q, \tau)]^2 \quad (5.31)$$

In an ideal experiment $A = 1$ and $\beta = 1$. For monodisperse spherical particles the first order autocorrelation function decays as a single exponential decay

$$g_{(1)}(q, \tau) = \exp(-\Gamma\tau) \quad (5.32)$$

where Γ is the decay rate, which is related to the translational diffusion coefficient D_t and may be derived at a single angle or at a range of angles depending on the wave vector q . They are related by

$$\Gamma = q^2 D_t \quad (5.33)$$

with

$$q = \frac{4\pi n_0}{\lambda} \sin\left(\frac{\theta}{2}\right) \quad (5.34)$$

where λ is the incident laser wavelength, n_0 is the refractive index of the sample and θ is angle at which the detector is located with respect to the sample cell. The translational diffusion coefficient depends via the Stokes-Einstein relation on the hydrodynamic radius R_h of the particle and the viscosity η of the carrier liquid

$$D_t = \frac{k_B T}{6\pi\eta R_h} \quad (5.35)$$

In most cases, samples are polydisperse. Thus, the amplitude autocorrelation function is a sum of the exponential decays corresponding to each of the species in the population.

$$g_{(1)}(q, \tau) = \sum_{i=1}^n G_i(\Gamma_i) \exp(-\Gamma_i \tau) = \int G(\Gamma) \exp(-\Gamma \tau) d\Gamma. \quad (5.36)$$

Since $G(\Gamma)$ is proportional to the relative scattering from each species, it contains information on the distribution of sizes. Unfortunately the amplitude autocorrelation function is not directly experimentally accessible. Experimentally available is the intensity autocorrelation function (see eq. 5.31). Many hardwares for autocorrelation automatically determine the baseline and supply a reduced intensity autocorrelation

$$g_{(2)}(\tau) - 1 = |g_{(1)}(\tau)|^2 = \left| \int_0^\infty G(\Gamma) \exp(-\Gamma \tau) d\Gamma \right|^2 \quad (5.37)$$

For the analysis one has to calculate first $g_{(1)}(\tau)$ from $g_{(2)}(\tau) - 1$. Often one just takes the square root of the reduced intensity autocorrelation to obtain the amplitude autocorrelation. As the amplitude autocorrelation function is always positive this is justified. However, due to noise the reduced intensity autocorrelation can also become negative for large relaxation times τ as $g_{(2)}(\tau) - 1 = |g_{(1)}(\tau)|^2 \rightarrow 0$ for $\tau \rightarrow \infty$. Simply neglecting negative reduced intensities autocorrelation values would produce systematic errors in the analysis. A more stable and reliable strategy, even though badly mathematically justified, is to set

$$g_{(1)}(\tau) = \text{sign}(g_{(2)}(\tau) - 1) \sqrt{|g_{(2)}(\tau) - 1|} \quad (5.38)$$

Another strategy is to make use of the faltungs theorem for Laplace transform.

$$g_{(2)}(\tau) - 1 = |g_{(1)}(\tau)|^2 = \int_0^\infty G(x) \exp(-x\tau) dx \times \int_0^\infty G(y) \exp(-y\tau) dy \quad (5.39)$$

Changing the variable $x + y = z$ one gets

$$\left| g_{(1)}(\tau) \right|^2 = \int_y^\infty G(y) G(z-y) \exp(-z\tau) dy dz \quad (5.40)$$

$$= \int_0^\infty G_{(2)}(z) \exp(-z\tau) dz = \mathcal{L}[G_{(2)}(\Gamma)] \quad (5.41)$$

where $G_{(2)}(\Gamma) = \int_{-\infty}^\infty G(y) G(z-y) dy$ and $\mathcal{L}[\cdot]$ denotes the Laplace transform. The faltung theorem for the Laplace transform leads to

$$\mathcal{L} \left[\int_{-\infty}^\infty G(y) G(z-y) dy \right] = \mathcal{L}[G(y)] \mathcal{L}[G(y)] \quad (5.42)$$

Pike [392] suggests to calculate first $G_2(\Gamma)$ but than taking the square root of the Laplace transformation and afterwards the inverse of that square root

$$G(\Gamma) = \mathcal{L}^{-1} \left[\sqrt{\mathcal{L} [G_{(2)}(\Gamma)]} \right] \quad (5.43)$$

The determination of $G_{(2)}(\Gamma)$ is also done by an inverse Laplace transform. However, this first transform can be done by regularization techniques. The other two are done directly. Pike [392] mentions that this looks as one has "gone around in a circle since, by cancelling out the two transforms under the square root, this is nothing but the original method" but also that "One can hardly dispute the experimental results that show a significant improvement in accuracy".

Goldin [165] is suggesting a mixture of both methods. He has shown that even when the value under the radical in eq. 5.38 is non-negative, calculating $g_1(\tau)$ from $\sqrt{g_2(\tau) - 1}$ increases the random error (relative to $g_2(\tau)$) and introduces a systematic error. He proposes to compute the distribution of interest in two stages. In the first stage, the self-convolution of the distribution of interest $G_{(2)}(\Gamma)$ is computed from the function $g_2(\tau) - 1$ like in [392]. The smoothed estimation of $g_2(\tau)$ is then computed and used to compute the first order correlation function $g_1(\tau)$. This is then used to calculate $G(\Gamma)$.

After determining the relaxation probability $G(\Gamma)$ function the size distribution function $N_h(R_h)$ has to be determined. The relaxation time Γ and the hydrodynamic radius are related via eq. 5.33, 5.34, and 5.35

$$\Gamma = \Gamma(R_h) = q^2 \frac{k_B T}{6\pi\eta R_h} \quad (5.44)$$

Furthermore the scattering intensity of the particle $I(q, R_h)$ also contributes as a weighting factor, i.e. how much a certain size contributes to the relaxation distribution function of the corresponding relaxation time $G(\Gamma)$.

$$G(\Gamma) = \frac{I(q, R_h) N_h(R_h) \Gamma(R_h)}{\int_0^\infty I(q, R_h) N_h(R_h) dR_h} \quad (5.45)$$

so that the size distribution of the hydrodynamic radius is proportional to

$$N_h(R_h) \propto \frac{G \left(q^2 \frac{k_B T}{6\pi\eta R_h} \right)}{\int_0^\infty I(q, R_h) N_h(R_h) dR_h} \quad (5.46)$$

The volume and intensity distribution $N_v(R_h)$ and $N_i R_h$ are than defined as

$$N_v(R_h) = R_h^3 N_h(R_h) \quad (5.47)$$

$$N_i(R_h) = R_h^6 N_h(R_h) \quad (5.48)$$

Eq. 5.46 or eq. 5.45 show, that the size distribution or decay rate distribution also depend on the q and size dependent scattering function $I(q, R_h)$. Analysing intensity correlation function at different angles simultaneously normally helps to get a more stable solution for the size distribution of particles.

5.2. Expectation Maximization (EM)

The EM algorithm has been first explained in [108]. The method is an iterative fixed point method for positive defined functions. (Other fixed point techniques are described for example in [189].) In [502] it has been shown how the EM method can be applied to solve Fredholm integrals for the domain of nonnegative real valued functions. The method described there is equivalent to the Lucy-Richardson method [418, 317]. For calculating size distribution from scattering data the method has been applied e.g. by [536, 26, 25, 12]. For inverting scattering data to pair distance distribution functions the condition of nonnegativity of the involved functions does not hold anymore as both the kernel of the Fredholm integral as well as the pair distance distribution function can take negative values. In [82] it has been shown, how the EM algorithm can be reformulated for non-density functions, i.e. to functions which also can take negative values.

Writing the Fredholm integral in eq. 5.3 or 5.2 in discrete form according to 5.9

$$b_i = \sum_{j=0}^{N-1} A_{i,j} x_j \quad (5.49)$$

the EM iteration scheme or Lucy-Richardson inversion method reads as

$$x_j^{(k+1)} = x_j^{(k)} + \Delta x_j^{(k)} = \mathcal{O}_{\text{EM}} \left[x_j^{(k)} \right] \quad (5.50)$$

$$\Delta x_j^{(k)} = x_j^{(k)} \left[\sum_{i=0}^{M-1} \frac{A_{ij}}{\left(\sum_{m=0}^{M-1} A_{mj} \right) \sum_{n=0}^{N-1} A_{in} x_n^{(k)}} - 1 \right] \quad (5.51)$$

where \mathcal{O}_{EM} is the fixed point operator. It has been shown, that the convergence is assured since the algorithm is guaranteed to increase the likelihood at each iteration. On the other side the algorithm is known to converge quite slow.

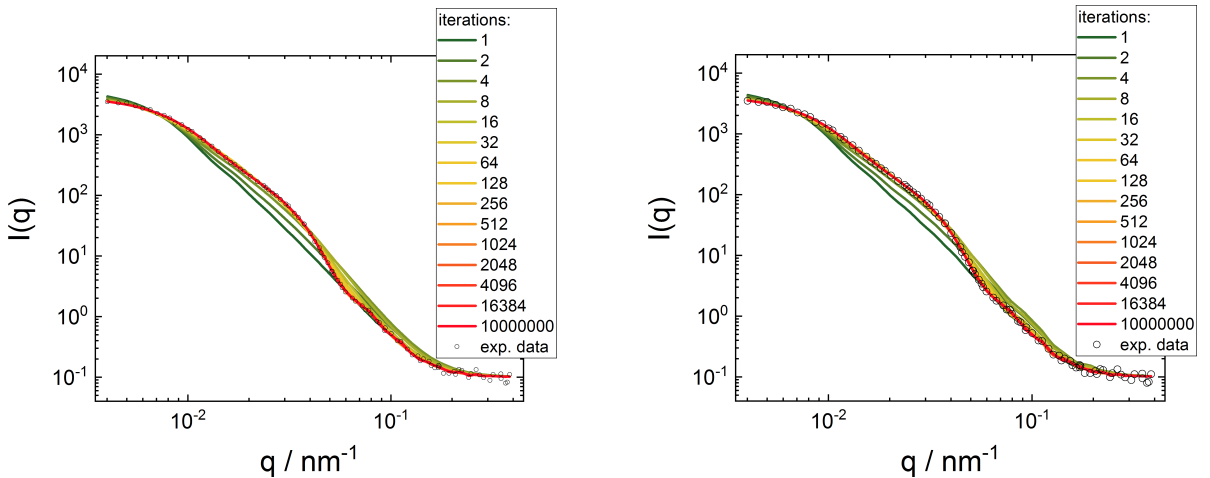


FIGURE 5.1. Scattering curve evolution for increasing number of iterations for a constant seed value (left) and random seed values (right).

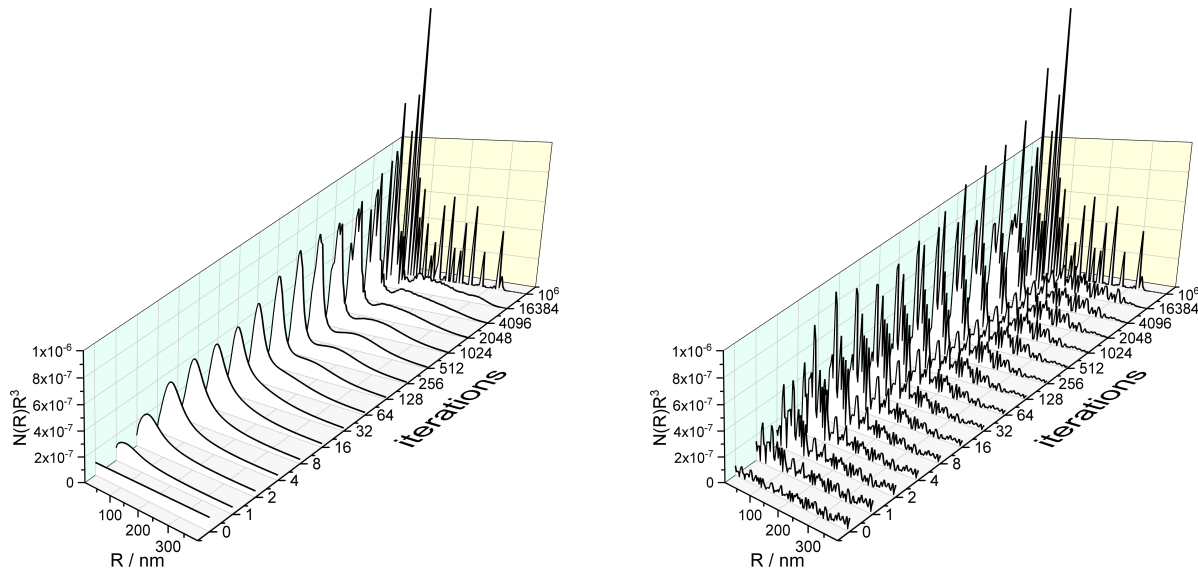


FIGURE 5.2. Size distribution evolution for increasing number of iterations for a constant seed value (left) and random seed values (right).

In figure 5.1 and 5.2 the progress of the EM-fixed point algorithm as a function of the number of iteration steps is shown. The starting values of the size distribution are assumed to be a constant (left) and random (right). In both cases the EM-scheme converges in that example finally to the same solution. However, assuming constant initial values the size distribution looks relatively smooth until the goodness-of-fit parameter approaches its final value in contrast to random seed values for the size distribution, where the initial roughness is never smoothed out by the EM scheme. In figure 5.3 the goodness-of-fit parameters are shown as a function of iterations. For this three variants of the goodness-of-fit definitions are used, the classical χ_r^2 of reduced weighted sums of squared residuals, the \mathcal{G} -test which is directly related to the Kullback-Leibler divergency of two probability function and the Pearson's χ_P^2 -test, which is obtained by a second order Taylor expansion of the natural logarithm around 1 of the \mathcal{G} -test.

$$\chi_r^2 = \sum_i^N \frac{1}{N} \left(\frac{I_{\text{th}}(q_i) - I_{\text{exp}}(q_i)}{\Delta I_{\text{exp}}(q_i)} \right)^2 \quad \text{weighted sum of squared residuals} \quad (5.52)$$

$$\chi_P^2 = \sum_i \frac{(I_{\text{th}}(q_i) - I_{\text{exp}}(q_i))^2}{I_{\text{th}}(q_i)} \quad \text{Pearson's } \chi^2\text{-test} \quad (5.53)$$

$$\mathcal{G} = 2 \sum_i \mathcal{J}_{\text{exp}}(q_i) \ln \left(\frac{\mathcal{J}_{\text{exp}}(q_i)}{\mathcal{J}_{\text{th}}(q_i)} \right) \quad \mathcal{G}\text{-test} \quad (5.54)$$

with $\mathcal{J}_{\text{exp}}(q_i) = I_{\text{exp}}(q_i) / \sum_i I_{\text{exp}}(q_i)$ and $\mathcal{J}_{\text{th}}(q_i) = I_{\text{th}}(q_i) / \sum_i I_{\text{th}}(q_i)$. Furthermore the roughness of the resulting size distribution is plotted which has been described by either the sum of the squared first or second derivatives for all radii, i.e. $\sum_i |\text{d}N(R_i)/\text{d}R_i|^2$ or $\sum_i |\text{d}^2N(R_i)/\text{d}R_i^2|^2$.

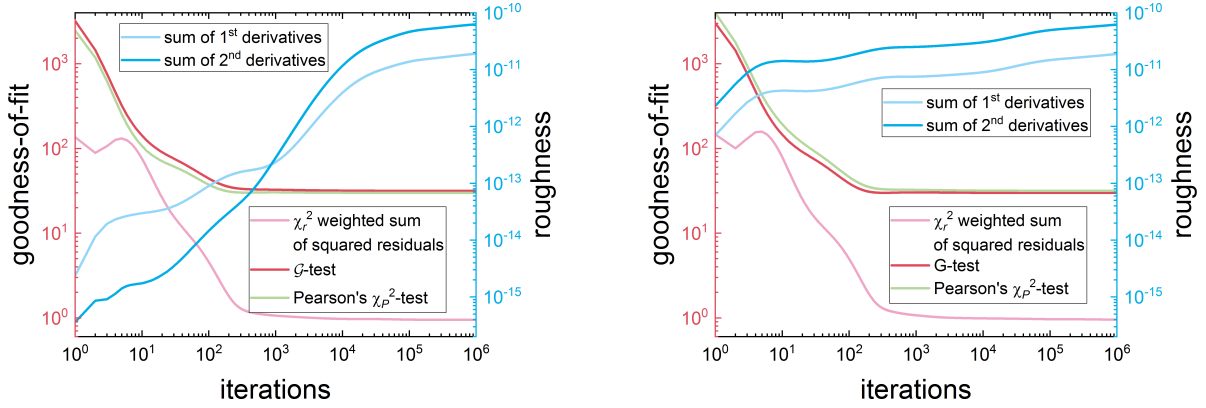


FIGURE 5.3. Dependency of goodness-of-fit and roughness on number of iterations for a constant seed value (left) and random seed values (right).

The roughness parameter and the goodness-of-fit parameter are then combined in figure 5.4 on loglog-scale showing somehow a similar behaviour as the L-curve in regularization techniques solving ill-posed problems. From a certain number of iterations the goodness-of-fit only improves infinitesimal but the roughness still continuous for a quite large number of iterations before it reaches the fixed point.

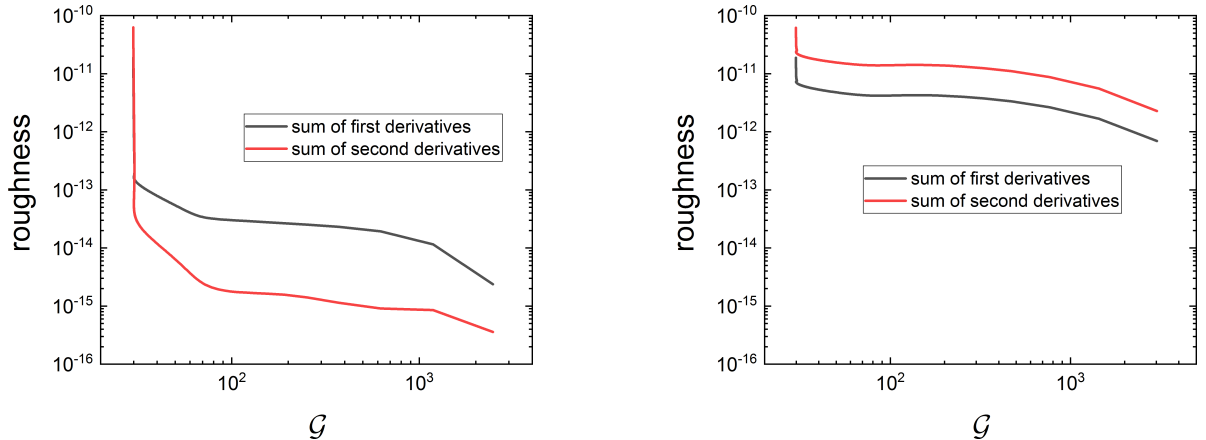


FIGURE 5.4. L-curve showing the dependency of the roughness parameters on the goodness-of-fit parameters for a constant seed value (left) and random seed values (right).

Even though the fixed point of the EM operator does not seem to depend on the initialization of the starting values but it will probably depend on the actual noise on the data, i.e. if the curve would be measured a second time with similar statistics the two curves would differ within their noise level and the EM fixed point would then very likely be slightly different, which is caused by the ill-posed nature of the Fredholm integral. Two strategies for overcoming this problem has been tested. One strategy introducing a smoothing operator into the iteration loop and a second strategy to introduce a classical regularization term in the EM scheme, which both then require a determination of the smoothing or regularization parameter.

5.2.1. EM with linear and non-linear smoothing operator.

Without any additional smoothing the EM scheme does not converge to a stable solution for scattering curves measured several times with the same statistics. Several stabilization methods have been suggested. One of them is to add an additional smoothing operator into the iteration sequence. In **SASfit** the smoothing operation suggested by [116, 117, 73] has been implemented. They suggest to add before or/and after each normal EM step (eq. 5.50) an additional smoothing step so that the EM algorithm takes the form.

$$x_j^{(k+1/2)} = x_j^{(k)} + \Delta x_j^{(k)} \quad (5.55)$$

$$x_j^{(k+1)} = \sum_{i=0}^{M-1} S_{ij}^{(h)} x_j^{(k+1/2)} \quad (5.56)$$

with the smoothing operator

$$\hat{\mathbf{S}}^{(h)} = \begin{pmatrix} 1-h & h & 0 & \cdots & 0 & 0 \\ h & 1-2h & h & \cdots & 0 & 0 \\ 0 & h & 1-2h & \cdots & 0 & 0 \\ \vdots & \vdots & \vdots & \ddots & \vdots & \vdots \\ 0 & 0 & 0 & \cdots & 1-2h & h \\ 0 & 0 & 0 & \cdots & h & 1-h \end{pmatrix} \quad (5.57)$$

whereby $0 < h \lesssim 0.3$. In case of a double smoothing they suggested a nonlinear smoothing operator before each EM step so that a complete smoothed EM step reads as

$$x_j^{(k+1/3)} = \exp \left(\sum_{i=0}^{M-1} S_{ij}^{(h)} \log(x_j^{(k)}) \right) \quad (5.58)$$

$$x_j^{(k+2/3)} = x_j^{(k+1/3)} + \Delta x_j^{(k+1/3)} \quad (5.59)$$

$$x_j^{(k+1)} = \sum_{i=0}^{M-1} S_{ij}^{(h)} x_j^{(k+2/3)} \quad (5.60)$$

The proper choice of the parameter h arises and its selection might follow similar strategies than for the regularization parameter in ill-posed problems. In contrast to regularization methods in this iteration scheme there is not directly a cost function for strongly oscillating solution involved like the sum of first or second derivatives of the solution vector or the entropy of the solution vector like in maximum entropy methods. However, these quantity can easily be calculated from the solution vector. Figure 5.4 shows the logarithm of a roughness term, namely the sum of 1st and 2nd derivatives of the resulting size distribution and the entropy against the goodness-of-fit parameter from eq. 5.54, namely the “ \mathcal{G} -test” parameter. The optimum smoothing parameter has been defined via the corner of the L-curve defined by $(\log(\mathcal{G}), \log(\|\hat{\mathbf{L}}\mathbf{x}\|^2))$, with $\hat{\mathbf{L}}$ being the first or second-order discrete derivative operator defined in eq. 5.78 or 5.80 and by $(\log(\mathcal{G}), \log(S))$ with S being the entropy defined in eq. 5.61. The corners were

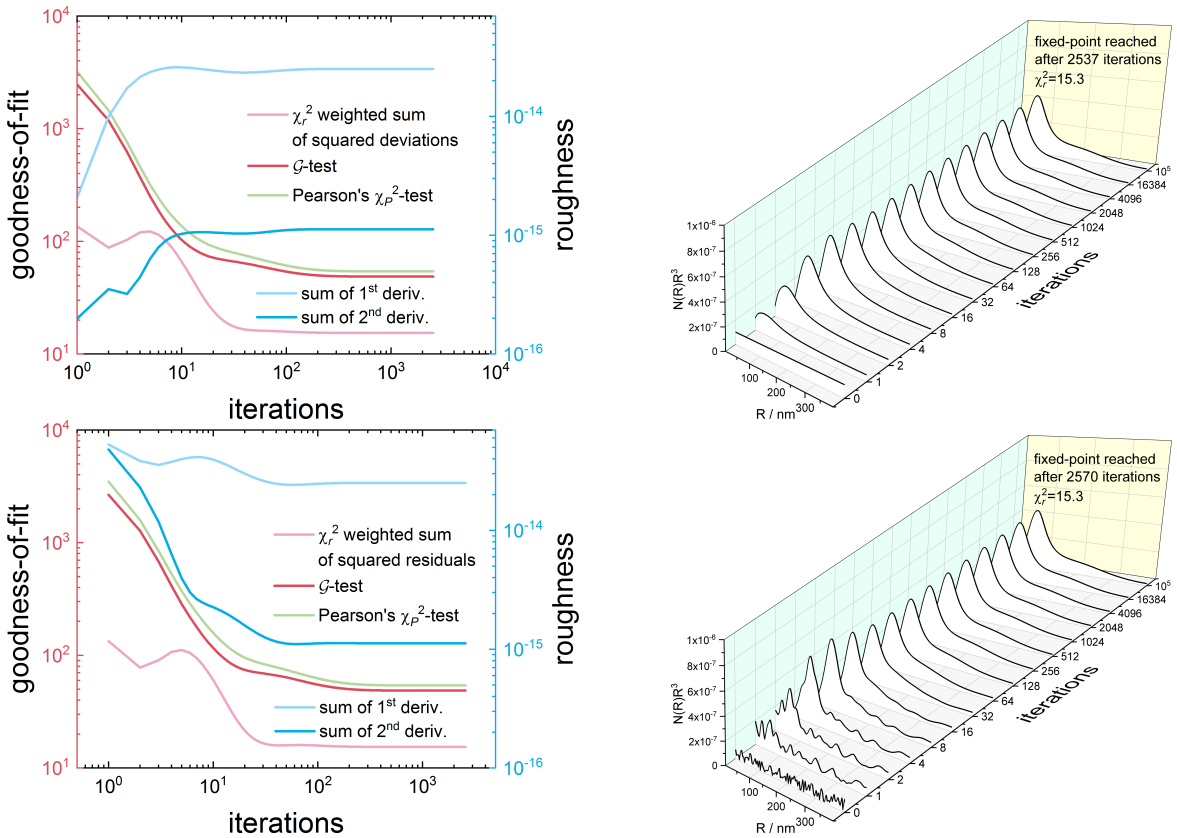


FIGURE 5.5. Roughness and goodness-of-fit parameters as well as the resulting volume distribution $N(R)R^3$ as a function of iterations for a constant seed value (top) and random seed values (bottom) for a large smoothing parameter $h = 0.3$ leading to $\chi_r^2 = 15.3$.

determined numerically as they are defined by having the maximum curvature. They are marked in fig. 5.7 by a symbols. The whole analysis does not make use of the uncertainties of the measured intensities. If the error bars are trustable and the model for the form factor is correct the weighted sum of squared residuals should be $\chi_r^2 = 1$. This can also be used as a condition for determining the smoothing parameter h . In the case of the present analysed data both strategies yield similar results as can be seen in fig. 5.8.

5.2.2. EM with maximum entropy regularization.

The Lucy-Richardson method [418, 317] has been extended by an additional penalty function, namely the entropy, by Lucy [318]. He introduces two variants, how the maximum entropy penalty can be introduced in the iteration algorithm by knowing either a fixed or assuming an adaptive prior for the solution vector. The entropy S is

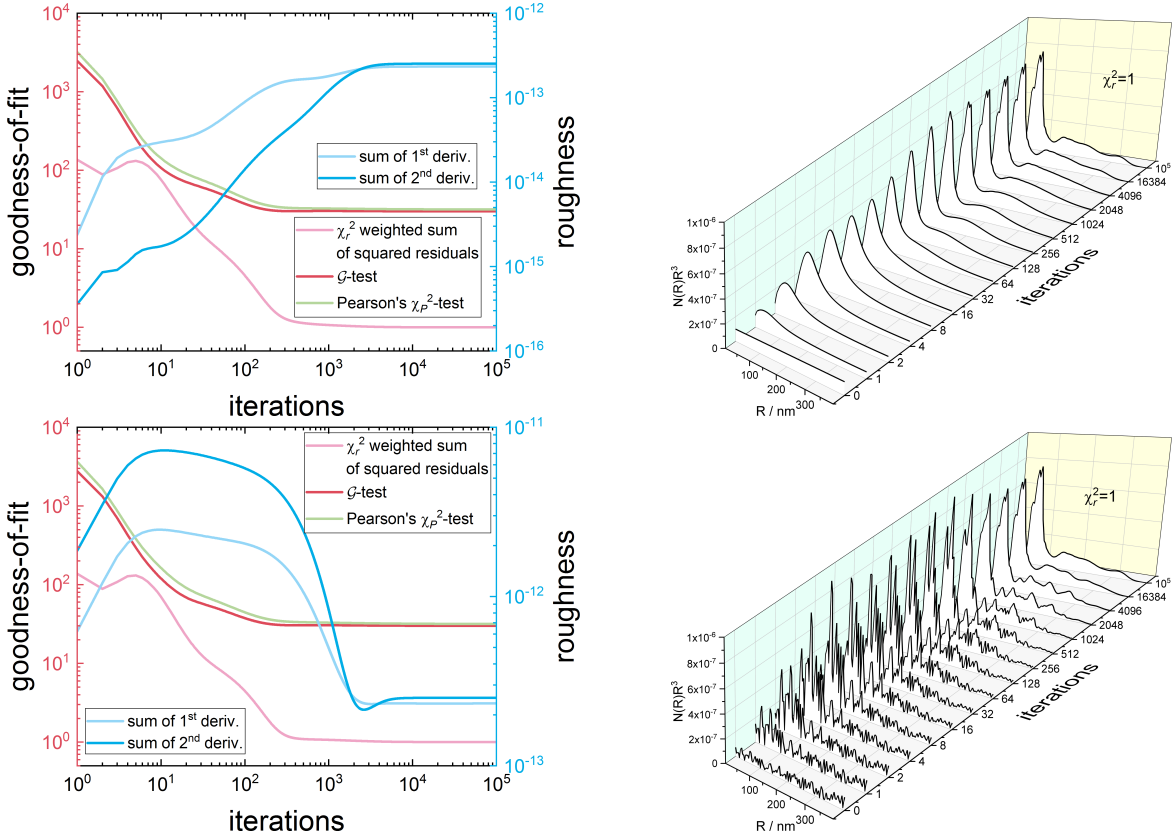


FIGURE 5.6. Roughness and goodness-of-fit parameters as well as the resulting volume distribution $N(R)R^3$ as a function of iterations for a constant seed value (top) and random seed values (bottom) for an optimum soothing parameter $h = 1.87 \times 10^{-4}$ leading to $\chi_r^2 = 1$.

given by

$$S = \sum_{j=0}^{N-1} -x_j \ln(x_j/m_j) + x_j - m_j \quad (5.61)$$

with \mathbf{m} being the prior estimate of \mathbf{x} . The update scheme in eq. 5.50 has to be extended as

$$x_j^{(k+1)} = x_j^{(k)} + \Delta x_j^{(k)} + \Delta s_j^{(k)} = \mathcal{O}_{\text{EM,ME,const}}[x_j^{(k)}] \quad (5.62)$$

with

$$\Delta x_j^{(k)} = x_j^{(k)} \left[\sum_{i=0}^{M-1} \frac{A_{ij}}{\left(\sum_{m=0}^{M-1} A_{mj} \right)} \frac{b_i}{\sum_{n=0}^{N-1} A_{in} x_n^{(k)}} - 1 \right] \quad (5.63)$$

$$\Delta s_j^{(k)} = \lambda x_j^{(k)} \left(-\ln \frac{x_j}{m_j} + \frac{1}{\sum_{j=0}^{N-1} x_j^{(k)}} \sum_{j=0}^{N-1} x_j^{(k)} \ln \frac{x_j^{(k)}}{m_j} \right) \quad (5.64)$$

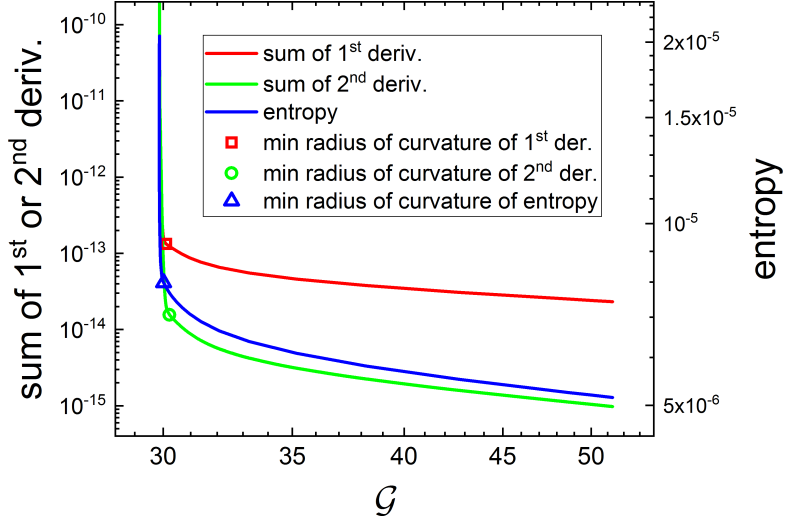


FIGURE 5.7. Optimum smoothing parameter h given by the corner of the L-curve.

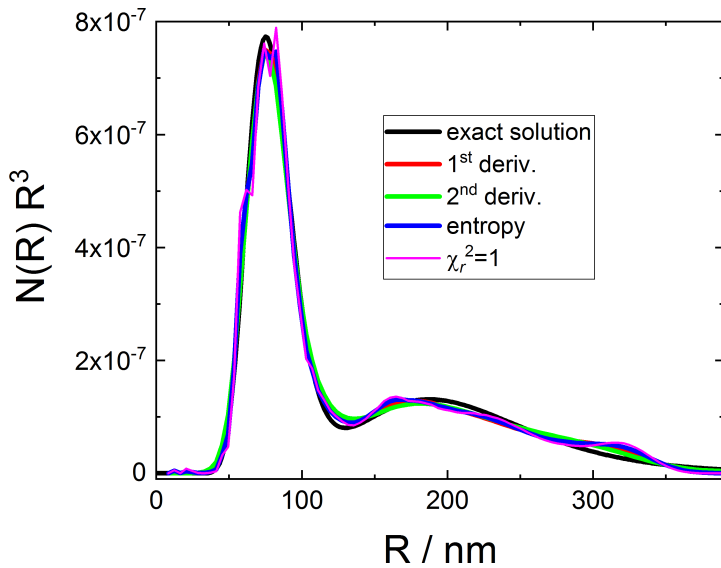


FIGURE 5.8. The smoothing parameters has been obtained by the corners of the L-curves in fig. 5.7 and the solution of the EM iteration scheme with double smoothing is compared with the exact solution.

in case of a known prior. If a prior is not known a constant prior can be chosen. However, even if no model for the prior is known, one can try to construct one adaptively according to Horne [221] by applying for example a Gaussian point spread function to the actual solution and using this as a prior for the next iteration step. In this case the update

scheme looks as

$$x_j^{(k+1)} = x_j^{(k)} + \Delta x_j^{(k)} + \Delta s_j^{(k)} = \mathcal{O}_{\text{EM,ME,adaptive}} \left[x_j^{(k)} \right] \quad (5.65)$$

$$\Delta x_j^{(k)} = x_j^{(k)} \left[\sum_{i=0}^{M-1} \frac{A_{ij}}{\left(\sum_{m=0}^{M-1} A_{mj} \right)} \frac{b_i}{\sum_{n=0}^{N-1} A_{in} x_n^{(k)}} - 1 \right] \quad (5.66)$$

$$\Delta s_j^{(k)} = \lambda x_j^{(k)} \left(-\ln \frac{x_j}{m_j^{(k)}} + \frac{1}{\sum_{j=0}^{N-1} x_j^{(k)}} \sum_{j=0}^{N-1} x_j^{(k)} \ln \frac{x_j^{(k)}}{m_j^{(k)}} - 1 + \sum_{i=0}^{N-1} \Pi_{ij} \frac{x_i^{(k)}}{m_i^{(k)}} \right) \quad (5.67)$$

$$m_i^{(k)} = \sum_{j=0}^{N-1} \Pi_{ij} x_j^{(k)} \quad (5.68)$$

As a smoothing operator for the prior

$$\Pi_{ij} = \frac{1}{c} \exp \left(-\frac{(i-j)^2}{2\sigma^2} \right) \quad (5.69)$$

has been assumed with the normalization constant $c = \sum_j \Pi_{ij}$ and a σ^2 typically between $\frac{1}{2}$ and 2. For large values of σ^2 the results converge to that one of a constant prior. For too small values the regularization is suppressed as the prior converges to the k^{th} iteration step.

The optimum regularization parameter λ can be determined similar to the previous section via the corner in the L-curve. The L-curves for both a constant and adaptive prior are shown in fig. 5.9 using the same data than shown in fig. 5.1. The optimum Lagrange parameter in the corner are marked with a symbol. The corresponding size distribution are shown in fig. 5.10 together with the exact solution and for a Lagrange parameter leading to $\chi_r^2 = 1$. From the L-curves in fig. 5.9 one can see, that the \mathcal{G} -test parameter for the constant prior varies over orders of magnitudes whereas for the adaptive prior also for a Lagrange parameter far away from its optimum value leads to a reasonable good result. Therefore the L-curve shows for the adaptive prior a much smaller range on the x -axis.

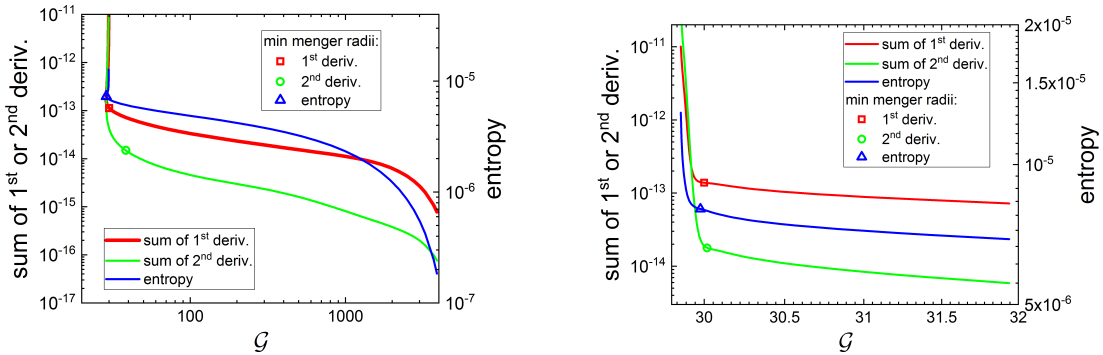


FIGURE 5.9. Determine optimum smoothing parameter λ by the corner of the L-curve, which is determined by a minimum radius of curvature. (left) constant prior, (right) adaptive prior

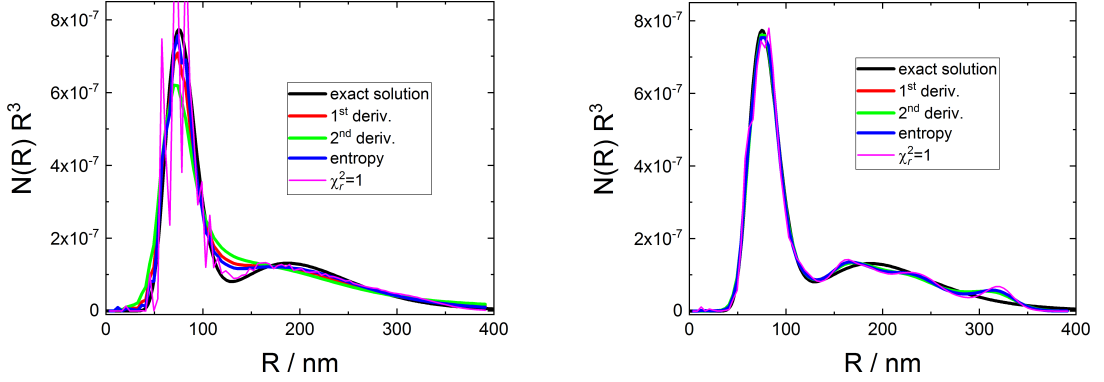


FIGURE 5.10. The smoothing parameters has been obtained by the corners of the L-curves in fig. 5.9 and the solution of the EM iteration scheme using Maximum Entropy term with constant and adaptive prior is compared with the exact solution as well as for a Lagrange parameter leading to weighted sum of squared residuals of $\chi_r^2 = 1$.

5.2.3. Acceleration of EM iteration scheme.

There exist several very efficient algorithms to increase the convergence rate of contractive fixed point operators. A few of them are listed below.

Lewitt et al. [300] have suggested to increase the convergence rate by introducing an overrelaxation parameter in the iteration loop

$$x_j^{(k+1)} = x_j^{(k)} + \lambda^{(k)} \Delta x_j^{(k)} \quad (5.70)$$

where $\lambda^{(k)}$ is the overrelaxation parameter ($\lambda^{(k)} > 1$) whose purpose is to accelerate the iterative process, and whose value is not so large as to violate the nonnegativity condition $x_j^{(k+1)} > 0$. To ensure that the overrelaxation of negative corrections to the solution vector does not decrease the value of any solution vector component below zero they suggest the following algorithm: first a pseudorelaxation parameter $\mu_j^{(k)}$ is calculated where

$$\mu_j^{(k)} = \begin{cases} \infty, & \text{if } x_j^{(k)} \geq 0 \\ \left| \frac{x_j^{(k)}}{\Delta x_j^{(k)}} \right|, & \text{otherwise.} \end{cases} \quad (5.71)$$

Then they defined a critical relaxation parameter as follows:

$$\hat{\lambda}^{(k)} = \min_j \mu_j^{(k)} \quad (5.72)$$

Finally the overrelaxation parameter $\lambda^{(k)}$ was chosen according to

$$\lambda^{(k)} = \min \left[\left(\hat{\lambda}^{(k)} - 1 \right) / 2, \lambda^{\max} \right] \quad (5.73)$$

with $\lambda^{\max} \simeq 4$ so that $1 \leq \lambda^{(k)} \leq \lambda^{\max}$.

Another more efficient method to accelerate the convergence rate of the EM iteration scheme is the so called Anderson acceleration [4] to solve fixed point problems (see also [515, 487]), which also has been suggested for the EM iteration scheme [211]. In **SASfit**

Algorithm 1 Biggs-Andrews vector extrapolation acceleration of order $o = 0, 1, 2$

```

1: procedure UPDATE_VECTORS( $\mathbf{g}^{(n-2)}, \mathbf{g}^{(n-1)}, \mathbf{x}^{(n+1)}, \mathbf{x}^{(n)}, \mathbf{x}^{(n-1)}, \mathbf{x}^{(n-2)}$ )
2:    $\mathbf{g}^{(n-2)} \leftarrow \mathbf{g}^{(n-1)}$ 
3:    $\mathbf{g}^{(n-1)} \leftarrow \mathbf{x}^{(n+1)} - \mathbf{x}^{(n)}$ 
4:    $\mathbf{x}^{(n-2)} \leftarrow \mathbf{x}^{(n-1)}$ 
5:    $\mathbf{x}^{(n-1)} \leftarrow \mathbf{x}^{(n)}$ 
6:    $\mathbf{x}^{(n)} \leftarrow \mathbf{x}^{(n+1)}$ 
7:   ▷ Acceleration of the fixed point operator  $\mathcal{O}[\mathbf{x}] = \mathbf{x}$ 
8: procedure BIGGS_ANDREWS_ACCELERATION( $\mathcal{O}[], \mathbf{x}^{(0)}, o$ )
9:    $\alpha \leftarrow 0$ 
10:   $\mathbf{x}^{(n)} \leftarrow \mathbf{x}^{(0)}$ 
11:   $\mathbf{x}^{(n+1)} \leftarrow \mathcal{O}[\mathbf{x}^{(n)}]$ 
12:  UPDATE_VECTORS( $\mathbf{g}^{(n-2)}, \mathbf{g}^{(n-1)}, \mathbf{x}^{(n+1)}, \mathbf{x}^{(n)}, \mathbf{x}^{(n-1)}, \mathbf{x}^{(n-2)}$ )
13:   $\mathbf{x}^{(n+1)} \leftarrow \mathcal{O}[\mathbf{x}^{(n)}]$ 
14:  UPDATE_VECTORS( $\mathbf{g}^{(n-2)}, \mathbf{g}^{(n-1)}, \mathbf{x}^{(n+1)}, \mathbf{x}^{(n)}, \mathbf{x}^{(n-1)}, \mathbf{x}^{(n-2)}$ )
15:   $\mathbf{y}^{(n)} \leftarrow \mathbf{x}^{(n+1)}$ 
16:  while ( $\mathcal{O}[]$  not converged) do
17:    ▷  $\alpha$  needs to be updated first
18:     $\alpha = \frac{(\mathbf{g}^{(n-1)})^T \mathbf{g}^{(n-2)}}{(\mathbf{g}^{(n-2)})^T \mathbf{g}^{(n-2)}}$ 
19:     $\alpha \leftarrow \max(\min(\alpha, 1), 0)$ 
20:     $\mathbf{x}^{(n+1)} \leftarrow \mathcal{O}[\mathbf{y}^{(n)}]$ 
21:    ▷ guess of next virtual step  $\mathbf{y}^{(n)}$  calculated up to  $o^{\text{th}}$ -order
22:    if  $\alpha = 0 \wedge o = 0$  then
23:       $\mathbf{y}^{(n)} \leftarrow \mathbf{x}^{(n)}$ 
24:    else if  $\alpha > 0 \vee o = 1$  then
25:       $\mathbf{y}^{(n)} \leftarrow \mathbf{x}^{(n)} + \alpha (\mathbf{x}^{(n)} - \mathbf{x}^{(n-1)})$ 
26:    else
27:       $\mathbf{y}^{(n)} \leftarrow \mathbf{x}^{(n)} \mathbf{x}^{(n)} + \alpha (\mathbf{x}^{(n)} - \mathbf{x}^{(n-1)}) + \frac{\alpha^2}{2} (\mathbf{x}^{(n)} + 2\mathbf{x}^{(n-1)} - \mathbf{x}^{(n-2)})$ 
28:    ▷ now all the other temporary vectors are updated
29:  UPDATE_VECTORS( $\mathbf{g}^{(n-2)}, \mathbf{g}^{(n-1)}, \mathbf{x}^{(n+1)}, \mathbf{x}^{(n)}, \mathbf{x}^{(n-1)}, \mathbf{x}^{(n-2)}$ )

```

several fixed point accelerations are supplied by making use of the sundials library [213]. However, only the supplied Anderson acceleration speeds up the fixed point iterations whereas all the others like GMRES [430], FGMRES [429], Bi-CGStab [496] or TFQMR [136] become instable and do not converge.

In [37, 36, 35, 517, 243] an acceleration process has been suggested basing on vector extrapolation which does not require an extra evaluation of the fixed point operator \mathcal{O}_{EM} in eq. 5.50. The method just needs to remember one or two previous solution vectors for calculating either the first or additionally the second derivative for guessing the next virtual solution vector, which is then used as an input vector for the next step of the fixed point iteration. The algorithm is described in alg. 1. The convergence behaviour of the different acceleration schemes are shown in fig. 5.11. Quite good acceleration has been achieved by the Biggs-Andrews method as well as Anderson acceleration, whereas other classical methods like GMRES, Bi-CGSab or TFQMR failed. The Picard iteration scheme and overrelaxation method need orders of magnitudes more iterations to reach the true fixed point solution. The preferred acceleration scheme therefore becomes the Biggs-Andrews methods.

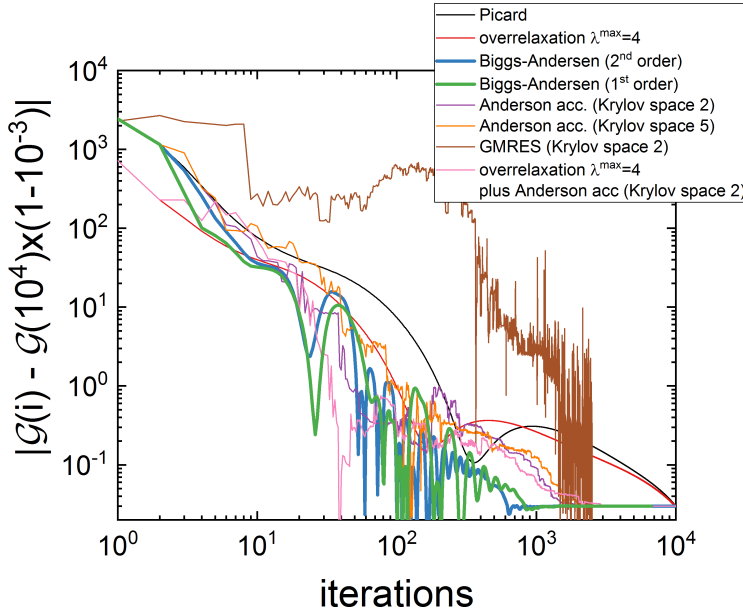


FIGURE 5.11. Convergence behaviour of a few acceleration schemes compared to the non-accelerated Picard iteration.

5.3. Linear least square regularization (LLS)

Linear least square regularization has been implemented using the GNU scientific library (**gs1**). It supplies routines to solve ill-posed problems including a regularization term in the least squares minimization

$$\chi^2 = \|\mathbf{b} - \hat{\mathbf{A}}\mathbf{x}\|_w^2 + \lambda^2 \|\hat{\mathbf{L}}\mathbf{x}\|^2 \quad (5.74)$$

Here $\|\dots\|_w^2$ denotes the weighted sum of squared residuals

$$\|\hat{\mathbf{A}}\mathbf{x} - \mathbf{b}\|_w^2 = (\mathbf{x}^T \hat{\mathbf{A}}^T \hat{\mathbf{w}}^T - \mathbf{b}^T \hat{\mathbf{w}}^T) (\hat{\mathbf{w}} \hat{\mathbf{A}} \mathbf{x} - \hat{\mathbf{w}} \mathbf{b}) \quad (5.75)$$

$$= \mathbf{x}^T \hat{\mathbf{A}}^T \hat{\mathbf{w}}^T \hat{\mathbf{w}} \hat{\mathbf{A}} \mathbf{x} - 2\mathbf{x}^T \hat{\mathbf{A}}^T \hat{\mathbf{w}}^T \hat{\mathbf{w}} \mathbf{b} + \mathbf{b}^T \hat{\mathbf{w}}^T \hat{\mathbf{w}} \mathbf{b} \quad (5.76)$$

with

$$\hat{\mathbf{w}} = \begin{pmatrix} \frac{1}{\Delta b_0} & 0 & \dots & 0 \\ 0 & \frac{1}{\Delta b_1} & \dots & 0 \\ \vdots & \vdots & \ddots & \vdots \\ 0 & 0 & \dots & \frac{1}{\Delta b_{M-1}} \end{pmatrix} \quad (5.77)$$

where Δb_i are the experimental errors (standard deviation, Gaussian error or root-mean-square error) of the measured quantities b_i . $\hat{\mathbf{L}}$ describes the penalty contribution and λ is the regularization parameter. To determine a suitable value for it automatically several routines are supplied in the **gs1** library. Several choices for the penalty term $\hat{\mathbf{L}}$ are supplied. In the simplest case the penalty term is the identity matrix $\hat{\mathbf{L}} = \hat{\mathbf{I}}$ so that the overall length of the solution vector is also tried to be minimized. As a second choice

for the penalty term is the first-order discrete derivative operator [111]

$$\hat{\mathbf{L}}_{1^{\text{st}}} = \begin{pmatrix} -1 & 1 & & \\ & \ddots & \ddots & \\ & & -1 & 1 \end{pmatrix} \in \mathbb{R}^{(N-1) \times N} \quad (5.78)$$

Since nonsingular regularization matrices are easier to handle than singular ones a common approach is to use small perturbations. If the perturbation is small enough the smoothing property is not deteriorated significantly. With a small diagonal element $\epsilon > 0$

$$\hat{\mathbf{L}}_{1^{\text{st}}} = \begin{pmatrix} \epsilon & & & \\ -1 & 1 & & \\ & \ddots & \ddots & \\ & & -1 & 1 \end{pmatrix} \text{ or } \hat{\mathbf{L}}_{1^{\text{st}}} = \begin{pmatrix} -1 & 1 & & \\ & \ddots & \ddots & \\ & & -1 & 1 \\ & & & \epsilon \end{pmatrix} \in \mathbb{R}^{N \times N} \quad (5.79)$$

The additional element ϵ forces either the first or last element to have small magnitude. A further common regularization matrix is the discrete second-order derivative [111] operator

$$\hat{\mathbf{L}}_{2^{\text{n}}} = \begin{pmatrix} -1 & 2 & -1 & & \\ & \ddots & \ddots & \ddots & \\ & & -1 & 2 & -1 \end{pmatrix} \in \mathbb{R}^{(N-2) \times N} \quad (5.80)$$

Also for this case a nonsingular squared matrix can be used as an approximation by adding one row at the top and one row at the bottom and assuming either Dirichlet boundary conditions or Neumann boundary conditions

$$\hat{\mathbf{L}}_{2^{\text{nd}}}^{\text{DD}} = \begin{pmatrix} 2 & -1 & & \\ -1 & 2 & -1 & \\ & \ddots & \ddots & \ddots & \\ & & -1 & 2 & -1 \\ & & & -1 & 2 \end{pmatrix} \in \mathbb{R}^{N \times N} \quad (5.81)$$

or

$$\hat{\mathbf{L}}_{2^{\text{nd}}}^{\text{NN}} = \begin{pmatrix} 1 & -1 & & \\ -1 & 2 & -1 & \\ & \ddots & \ddots & \ddots & \\ & & -1 & 2 & -1 \\ & & & -1 & 1 \end{pmatrix} \in \mathbb{R}^{N \times N} \quad (5.82)$$

Also mixed boundary condition with Dirichlet boundary condition at the left end point and the Neumann boundary condition at the right one or vice versa.

$$\hat{\mathbf{L}}_{2^{\text{nd}}}^{\text{ND}} = \begin{pmatrix} 2 & -1 & & \\ -1 & 2 & -1 & \\ \ddots & \ddots & \ddots & \\ & -1 & 2 & -1 \\ & & -1 & 1 \end{pmatrix} \in \mathbb{R}^{N \times N} \quad (5.83)$$

or

$$\hat{\mathbf{L}}_{2^{\text{nd}}}^{\text{DN}} = \begin{pmatrix} 1 & -1 & & \\ -1 & 2 & -1 & \\ \ddots & \ddots & \ddots & \\ & -1 & 2 & -1 \\ & & -1 & 2 \end{pmatrix} \in \mathbb{R}^{N \times N} \quad (5.84)$$

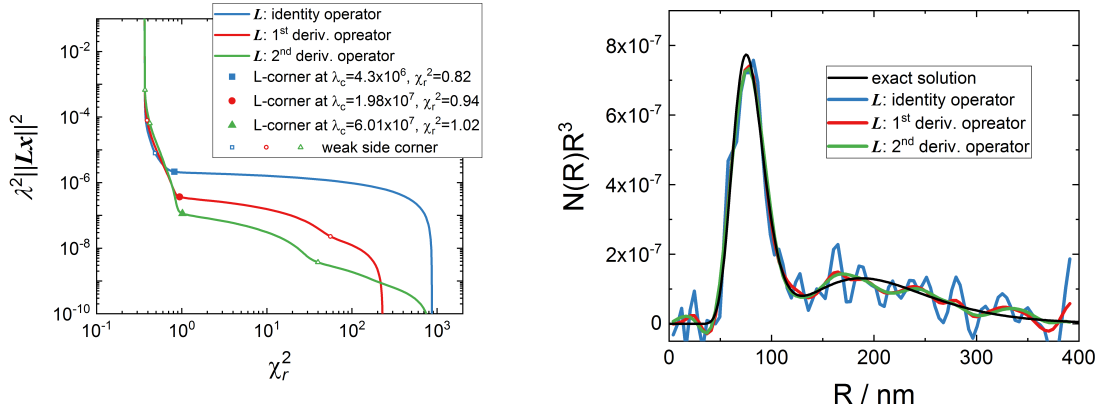


FIGURE 5.12. The optimum Lagrange parameters λ_c have been obtained by the corners of the L-curves for $\hat{\mathbf{L}} = \hat{\mathbf{1}}$, $\hat{\mathbf{L}} = \hat{\mathbf{L}}_{1^{\text{st}}}$ and $\hat{\mathbf{L}} = \hat{\mathbf{L}}_{2^{\text{nd}}}$.

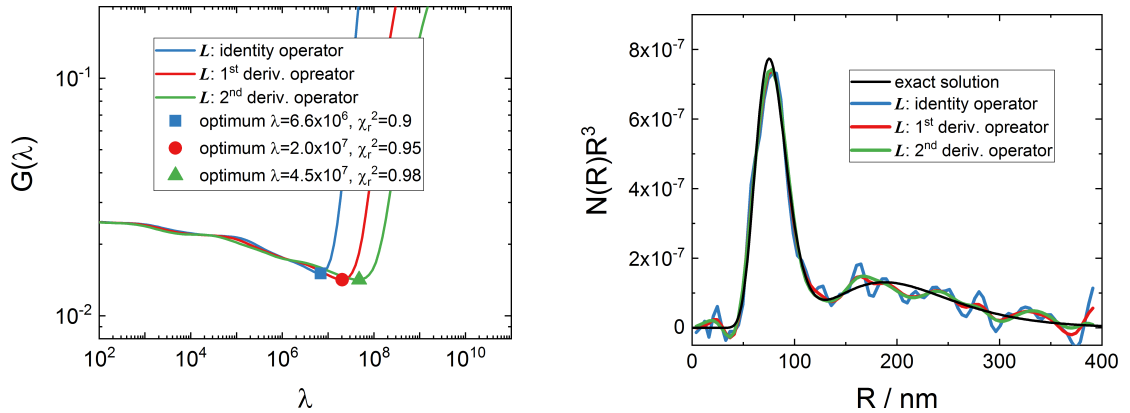


FIGURE 5.13. The optimum Lagrange parameters λ have been obtained by minimizing the “Generalized Cross Validation” function.

5.4. Non-negative linear least square regularization (NNLLS)

The non-negative linear least square solver used here is taken from [288] and are also available at netlib under <http://www.netlib.org/lawson-hanson/> as Fortran source code which has been translated to C by f2c. **SASfit** is using this routine to solves the same ill-posed problems including a regularization term as in eq. 5.74 of section 5.3 just with an additional constrain of non-negativity.

5.5. Chahine inversion scheme

Obtaining particle size distributions from forward scattered light using the Chahine inversion scheme has been introduced by [432] and later on applied to SANS by [448].

CHAPTER 6

Numerical solutions of the Ornstein Zernike equations

During an internship project in summer 2013 Evgeniy Ponomarev has implemented the core routine for solving the Ornstein Zernike equations. This algorithm numerically calculates structure factors $S(q)$, radial distribution functions $g(r)$ and direct correlation functions $c(r)$ of a systems with known pair interaction potential $U(r)$.

6.1. Background

The central part of this package is iterative solution of Ornstein-Zernike equation [366]. The theoretical background can be found in great detail in [355, 48, 192, 44, 74, 302]. The Ornstein-Zernike equation reads

$$h(\mathbf{r}_{12}) = c(\mathbf{r}_{12}) + \int c(\mathbf{r}_{13})\rho(\mathbf{r}_3)h(\mathbf{r}_{32})d\mathbf{r}_3 + \dots \quad (6.1)$$

where $h(\mathbf{r}_{12})$ is the total correlation function, $c(\mathbf{r}_{12})$ the direct correlation function (direct effect of particle 1 on particle 2), $c(\mathbf{r}_{13})$ the in direct correlation function describing the effect of particle 1 on particle 3 which influences particle 2, and ρ the particle number density of the colloids, molecules, or atoms that form the liquid. If the fluid is uniform and isotropic, the Ornstein-Zernike relation becomes

$$h(r) = c(r) + \rho \int c(|\mathbf{r} - \mathbf{r}'|)h(r')d\mathbf{r}' \quad (6.2)$$

$$= c(r) + \gamma(r) \quad (6.3)$$

The basic idea of this equation is that total correlation between positions of two particles is a combination of their direct and indirect (through neighboring particles) interactions. The first contribution to $h(r)$ is the direct correlation function $c(r)$ that represents the correlation between a particle of a pair with its closest neighbor separated by a distance r . The second contribution is the indirect correlation function $\gamma(r)$, which represents the correlation between the selected particle of the pair with the rest of the fluid constituents.

$g(r)$ is known as the radial or pair distribution function, which measures the probability that given a particle at the origin, another particle of the fluid can be found at a distance r from it. When the distance separating a pair of particles tends to infinity, the correlations vanish and $g(r)$ tends to 1. This means that the total correlation function defined as $h(r) = g(r) - 1$ tends to 0. The Fourier transform $\mathcal{F}\{\}$ of $g(r)$ and $h(r)$ are directly related to the structure factor $S(q)$ that is experimentally measurable by x-ray or neutron scattering

$$S(q) = 1 + \rho \int [g(r) - 1] \exp(-i\mathbf{q} \cdot \mathbf{r}) d\mathbf{r} \quad (6.4)$$

and

$$S(q) = 1 + \rho \tilde{h}(q) \quad (6.5)$$

where $\tilde{h}(q) = \mathcal{F}\{h(r)\}$ is the Fourier transform of the total correlation function $h(r)$, so that

$$\tilde{h}(q) = \int h(r) \exp(-\imath \mathbf{q} \cdot \mathbf{r}) dr \quad (6.6)$$

Via inverse Fourier transform $\mathcal{F}^{-1}\{\}$ of the structure factor the pair correlation function is obtained

$$\rho [g(r) - 1] = \mathcal{F}^{-1}\{S(q) - 1\} = \frac{1}{(2\pi)^3} \int (S(q) - 1) \exp(\imath \mathbf{q} \cdot \mathbf{r}) d\mathbf{q} \quad (6.7)$$

As for $g(r)$ also the direct correlation function $c(r)$ can be, in principle, derived from experiment as

$$\rho c(r) = \frac{1}{(2\pi)^3} \int \left(1 - \frac{1}{S(q)}\right) \exp(\imath \mathbf{q} \cdot \mathbf{r}) d\mathbf{q} \quad (6.8)$$

or

$$S(q) = \frac{1}{1 - \rho \tilde{c}(q)} \quad (6.9)$$

By Fourier transformation of eq. 6.2, one obtains

$$\tilde{h}(q) = \frac{\tilde{c}(q)}{1 - \rho \tilde{c}(q)} \quad (6.10)$$

where $\tilde{c}(q) = \mathcal{F}\{c(r)\}$ is the Fourier Transform of $c(r)$. In order to determine the two correlation functions $h(r)$ and $c(r)$ for a given pair potential $u(r)$, eq. 6.2 must be supplemented by an auxiliary closure relation. Furthermore the Fourier transform of eq. 6.3 in combination with eq. 6.10 allows to write the Fourier transform of the indirect correlation function as

$$\mathcal{F}\{\gamma(r)\} = \tilde{\gamma}(q) = \tilde{h}(q) - \tilde{c}(q) = \frac{\rho \tilde{c}^2(q)}{1 - \rho \tilde{c}(q)} \quad (6.11)$$

The closure is not complete as long the bridge function is unknown. Even though the bridge function is exactly defined the function is an unknown function of interparticle distance and only approximations can be given. The direct correlation function can be written in terms of the indirect correlation function, the interaction potential and the bridge function as

$$\begin{aligned} c(r) &= \exp[-\beta u(r) + \gamma(r) + B(r)] - \gamma(r) - 1 \\ &= g(r) - \gamma(r) - 1 \end{aligned} \quad (6.12)$$

$$\text{and } h(r) + 1 = g(r) = \exp[-\beta u(r) + \gamma(r) + B(r)] \quad (6.13)$$

where $u(r)$ is the pair interaction potential, $\beta = 1/(k_B T)$ the inverse temperature, with k_B being Boltzmann's constant, T is the absolute temperature, $\gamma(r)$ being the indirect correlation function and ρ is the number density of the molecules or atoms that form the liquid. $B(r)$ is the bridge function. The analytic expression of $B(r)$ is, in general, unknown. Unfortunately, the bridge function has to be approximated in practice. Though a number of theoretical and simulation procedures have been derived in recent years in order to get an approximate estimate of $B(r)$ for different fluid models, the exact bridge function is not known for any system.

6.2. Numerical implementation of the iterative algorithm in SASfit

The easiest algorithm for solving the Ornstein Zernike (OZ) equation 6.2 together with the closure equation 6.12 is direct iteration using fast Fourier transformation (see e.g. [219]). The solution of the OZ equations can be treated either as a fixed point problem for the unknown function $\gamma(r)$, so that $T_f^{\text{OZ}}(\gamma) = \gamma$ or as a multidimensional root finding problem $F_r^{\text{OZ}}(\gamma) = T_f^{\text{OZ}}(\gamma) - \gamma = 0$. In SASfit the fix point problem $T_f^{\text{OZ}}(\gamma) = \gamma$ is implemented as:

- (1) using a starting value for $\gamma(r)$, e.g. set $\gamma(r) \equiv 0$
- (2) Calculate a bridge function. Many different theories how to calculate the bridge function have been published. A few of them are described in the next section. The bridge function is often expressed in terms of the known potential $u(r)$ and the indirect correlation function $\gamma(r)$, which needs to be determined.
- (3) Calculate the direct correlation function according to eq. 6.12.
- (4) Calculate the Fourier transform $\tilde{c}(q)$ of the direct correlation function.
- (5) Use eq. 6.11 to get $\tilde{\gamma}(q)$.
- (6) Calculate the inverse Fourier transform of $\tilde{\gamma}(q)$ to get the new guess for $\gamma(r)$.

In the above algorithm to iteratively solve the Ornstein-Zernike equation two Fourier transforms have to be performed:

$$c(r) \xrightarrow{\mathcal{F}\{\cdot\}} \tilde{c}(q) \quad (\text{in step 4}) \quad (6.14)$$

$$\tilde{\gamma}(q) \xrightarrow{\mathcal{F}^{-1}\{\cdot\}} \gamma(r) \quad (\text{in step 6}) \quad (6.15)$$

As we assume that the system is isotropic, i.e. $c(r)$ and $\gamma(r)$ are only functions of the modulus of $|\mathbf{r}| = r$ the Fourier transforms can be written as

$$\tilde{c}(q) = \int c(r) \exp(-i\mathbf{q} \cdot \mathbf{r}) dr = \int_0^\infty 4\pi r^2 c(r) \frac{\sin(qr)}{qr} dr \quad (6.16)$$

$$\gamma(r) = \frac{1}{(2\pi)^3} \int \tilde{\gamma}(q) \exp(i\mathbf{q} \cdot \mathbf{r}) d\mathbf{q} = \frac{1}{(2\pi)^3} \int_0^\infty 4\pi q^2 \tilde{\gamma}(q) \frac{\sin(qr)}{qr} dq \quad (6.17)$$

To calculate these transforms numerically on a discrete grid of points one has to substitute the integration by a summation. Herby $\int_0^\infty dr$ is replaced by $\sum_{j=0}^{N_p-1} \Delta r$, $r_j = (j+1)\Delta r$, $q_j = (j+1)\Delta q$, and $\int_0^\infty dq$ is replaced by $\sum_{j=0}^{N_p-1} \Delta q$. The step width Δr in real space has to be defined by the user as well as the number of grid points N_p . The step width in reciprocal space is than obtained by $\Delta q = \frac{\pi}{(N_p+1)\Delta r}$. It is important to mention that the values of the first elements of the arrays r_i and k_i equals Δr and Δq , respectively ($r_0 = \Delta r$, $q_0 = \Delta q$).

$$\tilde{c}_i = \frac{4\pi\Delta r^2}{(i+1)\Delta q} \sum_{j=0}^{N_p-1} c_j(j+1) \sin\left(\frac{\pi(j+1)(i+1)}{N_p+1}\right) \quad (6.18)$$

$$\gamma_i = \frac{1}{(2\pi)^3} \frac{4\pi\Delta q^2}{(i+1)\Delta r} \sum_{j=0}^{N_p-1} \tilde{\gamma}_j(j+1) \sin\left(\frac{\pi(j+1)(i+1)}{N_p+1}\right) \quad (6.19)$$

For calculating the Fourier transformation the library FFTW for fast fourier transformation [139, 138] has been used. The library (source code available at <http://www.fftw.org/>) supplies a discrete sin transformation (type-I DST) named FFTW_RODFT00 which is doing the transformation

$$Y_k = 2 \sum_{j=0}^{N_p-1} X_j \sin \left(\frac{\pi(j+1)(k+1)}{N_p + 1} \right) \quad (6.20)$$

The unnormalized inverse of FFTW_RODFT00 is FFTW_RODFT00 itself. The same routine can be used for both transformations.

For the fix point problem $T_f^{\text{OZ}}(\gamma) = \gamma$ several iteration schemes are implemented. Tests have shown, that one can not easily make a prediction which one converges fastest or in case of e.g. very high volume or strong attraction converges at all. Next to some simple iteration schemes also a the very efficient Anderson Acceleration for fixed-point iteration [4, 515, 487] has been implemented.

The following iteration schemes are implemented:

Picard iteration [389]:

$$\gamma_{n+1} = T_f^{\text{OZ}}(\gamma_n) \quad (6.21)$$

Krasnoselskij iteration [277]:

$$\gamma_{n+1} = (1 - \alpha)\gamma_n + \alpha T_f^{\text{OZ}}(\gamma_n) \quad (6.22)$$

with $\alpha \in (0, 1]$ beeing a constant independent of n

Mann iteration [326]:

$$\gamma_{n+1} = (1 - \alpha_n)\gamma_n + \alpha_n T_f^{\text{OZ}}(\gamma_n) \quad (6.23)$$

with $\alpha_n \in (0, 1]$

Picard-Mann hybrid iteration (PMH) [264]:

$$y_n = (1 - \beta_n)\gamma_n + \beta_n T_f^{\text{OZ}}(\gamma_n) \quad (6.24)$$

$$\gamma_n = T_f^{\text{OZ}}(y_n) \quad (6.25)$$

with $\beta_n \in (0, 1]$

Mann II iteration [252]:

$$y_n = (1 - \beta_n)\gamma_n + \beta_n T_f^{\text{OZ}}(\gamma_n) \quad (6.26)$$

$$\gamma_n = (1 - \alpha_n)y_n + \alpha_n T_f^{\text{OZ}}(y_n) \quad (6.27)$$

with $\alpha_n, \beta_n \in (0, 1]$

S iteration [253, 1]:

$$y_n = (1 - \beta_n)\gamma_n + \beta_n T_f^{\text{OZ}}(\gamma_n) \quad (6.28)$$

$$\gamma_n = (1 - \alpha_n)T_f^{\text{OZ}}(\gamma_n) + \alpha_n T_f^{\text{OZ}}(y_n) \quad (6.29)$$

with $\alpha_n, \beta_n \in (0, 1]$

Ishikawa iteration [233]:

$$y_n = (1 - \beta_n)\gamma_n + \beta_n T_f^{\text{OZ}}(\gamma_n) \quad (6.30)$$

$$\gamma_n = (1 - \alpha_n)\gamma_n + \alpha_n T_f^{\text{OZ}}(y_n) \quad (6.31)$$

with $\alpha_n, \beta_n \in (0, 1]$

SP iteration [388]:

$$z_n = (1 - \xi_n)x_n + \xi_n T_f^{\text{OZ}}(\gamma_n) \quad (6.32)$$

$$y_n = (1 - \beta_n)z_n + \beta_n T_f^{\text{OZ}}(z_n) \quad (6.33)$$

$$\gamma_n = (1 - \alpha_n)y_n + \alpha_n T_f^{\text{OZ}}(y_n) \quad (6.34)$$

with $\alpha_n, \beta_n, \xi_n \in (0, 1]$

Noor iteration [360]:

$$z_n = (1 - \xi_n)x_n + \xi_n T_f^{\text{OZ}}(\gamma_n) \quad (6.35)$$

$$y_n = (1 - \beta_n)x_n + \beta_n T_f^{\text{OZ}}(z_n) \quad (6.36)$$

$$\gamma_n = (1 - \alpha_n)x_n + \alpha_n T_f^{\text{OZ}}(y_n) \quad (6.37)$$

with $\alpha_n, \beta_n, \xi_n \in (0, 1]$

CR iteration [90]:

$$z_n = (1 - \xi_n)x_n + \xi_n T_f^{\text{OZ}}(\gamma_n) \quad (6.38)$$

$$y_n = (1 - \beta_n)T_f^{\text{OZ}}(\gamma_n) + \beta_n T_f^{\text{OZ}}(z_n) \quad (6.39)$$

$$\gamma_n = (1 - \alpha_n)y_n + \alpha_n T_f^{\text{OZ}}(y_n) \quad (6.40)$$

with $\alpha_n, \beta_n, \xi_n \in (0, 1]$

Picard-S iteration [180]:

$$z_n = (1 - \beta_n)x_n + \beta_n T_f^{\text{OZ}}(\gamma_n) \quad (6.41)$$

$$y_n = (1 - \alpha_n)T_f^{\text{OZ}}(\gamma_n) + \alpha_n T_f^{\text{OZ}}(z_n) \quad (6.42)$$

$$\gamma_n = T_f^{\text{OZ}}(y_n) \quad (6.43)$$

with $\alpha_n, \beta_n \in (0, 1]$

S* iteration [253]:

$$z_n = (1 - \xi_n)x_n + \xi_n T_f^{\text{OZ}}(\gamma_n) \quad (6.44)$$

$$y_n = (1 - \beta_n)T_f^{\text{OZ}}(\gamma_n) + \beta_n T_f^{\text{OZ}}(z_n) \quad (6.45)$$

$$\gamma_n = (1 - \alpha_n)T_f^{\text{OZ}}(\gamma_n) + \alpha_n T_f^{\text{OZ}}(y_n) \quad (6.46)$$

with $\alpha_n, \beta_n, \xi_n \in (0, 1]$

α_n , β_n , and ξ_n are series of constants between $(0; 1]$. In **SASfit** the parameters α_n , β_n , and ξ_n have been chosen to be the same for each iteration n . Furthermore two series schemes have been implemented. The starting values for $n = 0$ of the series is the modulus of the mixing parameter m_{mix} , which can be changed in the GUI. The default value is $+0.5$. As $\alpha_n, \beta_n, \xi_n \in (0, 1]$ the series is in **SASfit** is defined for positive mixing parameters as $\alpha_n = \beta_n = \xi_n = (1 - m_{\text{mix}}) \exp(-\log_{10}(\|T_f^{\text{OZ}}(\gamma_n) - \gamma_n\|/\Delta_{\text{rel}})) + m_{\text{mix}}$ where Δ_{rel} is a user defined relative iteration precision. The default value is $\Delta_{\text{rel}} = 10^{-12}$. If one supplies a negative mixing parameter the series is defined as $\alpha_n = \beta_n = \xi_n = -m_{\text{mix}} + (i_n/i_{\text{max}})(1 + m_{\text{mix}})$. **SASfit** uses for the moment $i_{\text{max}} = 20$. i_n is incremented by 1 in case the relative error has been reduced and decremented by 1 if the relative error

increased in one iteration step. Decrementation and incrementation is only performed in the interval $[0, i_{\max}]$.

Instead of solving the OZ-fixed point problem $T_f^{\text{OZ}}(\gamma) = \gamma$ one can also use multi-dimensional root-finding algorithms for solving $F_r^{\text{OZ}}(\gamma) = T_f^{\text{OZ}}(\gamma) - \gamma = 0$. Some root finding algorithms are supplied from the gnu scientific library gsl for functions without derivatives namely the Hybrid algorithm which replaces calls to the Jacobian function by its finite difference approximation (**Hybrid**), a finite difference version of the Hybrid algorithm without internal scaling (**Hybrids (int. sc.)**), the discrete Newton algorithm (**dNewton**), and the Broyden algorithm (**Broyden**). All of them have the disadvantage to fill a Jacobian matrix and to calculate its inverse.

Next to the gsl root finding algorithms also several very efficient nonlinear system solver based on Newton-Krylov solver technology, like GMRES (Generalized Minimal RESidual)[[430](#), [260](#)], FGMRES (Flexible Generalized Minimal RESidual) [[429](#)], Bi-CGStab (Bi-Conjugate Gradient Stabilized) [[496](#), [260](#)], and TFQMR (Transpose-Free Quasi-Minimal Residual) [[136](#), [260](#)] are supplied. The nonlinear system solver are supplied using the "kinsol" library which is part of the SUNDIALS package [[213](#)] available at <https://computation.llnl.gov/casc/sundials/main.html>

Test have shown that either the Anderson acceleration, GMRES or FGMRES seems to be the most efficient algorithm to solve the Ornstein-Zernike with a minimum number of calls to the procedure evaluating the self consistent operator $F_r^{\text{OZ}}(\gamma)$ or $T_f^{\text{OZ}}(\gamma)$. The best choice for the iteration method depends often on the problem, i.e. the type of closure and the potential and also on the volume fraction. Therefore there are still all methods mentioned above available, which might change after getting some more experience with them.

6.3. Thermodynamic Parameters and Consistency Tests

Thermodynamic consistencies have been an important tool finding a good bridge function. The Ornstein-Zenike equations in combination with a closure relation enable us to calculate the direct $c(r)$ and total $h(r)$ correlation function as well as the pair distribution function $g(r)$. From these functions thermodynamic properties via different routes can be calculated.

The thermodynamic routes are:

compressibility route:

$$\left(\frac{\beta \partial P}{\partial \rho} \right)_T = (\rho k_B T \kappa_T)^{-1} \Leftrightarrow \kappa_T = \frac{1}{\rho} \left(\frac{\partial P}{\partial \rho} \right)_T^{-1} \quad (6.47)$$

The compressibility can also be related to the static structure factor in the long-wavelength limit:

$$\begin{aligned}\kappa_T &= \frac{\beta}{\rho} \left[1 + \rho \int 4\pi r^2 h(r\rho, T) dr \right] \\ &= \frac{\beta}{\rho} \left[1 + \rho \int 4\pi r^2 [g(r; \rho, T) - 1] dr \right] \\ &= \frac{\beta}{\rho} \left[1 - \rho \int 4\pi r^2 c(r) dr \right]^{-1} \\ &= \frac{\beta}{\rho} S(q = 0, \rho, T)\end{aligned}\tag{6.48}$$

energy route:

The internal energy U is

$$U = U_{\text{id}} + U_{\text{ex}}\tag{6.49}$$

where $U_{\text{id}} = \frac{3}{2}Nk_B T$ is the internal energy of an ideal gas and the excess internal energy per particle is given by

$$\frac{U_{\text{ex}}}{N} = 2\pi\rho \int g(r)u(r)r^2 dr\tag{6.50}$$

The excess internal energy U_{ex} is related to the excess Helmholtz free energy F_{ex} by

$$U_{\text{ex}} = \left(\frac{\partial \beta F_{\text{ex}}}{\partial \beta} \right)_V\tag{6.51}$$

The excess pressure P_{ex} ($P = P_{\text{id}} + P_{\text{ex}}$ and $P_{\text{id}} = \rho/\beta$) is than obtained as

$$P_{\text{ex}} = -\frac{\partial F_{\text{ex}}}{\partial V}\tag{6.52}$$

where $\beta F_{\text{ex}} = \int_0^\beta U(\beta', \rho) d\beta'$.

virial route:

The pressure or virial equation is given as

$$\frac{\beta P}{\rho} = 1 + \frac{2}{3}\beta\pi\rho \int g(r)r^3 \frac{du(r)}{dr} dr\tag{6.53}$$

where $\rho = N/V$ is the average number density of particles in the system. As for discontinuous potentials also $g(r)$ becomes discontinuous it might be an advantage to rewrite this equation in terms of $e(r) = \exp(-\beta u(r))$ and the cavity function $y(r) = (h(r) + 1)/e(r) = g(r)\exp(\beta u(r))$ where the cavity function is always a continuous function by using

$$g(r) \frac{du(r)}{dr} = y(r)e(r) \left(-\frac{1}{\beta e(r)} \frac{de(r)}{dr} \right) = \frac{y(r)}{\beta} \frac{de(r)}{dr}\tag{6.54}$$

so that

$$\frac{\beta P}{\rho} = 1 + \frac{2}{3}\pi\rho \int r^3 \frac{de(r)}{dr} y(r) dr\tag{6.55}$$

In case of potentials with a hard core or a step in the potential also $g(r)$ as well as $u(r)$ are discontinuous. The cavity function is a continuous function and helps to solve the integral. For discontinuous potentials the integration has to be done in parts and the discontinuity needs to be handled separately. It can be shown [456], that at a discontinuity of the potential, let say at $r = \sigma$, the discontinuity contributes to the integral with

$$\frac{2\pi}{3}\rho\sigma^3(g(\sigma^+) - g(\sigma^-))/\beta \quad (6.56)$$

To determine mixing parameters in various closures one often compare the pressures calculated via the three different routes leading to two consistency equations.

$P_v - \kappa_T$ consistency:

Via the virial route the pressure can be calculated by eq. 6.53 or 6.55. Its partial derivative according to the number density yield the isothermal compressibility (eq. 6.47), which is known from the structure factor in the long-wavelength limit at $q = 0$ according to eq. 6.48. This consistency condition can be written as an integral which has to be become zero [332, 508]

$$I(\rho, T) = 0 = \int \left[c(r) - \frac{r}{6} \frac{d(\beta u(r))}{dr} \left(2g(r) + \rho \frac{\partial g(r)}{\partial \rho} \right) \right] r^2 dr \quad (6.57)$$

$dU - dP$ consistency:

The Helmholtz free energy F obeys the Gibbs-Helmholtz relation

$$d(\beta F) = U d\beta - (\beta P) dV \quad (6.58)$$

In order for F to be an exact differential, the cross partial derivatives should be equal

$$\left(\frac{\partial U}{\partial V} \right)_T = \left(\frac{\partial(\beta P)}{\partial \beta} \right)_V = T^2 \frac{\partial}{\partial T} \left(\frac{P}{T} \right)_V \quad (6.59)$$

The internal energy U can be calculated via the energy route by eq. 6.50 and the pressure P again via the virial route by eq. 6.53 or 6.55. Also this consistency condition can be written in integral form as

$$J(\rho, T) = 0 = \int \left[u(r) \left(g(r) + \rho \frac{\partial g(r)}{\partial \rho} \right) + \frac{r}{3} \frac{du(r)}{dr} \left(g(r) - T \frac{\partial g(r)}{\partial T} \right) \right] r^2 dr \quad (6.60)$$

In practise the calculation of the integrals $I(\rho, T)$ and $J(\rho, T)$ involves the numerical partial derivation of the pair distribution function $g(r)$ with respect to the particle number density ρ and the temperature T , which can be approximated by

$$\frac{\partial g(r, \rho, T)}{\partial \rho} \simeq \frac{g(r, \rho + \Delta\rho, T) - g(r, \rho - \Delta\rho, T)}{2\Delta\rho} \quad (6.61)$$

$$\frac{\partial g(r, \rho, T)}{\partial T} \simeq \frac{g(r, \rho, T + \Delta T) - g(r, \rho, T - \Delta T)}{2\Delta T} \quad (6.62)$$

The integral equations therefore needs to be solved for five different thermodynamic states, namely at (ρ, T) , $(\rho + \Delta\rho, T)$, $(\rho - \Delta\rho, T)$, $(\rho, T + \Delta T)$, and $(\rho, T - \Delta T)$.

6.4. Closures

The closures implemented in **SASfit** have been taken from the overview papers from Bomont [44] and Caccamo [74] and the references in there.

6.4.1. Hypernetted-chain(HNC) approximation.

The HNC is one of the earliest and most applied integral equation theory of fluids [192]. It simply assumes for completing the closure relation 6.12 a negligible bridge function [74, 44, 192].

$$B_{\text{HNC}}(r) \equiv 0 \quad (6.63)$$

$$g(r) = \exp[-\beta u(r) + \gamma(r)] \quad (6.64)$$

The HNC equation is a special case insofar as it corresponds to a well-defined free-energy functional, and differentiation of that free energy with respect to volume can be shown to give the same result as the virial equation. The energy and virial routes to the equation of state are therefore equivalent. The HNC closure is often used for long range repulsive potentials. For short range repulsive potentials the PY approximation yields somehow better results.

6.4.2. Reference hypernetted chain closure (RHNC).

This closure is an extension of the HNC closure, which requires that a reference system is known and only need to be corrected for a small perturbation. Therefore the potential needs to be written as a sum of a reference and perturbation potential $u(r) = u_{\text{ref}} + u_{\text{pert}}(r)$. By that the indirect correlation function is given by $\gamma(r) = \gamma_{\text{ref}}(r) + \gamma_{\text{pert}}(r)$ and the direct correlation function by

$$c(r) = g_{\text{ref}}(r) \exp(\gamma_{\text{pert}} - \beta u_{\text{pert}}) - \gamma(r) - 1 \quad (6.65)$$

with $g_{\text{ref}}(r)$ being the radial distribution function of the reference system. To solve the OZ equation for the reference system the Martynov-Sarkisov (MS) closure (sec. 6.4.13) is used in SASfit as it yields results with relative good thermodynamic consistency for hard sphere potentials, at least better than the PY closure.

6.4.3. modified hypernetted chain closure (MHNC).

The modified hypernetted chain closure was introduced by Resnfeld and Ashcroft [426]. They suggested to approximate the bridge $B_{\text{MHNC}}(r)$ function by the one of hard spheres $B_{\text{PY}}(r, \eta^*)$ however with an effective volume fraction η^* to get thermodynamic

consistency. The bridge function in PY approximation they is given by

$$B_{\text{PY}}(r) = \begin{cases} c_{\text{PY}}(r) + 1 + \ln[-c_{\text{PY}}(r)] & \text{for } r < \sigma \\ -g_{\text{PY}}(r) + 1 + \ln[g_{\text{PY}}(r)] & \text{for } r > \sigma \end{cases} \quad (6.66)$$

The direct correlation function $c_{\text{PY}}(r)$ and radial distribution function $g_{\text{PY}}(r)$ are taken from the analytical solution for $c_{\text{PY}}(r)$ given by Wertheim [522] and $g_{\text{PY}}(r)$ by [488, 489]. SASfit is searching within the interval $\eta^* \in [0.02, 0.6]$ for a thermodynamic consistent solution.

6.4.4. Kovalenko-Hirata or partially linearized HNC closure (PLHNC).

Kovalenko and Hirata [274] introduced a closure (KH-closure) for studying self-consistent description of a metal–water interface and which has been used later on e.g. by [228] to study core-softened potentials. This closure is also named partially linearized hypernetted chain closure PLHNC. Their bridge function reads as

$$B_{\text{KH}}(r) = \begin{cases} 0 & \text{for } -\beta u(r) + \gamma(r) \leq 0 \\ \beta u(r) - \gamma(r) + \ln(-\beta u(r) + \gamma(r) + 1) & \text{for } -\beta u(r) + \gamma(r) > 0 \end{cases} \quad (6.67)$$

6.4.5. Percus-Yevick (PY) approximation.

This approximation has been successfully been used to find an analytical solution for the OZ equations for a Hard Sphere potential as well as a Sticky Hard Sphere potential. Also analytical solution for both Hard Sphere [385, 522] and Sticky Hard Sphere [18] with a size distribution has been found. The bridge function of this approximation reads as

$$B_{\text{PY}}(r) = \ln[\gamma(r) - 1] - \gamma(r) \quad (6.68)$$

$$g(r) = \exp[-\beta u(r)] (1 + \gamma(r)) \quad (6.69)$$

The PY equation proves to be more successful than the HNC approximation when the potential is strongly repulsive and short ranged. The PY equation is of particular interest in the theory of simple liquids because it is soluble analytically in the important case of the hard-sphere fluid.

6.4.6. Mean Spherical Approximation (MSA).

This approximation has originally been proposed by Lebowitz and Percus [294]. It has been mainly successfully applied to spherical potentials interacting through an

infinitely repulsive potential at short range. It uses the ansatz

$$g(r) = 0 \quad \text{for } \beta u(r) = +\infty \quad (6.70)$$

$$c(r) = -\beta u(r) \text{ for } \beta u(r) \neq +\infty \quad (6.71)$$

Analytical solutions have been obtained for charged hard spheres and hard core Yukawa potentials [74].

6.4.7. Rescaled Mean Spherical Approximation (RMSA).

The mean spherical approximation can especially for dilute cases result in a negative $g(r)$ at the contact point σ^+ , which is just out of the hard core radius, i.e. the first distance for which $\exp(-\beta u(r)) > 0$. The rescaled mean spherical approximation (RMSA) [191] is searching for the smallest apparent contact point $\tilde{\sigma}^+$ for which $g(\tilde{\sigma}^+) > 0$.

6.4.8. "Soft core" MSA (SMSA) Approximation.

This closure has been motivated because the Percus-Yevick (PY) approximation is not accurate for attractive potentials. The SMSA [321, 88] is a generalisation of the MSA closure. This has been done by incorporating the division scheme as of Weeks et al. [520] by dividing the potential in a entirely repulsive part and a attractive part $u(r) = u_R(r) + u_A(r)$. The SMSA bridge function reads as

$$B_{\text{SMSA}}(r) = \ln [1 + \gamma^*(r)] - \gamma^*(r) \quad (6.72)$$

with $\gamma^*(r) = \gamma(r) - \beta u_A(r)$. Normally $u_R(r)$ describes a short range repulsive interaction like hard sphere interaction or as in the division scheme from Weeks et al. the potential up to the minimum r_m . For $r > r_m$ or $r > \sigma^{\text{HS}}$ the closure reduces to the MSA approximation $c(r) = -\beta u(r)$. In a case of a purely repulsive interaction, one has $r_m \rightarrow \infty$ and $u_A(r) \equiv 0$. In this case the closure reduces to the PY closure. The SMSA interpolates between PY and MSA [44].

6.4.9. modified MSA (mMSA) Approximation.

This closure has been reported in [147, 146] where the direct correlation function $c(r)$ is set to the Mayer-f function, so that it reads as

$$g(r) = 0 \quad \text{for } \beta u(r) = +\infty \quad (6.73)$$

$$c(r) = \exp(-\beta u(r)) - 1 \text{ for } \beta u(r) \neq +\infty \quad (6.74)$$

6.4.10. Verlet Approximation.

A semi-phenomenological equation for the radial distribution function was proposed by Verlet [503, 504] for the case of hard spheres with the following bridge function

$$B_{\text{Verlet}}(r) = \frac{-\gamma^2(r)}{2 \left(1 + \frac{4}{5}\gamma(r)\right)} \quad (6.75)$$

The approximation yield very good results for both thermodynamic as well as structural properties. This closure has been extended and refined by others and are listed below.

6.4.11. Choudhury-Gosh (CG) Approximation.

Choudhury and Gosh [89] proposed a bridge function based on the closure of Verlet which reads as

$$B_{\text{CG}}(r) = \frac{-\gamma^{*2}}{2(1 + \alpha\gamma^*(r))} \quad (6.76)$$

with $\alpha = 1.0175 - 0.275\rho\sigma^3$ and $\gamma^*(r) = \gamma(r) - \beta u_A(r)$.

6.4.12. Duh-Haymet (DH) Approximation.

Duh-Haymet [113] introduced a closure for the Lennard-Jones potential, where they partitioned the potential slightly differently than Weeks et al. [520]. As the perturbation potential they used

$$u_{\text{pert}}^{\text{LR,DH}}(r) = -4k_B T \epsilon \left(\frac{\sigma}{r}\right)^6 \times \exp\left(-\frac{k_B T \epsilon}{\rho^*} \left(\frac{\sigma}{r}\right)^6\right) \quad (6.77)$$

with the reduced density taken as $\rho^* = \rho\sigma^3$. Their bridge function reads

$$B_{\text{DH}}(r) = \frac{-\gamma^{*2}(r)}{2 \left[1 + \frac{5\gamma^*(r)+11}{7\gamma^*(r)+9}\gamma^*(r)\right]} \quad (6.78)$$

with $\gamma^*(r) = \gamma(r) - \beta u_A(r)$ or in case of the Lennard-Jones potential $\gamma^*(r) = \gamma(r) - \beta u_{\text{pert}}^{\text{LR,DH}}(r)$

6.4.13. Martynov-Sarkisov (MS) Approximation.

An approximation proposed by Martynov and Sarkisov [331] sets the bridge function as

$$B_{\text{MS}}(r) = [1 + 2\gamma(r)]^{1/2} - 1 - \gamma(r) \quad (6.79)$$

This approximation has been originally applied to hard spheres without an additional adjustable parameter. Compared to PY or HNC this closure reduces considerably the thermodynamic inconsistency.

6.4.14. Ballone, Pastore, Galli, and Gazzillo (BPGG) approximations.

Ballone, Pastore, Galli, and Gazzillo [13] improved the MS approximation by assuming a bridge function of the form

$$B_{\text{BPGG}}(r) = [1 + s\gamma(r)]^{1/s} - 1 - \gamma(r) \quad (6.80)$$

For $s = 1$ the HNC is recovered and for $s = 2$ the MS closure. s is used here to obtain a thermodynamic consistency condition.

6.4.15. Vompe-Martynov (VM) Approximation.

The MS bridge function [331] has been refined by Vompe and Martynov [508]. Their extended bridge function reads

$$B_{\text{VM}}(r) = \sqrt{1 + 2\gamma^*(r)} - 1 - \gamma^*(r) \quad (6.81)$$

with $\gamma^*(r) = \gamma(r) - \beta u_{\text{LR}}(r)$

6.4.16. Bomont-Bretonnet (BB) Approximation.

Bomont and Bretonnet [45, 46] have suggested an extension of the MS approximation with the bridge function

$$B_{\text{BB}}(r) = \sqrt{1 + 2\gamma^*(r) + f\gamma^{*2}(r)} - 1 - \gamma^*(r) \quad (6.82)$$

The adjustable parameter f interpolates between the HNC for $f = 1$ and the VM for $f = 0$.

6.4.17. Charpentier-Jakse' semi-empirical extension of VM approximation (CJ-VM).

A similar semi-empirical approach has been suggested by Charpentier and Jakse [83]

$$B_{\text{CJ-VM}}(r) = \frac{1}{2\alpha} \left[\sqrt{1 + 4\alpha\gamma^*(r)} - 1 - 2\alpha\gamma^*(r) \right] \quad (6.83)$$

Also here α can be chosen so that thermodynamic consistency is obtained.

6.4.18. HNC-SMSA (HMSA) Approximation.

The HNC-SMSA (HMSA) closure from Zerah and Hansen [540] has been proposed for the Lennard-Jones fluid. It interpolates between HNC and SMSA. The HMSA has strong theoretical basis since it can be derived from Percus' functional expansion formalism and its bridge function expresses as a functional of the renormalised indirect correlation function $\gamma^*(r) = \gamma(r) - \beta u_R(r)$ so that

$$B_{\text{HMSA}}(r) = \ln \left[1 + \frac{\exp[f(r, \alpha)\gamma^*(r)] - 1}{f(r, \alpha)} \right] - \gamma^*(r) \quad (6.84)$$

where $f(r, \alpha)$ is the switching function defined as

$$f(r, \alpha) = 1 - \exp(-\alpha r) \quad (6.85)$$

The parameter α is varied in a self-consistent manner until virial and compressibility routes for the pressure coincide. The HMSA closure reduces to HNC for $f(r, \alpha) \xrightarrow{\alpha \rightarrow \infty} 1$ and to SMSA when $f(r, \alpha) \xrightarrow{\alpha \rightarrow 0} 0$.

6.4.19. Roger-Young (RY) closure.

Roger and Young have introduced a closure to interpolate continuously between HNC and PY theory [424]

$$B_{\text{RY}}(r) = \ln \left[1 + \frac{\exp[f(r, \alpha)\gamma(r)] - 1}{f(r, \alpha)} \right] - \gamma(r) \quad (6.86)$$

where $f(r, \alpha)$ is a "switching function", which they defined as

$$f(r, \alpha) = 1 - \exp(-\alpha r) \quad (6.87)$$

For $\alpha \rightarrow \infty$ the switching function becomes $f(r, \alpha) = 1$ and the closure becomes the HNC closure. For $\alpha \rightarrow 0$ the switching function becomes $f(r, \alpha) = 0$ and the closure converges to the PY closure. The parameter α is varied until the virial-compressibility consistency condition is satisfied.

6.4.20. Zero separation theorem based closure (ZSEP).

The closure based on the zero separation theorem (ZSEP) has been introduced by Lloyd L. Lee [295, 315]. The closure is basing on the one from Verlet [503] and has the form

$$B_{\text{ZSEP}}(r) = -\frac{\zeta \gamma^*(r)^2}{2} \left[1 - \frac{\alpha \phi \gamma^*(r)}{1 + \alpha \gamma^*(r)} \right] \quad (6.88)$$

6.5. Interaction Potentials

Many of the interaction potentials described below are discussed in [302]. The different closures of the previous section require partly that the interaction potential $u(r, \dots)$ is partitioned in a reference $u_{\text{ref}}(r, \dots)$ and perturbation $u_{\text{pert}}(r, \sigma, \dots)$, or a short range $u_{\text{SR}}(r, \sigma, \dots)$ and long range $u_{\text{LR}}(r, \sigma, \dots)$, or an attractive $u_{\text{A}}(r, \sigma, \dots)$ and repulsive $u_{\text{R}}(r, \sigma, \dots)$ potential part. One famous partition has been introduced by Weeks-Chandler-Andersen (WCA) [520]. They partitioned the potential $u(r) = u_{\text{R}}(r) + u_{\text{A}}(r)$ in a repulsive part $u_{\text{R}}(r)$ with an additional condition that $u_{\text{R}}(r) \xrightarrow{r \rightarrow \infty} 0$, and an attractive part $u_{\text{A}}(r)$. In some other closures the partition is done in a reference and perturbation $u(r) = u_{\text{ref}}(r) + u_{\text{pert}}(r)$ or a short range and long range part $u(r) = u_{\text{SR}}(r) + u_{\text{LR}}(r)$. The definitions together with the different ways of partitioning the potentials are defined below for each potential.

6.5.1. Hard Sphere Potential.

Hard spheres are the simplest model which are defined simply as impenetrable spheres that cannot overlap in space. They mimic the extremely strong repulsion that atoms and spherical molecules experience at very close distances. Hard spheres of diameter σ are particles with the following pairwise interaction potential:

$$u^{\text{HS}}(r, \sigma) = \begin{cases} \infty & \text{if } r < \sigma \\ 0 & \text{if } r \geq \sigma \end{cases} \quad (6.89)$$

A splitting of the simple hard sphere potential is not required, so that

$$u_{\text{ref}}^{\text{HS}}(r, \sigma) = u_{\text{SR}}^{\text{HS}}(r, \sigma) = u_{\text{R}}^{\text{HS}}(r, \sigma) = \begin{cases} \infty & \text{if } r < \sigma \\ 0 & \text{if } r \geq \sigma \end{cases} \quad (6.90)$$

and

$$u_{\text{pert}}^{\text{HS}}(r, \sigma) = u_{\text{LR}}^{\text{HS}}(r, \sigma) = u_{\text{A}}^{\text{HS}}(r, \sigma) \equiv 0 \quad (6.91)$$

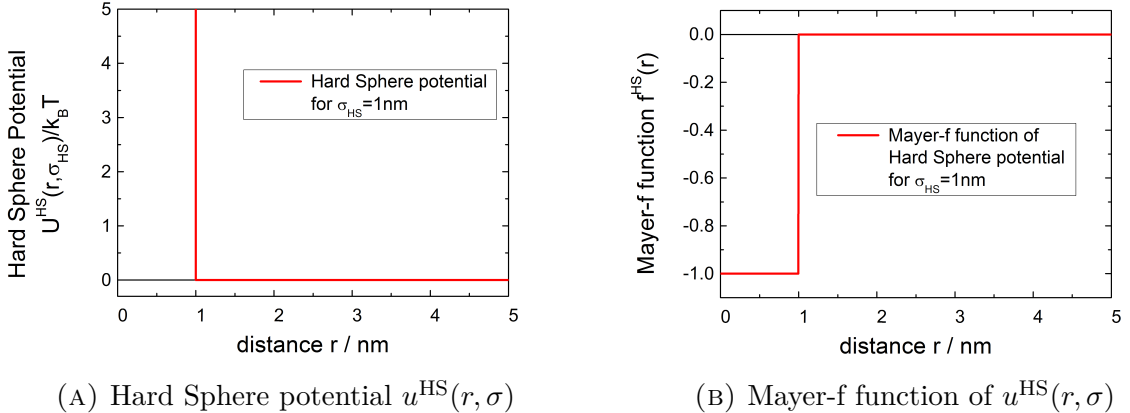


FIGURE 6.1. potential $u^{\text{HS}}(r, \sigma)$ and it's Mayer-f function
 $\exp\left(-\frac{u^{\text{HS}}(r, \sigma)}{k_B T}\right) - 1$

6.5.2. Sticky Hard Sphere Potential (SHS).

The original model of “adhesive” or “sticky” hard spheres potential was proposed by Baxter in 1968 [18]. This potential adds to a hard sphere interparticle repulsion an infinitely strong attraction when molecular surfaces come to contact. The adhesive surface contribution was defined by a particular limiting case of a square well tail, in which the well depth goes to infinity as the width goes to zero, in such a way that the contribution to the second osmotic virial coefficient B_2 remains finite but not zero (Baxter’s “sticky limit”). More explicitly, in the one-component case, the square well potential reads as

$$u^{\text{SHS}}(r) = \begin{cases} \infty, & 0 < r < \sigma \\ \epsilon, & \sigma \leq r \leq \sigma + \Delta \\ 0, & r > \sigma + \Delta \end{cases} \quad (6.92)$$

with

$$\epsilon = k_B T \ln \left(\frac{12\tau\Delta}{\sigma + \Delta} \right) \quad (6.93)$$

The height of the square well ϵ is positive for $\tau > (\sigma + \Delta)/(12\Delta)$. Therefore the splitting in attractive and repulsive potential is done as

$$u_A^{\text{SHS}}(r) = \begin{cases} \epsilon & \tau < \frac{\sigma+\Delta}{12\Delta} \wedge r \leq \sigma + \Delta \\ 0 & \text{otherwise} \end{cases} \quad (6.94)$$

$$u_R^{\text{SHS}}(r) = \begin{cases} \infty & r < \sigma \\ \epsilon & \tau > \frac{\sigma+\Delta}{12\Delta} \wedge \sigma \leq r \leq \sigma + \Delta \\ 0 & \tau < \frac{\sigma+\Delta}{12\Delta} \wedge \sigma \leq r \leq \sigma + \Delta \\ 0 & \text{otherwise} \end{cases} \quad (6.95)$$

The partitioning in reference and perturbation is done by

$$u_{\text{ref}}^{\text{SHS}}(r) = \begin{cases} \infty & r < \sigma \\ 0 & \text{otherwise} \end{cases} \quad (6.96)$$

$$u_{\text{pert}}^{\text{SHS}}(r) = \begin{cases} \epsilon & r \leq \sigma + \Delta \\ 0 & \text{otherwise} \end{cases} \quad (6.97)$$

A partitioning in long range and short range is not done. The long range potential is set to be always $u_{\text{LR}}^{\text{SHS}}(r) \equiv 0$, so that $u_{\text{SR}}^{\text{SHS}}(r) = u^{\text{SHS}}(r)$.

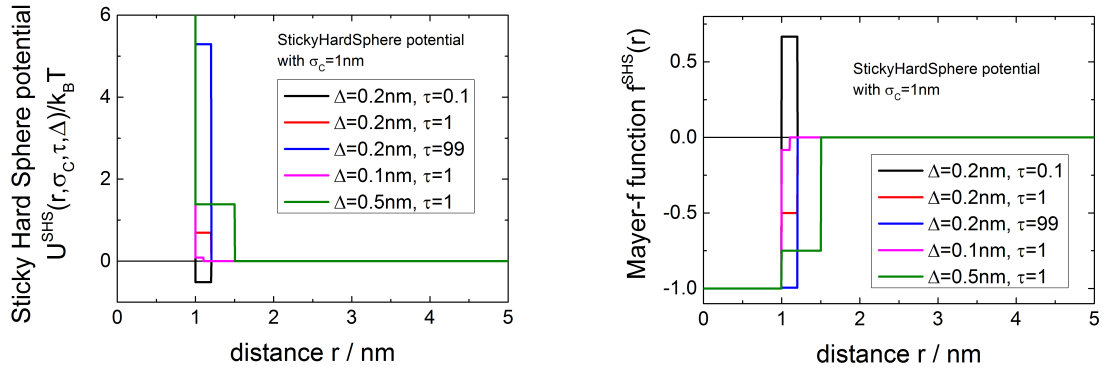
(A) sticky hard sphere potential $u^{\text{SHS}}(r, \sigma)$ e(B) Mayer-f function of $u^{\text{SHS}}(r, \sigma)$

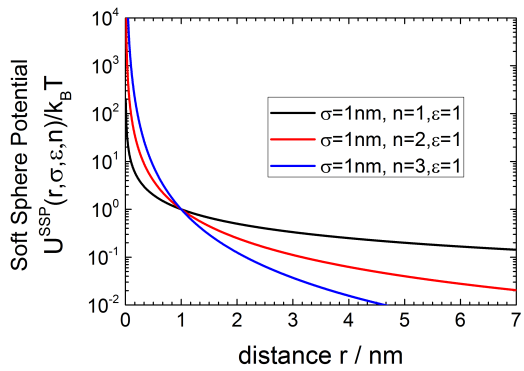
FIGURE 6.2. potential $u^{\text{SHS}}(r, \sigma)$ and it's Mayer-f function
 $\exp\left(-\frac{u^{\text{SHS}}(r, \sigma)}{k_B T}\right) - 1$

6.5.3. Soft Sphere Potential.

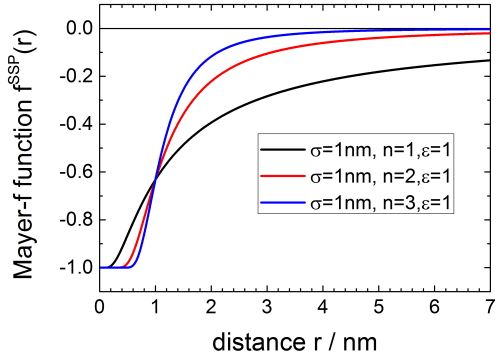
The soft sphere potential is defined as

$$u^{\text{SSP}}(r, \sigma, \epsilon) = k_B T \epsilon \left(\frac{\sigma}{r} \right)^n \quad (6.98)$$

σ is the nominal particle diameter, ϵ establishes the energy scale, and n controls the stiffness of the potential (the softness is $1/n$). Indeed for microgel particles this potential form has been used to interpret experimentally measured physical properties. $n \rightarrow \infty$ is the hard sphere limit, and this and intermediate n values (particularly $n = 12$) have been studied many times in the literature. For $n \leq 3$ this potential does not lead to a thermodynamically stable system as the volume integral of the potential diverges.



(A) Soft Sphere Potential $u^{\text{SSP}}(r, \sigma, \dots)$



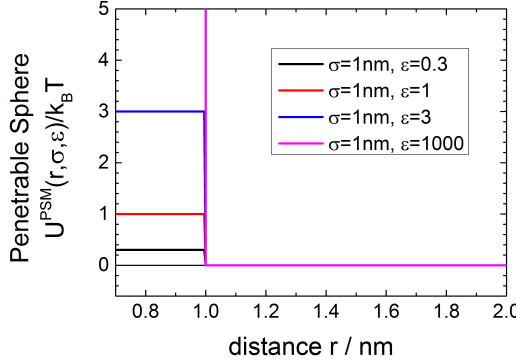
(B) Mayer-f function of $u^{\text{SSP}}(r, \sigma, \dots)$

FIGURE 6.3. potential $u^{\text{SSP}}(r, \sigma, \dots)$ and it's Mayer-f function $\exp\left(-\frac{u^{\text{SSP}}(r, \sigma, \dots)}{k_B T}\right) - 1$

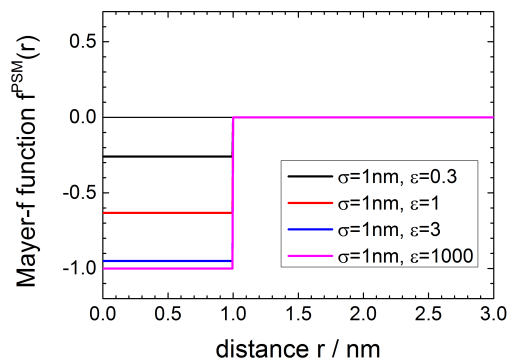
6.5.4. Penetrable Sphere Model.

The penetrable sphere model was used by Marquist and Witten [330] who suggested it as a prototype for the interaction between micelles in a solvent. The potential is defined as [330, 506]

$$u^{\text{PSM}}(r, \sigma, \epsilon) = \begin{cases} k_B T \epsilon & \text{for } r \leq \sigma \\ 0 & \text{for } r > \sigma \end{cases} \quad (6.99)$$



(A) Potential of the Penetrable Sphere Model (PSM) $u^{\text{PSM}}(r, \sigma, \dots)$



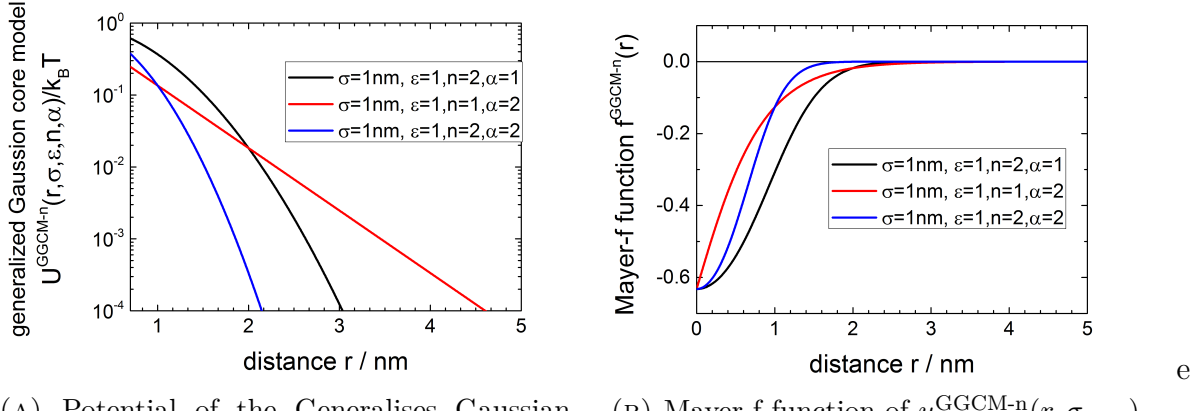
(B) Mayer-f function of $u^{\text{PSM}}(r, \sigma, \dots)$

FIGURE 6.4. potential $u^{\text{PSM}}(r, \sigma, \dots)$ and it's Mayer-f function $\exp\left(-\frac{u^{\text{PSM}}(r, \sigma, \dots)}{k_B T}\right) - 1$

6.5.5. Generalized Gaussian Core Model Potential - GGCM-n Potential.

The effective interaction between the centers of mass of two polymer chains in an athermal solvent can be described in very good approximation by an interaction of a Gaussian form $u^{\text{GCM}}(r) = k_B T \epsilon \exp\left(-\left(r/\sigma\right)^2\right)$. A generalisation of this form has been discussed in [341, 316] and has the form

$$u^{\text{GGCM-n}}(r) = k_B T \epsilon \exp\left(-\alpha \left(\frac{r}{\sigma}\right)^n\right) \quad (6.100)$$



(A) Potential of the Generalised Gaussian Code Model (GGCM-n) $u^{\text{GGCM-n}}(r, \sigma, \dots)$

(B) Mayer-f function of $u^{\text{GGCM-n}}(r, \sigma, \dots)$

FIGURE 6.5. potential $u^{\text{GGCM-n}}(r, \sigma, \dots)$ and it's Mayer-f function $\exp(-u^{\text{GGCM-n}}(r, \sigma, \dots)/k_B T) - 1$

6.5.6. Fermi Distribution Model.

$$u^{\text{FDM}}(r, \sigma, \epsilon, \xi) = k_B T \epsilon \frac{1 + \exp(-\sigma/\xi)}{1 + \exp((r - \sigma)/\xi)} \quad (6.101)$$

For $\xi = 0$ the Fermi Potential goes over into the Penetrable Sphere Model.

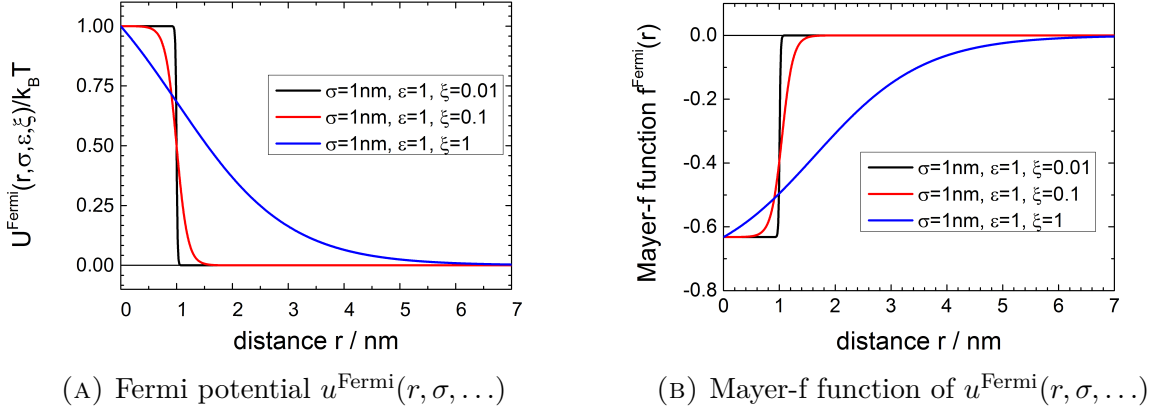


FIGURE 6.6. potential $u^{\text{Fermi}}(r, \sigma, \dots)$ and it's Mayer-f function $\exp(-u^{\text{Fermi}}(r, \sigma, \dots)/k_B T) - 1$

6.5.7. Star Polymer Potential.

Star polymers with tunable number f and size of arms, and thus interactions, represent ideal model systems for exploring the regime of soft material behaviour that interpolates between hard spheres and polymeric coils. Likos et al. [305, 302] have proposed an effective potential that describes the interaction between two stars. The potential is given by

$$u^{\text{star1}}(r, \sigma, f) = k_B T \frac{5}{8} f^{3/2} \begin{cases} \left(\frac{1}{1+\sqrt{f}} - \ln \left(\frac{r}{\sigma} \right) \right) & \text{for } r \leq \sigma \\ \frac{1}{1+\sqrt{f}} \frac{\sigma}{r} \exp \left(-\frac{\sqrt{f}(r-\sigma)}{2\sigma} \right) & \text{for } r > \sigma \end{cases} \quad (6.102)$$

where σ is the effective corona diameter (e.g., $\sigma \propto f^{1/5} N_a^{3/5}$ for good solvents, N_a being the arm degree of polymerization and f the functionality of the star). In equation 6.102 above, $\sigma/2$ is a length scale that extends from the star center to the middle of the outermost Daoud–Cotton blob [303]. Extensive comparisons with simulations have set this scale to $\sigma \cong 1.32 R_g$, where R_g is the star radius of gyration. The effective potential shows a soft, logarithmic divergence at close approaches, followed by a crossover to a Yukawa form as the center-to-center separation r grows. The potential becomes harder with increasing f , tending eventually to a hard-sphere interaction formally obtained in the limit $f \rightarrow \infty$.

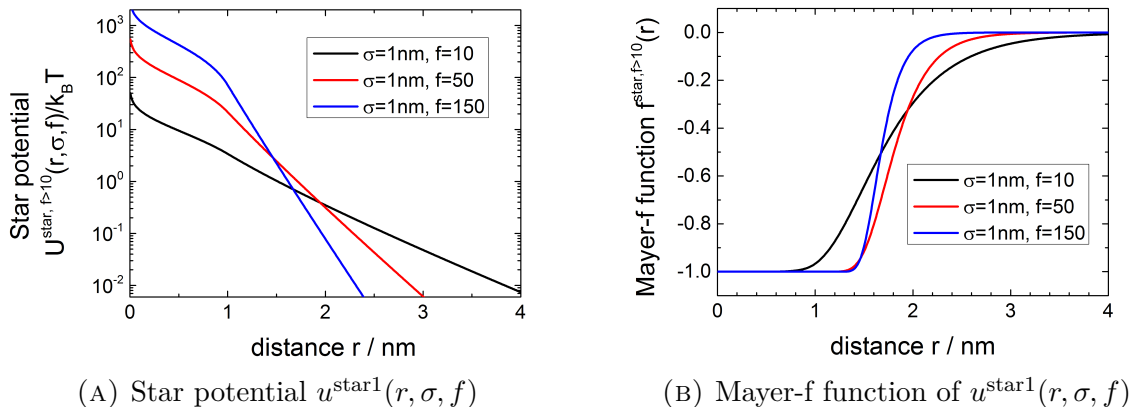


FIGURE 6.7. potential $u^{\text{star1}}(r, \sigma, f)$ and it's Mayer-f function $\exp(-u^{\text{star1}}(r, \sigma, f)/k_B T) - 1$

The effective potential valid for $f \leq 10$ has the form [248, 115, 302]:

$$u^{\text{star2}}(r, \sigma, f) = k_B T \frac{5}{8} f^{3/2} \begin{cases} \left(\frac{1}{2\tau^2 \sigma^2} - \ln \left(\frac{r}{\sigma} \right) \right) & \text{for } r \leq \sigma \\ \frac{1}{2\tau^2 \sigma^2} \exp \left(-\tau^2 (r^2 - \sigma^2) \right) & \text{for } r > \sigma \end{cases} \quad (6.103)$$

$$\text{with } \tau = \left(\frac{1.12}{3\sigma} - \frac{1.03}{3\sigma} \right) f + \frac{1.03}{\sigma} \quad (6.104)$$

τ is a free parameter of the order and is obtained by fitting to computer simulation results [115].

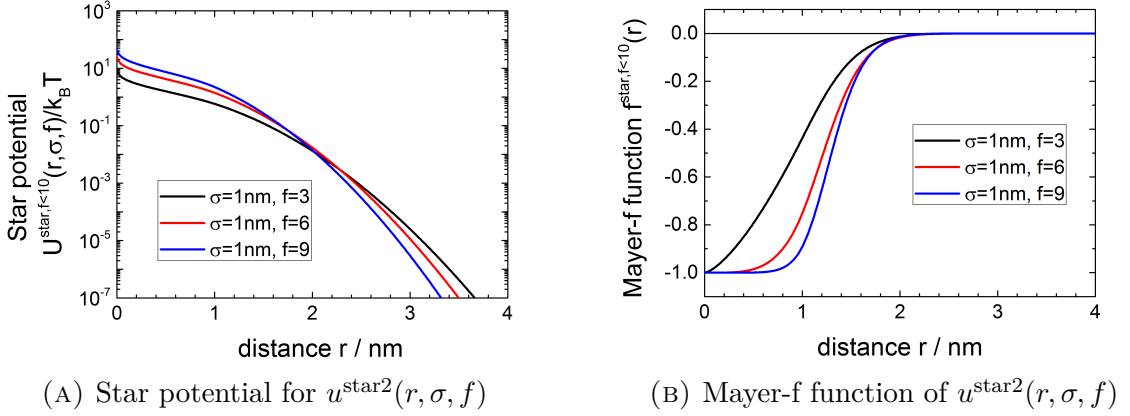


FIGURE 6.8. potential $u^{\text{star}2}(r, \sigma)$ and it's Mayer-f function $\exp(-u^{\text{star}2}(r, \sigma, f)/k_B T) - 1$

6.5.8. Lennard-Jones Potential.

The Lennard-Jones potential is a mathematically simple model that approximates the interaction between a pair of neutral atoms or molecules. A form of the potential was first proposed in 1924 by John Lennard-Jones [246].

$$u^{\text{LJ}}(r, \sigma, \dots) = 4k_B T \epsilon \left[\left(\frac{\sigma}{r}\right)^{12} - \left(\frac{\sigma}{r}\right)^6 \right] \quad (6.105)$$

The Lennard-Jones (LJ) potential has a minimum at $r_m = 2^{1/6}\sigma$, so that the potential can be written in parts of

$$u_{\text{ref}}^{\text{LJ}}(r) \equiv 0 \quad (6.106)$$

$$u_{\text{SR}}^{\text{LJ}}(r) = u_{\text{R}}^{\text{LJ}}(r) = \begin{cases} u^{\text{LJ}}(r) - u^{\text{LJ}}(r_m) & \text{if } r < r_m \\ 0 & \text{if } r \geq r_m \end{cases} \quad (6.107)$$

and

$$u_{\text{pert}}^{\text{LJ}}(r) = u^{\text{LJ}}(r) \quad (6.108)$$

$$u_{\text{LR}}^{\text{LJ}}(r) = u_{\text{A}}^{\text{LJ}}(r) = \begin{cases} u^{\text{LJ}}(r_m) & \text{if } r < r_m \\ u_{\text{LR}}^{\text{LJ}}(r) & \text{if } r \geq r_m \end{cases} \quad (6.109)$$

The LJ potential is not splitted in a reference and perturbation part, i.e. the reference part is set to 0.

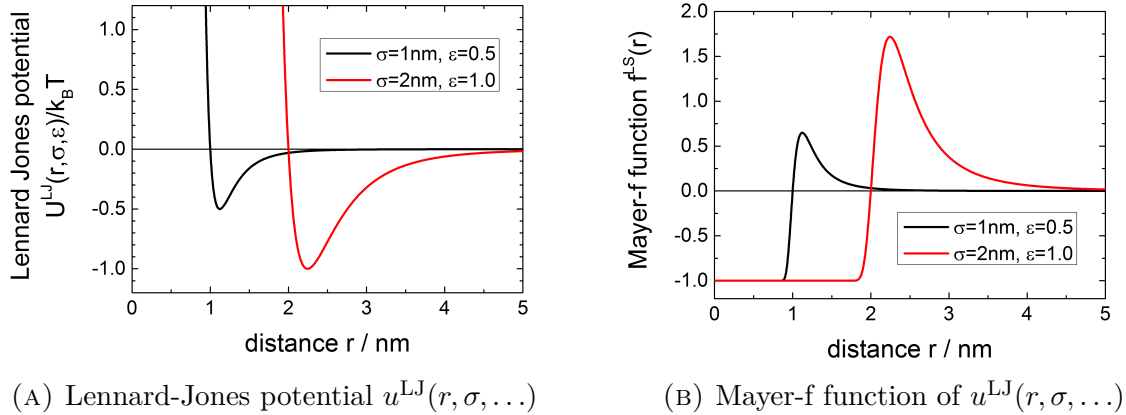


FIGURE 6.9. potential $u^{\text{LJ}}(r, \sigma, \dots)$ and it's Mayer-f function $\exp(-u^{\text{LJ}}(r, \sigma, \dots)/k_B T) - 1$

6.5.9. Depletion Potential.

The pair interaction potential of spheres by a depleting agent is implemented depending on the shape of the depleting agent. Analytical expressions have been developed for spherical, disc-like or rod-like shapes [367, 296].

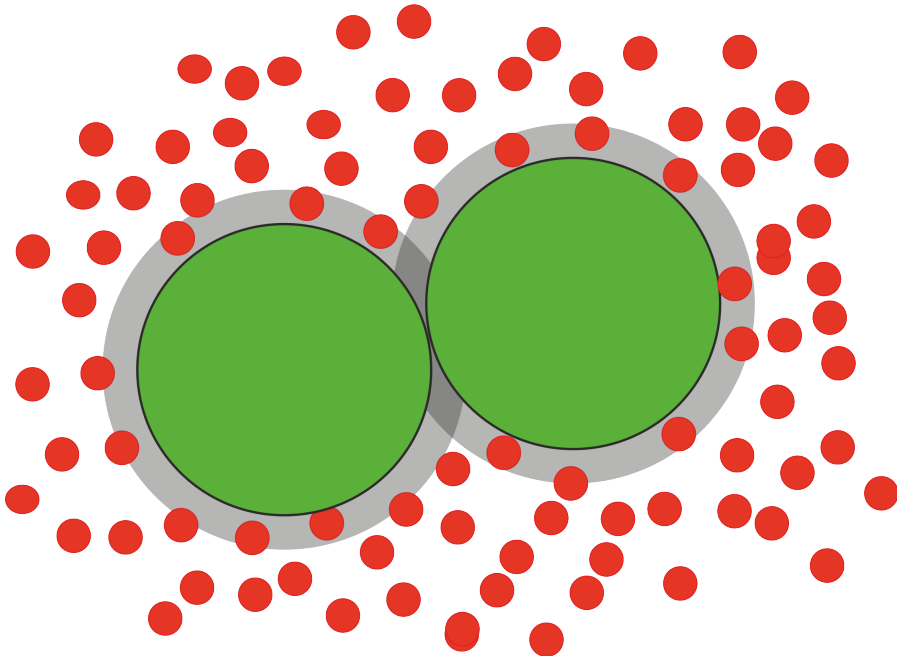
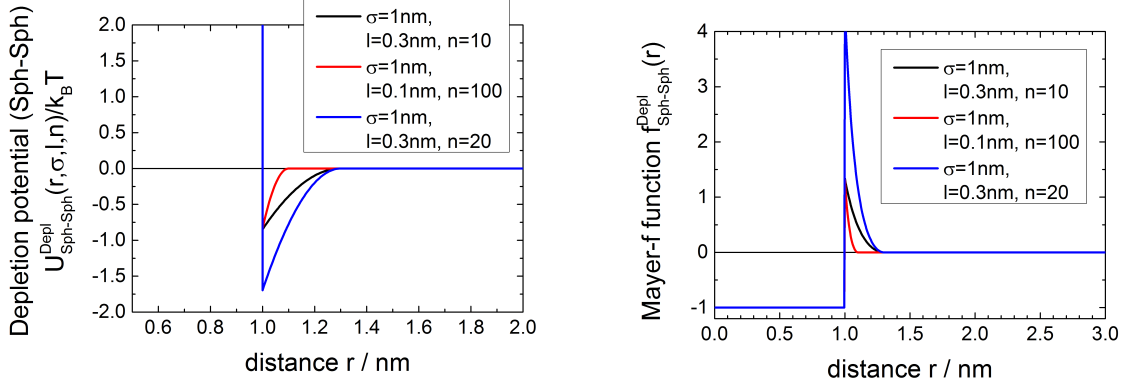


FIGURE 6.10. Attractive depletion forces between large spheres due to small spheres as depleting agent.



(A) potential between two large spheres and spherical depleting agents $u_{\text{sph}}^{\text{depl}}(r, \sigma, \dots)$

(B) Mayer-f function of $u_{\text{sph}}^{\text{depl}}(r, \sigma, \dots)$

FIGURE 6.11. potential $u_{\text{sph}}^{\text{depl}}(r, \sigma, \dots)$ and it's Mayer-f function $\exp(-u_{\text{sph}}^{\text{depl}}(r, \sigma, \dots)/k_B T) - 1$

The potential between two large spheres and spherical depleting agents of diameter l is given by

$$u_{\text{sph}}^{\text{depl}}(r) = \begin{cases} \infty & \text{for } r < \sigma \\ -k_B T(N_{\text{I}} + N_{\text{II}} - N_{\text{III}}) & \text{for } r \geq \sigma \end{cases} \quad (6.110)$$

$$N_{\text{I}} = n_d \frac{2}{3} \left(\frac{l}{2} - \frac{r - \sigma}{2} \right)^2 \left(\frac{3\sigma}{2} + l + \frac{r - \sigma}{2} \right) \quad (6.111)$$

$$N_{\text{II}} = N_{\text{III}} = 0 \quad (6.112)$$

Also a splitting of the potential in repulsive-attractive, reference-perturbation, shortrange-longrange has been implemented as

$$u_{\text{sph,R}}^{\text{depl}}(r) = \begin{cases} u_{\text{sph}}^{\text{depl}}(r) & \text{for } r < \sigma \\ 0 & \text{for } r \geq \sigma \end{cases} \quad (6.113a)$$

$$u_{\text{sph,A}}^{\text{depl}}(r) = \begin{cases} u_{\text{sph}}^{\text{depl}}(\sigma) & \text{for } r < \sigma \\ u_{\text{sph}}^{\text{depl}}(r) & \text{for } r \geq \sigma \end{cases} \quad (6.113b)$$

$$u_{\text{sph,ref}}^{\text{depl}}(r) = \begin{cases} u_{\text{sph}}^{\text{depl}}(r) & \text{for } r < \sigma \\ 0 & \text{for } r \geq \sigma \end{cases} \quad (6.113c)$$

$$u_{\text{sph,pert}}^{\text{depl}}(r) = \begin{cases} u_{\text{sph}}^{\text{depl}}(\sigma) & \text{for } r < \sigma \\ u_{\text{sph}}^{\text{depl}}(r) & \text{for } r \geq \sigma \end{cases} \quad (6.113d)$$

$$u_{\text{sph,SR}}^{\text{depl}}(r) = \begin{cases} u_{\text{sph}}^{\text{depl}}(r) & \text{for } r < \sigma \\ 0 & \text{for } r \geq \sigma \end{cases} \quad (6.113e)$$

$$u_{\text{sph,LR}}^{\text{depl}}(r) = \begin{cases} u_{\text{sph}}^{\text{depl}}(\sigma) & \text{for } r < \sigma \\ u_{\text{sph}}^{\text{depl}}(r) & \text{for } r \geq \sigma \end{cases} \quad (6.113f)$$

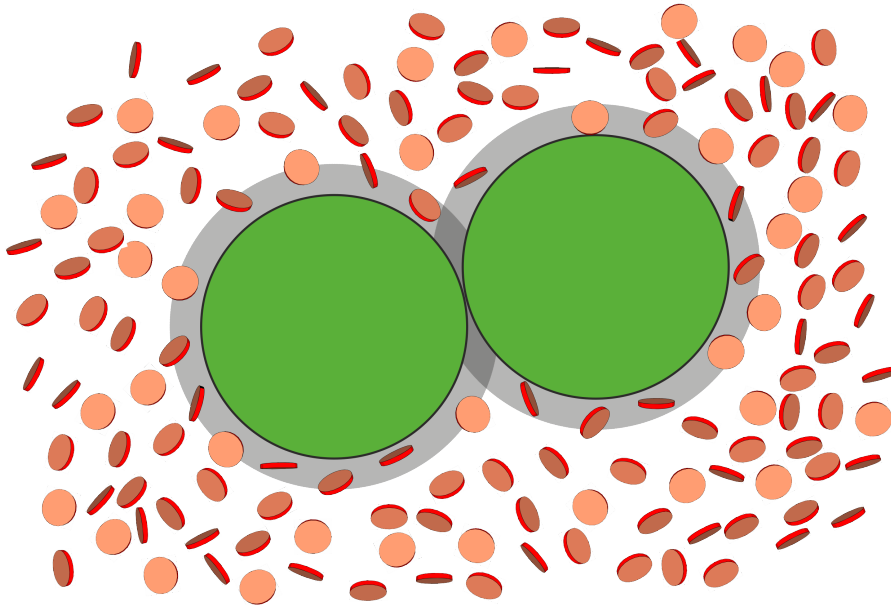
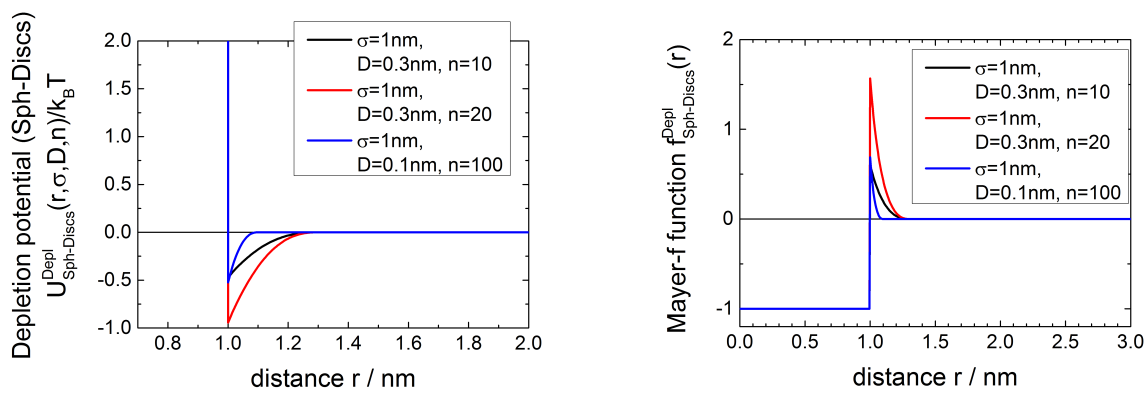


FIGURE 6.12. Attractive depletion forces between large spheres due to depletion forces of infinitesimal thin discs of diameter D as a depleting agents



(A) potential between two large spheres and dislike depleting agents $u_{\text{discs}}^{\text{depl}}(r, \sigma, \dots)$

(B) Mayer-f function of $u_{\text{discs}}^{\text{depl}}(r, \sigma, \dots)$

FIGURE 6.13. potential $u_{\text{discs}}^{\text{depl}}(r, \sigma, \dots)$ and it's Mayer-f function $\exp(-u_{\text{discs}}^{\text{depl}}(r, \sigma, \dots)/k_B T) - 1$

The potential between two large spheres and infinitesimal thin discs of diameter D as a depleting agents is given by

$$u_{\text{discs}}^{\text{depl}}(r) = -k_B T(N_I + N_{\text{II}} - N_{\text{III}}) \quad (6.114)$$

$$N_I = n_d \frac{\pi}{6} \sigma D^2 \left(1 - \frac{r - \sigma}{D}\right)^2 \left(\frac{3}{2} + \frac{D}{\sigma} + \frac{1}{2} \frac{r - \sigma}{\sigma}\right) \quad (6.115)$$

$$\begin{aligned} N_{\text{II}} - N_{\text{III}} &= \frac{\pi}{6} n_d D^2 \sigma \left\{ -\frac{3}{2} \left(1 - \frac{r - \sigma}{D}\right)^2 - \frac{3}{4} \pi \frac{r - \sigma}{D} \right. \\ &\quad \left. + \frac{3}{2} \frac{r - \sigma}{D} \arcsin \frac{r - \sigma}{D} \right. \\ &\quad \left. + \left(1 + \frac{1}{2} \left(\frac{r - \sigma}{D}\right)^2\right) \sqrt{1 - \left(\frac{r - \sigma}{D}\right)^2} \right\} \end{aligned} \quad (6.116)$$

Also a splitting of the potential in repulsive-attractive, reference-perturbation, shortrange-longrange has been implemented as

$$u_{\text{discs,R}}^{\text{depl}}(r) = \begin{cases} u_{\text{discs}}^{\text{depl}}(r) & \text{for } r < \sigma \\ 0 & \text{for } r \geq \sigma \end{cases} \quad (6.117a)$$

$$u_{\text{discs,A}}^{\text{depl}}(r) = \begin{cases} u_{\text{discs}}^{\text{depl}}(\sigma) & \text{for } r < \sigma \\ u_{\text{discs}}^{\text{depl}}(r) & \text{for } r \geq \sigma \end{cases} \quad (6.117b)$$

$$u_{\text{discs,ref}}^{\text{depl}}(r) = \begin{cases} u_{\text{discs}}^{\text{depl}}(r) & \text{for } r < \sigma \\ 0 & \text{for } r \geq \sigma \end{cases} \quad (6.117c)$$

$$u_{\text{discs,pert}}^{\text{depl}}(r) = \begin{cases} u_{\text{discs}}^{\text{depl}}(\sigma) & \text{for } r < \sigma \\ u_{\text{discs}}^{\text{depl}}(r) & \text{for } r \geq \sigma \end{cases} \quad (6.117d)$$

$$u_{\text{discs,SR}}^{\text{depl}}(r) = \begin{cases} u_{\text{discs}}^{\text{depl}}(r) & \text{for } r < \sigma \\ 0 & \text{for } r \geq \sigma \end{cases} \quad (6.117e)$$

$$u_{\text{discs,LR}}^{\text{depl}}(r) = \begin{cases} u_{\text{discs}}^{\text{depl}}(\sigma) & \text{for } r < \sigma \\ u_{\text{discs}}^{\text{depl}}(r) & \text{for } r \geq \sigma \end{cases} \quad (6.117f)$$

Another depletion potential of two hard spheres of diameter σ surrounded by infinitely thin hard rods of length L is given by

$$u_{\text{rods}}^{\text{depl}}(r) = -k_B T(N_I + N_{\text{II}} - N_{\text{III}}) \quad (6.118)$$

$$N_I = n_d \frac{\pi}{12} \sigma L^2 \left(1 - \frac{r - \sigma}{L}\right)^2 \left(3 + 2 \frac{L}{\sigma} + \frac{r - \sigma}{\sigma}\right) \quad (6.119)$$

$$N_{\text{II}} - N_{\text{III}} = \frac{\pi}{12} n_d L^2 \sigma \left\{ -2 - \left(\frac{r - \sigma}{D}\right)^3 + 3 \frac{r - \sigma}{D} \right\} \quad (6.120)$$

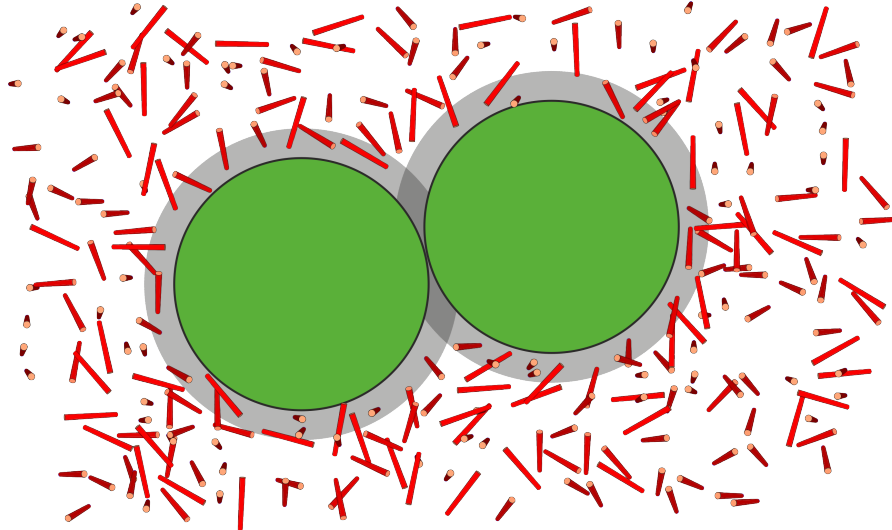


FIGURE 6.14. Attractive depletion forces between large spheres due to depletion forces of infinitely thin hard rods of length L as depleting agent.

Also a splitting of the potential in repulsive-attractive, reference-perturbation, shortrange-longrange has been implemented as

$$u_{\text{rods,R}}^{\text{depl}}(r) = \begin{cases} u_{\text{rods}}^{\text{depl}}(r) & \text{for } r < \sigma \\ 0 & \text{for } r \geq \sigma \end{cases} \quad (6.121\text{a})$$

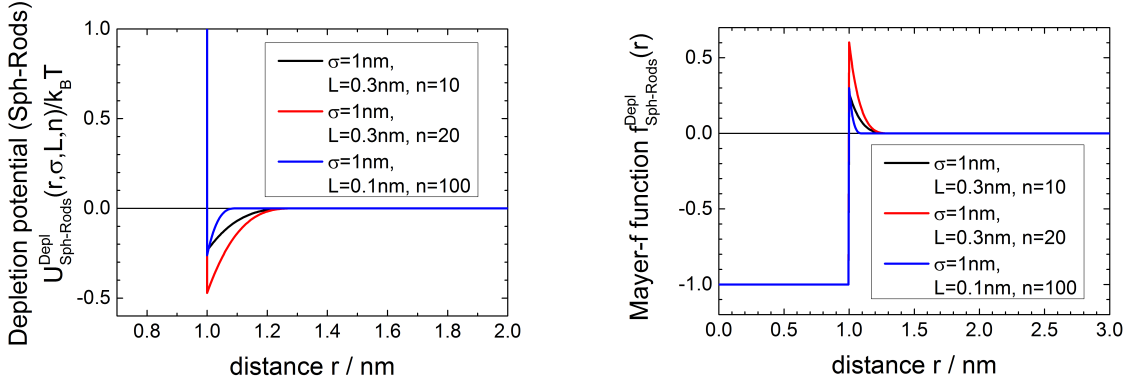
$$u_{\text{rods,A}}^{\text{depl}}(r) = \begin{cases} u_{\text{rods}}^{\text{depl}}(\sigma) & \text{for } r < \sigma \\ u_{\text{rods}}^{\text{depl}}(r) & \text{for } r \geq \sigma \end{cases} \quad (6.121\text{b})$$

$$u_{\text{rods,ref}}^{\text{depl}}(r) = \begin{cases} u_{\text{rods}}^{\text{depl}}(r) & \text{for } r < \sigma \\ 0 & \text{for } r \geq \sigma \end{cases} \quad (6.121\text{c})$$

$$u_{\text{rods,pert}}^{\text{depl}}(r) = \begin{cases} u_{\text{rods}}^{\text{depl}}(\sigma) & \text{for } r < \sigma \\ u_{\text{rods}}^{\text{depl}}(r) & \text{for } r \geq \sigma \end{cases} \quad (6.121\text{d})$$

$$u_{\text{rods,SR}}^{\text{depl}}(r) = \begin{cases} u_{\text{rods}}^{\text{depl}}(r) & \text{for } r < \sigma \\ 0 & \text{for } r \geq \sigma \end{cases} \quad (6.121\text{e})$$

$$u_{\text{rods,LR}}^{\text{depl}}(r) = \begin{cases} u_{\text{rods}}^{\text{depl}}(\sigma) & \text{for } r < \sigma \\ u_{\text{rods}}^{\text{depl}}(r) & \text{for } r \geq \sigma \end{cases} \quad (6.121\text{f})$$



(A) potential between two large spheres and rodlike depleting agents $u_{\text{rods}}^{\text{depl}}(r, \sigma, \dots)$

(B) Mayer-f function of $u_{\text{rods}}^{\text{depl}}(r, \sigma, \dots)$

FIGURE 6.15. potential $u_{\text{rods}}^{\text{depl}}(r, \sigma, \dots)$ and it's Mayer-f function $\exp(-u_{\text{rods}}^{\text{depl}}(r, \sigma, \dots)/k_B T) - 1$

6.5.10. Ionic Microgel Potential.

According to [304] the effective potential in ionic microgels can be partitioned in a contribution $\Phi_{r \leq \sigma}(r)$ for the overlap region $r \leq \sigma$ and one $\Phi_{r > \sigma}(r)$ for $r > \sigma$.

$$u^{\text{im}}(r) = k_B T \begin{cases} \Phi_{r \leq \sigma}(r) & \text{for } r \leq \sigma \\ \Phi_{r > \sigma}(r) & \text{for } r > \sigma \end{cases} \quad (6.122)$$

For the overlapping particle it has the form

$$\Phi_{r \leq \sigma}(r) = \frac{2Z^2 e^2}{\epsilon \sigma} \left[\frac{6}{5} - 2 \left(\frac{r}{\sigma} \right)^2 + \frac{3}{2} \left(\frac{r}{\sigma} \right)^3 - \frac{1}{5} \left(\frac{r}{\sigma} \right)^5 \right] - \frac{72Z^2 e^2}{\epsilon \kappa^4 \sigma^4 r} \Phi_{\text{ind}}(r) \quad (6.123)$$

where $\Phi_{\text{ind}}(r)$ is given by the expression

$$\begin{aligned} \Phi_{\text{ind}}(r) = & \left(1 - e^{-\kappa r} + \frac{1}{2} \kappa^2 r^2 + \frac{1}{24} \kappa^4 r^4 \right) \left(1 - \frac{4}{\kappa^2 \sigma^2} \right) \\ & + \frac{4}{\kappa \sigma} e^{-\kappa \sigma} \sinh(\kappa r) \\ & + \left[e^{-\kappa \sigma} \sinh(\kappa \sigma) + \kappa^2 \sigma r + \frac{1}{6} \kappa^4 (\sigma^3 r + r^3 \sigma) \right] \left(1 + \frac{4}{\kappa^2 \sigma^2} \right) \\ & - \frac{4r}{\sigma} \left(1 + \frac{1}{2} \kappa^2 \sigma^2 + \frac{1}{30} \kappa^4 \sigma^4 \right) \\ & - \frac{8r^3}{3\sigma^3} \left(\frac{\kappa^2 \sigma^2}{4} + \frac{\kappa^4 \sigma^4}{12} \right) - \frac{1}{180} \frac{\kappa^4}{\sigma^2} r^6 \end{aligned} \quad (6.124)$$

For the nonoverlapping distances the effective potential becomes

$$\Phi_{r > \sigma}(r) = \frac{144Z^2 e^2}{\epsilon \kappa^4 \sigma^4} \left[\cosh(\kappa \sigma / 2) - \frac{2 \sinh(\kappa \sigma / 2)}{\kappa \sigma} \right]^2 \frac{e^{-\kappa r}}{r} \quad (6.125)$$

6.5.11. DLVO Potential.

For the past half century or so, the stability of charged colloidal systems has generally been described in terms of the DLVO (Derjaguin-Landau-Verwey-Overbeek) potential between two colloidal particles. The DLVO potential is composed of a long-range screened Coulomb repulsion part $u^{\text{el}}(r)$ and a short-range van der Waals attraction part $u^{\text{vdW}}(r)$ [354].

$$u^{\text{DLVO}}(r) = \begin{cases} \infty & \text{if } r \leq \sigma \\ u^{\text{vdW}}(r) + u^{\text{el}}(r) & \text{if } r > \sigma \end{cases} \quad (6.126)$$

with

$$u^{\text{vdW}}(r) = -k_B T \frac{A_H}{12} \left(\frac{\sigma^2}{(r^2 - \sigma^2)} + \left(\frac{\sigma}{r} \right)^2 + 2 \ln \left(1 - \left(\frac{\sigma}{r} \right)^2 \right) \right) \quad (6.127)$$

$$u^{\text{el}}(r) = k_B T L_B Z_{\text{eff}}^2 \frac{1}{(1 + \kappa\sigma/2)^2} \frac{\exp(-\kappa(r - \sigma))}{r} \quad (6.128)$$

A_H is the Hamaker constant. $L_B = \frac{e^2}{4\pi\epsilon_r\epsilon_0 k_B T}$ is the so-called Bjerrum length¹. The vacuum permittivity is $\epsilon_0 = 8.854187817 \times 10^{-12} \left[\frac{\text{F}}{\text{m}} \right]$ and the elementary electric charge $e = 1.602176565(35) \times 10^{-19}$ coulombs². For water at 278 K with a relative permittivity of $\epsilon_r = 78.7$ the Bjerrum length is $L_B = 0.713 \text{ nm}$. The effective macroion valency is denoted Z_{eff} , and κ^{-1} is the Debye-Hückel screening length due to all macroions. This length characterize the typical distance at which the charge at the origin is screened by the other charges. It is given by $\kappa^2 = 4\pi L_B \sum_{i=1}^N n_i Z_i$, where n_i is the number density of ion i in the bulk solution, Z_i is the charge number or valency of that ion, and the sum is taken over all ions in the solution. A discussion about effective parameters can be found in [3, 492].

¹In Gaussian units, $4\pi\epsilon_0 = 1$ and the Bjerrum length has the simpler form $L_B = \frac{e^2}{\epsilon_r k_B T}$.

²The Gaussian units use the statcoulomb (statC) instead. The conversion between C and statC is different in different contexts. In case of electric charges 1C = 2997924580 statC $\approx 3.00 \times 10^9$ statC.

Also a splitting of the potential in repulsive-attractive, reference-perturbation, shortrange-longrange has been implemented as

$$u_{\text{ref}}^{\text{DLVO}}(r, \dots) = \begin{cases} \infty & \text{for } r \leq \sigma \\ 0 & \text{for } r > \sigma \end{cases} \quad (6.129\text{a})$$

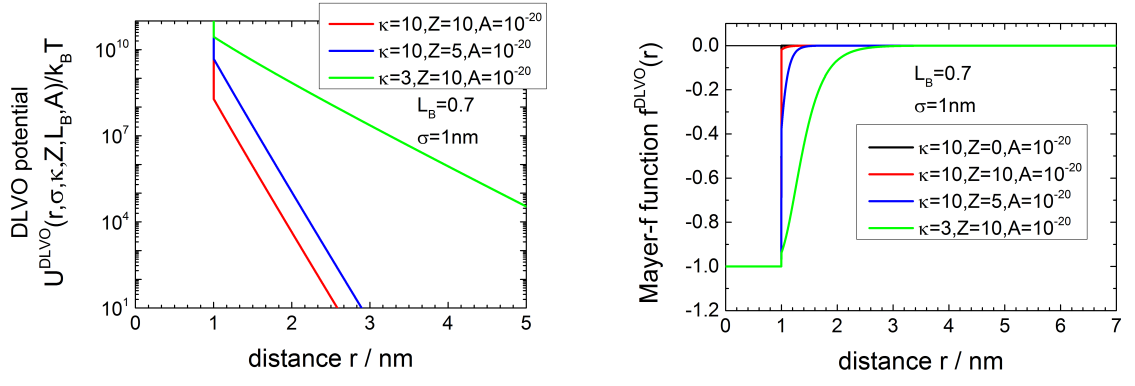
$$u_{\text{pert}}^{\text{DLVO}}(r, \dots) = \begin{cases} 0 & \text{for } r \leq \sigma \\ u^{\text{vdW}}(r) + u^{\text{el}}(r) & \text{for } r > \sigma \end{cases} \quad (6.129\text{b})$$

$$u_{\text{SR}}^{\text{DLVO}}(r, \dots) = \begin{cases} \infty & \text{for } r \leq \sigma \\ u^{\text{vdW}}(r) & \text{for } r > \sigma \end{cases} \quad (6.129\text{c})$$

$$u_{\text{LR}}^{\text{DLVO}}(r, \dots) = \begin{cases} u^{\text{el}}(\sigma) & \text{for } r \leq \sigma \\ u^{\text{el}}(r) & \text{for } r > \sigma \end{cases} \quad (6.129\text{d})$$

$$u_{\text{R}}^{\text{DLVO}}(r, \dots) = \begin{cases} \infty & \text{for } r \leq \sigma \\ u^{\text{el}}(r) & \text{for } r > \sigma \end{cases} \quad (6.129\text{e})$$

$$u_{\text{A}}^{\text{DLVO}}(r, \dots) = \begin{cases} 0 & \text{for } r \leq \sigma \\ u^{\text{vdW}}(r) & \text{for } r > \sigma \end{cases} \quad (6.129\text{f})$$



(A) DLVO potential (Derjaguin and Landau, Verwey and Overbeek) $u^{\text{DLVO}}(r, \sigma, \dots)$

(B) Mayer-f function of $u^{\text{DLVO}}(r, \sigma, \dots)$

FIGURE 6.16. potential $u^{\text{DLVO}}(r, \sigma, \dots)$ and it's Mayer-f function $\exp(-u^{\text{DLVO}}(r, \sigma, \dots)/k_B T) - 1$

6.5.12. Hard Core 3Yukawa Potential.

This potential is useful for systems with complicated potentials. Next to the hard core repulsion three Yukawa contributions are allowed. The potential reads

$$u^{\text{HC3Y}}(r, \dots) = \begin{cases} \infty & \text{for } r < \sigma \\ k_B T \sum_{i=1}^{N=3} -K_i \frac{\exp(-Z_i(\frac{r}{\sigma} - 1))}{r/\sigma} & \text{for } r \geq \sigma \end{cases} \quad (6.130)$$

The sign of K_i defines, if the potential is repulsive ($K_i < 0$) or attractive ($K_i > 0$) and the modulus of $|K_i|$ defines the strength of the interaction. $Z_i = 1/\lambda_i$ defines the range of the interaction and should be always a positive number. λ_i is the screening length.

Also a splitting of the potential in repulsive-attractive, reference-perturbation, shortrange-longrange has been implemented as

$$u_{\text{ref}}^{\text{HC3Y}}(r, \dots) = \begin{cases} \infty & \text{for } r < \sigma \\ 0 & \text{for } r \geq \sigma \end{cases} \quad (6.131\text{a})$$

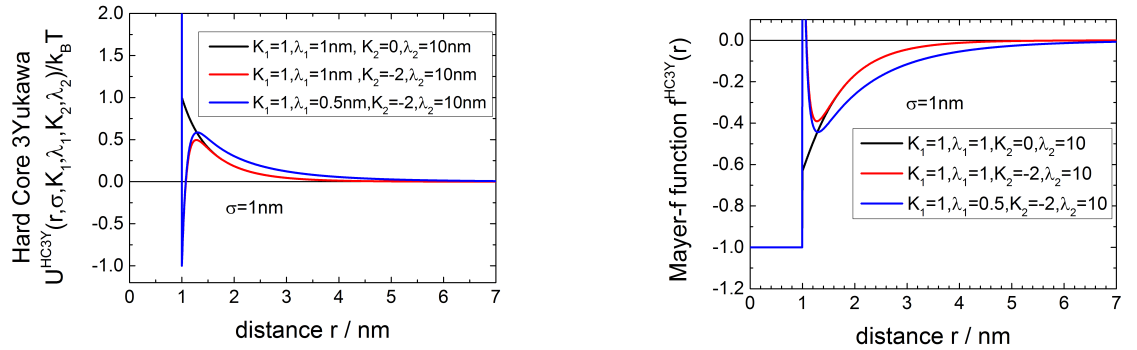
$$u_{\text{pert}}^{\text{HC3Y}}(r, \dots) = \begin{cases} u_{\text{ref}}^{\text{HC3Y}}(\sigma, \dots) & \text{for } r < \sigma \\ u_{\text{ref}}^{\text{HC3Y}}(r, \dots) & \text{for } r \geq \sigma \end{cases} \quad (6.131\text{b})$$

$$u_{\text{SR}}^{\text{HC3Y}}(r, \dots) = u_{\text{ref}}^{\text{HC3Y}}(r, \dots) \quad (6.131\text{c})$$

$$u_{\text{LR}}^{\text{HC3Y}}(r, \dots) = u_{\text{pert}}^{\text{HC3Y}}(r, \dots) \quad (6.131\text{d})$$

$$u_{\text{R}}^{\text{HC3Y}}(r, \dots) = \begin{cases} \infty & \text{for } r < \sigma \\ k_B T \sum_{\forall K_i < 0} -K_i \frac{\exp(-Z_i(\frac{r}{\sigma} - 1))}{r/\sigma} & \text{for } r \geq \sigma \end{cases} \quad (6.131\text{e})$$

$$u_{\text{A}}^{\text{HC3Y}}(r, \dots) = \begin{cases} k_B T \sum_{\forall K_i > 0} -K_i & \text{for } r < \sigma \\ k_B T \sum_{\forall K_i > 0} -K_i \frac{\exp(-Z_i(\frac{r}{\sigma} - 1))}{r/\sigma} & \text{for } r \geq \sigma \end{cases} \quad (6.131\text{f})$$



(A) Hard Core Yukawa potential with three linear combinations of Yukawa tails $u^{\text{HC3Y}}(r, \sigma, \dots)$

(B) Mayer-f function of $u^{\text{HC3Y}}(r, \sigma, \dots)$

FIGURE 6.17. potential $u^{\text{HC3Y}}(r, \sigma, \dots)$ and it's Mayer-f function $\exp(-u^{\text{HC3Y}}(r, \sigma, \dots)/k_B T) - 1$

6.6. GUI interface for the Ornstein Zernike solver

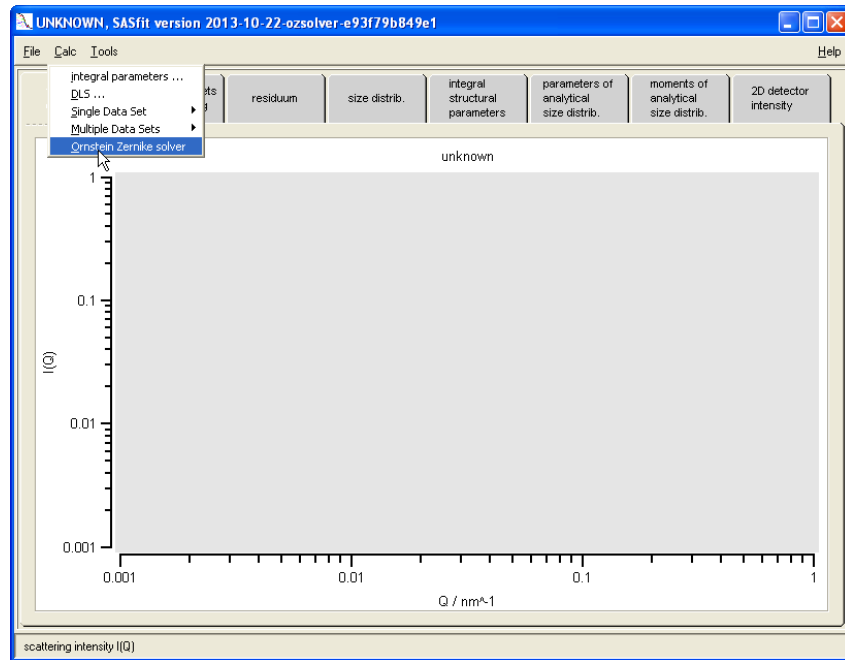


FIGURE 6.18. Starting the menu for OZ-solver.

The OZ-solver in **SASfit** does not allow at the moment an optimization of the parameters of the pair interaction potential in the fitting routine to fit the corresponding structure factor for single or multiple data sets. The main reason for that is, that in the implemented Levenberg-Marquardt-algorithmus the partial derivatives have to be calculated for every q-value. To do this with the implemented routine for the OZ-solver would be too time consuming at the moment. Nevertheless, **SASfit** allows to have access

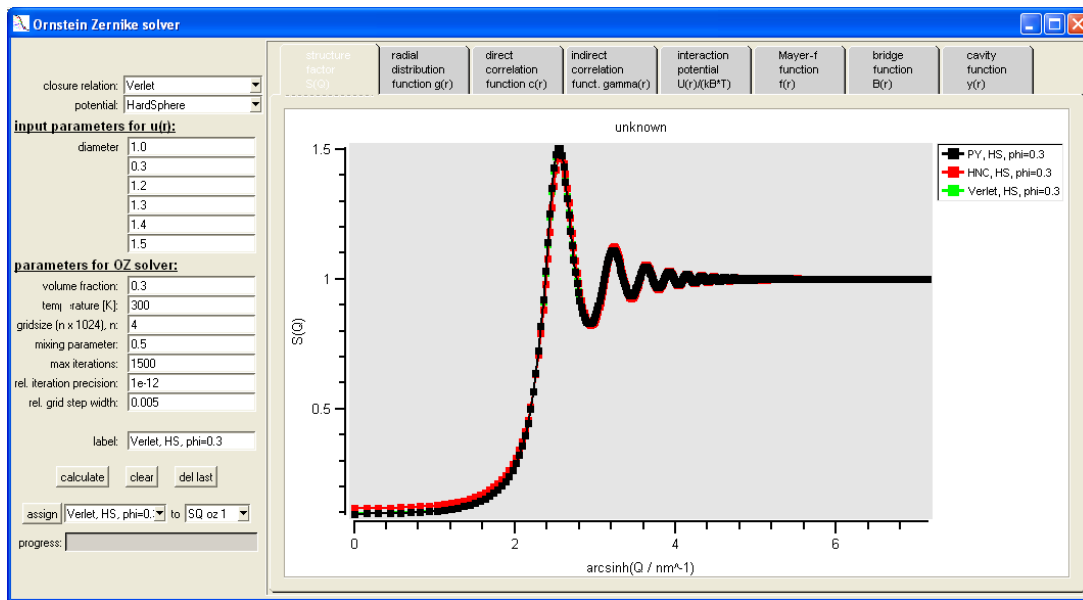


FIGURE 6.19. Main GUI for solving the Ornstein Zernike equation.

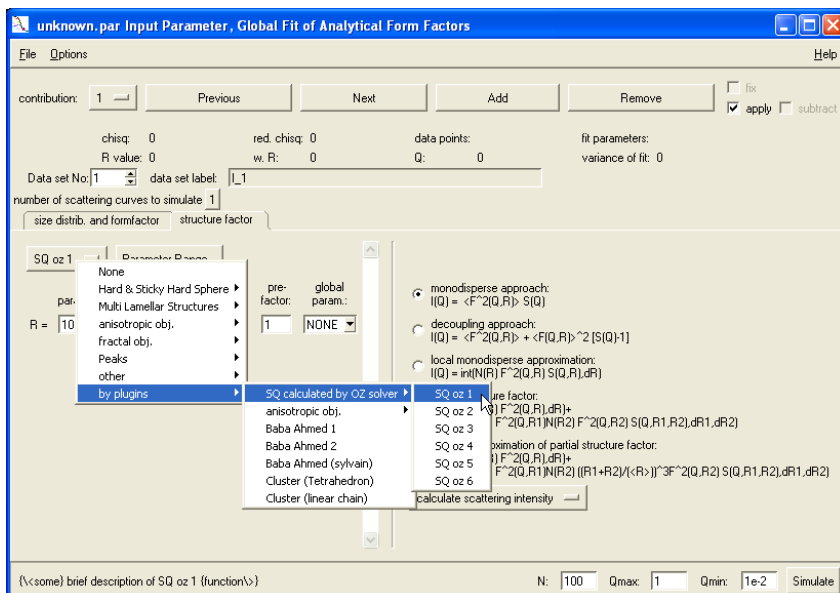


FIGURE 6.20. Access to the solutions of the OZ-solver.

up to 6 pre-calculated solutions of the OZ equations. These solutions can be stored as splines under the names "SQ oz 1", "SQ oz 2" to "SQ oz 6" in the menu interface of the OZ-solver. These splines functions are made available in the menu for calculating structure factors under the names [by plugins|SQ calculated by OZ solver|SQ oz 1] ... [by plugins|SQ calculated by OZ solver|SQ oz 6]. The extrapolation to $Q = 0$ is done by the OZ-solver by a quadratic extrapolation to zero of the first three $S(Q)$. For $Q > Q_{\max}$ it is assumed that $S(Q > Q_{\max}) \equiv 1$. As at the moment all

implemented potentials scale with a size parameter (diameter D), i.e. that the structure factor for different diameters $D = 2R$ scales as $S(QD) = S(Q2R)$ for all D . Therefore only the radius is an input values for the structure factors "SQ oz 1"- "SQ oz 6" and can be fitted.

CHAPTER 7

Size Distributions

Several distribution functions are supplied in **SASfit** for smearing parameters. In principle any parameter of the form factor can be assigned with a distribution function. It does not need to be a parameter describing a size or length quantity of the scattering object. As also the inclusion of the structure factor is effected by the size distribution details about this can be found in section 4.1. In the simplest case, let say a distribution of radii $N f_{\text{pdf}}(x)$ is needed to describe a system, the integration to be performed is

$$I(q) = \int_0^\infty N f_{\text{pdf}}(x) P(q, x) dx \quad (7.1)$$

which is an improper integral with an upper bound approaching infinity. The distribution function available are all probability distribution functions normalized on 1 for the definition range between 0 and ∞ and N is the scaling factor describing typically the number density of particles if the scattering intensity is given in units of 1/cm. Specialized code for such integrals are available and also implemented in **SASfit**. However, in cases where the size distribution shows a very narrow peak these algorithm might miss the peak. Therefore for all distribution functions it has been tried to find proper finite lower and upper integration limits. The routine for finding a suitable integration range also takes into account, that the form factor can scale with up to the 6th power of its size parameter. Therefore at the moment for each size distribution also the internal function for finding the proper integration limits needs to be extended.

Another way of performing the integration is to make use of the quantile distribution function. For many analytically available probability distribution function $f_{\text{pdf}}(x)$ also their cumulative distribution function $F_{\text{cdf}}(x)$ is analytically known

$$F_{\text{cdf}}(x) = \int_{-\infty}^x f_{\text{pdf}}(x') dx' = p \quad (7.2)$$

as well as its quantile distribution function

$$Q_{\text{qdf}}(p) = (F_{\text{cdf}}(x))^{-1}(p) = x, \quad (7.3)$$

which is the inverse of the cumulative distribution function $F(x)$. The quantile density function $q_{\text{qdf}}(p)$ is then given by

$$q_{\text{qdf}}(p) = \frac{dQ_{\text{qdf}}(p)}{dp} = \frac{dx}{dp} \quad (7.4)$$

and its reciprocal is related to the probability distribution function by

$$\frac{1}{q_{\text{qdf}}(p)} = f_{\text{pdf}}(F_{\text{cdf}}(x)) \quad (7.5)$$

We therefore can write the integral 7.1 as

$$I(q) = \int_0^\infty N f_{\text{pdf}}(x) P(q, x) dx \quad (7.6)$$

$$= \int_0^\infty N f_{\text{pdf}}(F_{\text{cdf}}(x)) P(q, x) dx \quad (7.7)$$

$$= \int_{F_{\text{cdf}}(0)}^{F_{\text{cdf}}(\infty)} N f_{\text{pdf}}(p) P(q, Q_{\text{qdf}}(p)) q_{\text{qdf}}(p) dp \quad (7.8)$$

$$= \int_{F_{\text{cdf}}(0)}^1 N P(q, Q_{\text{qdf}}(p)) dp \quad (7.9)$$

By this variable transformation the integral become a proper integral over the box $(F_{\text{cdf}}(0); 1)$ and behaves well both for very sharp as well as broad probability distribution functions as the integration is performed over the cumulative value dp of the probability distribution.

7.1. Delta

Choosing **Delta** as a size distribution simply scales the form factor with a constant value N without performing any integration.

Input Parameters for size distribution **Delta**:

N: particle number density N

7.2. Uniform distribution

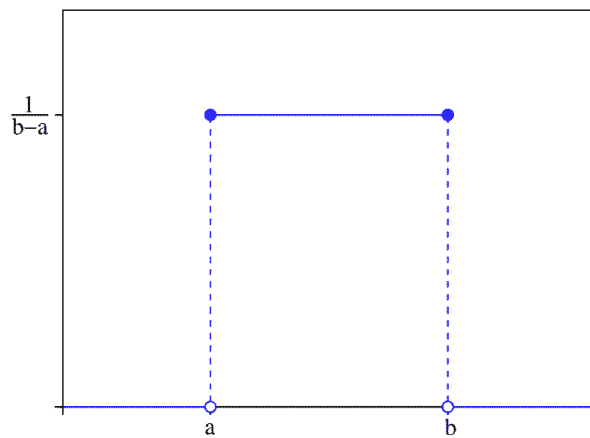


FIGURE 7.1. Uniform distribution function. $x_{\min}, x_{\max} \in (-\infty, \infty)$,
 $x_{\max} > x_{\min}$, $x_{\min} \leq x \leq x_{\max}$

The uniform distribution defines equal probability over a given range for a continuous distribution. The support is defined by the two parameters, x_{\min} and x_{\max} , which are its minimum and maximum values.

$$\text{Uniform}(x|N, x_{\min}, x_{\max}) = \begin{cases} \frac{N}{x_{\max} - x_{\min}} & \text{for } x_{\min} \leq x \leq x_{\max}, \\ 0 & \text{for } x < x_{\min} \text{ or } x > x_{\max} \end{cases} \quad (7.10a)$$

Input Parameters for size distribution **Uniform**:

N: particle number density N

Xmin: minimum value of the distribution (x_{\min})

Xmax: maximum value of the distribution (x_{\max})

7.3. Triangular distribution

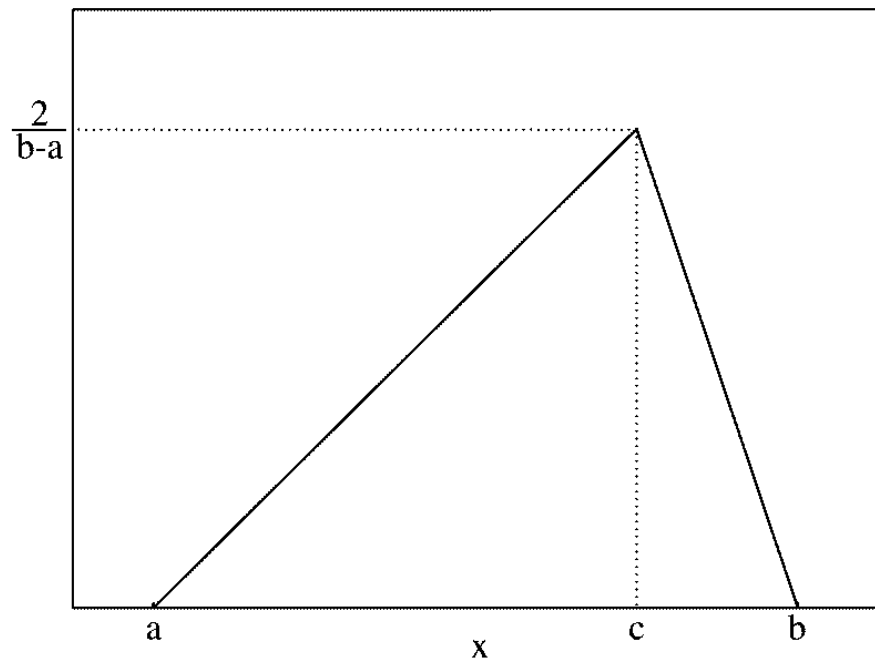


FIGURE 7.2. Triangular distribution function. $x_{\min}, x_{\text{mode}}, x_{\max} \in (-\infty, \infty)$, $x_{\max} > x_{\min}$, $x_{\min} \leq x_{\text{mode}} \leq x_{\max}$, $x_{\min} \leq x \leq x_{\max}$

$$\text{Triangular}(x|x_{\min}, x_{\max}, x_{\text{mode}}) = \begin{cases} \frac{2(x - x_{\min})}{(x_{\max} - x_{\min})(x_{\text{mode}} - x_{\min})} & \text{for } x_{\min} < x \leq x_{\text{mode}} \\ \frac{2(x_{\max} - x)}{(x_{\max} - x_{\min})(x_{\max} - x_{\text{mode}})} & \text{for } x_{\text{mode}} < x \leq x_{\max} \end{cases} \quad (7.11a)$$

7.4. Log-Normal distribution

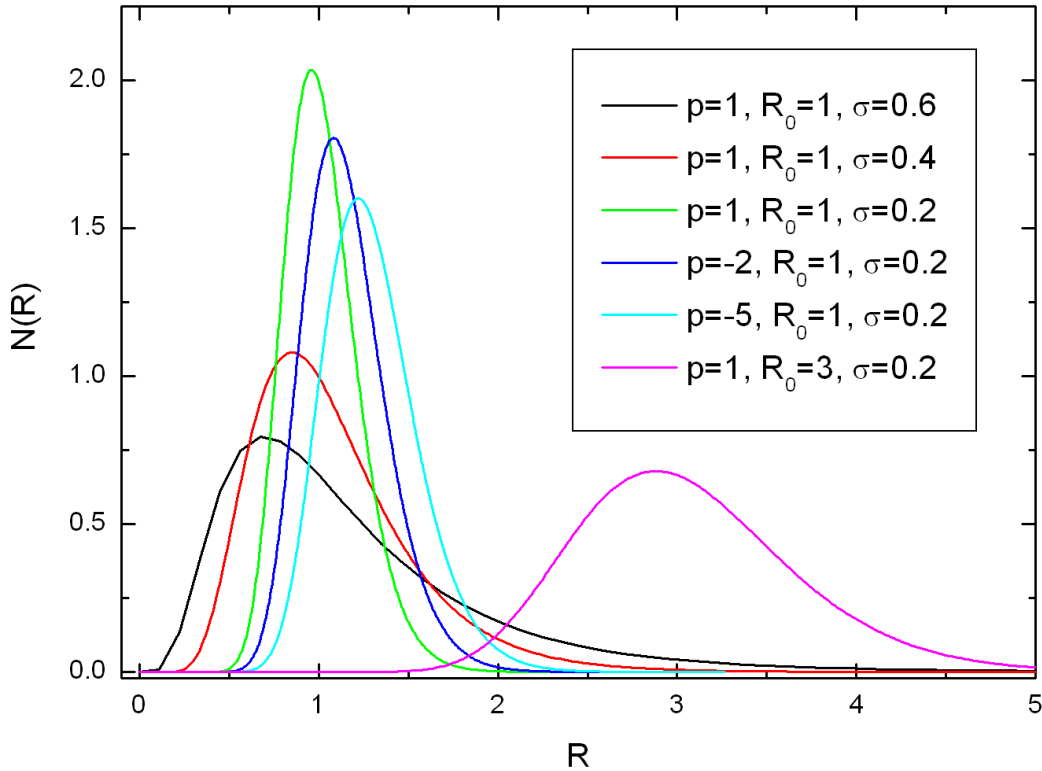


FIGURE 7.3. LogNormal distribution function ($R_0 = 1$ and $p = 1$ has been set both to one here). Valid parameter ranges: $R \in (0, \infty)$, $R_0 \in (0, \infty)$, $\sigma \geq 0$, $p \in (-\infty, \infty)$

The `LogNorm` distribution is a continuous distribution in which the logarithm of a variable has a normal distribution.

$$\text{LogNorm}(X, \mu, \sigma, p) = \frac{N}{c_{\text{LN}}} \frac{1}{X^p} \exp\left(-\frac{\ln(X/\mu)^2}{2\sigma^2}\right) \quad (7.12a)$$

$$c_{\text{LN}} = \sqrt{2\pi} \sigma \mu^{1-p} \exp\left((1-p)^2 \frac{\sigma^2}{2}\right) \quad (7.12b)$$

where σ is the width parameter, p a shape parameter, μ is the location parameter. c_{LN} is chosen so that $\int_0^\infty \text{LogNorm}(X, \mu, \sigma, p) dX = N$. The mode of the distribution X_{mode} and the variance $\text{Var}(X)$ are defined as

$$X_{\text{mode}} = \mu e^{-p\sigma^2} \quad (7.13)$$

$$X_{\text{mean}} = \mu e^{-\frac{1}{2}\sigma^2(2p-3)} \quad (7.14)$$

$$X_{\text{median}} = \mu e^{-\sigma^2(p-1)} \quad (7.15)$$

$$\text{Var}(X) = \mu^2 (e^{\sigma^2} - 1) e^{(3-2p)\sigma^2} \quad (7.16)$$

and the m^{th} moment $\langle X^m \rangle$ of the **LogNorm** distribution as

$$\langle X^m \rangle = \frac{\int X^m \text{LogNorm}(X) dX}{\int \text{LogNorm}(X) dX} = \mu^m e^{\frac{1}{2}\sigma^2 m(2-2p+m)}. \quad (7.17)$$

The cumulative distribution function is given by

$$F_{\text{LogNorm}}(X) = 1/2 \operatorname{erf} \left[\frac{(p-1)\sigma^2 + \ln(X/\mu)}{\sqrt{2}\sigma} \right] = Y \quad (7.18)$$

and its quantile function by

$$Q_{\text{LogNorm}}(Y) = \mu \exp \left(\sqrt{2}\sigma \operatorname{erf}^{-1}(2Y) - (p-1)\sigma^2 \right) = X \quad (7.19)$$

7.5. Schulz-Zimm (Flory) distribution

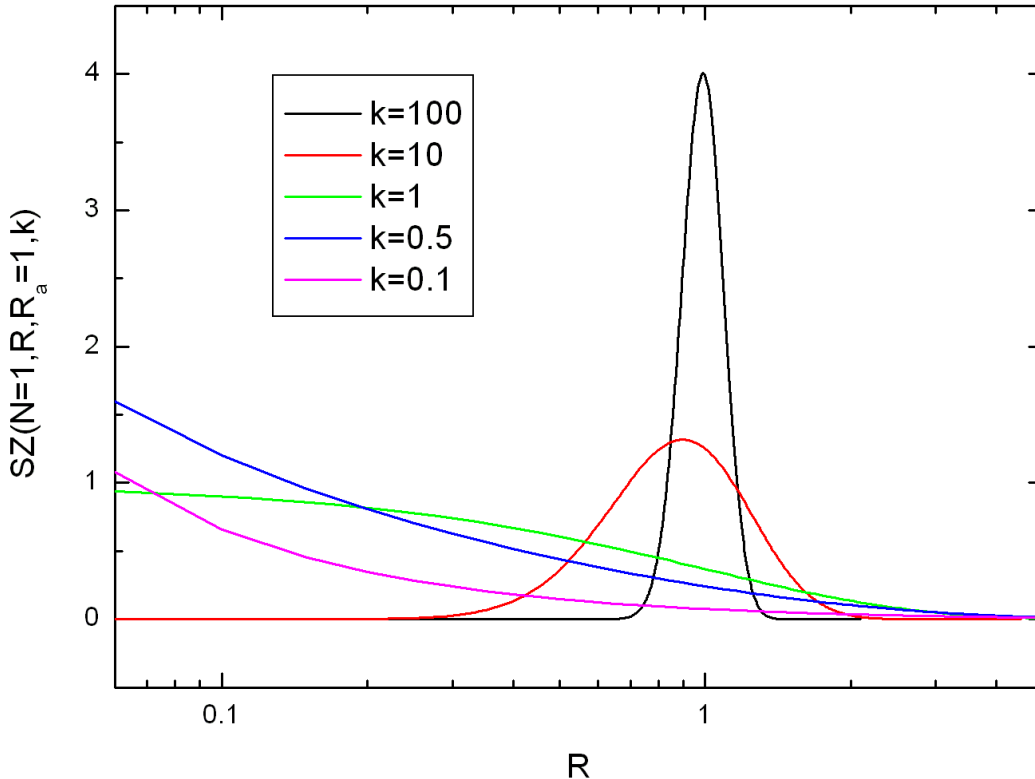


FIGURE 7.4. The $SZ(X, N, X_a, k)$ distribution function. Valid parameter ranges: $X \in [0, \infty)$, $X_a \in (0, \infty)$, $k = X_a^2/\sigma^2 > 0$

A function commonly used to present polymer molecular weight distributions is the Schulz-Zimm function [544]

$$SZ_n(X, N, X_a, k) = \frac{N}{X_a} \left(\frac{X}{X_a} \right)^{k-1} \frac{k^k \exp(-kX/X_a)}{\Gamma(k)} \quad (7.20)$$

$SZ_n(X, N, X_a, k)$ is normalized so that $\int_0^\infty SZ_n(X, N, X_a, k) dX = N$. In polymer science X would be the molecular weight M , $\bar{M}_n = X_a$, and $\bar{M}_w = \bar{M}_n \frac{k+1}{k}$, and $\Gamma(k)$ is the gamma function. The above form (7.20) gives the number distribution. Its mode, mean, variance and m^{th} -moment are given by

$$X_{\text{mode}} = X_a \left(1 - \frac{1}{k} \right) \quad (7.21a)$$

$$X_{\text{mean}} = X_a \quad (7.21b)$$

$$\text{Var}(X) = \sigma^2 = \frac{X_a^2}{k} \quad (7.21c)$$

$$\langle X^m \rangle = \left(\frac{X_a}{k} \right)^m \frac{\Gamma(k+m)}{\Gamma(k)} \quad (7.21d)$$

The number distribution as well as the weight distribution described below can be expressed by a gamma distribution described in eq. 7.24 by $\text{SZ}_n(X, N, X_a, k) = \text{gammaSD}(x, N, X_a(1 - 1/k), R_a^2/k)$.

The corresponding weight distribution is

$$\text{SZ}_w(X, N, X_a, k) = \frac{X}{X_a} \text{SZ}_n(X, N, X_a, k) = \frac{NX^k \left(\frac{k}{X_a}\right)^{k+1} e^{-\frac{kX}{X_a}}}{\Gamma(k+1)} \quad (7.22)$$

Also $\text{SZ}_w(X, N, X_a, k)$ is normalized so that $\int_0^\infty \text{SZ}_w(X, N, X_a, k) dX = N$. The mode, mean, variance and m^{th} -moment of the weight distribution are given by

$$X_{\text{mode}} = X_a \quad (7.23a)$$

$$X_{\text{mean}} = X_a \frac{1+k}{k} \quad (7.23b)$$

$$\text{Var}(X) = \sigma^2 = X_a^2 \frac{1+k}{k^2} \quad (7.23c)$$

$$\langle X^m \rangle = \left(\frac{X_a}{k}\right)^m \frac{\Gamma(k+m+1)}{\Gamma(k+1)} \quad (7.23d)$$

The weight distribution can be expressed by a gamma distribution described in eq. 7.24 by $\text{SZ}_w(X, N, X_a, k) = \text{gammaSD}(x, N, X_a, R_a^2(1+k)/k^2)$.

7.6. Gamma distribution

The Gamma distribution is a two parameter continuous distribution with a scale parameter θ and a shape parameter k .

$$\text{gammaSD}(x, N, \theta, \kappa) = \frac{N}{\theta} \left(\frac{x}{\theta} \right)^{\kappa-1} \frac{\exp(-x/\theta)}{\Gamma(\kappa)} \quad (7.24)$$

The mean x_{mean} , mode x_{mode} and variance σ^2 of the distribution are given by

$$x_{\text{mean}} = \kappa\theta \quad (7.25)$$

$$x_{\text{mode}} = (\kappa - 1)\theta \text{ for } \kappa \geq 1 \quad (7.26)$$

$$\sigma^2 = \kappa\theta^2 \quad (7.27)$$

The gamma distribution is more flexible than the exponential or χ^2 distribution function which are special cases of the gamma distribution function. When κ is large, the gamma distribution closely approximates a normal distribution with the advantage that the gamma distribution has density only for positive real numbers. For small values of κ the distribution becomes a right tailed distribution. The gamma distribution is equivalent to the Schulz-Zimm distribution $\text{SZ}_n()$ (sec. 7.5), which is using the mean value instead of $\theta = x_{\text{mean}}/\kappa$ for the parametrization. Also the Pearson III 7.7 is just another name for this distribution.

The m^{th} moment $\langle X^m \rangle$ of the size distribution is given by

$$\langle X^m \rangle = \theta^m \frac{\Gamma(\kappa + m)}{\Gamma(\kappa)}. \quad (7.28)$$

In the present version the Gamma distribution is re-parameterised as a function of the mode and variance, i.e.

$$\kappa = \frac{x_{\text{mode}} \sqrt{x_{\text{mode}}^2 + 4\sigma^2} + x_{\text{mode}}^2 + 2\sigma^2}{2\sigma^2} \quad (7.29)$$

and

$$\theta = \frac{1}{2} \left(\sqrt{x_{\text{mode}}^2 + 4\sigma^2} - x_{\text{mode}} \right) \quad (7.30)$$

$\text{gammaSD}(x, N, x_{\text{mode}}, \sigma)$ is normalized so that $\int_0^\infty \text{gammaSD}(x, N, x_{\text{mode}}, \sigma) dx = N$.

Input parameters for the size distribution `gammaSD`:

N: N

mode: mode of the distribution (maximum, most probable size) $x_{\text{mode}} > 0$

sigma: width parameter $\sigma > 0$. The variance of the distribution is σ^2 .

Note:

- The parameters **mode** and **sigma** needs to be positive.

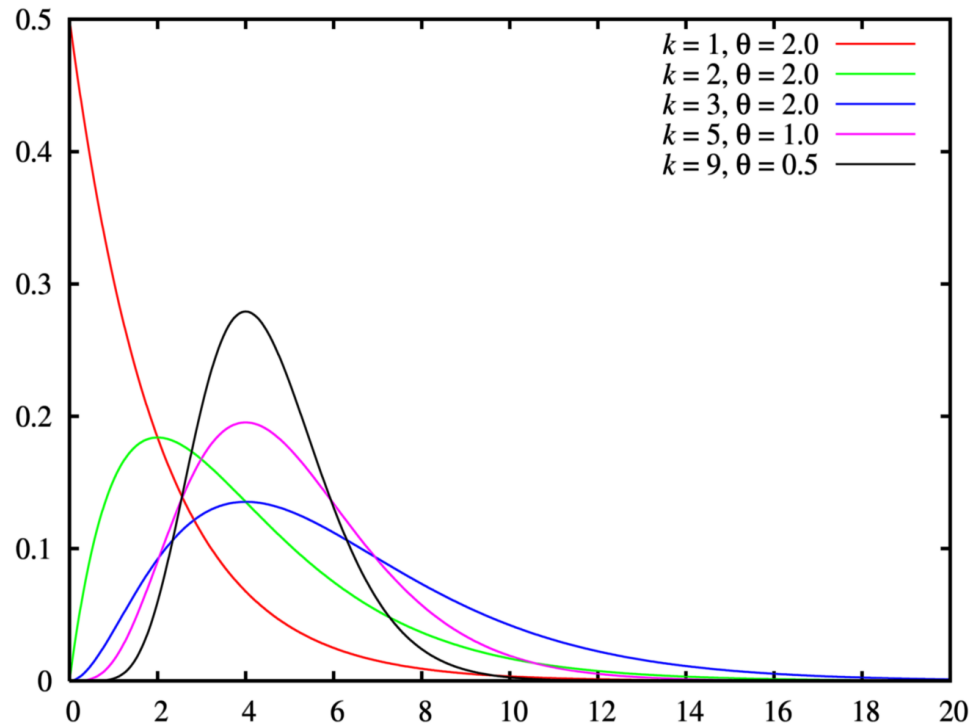


FIGURE 7.5. The $\text{gammaSD}(R, N, x_{\text{mode}}, \sigma)$ distribution function. Valid parameter ranges: $x \in [0, \infty)$, $x_{\text{mode}} \in (0, \infty)$, $\sigma > 0$

7.7. PearsonIII distribution

The Pearson distribution is a family of probability distributions that are a generalisation of the normal distribution. The Pearson Type III distribution is given by the probability density function

$$f(x) = \frac{1}{\beta \Gamma(p)} \left(\frac{x - \alpha}{\beta} \right)^{p-1} e^{-(x-\alpha)/\beta}, \quad (7.31)$$

where $x \in [\alpha, \infty)$ and α, β and p are parameters of the distribution with $\beta > 0$ and $p > 0$ (Abramowitz and Stegun 1954, p. 930). Here, $\Gamma()$ denotes the Gamma function.

- Mean:

$$\alpha + p\beta$$

- Variance:

$$p\beta^2$$

- Skewness:

$$\frac{2}{\sqrt{p}}$$

- Kurtosis:

$$\frac{6}{p}$$

The Pearson Type III distribution is identical to the Gamma distribution (7.24). When $\alpha = 0$, $\beta = 2$, and p is half-integer, the Pearson Type III distribution becomes the χ^2 distribution of $2p$ degrees of freedom.

7.8. Gauss distribution

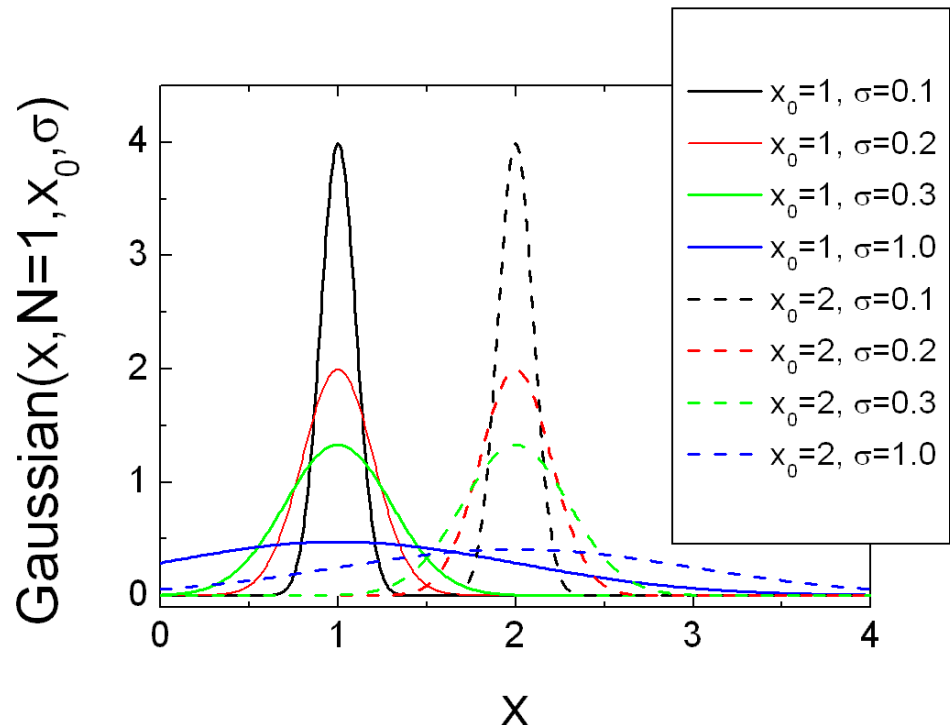


FIGURE 7.6. Normal or Gauss distribution function ($R_0 = \mu = 0$ has been chosen in the plot). Valid parameter ranges: $R \in (0, \infty)$, $R_0 \in (-\infty, \infty)$, $\sigma > 0$

$$\text{Gauss}(R, N, \sigma, R_0) = \frac{N}{c_{\text{Gauss}}} e^{-\frac{(R-R_0)^2}{2\sigma^2}} \quad (7.32a)$$

$$c_{\text{Gauss}} = \sqrt{\frac{\pi}{2}} \sigma \left(1 + \text{erf} \left(\frac{R_0}{\sqrt{2}\sigma} \right) \right) \quad (7.32b)$$

c_{Gauss} is chosen so that $\int_0^\infty \text{Gauss}(R, \sigma, R_0) dR = N$

7.9. Generalized exponential distribution (GEX)

The generalised exponential distribution is a three parameter distribution.

$$\text{GEX}(x, \beta, \lambda, \gamma) = N \frac{|\beta|}{\gamma} \left(\frac{x}{\gamma} \right)^{\lambda+1} \frac{e^{-(x/\gamma)^\beta}}{\Gamma(\frac{\lambda+2}{\beta})} \quad (7.33)$$

$$\text{GEX}(x, \beta, p, \gamma) = N \frac{|\beta|}{\gamma} \left(\frac{x}{\gamma} \right)^{p-1} \frac{e^{-(x/\gamma)^\beta}}{\Gamma(\frac{p}{\beta})} \quad (7.34)$$

For $\lambda + 2 = p = \beta$ it will transform in the Weibull distribution (eq. 7.43). For $\beta = 1$ one yields the Schulz-Zimm distribution (eq. 7.20) or the equivalent gamma distribution (eq. 8.31). In the limit $(\beta, \lambda) \rightarrow (0, \infty)$ whereas the product $\beta(\lambda + 2) \rightarrow \sigma$ is finite and the GEX distribution transforms into a Lognormal distribution.

$$\lim_{(\beta, \lambda) \rightarrow (0, \infty)} \text{GEX}(x, \beta, \lambda, \gamma) = \frac{1}{\sqrt{2\pi} \sigma x} \exp \left(-\frac{(\log x - \log \gamma)^2}{2\sigma^2} \right) \quad (7.35)$$

$$\text{with } \lim_{(\beta, \lambda) \rightarrow (0, \infty)} \beta(\lambda + 2) = \sigma \quad (7.36)$$

The mode x_{mode} , mean x_{mean} , and variance σ^2 of this distribution are given by

$$x_{\text{mode}} = \gamma \left(\frac{\lambda + 1}{\beta} \right)^{\frac{1}{\beta}} \quad (7.37)$$

$$x_{\text{mean}} = \begin{cases} \gamma \Gamma(\frac{\lambda+3}{\beta}) / \Gamma(\frac{\lambda+2}{\beta}) & \text{for } \beta > 0 \wedge \lambda > -3 \\ \text{undefined} & \text{otherwise} \end{cases} \quad (7.38)$$

$$\sigma^2 = \begin{cases} \gamma^2 \left(\frac{\Gamma(\frac{\lambda+4}{\beta})}{\Gamma(\frac{\lambda+2}{\beta})} - \left(\frac{\Gamma(\frac{\lambda+3}{\beta})}{\Gamma(\frac{\lambda+2}{\beta})} \right)^2 \right) & \text{for } \beta > 0 \wedge \lambda > -3 \\ \text{undefined} & \text{otherwise} \end{cases} \quad (7.39)$$

7.10. Generalized extreme value distribution (GEV)

FIGURE 7.7. The shape parameter governs the tail behaviour of the distribution, the sub-families defined by $\xi \rightarrow 0$, $\xi > 0$ and $\xi < 0$ correspond, respectively, to the Gumbel, Fréchet and Weibull families, whose cumulative distribution functions are reminded below. Gumbel or type I extreme value distribution

$$\text{GEV}(R, \mu, \sigma, \xi) = \frac{N}{c_1} \frac{e^{-(1+\frac{\xi(R-\mu)}{\sigma})^{-1/\xi}}}{\sigma \left(1 + \frac{\xi(R-\mu)}{\sigma}\right)^{1+1/\xi}} \quad (7.40)$$

with

$$c_1 = \begin{cases} 1 & \text{for } \xi > 0 \\ 1 - \exp\left(-\left(1 - \frac{\xi\mu}{\sigma}\right)^{-\frac{1}{\xi}}\right) & \text{for } \xi < 0 \end{cases} \quad (7.41)$$

The shape parameter ξ governs the tail behaviour of the distribution, the sub-families defined by $\xi \rightarrow 0$, $\xi > 0$ and $\xi < 0$ correspond, respectively, to the Gumbel, Fréchet and Weibull families, whose cumulative distribution functions are reminded below.

- Gumbel or type I extreme value distribution

$$F(x; \mu, \sigma) = e^{-e^{-(x-\mu)/\sigma}} \quad \text{for } x \in \mathbb{R}$$

- Fréchet or type II extreme value distribution

$$F(x; \mu, \sigma, \alpha) = \begin{cases} 0 & x \leq \mu \\ e^{-((x-\mu)/\sigma)^{-\alpha}} & x > \mu \end{cases}$$

- Weibull or type III extreme value distribution

$$F(x; \mu, \sigma, \alpha) = \begin{cases} e^{-(-(x-\mu)/\sigma)^{-\alpha}} & x < \mu \\ 1 & x \geq \mu \end{cases}$$

where $\xi > 0$ and $\xi > 0$

Remark I: For reliability issues the Weibull distribution is used with the variable $t = \mu - x$, the time, which is strictly positive. Thus the support is positive - in contrast to the use in extreme value theory.

Remark II: Be aware of an important distinctive feature of the three extreme value distributions: The support is either unlimited, or it has an upper or lower limit.

- Parameters

$\mu \in [-\infty, \infty]$ location (real)

$\sigma \in (0, \infty]$ scale (real)

$\xi \in [-\infty, \infty]$ shape (real)

- Support

$$x > \mu - \sigma/\xi \ (\xi > 0)$$

$$x < \mu - \sigma/\xi \ (\xi < 0)$$

$$x \in [-\infty, \infty] \ (\xi = 0)$$

[1] http://en.wikipedia.org/wiki/Generalized_extreme_value_distribution

7.11. Maxwell distribution

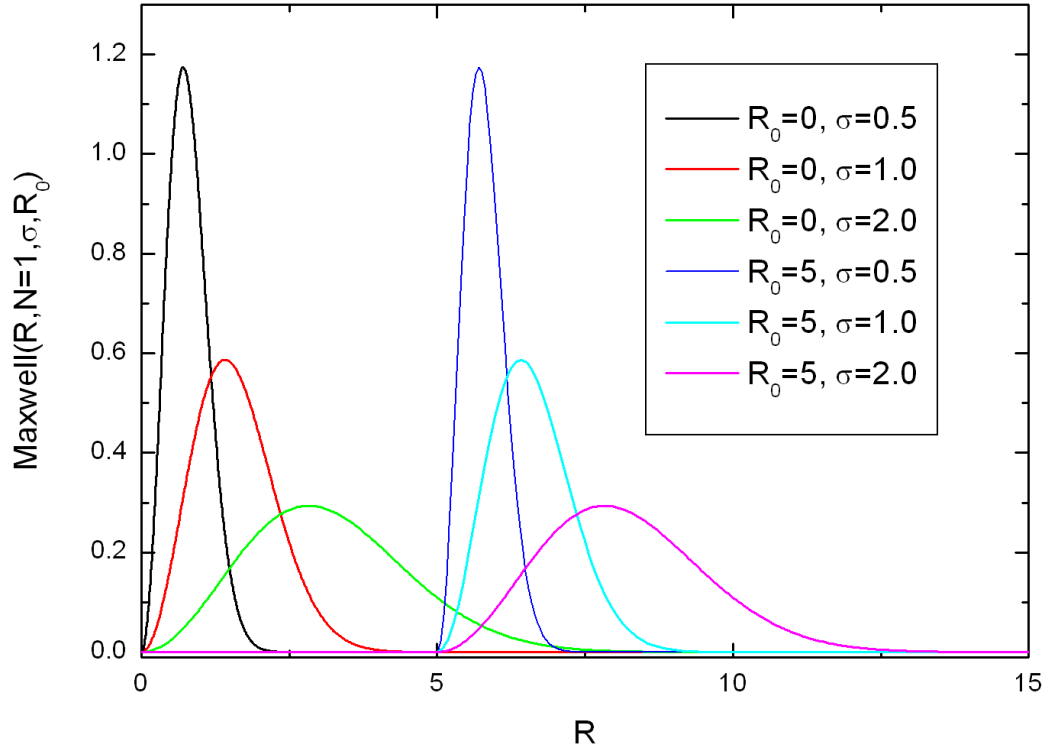


FIGURE 7.8. Maxwell distribution function. Valid parameter ranges: $R \in [0, \infty)$, $R_0 \in (-\infty, \infty)$, $\sigma > 0$

$$\text{Maxwell}(R, R_0, \sigma) = \begin{cases} \text{if } R \geq R_0: & N \frac{c}{c_{\text{mw}}} (R - R_0)^2 e^{-(R-R_0)^2/(2\sigma^2)} \\ \text{else:} & 0 \end{cases} \quad (7.42a)$$

$$c = \frac{4}{\sqrt{\pi}} (2\sigma^2)^{-3/2} \quad (7.42b)$$

$$c_{\text{mw}} = \begin{cases} \text{if } R_0 < 0: & 1 - \frac{1}{\sigma} \sqrt{\frac{2}{\pi}} \frac{R_0}{\sqrt{\exp(R_0^2/\sigma^2)}} + \text{erf}\left(\frac{R_0}{\sqrt{2}\sigma}\right) \\ \text{else:} & 1 \end{cases} \quad (7.42c)$$

7.12. Weibull distribution

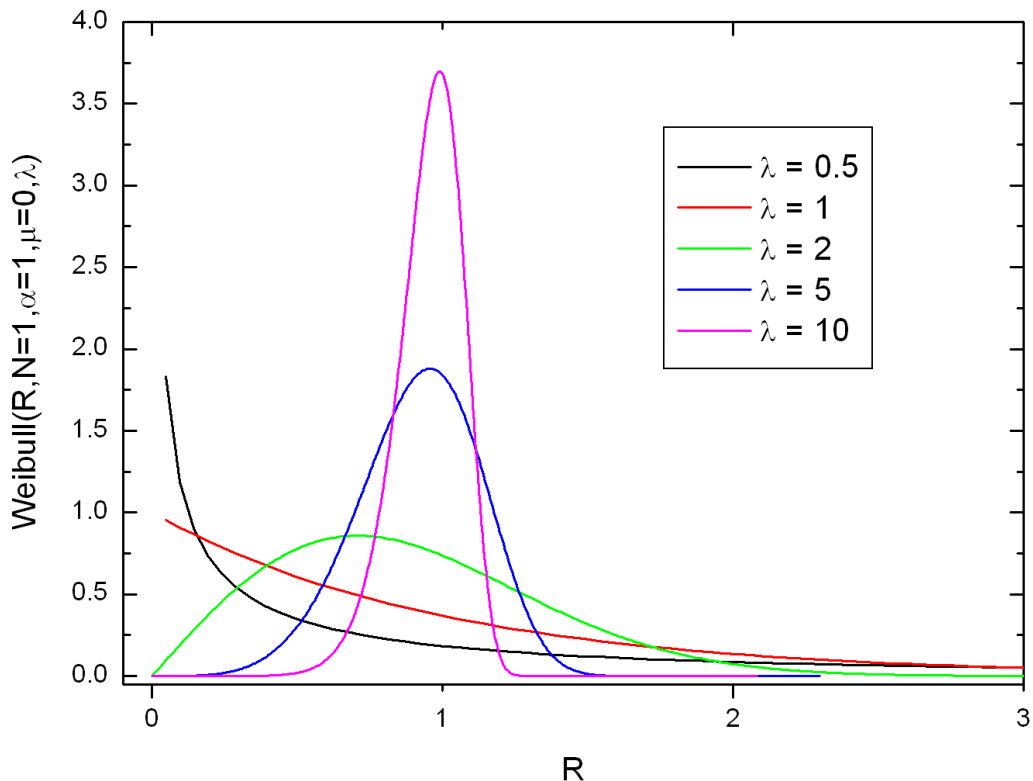


FIGURE 7.9. Weibull distribution function ($\mu = 0, \alpha = 1$ has been chosen in the plot). Valid parameter ranges: $R \in [0, \infty), \mu \in [0, \infty), \alpha > 0, \lambda > 0$

$$\text{Weibull}(R, \alpha, \lambda, \mu) = \frac{N\lambda}{\alpha} \left(\frac{R - \mu}{\alpha} \right)^{\lambda-1} e^{-\left(\frac{R-\mu}{\alpha}\right)^\lambda} e^{-\left(\frac{\mu}{\alpha}\right)^\lambda} \quad (7.43)$$

where λ is the shape parameter, μ is the location parameter and α is the scale parameter.

7.13. fractal size distribution

FIGURE 7.10. fractal size distribution function. Valid parameter ranges:
 $R \in [R_{\min}, R_{\max}]$, $f_D \in (-1, \infty)$, $R_{\max} > R_{\min} > 0$

$$\text{fractalSD}(R, N, R_{\min}, R_{\max}, f_D) = \frac{Nf_D}{R_{\min}^{-f_D} - R_{\max}^{-f_D}} R^{-(1+f_D)} \quad (7.44)$$

CHAPTER 8

Peak functions

8.1. Beta

The Beta distribution is a very versatile function which can be used to model several different shapes of probability density curves. In probability theory and statistics, the beta distribution is a family of continuous probability distributions defined on the interval $[0, 1]$ parameterized by two positive shape parameters, typically denoted by α and β .

$$p_{\text{Beta}}(x; \alpha, \beta) = \begin{cases} \frac{1}{B(\alpha, \beta)} x^{\alpha-1} (1-x)^{\beta-1} & \text{for } 0 < x < 1 \\ 0 & \text{otherwise} \end{cases} \quad (8.1)$$

The beta function, B , appears as a normalization constant to ensure that the total probability integrates to unity. α and β are positive numbers that define the shape parameters. The mode of the beta distribution for shape parameters $\alpha > 1$ and $\beta > 1$ is given by

$$\text{mode}(p_{\text{Beta}}) = \frac{\alpha - 1}{\alpha + \beta - 2} \quad (8.2)$$

8.1.1. Beta (Amplitude).

$$y_{\text{Beta(ampl)}}(x; A, x_{\min}, x_{\max}, \alpha, \beta, c_0) = A \frac{p_{\text{Beta}}\left(\frac{x-x_{\min}}{x_{\max}-x_{\min}}; \alpha, \beta\right)}{p_{\text{Beta}}\left(\frac{\alpha-1}{\alpha+\beta-2}; \alpha, \beta\right)} + c_0 \quad (8.3)$$

Required parameters:

ampl.: amplitude A of the Beta peak

xmin: continuous lower boundary parameters x_{\min}

xmax: continuous upper boundary parameters x_{\max}

alpha: first shape parameter $\alpha > 1$

beta: second shape parameter $\beta > 1$

backgr: offset c_0

Note

- Both shape parameter needs to be larger than one ($\alpha, \beta > 1$), as only than the distribution has a peak shape.
- where the Beta distribution is not defined the offset value is returned:
 $\forall x \notin (x_{\min}, x_{\max}) \quad y_{\text{Beta(ampl)}}(x) = c_0$
- Default (size) distribution: Monodisperse

8.1.2. Beta (Area).

$$y_{\text{Beta(area)}}(x; A, x_{\min}, x_{\max}, \alpha, \beta, c_0) = A \frac{p_{\text{Beta}}\left(\frac{x-x_{\min}}{x_{\max}-x_{\min}}; \alpha, \beta\right)}{x_{\max} - x_{\min}} + c_0 \quad (8.4)$$

Required parameters:

area: area A of the beta distribution

xmin: continuous lower boundary parameters x_{\min}

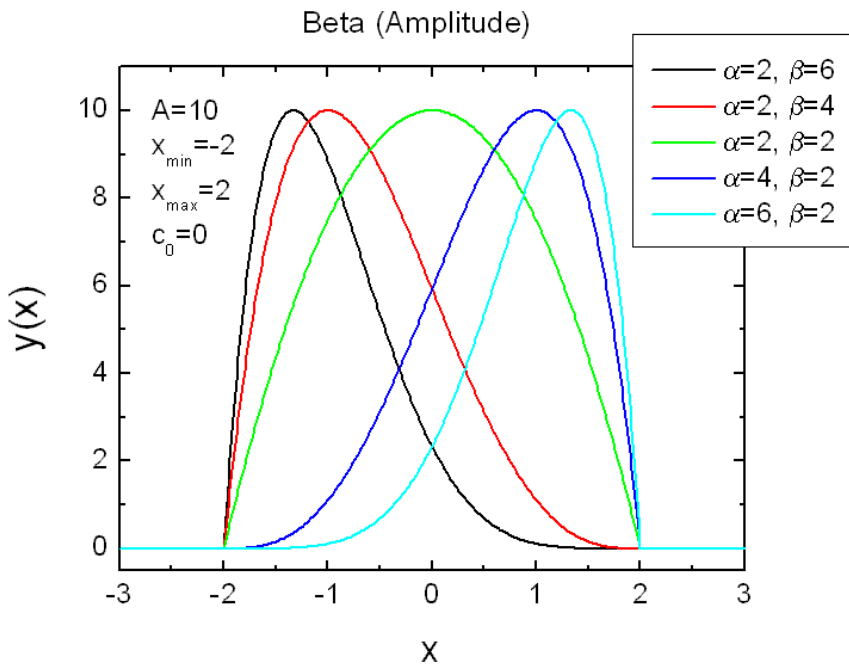


FIGURE 8.1. Plot of Beta (Amplitude) distribution.

xmax: continuous upper boundary parameters x_{\max}

alpha: first shape parameter $\alpha > 0$

beta: second shape parameter $\beta > 0$

backgr: offset c_0

Note

- Both shape parameter needs to be larger than zero ($\alpha, \beta > 0$)
- where the Beta distribution is not defined the offset value is returned:
 $\forall x \notin (x_{\min}, x_{\max}) \quad y_{\text{Beta(area)}}(x) = c_0$
- Default (size) distribution: Monodisperse

8.2. Chi-Squared

¹In probability theory and statistics, the chi-square distribution (also chi-squared or ξ^2 distribution) is one of the most widely used theoretical probability distributions in inferential statistics, e.g., in statistical significance tests. It is useful because, under reasonable assumptions, easily calculated quantities can be proven to have distributions that approximate to the chi-square distribution if the null hypothesis is true.

The best-known situations in which the chi-square distribution are used are the common chi-square tests for goodness of fit of an observed distribution to a theoretical one, and of the independence of two criteria of classification of qualitative data. Many other statistical tests also lead to a use of this distribution, like Friedman's analysis of variance by ranks.

A probability density function of the chi-square distribution is

$$f(x; k) = \begin{cases} \frac{1}{2^{k/2}\Gamma(k/2)} x^{(k/2)-1} e^{-x/2} & \text{for } x > 0 \\ 0 & \text{for } x \leq 0 \end{cases} \quad (8.5)$$

where Γ denotes the Gamma function, which has closed-form values at the half-integers. The mode of the distribution is

$$\text{mode} = k - 2 \text{ if } k \geq 2. \quad (8.6)$$

The χ^2 distribution is a special case of the gamma distribution 8.8 where $\theta = 2$ in the equation 8.31.

8.2.1. Chi-Squared (Amplitude).

$$\chi^2(x; A, x_c, \sigma, k, c_0) = \begin{cases} c_0 + A_0 (z + u)^v \exp\left(-\frac{z+u}{2}\right) & \text{for } z + u \geq 0 \\ c_0 & \text{otherwise} \end{cases} \quad (8.7)$$

with

$$z = \frac{x - x_c}{\sigma} \quad (8.8)$$

$$u = k - 2 \quad (8.9)$$

$$v = \frac{k}{2} - 1 \quad (8.10)$$

$$A_0 = \frac{A \exp(v)}{u^v} \quad (8.11)$$

The standard statistical form has been reparameterized. The parameter x_c has been added to enable variable x positioning, and σ to enable scaling. The mode is x_c . The function returns 0 for those x where it is undefined ($z + u < 0$).

Required parameters:

amplitude: amplitude a of the Gamma peak

center: location parameter (mode) x_c

¹Description taken partly from Wikipedia, the free encyclopedia

width: scaling parameter $\sigma > 0$

shape: shape parameter $k > 2$

backgr: offset c_0

Note

- The width parameter needs to be larger than zero ($\sigma > 0$).
- The shape parameter needs to be larger than two ($k > 2$)
- Default (size) distribution: Monodisperse

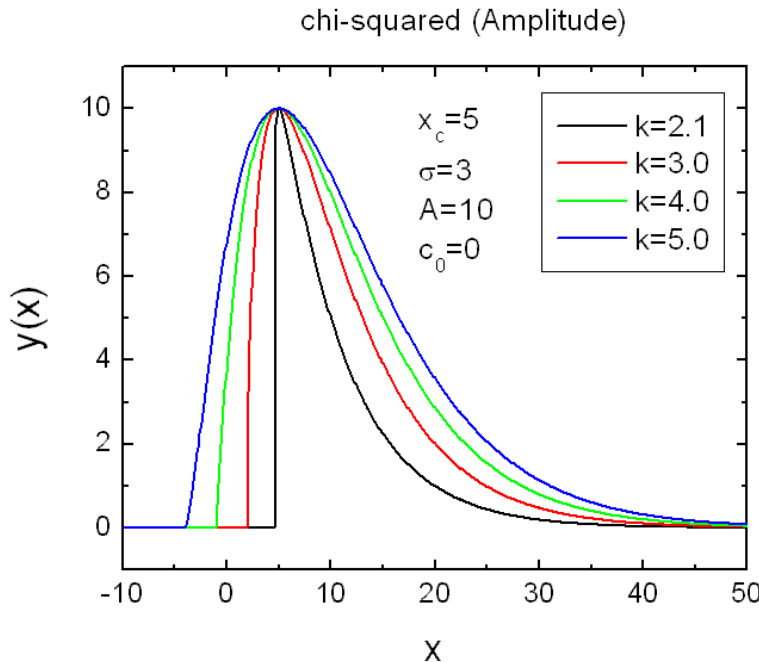


FIGURE 8.2. Plot of Chi-Squared (Amplitude) distribution.

8.2.2. Chi-Squared (Area).

$$\chi^2(x; A, x_c, \sigma, k, c_0) = \begin{cases} c_0 + A_0 (z + u)^v \exp\left(-\frac{z+u}{2}\right) & \text{for } z + u \geq 0 \\ c_0 & \text{otherwise} \end{cases} \quad (8.12)$$

with

$$z = \frac{x - x_c}{\sigma} \quad (8.13)$$

$$u = k - 2 \quad (8.14)$$

$$v = \frac{k}{2} - 1 \quad (8.15)$$

$$A_0 = \frac{A}{2^{\frac{k}{2}} \sigma \Gamma\left(\frac{k}{2}\right)} \quad (8.16)$$

The standard statistical form has been reparameterized. The parameter x_c has been added to enable variable x positioning, and σ to enable scaling. The mode is x_c . The function returns 0 for those x where it is undefined ($z + u < 0$).

Required parameters:

- area:** area a of the Gamma peak
- center:** location parameter (mode) x_c
- width:** scaling parameter $\sigma > 0$
- shape:** shape parameter $k > 2$
- backgr:** offset c_0

Note

- The width parameter needs to be larger than zero ($\sigma > 0$).
- The shape parameter needs to be larger than two ($k > 2$)
- Default (size) distribution: Monodisperse

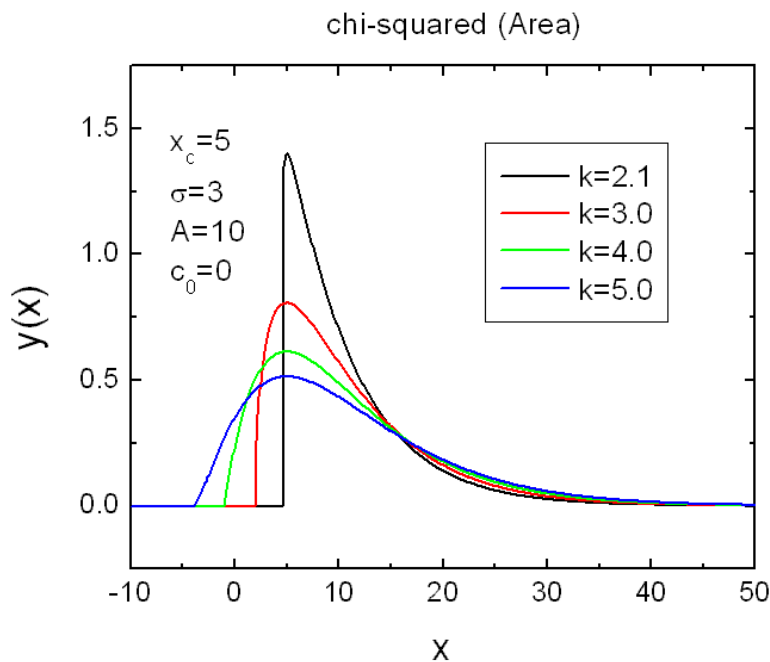


FIGURE 8.3. Plot of Chi-Squared (Area) distribution.

8.3. Erfc peak

8.3.1. Erfc (Amplitude).

$$y(x; a, x_c, \sigma, c_0) = a \operatorname{erfc} \left(\left(\frac{x - x_c}{\sigma} \right)^2 \right) + c_0 \quad (8.17)$$

Required parameters:

ampl.: amplitude a of the erfc peak

center: location parameter (mode) x_c

width: scaling parameter $\sigma > 0$

backgr: offset c_0

Note

- The width parameter needs to be non-zero ($\sigma \neq 0$).
- Default (size) distribution: Monodisperse

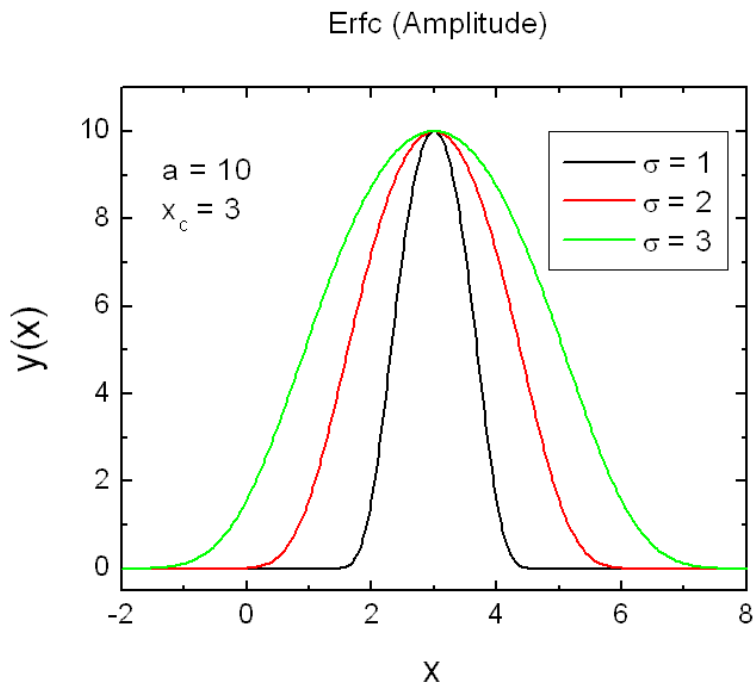


FIGURE 8.4. Plot of Erfc (Amplitude) distribution.

8.3.2. Erfc (Area).

$$y(x; a, x_c, \sigma, c_0) = a \frac{\operatorname{erfc}\left(\left(\frac{x-x_c}{\sigma}\right)^2\right)}{\int_{-\infty}^{\infty} \operatorname{erfc}\left(\left(\frac{x-x_c}{\sigma}\right)^2\right) dx} + c_0 \quad (8.18)$$

Required parameters:

area: area a below the erf c peak

center: location parameter (mode) x_c

width: scaling parameter $\sigma > 0$

backgr: offset c_0

Note

- The width parameter needs to be non-zero ($\sigma \neq 0$).
- Default (size) distribution: Monodisperse

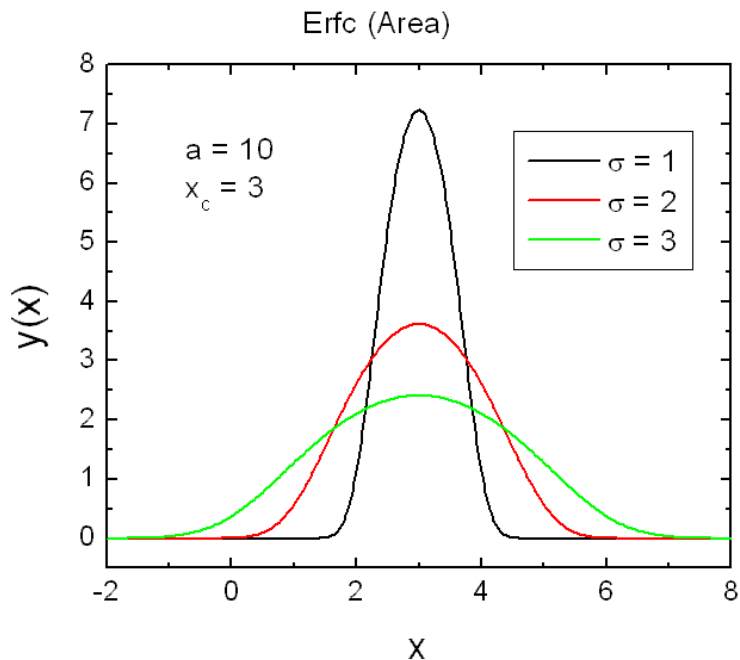


FIGURE 8.5. Plot of Erfc (Area) distribution.

8.4. Error peak

8.4.1. Error (Amplitude).

$$y(x; a, x_c, \sigma, k, c_0) = a \exp\left(-\frac{1}{2} \frac{|x - x_c|^{\frac{2}{k}}}{|\sigma|}\right) + c_0 \quad (8.19)$$

Required parameters:

ampl.: amplitude a of the error distribution

center: location parameter (mode) x_c

width: scaling parameter $\sigma \neq 0$

shape: shape parameter $k > 0$

backgr: offset c_0

Note

- The width parameter needs to be non-zero ($\sigma \neq 0$).
- The shape parameter needs to be larger than zero ($k > 0$).
- Default (size) distribution: Monodisperse

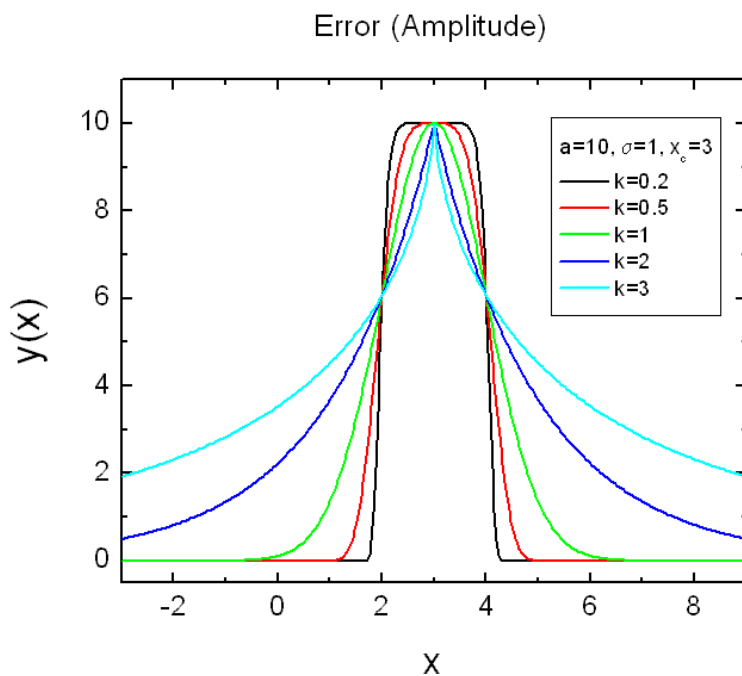


FIGURE 8.6. Plot of Error (Amplitude) distribution.

8.4.2. Error (Area).

$$y(x; a, x_c, \sigma, k, c_0) = \frac{a}{|\sigma|^{\frac{k}{2}} 2^{\frac{k}{2}+1} \Gamma\left(\frac{k}{2} + 1\right)} \exp\left(-\frac{1}{2} \frac{|x - x_c|^{\frac{2}{k}}}{|\sigma|}\right) + c_0 \quad (8.20)$$

Required parameters:

area: area a below the error distribution

center: location parameter (mode) x_c

width: scaling parameter $\sigma \neq 0$

shape: shape parameter $k > 0$

backgr: offset c_0

Note

- The width parameter needs to be non-zero ($\sigma \neq 0$).
- The shape parameter needs to be larger than zero ($k > 0$).
- Default (size) distribution: Monodisperse

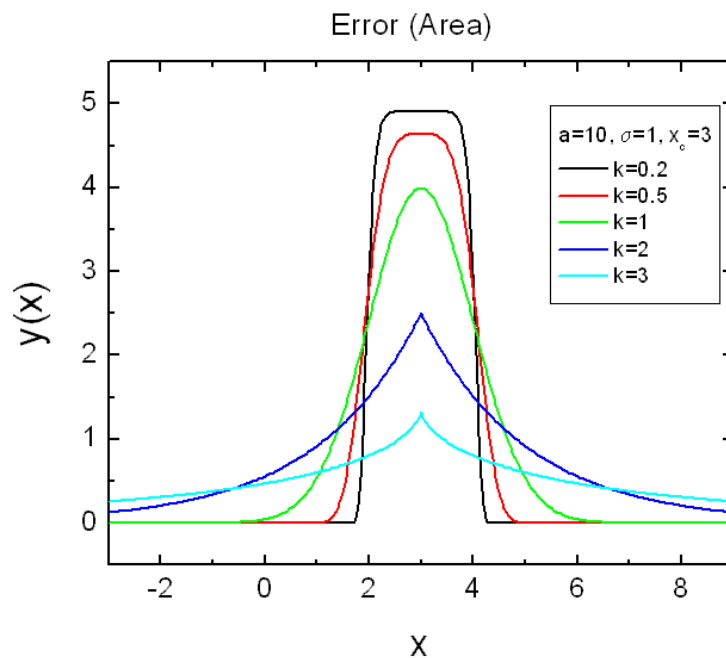


FIGURE 8.7. Plot of Error (Area) distribution.

8.5. Exponentially Modified Gaussian

8.5.1. Exponentially Modified Gaussian (Amplitude).

$$y(x; a, x_c, \sigma, \gamma, c_0) = \frac{a}{\text{const}} \exp \left(\frac{\sigma^2}{2\gamma^2} + \frac{x_c - x}{\gamma} \right) \left[\text{erf} \left(\frac{x - x_c}{\sqrt{2}\sigma} - \frac{\sigma}{\sqrt{2}\gamma} \right) + \frac{\gamma}{|\gamma|} \right] + c_0 \quad (8.21)$$

const is calculated numerically so that "a" represents the amplitude of the distribution.

Required parameters:

ampl.: amplitude a of the distribution

center: location parameter x_c

width: scaling parameter $\sigma > 0$

distortion: distortion parameter $\gamma \neq 0$

backgr: offset c_0

Note

- The width parameter needs to be non-zero ($\sigma \neq 0$).
- The distortion parameter needs to be non-zero ($\gamma \neq 0$).
- Default (size) distribution: Monodisperse

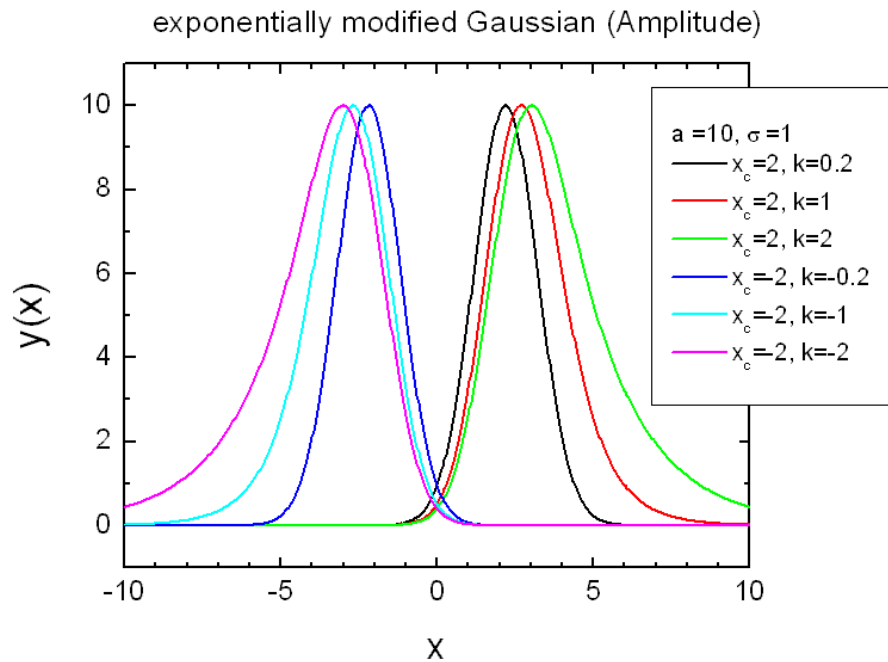


FIGURE 8.8. Plot of Exponentially Modified Gaussian (Amplitude) distribution.

8.5.2. Exponentially Modified Gaussian (Area).

$$y(x; a, x_c, \sigma, \gamma, c_0) = \frac{a}{2\gamma} \exp \left(\frac{\sigma^2}{2\gamma^2} + \frac{x_c - x}{\gamma} \right) \left[\operatorname{erf} \left(\frac{x - x_c}{\sqrt{2}\sigma} - \frac{\sigma}{\sqrt{2}\gamma} \right) + \frac{\gamma}{|\gamma|} \right] + c_0 \quad (8.22)$$

Required parameters:

area: area a below the distribution

center: location parameter x_c

width: scaling parameter $\sigma > 0$

distortion: distortion parameter $\gamma \neq 0$

backgr: offset c_0

Note

- The width parameter needs to be non-zero ($\sigma > 0$).
- The distortion parameter needs to be non-zero ($\gamma \neq 0$).
- Default (size) distribution: Monodisperse

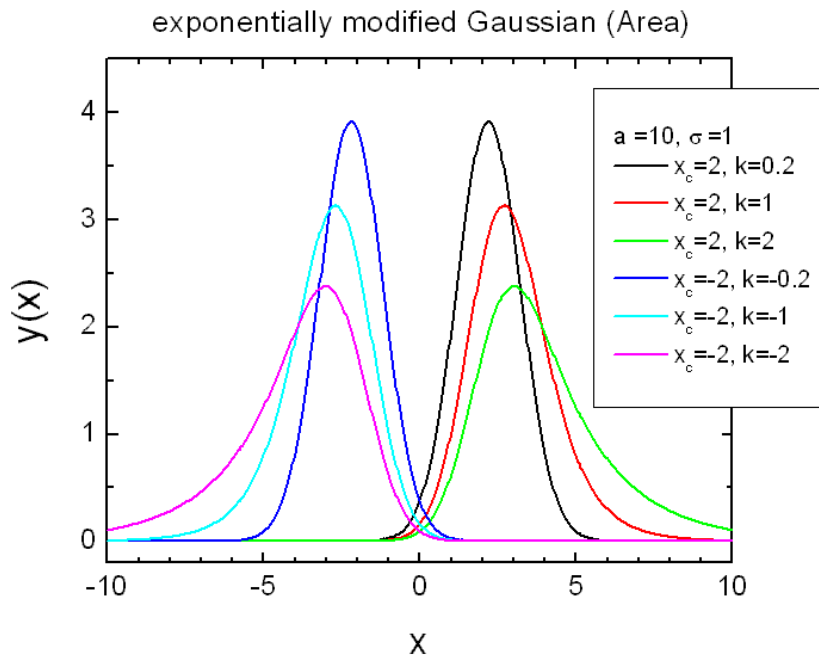


FIGURE 8.9. Plot of Exponentially Modified Gaussian (Area) distribution.

8.6. Extreme Value

8.6.1. Extreme Value (Amplitude).

$$y(x; a, x_c, \sigma, c_0) = a \exp \left[-\exp \left(-\frac{x - x_c}{|\sigma|} \right) - \frac{x - x_c}{|\sigma|} + 1 \right] + c_0 \quad (8.23)$$

Required parameters:

ampl.: amplitude a of the peak

center: location parameter (mode) x_c

width: scaling parameter $\sigma \neq 0$

backgr: offset c_0

Note

- The width parameter needs to be non-zero ($\sigma \neq 0$).
- Default (size) distribution: Monodisperse

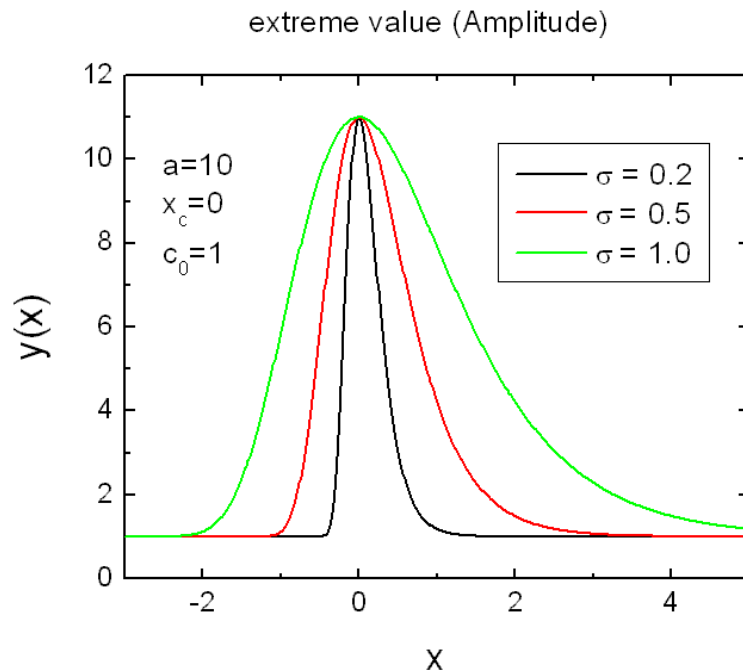


FIGURE 8.10. Plot of extreme value (Amplitude) distribution.

8.6.2. Extreme Value (Area).

$$y(x; a, x_c, \sigma, c_0) = \frac{a}{|\sigma|} \exp \left[-\exp \left(-\frac{x - x_c}{|\sigma|} \right) - \frac{x - x_c}{|\sigma|} \right] + c_0 \quad (8.24)$$

Required parameters:

area: area a below the peak

center: location parameter (mode) x_c

width: scaling parameter $\sigma \neq 0$

backgr: offset c_0

Note

- The width parameter needs to be non-zero ($\sigma \neq 0$).
- Default (size) distribution: Monodisperse

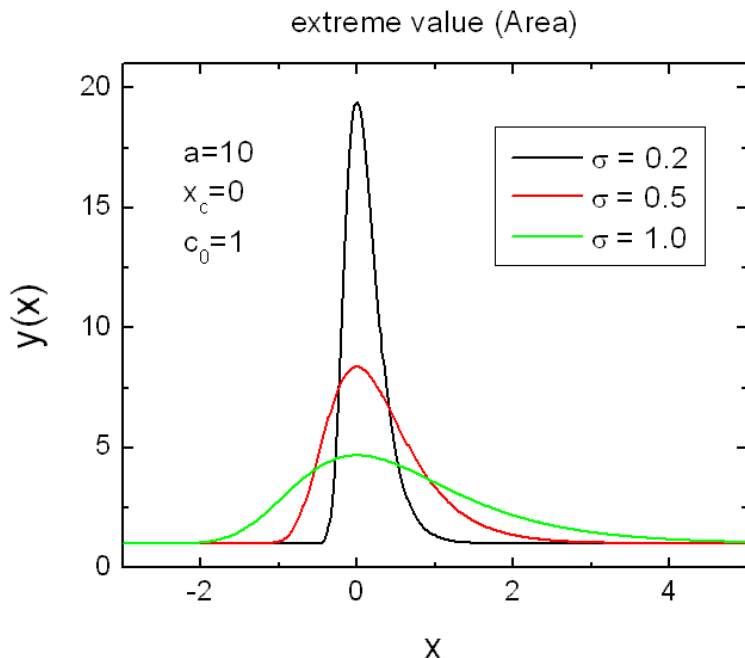


FIGURE 8.11. Plot of `extreme value (Area)` distribution.

8.7. F-Variance

In probability theory and statistics, the F-distribution is a continuous probability distribution. It is also known as Snedecor's F distribution or the Fisher-Snedecor distribution. The probability density is given by

$$p_{F-\text{var}}(x, \nu_1, \nu_2) = \frac{\sqrt{\frac{(\nu_1 x)^{\nu_1} \nu_2^{\nu_2}}{(\nu_1 x + \nu_2)^{\nu_1 + \nu_2}}}}{x B\left(\frac{\nu_1}{2}, \frac{\nu_2}{2}\right)} \quad (8.25)$$

for real $x \geq 0$, where $\nu > 1$ and ν_2 are positive, and $B()$ is the beta function. For $\nu_1 > 2$ the mode of the distribution is defined by

$$\text{mode}_F(\nu_1, \nu_2) = \frac{\nu_1 - 2}{\nu_1} \frac{\nu_2}{\nu_2 + 2} \quad (8.26)$$

8.7.1. F-Variance (Amplitude).

The amplitude version represents a re-parametrization of the standard statistical form.

$$y(x; a, x_c, \sigma, \nu_1, \nu_2) = \begin{cases} c_0 + a \frac{p_{F-\text{var}}(z, \nu_1, \nu_2)}{p_{F-\text{var}}(\text{mode}_F(\nu_1, \nu_2), \nu_1, \nu_2)} & \text{for } z > 0 \\ c_0 & \text{otherwise} \end{cases}$$

$$= \begin{cases} c_0 + a \frac{z^{\frac{\nu_1}{2}-1} \left(1+\frac{\nu_1-2}{\nu_2+2}\right)^{\frac{\nu_1+\nu_2}{2}}}{(1+\frac{\nu_1}{\nu_2}z)^{\frac{\nu_1+\nu_2}{2}} \left(\frac{\nu_2}{\nu_1} \frac{\nu_1-2}{\nu_2+2}\right)^{\frac{\nu_1}{2}-1}} & \text{for } z > 0 \\ c_0 & \text{otherwise} \end{cases} \quad (8.27)$$

with

$$z = \frac{x - x_c}{\sigma} + \frac{\nu_1 - 2}{\nu_1} \frac{\nu_2}{\nu_2 + 2} \quad (8.28)$$

The location parameter x_c has been added to enable variable x positioning, and σ to enable scaling. The mode of the distribution function is x_c due to the additional term $\frac{\nu_1-2}{\nu_1} \frac{\nu_2}{\nu_2+2}$ in the definition of z . The distribution function returns the offset c_0 for values $z \leq 0$.

Required parameters:

ampl.: amplitude a of the F-distribution

center: location parameter (mode) x_c

width: scaling parameter $\sigma > 0$

shape1: shape parameter $\nu_1 > 2$

shape2: shape parameter $\nu_2 > 2$

backgr: offset c_0

Note

- The scale parameter needs to be larger than zero $\sigma > 0$

- The first shape parameter needs to be larger than zero $\nu_1 > 2$
- The second shape parameter needs to be larger than zero $\nu_2 > 2$
- Default (Size) distribution: Monodisperse

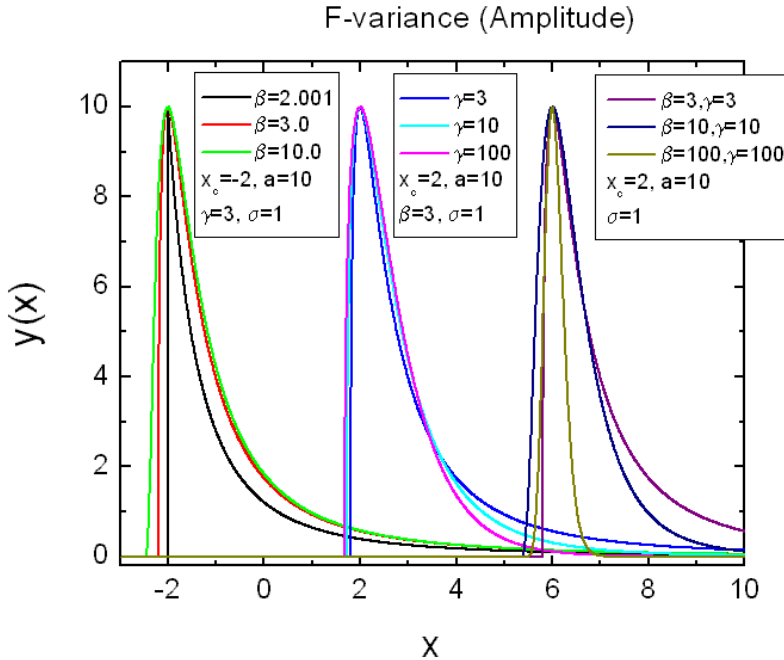


FIGURE 8.12. Plot of F-variance (Amplitude) distribution.

8.7.2. F-Variance (Area).

The area version represents a re-parametrization of the standard statistical form.

$$y(x; a, x_c, \sigma, \nu_1, \nu_2) = \begin{cases} c_0 + \frac{a}{\sigma} p_{F-\text{var}}(z, \nu_1, \nu_2) & \text{for } z > 0 \\ c_0 & \text{otherwise} \end{cases} \quad (8.29)$$

with

$$z = \frac{x - x_c}{\sigma} + \frac{\nu_1 - 2}{\nu_1} \frac{\nu_2}{\nu_2 + 2} \quad (8.30)$$

The location parameter x_c has been added to enable variable x positioning, and σ to enable scaling. The mode of the distribution function is x_c due to the additional term $\frac{\nu_1 - 2}{\nu_1} \frac{\nu_2}{\nu_2 + 2}$ in the definition of z . The distribution function returns the offset c_0 for values $z \leq 0$.

Required parameters:

area: area a of the F-distribution

center: location parameter (mode) x_c

width: scaling parameter $\sigma > 0$

shape1: shape parameter $\nu_1 > 2$

shape2: shape parameter $\nu_2 > 2$

backgr: offset c_0

Note

- The scale parameter needs to be larger than zero $\sigma > 0$
- The first shape parameter needs to be larger than zero $\nu_1 > 2$
- The second shape parameter needs to be larger than zero $\nu_2 > 2$
- Default (Size) distribution: Monodisperse

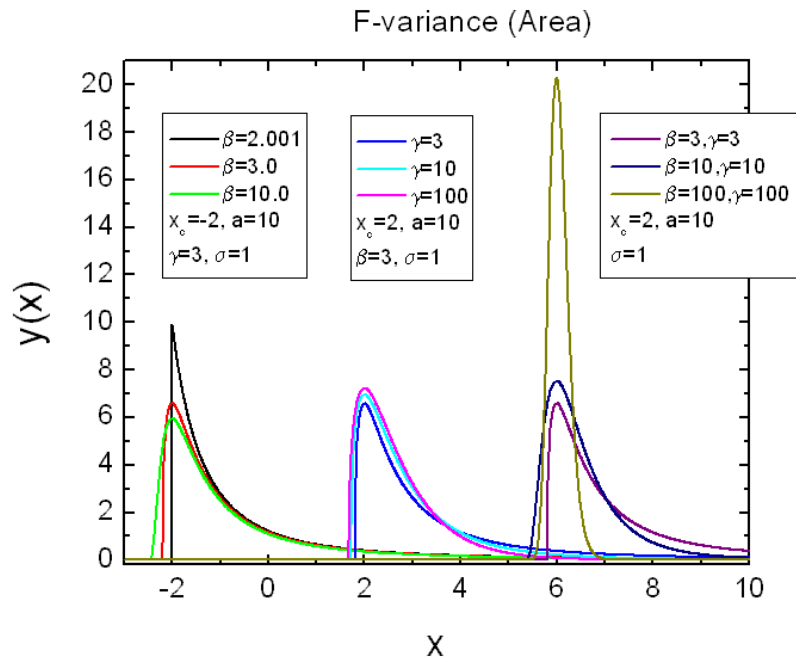


FIGURE 8.13. Plot of F-variance (Area) distribution.

8.8. Gamma

The gamma distribution models sums of exponentially distributed random variables.

The gamma distribution family is based on two parameters. The chi-square and exponential distributions, which are children of the gamma distribution, are one-parameter distributions that fix one of the two gamma parameters. The standard form is given by

$$p(x; k, \theta) = x^{k-1} \frac{e^{-x/\theta}}{\theta^k \Gamma(k)} \text{ for } x > 0 \text{ and } k, \theta > 0. \quad (8.31)$$

When k is large, the gamma distribution closely approximates a normal distribution with the advantage that the gamma distribution has density only for positive real numbers. In probability theory and statistics, the gamma distribution is a two-parameter family of continuous probability distributions. It has a scale parameter θ and a shape parameter k . If k is an integer then the distribution represents the sum of k independent exponentially distributed random variables, each of which has a mean of θ (which is equivalent to a rate parameter of θ^{-1}).

Alternatively, the gamma distribution can be parameterized in terms of a shape parameter $\alpha = k$ and an inverse scale parameter $\beta = 1/\theta$, called a rate parameter:

$$p(x; \alpha, \beta) = x^{\alpha-1} \frac{\beta^\alpha e^{-\beta x}}{\Gamma(\alpha)} \text{ for } x > 0. \quad (8.32)$$

8.8.1. Gamma (Amplitude).

The parameter x_c has been added to enable variable x positioning, whereas the $+z(k-1)$ adjusts x_c so that it represents the mode. c_0 is the offset value. The function returns the offset c_0 for those x where it is undefined

$$y(x) = \begin{cases} c_0 + a \exp(-z) \left(\frac{z+k-1}{k-1} \right)^{k-1} & \text{for } (z+k-1) > 0 \\ c_0 & \text{otherwise} \end{cases} \quad (8.33)$$

with $z = \frac{x-x_c}{\theta}$

Required parameters:

ampl.: amplitude a of the Gamma peak

center: location parameter (mode) x_c

width: scaling parameter $\theta > 0$

backgr: offset c_0

Note

- The shape parameter needs to be larger than one $k > 1$.
- The scale parameter needs to be larger than zero $\theta > 0$
- Default (Size) distribution: Monodisperse

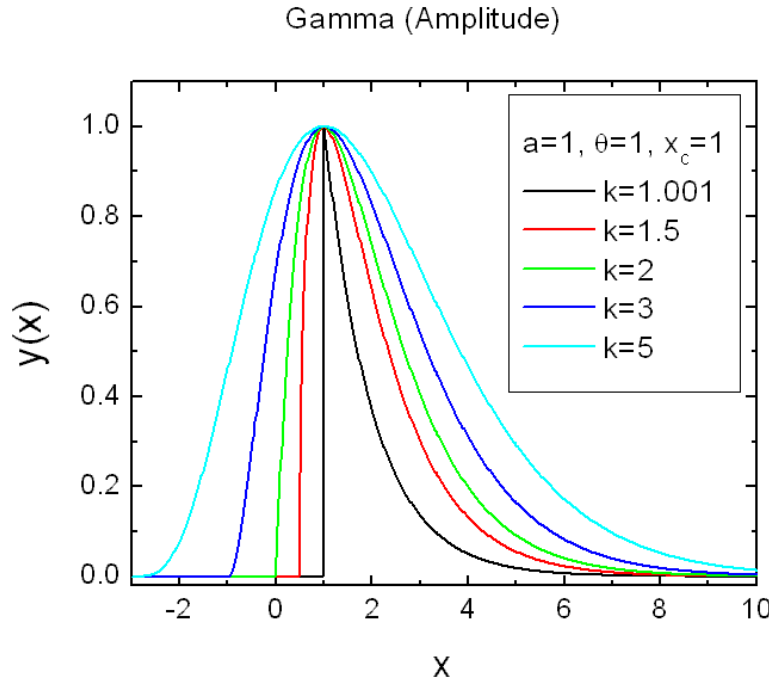


FIGURE 8.14. Plot of Gamma (Amplitude) distribution.

8.8.2. Gamma (Area).

The parameter x_c has been added to enable variable x positioning, whereas the $+\theta(k - 1)$ adjusts x_c so that it represents the mode. c_0 is the offset value. The function returns the offset c_0 for those x where it is undefined

$$y(x) = \begin{cases} c_0 + \frac{a}{\theta\Gamma(k)} \exp(-z) z^{k-1} & \text{for } z > 0 \\ c_0 & \text{otherwise} \end{cases} \quad (8.34)$$

with $z = \frac{x-x_c}{\theta} + k - 1$

Required parameters:

area: area a of the Gamma peak

center: location parameter (mode) x_c

width: scaling parameter $\theta > 0$

backgr: offset c_0

Note

- The shape parameter needs to be larger than one $k > 1$.
- The scale parameter needs to be larger than zero $\theta > 0$
- Default (Size) distribution: Monodisperse

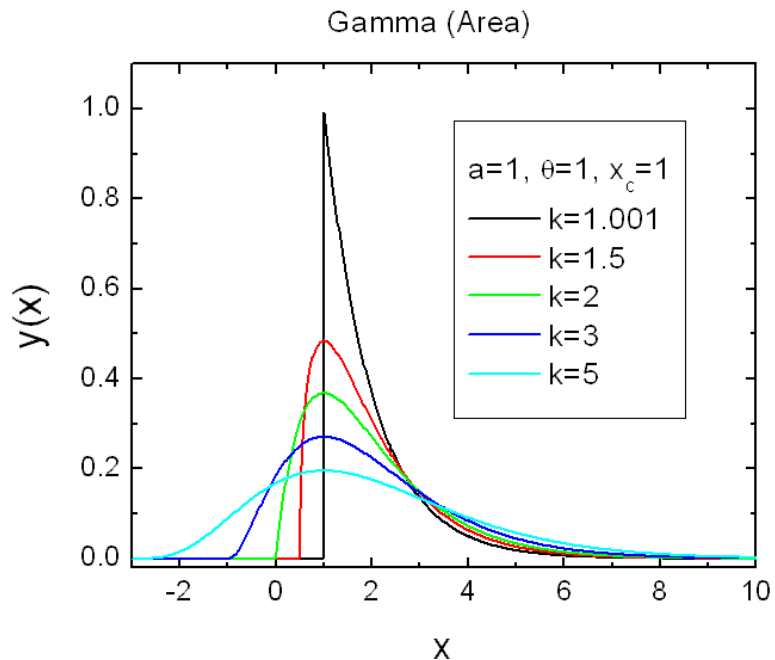


FIGURE 8.15. Plot of Gamma (Area) distribution.

8.9. Gaussian or Normal distribution

8.9.1. Gaussian (Amplitude).

$$y(x; a, x_c, \sigma, c_0) = a \exp \left[-\frac{1}{2} \left(\frac{x - x_c}{|\sigma|} \right)^2 \right] + c_0 \quad (8.35)$$

Required parameters:

ampl.: amplitude a of the peak

center: location parameter (mode) x_c

width: scaling parameter $\sigma \neq 0$

backgr: offset c_0

Note

- The width parameter needs to be non-zero ($\sigma \neq 0$).
- Default (size) distribution: Monodisperse

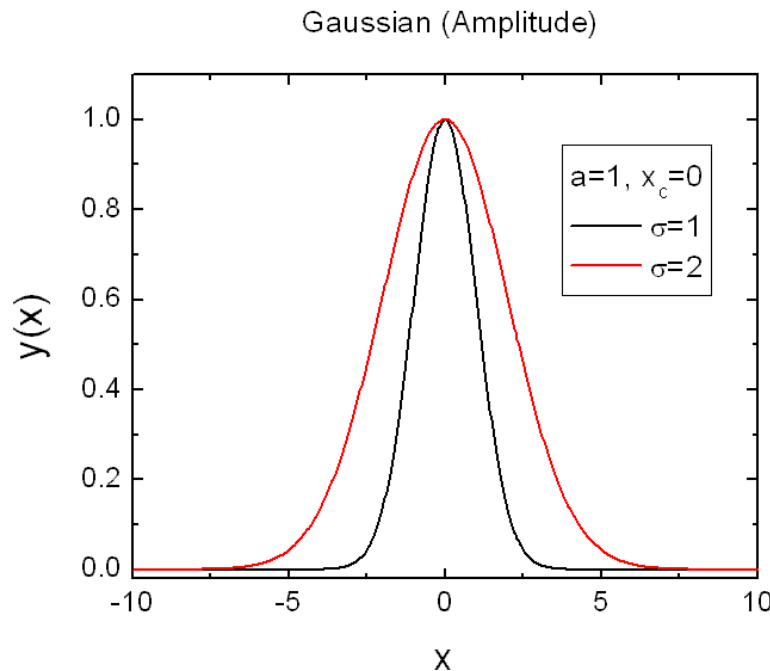


FIGURE 8.16. Plot of Gaussian (Amplitude) distribution.

8.9.2. Gaussian (Area).

$$y(x; a, x_c, \sigma, c_0) = \frac{a}{|\sigma| \sqrt{2\pi}} \exp \left[-\frac{1}{2} \left(\frac{x - x_c}{|\sigma|} \right)^2 \right] + c_0 \quad (8.36)$$

Required parameters:

area: area a below the peak

center: location parameter (mode) x_c

width: scaling parameter $\sigma \neq 0$

backgr: offset c_0

Note

- The width parameter needs to be non-zero ($\sigma \neq 0$).
- Default (size) distribution: Monodisperse

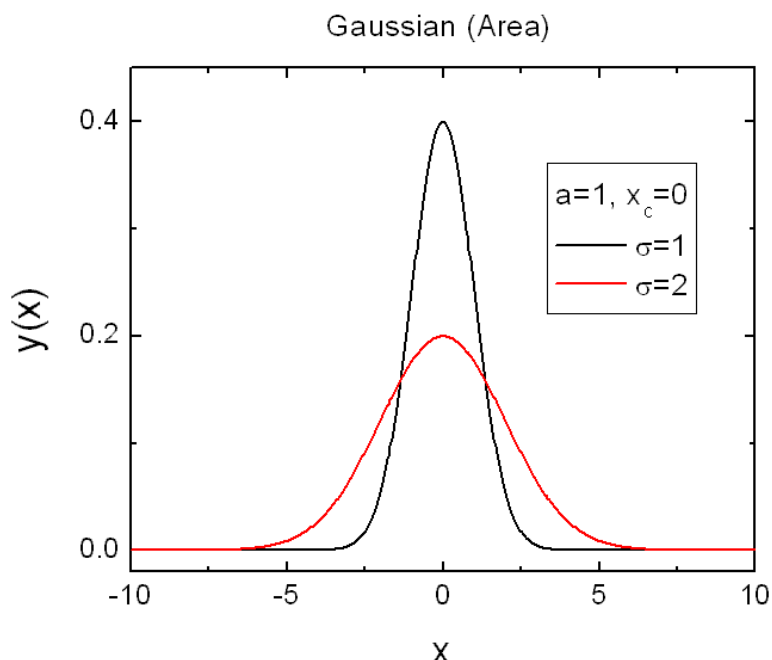


FIGURE 8.17. Plot of Gaussian (Area) distribution.

8.10. Gaussian-Lorentzian cross product

This distribution function is a Voigt approximation. It combines a Gaussian and Lorentzian in a multiplicative form. The shape parameter ν varies from 0 to 1. The pure Lorentzian occurs with $\nu = 1$ and the pure Gaussian with $\nu = 0$ but the transition from Lorentzian to Gaussian shape is not a linear function of ν

8.10.1. Gaussian-Lorentzian cross product (Amplitude).

$$y(x, a, x_c, \sigma, \nu, c_0) = a \frac{\exp\left(-\frac{1-\nu}{2} \left(\frac{x-x_c}{|\sigma|}\right)^2\right)}{1 + \nu \left(\frac{x-x_c}{|\sigma|}\right)^2} + c_0 \quad (8.37)$$

Required parameters:

amplitude: amplitude a of the peak

center: location parameter (mode) x_c

shape: shape parameter $\nu \in [0, 1]$

width: scaling parameter $\sigma \neq 0$

backgr: offset c_0

Note

- The width parameter needs to be non-zero ($\sigma \neq 0$).
- The shape parameter need to be between 0 and 1 ($\nu \in [0, 1]$)
- Default (size) distribution: Monodisperse

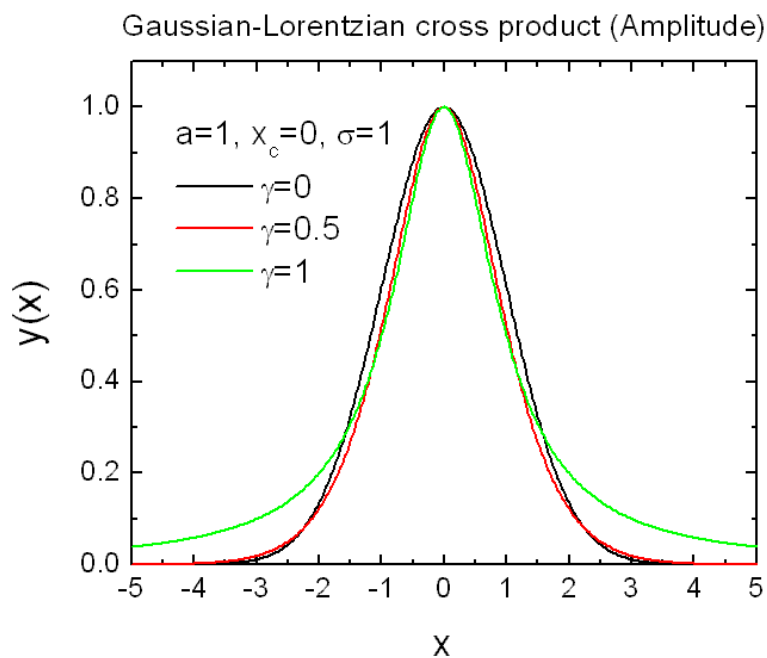


FIGURE 8.18. Plot of Gaussian-Lorentzian cross product (Amplitude) distribution.

8.10.2. Gaussian-Lorentzian cross product (Area).

$$y(x, a, x_c, \sigma, \nu, c_0) = a \frac{\sqrt{\nu}}{|\sigma|\pi} \frac{\exp\left(-\frac{1-\nu}{2\nu}\right)}{\operatorname{erfc}\left(\sqrt{\frac{1-\nu}{2\nu}}\right)} \frac{\exp\left(-\frac{1-\nu}{2} \left(\frac{x-x_c}{|\sigma|}\right)^2\right)}{1 + \nu \left(\frac{x-x_c}{|\sigma|}\right)^2} + c_0 \quad (8.38)$$

Required parameters:

- area:** area a below the peak
- center:** location parameter (mode) x_c
- shape:** shape parameter $\nu \in [0, 1]$
- width:** scaling parameter $\sigma \neq 0$
- backgr:** offset c_0

Note

- The width parameter needs to be non-zero ($\sigma \neq 0$).
- The shape parameter need to be between 0 and 1 ($\nu \in [0, 1]$)
- Default (size) distribution: Monodisperse

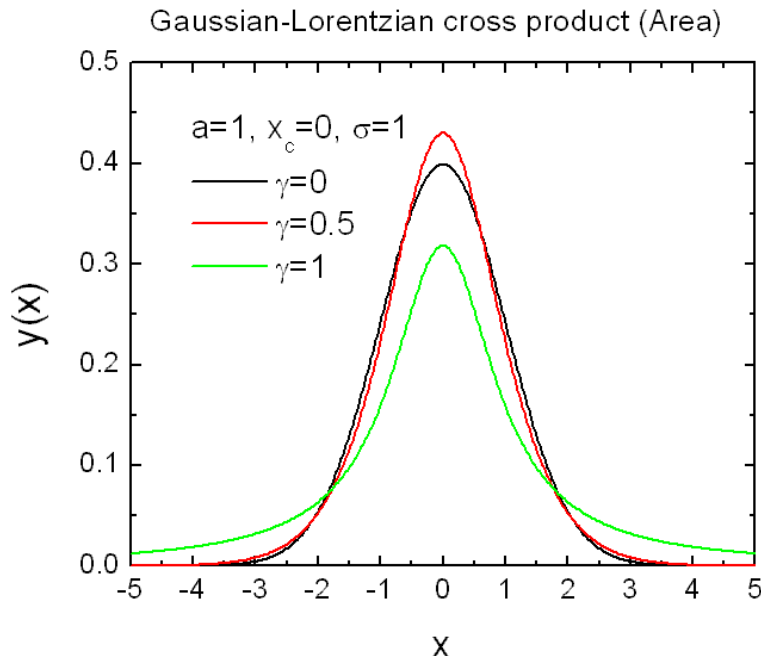


FIGURE 8.19. Plot of Gaussian-Lorentzian cross product (Area) distribution.

8.11. Gaussian-Lorentzian sum

This distribution function is another Voigt approximation, which is simply a sum of Lorentzian and Gaussian with equal FWHM. The shape parameter ν varies from 0 to 1. The pure Lorentzian occurs with $\nu = 1$ and the pure Gaussian with $\nu = 0$. The width parameter σ directly computes the full-width at half-maximum (FWHM).

8.11.1. Gaussian-Lorentzian sum (Amplitude).

$$y(x, a, x_c, \sigma, \nu, c_0) = a \frac{\frac{\nu}{|\sigma|} \sqrt{\frac{\ln 2}{\pi}} \exp\left(-4 \ln 2 \left(\frac{x-x_c}{|\sigma|}\right)^2\right) + \frac{1-\nu}{\pi |\sigma| \left[1+4\left(\frac{x-x_c}{|\sigma|}\right)^2\right]} + c_0}{\frac{\nu}{|\sigma|} \sqrt{\frac{\ln 2}{\pi}} + \frac{1-\nu}{\pi |\sigma|}} \quad (8.39)$$

Required parameters:

amplitude: amplitude a of the peak

center: location parameter (mode) x_c

shape: shape parameter $\nu \in [0, 1]$

width: scaling parameter $\sigma \neq 0$

backgr: offset c_0

Note

- The width parameter needs to be non-zero ($\sigma \neq 0$).
- The shape parameter need to be between 0 and 1 ($\nu \in [0, 1]$)
- Default (size) distribution: Monodisperse

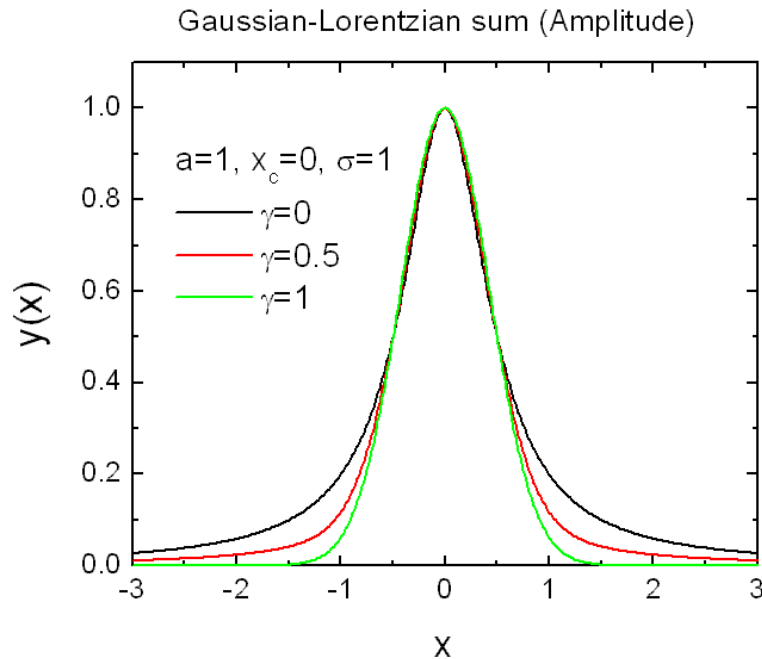


FIGURE 8.20. Plot of Gaussian-Lorentzian sum (Amplitude) distribution.

8.11.2. Gaussian-Lorentzian sum (Area).

$$y(x, a, x_c, \sigma, \nu, c_0) = 2a \left[\frac{\nu}{|\sigma|} \sqrt{\frac{\ln 2}{\pi}} \exp \left(-4 \ln 2 \left(\frac{x - x_c}{|\sigma|} \right)^2 \right) + \frac{1 - \nu}{\pi |\sigma| \left[1 + 4 \left(\frac{x - x_c}{|\sigma|} \right)^2 \right]} \right] + c_0 \quad (8.40)$$

Required parameters:

area: area a below the peak

center: location parameter (mode) x_c

shape: shape parameter $\nu \in [0, 1]$

width: scaling parameter $\sigma \neq 0$

backgr: offset c_0

Note

- The width parameter needs to be non-zero ($\sigma \neq 0$).
- The shape parameter need to be between 0 and 1 ($\nu \in [0, 1]$)
- Default (size) distribution: Monodisperse

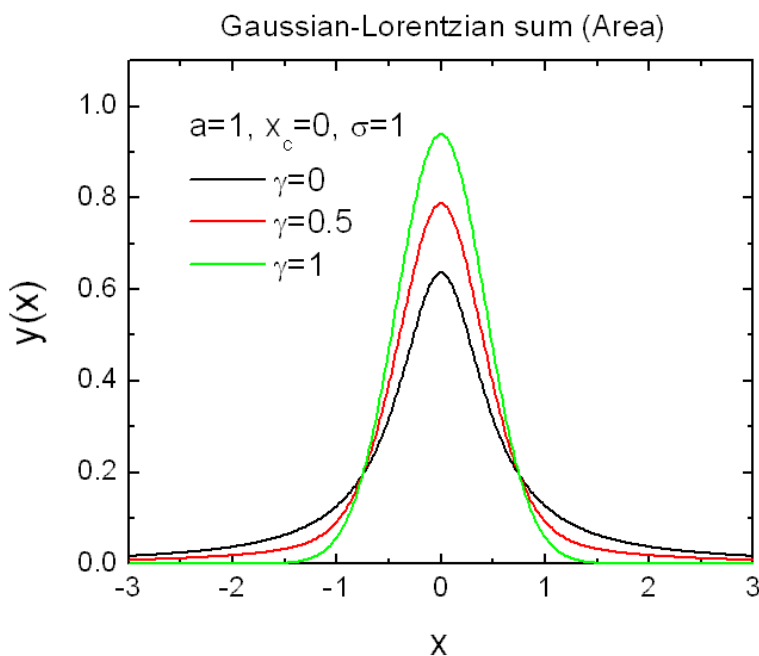


FIGURE 8.21. Plot of Gaussian-Lorentzian sum (Area) distribution.

8.12. generalized Gaussian 1

The generalized Gaussian distribution is one of two families of continuous probability distributions, which has an additional shape parameter to the normal distribution. Known also as the exponential power distribution, or the generalized error distribution, this is a parametric family of symmetric distributions. It includes all normal and Laplace distributions, and as limiting cases it includes all continuous uniform distributions on bounded intervals of the real line.

This family includes the normal distribution when $\beta = 2$ (with mean μ and variance $\frac{\alpha^2}{2}$) and it includes the Laplace distribution when $\beta = 1$. As $\beta \rightarrow \infty$, the density converges pointwise to a uniform density on $(\mu - \alpha, \mu + \alpha)$.

8.12.1. generalized Gaussian 1 (Amplitude).

$$y(x, a, \mu, \alpha, \beta) = ae^{-|x-\mu|^{\frac{2}{\alpha}}^{\beta}} \quad (8.41)$$

Required parameters:

amplitude: amplitude a of the peak

center: location parameter (mode) μ

width: scaling parameter $\alpha \neq 0$

shape: shape parameter β

backgr: offset c_0

Note

- The width parameter needs to be non-zero ($\alpha \neq 0$).
- The area parameter needs to be positive ($\beta > 0$).
- Default (size) distribution: Monodisperse

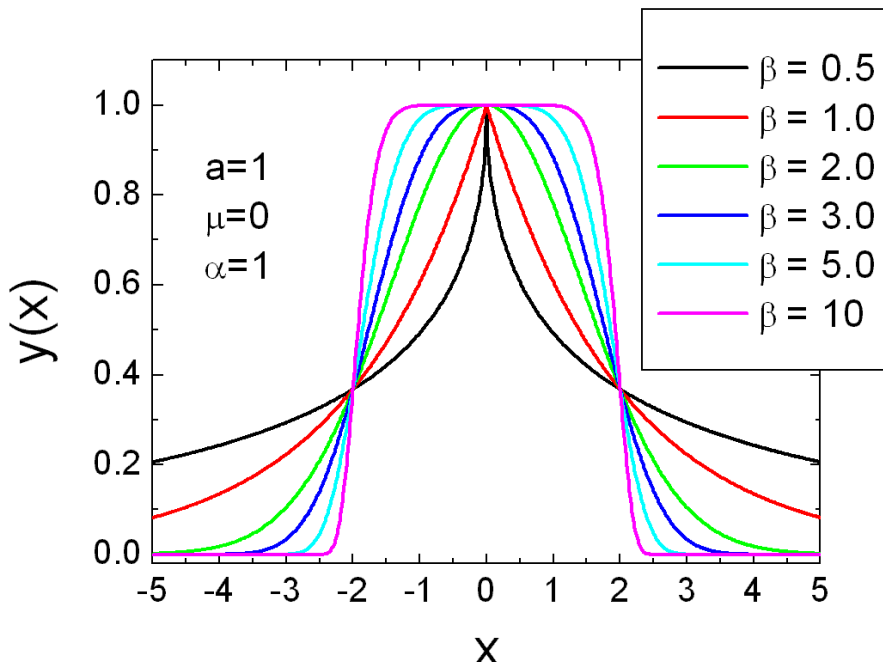


FIGURE 8.22. Plot of generalized Gaussian 1 (Amplitude) distribution.

8.12.2. generalized Gaussian 1 (Area).

$$y(x, a, \mu, \alpha, \beta) = a \frac{\beta}{2\alpha\Gamma(1/\beta)} e^{-|\frac{x-\mu}{\alpha}|^\beta} \quad (8.42)$$

Required parameters:

- area:** area a below the peak
- center:** location parameter (mode) μ
- width:** scaling parameter $\alpha \neq 0$
- shape:** shape parameter β
- backgr:** offset c_0

Note

- The scaling parameter needs to be positive ($\alpha > 0$).
- Default (size) distribution: Monodisperse

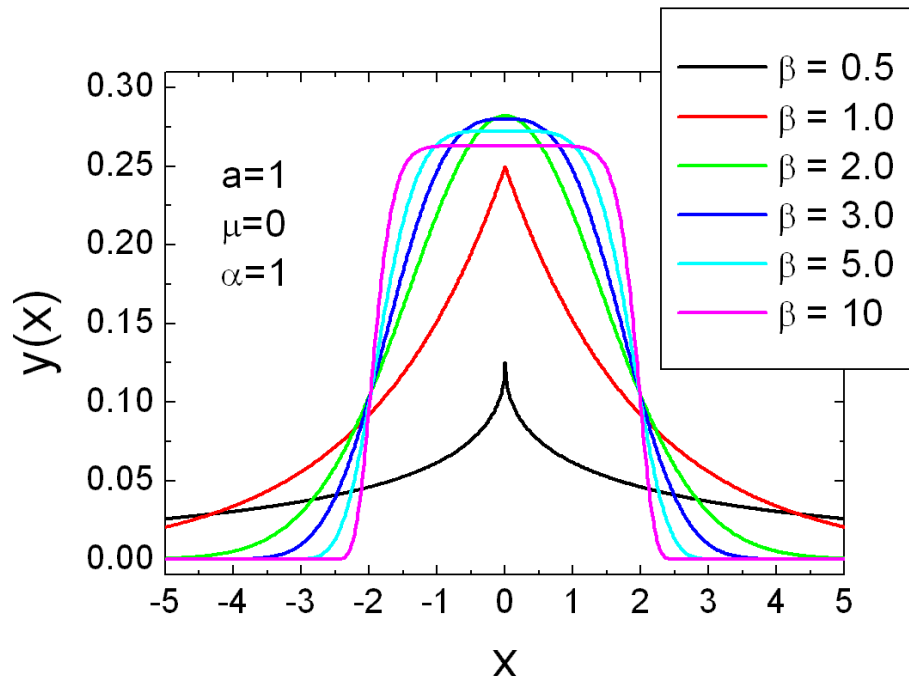


FIGURE 8.23. Plot of generalized Gaussian 1 (Area) distribution.

8.13. generalized Gaussian 2

$$x_{\text{mode}} = \begin{cases} \frac{\alpha}{\kappa} - \frac{\alpha}{\kappa} e^{-\kappa^2/2} + \xi & \text{if } \kappa \neq 0 \\ \xi & \text{if } \kappa = 0 \end{cases} \quad (8.43)$$

8.13.1. generalized Gaussian 2 (Amplitude).

$$y(x) = A \alpha \sqrt{2\pi} \exp\left(-\frac{\kappa^2}{2}\right) \frac{\phi(u)}{\alpha - \kappa(x - \xi)} + c_0 \quad (8.44)$$

where

$$u = \begin{cases} -\frac{1}{\kappa} \log \left[1 - \frac{\kappa(x-\xi)}{\alpha} \right] & \text{if } \kappa \neq 0 \\ \frac{x-\xi}{\alpha} & \text{if } \kappa = 0 \end{cases} \quad (8.45)$$

where

$$\phi(x) = \frac{1}{\sqrt{2\pi}} \exp\left(-\frac{x^2}{2}\right) \quad (8.46)$$

Required parameters:

amplitude: amplitude A of the peak

location: location parameter ξ

width: scaling parameter $\alpha > 0$

shape: shape parameter κ

backgr: offset c_0

Note

- The scaling parameter needs to be positive ($\alpha > 0$).
- Default (size) distribution: Monodisperse

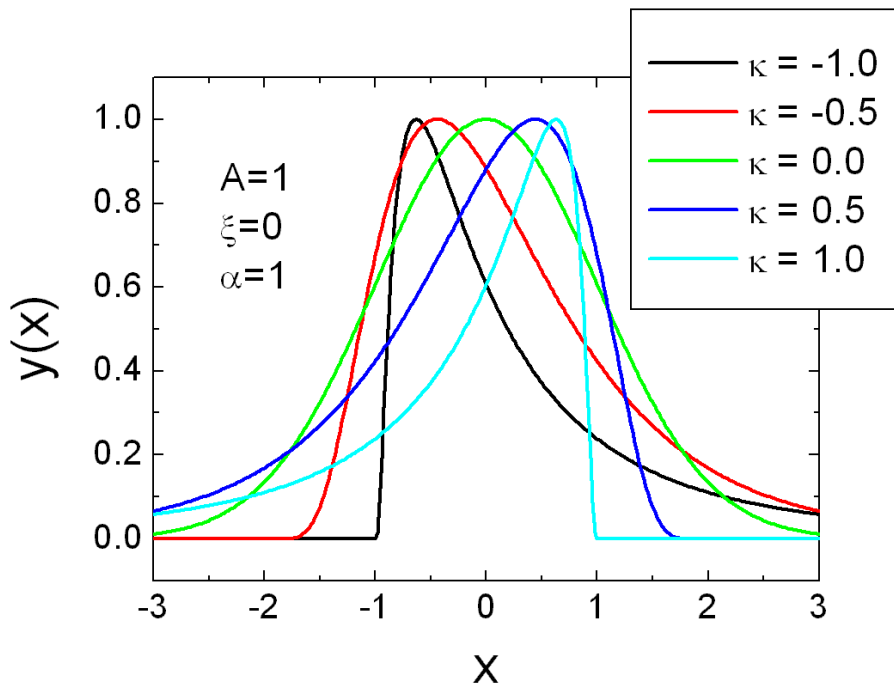


FIGURE 8.24. Plot of generalized Gaussian 2(Amplitude) distribution.

8.13.2. generalized Gaussian 2 (Area).

$$y(x) = A \frac{\phi(u)}{\alpha - \kappa(x - \xi)} + c_0 \quad (8.47a)$$

where

$$u = \begin{cases} -\frac{1}{\kappa} \log \left[1 - \frac{\kappa(x-\xi)}{\alpha} \right] & \text{if } \kappa \neq 0 \\ \frac{x-\xi}{\alpha} & \text{if } \kappa = 0 \end{cases} \quad (8.47b)$$

and

$$\phi(u) = \frac{1}{\sqrt{2\pi}} \exp \left(-\frac{u^2}{2} \right) \quad (8.47c)$$

Required parameters:

- area:** area A below the peak
- location:** location parameter ξ
- width:** scaling parameter $\alpha > 0$
- shape:** shape parameter κ
- backgr:** offset c_0

Note

- The scaling parameter needs to be positive ($\alpha > 0$).
- Default (size) distribution: Monodisperse

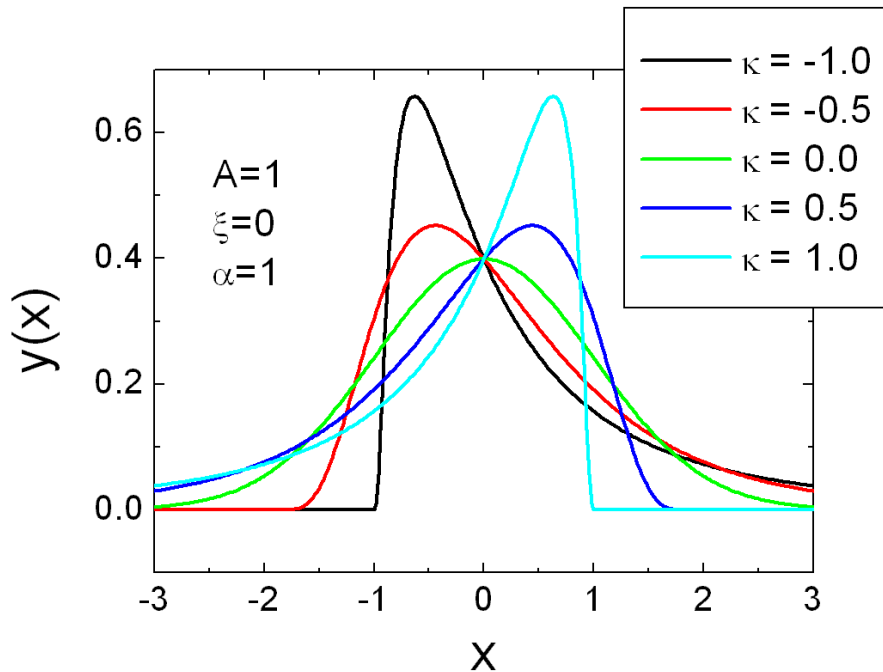


FIGURE 8.25. Plot of generalized Gaussian 2 (Area) distribution.

8.14. Giddings

The Giddings equation was derived by J. C. Giddings (Dynamics of Chromatography, Part I, Marcel Decker, New York, 1965). The equation provides a theoretical description for chromatographic peaks. The used formulae have been taken from the Manual of the Peakfit Software package (SeaSolve Software Inc.), which contains an expression for the Giddings (Area). As the mode x_{mode} of the peak can not be calculated analytical the amplitude version of this peaks Giddings (Amplitude) calculates first numerically the mode of the peak and than normalizes the value at x_{mode} to be $y(x_{\text{mode}}) = A$.

8.14.1. Giddings (Amplitude).

As the mode x_{mode} of this peak can not be calculated analytical this version of the Giddings peak calculates first numerically the mode of the peak and than normalizes the value at x_{mode} to be $y(x_{\text{mode}}) = A$.

$$y(x) = \frac{A}{c} \sqrt{\frac{\beta}{x}} I_1 \left(\frac{2\sqrt{\beta x}}{\sigma} \right) \exp \left(-\frac{x + \beta}{\sigma} \right) \quad (8.48a)$$

with

$$c = \sqrt{\frac{\beta}{x_{\text{mode}}}} I_1 \left(\frac{2\sqrt{\beta x_{\text{mode}}}}{\sigma} \right) \exp \left(-\frac{x_{\text{mode}} + \beta}{\sigma} \right) \quad (8.48b)$$

Required parameters:

amplitude: amplitude A of the peak

location: location parameter β

width: scaling parameter $\sigma > 0$

backgr: offset c_0

Note

- The scaling parameter needs to be positive ($\sigma > 0$).
- Default (size) distribution: Monodisperse

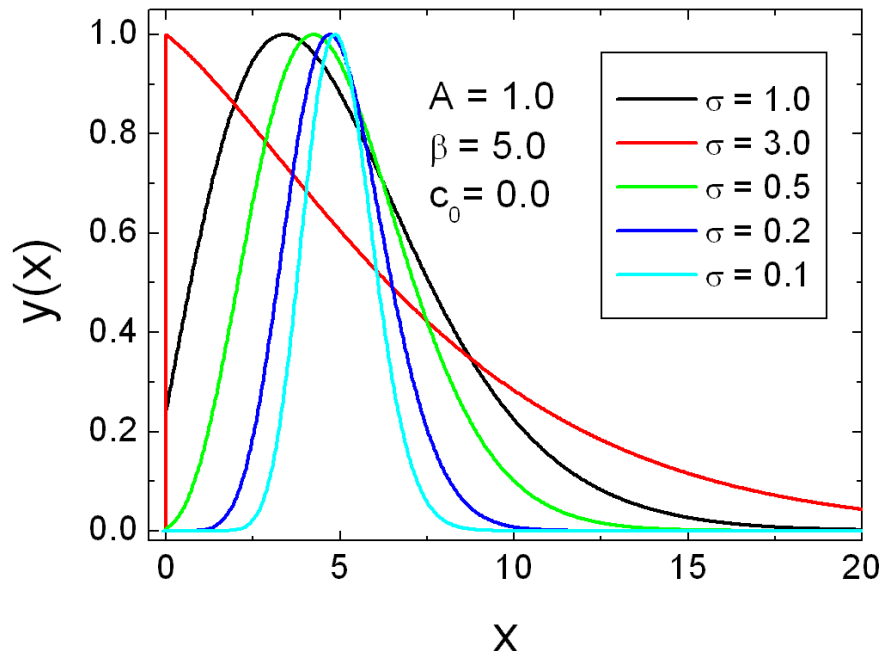


FIGURE 8.26. Plot of Giddings (Amplitude) distribution.

8.14.2. Giddings (Area).

$$y(x) = \frac{A}{1 - \exp\left(-\frac{\beta}{\sigma}\right)} \frac{1}{\sigma} \sqrt{\frac{\beta}{x}} I_1\left(\frac{2\sqrt{\beta x}}{\sigma}\right) \exp\left(-\frac{x + \beta}{\sigma}\right) \quad (8.49)$$

Required parameters:

area: area A below the peak

location: location parameter β

width: scaling parameter $\sigma > 0$

backgr: offset c_0

Note

- The scaling parameter needs to be positive ($\sigma > 0$).
- Default (size) distribution: Monodisperse

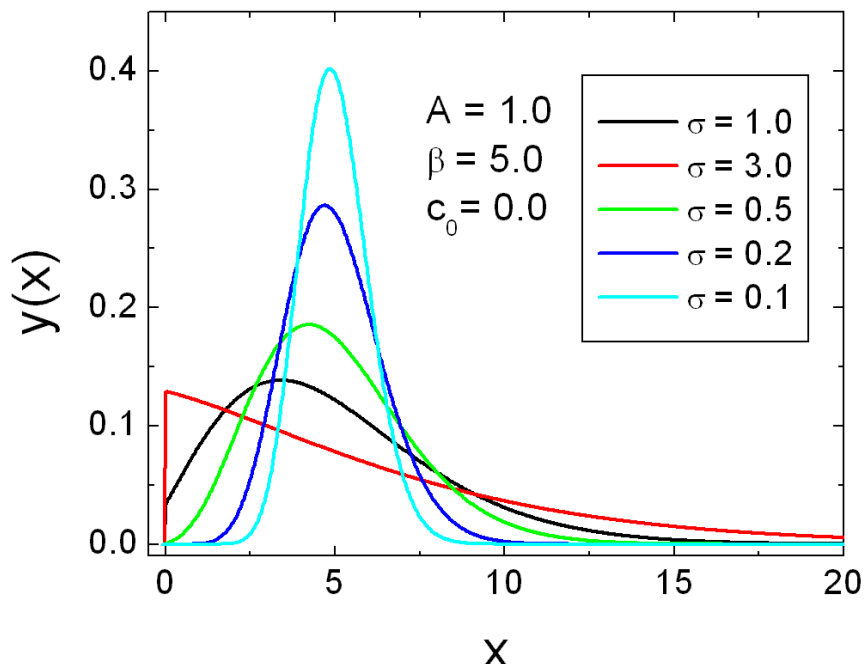


FIGURE 8.27. Plot of Giddings (Area) distribution.

8.15. Haarhoff - Van der Linde (Area)

$$HVL(x) = \frac{\frac{A\sigma}{\mu\delta\sqrt{2\pi}} \exp\left[-\frac{1}{2}\left(\frac{x-\mu}{\sigma}\right)^2\right]}{\left(\exp\left(\frac{\mu\delta}{\sigma^2}\right) - 1\right)^{-1} + \frac{1}{2}\left[1 + \operatorname{erf}\left(\frac{x-\mu}{\sqrt{2}\sigma}\right)\right]} \quad (8.50)$$

for $\delta \rightarrow 0$ one get the Gaussian distribution as a limiting case

$$\lim_{\delta \rightarrow 0} HVL(x) = \frac{A}{\sigma\sqrt{2\pi}} \exp\left[-\frac{1}{2}\left(\frac{x-\mu}{\sigma}\right)^2\right] \quad (8.51)$$

as well as for $\mu \rightarrow 0$

$$\lim_{\mu \rightarrow 0} HVL(x) = \frac{A}{\sigma\sqrt{2\pi}} \exp\left[-\frac{1}{2}\left(\frac{x}{\sigma}\right)^2\right] \quad (8.52)$$

Required parameters:

- area:** area A below the peak
- width:** scaling parameter $\sigma > 0$
- backgr:** offset c_0

Note

- The location parameter needs to be positive ($\mu > 0$).
- The scaling parameter needs to be positive ($\sigma > 0$).
- The distortion parameter needs to be nonzero ($\delta \neq 0$).
- Default (size) distribution: Monodisperse

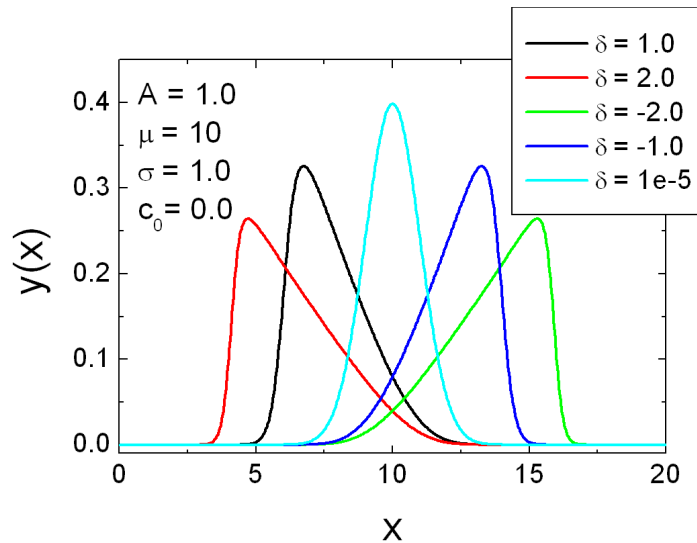


FIGURE 8.28. Plot of HaarhoffVanderLinde (Area) distribution.

8.16. Half Gaussian Modified Gaussian (Area)

The Half Gaussian Modified Gaussian (Area) is the mathematical convolution of a Gaussian with a half-Gaussian response function. There are only two components to this model, a primary Gaussian, and a response function which convolves or smears the Gaussian as in the profiles above. As the width of the half-Gaussian response increases, peaks become more asymmetric or tailed. This function directly fit both tailed and fronted peaks. The transition from tailed to smooth is continuous and occurs at $\delta = 0$. The formula has been taken from the Manual of the Peakfit Software package (SeaSolve Software Inc.).

$$y(x) = A \frac{\exp\left(-\frac{1}{2} \frac{(x-\mu)^2}{\sigma^2 + \delta^2}\right) \left[1 + \operatorname{erf}\left(\frac{\delta(x-\mu)}{\sqrt{2}\sigma\sqrt{\sigma^2 + \delta^2}}\right)\right]}{\sqrt{2\pi} \sqrt{\sigma^2 + \delta^2}} \quad (8.53)$$

Required parameters:

area: area A below the peak

location: location parameter μ

width: scaling parameter $\sigma > 0$

distortion: distortion parameter $\delta \neq 0$

backgr: offset c_0

Note

- The scaling parameter needs to be positive ($\sigma > 0$).
- The distortion parameter needs to be nonzero ($\delta \neq 0$).
- Default (size) distribution: Monodisperse

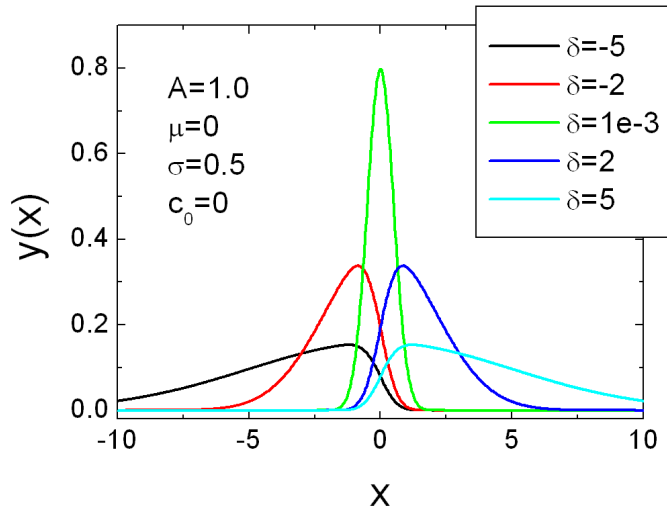


FIGURE 8.29. Plot of Half Gaussian Modified Gaussian (Area) distribution.

8.17. Inverted Gamma

The inverse gamma distribution is a two-parameter family of continuous probability distributions on the positive real line, which is the distribution of the reciprocal of a variable distributed according to the gamma distribution. The inverse gamma distribution's probability density function is defined over the support $x > 0$. The probability density function is given by

$$p(x) = \frac{\beta^\alpha}{\Gamma(\alpha)} x^{-\alpha-1} \exp\left(\frac{-\beta}{x}\right) \quad (8.54)$$

the mode x_{mode} of the probability function is given by $x_{\text{mode}} = \frac{\beta}{\alpha+1}$. The shape parameter α needs to be positive and non-zero as well as the scale parameter β ($\alpha > 0$, $\beta > 0$). The **SASfit** version represents a reparametrization of the standard statistical form. The parameter μ has been added to enable variable x positioning. Adjustment terms have been added so that μ is the mode x_{mode} . The function returns c_0 for those x where it is undefined. Note that the amplitude form is much faster.

8.17.1. Inverted Gamma (Amplitude).

$$y(x) = A \frac{\beta \exp\left(\frac{(x-\mu)(\alpha+1)^2}{x(\alpha+1)+\beta-\mu(\alpha+1)}\right) \left(\frac{x(\alpha+1)-\mu(\alpha+1)}{\beta} + 1\right)^{-\alpha}}{x(\alpha+1) + \beta - \mu(\alpha+1)} + c_0 \quad (8.55)$$

Required parameters:

amplitude: amplitude A of the peak

location: location parameter μ

width: scaling parameter $\beta > 0$

shape: shape parameter $\alpha > 0$

backgr: offset c_0

Note

- The scaling parameter needs to be positive ($\beta > 0$).
- The shape parameter needs to be positive ($\alpha > 0$).
- Default (size) distribution: Monodisperse

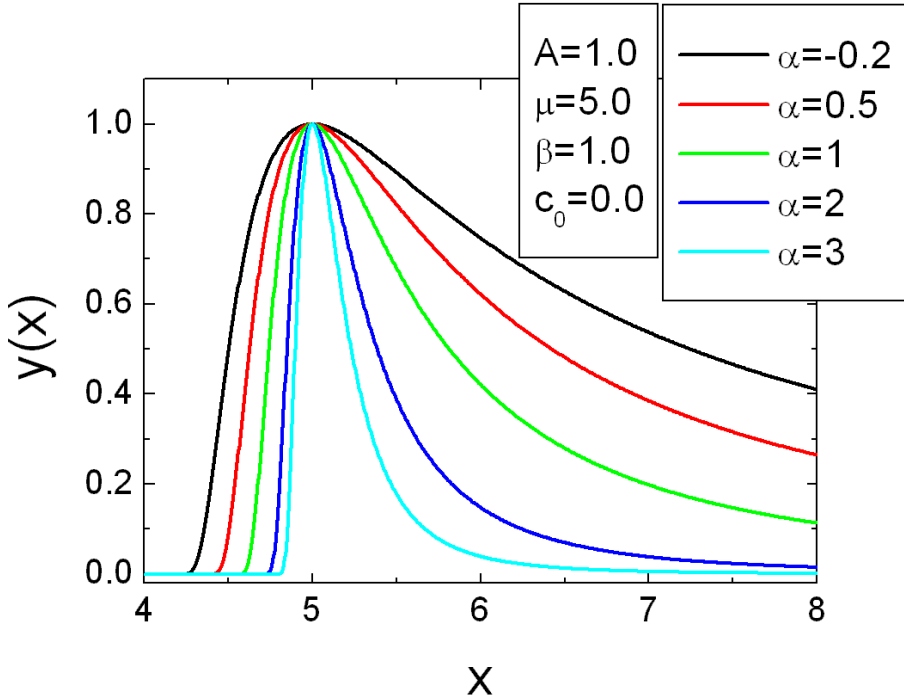


FIGURE 8.30. Plot of inverted Gamma (Amplitude) distribution.

8.17.2. Inverted Gamma (Area).

$$y(x) = A \frac{(\alpha + 1) \exp\left(\frac{\beta(\alpha+1)}{x(\alpha+1)+\beta-\mu(\alpha+1)}\right) \left(\frac{\beta(\alpha+1)}{x(\alpha+1)+\beta-\mu(\alpha+1)}\right)^\alpha}{(x(\alpha + 1) + \beta - \mu(\alpha + 1)) \Gamma(\alpha)} + c_0 \quad (8.56)$$

Required parameters:

area: area A below the peak

location: location parameter μ

width: scaling parameter $\beta > 0$

shape: shape parameter $\alpha > 0$

backgr: offset c_0

Note

- The scaling parameter needs to be positive ($\beta > 0$).
- The shape parameter needs to be positive ($\alpha > 0$).
- Default (size) distribution: Monodisperse

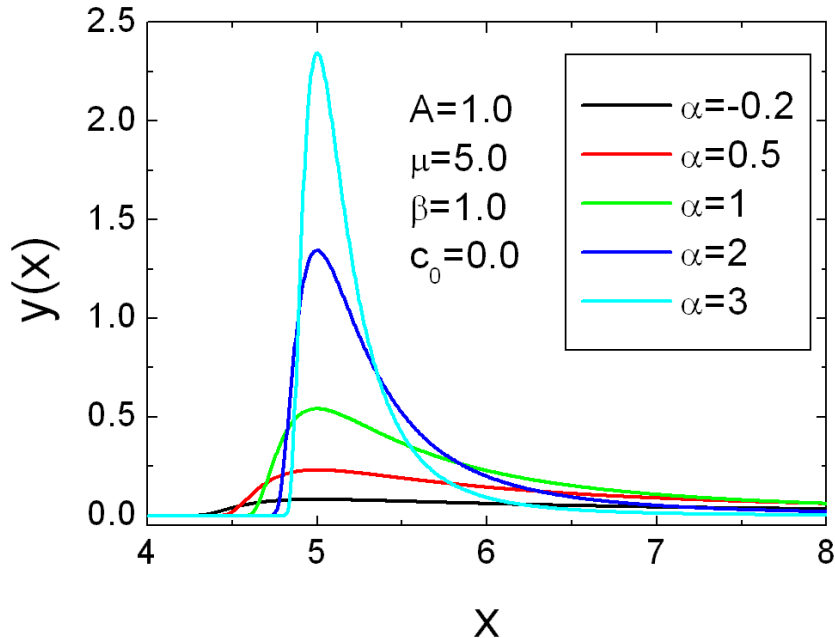


FIGURE 8.31. Plot of inverted Gamma (Area) distribution.

8.18. Kumaraswamy

The Kumaraswamy's double bounded distribution is a family of continuous probability distributions defined on the interval $[0, 1]$ differing in the values of their two non-negative shape parameters, a and b . It is similar to the Beta distribution, but much simpler to use especially in simulation studies due to the simple closed form of both its probability density function and cumulative distribution function. The probability density function of the Kumaraswamy distribution is

$$p(x; \alpha, \beta) = \alpha\beta x^{\alpha-1} (1-x^\alpha)^{\beta-1}. \quad (8.57)$$

For $\alpha > 1$ and $\beta > 1$ the mode of the distribution reads as

$$x_{\text{mode}} = \left(\frac{\alpha - 1}{\alpha\beta - 1} \right)^{1/\alpha} \quad (8.58)$$

8.18.1. Kumaraswamy (Amplitude).

$$y(x) = \begin{cases} \frac{A\alpha\beta \left(\frac{x+x_{\min}}{x_{\max}-x_{\min}} \right)^{\alpha-1} \left(1 - \left(\frac{x+x_{\min}}{x_{\max}-x_{\min}} \right)^\alpha \right)^{\beta-1}}{\alpha\beta x_{\text{mode}}^{\alpha-1} (1-x_{\text{mode}}^\alpha)^{\beta-1}} + c_0 & \text{for } x \in [x_{\min}, x_{\max}] \\ c_0 & \text{for } x \notin [x_{\min}, x_{\max}] \end{cases} \quad (8.59)$$

Required parameters:

- ampl.:** amplitude A of the Kumaraswamy peak
- xmin:** continuous lower boundary parameters x_{\min}
- xmax:** continuous upper boundary parameters x_{\max}
- alpha:** first shape parameter $\alpha > 1$
- beta:** second shape parameter $\beta > 1$
- backgr:** offset c_0

Note

- Both shape parameter needs to be larger than one ($\alpha, \beta > 1$), as only than the distribution has a peak shape.
- where the Kumaraswamy distribution is not defined the offset value is returned:
 $\forall x \notin (x_{\min}, x_{\max}) \quad y_{\text{Beta(ampl)}}(x) = c_0$
- Default (size) distribution: Monodisperse

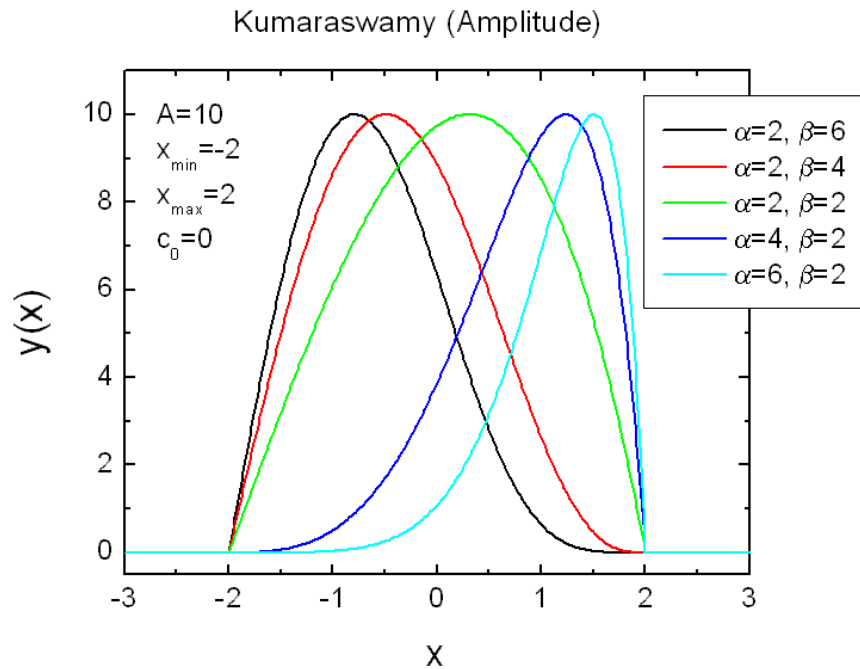


FIGURE 8.32. Plot of Kumaraswamy (Amplitude) distribution.

8.19. Kumaraswamy (Area)

$$y(x) = \begin{cases} \frac{A\alpha\beta\left(\frac{x+x_{\min}}{x_{\max}-x_{\min}}\right)^{\alpha-1}\left(1-\left(\frac{x+x_{\min}}{x_{\max}-x_{\min}}\right)^{\alpha}\right)^{\beta-1}}{x_{\max}-x_{\min}} + c_0 & \text{for } x \in [x_{\min}, x_{\max}] \\ c_0 & \text{for } x \notin [x_{\min}, x_{\max}] \end{cases} \quad (8.60)$$

Required parameters:

area: area A of the Kumaraswamy distribution

xmin: continuous lower boundary parameters x_{\min}

xmax: continuous upper boundary parameters x_{\max}

alpha: first shape parameter $\alpha > 0$

beta: second shape parameter $\beta > 0$

backgr: offset c_0

Note

- Both shape parameter needs to be larger than zero ($\alpha, \beta > 0$)
- where the Kumaraswamy distribution is not defined the offset value is returned:
 $\forall x \notin (x_{\min}, x_{\max}) \quad y_{\text{Beta}(area)}(x) = c_0$
- Default (size) distribution: Monodisperse

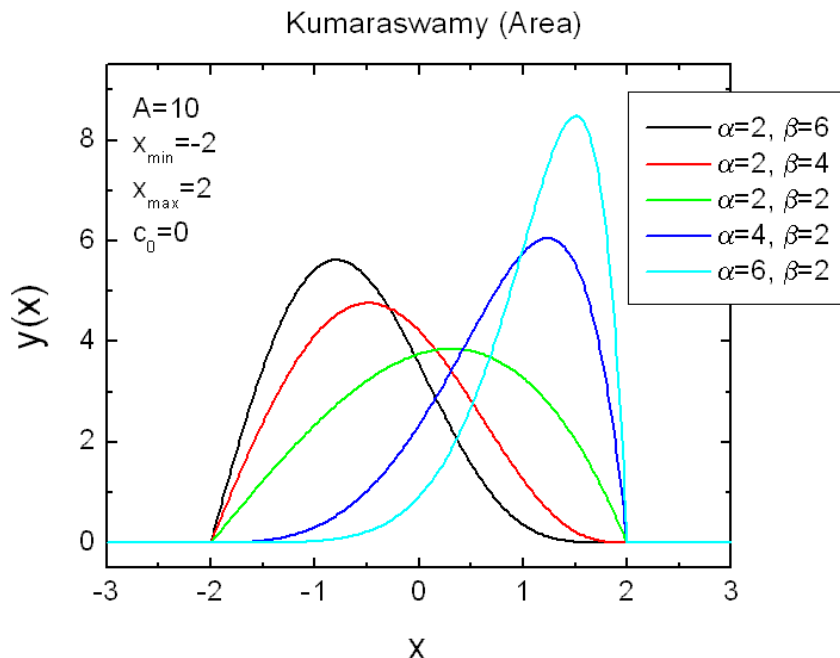


FIGURE 8.33. Plot of Kumaraswamy (Area) distribution.

8.20. Laplace

A random variable has a Laplace distribution if its probability density function is

$$p(x; x_0, \sigma) = \frac{1}{2\sigma} \exp\left(-\frac{|x - x_0|}{\sigma}\right) \quad (8.61)$$

Here, x_0 is a location parameter and $\sigma > 0$ is a scale parameter. The Laplace distribution is also sometimes called the double exponential distribution, because it can be thought of as two exponential distributions (with an additional location parameter) spliced together back-to-back, but the term double exponential distribution is also sometimes used to refer to the Gumbel distribution.

8.20.1. Laplace (Amplitude).

$$y(x; x_0, \sigma) = A \exp\left(-\frac{|x - x_0|}{\sigma}\right) + c_0 \quad (8.62)$$

Required parameters:

amplitude: amplitude A of the Laplace distribution

center: peak center (mode) x_0 of the Laplace distribution

width: width parameter $\sigma > 0$

backgr: offset c_0

Note

- Width parameter needs to be larger than zero ($\sigma > 0$)
- Default (size) distribution: Monodisperse

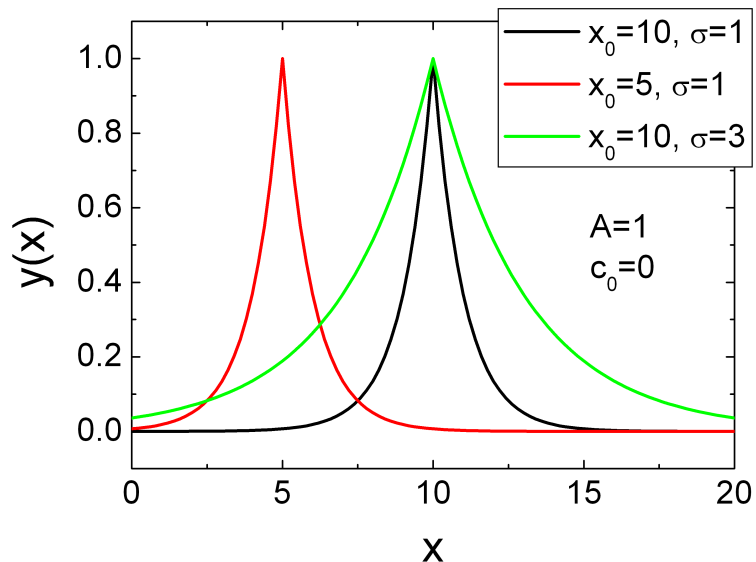


FIGURE 8.34. Plot of Laplace (Amplitude) distribution.

8.20.2. Laplace (Area).

$$y(x; x_0, \sigma) = \frac{A}{2\sigma} \exp\left(-\frac{|x - x_0|}{\sigma}\right) + c_0 \quad (8.63)$$

Required parameters:

area: area A of the Laplace distribution

center: peak center (mode) x_0 of the Laplace distribution

width: width parameter $\sigma > 0$

backgr: offset c_0

Note

- Width parameter needs to be larger than zero ($\sigma > 0$)
- Default (size) distribution: Monodisperse

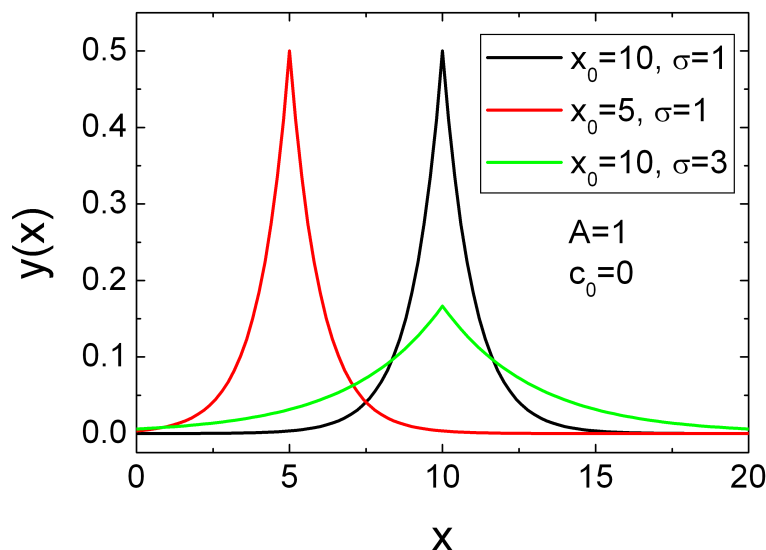


FIGURE 8.35. Plot of Laplace (Area) distribution.

8.21. Logistic

The logistic distribution is a continuous probability distribution. It resembles the normal distribution in shape but has heavier tails (higher kurtosis). The probability density function (pdf) of the logistic distribution is given by:

$$p(x; x_0, \sigma) = \frac{\exp\left(-\frac{x-x_0}{\sigma}\right)}{\sigma \left(1 + \exp\left(-\frac{x-x_0}{\sigma}\right)\right)^2} = \frac{1}{4\sigma} \operatorname{sech}^2\left(\frac{x-x_0}{2\sigma}\right). \quad (8.64)$$

Because the pdf can be expressed in terms of the square of the hyperbolic secant function sech , it is sometimes referred to as the sech-squared distribution. The mode, mean and median values are x_0 .

8.21.1. Logistic (Amplitude).

$$y(x; x_0, \sigma) = 4A \frac{\exp\left(-\frac{x-x_0}{\sigma}\right)}{\left(1 + \exp\left(-\frac{x-x_0}{\sigma}\right)\right)^2} \quad (8.65)$$

Required parameters:

amplitude: amplitude A of the Logistic distribution

x0: location parameter (mode) x_0

sigma: width parameters σ

backgr: offset c_0

Note

- the width parameter needs to be larger than zero $\sigma > 0$
- Default (size) distribution: Monodisperse

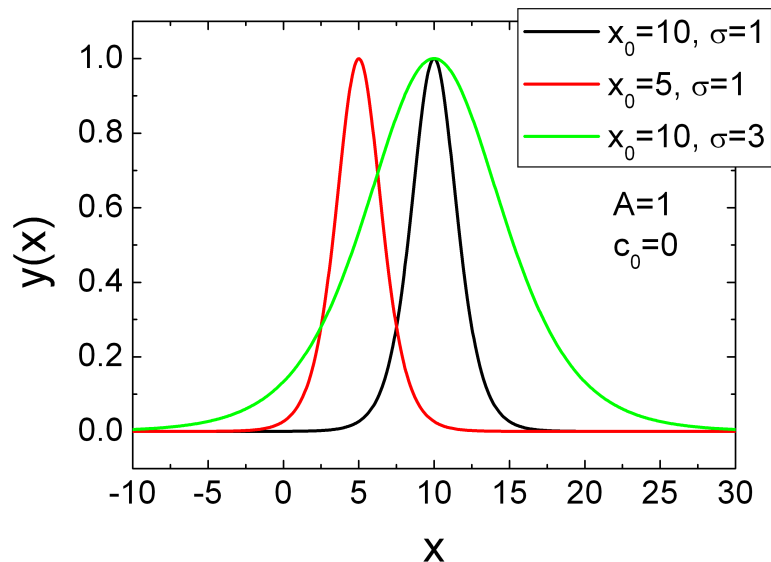


FIGURE 8.36. Plot of Logistic (Amplitude) distribution.

8.21.2. Logistic (Area).

$$y(x; x_0, \sigma) = A \frac{\exp\left(-\frac{x-x_0}{\sigma}\right)}{\sigma \left(1 + \exp\left(-\frac{x-x_0}{\sigma}\right)\right)^2} \quad (8.66)$$

Required parameters:

area: area A of the Logistic distribution

x0: location parameter (mode) x_0

sigma: width parameters σ

backgr: offset c_0

Note

- the width parameter needs to be larger than zero $\sigma > 0$
- Default (size) distribution: Monodisperse

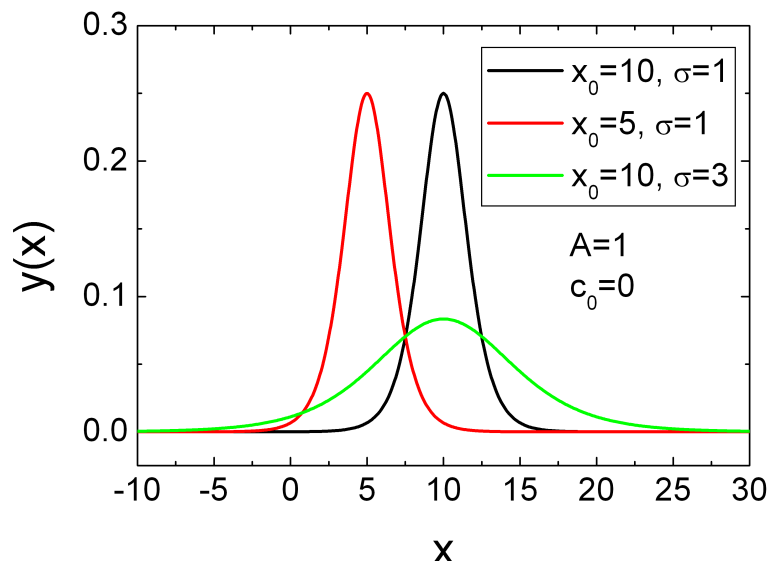


FIGURE 8.37. Plot of Logistic (Area) distribution

8.22. LogitNormal

The Logit-Normal distribution is a continuous probability distribution on a bounded interval of a random variable, whose logit has a normal distribution. The probability density function (pdf) of the logistic distribution is given by:

$$p(x; \mu, \sigma) = \frac{\exp\left(-\frac{(\text{logit}(x) - \mu)^2}{2\sigma^2}\right)}{\sigma\sqrt{2\pi} (x(1-x))} \quad (8.67)$$

$$\text{logit}(x) = \log\left(\frac{x}{1-x}\right) \quad (8.68)$$

Because the pdf can be expressed in terms of the square of the hyperbolic secant function sech, it is sometimes referred to as the sech-squared distribution. The mode, mean and median values are x_0 .

8.22.1. LogitNormal (Amplitude).

$$y(x; A, x_{\min}, x_{\max}, \mu, \sigma) = \frac{A \exp\left(-\frac{(\text{logit}(z) - \mu)^2}{2\sigma^2}\right)}{c \sigma\sqrt{2\pi} (z(1-z))} \quad (8.69)$$

$$z = \frac{(x - x_{\min})}{x_{\max} - x_{\min}} \quad (8.70)$$

The scaling variable c is chosen so that at the mode x_{mode} of the distribution its value becomes $y(x_{\text{mode}}; A, \dots) = A$. The mode itself is numerically calculated as for this distribution there does not exist an analytical definition of it.

Required parameters:

amplitude: amplitude A of the LogitNormal distribution

xmin: lower bound x_{\min}

xmax: upper bound x_{\max}

mu: location parameters μ

sigma: width parameters σ

backgr: offset c_0

Note

- the width parameter needs to be non-zero $\sigma^2 > 0$
- width of the boundary interval needs to be finite, i.e. $|x_{\max} - x_{\min}| > 0$
- Default (size) distribution: Monodisperse

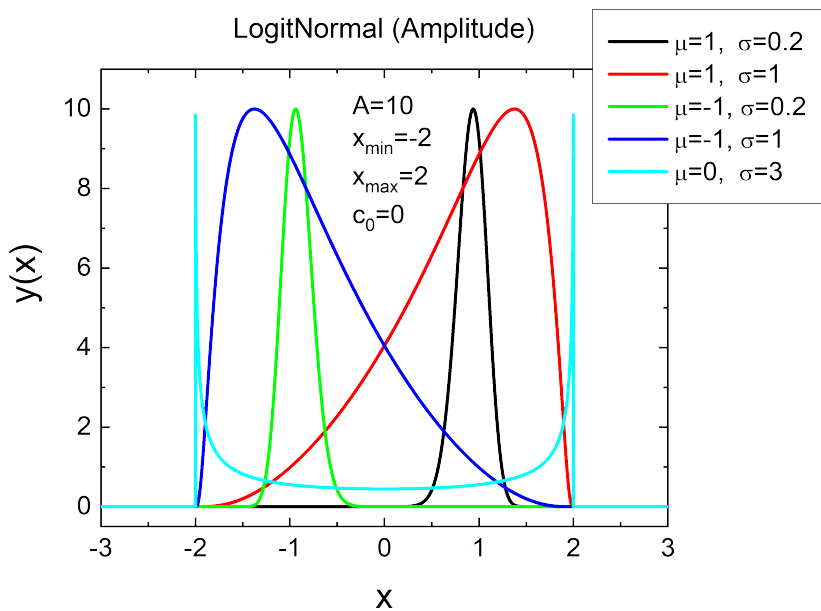


FIGURE 8.38. Plot of LogitNormal (Amplitude) distribution.

8.22.2. LogitNormal (Area).

$$y(x; A, x_{\min}, x_{\max}, \mu, \sigma) = \frac{A}{(x - x_{\min})} \frac{\exp\left(-\frac{(\log(z) - \mu)^2}{2\sigma^2}\right)}{\sigma\sqrt{2\pi} (z(1 - z))} \quad (8.71)$$

$$z = \frac{(x - x_{\min})}{x_{\max} - x_{\min}} \quad (8.72)$$

Required parameters:

area: area A below LogitNormal distribution

xmin: lower bound x_{\min}

xmax: upper bound x_{\max}

mu: location parameters μ

sigma: width parameters σ

backgr: offset c_0

Note

- the width parameter needs to be non-zero $\sigma^2 > 0$
- width of the boundary interval needs to be finite, i.e. $|x_{\max} - x_{\min}| > 0$
- Default (size) distribution: Monodisperse

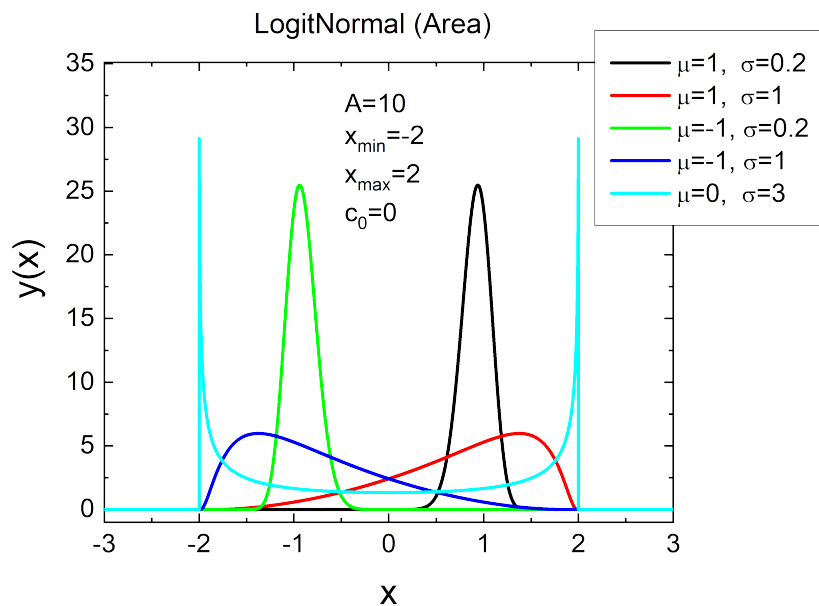


FIGURE 8.39. Plot of LogitNormal (Area) distribution

8.23. LogLogistic

As may be indicated by the name, the loglogistic (known as the Fisk distribution in economics) distribution has certain similarities to the logistic distribution. A random variable is loglogistically distributed if the logarithm of the random variable is logistically distributed. The **LogLogistic** distribution is a two-parameter distribution with parameters σ and x_0 . It is similar in shape to the log-normal distribution but has heavier tails.

The pdf for this distribution is given by:

$$p(x; \mu, \sigma) = \frac{\exp\left(-\frac{\log(x)-\log(\mu)}{\sigma}\right)}{\sigma(x)\left(1+\exp\left(-\frac{\log(x)-\log(\mu)}{\sigma}\right)\right)^2} = \frac{\left(\frac{x}{\mu}\right)^{-1/\sigma}}{x\sigma\left[1+\left(\frac{x}{\mu}\right)^{-1/\sigma}\right]^2}. \quad (8.73)$$

where $0 < x < \infty$, $-\infty < x_0 < \infty$ and $0 < \sigma < \infty$. The mode of the **LogLogistic** distribution, if $\sigma < 1$, is given by:

$$\text{mode} = \mu \left(\frac{1-\sigma}{1+\sigma}\right)^\sigma \quad (8.74)$$

8.23.1. LogLogistic (Amplitude).

$$y(x) = \begin{cases} A \frac{\left(\frac{x-x_0}{\mu}\right)^{-1/\sigma}}{(x-x_0)\sigma\left[1+\left(\frac{x-x_0}{\mu}\right)^{-1/\sigma}\right]^2} + c_0 & \text{for } x \geq x_0 \\ c_0 & \text{for } x < x_0 \end{cases} \quad (8.75)$$

Required parameters:

amplitude: amplitude A of the LogLogistic distribution

x0: location parameter x_0

mu: scale parameter μ

sigma: shape parameters σ

backgr: offset c_0

Note

- the width parameter needs to be larger than zero $0 < \sigma < 1$
- Default (size) distribution: Monodisperse

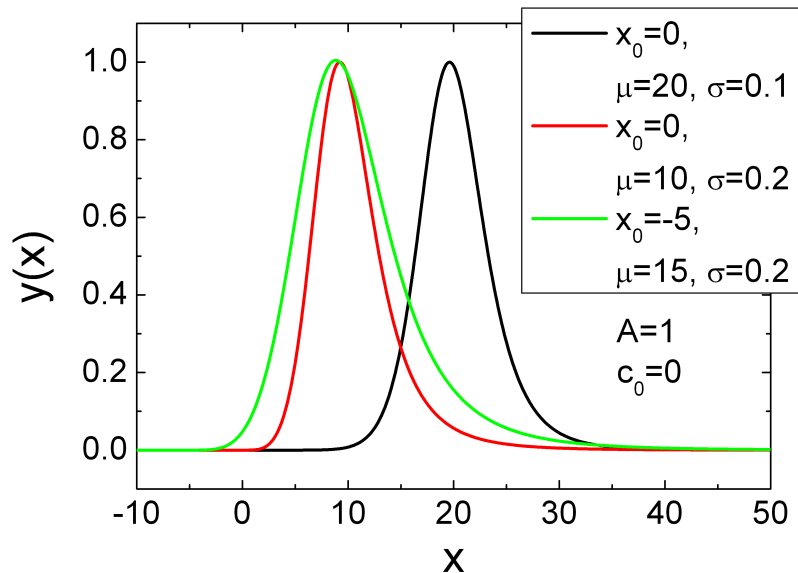


FIGURE 8.40. Plot of LogLogistic (Amplitude) distribution.

8.23.2. LogLogistic (Area).

$$y(x) = A \frac{\left(\frac{x}{x_0}\right)^{-1/\sigma}}{x\sigma \left[1 + \left(\frac{x}{x_0}\right)^{-1/\sigma}\right]^2}. \quad (8.76)$$

Required parameters:

area: area A of the LogLogistic distribution

x0: location parameter x_0

mu: scale parameter μ

sigma: shape parameters $0 < \sigma < 1$

backgr: offset c_0

Note

- the width parameter needs to be larger than zero $\sigma > 0$
- Default (size) distribution: Monodisperse

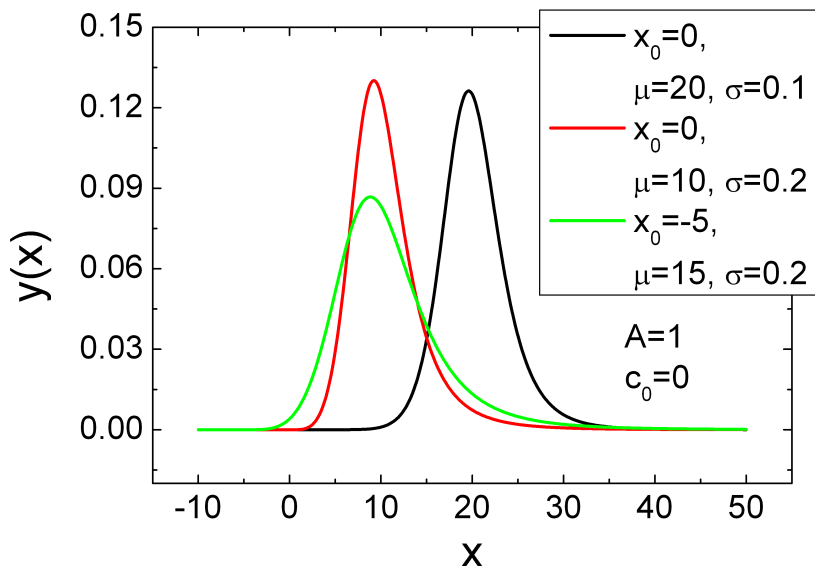


FIGURE 8.41. Plot of LogLogistic (Area) distribution.

8.24. Lognormal 4-Parameter

8.24.1. Lognormal 4-Parameter (Amplitude).

$$y(x) = \begin{cases} c_0 + A \exp \left[-\frac{\ln(2) \ln \left(\frac{(x-x_0)(\gamma^2-1)}{\sigma\gamma} + 1 \right)^2}{\ln(\gamma)} \right] & \text{for } \gamma \neq 1, \gamma > 0 \\ c_0 + A 2^{-4 \left(\frac{x-x_0}{\sigma} \right)^2} & \text{for } \gamma = 1 \end{cases} \quad (8.77)$$

For $(x \geq x_0 - \frac{\sigma\gamma}{\gamma^2-1} \wedge \gamma < 1) \vee (x \leq x_0 - \frac{\sigma\gamma}{\gamma^2-1} \wedge \gamma > 1)$ the function returns c_0 .

Required parameters:

amplitude: amplitude A of the LogLogistic distribution

x0: location parameter x_0

sigma: width parameter $\sigma > 0$

gamma: shape parameters $\gamma > 0$

backgr: offset c_0

Note

- the width parameter needs to be larger than zero $\sigma > 0$
- the shape parameter needs to be larger than zero $\gamma > 0$
- Default (size) distribution: Monodisperse

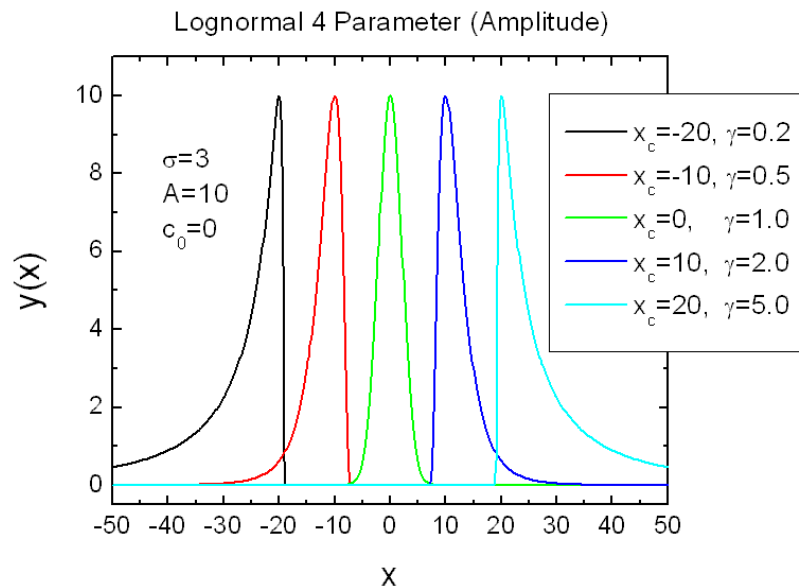


FIGURE 8.42. Plot of Lognormal 4-Parameter (Amplitude) distribution.

8.24.2. Lognormal 4-Parameter (Area).

$$y(x) = \begin{cases} c_0 + A \frac{\sqrt{\ln 2}(\gamma^2 - 1)}{\sigma\gamma \ln(\gamma)\sqrt{\pi} \exp\left(\frac{\ln(\gamma^2)}{4\ln 2}\right)} \exp\left[-\frac{\ln(2) \ln\left(\frac{(x-x_0)(\gamma^2-1)}{\sigma\gamma}+1\right)^2}{\ln(\gamma)}\right] & \text{for } \gamma \neq 1, \gamma > 0 \\ c_0 + A \frac{\sqrt{\ln 2}}{\sigma\sqrt{\pi}} 2^{-4\left(\frac{x-x_0}{\sigma}\right)^2} & \text{for } \gamma = 1 \end{cases} \quad (8.78)$$

For $(x \geq x_0 - \frac{\sigma\gamma}{\gamma^2-1} \wedge \gamma < 1) \vee (x \leq x_0 - \frac{\sigma\gamma}{\gamma^2-1} \wedge \gamma > 1)$ the function returns c_0 .

Required parameters:

area: area A of the LogLogistic distribution

x0: location parameter x_0

sigma: width parameter $\sigma > 0$

gamma: shape parameters $\gamma > 0$

backgr: offset c_0

Note

- the width parameter needs to be larger than zero $\sigma > 0$
- the shape parameter needs to be larger than zero $\gamma > 0$
- Default (size) distribution: Monodisperse

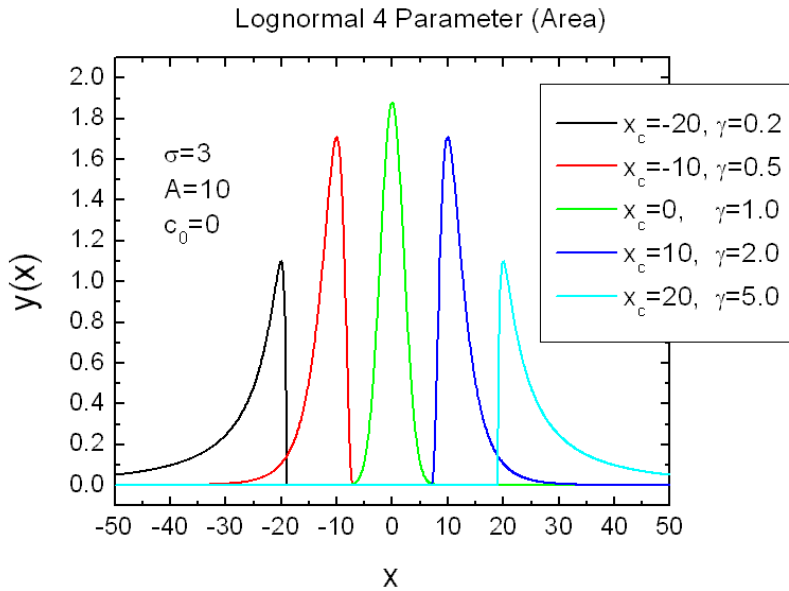


FIGURE 8.43. Plot of Lognormal 4-Parameter (Area) distribution.

8.25. LogNormal

The LogNormal distribution is defined with reference to the normal distribution. A random variable is Lognormally distributed if the logarithm of the random variable is normally distributed.

The LogNormal distribution is commonly used for general reliability analysis, cycles-to-failure in fatigue, material strengths and loading variables in probabilistic design. Another advantage of the LogNormal distribution is that it is positive-definite, so it is often useful for representing quantities that cannot have negative values. LogNormal distributions have proven useful as distributions for rainfall amounts, for the size distributions of aerosol particles or droplets, and for many other cases. The log-normal distribution has the probability density function

$$f(x') = \frac{1}{\sigma\sqrt{2\pi}} \exp\left(-\frac{1}{2} \left(\frac{x' - \mu'}{\sigma}\right)^2\right) \quad (8.79)$$

where $\mu' = \ln(\mu)$ and $x' = \ln(x)$. The lognormal pdf can be obtained, realizing that for equal probabilities under the normal and lognormal pdfs, incremental areas should also be equal, or:

$$f(x; \mu, \sigma) dx = f(x'; \mu, \sigma) dx' \quad (8.80)$$

Taking the derivative yields:

$$dx' = \frac{dx}{x} \quad (8.81)$$

Substitution yields:

$$f(x; \mu, \sigma) = \frac{f(x'; \mu, \sigma)}{x} \quad (8.82)$$

where:

$$f(x; \mu, \sigma) = \frac{1}{x\sigma\sqrt{2\pi}} \exp\left(-\frac{1}{2} \left(\frac{\ln(x) - \ln(\mu)}{\sigma}\right)^2\right) \quad (8.83)$$

for $x \in (0, \infty]$, where $\mu > 0$ and $\sigma \neq 0$ are the location and scale parameter. The mode of the distribution is

$$\text{mode} = \mu \exp(-\sigma^2) \quad (8.84)$$

8.25.1. LogNormal (Amplitude).

$$y(x) = \begin{cases} \frac{A \exp(-\frac{1}{2}\sigma^2)\mu}{x-x_0} \exp\left(-\frac{1}{2}\left(\frac{\ln(x-x_0)-\ln(\mu)}{\sigma}\right)^2\right) + c_0 & \text{for } x > x_0 \\ c_0 & \text{for } x \leq x_0 \end{cases} \quad (8.85)$$

Required parameters:

amplitude: amplitude A of the LogNormal distribution

mu: location parameter μ

sigma: width parameter $\sigma > 0$

x0: shift parameters x_0

backgr: offset c_0

Note

- the width parameter needs to be larger than zero $\sigma > 0$
- the location parameter needs to be larger than the shift parameter $\mu > x_0$
- Default (size) distribution: Monodisperse

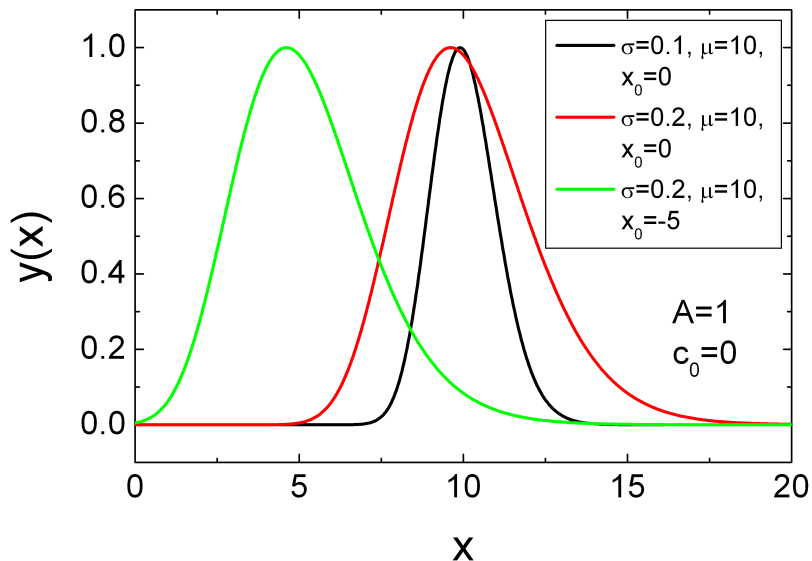


FIGURE 8.44. Plot of LogNormal (Amplitude) distribution.

8.25.2. LogNormal (Area).

$$y(x) = \begin{cases} \frac{A}{(x-x_0)\sigma\sqrt{2\pi}} \exp\left(-\frac{1}{2}\left(\frac{\ln(x-x_0)-\ln(\mu)}{\sigma}\right)^2\right) + c_0 & \text{for } x > x_0 \\ c_0 & \text{for } x \leq x_0 \end{cases} \quad (8.86)$$

Required parameters:

area: area A of the LogNormal distribution

mu: location parameter μ

sigma: width parameter $\sigma > 0$

x0: shift parameters x_0

backgr: offset c_0

Note

- the width parameter needs to be larger than zero $\sigma > 0$
- the location parameter needs to be larger than the shift parameter $\mu > x_0$
- Default (size) distribution: Monodisperse

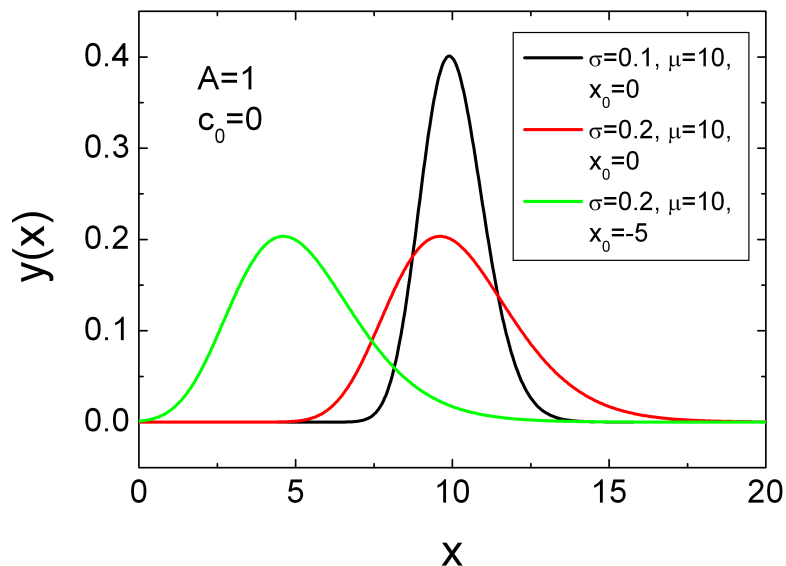


FIGURE 8.45. Plot of LogNormal (Area) distribution.

8.26. Lorentzian or Cauchy distribution

The Cauchy-Lorentz Distribution, named after Augustin Cauchy and Hendrik Lorentz, is a continuous probability distribution. As a probability distribution, it is known as the Cauchy distribution, while among physicists, it is known as a Lorentz distribution, or a Lorentz(ian) function or the Breit-Wigner distribution. Its importance in physics is due to it being the solution to the differential equation describing forced resonance. The Lorentzian distribution has the probability density function

$$\begin{aligned} f(x; x_0, \sigma) &= \frac{1}{\pi \sigma \left[1 + \left(\frac{x-x_0}{\sigma} \right)^2 \right]} \\ &= \frac{1}{\pi} \left[\frac{\sigma}{(x - x_0)^2 + \sigma^2} \right] \end{aligned} \quad (8.87)$$

where x_0 is the location parameter, specifying the location of the peak of the distribution, and σ is the scale parameter which specifies the half-width at half-maximum (HWHM).

8.26.1. Lorentzian (Amplitude).

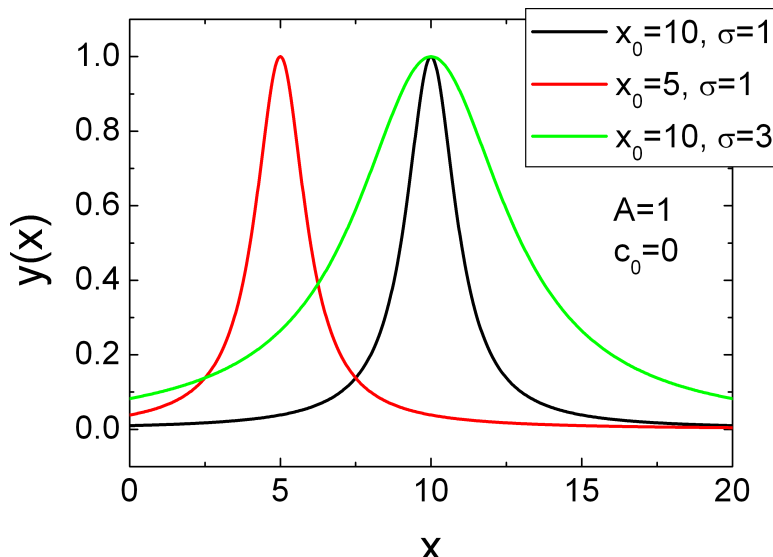


FIGURE 8.46. Plot of Lorentzian (Amplitude) distribution.

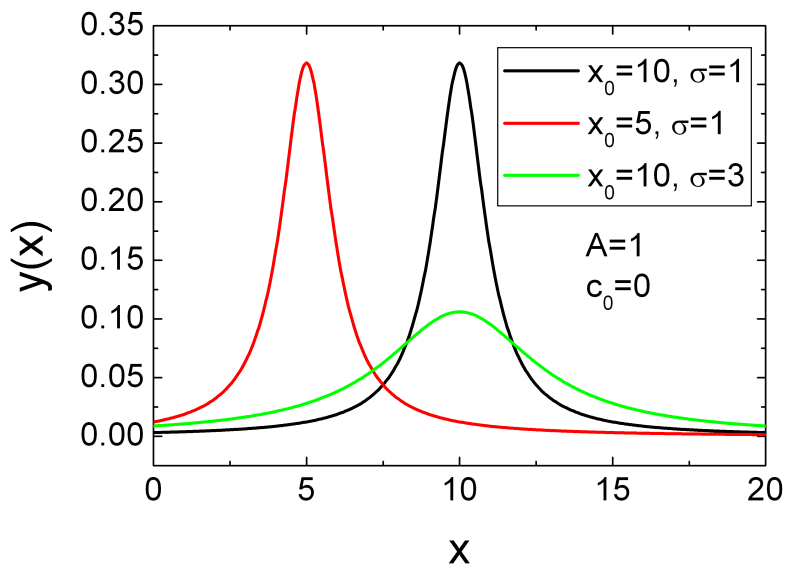
8.26.2. Lorentzian (Area).

FIGURE 8.47. Plot of Lorentzian (Area) distribution.

8.27. Maxwell-Boltzmann distribution

The Maxwell-Boltzmann distribution describes particle speeds in gases, where the particles do not constantly interact with each other but move freely between short collisions. It describes the probability of a particle's speed (the magnitude of its velocity vector) being near a given value as a function of the temperature of the system, the mass of the particle, and that speed value. This probability distribution is named after James Clerk Maxwell and Ludwig Boltzmann.

The Maxwell-Boltzmann distribution is usually thought of as the distribution for molecular speeds, but it can also refer to the distribution for velocities, momenta, and magnitude of the momenta of the molecules, each of which will have a different probability distribution function, all of which are related. Two Maxwell distributions have been implemented, one distribution for speed and a generalized Maxwell distribution, which includes also the energy distribution.

The generalized Maxwell distribution is here defined as

$$p(x; x_0, \sigma, n, m) = \begin{cases} 0 & \text{for } x < x_0 \\ \frac{(x-x_0)^m \exp\left(-\frac{1}{2}\left(\frac{x-x_0}{|\sigma|}\right)^n\right)}{2^{(1+m)/n} |\sigma|^{1+m} \frac{1}{|n|} \Gamma\left(\frac{1+m}{n}\right)} & \text{for } x \geq x_0. \end{cases} \quad (8.88)$$

where x_0 is the location parameter, specifying the location of the peak of the distribution, and σ is the scale parameter which specifies the width. The mode of the distribution is given by

$$x_{\text{mode}} = \left(\frac{2m}{n}\right)^{1/n} |\sigma| + x_0. \quad (8.89)$$

For the case $m = n = 2$ one gets the "Maxwell-Boltzmann distribution" to refers to the distribution of speed. To get the distribution for the energy one has to set $m = 1/2$ and $n = 1$. In case of the width parameter σ always the modulus is used in the calculation of the distribution function to avoid negative values for which the function is not always well defined. For $\sigma = 0$ the distribution function is not defined.

8.27.1. Maxwell (Amplitude).

$$y(x; A, \sigma, x_0, y_0) = \begin{cases} y_0 & \text{for } x < x_0 \\ y_0 + A \frac{(x-x_0)^2}{(x_{\text{mode}}-x_0)^2} \frac{\exp\left(-\frac{1}{2}\left(\frac{x-x_0}{\sigma}\right)^2\right)}{\exp\left(-\frac{1}{2}\left(\frac{x_{\text{mode}}-x_0}{\sigma}\right)^2\right)} & \text{for } x \geq x_0 \end{cases} \quad (8.90)$$

with $x_{\text{mode}} = \sqrt{2}|\sigma| + x_0$.

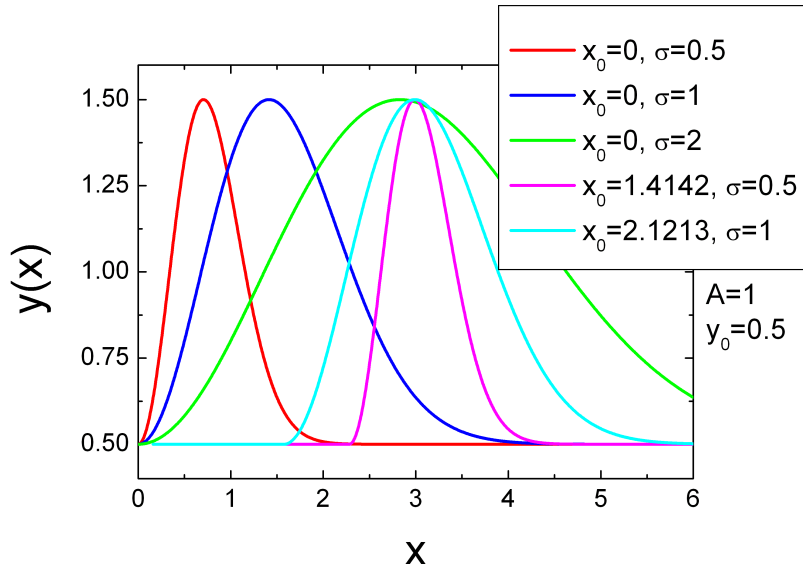


FIGURE 8.48. Plot of Maxwell (Amplitude) distribution.

8.27.2. Maxwell (Area).

$$y(x; A, \sigma, x_0, y_0) = \begin{cases} y_0 & \text{for } x < x_0 \\ y_0 + \sqrt{\frac{2}{\pi}} \frac{A(x-x_0)^2}{\sigma^3} \exp\left(-\frac{1}{2}\left(\frac{x-x_0}{\sigma}\right)^2\right) & \text{for } x \geq x_0 \end{cases} \quad (8.91)$$

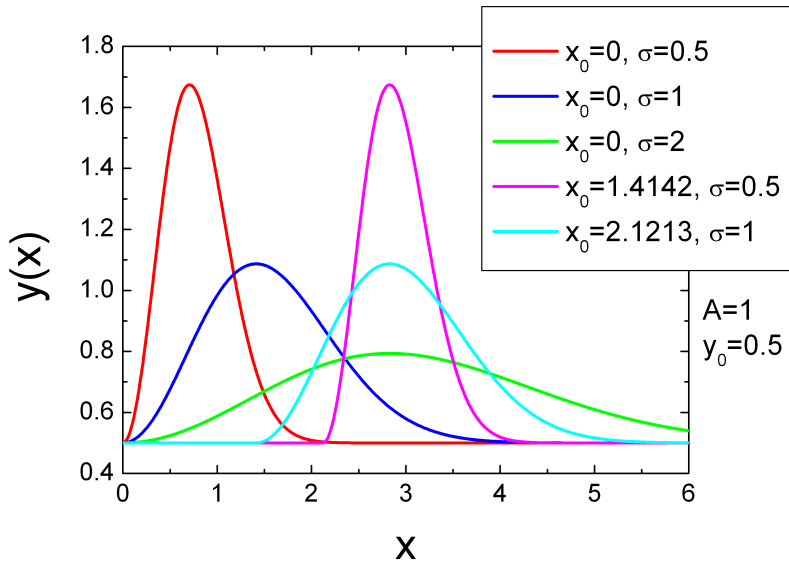


FIGURE 8.49. Plot of Maxwell (Area) distribution.

8.27.3. generalized Maxwell (Amplitude).

$$y(x; x_0, \sigma, n, m) = \begin{cases} y_0 & \text{for } x < x_0 \\ y_0 + A \frac{(x-x_0)^m \exp\left(-\frac{1}{2}\left(\frac{x-x_0}{|\sigma|}\right)^n\right)}{(x_{\text{mode}}-x_0)^m \exp\left(-\frac{1}{2}\left(\frac{x_{\text{mode}}-x_0}{|\sigma|}\right)^n\right)} & \text{for } x \geq x_0 \end{cases} \quad (8.92)$$

with $x_{\text{mode}} = \left(\frac{2m}{n}\right)^{1/n} |\sigma| + x_0$.

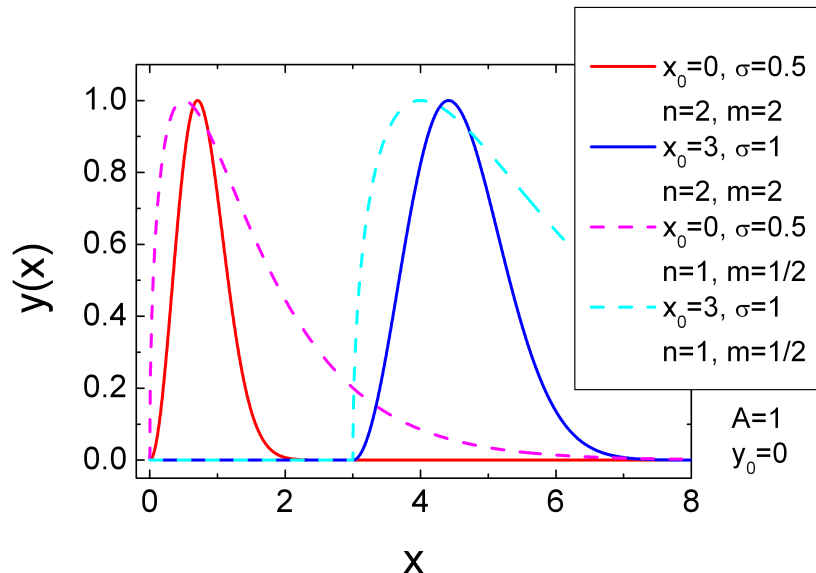


FIGURE 8.50. Plot of generalized Maxwell (Amplitude) distribution.

8.27.4. generalized Maxwell (Area).

$$y(x; x_0, \sigma, n, m) = \begin{cases} 0 & \text{for } x < x_0 \\ A \frac{(x-x_0)^m \exp\left(-\frac{1}{2}\left(\frac{x-x_0}{|\sigma|}\right)^n\right)}{2^{(1+m)/n} |\sigma|^{1+m} \frac{1}{|n|} \Gamma\left(\frac{1+m}{n}\right)} & \text{for } x \geq x_0. \end{cases} \quad (8.93)$$

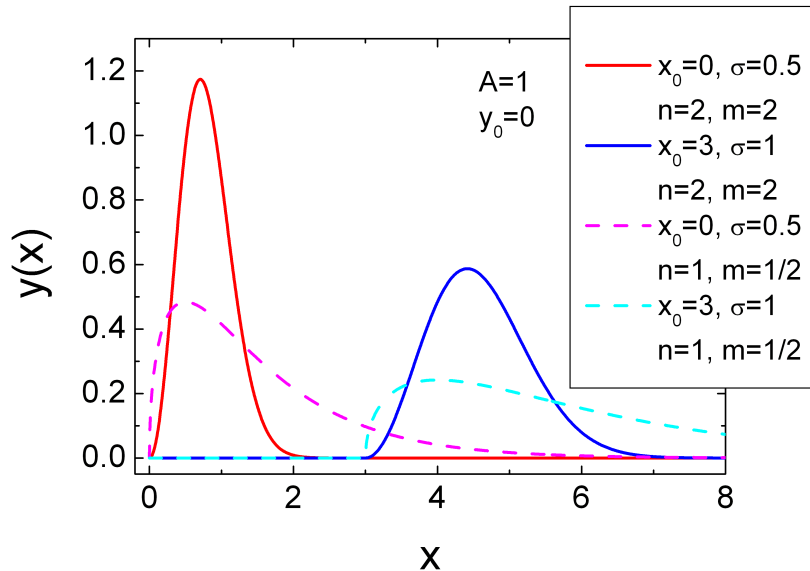


FIGURE 8.51. Plot of generalized Maxwell (Area) distribution.

8.28. Pearson-IV

Pearson type IV distribution:

$$p(x) = \frac{\left| \frac{\Gamma(m + \frac{\nu}{2}i)}{\Gamma(m)} \right|^2}{\alpha B\left(m - \frac{1}{2}, \frac{1}{2}\right)} \left[1 + \left(\frac{x - \lambda}{\alpha} \right)^2 \right]^{-m} \exp \left[-\nu \arctan \left(\frac{x - \lambda}{\alpha} \right) \right]. \quad (8.94)$$

The normalizing constant involves the complex Gamma function (Γ) and the Beta function (B). For the distribution the mode, mean and variance are given by

$$\text{mode} = \mathcal{M} = \lambda - \frac{\alpha\nu}{2m} \quad (8.95)$$

$$\text{mean} = \langle x \rangle = \lambda - \frac{\alpha\nu}{2(m-1)} \quad ((m > 1)) \quad (8.96)$$

$$\text{variance} = \langle (x - \langle x \rangle)^2 \rangle = \frac{\alpha^2}{r^2(r-1)} (r^2 + \nu^2) \quad \text{for } m > \frac{3}{2} \quad (8.97)$$

$$\text{with } r = 2(m-1)$$

The shape parameter ν of the Pearson type IV distribution controls its skewness. If we fix its value at zero, we obtain a symmetric three-parameter family. This special case is known as the Pearson type VII distribution 8.29.

8.28.1. Pearson-IV (Amplitude).

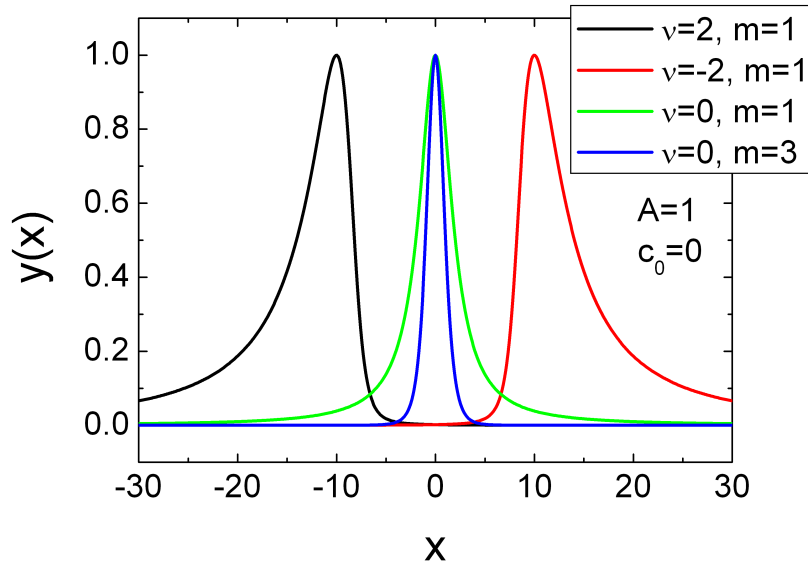


FIGURE 8.52. Plot of Pearson-IV (Amplitude) distribution.

8.28.2. Pearson-IV (Area).

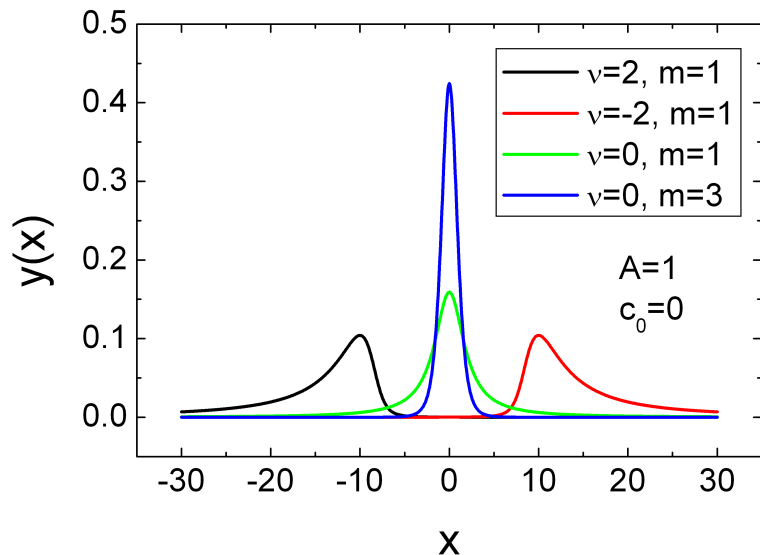


FIGURE 8.53. Plot of Pearson-IV (Area) distribution.

8.29. Pearson-VII

The Pearson-VII model has been used as an approximation for the Voigt function. The parameter σ is the FWHM (full-width at half-maxima). When m is 1.0, the function is an exact Lorentzian. As the m -power term increases, the function tends toward the Gaussian. For $m \sim 50$, the function is essentially Gaussian. The Pearson VII function is a different parametrization of the Student-t distribution function and reads as

$$p(x) = \frac{1}{\alpha B(m - \frac{1}{2}, \frac{1}{2})} \left[1 + \left(\frac{x - \lambda}{\alpha} \right)^2 \right]^{-m} \quad (8.98)$$

where B is the Beta function $B(a, b) = \Gamma(a)\Gamma(b)/\Gamma(a+b)$, with a and b not being negative integers. The mode \mathcal{M} of the distribution is equals $\mathcal{M} = \lambda$.

Sometimes distribution function are described by the mode \mathcal{M} and integral peak width or peak breadth β . The peak breadth is given by $\beta = p(\mathcal{M}) / \int_{-\infty}^{\infty} p(x) dx = \alpha B(m - \frac{1}{2}, \frac{1}{2})$, so that

$$p(x) = \frac{1}{\beta} \left[1 + B^2 \left(m - \frac{1}{2}, \frac{1}{2} \right) \left(\frac{x - \mathcal{M}}{\beta} \right)^2 \right]^{-m} \quad (8.99)$$

An alternative parameterization (and slight specialization) of the type VII distribution is obtained by letting $\alpha = \sigma\sqrt{2m-3}$, which requires $m > 3/2$. By this constrain the variance of the distribution exists and is equal to σ^2 .

$$p(x) = \frac{1}{\sigma\sqrt{2m-3}B(m - \frac{1}{2}, \frac{1}{2})} \left[1 + \left(\frac{x - \lambda}{\sigma\sqrt{2m-3}} \right)^2 \right]^{-m} \quad (8.100)$$

Now the parameter m only controls the kurtosis of the distribution. If m approaches infinity as λ and σ are held constant, the normal distribution arises as a special case:

$$\begin{aligned} & \lim_{m \rightarrow \infty} \frac{1}{\sigma\sqrt{2m-3}B(m - \frac{1}{2}, \frac{1}{2})} \left[1 + \left(\frac{x - \lambda}{\sigma\sqrt{2m-3}} \right)^2 \right]^{-m} \\ &= \frac{1}{\sigma\sqrt{2}\Gamma(\frac{1}{2})} \times \lim_{m \rightarrow \infty} \frac{\Gamma(m)}{\Gamma(m - \frac{1}{2})\sqrt{m - \frac{3}{2}}} \times \lim_{m \rightarrow \infty} \left[1 + \frac{\left(\frac{x - \lambda}{\sigma} \right)^2}{2m-3} \right]^{-m} \\ &= \frac{1}{\sigma\sqrt{2\pi}} \times 1 \times \exp \left[-\frac{1}{2} \left(\frac{x - \lambda}{\sigma} \right)^2 \right] \end{aligned}$$

For $m > \frac{5}{2}$ the distribution could also be expressed in terms of excess kurtosis γ_2 or kurtosis κ by letting

$$m = \frac{5}{2} + \frac{3}{\gamma_2} \quad (8.101)$$

$$\text{or } m = \frac{5}{2} + \frac{3}{\kappa - 3} \quad (8.102)$$

It is also possible to express the Pearson distribution in terms of the full width of half maximum ω_{FWHM} by substituting $\alpha = \omega_{\text{FWHM}} / (2\sqrt{2^{1/m} - 1})$. This leads to

$$p(x) = \frac{2\sqrt{2^{1/m} - 1}}{\omega_{\text{FWHM}} \text{B}\left(m - \frac{1}{2}, \frac{1}{2}\right)} \left[1 + 4 \left(\sqrt{2^{1/m} - 1} \right) \left(\frac{x - \lambda}{\omega_{\text{FWHM}}} \right)^2 \right]^{-m} \quad (8.103)$$

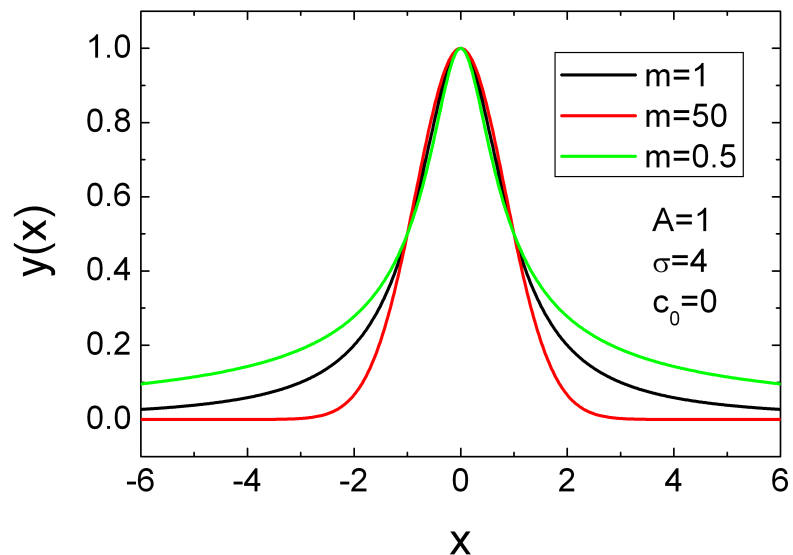
8.29.1. Pearson-VII (Amplitude).

FIGURE 8.54. Plot of Pearson-VII (Amplitude) distribution.

8.29.2. Pearson-VII (Area).

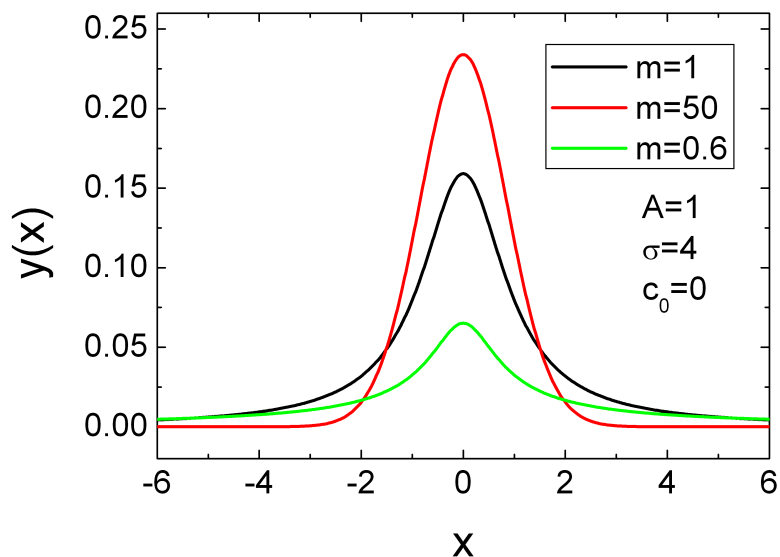


FIGURE 8.55. Plot of Pearson-VII (Area) distribution.

8.30. Pulse Peak

$$p(x) = \frac{2}{\sigma} \exp\left(\frac{x - x_0}{\sigma}\right) \left(1 - \exp\left(\frac{x - x_0}{\sigma}\right)\right) \quad (8.104)$$

$$\text{mode} = x_0 - \sigma \ln\left(\frac{1}{2}\right) \quad (8.105)$$

8.30.1. Pulse Peak (Amplitude).

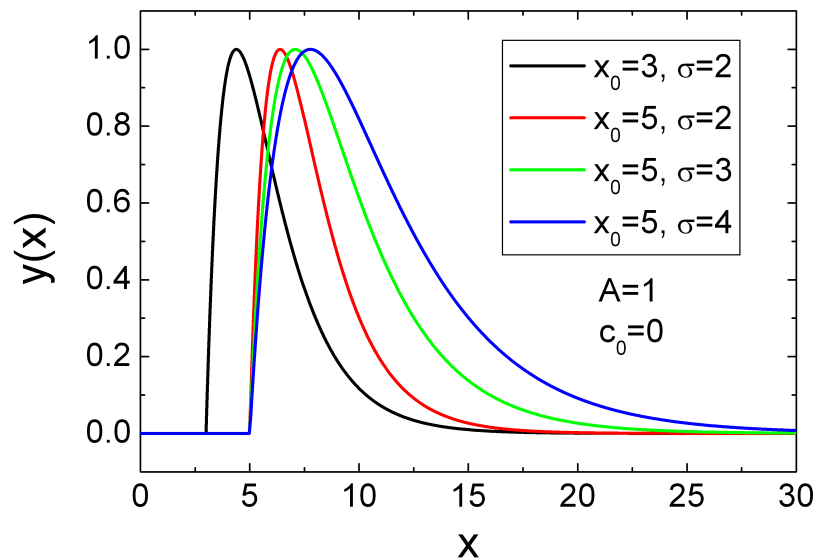


FIGURE 8.56. Plot of Pulse Peak (Amplitude) distribution.

8.30.2. Pulse Peak (Area).

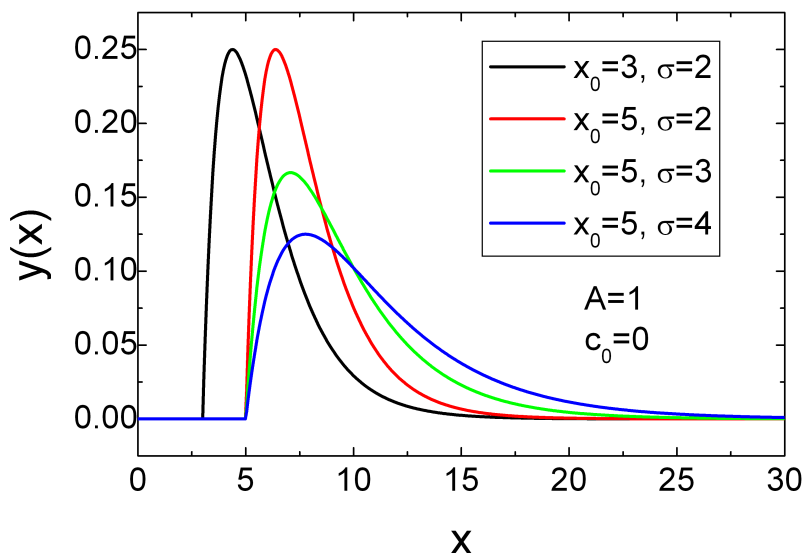


FIGURE 8.57. Plot of Pulse Peak (Area) distribution.

8.31. Pulse Peak with 2nd Width Term

$$p(x) = \frac{\sigma_1 + \sigma_2}{\sigma_2^2} \left(1 - \exp \left(\frac{x - x_0}{\sigma_1} \right) \right) \exp \left(\frac{x - x_0}{\sigma_2} \right) \quad (8.106)$$

$$\text{mode} = x_0 - \sigma_1 \ln \left(\frac{\sigma_1}{\sigma_2 + \sigma_1} \right) \quad (8.107)$$

8.31.1. Pulse Peak with 2nd Width Term (Amplitude).

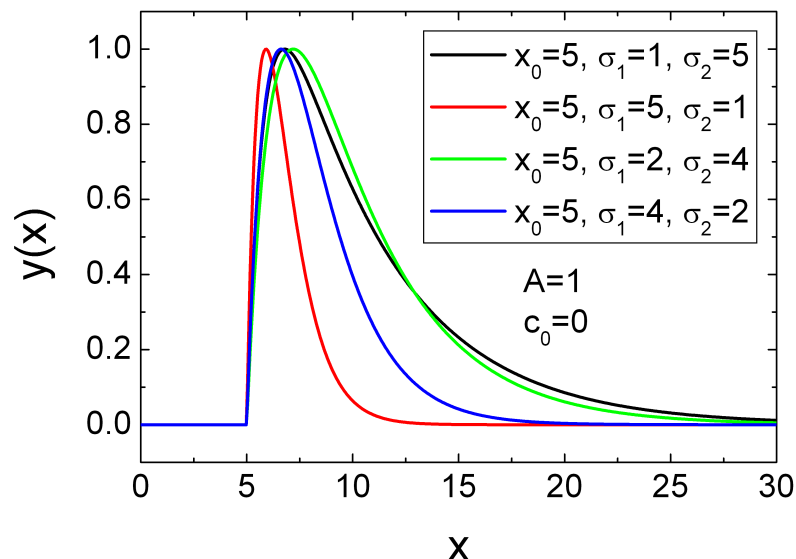


FIGURE 8.58. Plot of pulse with 2nd width (Amplitude) distribution.

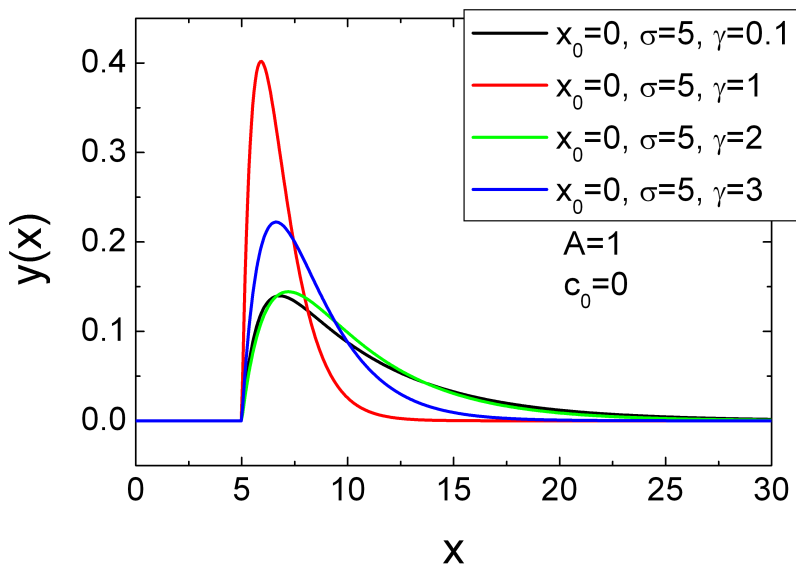
8.31.2. Pulse Peak with 2nd Width Term (Area).

FIGURE 8.59. Plot of pulse with 2nd width (Area) distribution.

8.32. Pulse Peak with Power Term

$$p(x) = \frac{\gamma + 1}{\sigma} \left(1 - \exp\left(\frac{x - x_0}{\sigma}\right)\right)^\gamma \exp\left(\frac{x - x_0}{\sigma}\right) \quad (8.108)$$

$$\text{mode} = x_0 - \sigma \ln\left(\frac{1}{\gamma + 1}\right) \quad (8.109)$$

8.32.1. Pulse Peak with Power Term (Amplitude).

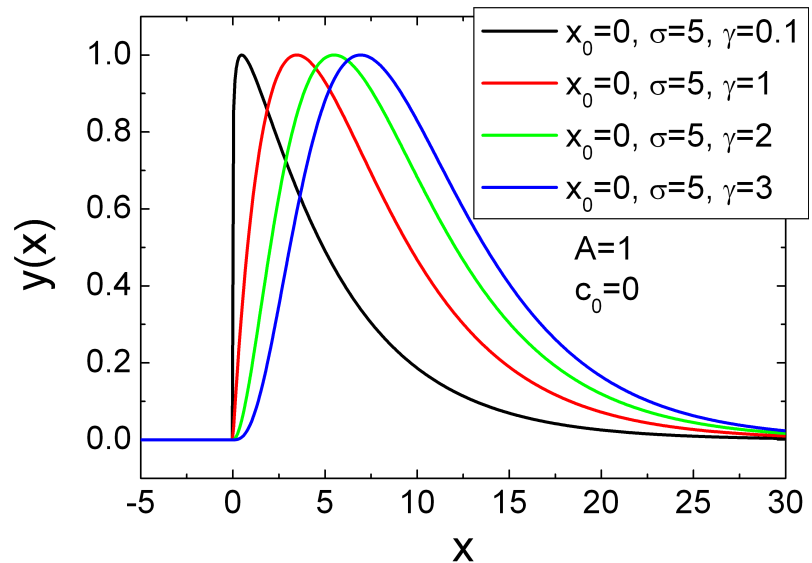


FIGURE 8.60. Plot of pulse with power term (Amplitude) distribution.

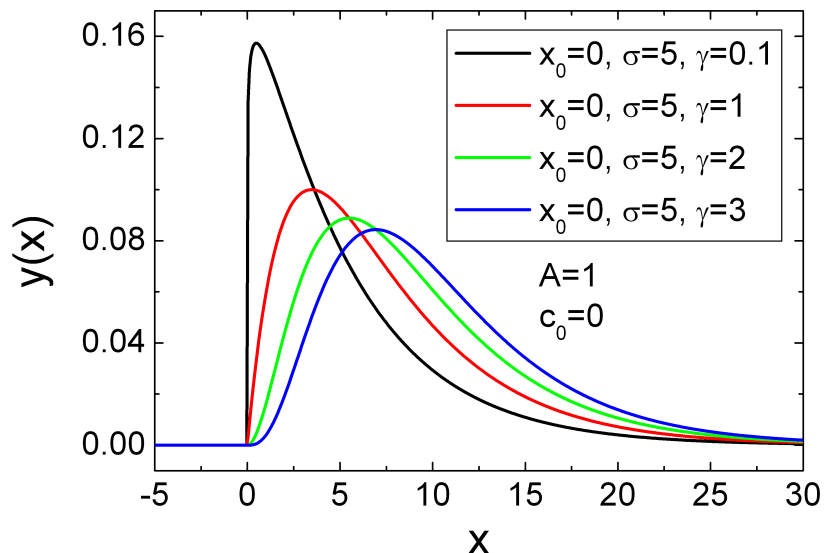
8.32.2. Pulse Peak with Power Term (Area).

FIGURE 8.61. Plot of pulse with power term (Area) distribution.

8.33. Student-t

$$p(x) = \frac{\Gamma(\frac{\nu+1}{2})}{\sqrt{\nu\pi}\Gamma(\frac{\nu}{2})} \left(1 + \frac{x^2}{\nu}\right)^{-(\frac{\nu+1}{2})} \quad (8.110)$$

8.33.1. Student-t (Amplitude).

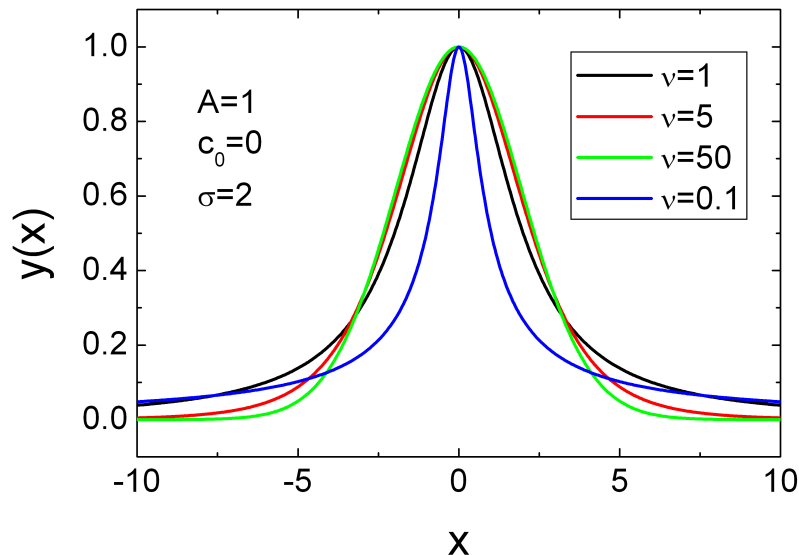


FIGURE 8.62. Plot of Student-t (Amplitude) distribution.

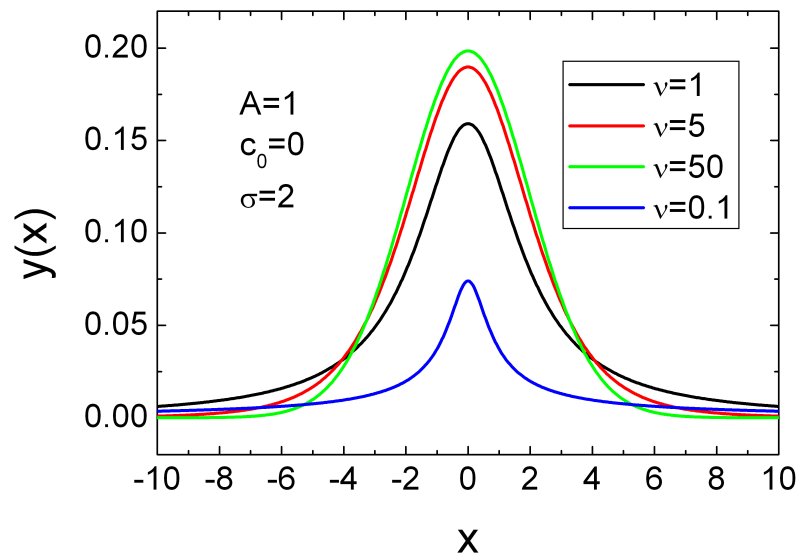
8.33.2. Student-t (Area).

FIGURE 8.63. Plot of Student-t (Area) distribution.

8.34. Trapezoidal peak

Trapezoidal distributions may be appropriate for modeling processes that can be represented by the following three stages:

- a growth stage
- a period of relative stability stage
- a decay stage

The trapezoidal model is probably the simplest model of this type (i.e., the growth and decline stages are linear and the stability stage is constant). The probability function is defined as

$$p_t(x|\alpha, \beta, \gamma, \delta) = u \begin{cases} \frac{x-\alpha}{\beta-\alpha} & \text{for } \alpha \leq x < \beta \\ 1 & \text{for } \beta \leq x < \gamma \\ \frac{\delta-x}{\delta-\gamma} & \text{for } \gamma \leq x \leq \delta \\ 0 & \text{otherwise} \end{cases} \quad (8.111)$$

$$u = \frac{2}{\gamma + \delta - \alpha - \beta} \quad (8.112)$$

α and δ are the lower and upper bound beyond which the probability is always zero. In addition, there are two sharp bending points (non-differentiable discontinuities) within the probability distribution named β and γ , so that $\alpha \leq \beta \leq \gamma \leq \delta$.

8.34.1. Trapezoidal peak (Area).

Next to the trapezoidal distribution also a symmetric variant is implemented, whereas the symmetric variant is parameterized in terms of location parameter l , width parameter for plateau σ_p and width parameter for growth and decay stage σ_e .

$$y_t(x|\alpha, \beta, \gamma, \delta, A, c_0) = Ap_t(x|\alpha, \beta, \gamma, \delta) + c_0 \quad (8.113)$$

$$y_{st}(x|l, \sigma_p, \sigma_e, A, c_0) = Ap_t\left(x|l - \frac{\sigma_p+\sigma_e}{2}, l - \frac{\sigma_p}{2}, l + \frac{\sigma_p}{2}, l + \frac{\sigma_p+\sigma_e}{2}\right) + c_0 \quad (8.114)$$

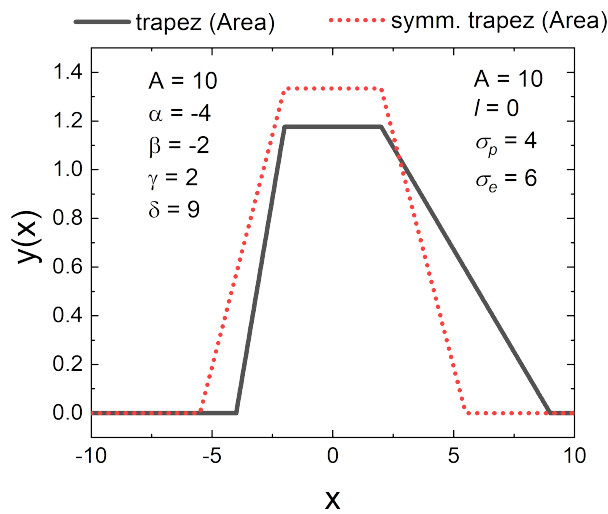


FIGURE 8.64. Plot of trapez (Area) distribution.

8.34.2. Trapezoidal peak (Ampl).

The corresponding peak function in terms of an amplitude instead of area parameter defined in the previous section is given by

$$y_t(x|\alpha, \beta, \gamma, \delta, A, c_0) = \frac{A}{u} p_t(x|\alpha, \beta, \gamma, \delta) + c_0 \quad (8.115)$$

$$y_{st}(x|l, \sigma_p, \sigma_e, A, c_0) = \frac{A}{u} p_t\left(x|l - \frac{\sigma_p + \sigma_e}{2}, l - \frac{\sigma_p}{2}, l + \frac{\sigma_p}{2}, l + \frac{\sigma_p + \sigma_e}{2}\right) + c_0 \quad (8.116)$$

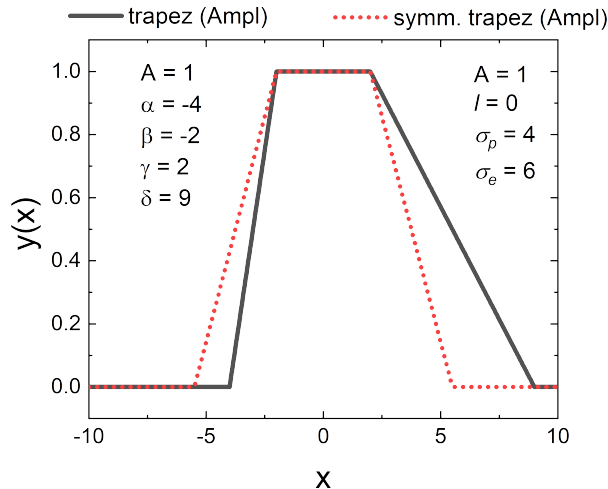


FIGURE 8.65. Plot of `trapez (Ampl)` distribution.

8.35. Generalized trapezoidal peak

The generalized trapezoidal distribution allows more flexibility in modeling in the growth, relative stability, and decay stages compared to the trapezoidal distribution. Specifically, the growth and decay stages may exhibit nonlinear convex or concave behaviour. In addition, the stability stage may be linearly increasing or decreasing. The generalized trapezoid distribution [497] has the following probability density function:

$$p_{gt}(x|\alpha, \beta, \gamma, \delta, \phi, n_1, n_3) = u \begin{cases} \phi \left(\frac{x-\alpha}{\beta-\alpha} \right)^{n_1-1} & \text{for } \alpha \leq x < \beta \\ (\phi - 1) \frac{\gamma-x}{\gamma-\beta} + 1 & \text{for } \beta \leq x < \gamma \\ \left(\frac{\delta-x}{\delta-\gamma} \right)^{n_3-1} & \text{for } \gamma \leq x \leq \delta \\ 0 & \text{otherwise} \end{cases} \quad (8.117)$$

with

$$u = \frac{2n_1n_3}{2\phi(\beta-\alpha)n_3 + (\phi+1)(\gamma-\beta)n_1n_3 + 2(\gamma-\delta)n_1} \quad (8.118)$$

The generalized trapezoidal distributions inherit the four basic trapezoidal parameters α, β, δ , and γ and need, for complete specification, two additional parameters n_1 and n_3 specifying the growth rate and decay rate in the first and third stage of the distribution, in addition to the boundary ratio parameter ϕ describing a linear increase or decrease in the plateau region.

8.35.1. Generalized trapezoidal peak (Area).

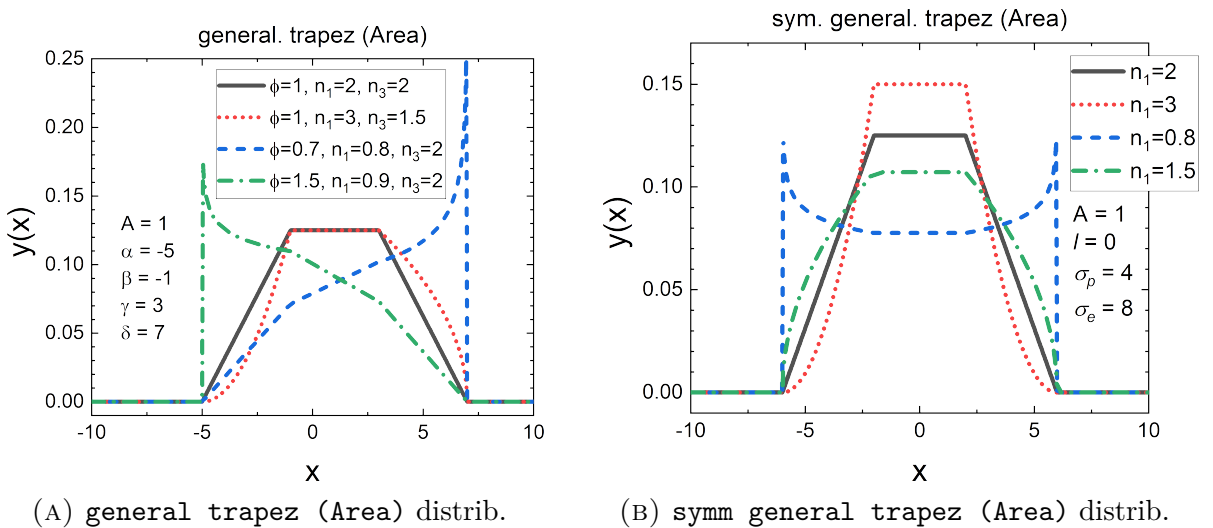


FIGURE 8.66. general trapezoidal peak

Next to the generalized trapezoidal distribution also a symmetric variant is implemented, whereas the symmetric variant is parameterized in terms of location parameter

l , width parameter for plateau σ_p and width parameter for growth and decay stage σ_e .

$$y_{\text{gt}}(x|\alpha, \dots) = A p_{\text{gt}}(x|\alpha, \dots) + c_0 \quad (8.119)$$

$$y_{\text{sgt}}(x|l, \sigma_p, \sigma_e, \dots) = A p_{\text{gt}}(x|\alpha, \beta, \gamma, \delta, 1, n_1, n_1) + c_0 \quad (8.120)$$

$$\begin{aligned} \alpha &= \frac{2l - \sigma_p - \sigma_e}{2} & \beta &= \frac{2l - \sigma_p}{2} \\ \gamma &= \frac{2l + \sigma_p}{2} & \delta &= \frac{2l + \sigma_p + \sigma_e}{2} \end{aligned} \quad (8.121)$$

8.35.2. Generalized trapezoidal peak (Ampl).

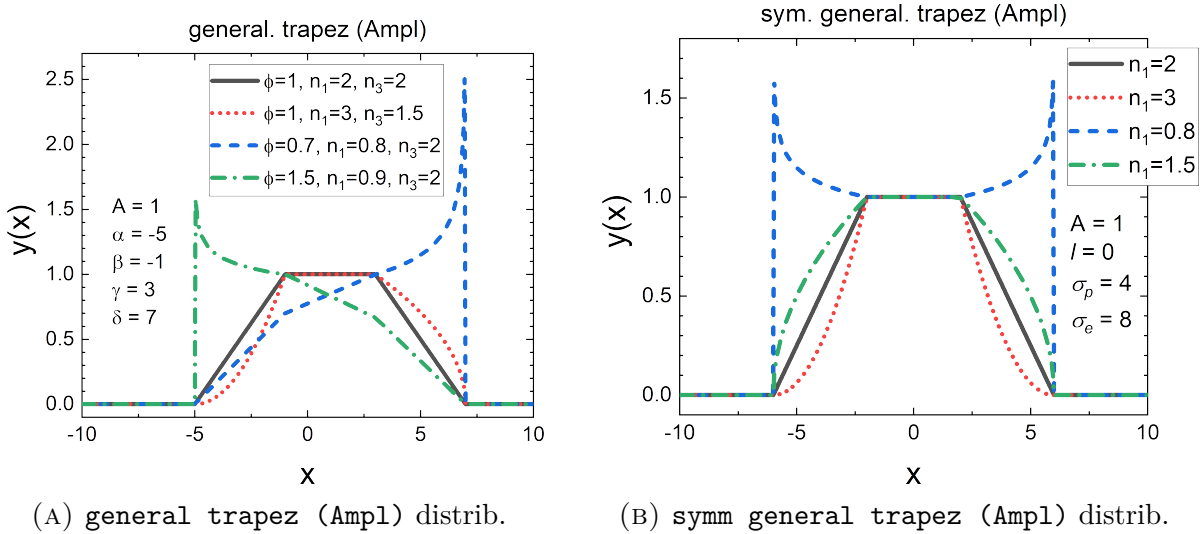


FIGURE 8.67. general trapezoidal peak

The corresponding peak function in terms of an amplitude instead of area parameter defined in the previous section is given by

$$y_{\text{gt}}(x|\alpha, \dots) = \frac{A}{\max \{\phi u, u\}} p_{\text{gt}}(x|\alpha, \dots) + c_0 \quad (8.122)$$

$$y_{\text{sgt}}(x|l, \sigma_p, \sigma_e, \dots) = \frac{A}{\max \{\phi u, u\}} p_{\text{gt}}(x|\alpha, \beta, \gamma, \delta, 1, n_1, n_1) + c_0 \quad (8.123)$$

$$\begin{aligned} \alpha &= \frac{2l - \sigma_p - \sigma_e}{2} & \beta &= \frac{2l - \sigma_p}{2} \\ \gamma &= \frac{2l + \sigma_p}{2} & \delta &= \frac{2l + \sigma_p + \sigma_e}{2} \end{aligned} \quad (8.124)$$

8.36. smoothed symmetric trapezoidal peak

This peak describes the convolution of two unit boxes of width $\Pi((x - x_0)/w_1)$ and $\Pi((x - x_0)/w_2)$, which results in a trapezoidal shape. Additional another convolution with a Gaussian function of width σ is performed for smoothing shape corners of the trapezoidal peak.

$$y_{\text{sst}}(x|w_1, \dots) = p_G(x - x_0, \sigma) * [\Pi((x - x_0)/w_1) * \Pi((x - x_0)/w_2)] + c_0 \quad (8.125)$$

$$\Pi(x) = \text{rect}(x) = \begin{cases} 0, & \text{if } |x| > \frac{1}{2} \\ \frac{1}{2}, & \text{if } |x| = \frac{1}{2} \\ 1, & \text{if } |x| < \frac{1}{2} \end{cases} \quad (8.126)$$

$$p_G(x, \sigma) = \frac{1}{\sigma\sqrt{2\pi}} \exp\left(-\frac{x^2}{2\sigma^2}\right) \quad (8.127)$$

The operator $*$ denotes the standard convolution operator in mathematics. Both convolution integrals can be solved analytically. An amplitude as well as an area normalized variants are available.

8.36.1. smoothed symmetric trapezoidal peak (Area).

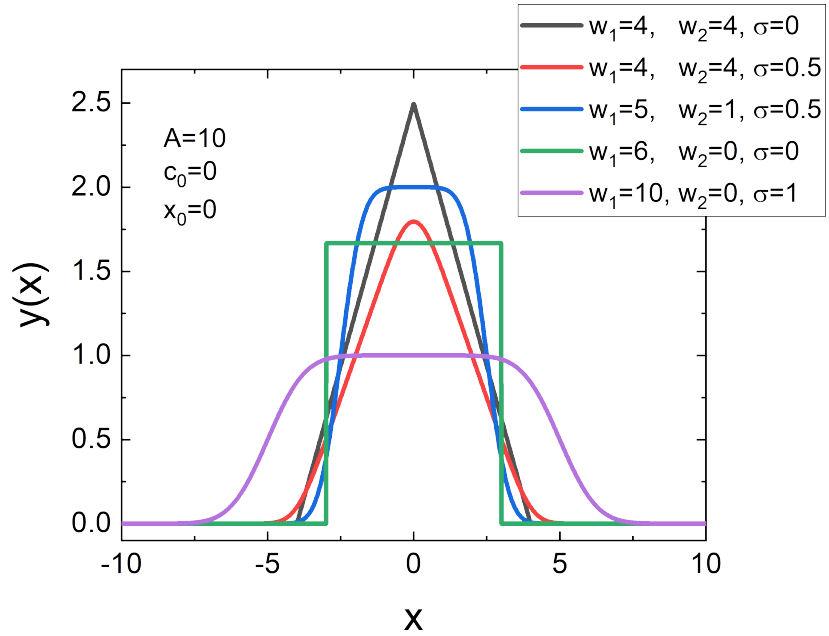


FIGURE 8.68. Plot of smoothed symm. trapez (Area) distribution.

This function contains next to the two width parameter w_1 and w_2 also a smoothing parameter σ , a location parameter x_0 as well as a scaling parameter A defining the area below the curve $y(x)$ and an offset or background parameter c_0 . The function is define over the whole domain of real numbers.

8.36.2. smoothed symmetric trapezoidal peak (Ampl).

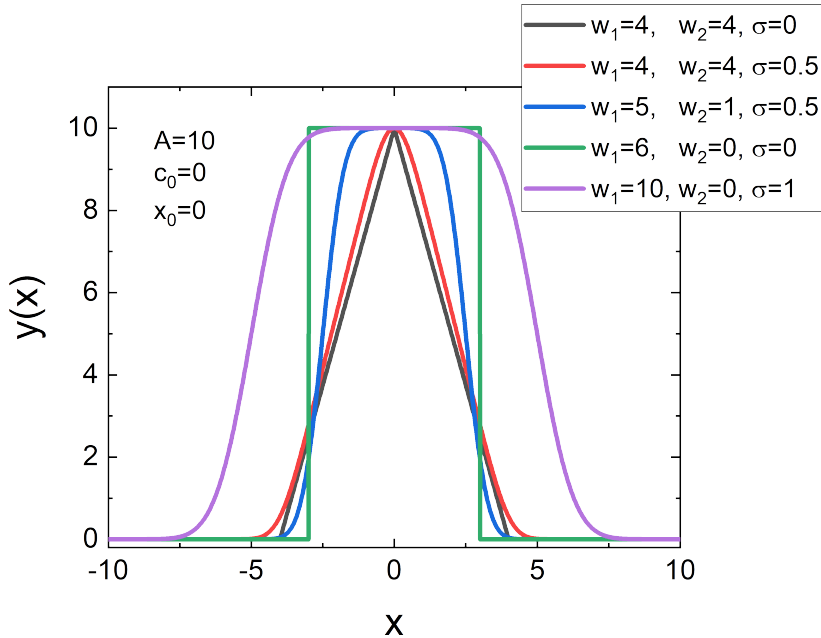


FIGURE 8.69. Plot of smoothed symm. trapez (Ampl) distribution.

This function contains next to the two width parameter w_1 and w_2 also a smoothing parameter σ , a location parameter x_0 as well as a scaling parameter A so that $y(x_0) = A + c_0$ and an offset or background parameter c_0 . The function is define over the whole domain of real numbers.

8.37. Voigt

The Voigt profile is a spectral line profile found in all branches of spectroscopy in which a spectral line is broadened by two types of mechanisms, one of which alone would produce a Gaussian profile (usually, as a result of the Doppler broadening), and the other would produce a Lorentzian profile. The Voigt profile is then a convolution of a Lorentz profile and a Gaussian profile:

$$V(x, x_c | \sigma, \gamma) = \int_{-\infty}^{\infty} D(x' | \sigma) L(x - x_c - x' | \gamma) dx' \quad (8.128a)$$

where $x - x_c$ is distance from line center x_c , $D(x | \sigma)$ is the centered Doppler profile:

$$D(x | \sigma) = \frac{e^{-x^2/2\sigma^2}}{\sigma\sqrt{2\pi}} \quad (8.128b)$$

and $L(x - x_c | \gamma)$ is the centered Lorentzian profile:

$$L(x - x_c | \gamma) = \frac{\gamma}{\pi((x - x_c)^2 + \gamma^2)}. \quad (8.128c)$$

The defining integral can be evaluated as [100, 229]:

$$V(x, x_c) = \frac{\Re[w(z)]}{\sigma\sqrt{2\pi}} \quad (8.128d)$$

where $\Re[w(z)]$ is the real part of the complex error function of z and

$$z = \frac{x - x_c + i\gamma}{\sigma\sqrt{2}} \quad (8.128e)$$

The full width at half maximum (FWHM) of the Voigt profile can be found from the widths of the associated Gaussian and Lorentzian widths. The FWHM of the Gaussian profile is $f_G = 2\sigma\sqrt{2\ln(2)}$. The FWHM of the Lorentzian profile is just $f_L = 2\gamma$. Define $\phi = f_L/f_G$. Then the FWHM of the Voigt profile (f_V) can be estimated as:

$$f_V \approx f_G \left(1 - c_0 c_1 + \sqrt{\phi^2 + 2c_1\phi + c_0^2 c_1^2} \right) \quad (8.129)$$

where $c_0 = 2.0056$ and $c_1 = 1.0593$. This estimate will have a standard deviation of error of about 2.4 percent for values of ϕ between 0 and 10. Note that the above equation will have the proper behavior in the limit of $\phi = 0$ and $\phi = \infty$. A different approximation was given by [363, 313]

$$f_V \approx 0.5346 f_L + \sqrt{0.2166 f_L^2 + f_G^2} \quad (8.130)$$

with an accuracy of 0.02

8.37.1. Voigt (Amplitude).

The amplitude version of the Voigt peak is parameterized as

$$V_{\text{Amplitude}}(x|A, \sigma, \gamma) = A \frac{\int_{-\infty}^{\infty} \frac{\exp(-u^2)}{\frac{\gamma^2}{2\sigma^2} + \left(\frac{x-x_c}{\sqrt{2}\sigma} - u\right)^2} du}{\int_{-\infty}^{\infty} \frac{\exp(-u^2)}{\frac{\gamma^2}{2\sigma^2} + u^2} du} = A \frac{V(x, x_c|\sigma, \gamma)}{V(x_c, x_c|\sigma, \gamma)} \quad (8.131)$$

Required parameters:

ampl.: amplitude A of the Voigt peak

center: location parameter (mode) x_c

sigma: width of Doppler (Gaussian) contribution $\sigma > 0$

gamma: width of Lorentzian contribution $\gamma > 0$

backgr: offset c_0

Note

- The Doppler (Gaussian) width parameter needs to be larger than 0 $\sigma > 0$.
- The Lorentzian width parameter needs to be larger than 0 $\gamma > 0$.
- Default (Size) distribution: Monodisperse

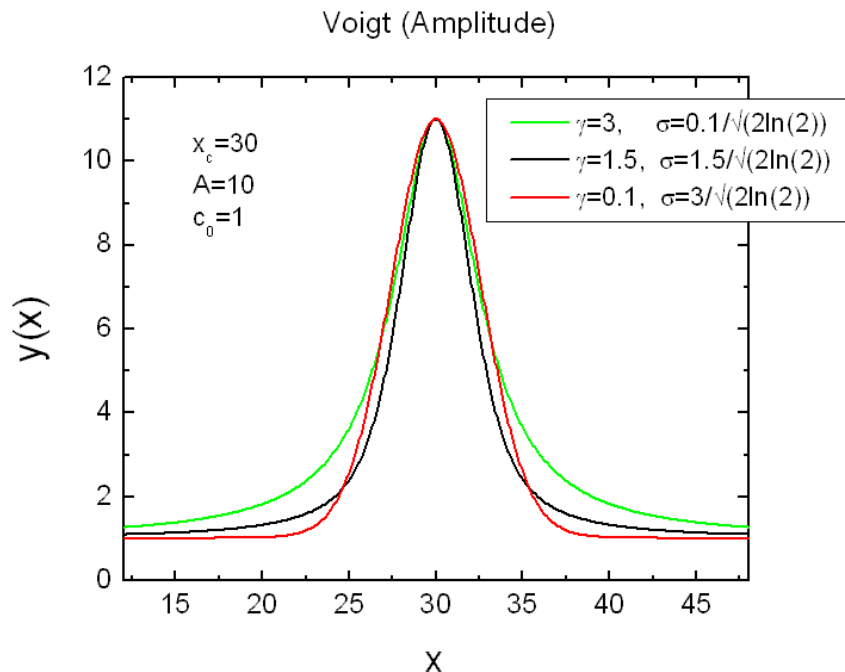


FIGURE 8.70. Plot of Voigt (Amplitude) distribution.

8.37.2. Voigt (Area).

The area version of the Voigt peak is parameterized as

$$V_{\text{Area}}(x|A, \sigma, \gamma) = A \frac{\gamma}{2\pi\sqrt{\pi}\sigma^2} \int_{-\infty}^{\infty} \frac{\exp(-u^2)}{\frac{\gamma^2}{2\sigma^2} + \left(\frac{x-x_c}{\sqrt{2}\sigma} - u\right)^2} du = A V(x, x_c|\sigma, \gamma) \quad (8.132)$$

Required parameters:

area: area A of the Voigt peak

center: location parameter (mode) x_c

sigma: width of Doppler (Gaussian) contribution $\sigma > 0$

gamma: width of Lorentzian contribution $\gamma > 0$

backgr: offset c_0

Note

- The Doppler (Gaussian) width parameter needs to be larger than 0 $\sigma > 0$.
- The Lorentzian width parameter needs to be larger than 0 $\gamma > 0$.
- Default (Size) distribution: Monodisperse

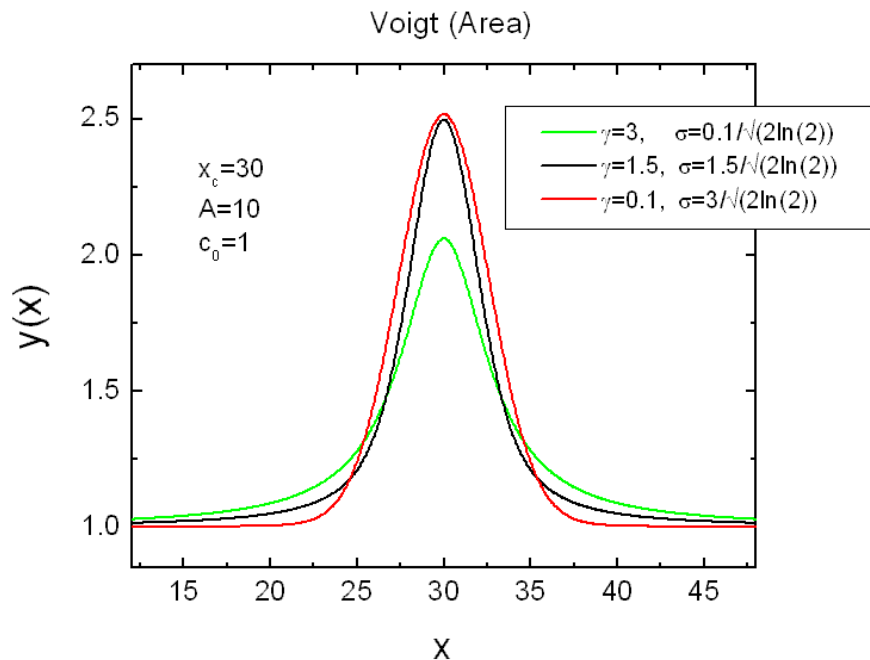


FIGURE 8.71. Plot of Voigt (Area) distribution.

8.37.3. Weibull.

The Weibull distribution is a continuous probability distribution. It is named after Waloddi Weibull who described it in detail in 1951, although it was first identified by Fréchet (1927) and first applied by Rosin & Rammler (1933) to describe the size distribution of particles. The probability density function of a Weibull random variable x is:

$$p(x; \lambda, k) = \begin{cases} \frac{k}{\lambda} \left(\frac{x}{\lambda}\right)^{k-1} e^{-(x/\lambda)^k} & x \geq 0 \\ 0 & x < 0 \end{cases} \quad (8.133)$$

where $k > 0$ is the shape parameter and $\lambda > 0$ is the scale parameter of the distribution. For $k > 1$ the mode is given by

$$\text{mode} = \lambda \left(\frac{k-1}{k} \right)^{\frac{1}{k}} \text{ if } k > 1. \quad (8.134)$$

8.37.4. Weibull (Amplitude).

The amplitude version represents a reparametrization of the standard statistical form. The parameter x_0 has been added to enable variable x positioning. An additional adjustment term has been added so that x_0 represents the mode. The function returns c_0 for those x where it is undefined.

$$\begin{aligned} u &= \frac{k-1}{k} \\ z &= \frac{x - x_0}{\lambda} + u^{1/k} \\ y(x; x_0, k, \lambda, c_0, A) &= \begin{cases} c_0 + Au^{-u}z^{k-1} \exp(-z^k) & z \geq 0 \\ c_0 & z < 0 \end{cases} \end{aligned} \quad (8.135)$$

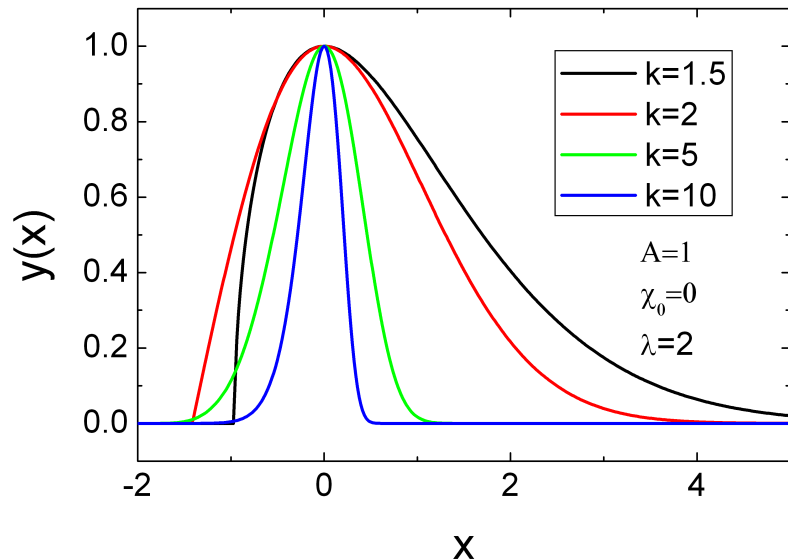


FIGURE 8.72. Plot of Weibull (Amplitude) distribution.

8.37.5. Weibull (Area).

The area version represents a reparametrization of the standard statistical form. The parameter x_0 has been added to enable variable x positioning. An additional adjustment term has been added so that x_0 represents the mode. The function returns c_0 for those x where it is undefined.

$$z = \frac{x - x_0}{\lambda} + \left(\frac{k - 1}{k} \right)^{1/k}$$

$$y(x; x_0, k, \lambda, c_0, A) = \begin{cases} c_0 + A \frac{k}{\lambda} z^{k-1} \exp(-z^k) & z \geq 0 \\ c_0 & z < 0 \end{cases} \quad (8.136)$$

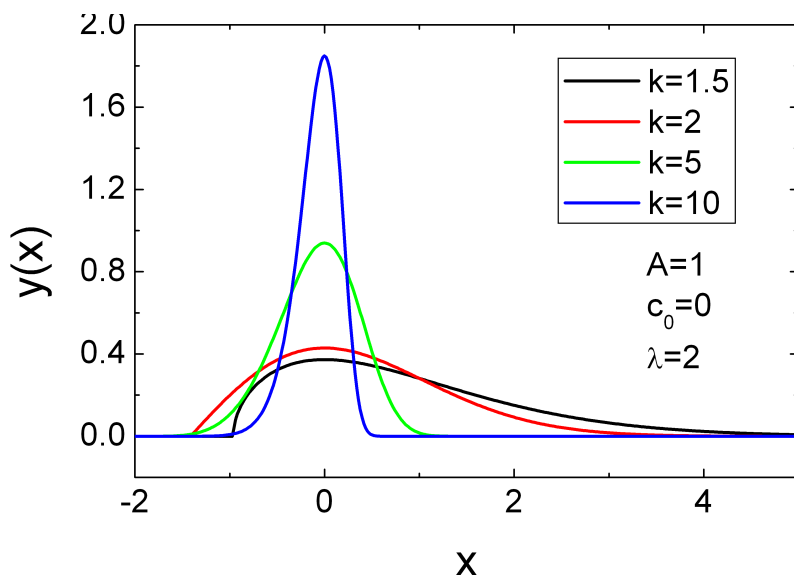


FIGURE 8.73. Plot of Weibull (Area) distribution.

CHAPTER 9

Plugin functions for form factors

9.1. Non spherical-symmetric randomly oriented particles

9.1.1. Rectangular parallelepiped.

In a rectangular parallelepiped, all angles are right angles, and opposite faces of a parallelepiped are equal. Also the terms rectangular cuboid or orthogonal parallelepiped are used to designate this polyhedron. Four variants of rectangular parallelepipeds have been implemented, where either none, one, two, or all three axis have a common size distribution. The scattering intensity of a monodisperse randomly oriented rectangular

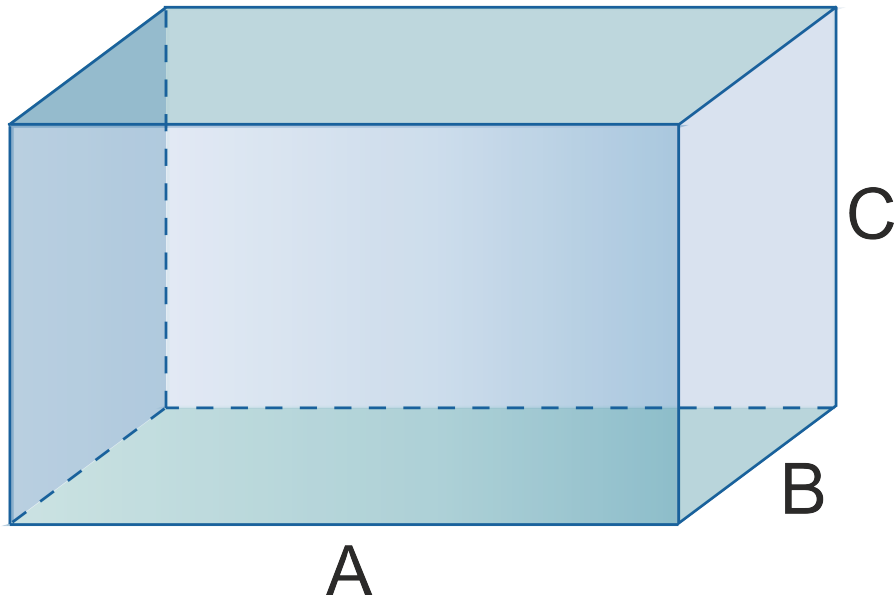


FIGURE 9.1. Rectangular parallelepiped with edge lengths A , B , and C .

parallelepiped with the edge lengths A , B , C , and a scattering length density contrast $\Delta\eta$ is given by

$$I_{\text{rPE}}(Q, A, B, C, \Delta\eta) = \int_0^{\pi} \int_0^{\pi/2} \frac{2}{\pi} \left[\text{sinc}\left(\frac{QA}{2} \sin(\alpha) \cos(\varphi)\right) \right. \\ \left. \text{sinc}\left(\frac{QB}{2} \sin(\alpha) \sin(\varphi)\right) \right. \\ \left. \text{sinc}\left(\frac{QC}{2} \cos(\alpha)\right) ABC \Delta\eta \right]^2 \sin(\alpha) d\alpha d\varphi \quad (9.1)$$

An additional size distribution is implemented in several ways either linearly, quadratically or cubically, depending if one two or all three axis scale with a single size distribution

$$I_{rPE,1}(Q, \sigma, a, b, c, \Delta\eta) = \int_0^{\infty} \text{LogNorm}(\nu, \sigma) I_{rPE}(Q, \nu a, b, c, \Delta\eta) d\nu \quad (9.2)$$

$$I_{rPE,2}(Q, \sigma, a, b, c, \Delta\eta) = \int_0^{\infty} \text{LogNorm}(\nu, \sigma) I_{rPE}(Q, \nu a, \nu b, c, \Delta\eta) d\nu \quad (9.3)$$

$$I_{rPE,3}(Q, \sigma, a, b, c, \Delta\eta) = \int_0^{\infty} \text{LogNorm}(\nu, \sigma) I_{rPE}(Q, \nu a, \nu b, \nu c, \Delta\eta) d\nu \quad (9.4)$$

with

$$\text{LogNorm}(\nu, \sigma) = \frac{1}{\sqrt{2\pi}\sigma} \exp\left(-\frac{\ln^2(\nu)}{2\sigma^2}\right) \quad (9.5)$$

Input Parameters for model Parallelepiped_abc:

A: width A

B: depth B

C: hight C

dummy: not used

eta: scattering length density contrast $\Delta\eta$

Input Parameters for models Parallelepiped_abcl, Parallelepiped_abc2, and Parallelepiped_abc3:

A: width A

B: depth B

C: hight C

sigma: width parameter σ assuming a LogNorm-distribution

eta: scattering length density contrast $\Delta\eta$

Note:

- The form factor is needs especially for large q -values quite some computational resources. In case of a parallelepiped with edge length differing a lot in size faster approximations are available 9.1.2 which make use of approximations used for thin or flat objects like in 9.2.
- The integration routine for orientational average can be configured via the GUI interface. The orientational averaging is typically the time consuming task and a test of the different integration algorithms for orientational averaging might differ significantly in computational time.
- One version is assuming a monodisperse size distribution and the other three already have included a lognormal distribution either for one edge length, or simultaneous size distribution for either two or three edge lengths.

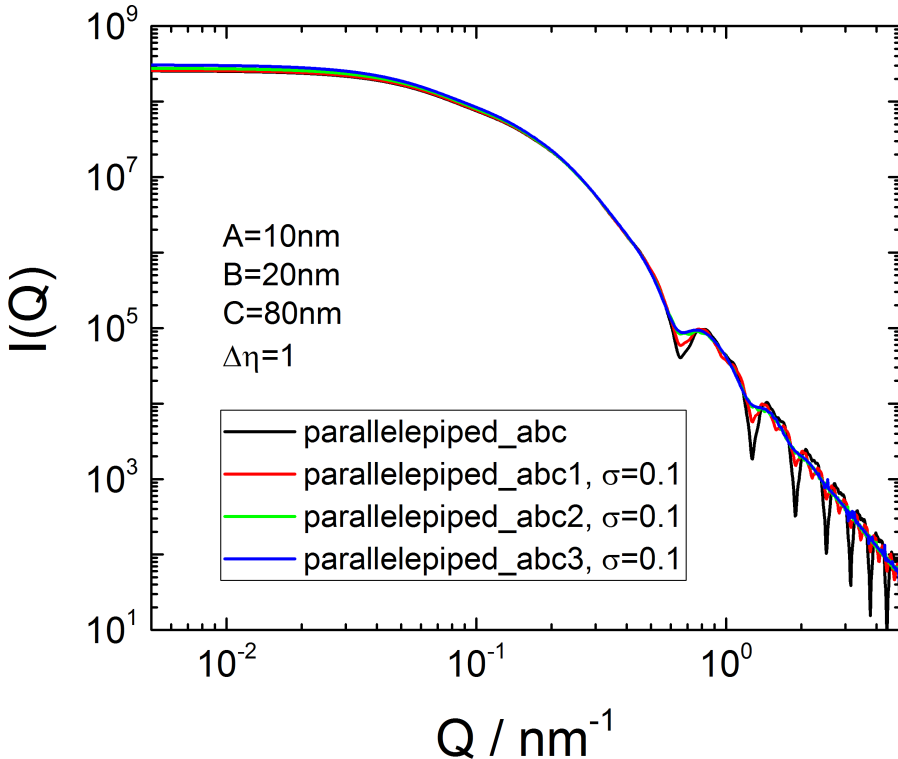


FIGURE 9.2. Scattering curves for parallelepiped with optional size distribution a single edge length (parallelepiped_abc1), of a surface area (parallelepiped_abc2), or volume parallelepiped_abc3.

9.1.2. Ribbon.

A ribbon is called here a long and thin parallelepiped, where the parallelepiped is parametrized like in section 9.1.1. However, now the three edge lengths (A , B , C) differ a lot in length. In such a case the form factor can be factorized like for thin or flat objects as discussed in 9.2. The form factor of this plugin has been taken from [468] for a long straight ribbon with edge length $C \gg B \gg A$.

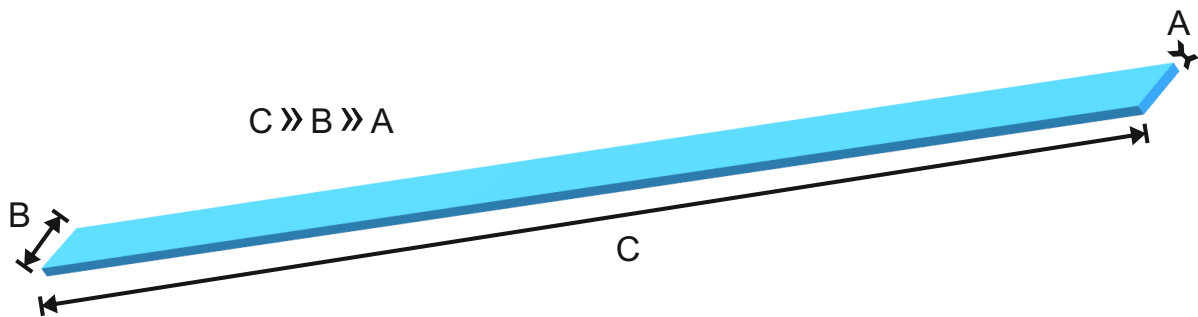


FIGURE 9.3. Long and thin ribbon with edge lengths $C \gg B \gg A$.

The form factor of a straight long and thin ribbon reads as

$$I_{\text{ribbon}}(q) = P'(q, C) \frac{(\Delta\eta AB)^2}{2} \left[\frac{\sin(qA/2)}{qA/2} \right]^2 {}_1F_2 \left(\frac{1}{2}; \frac{3}{2}, 2; -q^2 B^2/4 \right) \quad (9.6)$$

$$P'(q, C) = C^2 \left(2 \frac{\text{Si}(qC)}{qC} - \frac{\sin^2(qC/2)}{(qC/2)^2} \right) \quad (9.7)$$

where ${}_1F_2$ is a hypergeometric function and Si the sinus integral. $P'(q, C)$ is the form factor of an infinitesimal thin rod 9.47. Instead of the function for the thin rod one also could use the one of a wormlike structure 9.2.4.3, if the q -range is sufficient and the ribbon is bended like a wormlike structure. Due to the approximate factorization [468] the shape of the cross-section changes slightly from a regular rectangle of thickness A and width B to a rectangle with its two ends rounded.

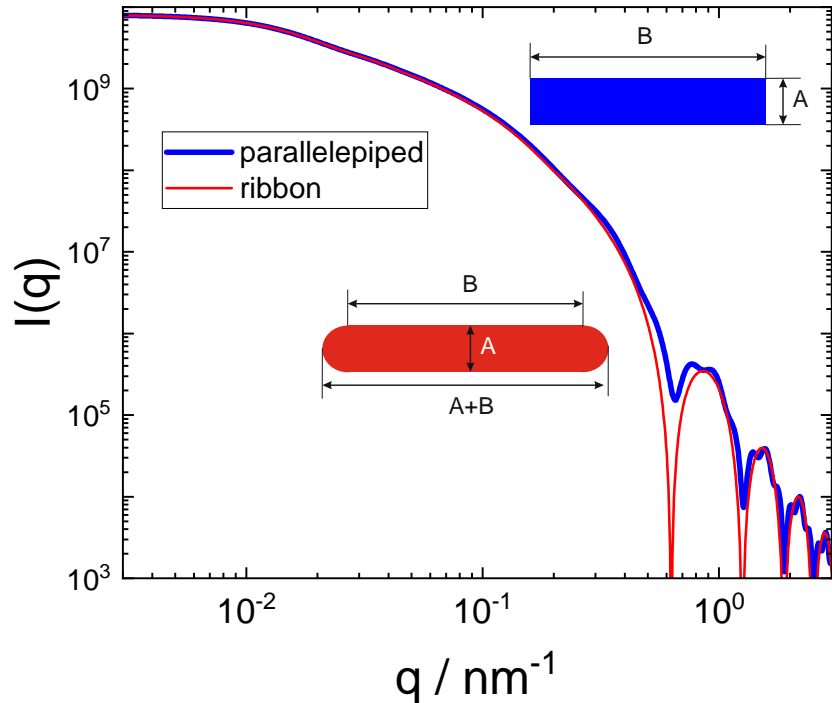


FIGURE 9.4. Comparison of scattering curves from a ribbon (red) and a parallelepiped (blue) with edge lengths ($A = 10\text{nm}$, $B = 30\text{nm}$, $C = 300\text{nm}$)

As the form factor can be factorized due to its three dimensions which differ a lot in lengths, size distributions can be easily implemented. Assuming a gamma distribution

for the two smaller dimensions the integration can be even performed analytically.

$$I_{\text{ribbonSD}}(q) = P'(q, C) \frac{\Delta\eta^2}{2} \int_0^\infty p_\Gamma(A; A_0, \sigma_A) A^2 \left[\frac{\sin(qA/2)}{qA/2} \right]^2 dA \times \\ \int_0^\infty p_\Gamma(B; B_0, \sigma_B) B^2 {}_1F_2 \left(\frac{1}{2}, \frac{3}{2}, 2; -q^2 B^2/4 \right) dB \quad (9.8)$$

$$= \Delta\eta^2 P'(q, C) \frac{2}{q^2} \left\{ 1 - \Re \left[\left(1 + \frac{i q \sigma_A^2}{A_0} \right)^{(A_0/\sigma_A)^2} \right] \right\} \times \\ (B_0^2 + \sigma_B^2) {}_3F_2 \left(\frac{1}{2}, 1 + \frac{B_0^2}{2\sigma_B^2}, \frac{3}{2} + \frac{B_0^2}{2\sigma_B^2}; \frac{3}{2}, 2; -q^2 \sigma_B^4 / B_0^2 \right) \quad (9.9)$$

$$p_\Gamma(x; x_0, \sigma) = \frac{\exp(-x_0 x / \sigma^2) (x_0 x / \sigma^2)^{x_0^2 / \sigma^2}}{x \Gamma(x_0^2 / \sigma^2)} \quad (9.10)$$

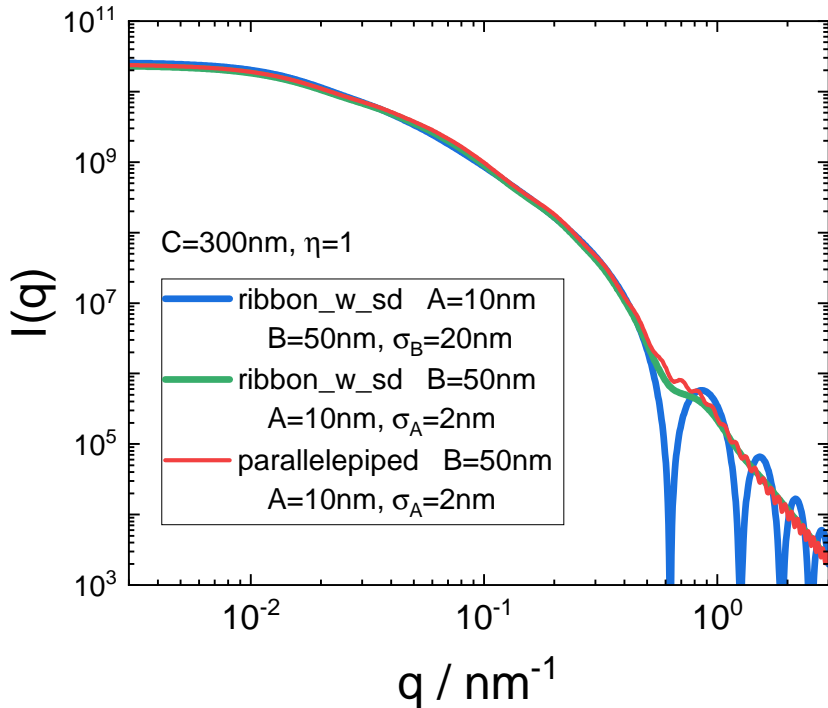


FIGURE 9.5. Comparison of scattering curves from a ribbon (red) with a size distribution in B and A (green) as well as a parallelepiped (blue) with size distribution in A .

Input Parameters for model `ribbon_mono`:

A: thickness A

dummy: not used

B: depth B

dummy: not used

C: length C

dummy: not used

eta: scattering length density contrast $\Delta\eta$

Input Parameters for models **ribbon_w_sd**:

A: thickness A_0

sigma_A: width parameter of gamma size distribution σ_A

B: depth B_0

sigma_B: width parameter of gamma size distribution σ_B

C: length C

dummy: not used

eta: scattering length density contrast $\Delta\eta$

Note:

- The polydisperse version still shows some numerical instabilities for very narrow and very broad distributions for with large σ_B/B_0 as well as very small q -values

9.2. Very thin particles (local planar & local cylindrical objects)

For very thin random orientated particles the form factor can be factorize according to Porod [393] in a cross section term $P_{\text{cs}}(Q)$ for the shorter or thin dimension and a shape factor $P'(Q)$ for the long dimension.

$$I(Q) = P'(Q)P_{\text{cs}}(Q). \quad (9.11)$$

In this plugin the form factors of two types of thin particles are collected, those with a local cylindrical and with a local planar geometry. In case of local planar objects the cross section term $P_{\text{cs}}(Q)$ can be homogeneous, a centro-symmetric bilayer, a gaussian bilayer, etc. . This cross section factor can than be combined with the overall shape factor $P'(Q)$ of for examples a thin spherical shell of elliptical shell, a thin cylindrical shell or a thin disc. As the total form factor is the product of the cross-section form factor and a shape form factor one can either programm all combination of cross-section and shape factors into individual form factor functions or one can programm the cross-section factors as form factor and the shape factor as a structure factors. Using the monodisperse approximation yields than the same result.

In this plugin the product of the cross-section and shape term have been implemented as form factor under "[by plugin|thin obj.|local planar obj.]" and "[by plugin|thin obj.|local cylindrical obj.]". The cross-section terms alone are also implemented as form factors under "[by plugin|thin obj.|Pcs(Q) for planar obj.]" and "[by plugin|thin obj.|Pcs(Q) for cylindrical obj.]". The shape factors are also available as structure factors under "[by plugin|thin obj.|P'(Q): local planar obj.]" and "[by plugin|thin obj.|P'(Q): local cylindrical obj.]".

The cross-section form factors can be easily calculated if the scattering length density contrast profile $\Delta\eta_{\text{cs}}(r)$ is known. For structures with a local planar geometry and a symmetric cross-section the form factor is given by

$$P_{\text{cs}}^{\text{planar}}(Q) = \left[2 \int_0^{\infty} \Delta\eta_{\text{cs}}(r) \cos(Qr) dr \right]^2 \quad (9.12)$$

In case of local cylindrical particles with a centro-symmetric scattering length density distribution the form factor is given by

$$P_{\text{cs}}^{\text{cylindrical}}(Q) = \left[2\pi \int_0^{\infty} \Delta\eta_{\text{cs}}(r) J_0(Qr) r dr \right]^2 \quad (9.13)$$

9.2.1. $P_{cs}(Q)$ for planar obj.

The cross-section form factors with local planar geometry are valid when the cross-section dimension is much smaller than the radius of curvature of the locally planar structure.

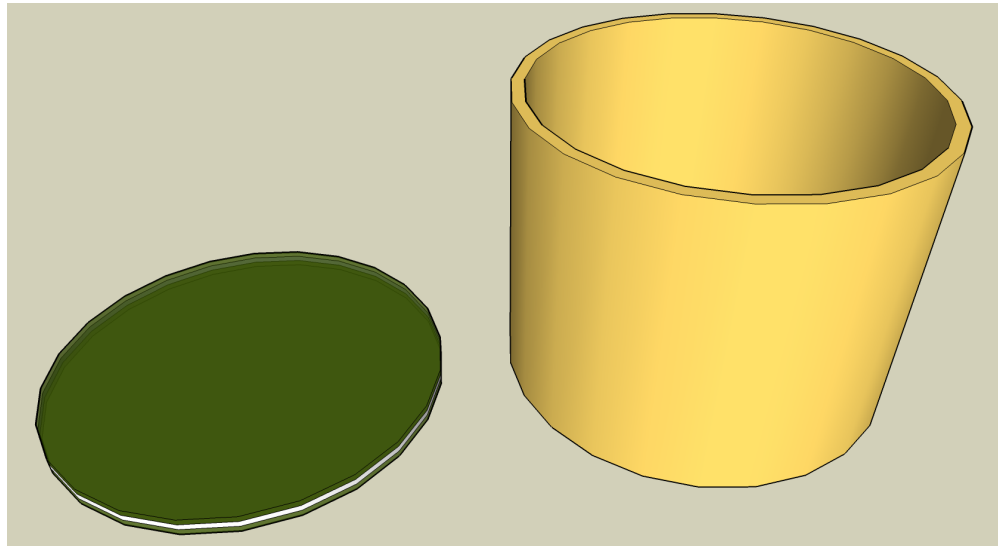


FIGURE 9.6. for local planar particles the cross section dimension is much smaller than the radius of curvature of the particle

Several cross-section profiles for local planar objects have been implemented, like a homogeneous cross-section, cross-section with two infinitely thin plates, layered centrosymmetric cross-section, bilayer with a Gaussian scattering length density profile, layer with Gaussian chains attached to the surface. These form factors are supposed to be combined with a shape factor for local planar objects which are implemented as structure plugins under "[by plugin|thin obj.| $P'(Q)$: local planar obj.]".

9.2.1.1. $P_{cs}(Q)$ for a homogeneous cross-section.

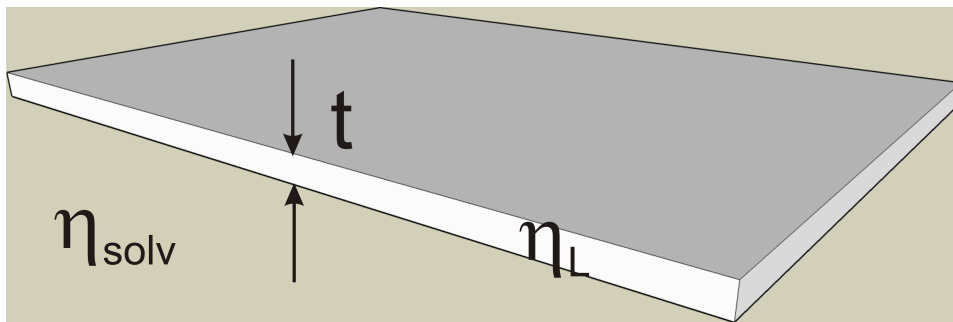


FIGURE 9.7. Plane with a homogeneous cross-section of thickness t .

This cross-section form factor describes the scattering of a layer with homogeneous scattering length density η_L in a matrix of a scattering length density η_{solv} . The thickness can have a distribution described by a log-normal distribution according to eq. 7.12b.

$$P_{cs}(Q, \sigma_t, t) = \int_0^{\infty} \text{LogNorm}(x, 1, \sigma_t, 1, t) \left[(\eta_L - \eta_{\text{solv}}) x \frac{\sin(Qx/2)}{Qx/2} \right]^2 dx \quad (9.14)$$

Input parameters for Pcs:homogeneousPlate:

t: most probable layer thickness t
sigm_t: width σ_t of thickness distribution (LogNorm)
dummy: unused disabled parameter
dummy: unused disabled parameter
eta_l: scattering length density of layer η_L
eta_solv: scattering length density of solvent η_{solv}

Note

- This form factor is supposed to be combined with a shape factor for local planar objects which are implemented as structure plugins under "[by plugin|thin obj.|P'(Q): local planar obj.]".
- As the form factor already have the width distribution included one normally uses in SASfit as a size distribution the Delta-distribution.

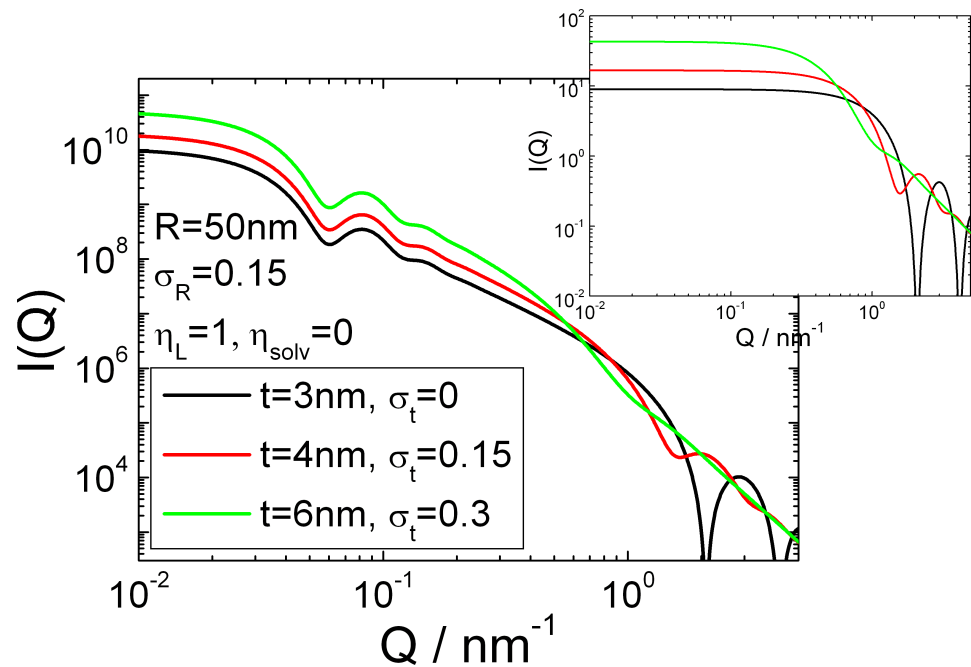


FIGURE 9.8. Scattering curve for the form factor "Pcs:homogeneousPlate" only (insert) and in combination with a structure factor "P'(Q): Thin Spherical Shell".

9.2.1.2. $P_{cs}(Q)$ for two infinitely thin parallel layers.

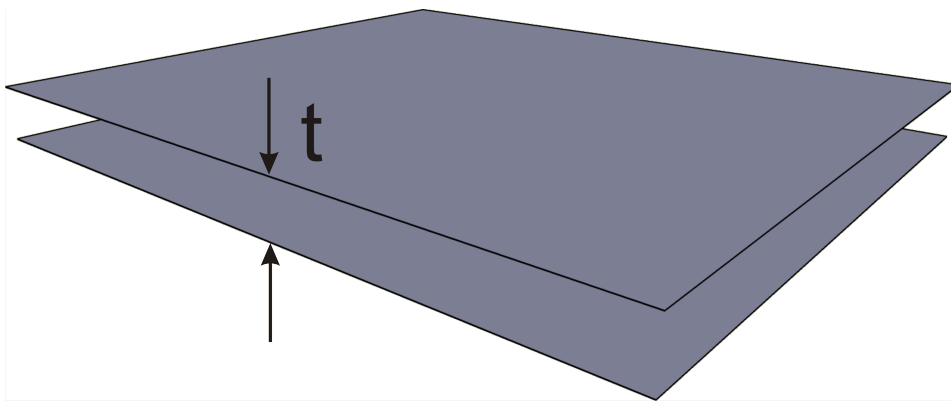


FIGURE 9.9. Two infinitely thin parallel layers separated by a distance t .

This cross-section form factor describes the scattering of two infinitely thin parallel layers. The separation distance can have a distribution described by a log-normal distribution according to eq. 7.12b.

$$P_{cs}(Q, \sigma_t, t) = \int_0^{\infty} \text{LogNorm}(x, 1, \sigma_t, 1, t) \cos^2(Qx/2) dx \quad (9.15)$$

Input parameters for `Pcs:TwoInfinitelyThinLayers`:

t: most probable layer separation t

sigm_t: width σ_t of separation distribution (LogNorm)

Note

- This form factor is supposed to be combined with a shape factor for local planar objects which are implemented as structure plugins under "[by plugin|thin obj.|P'(Q): local planar obj.]".
- As the form factor already have the width distribution included one normally uses in SASfit as a size distribution the Delta-distribution.

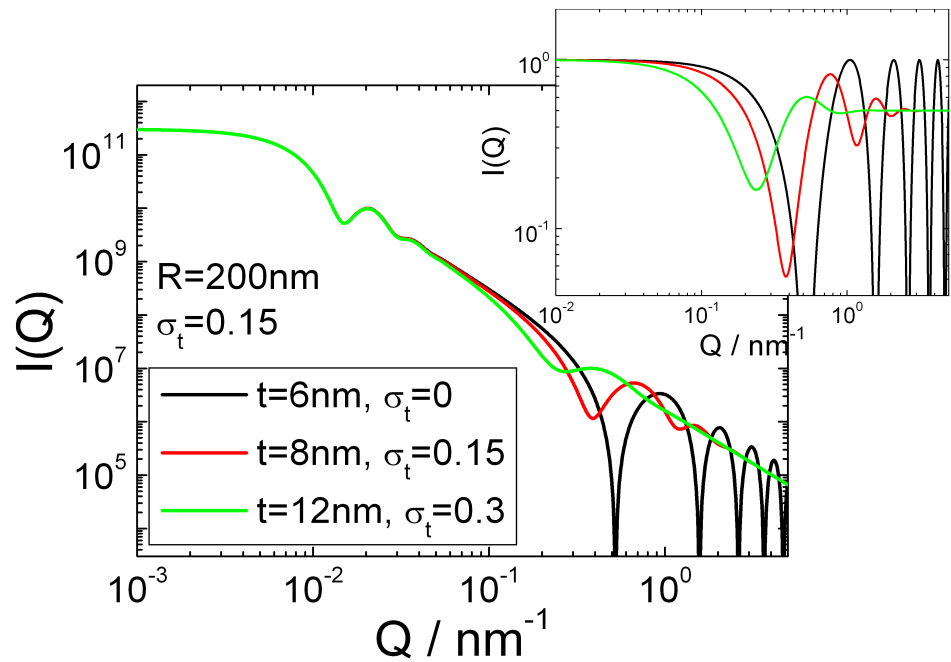


FIGURE 9.10. Scattering curve for the form factor "Pcs:TwoInfinitelyThinLayers" only (insert) and in combination with a structure factor "P'(Q): Thin Spherical Shell".

9.2.1.3. $P_{cs}(Q)$ for a layered centro symmetric cross-section structure.

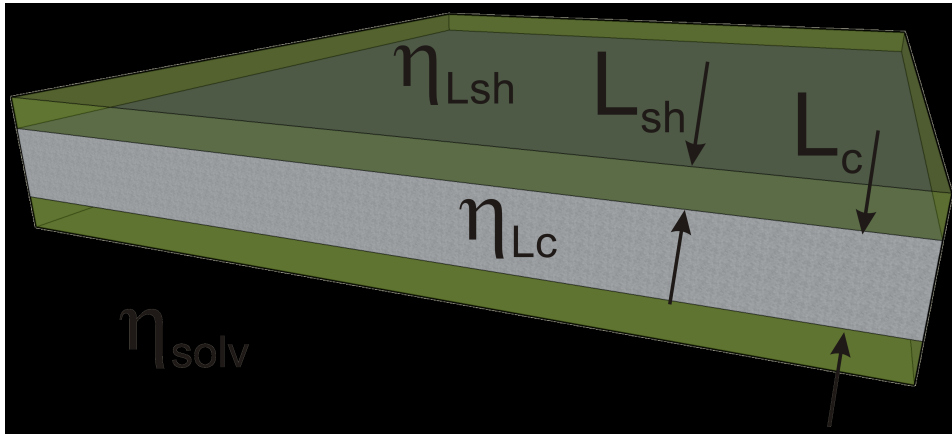


FIGURE 9.11. Two layered centro symmetric structure with a core thickness of L_c and an outer layer thickness L_{sh} . The corresponding scattering length densities of the core, the shell layer and the solvent are η_{L_c} , $\eta_{L_{sh}}$, and $\eta_{L_{solv}}$.

This cross-section form factor describes the scattering of a layered centro symmetric cross-section structure. Both the core thickness as well as the shell thickness can have a distribution described by a log-normal distribution as defined in eq. 7.12b.

$$\begin{aligned}
 P_{cs}(Q, \sigma_{L_c}, L_c, \sigma_{L_{sh}}, L_{sh}, \eta_{L_c}, \eta_{L_{sh}}, \eta_{solv}) = \\
 \int_0^{\infty} \text{LogNorm}(v, 1, \sigma_{L_c}, 1, L_c) \int_0^{\infty} \text{LogNorm}(u, 1, \sigma_{L_{sh}}, 1, L_{sh}) \\
 \left[\frac{(\eta_{L_{sh}} - \eta_{solv})(v + 2u) \sin(Q \frac{v+2u}{2})}{Q \frac{v+2u}{2}} - \frac{(\eta_{L_{sh}} - \eta_{L_c})v \sin(Q \frac{v}{2})}{Q \frac{v}{2}} \right]^2 du dv \quad (9.16)
 \end{aligned}$$

Input parameters for `Pcs:LayeredCentroSymmetricXS`:

L_c: most probable layer separation L_c

sigm_Lc: width σ_{L_c} of core thickness distribution (LogNorm)

L_sh: most probable shell thickness L_{sh}

sigm_Lsh: width $\sigma_{L_{sh}}$ of shell thickness distribution (LogNorm)

eta_Lc: scattering length density of core layer η_{L_c}

eta_Lsh: scattering length density of shell layer $\eta_{L_{sh}}$

eta_solv: scattering length density of solvent η_{solv}

Note

- This form factor is supposed to be combined with a shape factor for local planar objects which are implemented as structure plugins under "[by plugin|thin obj.|P'(Q): local planar obj.]".

- As the form factor already have the width distribution included one normally uses in SASfit as a size distribution the Delta-distribution.

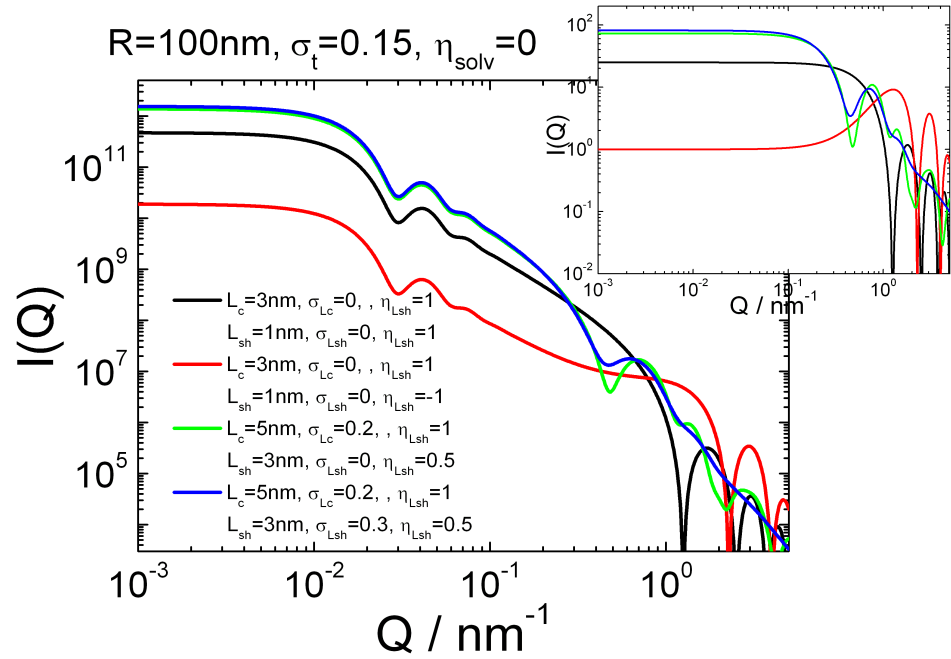


FIGURE 9.12. Scattering curve for the form factor "Pcs:LayeredCentroSymmetricXS" only (insert) and in combination with a structure factor "P'(Q): Thin Spherical Shell".

9.2.1.4. $P_{cs}(Q)$ for a bilayer with a Gaussian electron density profile.

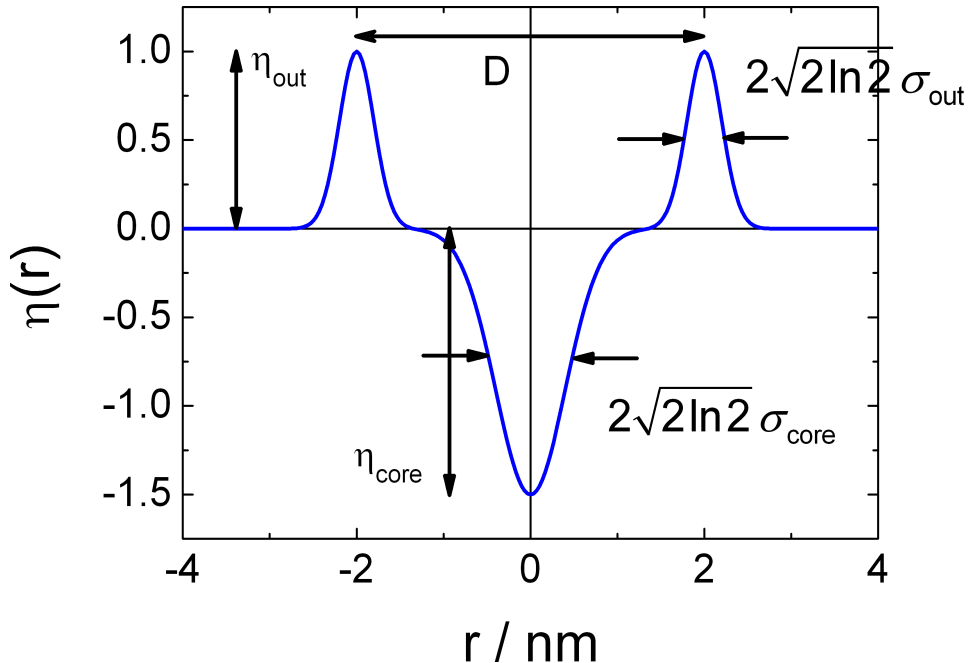


FIGURE 9.13. The plot shows a model for the Gaussian description of the bilayer electron density profile according to eq. 9.17. The origin of the profile is set to the bilayer centre. The model encountering a single Gaussian for the head group at $\pm t/2$. η_{out} is the amplitude of the head-group Gaussian and η_{core} that of the hydrocarbon chains with respect to the average electron density of water. The FWHM of the Gaussian profiles are $2\sqrt{2 \ln 2} \sigma_{\text{out}}$ and $2\sqrt{2 \ln 2} \sigma_{\text{core}}$.

This model for a bilayer is using a real-space representation of the electron density profile using a Gaussian description [371, 370]. In comparison to other models it is simpler and requiring the adjustment of only four parameters. The electron density profile (Fig. 9.13) is described by

$$\eta(r) = \eta_{\text{out}} \left[\exp \left(-\frac{(r - \frac{t}{2})^2}{2\sigma_{\text{out}}^2} \right) + \exp \left(-\frac{(r + \frac{t}{2})^2}{2\sigma_{\text{out}}^2} \right) \right] + \eta_{\text{core}} \exp \left(-\frac{r^2}{2\sigma_{\text{core}}^2} \right) \quad (9.17)$$

The scattering intensity of this cross section profile of a planar object can be calculated by eq. 9.12 and computes as

$$F_{\text{out}}(Q, D, \sigma_{\text{out}}, \eta_{\text{out}}) = \sqrt{2\pi} \sigma_{\text{out}} \eta_{\text{out}} \exp \left(-\frac{1}{2} (Q\sigma_{\text{out}})^2 \right) \cos \left(Q \frac{t}{2} \right) \quad (9.18)$$

$$F_{\text{core}}(Q, \sigma_{\text{core}}, \eta_{\text{core}}) = \sqrt{2\pi} \sigma_{\text{core}} \eta_{\text{core}} \exp \left(-\frac{1}{2} (Q\sigma_{\text{core}})^2 \right) \quad (9.19)$$

so that

$$P_{\text{cs}}(Q) = [F_{\text{core}}(Q, \sigma_{\text{core}}, \eta_{\text{core}}) + 2F_{\text{out}}(Q, D, \sigma_{\text{out}}, \eta_{\text{out}})]^2 \quad (9.20)$$

Input parameters for Pcs:BilayerGauss:

sigma_core: width σ_{core} of the central Gaussian profile

eta_core: scattering length density contrast of the central Gaussian profile

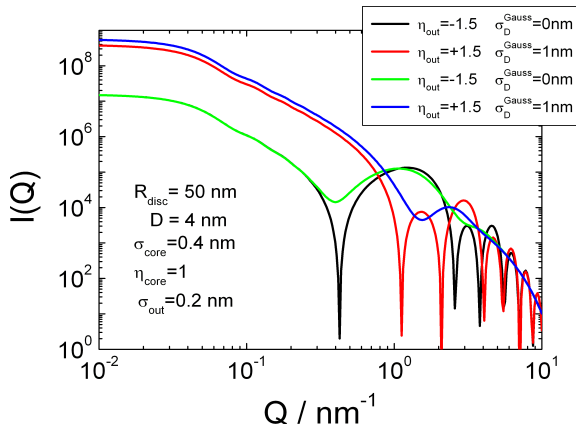
sigma_out: width σ_{out} of the two outer Gaussian profiles

eta_out: scattering length density contrast of the two outer Gaussian profiles

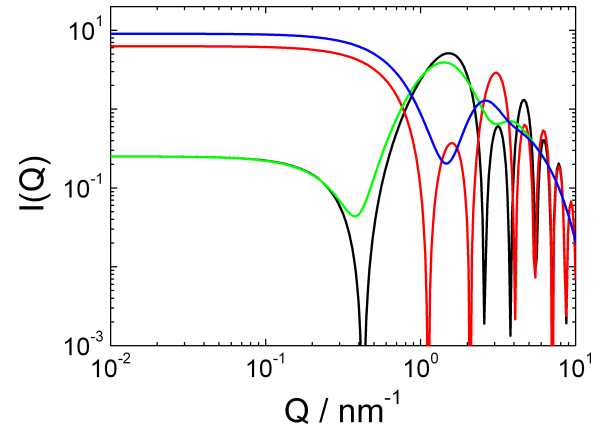
t: distance between the centers of the outer Gaussian profiles

Note

- This form factor is supposed to be combined with a shape factor for local planar objects which are implemented as structure plugins under "[by plugin|thin obj.|P'(Q) : local planar obj.]".



(A) Plot of the cross section form factor P_{cs} in combination with a structure factor "P'(Q) : Thin Disc" as the shape factor $P'(Q)$:



(B) Plot of the cross section form factor P_{cs} only according to eq. 9.20. The parameters for the profile are the same than in Fig. 9.14a

FIGURE 9.14. Scattering curve for the cross-section form factor "Pcs:BilayerGaussian". For some of the curves a distance distribution of the heads groups are assumed being Gaussian (see eq. 7.32a), i.e. calculating $\int_0^\infty \text{Gauss}(D, 1, \sigma_D^{\text{Gauss}}, D_0) P_{\text{cs}}(Q, D) dD$.

9.2.2. $P_{cs}(Q)$ for cylindrical obj.

The cross-section form factors with cylindrical geometry are valid when the cross-section dimension is much smaller than the segment length or Kuhn length of the local cylindrical structure.

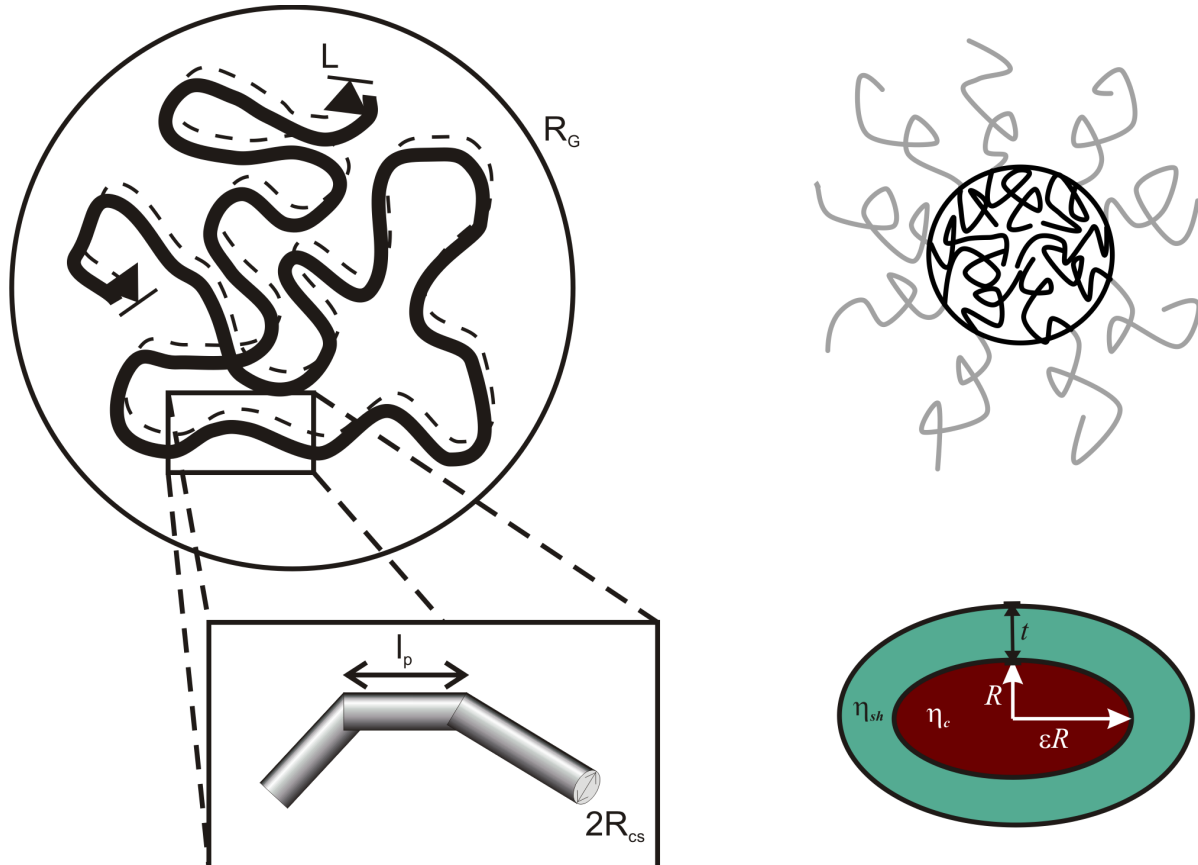


FIGURE 9.15. Sketch of wormlike structures which represent local cylindrical structures. The cross-section $2R_{cs}$ is much smaller than the Kuhn length l_p , which is a typical length scale where a freely jointed chain can randomly orient in any direction without the influence of any forces, independent of the directions taken by other segments. For the cross-section term several profiles have been implemented, like homogeneous round profile or elliptical shell profile

9.2.2.1. $P_{cs}(Q)$ for homogeneous cross-section of a cylinder.

This cross-section form factor describes the scattering of circular and homogeneous cross section. The cross-section radius R can have a distribution described by a log-normal distribution according to eq. 7.12b.

$$P_{cs}(Q, \sigma_R, R) = \int_0^{\infty} \text{LogNorm}(x, 1, \sigma_R, 1, R) \left((\eta_{\text{core}} - \eta_{\text{solv}}) \pi x^2 \frac{2J_1(Qx)}{Qx} \right)^2 dx \quad (9.21)$$

Input parameters for `Pcs:homogeneousCyl`:

R: most probable radius R

sigm_R: width σ_R of radius distribution (LogNorm)

dummy: not used

eta_core: scattering length density of the core η_{core}

dummy: not used

eta_solv: scattering length density of the solvent η_{solv}

Note

- This form factor is supposed to be combined with a shape factor for local cylindrical objects which are implemented as structure plugins under "[by plugin|thin obj.|P'(Q): local cylindrical obj.]".
- As the form factor already have the width distribution included one normally uses in SASfit as a size distribution the Delta-distribution.

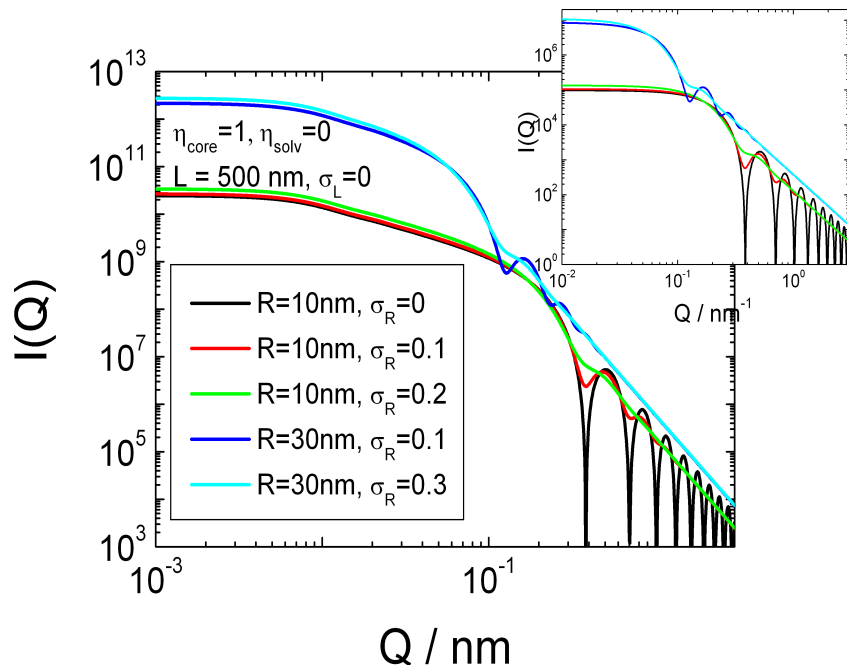


FIGURE 9.16. Scattering curve for the form factor "Pcs:homogeneousCyl" only (insert) and in combination with a structure factor "P'(Q): Thin Rod".

9.2.2.2. $P_{cs}(Q)$ for cross-section of a cylindrical shell with elliptical cross section.

This cross-section form factor describes the scattering of an elliptical core-shell cross-section. The cross-section radius R can have a distribution with a width of σ_R as described by a log-normal distribution according to eq. 7.12b.

$$P_{cs}(Q) = \int_0^{\infty} \text{LogNorm}(t', 1, \sigma_t, 1, t) \int_0^{\infty} \text{LogNorm}(R', 1, \sigma_{R_0}, 1, R) \times \\ \int_0^{\pi/2} \left[(\eta_{\text{shell}} - \eta_{\text{solv}}) F_{\text{cs,ell}}(Q, R' + t', \epsilon, \phi) \right. \\ \left. + (\eta_{\text{core}} - \eta_{\text{shell}}) F_{\text{cs,ell}}(Q, R', \epsilon, \phi) \right]^2 d\phi dR' dt' \quad (9.22)$$

with

$$F_{\text{cs,ell}}(Q, R, \epsilon, \Delta\eta\phi) = \frac{2J_1(Qr(R, \epsilon, \phi))}{Qr(R, \epsilon, \phi)} \quad (9.23a)$$

$$r(R, \epsilon, \phi) = R\sqrt{\sin^2\phi + \epsilon^2 \cos^2\phi} \quad (9.23b)$$

Input parameters for Pcs:ellCylSh:

R_0: most probable radius R_0

sigm_R0: width σ_{R_0} of radius distribution (LogNorm)

epsilon: stretching factor ϵ of elliptical cross-section

t: most probable shell thickness t

dummy: width σ_t of shell thickness distribution (LogNorm)

dummy: not used

dummy: not used

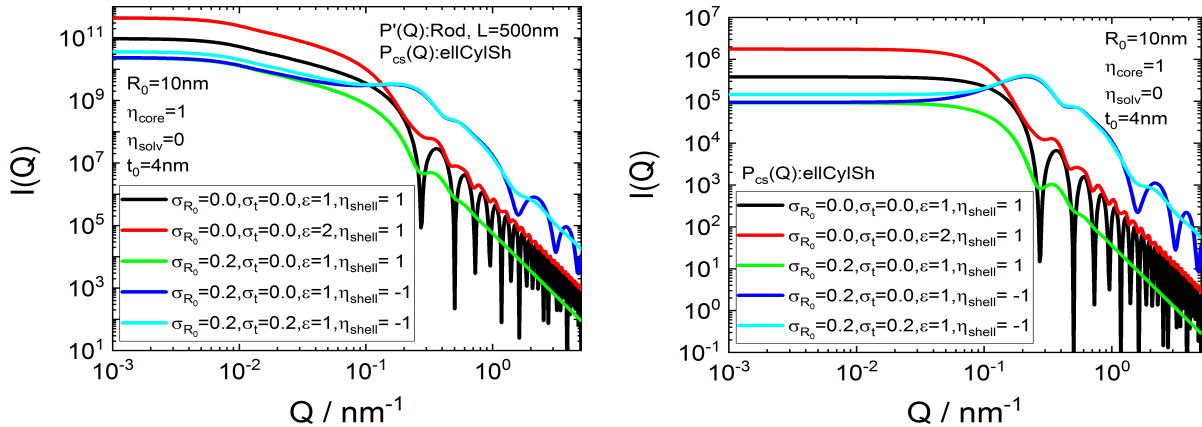
eta_core: scattering length density of the core η_{core}

eta_shell: scattering length density of the shell η_{shell}

eta_solv: scattering length density of the solvent η_{solv}

Note

- This form factor is supposed to be combined with a shape factor for local cylindrical objects which are implemented as structure plugins under "[by plugin|thin obj.|P'(Q): local cylindrical obj.]".
- As the form factor already has the width distribution included one normally uses in SASfit as a size distribution the Delta-distribution.



(A) Plot of the cross section form factor P'_{cs} in combination with a structure factor " $P'(Q)$: Rod" as the shape factor $P'(Q)$.

(B) [Plot of the cross section form factor P'_{cs} only according to eq. 9.22. The parameters for the profile are the same than in Fig. 9.17a

FIGURE 9.17. Scattering curve for the cross-section form factor "P_{cs}:ellCylSh".

9.2.2.3. $P_{cs}(q)$ for cross-section of circular core and shell with linear contrast.

The model already has been used for spherical symmetric particles with the same radial profile but in spherical coordinates 9.3.4. Form factor of a spherical shell with a core

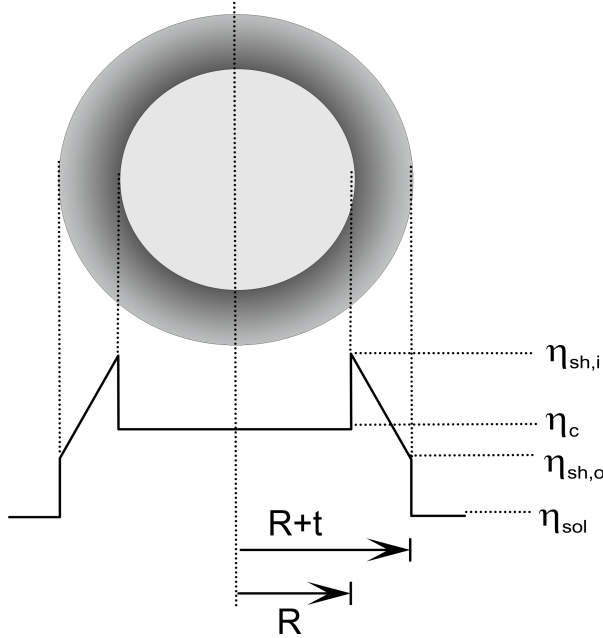


FIGURE 9.18. Radial profile for calculating the form factor of a thin cylindrical objects with a cross-section of a homogenous core and a linear scattering length density profile in the shell. The core has a radius of R and a shell thickness is t having a linear varying contrast profile.

radius R and a shell thickness of t . Here a linear contrast profile within the shell has been assumed.

$$\eta(r) = \begin{cases} \eta_c & \text{for } |r| < R \\ m|r| + b & \text{for } |r| \in [R, R+t] \\ \eta_{sol} & \text{for } |r| > R+t \end{cases} \quad (9.24)$$

$$m = (\eta_{sh,o} - \eta_{sh,i})/t \quad (9.25)$$

$$b = -mR + \eta_{sh,i} \quad (9.26)$$

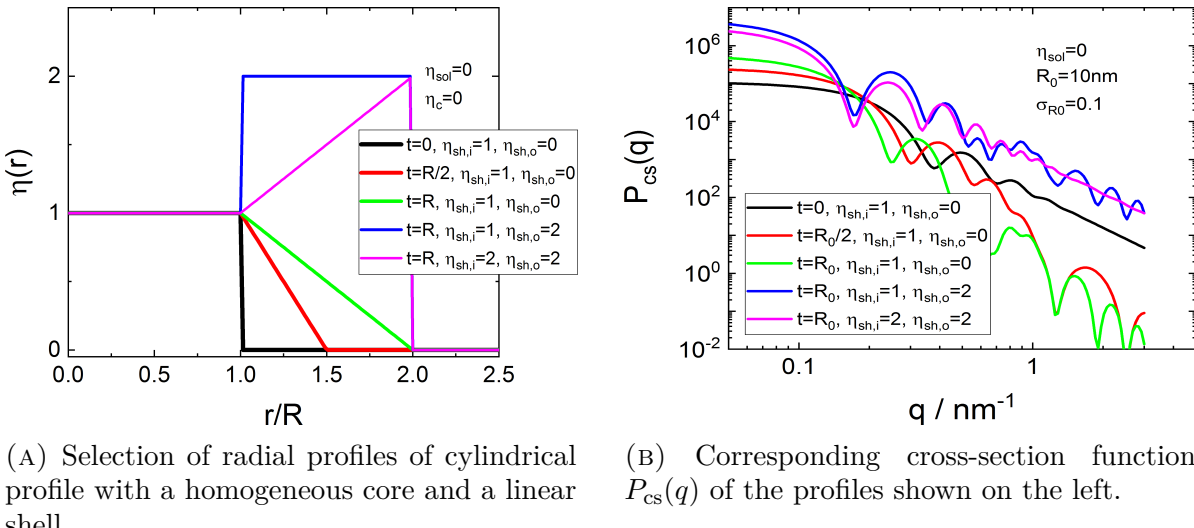
$\eta_{sh,i}$: scattering length density at R

$\eta_{sh,o}$: scattering length density at $R+t$

The scattering intensity is then given by

$$P_{\text{cs}}(q) = \left(\frac{1}{tq^2} \left\{ \pi \left[2qt \left\{ [\eta_c - \eta_{\text{sh},i}] RJ_1(qR) + [\eta_{\text{sh},o} - \eta_{\text{sol}}] (R+t)J_1(q(R+t)) \right\} \right. \right. \right. \right. \\ \left. \left. \left. \left. + \pi [\eta_{\text{sh},i} - \eta_{\text{sh},o}] \left\{ (R+t)J_1(q(R+t)) - RJ_1(qR)H_0(qR)H_0(q(R+t)) \right. \right. \right. \right. \\ \left. \left. \left. \left. + RJ_0(qR)H_1(qR) - (t+R)J_0(q(t+R))H_1(q(t+R)) \right\} \right] \right\} \right)^2 \quad (9.27)$$

$H_\alpha(x)$ is the Struve function of order α and $J_n(x)$ are the regular cylindrical Bessel function of order n .



(A) Selection of radial profiles of cylindrical profile with a homogeneous core and a linear shell.

(B) Corresponding cross-section function $P_{\text{cs}}(q)$ of the profiles shown on the left.

FIGURE 9.19. Radial profiles and scattering curve for the cross-section form factor "Pcs:linear shell cyl.". The scattering functions have been calculated with a narrow lognormal distribution with a width of $\sigma_{R_0} = 0.1$.

Input parameters for Pcs:linear shell cyl.:

R_0: most probable radius R_0

sigma_R0: width σ_{R_0} of radius distribution (LogNorm)

t: thickness t of the shell with linear scattering length density profile

sigma: width of fuzzy interface σ

dummy: not used

dummpy: not used

eta_c: scattering length density of core η_c

eta_sh_i: scattering length density $\eta_{\text{sh},i}$ at $r = R$

eta_sh_o: scattering length density $\eta_{\text{sh},o}$ at $r = R + t$

eta_sol: scattering length density η_{sol} of solvent

Input parameters for profile:linear shell cyl.:

R: radius R

dummy: not used, the profile plugin does not include a size distribution

t: thickness t of the shell with linear scattering length density profile

sigma: width of fussy interface σ

dummy: not used

dummy: not used

eta_c: scattering length density of core η_c

eta_sh_i: scattering length density $\eta_{sh,i}$ at $r = R$

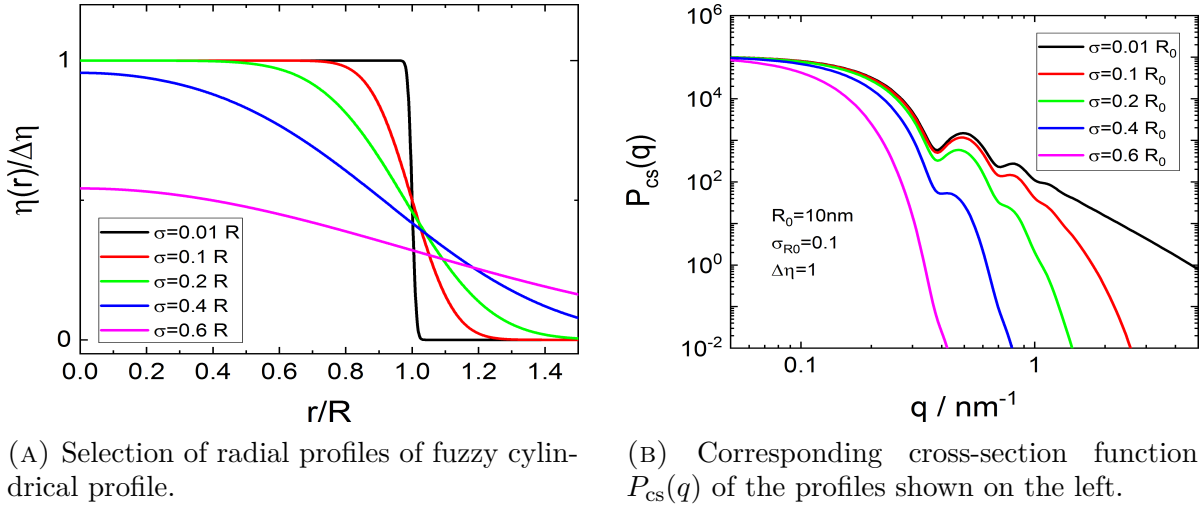
eta_sh_o: scattering length density $\eta_{sh,o}$ at $r = R + t$

eta_sol: scattering length density η_{sol} of solvent

Note

- This form factor is supposed to be combined with a shape factor for local cylindrical objects which are implemented as structure plugins under "[by plugin|thin obj.|P'(Q): local cylindrical obj.]".
- As the form factor already has the width distribution included one normally uses in SASfit as a size distribution the Delta-distribution.
- In case the shape factor is set to 1 or "None" the cross-section term can be interpreted as a perfect aligned cylindrical objects along the beam axis with a linear contrast profile of its shell

9.2.2.4. $P_{\text{cs}}(q)$ for circular cross-section folded with a Gaussian.



(A) Selection of radial profiles of fuzzy cylindrical profile.

(B) Corresponding cross-section function $P_{\text{cs}}(q)$ of the profiles shown on the left.

FIGURE 9.20. Radial profiles and scattering curve for the cross-section form factor "Pcs:fuzzy cyl.". The scattering functions have been calculated with a narrow lognormal distribution with a width of $\sigma_{R_0} = 0.1$.

Similar to the fuzzy sphere plugin described in section 9.3.2 also here the circular cross-section of the cylinder is folded with a Gaussian function, however, this time in two dimensions.

$$\begin{aligned}\eta_{\text{FuzzyCyl}}(|\mathbf{r}|) &= (\eta_{\text{circular}} \star \eta_{\text{Gauss}})(\mathbf{r}) \\ &= \int_{\mathbb{R}^2} \eta_{\text{circular}}(\boldsymbol{\tau}) \eta_{\text{Gauss}}(\mathbf{r} - \boldsymbol{\tau}) d\boldsymbol{\tau}\end{aligned}\quad (9.28)$$

with

$$\eta_{\text{circular}}(|\mathbf{r}|) = \begin{cases} (\eta_{\text{cyl}} - \eta_{\text{sol}}) & \text{for } |\mathbf{r}| \leq R \\ 0 & \text{for } |\mathbf{r}| > R \end{cases}\quad (9.29a)$$

$$\eta_{\text{Gauss}}(|\mathbf{r}|) = \frac{1}{2\pi\sigma^2} \exp\left[-\frac{\mathbf{r}^2}{2\sigma^2}\right]\quad (9.29b)$$

The convolution has to be done in \mathbb{R}^2 . As the circular cross-section of a homogeneous cylinder and Gaussian functions are radial symmetric also the profile of the fuzzy cylinder only depends on $|\mathbf{r}|$. By defining the interface via a convolution the form factor can be easily calculated because the Fourier transform of a convolution is the pointwise product of the Fourier transforms according to the convolution theorem, i.e.

$$P_{\text{cs}}(q) = \left[2\pi (\eta_{\text{cyl}} - \eta_{\text{sol}}) R^2 \frac{J_1(qR)}{qR} \exp\left(-\frac{1}{2}q^2\sigma^2\right) \right]^2\quad (9.30)$$

As the 2D Fourier transform of radial symmetric functions can be written as a Hankel transform of zero order [268] and the Hankel transform is its own inverse the scattering

length density profile can be written as

$$\eta_{\text{circular}}(r) = \int_0^{\infty} (\eta_{\text{cyl}} - \eta_{\text{sol}}) R^2 \frac{J_1(qR)}{qR} \exp\left(-\frac{1}{2} q^2 \sigma^2\right) J_0(qr) q dq \quad (9.31)$$

$$\stackrel{\sigma \ll R}{\approx} \frac{\eta_{\text{cyl}} - \eta_{\text{sol}}}{2} \left(1 - \operatorname{erf}\left(\frac{|r| - R}{\sqrt{2}\sigma}\right) \right) \quad (9.32)$$

Input parameters for `Pcs:fuzzy cyl.`:

R_0: most probable radius R_0

sigma_R0: width σ_{R_0} of radius distribution (LogNorm)

dummy: not used

sigma: width of fussy interface σ

dummy: not used

dummy: not used

dummy: not used

eta_cyl: scattering length density of cylindrical core η_{cyl}

eta_sol: scattering length density of solvent/matrix η_{sol}

Input parameters for `profile:fuzzy cyl.`:

R: radius R

dummy: not used, the profile plugin does not include a size distribution

dummy: not used

sigma: width of fussy interface σ

dummy: not used

dummy: not used

dummy: not used

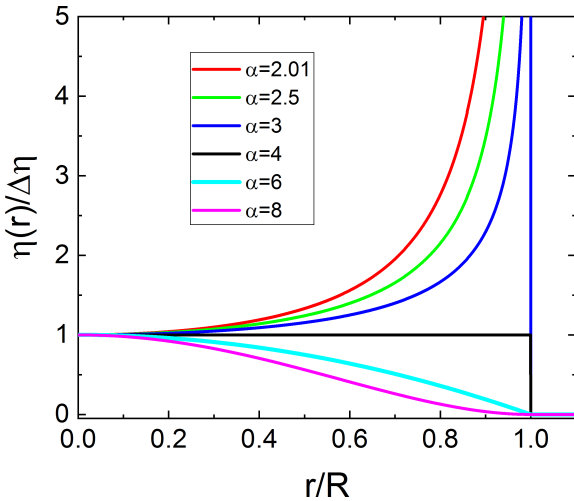
eta_cyl: scattering length density of cylindrical core η_{cyl}

eta_sol: scattering length density of solvent/matrix η_{sol}

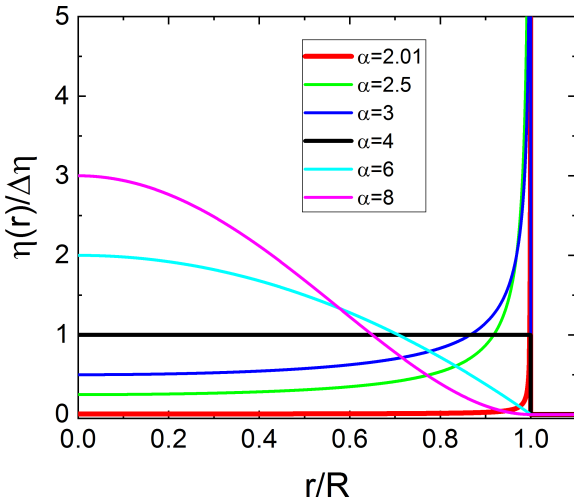
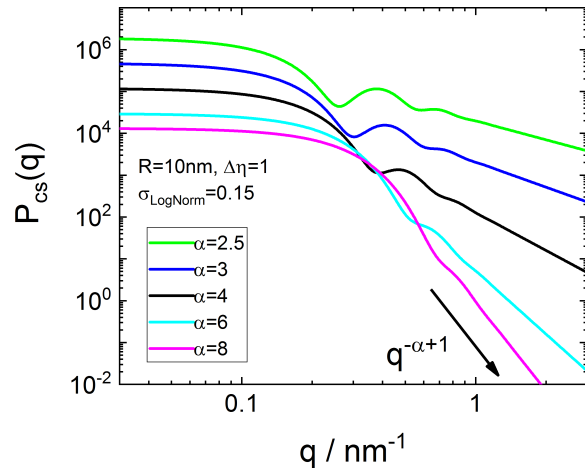
Note

- This form factor is supposed to be combined with a shape factor for local cylindrical objects which are implemented as structure plugins under "[by plugin|thin obj.|P'(Q): local cylindrical obj.]".
- As the form factor already has the width distribution included one normally uses in SASfit as a size distribution the Delta-distribution.
- In case the shape factor is set to 1 or "None" the cross-section term can be interpreted as a perfect aligned cylindrical objects along the beam axis with a fuzzy cross-section profile

9.2.2.5. $P_{\text{cs}}(q)$ for circular cross-section with a Boucher contrast profile.



(A) radial profiles with $\eta_0 = \Delta\eta$ for several values of α



(C) Scattering curves of `Pcs:Boucher cyl` for several α with a narrow LogNormal size distribution of $\sigma = 0.15$. As the excess scattering lenght β diverges for $\alpha \leq 2$ these values are not allowed.

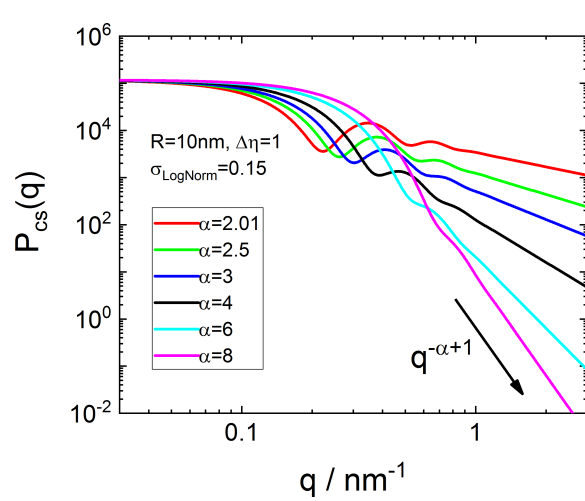


FIGURE 9.21. Two implemented cases for the radial profiles and their scattering profiles according to Boucher [49], but now applied for cylindrical objects

The idea of form factor is taken from section 9.3.7 but applied to cylindrical geometry. The cross-section term is valid for perfectly oriented cylinders with the cylinder axis pointing into the beam direction. In case of random oriented cylinders the cross-section term has to be multiplied by a shape factor $P'(q)$ according to eq. 12.77.

The radial profile of Boucher [49] reads as

$$\eta(r) = \eta_0 \begin{cases} \left(1 - \left(\frac{r}{R}\right)^2\right)^{\alpha/2-2}, & \text{if } r \leq R \\ 0, & \text{otherwise.} \end{cases} \quad (9.33)$$

For cylindrical geometry the scattering intensity is calculated as

$$P_{\text{cs}}(q) = \left[\int_0^\infty 2\pi J_0(qr) r \eta(r) dr \right]^2 = \beta^2 \left[{}_0F_1 \left(\frac{\alpha}{2}, -\frac{1}{4}q^2 R^2 \right) \right]^2 \quad (9.34)$$

$$(9.35)$$

with the excess scattering contribution β of the cross-section profile equals to

$$\beta = \eta_0 \pi R^2 \frac{2}{\alpha - 2} \quad (9.36)$$

The input value $\Delta\eta$ for this profile is the scatter contrast at $r = 0$, i.e.

$$\eta_0 = \Delta\eta \quad (\text{case Pcs:Boucher cyl.}) \quad (9.37)$$

The special case of $\alpha = 4$ corresponds to a homogeneous circular cross-section with a scattering contrast $\Delta\eta$ for which the excess scattering contribution becomes $\beta_{\text{cyl}} = \Delta\eta\pi R^2$.

Also a second variant of the form factor has been implemented. In the second case the excess scattering length is normalised to the one of a homogeneous circular cross-section with contrast $\Delta\eta$, so that the excess scattering length is for all α equal to $\beta_{\text{cyl}} = \Delta\eta\pi R^2$. This is done by setting the contrast at $r = 0$ in eq. ?? to

$$\eta_0 = \Delta\eta \frac{\alpha - 2}{2} \quad (\text{case Pcs:Boucher2 cyl.}) \quad (9.38)$$

By this normalisation the excess scattering contribution β is for all α equal to the one of a homogeneous cylinder with a scattering contrast $\Delta\eta$, i.e. $\beta_{\text{cyl}} = \Delta\eta\pi R^2$.

The scattering function $P_{\text{cs}}(q)$ decays at large q -values with a potential law of $q^{-\alpha+1}$. As the cross-section term has to be multiplied with a shape factor $P'(q)$ for cylindrical symmetric objects which decays at large q -values with q^{-1} the parameter α defines the overall power law at large scattering vectors similar to section 9.3.7 using the same radial profile for spherical symmetric objects.

Input parameters for Pcs:Boucher cyl. and Pcs:Boucher2 cyl.:

R_0: most probable radius R_0

sigma_R0: width σ_{R_0} of radius distribution (LogNorm)

dummy: not used

alpha: shape parameter α

dummy: not used

dummy: not used

dummy: not used

Delta_eta: scattering length density contrast $\Delta\eta$

Input parameters for `profile:Boucher cyl.` and `profile:Boucher2 cyl.:`

R: radius R

dummy: the profile plugins do not include a size distribution

dummy: not used

alpha: shape parameter α

dummy: not used

dummy: not used

dummy: not used

Delta_eta: scattering length density contrast $\Delta\eta$

Note

- This form factor is supposed to be combined with a shape factor for local cylindrical objects which are implemented as structure plugins under "[by plugin|thin obj.|P'(Q): local cylindrical obj.]".
- As the form factor already has the width distribution included one normally uses in **SASfit** as a size distribution the **Delta**-distribution.
- In case the shape factor is set to 1 or "None" the cross-section term can be interpreted as a perfect aligned cylindrical objects along the beam axis with a Boucher cross-section profile

9.2.3. $P'(Q)$ for local planar obj.

As local planar objects the following shapes have been implemented:

- (1) thin disc
- (2) thin spherical shell
- (3) thin ellipsoidal shell
- (4) thin hollow cylinder with closed ends

9.2.3.1. $P'(Q)$: thin discs.

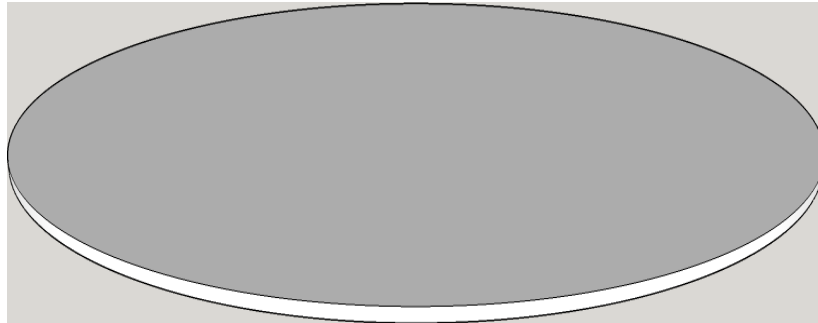


FIGURE 9.22. Sketch of a thin disc with a radius R . The thickness of the disc is assumed to be much smaller than its radius.

$$P'(Q) = \int_0^{\infty} \text{LogNorm}(R', \sigma, 1, R) \pi^2 R'^4 \frac{2}{(R'Q)^2} \left(1 - \frac{2J_1(2QR')}{2QR'}\right) dR' \quad (9.39)$$

Input parameters for $P'(Q)$: Thin Disc:

R: most probable radius R

dummy: not used

sigma: width σ of radius distribution (LogNorm)

Note

- This structure factor is supposed to be combined with a form factor of local planar objects which are implemented as form factor plugins under "[by plugin|thin obj.|Pcs(Q): local planar obj.]".
- The structure factor already has a log-normal width distribution for one parameter included.

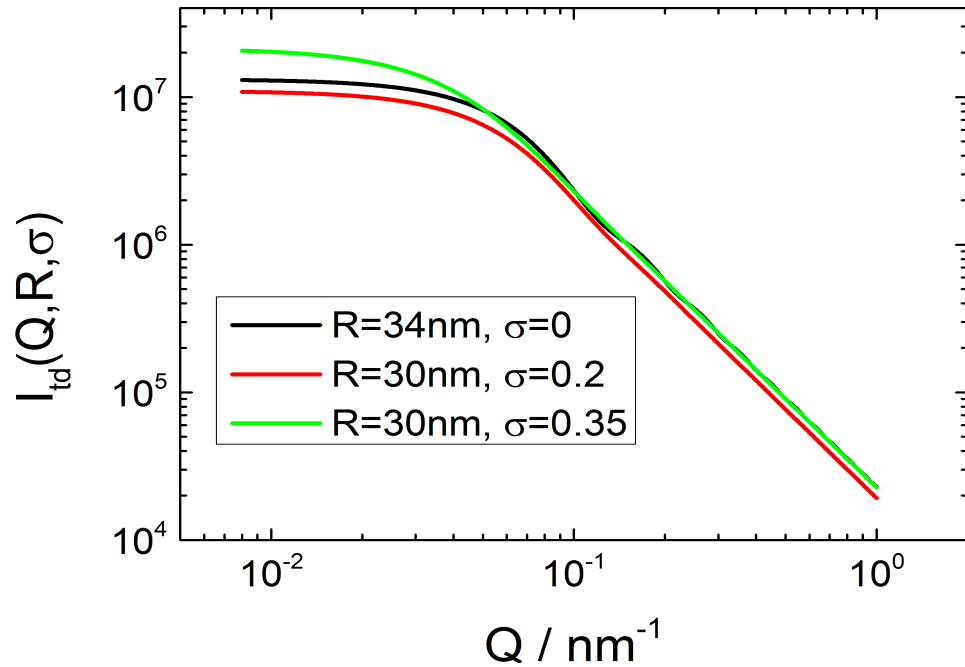


FIGURE 9.23. Scattering curve for the structure factor "P'(Q): Thin Disc" in combination with a constant background of 1".

9.2.3.2. $P'(Q)$: thin spherical shell.

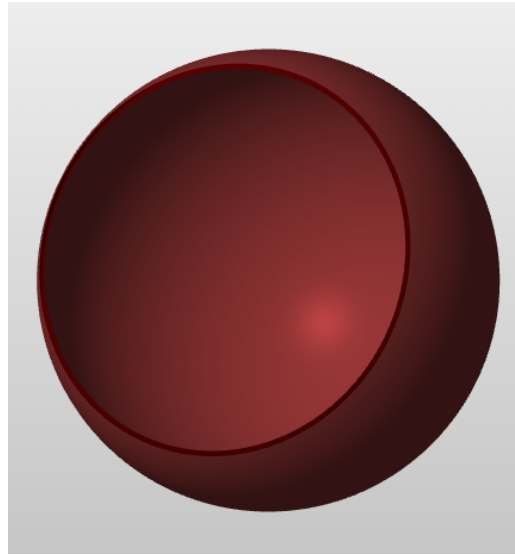


FIGURE 9.24. Sketch of a thin spherical shell with a radius R . The thickness of the shell is assumed to be much smaller than the radius of the sphere.

$$P'(Q) = \int_0^{\infty} \text{LogNorm}(R', \sigma, 1, R) \left(\frac{4\pi R'^2 \sin(QR')}{QR'} \right)^2 dR' \quad (9.40)$$

Input parameters for $P'(Q)$: Thin Spherical Shell:

R: most probable radius R

dummy: not used

sima: width σ of radius distribution (LogNorm)

Note

- This structure factor is supposed to be combined with a form factor of local planar objects which are implemented as form factor plugins under "[by plugin|thin obj.|Pcs(Q): local planar obj.]".
- The structure factor already has a log-normal width distribution for one parameter included.

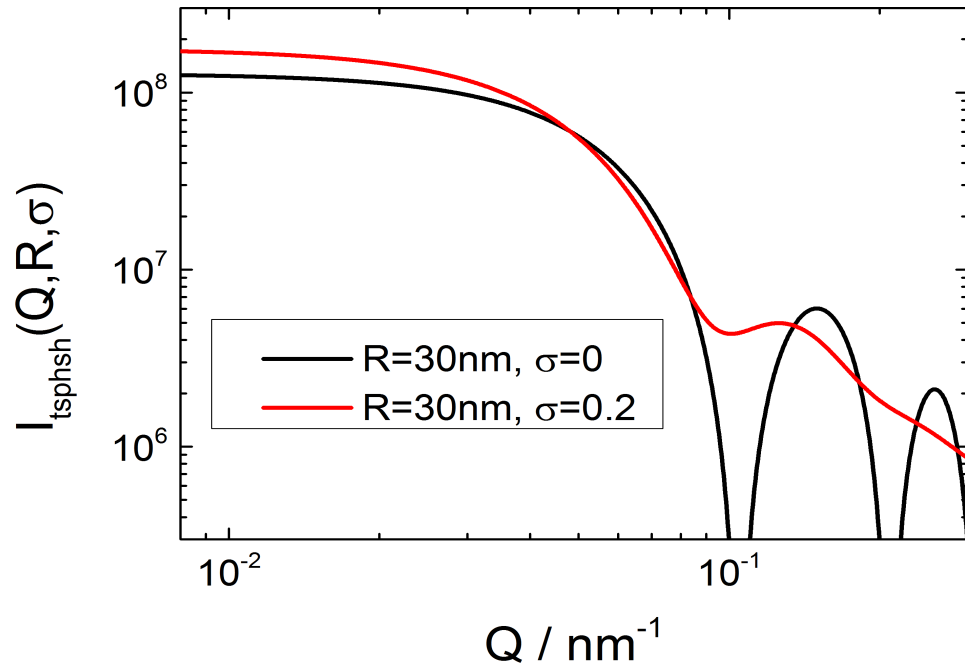


FIGURE 9.25. Scattering curve for the structure factor "P'(Q): Thin Spherical Shell" in combination with a constant background of 1".

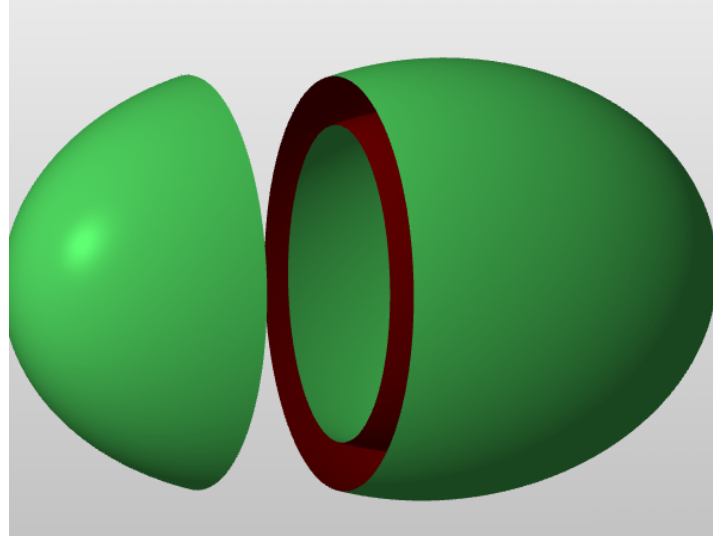
9.2.3.3. $P'(Q)$: thin ellipsoidal shell.

FIGURE 9.26. Sketch of a thin ellipsoidal shell with a radius R and stretching factor ϵ . The thickness of the shell is assumed to be much smaller than the two radii of the elliptical shell.

$$S(R, \epsilon) = 2\pi R^2 \left(1 + \epsilon^2 {}_2F_1 \left(\frac{1}{2}, 1; \frac{3}{2}; 1 - \epsilon^2 \right) \right) \quad (9.41)$$

$$u = QR' \sqrt{\sin^2 \alpha + \epsilon^2 \cos^2 \alpha} \quad (9.42)$$

$$P'(Q, R, \epsilon) = \int_0^\infty \text{LogNorm}(R', \sigma, 1, R) S^2(R', \epsilon) j_0^2(Qu) \sin \alpha d\alpha dR' \quad (9.43)$$

with j_0 being the regular spherical Bessel function of zeroth order.

Input parameters for $P'(Q)$: Thin Ellipsoidal Shell:

R: most probable radius R

epsilon: stretching factor ϵ

sima_R: width σ_R of radius distribution (LogNorm)

Note

- This structure factor is supposed to be combined with a form factor of local planar objects which are implemented as form factor plugins under "[by plugin|thin obj.|Pcs(Q): local planar obj.]".
- The structure factor already has a log-normal width distribution for one parameter included.

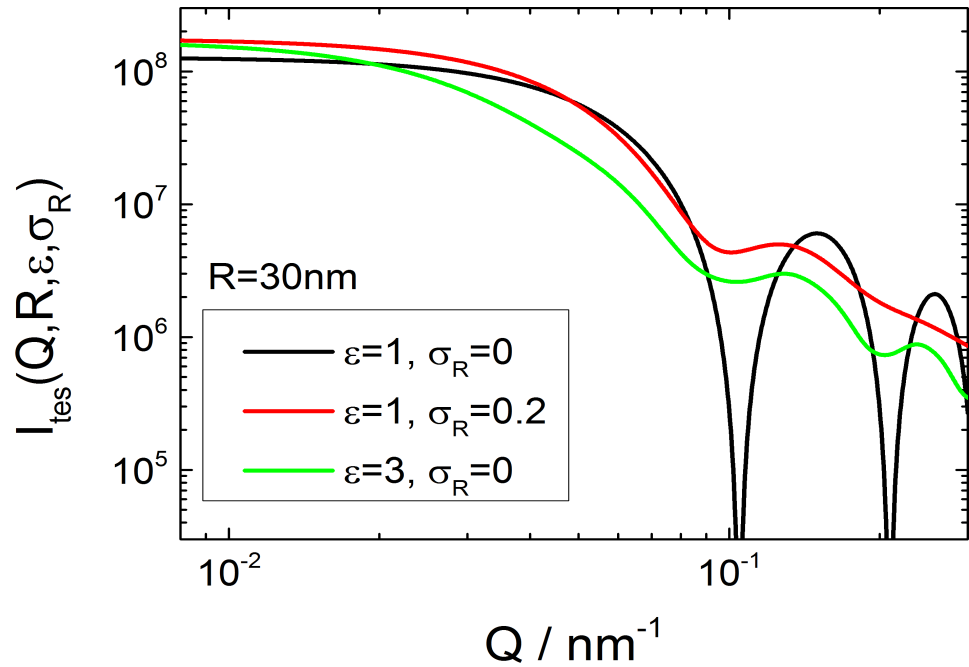


FIGURE 9.27. Scattering curve for the structure factor "P'(Q): Thin Ellipsoidal Shell" in combination with a constant background of 1".

9.2.3.4. $P'(Q)$: thin-walled hollow cylinder.

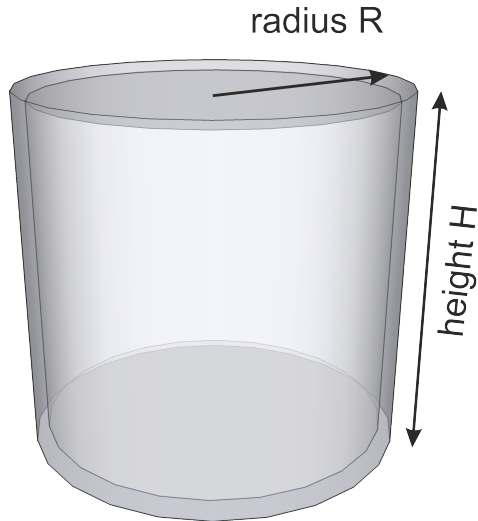


FIGURE 9.28. Sketch of a thin hollow cylinder of height H and radius R . The thickness of the wall is assumed to be much smaller than the outer dimensions of the cylinder.

$$\Xi(Q, R, H, \alpha) = 2\pi R \left[R \frac{J_1(QR \sin \alpha)}{QR \sin \alpha} + H J_0 \left(\frac{QH}{2} \cos \alpha \right) \frac{\sin \left(\frac{QH}{2} \cos \alpha \right)}{\frac{QH}{2} \cos \alpha} \right] \quad (9.44)$$

$$P_{\text{thc}}(Q, R, H) = \int_0^{\pi/2} \Xi^2(Q, R, H, \alpha) \sin \alpha d\alpha \quad (9.45)$$

$$P'_{\text{thc}}(Q, R, H) = \int_0^\infty \int_0^\infty \text{LogNorm}(r, 1, \sigma_R, 1, R, 1) \text{LogNorm}(h, 1, \sigma_H, 1, H, 1) P_{\text{thc}}(Q, r, h) dh dr \quad (9.46)$$

Input parameters for $P'(Q)$: Thin Hollow Cylinder:

R: most probable cylinder radius R

H: most probable cylinder height H

sima_R: width σ_R of radius distribution (LogNorm)

sima_H: width σ_H of height distribution (LogNorm)

Note

- This structure factor is supposed to be combined with a form factor of local planar objects which are implemented as form factor plugins under "[by plugin|thin obj.|Pcs(Q): local planar obj.]".
- The structure factor already has a log-normal width distribution for one parameter included.

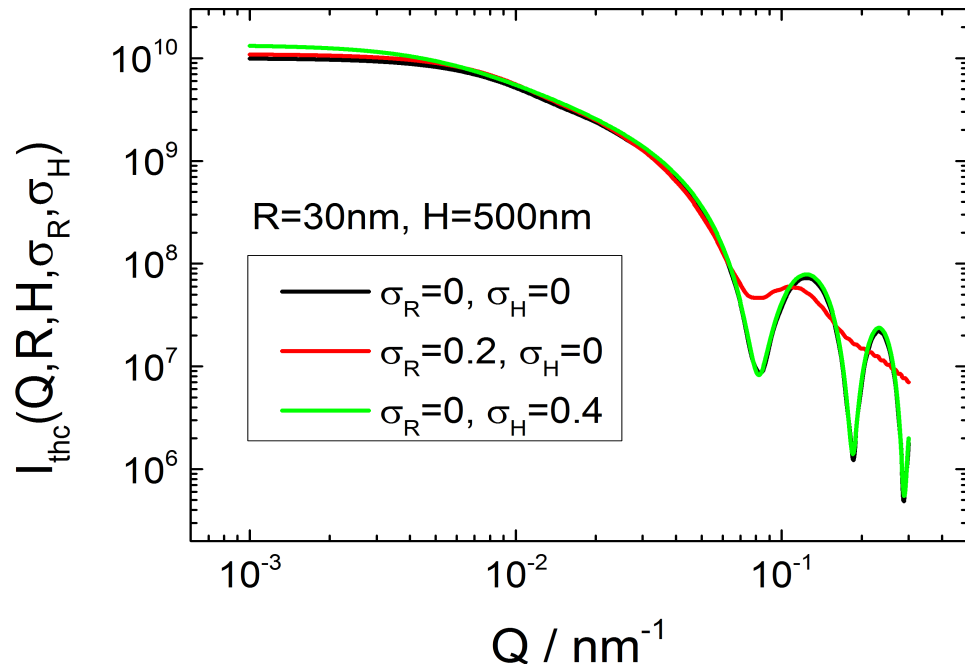


FIGURE 9.29. Scattering curve for the structure factor "P'(Q): Thin Hollow Cylinder" in combination with a constant background of 1'.

9.2.4. $P'(Q)$ for local cylindrical obj.

- (1) thin rigid rod
- (2) worm-like or semi-flexible structure

9.2.4.1. $P'(Q)$: Rod.

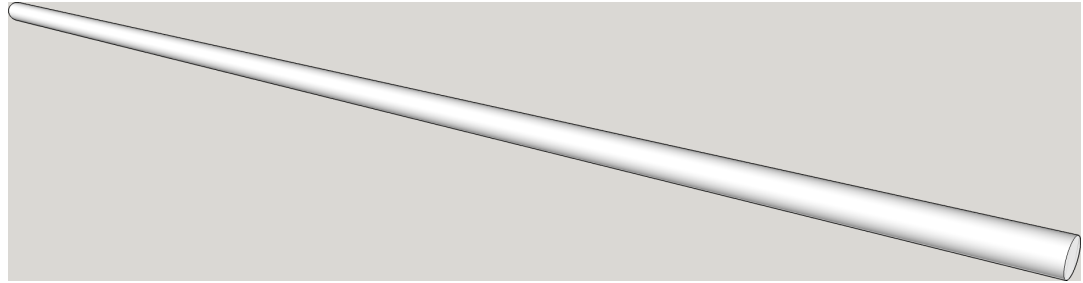


FIGURE 9.30. Sketch of a thin Rod of Length L . The diameter of the rod is assumed to be much smaller than its length.

$$P'(Q) = \int_0^{\infty} L'^2 \text{LogNorm}(L', \sigma_L, 1, L) \left(2 \frac{\text{Si}(QL')}{QL'} - \frac{\sin^2(QL'/2)}{(QL'/2)^2} \right) dL' \quad (9.47)$$

where $\text{Si}(z) = \int_0^z \frac{\sin t}{t} dt$ is the sine integral.

Input Parameters for model P'(Q): Rod:

L: most probable length L of rod

sigma_L: width LogNorm length distribution σ_L

Note

- This structure factor is supposed to be combined with a form factor with local cylindrical geometry which are implemented as form factor plugins under "[by plugin|thin obj.|Pcs(Q): local cylindrical obj.]".
- The structure factor already has a log-normal width distribution for one parameter included.

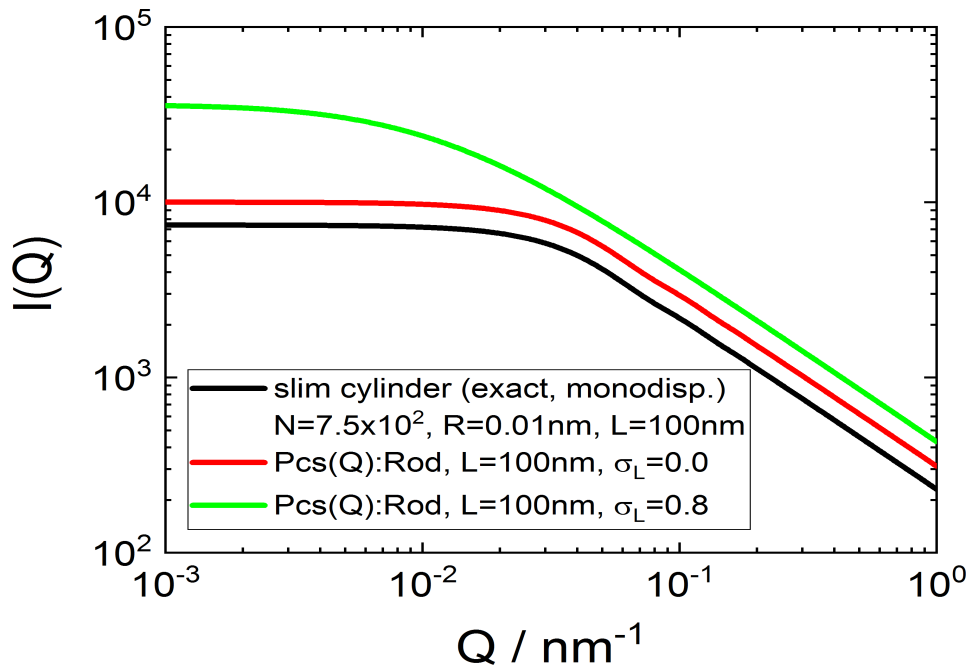


FIGURE 9.31. Scattering curve for the structure factor "P" (Q): Rod alone without $P_{cs}(Q)$.

9.2.4.2. $P'(Q)$: freely joined chain of rods.

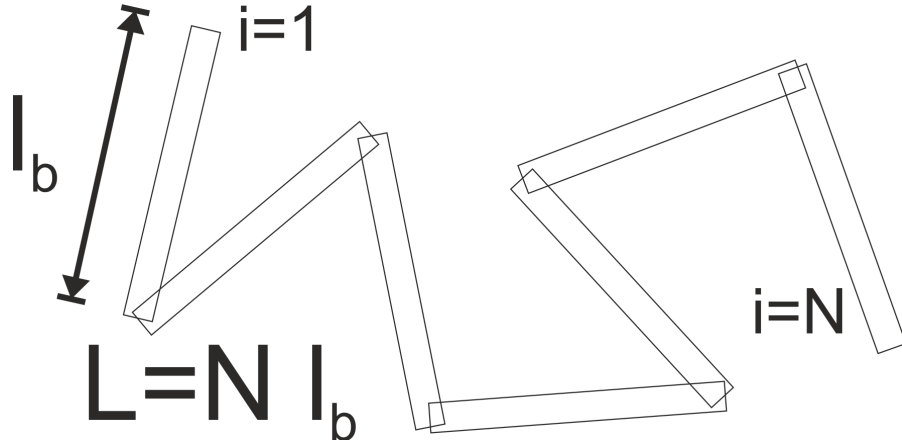


FIGURE 9.32. Sketch of a freely joined chain of rods.

This form factor describes a freely joined chain of infinitesimal thin rigid rods [212].

$$P'(Q, L, l_b) = L^2 \left(\frac{2l_b}{L} \left(\Lambda(\beta) - \frac{1}{2} \left(\frac{\sin(\beta/2)}{\beta/2} \right)^2 \right) \right) \quad (9.48)$$

$$+ L^2 \Lambda^2(\beta) \left(\frac{2l_b}{L} \frac{1}{1-\gamma} - \frac{2l_b^2}{L^2} \frac{1-\gamma^{L/l_b}}{(1-\gamma)^2} \right) \quad (9.49)$$

$$\beta = ql_b \quad (9.49)$$

$$\gamma = \frac{\sin(\beta)}{\beta} \quad (9.50)$$

$$\Lambda(\beta) = \frac{\text{Si}(\beta)}{\beta} \quad (9.51)$$

$$\text{Si}(x) = \int_0^x \frac{\sin t}{t} dt \quad (9.52)$$

Input Parameters for model $P'(Q)$ freely joined chain of rods:

1b: Kuhn length l_B of semi-flexible worm-like structure

L: contour length L of semi-flexible worm-like structure

Note

- This structure factor is supposed to be combined with a form factor with local cylindrical geometry which are implemented as form factor plugins under "[by plugin|thin obj.|Pcs(Q): local cylindrical obj.]".
- scattering function is normalized to $P'(Q, L, l_b) \xrightarrow[Q \rightarrow 0]{} L^2$

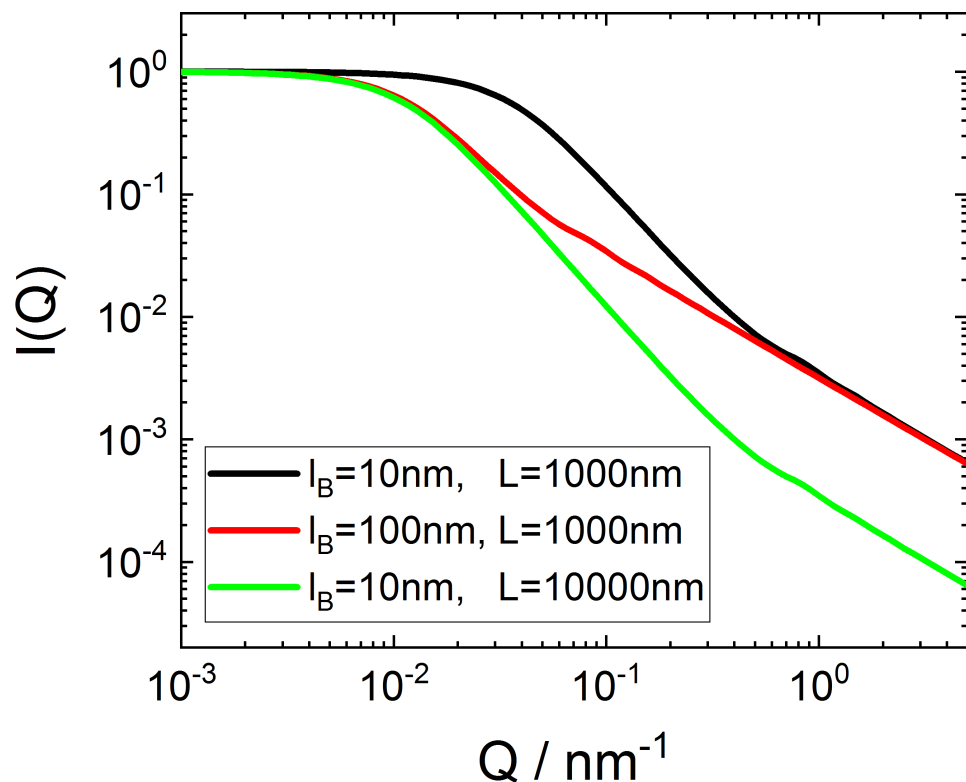


FIGURE 9.33. Scattering curve for the structure factor "P' (Q): freely joined chain of rods" alone without $P_{\text{cs}}(Q)$.

9.2.4.3. $P'(Q)$: Koyama worm.
[275, 276, 394]

$$P'(Q, L, l_b) = L^2 \frac{2}{X^2} \int_0^X (X - x) \phi(x) dx \quad (9.53)$$

$$X = \frac{2L}{l_b} \quad (9.54)$$

$$\phi(x) = \exp\left(-\frac{s^2}{3}xf(x)\right) \frac{\sin(sxg(x))}{sxg(x)} \quad (9.55)$$

$$s = \frac{1}{2}ql_b \quad (9.56)$$

$$xf(x) = \frac{2\langle r^2 \rangle}{l_b^2} - \frac{1}{2}x^2 g^2(x) \quad (9.57)$$

$$x^2 g^2(x) = \frac{2\langle r^2 \rangle}{l_b^2} \sqrt{10} \sqrt{1 - \frac{3}{5}K} \quad (9.58)$$

$$K = \frac{\langle r^4 \rangle}{\langle r^2 \rangle^2} \quad (9.59)$$

$$\langle r^2 \rangle = \frac{l_b^2}{2} \left(x - (1 - e^{-x}) \right) \quad (9.60)$$

$$\langle r^4 \rangle = \frac{l_b^4}{4} \left\{ \frac{5}{3}x^2 - \frac{52}{9}x - \frac{2}{27}(1 - e^{-3x}) + 8(1 - e^{-x}) - 2xe^{-x} \right\} \quad (9.61)$$

Input Parameters for model P'(Q) Koyama worm:

lb: Kuhn length l_B of semi-flexible worm-like structure
L: contour length L of semi-flexible worm-like structure

Note

- This structure factor is supposed to be combined with a form factor with local cylindrical geometry which are implemented as form factor plugins under "[by plugin|thin obj.|Pcs(Q): local cylindrical obj.]".
- scattering function is normalized to $P'(Q, L, l_b) \xrightarrow[Q \rightarrow 0]{} L^2$

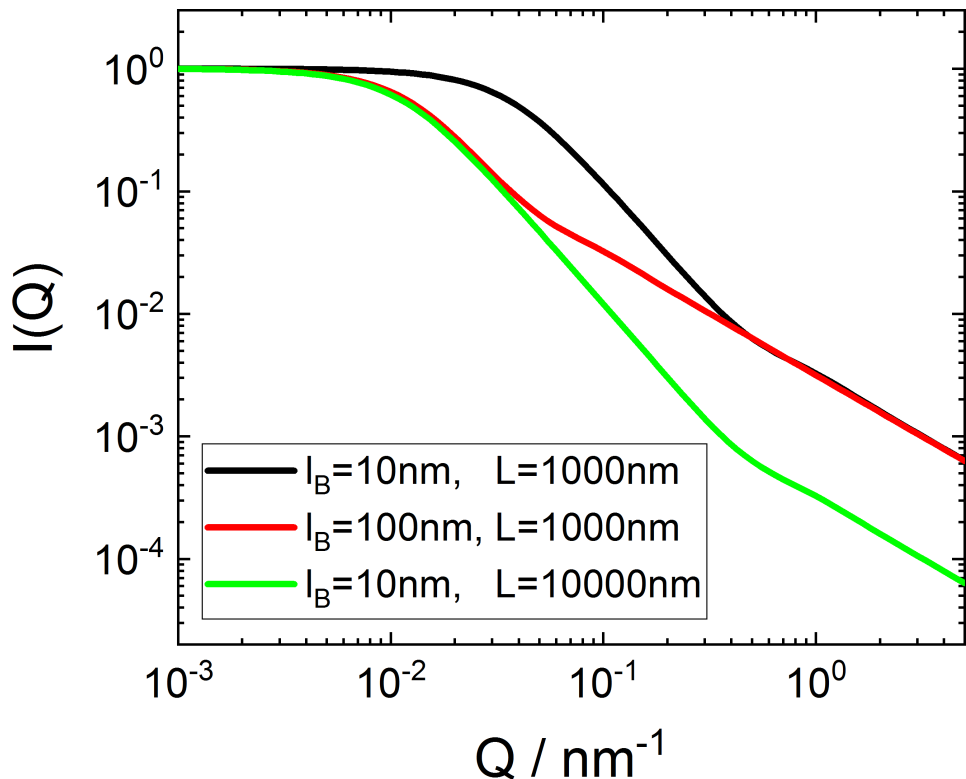


FIGURE 9.34. Scattering curve for the structure factor "P' (Q) : Koyama worm" alone without $P_{\text{cs}}(Q)$.

9.2.4.4. $P'(Q)$: Kholodenko's worm.

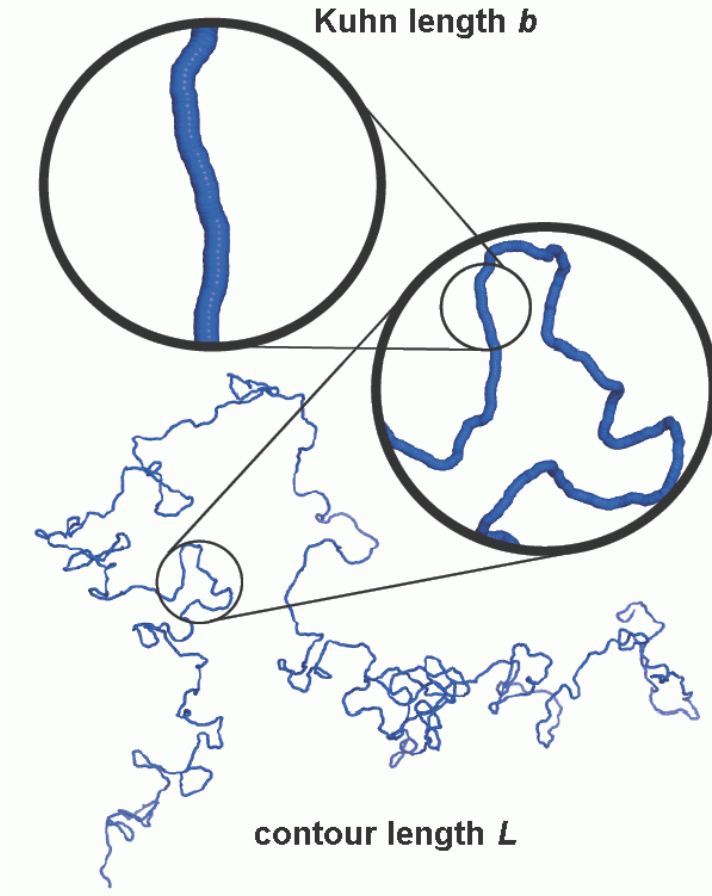


FIGURE 9.35

By using the analogy between Dirac's fermions and semi-flexible polymers Kholodenko [265] could give a simple expression for the scattering behaviour of wormlike structures. The form factor $P_0(Q)$ resulting from Kholodenko's approach is designed to reproduce correctly the rigid-rod limit and the random-coil limit. Defining $x = 3L/l_b$ (L : contour length, l_b : Kuhn length), it is given by

$$P'(Q, L, l_b) = L^2 \frac{2}{x} \left[I_{(1)} - \frac{1}{x} I_{(2)} \right] \quad (9.62)$$

where

$$I_{(n)}(x) = \int_0^x f(z) z^{n-1} dz \quad (9.63)$$

together with

$$f(z) = \begin{cases} \frac{1}{E} \frac{\sinh(Ez)}{\sinh(z)} & \text{for } Q \leq \frac{3}{l_b} \\ \frac{1}{F} \frac{\sin(Fz)}{\sinh(z)} & \text{for } Q > \frac{3}{l_b} \end{cases} \quad (9.64)$$

and

$$E = \sqrt{1 - \left(\frac{l_b Q}{3}\right)^2} \quad \text{and} \quad F = \sqrt{\left(\frac{l_b Q}{3}\right)^2 - 1} \quad (9.65)$$

Input Parameters for model P' (Q) Kholodenko Worm:

1b: Kuhn length¹ l_B of semi-flexible worm-like structure

L: contour length L of semi-flexible worm-like structure

Note

- This structure factor is supposed to be combined with a form factor with local cylindrical geometry which are implemented as form factor plugins under "[by plugin|thin obj.|Pcs(Q): local cylindrical obj.]".
- The equivalent solution of J.S. Pedersen [380] would be the expressions of worm-like structures without excluded volume effects.
- scattering function is normalized to $P'(Q, L, l_b) \xrightarrow[Q \rightarrow 0]{} L^2$

¹The Kuhn length l_b is related to the length a of locally stiff segment simply via $l_b = 2a$

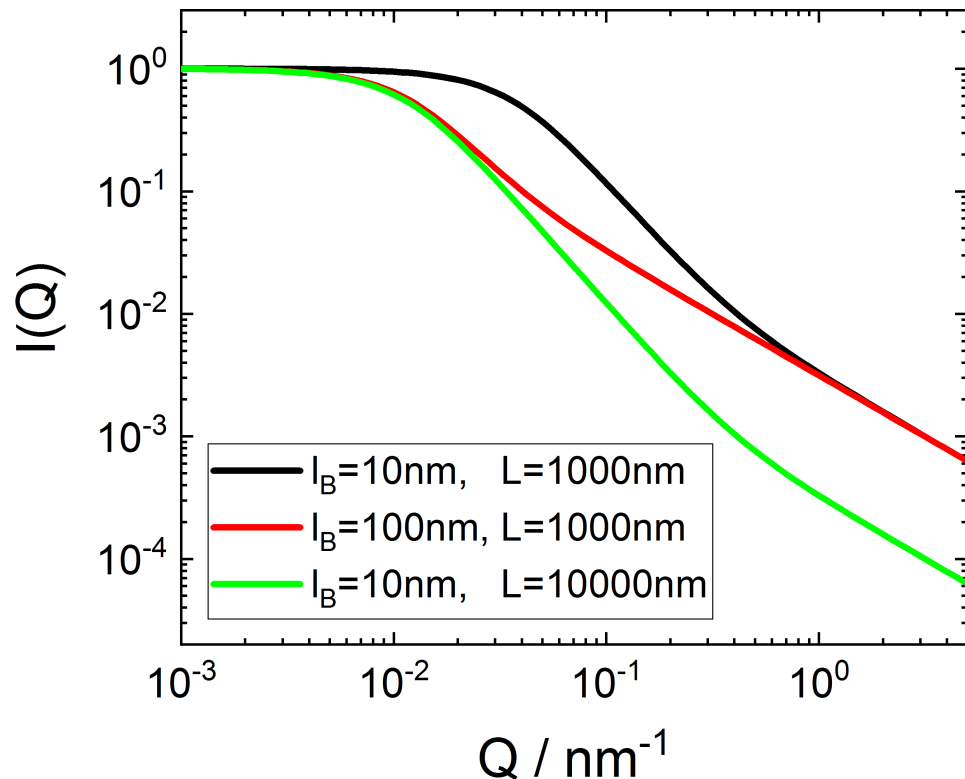


FIGURE 9.36. Scattering curve for the structure factor "P' (Q) : Kholodenko worm" alone without $P_{\text{cs}}(Q)$.

9.2.4.5. $P'(Q)$: wormlike PS1.

For worm-like micelles J.S. Pedersen [380] has developed three models, from which one is basing on a method developed by Yoshizaki et al. [537]. This first version has been developed both with and without excluded volume effects.

Without Excluded Volume Effects.

This first of the three solutions given by J.S. Pedersen [380] for worm-like micelles starts from the expression for the scattering function as follows:

$$S_{\text{WC}}(Q, L, l_B) = L^2 [(1 - \chi(Q, L, l_B)) S_{\text{chain}}(Q, L, l_B) + \chi(Q, L, l_B) S_{\text{rod}}(Q, L)] \Gamma(Q, L, l_B) \quad (9.66)$$

where $S_{\text{chain}}(Q, L, l_B)$ is the scattering function of a flexible chain without excluded volume effects and $S_{\text{rod}}(Q, L)$ is the scattering function of a rod. Furthermore, $\chi(Q, L, l_b)$ is a crossover function, and the function $\Gamma(q, L, b)$ corrects the crossover region. The function $S_{\text{chain}}(Q, L, l_B)$ is given by the Debye function:

$$S_{\text{chain}}(Q, L, l_B) = S_{\text{Debye}}(Q, L, l_B) = 2 [\exp(-u) + u - 1] / u^2 \quad (9.67)$$

with $u = \langle R_g^2 \rangle_0 Q^2$, where $\langle R_g^2 \rangle_0$ is the ensemble average of the square of the radius of gyration and given by

$$\langle R_g^2 \rangle_0 = \frac{Ll_B}{6} \left[1 - \frac{3}{2n_B} + \frac{3}{2n_B^2} - \frac{3}{4n_B^3} [1 - \exp(-2n_B)] \right] \quad (9.68)$$

where $n_B = L/l_B$ b is the number of statistical segments of the chain. The function $S_{\text{rod}}(Q, L)$ in 9.66 is the scattering function of an infinitely thin rod

$$S_{\text{rod}}(Q, L) = 2\text{Si}(Q, L)/(QL) - 4 \sin^2(QL/2)/(QL)^2 \quad (9.69)$$

where

$$\text{Si}(Q, L) = \int_0^x t^{-1} \sin t \, dt \quad (9.70)$$

Furthermore we have

$$\chi(Q, L, l_B) = \exp(-\xi^{-5}) \quad (9.71)$$

The parameter ξ is given by

$$\xi = Q \frac{\pi}{2L} \langle R_g^2 \rangle_0 \quad (9.72)$$

The function $\Gamma(Q, L, l_B)$ is given by

$$\Gamma(Q, L, l_B) = 1 + (1 - \chi) \sum_{i=2}^5 A_i \xi^i + \chi \sum_{i=0}^2 B_i \xi^{-i} \quad (9.73)$$

TABLE 1. Values for the parameters in the numerical expressions for the scattering function for worm-like chains **without** excluded volume effects [380]

$a1(2, 0)$	0.3054		$b_1(0, 0)$	-0.0162			
$a1(3, 0)$	0.05777		$b_1(1, 0)$	0.09046			
$a1(4, 0)$	-0.00604		$b_1(2, 0)$	0.1213			
$a1(5, 0)$	-0.03902		$b_1(0, 1)$	-0.3565	$b_2(0, 1)$	-0.3946	
$a1(2, 1)$	0.2316	$a2(2, 1)$	-0.4963	$b_1(1, 1)$	0.1909	$b_2(1, 1)$	-0.2231
$a1(3, 1)$	0.26531	$a2(3, 1)$	0.03688	$b_1(2, 1)$	0.15634	$b_2(2, 1)$	-0.2546
$a1(4, 1)$	0.3706	$a2(4, 1)$	0.30570	$b_1(0, 2)$	-0.3078	$b_2(0, 2)$	1.1361
$a1(5, 1)$	-1.0081	$a2(5, 1)$	0.39013	$b_1(1, 2)$	0.05176	$b_2(1, 2)$	-0.01615
$a1(2, 2)$	-22.779	$a2(2, 2)$	-0.4678	$b_1(2, 2)$	0.01568	$b_2(2, 2)$	-0.07606
$a1(3, 2)$	23.2457	$a2(3, 2)$	0.3365				
$a1(4, 2)$	8.1092	$a2(4, 2)$	0.4290				
$a1(5, 2)$	-3.3603	$a1(5, 2)$	0.3737				

where

$$A_i = \sum_{j=0}^2 a_1(i, j) \left(\frac{L}{l_B}\right)^{-j} \exp(-10l_B/L) + \sum_{j=1}^2 a_2(i, j) \left(\frac{L}{l_B}\right)^j \exp(-2L/l_B) \quad (9.74)$$

and

$$B_i = \sum_{j=0}^2 b_1(i, j) \left(\frac{L}{l_B}\right)^{-j} + \sum_{j=1}^2 b_2(i, j) \left(\frac{L}{l_B}\right)^j \exp(-2L/l_B) \quad (9.75)$$

The values of $a_1(i, j)$, $a_2(i, j)$, $b_1(i, j)$, and $b_2(i, j)$ are listed in table 1

With Excluded Volume Effects.

To include excluded volume effects in eq. 9.66 the function for a flexible chain $S_{\text{chain}}(Q, L, l_B)$ needs to be replaced by one with excluded volume effects included

$$S_{\text{WC}}(Q, L, l_B) = L^2 [(1 - \chi(Q, L, l_B)) S_{\text{exv}}(Q, L, l_B) + \chi(Q, L, l_B) S_{\text{rod}}(Q, L)] \Gamma(Q, L, l_B) \quad (9.76)$$

The scattering of a chain with excluded volume effects is given by

$$S_{\text{exv}}(Q, L, l_B) = w(Q, R_g) S_{\text{Debye}}(Q, L, l_B) + [1 - w(qR_g) [C_1 (QR_g)^{-1/\nu} + C_2 (QR_g)^{-2/\nu} + C_3 (QR_g)^{-3/\nu}]] \quad (9.77)$$

where $S_{\text{Debye}}(Q, L, l_B)$ is given by eq. 9.67 and

$$R_g^2 = \alpha(L/l_B)^2 \langle R_g^2 \rangle_0 \quad (9.78)$$

with $\alpha(L/l_B)$ being an expansion factor following the expression:

$$\alpha(x)^2 = [1 + (x/3.12)^2 + (x/8.67)^3]^{\epsilon/3} \quad (9.79)$$

and $\epsilon = 0.170$. The function $w(x)$ is another emical cross-over function chosen as:

$$w(x) = \left[1 + \tanh \left(\frac{x - C_4}{C_5} \right) / C_5 \right] / 2 \quad (9.80)$$

The parameters C_i have been given in [380] as $C_1 = 1.220$, $C_2 = 0.4288$, $C_3 = -1.651$, $C_4 = 1.523$, and $C_5 = 0.1477$.

Furthermore the parameter ξ in the cross-over function $\chi(Q, L, l_B)$ needs to be chosen as

$$\xi = Ql_B \left(\frac{\pi l_B}{1.103L} \right)^{3/2} \left[\frac{R_g^2}{l_B^2} \right]^{1.282} \quad (9.81)$$

with R_g^2 defined in eq. 9.78. Last, but not least the values of $a_1(i, j)$, $a_2(i, j)$, $b_1(i, j)$, and $b_2(i, j)$ need to be taken from table 2.

Input Parameters for model P' (Q) Worm(PS1) (with excluded volume effects):

1b: Kuhn length² l_B of semi-flexible worm-like structure

L: contour length L of semi-flexible worm-like structure

exvol: input flag to select the variant with or without excluded volume effects: $\text{exvol} \geq 1$ with excluded volume effects, $\text{exvol} < 1$ without excluded volume effects

Note

- This structure factor is supposed to be combined with a form factor with local cylindrical geometry which are implemented as form factor plugins under "[by plugin|thin obj.|Pcs(Q): local cylindrical obj.]".

²The Kuhn length l_b is related to the length a of locally stiff segment simply via $l_b = 2a$

TABLE 2. Values for the parameters in the numerical expressions for the scattering function for worm-like chains **with** excluded volume effects [380]

$a1(2, 0)$	-0.1222		$b_1(0, 0)$	-0.0699			
$a1(3, 0)$	0.3051		$b_1(1, 0)$	-0.0900			
$a1(4, 0)$	-0.0711		$b_1(2, 0)$	0.2677			
$a1(5, 0)$	0.0584		$b_1(0, 1)$	0.1342	$b_2(0, 1)$	-0.5171	
$a1(2, 1)$	1.761	$a2(2, 1)$	0.1212	$b_1(1, 1)$	0.0138	$b_2(1, 1)$	-0.2028
$a1(3, 1)$	2.252	$a2(3, 1)$	-0.4169	$b_1(2, 1)$	0.1898	$b_2(2, 1)$	-0.3112
$a1(4, 1)$	-1.291	$a2(4, 1)$	0.1988	$b_1(0, 2)$	-0.2020	$b_2(0, 2)$	0.6950
$a1(5, 1)$	0.6994	$a2(5, 1)$	0.3435	$b_1(1, 2)$	-0.0114	$b_2(1, 2)$	-0.3238
$a1(2, 2)$	-26.04	$a2(2, 2)$	0.0170	$b_1(2, 2)$	0.0123	$b_2(2, 2)$	-0.5403
$a1(3, 2)$	20.00	$a2(3, 2)$	-0.4731				
$a1(4, 2)$	4.382	$a2(4, 2)$	0.1869				
$a1(5, 2)$	1.594	$a1(5, 2)$	0.3350				

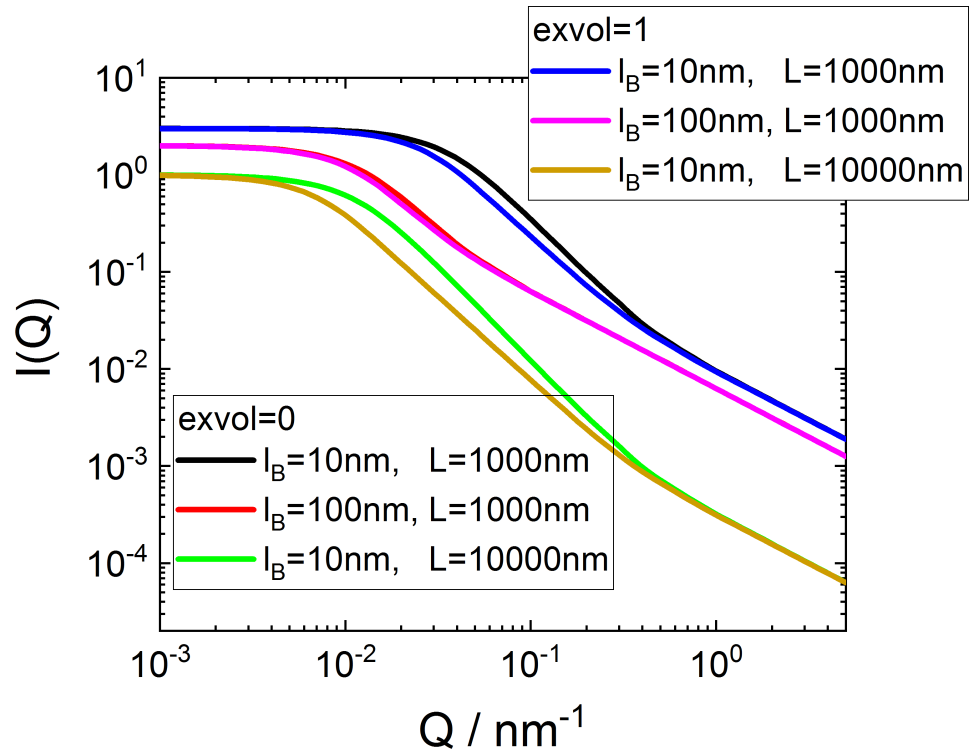


FIGURE 9.37. Scattering curve for the structure factor "P'(Q) : Worm(PS1)" alone without $P_{cs}(Q)$.

9.2.4.6. $P'(Q)$: wormlike PS2.

For this version of the wormlike structure [380] parameterized the structure factor in one for long and short wormlike micelles depending on their ratio $n_b = \frac{L}{l_B}$ is larger or smaller than 2.

$$S_{\text{PS2}}(Q, L, l_B) = L^2 \begin{cases} S_{\text{SB}}(Q, L, l_B)f_1 + S_{\text{loc}}(Q, L, l_B)1(1 - f_1) & \text{for } n_b > 2 \\ S_{\text{Debye}}(Q, Q^2 \langle R_g^2 \rangle_0)f_2 + S_{\text{loc}}(Q, L, l_B, a_1)(1 - f_2) & \text{for } n_b \leq 2 \end{cases} \quad (9.82)$$

with $\langle R_g^2 \rangle_0 = Ll_B/6 \left(1 - \frac{3}{2n_b} + \frac{3}{2n_b^2} - \frac{3}{4n_b^3} [1 - \exp(-2n_b)] \right)$. The transition functions are defined as

$$f_1 = \exp \left[- \left(\frac{Ql_B}{q_1} \right)^{p_1} \right] \quad (9.83)$$

$$f_2 = \exp \left[- \left(\frac{Ql_B}{q_2} \right)^{p_2} \right] \quad (9.84)$$

The Debye function is given by

$$S_{\text{Debye}}(Q, u) = 2 [\exp(-u) + u - 1] / u^2 \quad (9.85)$$

For large wormlike micelles in the small Q region the scattering function calculated for the Daniels approximation [95] according to [451, 380] is

$$S_{\text{SB}}(Q, L, l_B) = S_{\text{Debye}}(Q, Q^2 R_g^2) + \frac{\left[\frac{4}{15} + \frac{7}{15u} - \left(\frac{11}{15} + \frac{7}{15u} \right) \exp(-u) \right]}{n_b} \quad (9.86)$$

$$R_g^2 = Ll_B/6 \quad (9.87)$$

and in the large Q range

$$S_{\text{loc}}(Q, L, l_B, a_1) = \frac{a_1}{Ll_B Q^2} + \frac{\pi}{LQ} \quad (9.88)$$

The optimized values of the parameters q_1, p_1, a_1, a_2, q_2 , and p_2 are $q_1 = 5.53$, $p_1 = 5.33$, $a_1 = 0.0625$, $a_2 = 11.7$, $p_2 = 3.95$ and $q_2 = a_2/n_b$.

Input Parameters for model P' (Q) Worm(PS2) (always without excluded volume effects):

1b: Kuhn length³ l_B of semi-flexible worm-like structure

L: contour length L of semi-flexible worm-like structure

Note

- This structure factor is supposed to be combined with a form factor with local cylindrical geometry which are implemented as form factor plugins under "[by plugin|thin obj.|Pcs(Q): local cylindrical obj.]".

³The Kuhn length l_b is related to the length a of locally stiff segment simply via $l_b = 2a$

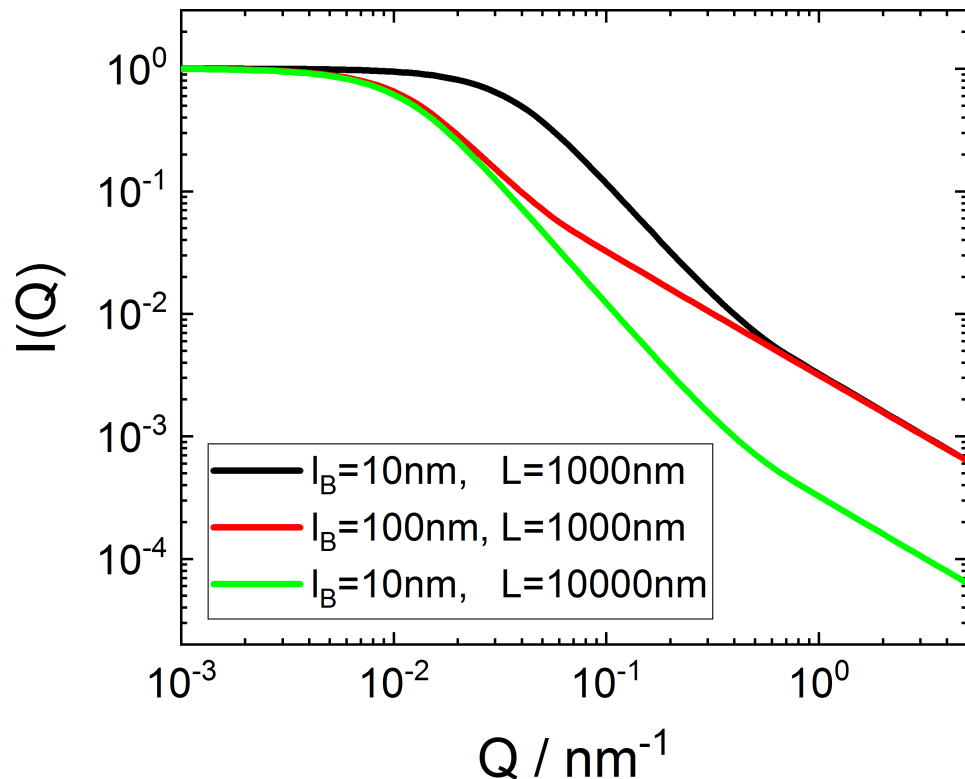


FIGURE 9.38. Scattering curve for the structure factor "P'(Q): Worm(PS2)" alone without $P_{\text{cs}}(Q)$.

9.2.4.7. $P'(Q)$: wormlike PS3.

This version of the worm-like structure model originally from [380] is implemented together with the suggestions for corrections given in [87].

$$q_0 = \begin{cases} 3.1 & \text{for } L > 4l_B \\ \max \{a_3 l_B / R_G, 4\} & \text{for } L \leq 4l_B \wedge \text{without excl. vol.} \\ \max \{a_3 l_B / R_G, 3\} & \text{for } L \leq 4l_B \wedge \text{with excl. vol.} \end{cases} \quad (9.89)$$

$$R_G^2 = \begin{cases} \frac{Ll_B}{6} & \text{for } L > 4l_B \wedge \text{without excl. vol.} \\ \frac{Ll_B}{6} f\left(\frac{L}{l_B}\right) & \text{for } L > 4l_B \wedge \text{with excl. vol.} \\ \frac{Ll_B}{6} f\left(\frac{L}{l_B}\right) & \text{for } L \leq 4l_B \wedge \text{without excl. vol.} \\ \frac{Ll_B}{6} f\left(\frac{L}{l_B}\right) \alpha^2\left(\frac{L}{l_B}\right) & \text{for } L \leq 4l_B \wedge \text{with excl. vol.} \end{cases} \quad (9.90)$$

$$f(x) = 1 - \frac{3}{2x} + \frac{3}{2(x)^2} - \frac{3}{4(x)^3} [1 - \exp(-2x)] \quad (9.91)$$

$$\alpha(x) = \left(1 + (x/3.12)^2 + (x/8.67)^3\right)^{\epsilon/3} \quad (9.92)$$

$$\epsilon = 0.170 \quad (9.93)$$

$$C\left(\frac{L}{l_B}\right) = \begin{cases} a_4 / \left(\frac{L}{l_B}\right)^{p_3} & \text{for } L > 10l_B \wedge \text{with excl. vol.} \\ 1 & \text{otherwise} \end{cases} \quad (9.94)$$

with $a_3 = 2.02$, $a_4 = 3.06$, and $p_3 = 0.44$.

$$S(Q, L, l_B) = L^2 \begin{cases} L^2 S_{\text{small } Q}(Q, L, l_B) & \text{for } Ql_B < q_0 \\ L^2 \left(\frac{a_1}{(Ql_B)^{p_1}} + \frac{a_2}{(Ql_B)^{p_2}} + \frac{\pi}{QL}\right) & \text{for } Ql_B \geq q_0 \end{cases} \quad (9.95)$$

$$p_1 = \begin{cases} 4.95 & \text{for } L > 4l_B \wedge \text{without excl. vol.} \\ 5.13 & \text{for } L \leq 4l_B \wedge \text{without excl. vol.} \\ 4.12 & \text{for } L > 4l_B \wedge \text{with excl. vol.} \\ 5.36 & \text{for } L \leq 4l_B \wedge \text{with excl. vol.} \end{cases} \quad (9.96)$$

$$p_2 = \begin{cases} 5.29 & \text{for } L > 4l_B \wedge \text{without excl. vol.} \\ 7.47 & \text{for } L \leq 4l_B \wedge \text{without excl. vol.} \\ 4.42 & \text{for } L > 4l_B \wedge \text{with excl. vol.} \\ 5.62 & \text{for } L \leq 4l_B \wedge \text{with excl. vol.} \end{cases} \quad (9.97)$$

The parameters a_1 and a_2 are defined by the condition that for $Ql_B = q_0$ the small and large Q region are continuous and smooth, i.e. that also the first derivative of $dS(q, L, l_B)/dq|_{q=q_0/l_B}$ is continuous.

$$S_{\text{small } Q}(Q, L, l_B) = \begin{cases} S_{\text{SB}}(Q, R_G) & \text{for } L > 4l_B \\ S_{\text{Debye}}(Q, R_G) & \text{for } L \leq 4l_B \wedge \text{without excl. vol.} \\ S_{\text{cexv}}(Q, R_G) & \text{for } L \leq 4l_B \wedge \text{with excl. vol.} \end{cases} \quad (9.98)$$

where

$$S_{\text{SB}}(Q, R_G) = S_{\text{Debye}}(Q, Q^2 R_g^2) + \frac{\left[\frac{4}{15} + \frac{7}{15u} - \left(\frac{11}{15} + \frac{7}{15u}\right) \exp(-u)\right]}{L/l_B} \quad (9.99)$$

$$S_{\text{Debye}}(Q, R_G) = 2(\exp(-u) + u - 1)/u^2 \quad (9.100)$$

$$S_{\text{cexv}}(Q, R_G) = S_{\text{EXV}}(Q, R_G) + C \left(\frac{L}{l_B}\right) \frac{\frac{4}{15} + \frac{7}{15u} - \left(\frac{11}{15} + \frac{7}{15u}\right) \exp(-u)}{L/l_B} \quad (9.101)$$

$$u = Q^2 R_G^2 \quad (9.102)$$

$$x = QR_G \quad (9.103)$$

$$S_{\text{EXV}}(Q, R_G) = (1 - w) S_{\text{Debye}}(Q, R_G) \quad (9.104)$$

$$\begin{aligned} &+ wf_{\text{corr}}(Q) (C_1 x^{-1/\nu} + C_2 x^{-2/\nu} + C_3 x^{-3/\nu}) \\ w = \frac{1}{2} (1 + \tanh((x - 1.523)/0.1477)) \end{aligned} \quad (9.105)$$

with the optimized parameters $C_1 = 1.2220$, $C_2 = 0.4288$, and $C_3 = -1.651$. As S_{EXV} should be a monotonic decreasing function also at very small Q -values the correction factor $f_{\text{corr}}(Q, R_G)$ has been introduced by [87]

$$f_{\text{corr}}(Q, R_G) = \begin{cases} 1 & \text{for } \frac{dS_{\text{cexv}}(Q, R_G)}{dQ} \leq 0 \\ 0 & \text{otherwise} \end{cases} \quad (9.106)$$

Input Parameters for model P'(Q) Worm(PS3) (with/without excluded volume effects):

1b: Kuhn length⁴ l_B of semi-flexible worm-like structure

L: contour length L of semi-flexible worm-like structure

exvol: input flag to select the variant with or without excluded volume effects: exvol ≥ 1 with excluded volume effects, exvol < 1 without excluded volume effects

Note

- This structure factor is supposed to be combined with a form factor with local cylindrical geometry which are implemented as form factor plugins under "[by plugin|thin obj.|Pcs(Q): local cylindrical obj.]".

⁴The Kuhn length l_b is related to the length a of locally stiff segment simply via $l_b = 2a$

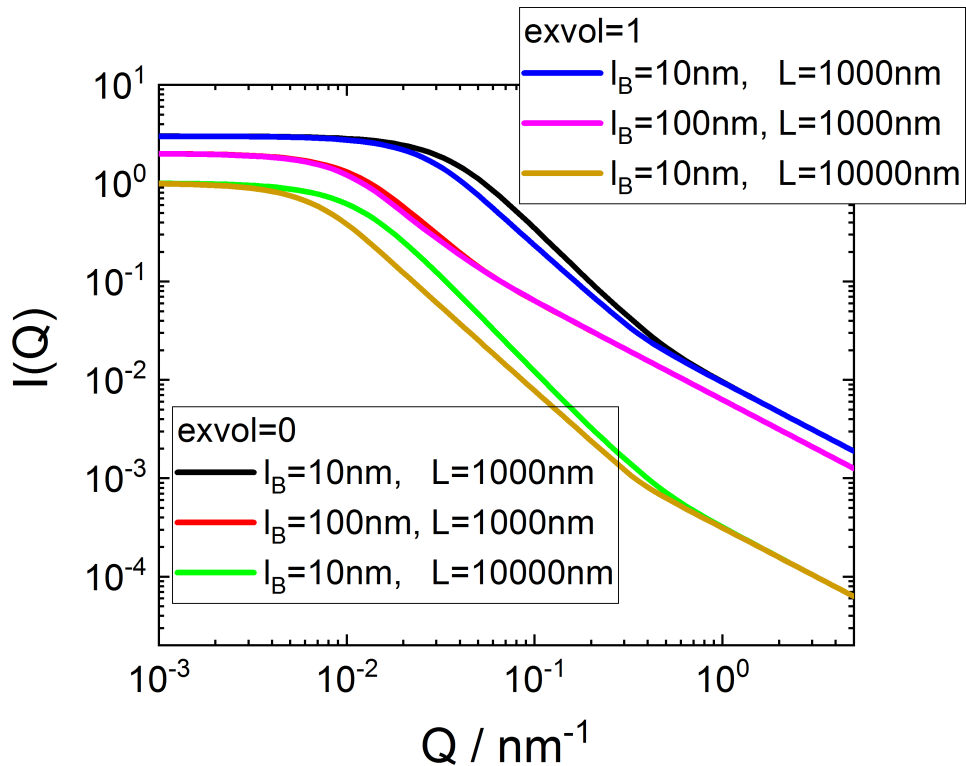


FIGURE 9.39. Scattering curve for the structure factor "P'(Q): Worm(PS3)" alone without $P_{cs}(Q)$.

9.2.4.8. $P'(Q)$: semi-dilute wormlike PS3.

For describing the structure factor of interacting worm-like micelles the RPA (random phase approximation) and PRISM (polymer reference interaction site model) approach has been used [382, 241, 76, 77, 381, 377]. The corresponding structure factors are

$$S_{\text{RPA}}(q) = \frac{1}{1 + \beta P_{\text{WLM}}(q)} \quad (9.107)$$

$$S_{\text{PRISM}}(q) = \frac{1}{1 + \beta c(q) P_{\text{WLM}}(q)} \quad (9.108)$$

with $\beta = (1 - S(0))/S(0)$. For the structure factor the worm-like model in section 9.2.4.7 has been used including an exponential contour length distribution so that

$$P_{\text{WLM}}(q) \int_0^\infty \frac{1}{\langle L \rangle} \exp(-L/\langle L \rangle) P'(q, L, l_B) dL \quad (9.109)$$

with $P'(q, L, l_B)$ given by eq. 9.95. The exponential length distribution describes well the the contour length distribution of the worm-like micelles and has the additional advantage not to introduce an additional parameter.

Depending on the regime of Coulomb interaction different approximations for $c(q)$ have been favored and confirmed both by experiment and MC simulations:

- micelles which are neutral or in solutions with high salt concentrations
For these micelles either the RPA approximation or the PRISM approximation has been used with

$$c(q) = \left[2\text{Si}(qL_c)/(qL_c) - 4 \sin^2(qL_c/2)/(qL_c)^2 \right] \quad (9.110)$$

where L_c is the characteristic length of the function, with magnitude between the overall size of the chains and the cross-section dimension of the micelle. The forward scattering is written as a function of a reduced concentration $X \approx c/c^*$

$$\begin{aligned} S^{-1}(0) &= 1 + \frac{1}{8} \left(9X - 2 + \frac{2 \ln(1+X)}{X} \right) \\ &\quad \exp \left(\frac{1}{2.565} \left[\frac{1}{X} + \left(1 - \frac{1}{X^2} \right) \ln(1+X) \right] \right) \end{aligned} \quad (9.111)$$

- highly charged micelles at high ionic strength

$$c(q) = \frac{\sin q2R' - q2R' \cos q2R'}{(q2R')^3} \quad (9.112)$$

with $R' \approx R + \lambda_D$, where λ_D is the Debye screening length. The forward scattering is given by

$$S(0) = \frac{(1 - B - C)^4}{[1 + 2(B + C)]^2 + 2D[1 + B + \frac{5}{4}C]} \quad (9.113)$$

where $B = \pi R^2 L n$, $C = \frac{4}{3}\pi R^3 n$, $D = \frac{1}{2}\pi R L^2 n$, with n being the number density of micelles.

- ionic micelles interacting with a screened Coulomb potential

$$c(q) = \frac{\sin qR_c}{qR_c} \exp(-\sigma^2 q^2) \quad (9.114)$$

with $R_c = 2 \ln \sigma + 2$. The forward scattering follow a behaviour similar to neutral chains with

$$S^{-1}(0) = 1 + \frac{1}{8} \left(9X - 2 + \frac{2 \ln(1+X)}{X} \right) \exp \left(0.8 \left[\frac{1}{X} + \left(1 - \frac{1}{X^2} \right) \ln(1+X) \right] \right) \quad (9.115)$$

where $X \approx 42.1\eta_r$ with

$$\eta_r = \left(\frac{\lambda_D + R}{R} \right) \left(\frac{R_g}{R_{g,u}} \right)^3 \eta \quad (9.116)$$

In this expression, R_g is the radius of gyration of the chains and $R_{g,u}$ is the radius of gyration of the uncharged chains of the same length, and η is the volume fraction of the chains.

9.2.5. local planar obj.

A few selected combinations of the cross-sections $P_{\text{cs}}(Q)$ and shape factors $P'(Q)$ have been collected for thin planar objects in this subsection to give access to structure factor effects on these systems. The list can easily be extended on request.

9.2.5.1. Disc+SD+BiLayerGauss.

In this form factor the cross section term of a lipid bilayer (eq. 9.20) is combined with a shape factor of a disc (eq. 9.39).

Input Parameters for model Disc+SD+BiLayerGauss:

t: most probable layer distance between layer centers t
sigma_t: width of distance distribution σ_t
R0: most probable disc radius R_0
sigma_R0: width of radii distribution σ_{R_0}
dummy: not used
dummy: not used
sigma_out: width of scattering density distribution in the head groups of the lipids forming the outer layers of the bilayer σ_{out}
b_out: excess scattering length of the head groups b_{out}
sigma_core: width of scattering density distribution in the tail groups of the lipids forming the core of the bilayer σ_{core}
b_core: excess scattering length of the tail groups b_{core}

9.2.5.2. Disc+SD+homoXS.

In this form factor the cross section term of a homogeneous plate (eq. 9.14) is combined with a shape factor of a disc (eq. 9.39).

Input Parameters for model Disc+SD+homoXS:

t: most probable layer thickness t
sigma_t: width of thickness distribution σ_t
R0: most probable disc radius R_0
sigma_R0: width of radii distribution σ_{R_0}
dummy: not used
dummy: not used
eta_l: scattering length density of layer η_l
eta_sol: scattering length density of solvent η_{sol}

9.2.5.3. EllSh+SD+BiLayerGauss.

In this form factor the cross section term of a lipid bilayer (eq. 9.20) is combined with a shape factor of a thin ellipsoidal shell (eq. 9.43).

Input Parameters for model EllSh+SD+BiLayerGauss:

t: most probable layer distance between layer centers t
sigma_t: width of distance distribution σ_t
R0: most probable disc radius R_0
sigma_R0: width of radii distribution σ_{R_0}
epsilon: stretching factor
dummy: not used
sigma_out: width of scattering density distribution in the head groups of the lipids forming the outer layers of the bilayer σ_{out}
b_out: excess scattering length of the head groups b_{out}
sigma_core: width of scattering density distribution in the tail groups of the lipids forming the core of the bilayer σ_{core}
b_core: excess scattering length of the tail groups b_{core}

9.2.5.4. *EllSh+SD+homoXS.*

In this form factor the cross section term of a homogeneous plate (eq. 9.14) is combined with a shape factor of a thin ellipsoidal shell (eq. 9.43).

Input Parameters for model EllSh+SD+homoXS:

t: most probable layer thickness t
sigma_t: width of thickness distribution σ_t
R0: most probable disc radius R_0
sigma_R0: width of radii distribution σ_{R_0}
epsilon: stretching factor
dummy: not used
eta_l: scattering length density of layer η_l
eta_sol: scattering length density of solvent η_{sol}

9.2.5.5. *CylSh+SD+BiLayerGauss.*

In this form factor the cross section term of a lipid bilayer (eq. 9.20) is combined with a shape factor of a thin walled cylinder with closed ends (eq. 9.46).

Input Parameters for model CylSh+SD+BiLayerGauss:

t: most probable layer distance between layer centers t

sigma_t: width of distance distribution σ_t
R0: most probable cylinder radius R_0
sigma_R0: width of radii distribution σ_{R_0}
R0: most probable cylinder height H_0
sigma_H0: width of height distribution σ_{H_0}
sigma_out: width of scattering density distribution in the head groups of the lipids
 forming the outer layers of the bilayer σ_{out}
b_out: excess scattering length of the head groups b_{out}
sigma_core: width of scattering density distribution in the tail groups of the lipids
 forming the core of the bilayer σ_{core}
b_core: excess scattering length of the tail groups b_{core}

9.2.5.6. *CylSh+SD+homoXS*.

In this form factor the cross section term of a homogeneous plate (eq. 9.14) is combined with a shape factor of a thin walled cylinder with closed ends (eq. 9.46).

Input Parameters for model CylSh+SD+homoXS:

t: most probable layer thickness t
sigma_t: width of thickness distribution σ_t
R0: most probable cylinder radius R_0
sigma_R0: width of radii distribution σ_{R_0}
R0: most probable cylinder height H_0
sigma_H0: width of height distribution σ_{H_0}
eta_l: scattering length density of layer η_l
eta_sol: scattering length density of solvent η_{sol}

9.2.6. local cylindrical obj.

A few selected combinations of the cross-sections $P_{\text{cs}}(Q)$ and shape factors $P'(Q)$ have been collected for thin cylindrical objects in this subsection to give access to structure factor effects on these systems. The list can easily be extended on request.

9.2.6.1. Rod+SD+EllCylSh.

In this form factor the cross section term of a homogeneous plate (eq. ??) is combined with a shape factor of a infinitesimal thin rod of length L (eq. 9.47).

Input Parameters for model Rod+SD+EllCylSh:

R0: most probable core radius R_0

sigma_R0: width of core radius distribution σ_{R_0} (LogNorm)

epsilon: stretching factor ϵ of the elliptical cross-section

T0: most probable shell thickness t_0

sigma_t0: width of thickness distribution σ_{t_0} (LogNorm)

L0: most probable rod length L_0

sigma_L0: width of lengths distribution σ_{L_0} (LogNorm)

eta_core: scattering length density of core η_{core}

eta_shell: scattering length density of shell η_{shell}

eta_sol: scattering length density of solvent η_{sol}

9.2.7. Liposomal structures.

In this section some specialized spherical multi-shell structures are summarized which describe a few types of liposomal vesicular structures. The main characteristics of a vesicle are shown in fig. 9.40. In first approximation these vesicles are described as spherical shell structures, where the lipid hydrophobic tail groups from the core of the spherical membrane and the hydrophilic head groups the inner and outer shell of this spherical membrane. This containment has aqueous solution inside and outside. As the lipids are in general very well known one likes to extend the models of a bilayer as described in section 3.1.5 or 9.2.5.3 by known molecular constrains like in section 3.2.4 about diblock copolymer micelles.

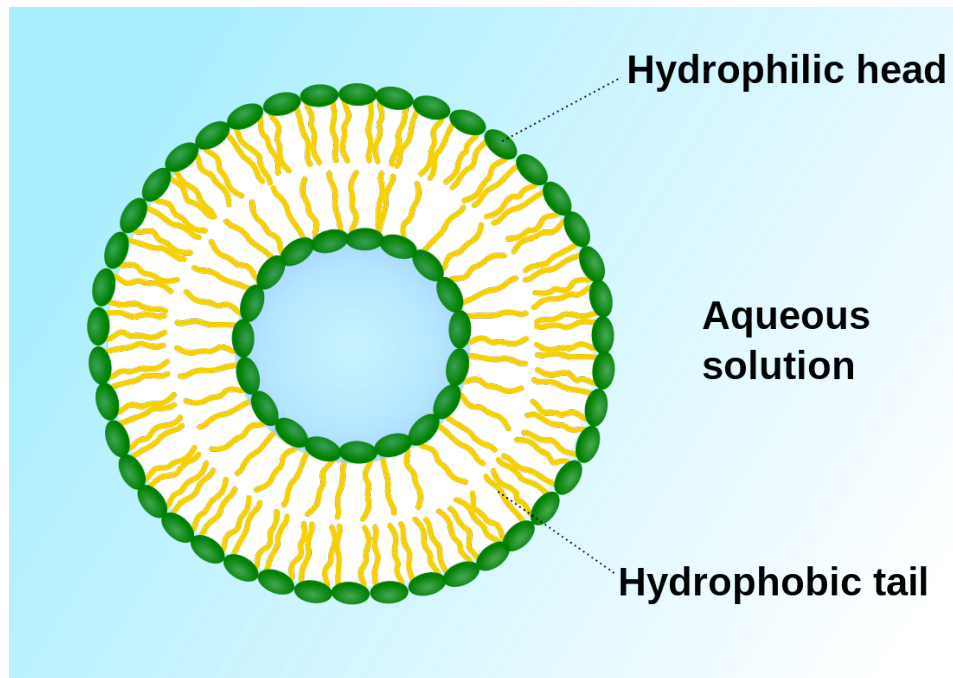


FIGURE 9.40. scheme of a liposomal vesicular structure

In pharmaceutical applications these vesicles are sometimes decorated with PEG molecules to increase their circulation time in a living body, as they give them a sort of stealth properties against the immune system. depending on the synthesis procedure the PEG molecules are either attached on both sides or mainly from the outside as shown in fig. 9.41.

The dimension in the vesicle are typically such, that the thickness of the bilayer is much smaller than the overall diameter of a micelle. Therefore next to a full 3D Fourier transform of the scattering length density profile also an approximation factorizing the contribution of the small object dimension and from the large object dimension can be performed. For very thin random orientated particles the form factor can be factorize according to Porod [393] in a cross section term $P_{cs}(Q)$ for the shorter or thin dimension and a shape factor $P'(Q)$ for the long dimension. For a small number of cross-section types and shapes these functions are supplied in section 9.2.1 and 9.2.3. In the

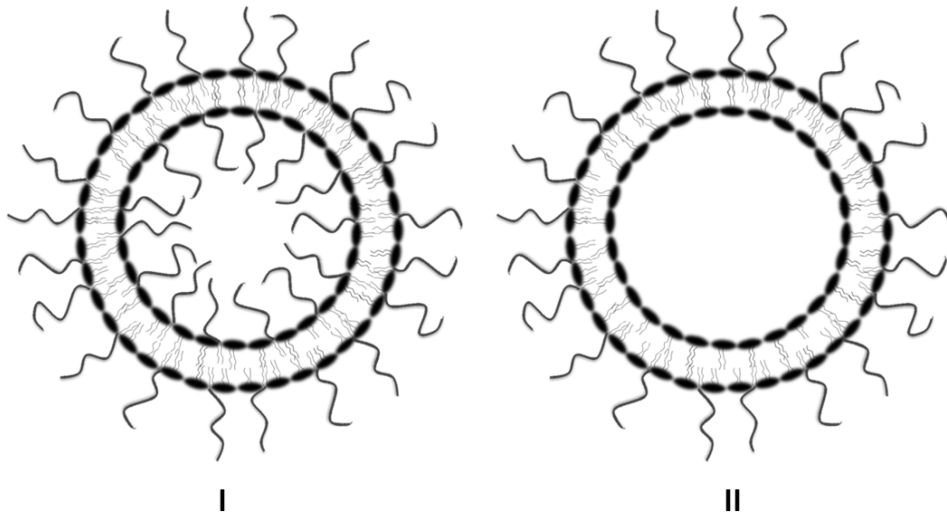


FIGURE 9.41. scheme of pegylated vesicle with PEG molecules both inside and outside or only outside the vesicle

cases discussed in this section knowledge about molecular properties are tried to taken into account by parameterizing the model by known molecular properties following the concept developed for block copolymer micelles [378].

9.2.7.1. PEGylated liposome with piecewise constant bilayer scattering length density profile.

This version of a pegylated vesicle is following the formalism used in [8] and [357]. The lipid bilayer is described in by spherical multi-shell model. Inside and outside the shell is solvent and the shell itself is formed by the lipids. The head groups point towards the solvent and the tail groups form the core like a centro-symmetric cross-section as shown in fig. 9.42. The scattering intensity can be described as

$$I(q) = I_{vv}(q) + I_{\text{chain}}(q) + I_{oo}(q) + I_{ii}(q) + I_{io}(q) + I_{vo}(q) + I_{vi}(q) \quad (9.117)$$

where $I_{vv}(q)$ is the scattering from the lipid vesicles themselves and $I_{\text{chain}}(q)$ is the scattering from the PEG-chains alone. The next terms, $I_{ii}(q)$ and $I_{oo}(q)$, are the interference terms between PEG chains attached to the inner surface of the vesicles and between the PEG chains on the outer surface, respectively, while $I_{io}(q)$ is the inter-interference between the inner and outer PEG chains. Furthermore, the terms $I_{vi}(q)$ and $I_{vo}(q)$ are the interference cross-terms of the inner and outer chains with the bilayer. These seven

terms can be written as

$$I_{\text{chain}}(q) = (n_i + n_o)\beta_{\text{PEG}}^2 2 \frac{e^{-q^2 R_g^2} - 1 + q^2 R_g^2}{(qR_g)^4} \quad (9.118)$$

$$I_{oo}(q) = n_o(n_o - 1)\beta_{\text{PEG}}^2 \left[\frac{1 - e^{-q^2 R_g^2}}{q^2 R_g^2} \right]^2 \left[\frac{\sin(q(R_o + H_o + R_g))}{q(R_o + H_o + R_g)} \right]^2 \quad (9.119)$$

$$I_{ii}(q) = n_i(n_i - 1)\beta_{\text{PEG}}^2 \left[\frac{1 - e^{-q^2 R_g^2}}{q^2 R_g^2} \right]^2 \left[\frac{\sin(q(R_i - H_i - R_g))}{q(R_i - H_i - R_g)} \right]^2 \quad (9.120)$$

$$I_{io}(q) = 2n_i n_o \beta_{\text{PEG}}^2 \left[\frac{1 - e^{-q^2 R_g^2}}{q^2 R_g^2} \right]^2 \left[\frac{\sin(q(R_i - H_i - R_g))}{q(R_i - H_i - R_g)} \right] \left[\frac{\sin(q(R_o + H_o + R_g))}{q(R_o + H_o + R_g)} \right] \quad (9.121)$$

$$F_{\text{sp}}(q, R) = 3 \frac{\sin qR - qR \cos qR}{(qR)^3} \quad (9.122)$$

$$\begin{aligned} F_{\text{bi,m}}(q) &= (\eta_h - \eta_{\text{sol}}) \left(\frac{4}{3}\pi(R_o + H_o)^3 F_{\text{sp}}(q, R_o + H_o) - \frac{4}{3}\pi R_o^3 F_{\text{sp}}(q, R_o) \right) \\ &\quad (\eta_t - \eta_{\text{sol}}) \left(\frac{4}{3}\pi R_o^3 F_{\text{sp}}(q, R_o) - \frac{4}{3}\pi R_i^3 F_{\text{sp}}(q, R_i) \right) \\ &\quad (\eta_h - \eta_{\text{sol}}) \left(\frac{4}{3}\pi R_i^3 F_{\text{sp}}(q, R_i) - \frac{4}{3}\pi(R_i - H_i)^3 F_{\text{sp}}(q, R_i - H_i) \right) \end{aligned} \quad (9.123)$$

$$I_{vv}(q) = F_{\text{bi,m}}^2(q) \quad (9.124)$$

$$I_{vi}(q) = 2n_i \beta_{\text{PEG}} F_{\text{bi,m}}(q) \frac{\sin(q(R_i - H_i - R_g))}{q(R_i - H_i - R_g)} \quad (9.125)$$

$$I_{vo}(q) = 2n_o \beta_{\text{PEG}} F_{\text{bi,m}}(q) \frac{\sin(q(R_o + H_o + R_g))}{q(R_o + H_o + R_g)} \quad (9.126)$$

$$\beta_{\text{PEG}} = (\eta_{\text{PEG}} - \eta_{\text{sol}}) V_{\text{PEG}} \quad (9.127)$$

The seven term are parameterized by the radius of gyration R_g of the PEG molecules, the thickness of the lipid head group layer on the inner side of the vesicle membrane H_i , as well as at the outside H_o , the radius pointing to the interface between head and tail group layer at the inside R_i and its counter part at the outside of the vesicle R_o . Further parameters are the excess scattering length of the PEG molecules β_{PEG} and the numbers of molecules n_i attached inside to the lipids and n_o attached outside to the lipids. η_h , η_t , and η_{sol} are the scattering length densities of the lipid head group, of the lipid tail group and of the solvent.

These parameters now needs to be expressed by known properties of the involved macro molecules. Scattering length densities are typically calculated from the known chemical sum formula and the bulk density of the molecules. The sum formula allows to calculate the molecular mass as well as the overall scattering length of the molecule, which then would allow to calculate the scattering length density of the molecule. However, in a solvent the molecular volume might change. Therefore volumetric measurements of the molecular volume in the used solvent are more precise and preferable, if

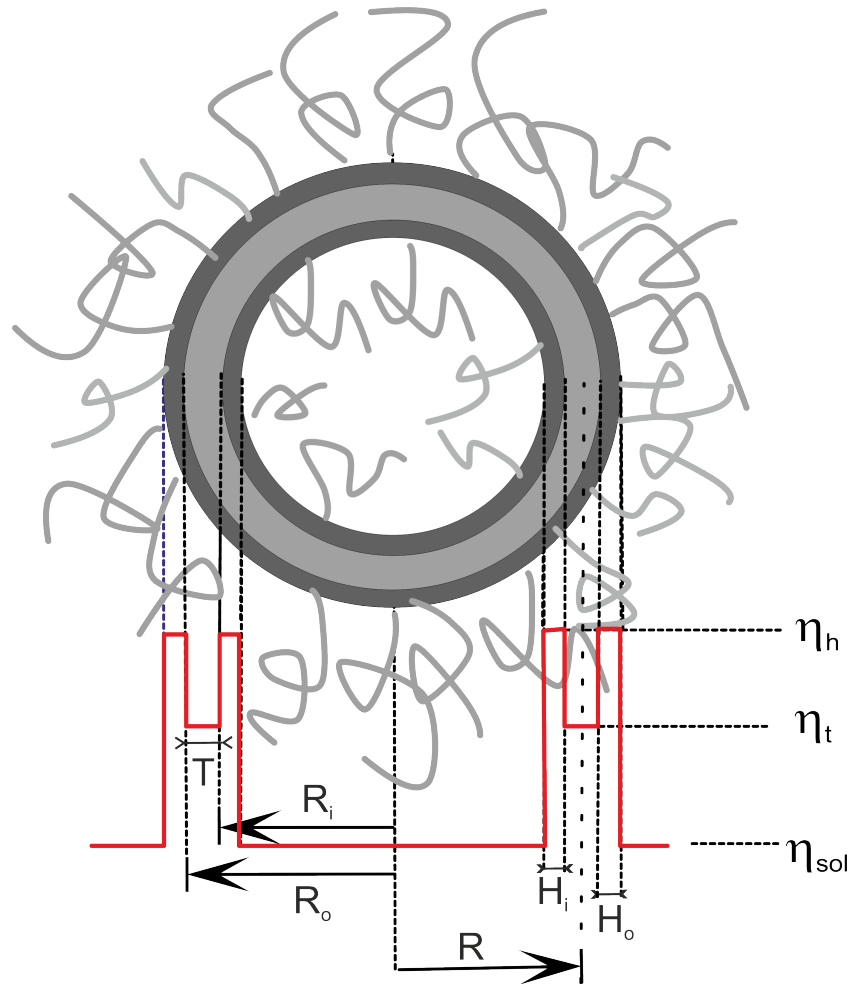


FIGURE 9.42. scheme of PEGylated vesicle with PEG molecules attached in as well outside the vesicle but otherwise a piecewise constant scattering cross section of the membrane

available. Also literature values for the molecular volume of the head group V_h separated from the molecular volume of the tail group V_t are available.

These molecular volumes then can be used to determine the number of lipids per vesicle and the relative volume of the head group shells and the tail core in the membrane layer. If the thickness T of the tail group layer and the radius of the vesicle R are given

the other quantities can be calculated by

$$R_i = R - \frac{T}{2} \quad (9.128)$$

$$R_o = R + \frac{T}{2} \quad (9.129)$$

$$n_{l,i} = \frac{4\pi}{3V_t} (R^3 - R_i^3) \quad (9.130)$$

$$n_{l,o} = \frac{4\pi}{3V_t} (R_o^3 - R^3) \quad (9.131)$$

$$V_{v,h,i} = n_{l,i} V_h \quad (9.132)$$

$$V_{v,h,o} = n_{l,o} V_h \quad (9.133)$$

$$n_i = n_{l,i} f_{PEG,i} \quad (9.134)$$

$$n_o = n_{l,o} f_{PEG,o} \quad (9.135)$$

$$H_i = R - \frac{T}{2} - \frac{1}{2} \left[(2R - T)^3 - (12R^2T - 6RT^2 + T^3) \frac{V_h}{V_t} \right]^{1/3} \quad (9.136)$$

$$H_o = -R - \frac{T}{2} + \frac{1}{2} \left[(2R + T)^3 + (12R^2T + 6RT^2 + T^3) \frac{V_h}{V_t} \right]^{1/3} \quad (9.137)$$

Further model input parameters are the fraction of lipids decorated with PEG inside the vesicle $f_{PEG,i}$ and outside the vesicle $f_{PEG,o}$. In this model it is assumed that neither the tail layer nor the head group layers contain any solvent. The distance of the center of mass for the attached PEG molecules is assumed to be equal to its radius of gyration R_g .

9.2.7.2. PEGylated liposome with smeared scattering length density profile.

In practise it could be shown [369, 57] that at least for x-rays the scattering length density profiles across a membrane are better modelled by a smooth transition and gaussian scattering length density profile have been suggested and successfully been used. However, using Gaussian profiles the use of known molecular parameters like molecular volume are not so straight forward to be integrated as constrains for the input parameters. Here we therefore introduce a smooth transition between the scattering length density of the hydrocarbon chain and the phospholipid head group as well as between the head group and the solvent. The transition can be performed with any sigmoidal function which smoothly varies between 0 and 1. In practice all cumulative distribution functions are such functions and are therefore typically used for this task

are

$$w_{\text{logistic}}(x) = \frac{1}{1 + \exp(-x)} \quad (9.138\text{a})$$

$$w_{\text{Laplace}}(x) = \begin{cases} \frac{1}{2} \exp(x), & \text{if } x \leq 0 \\ 1 - \frac{1}{2} \exp(-x), & \text{otherwise.} \end{cases} \quad (9.138\text{b})$$

$$w_{\text{Cauchy}}(x) = \frac{1}{\pi} \arctan(x) + \frac{1}{2} \quad (9.138\text{c})$$

$$w_{\text{Normal}}(x) = \frac{1}{2} [1 + \text{erf}(x/\sqrt{2})] \quad (9.138\text{d})$$

$$w_{\text{Rayleigh}}(x) = \begin{cases} 0, & \text{if } x \leq 0 \\ 1 - \exp(-x/\sqrt{2}), & \text{otherwise.} \end{cases} \quad (9.138\text{e})$$

$$w_{\text{algebraic}}(x) = \frac{1}{2} + \frac{1}{2} \frac{x}{\sqrt{1+x^2}} \quad \text{algebraic transition function} \quad (9.138\text{f})$$

$$w_{\text{Fermi}}(x) = 1 - \frac{1}{1 + \exp(x)} \quad (9.138\text{g})$$

$$w_{\text{Gudermannian}}(x) = \frac{2}{\pi} \arctan(\tanh(x/2)) + \frac{1}{2} \quad (9.138\text{h})$$

$$w_{\text{tanh}}(x) = \frac{1}{2} + \frac{1}{2} \tanh(x) \quad (9.138\text{i})$$

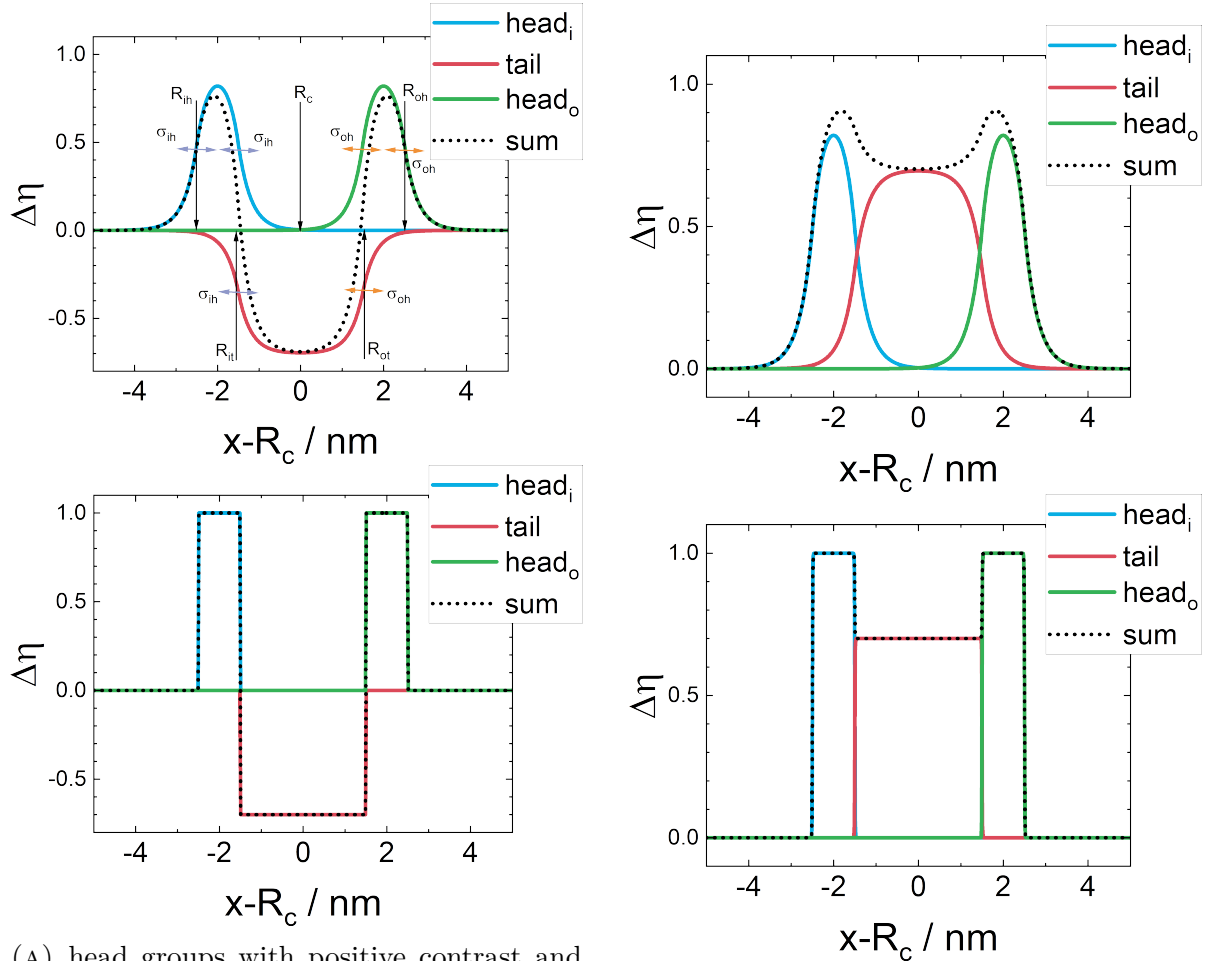
These transition function are here used to describe the rise and fall of the scattering length density profiles at interfaces. The scattering length density profile $\eta_{l,i}(x)$ of layer i is then given by

$$\eta_{l,\text{type},i}(x) = (\eta_i - \eta_{\text{sol}}) w_{\text{type},i} \left(\frac{x - R_i}{\sigma_i} \right) \left[1 - w_{\text{type},i+1} \left(\frac{x - R_{i+1}}{\sigma_{i+1}} \right) \right] \quad (9.139)$$

The falling profile $\left[1 - w_{\text{type},i+1} \left(\frac{x - R_{i+1}}{\sigma_{i+1}} \right) \right]$ of the i^{th} -layer is assumed being of the same type and with the same input parameters as the rising profile $w_{\text{type},i+1} \left(\frac{x - R_{i+1}}{\sigma_{i+1}} \right)$ of the $(i+1)^{\text{th}}$ -layer. By this we assume within the overlap region a mixture of the elements of both layers, with a smooth transition.

The scattering intensity for a smoothed profile contains the same contribution as for a piecewise constant profile according to equation 9.117. However, the scattering contribution $I_{\text{vv}}(q)$, as well as $I_{\text{vi}}(q)$ $I_{\text{vo}}(q)$ from the lipid vesicle needs to be calculated of layers with a smooth scattering length density profile according to eq. 9.139. In the following we use $w_{\text{Laplace}}(x)$ as for such a profile all needed Fourier transformations can be calculated analytically. The scattering length density profile of a lipid bilayer $\eta_{\text{bilayer}}(r)$ then reads as

$$\begin{aligned} \eta_{\text{bilayer}}(r) = & \eta_{l,\text{Laplace},ih}(r, \sigma_{ih}, R_{ih}, \sigma_{ih}, R_{it}, \eta_h, \eta_{\text{sol}}) \\ & + \eta_{l,\text{Laplace},t}(r, \sigma_{ih}, R_{it}, \sigma_{oh}, R_{ot}, \eta_t, \eta_{\text{sol}}) \\ & + \eta_{l,\text{Laplace},oh}(r, \sigma_{oh}, R_{ot}, \sigma_{oh}, R_{oh}, \eta_h, \eta_{\text{sol}}) \end{aligned} \quad (9.140)$$



(A) head groups with positive contrast and tail group with negative contrast relative to solvent. Top picture is calculated with smeared interfaces and bottom one with sharp interfaces.

(B) head and tail group have both positive contrast relative to solvent. Top picture is calculated with smeared interfaces and bottom one with sharp interfaces.

FIGURE 9.43. scattering length density profiles across liposome membrane

The scattering amplitude is the Fourier transform of this profile

$$F_{\text{bilayer}}(q) = \int_0^\infty 4\pi r^2 \eta_{\text{bilayer}}(r) \frac{\sin qr}{qr} dr \quad (9.141)$$

and can be performed fully analytically but is quite lengthy and has been obtained by a symbolic algebra software [230]. The overall volume of the tail groups as well as those of the headgroups in and outside the vesicles are obtained by integrating 9.139 and using

a scattering length density contrast of 1

$$V_{ih} = \int_0^{\infty} 4\pi r^2 \eta_{l,\text{Laplace},ih}(r) dr \quad (9.142)$$

$$V_t = \int_0^{\infty} 4\pi r^2 \eta_{l,\text{Laplace},t}(r) dr \quad (9.143)$$

$$V_{oh} = \int_0^{\infty} 4\pi r^2 \eta_{l,\text{Laplace},oh}(r) dr \quad (9.144)$$

As the form factor is parameterized in terms of the molecular volume of the head V_{head} and tail V_{tail} groups of a lipid molecule the following constraints need to be fulfilled

$$\frac{V_{ih}}{\frac{1}{2}V_t} = \frac{V_{\text{head}}}{V_{\text{tail}}} \quad (9.145)$$

$$\frac{V_{oh}}{\frac{1}{2}V_t} = \frac{V_{\text{head}}}{V_{\text{tail}}} \quad (9.146)$$

This is done by adapting the head group layer widths H_i and H_o using a root finding algorithm. Hereby $H_i = R - R_i$ and $H_o = R_o - R$ according to the sketch in fig. 9.42.

Input Parameters for model BilayeredVesicle:

R: vesicle radius R (center of vesicle to center of lipid bilayer)

sigma_R: size distribution width parameter σ_R

T: thickness of central tail layer T

sigma_T: size distribution width parameter σ_T

sigma_i: smearing width parameter of membrane interface inside vesicle

sigma_o: smearing width parameter of membrane interface outside vesicle

Rg: radius of gyration of attached PEG molecules

f_PEG_i: fraction of PEG decorated inner lipids where PEG is pointing towards inside of vesicle

f_PEG_o: fraction of PEG decorated outer lipids where PEG is pointing towards outside of vesicle

V_PEG: molecular volume of PEG V_{PEG}

eta_PEG: scattering length density of PEG η_{PEG}

V_head: molecular volume of lipid head group V_h

eta_head: scattering length density of lipid head group η_h

V_tail: molecular volume of lipid tail group V_t

eta_tail: scattering length density of lipid tail group η_t

eta_sol: scattering length density of solvent η_{sol}

9.3. Spherical core-shell structures with smooth or fuzzy interfaces

This plugin contains a collection of form factor for spherical core-shell structure with a smooth interface. The smooth interfaces are described by radial profiles of a form which are analytical integrable, i.e. for which the following integral for calculating the scattering amplitude $A_i(Q)$ of the i^{th} shell has an analytical solution.

$$A_i(Q) = \int_{R_i}^{R_i+t_i} \eta_i(r) 4\pi r^2 \frac{\sin(Qr)}{Qr} dr \quad (9.147)$$

Radial profiles for which this integral has been solved are

$$\eta_{a,i}(r) = (\eta_{out,i} - \eta_{in,i}) \frac{r - R}{t} + \eta_{in,i} \quad (9.148a)$$

$$\eta_{b,i}(r) = (\eta_{out,i} - \eta_{in,i}) \left(\frac{r - R}{t} \right)^2 + \eta_{in,i} \quad (9.148b)$$

$$\eta_{c,i}(r) = (\eta_{out,i} - \eta_{in,i}) \exp \left(\frac{r - R}{t} \right) + \eta_{in,i} \quad (9.148c)$$

9.3.1. JuelichCoreShell.

This model considers a dense core and original two shells [532]. Besides, it considers two different density profiles: a parabolic and a star-like profile for the second shell.

$$\eta_{\text{shell}}(r) \propto r^{-x} \quad \text{for starlike profile } x = 4/3 \quad (9.149)$$

$$\eta_{\text{shell}}(r) \propto 1 - \left(\frac{r}{L_p}\right)^2 \quad \text{for parabolic profile of thickness } L_p \quad (9.150)$$

Model parameters:

b_{solv} : scattering length density of the solvent

I_0 : forward scattering

M_{core} : molecular weight of core (g/mol)

M_{brush} : molecular weight brush (g/mol)

ρ_{core} : mass density of core matter (g/cm³)

ρ_{brush} : mass density of brush matter (g/cm³)

b_{core} : scattering length density of core material (cm⁻²)

b_{brush} : scattering length density of brush material (cm⁻²)

N_{agg} : aggregation number (real number)

d_c^+ : extra radius of core (compared to compact)

p_{12} : relative distribution of shell amount in (1stshell:2ndshell) (0 ... ∞)

d_1^+ : extra radius of first shell (compared to compact)

d_2^+ : extra radius of second shell (compared to compact)

σ_c : core smearing

σ_1 : smearing of 1st shell

σ_2 : smearing of 2nd shell

x_{star} : relative distribution of parabolic:starlike profile in 2nd shell, one has to put a very high value in order to consider only a star-like profile.

γ : for star-like profile the exponent is 4/3 and for a constant profile chose 0

L_p : thickness of parabolic brush (must fit in 2nd shell!)

$$I(Q) = [\Delta b_c F_c + \Delta b_b (F_1 + F_2)]^2 \quad (9.151)$$

$$\Delta b_c = b_{\text{core}} - b_{\text{solv}}(1 - f_{\text{core}}) \quad (9.152)$$

$$\Delta b_b = b_{\text{brush}} - b_{\text{solv}}(1 - f_{\text{brush}}) \quad (9.153)$$

V_c and V_b are the core and shell bulk volumes respectively.

Mass Conservation:

From the given values of the molecular weights of the two blocks and their densities, and an assumed aggregation number N_{agg} , the bulk volumes of the core and the shell, V_c and V_b , can be calculated.

Core:

$$\text{bulk core volume: } V_c = \frac{N_{\text{agg}} M_{\text{core}}}{\rho_{\text{core}} N_a} \quad (9.154)$$

$$\text{minimal radius of core: } R_c^0 = \left(\frac{3}{4\pi} V_c \right)^{1/3} \quad (9.155)$$

$$\text{effective core radius: } R_c = R_c^0 + d_c^+ \quad (9.156)$$

$$\text{swollen core volume: } V_{sc} = \frac{4}{3}\pi R_c^3 \quad (9.157)$$

$$\text{swelling factor: } s_c = \frac{V_{sc}}{V_c} \quad (9.158)$$

Shell:

$$\text{bulk shell volume: } V_b = \frac{N_{\text{agg}} M_{\text{shell}}}{\rho_{\text{shell}} N_a} \quad (9.159)$$

The relative amount of shell material in the first shell f_{shell1} is controlled by the parameter p_{12} , so that the portion of the second shell f_{shell2} can be obtained through:

$$f_{\text{shell1}} = \frac{p_{12}}{1 + p_{12}} \quad (9.160)$$

$$f_{\text{shell2}} = 1 - f_{\text{shell1}} \quad (9.161)$$

Shell 1:

$$\text{portion of the total shell volume in first shell: } V_{s1} = f_{\text{shell1}} V_b \quad (9.162)$$

$$\text{minimal radius of shell: } R_{c1} = \left(\frac{3}{4\pi} (V_{sc} + V_{s1}) \right)^{1/3} \quad (9.163)$$

$$\text{effective core radius: } R_1 = R_{c1} + d_1^+ \quad (9.164)$$

$$\text{swollen volume of first shell: } V_{s1s} = \frac{4}{3}\pi R_1^3 \quad (9.165)$$

$$\text{swelling factor: } s_{s1} = \frac{V_{s1s} - V_{sc}}{V_{s1}} \quad (9.166)$$

Shell 2:

$$\text{portion of the total shell volume in second shell: } V_{s2} = f_{\text{shell2}} V_b \quad (9.167)$$

$$\text{minimal radius of shell: } R_{c2} = \left(\frac{3}{4\pi} (V_{s1s} + V_{s2}) \right)^{1/3} \quad (9.168)$$

$$\text{effective core radius: } R_2 = R_{c2} + d_2^+ \quad (9.169)$$

$$\text{swollen volume of second shell: } V_{s2s} = \frac{4}{3}\pi R_2^3 \quad (9.170)$$

$$\text{swelling factor: } s_{s2} = \frac{V_{s2s} - V_{s1s}}{V_{s2}} \quad (9.171)$$

$$\text{fraction of star-like density profile in 2nd shell: } f_{\text{star}} = 2 \frac{\arctan(|p_{\text{star}}|)}{\pi} \quad (9.172)$$

Together with the profile functions $\Phi_c(r, R_c)$, $\Phi_1(r, R_1, R_2)$, $\Phi_2(r, R_1, R_2, f_{\text{star}})$ and

$$f_{\text{Fermi}}(x) = \frac{1}{1 + \exp(x)} \quad (9.173)$$

the volumes of the core and two shells and the corresponding form factor are determined by numerical integration.

Profiles:

$$\Phi_c(r, R_c) = f_{\text{Fermi}}(r - R_c) dr \quad (9.174)$$

$$\Phi_1(r, R_1, R_2) = (1 - f_{\text{Fermi}}(r - R_1)) f_{\text{Fermi}}(r - R_2) dr \quad (9.175)$$

for $r < R_1$

$$\begin{aligned} \Phi_2(r, R_1, R_2, f_{\text{star}}, \gamma) = & (1 - f_{\text{Fermi}}(r - R_1)) f_{\text{Fermi}}(r - R_2) \\ & \times \left[(1 - f_{\text{star}}) + \frac{f_{\text{star}}}{R_1^\gamma} \right] \end{aligned} \quad (9.176)$$

for $r > R_1$

$$\begin{aligned} \Phi_2(r, R_1, R_2, f_{\text{star}}, \gamma, L_p) = & (1 - f_{\text{Fermi}}(r - R_1)) f_{\text{Fermi}}(r - R_2) \\ & \times \left[(1 - f_{\text{star}}) \left(1 - \left(\frac{r - R_1}{L_p} \right)^2 \right) + \frac{f_{\text{star}}}{r^\gamma} \right] \end{aligned} \quad (9.177)$$

Input Parameters for model JuelichCoreShell:

C: scaling constant C

Mcore: molecular weight core (g/mol) M_{core}

Mbrush: molecular weight brush (g/mol) M_{brush}

rho_core: mass density core matter (g/cm³) ρ_{core}

rho_brush: mass density brush matter (g/cm³) ρ_{brush}

b_core: scattering length density of core material (cm⁻²) b_{core}

b_brush: scattering length density of brush material (cm⁻²) b_{brush}

Nagg: aggregation number N_{agg}

d1_plus: extra radius of shell1=core (compared to compact) d_c^+

part23: relative distribution of shell amount in (1stshell:2ndshell) (0...∞) p_{12}

d2_plus: extra radius of first shell2 (compared to compact) d_1^+

d3_plus: extra radius of second shell3 (compared to compact) d_2^+

sigma1: core smearing σ_c

sigma2: smearing of 1st shell2 σ_1

sigma3: smearing of 2nd shell3 σ_2

partstar: relative distribution of parabolic:starlike profile in shell3 x_{star} ; one usually puts a very high value in order to consider only a star-like profile.

gamma: star-like profile: exponent is $\gamma = 4/3$, constant profile: $\gamma = 0$

lparabol: thickness of parabolic brush L_p (must fit in shell3!)

f_brush: scattering length density correction factor brush

f_core: scattering length density correction factor core

rhosolv: scattering length density of solvent b_{solv}

9.3.2. Fuzzy Sphere.

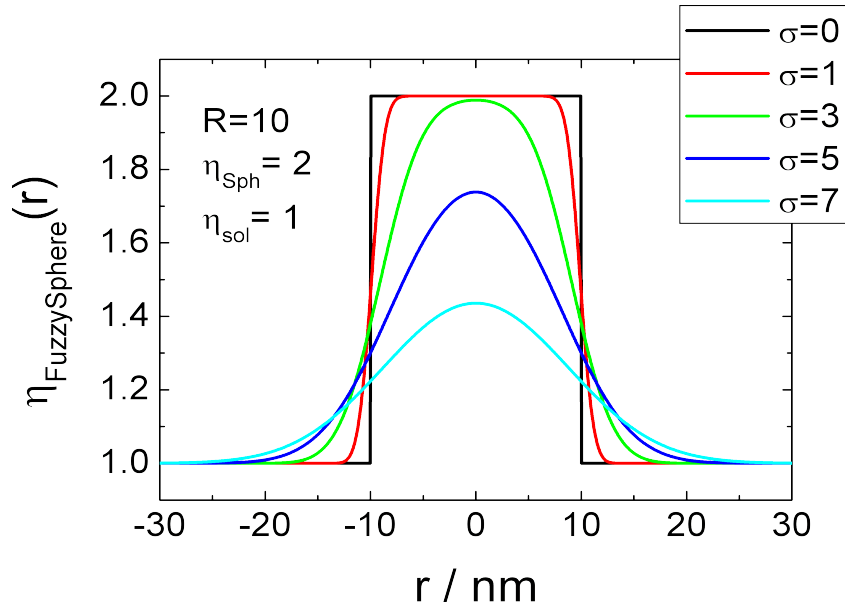


FIGURE 9.44. radial profile of a fuzzy sphere model

This model can be used to calculate the scattering from spherical particles with a "fuzzy" interface [464]. The fuzzy interface is obtained by convoluting the radial profile of a hard sphere with a Gaussian function.

$$\begin{aligned}\eta_{\text{FuzzySph}}(|\mathbf{r}|) &= (\eta_{\text{HS}} \star \eta_{\text{Gauss}})(\mathbf{r}) \\ &= \int_{\mathbb{R}^3} \eta_{\text{HS}}(\boldsymbol{\tau}) \eta_{\text{Gauss}}(\mathbf{r} - \boldsymbol{\tau}) d\boldsymbol{\tau}\end{aligned}\quad (9.178)$$

with

$$\eta_{\text{HS}}(|\mathbf{r}|) = \begin{cases} (\eta_{\text{sph}} - \eta_{\text{sol}}) & \text{for } |\mathbf{r}| \leq R \\ 0 & \text{for } |\mathbf{r}| > R \end{cases}\quad (9.179a)$$

$$\eta_{\text{Gauss}}(|\mathbf{r}|) = \frac{1}{2\sqrt{2}\pi^{3/2}|\sigma|^3} \exp\left[-\frac{|\mathbf{r}|^2}{2|\sigma|^2}\right]\quad (9.179b)$$

The convolution has to be done in \mathbb{R}^3 . As the hard sphere and Gaussian functions are radial symmetric also the profile of the fuzzy sphere only depends on $|\mathbf{r}|$. By defining the interface via a convolution the form factor can be easily calculated because the Fourier transform of a convolution is the pointwise product of the Fourier transforms according

to the convolution theorem, i.e.

$$\begin{aligned}
 F(Q) &= \mathcal{F} [\eta_{\text{FuzzySph}}(r)] \\
 &= \mathcal{F} [(\eta_{\text{HS}} \star \eta_{\text{Gauss}})(r)] = \mathcal{F} [\eta_{\text{HS}}(r)] \mathcal{F} [\eta_{\text{Gauss}}(r)] \\
 &= \int_0^\infty \eta_{\text{HS}}(r) 4\pi r^2 \frac{\sin(Qr)}{Qr} dr \int_0^\infty \eta_{\text{Gauss}}(r) 4\pi r^2 \frac{\sin(Qr)}{Qr} dr \\
 &= (\eta_{\text{sph}} - \eta_{\text{sol}}) 4\pi R^3 \frac{\sin(QR) - QR \cos(QR)}{(QR)^3} e^{-\frac{1}{2}\sigma^2 Q^2}
 \end{aligned} \tag{9.180}$$

Instead of calculating the convolution integral one also can get the radial profile of the fuzzy interface by the inverse Fourier transformation of the scattering amplitude

$$\eta_{\text{FuzzySph}}(r) = \int_0^\infty \frac{1}{(2\pi)^3} F(Q) 4\pi Q^2 \frac{\sin(Qr)}{Qr} dQ \tag{9.181}$$

$$\begin{aligned}
 \eta_{\text{FuzzySph}}(r) &= (\eta_{\text{sph}} - \eta_{\text{sol}}) \\
 &\left(\frac{\left(e^{-\frac{(r+R)^2}{2\sigma^2}} - e^{-\frac{(r-R)^2}{2\sigma^2}} \right) \sigma}{\sqrt{2\pi} r} + \frac{1}{2} \operatorname{erf} \left[\frac{r+R}{\sqrt{2}|\sigma|} \right] - \frac{1}{2} \operatorname{erf} \left[\frac{r-R}{\sqrt{2}|\sigma|} \right] \right)
 \end{aligned} \tag{9.182}$$

Finally the scattering intensity is given by

$$\begin{aligned}
 I_{\text{FuzzySph}}(Q) &= F^2(Q) = \\
 &\left[(\eta_{\text{sph}} - \eta_{\text{sol}}) 4\pi R^3 \frac{\sin(QR) - QR \cos(QR)}{(QR)^3} e^{-\frac{1}{2}\sigma^2 Q^2} \right]^2
 \end{aligned} \tag{9.183}$$

The intensity $I_{\text{FuzzySph}}(Q)$ and also the scattering length density profile $\eta_{\text{FuzzySph}}(r)$ are normalized so that

$$\begin{aligned}
 \lim_{Q \rightarrow 0} I_{\text{FuzzySph}}(Q) &= \left((\eta_{\text{sph}} - \eta_{\text{sol}}) \frac{4}{3}\pi R^3 \right)^2 \\
 \int_0^\infty 4\pi r^2 \eta_{\text{FuzzySph}}(r) dr &= \frac{4}{3}\pi R^3
 \end{aligned}$$

R = radius of the fuzzy sphere

σ = thickness of the fuzzy shell

η_{sph} : scattering length density of sphere

η_{sol} : scattering length density of the solvent

(9.184)

Input Parameters for model FuzzySphere and radial profile of FuzzySphere:

R: radius of the fuzzy sphere R

sigma: thickness of the fuzzy shell σ

eta_sph: scattering length density of sphere η_{sph}

eta_sol: scattering length density of solvent η_{sol}

Note:

- This form factor is only defined for positive radii $R > 0$.
- For $\sigma = 0$ the limiting case of a simple hard sphere form factor is used.
- In addition, scattering contributions arising from fluctuations of the microgel network are often included in this model expression as a Lorentzian function

$$I_{\text{fluct}}(Q) = \frac{I_{\text{fluct}}(0)}{1 + \xi^2 Q^2} \quad (9.185)$$

so that

$$I(Q) = I_{\text{FuzzySph}}(Q) + I_{\text{fluct}}(Q) \quad (9.186)$$

where $I_{\text{fluct}}(0)$ is the $Q = 0$ limiting intensity and ξ represents the correlation length of the fluctuations, which can be considered to be related to the blob or mesh size. It should be noted that the Lorentzian describes the ensemble average correlations in the polymer network.

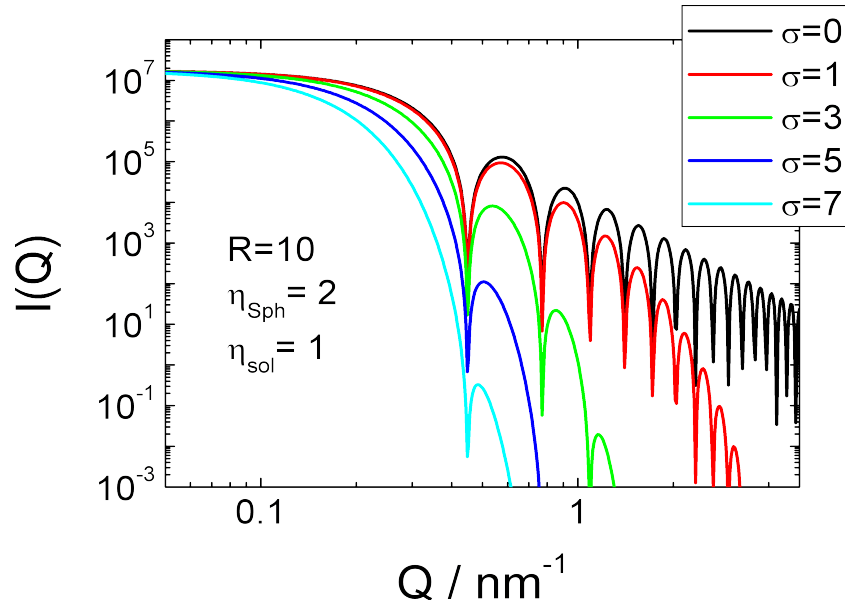


FIGURE 9.45. Scattering intensity of a fuzzy sphere. The scattering intensity has been calculated for a core radius $R = 10$, a scattering length density of the FuzzySphere of $\eta_{\text{Sph}} = 1$, a scattering length density of the solvent $\eta_{\text{sol}} = 1$, and several widths of the "fuzzy" shell

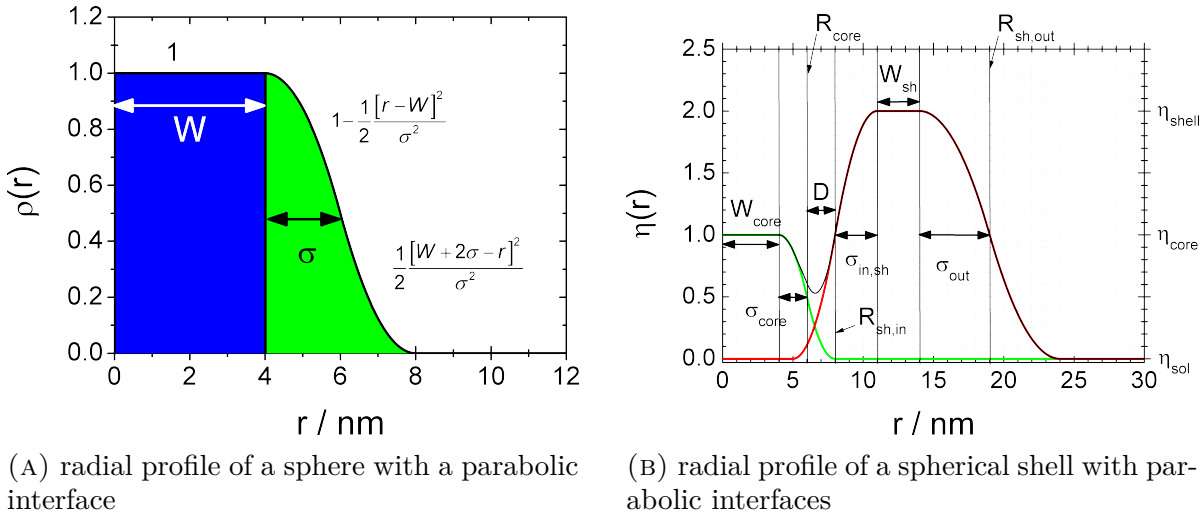


FIGURE 9.46. Profiles of core-shell microgel

9.3.3. CoreShellMicrogel. This model can be used to calculate the scattering from spherical particles with a parabolic "fuzzy" interface [30, 29, 31]. The radial profile is given by

$$\rho(r, R, \sigma) = \begin{cases} 1 & \text{for } r \leq R - \sigma \\ 1 - \frac{1}{2} \frac{((r-R)+\sigma)^2}{\sigma^2} & \text{for } R - \sigma < r \leq R \\ \frac{1}{2} \frac{((R-r)+\sigma)^2}{\sigma^2} & \text{for } R < r \leq R + \sigma \\ 0 & \text{for } r > R + \sigma \end{cases} \quad (9.187)$$

where $R = W + \sigma$. For such a radial profile the Fourier-transformation can be calculated analytically as

$$\begin{aligned} F(Q, R, \sigma) = \mathcal{F}[\rho(r, R, \sigma)] = \\ 4\pi \left(\left(\frac{R}{\sigma^2} + \frac{1}{\sigma} \right) \frac{\cos(q(R + \sigma))}{q^4} + \left(\frac{R}{\sigma^2} - \frac{1}{\sigma} \right) \frac{\cos(q(R - \sigma))}{q^4} \right. \\ \left. - 3 \frac{\sin(q(R + \sigma))}{q^5 \sigma^2} - 3 \frac{\sin(q(R - \sigma))}{q^5 \sigma^2} - 6 \frac{\sin(qR)}{q^5 \sigma^2} - 2R \frac{\cos(qR)}{q^4 \sigma^2} \right) \quad (9.188) \end{aligned}$$

The last term in the brackets needed to be corrected compared to the papers mentioned above due to a typo in the original papers. The radial scattering length density profile of a fuzzy core shell like in Fig. 9.46b can be obtained by

$$\begin{aligned} \eta_{core,sh}(r, W_{core}, \sigma_{core}, D, \sigma_{sh,in}, W_{sh}, \sigma_{sh,out}) = \eta_{sol} + (\eta_{shell} - \eta_{sol})\rho(r, R_{out}, \sigma_{out}) \\ + (\eta_{shell} - \eta_{sol})\rho(r, R_{sh,in}, \sigma_{sh,in}) + (\eta_{core} - \eta_{sol})\rho(r, R_{core}, \sigma_{core}) \quad (9.189) \end{aligned}$$

with

$$R_{\text{core}} = W_{\text{core}} + \sigma_{\text{core}} \quad (9.190\text{a})$$

$$R_{\text{sh,in}} = R_{\text{core}} + D \quad (9.190\text{b})$$

$$R_{\text{out}} = R_{\text{sh,in}} + \sigma_{\text{sh,in}} + W_{\text{sh}} + \sigma_{\text{sh,out}} \quad (9.190\text{c})$$

In the same way also the scattering amplitude $F_{\text{core,sh}}(Q, \dots)$ and the scattering intensity $I_{\text{core,sh}}(Q, \dots) = |F_{\text{core,sh}}(Q, \dots)|^2$ can be calculated

$$\begin{aligned} F_{\text{core,sh}}(Q, W_{\text{core}}, \sigma_{\text{core}}, D, \sigma_{\text{sh,in}}, W_{\text{sh}}, \sigma_{\text{sh,out}}) &= (\eta_{\text{shell}} - \eta_{\text{sol}})F(Q, R_{\text{out}}, \sigma_{\text{out}}) \\ &+ (\eta_{\text{shell}} - \eta_{\text{sol}})F(Q, R_{\text{sh,in}}, \sigma_{\text{sh,in}}) + (\eta_{\text{core}} - \eta_{\text{sol}})F(Q, R_{\text{core}}, \sigma_{\text{core}}) \end{aligned} \quad (9.191\text{a})$$

$$I_{\text{core,sh}}(Q, W_{\text{core}}, \sigma_{\text{core}}, D, \sigma_{\text{sh,in}}, W_{\text{sh}}, \sigma_{\text{sh,out}}) = |F_{\text{core,sh}}(Q, \dots)|^2 \quad (9.191\text{b})$$

Input parameters for "CoreShellMicrogel" and "radial profile of CoreShellMicrogel":

W_core: radius of center parts of core W_{core} with homogeneous scattering length density

sigma_core: interface half width of the core σ_{core}

W_shell: width of center parts of shell W_{sh} with homogeneous scattering length density

sigma_sh,in: half width of the inner interface of shell $\sigma_{\text{sh,in}}$

D: distance D between interface of core and in interface of shell

sigma_out: half width of the outer surface profile σ_{out}

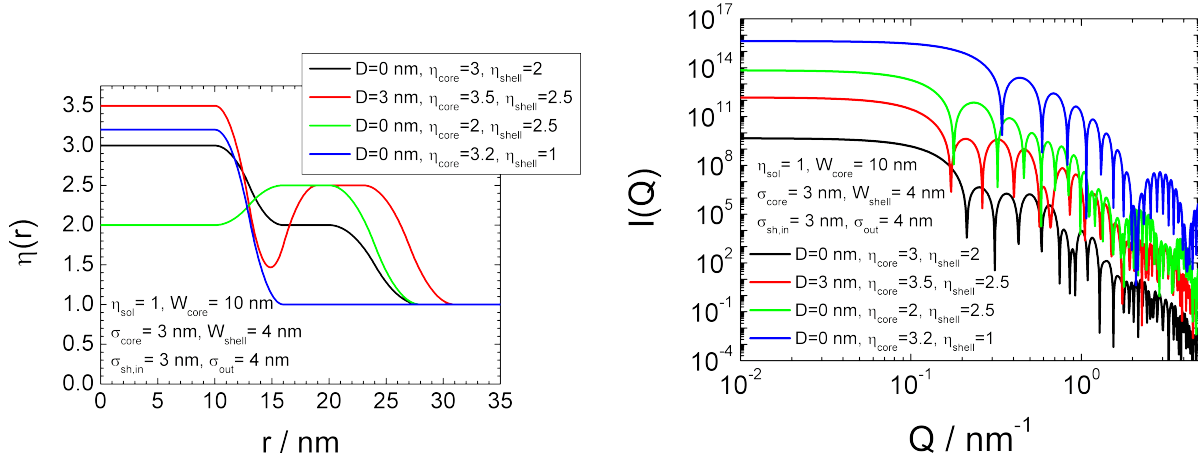
eta_core: scattering length density of homogeneous core part η_{core}

eta_shell: scattering length density of homogeneous shell part η_{shell}

eta_sol: scattering length density of solvent η_{sol}

Note

- If one like to simulate a simple step profile one should set $D = 0$ and $\sigma_{\text{core}} = \sigma_{\text{sh,in}}$. The last equality in case of fitting this parameter can be simply obtained by a global parameter under fitting multiple data sets.
- Instead of using the radii in eq. 9.190 as input parameters the thickness of the homogeneous parts of the core and the shell have been used to avoid a problems (negative dimensions) by applying an integration over a size distribution starting from 0 on the radii.



(A) Some radial profiles of spheres with a parabolic interfaces which have been used to calculate the scattering curve in Fig. 9.47b

(B) Scattering curves of the radial profiles shown in Fig. 9.47a.

FIGURE 9.47. The profiles and scattering curves have been calculated with the plugin functions "CoreShellMicrogel" and "Radial Profile of CoreShellMicrogel".

9.3.4. Spherical shell with linear varying contrast profile (LinShell).

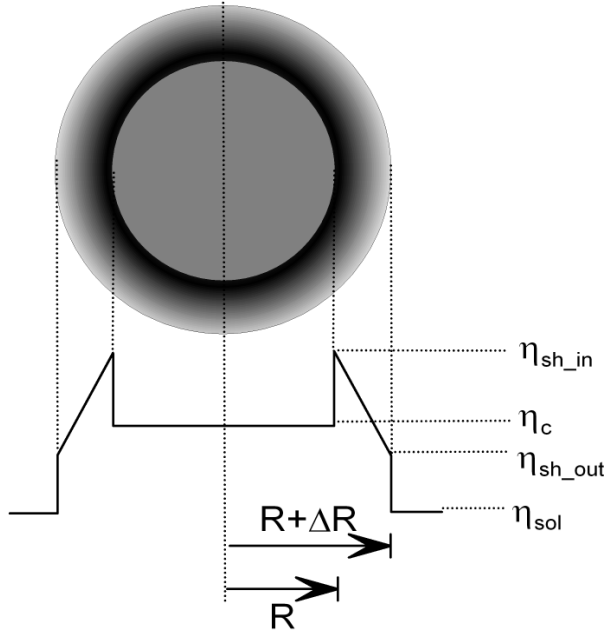


FIGURE 9.48. Radial profile for calculating the form factor of a spherical shell with a core radius R and a shell thickness of ΔR and a linear varying contrast profile.

Form factor of a spherical shell with a core radius R and a shell thickness of ΔR . Here a linear contrast profile within the shell has been assumed.

$$\eta(r) = \begin{cases} \eta_c & \text{for } r < R \\ mr + b & \text{for } r \in [R, R + \Delta R] \\ \eta_{\text{sol}} & \text{for } r > R + \Delta R \end{cases} \quad (9.192)$$

$$m = (\eta_{\text{sh_out}} - \eta_{\text{sh_in}})/\Delta R \quad (9.193)$$

$$b = -mR + \eta_{\text{sh_in}} \quad (9.194)$$

$$\eta_{\text{sh_in}} = (1 - x_{\text{in},\text{sol}}) \eta_{\text{sh}} + x_{\text{in},\text{sol}} \eta_{\text{sol}} - \eta_{\text{sol}} \quad (9.195)$$

: scattering length density at R

$$\eta_{\text{sh_out}} = (1 - x_{\text{out},\text{sol}}) \eta_{\text{sh}} + x_{\text{out},\text{sol}} \eta_{\text{sol}} - \eta_{\text{sol}} \quad (9.196)$$

: scattering length density at $R + \Delta R$

η_{sh} : scattering length density of pure shell material

η_c : scattering length density of core

$$F_{\text{sph}}(A, x) = \frac{4}{3}\pi x^3 \cdot 3 \frac{\sin(A) - A \cos(A)}{A^3} \quad (9.197)$$

$$F_{\text{shlin}}(A, x) = 4\pi x^4 \frac{2 \cos(A) + 2A \sin(A) - A^2 \cos(A)}{A^4} \quad (9.198)$$

$$\begin{aligned} I_{\text{LinShell}} = & \left[(\eta_c - \eta_{\text{sol}} - b) F_{\text{sph}}(QR, R) \right. \\ & - m F_{\text{shlin}}(QR, R) \\ & + m F_{\text{shlin}}(Q(R + \Delta R), R + \Delta R) \\ & \left. + b F_{\text{sph}}(Q(R + \Delta R), R + \Delta R) \right]^2 \end{aligned} \quad (9.199)$$

Input Parameters for model LinShell and radial profile of LinShell:

R: radius of core R

dR: thickness of the shell ΔR

eta_c: scattering length density η_c

eta_sh: scattering length density of non-swollen shell η_{sh}

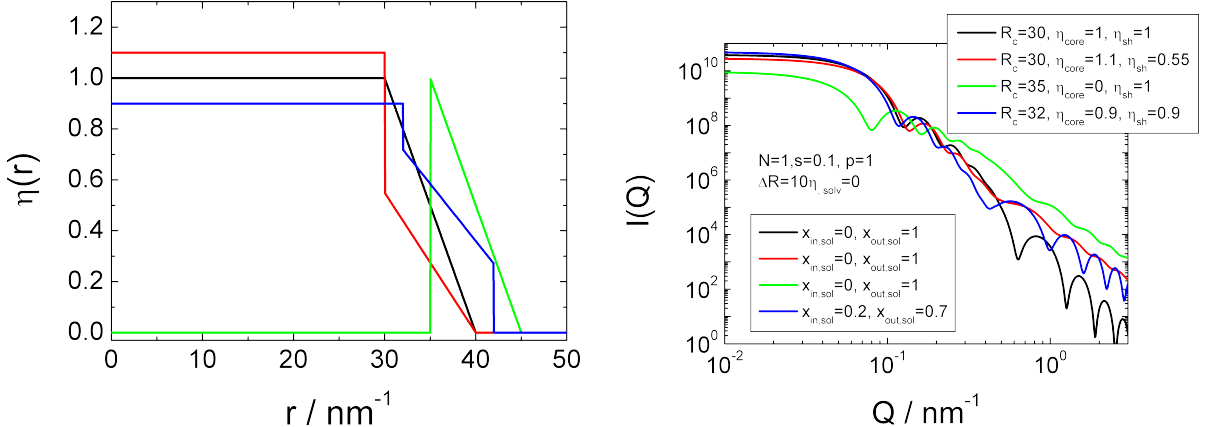
x_in: amount of solvent $x_{\text{in},\text{sol}}$ on core-shell interface at R

x_out: amount of solvent $x_{\text{out},\text{sol}}$ on shell-solvent interface at $R + \Delta R$

eta_sol: scattering length density of solvent η_{sol}

Note:

- $x_{\text{in},\text{sol}}$ and $x_{\text{out},\text{sol}}$ are only physical for values between 0 and 1.



(A) Some radial profiles of spheres with a linear interface profiles due to penetration of solvent into the shell which have been used to calculate the scattering curve in Fig. 9.49b.

(B) Scattering curves of the radial profiles shown in Fig. 9.49a.

FIGURE 9.49. Scattering intensity of a spherical shell with a linear shell profile. The scattering intensity has been calculated with a lognormal size distribution for the core radius R_c .

9.3.5. LinShell2.

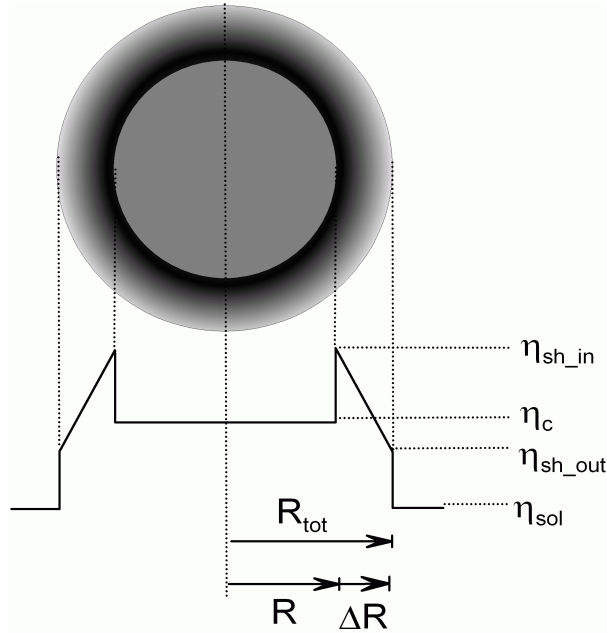


FIGURE 9.50. Radial profile for calculating the form factor of a spherical shell with a total radius R_{tot} , a shell thickness of ΔR , and a linear varying contrast profile.

Form factor of a spherical shell with a total radius R_{tot} and a shell thickness of ΔR . The definition are the same than for LinShell except that instead of the core radius R now the total radius R_{tot} is used to parameterize the form factor. The parameter definitions are the following:

$$R = \begin{cases} R_{\text{tot}} - \Delta R & \text{for } R_{\text{tot}} > \Delta R \\ 0 & \text{otherwise} \end{cases} \quad (9.200)$$

$$\Delta\eta(r) = \begin{cases} \eta_c & \text{for } r < R \\ mr + b & \text{for } r \in [R, R_{\text{tot}}] \\ \eta_{\text{sol}} & \text{for } r > R_{\text{tot}} \end{cases} \quad (9.201)$$

with

$$m = (\eta_{\text{sh_out}} - \eta_{\text{sh_in}})/\Delta R \quad (9.202)$$

$$b = -mR + \eta_{\text{sh_in}} \quad (9.203)$$

and

$$\eta_{\text{sh_in}} = (1 - x_{\text{in,sol}}) \eta_{\text{sh}} + x_{\text{in,sol}} \eta_{\text{sol}} \quad (9.204)$$

: scattering length density at R

$$\eta_{\text{sh_out}} = (1 - x_{\text{out,sol}}) \eta_{\text{sh}} + x_{\text{out,sol}} \eta_{\text{sol}} \quad (9.205)$$

: scattering length density at $R_{\text{tot}} = R + \Delta R$

η_{sh} : scattering length density of pure shell material

η_{c} : scattering length density of core

$x_{\text{in,sol}}$: amount of solvent at R

$x_{\text{out,sol}}$: amount of solvent at $R_{\text{tot}} = R + \Delta R$

$$F_{\text{sph}}(A, x) = \frac{4}{3}\pi x^3 \cdot 3 \frac{\sin(A) - A \cos(A)}{A^3} \quad (9.206)$$

$$F_{\text{shlin}}(A, x) = 4\pi x^4 \frac{2 \cos(A) + 2A \sin(A) - A^2 \cos(A)}{A^4} \quad (9.207)$$

$$I_{\text{LinShell2}} = \left[(\eta_{\text{c}} - \eta_{\text{sol}} - b) F_{\text{sph}}(QR, R) \right.$$

$$- m F_{\text{shlin}}(QR, R) \quad (9.208)$$

$$+ m F_{\text{shlin}}(QR_{\text{tot}}, R_{\text{tot}})$$

$$\left. + b F_{\text{sph}}(QR_{\text{tot}}, R_{\text{tot}}) \right]^2$$

Input Parameters for model LinShell2 and radial profile of LinShell2:

Rtot: total overall radius R_{tot}

dR: thickness of the shell ΔR

eta_c: scattering length density η_{c}

eta_sh: scattering length density of non-swollen shell η_{sh}

x_in: amount of solvent $x_{\text{in,sol}}$ on core-shell interface at R ($x_{\text{in,sol}} \in [0; 1]$)

x_out: amount of solvent $x_{\text{out,sol}}$ on shell-solvent interface at $R + \Delta R$ ($x_{\text{out,sol}} \in [0; 1]$).

eta_s: scattering length density of solvent η_{sol}

Note:

- $x_{\text{in,sol}}$ and $x_{\text{out,sol}}$ are only physical for values between 0 and 1.

9.3.6. ExpShell.

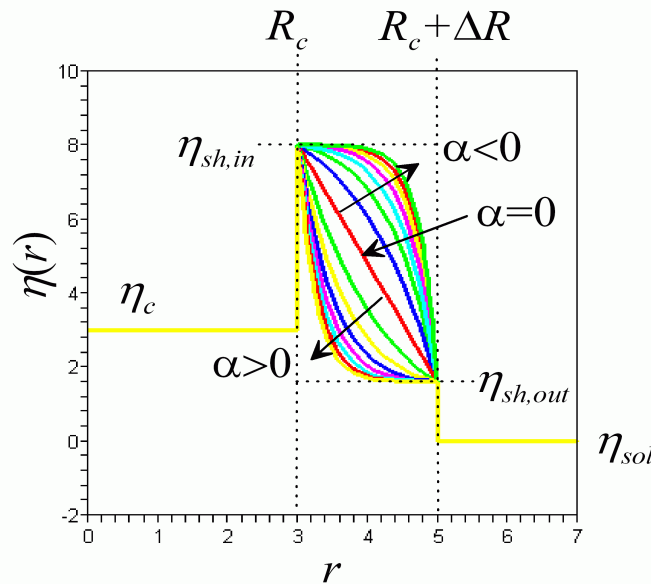


FIGURE 9.51. Radial profile for calculating the form factor of a spherical shell with a core radius R_c and a shell thickness of ΔR and a exponentially varying contrast profile. The profile shape can be varied by the parameter α describing the penetration of the solvent into the shell. A value of $\alpha = 0$ means linear profile and is equivalent to LinShell and LinShell2. For $\alpha > 0$ the solvent penetrates further into the shell and for $\alpha < 0$ less.

$$\eta_{\text{ExpShell}}(r, R_c, \Delta R, \alpha, \phi_{\text{in}}, \phi_{\text{out}}) = \begin{cases} \eta_c & r \leq R_c \\ \eta_{\text{exp}}\left(\frac{r-R_c}{\Delta R}\right) & R_c < r < R_c + \Delta R \\ \eta_{\text{sol}} & r > R_c + \Delta R \end{cases} \quad (9.209)$$

$$\eta_{\text{exp}}(x) = \begin{cases} \eta_{\text{sh,in}} + [\eta_{\text{sh,out}} - \eta_{\text{sh,in}}] x \exp([1-x]\alpha) & \alpha < 0 \\ [\eta_{\text{sh,in}} - \eta_{\text{sh,out}}] [1-x] \exp(-x\alpha) + \eta_{\text{sh,out}} & \alpha \geq 0 \end{cases} \quad (9.210)$$

$$\eta_{\text{sh,in}} = [\phi_{\text{in}} \eta_{\text{sol}} + (1 - \phi_{\text{in}}) \eta_{\text{sh}}] \quad (9.211)$$

$$\eta_{\text{sh,out}} = [\phi_{\text{out}} \eta_{\text{sol}} + (1 - \phi_{\text{out}}) \eta_{\text{sh}}] \quad (9.212)$$

The scattering intensity for the radial symmetric scattering length density profile $\eta_{\text{ExpShell}}(r)$ can be calculated analytical. The integral needed to be solved for that is

$$I_{\text{ExpShell}}(Q) = \int_0^\infty 4\pi r^2 \frac{\sin Qr}{Qr} \eta_{\text{ExpShell}}(r) dr \quad (9.213)$$

R_c = core radius

ΔR = shell thickness

$$\eta_{\text{sh,in}} = (1 - \phi_{\text{in,sol}}) \eta_{\text{sh}} + \phi_{\text{in,sol}} \eta_{\text{sol}} \quad (9.214)$$

: scattering length density at R_c

$$\eta_{\text{sh,out}} = (1 - \phi_{\text{out,sol}}) \eta_{\text{sh}} + \phi_{\text{out,sol}} \eta_{\text{sol}} \quad (9.215)$$

: scattering length density at $R_c + \Delta R$

η_{sh} : scattering length density of pure shell material

η_c : scattering length density of core

ϕ_{in} : amount of solvent at R_c

ϕ_{out} : amount of solvent at $R_c + \Delta R$

α : parameter for exponential diffuse profile of the shell (9.216)

Input Parameters for model ExpShell:

R_core: radius of core R_c

DR: thickness of the shell ΔR

eta_core: scattering length density η_c

eta_shell: scattering length density of non-swollen shell η_{sh}

x_in_sol: amount of solvent ϕ_{in} on core-shell interface at $r = R$

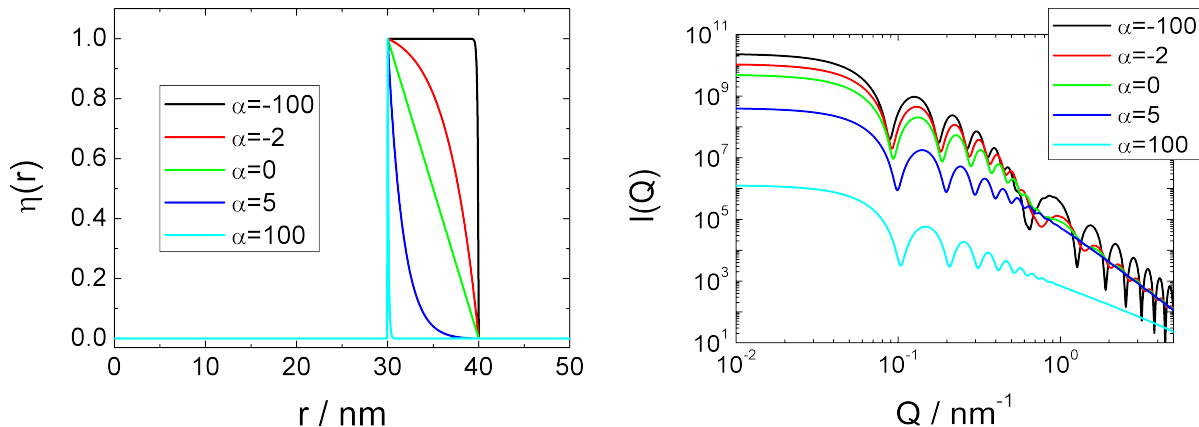
x_out_sol: amount of solvent ϕ_{out} on shell-solvent interface at $r = R + \Delta R$

alpha: a parameter (α) which describes the penetration profile of the solvent into the shell. A value of $\alpha = 0$ means linear profile and is equivalent to LinShell and LinShell2. For $\alpha > 0$ the solvent penetrates further into the shell and for $\alpha < 0$ less.

eta_solvent: scattering length density of solvent η_{sol}

Note:

- ϕ_{in} and ϕ_{out} are only physical for values between 0 and 1.

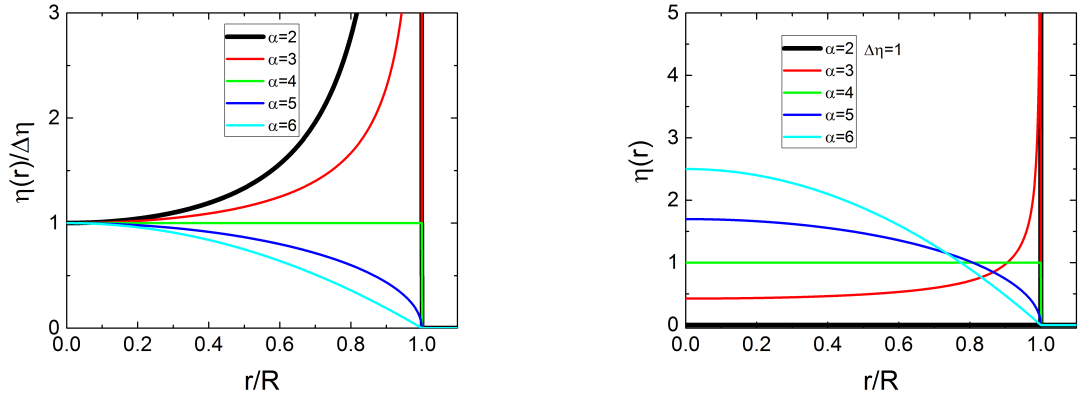


(A) Some radial profiles of spheres with a exponential interfaces which have been used to calculate the scattering curve in Fig. 9.52b

(B) Scattering curves of the radial profiles shown in Fig. 9.52a.

FIGURE 9.52. Scattering intensity of a spherical shell with an exponential shell profile. The scattering intensity has been calculated with a lognormal [$\text{LogNorm}(N = 1, \sigma = 0.05, p = 1, R = 30)$] size distribution for the core radius R_c . The scattering length density of the core η_c and the solvent η_{sol} are set to 0, $\eta_{\text{sh}} = 1$, $\phi_{\text{in}} = 0$, $\phi_{\text{out}} = 1$, and $\Delta R = 10$.

9.3.7. BoucherSphere, radial profile for a sphere resulting in a Porod law both below and above q^{-4} .



(A) Some radial profiles with $\eta_0 = \Delta\eta$ for several values of α .

(B) Radial profiles for several values of α with a normalised radial profile to assure α -independent excess scattering length.

FIGURE 9.53. The two implemented case for the radial profiles according to Boucher [49]

Boucher has described in [49] a simple analytical radial profile for which also the form factor can be calculated analytically. The radial profile is parameterized in a way that any potential law in the Porod regime can be obtained. The radial profile is defined by

$$\eta(r) = \eta_0 \begin{cases} \left[1 - \left(\frac{r}{R}\right)^2\right]^{\frac{\alpha}{2}-2} & \text{for } r \leq R \\ 0 & \text{for } r > R \end{cases} \quad (9.217)$$

The excess scattering β of such a particle is

$$\beta = \int_0^R \eta(r) 4\pi r^2 dr = \eta_0 R^3 \pi^{\frac{3}{2}} \frac{\Gamma\left(\frac{\alpha}{2} - 1\right)}{\Gamma\left(\frac{\alpha+1}{2}\right)} \quad (9.218)$$

The input value $\Delta\eta$ for this profile is the scatter contrast at $r = 0$, i.e.

$$\eta_0 = \Delta\eta \quad (\text{case BoucherSphere}) \quad (9.219)$$

The special case of $\alpha = 4$ corresponds to a homogeneous sphere with a scattering contrast $\Delta\eta$ for which the excess scattering length becomes $\beta_{sp} = \Delta\eta^{\frac{4}{3}}\pi R^3$.

Also a second variant of the form factor has been implemented. In the second case the excess scattering length is normalised to the one of a homogeneous sphere with contrast $\Delta\eta$, so that the excess scattering length is for all α equal to $\beta_{sp} = \Delta\eta^{\frac{4}{3}}\pi R^3$.

This is done by setting the contrast at $r = 0$ in eq. 9.217 to

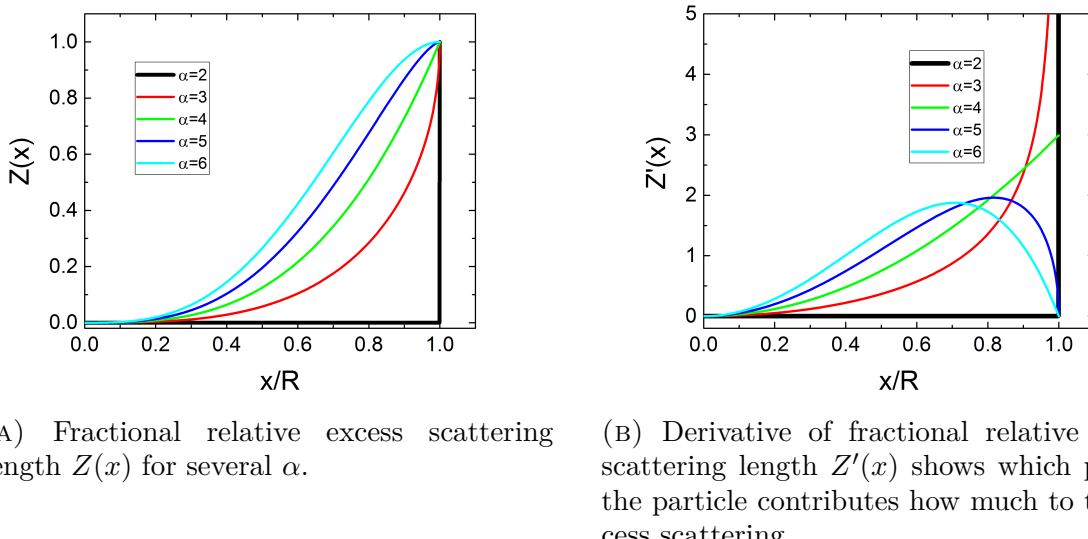
$$\eta_0 = \Delta\eta \frac{4}{3\sqrt{\pi}} \frac{\Gamma\left(\frac{\alpha+1}{2}\right)}{\Gamma\left(\frac{\alpha}{2} - 1\right)} \quad (\text{case BoucherSphere2}) \quad (9.220)$$

By this normalisation the excess scattering length is for all α equal to the one of a homogeneous sphere with a scattering contrast $\Delta\eta$, i.e. $\beta_{sp} = \Delta\eta \frac{4}{3}\pi R^3$.

To get a feeling which part of the spherical scattering length density profile contributes most to the scattering it is convenient to define a fractional relative excess scattering length according to [49] which reads as

$$\begin{aligned} Z(x) &= \frac{\int_0^x \left(1 - \frac{r^2}{R^2}\right)^{\frac{\alpha}{2}-2} 4\pi r^2 dr}{\int_0^R \left(1 - \frac{r^2}{R^2}\right)^{\frac{\alpha}{2}-2} 4\pi r^2 dr} \\ &= \frac{4}{3} \frac{x^3 \Gamma\left(\frac{\alpha+1}{2}\right)}{\sqrt{\pi} \Gamma\left(\frac{\alpha}{2} - 1\right) R^3} {}_2F_1\left(\frac{3}{2}, -\frac{\alpha}{2} + 2; \frac{5}{2}; \frac{x^2}{R^2}\right) \end{aligned} \quad (9.221)$$

$Z(x)$ is the excess scattering of the sub-domain of the spherical particle ranging from $r = 0$ to $r = x$ relative to the excess scattering of the whole particle. The derivative $Z'(x)$ then defines the fractional contribution of a sub-shell with radius $r = x$ and thickness dx of the spherical particle compared to its total excess scattering length of the particle.



(A) Fractional relative excess scattering length $Z(x)$ for several α .

(B) Derivative of fractional relative excess scattering length $Z'(x)$ shows which part of the particle contributes how much to the excess scattering.

FIGURE 9.54. For $\alpha = 2$ all the scattering is caused by an infinitesimal thin outer shell of the particle where all the fractional excess scattering length is located.

The scattering amplitude for the radial profile in eq. 9.217 can be calculated as

$$\begin{aligned}
 F(Q) &= \int_0^R \eta(r) 4\pi r^2 \frac{\sin Qr}{Qr} dr \\
 &= \beta \left(\frac{2}{QR} \right)^{\frac{\alpha-1}{2}} J_{\frac{\alpha-1}{2}}(QR) \Gamma \left(\frac{\alpha+1}{2} \right) \\
 &= \beta {}_0F_1 \left(\frac{\alpha+1}{2}; -\frac{(QR)^2}{4} \right)
 \end{aligned} \tag{9.222}$$

making use of the fact that the bessel function can be expressed in terms of generalised hypergeometric functions $J_\alpha(x) = \frac{(\frac{x}{2})^\alpha}{\Gamma(\alpha+1)} {}_0F_1(\alpha+1; -\frac{x^2}{4})$. The scattering amplitude simplifies in case of $\alpha = 4$ exactly to the one of a homogenous sphere and in case of $\alpha = 2$ to an infinitesimal thin spherical shell. For the scattering intensity $I(Q) = F^2(Q)$ we get in the Porod limit $Q \rightarrow \infty$

$$\lim_{Q \rightarrow \infty} I(Q) = \lim_{Q \rightarrow \infty} F^2(Q) = \beta^2 \frac{2^{\alpha-1}}{\pi} \Gamma^2 \left(\frac{\alpha+1}{2} \right) \frac{1}{(QR)^\alpha} \tag{9.223}$$

Input Parameters for model BoucherSphere and Boucher profile:

R: radius R

alpha: shape parameter of the profile α , which is also equal to the potential law at large Q -values

Delta_eta: scattering length density at $r = 0$, $\Delta\eta = \eta(r = 0)$

Note for model BoucherSphere and Boucher profile:

- For $\alpha < 4$ the scattering length density profile has a pole at $r = R$
- For $\alpha \leq 2$ the excess scattering length of the overall particle diverges and are therefore forbidden values.

Input Parameters for model BoucherSphere2 and Boucher profile2:

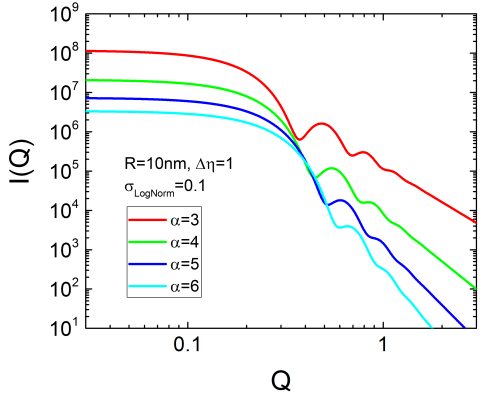
R: radius R

alpha: shape parameter of the profile α , which is also equal to the potential law at large Q -values

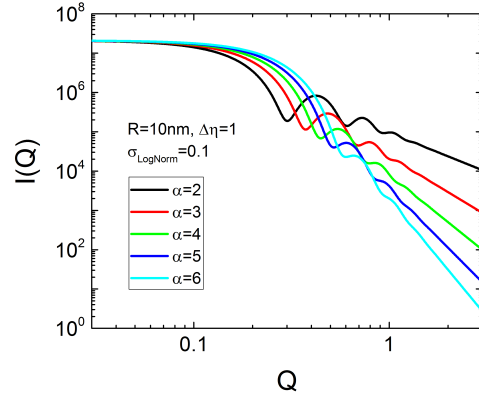
Delta_eta: is the average scattering length density so that the excess scattering length corresponds to the one of a homogeneous sphere with contrast $\Delta\eta$

Note for model BoucherSphere2 and Boucher profile:

- For $\alpha < 4$ the scattering length density profile has a pole at $r = R$
- There is no restriction for the input values of α in the form factor but in the profile, which only allows values for $\alpha > 2$. α -values below 2 do not have a standard physical interpretation.



(A) Scattering curves of `BoucherSpheres` for several α with a narrow LogNormal size distribution with $\sigma = 0.1$. As the excess scattering length diverges for $\alpha \leq 2$ these values are not allowed.



(B) Scattering curves of `BoucherSpheres2` for several α with a narrow LogNormal size distribution with $\sigma = 0.1$.

FIGURE 9.55. Scattering curves for the form factors `BoucherSpheres` and `BoucherSpheres2`.

9.3.8. Power law scattering profile (fuzzy sphere model).

The power law profile looks similar to the Boucher profile and is defined as

$$\eta_{\text{PowLaw}}(r) = \Delta\eta \begin{cases} 1 - \left(\frac{r}{R}\right)^\alpha, & \text{if } r < R \\ 0, & \text{otherwise.} \end{cases} \quad (9.224)$$

The scattering amplitude and the scattering intensity are then given by

$$F_{\text{PowLaw}}(Q, R, \alpha) = \frac{4\pi(\sin(QR) - QR \cos(QR))}{Q^3} - \frac{4\pi R^3 {}_1F_2\left(\frac{\alpha}{2} + \frac{3}{2}; \frac{3}{2}, \frac{\alpha}{2} + \frac{5}{2}; -\frac{1}{4}Q^2R^2\right)}{\alpha + 3} \quad (9.225)$$

$$I_{\text{PowLaw}}(Q, R, \alpha) = F_{\text{PowLaw}}^2(Q, R, \alpha) \quad (9.226)$$

Note

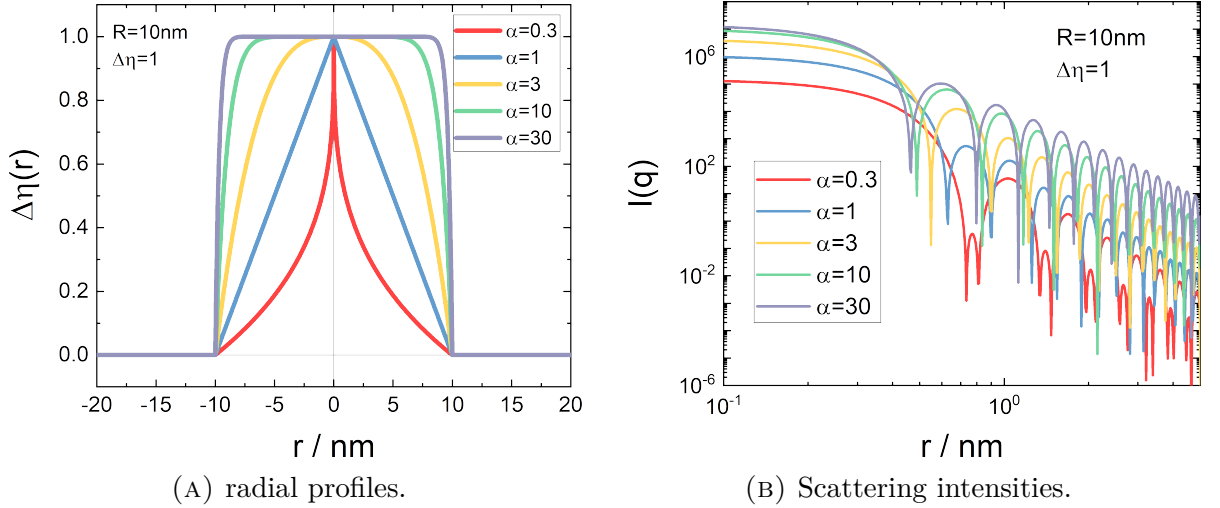
- the parameter α needs to be larger than -3.
- for α values smaller than 0 the radial profile has a pole at $r = 0$.

Input Parameters for model `power law Sphere` and `profile:power law Sphere`:

R: radius R

alpha: power law α in radial profile

Delta_eta: scattering length density contrast $\Delta\eta$

FIGURE 9.56. `powLaw Sphere`-model.

9.3.9. Generalized Exponential scattering profile (fuzzy sphere model).

In [218] the form factor of a variety of spherical profiles have been given. The Yukawa profiles have been summarized in this form factor called generalized exponential sphere. The radial scattering length density profile is defined as

$$\eta_{\text{genExp}}(r) = \Delta\eta \frac{((\alpha+3)(\alpha+4))^{\frac{\alpha+3}{2}} e^{-\frac{\sqrt{(\alpha+3)(\alpha+4)}r}{R_g}} \left(\frac{r}{R_g}\right)^\alpha}{\Gamma(\alpha+3)} \quad (9.227)$$

The corresponding scattering amplitude is then calculated as

$$F_{\text{genExp}}(Q, R_g) = 4\pi R^3 c_{\text{genExp}} \frac{\sin\left((\alpha+2) \arctan\left(\frac{QR}{\sqrt{(\alpha+3)(\alpha+4)}}\right)\right)}{(\alpha+2)QR} \quad (9.228)$$

$$c_{\text{genExp}} = ((\alpha+3)(\alpha+4))^{\frac{\alpha+3}{2}} \left(\alpha(\alpha+7) + Q^2 R^2 + 12\right)^{-\frac{\alpha}{2}-1} \quad (9.229)$$

$$I_{\text{genExp}}(Q, R, \alpha) = F_{\text{genExp}}^2(Q, R, \alpha) \quad (9.230)$$

The scattering intensity decays for large q -values as

$$\lim_{Q \rightarrow \infty} I_{\text{genExp}}(Q, R, \alpha) \propto Q^{-6-2\alpha} \quad (9.231)$$

A decay of Q^{-4} therefore occurs for $\alpha = -1$. This case give formally the same scattering intensity as the Debye-Anderson-Brumberger model in section 9.14.3. For certain values of α the form factor can be expressed by simple rational polynomials. A few examples

are

$$I_{\text{genExp}}(Q, R, \alpha = -2) = \left(4\pi R^3 \Delta\eta \frac{\arctan(QR/\sqrt{2})}{QR/\sqrt{2}} \right)^2 \quad (9.232)$$

$$I_{\text{genExp}}(Q, R, \alpha = -1) = \left(4\pi R^3 \Delta\eta \frac{1}{1 + \frac{1}{6}Q^2 R^2} \right)^2 \quad (9.233)$$

$$I_{\text{genExp}}(Q, R, \alpha = 0) = \left(4\pi R^3 \Delta\eta \frac{1}{\left(1 + \frac{1}{12}Q^2 R^2\right)^2} \right)^2 \quad (9.234)$$

$$I_{\text{genExp}}(Q, R, \alpha = 1) = \left(4\pi R^3 \Delta\eta \frac{1 - \frac{1}{60}Q^2 R^2}{\left(1 + \frac{1}{20}Q^2 R^2\right)^3} \right)^2 \quad (9.235)$$

$$I_{\text{genExp}}(Q, R, \alpha = 2) = \left(4\pi R^3 \Delta\eta \frac{1 - \frac{1}{30}Q^2 R^2}{\left(1 + \frac{1}{30}Q^2 R^2\right)^4} \right)^2 \quad (9.236)$$

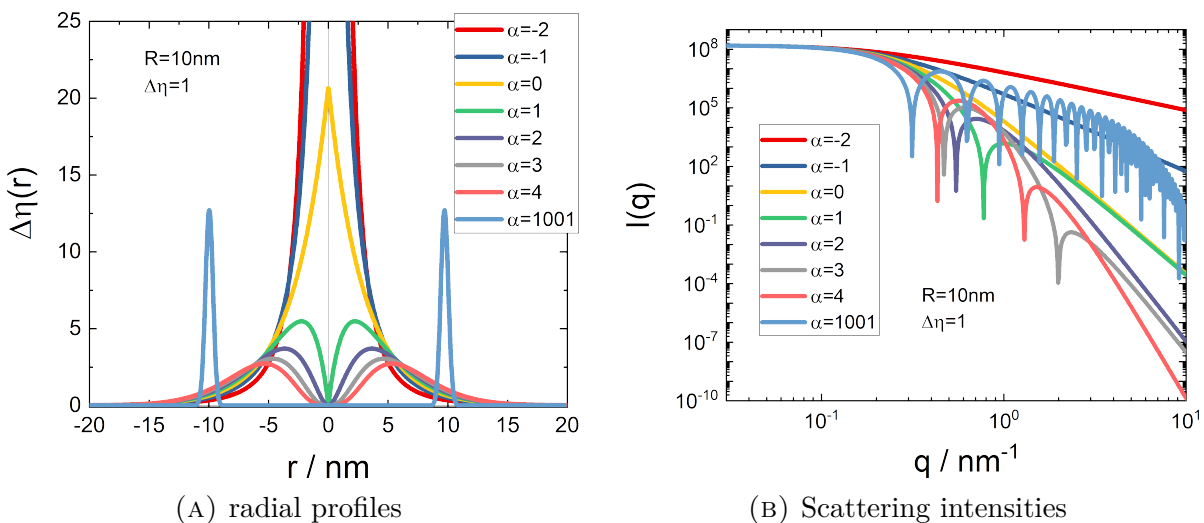


FIGURE 9.57. `genExp Sphere`-model.

Note

- the parameter α needs to be larger than -3.
- for α values smaller than 0 the radial profile has a pole at $r = 0$.

Input Parameters for model Gen. Exp. Sphere and profile:Gen. Exp. Sphere:

R: radius of gyration R_g

alpha: shape parameter α of radial profile

Delta_eta: scattering length density contrast $\Delta\eta$

9.3.10. Generalized Gaussian scattering profile (fuzzy sphere model).

In [218] the form factor of a variety of spherical profiles have been given. The hollow Gaussian profiles have been summarized in this form factor called generalized gaussian sphere. The radial scattering length density profile is defined as

$$\eta_{\text{genGauss}}(r) = \Delta\eta \frac{\left(\frac{r}{R_g}\right)^\alpha e^{-\frac{\alpha+3}{2}\frac{r^2}{R_g^2}} 2^{-\frac{\alpha+1}{2}} (3+\alpha)^{3+\alpha}}{\Gamma\left(\frac{\alpha+3}{2}\right)} \quad (9.237)$$

The corresponding scattering amplitude is then calculated as

$$F_{\text{genGauss}}(Q, R_g) = 4\pi R_g^3 {}_1F_1\left(\frac{\alpha+3}{2}, \frac{3}{2}, -\frac{R_g^2 Q^2}{2(\alpha+3)}\right) \quad (9.238)$$

$$I_{\text{genGauss}}(Q, R_g, \alpha) = F_{\text{genGauss}}^2(Q, R_g, \alpha) \quad (9.239)$$

The scattering intensity decays for large q -values and for positive and not even integer values of α as

$$\lim_{Q \rightarrow \infty} I_{\text{genGauss}}(Q, R_g, \alpha) \propto Q^{-2(3+\alpha)} \quad (9.240)$$

For positive and even integer values of α the decay at large Q -values is

$$\lim_{Q \rightarrow \infty} I_{\text{genGauss}}(Q, R_g, \alpha) \propto e^{-R_g^2 Q^2 / (6+2\alpha)} Q^{2\alpha} \quad (9.241)$$

A decay of Q^{-4} therefore occurs for $\alpha = -1$. For certain values of α the form factor can be expressed with simple functions. A few examples are

$$I_{\text{genGauss}}(Q, R_g, \alpha = -2) = \Delta\eta^2 V^2 \frac{\pi \operatorname{erf}^2\left(\frac{R_g Q}{\sqrt{2}}\right)}{2R_g^2 Q^2} \quad (9.242)$$

$$I_{\text{genGauss}}(Q, R_g, \alpha = -1) = \Delta\eta^2 V^2 \frac{4 D_F^2\left(\frac{R_g Q}{2}\right)}{R_g^2 Q^2} \quad (9.243)$$

$$I_{\text{genGauss}}(Q, R_g, \alpha = 0) = \Delta\eta^2 V^2 e^{-\frac{1}{3} R_g^2 Q^2} \quad (9.244)$$

$$I_{\text{genGauss}}(Q, R_g, \alpha = 1) = \Delta\eta^2 V^2 \frac{\left(\sqrt{2}(R_g^2 Q^2 - 4)4 D_F\left(\frac{R_g Q}{2}\right) - 2R_g Q\right)^2}{16R_g^2 Q^2} \quad (9.245)$$

$$I_{\text{genGauss}}(Q, R_g, \alpha = 2) = e^{-\frac{1}{5} R_g^2 Q^2} \left(1 - \frac{R_g^2 Q^2}{15}\right)^2 \quad (9.246)$$

$$I_{\text{genGauss}}(Q, R_g, \alpha = 4) = e^{-\frac{1}{7} R_g^2 Q^2} \left(1 + \frac{1}{175} R_g^2 Q^2 (R_g^2 Q^2 - 70)\right)^2 \quad (9.247)$$

where $D_F(x)$ is the Dawson integral.

Note

- the parameter α needs to be larger than -3.
- for α values smaller than 0 the radial profile has a pole at $r = 0$.

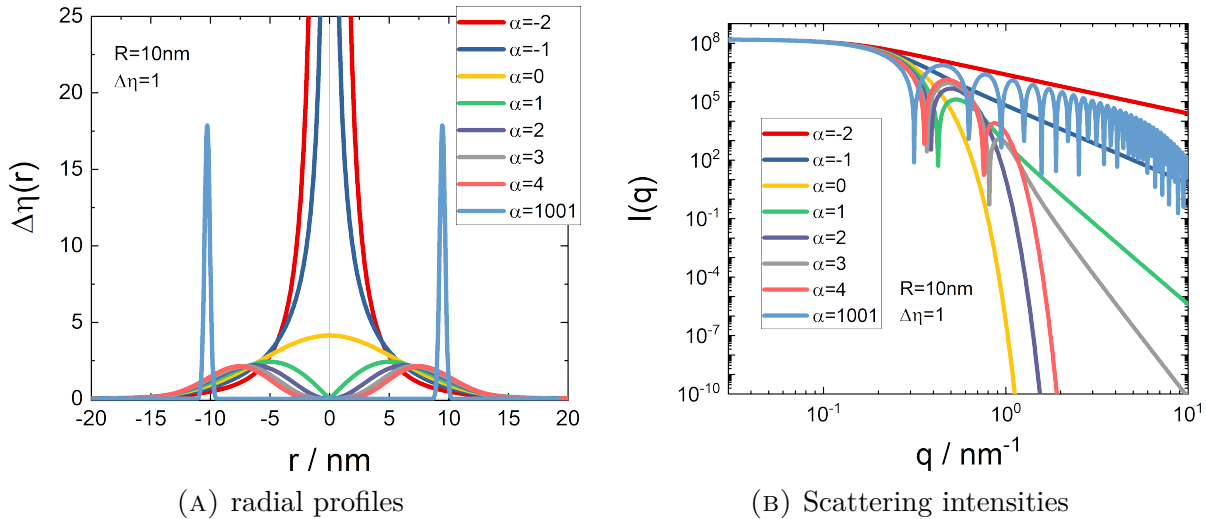


FIGURE 9.58. genGauss Sphere-model.

Input Parameters for model Gen. Gauss Sphere and profile:Gen. Gauss Sphere:
R: radius of gyration R_g
alpha: shape parameter α of radial profile
Delta_eta: scattering length density contrast $\Delta\eta$

9.4. Polymers and Micelles

9.4.1. Gaussian chain.

Consider a flexible polymer coil where each monomer located at a distance \mathbf{R}_m its scattering field amplitude is given by

$$F(\mathbf{q}, t) = \sum_{m=1}^N e^{-i\mathbf{q} \cdot \mathbf{R}_m(t)}. \quad (9.248)$$

The scattering intensity averaged over all molecule configurations reads

$$\langle |F(\mathbf{q})|^2 \rangle = \sum_{m,n} \langle e^{-i\mathbf{q} \cdot (\mathbf{R}_m - \mathbf{R}_n)} \rangle \quad (9.249)$$

As the monomer segments $\mathbf{R}_m - \mathbf{R}_n$ are Gaussian distributed the averages $\langle \dots \rangle$ can be written as

$$\langle e^{-i\mathbf{q} \cdot (\mathbf{R}_m - \mathbf{R}_n)} \rangle = e^{\frac{q^2}{6} \langle (\mathbf{R}_m - \mathbf{R}_n)^2 \rangle} \quad (9.250a)$$

$$= e^{-\frac{q^2 b^2}{6} |m-n|^{2\nu}} \quad (9.250b)$$

Here b is the statistical segment length and the contour length L equals $L = Nb$. The average of the segment inter-distances squares is kept in the general form

$$\langle (\mathbf{R}_m - \mathbf{R}_n)^2 \rangle = b^2 |m-n|^{2\nu}. \quad (9.251)$$

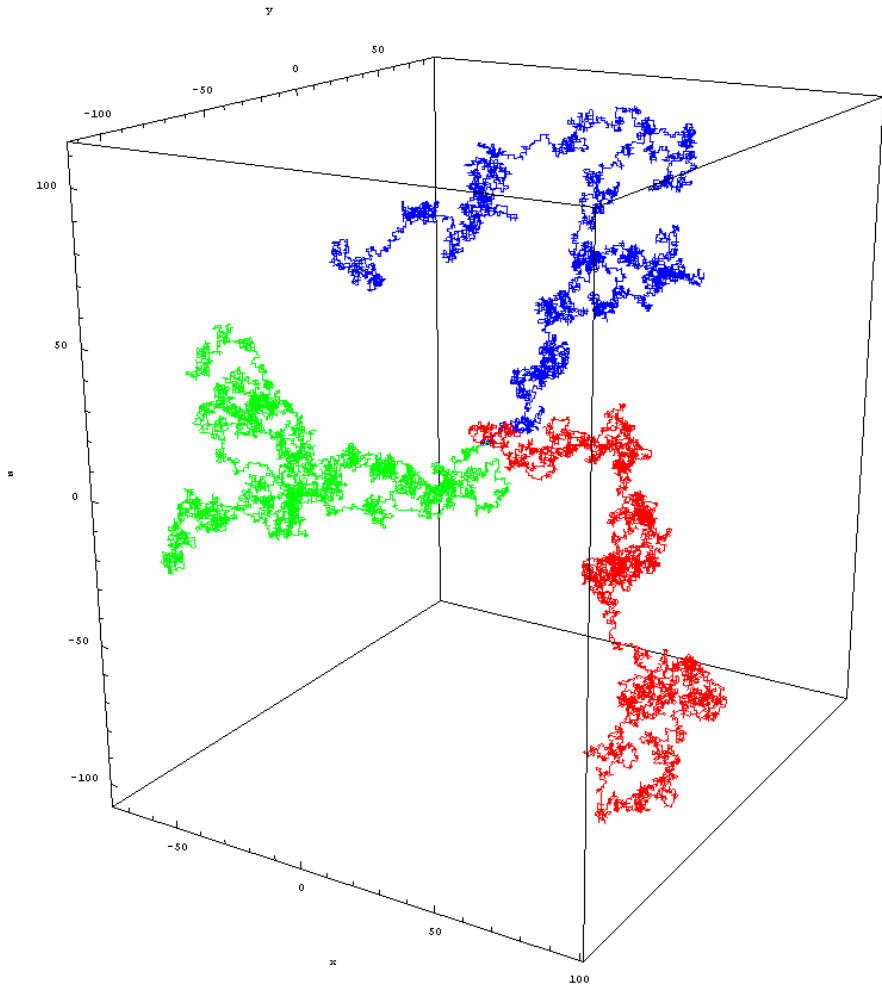


FIGURE 9.59. The underlying model for a polymer chain is an isotropic random walk on the Euclidean lattice \mathbb{Z}^3 . This picture shows three different walks after 10 000 unit steps, all three starting from the origin.

ν is the excluded volume parameter from the Flory mean field theory⁵⁶ of polymer solutions. The radius of gyration R_G is given by

$$R_G^2 = \frac{1}{2N^2} \sum_{m,n}^N \langle (\mathbf{R}_m - \mathbf{R}_n)^2 \rangle \quad (9.252a)$$

$$= \frac{1}{2N^2} \sum_{m,n}^N b^2 |m - n|^{2\nu} \quad (9.252b)$$

$$= \frac{b^2}{N} \sum_k^N \left(1 - \frac{k}{N}\right) k^{2\nu} \quad (9.252c)$$

$$= \frac{b^2}{(2\nu + 1)(2\nu + 2)} N^{2\nu} \quad (9.252d)$$

⁵P.J. Flory, "Statistical Mechanics of Chain Molecules", Interscience Publishers (1969)

⁶[Boualem Hammouda, the_SANS_toolbox.pdf](#)

Three cases are relevant:

- (1) Self-avoiding walk corresponds to swollen chains with $\nu = 3/5$, for which $R_G^2 = \frac{25}{176}b^2N^{6/5}$.
- (2) Pure random walk corresponds to chains in Θ -conditions (where solvent-solvent, monomer-monomer and solvent-monomer interactions are equivalent) with $\nu = 1/2$, for which $R_G^2 = \frac{1}{6}b^2N$.
- (3) Self attracting walk corresponds to collapsed chains with $\nu = 1/3$, for which $R_G^2 = \frac{9}{40}b^2N^{2/3}$.

Using the general identity

$$\sum_{i,j}^N y(|i - j|) = N + 2 \sum_{k=1}^N (N - k)y(k) \quad (9.253)$$

the form factor reads

$$P(q) = \frac{1}{N^2}|F(q)|^2 = \frac{1}{N^2} \left\{ N + 2 \sum_{k=1}^N (N - k)e^{-\frac{q^2 b^2}{6}k^{2\nu}} \right\} \quad (9.254)$$

Going to the continuous limit ($N \gg 1$), one obtains:

$$P(q) = 2 \int_0^1 dx (1 - x)e^{-\frac{q^2 b^2}{6}N^{2\nu}x^{2\nu}} \quad (9.255a)$$

$$= \frac{U^{\frac{1}{2\nu}}\Gamma\left(\frac{1}{2\nu}\right) - \Gamma\left(\frac{1}{\nu}\right) - U^{\frac{1}{2\nu}}\Gamma\left(\frac{1}{2\nu}, U\right) + \Gamma\left(\frac{1}{\nu}, U\right)}{\nu U^{1/\nu}} \quad (9.255b)$$

$$= \frac{1}{\nu U^{\frac{1}{2\nu}}} \gamma\left(\frac{1}{2\nu}, U\right) - \frac{1}{\nu U^{\frac{1}{\nu}}} \gamma\left(\frac{1}{\nu}, U\right) \quad (9.255c)$$

with the modified variable

$$U = \frac{q^2 b^2 N^{2\nu}}{6} = (2\nu + 1)(2\nu + 2) \frac{q^2 R_G^2}{6} \quad (9.256)$$

and the upper incomplete Gamma Function $\Gamma(a, x) = \int_x^\infty dt t^{a-1} \exp(-t)$ and lower incomplete Gamma Function $\gamma(a, x) = \int_0^x dt t^{a-1} \exp(-t)$ for a real and $x \geq 0$ and the Gamma function $\Gamma(a) = \Gamma(a, 0) = \gamma(a, \infty) = \Gamma(a, x) + \gamma(a, x) = \int_0^\infty dt t^{a-1} \exp(-t)$. Polymer chains follow Gaussian statistics in polymer solutions: they are swollen in good solvents $\nu = 3/5$, are thermally relaxed in "theta"-solvents $\nu = 1/2$ and partially precipitate in poor solvents $\nu = 1/3$. The familiar Debye function is recovered when $\nu = 1/2$. The asymptotic limit at large q -values of the generalized Gaussian chain is dominated by the $\frac{1}{\nu U^{\frac{1}{2\nu}}} \Gamma\left(\frac{1}{2\nu}\right)$ term which varies like $U^{-1/(2\nu)} \sim q^{-1/\nu}$. For $\nu = 1$ we get the limit of an infinitesimal thin rod and for $\nu = 1/4$ a compact object with a Porod law of q^{-4} .

SASfit has implemented the generalized form of a Gaussian (**generalized Gaussian coil**) coil and the standard Debye formula **Gauss**. In both cases three versions are implemented which only differ in their parametrization of the forward scattering. In case of the Debye-formula also the polydisperse **GaussPoly** is implemented.

9.4.1.1. *Gauss*.

Flexible polymer chains which are not self-avoiding and obey Gaussian statistics. Debye (1947) [105] has calculated the form factor of such chains:

$$I_{\text{Gauss}}(q) = I_0 2 \frac{\exp(-u) + u - 1}{u^2} \quad (9.257)$$

$$u = q^2 R_g^2 \quad (9.258)$$

Input Parameters for model Gauss:

Rg: radius of gyration R_g

I0: forward scattering I_0 for $q = 0$

9.4.1.2. *Gauss2*.

This form factor [105] differs only by the parametrization for the forward scattering $I_0 = (b_p - V\eta_s)^2$ from the Debye formula in eq. 9.257

$$I_{\text{Gauss2}}(q) = \beta^2 2 \frac{\exp(-u) + u - 1}{u^2} \quad (9.259)$$

$$u = q^2 R_g^2$$

$$\beta = b_p - V\eta_s,$$

where b_p is the scattering length of a polymer molecule of molecular volume V dissolved in a solvent of scattering length density η_s from which the excess scattering length of a polymer molecule β can be calculated. Combining this form factor with a **Delta** size distribution 7.1 is needed to scale the scattering intensity. With proper values for the form factor the parameter N of the **Delta**-distribution yields the particle number density.

Input Parameters for model Gauss2:

Rg: radius of gyration R_g

b_p: scattering length of polymer b_p in [cm]

V: molecular volume of a single polymer molecule V in [cm^3]

eta_s: scattering length density of solvent η_s in [cm^{-2}]

9.4.1.3. *Gauss3*.

This form factor [105] differs only by the parametrization for the forward scattering $I_0 = (b_p - \frac{M_w}{N_a \rho_p} \eta_s)^2$ from the Debye formula in eq. 9.257

$$I_{\text{Gauss3}}(q) = \beta^2 2 \frac{\exp(-u) + u - 1}{u^2} \quad (9.260)$$

with

$$u = q^2 R_g^2$$

$$\beta = b_p - V \eta_s$$

$$V = \frac{M_w}{N_a \rho_p}$$

N_a = Avogadro number

Input Parameters for model Gauss3:

Rg: radius of gyration R_g

b_p: scattering length of polymer b_p in [cm]

M_w: molecular weight of polymer M_w in [g/mol]

rho_p: mass density of polymer ρ_p in [g cm^{-3}]

eta_s: scattering length density of solvent η_s in [cm^{-2}]

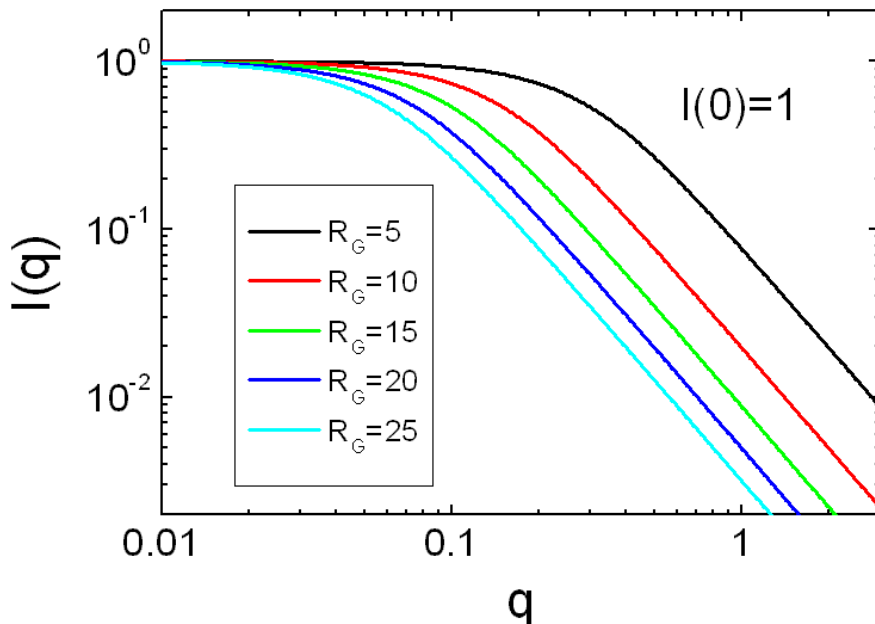


FIGURE 9.60. Scattering function of Gaussian coils plotted for several radii of gyration.

9.4.1.4. Polydisperse flexible polymers with Gaussian statistics. [376]

Polydispersity has been included in terms of a Schulz–Zimm mass distribution by Zimm (1948) [545] and Greschner (1973) [170]

$$\begin{aligned}
 I_{\text{GaussPoly}}(q) &= I_0 2 \frac{(1+Ux)^{-1/U} + x - 1}{(1+U)x^2} \\
 x &= q^2 R_g^2 / (1 + 2U) \\
 U &= \frac{M_w}{M_n} - 1
 \end{aligned} \tag{9.261}$$

Input Parameters for model GaussPoly:

- Rg: radius of gyration R_g
- M_w: weight averaged molecular weight M_w
- M_n: number averaged molecular weight M_n
- I0: forward scattering I_0 for $q = 0$

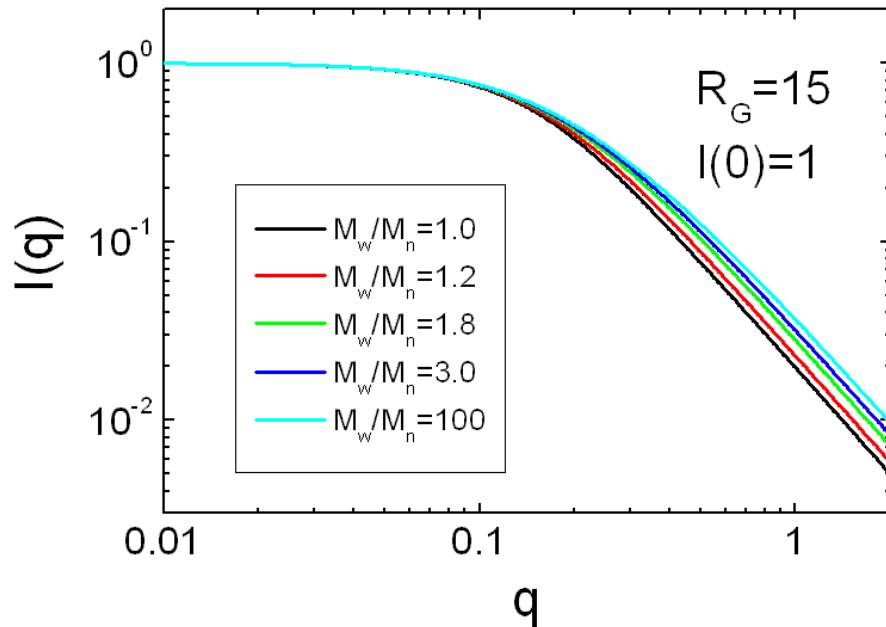


FIGURE 9.61. Scattering function of polydisperse Gaussian coil plotted for several ratios of M_w/M_n .

9.4.1.5. generalized Gaussian coil. [186, 184, 182, 185]

The scattering function for the generalized Gaussian coil is according to eq. 9.255c

$$I_{\text{gGc}}(q) = I_0 \left(\frac{1}{\nu U^{\frac{1}{2\nu}}} \gamma \left(\frac{1}{2\nu}, U \right) - \frac{1}{\nu U^{\frac{1}{\nu}}} \gamma \left(\frac{1}{\nu}, U \right) \right) \tag{9.262}$$

with the modified variable

$$U = (2\nu + 1)(2\nu + 2) \frac{q^2 R_G^2}{6} \quad (9.263)$$

and the lower incomplete Gamma Function $\gamma(a, x) = \int_0^x dt t^{a-1} \exp(-t)$. ν is the excluded volume parameter from the Flory mean field theory and typical values for them are

- $\nu = 1/3$: partially precipitate in poor solvents
- $\nu = 1/2$: thermally relaxed in "theta"-solvents
- $\nu = 3/5$: swollen in good solvents

Input Parameters for model generalized Gaussian coil:

- Rg:** radius of gyration R_g
- nu:** excluded volume parameter $\nu > 0$
- I0:** forward scattering I_0 for $q = 0$

Note:

- For large q -values to model decays with the law $\propto q^{-1/\nu}$ for $q \rightarrow 0$

9.4.1.6. generalized Gaussian coil 2. [186, 184]

The scattering function for the generalized Gaussian coil is according to eq. 9.255c and differs only by the parametrization for the forward scattering $I_0 = (b_p - V\eta_s)^2$ from the formula in eq. 9.262

$$I_{gGc2}(q) = (b_p - V\eta_s)^2 \left(\frac{1}{\nu U^{\frac{1}{2\nu}}} \gamma \left(\frac{1}{2\nu}, U \right) - \frac{1}{\nu U^{\frac{1}{\nu}}} \gamma \left(\frac{1}{\nu}, U \right) \right) \quad (9.264)$$

with the modified variable

$$U = (2\nu + 1)(2\nu + 2) \frac{q^2 R_G^2}{6} \quad (9.265)$$

Input Parameters for model generalized Gaussian coil 2:

- Rg:** radius of gyration R_g
- b_p:** scattering length of polymer b_p in [cm]
- V:** molecular volume of a single polymer molecule V in [cm^3]
- eta_s:** scattering length density of solvent η_s in [cm^{-2}]

Note:

- For large q -values to model decays with the law $\propto q^{-1/\nu}$ for $q \rightarrow 0$

9.4.1.7. generalized Gaussian coil 3. [186, 184]

The scattering function for the generalized Gaussian coil is according to eq. 9.255c and differs only by the parametrization for the forward scattering $I_0 = (b_p - \frac{M_w}{N_a \rho_p} \eta_s)^2$ from the formula in eq. 9.262

$$I_{\text{gGc3}}(q) = \left(b_p - \frac{M_w}{N_a \rho_p} \eta_s \right)^2 \left(\frac{1}{\nu U^{\frac{1}{2\nu}}} \gamma \left(\frac{1}{2\nu}, U \right) - \frac{1}{\nu U^{\frac{1}{\nu}}} \gamma \left(\frac{1}{\nu}, U \right) \right) \quad (9.266)$$

with the modified variable

$$U = (2\nu + 1)(2\nu + 2) \frac{q^2 R_G^2}{6} \quad (9.267)$$

Input Parameters for model generalized Gaussian coil 3:

Rg: radius of gyration R_g

b_p: scattering length of polymer b_p in [cm]

M_w: molecular weight of polymer M_w in [g/mol]

rho_p: mass density of polymer ρ_p in [g cm⁻³]

eta_s: scattering length density of solvent η_s in [cm⁻²]

Note:

- For large q -values to model decays with the law $\propto q^{-1/\nu}$ for $q \rightarrow 0$

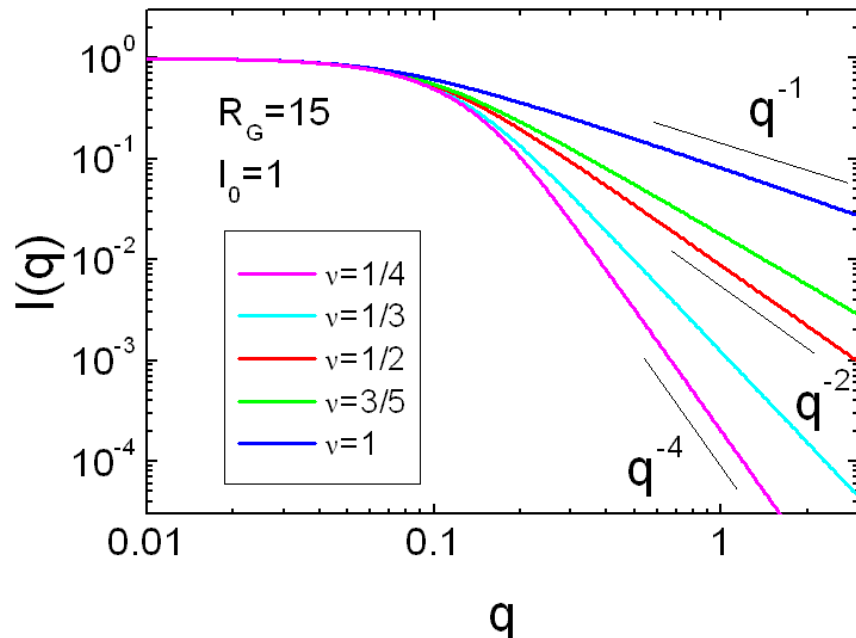


FIGURE 9.62. Scattering function of the generalized Gaussian coil plotted for several excluded volume parameters.

9.4.2. Star-shaped polymers.

Star-shaped polymers [531] are branched polymers consisting of several (more than three) linear chains connected to a central core [414]. The core of the star-shaped polymer is much smaller than the length of the arms and can be an atom, molecule, or macromolecule. Star-shaped polymers in which the arms are all equivalent in length and structure are considered homogeneous, and ones with variable lengths and structures are considered heterogeneous. For selected types of star-shaped polymers analytical expressions for the scattering intensity have been published and included in SASfit .

9.4.2.1. Star polymer with Gaussian statistic according to Benoit.

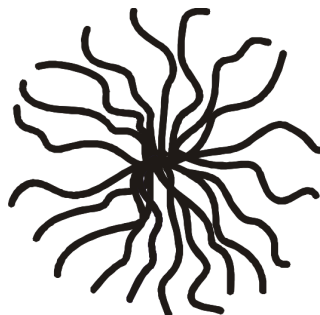


FIGURE 9.63. Sketch of a branched or star polymers with f number of arms

Benoit [23] derived an expression for the scattering from branched or star polymers with a number of arms f , which can be expressed in the following way:

$$I_{\text{Star}}(Q, R_G, f) = I_0 \frac{2}{f\nu^2} \left(\nu - [1 - e^{-\nu}] + \frac{f-1}{2} [1 - e^{-\nu}]^2 \right) \quad (9.268)$$

with $u = R_G^2 Q^2$, $\nu = \frac{uf}{3f-2}$ and $\lim_{Q=0} I_{\text{Star}}(Q, R_G, f) = I_0$. f denotes the number of arms and R_G the Guinier radius of a single arm.

Input Parameters for model BenoitStar:

I0: forward scattering I_0 for $q = 0$

RG: radius of gyration of the star polymer R_g

dummy: not used

dummy: not used

f: number of arms f

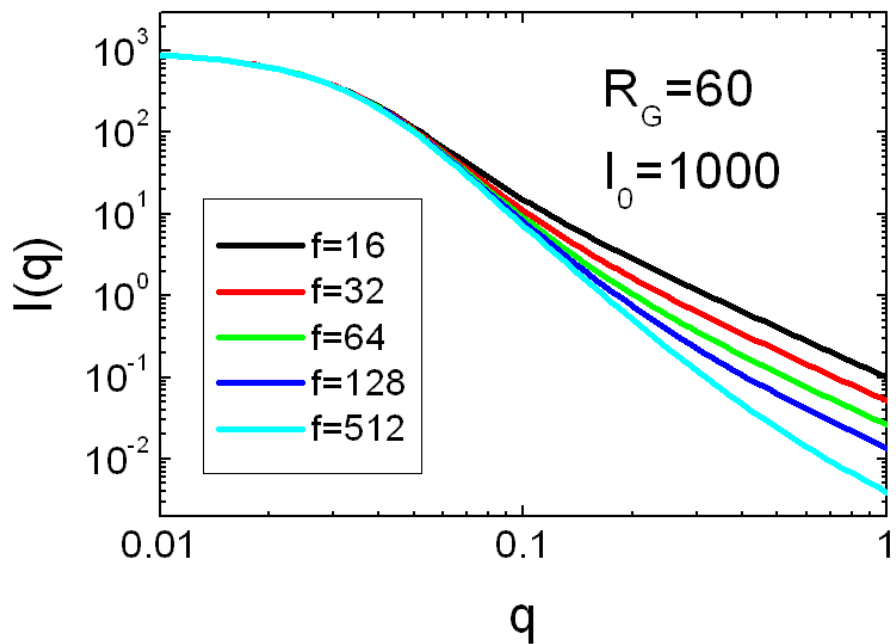


FIGURE 9.64. Scattering function of a star polymer according to Benoit.

9.4.2.2. *Star polymer with arms of rigid rods.*

[225]

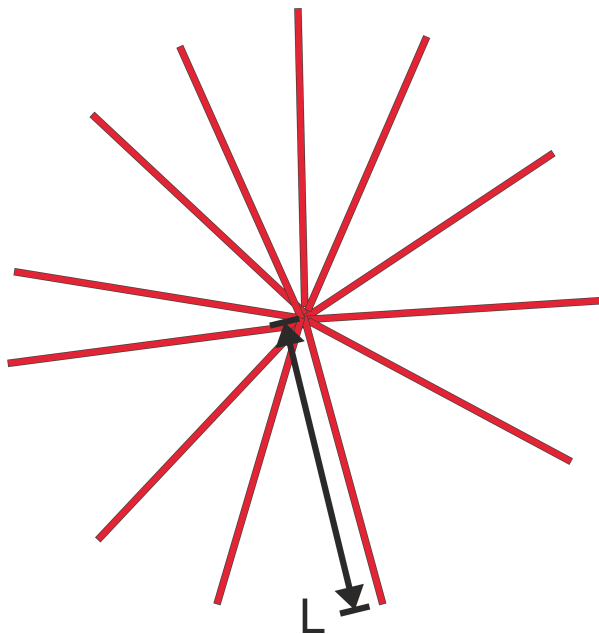


FIGURE 9.65. Star with arms of thin rigid rods

$$P_{\text{star}}(Q) = I_0/f (P_{\text{sb}} + (f - 1)P_{\text{ib}}) \quad (9.269)$$

$$P_{\text{sb}} = 2\text{Si}(qL)/(qL) - j_0(qL/2) \quad (9.270)$$

$$P_{\text{ib}} = (\text{Si}(qL)/(qL))^2 \quad (9.271)$$

with $j_0(x) = \frac{\sin(x)}{x}$ being the spherical Bessel function of first kind and zero order.

Input Parameters for model star polymer with arms of rigid rods:

I0: forward scattering I_0 for $q = 0$

L: length L of a single rigid infinitesimal thin rodlike arm

dummy: not used

dummy: not used

f: number of arms f

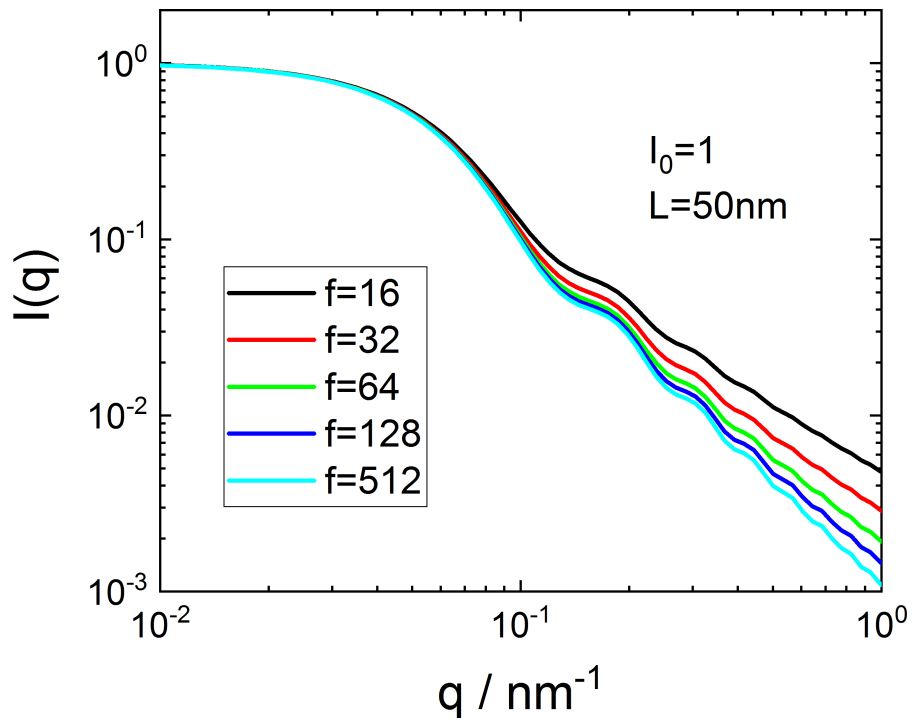


FIGURE 9.66. Scattering function of a star polymer with arms of thin rigid rods.

9.4.2.3. Star polymer with semi-flexible arms.

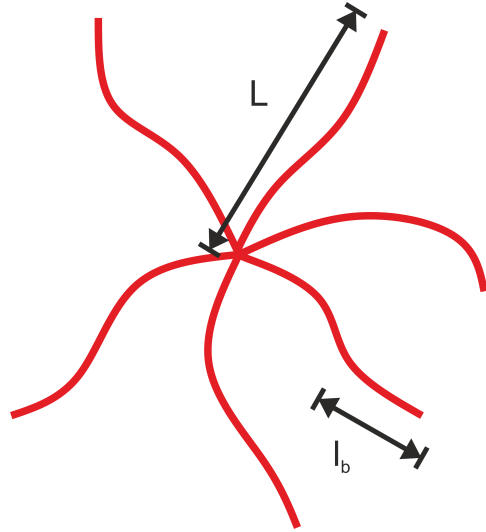


FIGURE 9.67. Star with arms of semi-flexible (wormlike) polymers

The derivation of the form factor of a star with semi-flexible arms can be found in [275, 276, 225, 394]. The resulting function for the scattering intensity is given by

$$P_{\text{star}}(Q) = I_0/f (P_{\text{sb}} + (f - 1)P_{\text{ib}}) \quad (9.272)$$

$$P_{\text{sb}} = \frac{2}{X^2} \int_0^X (X - x) \phi(x) dx \quad (9.273)$$

$$P_{\text{ib}} = \left(\frac{1}{X} \int_0^X \phi(x) dx \right)^2 \quad (9.274)$$

with

$$X = \frac{2L}{l_b} \quad (9.275)$$

$$\phi(x) = \exp \left(-\frac{s^2}{3} x f(x) \right) \frac{\sin(sxg(x))}{sxg(x)} \quad (9.276)$$

$$s = \frac{1}{2} ql_b \quad (9.277)$$

$$x f(x) = \frac{2\langle r^2 \rangle}{l_b^2} - \frac{1}{2} x^2 g^2(x) \quad (9.278)$$

$$x^2 g^2(x) = \frac{2\langle r^2 \rangle}{l_b^2} \sqrt{10} \sqrt{1 - \frac{3}{5} K} \quad (9.279)$$

and

$$K = \frac{\langle r^4 \rangle}{\langle r^2 \rangle^2} \quad (9.280)$$

$$\langle r^2 \rangle = \frac{l_b^2}{2} \left(x - (1 - e^{-x}) \right) \quad (9.281)$$

$$\langle r^4 \rangle = \frac{l_b^4}{4} \left\{ \frac{5}{3} x^2 - \frac{52}{9} x - \frac{2}{27} (1 - e^{-3x}) + 8 (1 - e^{-x}) - 2x e^{-x} \right\} \quad (9.282)$$

The radius of gyration of a star polymer with semi-flexible arms is [327, 225]

$$R_G = \left[(3f - 2) \frac{2L}{3l_b} + 1 - 2f + \frac{l_b}{L} + 2(f-1) \frac{l_b}{2L} x_1 - 2 \left(\frac{l_b}{2L} \right)^2 x_1 + \left(1 - x_1 \frac{l_b}{2L} \right)^2 \right] \frac{l_b^2}{4f} \quad (9.283)$$

$$x_1 = 1 - \exp(-2L/l_b) \quad (9.284)$$

The limiting cases

$$\lim_{l_b \rightarrow \infty} R_G = L^2/3 \quad (9.285)$$

$$\lim_{l_b \rightarrow 0} R_G = \frac{3f - 2}{6f} L l_b \quad (9.286)$$

correspond to the cases of a star with rigid rod and a star with Gaussian arms.

Input Parameters for model **star polymer with semi-flexible arms**:

I0: forward scattering I_0 for $q = 0$

L: contour length L of a single arm

lb: Kuhn length l_b of the polymer arm

dummy: not used

f: number of arms f

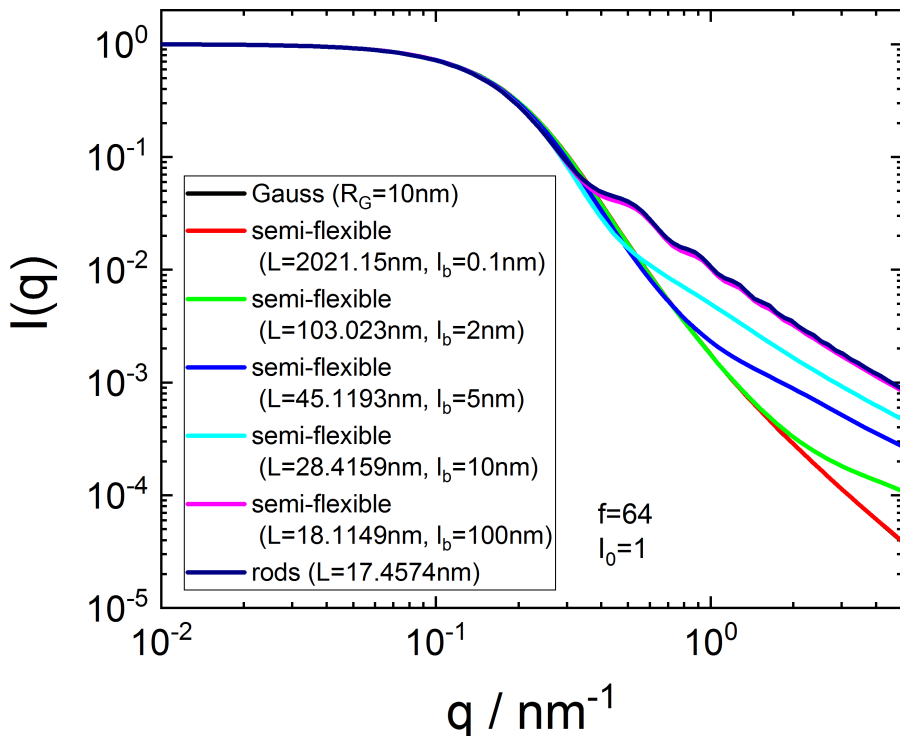


FIGURE 9.68. Scattering function of a star polymer with semi-flexible arms. In the limit $l_b \rightarrow 0$ and $l_b \rightarrow 0$ the form factor is approximated by a star with gaussian arms and in stars with arms of rigid rods. The contour length L and Kuhn length l_b have been chosen to get always the same radius of gyration of 10nm.

9.4.2.4. Star of gaussian polymer with excluded volume.

In [185] the star form factor including excluded volume effects takes the form factor of an individual polymer and combines it in terms of a combinatorial star according to [225]. For this the form factor of a chain with the contour length L of a single arm and that one with a contour length of twice a single arm $2L$ is needed. As the Radius of gyration of a single arm scales according to eq. 9.256 with $R_g \propto L^{2\nu}$ we get

$$P_{\text{star}}(q) = I_0/f (P_{\text{sb}}(q, R_G) + (f - 1)P_{\text{ib}}(q, R_G)) \quad (9.287)$$

$$P_{\text{sb}}(q, R_G) = \frac{1}{\nu U^{\frac{1}{2\nu}}} \gamma\left(\frac{1}{2\nu}, U\right) - \frac{1}{\nu U^{\frac{1}{\nu}}} \gamma\left(\frac{1}{\nu}, U\right) \quad (9.288)$$

$$P_{\text{ib}} = 2P_{\text{sb}}(q, 2^{2\nu}R_G) - P_{\text{sb}}(q, R_G) \quad (9.289)$$

with $\gamma(d, U)$ being the lower incomplete gamma-function and the definition of U as

$$\gamma(d, U) = \int_0^U \exp(-t)t^{d-1} dt \quad (9.290)$$

$$U = q^2 R_G^2 \frac{(2\nu + 1)(2\nu + 2)}{6} \quad (9.291)$$

Input Parameters for model star of polymer arms with excl. vol.:

I0: forward scattering I_0 for $q = 0$

Rg: radius of gyration R_G of a single arm

nu: Flory exponent ν of the polymer arm

dummy: not used

f: number of arms f

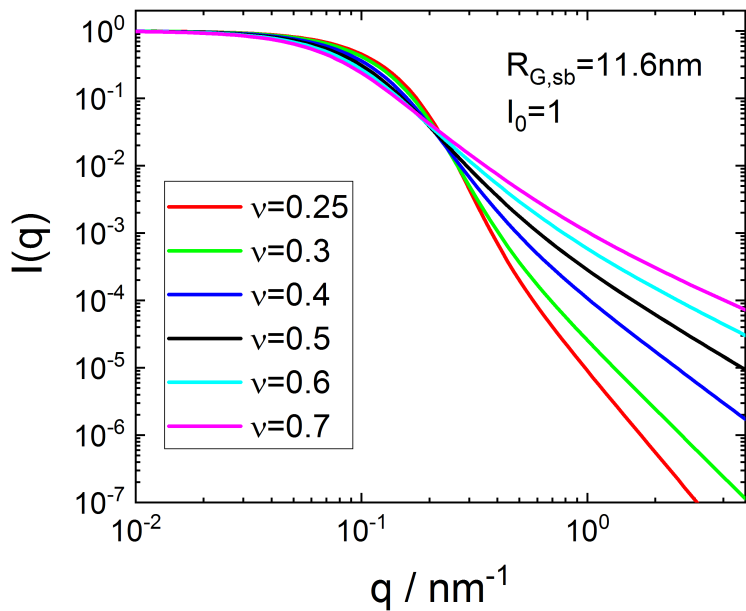


FIGURE 9.69. Scattering function of a star polymer with arms following Gaussian statistics with excluded volume effects. For $\nu = 1/2$ the scattering curves is identical to the BenoitStar.

9.4.2.5. *Polydisperse star polymer with Gaussian statistics [62].*

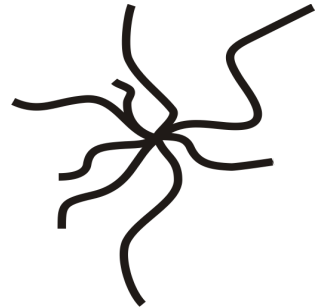


FIGURE 9.70. Polydisperse star polymer with Gaussian statistics

For a Schulz–Flory (most probable) distribution (Schulz–Zimm distribution with $z = 1$) for the mass distribution of the arms, Burchard [62] has given the form factor:

$$I_{\text{PolydisperseStar}}(Q) = I_0 \frac{1 + \frac{u^2}{3f}}{\left(1 + \frac{u^2(f+1)}{6f}\right)^2} \quad (9.292)$$

where f is the number of arms and $u^2 = \langle R_g^2 \rangle_z Q^2$, where $\langle R_g^2 \rangle_z$ is the z -average radius of gyration squared of an arm.

Input Parameters for model PolydisperseStar:

I0: forward scattering I_0

R_G: radius of gyration R_G

dummy: not used

dummy: not used

f: number of arms f

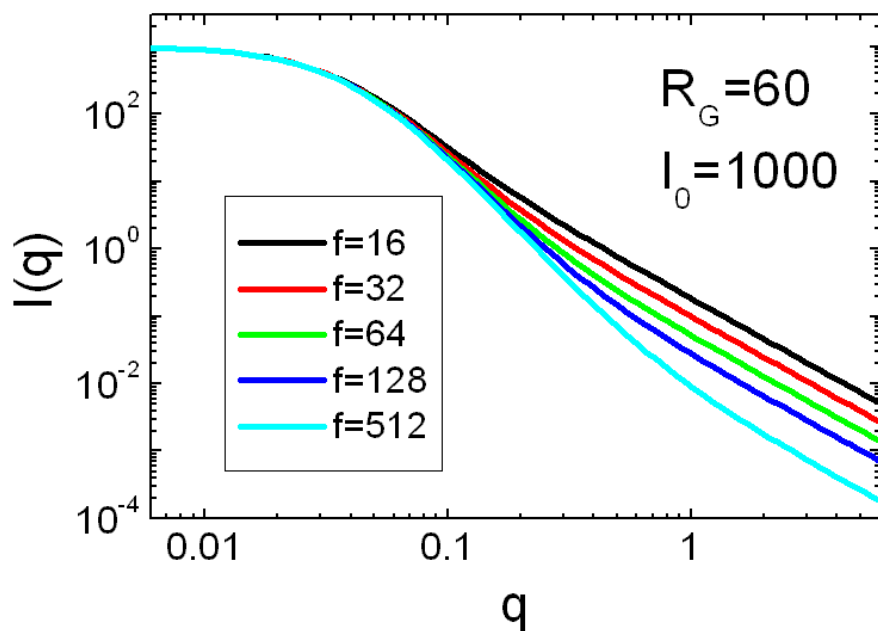


FIGURE 9.71. Scattering function of a polydisperse star polymer with Gaussian statistics.

9.4.2.6. Star polymer according to Dozier.

9.4.2.7. Dozier.

Branched polymers having all branches emanating from the center of the macromolecule

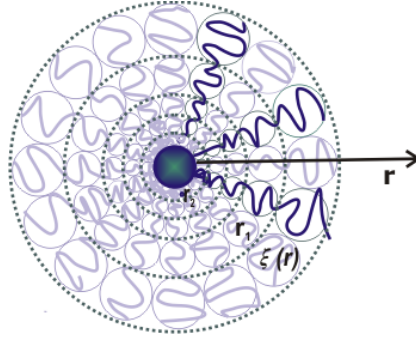


FIGURE 9.72. Star polymer according to Dozier

are commonly called star polymers. For a star polymer Dozier [112] has developed a scattering function which reads:

$$I_{\text{DozierStar}}(Q, I_0, R_G, \alpha, \nu, f) = I_0 \exp \left(-\frac{Q^2 R_G^2}{3} \right) + \frac{4\pi\alpha}{Q\xi} \Gamma(\mu) \frac{\sin(\mu \arctan(Q\xi))}{(1 + Q^2 \xi^2)^{\mu/2}} \quad (9.293)$$

with $\mu = 1/\nu - 1$ and $\xi = 2R_G/\sqrt{f}$.

I_0 : scale parameter

R_G : radius of gyration

α : scale parameter for fractal term

ν : Flory exponent, 3/5 in good solvent, 1/2 in Θ -solvent

f : number of arms in the star

Input Parameters for model Dozier:

I_0: scale parameter if the Gaussian term I_0

R_G: radius of gyration R_G

alpha: scale parameter for fractal term α

nu: excluded volume parameter or Flory exponent ν

f: number of arms f in the star

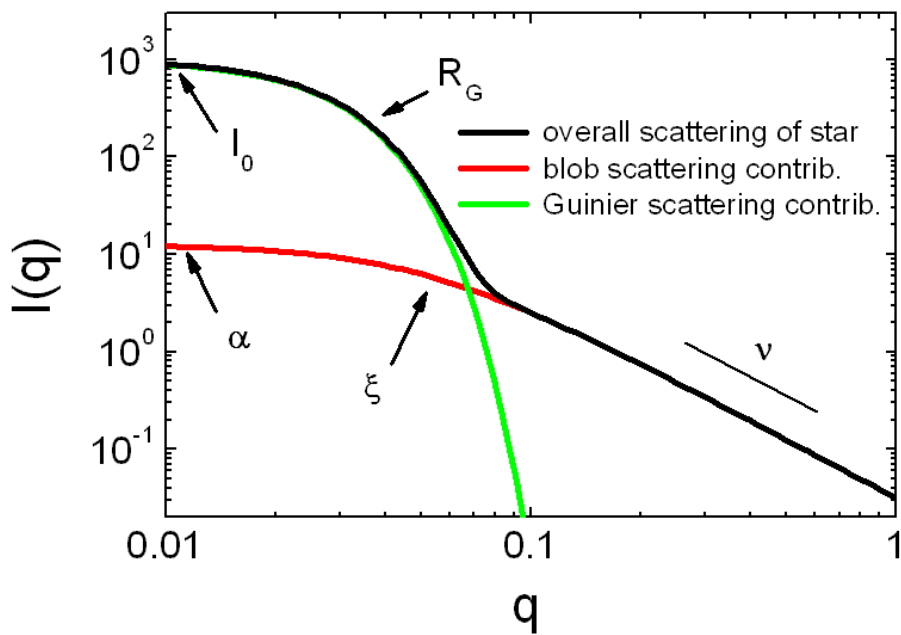


FIGURE 9.73. Scattering function of a star polymer according to Dozier:
 $I_0 = 10^3$, $R_g = 60$, $\alpha = 1$ $\xi = 20$, $\nu = 1/2$

9.4.2.8. *Dozier2*.

This is a re-parametrization of the **Dozier** form factor to scale the scattering of the overall star to the local scattering of the individual arms.

$$I_{\text{DozierStar2}}(Q, I_0, R_G, f, \nu) = \frac{I_0}{f} \left((f - 1) \exp \left(-\frac{Q^2 R_G^2}{3} \right) + \frac{\Gamma(\mu)}{Q\xi} \frac{\sin(\mu \arctan(Q\xi))}{(1 + Q^2 \xi^2)^{\mu/2}} \right) \quad (9.294)$$

with $\mu = 1/\nu - 1$ and $\xi = 2R_G/\sqrt{f}$.

I_0 : scale parameter

R_G : radius of gyration of the star

ξ : exponential damping length in mass fractal $\xi = 2R_G/\sqrt{f}$

ν : Flory exponent, 3/5 in good solvent, 1/2 in Θ -solvent

f : number of arms in the star

(9.295)

Input Parameters for model *Dozier2*:

I_0: scale parameter I_0

R_G: radius of gyration of the star R_G

dummy: not used

nu: Flory exponent, $\nu = 3/5$ in good solvent, $\nu = 1/2$ in Θ -solvent

f: number of arms f in the star from which the scale parameter for the fractal term is calculated.

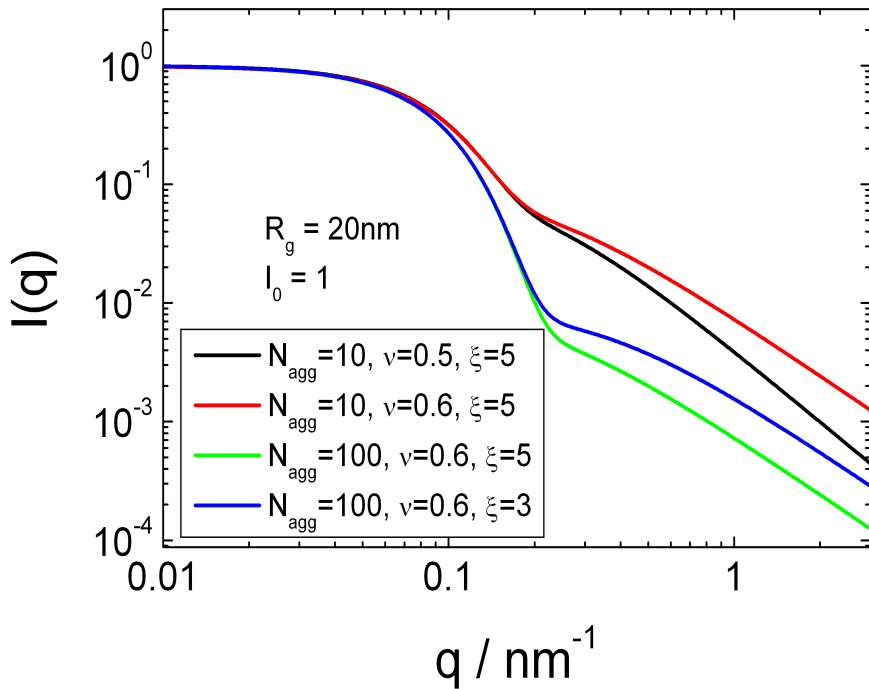


FIGURE 9.74. Scattering function of a star polymer according to Dozier but modified to scale the scattering of the overall star to the local scattering of the individual arms by the number of arms

9.4.3. Ring Polymers.

9.4.3.1. Flexible Ring Polymer.

Three different versions of a ring polymer have been implemented. The form factor of a cyclic chain under theta solvent conditions was first calculated by Casassa using the Gaussian approximation [79, 65]. The formalism has been extended to ring polymers with an excluded volume parameter or Flory parameter ν [24, 168].

The classical form factor of Casassa for a flexible ring polymer following Gaussian statistics in a theta solvent is given by

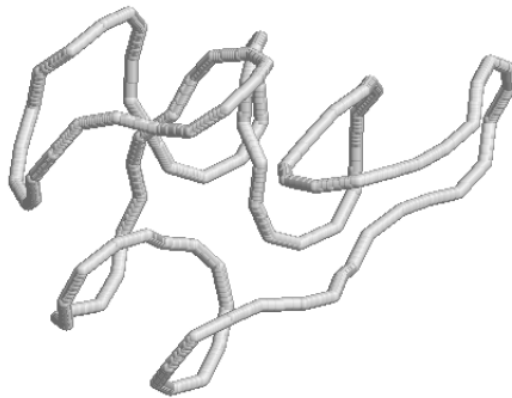


FIGURE 9.75. Sketch of a flexible ring polymer.

$$P_{1r}(q) = \sqrt{\frac{2}{u_{1r}^2}} D \left[\sqrt{\frac{u_{1r}^2}{2}} \right] \quad (9.296)$$

$$u_{1r}^2 = q^2 R_{g,1r}^2 \quad (9.297)$$

$$R_{g,1r}^2 = \frac{b^2 N}{12} \quad (9.298)$$

$$D(X) = \exp(X^2) \int_0^X \exp(t^2) dt \quad (9.299)$$

For ring polymers in a poor or very good solvent show excluded volume effects for which Bloomfeld and Zimm [42, 24, 168] have calculated the radius of gyration. The

corresponding scattering function can be found in [24].

$$P_{BZ,1r}(q) = 2 \int_0^1 (1-x) \exp\left(-\mu \frac{(1-x)^{1+\epsilon} x^{1+\epsilon}}{(1-x)^{1+\epsilon} + x^{1+\epsilon}}\right) dx \quad (9.300)$$

$$\mu = \frac{q^2 R_{g,1r}^2}{6 K_{BZ}} \quad (9.301)$$

$$K_{BZ} = \int_0^1 \frac{(1-X)^{2+\epsilon} X^{1+\epsilon}}{(1-X)^{1+\epsilon} + X^{1+\epsilon}} dX \quad (9.302)$$

$$\epsilon = 2\nu - 1 \quad (9.303)$$

Bensafi et al. [24] also have given a semi-empirical description of a ring polymer with excluded volume effects

$$P_{BMP,1r}(q) = 2 \int_0^1 (1-x) \exp\left(-\mu(1-x)^{1+\epsilon} x^{1+\epsilon}\right) dx \quad (9.304)$$

$$\mu = \frac{q^2 R_{g,1r}^2}{6 K_{BMB}} \quad (9.305)$$

$$K_{BMB} = \int_0^1 (1-X)^{2+\epsilon} X^{1+\epsilon} dX \quad (9.306)$$

$$\epsilon = 2\nu - 1 \quad (9.307)$$

Input Parameters for model RingPolymerCasassa:

Rg: radius of gyration R_G

dummy: not used

dummy: not used

I0: forward scattering I_0

Input Parameters for model RingPolymerBZ:

Rg: radius of gyration R_G

dummy: not used

nu: excluded volume parameter

I0: forward scattering I_0

Input Parameters for model RingPolymerBMB:

Rg: radius of gyration R_G

dummy: not used

nu: excluded volume parameter

I0: forward scattering I_0

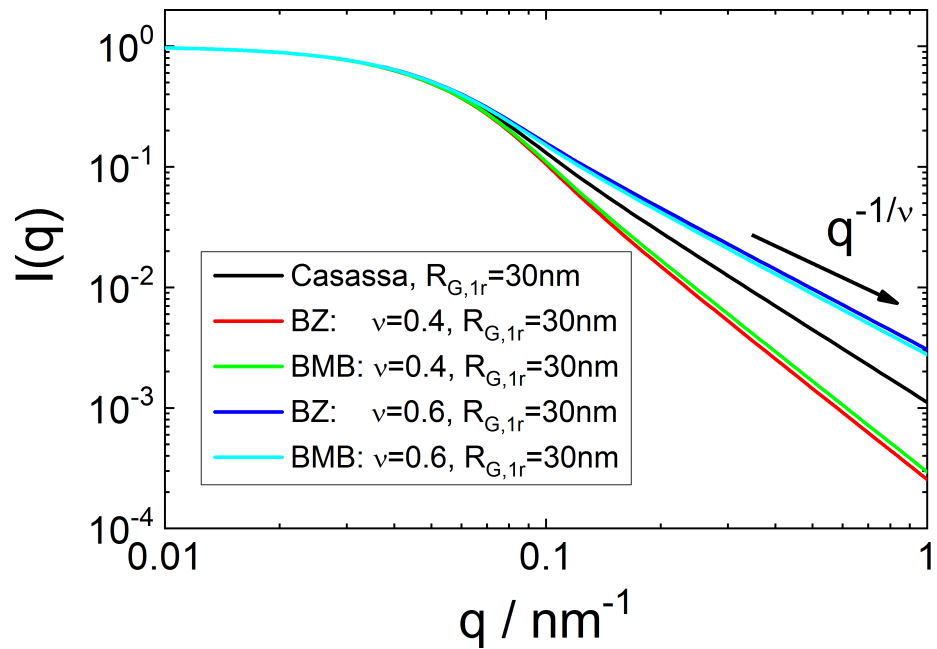


FIGURE 9.76. Scattering intensity of ring polymers of different radius of gyration.

9.4.3.2. *m-membered twisted ring.*

[65]

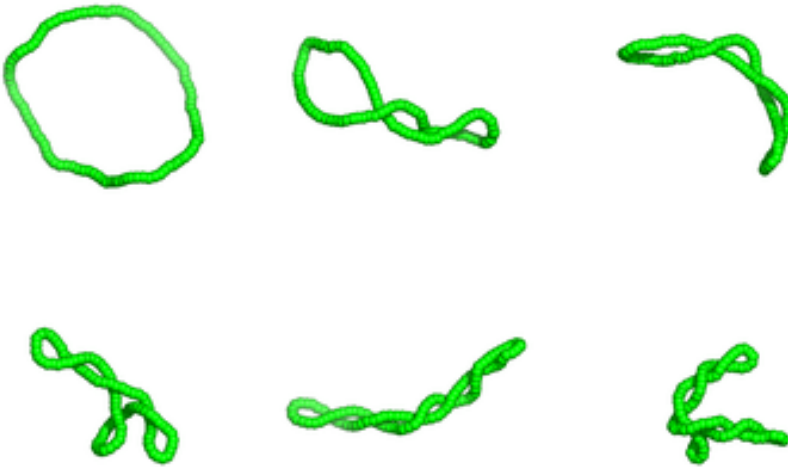


FIGURE 9.77. Sketch of ring polymers with different degree of twisting

$$P_{mr}(q) = I_0 \left(\frac{P_{1r}(q)}{m} + \frac{2}{m^2} P_{1r}^2(q) \sum_{j=1}^{m-1} (m-j) \exp\left(-\frac{q^2 R_{g,1r}^2}{2}(j-1)\right) \right) \quad (9.308)$$

$$P_{1r}(q) = \sqrt{\frac{2}{u_{1r}^2}} D \left[\sqrt{\frac{u_{1r}^2}{2}} \right] \quad (9.309)$$

$$u_{1r}^2 = q^2 R_{g,1r}^2 \quad (9.310)$$

$$R_{g,1r}^2 = \sqrt{\frac{b^2 N}{12}} \quad (9.311)$$

$$D(X) = \exp(X^2) \int_0^X \exp(t^2) dt \quad (9.312)$$

The above formula is defined for integer values of m larger or equal 1. For non-integer values of m a mixture between $\lfloor m \rfloor$ and $\lfloor m \rfloor + 1$ is assumed where $\lfloor m \rfloor$ denotes the greatest integer less than or equal to m . (floor-function). We finally get

$$P_r q = (1-w) P_{\lfloor m \rfloor r}(q) + w P_{(\lfloor m \rfloor + 1)r}(q) \quad (9.313)$$

with $w = m - \lfloor m \rfloor$.

Input Parameters for model `mMemberedTwistedRing`:

R_G,1r: radius of gyration $R_{G,1r}$ of one of m loop

m: number of twists m
I₀: forward scattering I_0

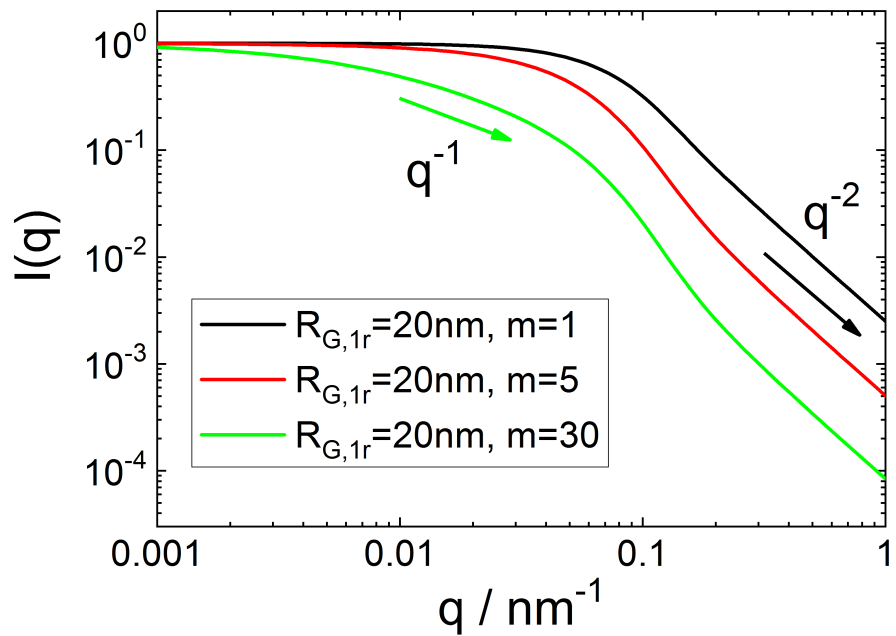


FIGURE 9.78. Scattering intensity of an m -membered twisted ring polymers with different values for m .

9.4.3.3. *Daisy-like Ring.*

[65]

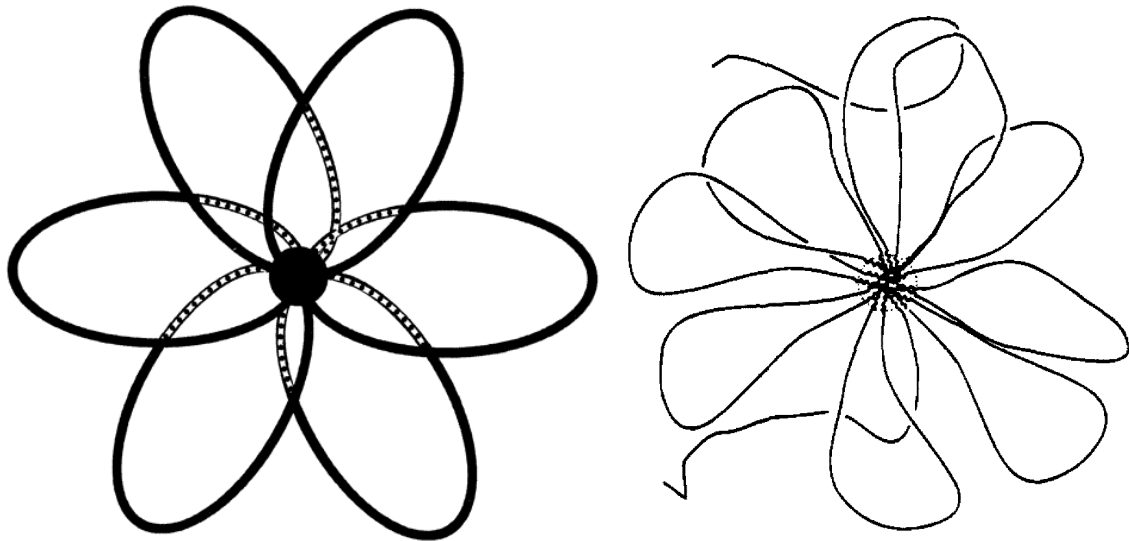


FIGURE 9.79. Sketch of a Daisy-like polymer.

$$P_{mr}(q) = \frac{I_0}{m} \left(P_{1r}(q) + (m-1)P_{1r}^2(q) \right) \quad (9.314)$$

$$P_{1r}(q) = \sqrt{\frac{2}{u_{1r}^2}} D \left[\sqrt{\frac{u_{1r}^2}{2}} \right] \quad (9.315)$$

$$u_{1r}^2 = q^2 R_{g,1r}^2 \quad (9.316)$$

$$R_{g,1r}^2 = \sqrt{\frac{b^2 N}{12}} \quad (9.317)$$

$$D(X) = \exp(X^2) \int_0^X \exp(t^2) dt \quad (9.318)$$

Input Parameters for model `DaisyLikeRing`:

R_G,1r: radius of gyration $R_{G,1r}$ of one of m loop

m: number of loops m

I0: forward scattering I_0

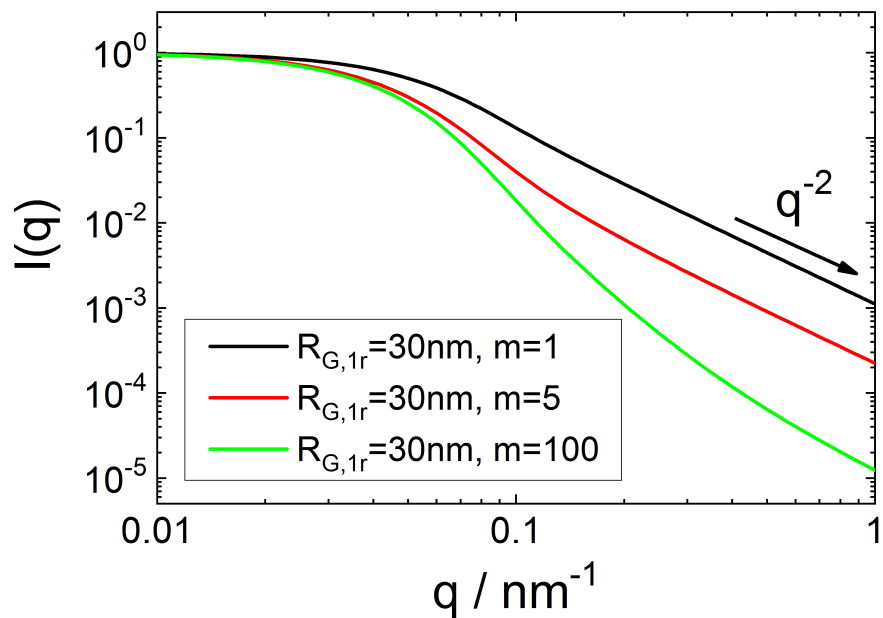
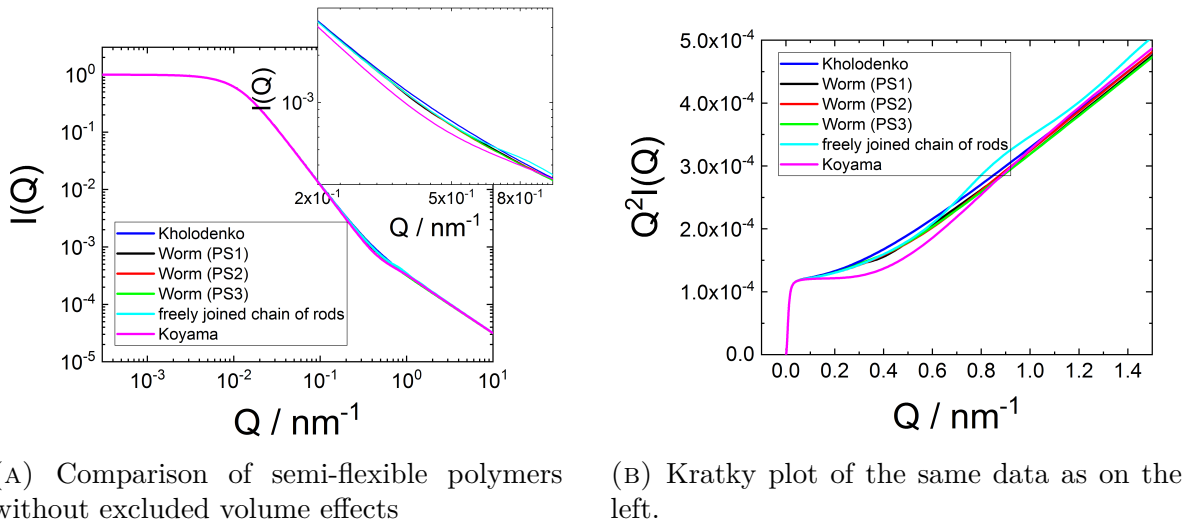


FIGURE 9.80. Scattering intensity of a Daisy-like ring polymers with different number of loops.

9.4.4. Semi-flexible or worm-like polymers.

Semi-flexible or worm-like structures have been implemented also as $P'(Q)$ for thin objects with local cylindrical geometry section 9.2.4. Here they are implemented for describing polymers with infinitesimal thin cross sections of the stiff Kuhn segments.



(A) Comparison of semi-flexible polymers without excluded volume effects (B) Kratky plot of the same data as on the left.

FIGURE 9.81. Comparison of model for semi-flexible or worm-like polymers

9.4.4.1. *wormlike polymer (PS1)*.

This first form factor for a semi-flexible polymer without excluded volume effects according to [380] is given in eq. 9.66 and with excluded volume effects in eq. 9.76. The form factors is normalized to $I(Q = 0) = I_0$.

Input Parameters for model Worms(PS1) (with and without excluded volume effects):

1b: Kuhn length l_B of semi-flexible worm-like structure

L: contour length L of semi-flexible worm-like structure

exvol: input flag to select the variant with or without excluded volume effects: $\text{exvol} \geq 1$
with excluded volume effects, $\text{exvol} < 1$ without excluded volume effects

I0: forward scattering $I(Q = 0) = I_0$

9.4.4.2. *wormlike polymer (PS2)*.

This second form factor for a semi-flexible polymer according to [380] only is available without excluded volume effects and is given in eq. 9.82. The form factors is normalized to $I(Q = 0) = I_0$.

Input Parameters for model Worms(PS2):

- lb:** Kuhn length l_B of semi-flexible worm-like structure
L: contour length L of semi-flexible worm-like structure
dummy: not used
I0: forward scattering $I(Q = 0) = I_0$

9.4.4.3. *wormlike polymer (PS3).*

This third form factor for a semi-flexible polymer without excluded volume effects according to [380] is given in eq. 9.95 for both without and with excluded volume effects. The form factors is normalized to $I(Q = 0) = I_0$.

Input Parameters for model Worms(PS3) (with and without excluded volume effects):

- lb:** Kuhn length l_B of semi-flexible worm-like structure
L: contour length L of semi-flexible worm-like structure
exvol: input flag to select the variant with or without excluded volume effects: $\text{exvol} \geq 1$ with excluded volume effects, $\text{exvol} < 1$ without excluded volume effects
I0: forward scattering $I(Q = 0) = I_0$

9.4.4.4. *Kholodenko worm.*

Kholodenko [265] has given a simple expression for semi-flexible polymers without excluded volume effects. The form factor has been given in section 9.2.4.4 by eq. 9.62. The form factors here is normalized to $I(Q = 0) = I_0$.

Input Parameters for model Kholodenko worm:

- lb:** Kuhn length l_B of semi-flexible worm-like structure
L: contour length L of semi-flexible worm-like structure
dummy: not used
I0: forward scattering $I(Q = 0) = I_0$

9.4.4.5. *Koyama worm.*

This form factors of semi-flexible polymers from Koyama [275, 276] given in eq. 9.54 but normalized here to $I(Q = 0) = I_0$.

Input Parameters for model Koyama worm:

1b: Kuhn length l_B of semi-flexible worm-like structure

L: contour length L of semi-flexible worm-like structure

dummy: not used

I0: forward scattering $I(Q = 0) = I_0$

9.4.4.6. *Freely joined chain of rigid rods.*

The form factors of freely joined chain of rigid rods by Hermans and Hermans [212] is given in eq. 9.48 but normalized here to $I(Q = 0) = I_0$.

Input Parameters for model freely joined chain of rods:

1b: Kuhn length l_B of semi-flexible worm-like structure

L: contour length L of semi-flexible worm-like structure

dummy: not used

I0: forward scattering $I(Q = 0) = I_0$

9.4.5. branched polymer.

Polymers can be synthesized in a large variety of architectures, like architectures of linear polymers, rings, branched polymers, dendrimers, combs, ladders, cross-linked polymers, etc. A few possible architectures are sketched in fig. 9.82.

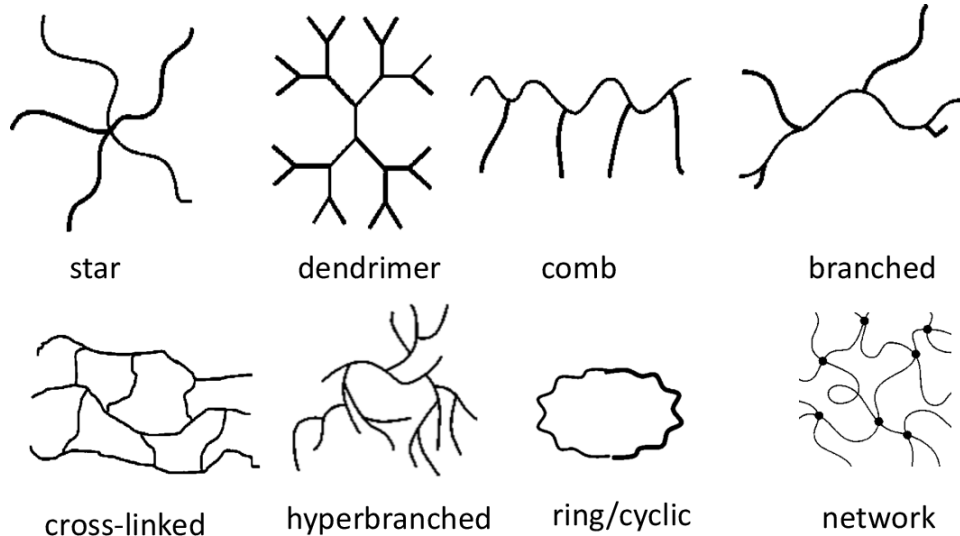


FIGURE 9.82. Some categories of polymer architectures

9.4.5.1. random f -functional polycondensates.

[250, 66, 67, 60]

$$I_{f-\text{pc}} = \frac{I_0}{1 + R_g^2 q^2 / 3} \quad (9.319)$$

$$R_g^2 = \frac{1}{2} \sigma^2 \left(\frac{\alpha(f-1)}{1 - \alpha(f-1)} + \frac{\alpha}{1 + \alpha} \right) \quad (9.320)$$

where f is the functionality, α the fraction of functionalities which have reacted and σ^2 may be defined as the mean-square distance between two units directly connected by a link.

9.4.5.2. hyperbranched polymer: fractal approach.

[59]

9.4.5.3. Hyper-branched AB_2 polymers perturbed by excluded volume interaction.

[66, 67]

9.4.5.4. comb.

Casassa and Berry have developed a model polymers with a comb-like architecture [80]. They assume sufficiently dilute solution at the Flory temperature, where the molecular configuration is described by random flight statistics. They describe in their paper three version, a regular, a random and a heterogenous comb architecture.

The form factor of a regular comb reads as [80, 509]

$$I_{\text{comb,reg}}(q) = \frac{2}{x^2} (A_{\text{reg}} + B_{\text{reg}} + C_{\text{reg}}) \quad (9.321)$$

$$A_{\text{reg}} = x - 1 + e^{-x\lambda} \quad (9.322)$$

$$B_{\text{reg}} = \left(1 - e^{-x(1-\lambda)/\zeta}\right) \left(\zeta + 2 \frac{1 - e^{-x\lambda\zeta/(\zeta+1)}}{1 - e^{x\lambda/(\zeta+1)}}\right) \quad (9.323)$$

$$C_{\text{reg}} = \left(1 - e^{-x(1-\lambda)/\zeta}\right)^2 \left(\frac{(\zeta - 1) \left(e^{x\lambda/(\zeta+1)} - 1\right) - \left(1 - e^{-x\lambda(\zeta-1)/(\zeta+1)}\right)}{\left(1 - e^{x\lambda/(\zeta+1)}\right)^2}\right) \quad (9.324)$$

with

$$x = q^2 a^2 \quad (9.325)$$

$$a^2 = N l_b^2 / 6 \quad (9.326)$$

$$N = N_0 + \zeta n_\zeta \quad (9.327)$$

$$\lambda = N_0 / N \quad (9.328)$$

where l_b is the length of a polymer chain element, ζ the number of side branches equally spaced along the back-bone, N the total number of chain (Kuhn) elements, N_0 the chain elements in the back-bone, n_ζ the number of chain elements in the side branch. a would be the radius of gyration of a linear polymer with the same number of chain elements than the comb shaped polymer.

The form factor of a random comb reads as [80]

$$I_{\text{comb,rnd}}(q) = \frac{2}{x^2} (A_{\text{rnd}} + B_{\text{rnd}} + C_{\text{rnd}}) \quad (9.329)$$

$$A_{\text{rnd}} = x + \left(e^{-x\lambda} - 1\right) \quad (9.330)$$

$$B_{\text{rnd}} = \left(1 - e^{-x(1-\lambda)/\zeta}\right) \zeta \left[1 + \frac{2}{x\lambda} \left(e^{-x\lambda} - 1\right)\right] \quad (9.331)$$

$$C_{\text{rnd}} = \left(1 - e^{-x(1-\lambda)/\zeta}\right)^2 \left[\frac{x\lambda + \left(e^{-x\lambda} - 1\right)}{x^2\lambda^2/(\zeta(\zeta-1))}\right] \quad (9.332)$$

The third case discussed in [80] includes a binomial distributed random ζ -branched comb, which they name heterogenous. The averaged random form factor (heterogeneous

comb) reads as

$$I_{\text{comb,h}}(q) = \frac{2}{\bar{x}^2} \frac{1}{1 + (1 - \bar{\lambda})^2/\zeta} (A_h + B_h + C_h) \quad (9.333)$$

$$A_h = \bar{x} + (e^{-\bar{x}\bar{\lambda}} - 1) \quad (9.334)$$

$$B_h = (1 - e^{-\bar{x}(1-\bar{\lambda})/\zeta}) \zeta \left[1 + \frac{2}{\bar{x}\bar{\lambda}} (e^{-\bar{x}\bar{\lambda}} - 1) \right] \quad (9.335)$$

$$C_h = (1 - e^{-\bar{x}(1-\bar{\lambda})/\zeta})^2 \left[\frac{\bar{x}\bar{\lambda} + (e^{-\bar{x}\bar{\lambda}} - 1)}{\bar{x}^2\bar{\lambda}^2/\zeta^2} \right] \quad (9.336)$$

where \bar{x} , $\bar{\lambda}$, and $\bar{\lambda}$ are averaged accordingly (details see [80]). In fig. 9.83 The scattering intensity of am comb with 10 branches is shown. The differences between the models are hardly visible in the loglog presentation, however, in the Kratky plot they become visible.

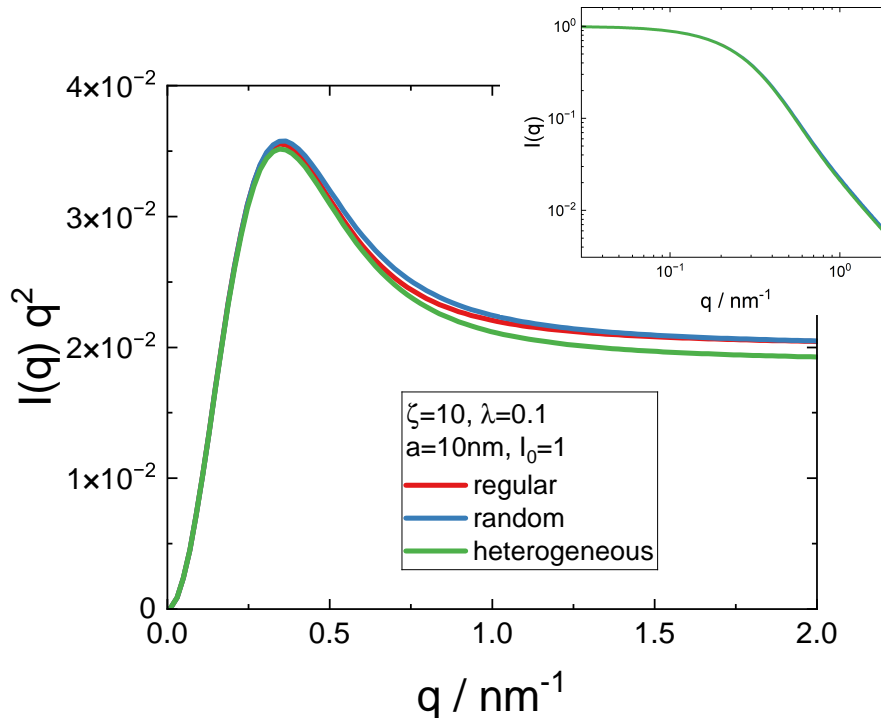


FIGURE 9.83. Scattering of a comb in a Kratky and Loglog plot.

Input Parameters for models `comb (regular)`, `comb (random)`, and `comb (heterogeneous)`:

- a:** radius of gyration of a linear chain with the same number of polymer units a as the comb
- zeta:** functionality or number of branches ζ
- lambda:** density of side chains λ
- I0:** forward scattering I_0

Note:

- $0 \leq \lambda \leq 1$
- $\zeta > 1$
- $a > 0$

9.4.5.5. bottle-brush polymer.

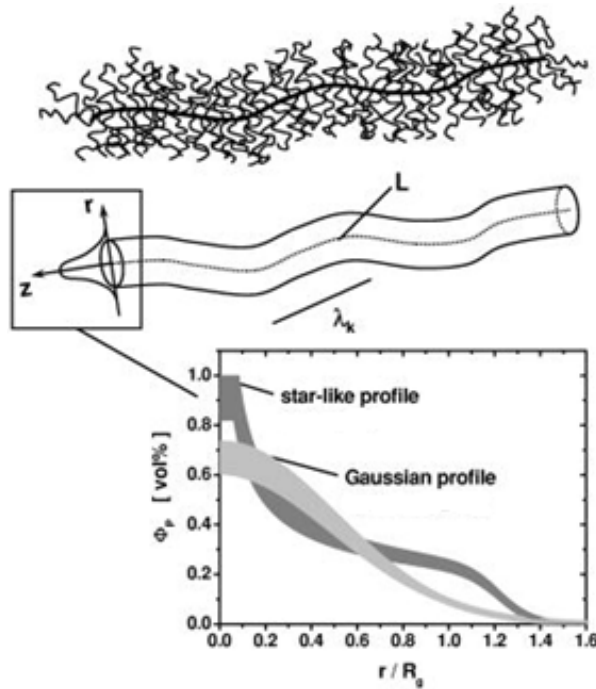


FIGURE 9.84. sketch of a bottle brush polymer [408].

For a bottle-brush polymer analytical expressions for the scattering length density profile of the brush cross-section have been suggested by [408], which is an empirical star-like profile, and by [223, 224] based on simulations. The corresponding profiles read as

$$\rho_{\text{emp}}(r) = \begin{cases} \eta, & \text{if } r \leq R_c \\ \eta \alpha r^{-k} \left\{ 1 + \exp \left(\frac{r-R_c}{\sigma_s} \right) \right\}^{-1}, & \text{otherwise.} \end{cases} \quad (9.337)$$

$$\rho_{\text{sim}}(r) = \frac{\sigma \eta}{1 + (r/R_1)^{x_1}} \exp [-(r/R_2)^{x_2}] \quad (9.338)$$

with η being the scattering contrast, $\alpha = R_c^k \left\{ 1 + \exp \left(\frac{R_c-R_s}{\sigma_s} \right) \right\}$ a scaling constant so that $\rho(R_c)$ is continuous, R_c the inner radius, up to which this profile is constant, k describes the power law decay to some outer radius R_s with σ_s to have a smooth transition to zero (Fermi function). In the second model σ describes the grafting density, R_1 and R_2 are the length scales for the algebraic decays ($R_1 \ll R_2$), and x_1 and x_2 are the

corresponding exponents. It is expected to have $x_1 \simeq (3\nu - 1)/(2\nu)$, where ν is the Flory parameter.

For this two profiles the cross-section term $P_{\text{cs}}(q)$ for thin rod-like structures as discussed in 9.2 using eq. 9.13 reads as

$$P_{\text{cs}}^{\text{emp}}(q) = \left[2\pi \int_0^{\infty} \rho_{\text{emp}}^{\text{sim}}(r) J_0(qr) r dr \right]^2 \quad (9.339)$$

Input Parameters for models `BottleBrush (emp.)` and `BottleBrush profile (emp.)`:

eta: contrast

Rc: core radius R_c

k: power law decay $k > 0$

Rs: outer radius $R_s > R_c$

sigma_s: transition width σ_s

Note:

- $R_s > R_c$
- $k > 0$
- $\sigma_s > 0$

Input Parameters for models `BottleBrush (sim)` and `BottleBrush profile (sim)`:

sigma_eta: grafting density times scattering contrast $\sigma\eta$

R_1: first length scales for the algebraic decays R_1

x_1: first power law decay $x_1 > 0$

R_2: second length scales for the algebraic decays $0 < R_1 \ll R_2$

x_2: second power law decay $x_2 > 0$

Note:

- $0 < R_1 \ll R_2$
- $x_1 > 0$
- $x_2 > 0$

9.4.5.6. soft sphere model.

[437, 61, 64]

9.5. Lorenz-Mie Form Factors for Static Light Scattering

Mie theory, also called Lorenz-Mie theory [337, 495, 43], is a complete mathematical-physical theory of the scattering of electromagnetic radiation by spherical particles. Mie theory is named after its developer German physicist Gustav Mie (1868 Rostock - 1957 Freiburg im Breisgau) and Danish physicist Ludvig Lorenz (1829-1891) who independently developed the theory of electromagnetic plane wave scattering by a dielectric sphere in 1908.

Mie scattering describes the scattering of electromagnetic radiation by spherical particles of any size r , relative to the wavelength, λ . Since the cases $r \ll \lambda$ and $r \gg \lambda$ are covered by Rayleigh (dipole) scattering and geometric scattering theories, respectively, Mie scattering often refers to the case of $r \sim \lambda$.

9.5.1. MieSphere.

The Mie scattering formulae are given in several books (Van de Hulst [495], Kerker [261], Deirmendjian, 1969) and by Dave [99, 97, 98], although not always in the forms most suited to computation. The algorithm used here is based on the MIEV0 package described in [533, 534]. The following input values are used:

$$\Theta = 2 \arcsin(Q\lambda/(4\pi)) \text{ with } Q < Q_{\max} = 4\pi/\lambda$$

R = radius of scattering sphere

λ = wavelength of incident plane wave inside the solvent

m = complex refractive index of sphere relative to surrounding medium

$$= m_{\text{re}} - im_{\text{im}}$$

$$|m| \geq 1 \text{ and } m_{\text{im}} \geq 0$$

or

$$|m| < 1 \text{ and } m_{\text{im}} = 0$$

$\text{pol} = 0$ unpolarized light

$\text{pol} = 1$ parallel to scattering plane polarized light

$\text{pol} = -1$ perpendicular to scattering plane polarized light

$|m| < 1$ would, for example, include visible light scattering from air bubbles in water.

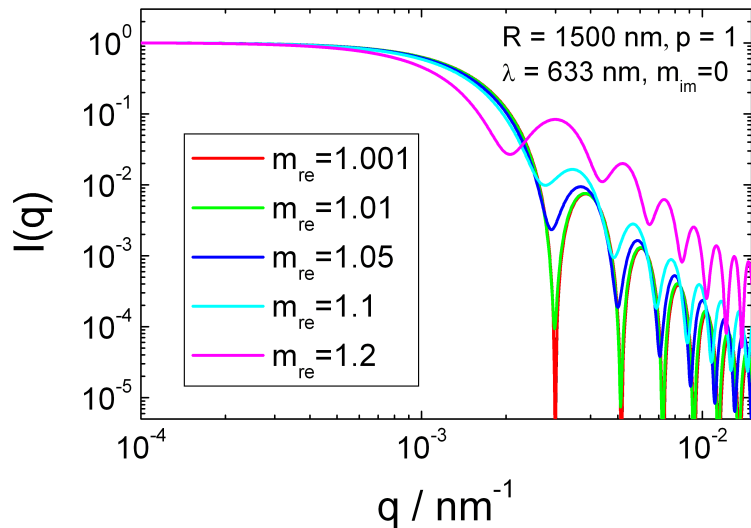


FIGURE 9.85. Scattering intensity of a sphere using the formalism for Mie scattering. The data are normalized to one for $q = 0$.

9.5.2. MieShell.

This form factor is basing on the version of MieLay, which computes electromagnetic scattering by a stratified sphere, i.e. a particle consisting of a spherical core surrounded by a spherical shell. The surrounding medium is assumed to have refractive index unity. The formulas, manipulated to avoid the ill-conditioning that plagued earlier formulations, were published in [486]. Further documentation, including definitions of input and output arguments, is inside the single precision version of this program (**SUBROUTINE MieLay**, available by anonymous ftp from `climate.gsfc.nasa.gov` in directory `pub/wiscombe`). The following input values are used:

$$\Theta = 2 \arcsin(Q\lambda/(4\pi)) \text{ with } Q < Q_{\max} = 4\pi/\lambda$$

R_c = radius of the core of scattering sphere

R_{sh} = thickness of the shell of scattering sphere

λ = wavelength of incident plane wave inside the solvent

m_c = complex refractive index of core relative to surrounding medium

$$= m_{c,re} - im_{c,im}$$

$$|m_c| \geq 1 \text{ and } m_{c,im} \geq 0$$

or

$$|m_c| < 1 \text{ and } m_{c,im} = 0$$

m_s = complex refractive index of core relative to surrounding medium

$$= m_{s,re} - im_{s,im}$$

$pol = 0$ unpolarized light

$pol = 1$ parallel to scattering plane polarized light

$pol = -1$ perpendicular to scattering plane polarized light

$|m| < 1$ would, for example, include visible light scattering from air bubbles in water.

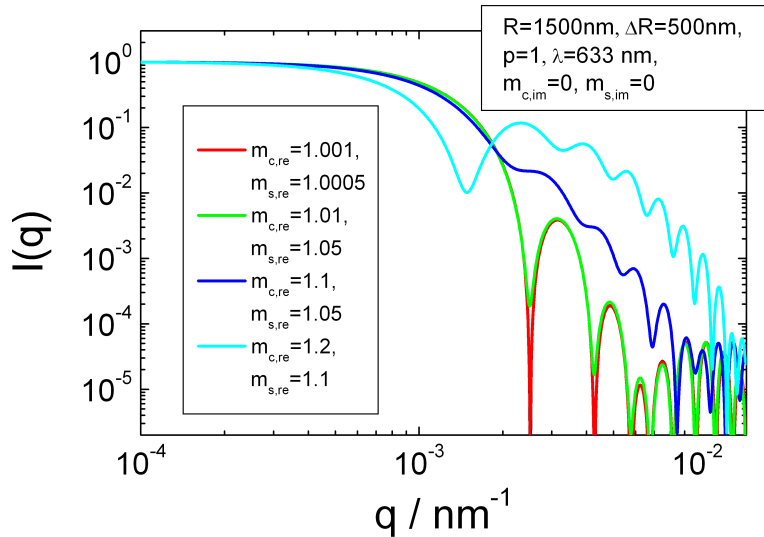


FIGURE 9.86. Scattering intensity of a spherical shell using the formalism for Mie scattering. The data are normalized to one for $q = 0$.

9.6. Ellipsoidal Objects

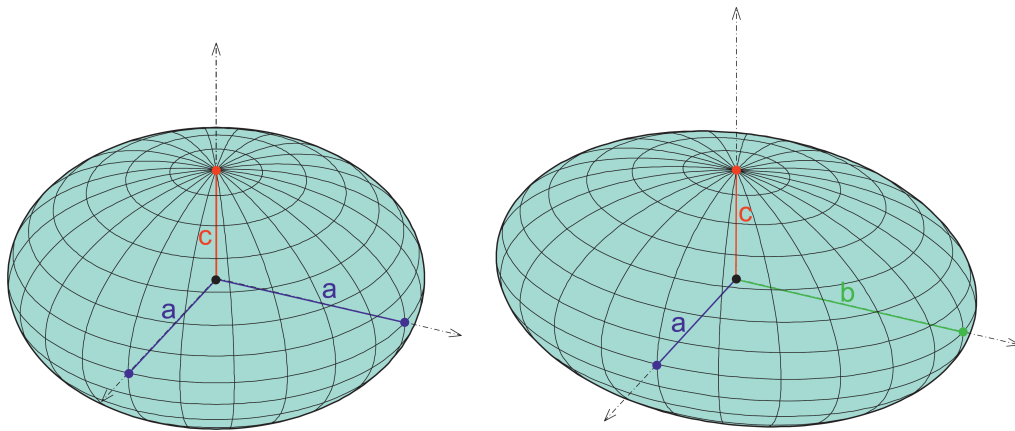


FIGURE 9.87. Ellipse of revolution (spheroid) and triaxial ellipse

The plugin "ellipsoidal obj." contains form factors of ellipsoidal object with rotational symmetry, which are called ellipsoid of revolution or spheroid, as well as triaxial ellipsoidal objects. The three axes of the ellipsoids are assumed to be orthogonal. Because of the non-spherical symmetry of the objects an orientational average has to be performed for random oriented ellipsoids, which requires for spheroids a single integration and for triaxial ellipsoids a double integration. An optional integration over the size distribution would then slow down the numerical evaluation of the scattering intensity and care has to be taken, to use an appropriate integration routine. At the moment **SASfit** makes use of the `pcubature` algorithm from Steven G. Johnson [245] instead of nested 1-dimensional integration routines used so far. Due to **SASfit** internals an optional integration over the size distribution was realized via the form factor itself instead of including it via the GUI to profit from the speed-up of routines optimized for multi-dimensional integration.

9.6.1. Ellipsoid of revolution or spheroid.

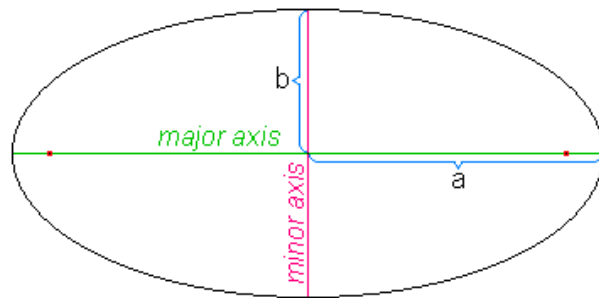


FIGURE 9.88. Ellipse, showing major and minor axes and parameters a and b

An ellipsoid is a quadric surface in three dimensions obtained by rotating an ellipse about one of its principal axes. Three particular cases of an ellipsoid are:

- If the ellipse is rotated about its major axis, the surface is a prolate spheroid.
- If the ellipse is rotated about its minor axis, the surface is an oblate spheroid.
- If the generating ellipse is a circle, the surface is a sphere.

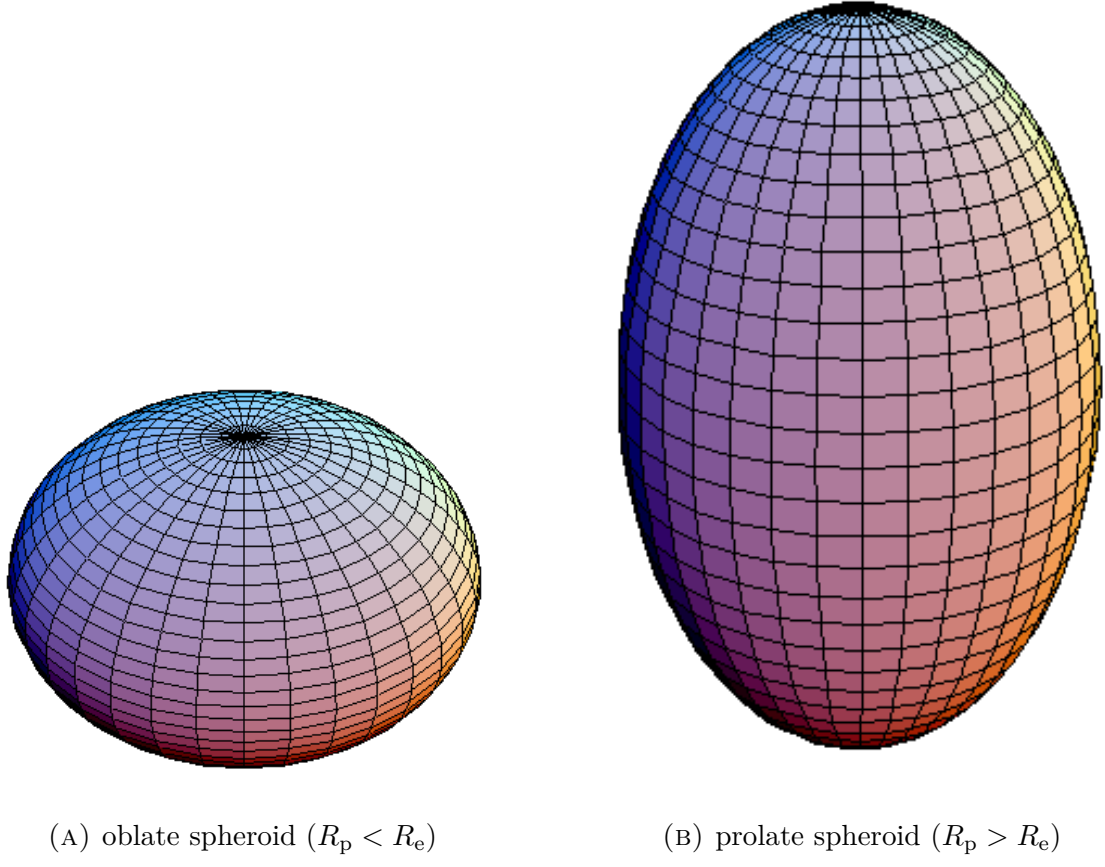


FIGURE 9.89. A spheroid is an ellipsoid having two equal equatorial semi-axes R_e . If the equatorial semi-axis are larger than the principal axis R_p the spheroid becomes oblate (a), if they are smaller it becomes prolate (b) and if they are equal the spheroid becomes a perfect sphere

The orientational averaged scattering amplitude and scattering intensity are given by [175]

$$\langle F_{\text{spheroid}}(Q, R_p, R_e, \Delta\eta) \rangle = V \Delta\eta \int_0^1 K \left(Q \sqrt{R_p^2 y^2 + R_e^2 (1-y)^2} \right) dy \quad (9.340)$$

$$I_{\text{spheroid}}(Q, R_p, R_e, \Delta\eta) = V^2 \Delta\eta^2 \int_0^1 K^2 \left(Q \sqrt{R_p^2 y^2 + R_e^2 (1-y)^2} \right) dy \quad (9.341)$$

with

$$V = \frac{4}{3}\pi R_e^2 R_p \quad (9.342)$$

$$K(x) = 3 \frac{\sin x - x \cos x}{x^3} \quad (9.343)$$

$$\Delta\eta = \eta_{\text{core}} - \eta_{\text{solv}} \quad (9.344)$$

The form factor of a spheroid has been implemented in three parametrisation variants. The variants **spheroid V** and **spheroid nu** replace the old variants **Ellipsoid i** and **Ellipsoid ii**, which are not anymore available. **spheroid R** is a new parametrisation variant. Their input parameters are

Input Parameters for model **spheroid nu**:

nu: ratio between radius of the polar axes and equatorial axis. Values of $\nu < 1$ describe oblate ellipsoids, a value of $\nu = 1$ a sphere, and $\nu > 1$ a prolate ellipsoids.

R_equatorial: length of the equatorial semi-axes R_e

dummy: not used

dummy: not used

dummy: not used

eta_core: scattering length density of spheroid

dummy: not used

eta_sol: scattering length density of solvent

Input Parameters for model **spheroid V**:

V: volume of spheroid

R_equatorial: length of equatorial semi-axes R_e

dummy: not used

dummy: not used

dummy: not used

eta_core: scattering length density of spheroid

dummy: not used

eta_sol: scattering length density of solvent

Input Parameters for model **spheroid R**:

R_polar: length of polar semi-axis R_p

R_equatorial: length of equatorial semi-axes R_e

dummy: not used

dummy: not used

dummy: not used

eta_core: scattering length density of spheroid

dummy: not used

eta_sol: scattering length density of solvent

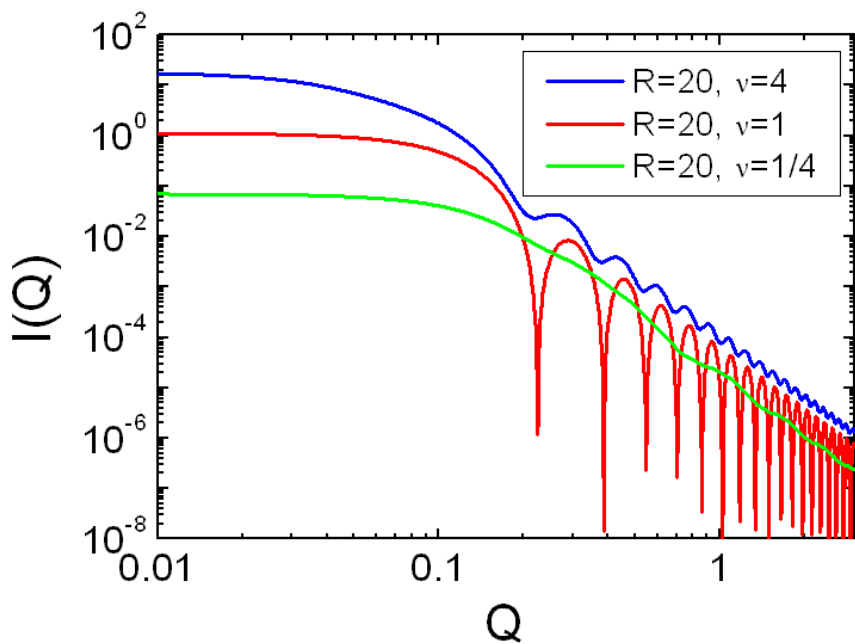


FIGURE 9.90. form factor of an ellipsoid with axis R , R and νR .

9.6.2. Spheroid with a Gamma size distribution.

The Gamma-distribution or Schulz-Zimm (Flory) distribution in section 7.6 or 7.5 has been used since many decades [441, 7, 444, 16, 206, 513, 128] to analytically integrate the form factor of a spherical particle or spheroids over a size distribution. The form factor of a homogeneous randomly oriented spheroid with a gamma distribution has been calculated by Schmidt in [441], where he performed the integration over the size distribution analytically.

$$I(q) = \Delta\eta^2 \int_0^\infty \int_0^1 N(R) V^2 \frac{9}{2} \pi \frac{J_{3/2}^2(qtR)}{(qtR)^3} dy dR \quad (9.345)$$

$$= \Delta\eta^2 \int_0^\infty \int_0^1 \frac{1}{\theta} \left(\frac{R}{\theta}\right)^{k-1} \frac{\exp(-R/\theta)}{\Gamma(k)} \left(\frac{4}{3}\pi\nu R^3\right)^2 \frac{9}{2} \pi \frac{J_{3/2}^2(qtR)}{(qtR)^3} dy dR \quad (9.346)$$

$$I(q) = \Delta\eta^2 \int_0^1 \frac{8\nu^2}{(qt)^6} \left((A-1)k(k+1) \left(C^{-\frac{k}{2}-1} \cos(B(k+2)) + 1 \right) - 2kqt\theta C^{-\frac{k}{2}-\frac{1}{2}} \sin(B(k+1)) - C^{-k/2} \cos(Bk) + 1 \right) dy \quad (9.347)$$

with

$$t = \sqrt{1 + (\nu^2 - 1) y^2} \quad (9.348)$$

$$\theta = R_e/(k-1) \quad (9.349)$$

$$\Delta\eta = \eta_c - \eta_s \quad (9.350)$$

$$A = 1 + (qt\theta)^2 \quad (9.351)$$

$$B = \arctan(2qt\theta) \quad (9.352)$$

$$C = 4A - 3 \quad (9.353)$$

Input Parameters for model spheroid w. g-size distr:

nu: ratio between radius of the polar axes R_p and equatorial axis R_e .

R_equatorial: length of the equatorial semi-axes R_e

dummy: not used

dummy: not used

k: width parameter of the gamma distribution ($k > 1$).

eta_core: scattering length density of spheroid η_c

dummy: not used

eta_sol: scattering length density of solvent η_s

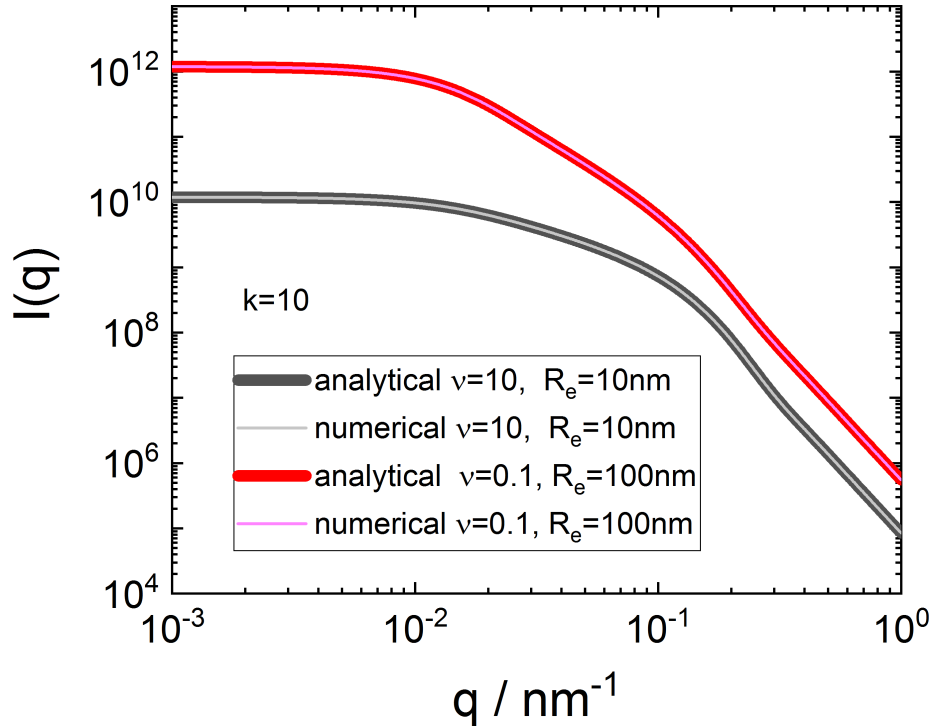


FIGURE 9.91. form factor of an spheroid with axis R_e , R_e and $R_p\nu R_e$. Values of $\nu < 1$ describe oblate ellipsoids, a value of $\nu = 1$ a sphere, and $\nu > 1$ a prolate ellipsoids. The plot show both the analytically integrated variant and the numerically averaged intensity using the same gamma size distribution.

Note:

- the width parameter needs to be larger than 1, $k > 1$. The most probable size and the size parameter θ are related by $R_e = (k - 1)\theta$ and the variance of the distribution is $\sigma^2 = k\theta^2$
- The stretching factor ν needs to be a nonzero positive number $\nu > 0$ as well as the equatorial axis $R_e > 0$.
- compared to the numerical integration over the size distribution this analytical one is especially much faster for large q -values which is in the numerical variant an integration over an oscillating function and numerically more demanding.

9.6.3. Ellipsoid with two equal equatorial semi-axis R and volume V .

$$I_i(Q, R, \nu) = (V\Delta\eta)^2 \int_0^{\frac{\pi}{2}} K^2 \left(Q, R\sqrt{\nu^2 \cos^2 \Theta + \sin^2 \Theta} \right) \sin \Theta d\Theta \quad (9.354)$$

with

$$\nu = \frac{V}{R^3} \frac{3}{4\pi} \quad \text{so that} \quad V = \frac{4}{3}\pi\nu R^3$$

and $\lim_{Q=0} I_i(Q, R, \nu) = (V\Delta\eta)^2$

Input Parameters for model Ellipsoid i:

R: radius of the rotational axes

V: total volume of the ellipsoid.

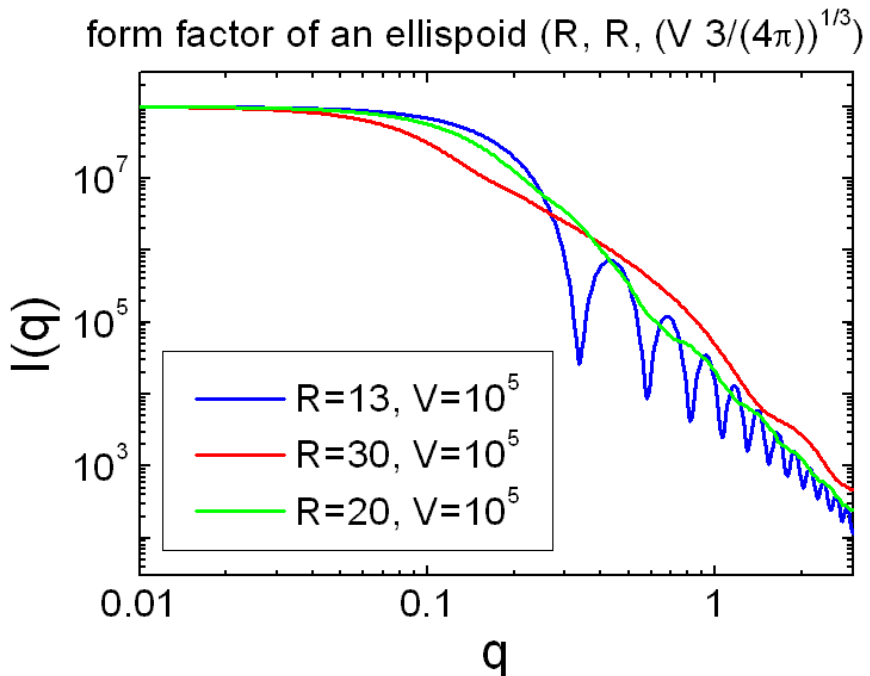


FIGURE 9.92. form factor of an ellipsoid with axis R , R and $\sqrt[3]{V \frac{3}{4\pi}}$.

9.6.4. Ellipsoidal core shell structure.

For these form factor plugins a size distribution parameter has been included directly in the form factor to avoid applying nested numerical integration routines. A routine for multi-dimensional integration (`pcubature` [245]) has been used instead.

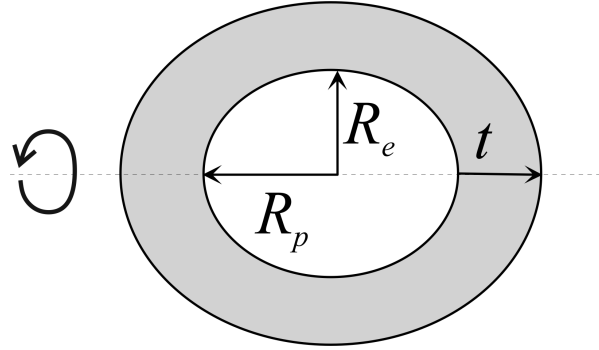


FIGURE 9.93. Ellipsoid of revolution with an outer shell of constant thickness t

$$I_{\text{ECSH}}(Q, R_p, R_e, t) = \langle F^2(Q, R_p, R_e, t) \rangle = \int_0^1 [F(Q, R_p, R_e, t, \mu)]^2 d\mu \quad (9.355)$$

$$\langle F(Q, R_p, R_e, t) \rangle = \int_0^1 F(Q, R_p, R_e, t, \mu) d\mu \quad (9.356)$$

with

$$F(Q, R_p, R_e, t, \mu) = (\eta_{\text{core}} - \eta_{\text{shell}}) V_c \left[\frac{3j_1(x_c)}{x_c} \right] + (\eta_{\text{shell}} - \eta_{\text{sol}}) V_t \left[\frac{3j_1(x_t)}{x_t} \right]$$

$$j_1(x) = \frac{\sin(x) - x \cos(x)}{x^2}$$

$$x_c = Q \sqrt{R_p^2 \mu^2 + R_e^2 (1 - \mu^2)}$$

$$x_t = Q \sqrt{(R_p + t)^2 \mu^2 + (R_e + t)^2 (1 - \mu^2)}$$

$$V_c = \frac{4}{3} \pi R_p R_e^2$$

$$V_t = \frac{4}{3} \pi (R_p + t)(R_e + t)^2$$

- η_{core} : scattering length density of core
- η_{shell} : scattering length density of shell
- η_{sol} : scattering length density of solvent
- R_p : polar semi-axes of elliptical core
- R_e : equatorial semi-axis of elliptical core
- t : thickness of shell
- V_c : volume of core
- V_t : total volume of core along with shell

Several variants including a size distribution have been implemented which just differ if only none, one or both axis scale with the same size distribution and if additionally also scales with that distribution.

$$\begin{aligned}
 \text{Ellipsoidal Shell} &: \langle F^n(Q, R_p, R_e, t) \rangle \\
 \text{Ellipsoidal Shell (t)} &: \int_0^{\infty} \text{LogNorm}(\nu, \sigma) \langle F^n(Q, R_p, R_e, \nu t) \rangle d\nu \\
 \text{Ellipsoidal Shell (R}_p\text{)} &: \int_0^{\infty} \text{LogNorm}(\nu, \sigma) \langle F^n(Q, \nu R_p, R_e, t) \rangle d\nu \\
 \text{Ellipsoidal Shell (R}_p\text{ t)} &: \int_0^{\infty} \text{LogNorm}(\nu, \sigma) \langle F^n(Q, \nu R_p, R_e, \nu t) \rangle d\nu \\
 \text{Ellipsoidal Shell (R}_e\text{)} &: \int_0^{\infty} \text{LogNorm}(\nu, \sigma) \langle F^n(Q, R_p, \nu R_e, t) \rangle d\nu \\
 \text{Ellipsoidal Shell (R}_e\text{ t)} &: \int_0^{\infty} \text{LogNorm}(\nu, \sigma) \langle F^n(Q, R_p, \nu R_e, \nu t) \rangle d\nu \\
 \text{Ellipsoidal Shell (R}_e\text{ R}_p\text{)} &: \int_0^{\infty} \text{LogNorm}(\nu, \sigma) \langle F^n(Q, \nu R_p, \nu R_e, t) \rangle d\nu \\
 \text{Ellipsoidal Shell (R}_e\text{ R}_p\text{ t)} &: \int_0^{\infty} \text{LogNorm}(\nu, \sigma) \langle F^n(Q, \nu R_p, \nu R_e, \nu t) \rangle d\nu
 \end{aligned}$$

with n being either 1 or 2 depending if the size averaged amplitude or the size averaged intensity needs to be calculated. As a size distribution a lognormal distribution is assumed where all parameters are scaled simultaneously. The used lognormal distribution is defined as

$$\text{LogNorm}(x, \sigma) = \frac{1}{\sqrt{2\pi}x} \exp\left(-\frac{\ln^2(x)}{2\sigma^2}\right)$$

Input Parameters for model Ellipsoidal Shell:

R_p: semi-principal polar axes of elliptical core R_p

R_e: equatorial semi-axis axes of elliptical core R_e

dummy: not used

t: thickness of shell t

dummy: not used

eta_core: scattering length density of core η_c

eta_shell: scattering length density of shell η_{sh}

eta_sol: scattering length density of solvent η_{sol}

Input Parameters for model Ellipsoidal Shell (t), Ellipsoidal Shell (R_p), Ellipsoidal Shell (R_p t), Ellipsoidal Shell (R_e), Ellipsoidal Shell (R_e t), Ellipsoidal Shell (R_e R_p), Ellipsoidal Shell (R_e R_p t):

R_p: semi-principal polar axes of elliptical core R_p

R_e: equatorial semi-axis axes of elliptical core R_e

dummy: not used

t: thickness of shell t

sigma: width of the LogNorm size distribution

eta_core: scattering length density of core η_c

eta_shell: scattering length density of shell η_{sh}

eta_sol: scattering length density of solvent η_{sol}

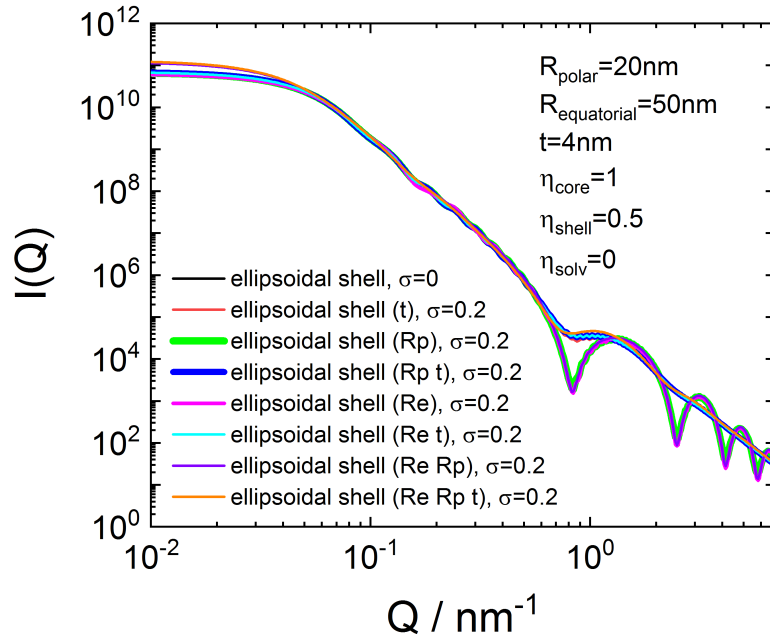


FIGURE 9.94. Form factor of an ellipsoidal core shell structure including a lognormal size distribution.

9.6.5. triaxial ellipsoidal core shell structure.

Also for these form factor plugins a size distribution parameter has been included directly in the form factor similar to the ellipsoidal shell of revolution to avoid applying nested numerical integration routines. As for the triaxial ellipsoid already a double integration for the orientational averaging is required it becomes even more important to have an optimized integration routine for including an additional size distribution, i.e an additional integration. The routine for multi-dimensional integration (pcubature [245]) has been used.

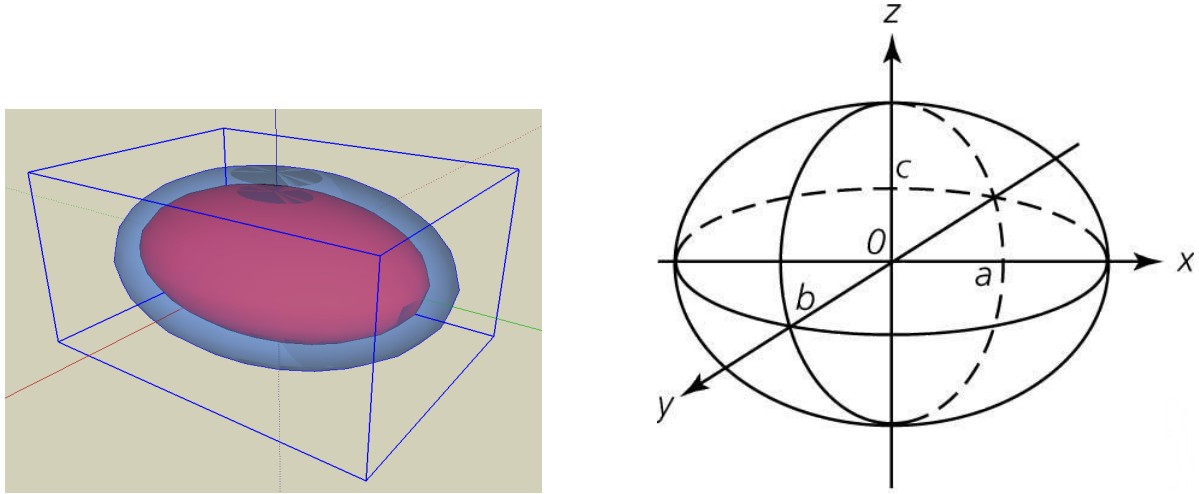


FIGURE 9.95. triaxial ellipsoidal core shell structure

$$I_{\text{triaxEllSh}}(Q) = \langle F^2(Q, a, b, c, t) \rangle = \int_0^1 \int_0^1 dx dy K_{\text{sh}}^2(Q, R, R_t) \quad (9.357)$$

$$\langle F(Q, a, b, c, t) \rangle = \int_0^1 \int_0^1 dx dy K_{\text{sh}}(Q, R, R_t) \quad (9.358)$$

with

$$K(QR) = 3 \frac{\sin QR - QR \cos QR}{(QR)^3} \quad (9.359)$$

$$K_{\text{sh}}(Q, R, R_t) = (\eta_c - \eta_{\text{sh}}) K(QR) + (\eta_{\text{sh}} - \eta_{\text{sol}}) K(QR_t) \quad (9.360)$$

$$R^2 = [a^2 \cos^2(\pi x/2) + b^2 \sin^2(\pi x/2)] (1 - y^2) + c^2 y^2$$

$$R_t^2 = [(a + t)^2 \cos^2(\pi x/2) + (b + t)^2 \sin^2(\pi x/2)] (1 - y^2) + (c + t)^2 y^2$$

$$V_c = \frac{4}{3}\pi abc$$

$$V_t = \frac{4}{3}\pi(a + t)(b + t)(c + t)$$

η_c : scattering length density of core
 η_{sh} : scattering length density of shell
 η_{sol} : scattering length density of solvent
 a : semi-axes of elliptical core
 b : semi-axes of elliptical core
 c : semi-axes of elliptical core
 t : thickness of shell
 V_c : volume of core
 V_t : total volume of core along with shell

Several variants including a size distribution have been implemented which just differ if only none, one or both axis scale with the same size distribution and if additionally also scales with that distribution.

$$\begin{aligned}
 & \text{triax ellip shell} : \langle F^n(Q, a, b, c, t) \rangle \\
 & \text{triax ellip shell t} : \int_0^{\infty} \text{LogNorm}(\nu, \sigma) \langle F^n(Q, a, b, c, \nu t) \rangle d\nu \\
 & \text{triax ellip shell 1} : \int_0^{\infty} \text{LogNorm}(\nu, \sigma) \langle F^n(Q, \nu a, b, c, t) \rangle d\nu \\
 & \text{triax ellip shell 1t} : \int_0^{\infty} \text{LogNorm}(\nu, \sigma) \langle F^n(Q, \nu a, b, c, \nu t) \rangle d\nu \\
 & \text{triax ellip shell 2} : \int_0^{\infty} \text{LogNorm}(\nu, \sigma) \langle F^n(Q, \nu a, \nu b, c, t) \rangle d\nu \\
 & \text{triax ellip shell 2t} : \int_0^{\infty} \text{LogNorm}(\nu, \sigma) \langle F^n(Q, \nu a, \nu b, c, \nu t) \rangle d\nu \\
 & \text{triax ellip shell 3} : \int_0^{\infty} \text{LogNorm}(\nu, \sigma) \langle F^n(Q, \nu a, \nu b, \nu c, t) \rangle d\nu \\
 & \text{triax ellip shell 3t} : \int_0^{\infty} \text{LogNorm}(\nu, \sigma) \langle F^n(Q, \nu a, \nu b, \nu c, \nu t) \rangle d\nu
 \end{aligned}$$

with n being either 1 or 2 depending if the size averaged amplitude or the size averaged intensity needs to be calculated. As a size distribution a lognormal distribution is assumed where all parameters are scaled simultaneously. The used lognormal distribution is defined as

$$\text{LogNorm}(x, \sigma) = \frac{1}{\sqrt{2\pi} x} \exp\left(-\frac{\ln^2(x)}{2\sigma^2}\right)$$

Input Parameters for model triax ellip shell:

a: semi-axes of elliptical core a
b: semi-axes of elliptical core b
c: semi-axes of elliptical core c
t: thickness of shell t
dummy: not used
eta_c: scattering length density of core η_c
eta_sh: scattering length density of shell η_{sh}
eta_sol: scattering length density of solvent η_{sol}

Input Parameters for model triax ellip shell t, triax ellip shell 1, triax ellip shell 1t, triax ellip shell 2, triax ellip shell 2t, triax ellip shell 3, triax ellip shell 3t:

a: semi-axes of elliptical core a
b: semi-axes of elliptical core b
c: semi-axes of elliptical core c
t: thickness of shell t
sigma: width of the LogNorm size distribution σ
eta_c: scattering length density of core η_c
eta_sh: scattering length density of shell η_{sh}
eta_sol: scattering length density of solvent η_{sol}

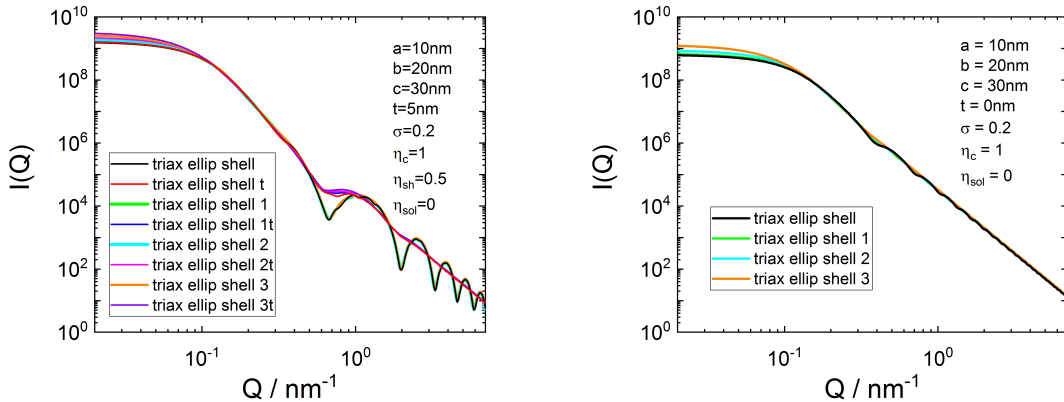


FIGURE 9.96. Form factor of a triaxial ellipsoidal core shell with semi axis a , b and c , with and without a shell thickness t plus an additional size distribution.

9.7. Cylindrical objects

9.7.1. Disc.



FIGURE 9.97

$$I_{\text{Disc}}(q, R) = \pi^2 R^4 \Delta\eta^2 \frac{2}{(qR)^2} \left(1 - \frac{1}{qR} J_1(2qR) \right) \quad (9.361)$$

with $\lim_{q \rightarrow 0} I_{\text{Disc}}(q, R) = \pi^2 R^4 \Delta\eta^2$

Input Parameters for model Disc:

R: radius of disc R

eta: scattering contrast $\Delta\eta$

Note:

- none

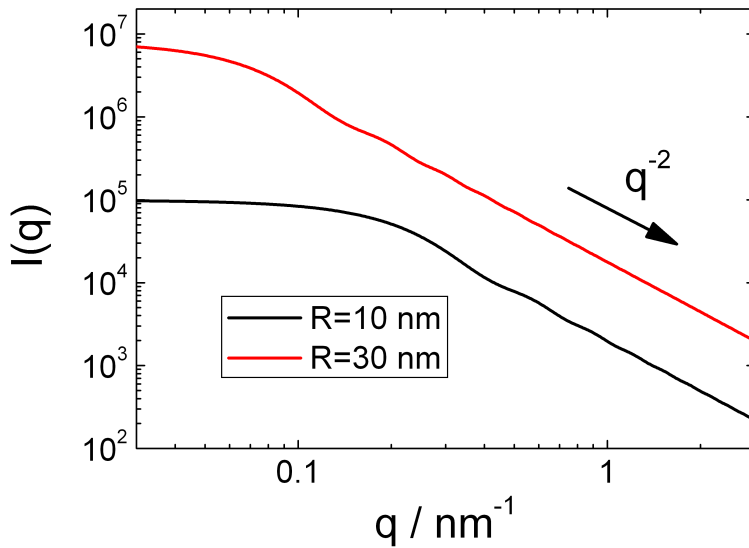


FIGURE 9.98. Scattering intensity of a disc with radii $R = 10$ nm and $R = 30$ nm. The scattering length density contrast is set to 1.

9.7.2. Rod.



FIGURE 9.99

$$I_{\text{Rod}}(q, L) = \Delta\eta^2 L^2 \left(\frac{2}{qL} \text{Si}(qL) - \left(\frac{\sin(qL/2)}{qL/2} \right)^2 \right) \quad (9.362)$$

with $\text{Si}(x) = \int_0^x \frac{\sin t}{t} dt$ and $\lim_{q \rightarrow 0} I_{\text{Rod}}(q, L) = \Delta\eta^2 L^2$

Input Parameters for model Rod:

L: length of rod L

eta: scattering contrast $\Delta\eta$

Note:

- none

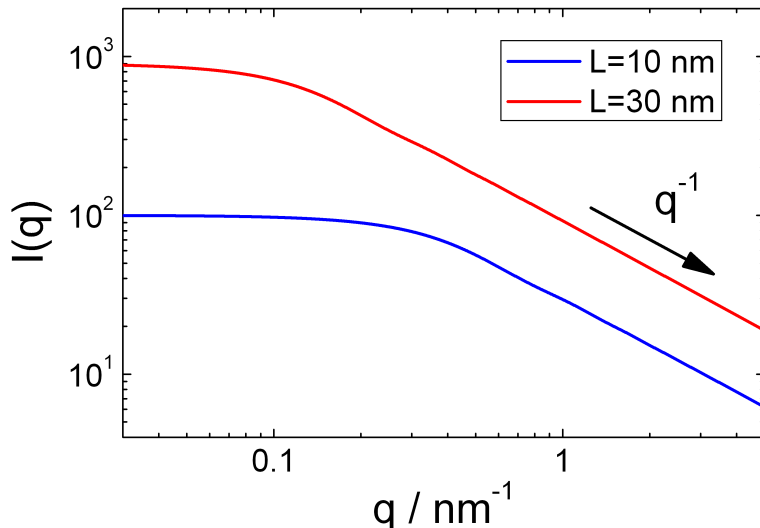


FIGURE 9.100. Scattering intensity of a rod of length $L = 10$ nm and $L = 30$ nm. The scattering length density contrast is set to 1.

9.7.3. Porod's approximation for a long cylinder. [393]

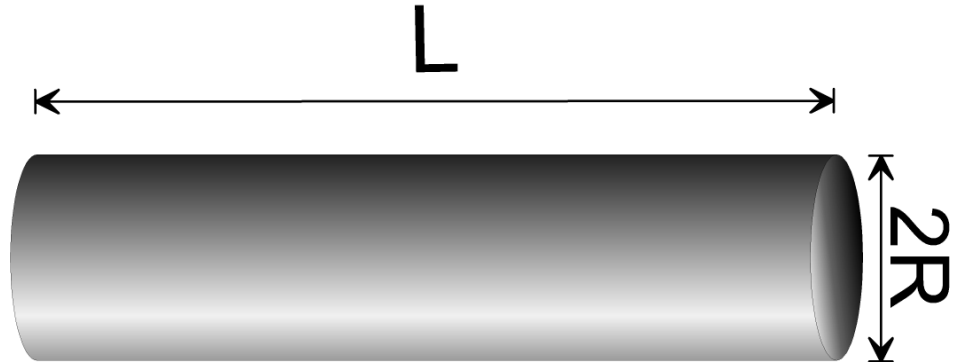


FIGURE 9.101

$$\text{Si}_{\frac{\pi}{2}}(x) = \left(\text{Si}(x) + \frac{\cos x}{x} + \frac{\sin x}{x^2} \right) \xrightarrow{x \rightarrow \infty} \frac{\pi}{2} \quad (9.363)$$

$$\Lambda_1(x) = \frac{2}{x} J_1(x) \quad (9.364)$$

$$\Lambda_2(x) = \frac{8}{x^2} J_2(x) \quad (9.365)$$

$$\omega(x) = \frac{8}{x^2} (3J_2(x) + J_0(x) - 1) \quad (9.366)$$

$$\Phi_{\text{long}}(q, R, L) = \left(\Delta\eta \pi R^2 L \right)^2 \frac{2}{QL} \times \left\{ \text{Si}_{\frac{\pi}{2}}(QL) \Lambda_1^2(QR) - \frac{\omega(2QR)}{QL} - \frac{\sin(QL)}{(QL)^2} \right\} \quad (9.367)$$

$J_n(x)$ are the regular cylindrical Bessel function of order n .

Input Parameters for model LongCylinder:

R: radius of cylinder R

L: length of cylinder L

eta: scattering contrast $\Delta\eta$

Note:

- The approximation is valid for $L > 2R$

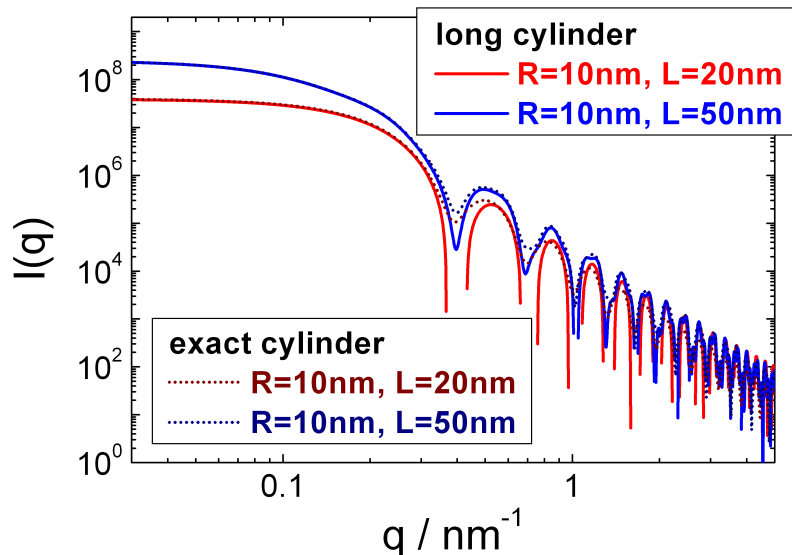


FIGURE 9.102. Scattering intensity of a cylinder with radius $R = 10$ nm and lengths of $L = 20$ nm and $L = 50$ nm. Next to Porod's approximation for long cylinders also the exact integral solution is shown for comparison. The scattering length density contrast is set to 1.

9.7.4. Porod's approximation for a flat cylinder. [393]

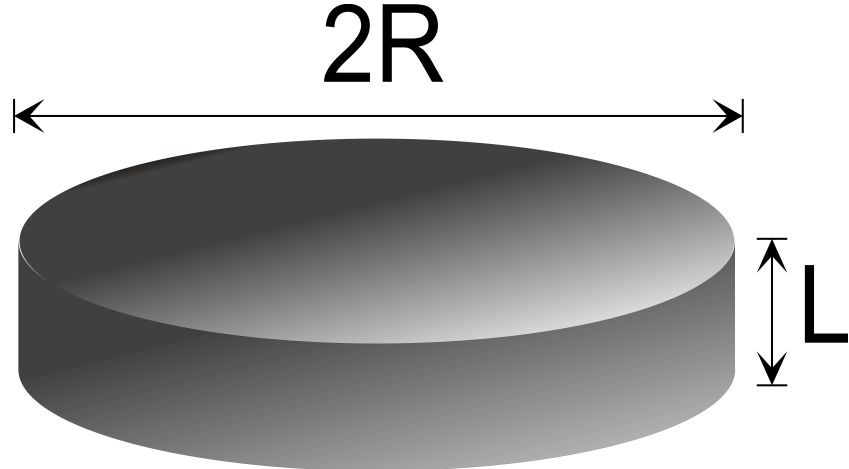


FIGURE 9.103

$$\Lambda_1(x) = \frac{2}{x} J_1(x) \quad (9.368)$$

$$I_1(x) = \int_0^x \Lambda_1(x') dx' = \quad (9.369)$$

$$2xJ_0(x) - 2J_1(x) - \pi x [J_0(x)H_1(x) - J_1(x)H_0(x)]$$

$$I_0(x) = \frac{I_1(x) + x\Lambda_1(x)}{2} \quad (9.370)$$

$$\Omega(x) = \frac{2}{x} [I_0(x) - 2J_1(x)] \quad (9.371)$$

$$\chi(x) = \left(\frac{\sin(x/2)}{x/2} \right)^2 \quad (9.372)$$

$$\Phi_{\text{flat}}(q, R, L) = \left(\Delta\eta\pi R^2 L \right)^2 \frac{8}{(2qR)^2} \quad (9.373)$$

$$\times \left\{ \chi(qL) + \frac{I_1(2QR) \Omega(qL)}{2qR} - \Lambda_1(2qR) \right\}$$

$H_\alpha(x)$ is the Struve function of order α and $J_n(x)$ are the regular cylindrical Bessel function of order n .

Input Parameters for model FlatCylinder:

R: radius of cylinder R

L: length of cylinder L

eta: scattering contrast $\Delta\eta$

Note:

- The approximation is valid for $L < 2R$

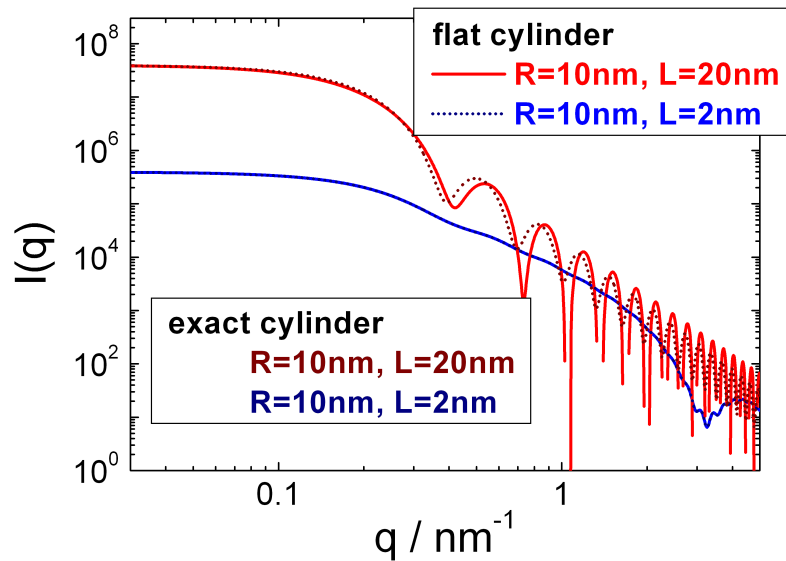


FIGURE 9.104. Scattering intensity of a cylinder with radius $R = 10$ nm and lengths of $L = 2$ nm and $L = 20$ nm. Next to Porod's approximation for flat cylinders also the exact integral solution is shown for comparison. The scattering length density contrast is set to 1.

9.7.5. Porod's approximations for cylinder. [393]

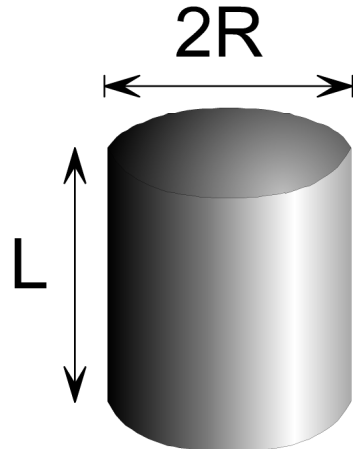


FIGURE 9.105

This form factor combines the two solutions of Porod for a long $\Phi_{\text{long}}(q, R, L)$ (9.367) and a flat $\Phi_{\text{flat}}(q, R, L)$ (9.373) cylinder by a linear combination of both. A simple linear transition at $L = 2R$ is assumed.

$$\Phi_{\text{Porod}}(q, R, L) = p \left(\frac{2R}{L} \right) \Phi_{\text{flat}}(q, R, L) + \left(1 - p \left(\frac{2R}{L} \right) \right) \Phi_{\text{long}}(q, R, L) \quad (9.374)$$

$$p(x) = \begin{cases} 1 & \text{for } x > \frac{5}{4} \\ 2 \left(x - \frac{3}{4} \right) & \text{for } \frac{3}{4} \leq x \leq \frac{5}{4} \\ 0 & \text{for } x < \frac{3}{4} \end{cases} \quad (9.375)$$

Input Parameters for model PorodCylinder:

R: radius of cylinder R

L: length of cylinder L

eta: scattering contrast $\Delta\eta$

Note:

- less good approximation for $L \sim 2R$

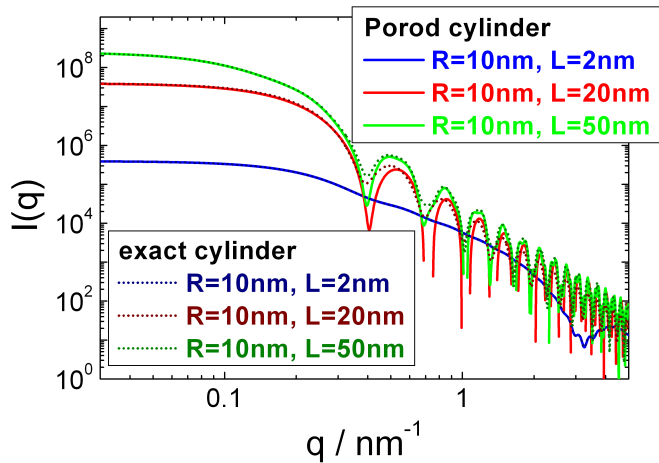


FIGURE 9.106. Scattering intensity of a cylinder with radius $R = 10$ nm and lengths of $L = 2$ nm, $L = 20$ nm, and $L = 50$ nm. Next to Porod's approximation for a cylinders also the exact integral solution is shown for comparison. The scattering length density contrast is set to 1.

9.7.6. Cylinder of length L , radius R and scattering contrast $\Delta\eta$.

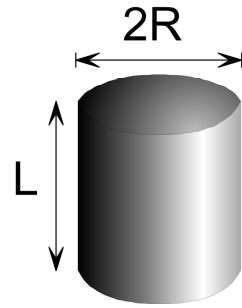


FIGURE 9.107

$$I_{\text{cyl}} = 16(\pi R^2 L)^2 \Delta\eta^2 \int_0^1 \left(\frac{J_1(QR\sqrt{1-x^2}) \sin(QLx/2)}{Q^2 R \sqrt{1-x^2} L x} \right)^2 dx \quad (9.376)$$

Input Parameters for model Cylinder:

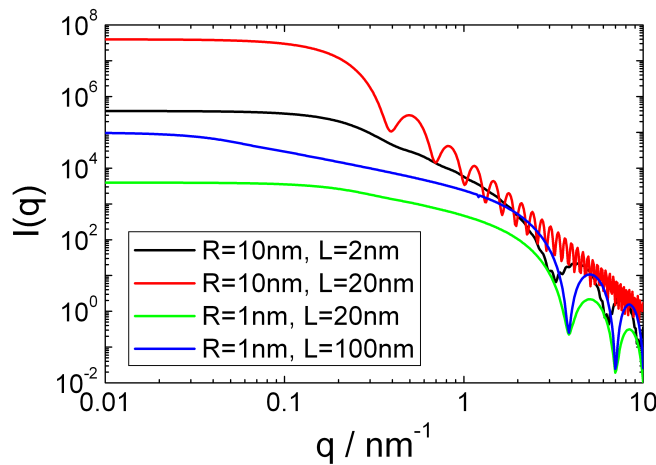
R: radius of cylinder R

L: length of cylinder L

eta: scattering contrast $\Delta\eta$

Note:

- None

FIGURE 9.108. Scattering intensity of a cylinder for different radii radius R nm and lengths L . The scattering length density contrast is set to 1.

9.7.7. Random oriented cylindrical shell with circular cross-section.

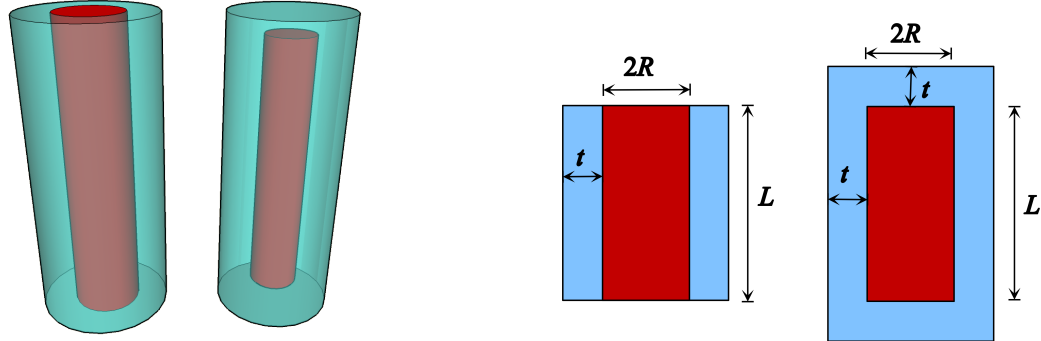


FIGURE 9.109. cylindrical shell with circular cross-section

To different versions for a random oriented cylindrical shell with a circular cross-section has been implemented. One without `CylShell1` and one with `CylShell2` capped flat ends. For very long cylinders a faster approximation for the uncapped version can be used `LongCylShell`

$$K_{\text{Cyl}}(Q, \Delta\eta, R, L, x) = 2\pi R^2 L \Delta\eta \frac{J_1(QR\sqrt{1-x^2})}{QR\sqrt{1-x^2}} \frac{\sin(QLx/2)}{QLx/2} \quad (9.377)$$

$$I_{\text{CylShell1}} = \int_0^1 \left(K_{\text{Cyl}}(Q, \eta_{\text{core}} - \eta_{\text{shell}}, R, L, x) + K_{\text{Cyl}}(Q, \eta_{\text{shell}} - \eta_{\text{solv}}, R + t, L, x) \right)^2 dx \quad (9.378)$$

$$I_{\text{CylShell2}} = \int_0^1 \left(K_{\text{Cyl}}(Q, \eta_{\text{core}} - \eta_{\text{shell}}, R, L, x) + K_{\text{Cyl}}(Q, \eta_{\text{shell}} - \eta_{\text{solv}}, R + t, L + 2t, x) \right)^2 dx \quad (9.379)$$

$$I_{\text{LongCylShell}}(Q) = P'(Q)P_{\text{cs}}(Q) \quad (9.380)$$

$$P'(Q) = 2 \frac{\text{Si}(QL)}{QL} - \left(\frac{\sin(QL/2)}{QL/2} \right)^2 \quad (9.381)$$

$$\text{Si}(x) = \int_0^x \frac{\sin t}{t} dt \quad (9.382)$$

$$P_{\text{cs}}(Q) = \left(2 \frac{J_1(QR)}{QR} (\eta_{\text{core}} - \eta_{\text{shell}}) R^2 L \pi + 2 \frac{J_1(Q(R+t))}{Q(R+t)} (\eta_{\text{shell}} - \eta_{\text{solv}}) (R+t)^2 L \pi \right)^2 \quad (9.383)$$

Input Parameters for models CylShell1, CylShell2 and LongCylShell:

R: core radius R

t: shell thickness t

L: cylinder length L

eta_core: scattering length density η_{core} of cylinder core

eta_shell: scattering length density η_{shell} of cylinder shell

eta_solv: scattering length density η_{solv} of solvent

Note:

- The approximation for a long cylindrical shell (LongCylShell) only holds for $L \gg 2R$.

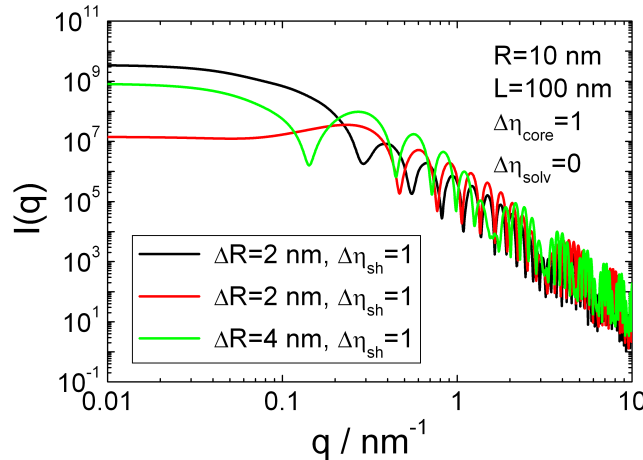


FIGURE 9.110. Scattering intensity of a cylinder shell CylShell1.

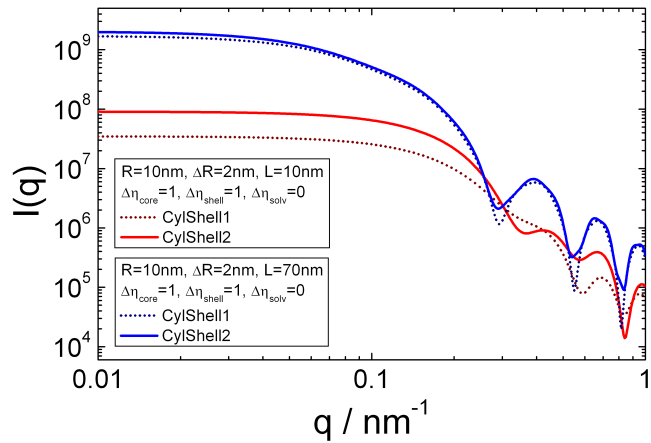


FIGURE 9.111. Scattering intensity of a cylinder shell CylShell2.

9.7.8. Random oriented cylindrical shell with elliptical cross-section.

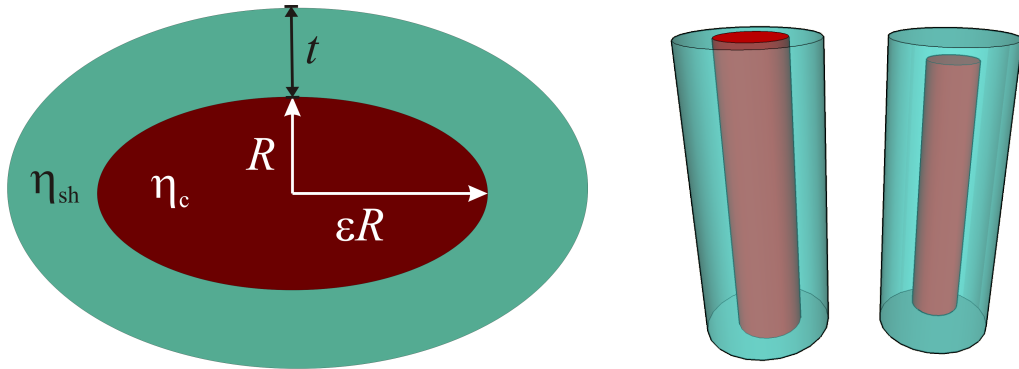


FIGURE 9.112. cylindrical shell with elliptical cross-section

To different versions for a random oriented cylindrical shell with an elliptical cross-section has been implemented. One without `ellCylShell1` and one with `ellCylShell2` capped flat ends.

$$K_{\text{ellCyl}}(q, \Delta\eta, R, \epsilon, L, t, \phi, \alpha) = \pi\epsilon R(\epsilon R + t)L\Delta\eta \quad (9.384)$$

$$\times \frac{2J_1(qr(R, \epsilon, t, \phi, \alpha))}{qr(R, \epsilon, t, \phi, \alpha)} \frac{\sin(q\frac{L}{2}\cos(\alpha))}{q\frac{L}{2}\cos(\alpha)}$$

$$r(R, \epsilon, t, \phi, \alpha) = \sqrt{(R+t)^2 \sin^2(\phi) + (\epsilon R + t)^2 \cos^2(\phi)} \quad (9.385)$$

$$I_{\text{ellCylShell1}}(q) = \frac{2}{\pi} \int_0^{\frac{\pi}{2}} \int_0^{\frac{\pi}{2}} \left(K_{\text{ellCyl}}(q, \eta_{\text{core}} - \eta_{\text{shell}}, R, \epsilon, L, 0, \phi, \alpha) \right. \quad (9.386)$$

$$\left. + K_{\text{ellCyl}}(q, \eta_{\text{shell}} - \eta_{\text{sol}}, R, \epsilon, L, t, \phi, \alpha) \right)^2 \sin(\alpha) d\alpha d\phi$$

$$I_{\text{ellCylShell2}}(q) = \frac{2}{\pi} \int_0^{\frac{\pi}{2}} \int_0^{\frac{\pi}{2}} \left(K_{\text{ellCyl}}(q, \eta_{\text{core}} - \eta_{\text{shell}}, R, \epsilon, L, 0, \phi, \alpha) \right. \quad (9.387)$$

$$\left. + K_{\text{ellCyl}}(q, \eta_{\text{shell}} - \eta_{\text{sol}}, R, \epsilon, L+2t, t, \phi, \alpha) \right)^2 \sin(\alpha) d\alpha d\phi$$

Input Parameters for models `ellCylShell1` and `ellCylShell2`:

R: core radius R

epsilon: stretching factor ϵ of cross-section

L: cylinder length L

t: shell thickness t

eta_core: scattering length density η_{core} of cylinder core
eta_shell: scattering length density η_{shell} of cylinder shell
eta_sol: scattering length density η_{sol} of solvent

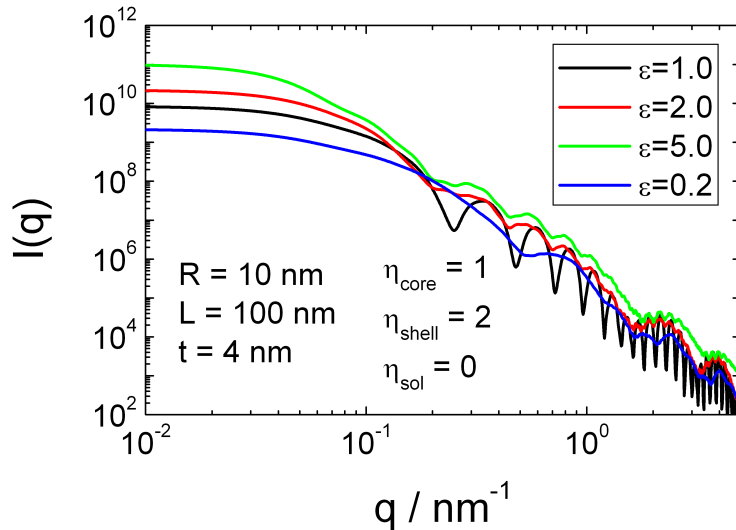


FIGURE 9.113. Scattering intensity of a cylinder with elliptical cross-section.

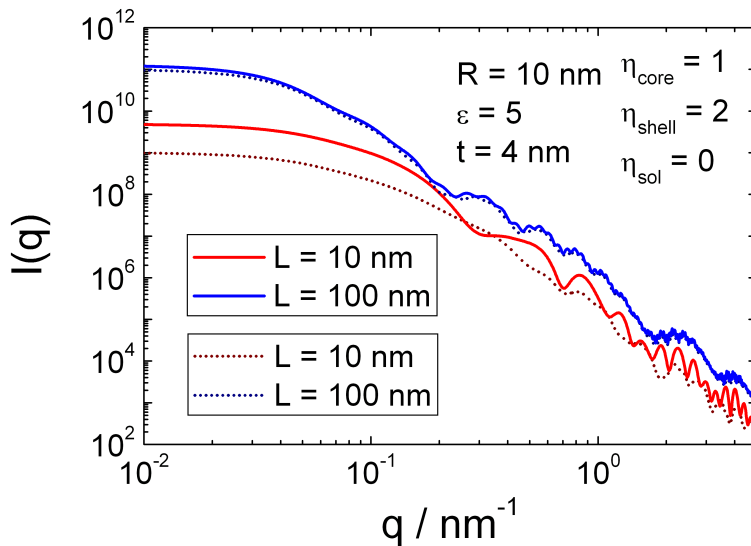


FIGURE 9.114. Scattering intensity of a cylinder with elliptical cross-section with and without capped flat ends.

For very long cylinders a faster approximation for the uncapped version can be used `Pcs:ellCylSh` combined with the structure factor `P'(Q):Rod`. The implemented approximation is the following

$$I_{\text{Long_ellCylShell}}(q) = P'(q)P_{\text{cs}}(q) \quad (9.388)$$

$$P'(q) = 2 \frac{\text{Si}(qL)}{qL} - \left(\frac{\sin(qL/2)}{qL/2} \right) \quad (9.389)$$

$$\text{Si}(x) = \int_0^x \frac{\sin t}{t} dt \quad (9.390)$$

$$r(R, \epsilon, t, \phi) = \sqrt{(R+t)^2 \sin^2(\phi) + (\epsilon R + t)^2 \cos^2(\phi)} \quad (9.391)$$

$$P_{\text{cs}}(q) = \frac{2}{\pi} \int_0^{\frac{\pi}{2}} \left(\frac{2J_1(qr(R, \epsilon, 0, \phi))}{qr(R, \epsilon, 0, \phi)} (\eta_{\text{core}} - \eta_{\text{shell}}) \epsilon R^2 L \pi + \frac{2J_1(q(r(R, \epsilon, t, \phi)))}{qr(R, \epsilon, t, \phi)} (\eta_{\text{shell}} - \eta_{\text{sol}}) (R+t)(\epsilon R + t) L \pi \right)^2 d\phi \quad (9.392)$$

Input Parameters for model `Pcs:ellCylSh`:

R: core radius R

epsilon: stretching factor ϵ of cross-section

t: shell thickness t

eta_core: scattering length density η_{core} of cylinder core

eta_shell: scattering length density η_{shell} of cylinder shell

eta_sol: scattering length density η_{sol} of solvent

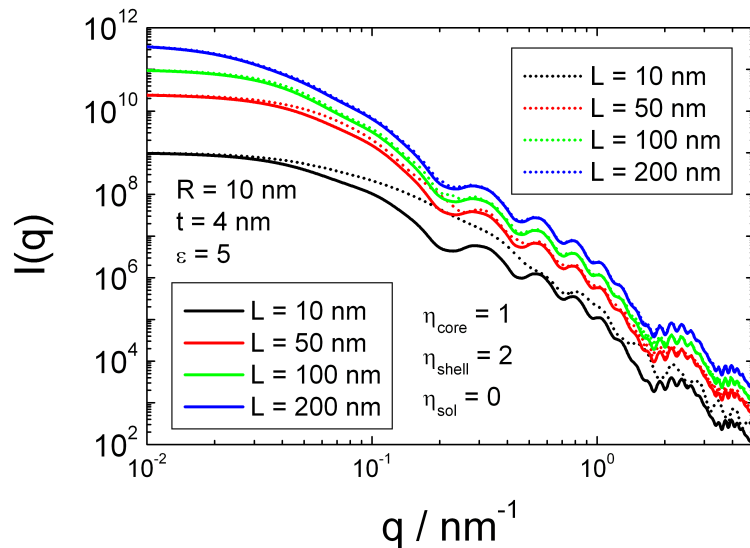


FIGURE 9.115. Scattering intensity of a cylinder with elliptical cross-section. The exact solutions `ellCylShell1` (dotted lines) are compared with `Pcs:ellCylSh` (solid lines), which is only valid for very long cylinders $L \gg 2R$.

9.7.9. Random oriented solid cylinder with circular cross-section and globular end caps.

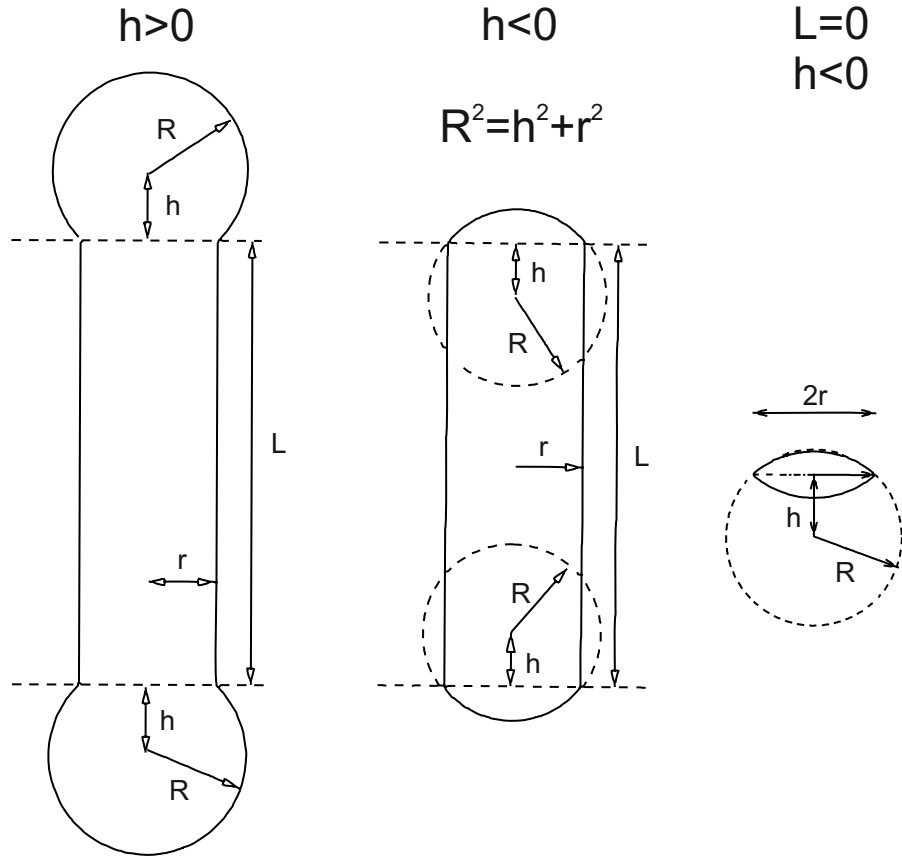


FIGURE 9.116. solid cylinders with circular cross-section and globular end caps

The scattering from cylinders with globular end caps have been studied by [255, 256]. There form factor also contain the special case of hemispherical end-caps given by [92]. They obtain for the scattering amplitude the expression

$$\begin{aligned}
 F(Q, r, L, h, \theta) = & \pi r^2 L \frac{\sin(QL/2 \cos(\theta))}{QL/2 \cos(\theta)} \frac{2 J_1(Qr \sin(\theta))}{Qr \sin(\theta)} \\
 & + 4\pi R^3 \int_{-h/R}^1 dt \cos(Q(Rt + h + L/2) \cos(\theta)) \\
 & \times (1 - t^2) \frac{J_1(QR \sin(\theta) \sqrt{1 - t^2})}{QR \sin(\theta) \sqrt{1 - t^2}}
 \end{aligned} \tag{9.393}$$

Here r is the radius of the cylinder, $R = \sqrt{h^2 + r^2}$ the radius of the globular end caps, h the offset of the globular end cap from the end of the cylinder and L is the length of the cylinder. For $h > 0$ the end caps are barbel like and for $h < 0$ they are flat.

The scattering intensity of a random oriented cylinder with globular end caps reads as

$$I(Q) = \int_0^{\pi/2} |F(Q, r, L, h, \theta)|^2 \sin \theta \, d\theta \quad (9.394)$$

Input Parameters for model capped_cylinder:

r: cylinder radius r

h: center offset of cap from surface h . ($h < 0$: flat end cap, $h > 0$: barbel end caps)

L: cylinder length L

eta: scattering length density η of cylinder

Note:

- r and L are only physical for values larger than 0.
- h can be positive or negative depending on the direction of the offset.
- the integration algorithm can be configured via GUI (via `integration strategy`)

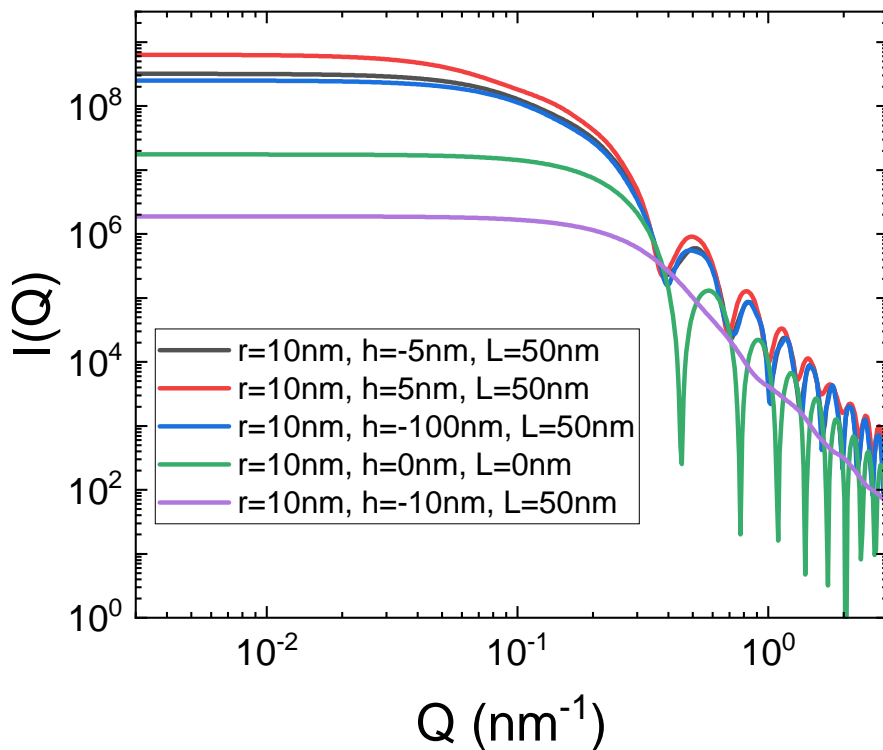


FIGURE 9.117. scattering curves of random oriented capped cylinders with circular cross-section and globular end caps

9.7.10. Cylinders packed in a hexagonal lattice with paracrystalline distortion.

Hashimoto has given in [203] an analytical expression for hexagonal packed infinite



FIGURE 9.118. hexagonal packed long cylinders

long cylinders with a paracrystalline disorder. In a first case the scattering perpendicular to the cylinder axis is derived but also the random oriented case is given, where simply a Lorentz factor of q^{-1} needs to be multiplied [452, 163]. In principle the two cases can be considered as the case of very thin rod-like structures as discussed in 9.2. For such thin random orientated particles the form factor can be factorized in a cross-section term $P_{cs}(Q)$ for the shorter or thin dimension and a shape factor $P'(Q)$ for the long dimension.

$$I(Q) = P'(Q)P_{cs}(Q). \quad (9.395)$$

The cross section term for cylinder-symmetric structures is the zero order Hankel transform of the radial scattering length density profile $\eta(\rho)$

$$P_{cs}(Q) \left| \int_0^\infty \eta(\rho) \rho J_0(Q\rho) \right|^2 \quad (9.396)$$

The cross-section term alone describes the scattering perpendicular to the cylinder axes and has to be used if the cylinder axis is perfectly aligned to the beam direction, i.e. perpendicular to the scattering vector, as e.g. done in [384] to analyse textured wood samples. In [203, 384] the cross section term $P_{cs}(Q)$ is named $P_{cs} = I_{cyl}(Q)$. The given model assumes, that also for the aligned cases only the cylinder axis are aligned to the

beam axis but otherwise random orientations around that axis is assumed.

$$I_{\text{cyl}}(Q) = \frac{1}{2\pi} \int_0^\infty I_\perp(Q, \psi) d\psi \quad (9.397\text{a})$$

$$I_\perp(Q, \psi) = \langle |F_{\text{cs}}(Q)^2| \rangle + |\langle F_{\text{cs}}(Q) \rangle|^2 (S(Q) - 1) \quad (9.397\text{b})$$

$$F_{\text{cs}}(Q, R) = \int_0^\infty \eta(\rho) \rho J_0(Q\rho) d\rho = \pi R^2 \frac{J_1(Qr)}{QR} \quad (9.397\text{c})$$

$$S(Q) = Z_1 Z_2 \quad (9.397\text{d})$$

$$Z_k = \frac{1 - |F_k|^2}{1 - 2|F_k| \cos(\mathbf{Q}\mathbf{a}_k) + |F_k|^2} \quad (9.397\text{e})$$

$$F_k = \exp \left(-\frac{1}{2} \left(\frac{\Delta a}{a} \right)^2 \left[(\mathbf{Q}\mathbf{a}_1)^2 + (\mathbf{Q}\mathbf{a}_2)^2 \right] \right) \quad (9.397\text{f})$$

$$\mathbf{Q}\mathbf{a}_1 = -aQ \cos(\psi - \pi/6) \quad (9.397\text{g})$$

$$\mathbf{Q}\mathbf{a}_2 = aQ \sin(\psi) \quad (9.397\text{h})$$

The lattice constant a is assumed to have a certain paracrystalline distortion quantified by Δa . The structure factor of the hexagonal lattice has been introduced using the decoupling approach [273], which involves two averages $\langle |F_{\text{cs}}(Q)^2| \rangle$ and $|\langle F_{\text{cs}}(Q) \rangle|^2$ of the cross-section amplitude. In case of a Gaussian distribution (see 7.8) of cylinder radii with \bar{R} being the maximum of the Gaussian distribution and $\Delta R = \sigma$ the width parameter according to eq. 7.32a so that

$$\langle F_{\text{cs}}(Q) \rangle = \int_0^\infty \text{Gauss}(R, 1, \Delta R, \bar{R}) F_{\text{cs}}(Q, R) dR \quad (9.398)$$

$$\langle F_{\text{cs}}^2(Q) \rangle = \int_0^\infty \text{Gauss}(R, 1, \Delta R, \bar{R}) F_{\text{cs}}^2(Q, R) dR \quad (9.399)$$

To suppress the upturn in the structure factor at small Q -values a modification of the lattice factor Z_k has been suggested in [384] by approximating the lattice factor by

$$Z_k = \begin{cases} Z_k(Q_0), & \text{if } Q \leq Q_0 \\ Z_k(Q), & \text{if } Q > Q_0 \end{cases} \quad (9.400)$$

$$Q_0 = 7.061 \times 10^{-5} a^2 - 0.007413a + 0.2465 \quad (9.401)$$

The polynomial dependencies of Q_0 has been determined in [384], where they found, that it is also almost independent on Δa .

9.7.10.1. Scattering perpendicular to paracrystalline hexagonal packed cylinders.

For the scattering of the hexagonal packed cylinders perpendicular to the cylinder axes the intensity is given by eq. 9.397a. If the correction of the lattice factor in eq.

[9.400](#) is used or not can be set via a flag parameter. If `vers` ≤ 0 the corrected lattice factor is used otherwise the original one in eq. [9.397e](#).

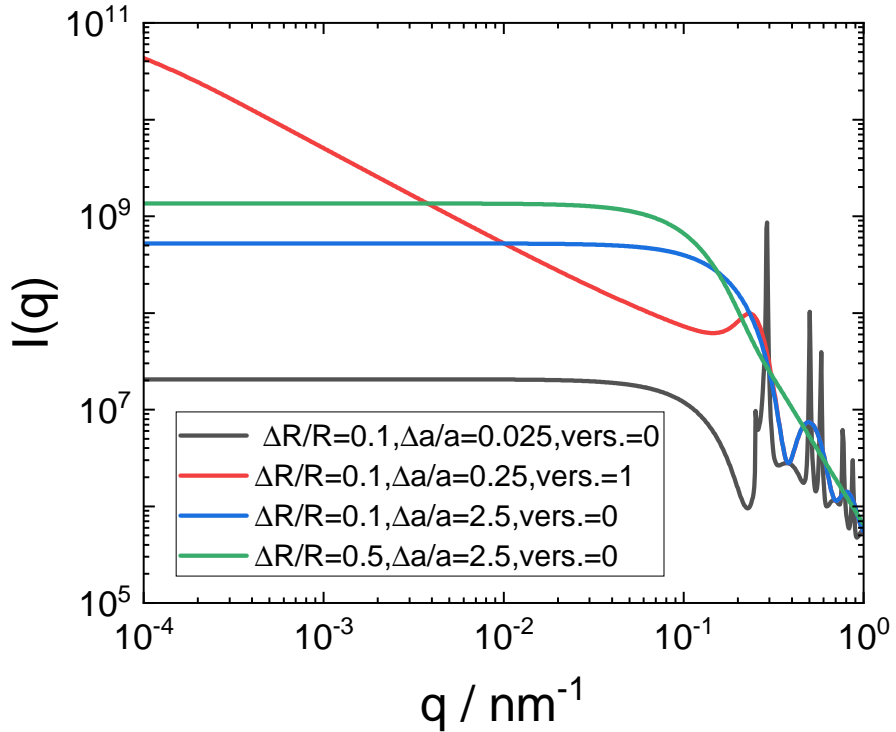


FIGURE 9.119. Scattering intensity perpendicular to paracrystalline hexagonal packed cylinders.

Input Parameters for model `paracryst_hex_cyl_perp`:

R: avg. cylinder radius R

dR_ratio: Gaussian width parameter ΔR divided by average radius $\Delta R/R$

dummy: not used

dummy: not used

a: lattice parameter a

da_ratio: paracrystalline distortion parameter Δa divided by lattice constant $\Delta a/a$

vers.: flag how the structure factor is calculated

Note:

- the integration algorithm can be configured via GUI (via `integration strategy`)

9.7.10.2. Scattering of randomly oriented bundles of paracrystalline hexagonal packed cylinders.

The random oriented version of the previous form factor is in principle also able to probe the length of the cylinders. The form factor is given by eq. 12.77 with the cross-section term of eq. 9.397a and $P'(Q)$ given by eq. 9.47 describing the scattering of a thin rod with a LogNorm length distribution. As for the previous version a parameter is introduced to define if the correction of the lattice factor in eq. 9.400 is used or not. The version can be set via a flag parameter. If $\text{vers} \leq 0$ the corrected lattice factor is used otherwise the original one in eq. 9.397e.

Input Parameters for model paracryst_hex_cyl_rnd:

R: avg. cylinder radius R

dR_ratio: Gaussian width parameter ΔR divided by average radius $\Delta R/R$

dummy: not used

dummy: not used

a: lattice parameter a

da_ratio: paracrystalline distortion parameter Δa divided by lattice constant $\Delta a/a$

vers.: flag how the structure factor is calculated

L: mode of cylinder length distribution L

sigma_L: LogNorm width parameter for cylinder length σ_L

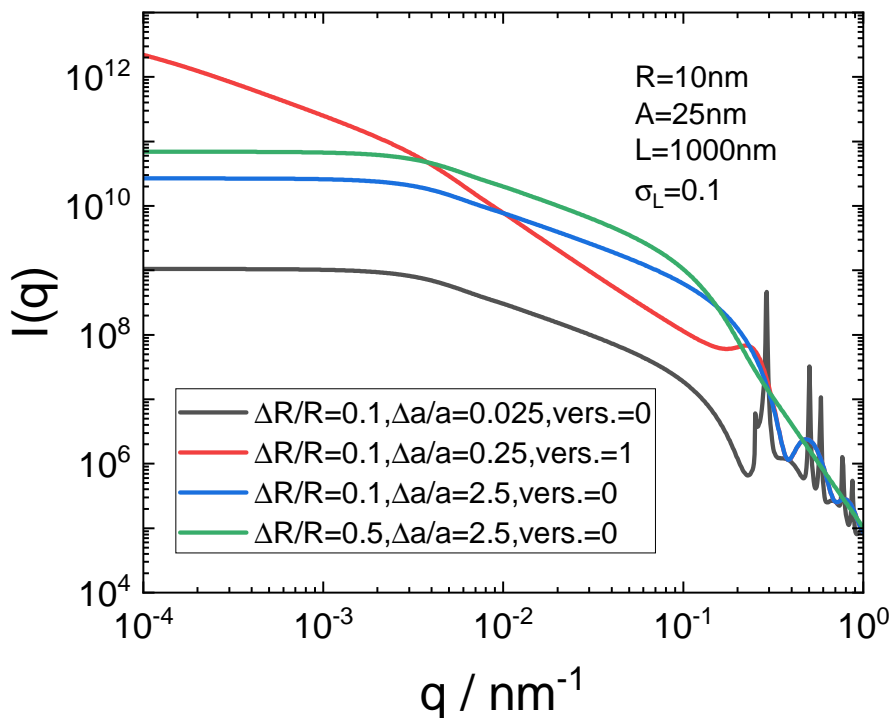


FIGURE 9.120. Scattering intensity randomly oriented bundles of paracrystalline hexagonal packed cylinders.

Note:

- the integration algorithm can be configured via GUI (via `integration strategy`)

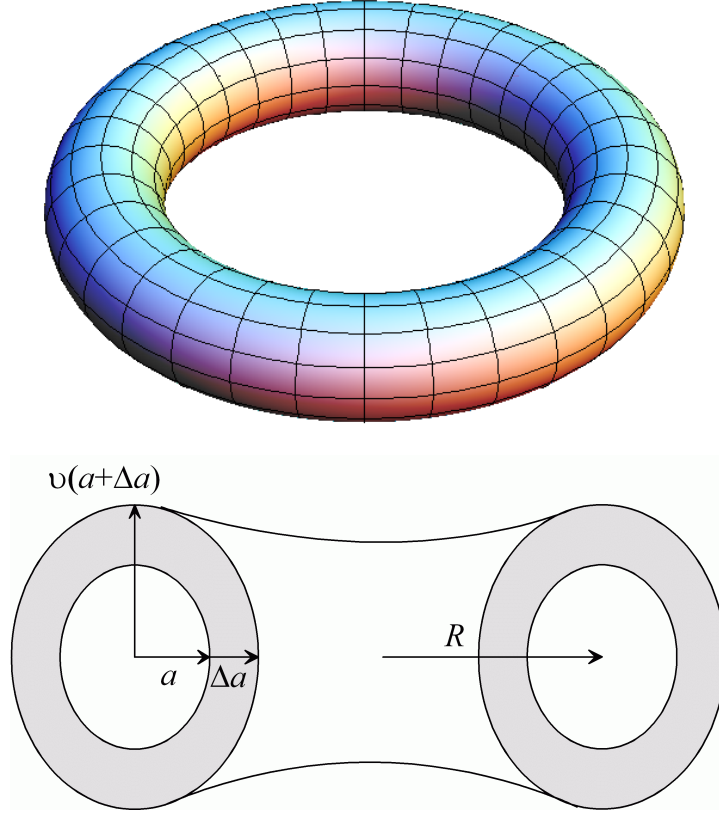
9.7.11. Torus with elliptical shell cross-section. [254, 127]


FIGURE 9.121

$$F_{\text{torus}}(Q, \Theta, R, x, \nu, \Delta\eta) = \int_{\max\{0, R-x\}}^{R+x} 4\pi r \Delta\eta \frac{J_0(Qr \sin \Theta) \sin(Q\gamma(r) \cos \Theta)}{Q \cos(\Theta)} dr \quad (9.402)$$

$$\text{with } \gamma(r) = \nu \sqrt{x^2 - (r - R)^2} \quad (9.403)$$

$$I_{\text{torus}}(Q, R, a, \nu, \Delta\eta) = \int_0^{\pi/2} |F_{\text{torus}}(Q, \Theta, R, a, \nu, \Delta\eta)|^2 \sin \Theta d\Theta \quad (9.404)$$

$$I_{\text{torus,sh}}(Q, R, a, \Delta a, \nu, \Delta\eta_{sh}, \Delta\eta_c) = \int_0^{\pi/2} \left| F_{\text{torus}}(Q, \Theta, R, a + \Delta a, \nu, \Delta\eta_{sh}) - F_{\text{torus}}(Q, \Theta, R, a, \nu, \Delta\eta_c) \right|^2 \sin \Theta d\Theta \quad (9.405)$$

An alternative form factor for F_{torus} following [127] is

$$F_{\text{torus}}(Q, \Theta, R, x, \nu, \Delta\eta) = 2\pi \int_{-x}^x \left[R_{(+)} J_1(QR_{(+)} \sin \theta) - R_{(-)} J_1(QR_{(-)} \sin \theta) \right] \frac{\cos(Qz \cos \theta)}{Q \sin \theta} dz \quad (9.406)$$

with $R_{(\pm)} = R \pm \nu \sqrt{x^2 - z^2}$

Input Parameters for model torus:

R: distance between center of tube to center of torus R

a: radius of tube core

Delta_a: shell thickness of tube shell Δa

nu: stretching factor of elliptical torus cross-section ν

eta_c: scattering length density of core η_c

eta_sh: scattering length density of shell η_{sh}

eta_sol: scattering length density of core η_{sol}

Note:

- the integration algorithm can be configured via GUI (via **integration strategy**)
- for $R - a - \Delta a < 0$ the integration in 9.402 starts at 0 as a lower limit. In the extreme case $R = 0$ the form factor is the one of an elliptical shell.

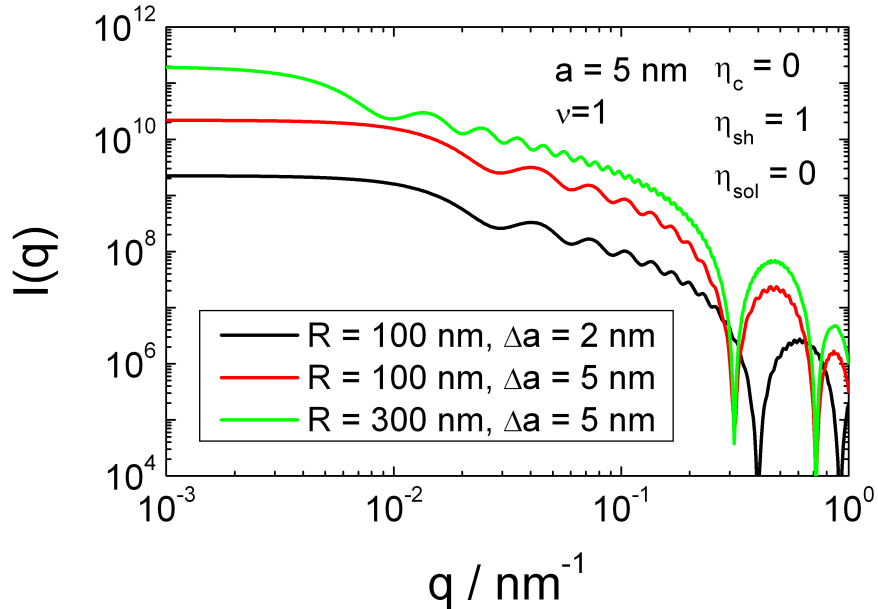


FIGURE 9.122. Scattering intensity of a torus.

9.7.12. Helical structures.

Several approaches for describing the small angle scattering signal from randomly oriented helical structures have been published. In [133, 403] a model of a double helix with a round cross section for each strand has been developed. For a fanlike cross section of a double helix a solution has been given by [442, 398]. Fukuda et al. [142] have extended the model to an arbitrary shaped cross section. In a model developed by Lebedev et al. [290] it is assumed, that beads are arranged on a helical path assuming a single strand. In all models the helix is straight and its length dimension is large compared to all other characteristic length of the helix. In [22] a solution of a single helical strand which can have a secondary coiling has been described. In this paper the cross section of the helical strand is assumed to be infinitesimal thin.

9.7.12.1. Fanlike helix.

Double helices with a fanlike cross section in the plane perpendicular to the helix axis have been described by Schmidt and Pringle [442, 398]. The model has been generalized by Fakuda et al. [142] for an arbitrarily shaped cross section and by Teixeira et al. [480] to a multi radial shell with fanlike cross section.

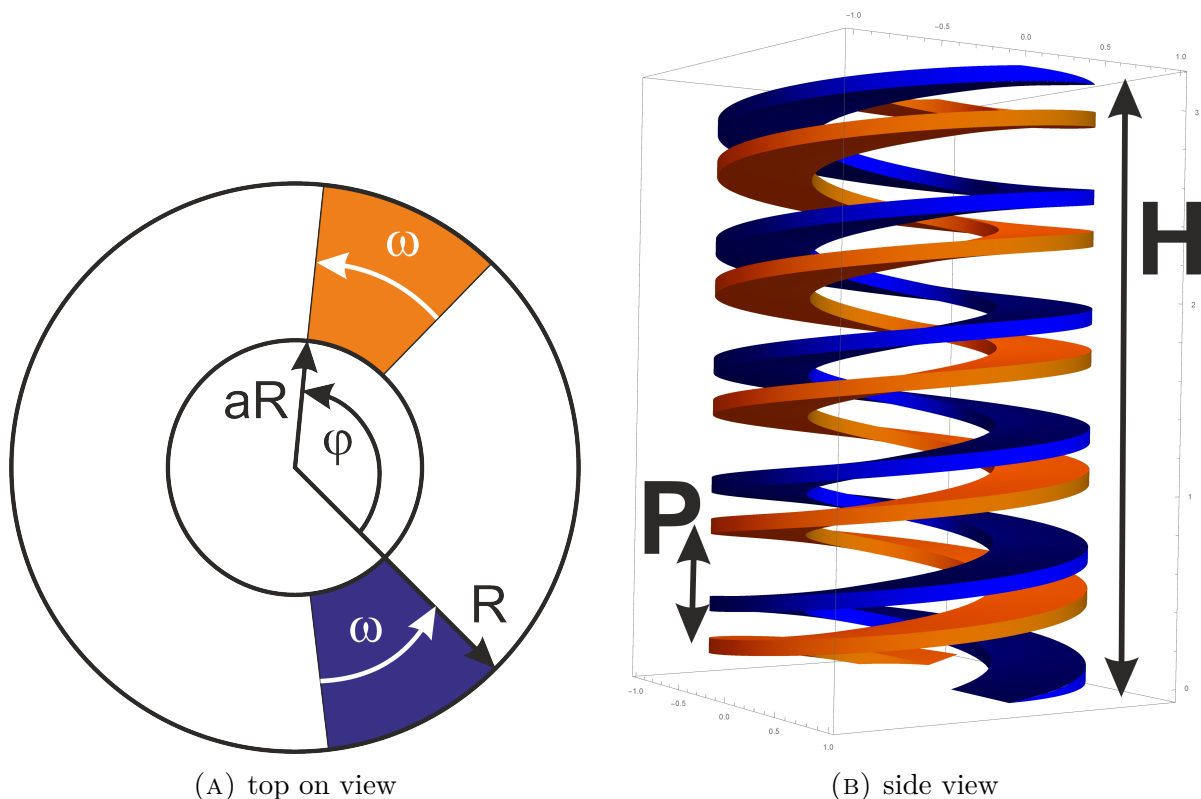


FIGURE 9.123. Double helix with strands of round cross sections.

$$I(Q) = P_{\text{rod}}(Q, H) \left((\eta_h - \eta_{\text{solv}}) \omega R^2 (1 - a^2) \right)^2 \\ \times \sum_{n=0}^{\infty} \epsilon_n \left(\cos(n\varphi/2) \frac{\sin(n\omega/2)}{n\omega/2} g_n(Q, R, a) \right)^2 \quad (9.407)$$

$$g_n(Q, R, a) = \frac{2}{R^2 (1 - a^2)} \int_{aR}^R r' J_n(Qr' (1 - q_n^2)) dr' \quad (9.408)$$

$$q_n = \begin{cases} \frac{2\pi n}{QP} & \text{for } Q \geq \frac{2\pi n}{P} \\ 1 & \text{for } Q < \frac{2\pi n}{P} \end{cases} \quad (9.409)$$

$$P_{\text{rod}}(Q, H) = H^2 \left(2 \frac{\text{Si}(QH)}{(QH)} - \left(\frac{\sin(QH/2)}{QH/2} \right)^2 \right) \quad (9.410)$$

with $\epsilon_n = 1$ for $n = 0$ and $\epsilon_n = 2$ for $n \geq 1$.

The sum converges very fast and for small Q -values the first few terms are already sufficient. However, SASfit is continuing the sum until the relative change of the sum is less than 10^{-10} .

The forward scattering of the model is normalized to the squared scattering length density contrast and squared total volume of the helix so that

$$I(Q = 0) = \left(H(\eta_h - \eta_{\text{solv}}) \omega R^2 (1 - a^2) \right)^2 \quad (9.411)$$

Input Parameters for model `fanlike helix`:

R: external helix radius R

a: inner helix radius aR , with $0 \leq a \leq 1$

omega: angular of the sector of material ω

phi: angle between the two sectors of material φ

dummy: not used

P: height of one helix period P

H: total length of helix H

eta_h: scattering length density of helix η_h

dummy: not used

eta_solv: scattering length density of solvent η_{solv}

Note:

- The helix is assumed to be stiff and long so that its scattering intensity can be factorized in a cross-section contribution and a shape contribution, whereas the shape contribution can be described by an infinitesimal thin rod of length H .
- R , P , and H are only physical for values larger than 0.
- The model is an approximation for the limit $H \gg P$ and $H \gg R$.
- $0 \leq a \leq 1$

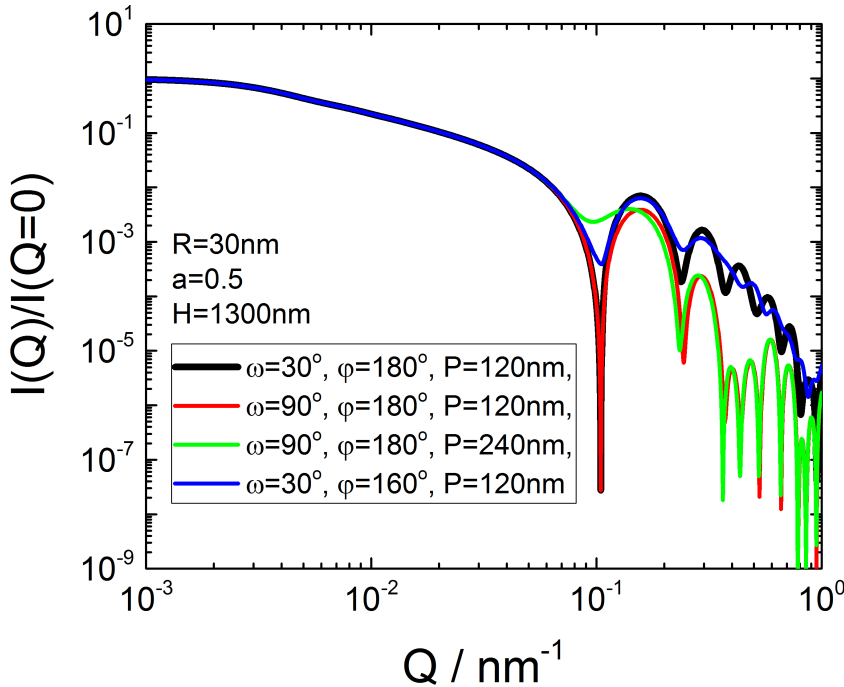


FIGURE 9.124. Normalized scattering curves of fanlike helices.

9.7.12.2. Helix with round cross-section.

Originally Franklin et al. [133] and Puigjaner et al. [403] have given the form factor of a cylinder with a groove of a double helix shape of round cross section. Fukada [142] is discussing the form factor of the random oriented double helices alone, but with arbitrary cross-sections.

$$I(Q) = P_{\text{rod}}(Q, H) \sum_{n=0}^{\infty} \epsilon_n \left(A_{1n}^2 + A_{2n}^2 + 2A_{1n}A_{2n} \cos n\alpha \right) \quad (9.412)$$

where

$$A_{in} = J_n(\delta_i Q_{\perp}) \pi R_i^2 (\eta_i - \eta_{\text{solv}}) \frac{2J_1(R_i Q_{\perp})}{R_i Q_{\perp}} \quad (9.413)$$

$$Q_{\perp}^2 = Q^2 - \left[\frac{2\pi n}{P} \right]^2 \quad (9.414)$$

with $\epsilon_j = 1$ for $j = 0$ and $\epsilon_j = 2$ for $j \geq 1$. Furthermore R_1 and R_2 are the radii of the round helical strands. δ_1 and δ_2 are the distances of the strands to the helix axis. The pitch of the helix is denoted by P , whereas α is the angle between the two strands.

The sum converges very fast and for small Q -values the first few terms are already sufficient. However, SASfit is continuing the sum until the relative change of the sum is less than 10^{-10} .

The forward scattering of the model is normalized to the squared scattering length density contrast and squared total volume of the helix so that

$$I(Q = 0) = H^2 \left((\eta_1 - \eta_{\text{solv}}) \pi R_1^2 + (\eta_2 - \eta_{\text{solv}}) \pi R_2^2 \right)^2 \quad (9.415)$$

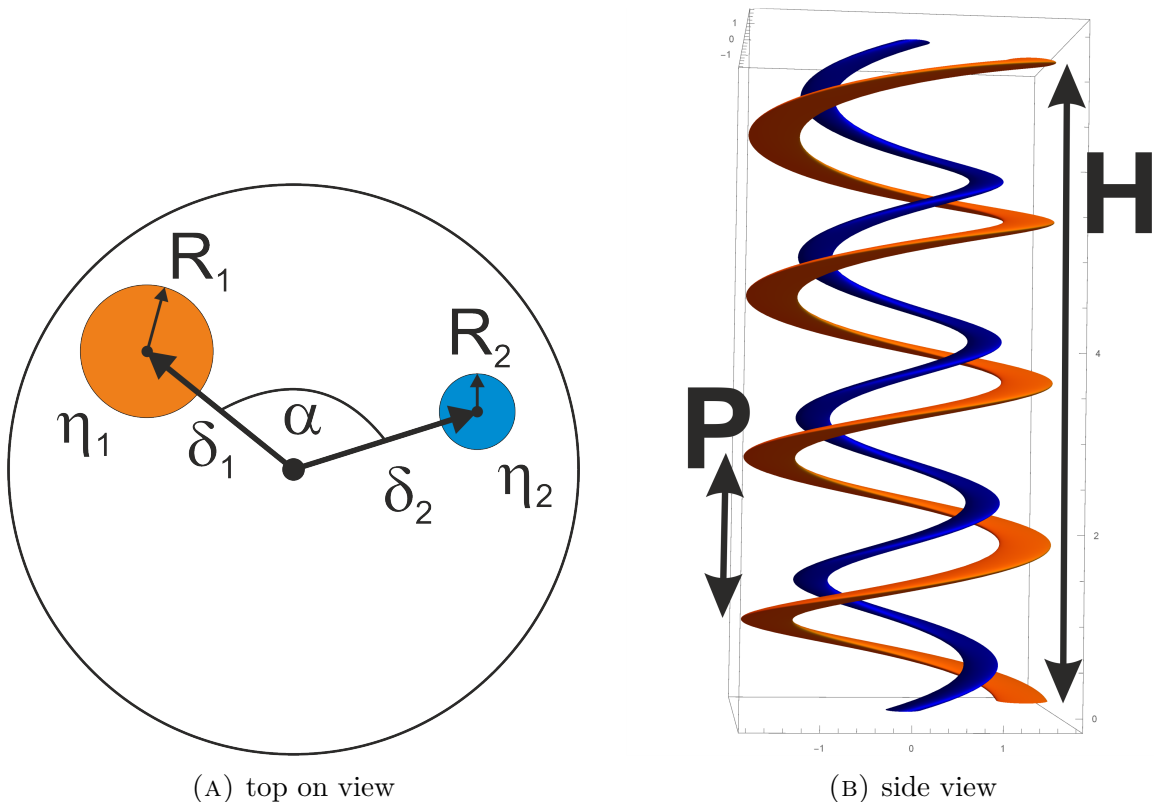


FIGURE 9.125. Double helix with strands of round cross sections. The cross-sections are round in the plane perpendicular to the helix axis.

Input Parameters for model **helix** with round XS:

R_1: radius of first strand thickness R_1

delta_1: distance of first strand to helix axis δ_1

R_2: radius of second strand thickness R_2

delta_2: distance of second strand to helix axis δ_2

alpha: angle α between the two strands

P: height of one helix period P

H: total length of helix H

eta 1: scattering length density of first strand η_1

eta 2: scattering length density of second strand η_2

eta_solv: scattering length density of solvent η_{solv}

Not

- The helix is assumed to be stiff and long so that its scattering intensity can be factorized in a cross-section contribution and a shape contribution, whereas the shape contribution can be described by an infinitesimal thin rod of length H .
 - R_1 , R_2 , δ_1 , δ_2 , P , and H are only physical for values larger than 0.
 - The model is an approximation for the limit $H \gg P$ and $H \gg R$.

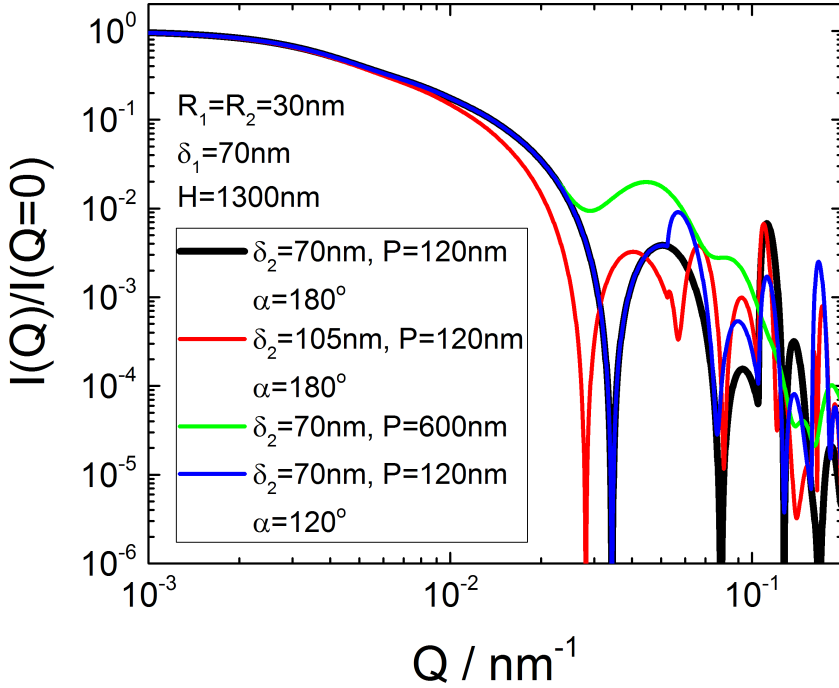


FIGURE 9.126. Normalized scattering curves of helices with round cross sections.

9.7.12.3. Beads model of a single helical strand.

In this model [290, 11] it is assumed that spherical beads are arranged along the path of a single helical strand. It is the product of the form factor of a sphere and the structure factor described by a helix with an infinitesimal thin single strand.

$$I(Q) = P_{\text{rod}}(Q, H) \sum_{j=-\infty}^{\infty} \left| \frac{nH}{P} \Psi_j \left(QD, \frac{2\pi j}{PQ} \right) \Phi(Q, R) \right|^2 \quad (9.416)$$

with

$$\Psi_j \left(QD, \frac{2\pi j}{PQ} \right) = \begin{cases} J_j \left(\frac{QD}{2} \sqrt{1 - \left(\frac{2\pi j}{PQ} \right)^2} \right) & \text{for } Q \geq \frac{2\pi |j|}{P} \\ 0 & \text{for } Q < \frac{2\pi |j|}{P} \end{cases} \quad (9.417)$$

$$\Phi(Q, R) = 3 \frac{4\pi}{3} R^3 (\eta_b - \eta_{\text{solv}}) \frac{\sin(QR) - QR \cos QR}{(QR)^3} \quad (9.418)$$

$$P_{\text{rod}}(Q, H) = H^2 \left(2 \frac{\text{Si}(QH)}{(QH)} - \left(\frac{\sin(QH/2)}{QH/2} \right)^2 \right) \quad (9.419)$$

where $\text{Si}(x) = \int_0^x \frac{\sin t}{t} dt$ is the sine integral. $P_{\text{rod}}(Q, H)$ is the form factor of an infinitesimal thin rod of length H . J_j is the regular cylindrical Bessel function, for which $J_j(x) = (-1)^{|j|} J_{-j}(x)$ if $j \in \mathbb{Z}$ (integer value) and $j \neq 0$. Therefore the sum in eq. 9.416

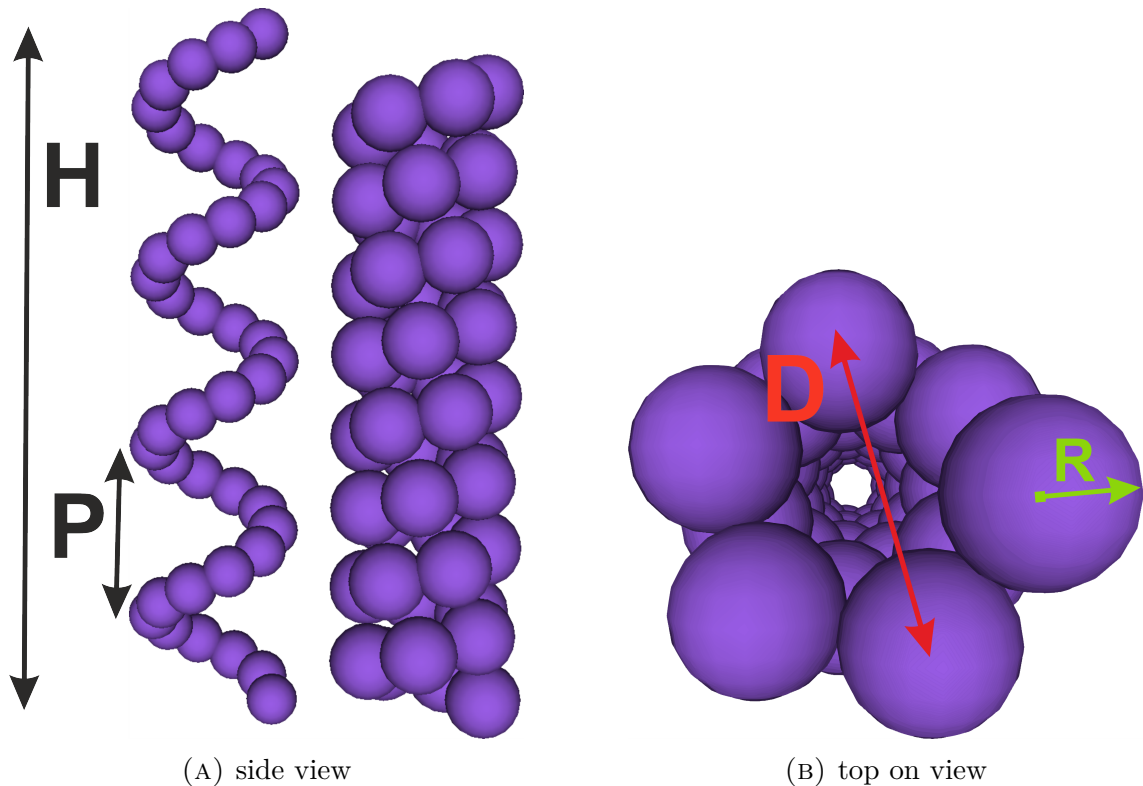


FIGURE 9.127. Bead model of a helix. In figure a) bead helices with different bead radius and different number of beads per turn are shown

can be written as

$$I(Q) = P_{\text{rod}}(Q, H) \sum_{j=0}^{\infty} \epsilon_j \left| \frac{nH}{P} \Psi_j \left(QD, \frac{2\pi j}{PQ} \right) \Phi(Q, R) \right|^2 \quad (9.420)$$

with $\epsilon_j = 1$ for $j = 0$ and $\epsilon_j = 2$ for $j \geq 1$.

The sum converges very fast and for small Q -values the first two term are already sufficient. However, **SASfit** is continuing the sum until either the argument below the square root becomes negative or the relative change of the sum is less than 10^{-10} .

The forward scattering of the model is normalized so that

$$I(Q=0) = \left(H \frac{nH}{P} \frac{4\pi}{3} R^3 (\eta_b - \eta_{solv}) \right)^2 \quad (9.421)$$

Input Parameters for model beads helix:

R: radius of monomer units/beads R

D: mean diameter of helix D

n : number of monomer beads per turn n

dummy: not used

dummy: not used

P : height of one helix period P

H: total length of helix H

eta_b: scattering length density of monomer beads η_b

dummy: not used

eta_solv: scattering length density of solvent η_{solv}

Note:

- The helix is assumed to be stiff and long so that its scattering intensity can be factorized in a cross-section contribution and a shape contribution, whereas the shape contribution can be described by an infinitesimal thin rod of length H .
- R , P , D , H , and n are only physical for values larger than 0.
- The model is an approximation for the limit $H \gg P$ and $H \gg D$.

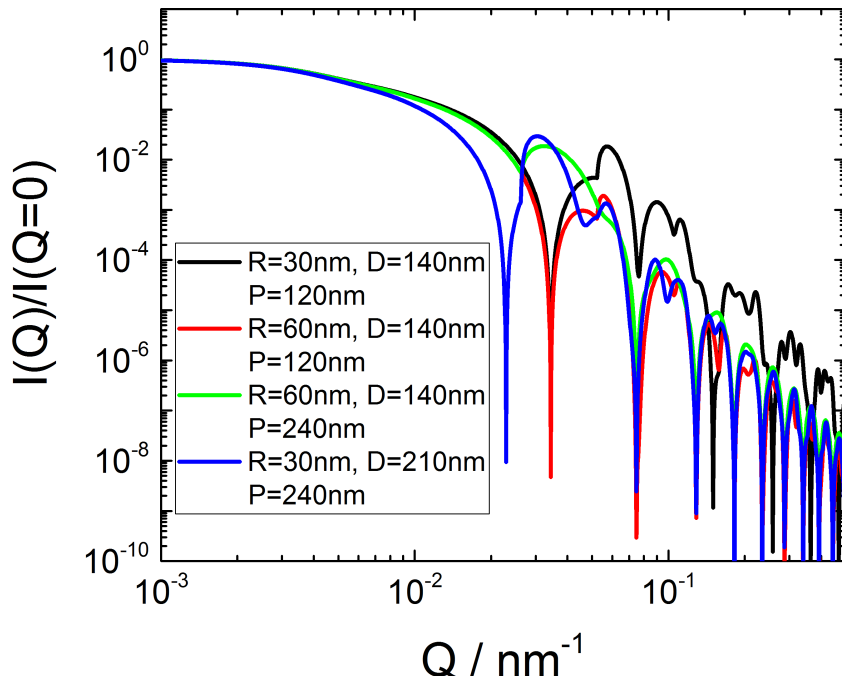


FIGURE 9.128. Normalized scattering curves of a single stranded helices formed by spherical beads.

9.7.12.4. straight superhelix.

Benham et al. [22] and Crick [91] describe single helices with a secondary helical curvature, which they call coiled superhelices or coiled coil. They assume in their analysis an infinitesimal thin helical strand. The straight superhelix is their starting geometry

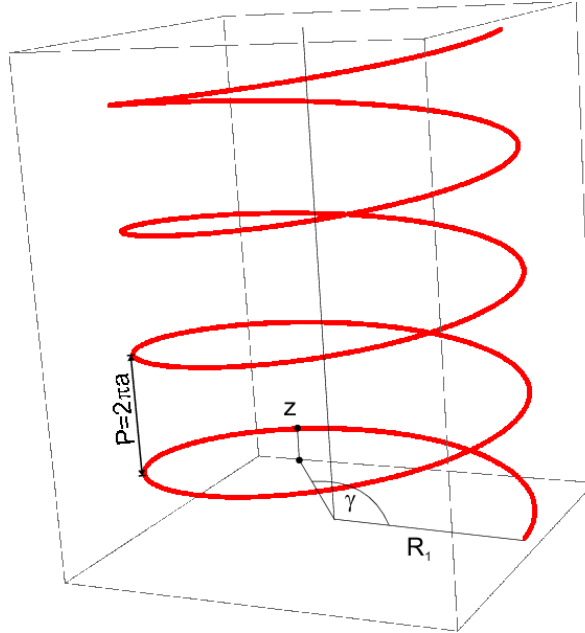


FIGURE 9.129. infinitesimal thin single stranded helix

without a secondary coiling. The expression for a random oriented straight superhelix of finite length can be written exact in form of a single integral and is given by

$$I(Q) = 2 \int_0^{\mathcal{L}} \frac{(\mathcal{L} - w) \sin Q\psi}{Q\psi} dw \quad (9.422)$$

$$\psi = + \sqrt{2R_1^2 \left[1 - \cos \left(\frac{w}{\sqrt{R_1^2 + a^2}} \right) \right] + \frac{a^2 w^2}{R_1^2 + a^2}} \quad (9.423)$$

$$\mathcal{L} = 2\pi \frac{H}{P} \sqrt{R_1^2 + a^2} \quad (9.424)$$

$$a = \frac{P}{2\pi} \quad (9.425)$$

\mathcal{L} is the arclength of the helix, R_1 the distance to the helix axis and P the pitch of the helix. The intensity is normalized to the squared arclength of the helix. i.e.

$$I(Q = 0) = \mathcal{L}^2 \quad (9.426)$$

Input Parameters for model **straight superhelix**:

R_1: distance to the helix axis R_1

dummy: not used

dummy: not used

dummy: not used

dummy: not used

P: height of one helix period P

H: total length of helix H

dummy: not used

dummy: not used

dummy: not used

Note:

- the model assumes an infinitesimal thin single helical strand.
- R_1 , P , and H are only physical for values larger than 0.
- The model is exact.

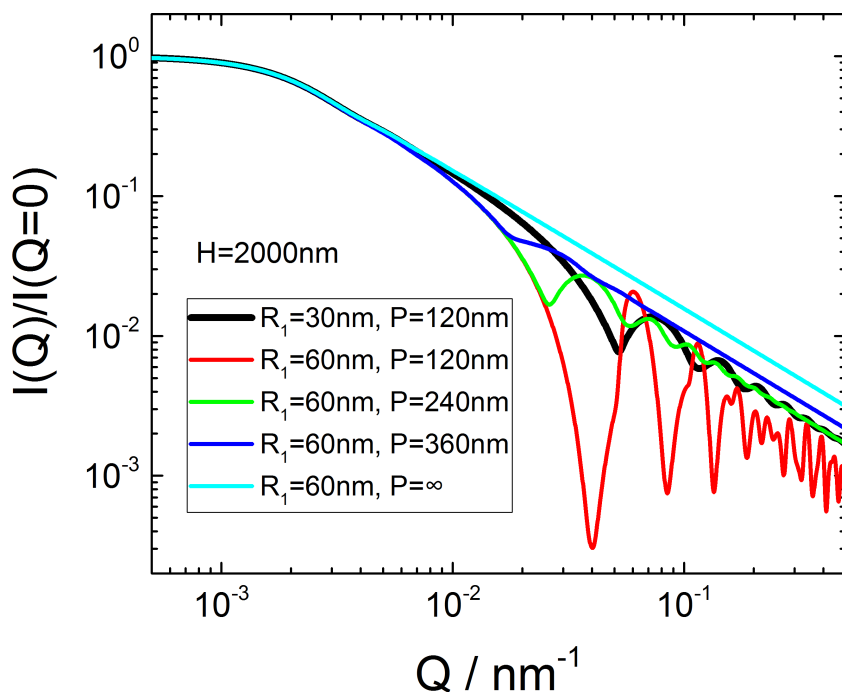
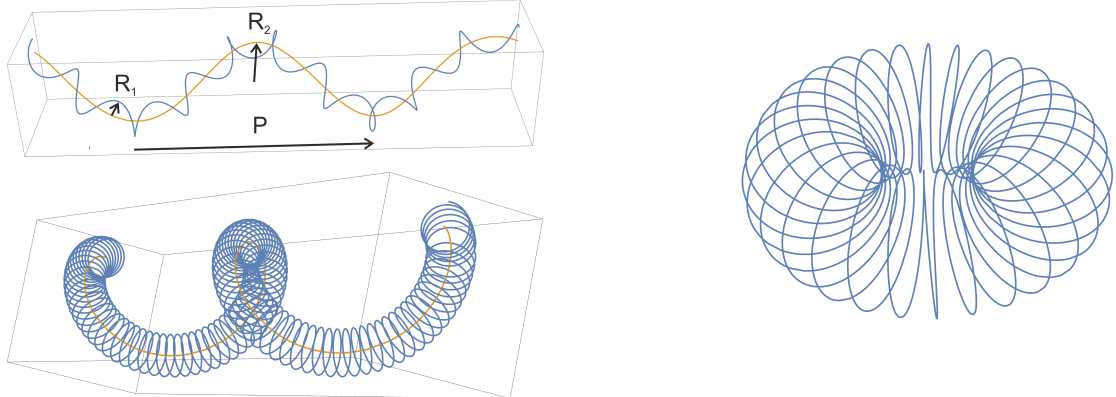


FIGURE 9.130. Normalized scattering curves of single infinitesimal thin stranded helices.

9.7.12.5. coiled superhelix.

A coiled superhelix or coiled coil is a helix with a small repeat whose axis is slightly deformed and follows a larger more graded helical path [22, 91].



(A) [A superhelix with primary and secondary turns. The bottom one has ten times more primary turns per secondary turn than the top one]

(B) A superhelix with zero pitch forms a toroidal helix

FIGURE 9.131. Combinations of two helical orders are referred to as coiled coils or coiled superhelix.

The points $p(\gamma) = [x(\gamma), y(\gamma), z(\gamma)]$ on the coiled superhelix are parametrized by

$$x(\gamma) = \cos(\gamma)(R_2 + R_1 \cos(N\gamma)) - R_1 \cos(\alpha_2) \sin(\gamma) \sin(N\gamma) \quad (9.427)$$

$$y(\gamma) = \sin(\gamma)(R_2 + R_1 \cos(N\gamma)) - R_1 \cos(\gamma) \sin(N\gamma) \cos(\alpha_2) \quad (9.428)$$

$$z(\gamma) = \frac{P}{2\pi}\gamma - R_1 \sin(\alpha_2) \sin(N\gamma) \quad (9.429)$$

R_1 and R_2 are the radii of the primary and secondary coiling of the superhelix. P is the pitch of the secondary coiling and $\alpha_2 = \arctan\left(\frac{2\pi R_2}{P}\right)$ its pitch angle. N is the number of first order turns in the primary coiling for each turn of the secondary coiling. The arc length of the helix \mathcal{L} can be calculated by

$$\mathcal{L} = \int_0^{\gamma_{\max}} \sqrt{f(\gamma)} d\gamma \quad (9.430)$$

with

$$f(\gamma) = R_2^2 + R_1^2 N^2 \left(\cos^2(N\gamma) + \sin^2(N\gamma) \cos^2(\alpha_2) \right) + \frac{P^2}{(2\pi)^2} + 2R_2 R_1 \cos(N\gamma) + 2R_1^2 N \cos(\alpha_2) \quad (9.431)$$

and

$$\gamma_{\max} = 2\pi N_{\text{2nd}} \quad (9.432)$$

where N_{2nd} is the number of secondary turns of the coiled superhelix. The scattering intensity is than given by

$$I(Q) = \int_0^{\gamma_{\max}} d\gamma_2 \int_0^{\gamma_{\max}} \sqrt{f(\gamma_2)f(\gamma_1)} \frac{\sin(Qr(\gamma_1, \gamma_2))}{Qr(\gamma_1, \gamma_2)} d\gamma_2 \quad (9.433)$$

with

$$r^2(\gamma_1, \gamma_2) = \left(\begin{pmatrix} x(\gamma_2) \\ y(\gamma_2) \\ z(\gamma_2) \end{pmatrix} - \begin{pmatrix} x(\gamma_1) \\ y(\gamma_1) \\ z(\gamma_1) \end{pmatrix} \right)^2 \quad (9.434)$$

The intensity is normalized to the squared arclength of the helix. i.e.

$$I(Q = 0) = \mathcal{L}^2 \quad (9.435)$$

Input Parameters for model `coiled_superhelix`:

R_1: distance to the primary helix axis R_1

R_2: distance to the primary helix axis R_1

dummy: not used

N: number of primary turns N per secondary turn

dummy: not used

P: pitch length of secondary helix P

turns: number of secondary turns N_{2nd}

dummy: not used

dummy: not used

dummy: not used

Note:

- the model assumes an infinitesimal thin single helical strand with an additional secondary coiling.
- $R_1, R_2, P, N_{\text{2nd}}$ and N are only physical for values larger than 0.
- The model is exact.
- The calculation of the scattering intensity requires a double integration, which is the reason for the longer computing time.

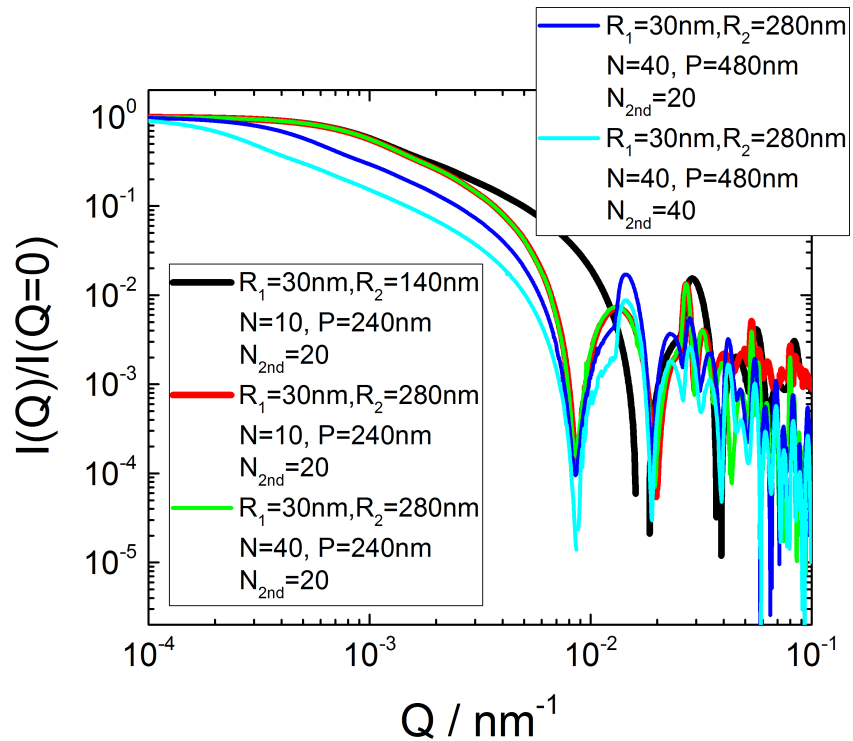


FIGURE 9.132. Normalized scattering curves of single stranded infinitesimal thin coiled helices.

9.8. Generalized form factor compliant for Titchmarsh transform

This generalized form factor include several special shapes like uniform spheres, spheres in Fraunhofer limit, thin randomly oriented platelets, long randomly oriented cylinder, etc. [121]. A list of shapes is given in table 3. They all have in common, that they only depend on one size parameter a . The parameter γ additionally allows that scattering object contain other size parameters which must, however, be out of the q -range of the SAS experiment.

TABLE 3. Explicit expressions for $I(q) = \frac{1}{q^\gamma} \frac{J_\nu^2(qa)}{(qa)^\beta} (V_0 a^\alpha)^2$ for several particle shapes. The values $n = \beta + 1$ and $m = 2\alpha - n$ are used for the Titchmarsh transform in the paper from Fedorova

shape	$I(q)/V_0^2$	ν	γ	β	n	m	α	s	p	d
1. uniform sphere	$\frac{J_{3/2}^2(qa)}{(qa)^3} a^6$	$\frac{3}{2}$	0	3	4	2	3	0	4	3
2. Long cylinder perpendicular to the plane of scattering										
3. Thin disc in scattering plane	$\frac{J_1^2(qa)}{(qa)^2} a^4$	1	0	2	3	1	2	0	3	2
4. Sphere (Fraunhofer diffraction)										
5. Long randomly oriented cylinder	$\frac{1}{q} \frac{J_1^2(qa)}{(qa)^2} a^4$	1	1	2	3	1	2	1	4	3
6. Spherical shell	$\frac{J_{1/2}^2(qa)}{qa} a^4$	$\frac{1}{2}$	0	1	2	2	2	0	2	2
7. Thin randomly oriented platelet	$\frac{1}{q^2} \frac{J_{1/2}^2(qa)}{qa} a^2$	$\frac{1}{2}$	2	1	4	0	1	2	4	3
8. Long cylinder (Fraunhofer diffraction)	$\frac{1}{q} \frac{J_{1/2}^2(qa)}{qa} a^2$	$\frac{1}{2}$	1	1	3	0	1	1	3	2
9. Thin rod perpendicular to the incident beam and in the plane of scattering	$\frac{J_{1/2}^2(qa)}{qa} a^2$	$\frac{1}{2}$	0	1	2	0	1	0	2	1
10. Hollow cylinder perpendicular to beam	$J_0^2(qa) a^2$	0	0	0	1	1	1	0	1	1
11. Randomly oriented long hollow cylinder	$\frac{1}{q} J_0^2(qa) a^2$	0	1	0	2	1	1	1	2	2

The generalized form factor is defined as

$$I(q) = \frac{1}{q^\gamma} \frac{J_\nu^2(qa)}{(qa)^\beta} (V_0 a^\alpha)^2 \quad (9.436)$$

$$= \frac{1}{q^\gamma} \frac{(V_0 a^\alpha)^2 4^{-\nu}}{(aq)^{\beta-2\nu} \Gamma(\nu+1)^2} {}_0F_1^2 (\{\}, \{\nu+1\}; -(qa)^2/4) \quad (9.437)$$

in the limits of $q \rightarrow 0$ and $q \rightarrow \infty$ the scattering intensities become

$$\lim_{q \rightarrow 0} I(q) = \frac{1}{q^\gamma} \frac{(V_0 a^\alpha)^2}{(aq)^{\beta-2\nu}} \frac{4^{-\nu}}{\Gamma(\nu+1)^2} \quad (9.438)$$

$$\lim_{q \rightarrow \infty} I(q) = \frac{1}{q^\gamma} \frac{(V_0 a^\alpha)^2}{\pi (aq)^{\beta+1}} \quad (9.439)$$

The parameter γ is not necessarily required and any value of it could be replaced by a proper correction of the values for α and β . However, the parameter α was introduced to describe how the volume of the objects, on which small angle scattering is sensitive, scales with the parameter a . For a homogeneous cylinder oriented randomly with its radius in the range of the SAS experiments the object dimension is $d = 3$. However, for an oriented cylinder where SAS is measured perpendicular to the cylinder axis the signal only probes the cross section and d is therefore 2. If a is the smaller or larger dimension of a very anisotropic object like thin local cylindrical objects or thin local planar objects the volume scales with $V_0 a^\alpha l^\gamma$ where $l \gg a$ or $l \ll a$ describes the larger or smaller dimensions of the object. The overall dimension of the object is $1 \leq d = \alpha + \gamma \leq 3$ and should lay between 1 and 3. Furthermore the overall dimension d of the object needs to be larger than α , i.e. $2 \geq \gamma \geq 0$. As only the dimension a is probed in the case of $l \gg a$ the larger dimension l leads to a potential law behaviour at small q -values with $s = \gamma$. This is an additional constrain leading to the lesser generalized form factor having three input parameters either (d, s, p) or (d, α, p) .

$$\begin{array}{lll} s = \gamma & \alpha = d - s & s = d - \alpha \\ s = \gamma + \beta - 2\nu & \beta = p - s - 1 & \Leftrightarrow \beta = \alpha + p - d - 1 \\ p = \gamma + \beta + 1 & \gamma = s & \gamma = s \\ d = \alpha + \gamma & \nu = \beta/2 & \nu = \beta/2 \end{array} \quad (9.440)$$

The other constraints on the parameters for physical meaningful two-phase models with sharp interfaces are $(3 \geq d \geq \alpha \geq 1)$, $(2 \geq s \geq 0)$, $(4 \geq p \geq 1)$, $(\beta, \nu \geq 0)$.

Input Parameters for model generalized form factor:

a: size parameter a

sigma_a: width σ_a of the size distribution (LogNorm)

alpha: dimensionality parameter α related to a .

beta: decay at large scattering vectors, q^p , with $p = \gamma + \beta + 1$

gamma: additional potential law $q^{-\gamma}$

nu: shape parameter ν

eta: scattering length density contrast $\Delta\eta$

Input Parameters for model lesser generalized form factor 1:

a: size parameter a

sigma_a: width σ_a of the size distribution (LogNorm)

alpha: dimensionality parameter α related to a .

dummy: not used

s: potential law at small q -values

p: potential law at large q -values

eta: scattering length density contrast $\Delta\eta$

Input Parameters for model lesser generalized form factor 2:

a: size parameter a

sigma_a: width σ_a of the size distribution (LogNorm)

dummy: not used

dim: overall dimension d of the particle ($1 \leq d \leq 3$)

s: potential law q^{-s} at small q -values

p: potential law q^{-p} at large q -values

eta: scattering length density contrast $\Delta\eta$

Note:

- ($3 \geq d \geq \alpha \geq 1$)
- ($2 \geq s \geq 0$)
- ($4 \geq p \geq 1$)
- ($\beta, \nu \geq 0$).

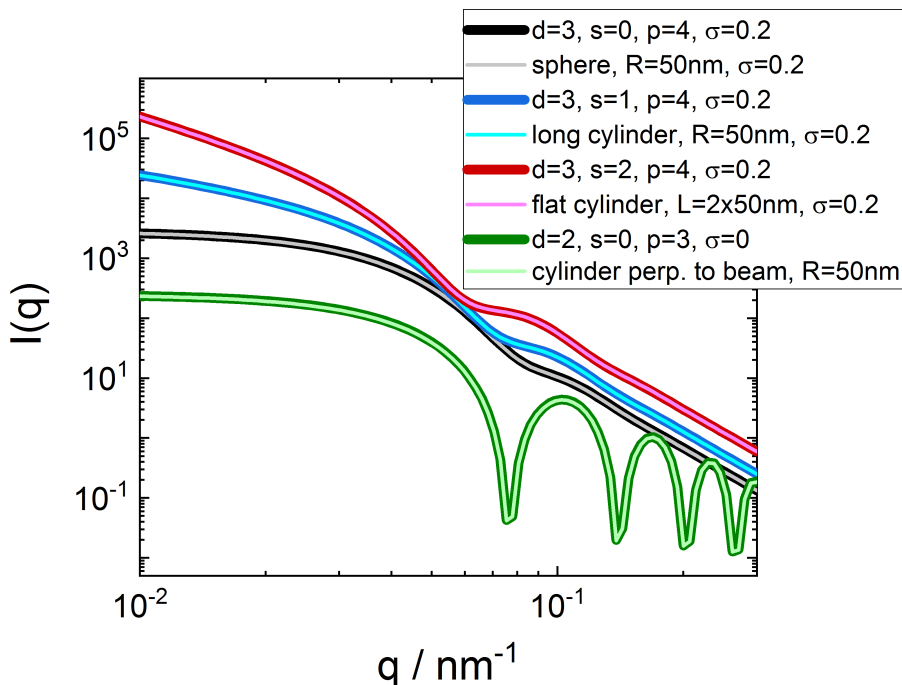


FIGURE 9.133. Comparison of generalized form factor with certain geometries namely Sphere, LongCylinder, FlatCylinder, cylinder (OPO) (cylinder perp. to beam).

9.9. Sheared and deformed objects

9.9.1. Non-equilibrium static form factor of a reptating chain.

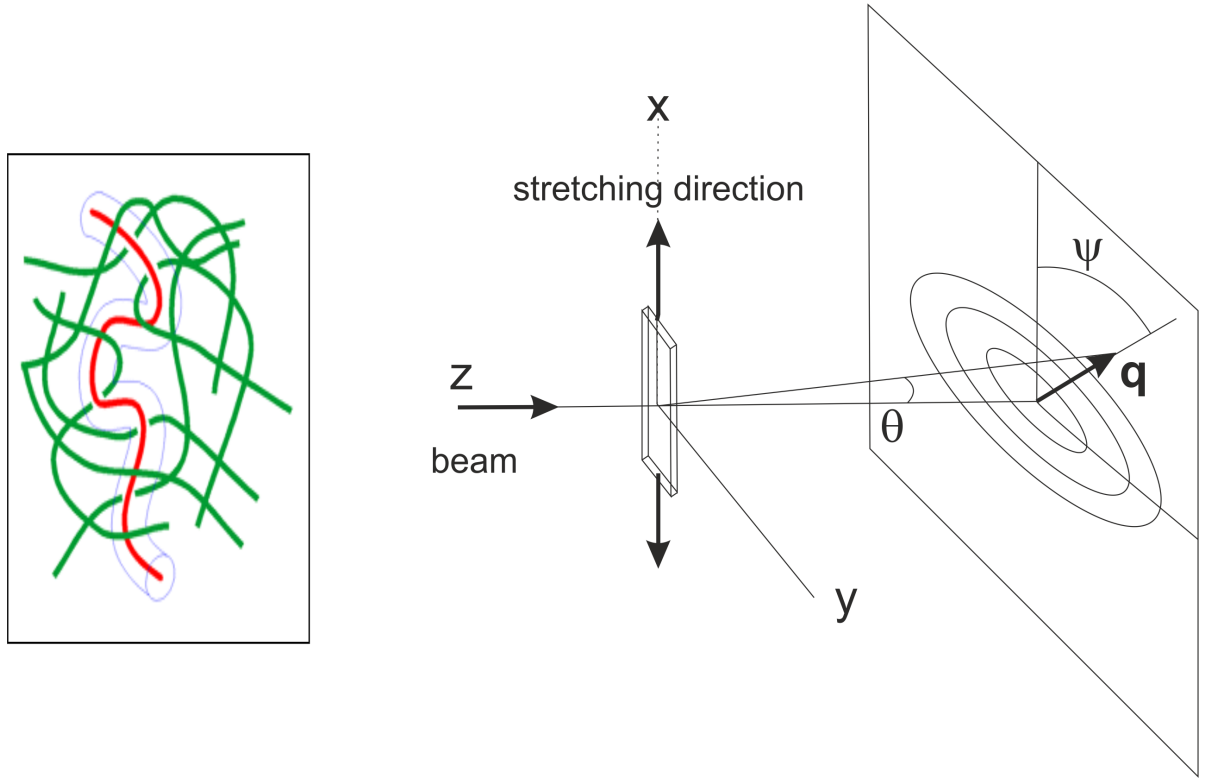


FIGURE 9.134. Sketch of experimental setup for stretching a polymer melt.

This model [220, 359] describes the scattering behaviour of an uniaxial deformed (stretched) Gaussian polymer chain as a function of the deformation ratio and Rouse relaxation time. The model might not include an up-to-date tube model but shows some main features of deformed polymer melts.

$$\begin{aligned} I\left(q, \frac{t}{\tau}\right) / I_0 = & D(\alpha) + \frac{1}{6}(\alpha - \beta)(1 + e^{-\alpha}) H\left(\alpha, \frac{t}{\tau}\right) \\ & + \frac{1}{6}(\alpha - \beta)^2 e^{-\beta} \int_0^1 dy y^3 e^{\beta y} (1 + e^{-\alpha y}) H\left(\alpha y, \frac{t}{\tau y^2}\right) \end{aligned} \quad (9.441)$$

with

$$H\left(x, \frac{t}{\tau}\right) = \frac{96}{\pi^2} \sum_{n=\text{odd}} \frac{1}{n^2 (n^2 \pi^2 + x^2)} e^{-n^2 \frac{t}{\tau}} \quad (9.442)$$

$D(x)$ is the Debye function $D(x) = 2(x - 1 + e^{-x})/x^2$, $\alpha = q^2 R_g^2$, R_g is the equilibrium radius of gyration of the chain and τ is the reptation time or tube disengagement time.

Furthermore λ is the uniaxial elongation factor, q_{\parallel} and q_{\perp} are respectively the components of the wave vector q in directions parallel and perpendicular to the direction of elongation which than define the parameter β as

$$\beta = \left(q_{\parallel}^2 \lambda^2 + q_{\perp}^2 / \lambda \right) R_g^2 / E \quad (9.443)$$

$$E = \frac{1}{2} \left\{ \lambda + \frac{\operatorname{asinh}(\sqrt{\lambda^3 - 1})}{\sqrt{\lambda(\lambda^3 - 1)}} \right\} \quad (9.444)$$

$$q_{\parallel} = q \cos(\psi - \theta_0) \quad (9.445)$$

$$q_{\perp} = q \sin(\psi - \theta_0) \quad (9.446)$$

Input Parameters for models reptating chain:

I0: forward scattering I_0

Rg: radius of gyration of unstretched polymer R_g

lambda: stretching factor λ

t/tau: relaxation time in units of Rouse time t/τ

theta_0: stretching direction θ_0 in the detector plane in degree

psi: q-direction ψ in the detector plane in degree

Note:

- The model only converges for $\lambda > 1$.

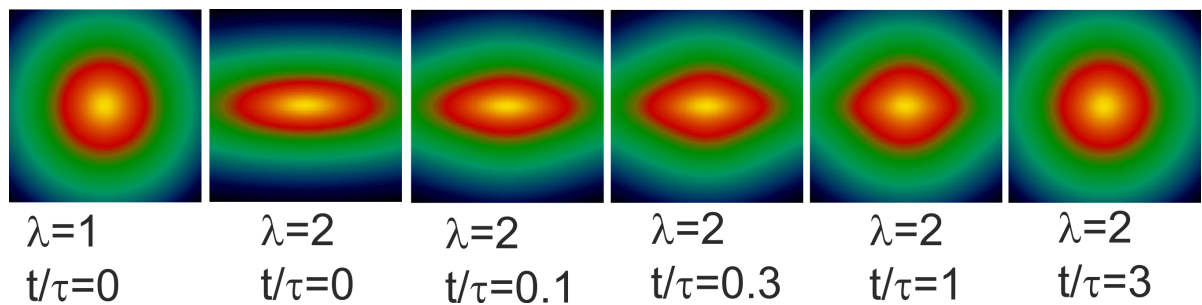


FIGURE 9.135. 2D scattering patterns for different relaxation times t/τ after a deformation step of $\lambda = 2$

9.9.2. step-deformed polymer networks.

Two slightly different tube models for labeled polymer chains in a deformed network are implemented in this plugin: the original one from Warner-Edwards (WE) [519] and a refined one from Heinrich-Straube-Helmis (HSH) [207], which have been extensively used to study uni-axial stretched polymer networks [465, 335, 524, 523, 525, 411]. The form factor of an uniaxial stretched polymer network with a stretching direction in the plane of the detector reads as

$$S(\mathbf{q}, \lambda) = \int_0^1 d\eta \int_0^1 d\eta' \prod_{\mu} e^{-(Q_{\mu} \lambda_{\mu})^2 |\eta - \eta'| - Q_{\mu}^2 (1 - \lambda_{\mu}^2) \xi \left\{ 1 - \exp \left(-\frac{|\eta - \eta'|}{\xi} \right) \right\}} \quad (9.447)$$

$$\xi = \frac{d_t^2}{2\sqrt{6}R_g^2} \quad (9.448)$$

$$Q_{\mu} = q_{\mu} R_g \quad (9.449)$$

$$\mu = x, y, z \quad (9.450)$$

$$\mathbf{q} = \begin{pmatrix} q_x \\ q_y \\ q_z \end{pmatrix} = \begin{pmatrix} q \cos(\psi - \delta) \\ q \sin(\psi - \delta) \\ 0 \end{pmatrix} \quad (9.451)$$

As the function of the integral kernel in eq. 9.447 only depends on $|\eta - \eta'|$ one can transform the 2D-integral into a 1D-integral by using the identity

$$\int_0^1 d\eta \int_0^1 d\eta' K(|\eta - \eta'|) = 2 \int_0^1 (1 - x) K(x) dx \quad (9.452)$$

The difference between the WE-model and the HSH-model is how the deformed tube diameter d_t is calculated. In case of the WE-model the projection d_{μ} of d_t onto the Cartesian axis are used, whereas the HSH-model uses an effective angle dependent diameter d_{ϕ} .

$$(\text{WE-model}): d_t = d_{\mu}^2 = d_0^2 \lambda_{\mu}^{2\nu} \quad (9.453)$$

$$(\text{HSH-model}): d_t = d_{\phi}^2 = d_0^2 \lambda_{\phi}^{2\nu} \quad (9.454)$$

If we assume an elongation ratio of λ in the x -direction

$$\lambda_x = \lambda_{\parallel} = \lambda, \quad \lambda_y = \lambda_z = \lambda_{\perp} = \frac{1}{\sqrt{\lambda}} \quad (9.455)$$

$$\lambda_{\phi}^2 = \lambda_{\parallel}^2 \cos^2(\psi - \delta) + \lambda_{\perp}^2 \sin^2(\psi - \delta) \quad (9.456)$$

where R_g the radius of gyration of the un-deformed polymer network λ_{μ} is the macroscopic stretch ratio in this Cartesian direction and the exponent ν is predicted to take a value of 1/2 in the case of networks [465, 410]. Nevertheless ν is kept as a fit parameter

in this plug-in function.

$$S^{\text{WE}}(\mathbf{q}, R_g, \lambda, \nu, d_0) = 2 \int_0^1 dx (1-x) e^{\left(\sum_{\mu} -Q_{\mu}^2 \lambda_{\mu}^2 x - (1-\lambda_{\mu}^2) Q_{\mu}^2 \xi_{\mu} \left\{ 1 - e^{\left(-\frac{x}{\xi_{\mu}} \right)} \right\} \right)} \quad (9.457)$$

$$S^{\text{HSH}}(\mathbf{q}, R_g, \lambda, \nu, d_0) = 2 \int_0^1 dx (1-x) e^{\left(\sum_{\mu} -Q_{\mu}^2 \lambda_{\mu}^2 x - (1-\lambda_{\mu}^2) Q_{\mu}^2 \xi_{\phi} \left\{ 1 - e^{\left(-\frac{x}{\xi_{\phi}} \right)} \right\} \right)} \quad (9.458)$$

with

$$\xi_{\mu} = \frac{d_{\mu}^2}{2\sqrt{6}R_g^2} \quad (9.459)$$

$$\xi_{\phi} = \frac{d_{\phi}^2}{2\sqrt{6}R_g^2} \quad (9.460)$$

In a work of [39] an additional retraction coefficient $\gamma(t)$ has been included so that the final equation for the HSH model reads as

$$S^{\text{HSH}}(\mathbf{q}, R_g, \lambda, \nu, \gamma, d_0) = 2 \int_0^1 dx (1-x) \exp \left(\sum_{\mu} Q_{\mu}^2 \left[-\lambda_{\mu}^2 \frac{x}{\gamma(t)} - \xi_{\phi} \left\{ 1 - e^{\left(-\frac{x}{\xi_{\phi} \gamma(t)} \right)} \right\} + \lambda_{\mu}^2 \xi_{\phi} \left\{ 1 - e^{\left(-\frac{x}{\xi_{\phi}} \right)} \right\} \right] \right) \quad (9.461)$$

The retraction coefficient is for short times $\gamma(t=0) = 1$ and becomes larger for increasing relaxation times $\gamma(t > 0) > 1$.

Input Parameters for models WE: deformed polym. netw.:

I0: forward scattering I_0

Rg: radius of gyration of unstretched polymer R_g

d0: equilibrium tube diameter d_0

nu: exponent ($\nu = 1/2$, $\nu = 1$:affine deformation)

lambda: deformation ratio λ along deformation axis

dummy: not used

psi: direction ψ of the scattering vector \mathbf{q} in the detector plane in degree

delta: stretching direction in the detector plane δ in degree

Input Parameters for models HSH: deformed polym. netw.:

I0: forward scattering I_0

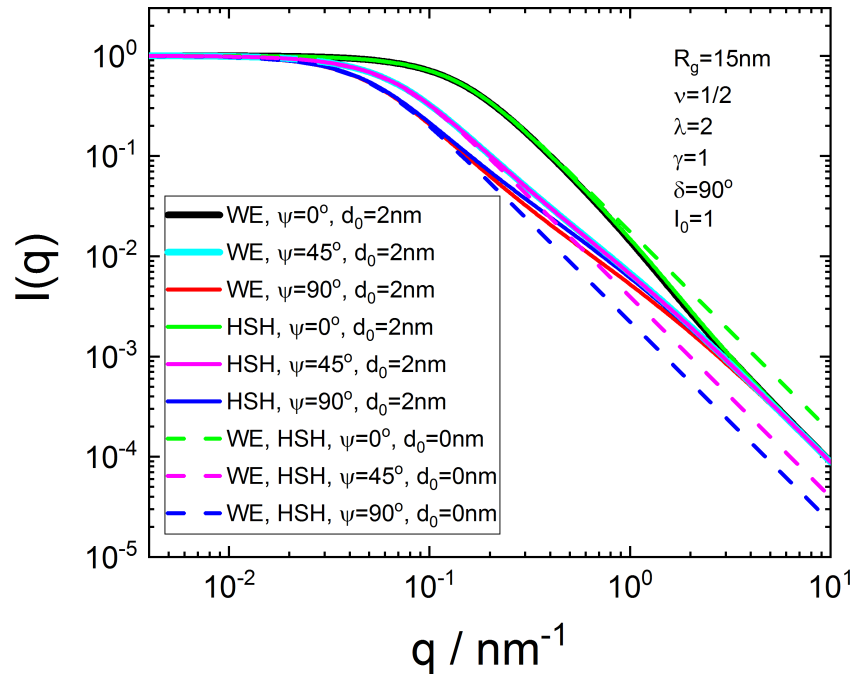


FIGURE 9.136. sector averaged scattering curves of the Warner-Edwards and Heinrich-Straube-Helmis model of step-deformed polymer networks for tube diameters d_0 of 2nm and zero nm

Rg: radius of gyration of unstretched polymer R_g

d0: equilibrium tube diameter d_0

nu: exponent ($\nu = 1/2$, $\nu = 1$:affine deformation)

lambda: deformation ratio λ along deformation axis

gamma: retraction coefficient ($1 < \gamma \lesssim 2$)

psi: direction ψ of the scattering vector \mathbf{q} in the detector plane in degree

delta: stretching direction in the detector plane δ in degree

Note:

- for large q -values the integration routines might fail to converge.

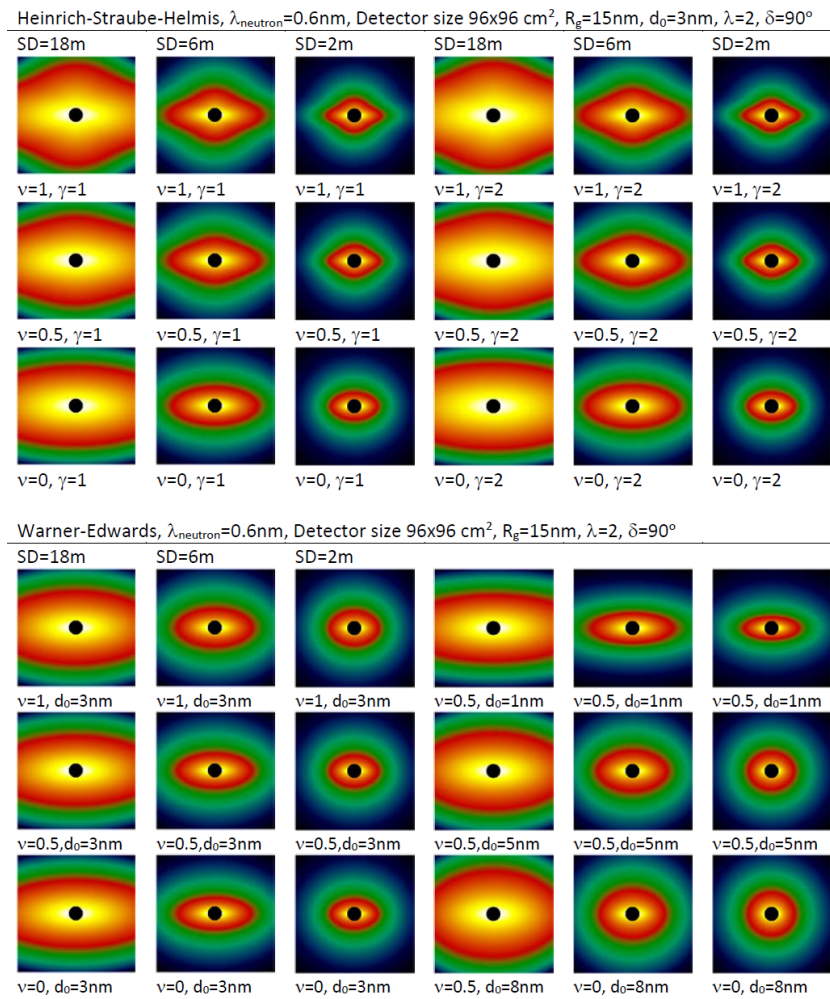
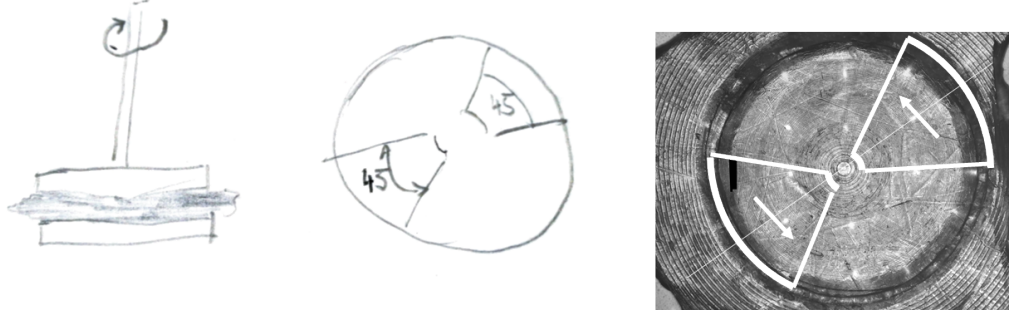


FIGURE 9.137. 2D scattering patterns of the Warner-Edwards and Heinrich-Straube-Helmis model of step-deformed polymer networks

9.9.3. polymer under shear flow.

This plugin is implemented for a certain experimental setup of a quenched shear sample using two different configuration. The sample has a disc shape of a few mm in diameter and was sheared in a cone-plate geometry. Therefore, the vorticity, flow and gradient direction are well described in a cylindrical coordinate system \mathbf{e}_ρ , \mathbf{e}_φ , and \mathbf{e}_z . The normal of the disc represents the gradient direction of the sheared sample $\mathbf{e}_z = \mathbf{e}_g$. The radial direction $\mathbf{e}_\rho = \mathbf{e}_v$ represents the vorticity direction and the azimuth direction the flow direction $\mathbf{e}_\varphi = \mathbf{e}_f$.

- (1) In one experimental geometry the normal \mathbf{e}_g (gradient direction) of the disc shaped sample is parallel to the incoming neutron beam \mathbf{e}_n . To separate the deformation in flow and vorticity direction apertures with a sector shape and two opposite openings of 45 degree each as marked in the image below are used. In this geometry the scattering in this setup is sensitive to in vorticity and flow direction only.



- (2) In a second setup a fully opened circular aperture (no sectors) of the same diameter as the sample is mounted and turned with the sample around the vertical axis by an angle θ_0 . Depending on the turning angle θ_0 the horizontal detector direction probes a mixture of the averaged flow/vorticity contribution and the scattering in gradient direction. The contributions depend on the projection of the scattering vector onto the plane of the disc and to the normal of the disc being the gradient direction



The form factors describing linear polymers under shear flow has been taken from [272]. In the original paper it is assumed that the shear-vorticity plane is the same than the detector plane. We slightly extend it here to any orientation defined by proper Euler angles.

The form factor of polymers is deduced from the mean squared distance (MSD) $\langle(\mathbf{q} \cdot \mathbf{r}_{nm})^2\rangle/2$ within a polymer chain and is given by a double integral

$$P(\mathbf{q}) = \frac{1}{N^2} \int_0^N dn \int_0^N dm \exp\left(-\frac{\langle(\mathbf{q} \cdot \mathbf{r}_{nm})^2\rangle}{2}\right) \quad (9.462)$$

If the mean squared distance function (MSD) $\langle(\mathbf{q} \cdot \mathbf{r}_{nm})\rangle/2$ can be written as a function of $\nu = |n - m|/N$, one can replace the double integral by a single integral.

$$P(\mathbf{q}) = 2 \int_0^1 (1 - \nu) \exp\left(-\frac{\langle(\mathbf{q} \cdot \mathbf{r}_{nm})^2\rangle}{2}\right) d\nu \quad (9.463)$$

Here the polymer consists of N flexible units where \mathbf{r}_{nm} is the vectorial distance between the centers of the n^{th} and m^{th} monomer unit. The scattering vector in the laboratory system is

$$\mathbf{q} = q \begin{pmatrix} \cos(\phi) \\ \sin(\phi) \\ 0 \end{pmatrix} \quad (9.464)$$

The vectorial distance between \mathbf{r}_{nm} is defined here in the coordination system of the applied flow

$$\mathbf{r}_{nm} = x_{v,nm}\mathbf{e}_{v,nm} + z_{f,nm}\mathbf{e}_f + y_{g,nm}\mathbf{e}_g \quad (9.465)$$

The averages to be taken are then

$$\begin{aligned} \langle (\mathbf{q} \cdot \mathbf{r}_{nm})^2 \rangle &= q_v^2 \langle x_{v,nm}^2 \rangle + q_f^2 \langle z_{f,nm}^2 \rangle + q_g^2 \langle y_{g,nm}^2 \rangle + \\ &\quad 2q_v q_f \langle x_{v,nm} z_{f,nm} \rangle + 2q_v q_g \langle x_{v,nm} y_{g,nm} \rangle + 2q_f q_g \langle z_{f,nm} y_{g,nm} \rangle \end{aligned} \quad (9.466)$$

with

$$q_g = \mathbf{q} \cdot \mathbf{e}_g \quad (9.467)$$

$$q_f = \mathbf{q} \cdot \mathbf{e}_f \quad (9.468)$$

$$q_v = \mathbf{q} \cdot \mathbf{e}_v \quad (9.469)$$

The unit vectors \mathbf{e}_g , \mathbf{e}_f , and \mathbf{e}_v are determined by the sample orientation and will be defined later on. In the following it is assumed, that the mixed terms in eq. 9.466 are negligible (this is exactly true for an undeformed linear polymer in equilibrium) and only the squared terms (which are symmetric for the undeformed polymer) contribute to the mean squared internal distance so that eq. 9.466 simplifies to

$$\langle (\mathbf{q} \cdot \mathbf{r}_{nm})^2 \rangle = q_v^2 \langle x_{v,nm}^2 \rangle + q_f^2 \langle z_{f,nm}^2 \rangle + q_g^2 \langle y_{g,nm}^2 \rangle \quad (9.470)$$

An undeformed linear polymer in equilibrium has an exact solution for the MSD

$$\langle (\mathbf{q} \cdot \mathbf{r}_{nm})^2 \rangle / 2 = a |n - m| / N \quad (9.471)$$

and is a straight line with a slope $a = q^2 R_g^2 = q^2 N \lambda^2 / 6$, where λ is the Kuhn length and R_g the equilibrium radius of gyration. N is the number of Kuhn segments of a single polymer chain. This leads to the scattering function

$$P_{\text{lin},\text{iso}}(\mathbf{q}) = \frac{2(e^{-a} - 1 + a)}{a^2} \quad (9.472)$$

9.9.4. linear polymer under shear flow.

For a sheared linear polymer the mean squared distance MSD in the flow, vorticity and gradient direction has been approximated in [272] by a piecewise linear approximation and with a limitation to just two segments. The approximation of the MSD by a series of two straight lines reads as

$$\frac{\langle (\mathbf{q} \cdot \mathbf{r}_{nm})^2 \rangle}{2} = \begin{cases} b |n - m| / N, & \text{if } |n - m| / N < f \\ c |n - m| / N + (b - c)f, & \text{otherwise.} \end{cases} \quad (9.473)$$

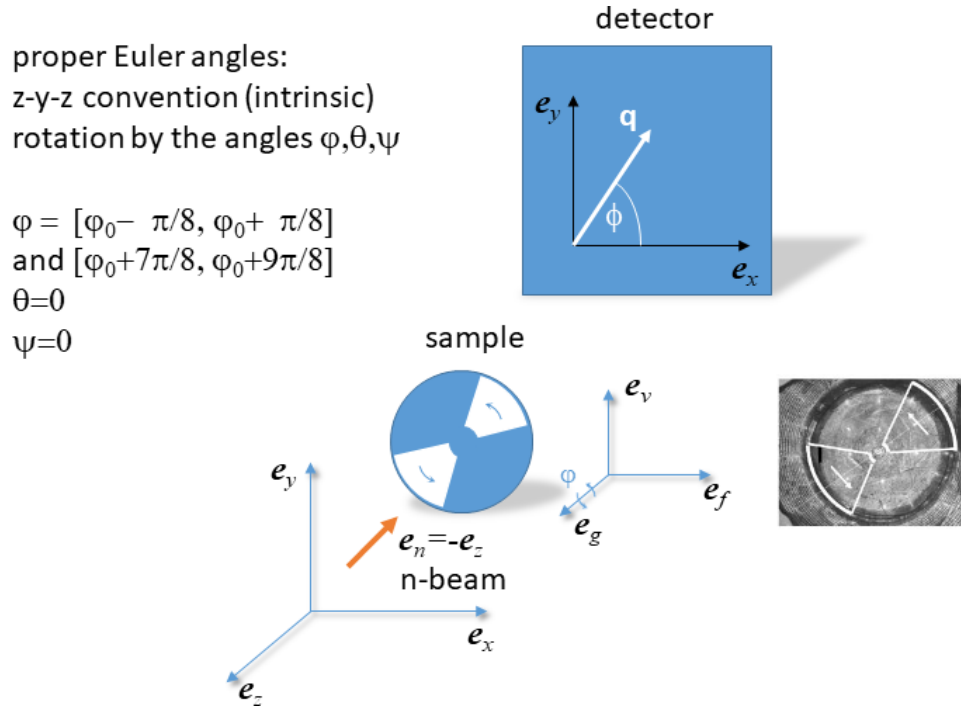


FIGURE 9.138. used coordination axis and Euler angles for case 1

with $f \in (0, 1)$. Depending on the orientation of the sample one probes in a certain scattering direction the contribution of the different projections of the shear axis on \mathbf{q} (only diagonal contributions are assumed). The slopes are given by

$$b = R_g^2 [\alpha^2 q_f^2 + \beta^2 q_v^2 + \gamma^2 q_g^2] \quad (9.474)$$

$$c = R_g^2 [A^2 q_f^2 + B^2 q_v^2 + \Gamma^2 q_g^2] \quad (9.475)$$

The form factor for such a slope in the MSD is given by

$$P_{\text{lin},2}(q, R_g, \alpha, \beta, \gamma, A, B, \Gamma) = \frac{2}{b^2} \left(b - 1 + \exp(-fb) \times \left\{ 1 + \left[\frac{b^2}{c^2} - 1 \right] \exp((f-1)c) + (1-f) \frac{b(b-c)}{c} \right\} \right) \quad (9.476)$$

with a radius of gyration $R_{g,\text{lin}}$

$$R_{g,\text{lin},2} = R_g \sqrt{c + (b-c)(3f-3f^2+f^3)} \quad (9.477)$$

The parametrization above does not automatically preserve the contour length of the polymer.

The last missing part is to define the orientation of the three shear vectors to get the projection q_g, q_f, q_v of them on \mathbf{q} (eqs. 9.467-9.469) as they are needed to calculate the slopes b and c in eq. 9.474 and 9.475.

To values for these vectors are obtained by rotation of the laboratory axis into the shear coordination system. This can be done by using Euler angles. For the chosen

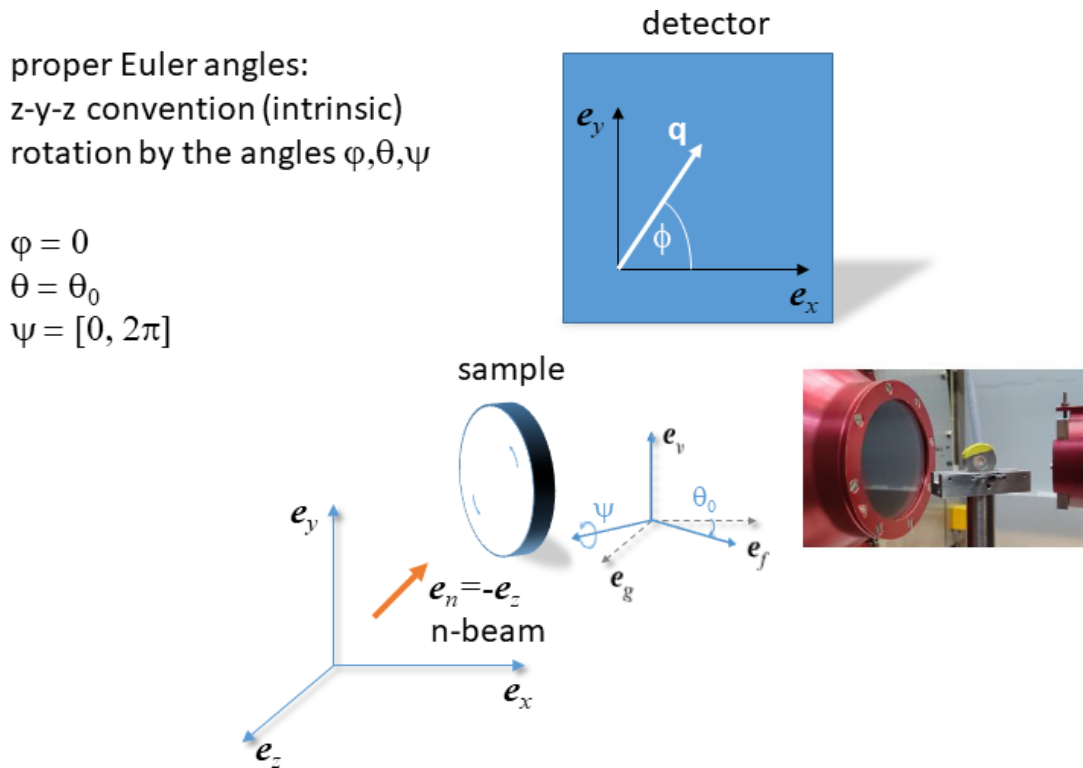


FIGURE 9.139. used coordination axis and Euler angles for case 2

coordination system proper Euler angles using z - y - z convention using the angles φ , θ , ψ are well suited [416]. Lets $\mathbf{M}_{\varphi,\theta,\psi}$ be the rotation matrix, then the shear vector are given by

$$\mathbf{e}_f = \mathbf{M}_{\varphi,\theta,\psi} \mathbf{e}_x \quad (9.478)$$

$$\mathbf{e}_v = \mathbf{M}_{\varphi,\theta,\psi} \mathbf{e}_y \quad (9.479)$$

$$\mathbf{e}_g = \mathbf{M}_{\varphi,\theta,\psi} \mathbf{e}_z \quad (9.480)$$

where $\mathbf{e}_x = (1, 0, 0)^T$, $\mathbf{e}_y = (0, 1, 0)^T$, and $\mathbf{e}_z = (0, 0, 1)^T$. The Euler matrix $\mathbf{M}_{\varphi,\theta,\psi}$ using z - y - z convention reads as

$$\mathbf{M}_{\varphi,\theta,\psi} = \begin{pmatrix} c_\theta c_\psi c_\varphi - s_\psi s_\varphi & -c_\theta c_\varphi s_\psi - c_\psi s_\varphi & c_\varphi s_\theta \\ c_\theta c_\psi s_\varphi + c_\varphi s_\psi & c_\psi c_\varphi - c_\theta s_\psi s_\varphi & s_\theta s_\varphi \\ -c_\psi s_\theta & s_\theta s_\psi & c_\theta \end{pmatrix} \quad (9.481)$$

with $c_x = \cos(x)$ and $s_x = \sin(x)$. By defining the shear vectors via a rotation matrix of the cartesian unit vectors the form factor now also depends on the Euler angles so that it becomes a function of $P(q, R_g, \alpha, \beta, \gamma, A, B, \Gamma, \varphi, \theta, \psi)$.

At least for the cases 1 and 2 mentioned at the beginning this allows to simply integrate over the orientations of the shear vectors defined by the turning angle of the sample and apertures shapes used.

For the case 1 the axis are shown in fig. 9.138. In this setup the sample is already placed with its gradient direction parallel to the beam. The aperture in front of the sample has only aperture opening of sector with for example $\Delta\varphi = 45^\circ = \pi/4$. As the

two sectors are not aligned to the x -axis but turned by φ_0 the aperture smearing can be included by

$$I_{\text{lin},2,a}(\mathbf{q}) = 2 \int_{\varphi_0 - \Delta\varphi/2}^{\varphi_0 + \Delta\varphi/2} P_{\text{lin},2}(q, R_g, \alpha, \beta, \gamma, A, B, \Gamma, \varphi, \theta = 0, \psi = 0) d\varphi \quad (9.482)$$

As the scattering intensity is symmetric and the second sector is turned by π it produces the same scattering contribution as the first one.

Also the second case, where the sample has been rotated in the beam by an angle θ_0 can easily be described. In that case the aperture in front of the sample has a full circular opening as shown in fig. 9.139, but is turned in the beam around the vertical y -axis by θ_0 . Therefore the scattering intensity for case 2 is given by

$$I_{\text{lin},2,b}(\mathbf{q}) = \int_0^{2\pi} P_{\text{lin},2}(q, R_g, \alpha, \beta, \gamma, A, B, \Gamma, \varphi = 0, \theta = \theta_0, \psi) d\psi \quad (9.483)$$

The intensity for $\theta = 0$ should not depend on the azimuthal angle ψ . However, in some case a certain anisotropy has been seen like shown in fig. 9.140.

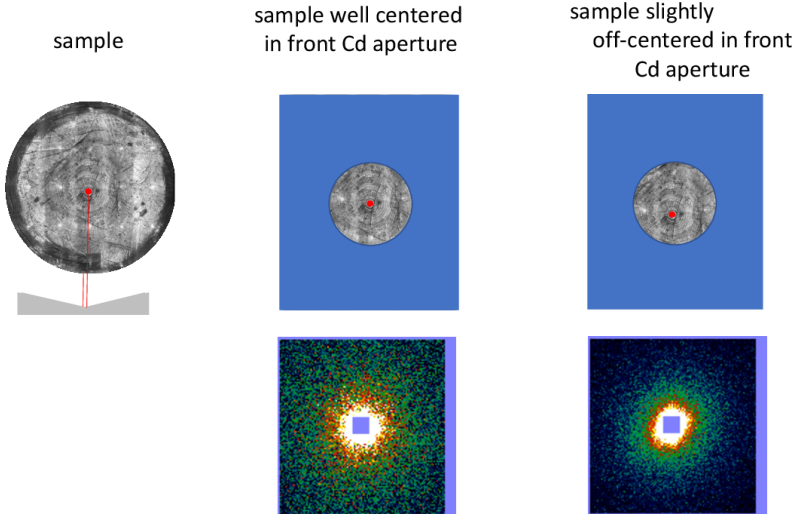


FIGURE 9.140. effect of off-centered samples in front of aperture

To account for a possible off-centered sample the azimuthal integration would need to be done including a certain orientation probability distribution $p(\psi, \psi_0, S_2, S_4)$ of the flow direction.

$$I_2(\mathbf{q}) = \frac{1}{2\pi} \int_0^{2\pi} f(\psi - \psi_0, S_2, S_4) P_{\text{lin}}(q, R_g, \alpha, \beta, \gamma, A, B, \Gamma, \varphi = 0, \theta, \psi) d\psi \quad (9.484)$$

The orientation distribution function is simply described in terms of Legendre polynomials.

$$f(\psi) = \sum_l c_l P_l(\cos \psi) = \sum_l \frac{2l+1}{2} S_l P_l(\cos \psi) \quad (9.485)$$

with the first three Legendre polynomials defined by

$$P_0(\cos \psi) = 1 \quad (9.486a)$$

$$P_1(\cos \psi) = \cos \psi \quad (9.486b)$$

$$P_2(\cos \psi) = \frac{1}{2} (3 \cos^2 \psi - 1) \quad (9.486c)$$

As the orientation distribution was assumed to be symmetric to ψ_0 only odd terms have been considered. In practice the off centered alignment could be sufficiently good corrected for using just the $P_0(\cos \psi)$ and $P_2(\cos \psi)$ with $c_0 = 1$ and c_2 and ψ_0 being fit parameters.

- a semi-empirical 3-parameter formula (B_x, B_y, ξ) to have a similar shape than the piecewise linear MSD function above.

$$\frac{\langle (\mathbf{q} \cdot \mathbf{r}_{nm})^2 \rangle}{2} = (qR_g)^2 \times \left\{ \left| \frac{n-m}{N} \right| + [B_x^2 \cos^2(\psi - \phi_0) - B_y^2 \sin^2(\psi - \phi_0)] \left| \frac{n-m}{N} \right|^\xi \right\} \quad (9.487)$$

To get the same endpoints than the piecewise linear MSD function the amplitudes should be $B_x = \sqrt{\nu\alpha^2 + (1-\nu)\gamma^2}$ and $B_y = \sqrt{\nu\beta^2 + (1-\nu)\delta^2}$. After making use of the identity 9.452 the scattering intensity is than given by

$$P(\mathbf{q}) = 2 \int_0^1 (1-x) \exp \left((qR_g)^2 \left(x + (B_x^2 q^2 \cos^2(\psi - \phi_0) + B_y^2 q^2 \sin^2(\psi - \phi_0)) x^\xi \right) \right) \quad (9.488)$$

- by applying the Rouse model [272] the MSD which reads as

$$\frac{\langle (\mathbf{q} \cdot \mathbf{r}_{nm})^2 \rangle}{2} = (qR_g)^2 \times \left[x + \frac{(\cos(\psi - \phi_0) \pi^2 \text{Wi}_{\text{lin}})^2}{180} x^2 (1 + x - x^2/4 - 2x^3 + x^4) \right] \quad (9.489)$$

with $x = \left| \frac{n-m}{N} \right|$ and the Weissenberg number $\text{Wi}_{\text{lin}} = \tau_1 \dot{\gamma}$.

9.9.5. Ring polymer under shear flow.

Ring polymers under shear flow also can be described using the Rouse model [491, 463] similarly to eq. 9.489. The mean square displacement then reads as

$$\frac{\langle (\mathbf{q} \cdot \mathbf{r}_{nm})^2 \rangle}{2} = 2 (qR_{g,\text{ring}})^2 \left[\mu + \frac{(\cos(\psi - \phi_0) \pi^2 \text{Wi}_{\text{ring}})^2}{1440} (\mu^2 + 2\mu^3) \right] \quad (9.490)$$

with $\mu = x(1-x)$, $x = \left| \frac{n-m}{N} \right|$, $\text{Wi}_{\text{ring}} = \tau_1 \dot{\gamma}$, and $R_{g,\text{ring}}^2 = \frac{Nb^2}{12} = R_{g,\text{lin}}^2/2$. The scattering intensity is then obtained by eq. 9.463

$$P(\mathbf{q}) = 2 \int_0^1 (1-x) \exp \left(-\frac{\langle (\mathbf{q} \cdot \mathbf{r}_{nm})^2 \rangle}{2} \right) dx \quad (9.491)$$

9.9.6. Sheared Cylinder according to Hayter and Penfold.

The orientation distribution of long cylinders in a shear cell has been studied by [439, 242, 205]. In contrast to the orientation distributions described in the next section this distribution also describes the tilting of the most probable orientation against the flow direction.

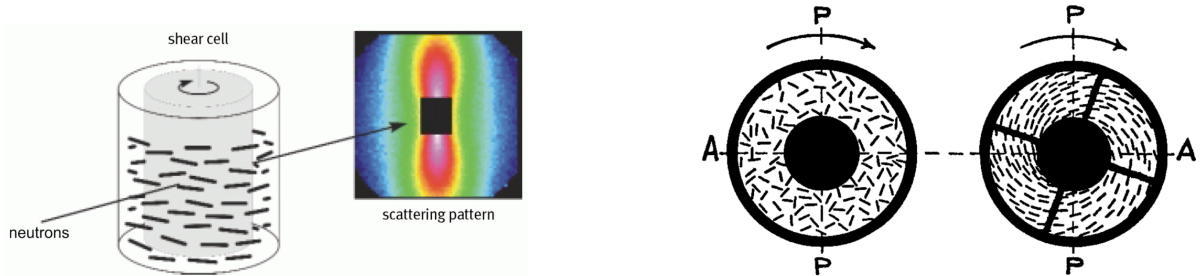


FIGURE 9.141. Shear orientation of micelles in a shear cell with the corresponding SANS-pattern. The orientation of rods at rest and under shear according to [439] are shown on the right as a top view on the cuvette cell.

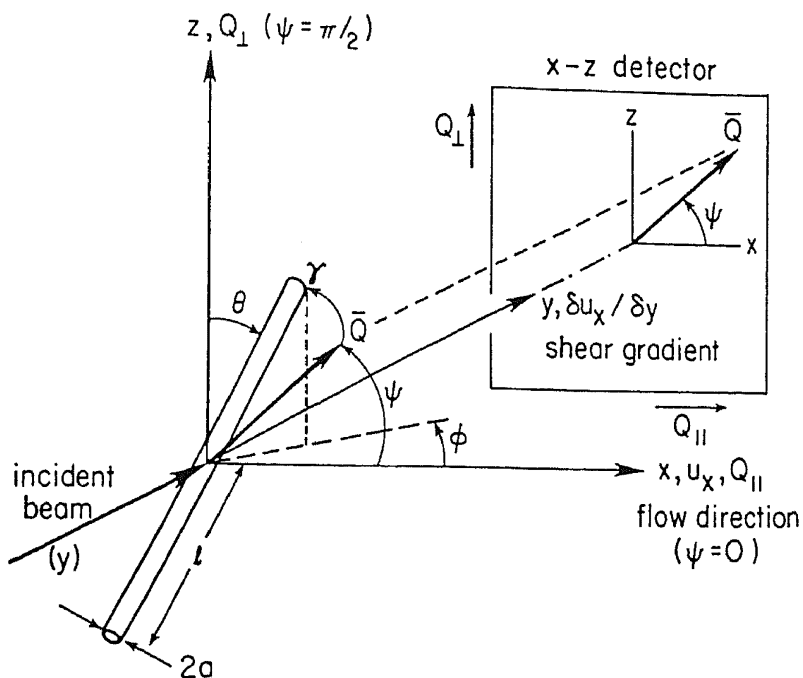


FIGURE 9.142. Cartesian and angular coordinates referred to the center of a cylindrical micelle at origin [205]. The relationship to the spectrometer geometry is shown schematically. The momentum transfer, Q , lies in the $z - x$ plane.

The scattering from monodisperse dilute (non-interacting) isotropic solution of anisotropic micelles is given by [205]

$$I(Q) = \left\langle |K_{\text{CylSh}}(Q)|^2 \right\rangle_Q \quad (9.492)$$

where $K(Q)$ is the form factor for a micelle at a given orientation relative to the momentum transfer Q and $\langle \rangle_Q$ denotes an average over all such orientations.

For a cylindrical shell of length L , core diameter $2R$, and shell thickness t the form factor is given by:

$$\begin{aligned} K_{\text{CylSh}}(Q, \dots, \gamma) = & K_{\text{Cyl}}(Q, \eta_{\text{core}} - \eta_{\text{shell}}, R, L, \gamma) \\ & + K_{\text{Cyl}}(Q, \eta_{\text{shell}} - \eta_{\text{solv}}, R + \Delta R, L, \gamma) \end{aligned} \quad (9.493)$$

with

$$K_{\text{Cyl}}(Q, \Delta\eta, R, L, \gamma) = 2\pi R^2 L \Delta\eta \frac{J_1(QR \sin \gamma)}{QR \sin \gamma} \frac{\sin\left(\frac{QL}{2} \cos \gamma\right)}{\frac{QL}{2} \cos \gamma} \quad (9.494)$$

where γ is the angle between \mathbf{Q} and the cylinder axis \mathbf{n} . η_{core} , η_{shell} , and η_{solv} are the scattering length densities of the cylinder core, shell and solvent. $J_1(x)$ is the first order Bessel function of the first kind. γ can be calculated from the orientation (θ, ϕ) of the cylinder and the direction of the scattering vector ψ in the plane of the detector by where γ is the angle between Q and the cylinder axis.

The scattering geometry for shear alignment is shown in Fig. 9.142. In general perfect alignment will not be achieved, and an orientation distribution must be employed such that the resultant scattering will be given by

$$I(Q, \psi) = \int_0^{2\pi} \int_0^\pi p_{\text{HP}}(\theta, \phi; \kappa) \left(K_{\text{CylSh}}^2(Q, \gamma^+) + K_{\text{CylSh}}^2(Q, \gamma^-) \right) \sin \theta d\theta d\phi \quad (9.495)$$

with

$$p_{\text{HP}}(\theta, \phi; \kappa) = \frac{(1 - \cos 2\Phi_0)(1 + \sin^2 \theta \cos 2\Phi_0)^{3/2}}{4\pi [1 - \sin^2 \theta \cos 2\Phi_0 \cos 2(\phi - \Phi_0)]^2} \quad (9.496)$$

and

$$2\Phi_0 = \arctan(8/\kappa) \quad (9.497)$$

$(\cos \Phi_0, \sin \Phi_0, 0)^T$ is the direction of the most probable orientation $(\theta = \frac{\pi}{2}; \phi = \Phi_0)$. Φ_0 varies between $\Phi_0 = \frac{\pi}{4}$ for the isotropic case ($\kappa = 0$) to $\Phi_0 = 0$ for perfect alignment ($\kappa \rightarrow \infty$). As the most probable direction is not the same as the flow direction, which is assumed to be the x -direction, and secondly that the beam is passing twice the cuvette cell with flow direction \mathbf{x} and $-\mathbf{x}$ we have to take the sum over two values for γ^\pm in eq. 9.495. The angle $\gamma^\pm = \angle(\mathbf{Q}, \mathbf{n}^\pm)$ between the scattering vector \mathbf{Q} and the director of the cylinder axis \mathbf{n}^\pm is

$$\frac{\mathbf{Q}}{|\mathbf{Q}|} = \begin{pmatrix} \cos \psi \\ 0 \\ \sin \psi \end{pmatrix} \quad \frac{\mathbf{n}^\pm}{|\mathbf{n}^\pm|} = \begin{pmatrix} \pm \sin \theta \cos \phi \\ \pm \sin \theta \sin \phi \\ \cos \theta \end{pmatrix} \quad (9.498)$$

$$\cos \angle(\mathbf{Q}, \mathbf{n}^\pm) = \cos \gamma^\pm = \frac{\mathbf{Q} \cdot \mathbf{n}^\pm}{|\mathbf{Q}| |\mathbf{n}^\pm|} = \pm \cos \psi \sin \theta \cos \phi + \sin \psi \cos \theta \quad (9.499)$$

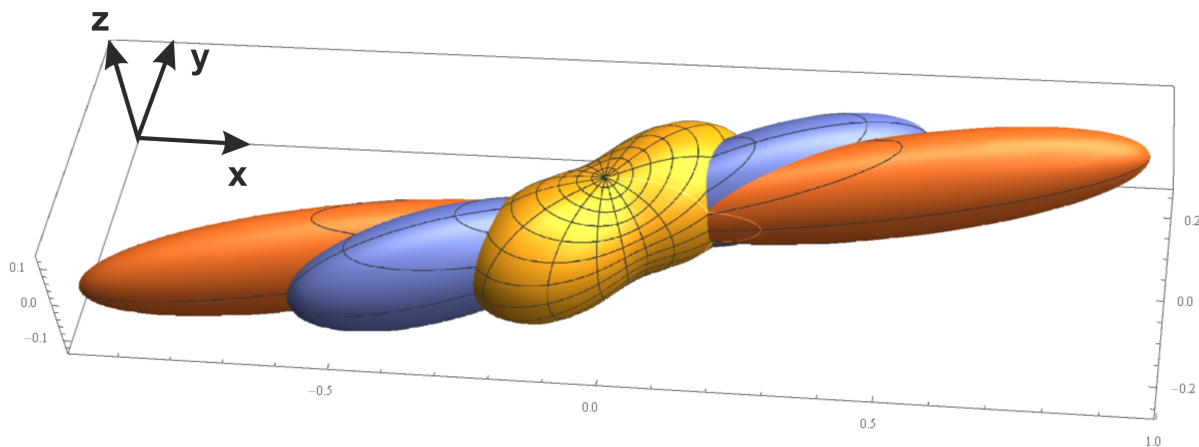


FIGURE 9.143. 3D plot of the orientation distributions $2p_{\text{HP}}(\theta, \phi; \kappa = 2)$ (yellow), $p_{\text{HP}}(\theta, \phi; \kappa=8)$ (blue), $\frac{1}{2}p_{\text{HP}}(\theta, \phi; \kappa=16)$ (orange).

For the reversed direction of the flow the x -component of the vector \mathbf{n}^- changes its sign. In the original paper [205] one finds $\cos \gamma_{\text{HP}}^- = \cos \psi \sin \theta \cos \phi - \sin \psi \cos \theta$, which, however, results to the same scattering intensity as the scattering intensity of a cylinder is invariant by a rotation of π , i.e. as $\cos(\pi + \gamma^-) = -\cos \gamma^- = \cos \gamma_{\text{HP}}^-$ the resulting scattering patterns are the same for both value γ^- and γ_{HP}^- .

Input Parameters for model Sheared Cylinders (HayterPenfold):

R: radius of cylinders R

t: shell thickness t

L: cylinder length L

eta_core: scattering length density of cylinder core η_{core}

eta_shell: scattering length density of cylinder shell η_{shell}

eta_solv: scattering length density of solvent η_{solv}

psi: direction of scattering vector on the detector ψ

sigma: width parameter of lognormal size distribution σ

kappa: orientation distribution parameter κ

Note:

- The size distribution is taken simultaneously over all parameters R , t and L , so that their aspect ratios stay always constant
- The most probable orientation is not the \mathbf{x} -direction but tilted by the angle Φ_0 . As in a rheometer with cuette geometry the sample is passing the sample twice the forward scattering is twice as large as in the model described in the next section.
- As the orientation distribution is also not rotational symmetric around the direction of the most probable orientation and additional tilted against \mathbf{x} -axis the scattering pattern look less anisotropic than the other models in the following sections with the same order parameter κ .

9.9.7. partly aligned anisotropic objects.

In contrast to the model of Hayter and Penfold [205] in section 9.9.6 here we use an orientation distribution with the most probable orientation along the x-axis and independent on the polar angle ϕ . Therefore the coordination system is slightly differently defined in the Hayter-Penfold model of sheared cylinders.

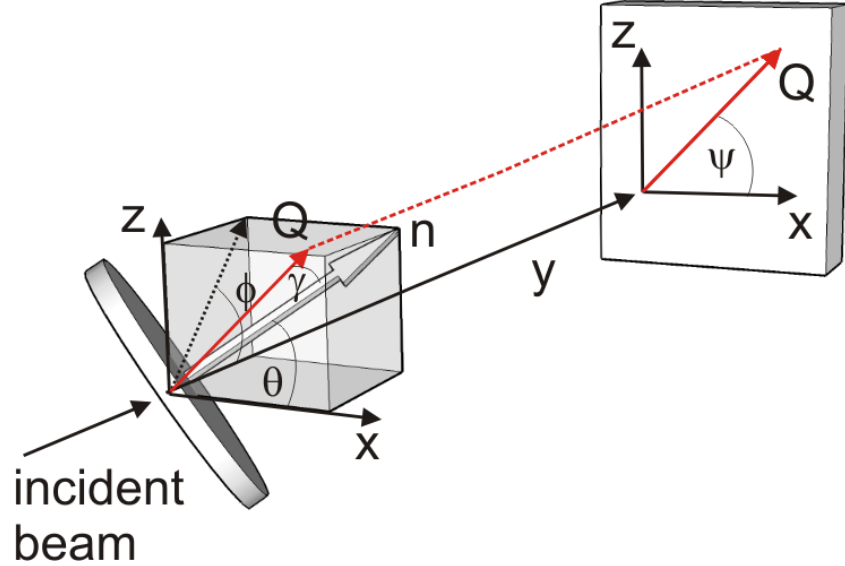


FIGURE 9.144. Sketch of relative orientation \mathbf{n} of partly aligned cylinders or discs to the scattering vector \mathbf{Q} .

The scattering amplitude of a cylindrical shell is given by

$$K_{\text{CylShell}}(Q, \dots, \gamma) = K_{\text{Cyl}}(Q, \eta_{\text{core}} - \eta_{\text{shell}}, R, L, \gamma) + K_{\text{Cyl}}(Q, \eta_{\text{shell}} - \eta_{\text{solv}}, R + \Delta R, L, \gamma) \quad (9.500)$$

with

$$K_{\text{Cyl}}(Q, \Delta\eta, R, L, \gamma) = 2\pi R^2 L \Delta\eta \frac{J_1(QR \sin \gamma)}{QR \sin \gamma} \frac{\sin\left(\frac{QL}{2} \cos \gamma\right)}{\frac{QL}{2} \cos \gamma} \quad (9.501)$$

where γ is the angle between \mathbf{Q} and the cylinder axis \mathbf{n} . L is the length of the cylinder, R its radius, $\Delta\eta$ the scattering length density contrast relative to the solvent and $J_1(x)$ is the first order Bessel function of the first kind.

The scattering amplitude of an ellipsoid of revolution is given by

$$K_{\text{Ell}}(Q, \Delta\eta, R_e, R_p, \gamma) = 4\pi R_e^2 R_p \Delta\eta \frac{j_1(Qs)}{Qs} \quad (9.502)$$

with $s = \sqrt{R_p \cos^2 \gamma + R_e \sin^2 \gamma}$ and $j_1(x)$ being the spherical bessel function of first kind. R_e and R_p are the equatorial and polar semi-axes of the spheroid, respectively.

The scattering amplitude of an ellipsoidal shell is given by

$$\begin{aligned} K_{\text{EllShell}}(Q, \dots, \gamma) = & K_{\text{Ell}}(Q, \eta_{\text{core}} - \eta_{\text{shell}}, R_p, R_e, \gamma) \\ & + K_{\text{Ell}}(Q, \eta_{\text{shell}} - \eta_{\text{solv}}, R_p + \Delta R, R_e + \Delta R, \gamma) \end{aligned} \quad (9.503)$$

γ can be calculated from the orientation (θ, ϕ) of the cylinder and the direction of the scattering vector ψ in the plane of the detector by

$$\frac{\mathbf{Q}}{|\mathbf{Q}|} = \begin{pmatrix} \cos \psi \\ 0 \\ \sin \psi \end{pmatrix} \quad \frac{\mathbf{n}}{|\mathbf{n}|} = \begin{pmatrix} \cos \theta \\ \sin \theta \cos \phi \\ \sin \theta \sin \phi \end{pmatrix} \quad (9.504)$$

$$\cos \angle(\mathbf{Q}, \mathbf{n}) = \cos \gamma = \frac{\mathbf{Q} \cdot \mathbf{n}}{|\mathbf{Q}| |\mathbf{n}|} = \cos \psi \cos \theta + \sin \psi \sin \theta \sin \phi \quad (9.505)$$

If the orientation distribution of the orientation vector \mathbf{n} is described by $p(\theta, \phi, \kappa)$ so that the scattering intensity is given by

$$I_{\text{p.a.CylShell}}(Q) = \int_0^\pi d\theta \int_0^{2\pi} d\phi K_{\text{CylShell}}^2(Q, \dots, \gamma) p(\theta, \phi; \kappa) \sin(\theta) \quad (9.506)$$

$$I_{\text{p.a.EllShell}}(Q) = \int_0^\pi d\theta \int_0^{2\pi} d\phi K_{\text{EllShell}}^2(Q, \dots, \gamma) p(\theta, \phi; \kappa) \sin(\theta) \quad (9.507)$$

For this form factor it is assumed that the orientation distribution is independent of ϕ , i.e. $p(\theta, \phi; \kappa) = p(\theta; \kappa)$ and that $p(\theta; \kappa) = p(\pi - \theta; \kappa)$, which means that turning the cylinder by 180° results in the same scattering intensity. Several orientation distributions have been implemented in a way that their resulting order parameter S_2 can have values between -0.5 and 1, which correspond to perfect alignment perpendicular to the x axis and perfect alignment parallel to it. All probability distributions have been normalized

$$\int_0^\pi \int_0^{2\pi} p(\theta, \phi; \kappa) \sin \theta d\theta d\phi = 1 \quad (9.508)$$

TABLE 4. Values for κ to obtain certain order parameters $S_2(\kappa)$ for the different orientation distributions $p(\theta, \phi, \kappa)$.

$p(\theta, \phi, \kappa)$	-0.45	-0.4	-0.2	0	0.2	0.4	0.6	0.8	0.9	0.95
Gauss	-3.739	-1.62	-1.128	0	0.83	1.220	1.686	2.576	3.762	5.4
Boltzmann	-7.141	-4.59	-1.431	0	1.114	2.218	3.581	5.989	9	13.08
Maier-Saupe	-15	-7.49	-1.874	0	1.367	2.709	4.444	8.241	15.59	30.54
Onsager	-28.43	-13.35	-2.918	0	2.042	3.629	6.313	13.92	28.96	58.99
Heavyside	-3.108	-2.157	-1.129	0	0.794	0.982	1.267	1.868	2.692	3.840
Hayter-Penfold	\emptyset	\emptyset	\emptyset	0	3.008	6.269	10.93	20.8	34.91	55.64

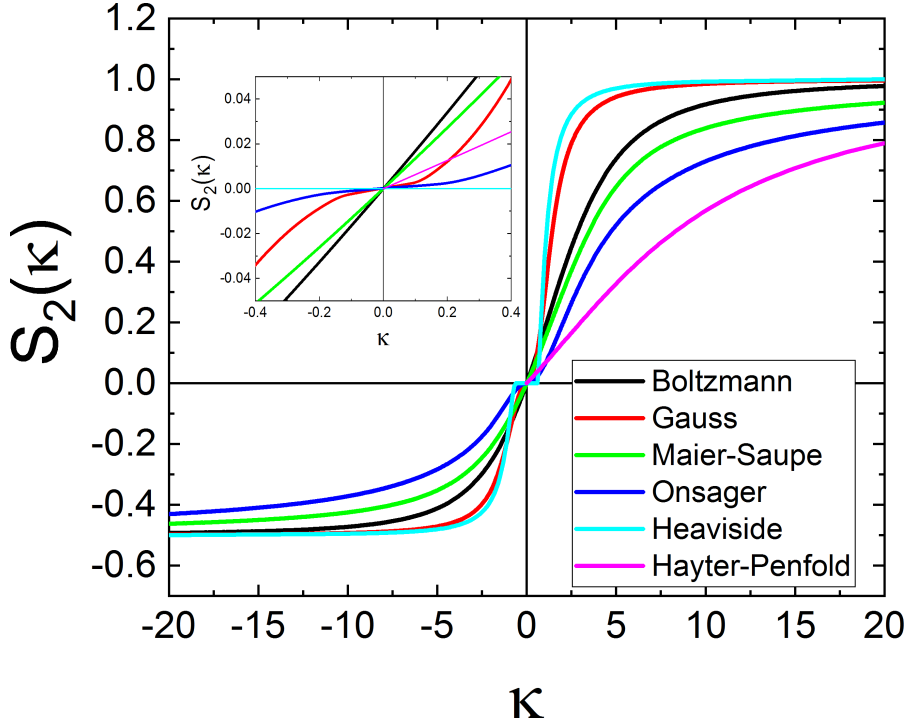


FIGURE 9.145. Order parameter $S_2(\kappa)$ for the orientation distributions described in the next subsections.

The order parameters S_2 can be calculated by

$$\begin{aligned} S_2(\kappa) &= \int_0^{\pi} \int_0^{2\pi} p(\theta, \phi; \kappa) \frac{1}{2} (3 \cos^2 \theta - 1) \sin \theta d\theta d\phi \\ &= \int_0^{\pi} 2\pi p(\theta; \kappa) \frac{1}{2} (3 \cos^2 \theta - 1) \sin \theta d\theta \end{aligned} \quad (9.509)$$

The order parameter for the Hayter-Penfold orientation distribution has been calculated by performing first a coordination transformation of the polar coordinates with \mathbf{z} being the polar axis to coordination system with a polar axis pointing into the direction of the most probable orientation. The order parameter $S_2(\kappa)$ in eq. 9.509 is then calculated in this new polar coordinate system.

The form factors additional contain already a size distribution to profit from the speed enhancement by using a specialized multidimensional integration routine. The size distribution is included as

$$I(Q) = \int_0^{\infty} \text{LogNorm}(\nu, \sigma, 1) I_{\text{p.a.CylShell}}(Q, R\nu, \Delta R\nu, L\nu) d\nu \quad (9.510)$$

$$(9.511)$$

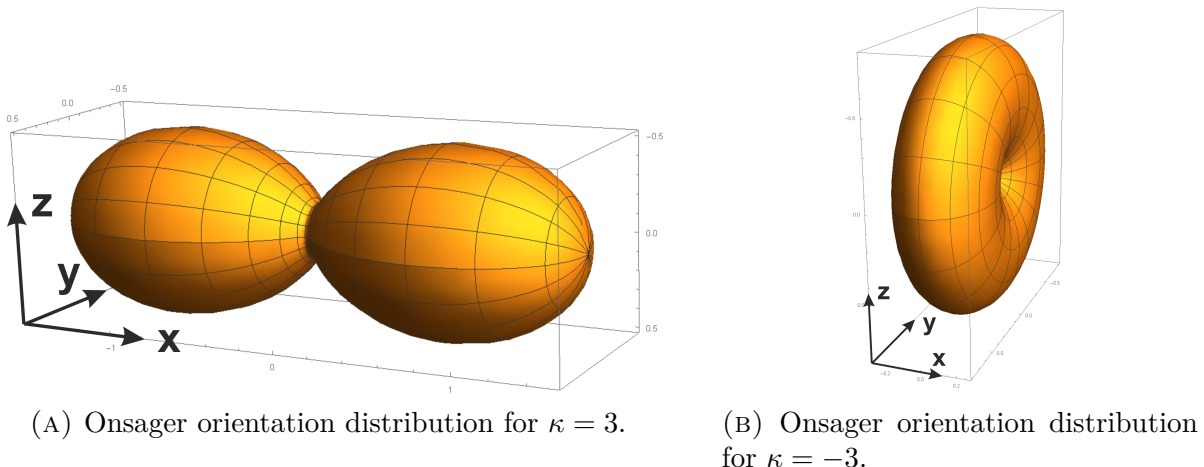


FIGURE 9.146. Orientation distributions are all independent on ϕ and have for $\kappa > 0$ a positive order parameter, i.e. the most probable orientation is in the \mathbf{x} -direction and for $\kappa < 0$ a negative order parameter, i.e. the most probable orientation lies in the $\mathbf{z}\mathbf{y}$ -plane

and

$$I(Q) = \int_0^\infty \text{LogNorm}(\nu, \sigma, 1) I_{\text{p.a.EllShell}}(Q, R_p \nu, \Delta R \nu, R_e \nu) d\nu \quad (9.512)$$

with

$$\text{LogNorm}(\nu, \sigma, \mu) = \frac{1}{\sqrt{2\pi}\sigma} \frac{1}{\nu} \exp\left(-\frac{(\ln(\nu/\mu))^2}{2\sigma^2}\right) \quad (9.513)$$

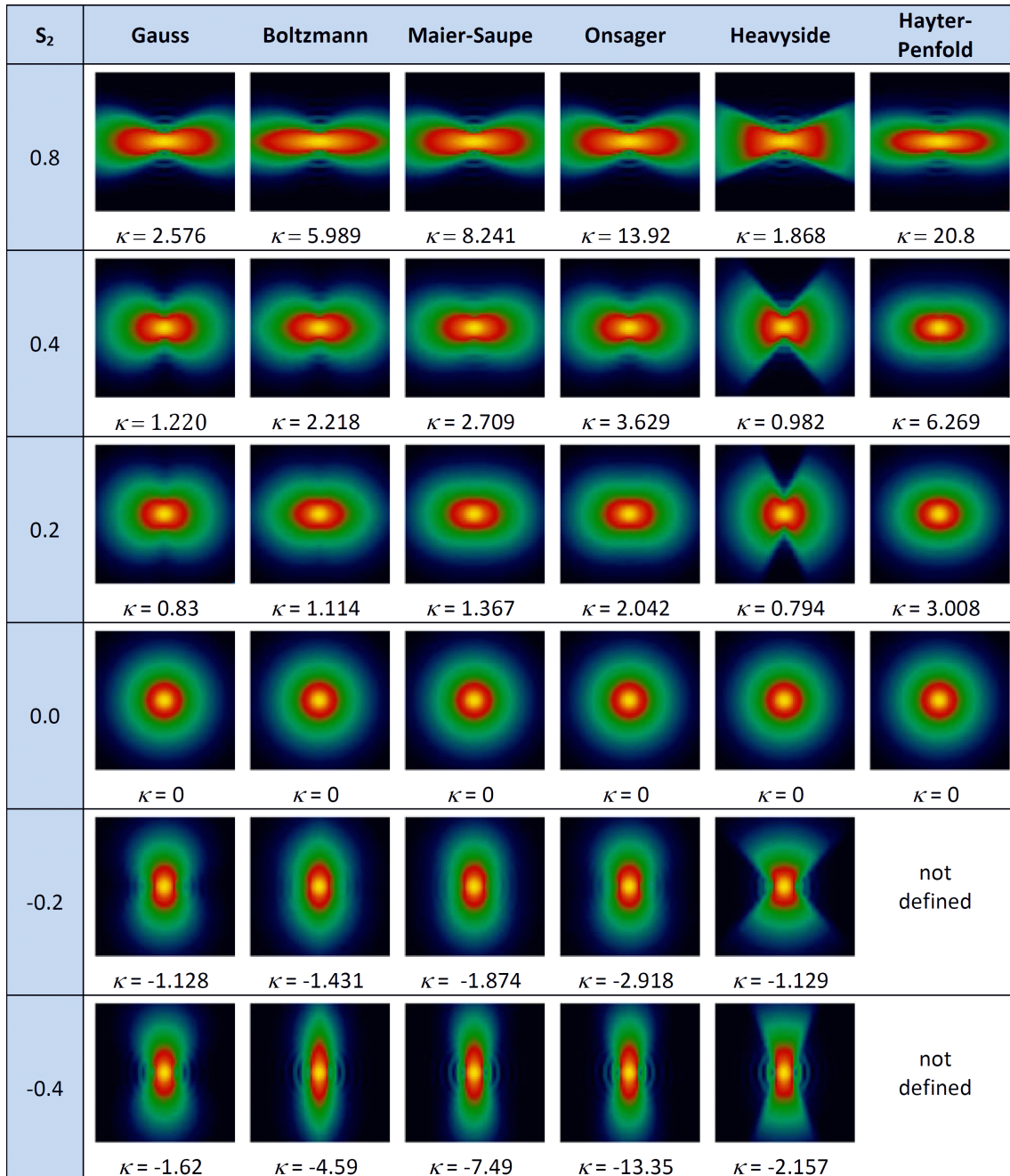


FIGURE 9.147. comparison of different orientation distributions with the same order parameter.

9.9.7.1. Maier-Saupe orientation distribution.

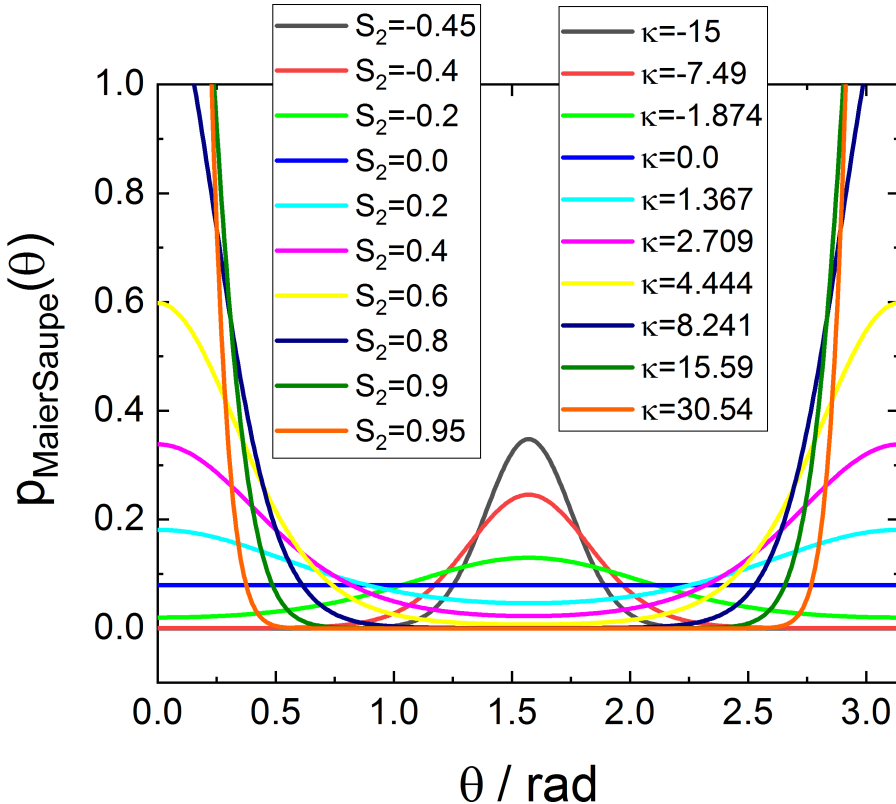


FIGURE 9.148. Maier-Saupe orientation distribution $p_{\text{MS}}(\theta, \kappa)$ for different values of κ , resulting in an order parameter as listed in table 4.

$$p(\theta, \phi; \kappa) = \frac{1}{c_{\text{MS}}} \exp(\kappa \cos^2 \theta) \quad (9.514)$$

with

$$c_{\text{MS}} = \begin{cases} 4\pi \exp(\kappa) \frac{D(\sqrt{\kappa})}{\sqrt{\kappa}} & \text{for } \kappa > 0 \\ 2\pi\sqrt{\pi} \frac{\text{erf}(\sqrt{|\kappa|})}{\sqrt{|\kappa|}} & \text{for } \kappa < 0 \\ 4\pi & \text{for } \kappa = 0 \end{cases} \quad (9.515)$$

with $D(x)$ being Dawson's integral $D(x) = e^{-x^2} \int_0^x e^{y^2} dy = \frac{1}{2}\sqrt{\pi} e^{-x^2} \text{erfi}(x)$

Input Parameters for model Sheared Cylinders (Maier-Saupe):

R: radius of cylinders R

t: shell thickness t

L: cylinder length L

eta_core: scattering length density of cylinder core η_{core}

eta_shell: scattering length density of cylinder shell η_{shell}

eta_solv: scattering length density of solvent η_{solv}

psi: direction of scattering vector on the detector ψ

sigma: width parameter of lognormal size distribution σ

kappa: orientation distribution parameter κ

Input Parameters for model Sheared Spheroids (Maier-Saupe):

R_equatorial: equatorial semi-axes of spheroids R_e

t: shell thickness t

R_polar: polar semi-axis of spheroids R_p

eta_core: scattering length density of cylinder core η_{core}

eta_shell: scattering length density of cylinder shell η_{shell}

eta_solv: scattering length density of solvent η_{solv}

psi: direction of scattering vector on the detector ψ

sigma: width parameter of lognormal size distribution σ

kappa: orientation distribution parameter κ

Note:

- The size distribution is taken simultaneously over all parameters R , t , L , and R_e , t , R_p respectively, so that their aspect ratios always stay constant.

9.9.7.2. Onsager orientation distribution.

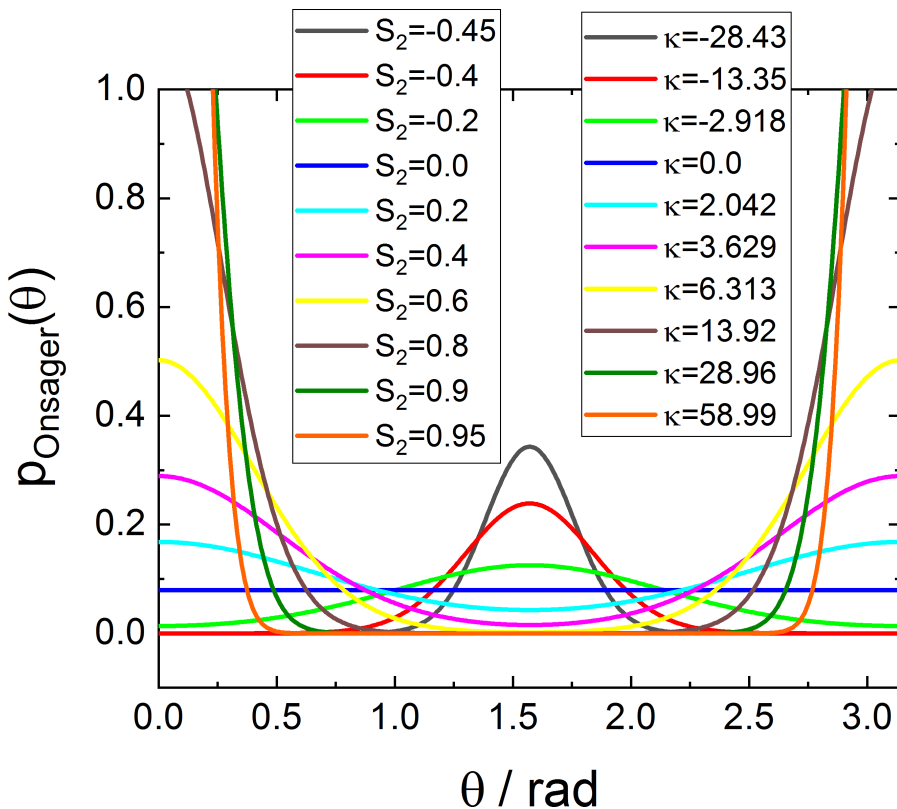


FIGURE 9.149. Onsager orientation distribution $p_O(\theta, \kappa)$ for different values of κ , resulting in an order parameter as listed in table 4.

$$p_O(\theta, \phi; \kappa) = \begin{cases} \frac{\kappa \cosh(\kappa \cos(\theta))}{4\pi \sinh(\kappa)} & \text{for } \kappa \geq 0 \\ \frac{\cosh(|\kappa| \sin(\theta))}{2\pi^2 L_1(|\kappa|)} & \text{for } \kappa < 0 \end{cases} \quad (9.516)$$

where $L_\nu(x)$ is the modified Struve function.

Input Parameters for model Sheared Cylinders (Onsager):

R: radius of cylinders R

t: shell thickness t

L: cylinder length L

eta_core: scattering length density of cylinder core η_{core}

eta_shell: scattering length density of cylinder shell η_{shell}

eta_solv: scattering length density of solvent η_{solv}

psi: direction of scattering vector on the detector ψ

sigma: width parameter of lognormal size distribution σ

kappa: orientation distribution parameter κ

Input Parameters for model Sheared Spheroids (Onsager:

R_equatorial: equatorial semi-axes of spheroids R_e

t: shell thickness t

R_polar: polar semi-axis of spheroids R_p

eta_core: scattering length density of cylinder core η_{core}

eta_shell: scattering length density of cylinder shell η_{shell}

eta_solv: scattering length density of solvent η_{solv}

psi: direction of scattering vector on the detector ψ

sigma: width parameter of lognormal size distribution σ

kappa: orientation distribution parameter κ

Note:

- The size distribution is taken simultaneously over all parameters R , t , L , and R_e , t , R_p respectively, so that their aspect ratios always stay constant.

9.9.7.3. Boltzmann orientation distribution.

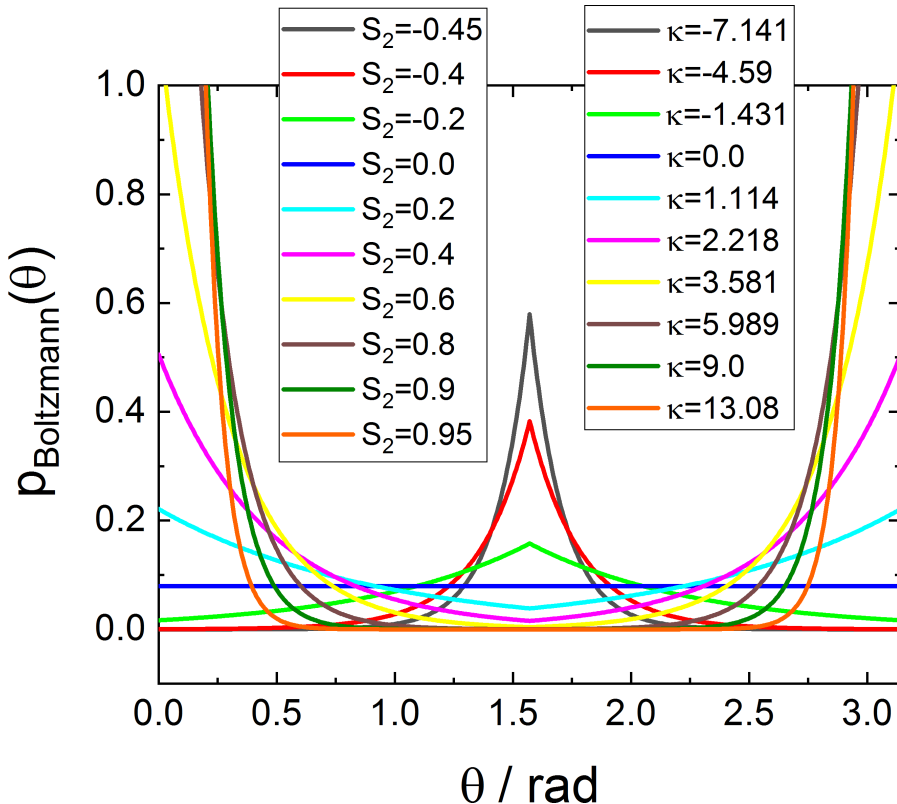


FIGURE 9.150. Boltzmann orientation distribution $p_B(\theta, \kappa)$ for different values of κ , resulting in an order parameter as listed in table 4.

$$p_B(\theta, \phi; \kappa) = \begin{cases} \frac{1}{2\pi c_B} \exp(-\theta\kappa) & \text{for } \theta \leq \frac{\pi}{2} \\ \frac{1}{2\pi c_B} \exp(-(\pi - \theta)\kappa) & \text{for } \theta > \frac{\pi}{2} \end{cases} \quad (9.517)$$

with

$$c_B = \frac{2 \left(1 - \kappa \exp\left(-\frac{\pi}{2}\kappa\right) \right)}{\kappa^2 + 1} \quad (9.518)$$

Input Parameters for model Sheared Cylinders (Boltzmann):

R: radius of cylinders R

t: shell thickness t

L: cylinder length L

eta_core: scattering length density of cylinder core η_{core}

eta_shell: scattering length density of cylinder shell η_{shell}

eta_solv: scattering length density of solvent η_{solv}
psi: direction of scattering vector on the detector ψ
sigma: width parameter of lognormal size distribution σ
kappa: orientation distribution parameter κ

Input Parameters for model Sheared Spheroids (Boltzmann):

R_equatorial: equatorial semi-axes of spheroids R_e
t: shell thickness t
R_polar: polar semi-axis of spheroids R_p
eta_core: scattering length density of cylinder core η_{core}
eta_shell: scattering length density of cylinder shell η_{shell}
eta_solv: scattering length density of solvent η_{solv}
psi: direction of scattering vector on the detector ψ
sigma: width parameter of lognormal size distribution σ
kappa: orientation distribution parameter κ

Note:

- The size distribution is taken simultaneously over all parameters R , t , L , and R_e , t , R_p respectively, so that their aspect ratios always stay constant.

9.9.7.4. Gaussian orientation distribution.

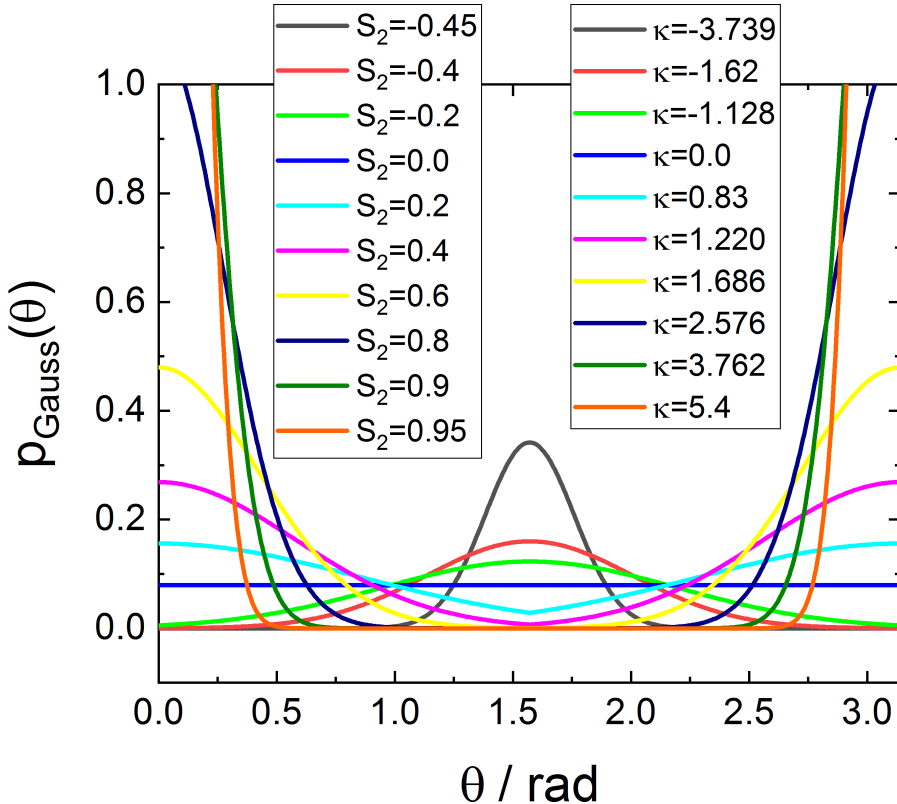


FIGURE 9.151. Gaussian orientation distribution $p_G(\theta, \kappa)$ for different values of κ , resulting in an order parameter as listed in table 4.

$$p_G(\theta, \phi; \kappa) = \begin{cases} \frac{1}{2\pi c_G} \exp(-\theta^2 \kappa^2) & \text{for } \kappa \geq 0 \text{ and } \theta \leq \frac{\pi}{2} \\ \frac{1}{2\pi c_G} \exp(-(\pi - \theta)^2 \kappa^2) & \text{for } \kappa \geq 0 \text{ and } \theta > \frac{\pi}{2} \\ \frac{1}{2\pi c_G} \exp\left(-\left(\frac{\pi}{2} - \theta\right)^2 |\kappa|^2\right) & \text{for } \kappa < 0 \end{cases} \quad (9.519)$$

with

$$c_G = \begin{cases} \frac{D(\kappa/2)}{\kappa} + \frac{\sqrt{\pi}}{2\kappa} e^{-\frac{1}{4\kappa^2}} \Re \left(\text{cerfi} \left(-\frac{1}{2\kappa} + i\frac{\pi}{2}\kappa \right) \right) & \text{for } \kappa \geq 0 \\ \frac{\sqrt{\pi}}{|\kappa|} e^{-\frac{1}{4\kappa^2}} \Im \left(\text{cerfi} \left(-\frac{1}{2|\kappa|} + i\frac{\pi}{2}|\kappa| \right) \right) & \text{for } \kappa < 0 \end{cases} \quad (9.520)$$

Input Parameters for model Sheared Cylinders (Gauss):

R: radius of cylinders R

t: shell thickness t

L: cylinder length L

eta_core: scattering length density of cylinder core η_{core}

eta_shell: scattering length density of cylinder shell η_{shell}

eta_solv: scattering length density of solvent η_{solv}

psi: direction of scattering vector on the detector ψ

sigma: width parameter of lognormal size distribution σ

kappa: orientation distribution parameter κ

Input Parameters for model Sheared Spheroids (Gauss):

R_equatorial: equatorial semi-axes of spheroids R_e

t: shell thickness t

R_polar: polar semi-axis of spheroids R_p

eta_core: scattering length density of cylinder core η_{core}

eta_shell: scattering length density of cylinder shell η_{shell}

eta_solv: scattering length density of solvent η_{solv}

psi: direction of scattering vector on the detector ψ

sigma: width parameter of lognormal size distribution σ

kappa: orientation distribution parameter κ

Note:

- The size distribution is taken simultaneously over all parameters R , t , L , and R_e , t , R_p respectively, so that their aspect ratios always stay constant.

9.9.7.5. *Boxed orientation distribution (HeavisidePi).*

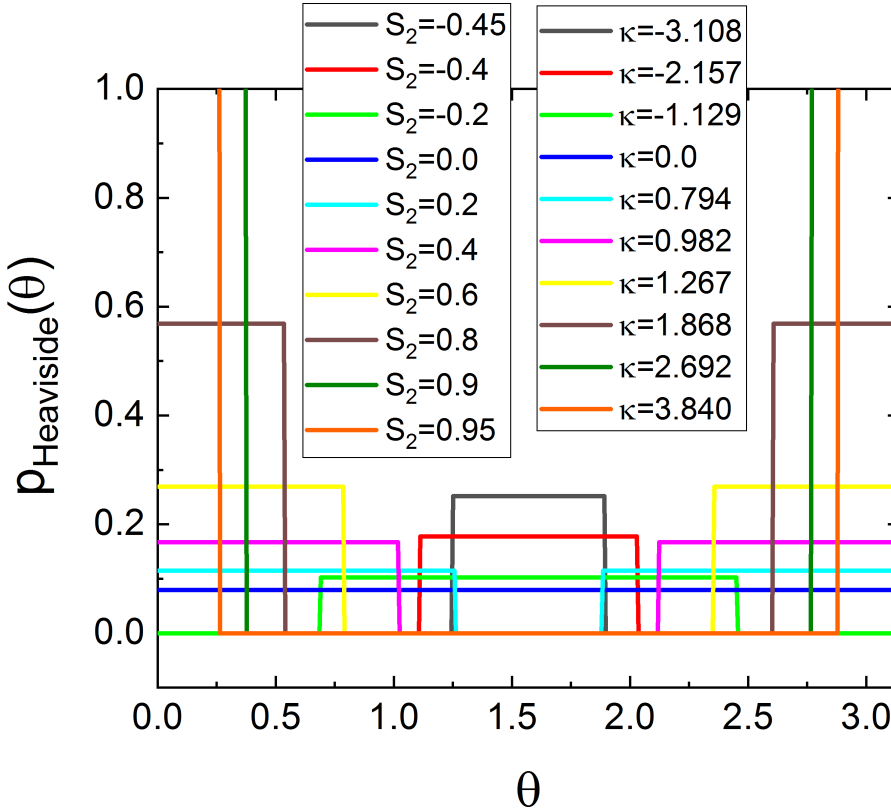


FIGURE 9.152. Heaviside orientation distribution $p_{HS}(\theta, \kappa)$ for different values of κ , resulting in an order parameter as listed in table 4.

$$p(\theta, \phi; \kappa) = \begin{cases} \frac{1}{4\pi(1 - \cos(1/\kappa))} \left(\Pi\left(\frac{x\kappa}{2}\right) + \Pi\left(\frac{(x - \pi)\kappa}{2}\right) \right) & \text{for } \kappa > \frac{2}{\pi} \\ \frac{1}{4\pi} & \text{for } |\kappa| \leq \frac{2}{\pi} \\ \frac{1}{4\pi \sin\left(\frac{1}{|\kappa|}\right)} \Pi\left(\frac{\left(x - \frac{\pi}{2}\right) |\kappa|}{2}\right) & \text{for } \kappa < -\frac{2}{\pi} \end{cases} \quad (9.521)$$

with the rectangle function $\Pi(x)$

$$\Pi(x) = \begin{cases} 0 & \text{for } |x| > \frac{1}{2} \\ \frac{1}{2} & \text{for } |x| = \frac{1}{2} \\ 1 & \text{for } |x| < \frac{1}{2} \end{cases} \quad (9.522)$$

Input Parameters for model Sheared Cylinders (Heaviside):

R: radius of cylinders R
t: shell thickness t
L: cylinder length L
eta_core: scattering length density of cylinder core η_{core}
eta_shell: scattering length density of cylinder shell η_{shell}
eta_solv: scattering length density of solvent η_{solv}
psi: direction of scattering vector on the detector ψ
sigma: width parameter of lognormal size distribution σ
kappa: orientation distribution parameter κ

Input Parameters for model Sheared Spheroids (Heaviside):

R_equatorial: equatorial semi-axes of spheroids R_e
t: shell thickness t
R_polar: polar semi-axis of spheroids R_p
eta_core: scattering length density of cylinder core η_{core}
eta_shell: scattering length density of cylinder shell η_{shell}
eta_solv: scattering length density of solvent η_{solv}
psi: direction of scattering vector on the detector ψ
sigma: width parameter of lognormal size distribution σ
kappa: orientation distribution parameter κ

Note:

- The size distribution is taken simultaneously over all parameters R , t , L , and R_e , t , R_p respectively, so that their aspect ratios always stay constant.
- For $|\kappa| < \frac{2}{\pi}$ the partial derivative $\delta/\delta\kappa$ of the model function is zero which will cause an error message in the minimization routine. This means the fitting procedure will not work in this domain of values.

9.10. Functions for analysing azimuthal averaged data

9.10.1. \sin^2 - \sin^4 azimuthal analysis.

This plugin can be used to describe azimuthal averaged data in case of e.g. magnetic scattering [527], where depending on the incident and scattered polarization and the dipole-dipole nature of the interaction of the neutron with a magnetic moment of an atom an angle dependent cross-section is observed even though the scattering objects are spherical. The spherical symmetry is broken by orienting the magnetic towards a applied magnetic field. Some detailed form factor for magnetic objects can be found in chapter 9.13. The scattering can be often decomposed in an isotropic term independent of the angle between the scattering vector and the applied field and anisotropic terms which anisotropy term is described by a $\sin^2(\psi)$ and $\sin^4(\psi)$ term.

$$I_{\text{rad}}(\psi) = A + B \sin^2(\psi - \delta) + C \sin^4(\psi - \delta) \quad (9.523)$$

$$I_{\text{deg}}(\psi) = A + B \sin^2\left((\psi - \delta) \frac{\pi}{180}\right) + C \sin^4\left((\psi - \delta) \frac{\pi}{180}\right) \quad (9.524)$$

Input Parameters for models A+Bsin2+Csin4 (deg) and A+Bsin2+Csin4 (rad):

A: isotropic scattering intensity A

B: anisotropic \sin^2 -dependent scattering intensity B

C: anisotropic \sin^4 -dependent scattering intensity C

delta: offset of deformation direction δ in degree or radian

Note: None.

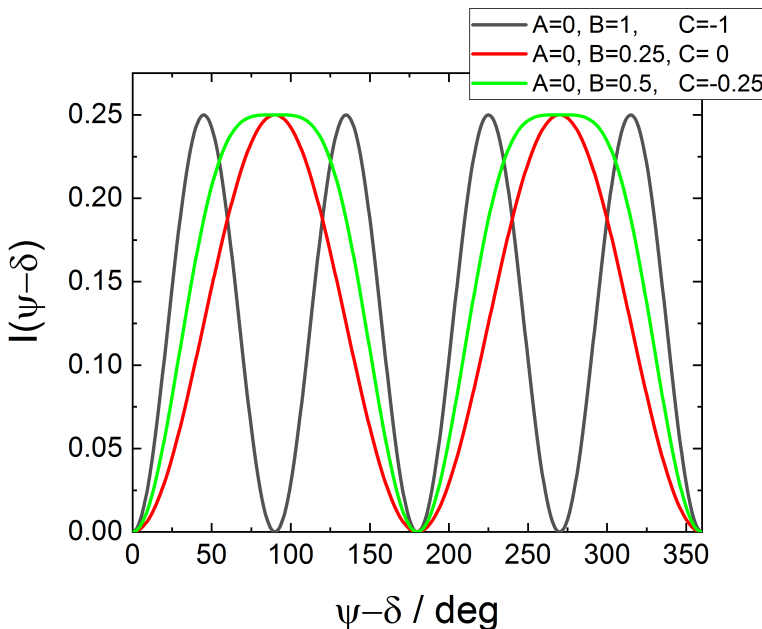


FIGURE 9.153. Azimuthal intensity distribution typical in the field of magnetic scattering

9.10.2. Ellipsoidal azimuthal analysis.

Instead of radial or sector averaged data this function describes azimuthal averaged data of deformed or textured samples with an anisotropic scattering pattern as described in [469, 338, 417, 188, 187, 436, 476, 173, 174]

$$I_{\text{rad}}(\psi) = \left(\left(\frac{\cos(\psi - \delta)}{A} \right)^2 + \left(\frac{\sin(\psi - \delta)}{B} \right)^2 \right)^{-N/2} + C \quad (9.525)$$

$$I_{\text{deg}}(\psi) = \left(\left(\frac{\cos((\psi - \delta)\frac{\pi}{180})}{A} \right)^2 + \left(\frac{\sin((\psi - \delta)\frac{\pi}{180})}{B} \right)^2 \right)^{-N/2} + C \quad (9.526)$$

Input Parameters for models elliptically averaged (deg) and elliptically averaged (rad):

A: semi-axis along $\psi - \delta = 0$ of iso-contours in reciprocal space

B: semi-axis along $\psi - \delta = \pi/2$ of iso-contours in reciprocal space

C: Amplitude A of the angle dependent intensity

delta: direction of the polarisation δ in degree or radian

Note: The reciprocal value of A and B are related to the corresponding correlation length of the scattering object in that direction.

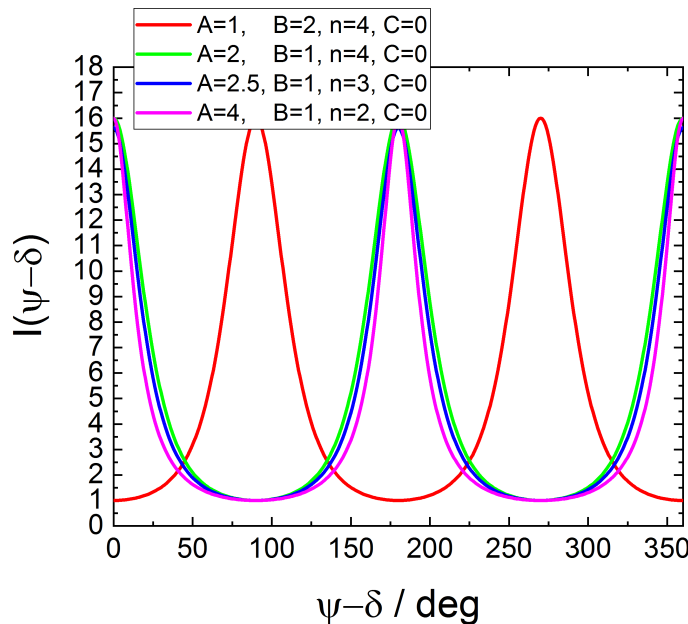


FIGURE 9.154. Azimuthal intensity distribution of the elliptically averaged model

9.10.3. affine shrinkage.

An affine deformation profile has been given by [507, 546] and reads as

$$\mathcal{I}_{\text{as}}(\psi) = \lambda^2 \frac{\cos^2 [\arctan (\lambda \tan \chi)]}{\cos^3(\chi)} \quad (9.527)$$

$$\chi = \psi - \delta \quad (9.528)$$

where λ is the degree of compression. The final model function is than normalized on the average intensity so that the azimuthal intensity distribution is given by

$$I_{\text{as}}(\chi) = I_0 + A \frac{\pi}{2} \frac{\mathcal{I}_{\text{as}}(\chi)}{\int_0^{\pi/2} \mathcal{I}_{\text{as}}(\chi) d\chi} \quad (9.529)$$

Input Parameters for models affine shrinkage (deg) and affine shrinkage (rad):

I0: flat background I_0

A: Amplitude A of the angle dependent intensity

lambda: shrinkage factor λ

delta: offset of shrinkage direction δ in degree or radian

Note: λ needs to be a positive nonzero number. $\lambda = 1$: no shrinkage, $\lambda > 1$: shrinkage, $0 < \lambda < 1$: swelling.

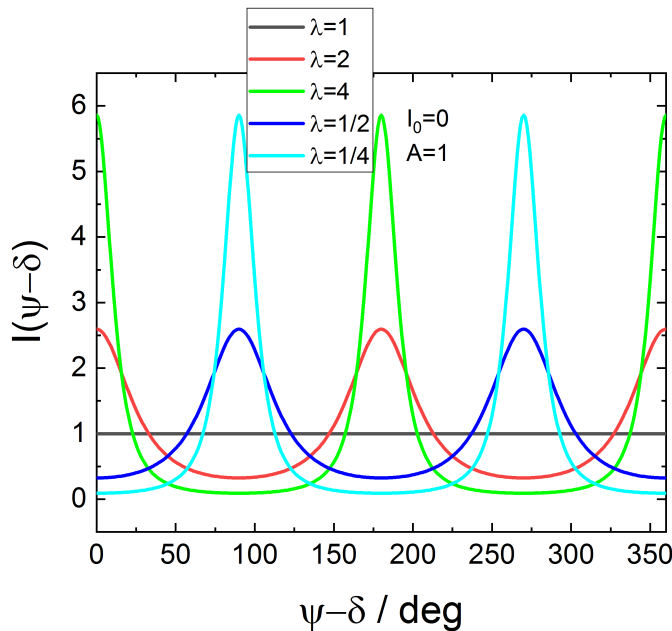


FIGURE 9.155. Azimuthal intensity distribution of the affine shrinkage model

9.10.4. Maier-Saupe azimuthal analysis.

In the Picken model [390, 120, 324] the azimuthal intensity reads as

$$\mathcal{I}_P(\chi) = \exp(\kappa \cos^2 \chi) \quad (9.530)$$

$$\chi = \psi - \delta \quad (9.531)$$

The final model function is than normalized on the average intensity so that the azimuthal intensity distribution is given by

$$I_P(\chi) = I_0 + A \frac{\pi}{2} \frac{\mathcal{I}_P(\chi)}{\int_0^{\pi/2} \mathcal{I}_P(\chi) d\chi} \quad (9.532)$$

Input Parameters for models MaierSaupe (deg) and MaierSaupe (rad):

I0: flat background I_0

A: Amplitude A of the angle dependent intensity

kappa: parameter for strength of orientation κ

delta: offset δ in degree or radian

Note: For $\kappa = 0$ the azimuthal intensity is flat, for $\kappa > 0$ the highest intensity is in the direction $\psi - \delta = 0$ and for $\kappa < 0$ in the direction $\psi - \delta = \pi/2$

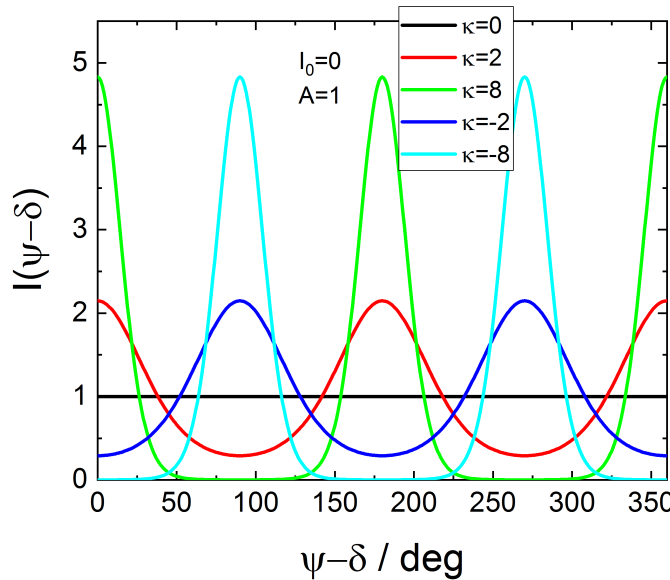


FIGURE 9.156. Azimuthal intensity distribution of the Maier-Saupe model from Picken [390]

9.10.5. azimuthal analysis of very long oriented structures with Maier-Saupe or Onsager orientation distribution.

X-ray scattering has been used to obtain order parameters of liquid crystals. A work of Leadbetter and Norris [289] describe the underlying assumptions and derived the equation

$$\mathcal{J}_{LN}(\chi) = \int_{\theta=\chi}^{\pi/2} \frac{p(\theta) \sin \theta}{\cos^2 \chi \sqrt{\tan^2 \theta - \tan^2 \chi}} d\theta \quad (9.533)$$

where $p(\theta) \sin \theta$ describe the orientation distribution of the molecular axis towards the preferred direction θ . Later on it was recognized by Burger and Ruland [68] that the formula contains an error and has to be corrected according to an equation derived earlier by Kratky [278]. The correct equation which was also re-derived by Mills [339] reads as [453, 2]

$$\mathcal{J}_K(\chi) = \int_{\theta=\chi}^{\pi/2} \frac{p(\theta) \sin \theta}{\sqrt{\cos^2 \chi - \cos^2 \theta}} d\theta = \int_{\theta=\chi}^{\pi/2} \frac{p(\theta) \sin \theta}{\sqrt{\sin^2 \theta - \sin^2 \chi}} d\theta \quad (9.534)$$

$$= \int_{\theta=\chi}^{\pi/2} \frac{p(\theta) \tan \theta}{\cos \chi \sqrt{\tan^2 \theta - \tan^2 \chi}} d\theta \quad (9.535)$$

with $\chi = \psi - \delta$. The final model function is than normalized on the average intensity so that the azimuthal intensity distribution is given by

$$I_{LN}(\chi) = I_0 + A \frac{\pi}{2} \frac{\mathcal{J}_{LN}(\chi)}{\int_0^{\pi/2} \mathcal{J}_{LN}(\chi) d\chi} \quad (9.536)$$

$$I_K(\chi) = I_0 + A \frac{\pi}{2} \frac{\mathcal{J}_K(\chi)}{\int_0^{\pi/2} \mathcal{J}_K(\chi) d\chi} \quad (9.537)$$

For the two approximations, the in principle obsolete Leadbetter and Norris one and the correct Kratky approximation, the Maier-Saupe and the Onsager orientation distribution have been implemented.

Input Parameters for models

azimuthal (long cyl.,MS,K,deg), azimuthal (long cyl.,MS,K,rad),
azimuthal (long cyl.,Onsager,K,deg), azimuthal (long cyl.,Onsager,K,rad),
azimuthal (long cyl.,MS,LN,deg), azimuthal (long cyl.,MS,LN,rad),
azimuthal (long cyl.,Onsager,LN,deg), azimuthal (long cyl.,Onsager,LN,rad):

I0: flat background I_0

A: Amplitude A of the angle dependent intensity

kappa: width κ of orientation distribution

delta: direction offset δ in degree or radian

Note:

- The integrals for $\mathcal{I}_K(\chi)$ and $\mathcal{I}_{LN}(\chi)$ around $\chi \simeq \pi/2$ become numerical unstable and are fixed to the value at $(1 - 10^{-4})\pi/2$.
- For the Maier-Saupe orientation distribution in the Kratky approximation the analytical solution given by [339] has been implemented.

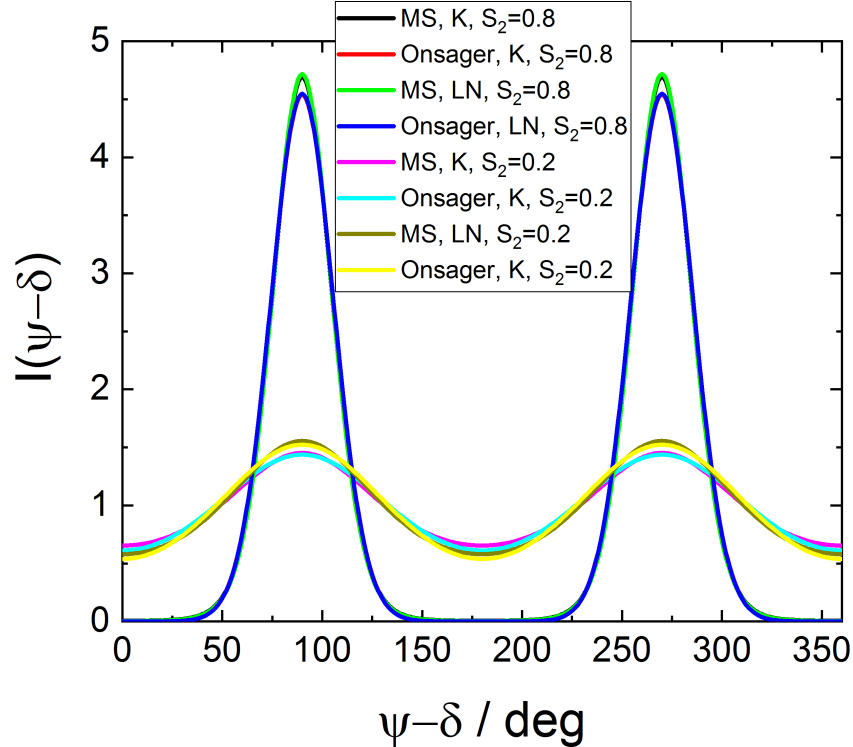
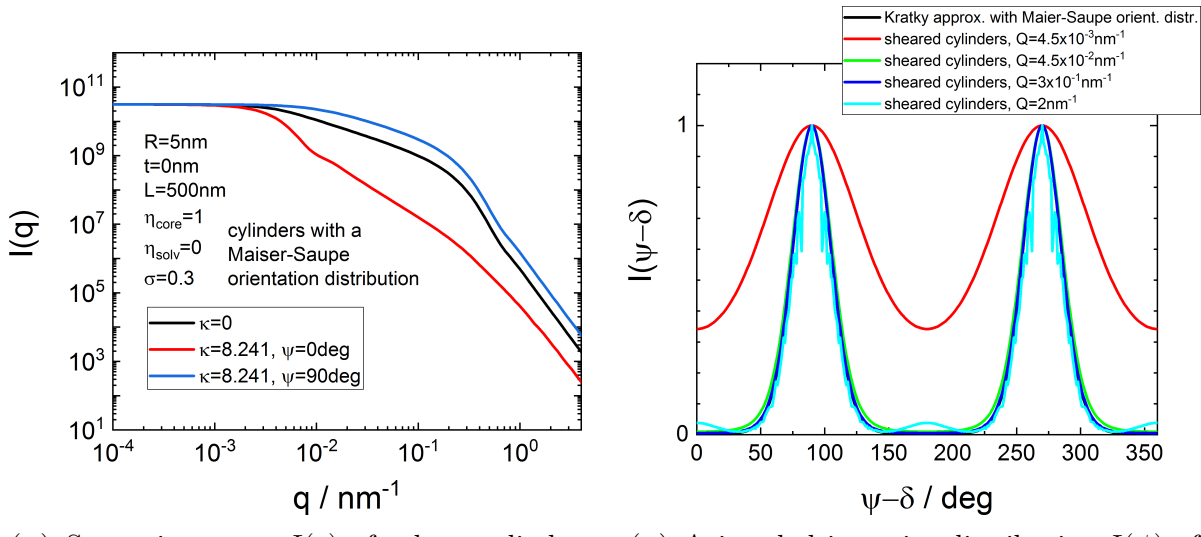


FIGURE 9.157. Azimuthal intensity distribution according to the correct Kratky approximation and the obsolete Leadbetter with a Maier-Saupe and Onsager orientation distribution. The parameters of the orientation distributions have been chosen so that their order parameter is $S_2 = 0.8$ and $S_2 = 0.2$.

9.10.6. azimuthal analysis of sheared or deformed structures.

A couple of models of sheared and deformed form factors are described in section 9.9. All these form factors have an parameter ψ describing the direction of the scattering vector towards the symmetry axis of the textured sample (e.g. due to shear or deformation). Some of these functions have been supplied so that they become a function of ψ instead of q , to be able to describe not sector averaged data $I(q; \psi, \dots)$ but rather azimuthal data at a fixed scattering vector $I(\psi; q, \dots)$. The form factor from section 9.9.6 and 9.9.7 have been made available. If the azimuthal plot is supplied by an appropriate q -value it is often an advantage not to use the full model description but rather the approximations given by the models in the previous sections 9.10.4 and 9.10.5.



(A) Scattering curve $I(q)$ of a long cylinder aligned according to a Maier-Saupe orientation distribution

(B) Azimuthal intensity distribution $I(\psi)$ of the same model as on the left

FIGURE 9.158. The approximations made by Kratky, Leadbetter and Pickens in the previous sections seems to hold in the intermediate q -range, but not in the Porod-regime or Guinier-regime of the cylinders

The input parameters are the same as those in 9.9.6 and 9.9.7, except that q and ψ have been exchanged.

Input Parameters for model

Sheared Cylinders (Maier-Saupe) azimuthal, Sheared Cylinders (Gauss) azimuthal,
Sheared Cylinders (Boltzmann) azimuthal, Sheared Cylinders (Onsager) azimuthal,
Sheared Cylinders (Heavyside) azimuthal, Sheared Cylinders (Hayter-Penfold) azimuthal:

R: radius of cylinders R

t: shell thickness t

L: cylinder length L

eta_core: scattering length density of cylinder core η_{core}

eta_shell: scattering length density of cylinder shell η_{shell}

eta_solv: scattering length density of solvent η_{solv}

Q: scattering vector Q

sigma: width parameter of lognormal size distribution σ

kappa: orientation distribution parameter κ

Input Parameters for model

Sheared Spheroids (Maier-Saupe) azimuthal, Sheared Spheroids (Gauss) azimuthal,

Sheared Spheroids (Boltzmann) azimuthal, Sheared Spheroids (Onsager) azimuthal,

Sheared Spheroids (Heavyside) azimuthal, Sheared Spheroids (Hayter-Penfold) azimuthal

R_equatorial: equatorial semi-axes of spheroids R_e

t: shell thickness t

R_polar: polar semi-axis of spheroids R_p

eta_core: scattering length density of cylinder core η_{core}

eta_shell: scattering length density of cylinder shell η_{shell}

eta_solv: scattering length density of solvent η_{solv}

Q: scattering vector Q

sigma: width parameter of lognormal size distribution σ

kappa: orientation distribution parameter κ

Note:

- The size distribution is taken simultaneously over all parameters R , t , L , and R_e , t , R_p respectively, so that their aspect ratios always stay constant.
- The numerics becomes unstable at large q -values and t the same time high order parameters.

9.11. anisotropic form factors of oriented primitive objects

In this section The scattering amplitudes of simple geometric objects are described having an arbitrary but fixed orientation as well as those which are obtained by an affine transformation. The most simple ones are unit spheres, unit cube and unit cylinder, and their affine deformed shapes of ellipsoid, oblique parallelepiped and oblique cylinder for which their \mathbf{Q} -dependent form factors $F(\mathbf{Q})$ are given analytically.

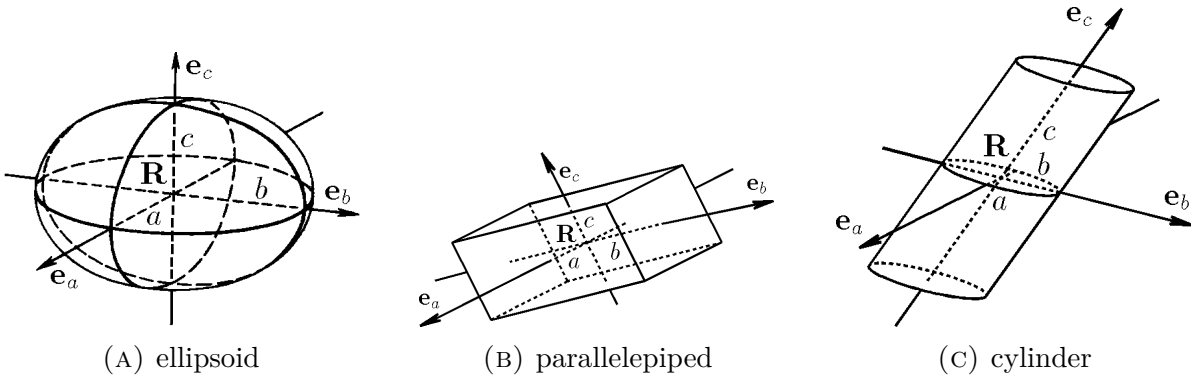


FIGURE 9.159. \mathbf{R} : object center, a, b, c : half axes/lengths, $\mathbf{e}_a, \mathbf{e}_b, \mathbf{e}_c$: directions of the half axes

The scattering amplitude $F(\mathbf{Q})$ of an object is given by the Fourier transform of the scattering length density distribution within the object

$$F(\mathbf{Q}) = \int_V d\mathbf{r} \eta(\mathbf{r}) e^{i\mathbf{Q}\mathbf{r}}, \quad (9.538)$$

where $\eta(\mathbf{r})$ is the scattering length density distribution of the scattering object and V the sample volume. In the following it is assumed that the particles have a homogeneous scattering length density η_P , embedded in a matrix of also homogeneous scattering length density $\eta_M = \eta_P - \Delta\eta$. The position, orientation and size of the objects is uniquely defined by the center of scattering length density \mathbf{R} , the half axes a, b and c , as well as the direction of the half axes $\mathbf{e}_a, \mathbf{e}_b$ and \mathbf{e}_c . The base vectors \mathbf{e}_i are normalized $|\mathbf{e}_i| = 1$ but do not need to be orthogonal to each other. For the scattering amplitude of an individual objects one gets after a translation by $-\mathbf{R}$ and a following change of basis $\underline{\mathbf{D}}$ from cartesian coordinates $O_{xyz} = \{\mathbf{e}_x, \mathbf{e}_y, \mathbf{e}_z\}$ into the coordinate system of the particle $O_{abc} = \{a\mathbf{e}_a, b\mathbf{e}_b, c\mathbf{e}_c\}$, so that $\mathbf{P}_{O_{abc}} = \underline{\mathbf{D}} \mathbf{P}_{O_{xyz}}$

$$F(\mathbf{Q}) = e^{-i\mathbf{Q}\mathbf{R}} \Delta\eta \int_{V(0)} d\mathbf{r} e^{i\mathbf{Q}(\underline{\mathbf{D}}^{-1} \underline{\mathbf{D}}\mathbf{r})} \quad (9.539)$$

$$= \det(\underline{\mathbf{D}}^{-1}) e^{-i\mathbf{Q}\mathbf{R}} \Delta\eta \int_{\underline{\mathbf{D}}V(0)} d\mathbf{r} e^{i\hat{\mathbf{Q}}\mathbf{r}} \quad (9.540)$$

with

$$\hat{\mathbf{Q}} = (\underline{\mathbf{D}}^{-1})^T \mathbf{Q} = \begin{pmatrix} a \mathbf{e}_a \mathbf{Q} \\ b \mathbf{e}_b \mathbf{Q} \\ c \mathbf{e}_c \mathbf{Q} \end{pmatrix} \quad (9.541)$$

$V(\mathbf{0})$ is the volume of the scattering object a scattering length density center located at the origin of the coordinate system and $\underline{\mathbf{D}}V(\mathbf{0})$ is the volume of the unit object, i.e. unit sphere, unit cube or unit cylinder. The transformation matrix $\underline{\mathbf{D}}$ and its inverse $\underline{\mathbf{D}}^{-1}$ are given by

$$\underline{\mathbf{D}}^{-1} = \begin{pmatrix} a e_{ax} & b e_{bx} & c e_{cx} \\ a e_{ay} & b e_{by} & c e_{cy} \\ a e_{az} & b e_{bz} & c e_{cz} \end{pmatrix} = (a\mathbf{e}_a, b\mathbf{e}_b, c\mathbf{e}_c) \quad (9.542)$$

$$\mathbf{Q}(\underline{\mathbf{D}}^{-1}\mathbf{r}) = ((\underline{\mathbf{D}}^{-1})^T \mathbf{Q})\mathbf{r}, \quad (9.543)$$

$$\det(\underline{\mathbf{D}}^{-1}) = abc(e_{ax}e_{by}e_{cz} + e_{ay}e_{bz}e_{cx} + e_{az}e_{bx}e_{cy} - e_{az}e_{by}e_{cx} - e_{ay}e_{bx}e_{cz} - e_{ax}e_{bz}e_{cy}) \quad (9.544)$$

$$\begin{aligned} \underline{\mathbf{D}} = (\underline{\mathbf{D}}^{-1})^{-1} &= \frac{1}{\det(\underline{\mathbf{D}}^{-1})} (\underline{\mathbf{D}}^{-1})^{\text{adj}} \\ &= \frac{1}{\det(\underline{\mathbf{D}}^{-1})} (b\mathbf{e}_b \times c\mathbf{e}_c, -a\mathbf{e}_a \times c\mathbf{e}_c, a\mathbf{e}_a \times b\mathbf{e}_b) \end{aligned} \quad (9.545)$$

whereas $\det(\underline{\mathbf{D}}) \det(\underline{\mathbf{D}}^{-1}) = \det(\underline{\mathbf{D}} \underline{\mathbf{D}}^{-1}) = \det(\mathbf{I}) = 1$

To reorient or rotate the objects one simply changes the direction of the base vectors \mathbf{e}_a , \mathbf{e}_b , \mathbf{e}_c which is done by introducing a rotation matrix $\underline{\mathbf{R}}_{\alpha\beta\gamma}$. The rotation matrix can be defined via Euler angles α , β , and γ . Its definition depends on the convention. There exist twelve possible sequences of rotation axes, divided in two groups: proper Euler angles (z - x - z , x - y - x , y - z - y , z - y - z , x - z - x , y - x - y), Tait–Bryan angles (x - y - z , y - z - x , z - x - y , x - z - y , z - y - x , y - x - z). The difference between the two conventions is that Tait–Bryan angles represent rotations about three distinct axes, while proper Euler angles use the same axis for both the first and third elemental rotations. **SASfit** allows internally to use any of the 12 conventions. However, as default conventions the yaw-pitch-roll is used (also named gier-nick-roll, east-north-up, north-East-Down, or z - y - x), so that

$$\hat{\mathbf{Q}} = \begin{pmatrix} a \underline{\mathbf{R}}_{\alpha\beta\gamma} \mathbf{e}_a \mathbf{Q} \\ b \underline{\mathbf{R}}_{\alpha\beta\gamma} \mathbf{e}_b \mathbf{Q} \\ c \underline{\mathbf{R}}_{\alpha\beta\gamma} \mathbf{e}_c \mathbf{Q} \end{pmatrix} \quad (9.546)$$

Next to the form factor of an oriented primitive object also the form factor of its fully randomly oriented version is made available. The orientational average is done by integrating over the full Ewald’s sphere, which is a double integration. **SASfit** supplies for this orientational average separate integration routines which can be configured via the GUI. Next to the multidimensional adaptive integration routines **pcubature** and **hcubature** from [245] also some other routines are supplied, which however are non-adaptive without error estimate of the integral but optimized for integrations over a

sphere surface. Nevertheless, these routines often need significant less function evaluations than a conventional multidimensional integration routines. The implemented methods are a 2D-GaussLegendre integration, Lebedev [291, 292, 293] and Fibonacci [356, 329] quadrature algorithm with a fixed and configurable number of function evaluations and without error estimation of the integral.

9.11.1. perfect and random oriented ellipsoid.

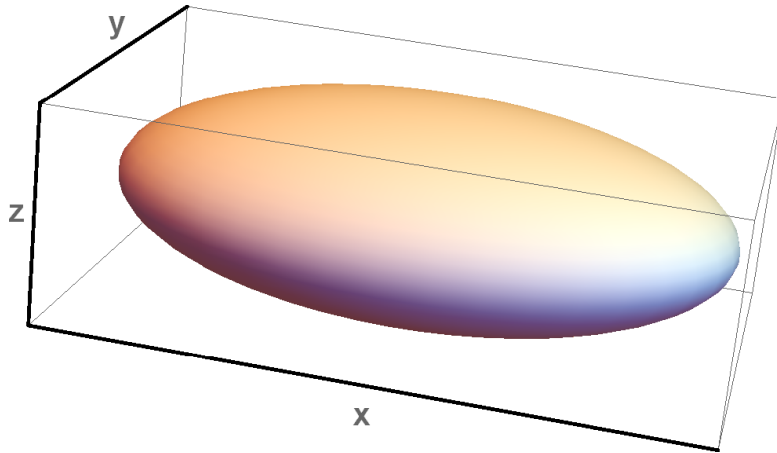


FIGURE 9.160. ellipsoid with semi-axis $(a : b : c) = (3 : 2 : 1)$ and $\alpha = \beta = \gamma = 0$

This form factor describes an oblique ellipsoid with half axis a , b , and c , which is obtained by an affine transformation of an unit sphere. The detector plane is in the xy -plane and the incident beam in the $-z$ -direction. The unit vectors \mathbf{e}_a , \mathbf{e}_b , and \mathbf{e}_c are assumed in this example pointing into the directions of the three orthogonal axis \mathbf{e}_x , \mathbf{e}_y , and \mathbf{e}_z and therefore represent a triaxial ellipsoid.

$$\begin{aligned} F_E(\mathbf{Q}) &= \det(\underline{\mathbf{D}}^{-1}) e^{-i\mathbf{QR}} \Delta\eta \int_0^1 dr r^2 \int_0^\pi d\theta \sin\theta \int_0^{2\pi} d\phi e^{i\hat{\mathbf{Q}}r} \\ &= 4\pi \det(\underline{\mathbf{D}}^{-1}) e^{-i\mathbf{QR}} \Delta\eta \frac{\sin|\hat{\mathbf{Q}}| - |\hat{\mathbf{Q}}|\cos|\hat{\mathbf{Q}}|}{|\hat{\mathbf{Q}}|^3} \end{aligned} \quad (9.547)$$

For a random oriented ellipsoid one either can integrate over all Euler-angle, which is a tripble integration or over all orientations of \mathbf{Q} , which is a double integration and performed for the randomized form factor. The corresponding scattering amplitude

$F_{E,rnd}$ and scattering intensity $P_{E,rnd}$ are then given by

$$F_{E,rnd}(Q) = \langle F_E(\mathbf{Q}) \rangle_{\mathbf{Q}} = \int_0^{\pi} d\theta \int_0^{2\pi} d\phi F_E \left(Q \begin{pmatrix} \cos(\phi) \sin(\theta) \\ \sin(\phi) \sin(\theta) \\ \cos(\theta) \end{pmatrix} \right) \quad (9.548)$$

$$P_{E,rnd}(Q) = \langle F_E^2(\mathbf{Q}) \rangle_{\mathbf{Q}} = \int_0^{\pi} d\theta \int_0^{2\pi} d\phi F_E^2 \left(Q \begin{pmatrix} \cos(\phi) \sin(\theta) \\ \sin(\phi) \sin(\theta) \\ \cos(\theta) \end{pmatrix} \right) \quad (9.549)$$

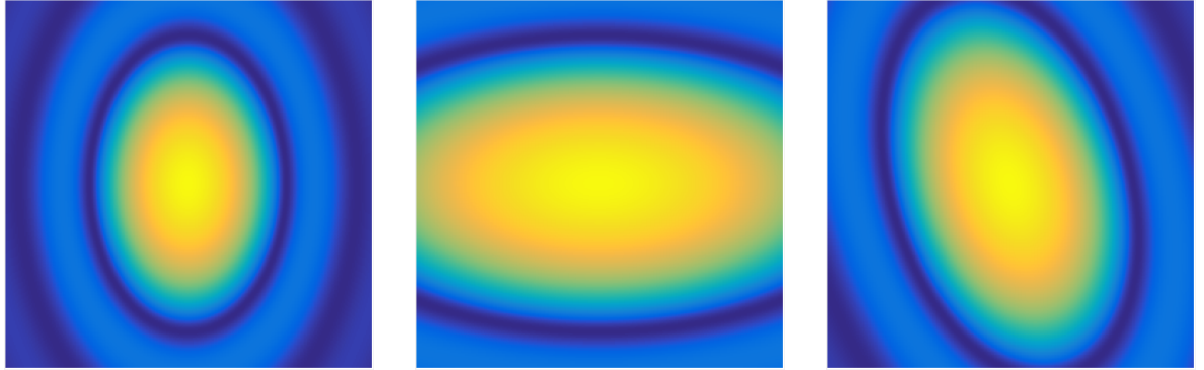


FIGURE 9.161. Scattering patterns at 18m detector distance and a wavelength of $\lambda = 0.6\text{nm}$. The ellipsoids are simulated with radii of $a = 30\text{nm}$, $b = 20\text{nm}$, and $c = 10\text{nm}$. The Tait–Bryan angles (yaw-pitch-roll) are $(\alpha = 0^\circ, \beta = 0^\circ, \gamma = 0^\circ)$, $(\alpha = 0^\circ, \beta = 90^\circ, \gamma = 0^\circ)$, and $(\alpha = 0^\circ, \beta = 45^\circ, \gamma = 45^\circ)$

Input Parameters for model `ellipsoid` (`opo`):

- a:** length of first half axis
- ea_x:** x -component of fist axis.
- ea_y:** y -component of fist axis.
- ea_z:** z -component of fist axis.
- b:** length of second half axis
- eb_x:** x -component of second axis.
- eb_y:** y -component of second axis.
- eb_z:** z -component of second axis.
- c:** length of third half axis
- ec_x:** x -component of third axis.
- ec_y:** y -component of third axis.
- ec_z:** z -component of third axis.
- eta_p:** scattering length density η_p of particle
- eta_m:** scattering length density η_m of matrix
- alpha:** first Euler angle
- beta:** second Euler angle
- gamma:** third Euler angle
- psi:** direction of \mathbf{Q} on detector ($\psi = 0$, x -direction, to the right)

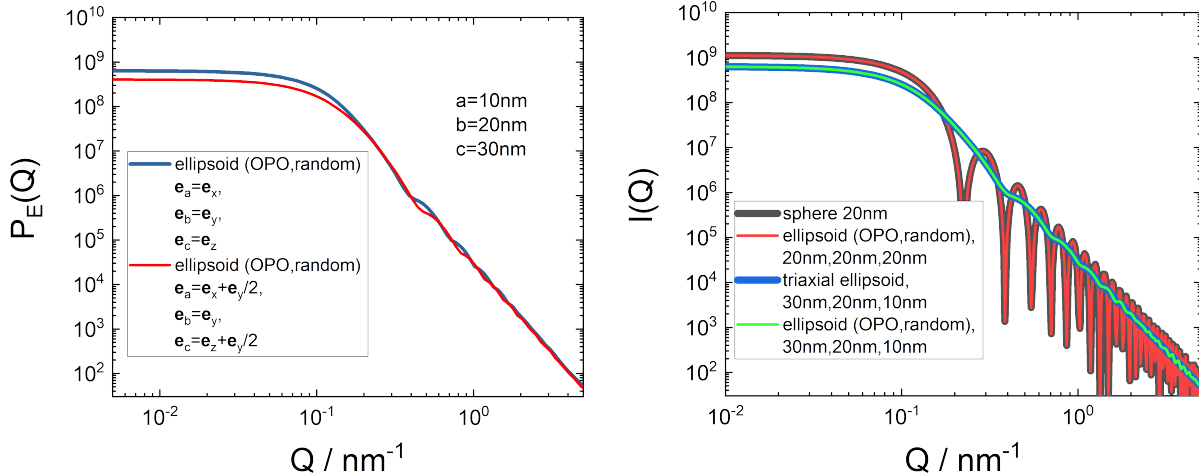


FIGURE 9.162. scattering curved of an oblique ellipsoid (OPO, random) (left) and a comparison with a sphere and a triaxial ellipsoid form factor (right)

Input Parameters for model ellipsoid (opo, random):

a: length of first half axis
ea_x: x -component of fist axis.
ea_y: y -component of fist axis.
ea_z: z -component of fist axis.
b: length of second half axis
eb_x: x -component of second axis.
eb_y: y -component of second axis.
eb_z: z -component of second axis.
c: length of third half axis
ec_x: x -component of third axis.
ec_y: y -component of third axis.
ec_z: z -component of third axis.
eta_p: scattering length density η_p of particle
eta_m: scattering length density η_m of matrix

Note:

- the unit vector \mathbf{e}_a , \mathbf{e}_b , and \mathbf{e}_c are internally normalized to 1 and need to be linear independent.
- the volume of the oblique ellipsoid is $V_E = \frac{4}{3} \det(\mathbf{D}^{-1})$

9.11.2. perfect and random oriented parallelepiped.

This form factor describes an oblique parallelepiped which is obtained by an affine transformation of an unit cube with half edge lengths of a , b , and c . The detector plane is in the xy -plane and the incident beam in the $-z$ -direction.

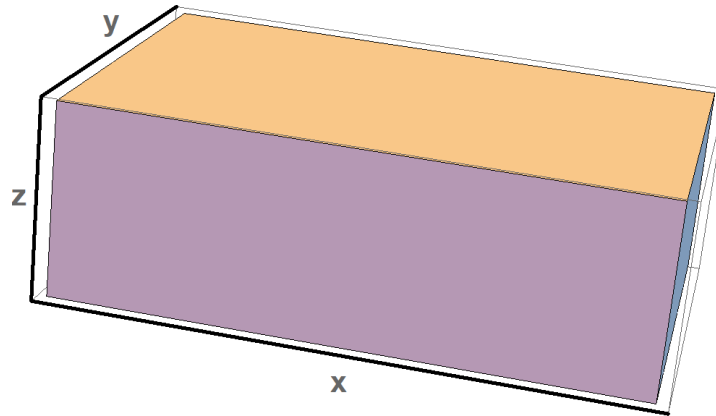


FIGURE 9.163. parallelepiped with half edge length $(a : b : c) = (3 : 2 : 1)$ and $\alpha = \beta = \gamma = 0$

$$\begin{aligned} F_P(\mathbf{Q}) &= \det(\underline{\mathbf{D}}^{-1}) e^{-i\mathbf{QR}} \Delta\eta \int_{-1}^1 dx \int_{-1}^1 dy \int_{-1}^1 dz e^{i\hat{\mathbf{Q}}\mathbf{r}} \\ &= 8 \det(\underline{\mathbf{D}}^{-1}) e^{-i\mathbf{QR}} \Delta\eta \frac{\sin \hat{\mathbf{Q}} \mathbf{e}_x}{\hat{\mathbf{Q}} \mathbf{e}_x} \frac{\sin \hat{\mathbf{Q}} \mathbf{e}_y}{\hat{\mathbf{Q}} \mathbf{e}_y} \frac{\sin \hat{\mathbf{Q}} \mathbf{e}_z}{\hat{\mathbf{Q}} \mathbf{e}_z} \end{aligned} \quad (9.550)$$

For a random oriented parallelepiped the orientation average is done over all directions of \mathbf{Q} . The corresponding scattering amplitude $F_{E,rnd}$ and scattering intensity $P_{E,rnd}$ are then given by

$$F_{P,rnd}(Q) = \langle F_P(\mathbf{Q}) \rangle_{\mathbf{Q}} = \int_0^\pi d\theta \int_0^{2\pi} d\phi F_P \left(Q \begin{pmatrix} \cos(\phi) \sin(\theta) \\ \sin(\phi) \sin(\theta) \\ \cos(\theta) \end{pmatrix} \right) \quad (9.551)$$

$$P_{P,rnd}(Q) = \langle F_P^2(\mathbf{Q}) \rangle_{\mathbf{Q}} = \int_0^\pi d\theta \int_0^{2\pi} d\phi F_P^2 \left(Q \begin{pmatrix} \cos(\phi) \sin(\theta) \\ \sin(\phi) \sin(\theta) \\ \cos(\theta) \end{pmatrix} \right) \quad (9.552)$$

Input Parameters for model parallelepiped (opo):

- a:** length of first half axis
- ea_x:** x -component of fist axis.
- ea_y:** y -component of fist axis.
- ea_z:** z -component of fist axis.
- b:** length of second half axis
- eb_x:** x -component of second axis.
- eb_y:** y -component of second axis.
- eb_z:** z -component of second axis.
- c:** length of third half axis
- ec_x:** x -component of third axis.
- ec_y:** y -component of third axis.
- ec_z:** z -component of third axis.

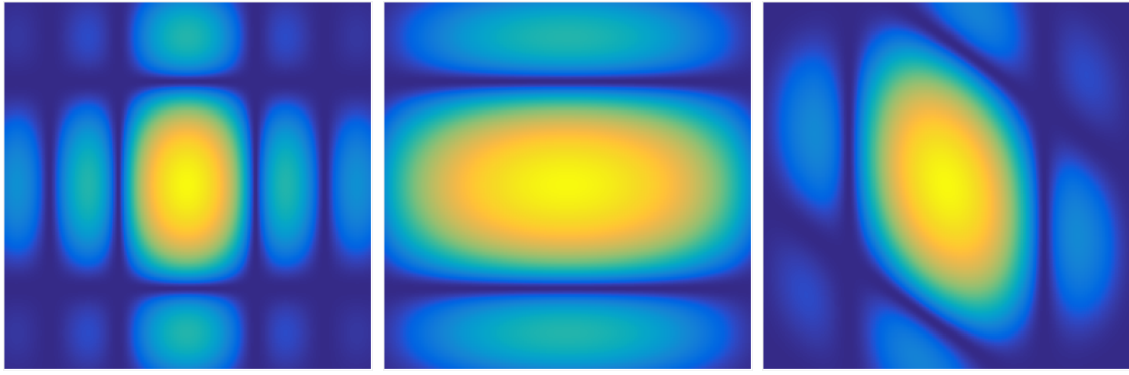


FIGURE 9.164. Scattering patterns at 18m detector distance and a wavelength of $\lambda = 0.6\text{nm}$. The parallelepipeds are simulated with half edge length of $a = 30\text{nm}$, $b = 20\text{nm}$, and $c = 10\text{nm}$. The Tait–Bryan angles (yaw–pitch–roll) are $(\alpha = 0^\circ, \beta = 0^\circ, \gamma = 0^\circ)$, $(\alpha = 0^\circ, \beta = 90^\circ, \gamma = 0^\circ)$, and $(\alpha = 0^\circ, \beta = 45^\circ, \gamma = 45^\circ)$

eta_p: scattering length density η_p of particle

eta_m: scattering length density η_m of matrix

alpha: first Euler angle

beta: second Euler angle

gamma: third Euler angle

psi: direction of \mathbf{Q} on detector ($\psi = 0$, x -direction, to the right)

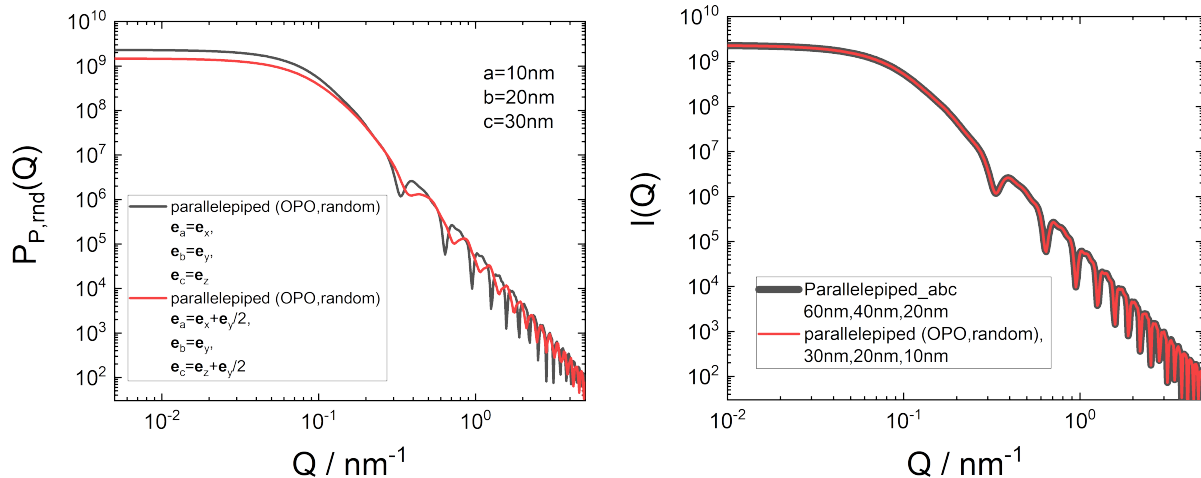


FIGURE 9.165. scattering curved of an oblique parallelepiped (OPO,random) (left) and a comparison of an parallelepiped (OPO,random) (using length of half axis) and Parallelepiped_abc (using full edge length) form factor (right)

Input Parameters for model parallelepiped (opo, random):

a: length of first half axis

ea_x: x -component of fist axis.
ea_y: y -component of fist axis.
ea_z: z -component of fist axis.
b: length of second half axis
eb_x: x -component of second axis.
eb_y: y -component of second axis.
eb_z: z -component of second axis.
c: length of third half axis
ec_x: x -component of third axis.
ec_y: y -component of third axis.
ec_z: z -component of third axis.
eta_p: scattering length density η_p of particle
eta_m: scattering length density η_m of matrix

Note:

- the unit vector \mathbf{e}_a , \mathbf{e}_b , and \mathbf{e}_c are internally normalized to 1 and need to be linear independent.
- the volume of the oblique parallelepiped is $V_P = 8 \det(\underline{\mathbf{D}}^{-1})$

9.11.3. perfect and random oriented cylinder.

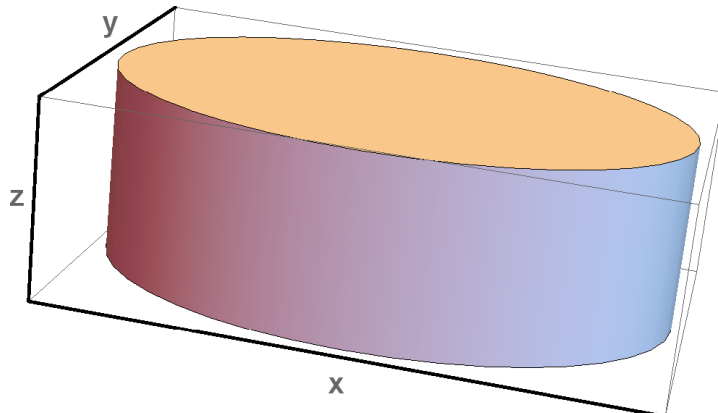


FIGURE 9.166. cylinder with radii a and b and half height c . The axis ratios of the cylinder shown are $(a : b : c) = (3 : 2 : 1)$ and $\alpha = \beta = \gamma = 0$

This form factor describes an oblique cylinder which is obtained by an affine transformation of an unit cylinder with radii a and b and half height c . The detector plane is in the xy -plane and the incident beam in the $-z$ -direction.

$$\begin{aligned}
F_C(\mathbf{Q}) &= \det(\underline{\mathbf{D}}^{-1}) e^{-i\mathbf{QR}} \Delta\eta \int_{-1}^1 dz \int_0^1 dr r \int_0^{2\pi} d\phi e^{i\hat{\mathbf{Q}}\mathbf{r}} \\
&= 4\pi \det(\underline{\mathbf{D}}^{-1}) e^{-i\mathbf{QR}} \Delta\eta \frac{\sin \hat{\mathbf{Q}}\mathbf{e}_z}{\hat{\mathbf{Q}}\mathbf{e}_z} \int_0^1 dr r J_0 \left(r \sqrt{(\hat{\mathbf{Q}}\mathbf{e}_x)^2 + (\hat{\mathbf{Q}}\mathbf{e}_y)^2} \right) \\
&= 8\pi \det(\underline{\mathbf{D}}^{-1}) e^{-i\mathbf{QR}} \Delta\eta \frac{\sin \hat{\mathbf{Q}}\mathbf{e}_z}{\hat{\mathbf{Q}}\mathbf{e}_z} \frac{J_1 \left(\sqrt{(\hat{\mathbf{Q}}\mathbf{e}_x)^2 + (\hat{\mathbf{Q}}\mathbf{e}_y)^2} \right)}{\sqrt{(\hat{\mathbf{Q}}\mathbf{e}_x)^2 + (\hat{\mathbf{Q}}\mathbf{e}_y)^2}} \quad (9.553)
\end{aligned}$$

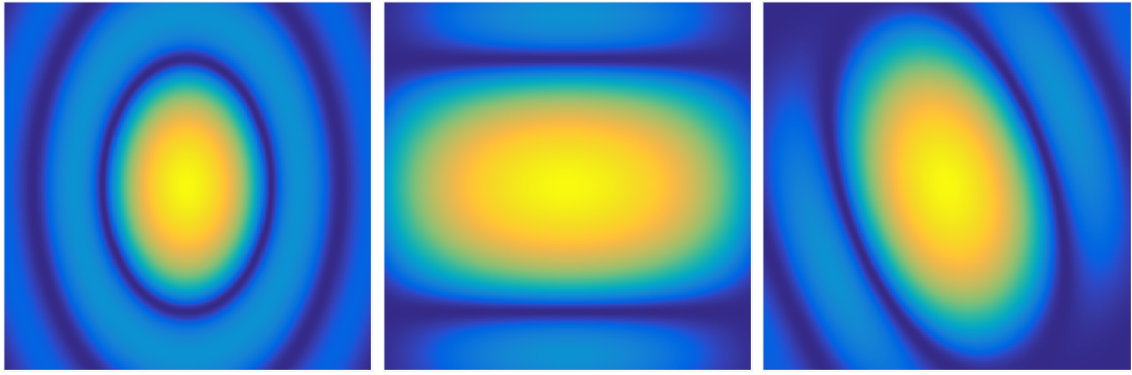


FIGURE 9.167. Scattering patterns at 18m detector distance and a wavelength of $\lambda = 0.6\text{nm}$. The cylinders are simulated with radii of $a = 30\text{nm}$, $b = 20\text{nm}$, and half height length $c = 10\text{nm}$. The Tait–Bryan angles (yaw–pitch–roll) are $(\alpha = 0^\circ, \beta = 0^\circ, \gamma = 0^\circ)$, $(\alpha = 0^\circ, \beta = 90^\circ, \gamma = 0^\circ)$, and $(\alpha = 0^\circ, \beta = 45^\circ, \gamma = 45^\circ)$

For a random oriented oblique cylinder the orientation average is done over all directions of \mathbf{Q} . The corresponding scattering amplitude $F_{C,rnd}$ and scattering intensity $P_{C,rnd}$ are then given by

$$F_{C,rnd}(Q) = \langle F_C(\mathbf{Q}) \rangle_{\mathbf{Q}} = \int_0^\pi d\theta \int_0^{2\pi} d\phi F_C \left(Q \begin{pmatrix} \cos(\phi) \sin(\theta) \\ \sin(\phi) \sin(\theta) \\ \cos(\theta) \end{pmatrix} \right) \quad (9.554)$$

$$P_{C,rnd}(Q) = \langle F_C^2(\mathbf{Q}) \rangle_{\mathbf{Q}} = \int_0^\pi d\theta \int_0^{2\pi} d\phi F_C^2 \left(Q \begin{pmatrix} \cos(\phi) \sin(\theta) \\ \sin(\phi) \sin(\theta) \\ \cos(\theta) \end{pmatrix} \right) \quad (9.555)$$

Input Parameters for model cylinder (opo):

- a:** length of first half axis
- ea_x:** x -component of fist axis.
- ea_y:** y -component of fist axis.
- ea_z:** z -component of fist axis.
- b:** length of second half axis

eb_x: x -component of second axis.
eb_y: y -component of second axis.
eb_z: z -component of second axis.
c: length of third half axis
ec_x: x -component of third axis.
ec_y: y -component of third axis.
ec_z: z -component of third axis.
eta_p: scattering length density η_p of particle
eta_m: scattering length density η_m of matrix
alpha: first Euler angle
beta: second Euler angle
gamma: third Euler angle
psi: direction of \mathbf{Q} on detector ($\psi = 0$, x -direction, to the right)

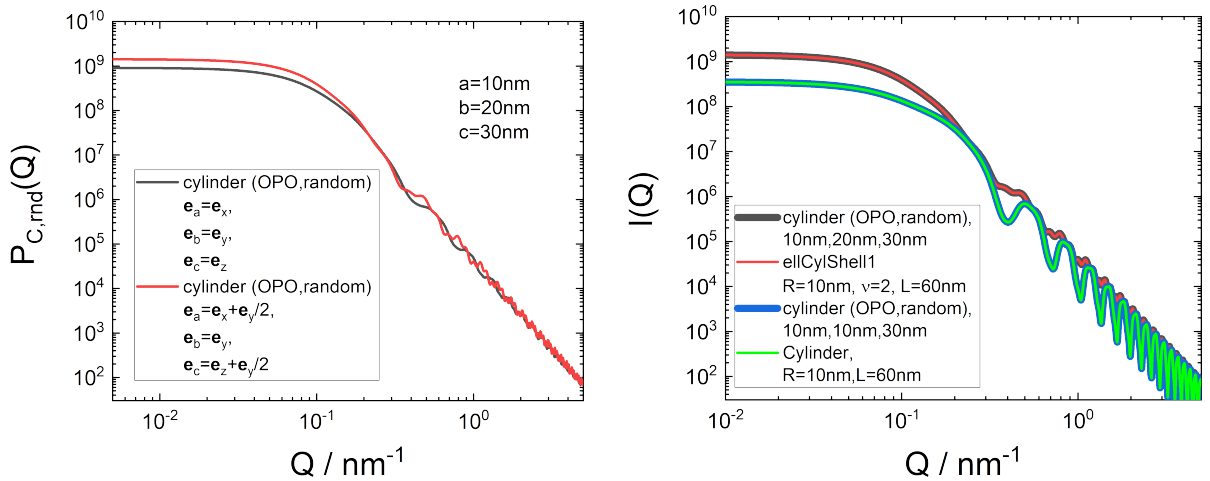


FIGURE 9.168. scattering curved of an oblique cylinder (OPO,random) (left) and a comparison of an parallelepiped (OPO,random) with an elliptical cylindrical shell ellCylShell1 and a random oriented solid cylinder form factor (right)

Input Parameters for model cylinder (opo, random):

a: length of first half axis
ea_x: x -component of fist axis.
ea_y: y -component of fist axis.
ea_z: z -component of fist axis.
b: length of second half axis
eb_x: x -component of second axis.
eb_y: y -component of second axis.
eb_z: z -component of second axis.
c: length of third half axis
ec_x: x -component of third axis.
ec_y: y -component of third axis.

ec_z: z -component of third axis.

eta_p: scattering length density η_p of particle

eta_m: scattering length density η_m of matrix

Note:

- the unit vector \mathbf{e}_a , \mathbf{e}_b , and \mathbf{e}_c are internally normalized to 1 and need to be linear independent.
- the volume of the oblique cylinder is $V_C = 2\pi \det(\mathbf{D}^{-1})$

9.11.4. oriented and random oriented cone.

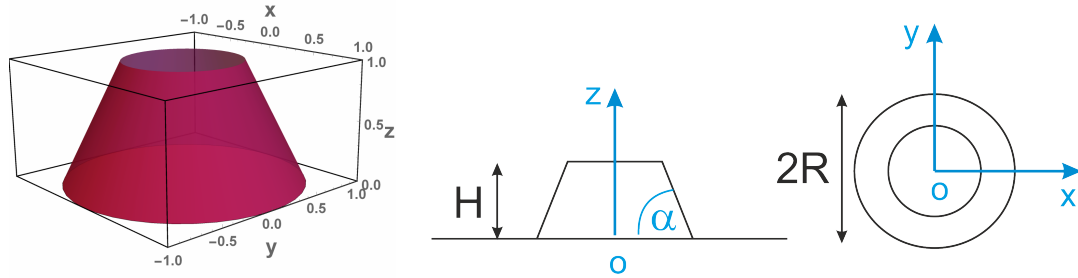


FIGURE 9.169. unit cone of radius $R = 1$, height H_R and tilting angle α_{tilt} .

The basic formula for the form factor of a blunted cone has been taken from [415]. The difference to that version is that the affine transformation from above is used to scale the size of the cone. This is also the reason why the ratio of the height and radius $H_R = \frac{H}{R}$ is used as an input parameter instead of H and R separately, i.e. a unit cone is assumed to have a radius of $R = 1$. The overall size is then scaled with the input parameters a , b and c . The shape does not have inversion symmetry and is therefore a complex function. The phase factor is taken so that the base plane lies in the xy -plane according to fig. 9.169. The form factor of the cone according to [415] is given as

$$F_{\text{cone}}(\mathbf{Q}, R, H, \alpha_{\text{tilt}}) = \int_0^H 2\pi R_z^2 \frac{J_1(q_{\parallel} R_z)}{q_{\parallel} R_z} e^{i\tilde{Q}_z z} dz \quad (9.556)$$

$$q_{\parallel} = \sqrt{\tilde{Q}_x^2 + \tilde{Q}_y^2} \quad (9.557)$$

$$R_z = R - z \cot(\alpha_{\text{tilt}}) \quad (9.558)$$

$$\frac{H}{R} < \tan(\alpha_{\text{tilt}}) \quad (9.559)$$

For a random oriented oblique cone the orientation average is done over all directions of \mathbf{Q} . The corresponding scattering amplitude $F_{\text{cone},rnd}$ and scattering intensity $P_{\text{cone},rnd}$

are then given by

$$F_{\text{cone},\text{rnd}}(Q) = \langle F_{\text{cone}}(\mathbf{Q}) \rangle_{\mathbf{Q}} = \int_0^{\pi} d\theta \int_0^{2\pi} d\phi F_{\text{cone}} \left(Q \begin{pmatrix} \cos(\phi) \sin(\theta) \\ \sin(\phi) \sin(\theta) \\ \cos(\theta) \end{pmatrix} \right) \quad (9.560)$$

$$P_{\text{cone},\text{rnd}}(Q) = \langle F_{\text{cone}}^2(\mathbf{Q}) \rangle_{\mathbf{Q}} = \int_0^{\pi} d\theta \int_0^{2\pi} d\phi F_{\text{cone}}^2 \left(Q \begin{pmatrix} \cos(\phi) \sin(\theta) \\ \sin(\phi) \sin(\theta) \\ \cos(\theta) \end{pmatrix} \right) \quad (9.561)$$

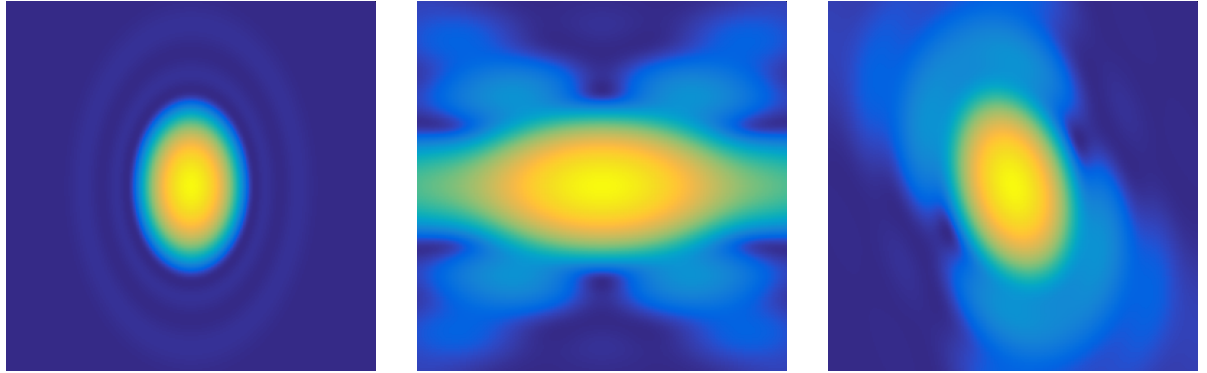


FIGURE 9.170. Scattering patterns at 18m detector distance and a wavelength of $\lambda = 0.6\text{nm}$. The cones are simulated with half axis length of $a = 30\text{nm}$, $b = 20\text{nm}$, and $c = 10\text{nm}$ and $\alpha_{\text{tilt}} = \arctan(2)$ and $H_R = 2$. The Tait–Bryan angles (yaw-pitch-roll) are $(\alpha = 0^\circ, \beta = 0^\circ, \gamma = 0^\circ)$, $(\alpha = 0^\circ, \beta = 90^\circ, \gamma = 0^\circ)$, and $(\alpha = 0^\circ, \beta = 45^\circ, \gamma = 45^\circ)$

Input Parameters for model cone (opo):

a: length of first half axis

ea_x: x -component of fist axis.

ea_y: y -component of fist axis.

ea_z: z -component of fist axis.

b: length of second half axis

eb_x: x -component of second axis.

eb_y: y -component of second axis.

eb_z: z -component of second axis.

c: length of third axis

ec_x: x -component of third axis.

ec_y: y -component of third axis.

ec_z: z -component of third axis.

eta_p: scattering length density η_p of particle

eta_m: scattering length density η_m of matrix

alpha: first Euler angle

beta: second Euler angle

gamma: third Euler angle

psi: direction of \mathbf{Q} on detector ($\psi = 0$, x -direction, to the right)

tilt: tilt angle α_{tilt} of conical side wall of unit cone

H_R: height of unit cone $H_R = H/R$

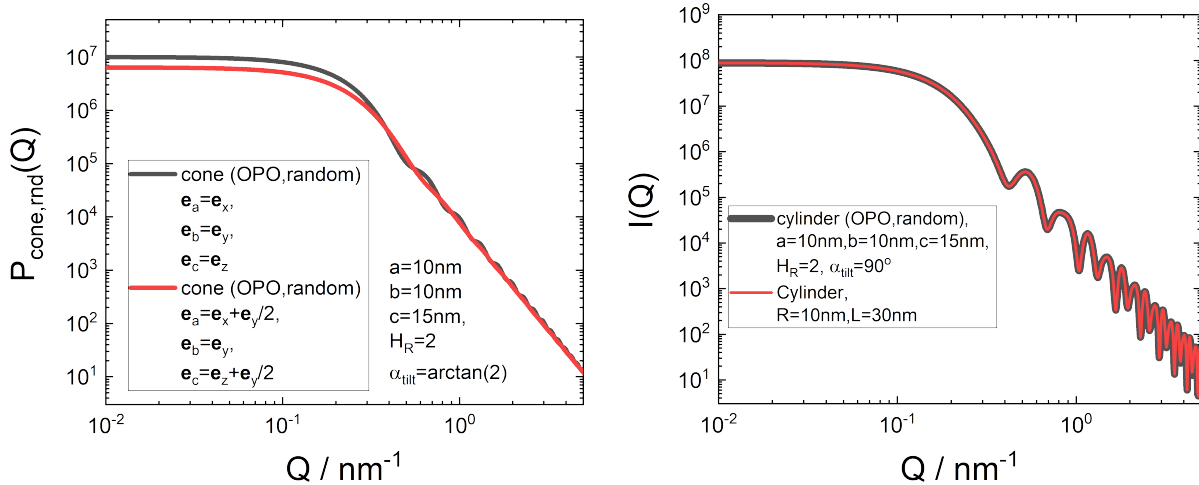


FIGURE 9.171. scattering curved of an oblique cone (OPO,random) (left) and a comparison of a cone (OPO,random) with a random oriented solid cylinder Cylinder form factor (right)

Input Parameters for model cone (opo, random):

a: length of first half axis
ea_x: x -component of fist axis.
ea_y: y -component of fist axis.
ea_z: z -component of fist axis.
b: length of second half axis
eb_x: x -component of second axis.
eb_y: y -component of second axis.
eb_z: z -component of second axis.
c: length of third axis
ec_x: x -component of third axis.
ec_y: y -component of third axis.
ec_z: z -component of third axis.
eta_p: scattering length density η_p of particle
eta_m: scattering length density η_m of matrix
dummy: not used
dummy: not used
dummy: not used
dummy: not used
tilt: tilt angle α_{tilt} of conical side wall of aunit cone
H_R: height of unit cone H_R

Note:

- the unit vector \mathbf{e}_a , \mathbf{e}_b , and \mathbf{e}_c are internally normalized to 1 and need to be linear independent.

- a and b are the half axis or radii of the elliptical base and cH_R the full height of the cone.
- the volume of the oblique cone is

$$V_{\text{cone}} = \frac{\pi}{3} \tan(\alpha_{\text{tilt}}) \left[1 - \left(1 - \frac{H_R}{\tan(\alpha_{\text{tilt}})} \right)^3 \right] \det(\underline{\mathbf{D}}^{-1})$$

9.11.5. oriented and random oriented cone with 6-fold symmetry.

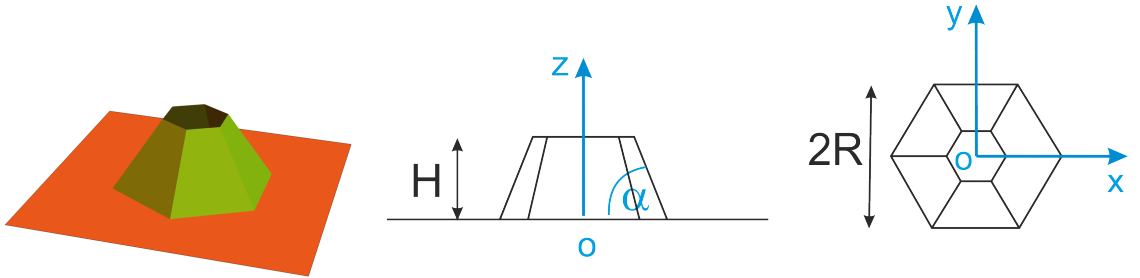


FIGURE 9.172. unit cone with 6-fold symmetry (blunted hexagonal pyramid), diameter of $2R = 2$, height H_R and tilting angle α_{tilt} .

The basic formula for the form factor of a cone with a 6-fold symmetry (blunted hexagonal pyramid) has been taken from [415]. The difference to that version is that the affine transformation from above is used to scale the size of the cone. This is also the reason why the ratio of the height and radius $H_R = \frac{H}{R}$ is used as an input parameter instead of H and R separately, i.e. a unit 6-fold symmetric cone is assumed to have a radius of $R = 1$. The overall size is then scaled with the input parameters a , b and c . The shape does not have inversion symmetry and is therefore a complex function. The phase factor is taken so that the base plane lies in the xy -plane according to fig. 9.172. The form factor of the cone according to [415] is given as

$$\begin{aligned} F_{\text{cone6}}(\mathbf{Q}, R, H, \alpha_{\text{tilt}}) = & \frac{4\sqrt{3}}{3\tilde{Q}_y^2 - \tilde{Q}_x^2} \int_0^H \left[\tilde{Q}_y^2 R_z^2 \frac{\sin(\tilde{Q}_x R_z / \sqrt{3})}{\tilde{Q}_x R_z / \sqrt{3}} \frac{\sin(\tilde{Q}_y R_z)}{\tilde{Q}_y R_z} \right. \\ & \left. + \cos(2\tilde{Q}_x R_z / \sqrt{3}) - \cos(\tilde{Q}_y R_z) \cos(\tilde{Q}_x R_z / \sqrt{3}) \right] \\ & \times e^{i\tilde{Q}_z z} dz \end{aligned} \quad (9.562)$$

$$R_z = R - z \cot(\alpha_{\text{tilt}}) \quad (9.563)$$

$$\frac{H}{R} < \tan(\alpha_{\text{tilt}}) \quad (9.564)$$

Input Parameters for model cone6 (opo):

a: length of first half axis

ea_x: x -component of first axis.

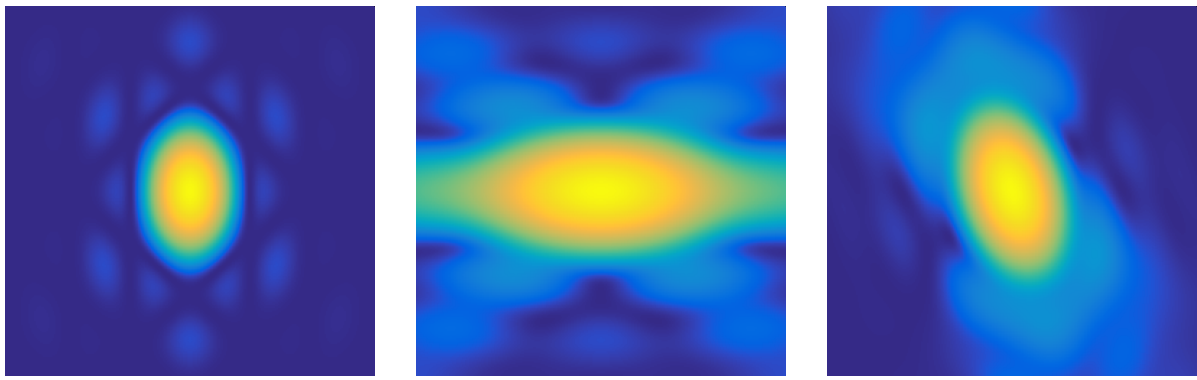


FIGURE 9.173. Scattering patterns at 18m detector distance and a wavelength of $\lambda = 0.6\text{nm}$. The cones with 6-fold symmetry are simulated with half axis length of $a = 30\text{nm}$, $b = 20\text{nm}$, and $c = 10\text{nm}$ and $\alpha_{\text{tilt}} = \arctan(2)$ and $H_R = 2$. The Tait–Bryan angles (yaw–pitch–roll) are $(\alpha = 0^\circ, \beta = 0^\circ, \gamma = 0^\circ)$, $(\alpha = 0^\circ, \beta = 90^\circ, \gamma = 0^\circ)$, and $(\alpha = 0^\circ, \beta = 45^\circ, \gamma = 45^\circ)$

ea_y: y -component of fist axis.

ea_z: z -component of fist axis.

b: length of second half axis

eb_x: x -component of second axis.

eb_y: y -component of second axis.

eb_z: z -component of second axis.

c: length of third axis

ec_x: x -component of third axis.

ec_y: y -component of third axis.

ec_z: z -component of third axis.

eta_p: scattering length density η_p of particle

eta_m: scattering length density η_m of matrix

alpha: first Euler angle

beta: second Euler angle

gamma: third Euler angle

psi: direction of \mathbf{Q} on detector ($\psi = 0$, x -direction, to the right)

tilt: tilt angle α_{tilt} of conical side wall of unit cone

H_R: height H_R of unit 6-fold symmetric cone

Input Parameters for model cone6 (opo, random):

a: length of first half axis

ea_x: x -component of fist axis.

ea_y: y -component of fist axis.

ea_z: z -component of fist axis.

b: length of second half axis

eb_x: x -component of second axis.

eb_y: y -component of second axis.

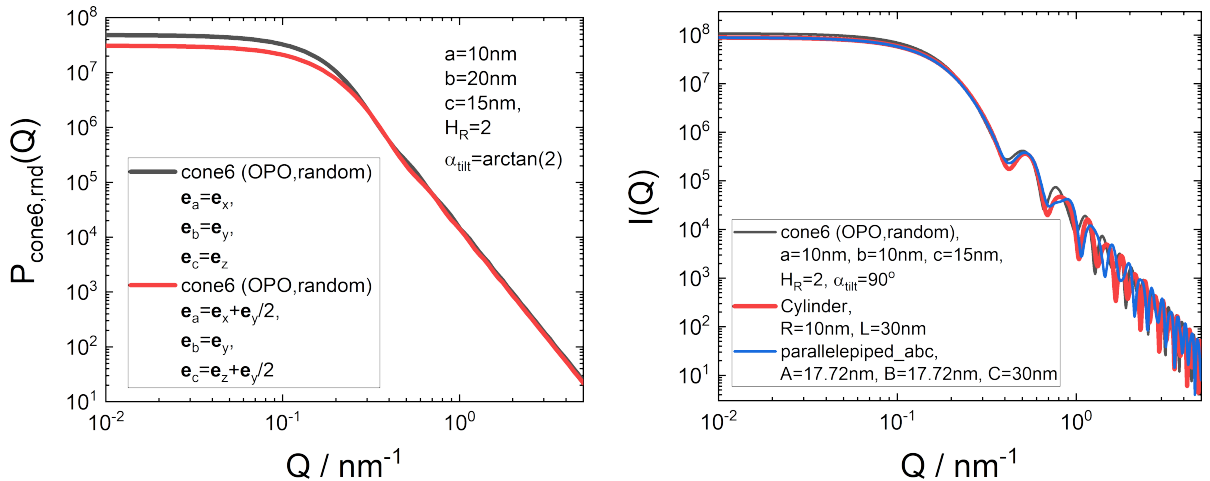


FIGURE 9.174. scattering curved of an oblique `cone6 (OPO,random)` (left) and a comparison of a `cone6 (OPO,random)` with a random oriented solid cylinder `Cylinder` form factor and a random oriented parallelepiped `parallelepiped_abc` (right)

eb_z: z -component of second axis.

c: length of third half axis

ec_x: x -component of third axis.

ec_y: y -component of third axis.

ec_z: z -component of third axis.

eta_p: scattering length density η_p of particle

eta_m: scattering length density η_m of matrix

dummy: not used

dummy: not used

dummy: not used

dummy: not used

tilt: tilt angle α_{tilt} of conical side wall of unit cone

H_R: height H_R of unit 6-fold symmetric cone

Note:

- the unit vector \mathbf{e}_a , \mathbf{e}_b , and \mathbf{e}_c are internally normalized to 1 and need to be linear independent.
- a and b are the half axis or radii of the elliptical base and cH_R the full height of the cone.
- the volume of the oblique 6-fold symmetric cone is

$$V_{\text{cone}} = \frac{2 \tan(\alpha_{\text{tilt}})}{\sqrt{3}} \left[1 - \left(1 - \frac{H_R}{\tan(\alpha_{\text{tilt}})} \right)^3 \right] \det(\underline{\mathbf{D}}^{-1})$$

9.11.6. oriented and random oriented tetrahedron.

[415]

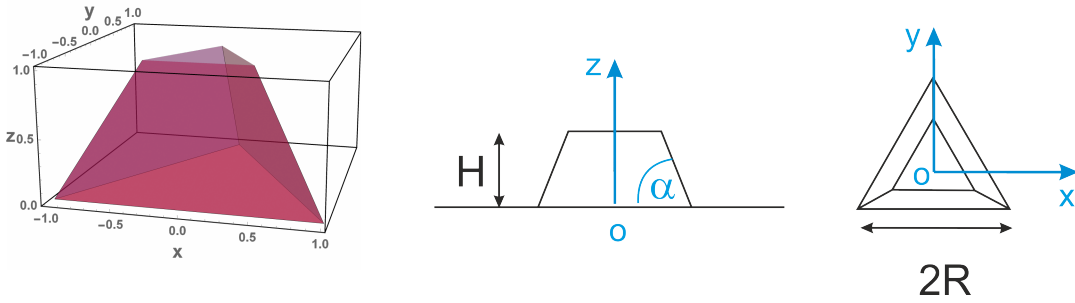


FIGURE 9.175. unit tetrahedron with base length of $2R = 2$, height H_R and tilting angle α .

$$F_{\text{th}}(\mathbf{Q}, R, H, \alpha) = \frac{H}{\sqrt{3}\tilde{Q}_x (\tilde{Q}_x^2 - 3\tilde{Q}_y^2)} e^{i\tilde{Q}_z R \tan(\alpha)/\sqrt{3}} \times \\ \left\{ -(\tilde{Q}_x + \sqrt{3}\tilde{Q}_y) \frac{\sin(q_1 H)}{q_1 H} e^{iq_1 L} + \right. \\ \left. (-\tilde{Q}_x + \sqrt{3}\tilde{Q}_y) \frac{\sin(q_2 H)}{q_2 H} e^{-iq_2 L} + 2\tilde{Q}_x \frac{\sin(q_3 H)}{q_3 H} e^{iq_3 L} \right\} \quad (9.565)$$

$$q_1 = \frac{1}{2} \left[\frac{\sqrt{3}\tilde{Q}_x - \tilde{Q}_y}{\tan(\alpha)} - \tilde{Q}_z \right] \quad (9.566)$$

$$q_2 = \frac{1}{2} \left[\frac{\sqrt{3}\tilde{Q}_x + \tilde{Q}_y}{\tan(\alpha)} + \tilde{Q}_z \right] \quad (9.567)$$

$$q_3 = \frac{1}{2} \left[\frac{2\tilde{Q}_y}{\tan(\alpha)} - \tilde{Q}_z \right] \quad (9.568)$$

$$L = \frac{2 \tan(\alpha) R}{\sqrt{3}} - H \quad (9.569)$$

$$\frac{H}{R} < \frac{\tan(\alpha)}{\sqrt{3}} \quad (9.570)$$

Note:

- the volume of the tetrahedron is

$$V_{\text{th}} = \frac{8}{3} \tan(\alpha) \left[R^3 - \left(R - \frac{\sqrt{3}H}{\tan(\alpha)} \right)^3 \right]$$

9.11.7. oriented and random oriented square basis pyramid.

The form factor of a square basis pyramid has been taken from [415].

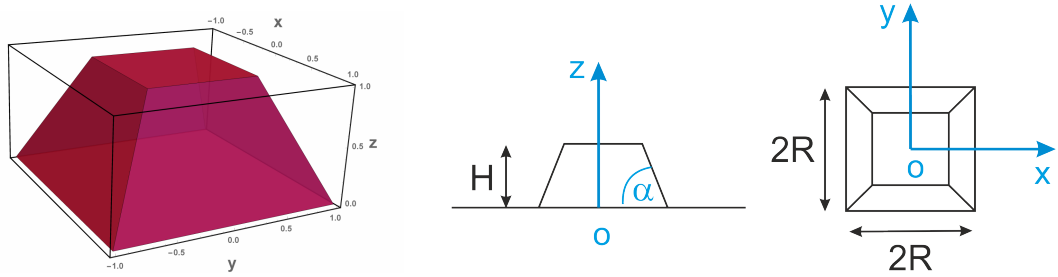


FIGURE 9.176. unit pyramid with base length of $2R = 2$, height H_R and tilting angle α .

$$F_{\text{py4}}(\mathbf{Q}, R, H, \alpha) = \frac{H}{\tilde{Q}_x \tilde{Q}_y} \left\{ K_1 \cos((\tilde{Q}_x - \tilde{Q}_y) R) + K_2 \sin((\tilde{Q}_x - \tilde{Q}_y) R) - K_3 \cos((\tilde{Q}_x + \tilde{Q}_y) R) - K_4 \sin((\tilde{Q}_x + \tilde{Q}_y) R) \right\} \quad (9.571)$$

$$q_1 = \frac{1}{2} \left[\frac{\tilde{Q}_x - \tilde{Q}_y}{\tan(\alpha)} + \tilde{Q}_z \right] \quad (9.572)$$

$$q_2 = \frac{1}{2} \left[\frac{\tilde{Q}_x - \tilde{Q}_y}{\tan(\alpha)} - \tilde{Q}_z \right] \quad (9.573)$$

$$q_3 = \frac{1}{2} \left[\frac{\tilde{Q}_x + \tilde{Q}_y}{\tan(\alpha)} + \tilde{Q}_z \right] \quad (9.574)$$

$$q_4 = \frac{1}{2} \left[\frac{\tilde{Q}_x + \tilde{Q}_y}{\tan(\alpha)} - \tilde{Q}_z \right] \quad (9.575)$$

$$K_1 = \frac{\sin(q_1 H)}{q_1 H} e^{i q_1 H} + \frac{\sin(q_2 H)}{q_2 H} e^{-i q_2 H} \quad (9.576)$$

$$K_2 = -i \frac{\sin(q_1 H)}{q_1 H} e^{i q_1 H} + i \frac{\sin(q_2 H)}{q_2 H} e^{-i q_2 H} \quad (9.577)$$

$$K_3 = \frac{\sin(q_3 H)}{q_3 H} e^{i q_3 H} + \frac{\sin(q_4 H)}{q_4 H} e^{-i q_4 H} \quad (9.578)$$

$$K_4 = -i \frac{\sin(q_3 H)}{q_3 H} e^{i q_3 H} + i \frac{\sin(q_4 H)}{q_4 H} e^{-i q_4 H} \quad (9.579)$$

$$\frac{H}{R} < \frac{\tan(\alpha)}{\sqrt{3}} \quad (9.580)$$

Note:

- the unit vector \mathbf{e}_a , \mathbf{e}_b , and \mathbf{e}_c are internally normalized to 1 and need to be linear independent.

- a and b are the half axis or radii of the elliptical base and cH_R the full height of the cone.
- the volume of the square basis pyramid: is

$$V_{\text{th}} = \frac{1}{3} \tan(\alpha) \left[R^3 - \left(R - \frac{H}{\tan(\alpha)} \right)^3 \right]$$

9.11.8. oriented and random oriented octahedron.

The octahedron can be represented as two regular pyramids with a quadrilateral base connected through this base. The form factor of a regular octahedron [301] with an

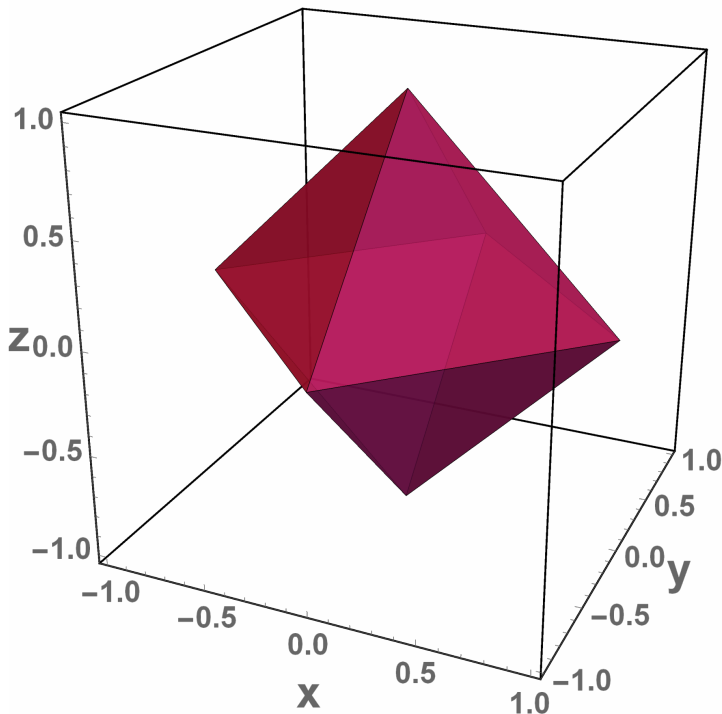


FIGURE 9.177. sketch of a regular octahedron composed of two regular pyramids with edge lengths of $2a$

edge length of $\sqrt{2}$ reads as

$$F_{\text{rOH}}(\mathbf{Q}) = \frac{V_{\text{rOH}}}{Q_x^2 - Q_y^2} (h(Q_y, Q_z) + h(Q_z, Q_x)) \quad (9.581)$$

$$V_{\text{rOH}} = \frac{4}{3} \quad (9.582)$$

$$h(Q_1, Q_2) = 8 \frac{Q_1 \sin Q_1 - Q_2 \sin Q_2}{Q_1^2 - Q_2^2} \quad (9.583)$$

To be consistent with the length definition of the other oriented primitive objects having an half axis length of a, b , and c we can use $\hat{\mathbf{Q}}$ as defined in 9.546 and $\det(\mathbf{D}^{-1})$ as defined

in 9.544 to also include an affine deformation and finally get

$$F_{\text{OH}}(\mathbf{Q}) = (\eta_p - \eta_m) \frac{\det(\underline{\mathbf{D}}^{-1})}{2\sqrt{2}} F_{\text{rOH}}(\hat{\mathbf{Q}}/\sqrt{2}) \quad (9.584)$$

$$P_{\text{OH}}(\mathbf{Q}) = F_{\text{OH}}^2(\hat{\mathbf{Q}}) \quad (9.585)$$

with η_p being the scattering length density of the particle and η_m that one of the matrix.

For a random oriented oblique octahedron the orientation average is done over all directions of \mathbf{Q} . The corresponding scattering amplitude $F_{\text{OH},\text{rnd}}(Q)$ and scattering intensity $P_{\text{OH},\text{rnd}}(Q)$ are then calculated in the same way as in eqs. 9.554 and 9.555.

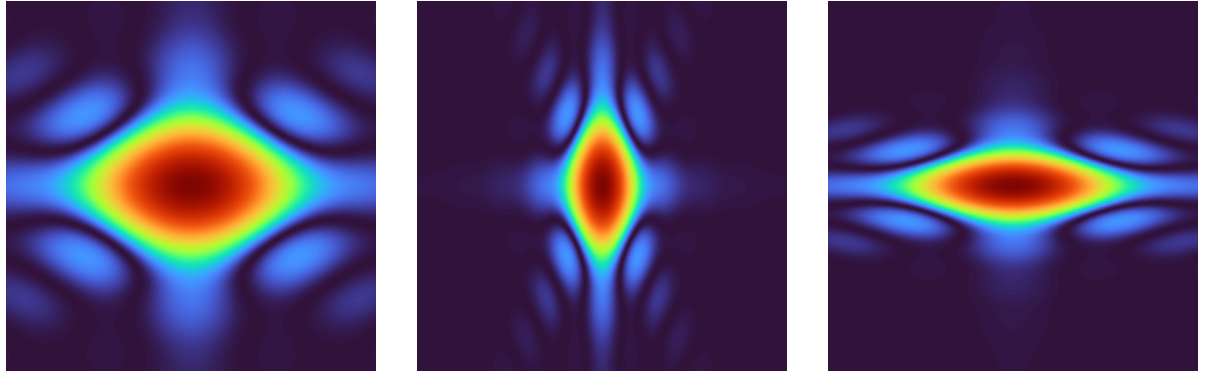


FIGURE 9.178. 2D scattering patterns of an oriented octahedron. The octahedrons are simulated with half axis length of $a = 1.5b = 5c$. The Tait–Bryan angles (yaw-pitch-roll) are $(\alpha = 0^\circ, \beta = 0^\circ, \gamma = 0^\circ)$, $(\alpha = 0^\circ, \beta = 90^\circ, \gamma = 0^\circ)$, and $(\alpha = 0^\circ, \beta = 0^\circ, \gamma = 90^\circ)$

Input Parameters for model octahedron (opo):

- a:** length of first half axis
- ea_x:** x -component of fist axis.
- ea_y:** y -component of fist axis.
- ea_z:** z -component of fist axis.
- nu:** length of second half axis $b = \nu a$
- eb_x:** x -component of second axis.
- eb_y:** y -component of second axis.
- eb_z:** z -component of second axis.
- mu:** length of third half axis $c = \mu a$
- ec_x:** x -component of third axis.
- ec_y:** y -component of third axis.
- ec_z:** z -component of third axis.
- eta_p:** scattering length density η_p of particle
- eta_m:** scattering length density η_m of matrix
- alpha:** first Euler angle
- beta:** second Euler angle
- gamma:** third Euler angle
- psi:** direction of \mathbf{Q} on detector ($\psi = 0$, x -direction, to the right)

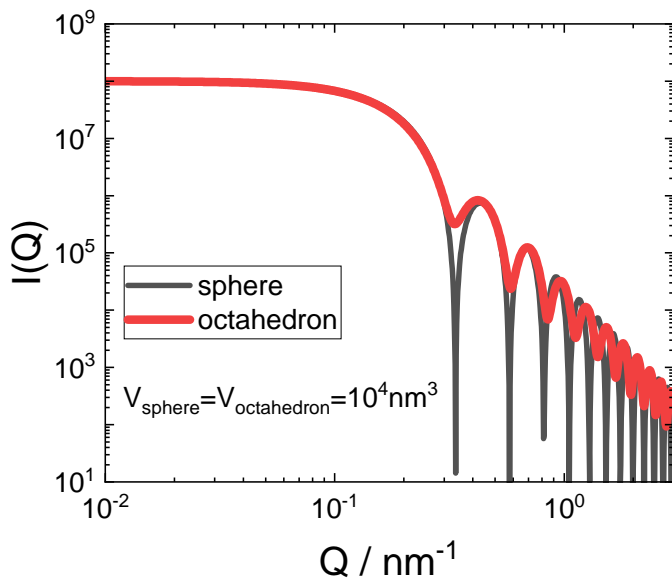


FIGURE 9.179. Scattering curves of an octahedron compared to a sphere of the same volume of 10^4 nm^3 .

Input Parameters for model octahedron (opo, random):

a: length of first half axis
ea_x: x -component of fist axis.
ea_y: y -component of fist axis.
ea_z: z -component of fist axis.
nu: length of second half axis $b = \nu a$
eb_x: x -component of second axis.
eb_y: y -component of second axis.
eb_z: z -component of second axis.
mu: length of third half axis $c = \mu a$
ec_x: x -component of third axis.
ec_y: y -component of third axis.
ec_z: z -component of third axis.
eta_p: scattering length density η_p of particle
eta_m: scattering length density η_m of matrix

Note:

- the unit vector \mathbf{e}_a , \mathbf{e}_b , and \mathbf{e}_c are internally normalized to 1 and need to be linear independent.
- the volume of the oblique octahedron is $V_{\text{OH}} = \frac{\sqrt{2}}{3} 8 \det(\mathbf{D}^{-1})$

9.11.9. oriented and random oriented rhombic dodecahedron.

A rhombic dodecahedron is composed of 6 pyramids with an edge length of $2R$ and height R and one cube with an edge length of $2R$ [247]. A rhombic dodecahedron is constructed by aligning the base of each pyramid with the faces of the cube.

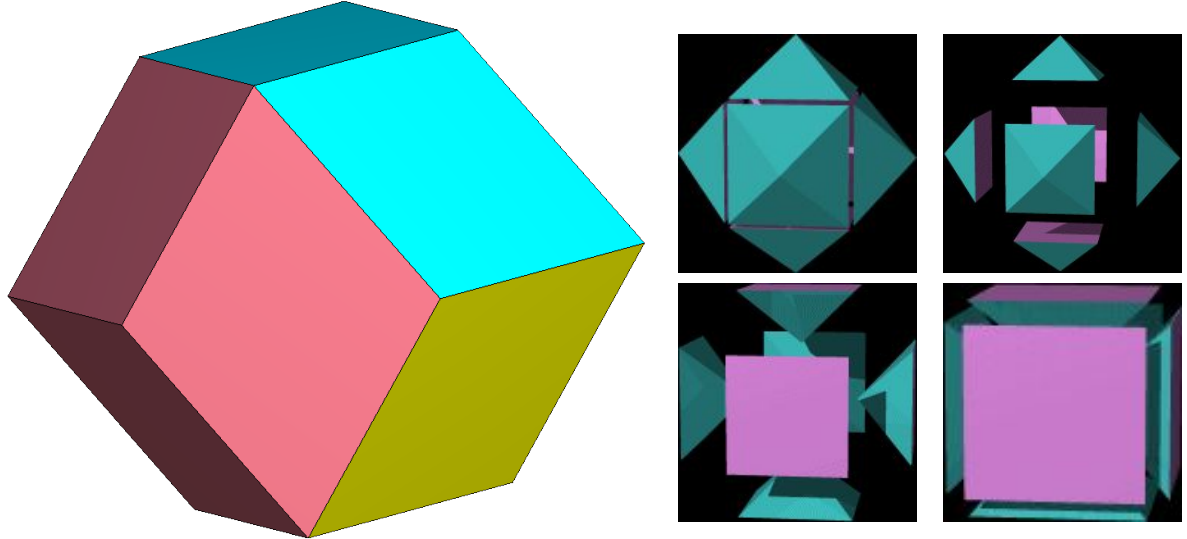


FIGURE 9.180. sketch of a rhombic dodecahedron composed of 12 pyramids with an edge length of $2R$ and height R

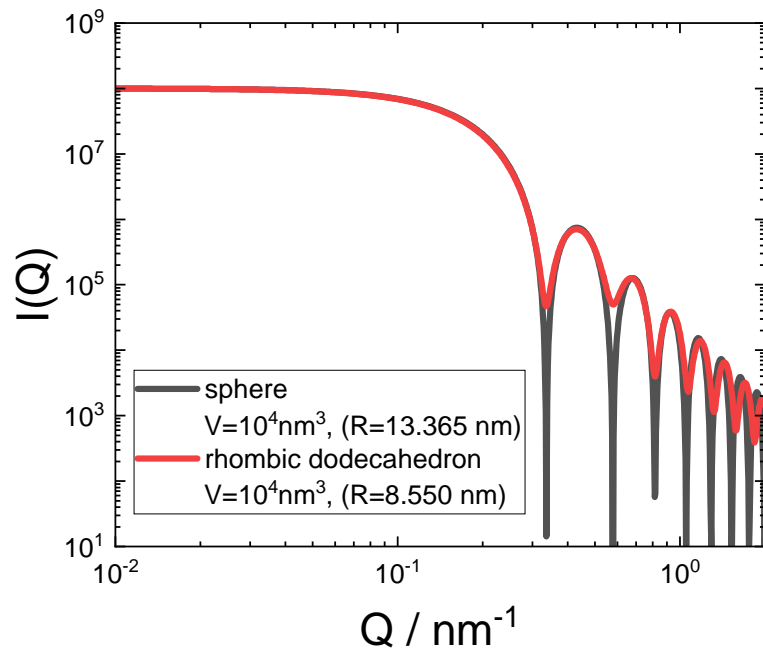


FIGURE 9.181. comparison of a random oriented rhombic dodecahedron and a sphere of the same volume

9.11.10. oriented superellipsoid.

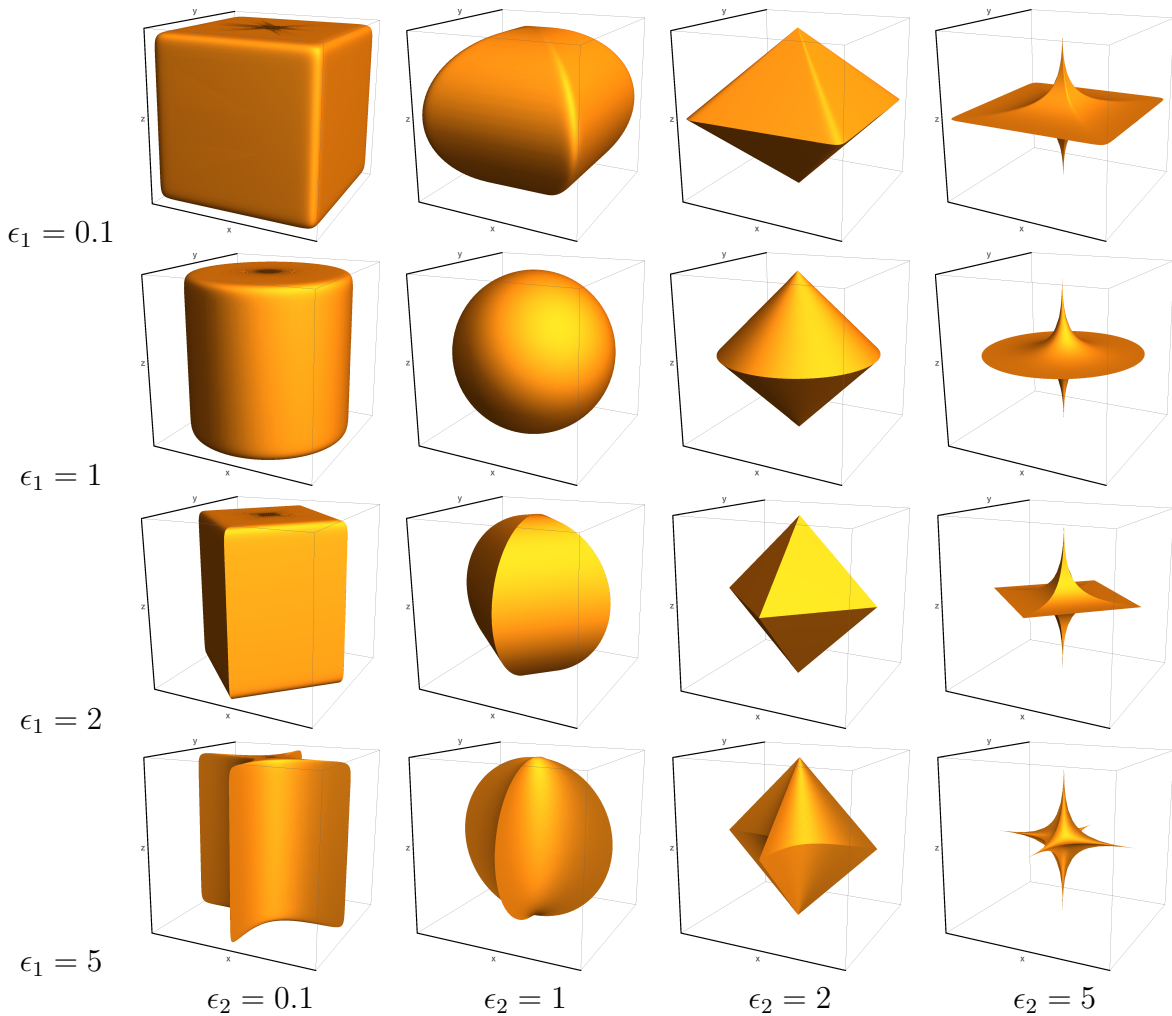


FIGURE 9.182. Typical superquadrics. The parameters for scale factors are $a_1 = a_2 = a_3 = 1$. The values for ϵ_2 vary horizontally by $\epsilon_2 = 0.1, 1, 2, 5$ and vertically by $\epsilon_1 = 0.1, 1, 2, 5$.

Superellipsoids belong to a class of shapes named superquadrics. The class of superquadrics have been widely used in computer graphics and were introduced by [15]. This class of shapes also include next to superellipsoids so called superhyperboloids and supertoroids. They all have both a parametric and an implicit representation. The parametric representation of the surface of a superellipsoid is defined by

$$\begin{pmatrix} x(a_1\theta, \phi) \\ y(a_2\theta, \phi) \\ z(a_3\theta, \phi) \end{pmatrix} = \begin{pmatrix} a_1 \text{sgnpow}(\cos \theta, \epsilon_2) \text{sgnpow}(\cos \phi, \epsilon_1) \\ a_2 \text{sgnpow}(\sin \theta, \epsilon_2) \text{sgnpow}(\cos \phi, \epsilon_1) \\ a_3 \text{sgnpow}(\sin \phi, \epsilon_1) \end{pmatrix} \quad (9.586)$$

whereas the signed power function is defined as

$$\text{sgn}(\epsilon) = \text{sgn}(t)|t|^\epsilon \quad (9.587)$$

$$\text{sgn}(t) = \begin{cases} -1 & \text{if } t < 0, \\ 0 & \text{if } t = 0, \\ 1 & \text{if } t > 0. \end{cases} \quad (9.588)$$

The implicit representation is given by

$$\left(\left| \frac{x}{a_1} \right|^{\frac{2}{\epsilon_2}} + \left| \frac{y}{a_2} \right|^{\frac{2}{\epsilon_2}} \right)^{\frac{\epsilon_2}{\epsilon_1}} + \left| \frac{z}{a_3} \right|^{\frac{2}{\epsilon_1}} \leq 1 \quad (9.589)$$

A supersphere is a special case of superellipsoid for which the two exponents are equal $\epsilon_1 = \epsilon_2$. The implicit representation then reads as $\left| \frac{x}{a_1} \right|^n + \left| \frac{y}{a_2} \right|^n + \left| \frac{z}{a_3} \right|^n \leq 1$ with $n = 1/\epsilon_1 = 1/\epsilon_2$. Another special case is the superegg for which one exponent is equal $\epsilon_1 = 1$ and the implicit representation then reads as $\left(\left| \frac{x}{a_1} \right|^2 + \left| \frac{y}{a_2} \right|^2 \right)^{1/\epsilon_2} + \left| \frac{z}{a_3} \right|^{2/\epsilon_2} \leq 1$. As the asymmetric superellipsoid is obtained by a scale transform, which is a special case of an affine transform only the Fourier transform of a unit superellipsoid has to be solved. All its affine transform than can be easily calculated by linear algebra.

The Fourier transform of a unit super-quadrics ($a_1 = a_2 = a_3 = 1$) is

$$\begin{aligned} F_{\text{SEll}}(\mathbf{Q}) &= \det(\underline{\mathbf{D}}^{-1}) e^{-i\mathbf{QR}} \Delta\eta \int_{-1}^1 dx \int_{-Y(x)}^{Y(x)} dy \int_{-Z(x,y)}^{Z(x,y)} dz e^{i\hat{\mathbf{Q}}r} \\ &= \det(\underline{\mathbf{D}}^{-1}) e^{-i\mathbf{QR}} \Delta\eta \end{aligned} \quad (9.590)$$

$$\begin{aligned} &\times \int_{-1}^1 dx \int_{-Y(x)}^{Y(x)} dy e^{i(\hat{Q}_x x + \hat{Q}_y y)} 2Z(x, y) \text{sinc}(\hat{Q}_z Z(x, y)) \\ &= \det(\underline{\mathbf{D}}^{-1}) e^{-i\mathbf{QR}} \Delta\eta \end{aligned} \quad (9.591)$$

$$\times \int_{-1}^1 dx \int_{-1}^1 ds e^{i(\hat{Q}_x x + \hat{Q}_y Y(x)s)} 2Z(x, Y(x)s) \text{sinc}(\hat{Q}_z Z(x, Y(x)s)) Y(x)$$

$$Y(x) = \left(1 - x^{\frac{2}{\epsilon_2}} \right)^{\frac{\epsilon_2}{2}} \quad (9.592)$$

$$Z(x, y) = \left(1 - \left(x^{\frac{2}{\epsilon_2}} + y^{\frac{2}{\epsilon_2}} \right)^{\frac{\epsilon_2}{\epsilon_1}} \right)^{\frac{\epsilon_1}{2}} \quad (9.593)$$

Input Parameters for model `superellipsoid (OPO)`:

a: length of first half axis

ea_x: x -component of fist axis.

ea_y: y -component of fist axis.

ea_z: z -component of fist axis.

mu: scaling factor of second half axis ($b = \mu a$) compared to first half axis

eb_x: x -component of second axis.

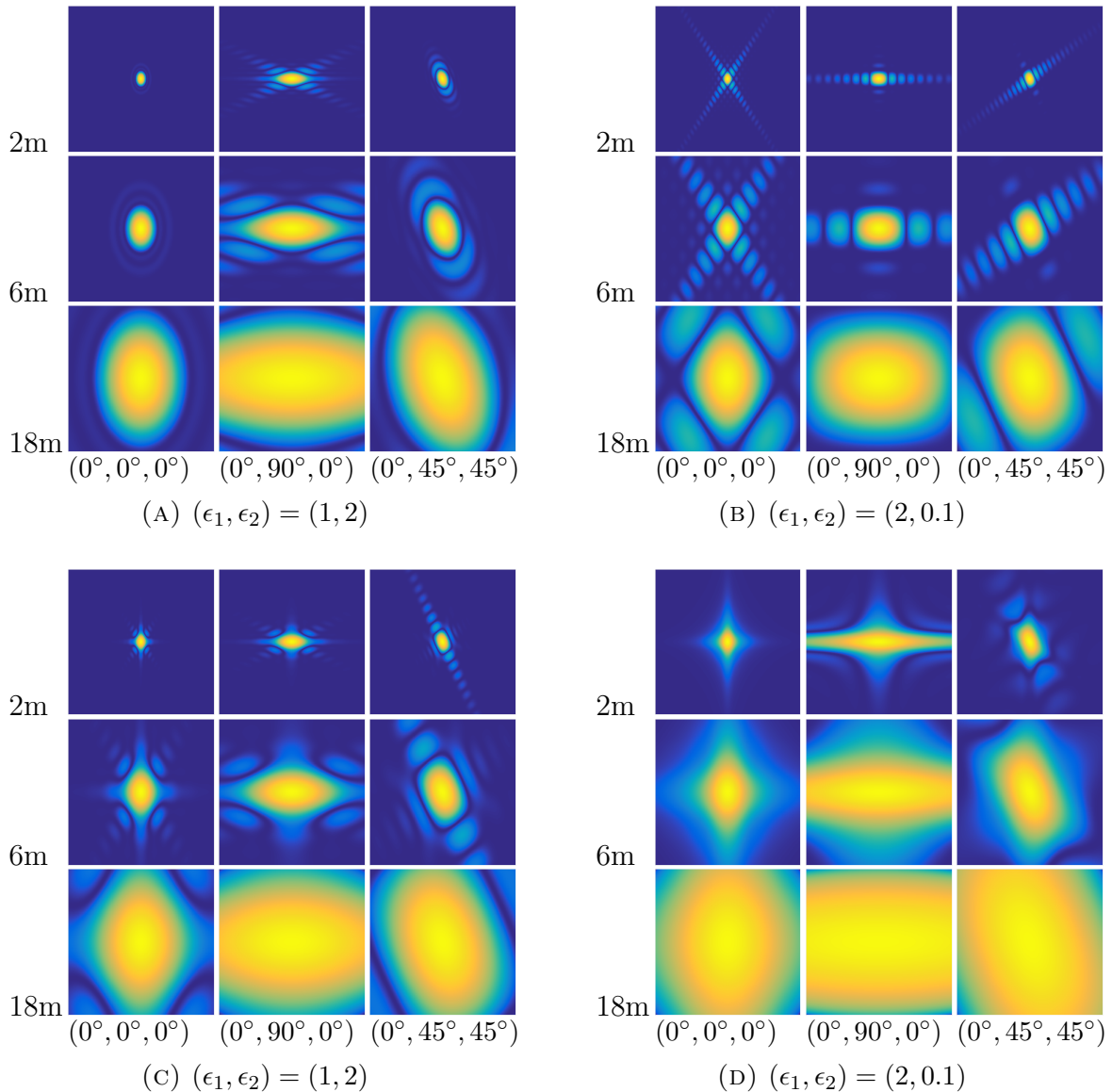


FIGURE 9.183. Scattering patterns for super-quadratics with scale factors are $a_1 = 30\text{nm}$, $a_2 = 20\text{nm}$, $a_3 = 10\text{nm}$ calculated for detector distances (2m, 6m, 18m) and a wavelength of 0.6nm are shown. Three orientation using Tait–Bryan angles (yaw- pitch-roll) are shown.

eb_y: y -component of second axis.

eb_z: z -component of second axis.

nu: scaling factor of third half axis ($c = \nu a$) compared to first half axis

ec_x: x -component of third axis.

ec_y: y -component of third axis.

ec_z: z -component of third axis.

eta_p: scattering length density η_p of particle

eta_m: scattering length density η_m of matrix

alpha: first Euler angle

beta: second Euler angle

gamma: third Euler angle

psi: direction of \mathbf{Q} on detector ($\psi = 0$, x -direction, to the right)

eps_2: shape parameter ϵ_2

eps_1: shape parameter ϵ_1

Input Parameters for model **superellipsoid** (OPO, random):

a: length of first half axis

ea_x: x -component of fist axis.

ea_y: y -component of fist axis.

ea_z: z -component of fist axis.

mu: scaling factor of second half axis ($b = \mu a$) compared to first half axis

eb_x: x -component of second axis.

eb_y: y -component of second axis.

eb_z: z -component of second axis.

nu: scaling factor of third half axis ($c = \nu a$) compared to first half axis

ec_x: x -component of third axis.

ec_y: y -component of third axis.

ec_z: z -component of third axis.

eta_p: scattering length density η_p of particle

eta_m: scattering length density η_m of matrix

dummy: not used

dummy: not used

dummy: not used

dummy: not used

eps_2: shape parameter ϵ_2

eps_1: shape parameter ϵ_1

Note:

- the unit vector \mathbf{e}_a , \mathbf{e}_b , and \mathbf{e}_c are internally normalized to 1 and need to be linear independent.
- shape parameter ϵ_1 needs to be a positive non-zero number, $\epsilon_1 > 0$
- shape parameter ϵ_2 needs to be a positive non-zero number, $\epsilon_2 > 0$
- The integration strategy for the double integral in eq. 9.591 can be configured via a menu interface as well as the integration routine for the random orientational average.

9.11.11. oriented super-egg.

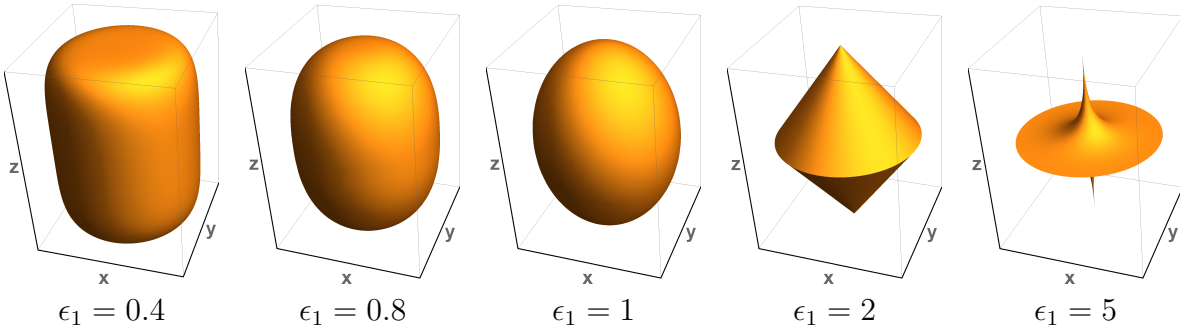


FIGURE 9.184. Supereggs. The parameters for the scale factors of the shown supereggs are $a = b = \frac{3}{4}c$. The values for $\epsilon_2 = 2$ and $\epsilon_1 = 0.4, 0.8, 1, 2, 5$.

The superegg is a superellipsoid whose horizontal cross-sections are ellipses, i.e. $\epsilon_2 = 1$. It is defined by the inequality [521]

$$\left(\sqrt{\left(\frac{x}{a_1}\right)^2 + \left(\frac{y}{a_2}\right)^2} \right)^{\frac{2}{\epsilon_1}} + \left(\frac{z}{a_3}\right)^{\frac{2}{\epsilon_1}} \leq 1 \quad (9.594)$$

For circular cross-sections the Fourier transform [328] can be written as a single integral. For the more general case of an elliptical cross-section the Fourier transform still can be written as a single integral, however, the orientation average becomes a double integral as the cylinder symmetry get lost.

$$\begin{aligned} F_{\text{SEgg}}(\mathbf{Q}) &= \det(\underline{\mathbf{D}}^{-1}) e^{-i\mathbf{QR}} \Delta\eta \\ &\times \int_0^1 \frac{4\pi r \sin\left(\hat{Q}_z \left(1 - r^{2/\epsilon_1}\right)^{\epsilon_1/2}\right) J_0\left(\sqrt{\hat{Q}_x^2 + \hat{Q}_y^2} r\right)}{\hat{Q}_z} dr \end{aligned} \quad (9.595)$$

Alternatively by using a different variable transformation the form factor can also be written as [328]

$$\begin{aligned} F_{\text{SEgg}}(\mathbf{Q}) &= \det(\underline{\mathbf{D}}^{-1}) e^{-i\mathbf{QR}} \Delta\eta \\ &\times \int_0^1 4\pi r^2(z) \frac{J_1\left(r(z)\sqrt{\hat{Q}_x^2 + \hat{Q}_y^2}\right)}{r(z)\sqrt{\hat{Q}_x^2 + \hat{Q}_y^2}} \cos(z\hat{Q}_z) dz \end{aligned} \quad (9.596)$$

$$r(z) = \left(1 - z^{2/\epsilon_1}\right)^{\epsilon_1/2} \quad (9.597)$$

Input Parameters for model superegg (OPO):

- a:** length of first half axis
- ea_x:** x -component of fist axis.
- ea_y:** y -component of fist axis.
- ea_z:** z -component of fist axis.

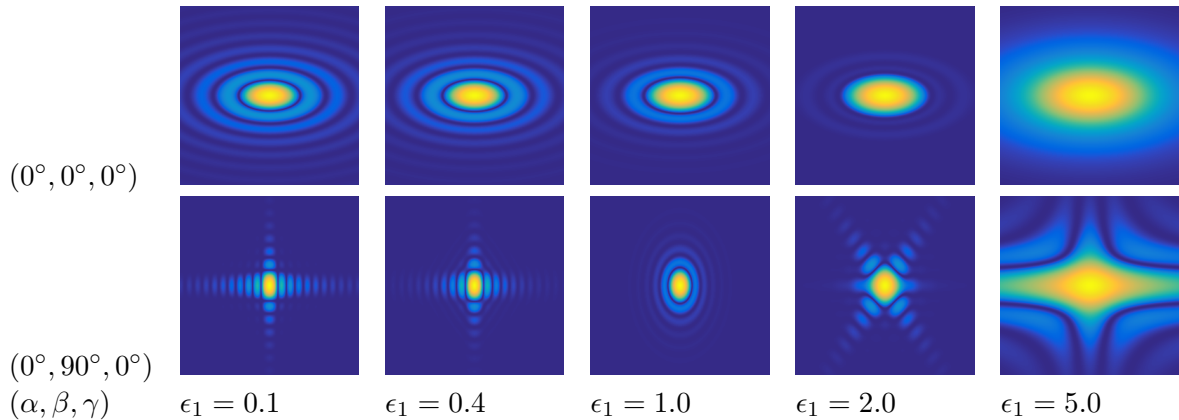


FIGURE 9.185. oriented superegg model with half axis length of $a = 10\text{nm}$, $b = \mu a = 20\text{nm}$, and $c = \nu a = 30\text{nm}$ and the corresponding axis pointing into $\mathbf{e}_a = \mathbf{e}_x$, $\mathbf{e}_b = \mathbf{e}_y$, and $\mathbf{e}_c = \mathbf{e}_z$. The scattering patterns have been calculated for two sets of Euler angles using Tait–Bryan angles (yaw–pitch–roll).

mu: scaling factor of second half axis ($b = \mu a$) compared to first half axis

eb_x: x -component of second axis.

eb_y: y -component of second axis.

eb_z: z -component of second axis.

nu: scaling factor of third half axis ($c = \nu a$) compared to first half axis

ec_x: x -component of third axis.

ec_y: y -component of third axis.

ec_z: z -component of third axis.

eta_p: scattering length density η_p of particle

eta_m: scattering length density η_m of matrix

alpha: first Euler angle

beta: second Euler angle

gamma: third Euler angle

psi: direction of \mathbf{Q} on detector ($\psi = 0$, x -direction, to the right)

eps1: shape parameter ϵ_1

Input Parameters for model `superegg` (OPO, random):

a: length of first half axis

ea_x: x -component of fist axis.

ea_y: y -component of fist axis.

ea_z: z -component of fist axis.

mu: scaling factor of second half axis ($b = \mu a$) compared to first half axis

eb_x: x -component of second axis.

eb_y: y -component of second axis.

eb_z: z -component of second axis.

nu: scaling factor of third half axis ($c = \nu a$) compared to first half axis

ec_x: x -component of third axis.

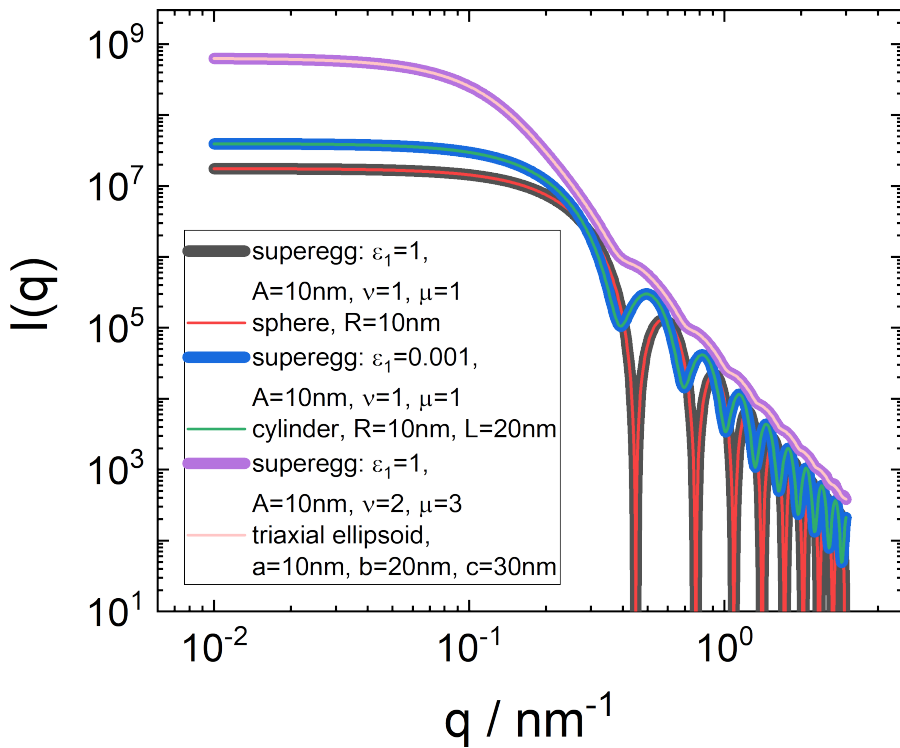


FIGURE 9.186. random oriented superegg model with parameters to test it against simple models like sphere, cylinder, and triaxial ellipsoid

ec_y: y -component of third axis.

ec_z: z -component of third axis.

eta_p: scattering length density η_p of particle

eta_m: scattering length density η_m of matrix

dummy: not used

dummy: not used

dummy: not used

dummy: not used

eps1: shape parameter ϵ_1

Note:

- the unit vector e_a , e_b , and e_c are internally normalized to 1 and need to be linear independent.
- shape parameter ϵ_1 needs to be a positive non-zero number, $\epsilon_1 > 0$

9.11.12. oriented super-shapes and rational super-shaped.
 Super-shapes [152, 9, 132] and rational super-shapes [38, 132] are a further general-

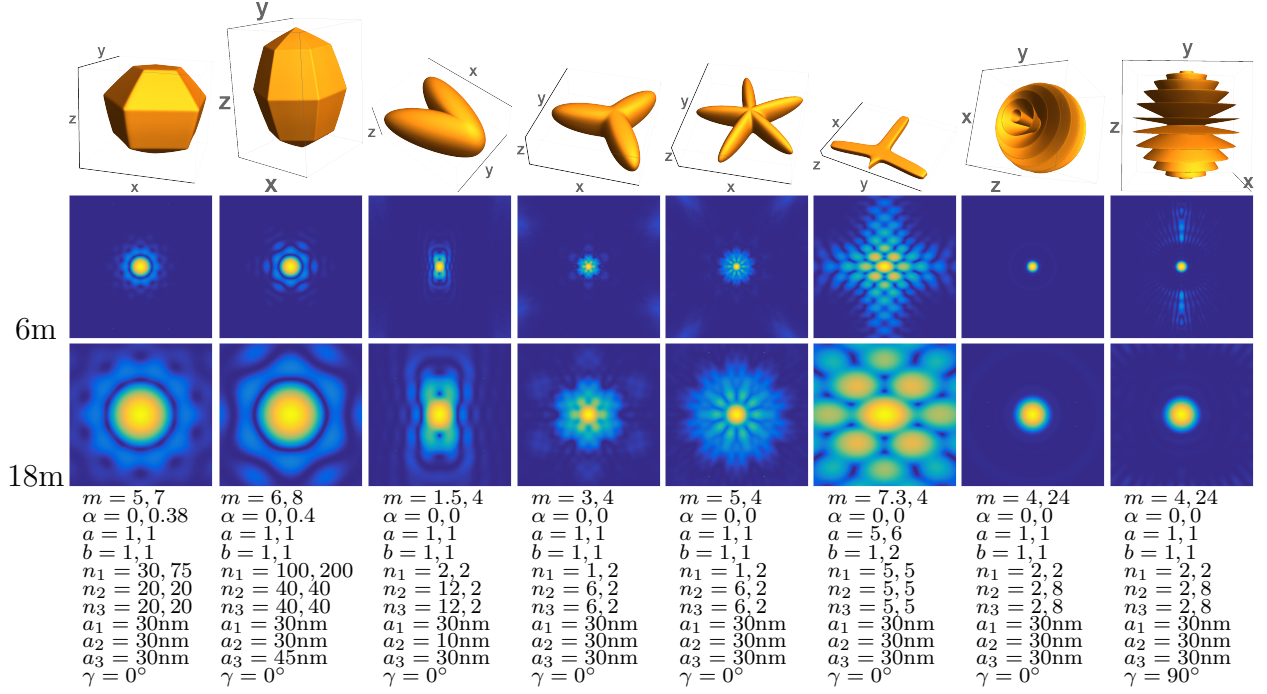


FIGURE 9.187. Supershapes: The scattering patterns are calculated for detector distances of 6 and 18 m at a wavelength of 0.6nm. The detector size is assumed to be $96 \times 96\text{cm}^2$. The values in the last row are the input values of eq. 9.598 for r_1 and r_2 (eqs. 9.615, 9.616). In the last example the incident beam direction is the x -directions instead of the z -direction.

ization of super-quadratics [15]. The parametric representation in two dimensions reads for super-shapes as [152]

$$r(\theta, \alpha, m, n_1, n_2, n_3, a, b) = \left(\left| \frac{\cos\left(\frac{m(\theta-\alpha)}{4}\right)}{a} \right|^{n_2} + \left| \frac{\sin\left(\frac{m(\theta-\alpha)}{4}\right)}{b} \right|^{n_3} \right)^{-\frac{1}{n_1}} \quad (9.598)$$

and for rational super-shapes [38, 132] as

$$r(\theta, \alpha, m, n_1, n_2, n_3, a, b) = 2^{\frac{-1}{n_1}} \left(\frac{1}{W(\theta - \alpha)n_1} + 1 - \frac{1}{n_1} \right) \quad (9.599)$$

with

$$W(\theta) = \frac{U(\theta)}{n_2 + (1 - n_2)U(\theta)} + \frac{V(\theta)}{n_3 + (1 - n_3)V(\theta)} \quad (9.600)$$

$$U(\theta) = \left| \frac{\cos\left(\frac{m\theta}{4}\right)}{a} \right| \quad \text{and} \quad V(\theta) = \left| \frac{\sin\left(\frac{m\theta}{4}\right)}{b} \right| \quad (9.601)$$

The generalization to extend the 2D parametric representation into 3D is done by a spherical product so that the parametrisation of a surface point \mathbf{S} or within the volume

\mathbf{V} read as

$$\mathbf{S} = \begin{pmatrix} x(a_1, \theta, \phi) \\ y(a_2, \theta, \phi) \\ z(a_3, \theta, \phi) \end{pmatrix} = \begin{pmatrix} a_1 r_1(\theta) \cos(\theta) r_2(\phi) \cos(\phi) \\ a_2 r_1(\theta) \sin(\theta) r_2(\phi) \cos(\phi) \\ a_3 r_2(\phi) \sin(\phi) \end{pmatrix} \quad (9.602)$$

$$\mathbf{V} = \tau \mathbf{S} \quad (9.603)$$

with

$$r_1(\theta) = r(\theta, \alpha, m, n_1, n_2, n_3, a, b) \quad (9.604)$$

$$r_2(\phi) = r(\phi, \beta, M, N_1, N_2, N_3, A, B) \quad (9.605)$$

where $\tau \in [0, 1]$, $\theta \in [-\pi, \pi]$ and $\phi \in [-\frac{\pi}{2}, \frac{\pi}{2}]$. For integer values of the degree of symmetries [129, 130, 131, 132] have given 2 implicit representations for the super-shapes.

$$1 \geq \frac{x^2 + y^2 + z^2 r_1^2(\theta)}{r_1^2(\theta) r_2^2(\phi)} \quad (9.606)$$

$$1 \geq 1 - \frac{1}{r_2(\phi)} \sqrt{\frac{x^2 + y^2 + z^2}{\cos^2(\phi) (r_1^2(\theta) - 1) + 1}} \quad (9.607)$$

The angles θ and ϕ are defined by

$$\begin{cases} \theta &= \arctan\left(\frac{y}{x}\right) \\ \phi &= \arctan\left(\frac{zr_1(\theta)\sin(\theta)}{y}\right) \\ &= \arctan\left(\frac{zr_1(\theta)\cos(\theta)}{x}\right) \end{cases} \quad (9.608)$$

The Jacobi determinant for both the super-shape as well as rational super-shape substitution is

$$\det \underline{\mathbf{J}} = \det \begin{pmatrix} \frac{\partial x(\tau, \theta, \phi)}{\partial \tau} & \frac{\partial y(\tau, \theta, \phi)}{\partial \tau} & \frac{\partial z(\tau, \theta, \phi)}{\partial \tau} \\ \frac{\partial x(\tau, \theta, \phi)}{\partial \theta} & \frac{\partial y(\tau, \theta, \phi)}{\partial \theta} & \frac{\partial z(\tau, \theta, \phi)}{\partial \theta} \\ \frac{\partial x(\tau, \theta, \phi)}{\partial \phi} & \frac{\partial y(\tau, \theta, \phi)}{\partial \phi} & \frac{\partial z(\tau, \theta, \phi)}{\partial \phi} \end{pmatrix} = \tau^2 \cos(\phi) r_1^2(\theta) r_2^3(\phi) \quad (9.609)$$

$$F_{\text{SuperSh}}(\mathbf{Q}) = \det(\underline{\mathbf{D}}^{-1}) e^{-i\mathbf{Q}\mathbf{R}} \Delta\eta \int_0^1 d\tau \int_{-\pi}^{\pi} d\theta \int_{-\pi/2}^{\pi/2} d\phi \det(\underline{\mathbf{J}}) e^{i\hat{\mathbf{Q}}\mathbf{r}} \quad (9.610)$$

$$= \det(\underline{\mathbf{D}}^{-1}) e^{-i\mathbf{Q}\mathbf{R}} \Delta\eta \int_{-\pi}^{\pi} d\theta \int_{-\pi/2}^{\pi/2} d\phi \cos(\phi) r_1^2(\theta) r_2^3(\phi) \quad (9.611)$$

$$\times \left(\frac{2\hat{q}_s \cos \hat{q}_s + (\hat{q}_s^2 - 2) \sin \hat{q}_s}{\hat{q}_s^3} + i \frac{(2 - \hat{q}_s^2) \cos \hat{q}_s - 2 + 2q_s \sin \hat{q}_s}{\hat{q}_s^3} \right)$$

$$\hat{q}_s = \hat{\mathbf{Q}}\mathbf{S} = \hat{Q}_x x(1, \theta, \phi) + \hat{Q}_y y(1, \theta, \phi) + \hat{Q}_z z(1, \theta, \phi) \quad (9.612)$$

```

rx[theta_, m_, a_, b_, n1_, n2_, n3_] := 2^(-1/n1) (1 - 1/n1
+ 1/( n1 (Abs[Cos[(m theta)/4]/a]/(n2 + (1 - n2) Abs[Cos[(m theta)/4]/a]) +
Abs[Sin[(m theta)/4]/a]/(n2 + (1 - n2) Abs[Sin[(m theta)/4]/a]))))
rx[theta_,m_,a_,b_,n1_,n2_,n3_] := Power[Abs[Cos[theta*m/4]/a]^n2+Abs[Sin[theta*m/4]/b]^n3,-1/n1]
Manipulate[
Grid[{{}
Grid[{{
{PolarPlot[With[{r1 = rx[([Theta] - alpha), m, a, b, n1, n2, n3]}, r1], {([Theta], -\[Pi], \[Pi]), Axes -> False, ImageSize -> {200, 200}, PlotLabel -> "superformula I"]},
{PolarPlot[With[{r2 = rx[([Phi] - beta), sm, sa, sb, sn1, sn2, sn3]}, r2], {([Phi], -\[Pi]/2, \[Pi]/2), Axes -> False, ImageSize -> {200, 200}, PlotLabel -> "superformula II (-pi/2,pi/2)"}],
{PolarPlot[With[{r3 = rx[([Phi] - beta), sm, sa, sb, sn1, sn2, sn3]}, r3], {([Phi], -\[Pi], \[Pi]), Axes -> False, ImageSize -> {200, 200}, PlotLabel -> "superformula II (-pi,pi)"} }]},
ParametricPlot3D[With[{r1=rx[([Theta]-alpha),m,a,b,n1,n2,n3], r2=rx[([Phi]-beta),sm,sa,sb,sn1,sn2,sn3]}, {r1 Cos[([Theta]) r2 Cos[([Phi]), r1 Sin[([Theta]) r2 Cos[([Phi]), r2 Sin[([Phi])]], {([Theta], -Pi, Pi}, {[Phi], -Pi/2, Pi/2}, Axes -> True, AxesLabel -> {"x", "y", "z"}, BaseStyle -> {FontWeight -> "Bold", FontSize -> 80}, PlotTheme -> "Normal", Ticks -> None, AxesStyle -> Thickness[0.005], Exclusions -> None, ImageSize -> {800, 600}, MaxRecursion -> ControlActive[1, 2], PlotPoints -> ControlActive[220, 220], PlotRange -> All, Mesh -> mesh }}],
{{mesh, False, "meshing"}, ImageSize -> Tiny}, {True -> "on", False -> "off"}, ControlType -> SetterBar}, Delimiter,
{{m, 5, "m"}, 1/10, 20, 1, ImageSize -> Tiny}, Delimiter,
{{n1, 30, Subscript["n", 1]}, 1/100, 100, 1, ImageSize -> Tiny},
{{n2, 20, Subscript["n", 2]}, 0, 100, 1, ImageSize -> Tiny},
{{n3, 20, Subscript["n", 3]}, 0, 100, 1, ImageSize -> Tiny}, Delimiter,
{{alpha, 0, "alpha"}, 0, 2*Pi, 0.1, ImageSize -> Tiny}, Delimiter,
{{a, 1, "a"}, 0.1, 2, ImageSize -> Tiny}, {{b, 1, "b"}, 0.2, 2, ImageSize -> Tiny}, Delimiter,
{{sm, 7, "M"}, 1/10, 20, 1, ImageSize -> Tiny}, Delimiter,
{{sn1, 75, Subscript["N", 1]}, 1/100, 100, 1, ImageSize -> Tiny},
{{sn2, 20, Subscript["N", 2]}, 0, 100, 1, ImageSize -> Tiny},
{{sn3, 20, Subscript["N", 3]}, 0, 100, 1, ImageSize -> Tiny}, Delimiter,
{{beta, 0.23, "beta"}, 0, 2*Pi, 0.1, ImageSize -> Tiny}, Delimiter,
{{sa, 1, "A"}, 0.1, 2, ImageSize -> Tiny}, {{sb, 1, "B"}, 0.2, 2, ImageSize -> Tiny},
{{xr, 1, "x scaling"}, 0.1, 10, ImageSize -> Tiny}, {{yr, 1, "y scaling"}, 0.1, 10, ImageSize -> Tiny},
{{zr, 1, "z scaling"}, 0.1, 10, ImageSize -> Tiny}, ControlPlacement -> Left, AutorunSequencing -> {2, 4, 6}]

```

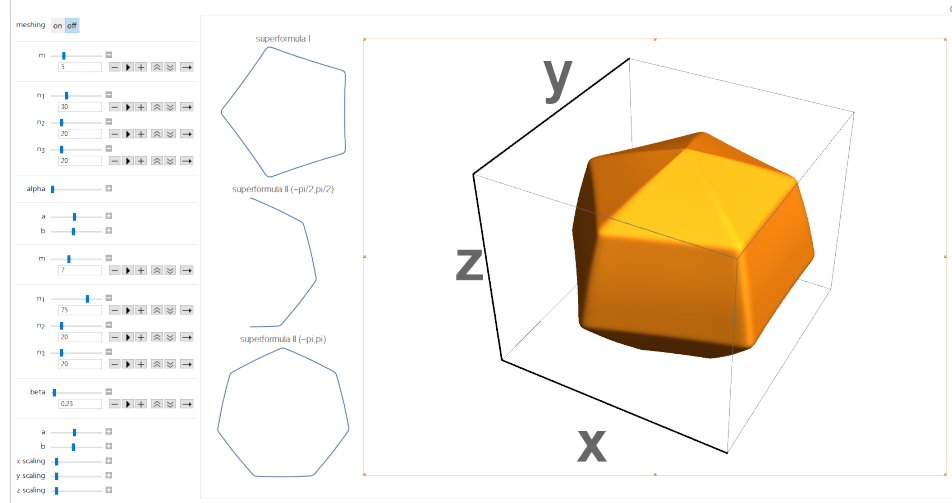


FIGURE 9.188. Mathematica interface to explore visually "super-shapes" as a function of their input parameters.

9.12. oriented super-toroid and super-helix

The super-toroid and super-helix are basing on the parametric representation in eq. 9.598 and the points on their surface \mathbf{S} and in the volume \mathbf{V} are defined as

$$\mathbf{S} = \begin{pmatrix} a_1 r_1(\theta, \alpha) \cos(\theta) [r_2(\phi, \beta + \gamma\theta) \cos(\phi) + R] \\ a_2 r_1(\theta, \alpha) \sin(\theta) [r_2(\phi, \beta + \gamma\theta) \cos(\phi) + R] \\ a_3 [r_2(\phi, \beta + \gamma\theta) \sin(\phi) + \frac{P\theta}{2\pi}] \end{pmatrix} \quad (9.613)$$

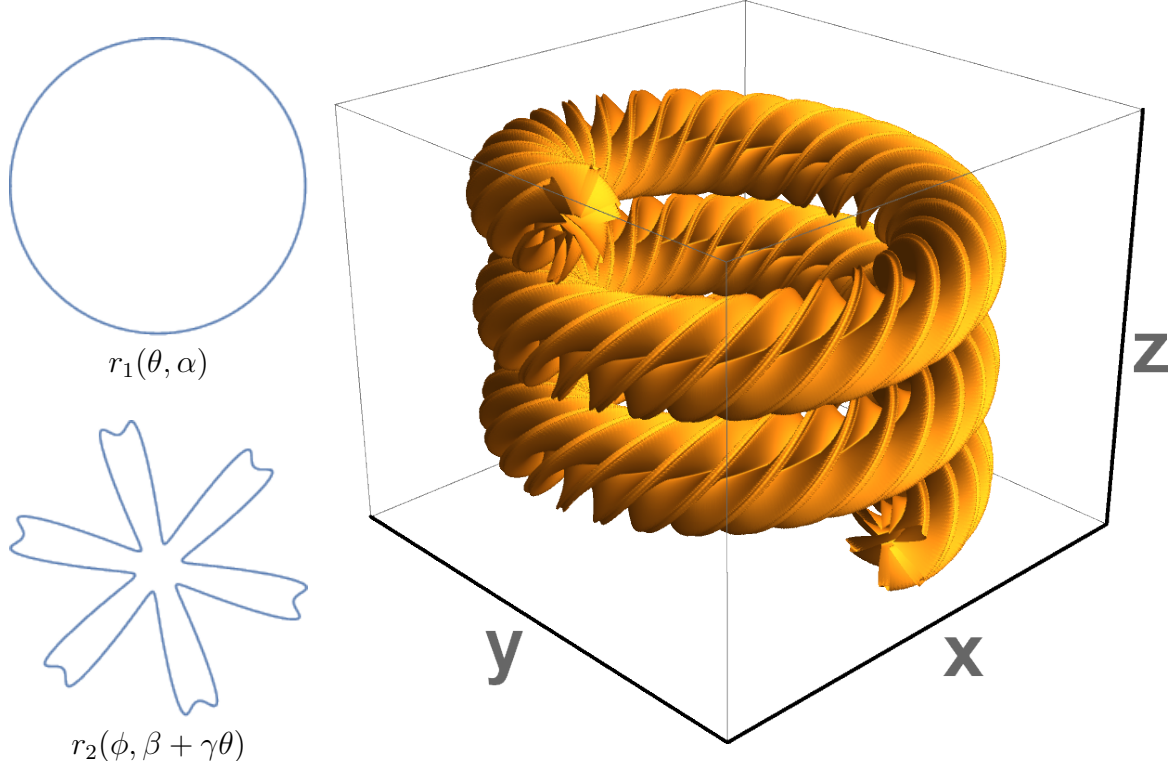
$$\begin{aligned} \mathbf{V} &= \begin{pmatrix} x(a_1, \tau, \theta, \phi) \\ y(a_2, \tau, \theta, \phi) \\ z(a_3, \tau, \theta, \phi) \end{pmatrix} \\ &= \begin{pmatrix} a_1 r_1(\theta, \alpha) \cos(\theta) [\tau r_2(\phi, \beta + \gamma\theta) \cos(\phi) + R] \\ a_2 r_1(\theta, \alpha) \sin(\theta) [\tau r_2(\phi, \beta + \gamma\theta) \cos(\phi) + R] \\ a_3 [\tau r_2(\phi, \beta + \gamma\theta) \sin(\phi) + \frac{P\theta}{2\pi}] \end{pmatrix} \end{aligned} \quad (9.614)$$

with

$$r_1(\theta, \alpha) = r(\theta, \alpha, m, n_1, n_2, n_3, a, b) \quad (9.615)$$

$$r_2(\phi, \beta + \gamma\theta) = r(\phi, \beta + \gamma\theta, M, N_1, N_2, N_3, A, B) \quad (9.616)$$

where $\tau \in [0, 1]$, $\theta \in [-T\pi, T\pi]$ and $\phi \in [-\pi, \pi]$. P is the pitch of the super-helix which is the height of one complete helix turn, measured parallel to the axis of the helix. T describes the number of turns. For a pitch of $P = 0$ and one turn ($T = 1$) one obtains a super-toroid. The parameter γ describes how many times the cross-section of the toroid/helix is twisted per turn. The Jacobi determinant for this substitution is



$$\det \underline{\mathbf{J}} = \det \begin{pmatrix} \frac{\partial x(a_1, \tau, \theta, \phi)}{\partial \tau} & \frac{\partial y(a_2, \tau, \theta, \phi)}{\partial \tau} & \frac{\partial z(a_3, \tau, \theta, \phi)}{\partial \tau} \\ \frac{\partial x(a_1, \tau, \theta, \phi)}{\partial \theta} & \frac{\partial y(a_2, \tau, \theta, \phi)}{\partial \theta} & \frac{\partial z(a_3, \tau, \theta, \phi)}{\partial \theta} \\ \frac{\partial x(a_1, \tau, \theta, \phi)}{\partial \phi} & \frac{\partial y(a_2, \tau, \theta, \phi)}{\partial \phi} & \frac{\partial z(a_3, \tau, \theta, \phi)}{\partial \phi} \end{pmatrix}$$

$$= a_1 a_2 a_3 \tau r_1^2(\theta, \alpha) r_2^2(\phi, \beta + \gamma \theta) [R + \tau r_2(\phi, \beta + \gamma \theta) \cos(\phi)] \quad (9.617)$$

9.13. Form factors of magnetic objects

9.13.1. Magnetic spin misalignment.

In [336] the autocorrelation function $C(r)$ of the spin misalignment has been published. The approach assumes the material to be close to magnetic saturation and considers uniform values for the exchange interaction and the saturation magnetization, i.e. it's a micro magnetic theory of single phase magnets. The correlation function is defined by

$$C(r) = \frac{KR^4}{H_i^2} \int_0^\infty \frac{j_0(qr)j_1^2(qR)}{(1 + l_H^2 q^2)^2} dq \quad (9.618)$$

where j_1 and j_2 are the spherical Bessel functions⁷ and $K = 8H_P^2/V$. H_i is the internal magnetic field, $l_H = \sqrt{2A/(\mu_0 M_s H_i)}$ the exchange length of the magnetic field, H_P the mean magnetic anisotropy field, A the exchange-stiffness constant, and μ_0 the permeability of free space. The internal magnetic field $H_i = H_0 - NM_s$ is the sum of the external applied magnetic field H_0 and the demagnetisation field $-NM_s$ (N : demagnetisation factor). V is the sample volume and M_s the saturation magnetisation.

It is assumed in this model that the magnetic anisotropy field, which perturbs the magnetization from the homogeneously magnetized state, is uniform (constant) within a spherical volume; the parameter R represents the corresponding "anisotropy-field" radius, and it is emphasized that R is not necessarily identical to the crystallite size.

The correlation is related to the scattering intensity by

$$C(r) = \frac{1}{2\pi^2} \int_0^\infty I(q)q^2 \frac{\sin(qr)}{qr} dq = \frac{1}{2\pi^2} \int_0^\infty I(q)q^2 j_0(qr) dq \quad (9.619)$$

Therefore the intensity $I(q)$ can be computed as

$$I(q) = \frac{KR^6}{H_i^2} \frac{2\pi^2}{(qR)^2} \frac{j_1^2(qR)}{(1 + l_H^2 q^2)^2} \quad (9.620)$$

Input Parameters for the models C(r) for spin misalignment and I(q) for spin misalignment:

K: $K = 8H_P^2/V$

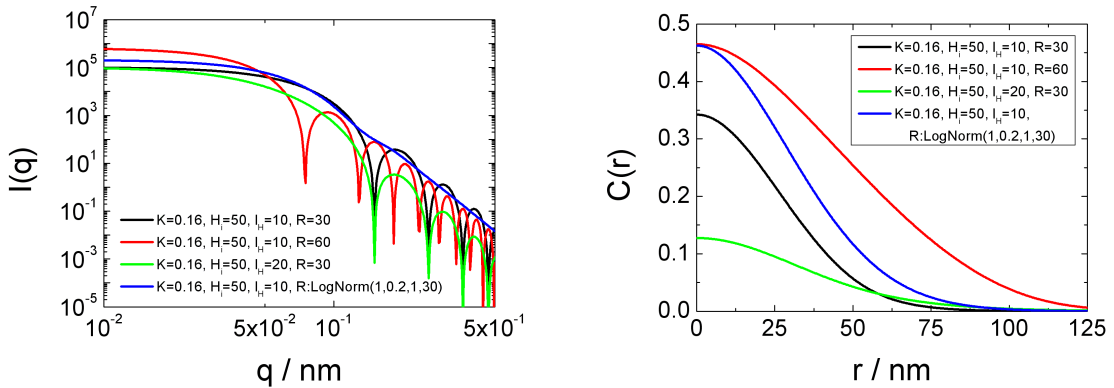
H_i: internal magnetic field H_i

l_H: exchange length of magnetic field l_H

R: anisotropy field radius R

Note: none

⁷the spherical Bessel functions j_n and y_n , and are related to the ordinary Bessel functions J_n and Y_n by: $j_n(x) = \sqrt{\frac{\pi}{2x}} J_{n+\frac{1}{2}}(x)$ and $y_n(x) = \sqrt{\frac{\pi}{2x}} Y_{n+\frac{1}{2}}(x) = (-1)^{n+1} \sqrt{\frac{\pi}{2x}} J_{-n-\frac{1}{2}}(x)$. The first two spherical Bessel function are computed by $j_0(x) = \frac{\sin(x)}{x}$ and $j_1(x) = \frac{\sin(x)}{x^2} - \frac{\cos(x)}{x}$



(A) The scattering curves for the correlation functions to the right

(B) correlation functions for the scattering curves to the left

FIGURE 9.189. Scattering curves and corresponding correlation functions. In one case the radius of the anisotropy field is assumed to have a lognormal size distribution.

9.13.2. Ferrofluids.

"Ferrofluids" and "Magnetic Liquids" are two common expressions for suspensions in which nanometer sized particles are dispersed in a carrier liquid. Figure 9.190 gives a schematic illustration. The particle material can be ferri- or ferromagnetic, and is often coated with a stabilizing dispersing agent (surfactant). The particle size is smaller than the size of magnetic domains of the corresponding bulk material. This means that every particle is single-domain ferri- or ferromagnetic. Additionally we assume in this model, that the metallic core has a shell structure to be able to model a thin oxidation layer with a reduced magnetisation on the surface. The surfactant molecules consist of a head and a polar tail. The head can coalesce with the magnetic particle, and the tail protrudes into the carrier liquid and can dissolve in it. This polar tails protruding into the liquid lead to repulsion between the colloids. Different substances like organic acids or polymers usually serve as surfactants. The carrier liquid is selected to meet the requirements for a particular applications: It can be hydrocarbon, ester, water or others. As a result of the small size of the particles they are very mobile due to Brownian motion. In zero field the magnetic moment is random oriented. Applying a magnetic field the orientation distribution of the magnetic moments of the ferrofluid particles follow a Langevin statistic.

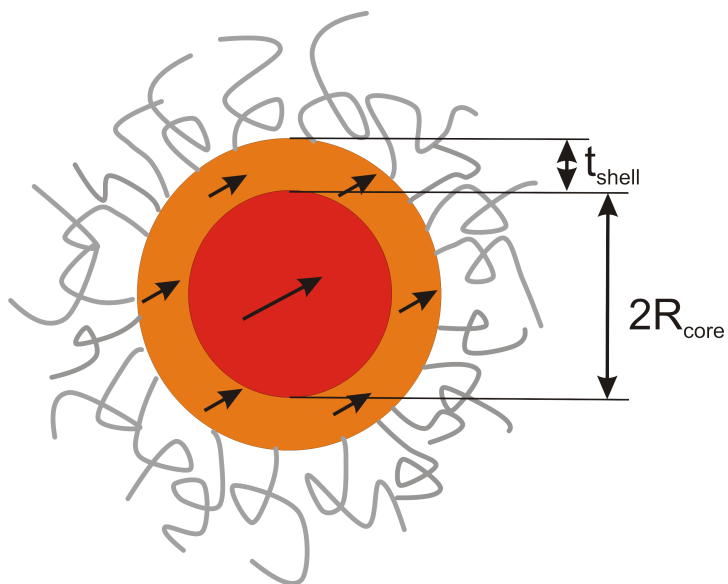


FIGURE 9.190. Sketch of a ferrofluid particle stabilised with surfactant molecules on its surface. The magnetic core can have a shell with lower magnetisation. The direction of the shell magnetisation is assumed to be parallel or antiparallel to the core magnetisation, depending on the signs of the magnetic scattering length densities.

In the present implementation of scattering function of superparamagnetic particles geometrical parameters are calculated like magnetic scattering length densities are calculated from the magnetization of the shell and the core, whereas the nuclear scattering length densities are an explicit input parameter. In such a case one has to be careful using the right units.

The relevant parameters to describe the ferrofluid particle in this model are:

- Radius of the R_{core} in reciprocal units of scattering vector q .
- Thickness of the metallic shell t_{shell} in reciprocal units of scattering vector q .
- Specific aggregation number of stabilizing surfactant molecules per surface area in units of cm^{-2} .
- Molecular volume V_{brush} of a single surfactant molecule in units of nm^3 . The scattering length density calculator of SASfit might be useful to supply this value.
- Nuclear scattering length density η_{core} of the solid ferromagnetic core.
- Nuclear scattering length density η_{sh} of an optional demagnetised shell of the solid ferromagnetic core.
- Nuclear scattering length density of the solvent η_{solv} .
- Magnetisation of the metallic core M_{core} . The magnetic scattering length density is calculated via eq. 9.621.
- Magnetisation of the metallic shell M_{sh} . Also here the magnetic scattering length density of the shell is calculated via eq. 9.621.
- Temperature T in Kelvin.
- External applied magnetic field B in Tesla or milliTesla depending of the units of q .
- Lagrange parameter α for describing superparamagnetic properties is calculated by ratio of the potential energy of the total magnetic moment of the superparamagnetic particle in the applied magnetic field to the thermal energy via eq. 9.624
- As aligned magnetic structures scatter anisotropically the angle ψ between scattering vector and the applied magnetic field needs to be supplied.
- using polarised neutrons the incident polarisation p needs to be known. p can have values $p \in [-1, 1]$.
- in case of full polarisation analysis also the transmission of the analyser needs to be known

The magnetic scattering length density η_{mag} in units of cm^{-2} is calculated from the magnetisation M given in units of A/m by

$$\eta_{\text{mag}} = D_M \mu_0 M \times 10^{-4} \quad (9.621)$$

$$D_M = 2.3161 \frac{1}{\text{Vs}} \quad (9.622)$$

$$\mu_0 = 4\pi \times 10^{-7} \text{Hm}^{-1} = 4\pi \times 10^{-7} \frac{\text{Vs}}{\text{Am}} \quad (9.623)$$

To get the magnetic scattering length density in cm^{-2} a multiplication factor of 10^{-4} has to be applied. By choosing the unit cm^{-2} for the magnetic scattering length density we have to use the corresponding units for the nuclear scattering length densities.

The other unit which has to be chosen with care is the molecular volume V_{brush} of a single surfactant molecule. From the specific aggregation and the molecular volume the excess scattering of the surfactant shell is calculated. In case that the q -values are given in units of nm^{-1} the molecular volume has to be in units of nm^3 and in case of \AA^{-1} for the q -values one also need to use \AA^3 units for the molecular volume.

The next parameter, where we need to use proper units is the Langevin parameter α , describing the ratio between potential energy of the magnetic moment of the particle to the thermal energy:

$$\alpha = \mu_{\text{FF}} B / (k_B T) \quad (9.624)$$

$$\mu_{\text{FF}} = \frac{4}{3} \pi [R_{\text{core}}^3 M_{\text{core}} + \{(R_{\text{core}} + t_{\text{shell}})^3 - R_{\text{core}}^3\} M_{\text{shell}}] \times \frac{10^{-27} \text{m}^3}{\text{nm}^3} \quad (9.625)$$

$$k_B = 1.3806488 \times 10^{-23} \text{m}^2 \text{kg s}^{-2} \text{K}^{-1} \quad (9.626)$$

The magnetic moment of a particle μ_{FF} as given in eq. 9.625 is calculated from the magnetisation of the core and the shell and their corresponding dimensions. The magnetisation has units of A/m whereas the radius and shell thickness have reciprocal dimensions of q . A magnetic moment is measured in ampere–square meters (Am^2) or in joules per tesla (JT^{-1}) which is equivalent: $1\text{Am}^2 = 1\text{JT}^{-1}$. In case that q values are given in \AA^{-1} the applied magnetic field should be given in units of mT instead of T.

The implemented form factor for ferrofluids is done for neutrons with or without incident polarisation as well as with polarisation analysis. In case of full polarisation analysis the measured intensity $I_m(\mathbf{Q})$ would depend on the incident polarisation, efficiency of the spin-flipper and in case of an opaque spin filter from its transmission values for the two spin states according to eq. 3.183. However here we just have implemented the intensities for a given incident polarisation without polarisation analysis (SANSPOL) and the intensities for POLARIS data are assumed to be corrected so that the resulting intensities correspond to perfect incident polarisation and perfect polarisation analysis. For calculating the scattering cross-section for the 4 scattering processes involved the differential cross-sections in the decoupling approach are given by

$$\frac{d\sigma_{\pm\pm}}{d\Omega}(\mathbf{Q}) = N \left\{ \left\langle \left| F_{\pm\pm}(\mathbf{Q}) \right|^2 \right\rangle + \left| \left\langle F_{\pm\pm}(\mathbf{Q}) \right\rangle \right|^2 (S(\mathbf{Q}) - 1) \right\} \quad (9.627)$$

The averages $\langle \rangle$ needs to be performed over the orientation distribution of the superparamagnetic moments of the ferrofluids and later on also about their size distribution. The averaging over the orientation distribution of the magnetic moments can be done analytically in terms of order parameters according to [527, 514, 269].

The spin dependent scattering amplitudes $F_{\pm\pm}(\mathbf{Q})$ can be calculated from the nuclear and magnetic amplitudes

$$F_{\pm\pm}(\mathbf{Q}) = F_N(\mathbf{Q}) \mp F_{M_{\perp x}}(\mathbf{Q}) \quad (9.628)$$

$$F_{\pm\mp}(\mathbf{Q}) = - (F_{M_{\perp y}}(\mathbf{Q}) \pm i F_{M_{\perp z}}(\mathbf{Q})) \quad (9.629)$$

The nuclear scattering amplitude is proportional to the nuclear excess scattering $\beta_N = F_N(Q = 0)$ and the nuclear form factor $f_N(\mathbf{Q})$

$$F_N(\mathbf{Q}) = \beta_N f_N(\mathbf{Q}) \quad (9.630)$$

The magnetic scattering amplitude $\mathbf{F}_{M_{\perp}}(\mathbf{Q})$ can be described as a vector, with

$$\mathbf{F}_{M_{\perp}}(\mathbf{Q}) = \hat{\boldsymbol{\mu}}_{\perp} D_M \mu_{\text{FF}} f_M(\mathbf{Q}) = \hat{\boldsymbol{\mu}}_{\perp} F_M(\mathbf{Q}) \quad (9.631)$$

where $f_M(Q)$ is the magnetic form factor, μ_{FF} the magnetic moment of the particle, $D_M = \frac{\gamma e}{2\pi\hbar}$, and $\hat{\mu}_\perp$ the Halpern-Johnson vector defined as

$$\hat{\mu}_\perp = \frac{\mathbf{Q}}{Q} \times \left(\frac{\mu_{\text{FF}}}{\mu_{\text{FF}}} \times \frac{\mathbf{Q}}{Q} \right) \quad (9.632)$$

It is assumed here that the neutron spin polarization is parallel or antiparallel to the axes \mathbf{e}_x which is the direction perpendicular to the incoming neutron beam.

In the following we derive the average over the squared scattering amplitude and the averaged scattering amplitude for superparamagnetic particles. The description of the nuclear scattering amplitude is based on the form factor described in [378, 375] for block copolymer micelles from Pedersen et al.

The different versions of form factor implemented in the plugin differ on one side on the model for describing the scattering of the molecules on the surface and on the other side how the data are pre-treated. At the moment three different model for the polymer chains on the surface are implemented, namely that the chains are noninteracting and follow random walk behaviour (`Chain,RW`), secondly they are interacting due to the high grafting density and a model for self avoiding walk (`Chain,SAW`) is applied, thirdly a parabolic scattering length density profile for the outer shell is used (`Chain,parabolic`). For each models a version for a sector cut in the direction ψ (`psi`), a radial averaged intensity (`rad. avg.`), the anisotropic scattering contribution, which follows a \sin^2 -law (`magnetic`), the angle dependent difference signal between two spin states (`cross-term`), as well as the radial averaged cross term (`cross-term (rad. avg.)`) has bee implemented. Also the for individual angle dependent cross-sections with full polarisation analysis are available. Finally we end up with the following possible combinations:

$$\left. \begin{array}{c} \text{FF+}(\text{Chain},\text{RW}) \\ \text{FF+}(\text{Chain},\text{SAW}) \\ \text{FF+}(\text{Chain},\text{parabolic}) \end{array} \right\} - \left\{ \begin{array}{l} \text{psi} \\ (\text{rad. avg.}) \\ \text{magnetic} \\ \text{cross-term} \\ \text{cross-term (rad. avg.)} \\ (++) \\ (-) \\ (+-) \\ (-+) \end{array} \right\} \quad (9.633)$$

9.13.3. Langevin statistics for averages of the form factor and averages of the squared form factor.

It is assumed here that the neutron spin polarization is parallel or antiparallel to the axes \mathbf{e}_x which is the direction perpendicular to the incoming neutron beam. If only the Halpern-Johnson vector $\hat{\mu}_\perp$ depends on the orientation distribution $f(\theta)$ of the magnetic moments μ of the particles but not the form factor $f_M(Q)$, which is valid for spherical symmetric particles or anisotropic shaped particles where the particle shape is not correlated to the direction of the magnetic moment, the averages in 9.627 can be

written in terms of the order parameters S_1 and S_2

$$\langle F_{\pm\pm}(\mathbf{Q}) \rangle = F_N(\mathbf{Q}) \mp F_M(\mathbf{Q}) S_1 \sin^2 \psi \quad (9.634a)$$

$$\langle F_{\pm\mp}(\mathbf{Q}) \rangle = F_M(\mathbf{Q}) S_1 \sin \psi \cos \psi \quad (9.634b)$$

$$\begin{aligned} \langle |F_{\pm\pm}(\mathbf{Q})|^2 \rangle &= |F_N(\mathbf{Q})|^2 + |F_M(\mathbf{Q})|^2 \left[S_2 \sin^4 \psi + \frac{1 - S_2}{3} \sin^2 \psi \right] \\ &\mp [F_M(\mathbf{Q}) F_N^*(\mathbf{Q}) + F_M^*(\mathbf{Q}) F_N(\mathbf{Q})] S_1 \sin^2 \psi \end{aligned} \quad (9.634c)$$

$$\langle |F_{\pm\mp}(\mathbf{Q})|^2 \rangle = |F_M(\mathbf{Q})|^2 \left[2 \frac{1 - S_2}{3} - S_2 \sin^4 \psi + \frac{4S_2 - 1}{3} \sin^2 \psi \right] \quad (9.634d)$$

The above equations for the spin dependent scattering intensities of magnetic particles with an orientation distribution $f(\theta, \phi)$ of its magnetic moment can be calculated in terms of order parameters S_l if one assumes that the particle are spherical symmetric or the orientation of the magnetic moment of a particle is not correlated to the particle orientation. Furthermore one has to assume that an external magnetic field is applied perpendicular to the incident neutron beam and that all orientations ϕ for a given angle θ , which is defined as the angle between the magnetisation vector of the particle and the direction of the external field \mathbf{B} have the same probability, i.e. the orientation distribution only depends on θ so that $f(\theta, \phi) = f(\theta)$. The orientation probability distribution function can be expanded in terms of a complete set of orthogonal functions. Expanding it in terms of Legendre polynomials $P_l(\cos \theta)$ gives

$$f(\theta) = \sum_l c_l P_l(\cos \theta) = \sum_l \frac{2l+1}{2} S_l P_l(\cos \theta) \quad (9.635)$$

The expansion coefficients can be calculated by

$$\begin{aligned} c_l &= \frac{2l+1}{2} \int_0^\pi f(\theta) P_l(\cos \theta) \sin \theta \, d\theta \\ \text{or} \end{aligned} \quad (9.636)$$

$$S_l = \int_0^\pi f(\theta) P_l(\cos \theta) \sin \theta \, d\theta$$

The first three Legendre polynomials are defined by

$$P_0(\cos \theta) = 1 \quad (9.637a)$$

$$P_1(\cos \theta) = \cos \theta \quad (9.637b)$$

$$P_2(\cos \theta) = \frac{1}{2} (3 \cos^2 \theta - 1) \quad (9.637c)$$

For superparamagnetic particle the orientation probability distribution is given by

$$f(\theta) = \frac{\alpha}{4\pi \sinh \alpha} \exp(\alpha \cos \theta) \quad (9.638)$$

with $\alpha = BM_p V_p / (k_B T)$ being the Langevin parameter. For this orientation probability distribution the first order parameters can be calculated as

$$S_0 = 1 \quad (9.639a)$$

$$S_1 = L(\alpha) = \coth \alpha - \frac{1}{\alpha} \quad (9.639b)$$

$$S_2 = 1 - 3 \frac{L(\alpha)}{\alpha} \quad (9.639c)$$

The spin-flip and spin-nonflip cross-section $\frac{d\sigma_{\pm\pm}}{d\Omega}(\mathbf{Q})$ can be obtained by combining 9.627 and 9.634. The cross-sections without polarization analysis $I_{\pm}(\mathbf{Q})$ and for unpolarized neutrons $I_{unp}(\mathbf{Q})$ are given by

$$\begin{aligned} I_{\pm}(\mathbf{Q}) &= I_{\pm\pm}(\mathbf{Q}) + I_{\pm\mp}(\mathbf{Q}) \\ &= \left[|F_N(\mathbf{Q})|^2 + |F_M(\mathbf{Q})|^2 S_1^2 \sin^2 \psi \right. \\ &\quad \left. \mp [F_M(\mathbf{Q}) F_N^*(\mathbf{Q}) + F_N^*(\mathbf{Q}) F_M(\mathbf{Q})] S_1 \sin^2 \psi \right] S(\mathbf{Q}) \\ &\quad |F_M(\mathbf{Q})|^2 \left(\frac{2}{3} (1 - S_2) + (S_2 - S_1^2) \sin^2 \psi \right) \end{aligned} \quad (9.640a)$$

$$\begin{aligned} I_{unp}(\mathbf{Q}) &= \frac{1}{2} (I_+(\mathbf{Q}) + I_-(\mathbf{Q})) \\ &= \left(|F_N(\mathbf{Q})|^2 + |F_M(\mathbf{Q})|^2 S_1^2 \sin^2 \psi \right) S(\mathbf{Q}) \\ &\quad + |F_M(\mathbf{Q})|^2 \left(\frac{2}{3} (1 - S_2) + (S_2 - S_1^2) \sin^2 \psi \right) \end{aligned} \quad (9.640b)$$

In the case of a Boltzmann orientation distribution $f(\theta) = \exp\left(\frac{B\mu}{k_B T}\right) = \exp\left(\frac{B\mu \cos \theta}{k_B T}\right)$ the order parameter S_l already have been given in eq. 9.639 and the spin dependent intensities can be written as

$$\begin{aligned} \frac{I_{\pm\pm}(\mathbf{Q})}{N} &= \left| F_M(\mathbf{Q}) L(\alpha) \sin^2 \psi \pm F_N(\mathbf{Q}) \right|^2 S(\mathbf{Q}) \\ &\quad + |F_M(\mathbf{Q})|^2 \left(\frac{L(\alpha)}{\alpha} \sin^2 \psi - \left(L^2(\alpha) - 1 + 3 \frac{L(\alpha)}{\alpha} \right) \sin^4 \psi \right) \end{aligned} \quad (9.641a)$$

$$\begin{aligned} \frac{I_{\mp\pm}(\mathbf{Q})}{N} &= (\sin^2 \psi - \sin^4 \psi) L^2(\alpha) |F_M(\mathbf{Q})|^2 S(\mathbf{Q}) \\ &\quad + |F_M(\mathbf{Q})|^2 \left((\sin^4 \psi - \sin^2 \psi) \left(L^2(\alpha) - 1 + 3 \frac{L(\alpha)}{\alpha} \right) + (2 - \sin^2 \psi) \frac{L(\alpha)}{\alpha} \right) \end{aligned} \quad (9.641b)$$

ψ is the angle between \mathbf{Q} and the horizontal axis in the plane of the detector. $L(\alpha) = \coth(\alpha) - \frac{1}{\alpha}$ is the Langevin function. In the case of a static field the superparamagnetic

particle are thermodynamic equilibrium and α is given by

$$\alpha = \frac{BM_P V_P}{k_B T}, \quad (9.642)$$

with M_P being the particle magnetization, V_P the particle volume, T the temperature in Kelvin and k_B the Boltzmann constant.

9.14. Bi-continuous and non-particulate structures

9.14.1. Stochastic models of disordered porous materials.

The stochastic models implemented base mainly on the paper from [166], where the different existing models have been compared. The "dead leaves"- model as well as the boolean models described for simplicity assuming spheres for the shapes of the grains, whereby the covariogram of a sphere is given by

$$K(r, R) = \frac{4\pi}{3} R^3 \left(1 - \frac{r}{2R}\right)^2 \left(1 + \frac{r}{4R}\right) \Theta(2R - r) \quad (9.643)$$

where $\Theta()$ is Heavyside's step function, taking the value 1 for a positive argument and 0 otherwise. A LogNormal size distribution $p_{LN}(R)$ can be taken into account analytically

$$\begin{aligned} K_{LN}(r) &= \int_0^\infty p_{LN}(R) K(r, R) dR \\ &= \frac{\pi}{24} r^3 \left(1 + \text{Erf}\left(\frac{\ln(2\mu/r)}{\sqrt{2}\sigma}\right)\right) - \\ &\quad \frac{\pi}{2} \mu^2 r e^{2\sigma^2} \left(1 + \text{Erf}\left(\frac{2\sigma^2 + \ln(2\mu/r)}{\sqrt{2}\sigma}\right)\right) + \\ &\quad \frac{2}{3} \pi e^{9\sigma^2/2} \mu^3 \left(1 + \text{Erf}\left(\frac{3\sigma^2 + \ln(2\mu/r)}{\sqrt{2}\sigma}\right)\right) \end{aligned} \quad (9.644)$$

with

$$p_{LN}(R, \mu, \sigma) = \frac{1}{R\sigma\sqrt{2\pi}} \exp\left(-\frac{1}{2} \left(\frac{\ln R - \ln \mu}{\sigma}\right)^2\right) \quad (9.645)$$

The Debye correlation function $\gamma(r)$ needs to be expressed in terms of the covariogram function $K(r)$ and the volume fractionas $\phi_0 = 1 - \phi_1$ of the pores or solid material. The knowledge of $\gamma(r)$ then allows to calculate the scattering intensity via

$$I_Q(q) = I(q) / \int_0^\infty I(q) 4\pi q^2 dq \quad (9.646)$$

$$= \frac{1}{(2\pi)^3} \int_0^\infty \gamma(r) \frac{\sin qr}{qr} 4\pi r^2 dr \quad (9.647)$$

9.14.1.1. *dead-leaves model.*

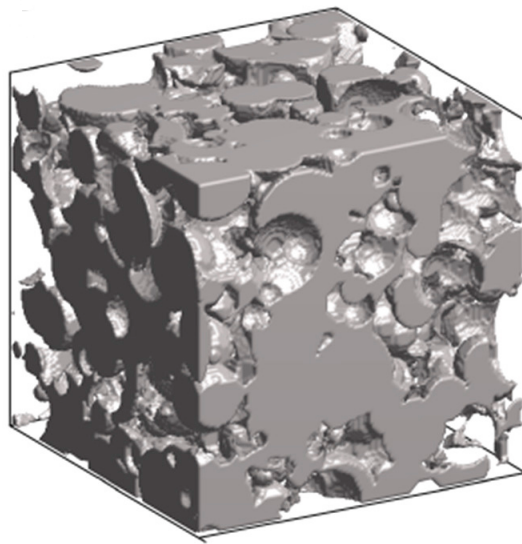


FIGURE 9.191. A real space realisation of a dead-leaves model [166].

A dead-leaves model of porous material is obtained by randomly covering an initially empty space by pore-like or solid-like spheres, and letting them overlap so that only the topmost sphere is visible. The process has to be continued until the entire space is covered either by pore-like or solid-like spheres.

For the dead leaves model the Debye correlation function is independent of the volume fraction of pores or particles and reads as

$$\gamma(r) = \frac{K_{LN}(r)}{2K_{LN}(0) - K_{LN}(r)} \quad (9.648)$$

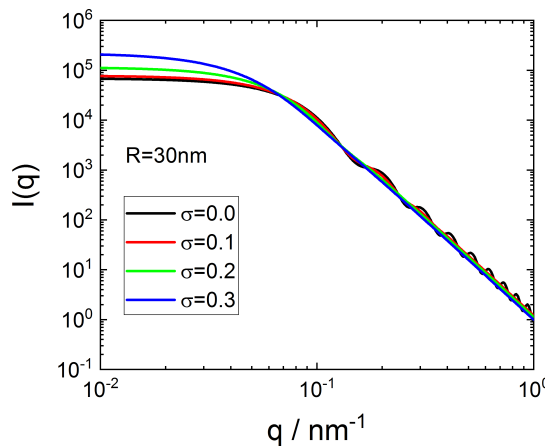


FIGURE 9.192. Dead-leaves model for different size distributions

Input Parameters for model `dead_leaves_model`:

scale: characteristic length for positional correlation ξ

dummy: not used

mu: median μ of LogNorm distribution

sigma: width σ of LogNorm distribution

Note:

- None

9.14.1.2. boolean (union model).

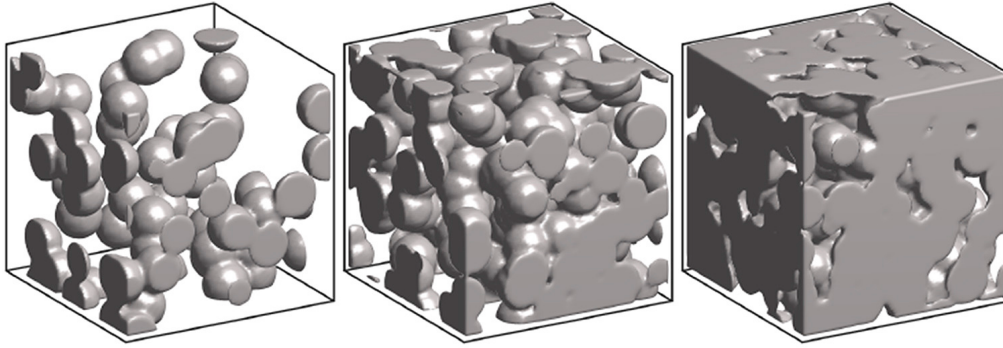


FIGURE 9.193. A real space realisation of a boolean union model of monodisperse spheres for $\phi_1 = 0.2, 0.5$, and 0.8 (taken from [166]).

The Boolean (union model) the structure is described as random positioned overlapping solid-like grains. The pore centers are positioned following a Poisson point process with density θ (average number density of grains). In the implemented model the grains are assumed being spheres with a size distribution. The geometrical covariogram is given by eq. 9.644. The corresponding Debye correlation function is than given by

$$\gamma(r) = \frac{\exp(\theta K_{LN}(r)) - 1}{\exp(\theta K_{LN}(0)) - 1} \quad (9.649)$$

$$= \frac{\exp(\theta K_{LN}(r)) - 1}{\frac{1}{\phi_0} - 1} \quad (9.650)$$

where $\phi_0 = 1 - \phi_1 = \exp(-\theta K_{LN}(0))$ is the volume fraction of pores.

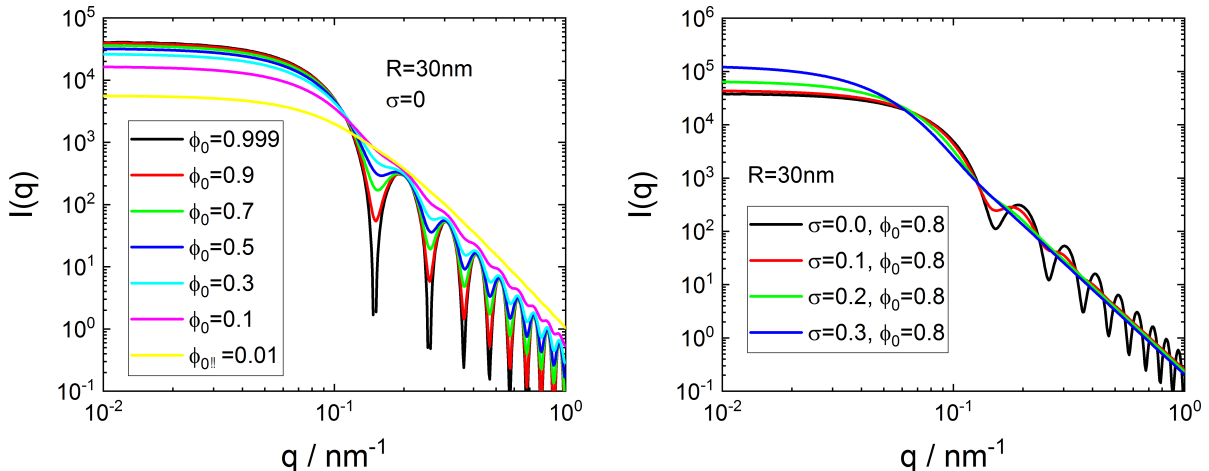


FIGURE 9.194. Boolean union model of spheres

Input Parameters for model `boolean union model`:

scale: characteristic length for positional correlation ξ

phi0: volume fraction ϕ_0 of pore-like phase

mu: median μ of LogNorm distribution

sigma: width σ of LogNorm distribution

Note:

- None

9.14.1.3. *boolean (intersection model).*

9.14.1.4. *clipped random fields.*

Clipped random field model are mathematically formalized geometrical models which have been applied to small angle scattering e.g. by [28, 483, 299, 420]. These class of models describe the morphology by stochastic standing wave $S(\mathbf{r})$ defined by

$$S(\mathbf{r}) = \frac{1}{\sqrt{N\langle A^2 \rangle}} \sum_{n=1}^N A_n \cos(\mathbf{q}_n \cdot \mathbf{r} + \phi_n) \quad (9.651)$$

ϕ_n and A_n are independent random variables, however the squared average amplitude need to be finite. For $N \rightarrow \infty$ the properties of $S(\mathbf{r})$ becomes independent of the distribution A_n and are therefore assumed to be $A_n = 1/\sqrt{2}$. The phase ϕ_n is assumed to be uniform distributed over $(0, 2\pi)$ and the direction of the random wave vector \mathbf{q}_n is uniformly distributed over all solid angle 4π . The distribution of the length of the wave vectors however follow a distribution $f(q)$ (spectral function), which than determines the properties of $S(\mathbf{r})$. The distribution is normalized so that $\int_0^\infty f(q) dq = 1$. The scattering length density $\rho(\mathbf{r})$ than takes values of ρ_1 or ρ_0 depending if $S(\mathbf{r})$ is larger or smaller than a threshold α , which can be written as

$$\rho(\mathbf{r}) = (\rho_1 - \rho_0) \Theta(S(\mathbf{r}) - \alpha) + \rho_0 \quad (9.652)$$

It is also possible to perform the definition via two thresholds α and β between which the value of $S(\mathbf{r})$ has to lay to be assigned to ρ_1 . An extension to a three phase system is also straight forward where then the phases are assigned according to the intervals $(-\infty, \alpha)$, (α, β) , and (β, ∞) . The two-point correlation function g_S of an isotropic gaussian random field is

$$g_S(\mathbf{r}) = g_S(r) = \langle S(\mathbf{r}) S(\mathbf{r} + \mathbf{x}) \rangle \quad (9.653)$$

$$= \int_0^\infty f(q) \frac{\sin qr}{qr} 4\pi q^2 dq \quad (9.654)$$

Single threshold:

For the single threshold model a two-phase system is described by a single threshold α . The volume fraction ϕ_1 of the solid phase with the scattering length density ρ_1 is than given by

$$\phi_1 = \frac{1}{2} - \frac{1}{2} \operatorname{erf}\left(\frac{\alpha}{\sqrt{2}}\right) \quad (9.655)$$

where erf is the error function and $\phi_0 = 1 - \phi_1$ the porosity. The covariance $C_{11}(r)$ than is defined as the probability that two gaussian fields $S(\mathbf{r})$ and $S(\mathbf{r} + \mathbf{x})$ takes values larger than α . Mathematically this is described equivalently by

$$C_{11}(r) = \frac{1}{2\pi} \int_0^{\arcsin(g_S(r))} \exp\left[\frac{-\alpha^2}{1 + \sin \theta}\right] d\theta + \phi_1^2 \quad (9.656)$$

The Debye correlation function is than given by

$$\gamma(r) = \frac{C_{11}(r) - \phi_1^2}{\phi_1 \phi_0} \quad (9.657)$$

from which the scattering intensity can be calculates as

$$I_Q(q) = \frac{1}{(2\pi)^3} \int_0^\infty \gamma(r) \frac{\sin qr}{qr} 4\pi r^2 dr \quad (9.658)$$

Two-cut model:

In the two-cut model, a solid phase is assumed where the random field has values between $-\alpha$ and α

$$\rho(\mathbf{r}) = (\rho_1 - \rho_0) \Theta(S(\mathbf{r}) - \alpha) \Theta(\alpha - S(\mathbf{r})) + \rho_0 \quad (9.659)$$

The volume fraction ϕ'_1 of the solid phase with the scattering length density ρ_1 is then given by

$$\phi'_1 = \operatorname{erf}\left(\frac{\alpha}{\sqrt{2}}\right) \quad (9.660)$$

The covariance $C'_{11}(r)$ is defined as the probability that two gaussian fields $S(\mathbf{r})$ and $S(\mathbf{r}+\mathbf{x})$ takes values between $\pm\alpha$ which is equivalent to

$$C'_{11}(r) = \frac{1}{\pi} \int_0^{\arcsin(g_S(r))} \exp\left[\frac{-\alpha^2}{1 + \sin \theta}\right] + \exp\left[\frac{-\alpha^2}{1 - \sin \theta}\right] d\theta + (\phi'_1)^2 \quad (9.661)$$

Two-cut intersection model:

In case of a two-cut intersection model one assumes that two independent clipped random fields with the same power spectrum must intersect to form the final structure. Therefore the probabilities have to be multiplied and the solid phase volume fraction is given by

$$\phi_1 = (\phi'_1)^2 \quad (9.662)$$

and

$$C_{11}(r) = (C'_{11}(r))^2 \quad (9.663)$$

To calculate the scattering intensity $I_Q(q)$ the spectral function $f(q)$ is assumed to be known as a parameterised function as well as its Fourier transformation, i.e. the two-point correlation function $g_S(r)$. In **SASfit** four parametrisation of the two-point correlation function $g_S(r)$ have been implemented, a simplified two parameter function

$g_{S,1}(r; \xi, d)$ [167, 166] and three 3-parameter functions. For this see e.g. [405, 419] $g_{S,2}(r; \xi, d, r_c)$ and [391] $g_{S,3}(r; \xi, d, r_c)$, [244] $g_{S,4}(r; \xi, d, r_c)$, or [86] $g_{S,5}(r; \xi, d, r_c)$.

$$g_{S,1}(r; \xi, d) = \frac{1}{\cosh(r/\xi)} \frac{\sin(2\pi r/d)}{2\pi r/d} \quad (9.664)$$

$$g_{S,2}(r; \xi, d, r_c) = \frac{\exp(-r/\xi) - r_c/\xi \exp(-r/r_c)}{1 - r_c/\xi} \frac{\sin(2\pi r/d)}{2\pi r/d} \quad (9.665)$$

$$g_{S,3}(r; \xi, d, r_c) = \frac{\sin(2\pi r/d)}{2\pi r/d} \frac{\frac{\xi}{r_c} \left(\frac{\xi}{r_c} + 1 \right)}{\left(\frac{\xi}{r_c} - 1 \right)^2} \quad (9.666)$$

$$\begin{aligned} g_{S,4}(r; \xi, d, r_c) &= \frac{4bc \left(a^2 + (b+c)^2 \right)^2}{(b+c)r} \\ &\times \left[e^{-cr} \left(\frac{a^2 - b^2 + c^2}{\left(4a^2b^2 + (a^2 - b^2 + c^2)^2 \right)^2} \right. \right. \\ &+ \frac{r}{4c \left((a^2 + b^2)^2 + 2(a^2 - b^2)c^2 + c^4 \right)} \\ &+ \frac{e^{-br}}{ab} \left(\frac{-8a^2b^2 + (a^2 + b^2)^2 + 2(a^2 - b^2)c^2 + c^4}{4 \left(4a^2b^2 + (a^2 - b^2 + c^2)^2 \right)^2} \right. \\ &\left. \left. \times \sin(ar) - \frac{ab(a^2 - b^2 + c^2)}{\left(4a^2b^2 + (a^2 - b^2 + c^2)^2 \right)^2} \cos(ar) \right) \right] \end{aligned} \quad (9.667)$$

$$\begin{aligned} g_{S,5}(r; \xi, d, r_c) &= \frac{1}{a^2 + (c-b)^2} \left\{ (a^2 + c^2 - b^2) \frac{\sin(ar)}{ar} \exp(-br) \right. \\ &\left. + 2b \frac{\exp(-cr) - \exp(-br) \cos(ar)}{r} \right\} \end{aligned} \quad (9.668)$$

where $a = 2\pi/d$, $b = 1/\xi$, and $c = 1/r_c$. Here d is the quasi-periodic distance responsible for the peak in the scattering data and ξ the decay length of that periodic structure, responsible for the width and height of the peak. The parameter r_c controls for the 2nd and 3rd model the transition to the large q -values a bit, whereas in the 4th and 5th model it also has a big influence at small q -value below the peak position given by d .

Input Parameters for model CRW 1:

scale: scaling factor for the intensity

d: quasi-periodic distance d

xi: decay length ξ of that periodic structure

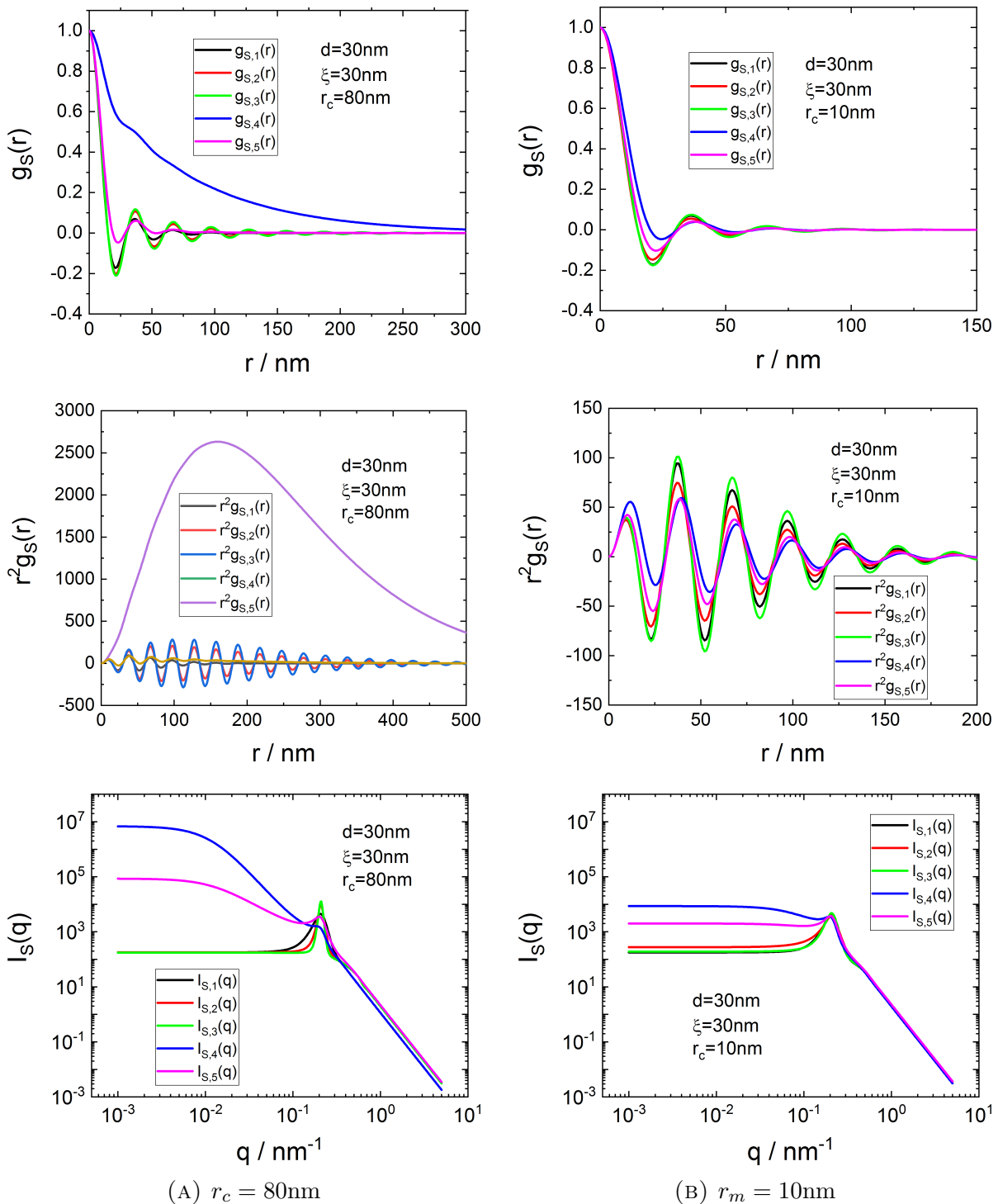


FIGURE 9.195. Two-point correlation functions $g_{S,1} \dots g_{S,5}$ and corresponding scattering intensities $I_{S,1}(q) \dots I_{S,5}(q)$

Input Parameters for models CRW 2, CRW 3, CRW 4, CRW 5:

scale: scaling factor for the intensity

d: quasi-periodic distance d

xi: decay length ξ of that periodic structure

r_c: cut-off length r_c

Note:

- for the models 2 and 3 $r_c \neq \xi$, otherwise **SASfit** returns an error message.
- Instead of assuming a two-point correlation function, one also can try to inverse the scattering data back into the spectral function $f(q)$ which e.g. has been realised in the software **SAXSMorph** [231].

9.14.2. Teubner-Strey.

The Teubner and Strey [484, 445, 460] phenomenological model often accurately describes scattering from bi-continuous micro-emulsions. The scattered intensity for this model is

$$I(q) = \frac{8\pi\langle\eta^2\rangle/\xi}{a^2 - 2bq^2 + q^4} \quad (9.669)$$

where $a^2 = (k^2 + 1/\xi^2)^2$ is a positive quantity, and $b = k^2 - 1/\xi^2$ can be a positive or negative depending on the relative magnitude of $d = 2\pi/k$ and ξ . A positive b , i.e. $\xi > d/2\pi$, leads to a peak at $q_{\max} = \sqrt{b}$ whereby for $\xi < d/2\pi$, hence negative b , no distinct peak appears. The length scale d represents a quasi-periodic repeat distance between water and oil regions within the solution, while the correlation length, ξ , corresponds to a characteristic length for positional correlation. k is defined as $2\pi/d$. The corresponding isotropic real space correlation function, $\gamma(r)$, that incorporates alternating regions of the two phases in the bi-continuous system⁸ (e.g. water and oil), is given by

$$\gamma(r) = \frac{\sin(kr)}{kr} \exp\left(-\frac{r}{\xi}\right) \quad (9.670)$$

The Fourier transformation of this function $\langle\eta^2\rangle \int_0^\infty 4\pi r^2 \frac{\sin qr}{qr} \gamma(r) dr$ leads to the scattering intensity in eq. 9.669. The correlation length defined by eq. 14.73

$$l_c = \frac{2}{\gamma(0)} \int \gamma(r) dr \quad (9.671)$$

leads to

$$l_c = \frac{d}{\pi} \arctan\left(\frac{2\pi\xi}{d}\right) \quad (9.672)$$

For large q -values the intensity decays as

$$I(q) \xrightarrow{q \rightarrow \infty} \frac{8\pi\langle\eta^2\rangle}{\xi} q^{-4} \quad (9.673)$$

The scattering invariant is given by (see also eq. 14.49)

$$\tilde{Q} = \int_0^\infty I(q) q^2 dq = 2\pi^2 \langle\eta^2\rangle \quad (9.674)$$

In case of a two phase model with sharp interphases, which have a contrast of $\Delta\rho$ one can write $\langle\eta^2\rangle = \Delta\rho^2 f_p(1 - f_p)$ (see also eq. 14.48). Next to the invariant also the first moment of the scattering curve is given analytically.

$$\int_0^\infty I(q) q dq = d\langle\eta^2\rangle \left(\frac{\pi}{2} - \arctan\left(\frac{d}{4\pi\xi} - \frac{\pi\xi}{d}\right) \right) \quad (9.675)$$

⁸In case of a correlation function $\gamma(r) = \exp\left(-\frac{r}{\xi}\right)$ the correlation length is $l_c = 2\xi$ and the expression of the scattering intensity is given by the form factor of Debye-Anderson-Brumberger in section 9.14.3 by $I(q) = I_0/(1 + (q\xi)^2)^2$

Therefore also a correlation length l_c (eq. 14.73 and 14.74) can be determined via

$$l_c = \pi \frac{\int_0^\infty I(q) q dq}{\int_0^\infty I(q) q^2 dq} = d \left(\frac{1}{4} - \frac{1}{2\pi} \arctan \left(\frac{d}{4\pi\xi} - \frac{\pi\xi}{d} \right) \right) \quad (9.676)$$

By using the identity $\frac{\pi}{4} - \frac{1}{2} \arctan \left(\frac{1}{4x} - x \right) = \arctan(2x)$ we get $l_c = \frac{d}{\pi} \arctan \left(\frac{2\pi\xi}{d} \right)$ which is consistent with eq. 9.672.

At $q_{\max} = \sqrt{b}$ the intensity is given by $I(q_{\max}) = \frac{d^2 \langle \eta^2 \rangle \xi}{2\pi}$ and for $q = 0$ one gets $I(0) = \frac{8\pi d^4 \langle \eta^2 \rangle \xi^3}{(d^2 + 4\pi^2 \xi^2)^2}$. In the limit of large values of d the form factor converges to the one from Debye-Anderson-Brumberger in section 9.14.3 which is $I(q) = I_0 / (1 + (q\xi)^2)^2$

Sometimes one finds the following parametrization

$$I(q) = \frac{I_0}{1 + c_1 q^2 + c_2 q^4} \quad (9.677)$$

As the intensity needs to be a positive number the conditions $c_2 > 0$ and $c_1 > -2\sqrt{c_2}$ have to hold. In this case the parameters are related to the above one via

$$I_0 = \frac{8\pi d^4 \langle \eta^2 \rangle \xi^3}{(d^2 + 4\pi^2 \xi^2)^2} \quad (9.678)$$

$$c_1 = \frac{2d^2 \xi^2 (d^2 - 4\pi^2 \xi^2)}{(d^2 + 4\pi^2 \xi^2)^2} \quad (9.679)$$

$$c_2 = \frac{d^4 \xi^4}{(d^2 + 4\pi^2 \xi^2)^2} \quad (9.680)$$

or

$$\xi^2 = 4 \frac{c_2}{c_1 + 2\sqrt{c_2}} \quad (9.681)$$

$$\langle \eta^2 \rangle = \frac{I_0 \xi / 2}{4\pi c_2} \quad (9.682)$$

$$d^2 = \frac{16\pi^2 c_2}{2\sqrt{c_2} - c_1} \quad (9.683)$$

Input Parameters for model Teubner-Strey:

xi: characteristic length for positional correlation ξ

d: characteristic domain size d

eta: $\langle \eta^2 \rangle$ is the mean square scattering length density fluctuation. In case of a two phase system with sharp interphases $\langle \eta^2 \rangle = \phi(1 - \phi)\Delta\rho^2$ where $\Delta\rho$ is the scattering contrast. In [466] a discussion about a smooth interface can be found.

Note:

- None

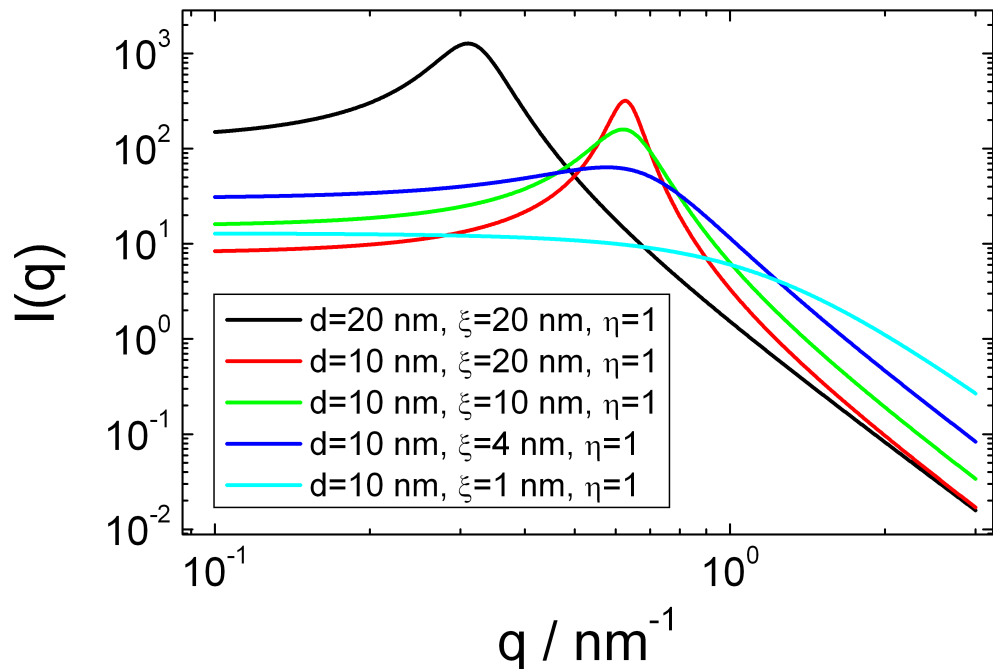


FIGURE 9.196. Some typical curves for the Teubner-Strey model function

9.14.3. Debye-Anderson-Brumberger(DAB).

This form factor calculates the scattering from a randomly distributed (i.e. non-particulate), two-phase system based on the Debye-Anderson-Brumberger (DAB) [106, 107] model for such systems. The two-phase system is characterized by a single length scale, the correlation length ξ^9 , which is a measure of the average spacing between regions of phase 1 and phase 2. The model also assumes smooth interfaces between the phases and hence exhibits Porod behavior ($I \propto q^{-4}$) at large q ($q\xi \gg 1$). The pair correlation function is given by [107]

$$\gamma(r) = \exp(-r/\xi) \quad (9.684)$$

The macroscopic scattering cross-section in the DBA model is given by

$$I_{\text{DAB}}(q) = \frac{(\pi \Delta \eta \xi^3)^2}{(1 + q^2 \xi^2)^2} \quad (9.685)$$

Input Parameters for model Debye-Anderson-Brumberger:

xi: correlation length ξ

eta: scattering length density contrast $\Delta\eta$

Note:

- None

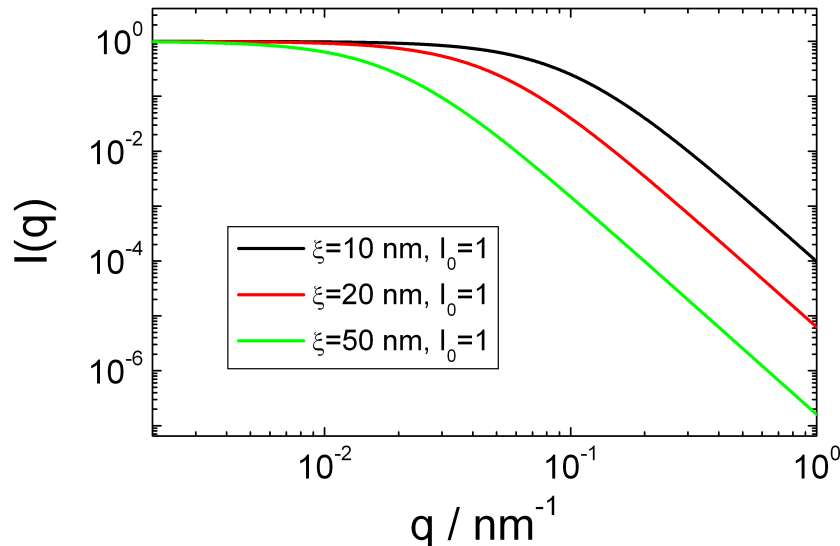


FIGURE 9.197. Some typical curves for the Debye-Anderson-Brumberger model function

⁹The Taylor series of the DAB model at small Q-values gives $I_{\text{DAB}}(Q \rightarrow 0, \xi) \sim 1 - 2\xi^2 Q^2 + 3\xi^4 Q^4$ whereas the Taylor series of a form factor in terms of the Guinier radius R_G or the Guinier law at small Q-values is $I(Q \rightarrow 0) \sim I_0 \exp(-R_G^2 Q^2/3) \sim I_0 (1 - R_G^2 Q^2/3)$, so that $\xi^2 = \frac{1}{6} R_G^2 = \frac{5}{18} R^2 = \frac{1}{3.6} R^2$

9.14.4. Generalization of the Debye-Anderson-Brumberger model.

The Debye-Anderson-Brumberger(DAB) model from the previous section 9.14.3 can be considered as a special case from a more general correlation function describing self-affine random density distributions [266, 226, 6]

$$\gamma_0(r) = \frac{2}{\Gamma(H)} \left(\frac{r}{2\xi} \right)^H K_H \left(\frac{r}{\xi} \right) \quad (9.686)$$

$$\tilde{\gamma}(r) = \gamma_0(r) \Delta\eta^2 \int_0^\infty \gamma_0(r) 4\pi r^2 dr = \frac{8\xi^3 \pi^{3/2} \Gamma(3/2 + H) \Delta\eta^2}{\Gamma(H)} \gamma_0(r) \quad (9.687)$$

where $K_n(x)$ is the modified Bessel function of the second kind and Γ is the Gamma function. H is the so-called Hurst exponent with typical value around $\frac{1}{2}$. For $H = \frac{1}{2}$ the gDAB-model results into the DAB model described in section 9.14.3. The scattering intensity is implemented as

$$I_{\text{gDAB}}(q) = \frac{\pi^3 \left((2\xi)^3 \Gamma(3/2 + H) \Delta\eta \right)^2}{\Gamma^2(H) [1 + (q\xi)^2]^{\frac{3}{2} + H}} \quad (9.688)$$

Input Parameters for model gDAB:

xi: correlation length ξ

H: Hurst exponent H

dummy: not used

eta: scattering length density contrast $\Delta\eta$

Note:

- For comparison with other models the relation of ξ to the radius of gyration R_g might be useful: $R_g^2 = \xi^2 \frac{3}{2} (3 + 2H)$
- H is constraint to $H > -3/2$
- For large q -values the model decays with the law $\propto q^{-3-2H}$

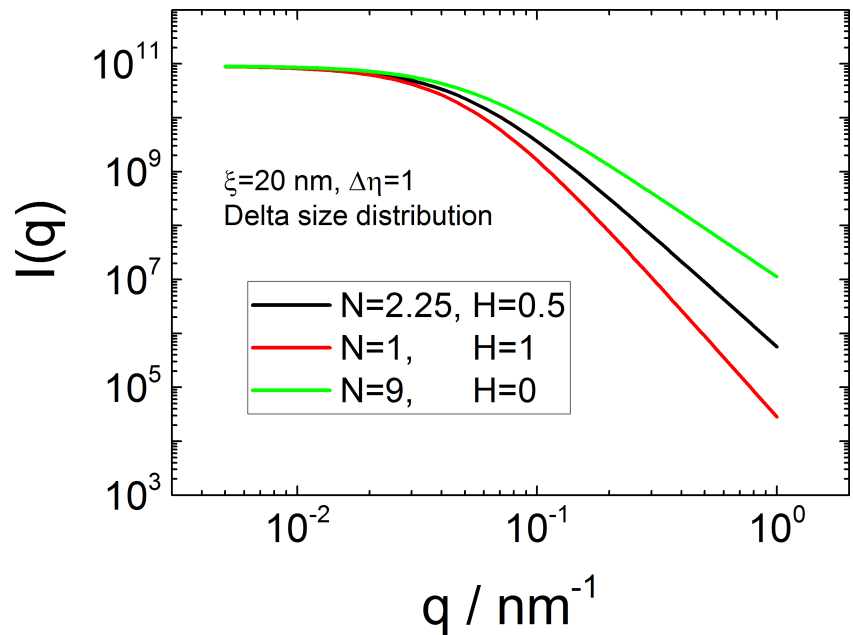


FIGURE 9.198. Some typical curves for the generalized Debye-Anderson-Brumberger model function

9.14.5. deformed random oriented Debye-Anderson-Brumberger model.

A second generalization of the DAB can be thought if the particles of the original model in section 9.14.3 first undergo a compression or an extensional deformation and secondly a random orientation averaging in the same way then for spheres becoming random oriented ellipsoids 9.6.3.

$$I_{\epsilon DAB}(q, \xi, \epsilon) = \int_0^{\pi/2} I_{DAB} \left(q\xi \sqrt{\sin^2 \theta + \epsilon^2 \cos^2 \theta} \right) \sin \theta \, d\theta \quad (9.689)$$

$$I_{DAB}(q\xi) = \frac{(\pi \Delta \eta \xi^3)^2}{(1 + q^2 \xi^2)^2} \quad (9.690)$$

The radial average can be done analytically and one gets for ϵ smaller and larger than 1 the expressions.

$$\frac{I_{\epsilon DAB}(q, \xi, \epsilon < 1)}{(\pi \Delta \eta \epsilon \xi^3)^2} = \frac{1}{4} \left(\frac{\log \left(\frac{p}{m} \right)}{\gamma u^2} + \frac{2}{mp} \right) \quad (9.691)$$

$$\frac{I_{\epsilon DAB}(q, \xi, \epsilon > 1)}{(\pi \Delta \eta \epsilon \xi^3)^2} = \frac{2\beta^2 \tan^{-1}(\alpha) - \beta^2 (\tan^{-1}(\alpha - \beta) + \tan^{-1}(\alpha + \beta)) + \alpha}{2u^2 \alpha (\epsilon^2 q^2 \xi^2 + 1)} \quad (9.692)$$

$$u = \sqrt{1 + q^2 \xi^2} \quad (9.693)$$

$$\alpha = \frac{1}{u} \sqrt{(\epsilon^2 - 1)(u^2 - 1)} \quad (9.694)$$

$$\beta = \frac{1}{u} \sqrt{1 + \epsilon^2 (u^2 - 1)} \quad (9.695)$$

$$\gamma = u \sqrt{(1 - \epsilon^2)(u^2 - 1)} \quad (9.696)$$

$$m = u^2 - \gamma \quad (9.697)$$

$$p = u^2 + \gamma \quad (9.698)$$

The limit $q \rightarrow 0$ is given by

$$\lim_{q \rightarrow 0} \frac{I_{\epsilon DAB}(q, \xi, \epsilon)}{(\pi \Delta \eta \epsilon \xi^3)^2} = 1 - \frac{2}{3} (q\xi)^2 (2 + \epsilon^2) \quad (9.699)$$

$$R_g^2 = \frac{\xi^2}{2(2 + \epsilon^2)} \quad (9.700)$$

For values of $\epsilon < 1$ the objects become disk-like and show a q^{-2} scattering behaviour at small q -values whereas for values of $\epsilon > 1$ an expected rod-like scattering behaviour of q^{-1} is observed at small q values.

Input Parameters for model epsilonDAB:

xi: correlation length ξ

epsilon: compression or extensional deformation factor of one axis ϵ

eta: scattering length density contrast $\Delta\eta$

Note:

- None

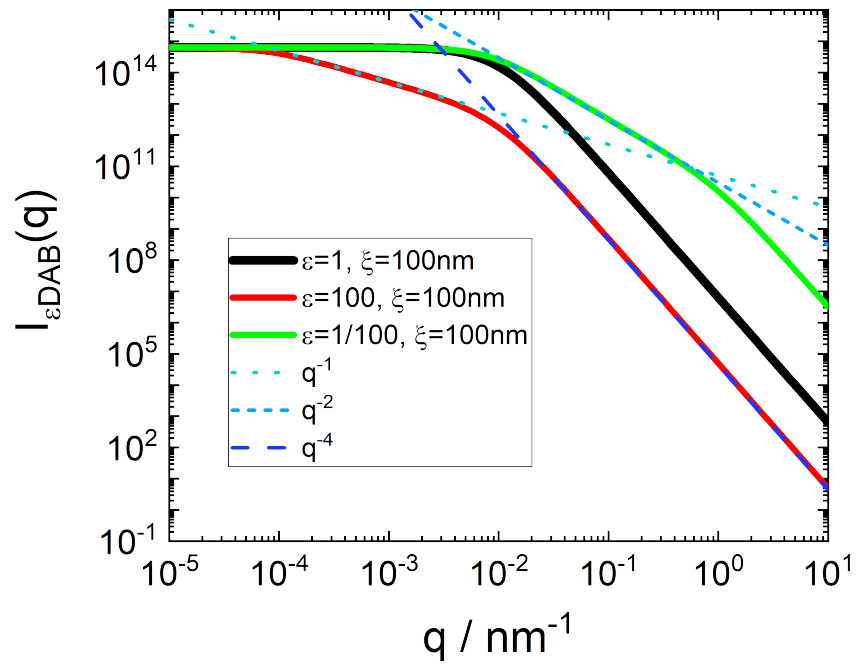


FIGURE 9.199. Some typical curves for a second generalized Debye-Anderson-Brumberger model function, this time extended by a compression or an extensional deformation and a subsequent random orientation averaging

9.14.6. Blob.

So called blob-scattering has been introduced to describe density fluctuations mainly within different polymer models like for star polymer using scaling concepts of [96] as described in [112] or similar for star-burst dendrimers in [407], which shows almost the same features than the fractal model of [19, 20]. All three models have been scaled so that at large q -values they are all proportional to $\lim_{q \rightarrow \infty} I(q) = c_P q^{-P}$ or $\lim_{q \rightarrow \infty} I(q) = c_\nu q^{-1/\nu}$

9.14.6.1. blob (beaucage).

This model is taken from [19, 20] and reads as

$$I_{b,\text{Beau}} = c_P \left(\frac{\left[\operatorname{erf} \left(qR_g / \sqrt{6} \right) \right]^3}{q} \right)^P \quad (9.701)$$

Input Parameters for model blob (beaucage):

Rg: radius of gyration R_g

P: potential law P

dummy: unused

c_P: scaling parameter c_P

Note:

- $R_g > 0$ and $q \geq 0$

9.14.6.2. blob (star).

This blob model has been introduced for star polymers by Dozier in [112] and reads after doing the scaling at large q -values as

$$I_{b,\text{star}}(q) = \frac{c_\nu}{c_N} \frac{4\pi\Gamma(\mu)}{q_b} \frac{\sin(\mu \arctan(q_b))}{(1 + q_b^2)^{\mu/2}} \quad (9.702)$$

$$\mu = \frac{1}{\nu} - 1 \quad (9.703)$$

$$q_b = \frac{2}{\sqrt{f}} q R_g \quad (9.704)$$

$$c_N = \left| 2^{1-\mu} f^{1/(2\nu)} \pi R_g^{-1/\nu} \cos(\pi/(2\nu)) \Gamma(\mu) \right| \quad (9.705)$$

Input Parameters for model blob (star):

Rg: radius of gyration R_g

nu: Flory-Huggins parameter $\frac{1}{3} < \nu \leq 1$

f: number of arms f

c_nu: scaling parameter c_ν

Note:

- $R_g > 0$ and $q \geq 0$
- $\frac{1}{3} < \nu \leq 1$
- $\lim_{q \rightarrow \infty} I_{\text{b,star}}(q) = c_\nu q^{-1/\nu}$

9.14.6.3. *blob (dendrimer)*.

This blob model has been introduced for star-burst dendrimers in [407] and reads after doing the scaling at large q -values as

$$I_{\text{b,dendrimer}}(q) = \frac{c_\nu}{c_N} \frac{4\pi\Gamma(\mu)}{q_b} \frac{\sin(\mu \arctan(q_b))}{(1 + q_b^2)^{\mu/2}} \quad (9.706)$$

$$\mu = \frac{1}{\nu} - 1 \quad (9.707)$$

$$q_b = \frac{q\xi}{[\operatorname{erf}(qR_g/\sqrt{6})]^3} \quad (9.708)$$

$$c_N = \left| 4\pi\xi^{-1/\nu} \cos(\pi/(2\nu))\Gamma(\mu) \right| \quad (9.709)$$

In the limiting case of $\xi/R_g \rightarrow \infty$ the intensity converges to

$$\lim_{\frac{\xi}{R_g} \rightarrow \infty} I_{\text{b,dendrimer}}(q) = I_{\text{b,Beau}}(q, P = \frac{1}{\nu}) \quad (9.710)$$

Input Parameters for model **blob (dendrimer)**:

- Rg:** radius of gyration R_g
nu: Flory-Huggins parameter $\frac{1}{3} < \nu \leq 1$
xi: correlation length ξ
c_nu: scaling parameter c_ν

Note:

- $R_g > 0$, $\xi > 0$, and $q \geq 0$
- $\frac{1}{3} < \nu \leq 1$
- $\lim_{q \rightarrow \infty} I_{\text{b,dendrimer}}(q) = c_\nu q^{-1/\nu}$

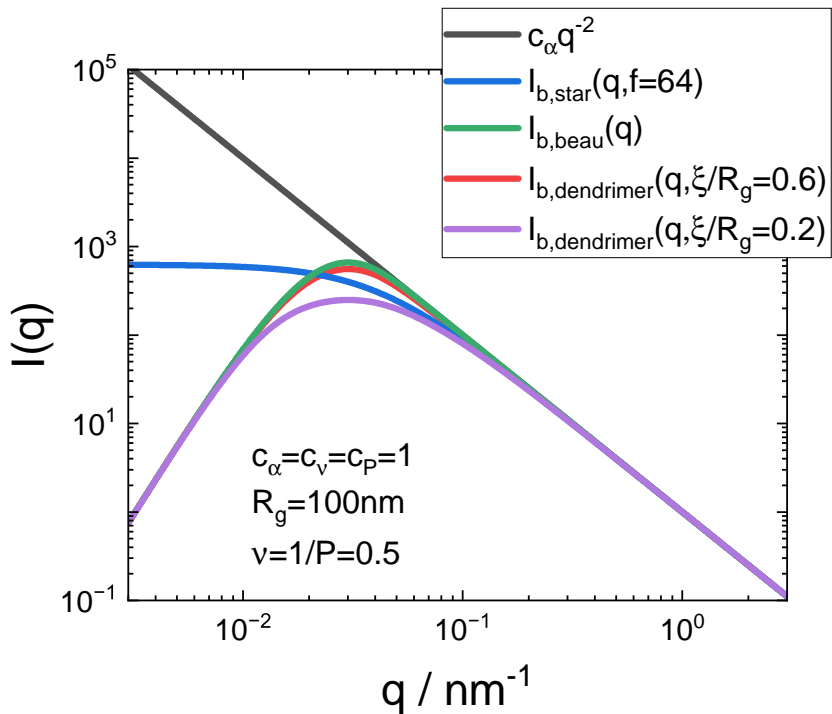


FIGURE 9.200. Comparison of scattering models for blob scattering.

9.14.7. Spinodal.

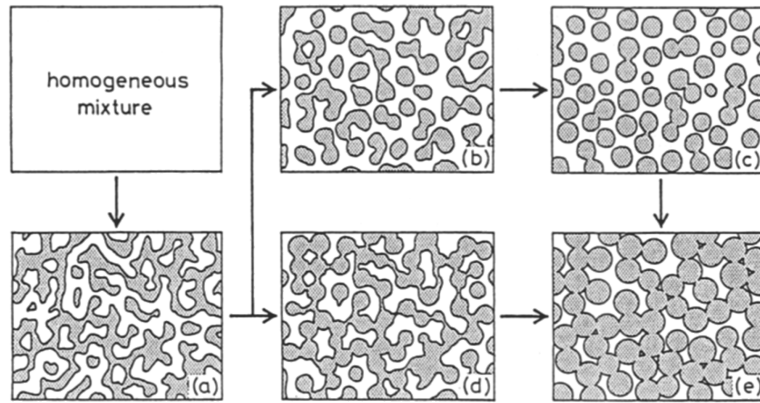


FIGURE 9.201. Schematic representation of a phase separation scheme resulting in a connected globule structure.

Spinodal decomposing systems show a characteristic small angle scattering signal with a correlation peak at some scattering value q_{\max} . The scattering curve $I(q)$ can be approximated by

$$I(q) = I_{\max} \frac{(1 + \gamma/2)x^2}{\gamma/2 + x^{2+\gamma}} \quad (9.711)$$

according to Furukawa [143], where $x = q/q_{\max}$. The position of the correlation peak at q_{\max} contain information about the size of the structures, which scatter. The exponent γ is equal to $\gamma = D + 1$ for off-critical mixtures and $\gamma = 2D$ for critical concentration mixtures, whereby D is the dimensionality of the system.

Input Parameters for model Spinodal:

I_{max}: scattering intensity at peak position I_{\max}

Q_{max}: peak maximum q_{\max}

gamma: exponent γ

Note:

- None

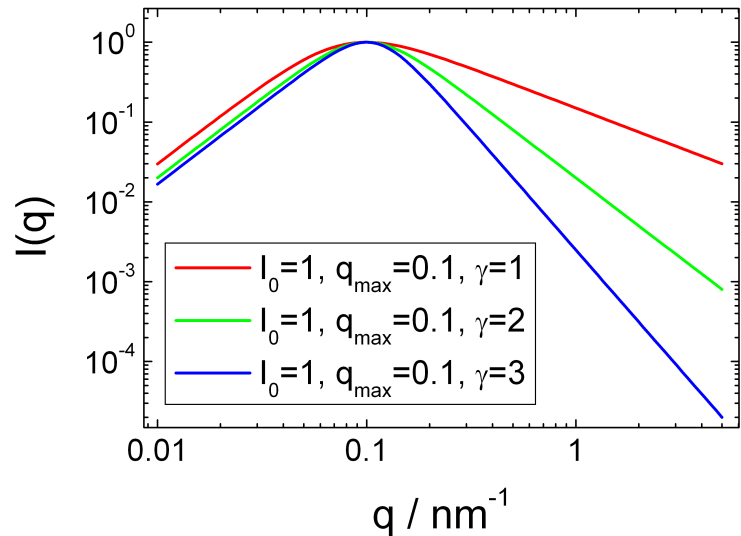


FIGURE 9.202. structure factor of the model spinodal for some selected values of γ .

9.14.8. Phase separation.

This phenomenological model describing phase separation has been supplied by Fratzl et al. [135]. They describe a heuristic "universal" formula for the scaled structure function following a quench into the miscibility gap which gives very good fits to a variety of experimental observations. A single adjustable parameter γ , is needed to fit data for alloys, binary fluids, polymer mixtures and computer simulation curves, which depends essentially only on the fraction of the volume of the minority phase. Minimizing the ratio of "surface area to volume" of the minority phase predicts a rough morphology of the system – its local character changes from spherical isolated droplets to interconnected plate-like objects as the minority fraction increases. By relating γ to this microstructure they obtain the value of γ correctly to within 10%. The scattering curve $I(q)$ can be approximated by

$$I(x = q/q_{\max}) = I_{\max} \frac{ax^4}{x^4 + c} \frac{b}{b + (x^2 - 1 + d)^2} \quad (9.712)$$

with

$$x = q/q_{\max} \quad (9.713)$$

$$b = \frac{4\gamma^2}{(1 - \gamma^2)^2} (1 - d)^2 \quad (9.714)$$

$$c = \frac{d}{b - d(1 - d)} \quad (9.715)$$

$$a = (1 + c) \left(1 + \frac{d^2}{b} \right) \quad (9.716)$$

The position of the correlation peak at q_{\max} contain information about the size of the structures, which scatter. The value of d seems to be close to 0.06. The parameter γ can be calculated from the volume fraction of the cluster and depend on their shape

$$\gamma = \begin{cases} \gamma = [4\pi\phi(1 - \phi)]^{-1}, & \text{plates, } \texttt{model} = 1 \\ \gamma = [4\sqrt{\pi\phi}(1 - \phi)]^{-1}, & \text{rods, } \texttt{model} = 2 \\ \gamma = \left[2 \left(\frac{4}{3}\pi \right)^{2/3} \phi^{1/3} (1 - \phi) \right]^{-1}, & \text{spheres, } \texttt{model} = 3 \\ \gamma = \gamma, & \text{otherwise.} \end{cases} \quad (9.717)$$

Input Parameters for model phase separation:

I_{max}: scattering intensity at peak position I_{\max}

Q_{max}: peak maximum q_{\max}

gamma/phi: γ : a measure for the width of the scaling curve. It can be calculated from the volume fraction ϕ .

d: $d \approx 0.06$

model: model to calculate $\gamma(\phi)$; 1: plates, 2: rods, 3: spheres, otherwise γ is input parameter

Note:

- for certain values of γ far away from 1 the intensity can become negative. In this case the plugin returns with an error message.

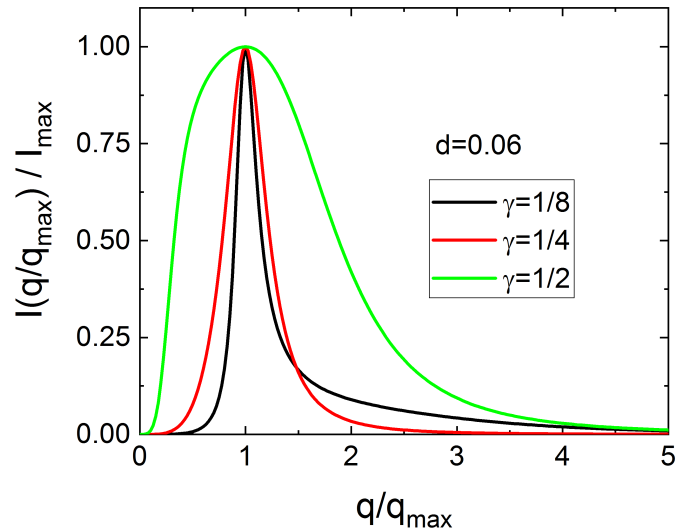


FIGURE 9.203. Scaled structure function for different values of γ .

9.14.9. OrnsteinZernike.

The low-angle scattering of thermal composition fluctuations can be described according to the Ornstein-Zernike formulation by a Lorentzian profile

$$I(q) = \frac{I_0}{1 + q^2\xi^2} \quad (9.718)$$

characterizing the exponential decay of the composition fluctuations correlation function, with correlation length ξ . The Fourier transform of a Lorentzian function corresponds to correlations dying out as $\gamma(r) \simeq \frac{1}{r} \exp(-r/\xi)$. Note that the low- Q limit of this emical form reproduces the Guinier law.

Input Parameters for model OrnsteinZernike:

I0: forward scattering I_0 at $q = 0$.

xi: correlation length ξ

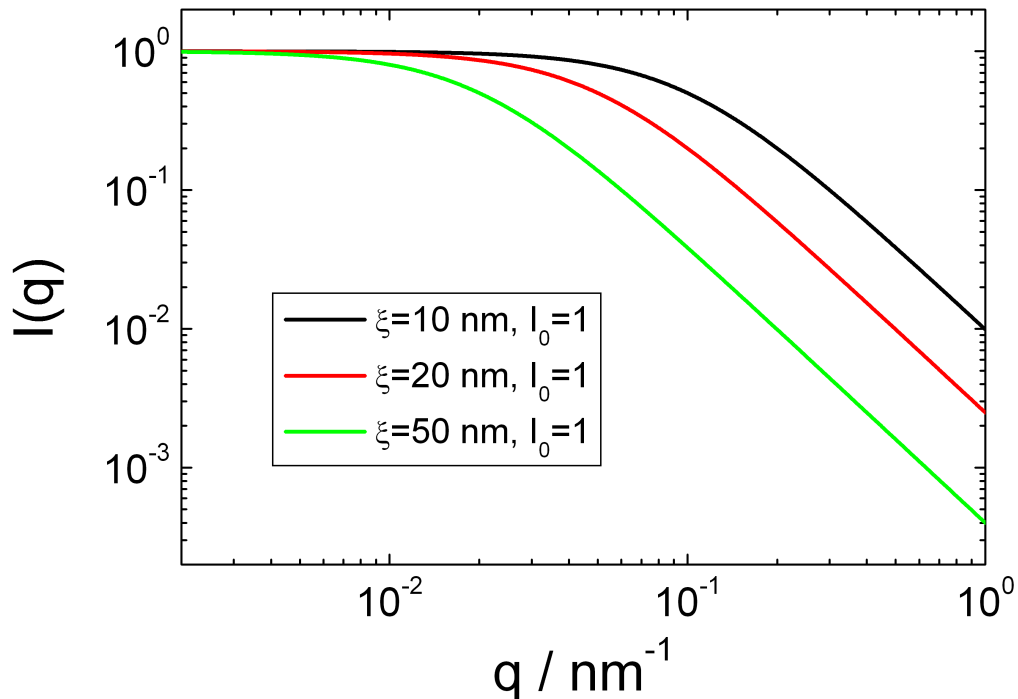


FIGURE 9.204. Ornstein-Zernike Scattering intensity $I(q)$ for different correlation lengths ξ

9.14.10. Broad-Peak.

Many SANS spectra are characterized by a broad peak even though they are from amorphous soft materials. The d -spacing corresponding to the broad peak is a characteristic distance between the scattering inhomogeneities (such as in lamellar, cylindrical, or spherical morphologies or for bicontinuous structures). The following simple functional form reproduces the broad peak feature:

$$I(q) = \frac{I_0}{(1 + (|q - q_0|\xi)^m)^p} \quad (9.719)$$

Here the peak position is related to the d -spacing as $q_0 = 2\pi/d$. Soft systems that show a SANS peak include copolymers, polyelectrolytes, multiphase systems, layered structures, etc.

Input Parameters for model Broad-Peak:

I0: scattering intensity $I(q)$ at $q = q_0$.

xi: correlation length ξ

m: exponent m

p: exponent p

Note:

- For $q_0 = 0$, $m = 2$ and $p = 1$ one gets the Ornstein-Zernike model.
- For $q_0 = 0$, $m = 2$ and $p = 2$ The Broad-Peak model is identical to the Debye-Anderson-Brumberger model.

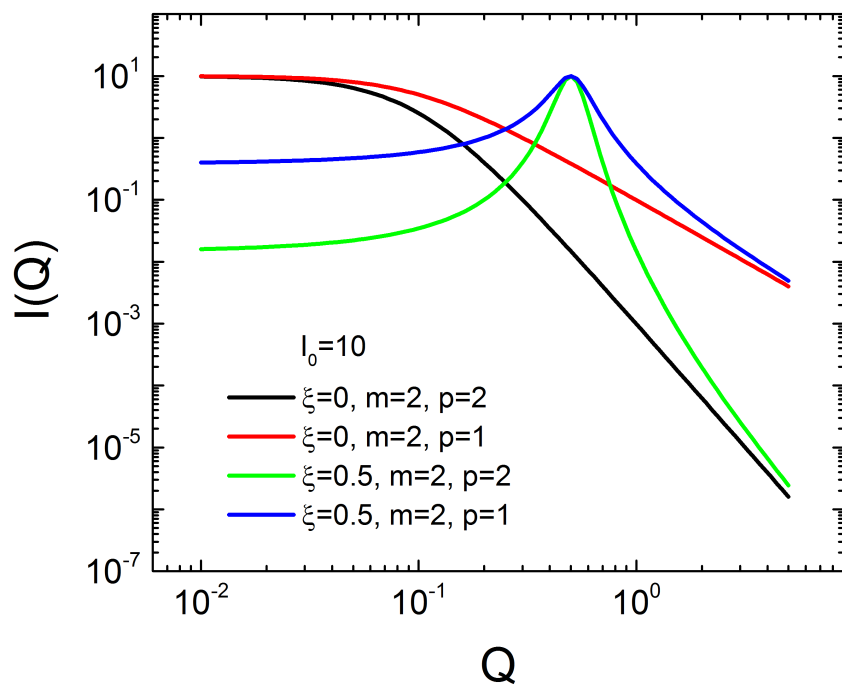


FIGURE 9.205. Empirical form factor of Broad-Peak

9.14.11. generalized Guinier approximation.

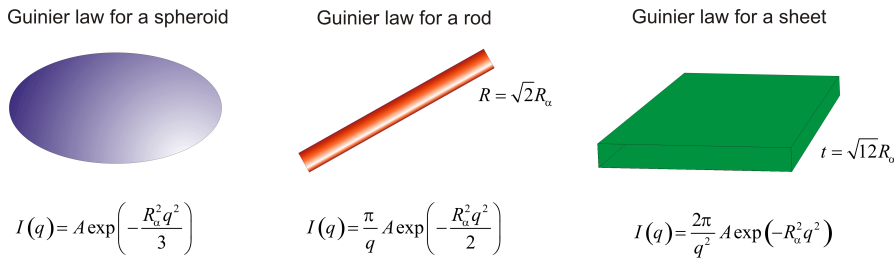


FIGURE 9.206. generalized Guinier approximation

Quantitative analysis of particle size and shape starts with the Guinier approximations. For three-dimensional objects the Guinier approximation is given by $I(q) = \exp(-Rg^2 q^2/3)$. This approximation can be extended also to rod-like and plane objects by [134, 217, 215, 216]

$$I(q) = \begin{cases} 1 & \text{for } \alpha = 0 \\ \alpha \pi q^{-\alpha} & \text{for } \alpha = 1, 2 \end{cases} A \exp\left(-\frac{R_\alpha^2 q^2}{3 - \alpha}\right) \quad (9.720)$$

$\alpha = 0$: spheroid

$\alpha = 1$: rod-like

$\alpha = 2$: plane

The apparent particle shape (also called the dimensionality) is represented in eq. 9.720 by α , which has integer values of 0, 1, and 2 for a point, a line, and a plane, respectively. Equation 9.720 states that there are q ranges, corresponding to length scales as q^{-1} , from which the particle dimension or shape, α , the radius of gyration, R_α , and the pre-factor, A , characteristic of α can be inferred. α has a value of 0 for a q range such that $qR_g < 1 - 1.3$ (the larger applies when the particle is known to be a spheroid), where R_g is the particle radius of gyration (computed about the particle centroid). In this case, the pre-factor A describes the excess differential cross-section per unit mass ($\text{cm}^2 \text{ g}^{-1}$) of a particle. If the particle has one dimension of length L , that is, much larger than the others (i.e., elongated, rod-like, or worm-like), then there is a q range such that $qR_c < 1 \ll qL$, where $\alpha = 1$. Here, R_c is the radius of gyration (computed about a line centered along L) of the cross-section perpendicular to L . If these conditions apply, the pre-factor A describes the excess differential cross section per unit length per unit mass ($\text{cm}^2 \text{ \AA}^{-1} \text{ g}^{-1}$). Finally, for planar shapes, including single bilayer vesicles, with two locally large dimensions, D , and planar cross-sectional radius of gyration (computed about a central plain), R_d , there may be a region of q such that $qR_d < 1 \ll qD$, where $\alpha = 2$. For such planar structures, the pre-factor is the excess differential cross-section per unit area per unit mass ($\text{cm}^2 \text{ \AA}^{-2} \text{ g}^{-1}$) of a sheet.

Input Parameters for model **generalized Guinier law**:

I0: scaling factor I_0 .

a: dimensionality parameter α for potential law at small Q -values; $\alpha = 0$: sphere, $\alpha = 1$: rod, $\alpha = 2$: lamellar

Ra: radius of gyration R_a

Note:

- parameter constrain: $3 > \alpha \geq 0$

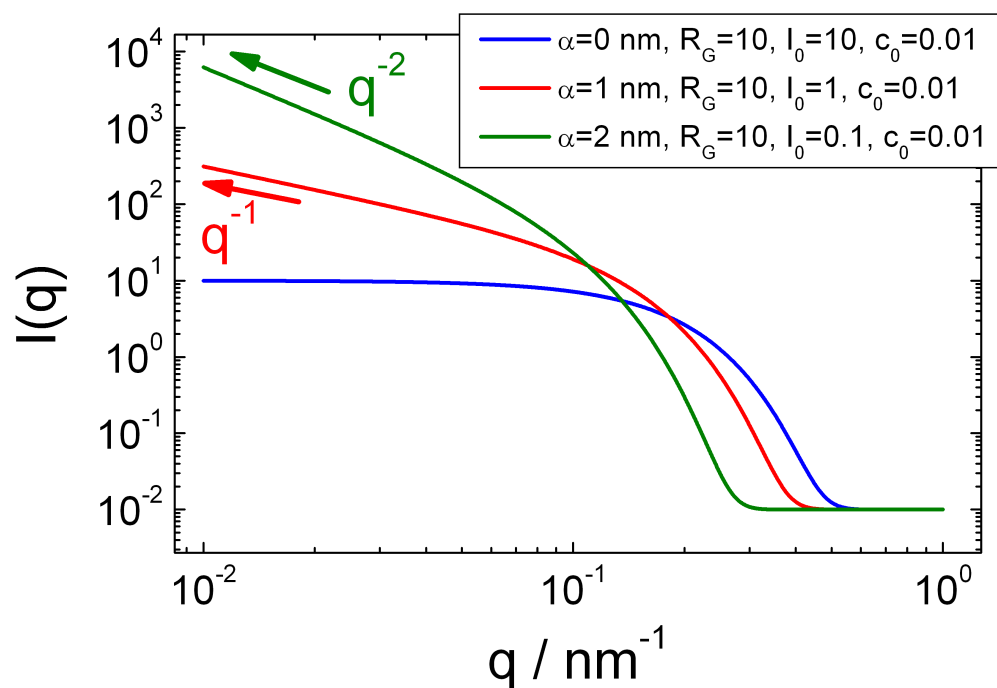


FIGURE 9.207. generalized Guinier law

9.14.12. generalized Guinier-Porod law.

The generalised Guinier-Porod approach from [183] combined the generalized Guinier approximation 9.14.11 with a potential law.

$$I(q) = \begin{cases} \frac{G_2}{Q^{s_2}} \exp\left(-\frac{Q^2 R_{g2}^2}{3-s_2}\right) & \text{for } Q \leq Q_2 \\ \frac{G_1}{Q^{s_1}} \exp\left(-\frac{Q^2 R_{g1}^2}{3-s_1}\right) & \text{for } Q_2 < Q \leq Q_1 \\ \frac{D}{Q^m} & \text{for } Q > Q_1 \end{cases} \quad (9.721)$$

To get a continuous function in $I(Q)$ and its derivative yield constrains for two parameters, which have been chosen to be Q_2 and G_2 , for which one get

$$Q_2 = \sqrt{\frac{s_1 - s_2}{\frac{2}{3-s_2} R_{g2}^2 - \frac{2}{3-s_1} R_{g1}^2}} \quad (9.722)$$

$$G_1 = G_2 \exp\left[-Q_2^2 \left(\frac{R_{g1}^2}{3-s_1} - \frac{R_{g2}^2}{3-s_2}\right)\right] Q_2^{(s_2-s_1)} \quad (9.723)$$

$$Q_1 = \frac{1}{R_{g1}} \sqrt{(m-s_1) \frac{3-s_1}{2}} \quad (9.724)$$

$$D = G_1 \exp\left(-\frac{Q_1^2 R_{g1}^2}{3-s_1}\right) Q_1^{m-s_1} \quad (9.725)$$

The constrains for the parameters are $R_{g2} > R_{g1}$, $3 > s_1 > s_2$, and $m > s_1$. The reason for that is, that the functions and their derivatives used in 9.721 are strongly monotonic decaying and the constrains are required to get a continuous function and derivative at Q_1 and Q_2 .

Input Parameters for model generalized Guinier-Porod law:

G2: scaling factor G_2 .

s2: potential law for the small Q -region, s_2 is a dimensionality parameter

RG2: radius of gyration R_{g2} (larger dimension)

s1: potential law in intermediate Q -range, s_1 is a dimensionality parameter

RG1: radius of gyration R_{g1} (smaller dimension)

m: potential law at large Q -value: Q^{-m}

Note:

- parameter constrain: $R_{g2} > R_{g1}$
- parameter constrain: $3 > s_1 > s_2$
- parameter constrain: $m > s_1$

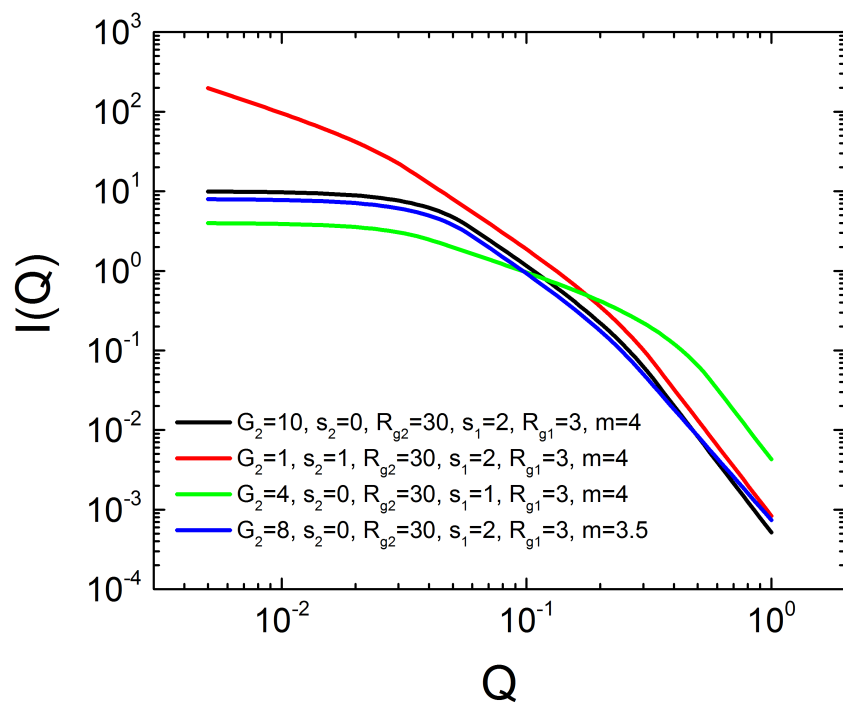


FIGURE 9.208. some examples showing the behaviour of the generalized Guinier-Porod law

9.15. Clustered Objects

9.15.1. Mass Fractal.

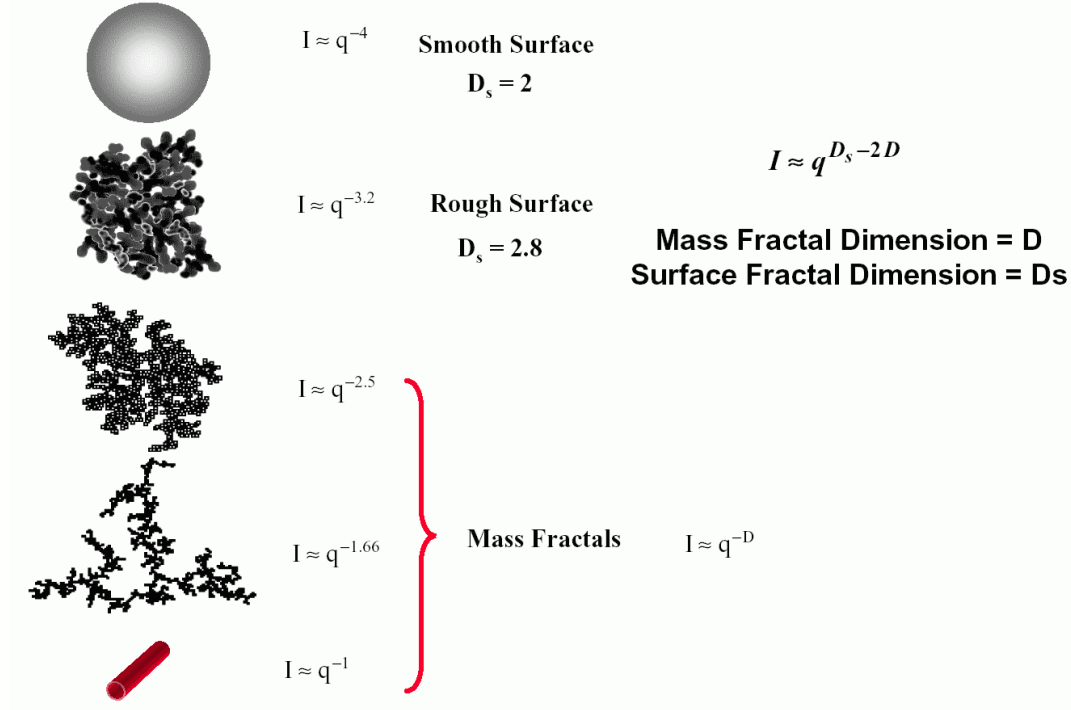


FIGURE 9.209

Aggregates and clusters often have a fractal morphology [459, 458, 227, 307, 308, 309, 310]. These self-similar clusters are well described by

$$N = k_0(R_g/r_0)^D \quad (9.726)$$

where N is the number of primary particles or monomers in the aggregate, k_0 is a constant of order unity, R_g is the radius of gyration of the aggregate, r_0 is the monomer radius, and D is the fractal dimension.

The scattering function and the density autocorrelation function of the aggregate are Fourier transform pairs; thus

$$I(q) = 4\pi \int_0^\infty g(r) r^2 \frac{\sin(qr)}{qr} dr \quad (9.727)$$

For a fractal aggregate the autocorrelation function has the form

$$g(r) \sim r^{D-d} h(r, \xi) \quad (9.728)$$

Here D is the fractal dimension, d the spatial dimension, and ξ a measure of the linear size of the aggregate proportional to the radius of gyration R_g . The function $h(r, \xi)$ is the cutoff function describing the perimeter of the aggregate. Its properties are that $h(r, \xi) \simeq 1$ for $r/\xi \lesssim 1$, but for large r/ξ it falls off faster than any power law.

TABLE 5. Scattering functions $I(q)$ for different cutoff functions $h(r, \xi)$.

SASfit-name	$h(r, \xi)$	ξ^2	$I(q)$	Ref.
Fisher-Burford	ca. $\exp\left[-\frac{r}{\xi}\right]$	$R_g^2/3$	$(1+\frac{2}{3D}q^2R_g^2)^{-D/2}$	[123]
MassFractExp	$\exp\left[-\frac{r}{\xi}\right]$	$\frac{2R_g^2}{D(D+1)}$	$\frac{\sin[(D-1)\arctan(q\xi)]}{(D-1)q\xi(1+q^2\xi^2)^{(D-1)/2}}$	[459]
MassFractGauss	$\exp\left[-\left(\frac{r}{\xi}\right)^2\right]$	$\frac{4R_g^2}{D}$	$e^{-\frac{q^2R_g^2}{D}} {}_1F_1\left[\frac{3-D}{2}, \frac{3}{2}, \frac{q^2R_g^2}{D}\right]$	[458]
Aggregate ($\text{Exp}(-x^\alpha)$ Cut-Off)	$\exp\left[-\left(\frac{r}{\xi}\right)^\alpha\right]$	—	numerical	[457]
Aggregate (OverlapSph Cut-Off)	$\begin{cases} \left(1+\frac{r}{4\xi}\right)\left(1-\frac{r}{2\xi}\right)^2, & r < 2\xi \\ 0, & r \geq 2\xi \end{cases}$	$\frac{(D+2)(D+5)}{2D(D+1)}R_g^2$	numerical	[227]
DLCAggregate	—	—	$\left[1 + \sum_{s=1}^4 C_s (qR_g)^{2s}\right]^{-D/8}$ $C_1 = \frac{8}{3D}, C_2 = 2.5$ $C_3 = -1.52, C_4 = 1.02$	[306]
RLCAGgregate	—	—	$C_1 = \frac{8}{3D}, C_2 = 3.13$ $C_3 = -2.58, C_4 = 0.95$	[306]

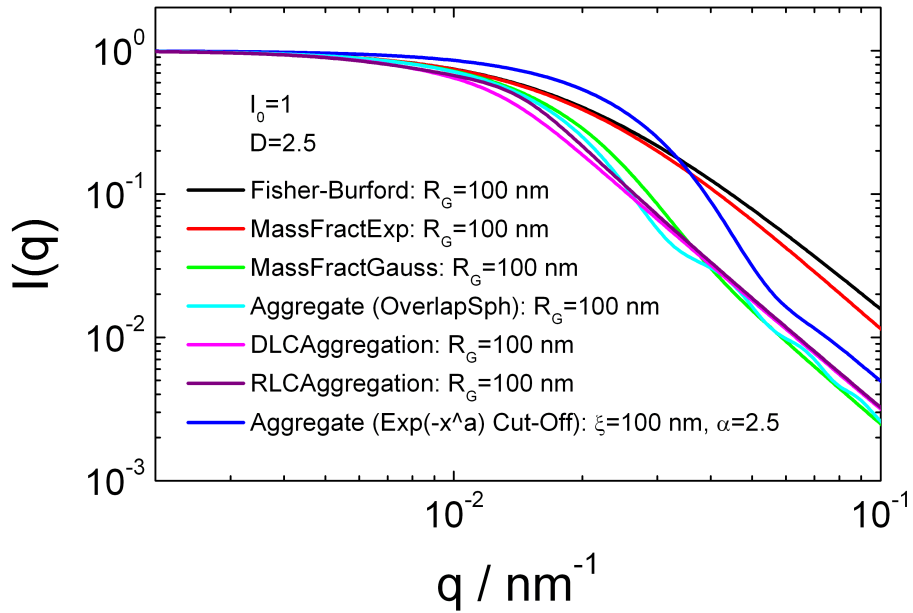


FIGURE 9.210. Form factor for the different types of mass fractals listed in 5.

9.15.2. Stacked Discs.



FIGURE 9.211. Sketch for a stack of discs with an additional surface layer

$$I_{\text{StackedDiscs}}(Q, R) = \int_0^{\pi/2} (\Delta\eta_l (V_t f_t - V_c f_c) + \Delta\eta_c V_c f_c)^2 S(Q, \Theta) \sin(\Theta) d\Theta \quad (9.729)$$

Here [280, 137, 493, 190] it is assumed that the nearest neighbor distance between the platelets obeys a Gaussian distribution and consider an internal structure factor, $S(Q, \Theta)$, first proposed by Kratky and Porod in 1949 [280]

$$S(Q, \Theta) = 1 + \frac{2}{n} \sum_{k=1}^{n-1} (n-k) \cos(kDQ \cos(\Theta)) \exp\left(-\frac{k}{2} (Q \cos(\Theta)\sigma_D)^2\right) \quad (9.730)$$

$$f_t = f_t = \frac{\sin\left(Q\left(\frac{d}{2} + h\right) \cos(\Theta)\right)}{Q\left(\frac{d}{2} + h\right) \cos(\Theta)} \cdot 2 \frac{J_1(QR \sin(\Theta))}{QR \sin(\Theta)} \quad (9.731)$$

$$f_c = f_c = \frac{\sin\left(Q\frac{d}{2} \cos(\Theta)\right)}{Q\frac{d}{2} \cos(\Theta)} \cdot 2 \frac{J_1(QR \sin(\Theta))}{QR \sin(\Theta)} \quad (9.732)$$

$$V_t = \pi R^2(d + 2h) \quad (9.733)$$

$$V_c = \pi R^2 d \quad (9.734)$$

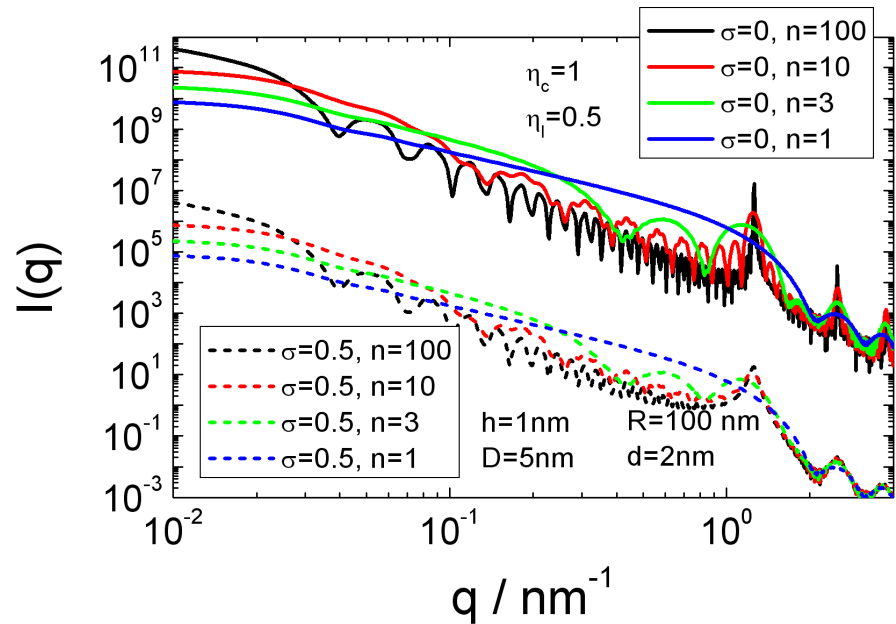


FIGURE 9.212. Scattering Intensity for a stack of discs with a layer.

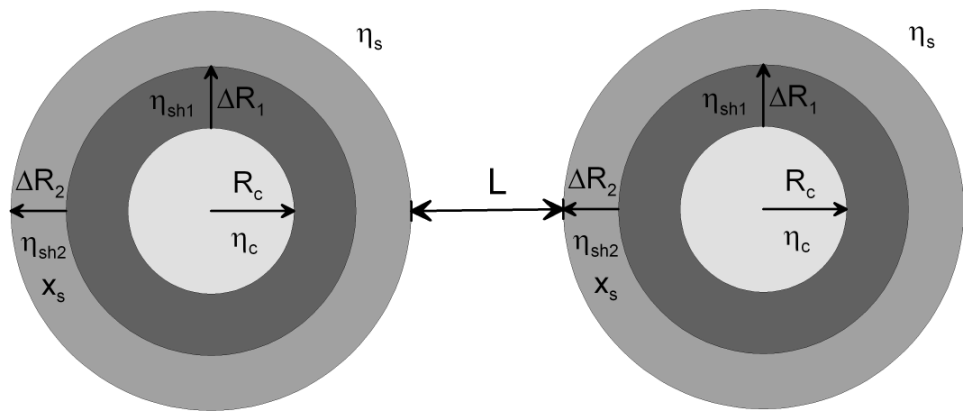
9.15.3. DumbbellShell.

FIGURE 9.213

9.15.4. DoubleShellChain.

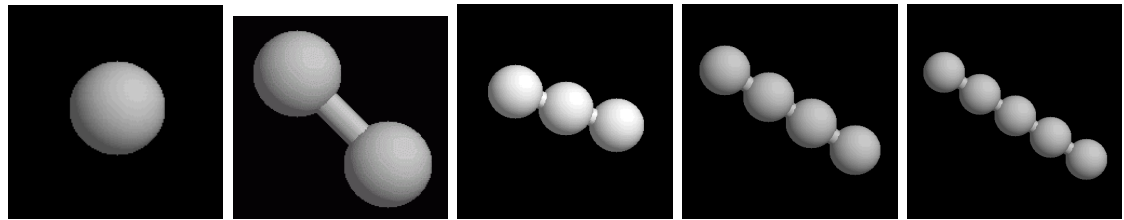


FIGURE 9.214

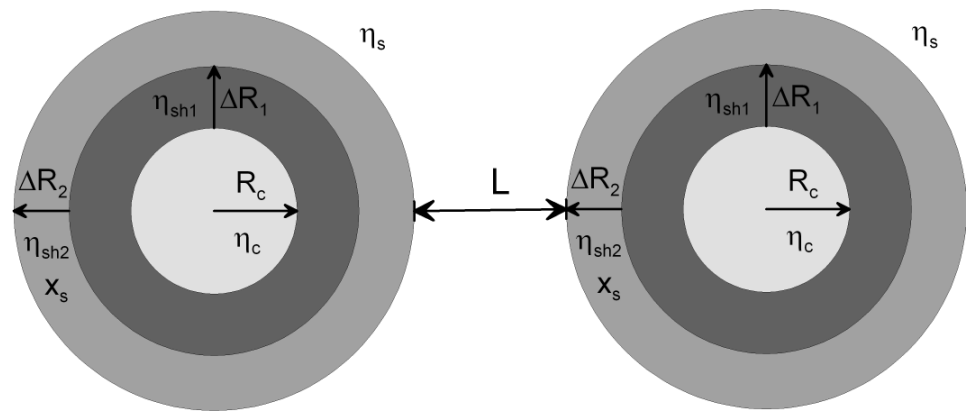


FIGURE 9.215

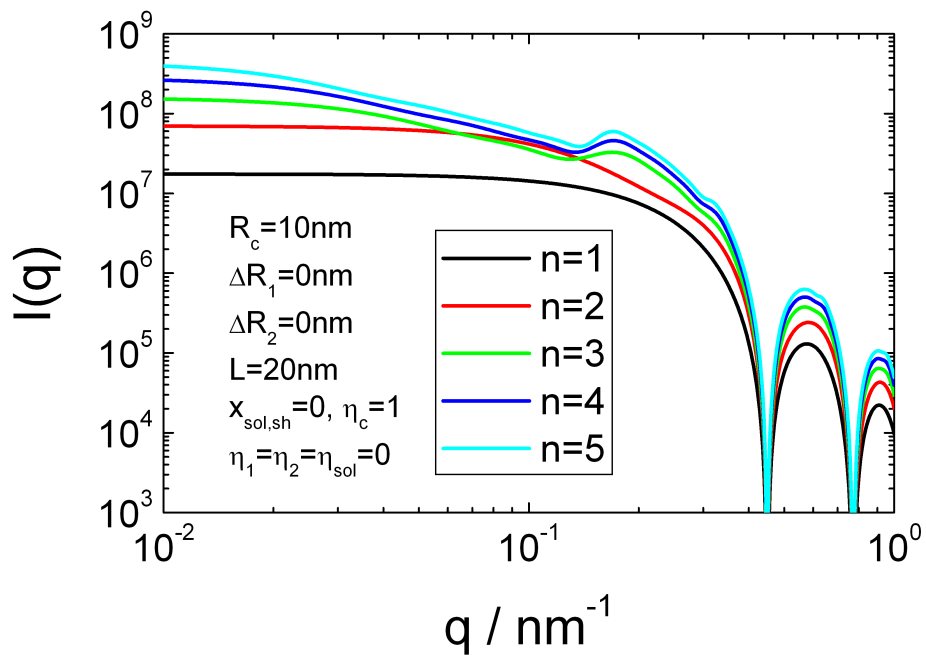


FIGURE 9.216

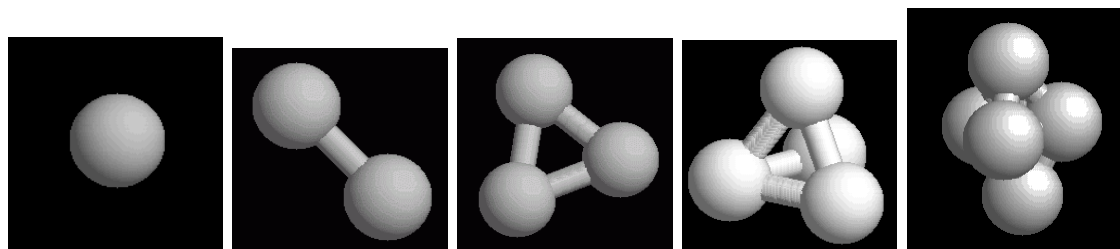


FIGURE 9.217

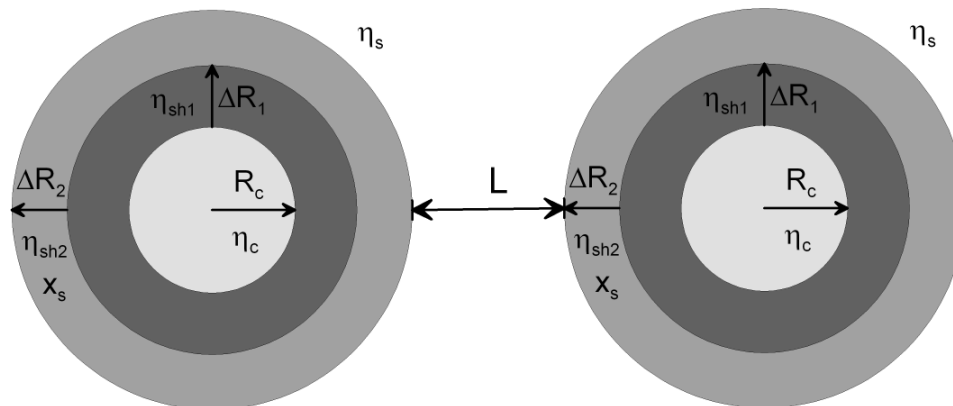


FIGURE 9.218

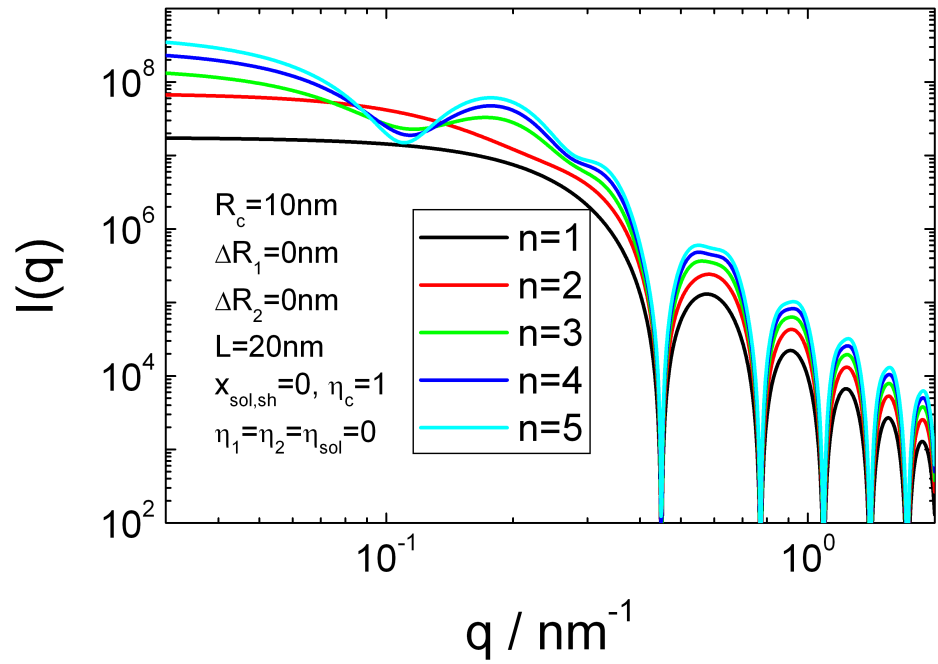


FIGURE 9.219

9.15.5. fractal size distribution of particles.

Scattering curves of samples having a fractal structure show on a log–log scale a linear behaviour. One way to define the fractal dimension of an object is to look how the mass m of an object scales with its size x . For an object with a fractal dimension of f_D the mass scales m with $m \propto x^{f_D}$. A similar behaviour also can be found if the sample contains particles with a size distribution $n(x)$ proportional to $\propto x^{-(1+f_D)}$.

$$n(x, N, f_D, x_{\min}, x_{\max}) = \begin{cases} x < x_{\min} & 0 \\ x_{\min} \leq x \leq x_{\max} & N \frac{x^{-(1+f_D)}}{\left(x_{\min}^{-f_D} - x_{\max}^{-f_D} \right) / f_D} \\ x > x_{\max} & 0 \end{cases} \quad (9.735)$$

The integral over size distribution $\int n(x, N, f_D, x_{\min}, x_{\max}) dx$ is normalized to N . In case the distribution follows such a potential law over a large enough size range a slope of $Q^{-(6-f_D)}$ in the scattering curve will be observed similar to the scattering behaviour of a surface fractal. Deviations of it can occur if the size range $[x_{\min}, x_{\max}]$ of such a size distribution is too narrow. The integration of a spherical form factor $I(Q) = \int_{\xi_{\min}}^{\xi_{\max}} N \frac{r^{-(1+f_D)}}{\left(R_{\min}^{-f_D} - R_{\max}^{-f_D} \right) / f_D} \left(\frac{4}{3} \pi r^3 \frac{\sin Qr - Qr \cos Qr}{(Qr)^3} \right)^2 dr$ has not been found yet. However, using the Debye-Anderson-Brumberger (DAB) model from 9.14.3 instead of the form factor for spheres allows to express the integral in terms of hypergeometric functions:

$$I_{f_D}(Q; N, f_D, \xi_{\min}, \xi_{\max}) = \int_0^\infty n(\xi, N, f_D, \xi_{\min}, \xi_{\max}) \xi^6 I_{\text{DAB}}(Q, \xi) d\xi \quad (9.736)$$

$$= \int_{\xi_{\min}}^{\xi_{\max}} N \frac{\xi^{-(1+f_D)}}{\left(\xi_{\min}^{-f_D} - \xi_{\max}^{-f_D} \right) / f_D} \frac{\xi^6}{(1 + \xi^2 Q^2)^2} d\xi \quad (9.737)$$

$$\begin{aligned} &= N \frac{(f_D - 4)f_D}{(f_D - 2)2Q^4 \left(\xi_{\max}^{f_D} - \xi_{\min}^{f_D} \right)} \left[\right. \\ &\quad \left. \xi_{\max}^2 \xi_{\min}^{f_D} {}_2F_1 \left(1, \frac{f_D - 2}{2}; \frac{f_D}{2}; -\frac{1}{Q^2 \xi_{\max}^2} \right) \right. \\ &\quad \left. - \xi_{\min}^2 \xi_{\max}^{f_D} {}_2F_1 \left(1, \frac{f_D - 2}{2}; \frac{f_D}{2}; -\frac{1}{Q^2 \xi_{\min}^2} \right) \right] \quad (9.738) \end{aligned}$$

$$+ N \frac{f_D Q^2 \left(\frac{\xi_{\min}^4 \xi_{\max}^{f_D}}{Q^2 \xi_{\min}^2 + 1} - \frac{\xi_{\max}^4 \xi_{\min}^{f_D}}{Q^2 \xi_{\max}^2 + 1} \right)}{2Q^4 \left(\xi_{\max}^{f_D} - \xi_{\min}^{f_D} \right)}$$

The DAB Model follows a Guinier law at small Q -values and the Porod law (Q^{-4}) at large Q values like a sphere. The term ξ^6 is added to account for the fact, that intensities scale with the squared volume of a particle. The correlation length ξ in the DAB model is related to the radius of gyration R_G or the radius of a sphere R via $\xi^2 = \frac{1}{6} R_G^2 = \frac{5}{18} R^2$.¹⁰

¹⁰The Taylor series of the DAB model at small Q -values gives $I_{\text{DAB}}(Q \rightarrow 0, \xi) \sim 1 - 2\xi^2 Q^2 + 3\xi^4 Q^4$ whereas the Taylor series of a form factor in terms of the Guinier radius R_G or the Guinier law at small Q -values is $I(Q \rightarrow 0) \sim I_0 \exp(-R_G^2 Q^2/3) \sim I_0 (1 - R_G^2 Q^2/3)$, so that $\xi^2 = \frac{1}{6} R_G^2 = \frac{5}{18} R^2 = \frac{1}{3.6} R^2$

This plugin has three variants of the above fractal size distribution implemented, namely a series of 1 to 3 of such distribution. The distributions are continuously continued when the fractal dimension is changing at a certain correlation length. For the form factor **fractal series 1** only one potential law with a fractal dimension $f_{D,1}$ is assumed. For the other cases we just assume a summation of k such distribution.

$$N(x) = \sum_{i=1}^k n(x, N_i, f_{D,i}, x_i, x_{i+1}) \quad (9.739)$$

We assume, that N is the overall number density of particles and normalize the size distribution accordingly

$$\int N(x)dx = N \quad (9.740)$$

To have a continuous sized distribution we also need to fulfill the conditions

$$n(x_{i+1}, N_i, f_{D,i}, x_i, x_{i+1}) = n(x_{i+1}, N_{i+1}, f_{D,i+1}, x_{i+1}, x_{i+2}) \forall i = 1, k - 1 \quad (9.741)$$

These conditions define the parameters N_i . Therefore we get

- (1) For **fractal series 1** we assume a single potential law, i.e. $k = 1$ and therefore only have $N_1 = N$
- (2) For **fractal series 2** we assume two potential laws. The first one ranges from x_{\min} to $x_{1,2}$ and the second one from $x_{1,2}$ to x_{\max} . Therefore N_1 and N_2 are calculated by

$$N_1 = N \frac{f_{D,2}x_{\max}^{f_{D,2}} (x_{1,2}^{f_{D,1}} - x_{\min}^{f_{D,1}})}{f_{D,2}x_{1,2}^{f_{D,1}} x_{\max}^{f_{D,2}} - x_{\min}^{f_{D,1}} (f_{D,1}x_{1,2}^{f_{D,2}} + (f_{D,2} - f_{D,1})x_{\max}^{f_{D,2}})} \quad (9.742)$$

$$N_2 = N \frac{f_{D,1}x_{\min}^{f_{D,1}} (x_{1,2}^{f_{D,2}} - x_{\max}^{f_{D,2}})}{x_{\min}^{f_{D,1}} (f_{D,1}x_{1,2}^{f_{D,2}} + (f_{D,2} - f_{D,1})x_{\max}^{f_{D,2}}) - f_{D,2}x_{1,2}^{f_{D,1}} x_{\max}^{f_{D,2}}} \quad (9.743)$$

- (3) For **fractal series 3** we assume three potential laws. The first one ranges from x_{\min} to $x_{1,2}$, the second one from $x_{1,2}$ to $x_{2,3}$ and the third from $x_{2,3}$ to x_{\max} . Therefore N_1 , N_2 and N_3 are calculated by

$$N_1 = N \left(f_{D,2}f_{D,3}x_{2,3}^{f_{D,2}} x_{\max}^{f_{D,3}} (x_{1,2}^{f_{D,1}} - x_{\min}^{f_{D,1}}) \right) \\ / \left\{ f_{D,2}f_{D,3}x_{1,2}^{f_{D,1}} x_{2,3}^{f_{D,2}} x_{\max}^{f_{D,3}} - x_{\min}^{f_{D,1}} (f_{D,1}f_{D,2}x_{1,2}^{f_{D,2}} x_{2,3}^{f_{D,3}} \right. \\ \left. + x_{\max}^{f_{D,3}} (f_{D,3}(f_{D,2} - f_{D,1})x_{2,3}^{f_{D,2}} - f_{D,1}(f_{D,2} - f_{D,3})x_{1,2}^{f_{D,2}})) \right\} \quad (9.744)$$

$$N_2 = N \left(f_{D,1}f_{D,3}x_{\min}^{f_{D,1}} x_{\max}^{f_{D,3}} (x_{1,2}^{f_{D,2}} - x_{2,3}^{f_{D,2}}) \right) \\ / \left\{ x_{\min}^{f_{D,1}} (f_{D,1}f_{D,2}x_{1,2}^{f_{D,2}} x_{2,3}^{f_{D,3}} + x_{\max}^{f_{D,3}} (f_{D,3}(f_{D,2} - f_{D,1})x_{2,3}^{f_{D,2}} \right. \\ \left. - f_{D,1}(f_{D,2} - f_{D,3})x_{1,2}^{f_{D,2}})) - f_{D,2}f_{D,3}x_{1,2}^{f_{D,1}} x_{2,3}^{f_{D,2}} x_{\max}^{f_{D,3}} \right\} \quad (9.745)$$

$$N_3 = N \left(f_{D,1}f_{D,2}x_{\min}^{f_{D,1}} x_{1,2}^{f_{D,2}} (x_{2,3}^{f_{D,3}} - x_{\max}^{f_{D,3}}) \right) \\ / \left\{ x_{\min}^{f_{D,1}} (f_{D,1}f_{D,2}x_{1,2}^{f_{D,2}} x_{2,3}^{f_{D,3}} + x_{\max}^{f_{D,3}} (f_{D,3}(f_{D,2} - f_{D,1})x_{2,3}^{f_{D,2}} \right. \\ \left. - f_{D,1}(f_{D,2} - f_{D,3})x_{1,2}^{f_{D,2}})) - f_{D,2}f_{D,3}x_{1,2}^{f_{D,1}} x_{2,3}^{f_{D,2}} x_{\max}^{f_{D,3}} \right\} \quad (9.746)$$

Input Parameters for the models **fractal series1**:

N: scaling factor, total number density of particles N

xi_min: minimum correlation length for DAB ξ_{\min}

fD1: first fractal dimension $f_{D,1}$

xi_max: maximum correlation length for DAB ξ_{\max}

Input Parameters for the models **fractal series2**:

N: scaling factor, total number density of particles N

xi_min: minimum correlation length for DAB ξ_{\min}

fD1: first fractal dimension $f_{D,1}$

xi_12: correlation length of DAB model where fractal dimension changes $\xi_{1,2}$

fD2: second fractal dimension $f_{D,2}$

xi_max: maximum correlation length for DAB ξ_{\max}

Input Parameters for the models **fractal series1**:

N: scaling factor, total number density of particles N

xi_min: minimum correlation length for DAB ξ_{\min}

fD1: first fractal dimension $f_{D,1}$

xi_12: correlation length of DAB model where fractal dimension changes $\xi_{1,2}$

fD2: second fractal dimension $f_{D,2}$

xi_23: correlation length of DAB model where fractal dimension changes $\xi_{2,3}$

fD3: third fractal dimension $f_{D,3}$

xi_max: maximum correlation length for DAB ξ_{\max}

Note: The fractal dimensions need to be larger than 0 as well as ξ_{\min} . For the numerical evaluation it is required that $0 > \xi_{\min} > \xi_{1,2} > \xi_{2,3} > \xi_{\max}$.

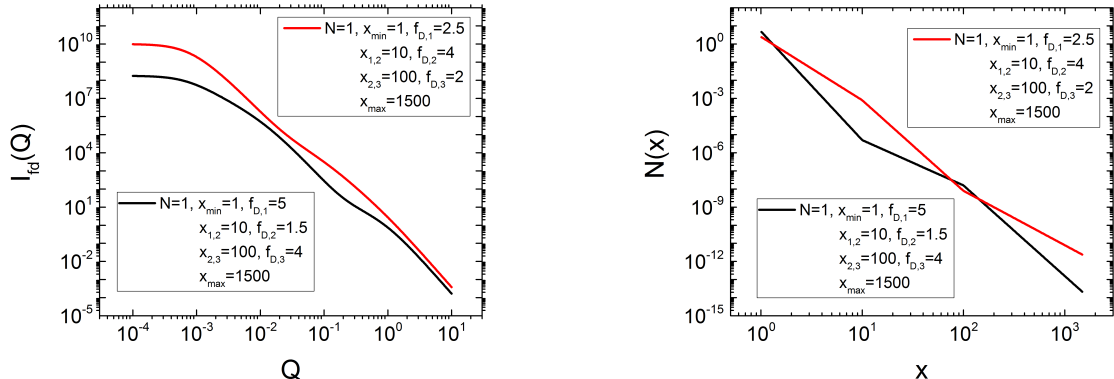


FIGURE 9.220. Scattering curve and corresponding size distribution for the plugin "fractal series 3".

9.16. Plugin functions for SESANS

An overview about the transformation cycle between the spherically symmetric correlation function, projected correlation function and differential cross section, which is relevant for the SESANS plugin functions, is described in detail in [268].

The depolarization of the neutron beam as a function of the spin-echo length z is given by

$$\frac{P_n(\delta)}{P_{n0}(\delta)} = \exp(\mathcal{G}(\delta) - \mathcal{G}(0)) \quad (9.747)$$

where the unnormalized SESANS correlation function reads as

$$\mathcal{G}(\delta) = \frac{1}{k_0^2} \int_{-\infty}^{\infty} \int_{-\infty}^{\infty} dQ_y dQ_z \frac{d\Sigma(\mathbf{Q})}{d\Omega} \frac{\cos(Q_z \delta)}{S} \quad (9.748)$$

$$= \frac{1}{k_0^2} \int_{-\infty}^{\infty} \int_{-\infty}^{\infty} dQ_y dQ_z \frac{d\sigma(\mathbf{Q})}{d\Omega} t \cos(Q_z \delta) \quad (9.749)$$

with $\mathbf{Q} = (0, Q_y, Q_z)^T$ and $\frac{d\Sigma(\mathbf{Q})}{d\Omega}$ being the macroscopic differential scattering cross-section in units of cm^2 and $\frac{d\sigma(\mathbf{Q})}{d\Omega} = \frac{1}{V} \frac{d\Sigma(\mathbf{Q})}{d\Omega}$ the differential scattering cross-section normalized on the sample volume $V = tS$ in units of cm^{-1} . t is the sample thickness and S the aperture cross-section defining the illuminated sample area. For isotropic scattering $\frac{d\sigma(\mathbf{Q})}{d\Omega} = \frac{d\sigma(Q)}{d\Omega}$, where the scattering only depends on the modulus of the scattering vector $Q = |\mathbf{Q}|$ the unnormalized SESANS correlation function simplifies to a Hankel transform of the scattering intensity multiplied by $\frac{\lambda^2 t}{2\pi}$. To see this, one has to change from cartesian coordinates $(0, Q_y, Q_z)$ to polar coordinates $Q(0, \sin \phi, \cos \phi)$ with $dQ_y dQ_z = Q dQ d\phi$. The integration over ϕ yield the cylindrical zeroth-order Bessel function

$$J_0(Qz) = \frac{1}{2\pi} \int_0^{2\pi} \cos(Q \cos(\phi) \delta) d\phi \quad (9.750)$$

so that one gets

$$\mathcal{G}(\delta) = \frac{2\pi t}{k_0^2} \int_0^{\infty} Q J_0(Q\delta) \frac{d\sigma(Q)}{d\Omega} dQ \quad (9.751)$$

$$= \frac{\lambda^2 t}{4\pi^2} 2\pi \underbrace{\int_0^{\infty} Q J_0(Q\delta) \frac{d\sigma(Q)}{d\Omega} dQ}_{\mathcal{H}_0\left[\frac{d\sigma(Q)}{d\Omega}\right](\delta)} = \frac{\lambda^2 t}{4\pi^2} 2\pi \mathcal{H}_0\left[\frac{d\sigma(Q)}{d\Omega}\right](\delta) = \lambda^2 t \tilde{G}(\delta) \quad (9.752)$$

where $\tilde{G}(\delta) = \frac{1}{2\pi} \mathcal{H}_0\left[\frac{d\sigma(Q)}{d\Omega}\right](\delta)$. $\mathcal{H}_0[\dots]$ denotes the Hankel transform of zeroth order.¹¹ Experimentally the differential cross-section is only measured up to a maximum

¹¹ There are several possible definitions of a Hankel transform $\mathcal{H}_\nu[f(r)]$ of order ν of a function $f(r)$ and its inverse $\mathcal{H}_\nu^{-1}[F_\nu(k)]$

(1) $F_\nu(k) = \int_0^\infty f(r) J_\nu(kr) r dr$ and its inverse $f(r) = \int_0^\infty F_\nu(k) J_\nu(kr) k dk$

scattering angle Θ_{\max} . Because of this **SASfit** supplies is clipping the Hankel transform of the model of the differential cross-section if the experimental data supplied with a fourth column containing the maximum scattering vector for each spin echo length $Q_{\max} = \frac{4\pi}{\lambda} \sin(\Theta_{\max}/2)$. This clipping is activated by activating the resolution option.

The instrument independent projected sample correlation function $\tilde{G}(\delta)$ can also be calculated via the Abel transform \mathcal{A} of the scattering length density autocorrelation function $\tilde{\gamma}(\mathbf{r}) = \int \rho(\mathbf{r}')\rho(\mathbf{r}' - \mathbf{r})d\mathbf{r}'$.

$$\tilde{G}(\delta) = 2 \int_z^\infty \frac{\tilde{\gamma}(r)r}{\sqrt{r^2 - z^2}} dr = \mathcal{A}[\tilde{\gamma}(r)](\delta) \quad (9.753)$$

The scattering intensity $I(Q)$ and $\tilde{\gamma}(r)$ are related by Fourier transform¹² $\mathcal{F}_{I,3D}[\dots]$

$$I(Q) = \int_0^\infty \tilde{\gamma}(r) \frac{\sin Qr}{Qr} 4\pi r^2 dr = \mathcal{F}_{I,3D}[\tilde{\gamma}(r)](Q) \quad (9.754)$$

In literature the expressions for the scattering length density autocorrelation function are often normalized to 1 for $r = 0$, i.e. the expressions $\gamma_0(r) = \tilde{\gamma}(r)/\tilde{\gamma}(0)$ are given. Also one finds that

$$\tilde{\gamma}(0) = \Delta\eta^2 V_P \quad (9.755)$$

and

$$\int_0^\infty \tilde{\gamma}(r) 4\pi r^2 dr = \Delta\eta^2 V_P^2 \quad \text{or} \quad \int_0^\infty \gamma_0(r) 4\pi r^2 dr = V_P \quad (9.756)$$

where in case of spherical particle $V_P = \frac{4}{3}\pi R^3$ In Fig. 9.221 it is shown how the functions $\tilde{\gamma}(r)$, $\tilde{G}(\delta)$ and $I(Q)$ are related to each other. However, the cycle is mathematically only exact for a one-dimensional Fourier transformation on a radial symmetric function. Such a transformation cycle is called the projection-slice theorem which is a standard analysis in imaging [51, 50]. The projection-slice theorem makes use of the fact that

$$\mathcal{H} \circ \mathcal{F}_{1D} \circ \mathcal{A} = \mathcal{F}_{1D} \circ \mathcal{A} \circ \mathcal{H} = \mathcal{A} \circ \mathcal{H} \circ \mathcal{F}_{1D} = \mathcal{I} \quad (9.757)$$

with $\mathcal{F}_{1D}(s) = \int_{-\infty}^\infty \exp(-i2\pi sr) f(r) dr$, i.e. using the pair (1) of Fourier as well pair (1) of Hankel transform conventions as given in footnote¹² and footnote¹¹. That the

(2) $F_\nu(k) = \int_0^\infty f(r) J_\nu(kr) \sqrt{kr} dr$ and its inverse $f(r) = \int_0^\infty F_\nu(k) J_\nu(kr) \sqrt{kr} dk$

(3) $F_\nu(k) = 2\pi \int_0^\infty f(r) J_\nu(2\pi kr) r dr$ and its inverse $f(r) = 2\pi \int_0^\infty F_\nu(q) J_\nu(2\pi qr) q dk$

¹²Similar to the Hankel transform also for the Fourier transform several conventions (spherical symmetric functions are assumed here) are in use which are

- (1) $\mathcal{F}_{I,3D}[f(r)](Q) = F(Q) = \int_0^\infty f(r) \frac{\sin 2\pi Qr}{2\pi Qr} 4\pi r^2 dr$ and
 $\mathcal{F}_{I,3D}^{-1}[F(Q)](r) = f(r) = \int_0^\infty F(Q) \frac{\sin 2\pi Qr}{2\pi Qr} 4\pi r^2 dQ$
- (2) $\mathcal{F}_{I,3D}[f(r)](Q) = F(Q) = \int_0^\infty f(r) \frac{\sin Qr}{Qr} 4\pi r^2 dr$ and
 $\mathcal{F}_{I,3D}^{-1}[F(Q)](r) = f(r) = \frac{1}{(2\pi)^3} \int_0^\infty F(Q) \frac{\sin Qr}{Qr} 4\pi r^2 dQ$
- (3) $\mathcal{F}_{I,3D}[f(r)](Q) = F(Q) = \frac{1}{(2\pi)^{3/2}} \int_0^\infty f(r) \frac{\sin Qr}{Qr} 4\pi r^2 dr$ and
 $\mathcal{F}_{I,3D}^{-1}[F(Q)](r) = f(r) = \frac{1}{(2\pi)^{3/2}} \int_0^\infty F(Q) \frac{\sin Qr}{Qr} 4\pi r^2 dQ$

In small angle scattering convention 2 is normally used.

\mathcal{FAS} cycle is still valid using the isotropic 3 dimensional Fourier transform $\mathcal{F}_{I,3D}$ as shown in fig. 9.221 has been shown in [268].

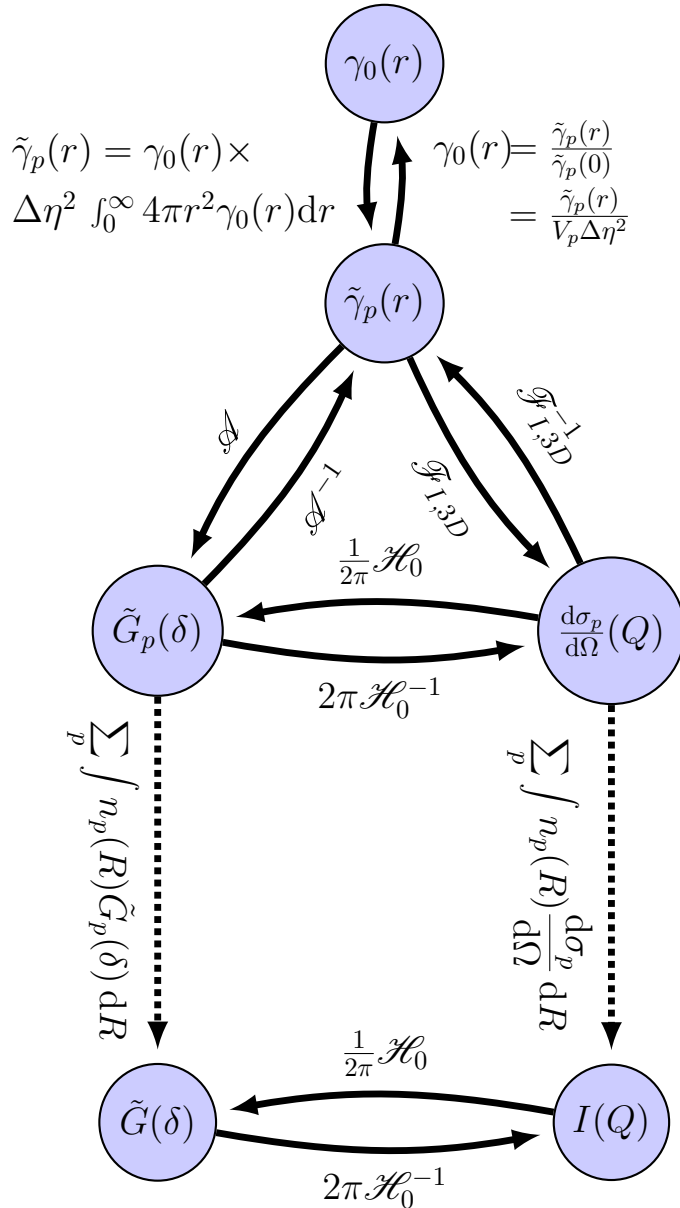


FIGURE 9.221. Transformation cycle between $\tilde{\gamma}(r)$, $I(q)$, and $\tilde{G}(\delta)$.

9.16.1. $G(\delta)$ of a sphere.

The scattering intensity for a single sphere is given by

$$I(Q) = \left(\frac{4}{3} \pi R^3 \Delta\eta \right)^2 \left(3 \frac{\sin QR - QR \cos QR}{Q^3 R^3} \right)^2 \quad (9.758)$$

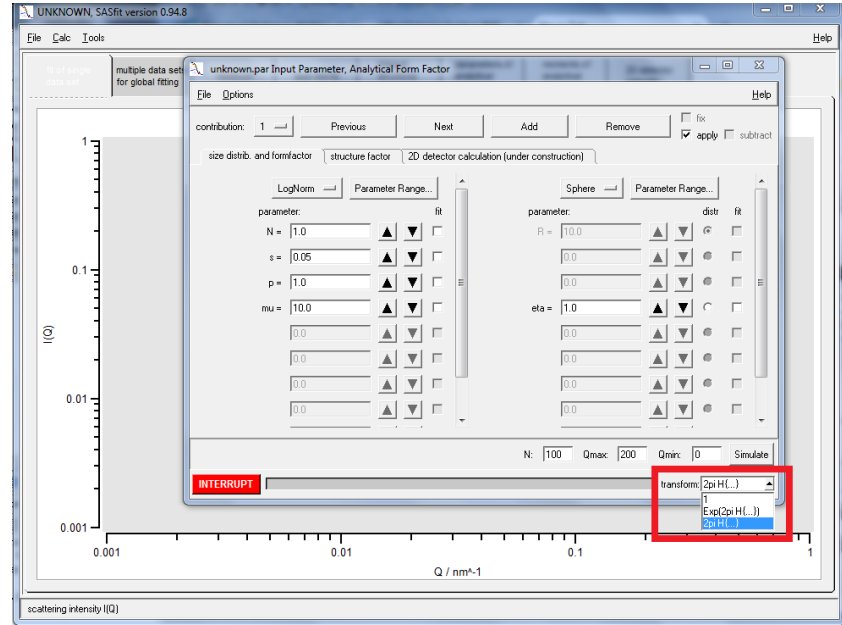


FIGURE 9.222. SASfit allows to perform a final transformation on the model function to convert a SANS signal into a SESANS signal

The unnormalized autocorrelation function for this sphere is given by

$$\tilde{\gamma}(r) = \begin{cases} \Delta\eta^2 \frac{4}{3}\pi R^3 \left(1 - \frac{3}{4}\frac{r}{R} + \frac{1}{16}\left(\frac{r}{R}\right)^3\right) & \text{for } r \leq 2R \\ 0 & \text{for } r > 2R \end{cases} \quad (9.759)$$

and the unnormalized SESANS correlation function

$$\begin{aligned} \tilde{G}_{\text{sph}}(\delta) &= \Delta\eta^2 \pi R^4 \\ &\times \left(\sqrt{1 - \xi^2} (2 + \xi^2) - \xi^2 (\xi^2 - 4) \ln \left(\frac{\xi}{1 + \sqrt{1 - \xi^2}} \right) \right) \end{aligned} \quad (9.760)$$

with $\xi = \frac{\delta}{2R}$.

Input Parameters for model G_Sphere(delta):

R: radius of sphere R

dummy: not used

dummy: not used

eta: scattering length density contrast $\Delta\eta$

Note:

- the function `G_Sphere(delta)` can be combined with a size distribution but should not be combined with a structure factor.

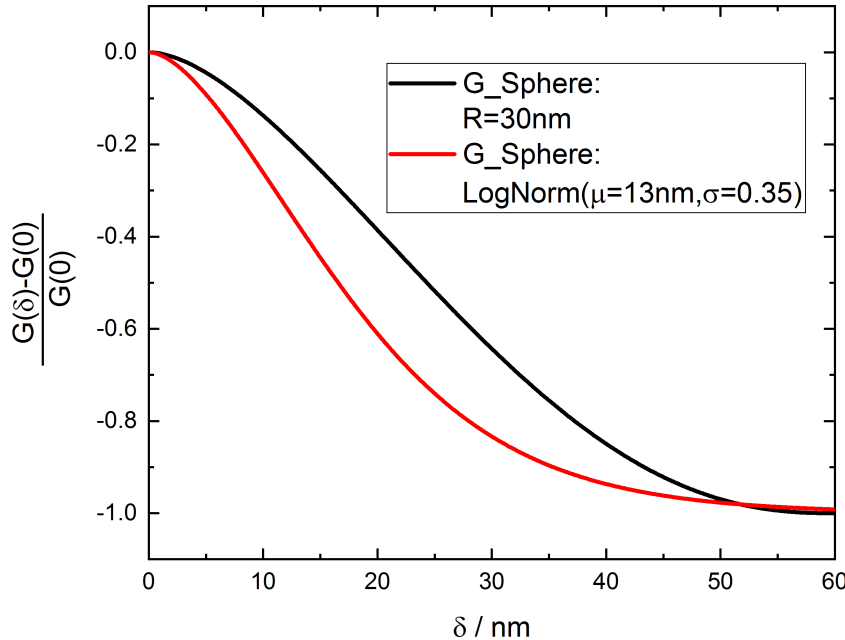


FIGURE 9.223. Projected correlation functions of monodisperse spheres and polydisperse Spheres, both with a $R_g = 24.5\text{nm}$

9.16.2. $G(\delta)$ of a randomly distributed, two-phase system (DAB) and its generalisation (gDAB).

The scattering intensity for a randomly distributed, two-phase system (DAB) is given by [107, 106, 6]

$$I(Q) = \frac{(8\pi\xi^3\Delta\eta)^2}{(1+Q^2\xi^2)^2} \quad (9.761)$$

The unnormalized autocorrelation function for the two-phase system reads as

$$\tilde{\gamma}(r) = \Delta\eta^2 8\pi\xi^3 \exp(-r/\xi) \quad (9.762)$$

and the unnormalized SESANS correlation function as

$$\tilde{G}_{\text{DAB}}(\delta) = 8\pi\xi^4 2\frac{\delta}{\xi} K_1\left(\frac{\delta}{\xi}\right) \quad (9.763)$$

The scattering intensity for a randomly distributed, self-affine two-phase system (gDAB) is given by [266, 226, 6]

$$I(Q) = \frac{V_P^2 \Delta\eta^2}{[1 + (q\xi)^2]^{\frac{3}{2}+H}} \quad (9.764)$$

The unnormalized autocorrelation function for this system is given by

$$\tilde{\gamma}(r) = \Delta\eta^2 V_P \gamma_0(r) \quad (9.765)$$

$$= \Delta\eta^2 V_P \frac{2}{\Gamma(H)} \left(\frac{r}{2\xi} \right)^H K_H \left(\frac{r}{\xi} \right) \quad (9.766)$$

$$V_P = \left(2\xi\sqrt{\pi} \right)^3 \frac{\Gamma\left(\frac{3}{2} + H\right)}{\Gamma(H)} \quad (9.767)$$

and the unnormalised SESANS correlation function

$$\tilde{G}_{gDAB}(\delta) = \frac{\Delta\eta^2 V_P^2}{2\pi\xi^2\Gamma\left(\frac{3}{2} + H\right)} \left(\frac{\delta}{2\xi} \right)^{\frac{1}{2}+H} K_{\frac{1}{2}+H} \left(\frac{\delta}{\xi} \right) \quad (9.768)$$

Input Parameters for model G_DAB(delta):

xi: correlation length ξ

dummy: not used

dummy: not used

eta: scattering length density contrast $\Delta\eta$

Input Parameters for model G_gDAB(delta):

xi: correlation length ξ

H: Hurst exponent

dummy: not used

eta: scattering length density contrast $\Delta\eta$

Note:

- the Hurst exponent needs to be in the interval $H \in (0, 1]$. Values of $H > 1$ as well as $H \in (-\frac{1}{2}, 0]$ will be accepted but might not have an established interpretation.
- the functions `G_DAB(delta)` and `G_gDAB(delta)` can be combined with a size distribution but should not be combined with a structure factor.

9.16.3. $G(\delta)$ for a generalized Gaussian coil (gGc).

The scattering intensity for a a generalized Gaussian coil (gGc) has been given by Hammouda [186, 184, 182, 185] (see also section 9.4.1.5) as

$$I_{gGc}(q) = I_0 \left(\frac{1}{\nu U^{\frac{1}{2\nu}}} \gamma \left(\frac{1}{2\nu}, U \right) - \frac{1}{\nu U^{\frac{1}{\nu}}} \gamma \left(\frac{1}{\nu}, U \right) \right) \quad (9.769)$$

with the modified variable

$$U = (2\nu + 1)(2\nu + 2) \frac{q^2 R_G^2}{6} \quad (9.770)$$

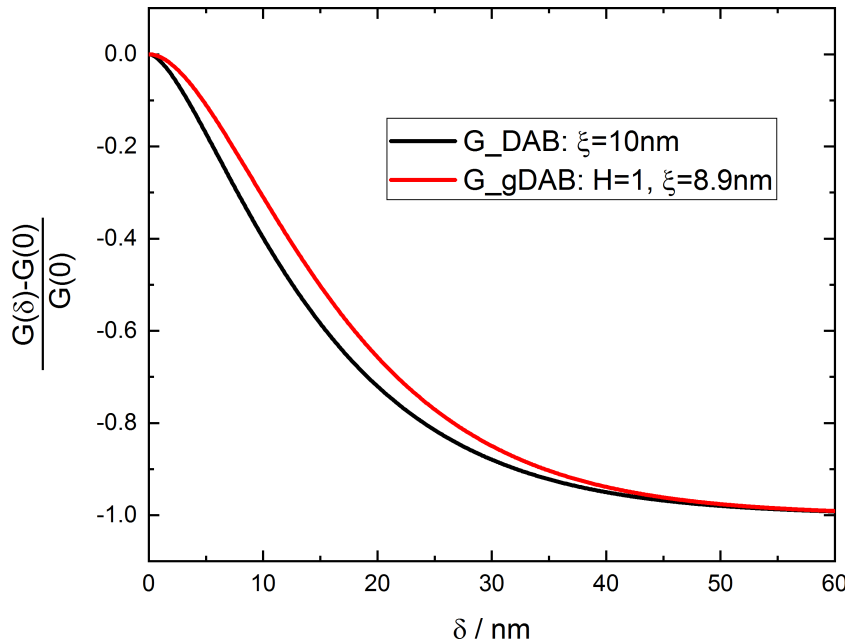


FIGURE 9.224. Projected correlation functions of the Debye-Andersson-Brumberger model and its generalisation with an Hurst exponent of $H = 1$ but both with a $R_g = 24.5\text{nm}$

and the lower incomplete Gamma Function $\gamma(a, x) = \int_0^x dt t^{a-1} \exp(-t)$. ν is the excluded volume parameter from the Flory mean field theory and typical values for them are

- $\nu = 1/3$: partially precipitate in poor solvents
- $\nu = 1/2$: thermally relaxed in "theta"-solvents
- $\nu = 3/5$: swollen in good solvents

To be able to perform the Hankel transform we start from eq. 9.255c which leads to eq. 9.769

$$P(q) = 2 \int_0^1 dx (1-x) e^{-q^2 R_g^2 (2\nu+1)(2\nu+2)x^{2\nu}} \quad (9.771)$$

The unnormalized autocorrelation function the order of integration over x and over q for the Hankel transform can be changed and one gets

$$\tilde{G}_{gGc}(\delta) = \frac{I_0 4\pi}{\nu \delta^2} \left(w^{\frac{1}{2\nu}} \Gamma \left(1 - \frac{1}{2\nu}, w \right) - w^{\frac{1}{\nu}} \Gamma \left(1 - \frac{1}{\nu}, w \right) \right) \quad (9.772)$$

$$w = \frac{3}{4} \frac{\delta^2}{(2\nu^2 + 3\nu + 1) R_g^2} \quad (9.773)$$

where $\Gamma(a, x) = \int_x^\infty dt t^{a-1} \exp(-t)$ is the upper incomplete Gamma Function. The limit $\tilde{G}_{gGc}(0)$ is only finite for $\nu \in (0, \frac{1}{2})$

$$\tilde{G}_{gGc}(0) = I_0 \frac{3\pi}{(4\nu^4 - 5\nu^2 + 1) R_g^2} \text{ for } \nu \in \left(0, \frac{1}{2} \right) \quad (9.774)$$

Input Parameters for model G_gGc(delta):

Rg: radius of gyration R_g

nu: Flory exponent

dummy: not used

beta^2: forward scattering or squared excess scattering length β^2

Note:

- For Flory exponents $\nu \geq \frac{1}{2}$: $\tilde{G}_{gGc}(0) \rightarrow \infty$.
- $\nu \in (0, \frac{1}{2})$
- the function G_gGc(delta) can be combined with a size distribution but should not be combined with a structure factor.

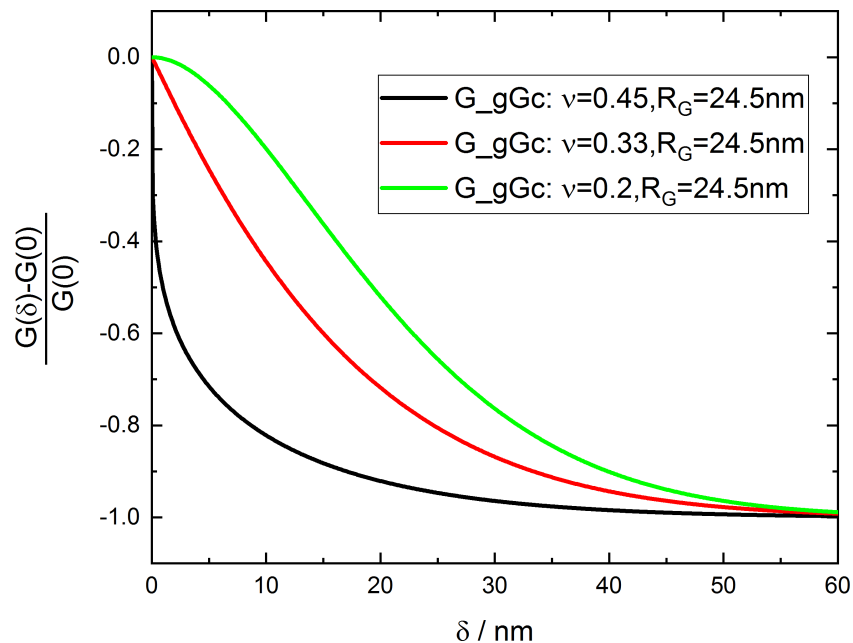


FIGURE 9.225. Projected correlation functions of the generalised Gaussian coil model with $R_g = 24.5\text{nm}$

9.17. Plugin functions for multiple scattering models

According to [438, 240] the multiple small angle scattering signal can be computed from the single scattering approximation via the intermediate function $i_1(r)$.

$$i_1(r) = 2\pi t \int_0^\infty J_0(qr) \frac{d\sigma_1}{d\Omega}(q) q dq = 2\pi t \mathcal{H}_0 \left[\frac{d\sigma_1}{d\Omega}(q) \right] (r) = 4\pi^2 t \tilde{G}(r) \quad (9.775)$$

$$i_m(r) = e^{-i_1(0)/k_0^2} k_0^2 \left(\exp \left(i_1(r)/k_0^2 \right) - 1 \right) \quad (9.776)$$

$$= k_0^2 \left[\exp \left(\frac{t}{k_0^2} (\tilde{G}(r) - \tilde{G}(0)) \right) - \exp \left(-\frac{t}{k_0^2} \tilde{G}(0) \right) \right] \quad (9.777)$$

$$\frac{d\sigma_m}{d\Omega}(q) = \frac{1}{2\pi t} \int_0^\infty J_0(qr) i_m(r) r dr = \frac{1}{2\pi t} \mathcal{H}_0 [i_m(r)] (q) \quad (9.778)$$

$$k_0 = \frac{2\pi}{\lambda} \quad (9.779)$$

where $\frac{d\sigma_m}{d\Omega}(q)$ is the measured scattering cross-section including multiple scattering contributions normalized on the sample volume and corrected for absorption and incoherent scattering, i.e. corrected for all beam attenuation effects except coherent small angle scattering. $\frac{d\sigma_1}{d\Omega}(q)$ is the corresponding single scattering cross-section per volume. It can be seen, that the intermediate function $i_1(r)$ is except a pre-factor identical to the projected correlation function $\tilde{G}(r)$ used in the theory of SESANS or SEMSANS analysis from section 9.16

$$i_1(r) = \tilde{G}(r) (2\pi)^2 t \quad (9.780)$$

At the moment all the analytical models for projected correlation functions SESANS from chapter 9.16 are also now available as scattering curves including multiple scattering effects. To include multiple scattering effects the scale parameter will be for all models the total scattering cross-section per sample volume $\Sigma_t = \tilde{G}(0)(2\pi)^2 = i_1(0)/t$. Furthermore all the models contain two parameters depending on the experimental conditions, which are the used wavelength λ and the sample thickness t . Similar to the arguments for SESANS [268] the units should be chosen so that λ has the reciprocal units of the scattering vector q , i.e. nm or Å, and the thickness should have the reciprocal units the scattering-cross section per volume, which are normally supplied in units of cm^{-1} . By this parametrisation the intermediate function $i_m(r)$ reads as

$$i_m(r) = k_0^2 \left[\exp \left(t\lambda^2 \Sigma_t \left(\frac{\tilde{G}(r) - \tilde{G}(0)}{\tilde{G}(0)} \right) \right) - \exp \left(-t\lambda^2 \Sigma_t \right) \right] \quad (9.781)$$

9.17.1. Multiple scattering of Spheres. This function uses the analytical expression for projected correlation function $\tilde{G}_{\text{sph}}(\delta)$ of monodisperse spheres as given in eq. 9.760 together with eq. 9.781 to calculate the scattering intensity considering multiple scattering effects.

Input Parameters for model MSAS Spheres:

R: radius of sphere R

dummy: not used

dummy: not used

Sigma_t: total scattering Σ_t

t: sample thickness t

lambda: wavelength of the beam λ

Note:

- the function MSAS Spheres should not be combined with a size distribution nor a structure factor.

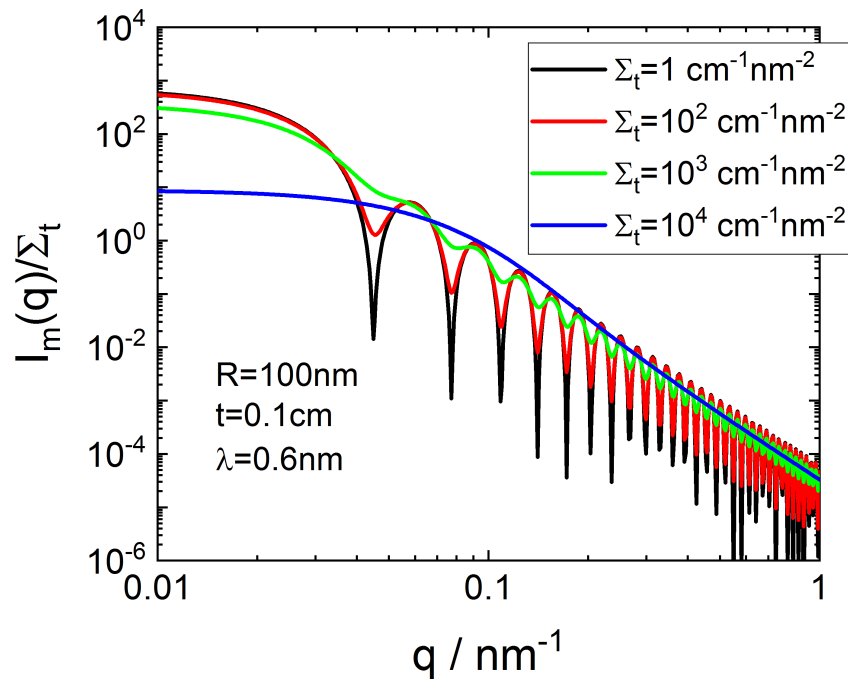


FIGURE 9.226. Multiple scattering of monodisperse Spheres depending on their total scattering.

9.17.2. Multiple scattering of polydisperse Spheres. This function uses the analytical expression for projected correlation function $\tilde{G}_{\text{sph}}(\delta)$ of monodisperse spheres as given in eq. 9.760 and first integrating this function over a LogNormal distribution before combining it with eq. 9.781 to calculate the scattering intensity considering multiple scattering effects.

Input Parameters for model MSAS polydisp. Spheres:

mu: mean radius of sphere μ

sigma: LogNorm width parameter σ

dummy: not used

Sigma_t: total scattering Σ_t

t: sample thickness t

lambda: wavelength of the beam λ

Note:

- the function MSAS polydisp. Spheres should not be combined with a size distribution nor a structure factor.

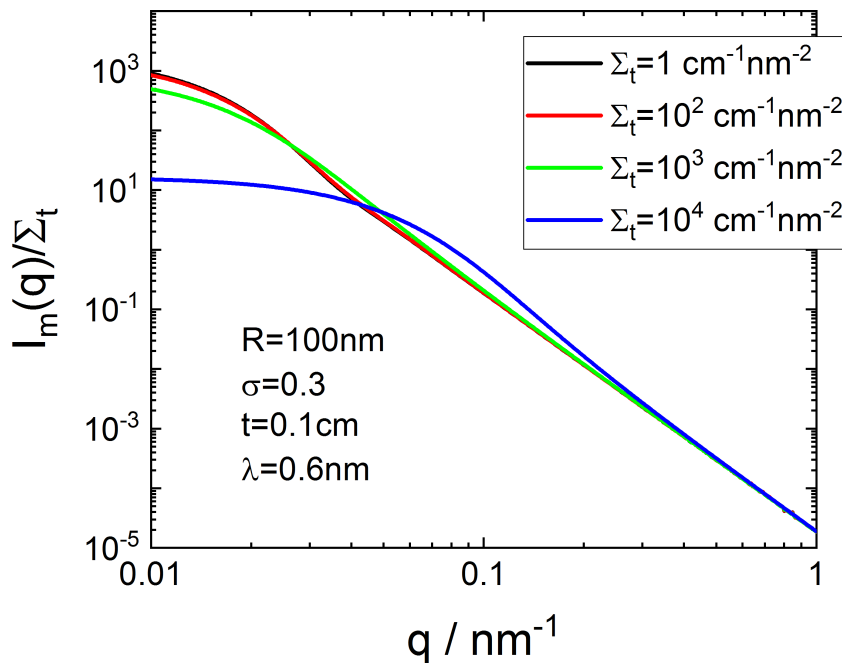


FIGURE 9.227. Multiple scattering of polydisperse Spheres following a LogNorm distribution depending on their total scattering.

9.17.3. Multiple scattering of Gaussian coils. This function uses the analytical expression for projected correlation function $\tilde{G}_{gGc}(\delta)$ of a generalised Gaussian polymer coil as given in eq. 9.772 and 9.774 together with eq. 9.781 to calculate the scattering intensity considering multiple scattering effects.

Input Parameters for model MSAS gGc:

Rg: radius of gyration R_g
nu: Flory exponent ν
dummy: not used
Sigma_t: total scattering Σ_t
t: sample thickness t
lambda: wavelength of the beam λ

Note:

- the function MSAS gGc should not be combined with a size distribution nor a structure factor.
- $\nu \in (0, \frac{1}{2})$

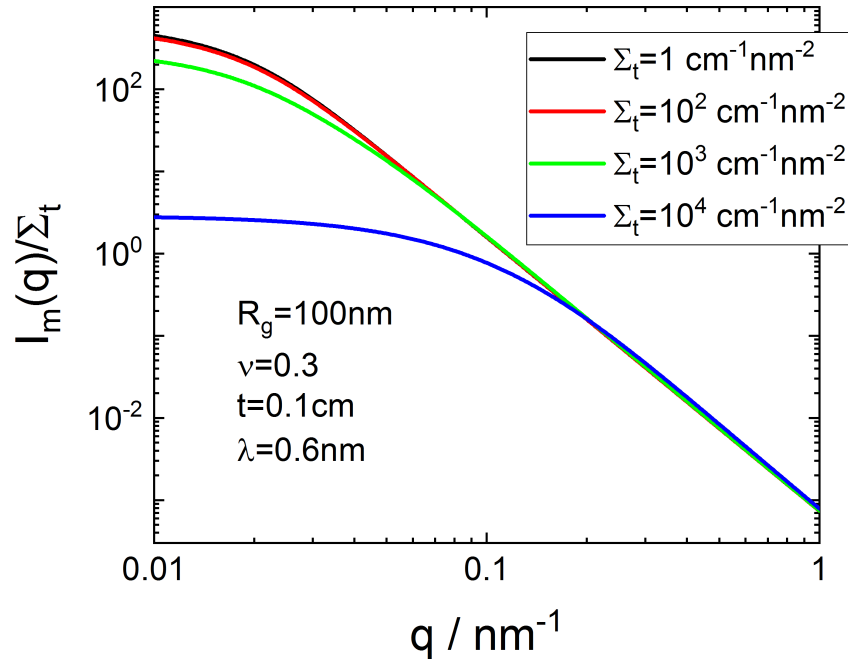


FIGURE 9.228. Multiple scattering of generalized Gaussian coil polymers depending on their total scattering.

9.17.4. Multiple scattering of a self-affine random distribution model. This function uses the analytical expression for projected correlation function $\tilde{G}_{\text{gDAB}}(\delta)$ of self-affine random distribution model as given in eq. 9.768 together with eq. 9.781 to calculate the scattering intensity considering multiple scattering effects.

Input Parameters for model MSAS gDAB:

xi: correlation length ξ

H: Hurst exponent H

dummy: not used

Sigma_t: total scattering Σ_t

t: sample thickness t

lambda: wavelength of the beam λ

Note:

- the function MSAS gDAB should not be combined with a size distribution nor a structure factor.
- H needs to be positive and non-zero: $H > 0$

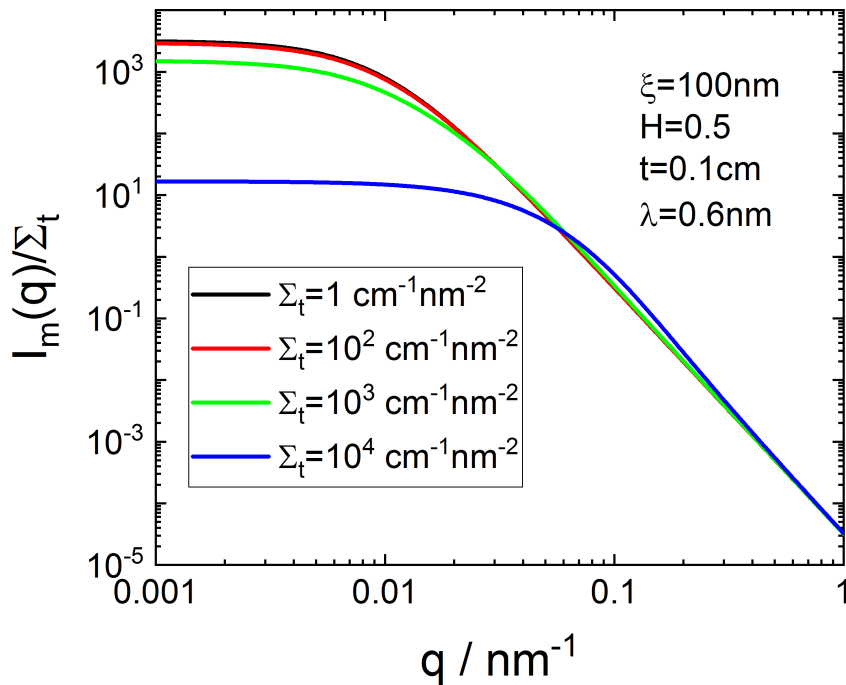


FIGURE 9.229. Multiple scattering of self-affine random distributions (gDAB) model depending on their total scattering.

CHAPTER 10

Plugin functions for size distributions

In practice scattering systems often do not consist of identical sized scatterer. In these cases it is necessary to average over an appropriate size distribution. If the scattering object is characterized by several size parameters like e.g. a rotational symmetric ellipsoid or a triaxial ellipsoid averages might need to be performed over all of the different length parameters of the scatterer. For non-spherical symmetric object also a texture or preferred orientation might need to be applied and an orientational average weighting by an orientational distribution function is required. The GUI of **SASfit** allows for assigning to a single parameter in the form factor a probability function. Assigning a probability function to multiple parameters is not foreseen so far. Even though size distributions can be added via the plugin option the integration range

10.1. LogNorm

The lognormal distribution is a heavy-right-tailed distribution defined on a left-bounded interval.

10.1.1. LogNorm_fp.

The **LogNorm** distribution is a continuous distribution in which the logarithm of a variable has a normal distribution.

$$\text{LogNorm}(x, N, \sigma, p, \mu) = \frac{N}{c_{\text{LN}}} \frac{1}{x^p} \exp\left(-\frac{\ln(x/\mu)^2}{2\sigma^2}\right) \quad (10.1a)$$

$$c_{\text{LN}} = \sqrt{2\pi} \sigma \mu^{1-p} \exp\left((1-p)^2 \frac{\sigma^2}{2}\right) \quad (10.1b)$$

where σ is the width parameter, p a shape parameter, μ is the location parameter. c_{LN} is chosen so that $\int_0^\infty \text{LogNorm}(x, \mu, \sigma, p) dR = N$. The mode of the distribution is defined as

$$x_{\text{mode}} = \mu e^{-p\sigma^2} \quad (10.2)$$

and the n^{th} moment $\langle X^n \rangle$ of the **LogNorm** distribution as

$$\langle X^n \rangle = \frac{\int X^n \text{LogNorm}(X) dX}{\int \text{LogNorm}(X) dX} = \mu^n e^{\frac{1}{2}\sigma^2 n(2-2p+n)}. \quad (10.3)$$

Instead of using the parameter N (particle number density) another Log-Normal size distribution namely **LogNorm_fp** with the volume fraction f_p as a parameter has been implemented. Using the volume fraction as a scaling parameter requires that the intensity is given in units of cm^{-1} and the scattering vector in nm^{-1} . Furthermore the scattering contrast needs to be supplied in units of cm^{-2} . More details about absolute intensity can be found in chapter ???. The volume fraction f_p can be obtained from the

`LogNorm`-distribution (eq. 10.1b) by integrating over the particle volume V_P . In case of spheres we get

$$f_p = 10^{21} \int_0^\infty \text{LogNorm}(R, N, \sigma, p, \mu) V_P(R) dR \quad (10.4)$$

$$= 10^{21} \int_0^\infty \text{LogNorm}(R, N, \sigma, p, \mu) \frac{4}{3} \pi R^3 dR = 10^{21} N \frac{4}{3} \pi \langle X^3 \rangle. \quad (10.5)$$

The scaling factor 10^{21} depends on the actual units. More details are given in section 12.4.

For other shapes than spheres the corresponding volume of the object has to be used in eq. 10.4. In case of cylinders the volume is given by $V_{\text{cyl}} = \pi R^2 L$. Depending whether the radius R or the cylinder length L has a size distribution the volume fraction f_p is calculated differently namely in case for a radius distribution by

$$f_p = 10^{21} \int_0^\infty \text{LogNorm}(R) V_{\text{cyl}}(R, L) dR \quad (10.6)$$

$$= 10^{21} \int_0^\infty \text{LogNorm}(R) \pi R^2 L dR = 10^{21} N \pi L \langle X^2 \rangle \quad (10.7)$$

and in case of a length distribution by

$$f_p = 10^{21} \int_0^\infty \text{LogNorm}(L) \pi R^2 L dL = 10^{21} N \pi R^2 \langle X \rangle. \quad (10.8)$$

As the cylinder volume depends on R^2 and L either the second or the first moment of the distribution function is involved in calculating the volume fraction depending which parameter has a distribution. For a spherical shell a sum of different moments has to be used as listed in table 1.

shape	form factor	distrib. param.	V			$N(f_p)$
			length2	length3	volume	
1	Sphere	R	not used	not used	whole sph.	$\frac{4}{3}\pi R^3$
2	Cylinder	R	L	not used	whole cyl.	$\pi R^2 L$
3	Cylinder	L	R	not used	whole cyl.	$\pi R^2 L$
4	Sph.Sh.iii	R	ΔR	not used	core+shell	$4\pi \left(R^2 \Delta R + R \Delta R^2 + \frac{1}{3} \Delta R^3 + \frac{1}{3} R^3 \right)$
5	Sph.Sh.iii	ΔR	R	not used	core+shell	$4\pi \left(R^2 \Delta R + R \Delta R^2 + \frac{1}{3} \Delta R^3 + \frac{1}{3} R^3 \right)$
6	Sph.Sh.iii	R	ΔR	not used	core	$\frac{4}{3}\pi R^3$
7	Sph.Sh.iii	ΔR	R	not used	core	$\frac{4}{3}\pi R^3$
8	Sph.Sh.iii	R	ΔR	not used	shell	$4\pi \left(R^2 \Delta R + R \Delta R^2 + \frac{1}{3} \Delta R^3 \right)$
9	Sph.Sh.iii	ΔR	R	not used	shell	$4\pi \left(R^2 \Delta R + R \Delta R^2 + \frac{1}{3} \Delta R^3 \right)$
10	CyShell1	R	ΔR	L	core+shell	$\pi L \left(\Delta R^2 + 2R\Delta R + R^2 \right)$
11	CyShell1	ΔR	R	L	core+shell	$\pi L \left(\Delta R^2 + 2R\Delta R + R^2 \right)$
12	CyShell1	L	R	ΔR	core+shell	$\pi L \left(\Delta R^2 + 2R\Delta R + R^2 \right)$
13	CyShell1	R	ΔR	L	core	$\pi L R^2$
14	CyShell1	ΔR	R	L	core	$\pi L R^2$
15	CyShell1	L	R	ΔR	core	$\pi L R^2$
16	CyShell1	R	ΔR	L	shell	$\pi L \left(\Delta R^2 + 2R\Delta R \right)$
17	CyShell1	ΔR	R	L	shell	$\pi L \left(\Delta R^2 + 2R\Delta R \right)$
18	CyShell1	L	R	ΔR	shell	$\pi L \left(\Delta R^2 + 2R\Delta R \right)$

TABLE 1. The number density N expressed in terms of volume fraction f_p and moments $\langle X^n \rangle$ of the distribution function for some particle shapes and different parameters having a distribution. The factor 10^{21} is needed due to unit conversion. It is assumed that the radius is given in nm, the intensity in cm^{-1} and the scattering length densities in cm^{-2} .

10.1.2. bi-LogNorm.

10.1.3. shifted LogNorm.

10.2. metalog distribution

The quantile function of the metalog distribution $Q(y) = M_k(y)$ is defined as [259, 257, 258]

$$M_k(y) = \begin{cases} a_1 + a_2 \ln \frac{y}{1-y}, & k = 2 \\ a_1 + a_2 \ln \frac{y}{1-y} + a_3(y - \frac{1}{2}) \ln \frac{y}{1-y}, & k = 3 \\ a_1 + a_2 \ln \frac{y}{1-y} + a_3(y - \frac{1}{2}) \ln \frac{y}{1-y} + a_4(y - \frac{1}{2}), & k = 4 \\ M_{k-1}(y) + a_k(y - \frac{1}{2})^{\frac{k-1}{2}}, & \text{odd } k \geq 5 \\ M_{k-1}(y) + a_k(y - \frac{1}{2})^{\frac{k}{2}-1} \ln \frac{y}{1-y}, & \text{even } k \geq 6 \end{cases} \quad (10.9)$$

and its PDF $p(x) = m_k(y)$ with $x = M_k(y)$ reads as

$$m_k(y) = \begin{cases} \frac{y(1-y)}{a_2}, & k = 2 \\ \left(\frac{a_2}{y(1-y)} + a_3 \left(\frac{y-\frac{1}{2}}{y(1-y)} + \ln \frac{y}{1-y} \right) \right)^{-1}, & k = 3 \\ \left(\frac{a_2}{y(1-y)} + a_3 \left(\frac{y-\frac{1}{2}}{y(1-y)} + \ln \frac{y}{1-y} \right) + a_4 \right)^{-1}, & k = 4 \\ \left(\frac{1}{m_{k-1}(y)} + a_k \frac{k-1}{2} (y - \frac{1}{2})^{(k-3)/2} \right)^{-1}, & \text{odd } k \geq 5 \\ \left(\frac{1}{m_{k-1}(y)} + a_k \left(\frac{(y-\frac{1}{2})^{\frac{k}{2}-1}}{y(1-y)} + (\frac{k}{2}-1)(y - \frac{1}{2})^{(\frac{k}{2}-2)} \ln \frac{y}{1-y} \right) \right)^{-1}, & \text{even } k \geq 6 \end{cases} \quad (10.10)$$

The metalog PDF as defined above is an unbounded distribution. In case of describing a size distribution it needs to be bounded (Logit metalog) or at least semi-bounded (bounded below, Log metalog). This can be easily done by a transformation of $z(x) = \ln(x - b_l)$ for a distribution with a lower bound b_l or $z(x) = \ln\left(\frac{x-b_l}{b_u-x}\right)$ with a lower bound b_l and an upper bound b_u , where z is then metalog-distributed. The corresponding quantile functions and PDF then reads as

$$M_k^{\log}(y) = \begin{cases} b_l + e^{M_k(y)}, & 0 < y < 1 \\ b_l, & y = 0 \end{cases} \quad (10.11)$$

$$m_k^{\log}(y) = \begin{cases} m_k(y)e^{-M_k(y)}, & 0 < y < 1 \\ 0, & y = 0 \end{cases} \quad (10.12)$$

$$M_k^{\text{logit}}(y) = \begin{cases} \frac{b_l+b_u e^{M_k(y)}}{1+e^{M_k(y)}}, & 0 < y < 1 \\ b_l, & y = 0 \\ b_u, & y = 1 \end{cases} \quad (10.13)$$

$$m_k^{\text{logit}}(y) = \begin{cases} m_k(y) \frac{(1+e^{M_k(y)})^2}{(b_u-b_l)e^{M_k(y)}}, & 0 < y < 1 \\ 0, & y = 0 \\ 0, & y = 1 \end{cases} \quad (10.14)$$

10.2.1. unbounded metalog distribution.

10.2.2. semi-bounded metalog distribution.

10.2.3. bounded metalog distribution.

10.3. Johnson's distribution

10.3.1. Johnson S_B .

10.3.2. Johnson S_L .

10.3.3. Johnson S_U .

10.3.4. Johnson S_N .

10.4. generalized Johnson's distribution

CHAPTER 11

Plugin functions for structure factors

11.1. Three dimensional structure factors for hard sphere systems

The rational function approximation method which is wholly compatible with the equation of state used for the fluid has been used for expressions of the hard sphere structure factor. In general, integral equation theories require a closure approximations, and they lead to different equations of state if one takes the virial or the compressibility routes (thermodynamic inconsistency problem). In contrast the rational function approximation method completely avoids the thermodynamic inconsistency problem, in that the compressibility factor is involved in the derivation of $S(Q)$ [538, 422, 102].

$$S(Q) = 1 - 24\eta \Re \left(\frac{t^2 G(t) - 1}{t^3} \Big|_{t=\nu Q\sigma} \right) \quad (11.1)$$

$$G(t) = \frac{t}{12\eta} \frac{1}{1 - \exp(t)\Phi(t)} \quad (11.2)$$

$$\Phi(t) = \frac{1 + S_1 t + S_2 t^2 + S_3 t^3 + S_4 t^4}{1 + L_1 t + L_2 t^2} \quad (11.3)$$

where the six coefficients S_1 , S_2 , S_3 , S_4 , L_1 , and L_2 may be evaluated in an algebraic form

$$L_1 = \frac{1}{2} \frac{\eta + 12\eta L_2 + 2 - 24\eta S_4}{2\eta + 1} \quad (11.4)$$

$$S_1 = \frac{3}{2} \eta \frac{-1 + 4L_2 - 8S_4}{2\eta + 1} \quad (11.5)$$

$$S_2 = -\frac{1}{2} \frac{-\eta + 8\eta L_2 + 1 - 2L_2 - 24\eta S_4}{2\eta + 1} \quad (11.6)$$

$$S_3 = \frac{1}{12} \frac{2\eta - \eta^2 + 12\eta^2 L_2 - 12\eta L_2 - 1 - 72\eta^2 S_4}{\eta(2\eta + 1)} \quad (11.7)$$

with

$$L_2 = -3(Z - 1)S_4 \quad (11.8)$$

$$S_4 = \frac{1 - \eta}{36\eta \left(Z - \frac{1}{3} \right)} \left[1 - \sqrt{1 + \frac{Z - \frac{1}{3}}{Z - Z_{\text{PY}}} \left(\frac{\chi}{\chi_{\text{PY}}} - 1 \right)} \right] \quad (11.9)$$

Here, $Z_{\text{PY}} = \frac{1+2\eta+3\eta^2}{(1-\eta)^2}$ and $\chi_{\text{PY}} = \frac{(1-\eta)^4}{(1+2\eta)^2}$ are the compressibility factor and isothermal susceptibility arising in the PY theory. The isothermal compressibility χ and the

compressibility factor Z are related by

$$\chi = \left(\frac{d(\rho Z)}{d\rho} \right)^{-1} = \left(Z + \eta \frac{dZ}{d\eta} \right)^{-1} \quad (11.10)$$

where $\eta = \frac{\pi}{6}\rho\sigma^3$ is the packing fraction of the spheres (ρ is the number density and σ the hard-sphere diameter). The only quantity which is left to calculate the structure factor is an explicit expression for the compressibility factor Z .

11.1.1. Carnahan and Starling. [78]

In this approximation eqs. 11.1-11.10 are used with $Z = Z^{\text{CS}}$, where

$$Z^{\text{CS}} = \frac{1 + \eta + \eta^2 - \eta^3}{(1 - \eta)^3} \quad (11.11)$$

Input parameters for 3D Hard Sphere (CS):

R: radius R

eta: volume fraction η

Note

- The structure factor accepts volume fractions between $\eta \in [0, 1]$.
- The model lead to physically meaningful structural properties in the whole definition range of volume fractions.

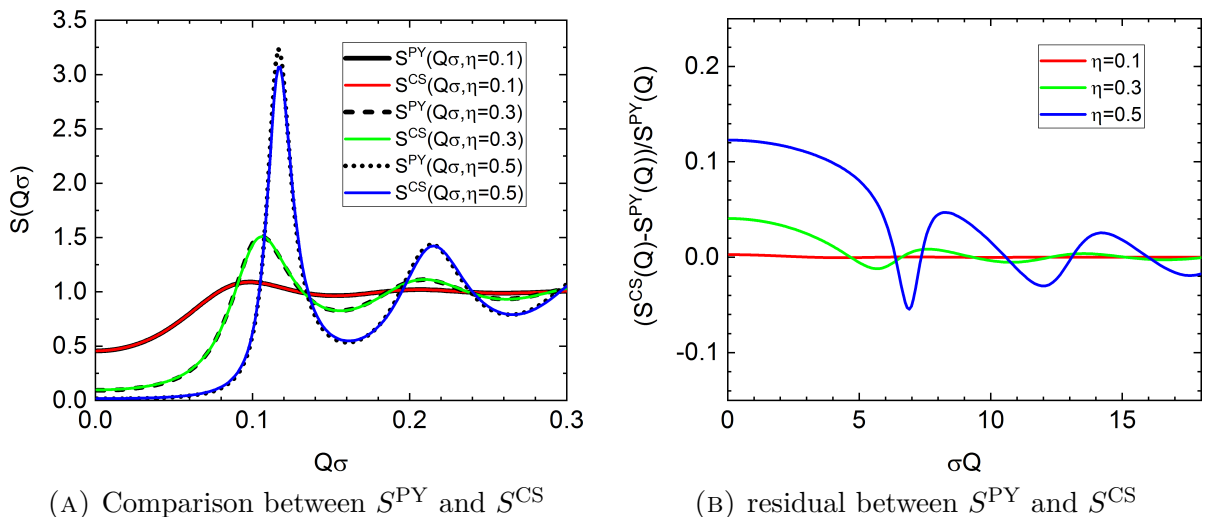


FIGURE 11.1. Comparison between analytical PY solution of hard sphere static structure factor and rational function approximation with a compressibility factor of Carnahan and Starling

11.1.2. Padé(4,3) of van Rensburg and Sánchez. [501, 431]

In this approximation eqs. 11.1-11.10 are used with $Z = Z^{(4,3)}$, where

$$Z^{(4,3)} = \frac{1 + 1.024385\eta + 1.104537\eta^2 - 0.4611472\eta^3 - 0.7430382\eta^4}{1 - 2.975615\eta + 3.007000\eta^2 - 1.097758\eta^3} \quad (11.12)$$

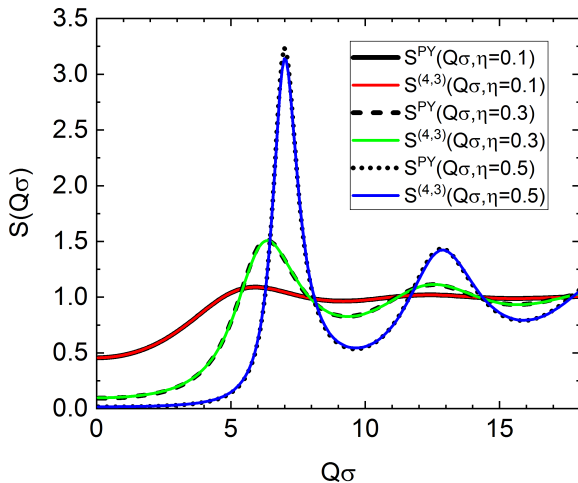
Input parameters for 3D Hard Sphere (4,3):

R: radius R

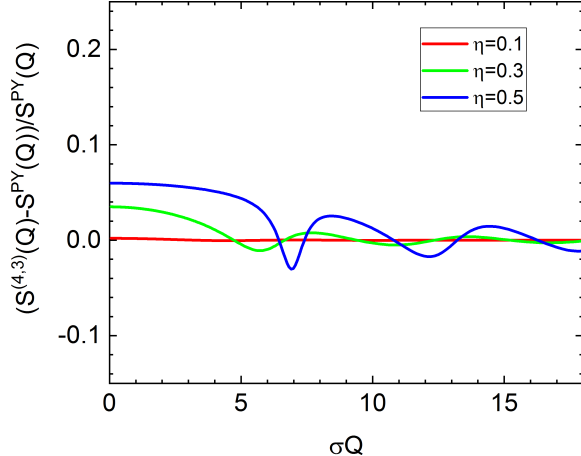
eta: volume fraction η

Note

- The structure factor accepts volume fractions between $\eta \in [0, 1]$.
- The threshold packing fraction (packing fraction at which a glass transition in the hard-sphere fluid takes place) of this model is $\eta_0^{(4,3)} = 0.5604$ beyond which no meaningful fluid structure can be derived [102].



(A) Comparison between S^{PY} and $S^{(4,3)}$



(B) residual between S^{PY} and $S^{(4,3)}$

FIGURE 11.2. Comparison between analytical PY solution of hard sphere static structure factor and rational function approximation with a compressibility factor of van Rensburg and Sánchez

11.1.3. Malijevský and Veverka. [325]

In this approximation eqs. 11.1-11.10 are used with $Z = Z^{\text{MV}}$, where

$$Z^{\text{MV}} = \frac{1 + 1.0560\eta + 1.6539\eta^2 + 0.3262\eta^3}{(1 - 3.8464\eta + 4.9574\eta^2 - 2.1639\eta^3)(1 - \eta)^3} \quad (11.13)$$

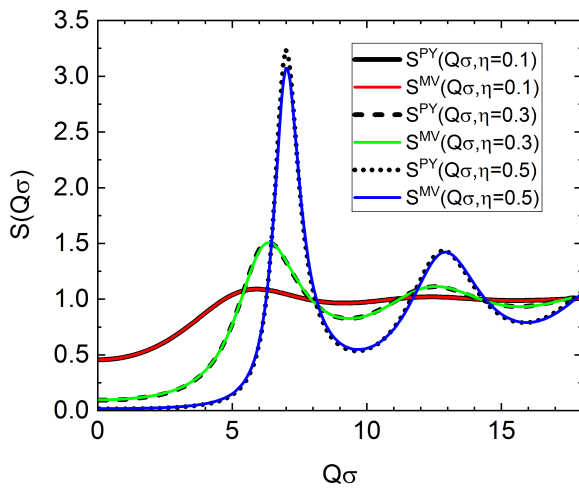
Input parameters for 3D Hard Sphere (MV):

R: radius R

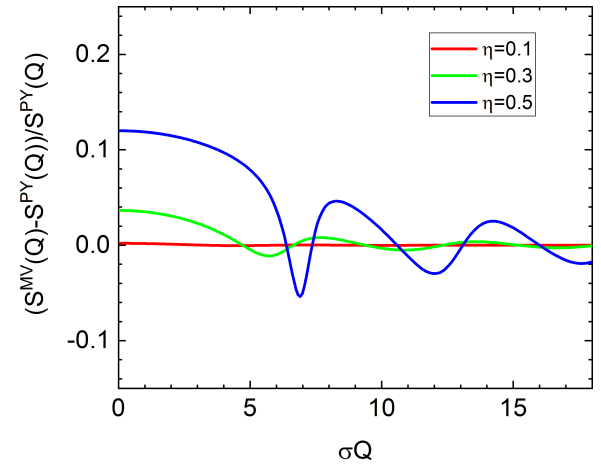
eta: volume fraction η

Note

- The structure factor accepts volume fractions between $\eta \in [0, 1]$.
- The model lead to physically meaningful structural properties in the whole definition range of volume fractions.



(A) Comparison between S^{PY} and S^{MV}



(B) residual between S^{PY} and S^{MV}

FIGURE 11.3. Comparison between analytical PY solution of hard sphere static structure factor and rational function approximation with a compressibility factor of Malijevský and Veverka

11.1.4. López de Haro and Robles. [423]

In this approximation eqs. 11.1-11.10 are used with $Z = Z^{\text{LHR}}$, where

$$Z^{\text{LHR}} = \frac{1 + 0.153555\eta - 0.428376\eta^2 - 2.7987\eta^3 - 0.317417\eta^4 - 0.105806\eta^5}{1 - 3.84644\eta + 4.9574\eta^2 - 2.16386\eta^3} \quad (11.14)$$

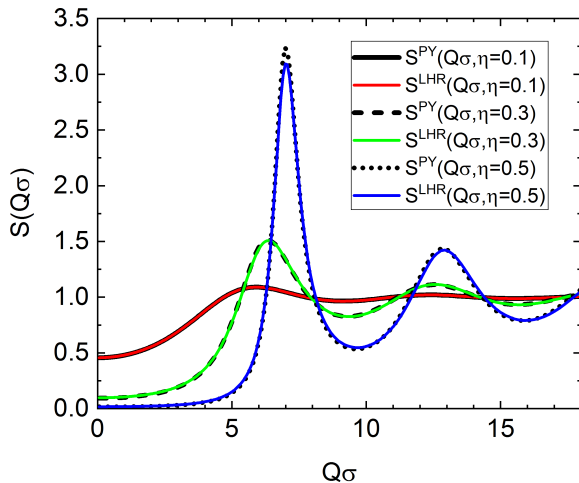
Input parameters for 3D Hard Sphere (LHR):

R: radius R

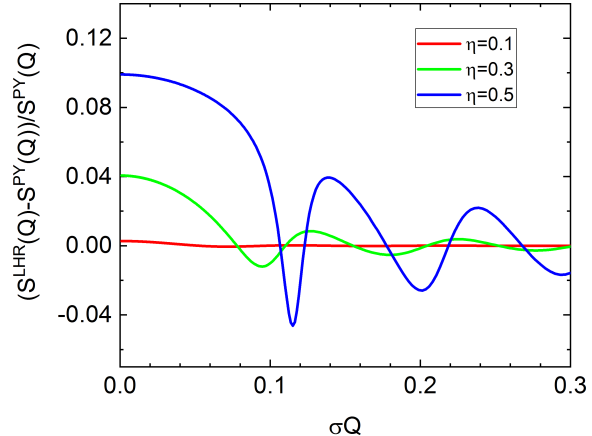
eta: volume fraction η

Note

- The structure factor accepts volume fractions between $\eta \in [0, 1]$.
- The threshold packing fraction (packing fraction at which a glass transition in the hard-sphere fluid takes place) of this model is $\eta_0^{\text{LHR}} = 0.5684$ beyond which no meaningful fluid structure can be derived [102].



(A) Comparison between S^{PY} and S^{LHR}



(B) residual between S^{PY} and S^{LHR}

FIGURE 11.4. Comparison between analytical PY solution of hard sphere static structure factor and rational function approximation with a compressibility factor of López de Haro and Robles

11.1.5. Grundke and Henderson.

In this approximation the structure factor in the Percus Yevick approximation is corrected to have thermodynamic consistency [210] so that both routes leads to the expression of Carnahan and Starling $pV/Nk_B T = \frac{1+\eta+\eta^2-\eta^3}{(1-\eta)^3}$

$$\sigma = 2R \quad (11.15)$$

$$(\sigma_0/\sigma)^3 = 1 - \eta/16 \quad (11.16)$$

$$\eta_0 = \eta(1 - \eta/16) \quad (11.17)$$

$$g_0(s, \eta_0) \simeq \frac{1 + \eta_0/2}{(1 - \eta_0)^2} - \frac{9}{2}\eta_0 \frac{1 + \eta_0}{(1 - \eta_0)^3}(s - 1) \quad (11.18)$$

$$\frac{C}{\sigma} = \frac{2 - \eta}{2(1 - \eta)^3} - g_0(\sigma/\sigma_0, \eta_0) \quad (11.19)$$

$$\begin{aligned} \frac{12\eta C}{m\sigma_0^2} &= \frac{(1 - \eta)^4}{1 + 4\eta + 4\eta^2 - 4\eta^3 + \eta^4} - \frac{(1 - \eta_0)^4}{(1 + 2\eta_0)^2} \\ &= 24\eta_0 \int_0^{\sigma/\sigma_0} g_0(s, \eta_0) s^2 ds \end{aligned} \quad (11.20)$$

$$S^{\text{GH}}(Q, \sigma, \eta) = S^{\text{PY}}(Q, \sigma_0, \eta_0) + \frac{6\eta}{\pi\sigma^3} \tilde{h}_{\text{GH}}(Q) \quad (11.21)$$

$$\begin{aligned} \tilde{h}_{\text{GH}}(Q) &= -\frac{4\pi\sigma_0}{Q\sigma_0} \int_1^{\sigma/\sigma_0} s g_0(s, \eta_0) \sin(Q\sigma_0 s) ds \\ &\quad + \frac{2\pi\sigma^3}{Q\sigma} \frac{C}{\sigma} \left\{ \frac{\cos(Q\sigma)}{\sigma} \left[\frac{Q + m}{m^2 + (Q + m)^2} + \frac{Q - m}{m^2 + (Q - m)^2} \right] \right. \\ &\quad \left. + \frac{\sin(Q\sigma)}{\sigma} \left[\frac{m}{m^2 + (Q + m)^2} + \frac{m}{m^2 + (Q - m)^2} \right] \right\} \end{aligned} \quad (11.22)$$

Input parameters for 3D Hard Sphere (GH):

R: radius R

eta: volume fraction η

Note

- The structure factor accepts volume fractions between $\eta \in [0, 1]$.

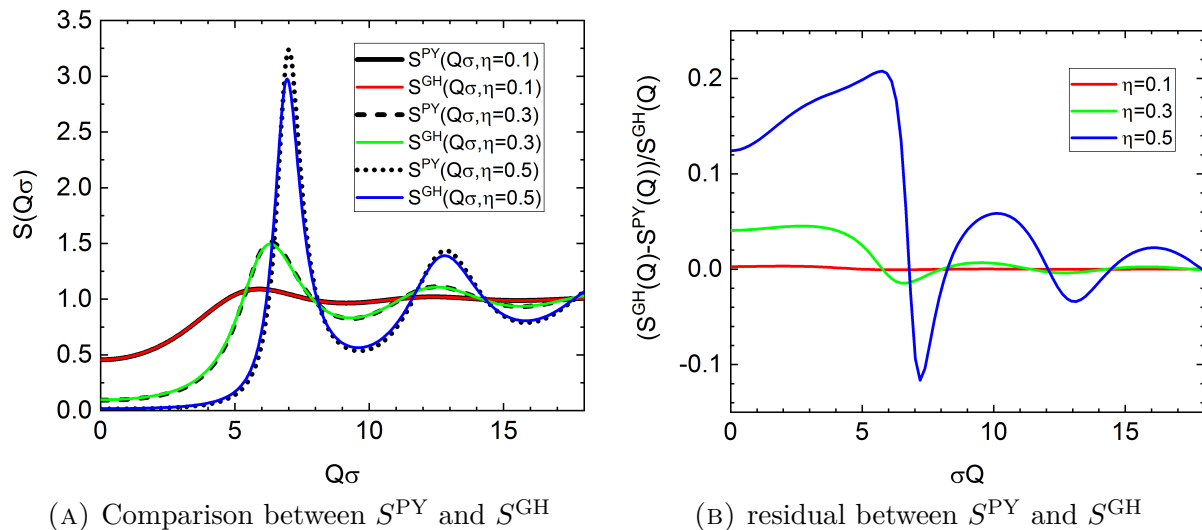


FIGURE 11.5. Comparison between analytical PY solution of hard sphere static structure factor and thermodynamically consistent correction as described by Henderson and Grundke

11.1.6. Hard Sphere (PY).

This is the classical analytical solution of the Percus-Yevick equations [385, 522, 512] for a hard sphere potential

$$U(r) = \begin{cases} \infty & \text{for } 0 < r < 2R \\ 0 & \text{for } r > 2R \end{cases} \quad (11.23)$$

The structure factor $S^{\text{PY}}(Q)$ can be calculated

$$\alpha = \frac{(1 + 2\eta)^2}{(1 - \eta)^4} \quad (11.24a)$$

$$\beta = -6\eta \frac{(1 + \eta/2)^2}{(1 - \eta)^4} \quad (11.24b)$$

$$\gamma = \frac{\eta\alpha}{2} \quad (11.24c)$$

$$A = 2RQ \quad (11.24d)$$

$$G(\eta, A) = \alpha \frac{\sin A - A \cos A}{A^2} + \beta \frac{2A \sin A + (2 - A^2) \cos A - 2}{A^3} + \gamma \frac{-A^4 \cos A + 4[(3A^2 - 6) \cos A + (A^3 - 6A) \sin A + 6]}{A^5} \quad (11.24e)$$

$$S^{\text{PY}}(Q, R, \eta) = \frac{1}{1 + 24\eta \frac{G(\eta, A)}{A}} \quad (11.24f)$$

Input parameters for 3D Hard Sphere (PY):

R: radius R

eta: volume fraction η

Note

- The structure factor accepts volume fractions between $\eta \in [0, 1]$.

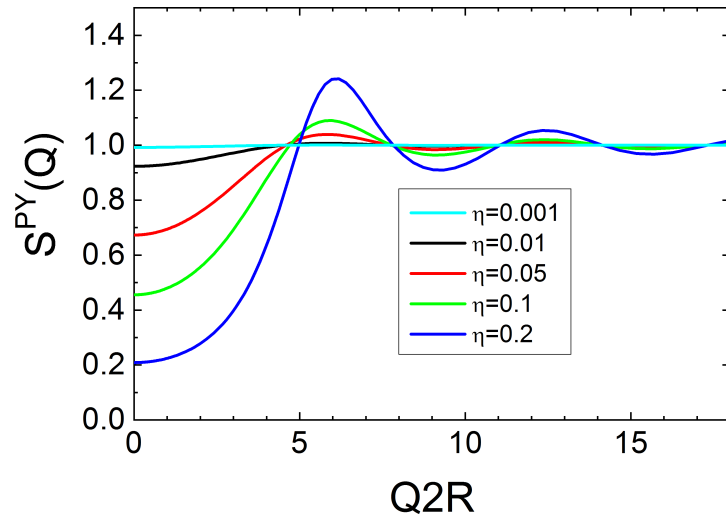


FIGURE 11.6. Structure factor $S^{PY}(Q)$ for a hard sphere interaction potential for the different volume fractions η .

11.2. Structure factor for a two dimensional hard spheres/disks fluid

The structure factor of hard disks or spheres with diameter/radius $\sigma = 2R$ in two dimensions with an interaction potential

$$U(r, \sigma) = \begin{cases} \infty & \text{for } r < \sigma \\ 0 & \text{for } r \geq \sigma \end{cases} \quad (11.25)$$

have been implemented in several variants. All the theories are developed for \mathbf{q} -vector in the plane of the two dimensional structure. However, in an experiment this plane might be tilted against the detection plane. Therefore in all cases two variants are implemented. One case is considering a certain direction of the normal of the two dimensional sample plane and a second one for a randomly oriented plane, i.e. the limit of a powder. The coordination system used to describe the normal of the 2D plane is defined in fig. 11.7. With the following definition for the scattering vector and the unit vector defining the

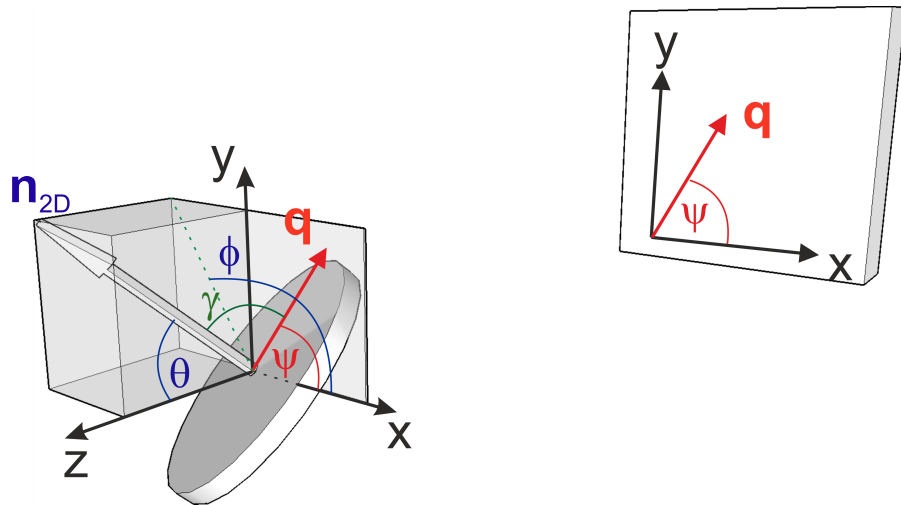


FIGURE 11.7. coordination system for 2D structure factors relative to the beam direction.

direction of the 1D structure

$$\mathbf{q} = q \begin{pmatrix} \cos \psi \\ \sin \psi \\ 0 \end{pmatrix} \quad \text{and} \quad \mathbf{n}_{2D} = \begin{pmatrix} \sin \theta \cos \phi \\ \sin \theta \sin \phi \\ \cos \theta \end{pmatrix} \quad (11.26)$$

$$(11.27)$$

the angle γ between \mathbf{q} and \mathbf{n}_{2D} is given as

$$\cos \gamma = \cos \psi \sin \theta \cos \phi + \sin \psi \sin \theta \sin \phi \quad (11.28)$$

11.2.1. Two dimensional hard sphere/disks fluid according to Rosenfeld.

An analytical form of the structure factor as a function of the disk radius R and surface coverage $\eta = \pi R^2 \rho$, where ρ is the number density of particles, have been given

by [425, 178]. Rosenfeld [425] gives the expression

$$\frac{1}{S_{\text{Rosenfeld}}(q \sin \gamma)} - 1 = 4\eta \left(A \frac{J_1^2(qR \sin \gamma)}{(qR \sin \gamma)^2} + B J_0(qR \sin \gamma) \frac{J_1(qR \sin \gamma)}{qR \sin \gamma} + G \frac{J_1(2qR \sin \gamma)}{qR \sin \gamma} \right) \quad (11.29)$$

with

$$A = (1 + (2\eta - 1)\chi + 2\eta G) / \eta \quad (11.30)$$

$$B = ((1 - \eta)\chi - 1 - 3\eta G) / \eta \quad (11.31)$$

$$G = \frac{1}{1 - \eta} \quad (11.32)$$

$$\chi = \frac{1 + \eta}{(1 - \eta)^2} \quad (11.33)$$

In the original paper from Rosenfeld the definition of χ seems to have a typo and has been corrected like in [119].

11.2.2. Two dimensional hard sphere/disks fluid according to Guo.

Guo [178] supplies the expression

$$S_{\text{Guo}}(q \sin \gamma) = \frac{1}{1 - \rho \tilde{c}(q \sin \gamma, r)} \quad (11.34)$$

$$\tilde{c}(q \sin \gamma, r) = 2\pi\sigma^2 \int_0^1 c(r', \eta) J_0(q \sin \gamma \sigma r') r' dr' \quad (11.35)$$

with

$$c(r', \eta) = \Theta(1 - r') \left[-\frac{1 - p\eta^2}{(1 - 2\eta + p\eta^2)^2} \right] \left\{ 1 - a^2\eta - a^2\eta \frac{2}{\pi} \left[\arccos \left(\frac{r'}{a} \right) - \frac{r'}{a} \sqrt{1 - \frac{r'^2}{a^2}} \right] \right\} \quad (11.36)$$

with $p = (4\sqrt{3}\pi - 12) / \pi^2$ and $\Theta()$ being the Heaviside function. The parameter a is the root of a non-linear equation, which has been solved numerically and then approximated via a polynomial fitting by

$$a = 0.3699\eta^4 - 1.2511\eta^3 + 2.0199\eta^2 - 2.2373\eta + 2.1 \quad (11.37)$$

Input Parameters for model 2D hard disks (Rosenfeld,aligned) as well as 2D hard disks (Guo,aligned):

R: radius of the disc R

eta: surface coverage η

theta: polar angle θ (polar axis = beam axis)

phi: azimuthal angle ϕ (in detector plane towards x -axis)

psi: azimuthal angle ψ for q towards x -axis

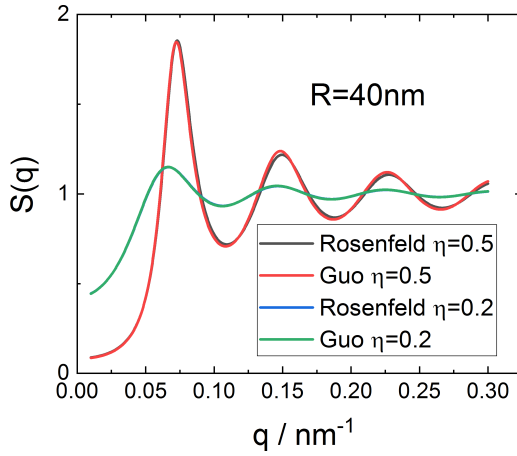
Input Parameters for model 2D hard disks (Rosenfeld,random) as well as 2D hard disks (Guo,random):

R: radius of the disc R

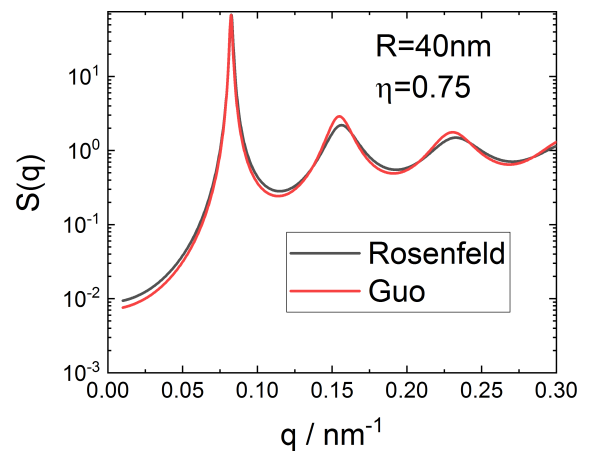
eta: surface coverage η

Note:

- Both models break down for surface coverage around $\eta > 0.75$. The densest possible lattice packing would be $\eta_{\max} = \frac{1}{6}\pi\sqrt{3} \simeq 0.907$.
- Values for surface coverage $0 < \eta < 1$ are accepted by the software.



(A) surface coverage of $\eta = 0.2$ and 0.5



(B) surface coverage of $\eta = 0.75$

FIGURE 11.8. Comparison between Rosenfeld's and Guo's results

11.3. One dimensional structure factors

for one dimensional structure factors the relative orientation of the 1D structure to the detection plane is relevant. The orientation has been defined by spherical coordinates with the polar axis pointing in the horizontal direction of the detection plane. With the

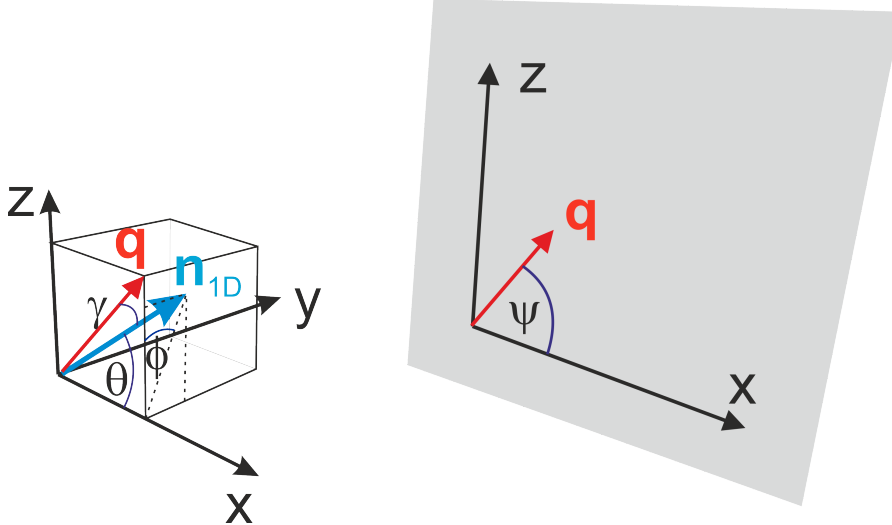


FIGURE 11.9. coordination system for 1D structure factors relative to the detection plane.

following definition for the scattering vector and the unit vector defining the direction of the 1D structure

$$\mathbf{q} = q \begin{pmatrix} \cos \psi \\ 0 \\ \sin \psi \end{pmatrix} \quad \text{and} \quad \mathbf{n}_{1D} = \begin{pmatrix} \cos \theta \\ \sin \theta \sin \phi \\ \sin \theta \cos \phi \end{pmatrix} \quad (11.38)$$

$$(11.39)$$

the angle γ between \mathbf{q} and \mathbf{n}_{1D} is given as

$$\cos \gamma = \cos \psi \cos \theta + \sin \psi \sin \theta \cos \phi \quad (11.40)$$

11.3.1. Structure factor for a hard spheres potential in one dimension.

The structure factor for hard spheres in one dimension has been solved in [298] and also implemented in the open source software `Jscatter` [34]. The structure factor is given by

$$S_{HS,1D,||}(q, \sigma, \eta) = \frac{1}{1 - \frac{\eta}{\sigma} \tilde{c}(q)} \quad (11.41)$$

$$\tilde{c}(q) = -2(A(q) + B(q)) \quad (11.42)$$

$$A(q) = \frac{\sigma}{1 - \eta} \frac{\sin q\sigma}{q\sigma} \quad (11.43)$$

$$B(q) = \frac{\eta}{\sigma} \frac{1}{(q(1 - \eta))^2} [1 - \cos q\sigma] \quad (11.44)$$

The above equation assumes that \mathbf{q} points along the one dimensional structure. In case of a certain angle γ , with $\cos \gamma = \mathbf{q} \cdot \mathbf{n}_{1D} / (|\mathbf{q}| |\mathbf{n}_{1D}|)$, between \mathbf{q} and the direction \mathbf{n}_{1D} of the one dimensional structure one has to take

$$S_{HS,1D}(q, \sigma, \eta, \gamma) = S_{HS,1D,||}(q \cos \gamma, \sigma, \eta) \quad (11.45)$$

For random oriented 1D structures the orientational average of the structure factor needs to be done in principle together with the form factor as shown for example in section 9.15.2 for stacked discs. However, if the individual stacked structures are spherical symmetric like a straight chain of spheres the form factor is isotropic and the average can be performed over the structure factor only which then reads as

$$S_{HS,1D,ran}(q, \sigma, \eta, \gamma) = \int_0^1 S_{HS,1D,||}(qx, \sigma, \eta) dx \quad (11.46)$$

11.3.2. One dimensional paracrystal.

$$S(q, \gamma) = 1 + \frac{2}{n} \sum_{k=1}^{n-1} (n - k) \cos(kDq \cos(\Theta)) \exp\left(-\frac{k}{2} (q \cos(\Theta) \sigma_D)^2\right) \quad (11.47)$$

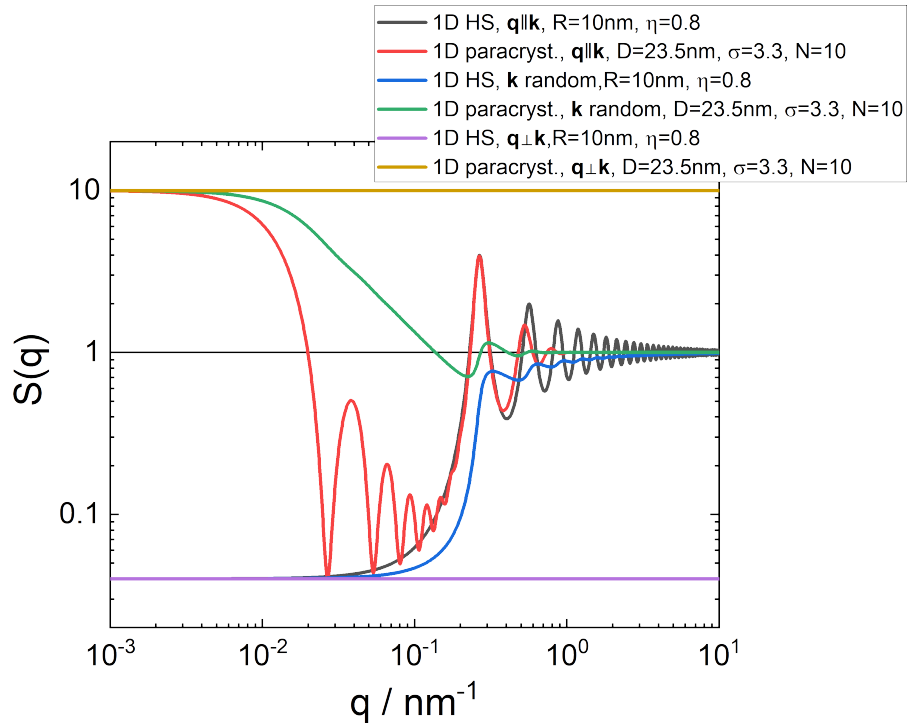


FIGURE 11.10. structure factor of aligned for both \mathbf{q} parallel and perpendicular to the direction of the 1D structure as well as and random oriented 1D structures.

11.4. three dimensional structure factor for sticky hard sphere systems

11.4.1. Sticky Hard Sphere.

In Baxter's model [18, 421, 283, 14, 333, 334] of adhesive hard spheres the pair interaction potential $U(r)$ is replaced by

$$\frac{U(r)}{k_B T} = \begin{cases} \infty & \text{for } 0 < r < \sigma \\ \ln \frac{12\tau\Delta}{\sigma+\Delta} & \text{for } \sigma < r < \sigma + \Delta \\ 0 & \text{for } r > \sigma + \Delta \end{cases} \quad (11.48)$$

after which, when applied, the limit $\Delta \rightarrow 0$ is taken. Thus, only a single parameter, the so-called stickiness parameter τ , characterizes the adhesive strength.

$$\kappa = 2qR_{\text{HS}} \quad (11.49a)$$

$$\eta = f_p \left(\frac{2R_{\text{HS}} + \Delta}{2R_{\text{HS}}} \right)^3 \quad (11.49b)$$

$$\epsilon = \tau + \frac{\eta}{1 - \eta} \quad (11.49c)$$

$$\gamma = f_p \frac{1 + \eta/2}{3(1 - \eta)^2} \quad (11.49d)$$

$$\lambda = \frac{6}{\eta} \left(\epsilon - \sqrt{\epsilon^2 - \gamma} \right) \quad (11.49e)$$

$$\mu = \lambda\eta(1 - \eta) \quad (11.49f)$$

$$\beta = -\frac{3\eta(2 + \eta)^2 - 2\mu(1 + 7\eta + \eta^2) + \mu^2(2 + \eta)}{2(1 - \eta)^4} \quad (11.49g)$$

$$\alpha = \frac{(1 + 2\eta - \mu)^2}{(1 - \eta)^4} \quad (11.49h)$$

$$C(q) = 2 \frac{\eta\lambda}{\kappa} \sin \kappa - 2 \frac{\eta^2\lambda^2}{\kappa^2} (1 - \cos \kappa) - \quad (11.49i)$$

$$\left\{ \alpha\kappa^3(\sin \kappa - \kappa \cos \kappa) + \beta\kappa^2(2\kappa \sin \kappa - (\kappa^2 - 2)\cos \kappa - 2) \right. \\ \left. + \frac{\eta\alpha}{2} ((4\kappa^3 - 24\kappa) \sin \kappa - (\kappa^4 - 12\kappa^2 + 24) \cos \kappa + 24) \right\} \times 24 \frac{\eta}{\kappa^6}$$

$$S_{\text{sHS}}(q, R_{\text{HS}}, f_p, \tau) = \frac{1}{1 - C(q)} \quad (11.49j)$$

Input Parameters for the structure factor model sticky hard sphere:

RHS: hard sphere radius

fp: volume fraction f_p

tau: stickiness parameter τ

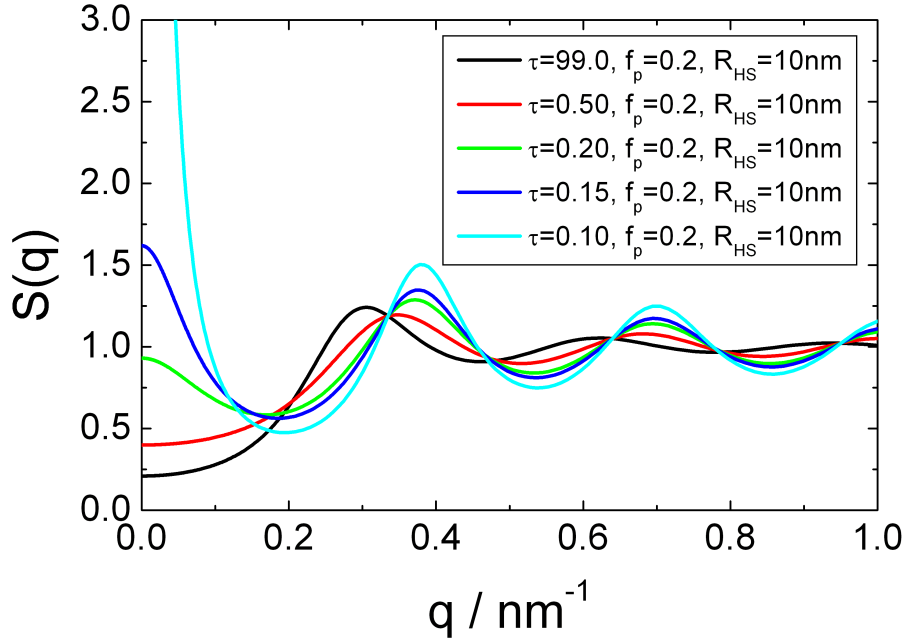


FIGURE 11.11. Structure factor $S(q)$ for a sticky hard sphere interaction potential for the different stickiness parameters τ .

Note:

- for stickiness parameters close to zero the root in eq. 11.49e becomes complex and is considered as a critical point where the system phase separates.

11.4.2. Sticky Hard Sphere (2nd version).

In Baxter's model of adhesive hard spheres the pair interaction potential $U(r)$ is replaced by

$$\frac{U(r)}{k_B T} = \begin{cases} \infty & \text{for } 0 < r < \sigma - \Delta \\ \ln \frac{12\tau\Delta}{\sigma + \Delta} & \text{for } \sigma - \Delta < r < \sigma \\ 0 & \text{for } r > \sigma \end{cases} \quad (11.50)$$

The structure factor for this potential has been implemented according to [412, 413] as

$$\sigma = 2R_{HS} + \Delta \quad (11.51)$$

$$\kappa = q\sigma \quad (11.52)$$

$$\phi = f_p \left(\frac{\sigma}{2R_{HS}} \right)^3 \quad (11.53)$$

$$\lambda_{\pm} = 6 \left(\frac{\tau}{\phi} + \frac{1}{1-\phi} \right) \pm \sqrt{36 \left[\frac{\tau}{\phi} + \frac{1}{1-\phi} \right]^2 - \frac{12}{\phi} \frac{1 + \frac{\phi}{2}}{(1-\phi)^2}} \quad (11.54)$$

$$\lambda = \begin{cases} \lambda_+ & \text{for } \lambda_+ < |\lambda_-| \\ \lambda_- & \text{otherwise} \end{cases} \quad (11.55)$$

$$\mu = \lambda\phi(1 - \phi) \quad (11.56)$$

$$A = \frac{1}{2} \frac{1 + 2\phi - \mu}{(1 - \phi)^2} \quad (11.57)$$

$$B = \frac{\sigma}{2} \frac{\mu - 3\phi}{2(1 - \phi)^2} \quad (11.58)$$

$$C = -A\sigma^2 - B\sigma + \lambda\sigma^2/12 \quad (11.59)$$

$$I_n(\kappa) = \int_0^1 x^n \cos(\kappa x) dx \quad (11.60)$$

$$J_n(\kappa) = \int_0^1 x^n \sin(\kappa x) dx \quad (11.61)$$

$$\alpha = 1 - 12f_p (C\sigma^{-2}I_0(\kappa) + B\sigma^{-1}I_1(\kappa) + AI_2(\kappa)) \quad (11.62)$$

$$\beta = 12f_p (C\sigma^{-2}J_0(\kappa) + B\sigma^{-1}J_1(\kappa) + AJ_2(\kappa)) \quad (11.63)$$

$$S(Q) = \frac{1}{\alpha^2 + \beta^2} \quad (11.64)$$

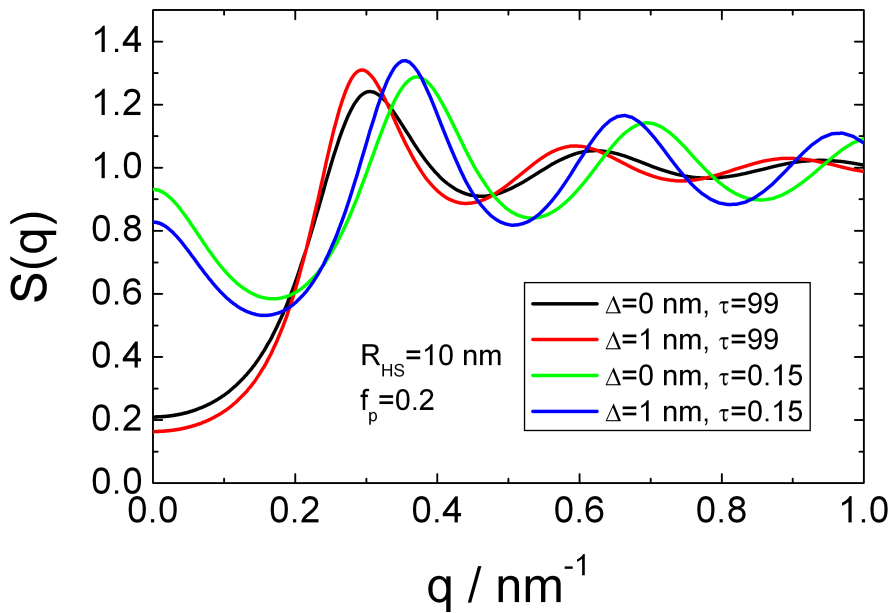


FIGURE 11.12. Structure factor $S(q)$ for a sticky hard sphere interaction potential for the different stickiness parameters τ .

Input Parameters for the structure factor model Sticky Hard Sphere 2:

RHS: hard sphere radius

fp: volume fraction f_p

tau: stickiness parameter τ

Delta: width Δ of stickiness potential

Note:

- for stickiness parameters close to zero the root in eq. 11.54 becomes complex and is considered as a critical point where the system phase separates.

11.4.3. Square Well Potential.

The Square well potential can be written as

$$U(r) = \begin{cases} \infty & \text{for } 0 < r < \sigma \\ -\epsilon & \text{for } \sigma < r < \lambda\sigma \\ 0 & \text{for } r > \lambda\sigma \end{cases} \quad (11.65)$$

where λ and ϵ correspond to the breadth and the depth of the square well potential. The structure factor $S(Q)$ is then given by the following relations [450]:

$$S(Q) = \frac{1}{1 - C(Q)} \quad (11.66a)$$

$$\begin{aligned} C(Q) = & -\frac{24\eta}{(Q\sigma)^6} \left\{ \alpha(Q\sigma)^3 [\sin(Q\sigma) - Q\sigma \cos(Q\sigma)] \right. \\ & + \beta(Q\sigma)^2 [2Q\sigma \sin(Q\sigma) - (Q^2\sigma^2 - 2) \cos(Q\sigma) - 2] \\ & + \gamma [4Q^3\sigma^3 - 24Q\sigma] \sin(Q\sigma) - (Q^4\sigma^4 - 12Q^2\sigma^2 + 24) \cos(Q\sigma) + 24 \\ & \left. - \frac{\epsilon}{k_B T} (Q\sigma)^3 [\sin(\lambda Q\sigma) - \lambda Q\sigma \cos(\lambda Q\sigma) + Q\sigma \cos(Q\sigma) - \sin(Q\sigma)] \right\} \end{aligned} \quad (11.66b)$$

where α , β and γ are given by

$$\alpha = \frac{(1 + 2\eta)^2 + \eta^3(\eta - 4)}{(1 - \eta)^4} \quad (11.66c)$$

$$\beta = -\frac{1}{3}\eta \frac{18 + 20\eta - 12\eta^2 + \eta^4}{(1 - \eta)^4} \quad (11.66d)$$

$$\gamma = \frac{1}{2}\eta \frac{(1 + 2\eta)^2 + \eta^3(\eta - 4)}{(1 - \eta)^4} \quad (11.66e)$$

Input Parameters for the structure factor model Square Well Potential:

RHS: hard sphere radius

fp: volume fraction f_p

epsi/kT: square well depth $\epsilon/k_B T$ in units of $k_B T$

lambda: relative square well width $\lambda > 1$, $\Delta = 2R_{HS}(\lambda - 1)$

Note:

- Values for the depth of $\epsilon > 1.5k_B T$ and for the volume fraction of $\eta > 0.08$ may give unphysical results when compared to Monte Carlo simulations according to [450].

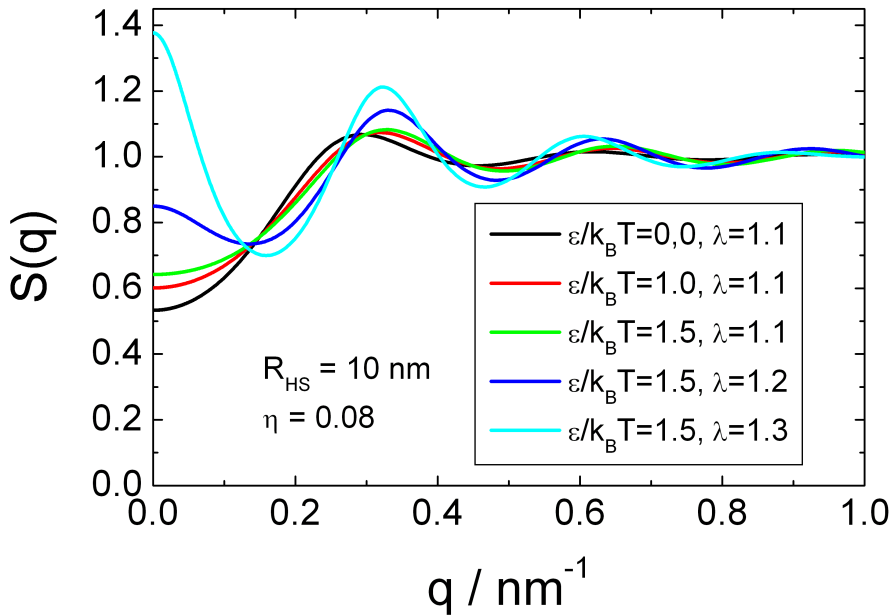


FIGURE 11.13. Structure factor $S(q)$ for a square well interaction potential.

11.4.4. Square Well Potential 2.

The Square well potential can be written as

$$U(r) = \begin{cases} \infty & \text{for } 0 < r < \sigma \\ -\epsilon & \text{for } \sigma < r < \sigma + \Delta \\ 0 & \text{for } r > \sigma + \Delta \end{cases} \quad (11.67)$$

where Δ and ϵ correspond to the width and the depth of the square well potential. The structure factor $S(Q)$ is then given by the following relations:

$$S(Q) = 1 - 4\pi\rho\sigma^3 \frac{\sin(Q\sigma) - Q\sigma \cos(Q\sigma)}{Q^3\sigma^3} + 4\pi\rho\sigma^2 \left[e^{\frac{\epsilon}{k_B T}} - 1 \right] \frac{\sin(Q\sigma)}{Q\sigma} \Delta \quad (11.68)$$

where σ is the particle diameter ($R_{HS} = \sigma/2$: hard sphere radius is requested by software as input parameter), Δ the width of the square well potential, ϵ (input value in software is ϵ/k_B , i.e. in Kelvin), T (in Kelvin) the sample temperature, the depth and ρ the colloid concentration, which is related to the colloid volume fraction η by $\eta = \pi\rho\sigma^3/6$.

Input Parameters for the structure factor model Square Well Potential 2:

RHS: hard sphere radius

fp: volume fraction f_p

epsi/kT: square well depth $\epsilon/k_B T$ in units of $k_B T$

Delta: square well width Δ

Note:

• .

11.4.5. Structure factor of fluids interacting via piece-wise constant potentials and a hard core.

The approach of Santos et al. [433, 434] allows to obtain for molecules interacting via potentials with a hard-core plus $n = 2$ piece-wise constant sections of different widths and heights a structure factor using a (semi-analytical) rational-function approximation method. The interaction potential with two piecewise constant domains can be written as

$$U(r) = \begin{cases} \infty & \text{for } 0 < r \leq \sigma \\ \epsilon_1 & \text{for } \sigma < r \leq \sigma\lambda_1 \\ \epsilon_2 & \text{for } \sigma\lambda_1 < r \leq \sigma\lambda_2 \\ 0 & \text{for } r > \sigma\lambda_2 \end{cases} \quad (11.69)$$

Negative values in ϵ_1 or ϵ_2 describes wells and positive values shoulders in the potential.

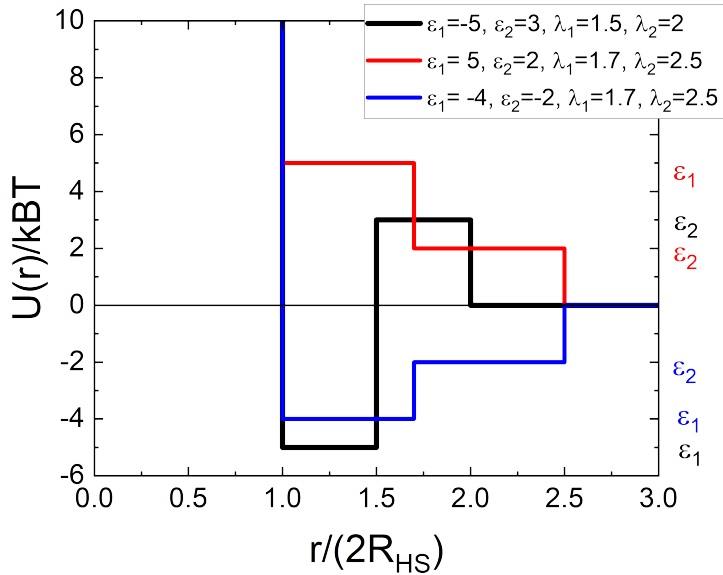


FIGURE 11.14. hard core piece-wise constant interaction potential.

A closure relation is not required in their derivation for calculating the structure factor.

$$S(q) = 1 + \rho \int d\mathbf{r} e^{-i\mathbf{qr}} [g(r) - 1] \quad (11.70)$$

$$= 1 - 12\eta \Re \left[\frac{G(s) - G(-s)}{s} \Big|_{s=iq} \right] \quad (11.71)$$

where ρ is the number density and $\eta = \rho \pi / (6(2R_{HS})^3)$ the volume fraction. The Laplace transform of $rg(r)$ has been written in terms of an auxiliary function $F(s)$ through

$$G(s) = s \frac{F(s)e^{-s}}{1 + 12\eta F(s)e^{-s}} \quad (11.72)$$

where

$$F(s) = R_0(s) + R_1(s)e^{-(\lambda_1-1)s} + R_2(s)e^{-(\lambda_2-1)s} \quad (11.73)$$

$$R_j(s) = -\frac{1}{12\eta} \frac{A_j + B_j s}{1 + S_1 s + S_2 s^2 + S_3 s^3}, \quad j = 0, 1, 2 \quad (11.74)$$

$$S_1 = -1 + B_0 - C^{(1)} \quad (11.75)$$

$$S_2 = \frac{1}{2} - B_0 + C^{(1)} + \frac{1}{2}C^{(2)} \quad (11.76)$$

$$S_3 = -\frac{1-2\eta}{12\eta} + \frac{1}{2}B_0 - \frac{1}{2}C^{(1)} - \frac{1}{2}C^{(2)} - \frac{1}{6}C^{(3)} \quad (11.77)$$

$$B_0 = C^{(1)} + \frac{\eta/2}{1+2\eta} (6C^{(2)} + 4C^{(3)} + C^{(4)}) + \frac{1+\eta/2}{1+2\eta} \quad (11.78)$$

$$C^{(k)} = \sum_{j=1}^2 [A_j (\lambda_j - 1)^k - k B_j (\lambda_j - 1)^{k-1}] \quad (11.79)$$

$$A_0 = e^{-\beta\epsilon_1} \quad (11.80)$$

$$A_1 = e^{-\beta\epsilon_2} - e^{-\beta\epsilon_1} \quad (11.81)$$

$$A_2 = 1 - e^{-\beta\epsilon_2} \quad (11.82)$$

with $\beta = 1/k_B T$. The above defined parameters all can be expressed in terms of B_1 and B_2 . These two last parameters are obtained by solving the coupled sets of equations:

$$\frac{B_1}{S_3} = \left[e^{\beta(\epsilon_1-\epsilon_2)} \right] \sum_{\nu=1}^3 \frac{s_\nu e^{(\lambda_1-1)s_\nu}}{S_1 + 2S_2 s_\nu + 3S_3 s_\nu^2} \\ \times (A_0 + B_0 s_\nu) \quad (11.83)$$

$$\frac{B_2}{S_3} = \left(e^{\beta\epsilon_2} - 1 \right) \sum_{\nu=1}^3 \frac{s_\nu e^{(\lambda_2-1)s_\nu}}{S_1 + 2S_2 s_\nu + 3S_3 s_\nu^2} \\ \times \left(A_0 + B_0 s_\nu + (A_1 + B_1 s_\nu) e^{-(\lambda_1-1)s_\nu} \right) \quad (11.84)$$

where $s_\nu (\nu = 1, 2, 3)$ are the roots of the equation

$$1 + S_1 s_\nu + S_2 s_\nu^2 + S_3 s_\nu^3 = 0 \quad (11.85)$$

11.5. ordered particle systems

This plugin contains the structure factor of ordered mesoscopic materials in case the domains are random orientated like in powder diffraction as described in [128]. For oriented domains the scattering pattern is not anymore radial symmetric and depends both on the direction and modulus of the scattering vector. For this case the structure factor are taken from [125]. This plugin tries to re-implement the functions which are originally supplied by the software package `scatter` described in [124]. The software package `scatter` is specialised on calculating and fitting ordered structures and has much more options and better GUI for this kind of studies. In both case the structure factor is approximated in the decoupling approach ([273]) as defined in 4.1.2 or in eq. 14.56 of section 14.2.4

In case of random oriented domains of three dimensional ordered particle systems the decoupling approach is implemented as

$$I(Q) = \langle \overline{F^2(Q)} \rangle_{or} + \langle \overline{F(Q)} \rangle_{or}^2 (S(Q) - 1) \quad (11.86)$$

The overline symbol denotes the average over a particle size distribution and the brackets $\langle \rangle_{or}$ for the orientational average. In the above case it is assumed that the position of the scatterer is independent of their size and orientation. For small size distributions and only small deviations from spherical symmetry of the scatterer the decoupling approximation works quite well. For two and one dimensional ordered particle systems the particles can be very anisotropic, i.e. very long cylindrical in case of 2D ordering and thin planar objects in case of 1D ordering. For this very anisotropic shaped particles the scattering amplitude and scattering intensity can be written as a product 9.2 in terms of a cross section term for the short dimension L_{short} and a shape factor for the long dimension L_{long} as well as there averages

$$F(Q, L_{\text{short}}, L_{\text{long}}) = F_{\text{cs}}(Q, L_{\text{short}})F'(Q, L_{\text{long}}) \quad (11.87a)$$

$$\langle \overline{F^2(Q, L_{\text{short}}, L_{\text{long}})} \rangle_{or} = \langle \overline{F_{\text{cs}}^2(Q, L_{\text{short}})} \rangle_{or} \langle \overline{F'^2(Q, L_{\text{long}})} \rangle_{or} \quad (11.87b)$$

$$\langle \overline{F(Q, L_{\text{short}}, L_{\text{long}})} \rangle_{or}^2 = \langle \overline{F_{\text{cs}}(Q, L_{\text{short}})} \rangle_{or}^2 \langle \overline{F'(Q, L_{\text{long}})} \rangle_{or}^2 \quad (11.87c)$$

In case of one (multi-lamellar structures) as well as of two dimensional (ordering of structures on a planar surface) ordered particles strongly anisotropic particles are often ordered along their short dimension, i.e. cylindrical pillar have their cylindrical axis often perpendicular to the ordering plane or in case of lamellar structures ordering happens always in the direction of the normal of the planar scattering objects. The averages, which needs to be performed in the decoupling approximation are

$$I(\mathbf{Q}) = \langle \langle \overline{F^2(\mathbf{Q})} \rangle_i \rangle_d + \langle \langle \overline{F(\mathbf{Q})} \rangle_i^2 (S(\mathbf{Q}) - 1) \rangle_d \quad (11.88a)$$

$$= \langle \langle \overline{F^2(\mathbf{Q})} \rangle_i \rangle_d + \langle \langle \overline{F(\mathbf{Q})} \rangle_i^2 (Z(\mathbf{Q}) - 1) G(\mathbf{Q}) \rangle_d \quad (11.88b)$$

with

$$S(\mathbf{Q}) = (Z(\mathbf{Q}) - 1) G(\mathbf{Q}) + 1 \quad (11.89)$$

In the last equation the structure factor $S(\mathbf{Q})$ has been expressed in terms of the lattice factor function $Z(\mathbf{Q})$ and the Debye-Waller factor $G((Q))$. The term $Z(\mathbf{Q})G(\mathbf{Q})$ describes the decay of the Bragg peaks due to displacement and $1 - G(\mathbf{Q})$ the concomitant increase of diffuse scattering. For a perfect lattice $G((Q)) = 1$. The orientation averages

is done here slightly different than in the paper from [125]. The orientational averaging of the scatterer within the domain are denoted by $\langle \dots \rangle_i$ and the orientation averaging of the whole domains by $\langle \dots \rangle_d$. In the appendix of [125] it is discussed under which conditions the orientation distribution over the structure factor and form factor can be factorized. If the orientation distribution of the scatterer in a domain is significant larger than the orientation distribution of the domains the averages can be factorized $\langle (\langle \dots \rangle_i)^2 \dots \rangle_d \simeq (\langle \dots \rangle_i)^2 \langle \dots \rangle_d$ and one obtains

$$I(\mathbf{Q}) = \langle \overline{F^2(\mathbf{Q})} \rangle_i + \langle \langle \overline{F(\mathbf{Q})} \rangle_i^2 (S(\mathbf{Q}) - 1) \rangle_d \quad (11.90a)$$

$$\simeq \langle \overline{F^2(\mathbf{Q})} \rangle_i + \langle \overline{F(\mathbf{Q})} \rangle_i^2 \langle (Z(\mathbf{Q}) - 1) G(\mathbf{Q}) \rangle_d \quad (11.90b)$$

The formula above is different to the one given in [125], where the orientational averaging is done after squaring the size average of the scattering amplitude $\langle \overline{F(\mathbf{Q})}^2 \rangle_{or}$ instead of doing the orientation averaging first $\langle \overline{F(\mathbf{Q})} \rangle_{or}^2$.

However, in case of a powder signal, where the orientation distribution within a domain is small and the domains are random oriented. Also the structures can be very anisotropic in two or one dimensional ordered structures and the periodicity is in most cases perpendicular to the long dimension of the scattering object.

11.5.1. Domains of ordered particle systems isotropically oriented.

For random oriented domains of ordered particle systems the structure factor can be written as

$$S(Q) = (Z_0(Q) - 1) G(Q) + 1 \quad (11.91)$$

$Z_0(Q)$ is the lattice factor got an ideal undistorted lattice and $G(Q)$ the Debye-Waller factor. The lattice factor expressed with Miller indices reads as

$$Z_0(Q) = \frac{(2\pi)^{d-1}}{nv_d \Omega_d Q^{d-1}} \sum_{\{hkl\}} m_{hkl} f_{hkl}^2 L_{hkl}(Q - Q_{hkl}) \quad (11.92)$$

where n is the number of particles per unit cell, f_{hkl} is the symmetry factor taking into account extinction rules, v_d is the volume ($d = 3$), surface ($d = 2$), or long-period ($d = 1$) of the d -dimensional unit cell, Ω_d is the d -dimensional solid angle, $L_{hkl}(Q - Q_{hkl})$ is a normalised peak-shape function, and m_{hkl} is the multiplicity. If the sum is done over all reflections $\{hkl\}$, i.e. $\sum_{\{hkl\}} = \sum_{h=-\infty}^{\infty} \sum_{k=-\infty}^{\infty} \sum_{l=-\infty}^{\infty}$, one automatically accounts for multiplicity but one the costs for summing over all combinations of $\{hkl\}$. For the normalized peak shape function $L_{hkl}(x)$ the user can choose between Lorentzian, Gaussian, and Pearson VII peak shape

$$L_{hkl}(x) = \begin{cases} \frac{2}{\pi\delta} \exp\left(-4\frac{x^2}{\pi\delta}\right) & \text{for Gaussian} \\ \frac{1}{2\pi} \frac{1}{x^2 + \left(\frac{\delta}{2}\right)^2} & \text{for Lorentzian} \\ \frac{\left(1+B^2\left(\nu-\frac{1}{2}, \frac{1}{2}\right)\left(\frac{x}{\delta}\right)^2\right)^{-\nu}}{\delta} & \text{for Pearson VII} \end{cases} \quad (11.93)$$

To describe the diffraction pattern one has to define the unit cell of the ordered structure and the position of the particles with in the unit cell. The unit cell can be

specified totally by six scalar quantities, which are called the unit cell dimensions or lattice parameters. These are (see also Fig. 11.15):

$$a, b, c, \alpha, \beta, \gamma$$

The first three parameters (a, b and c) represent the lengths of the unit cell edges, and the last three (α, β and γ) represent the angles between them. By convention, α is the angle between b and c , β is the angle between a and c , and γ is the angle between a and b .

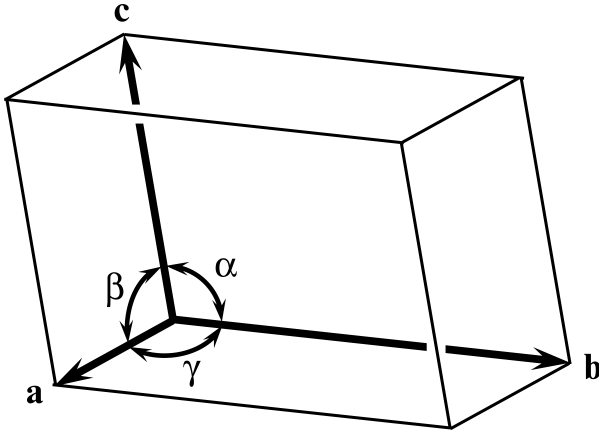


FIGURE 11.15. Unit cell in three dimensions.

If we assume that the vectors \mathbf{a} and \mathbf{b} are in the $x-y$ plane and $\mathbf{a} \parallel \mathbf{e}_x$ we can write the vector of the unit cell as

$$\mathbf{a} = a \begin{pmatrix} 1 \\ 0 \\ 0 \end{pmatrix} \quad \mathbf{b} = b \begin{pmatrix} \cos \gamma \\ \sin \gamma \\ 0 \end{pmatrix} \quad \mathbf{c} = c \begin{pmatrix} \frac{\cos \beta}{\cos \alpha - \cos \beta \cos \gamma} \\ \frac{\cos \alpha - \cos \beta \cos \gamma}{\sin \gamma} \\ \sqrt{1 - \cos^2 \beta - \left(\frac{\cos \alpha - \cos \beta \cos \gamma}{\sin \gamma} \right)^2} \end{pmatrix} \quad (11.94)$$

Next to the direct lattice with \mathbf{a} , \mathbf{b} , and \mathbf{c} be the elementary translations in a three-dimensional lattice a second lattice, reciprocal to the direct lattice, is defined by three elementary translations \mathbf{a}^* , \mathbf{b}^* and \mathbf{c}^*

$$\mathbf{a}^* = \frac{\mathbf{b} \times \mathbf{c}}{\mathbf{a} \cdot (\mathbf{b} \times \mathbf{c})} \quad \mathbf{b}^* = \frac{\mathbf{c} \times \mathbf{a}}{\mathbf{a} \cdot (\mathbf{b} \times \mathbf{c})} \quad \mathbf{c}^* = \frac{\mathbf{a} \times \mathbf{b}}{\mathbf{a} \cdot (\mathbf{b} \times \mathbf{c})} \quad (11.95)$$

For the scalar product between the direct and reciprocal lattice the following conditions holds:

$$\mathbf{a} \cdot \mathbf{a}^* = 1 \quad \mathbf{a} \cdot \mathbf{b}^* = 0 \quad \mathbf{a} \cdot \mathbf{c}^* = 0 \quad (11.96a)$$

$$\mathbf{b} \cdot \mathbf{a}^* = 0 \quad \mathbf{b} \cdot \mathbf{b}^* = 1 \quad \mathbf{b} \cdot \mathbf{c}^* = 0 \quad (11.96b)$$

$$\mathbf{c} \cdot \mathbf{a}^* = 0 \quad \mathbf{c} \cdot \mathbf{b}^* = 0 \quad \mathbf{c} \cdot \mathbf{c}^* = 1 \quad (11.96c)$$

For a two dimensional periodic lattice with the direct lattice vectors \mathbf{a}, \mathbf{b} and reciprocal lattice vector $\mathbf{a}^*, \mathbf{b}^*$ the orthogonal relations above also hold and by using eq. 11.95 with

$\mathbf{c} = (0, 0, 1)^T$ ($c = 1, \alpha = \beta = \pi/2$) one can calculate them in the same way.

$$\mathbf{a} = a \begin{pmatrix} 1 \\ 0 \\ 0 \end{pmatrix} \quad \mathbf{b} = b \begin{pmatrix} \cos \gamma \\ \sin \gamma \\ 0 \end{pmatrix} \quad (11.97a)$$

$$\mathbf{a}^* = \frac{1}{a} \begin{pmatrix} 1 \\ -\frac{\cos \gamma}{\sin \gamma} \\ 0 \end{pmatrix} \quad \mathbf{b}^* = \frac{1}{b} \begin{pmatrix} 0 \\ \frac{1}{\sin \gamma} \\ 0 \end{pmatrix} \quad (11.97b)$$

Last but not least, for a one dimensional lattice $\mathbf{a} = (a, 0, 0)^T$ the reciprocal lattice vector is simply $\mathbf{a}^* = \frac{1}{a} (1, 0, 0)^T$.

Diffraction peaks can occur at integer multiples, called Miller indices (hkl), of the reciprocal lattice

$$\mathbf{Q}_{hkl}^{3D} = 2\pi (h\mathbf{a}^* + k\mathbf{b}^* + l\mathbf{c}^*) \quad (11.98a)$$

$$\mathbf{Q}_{hk}^{2D} = 2\pi (h\mathbf{a}^* + k\mathbf{b}^*) \quad (11.98b)$$

$$\mathbf{Q}_h^{1D} = 2\pi h\mathbf{a}^* \quad (11.98c)$$

Due to the symmetry of the unit cell certain (hkl) reflections might be forbidden. This is described by the structure factor of the unit cell f_{hkl} . The structure factor depends next to the Miller indices also from the type and position of the scattering objects within the unit cell. The position $\mathbf{R}_i(u, v, w)$ of the i^{th} scatterer with the scattering amplitude $F_i(\mathbf{Q})$ in the unit cell is normally given in terms of the direct lattice vectors \mathbf{a} , \mathbf{b} , and \mathbf{c}

$$\mathbf{R}_i(u_i, v_i, w_i) = u_i \mathbf{a} + v_i \mathbf{b} + w_i \mathbf{c} \quad (11.99)$$

The scattering amplitude of the unit cell f_{hkl} is than given by

$$f_{hkl}(\mathbf{Q}_{hkl}) = \sum_{i=1}^N F_i(\mathbf{Q}_{hkl}) \exp(-i\mathbf{Q}_{hkl}\mathbf{R}_i) \quad (11.100a)$$

$$= \sum_{i=1}^N F_i(\mathbf{Q}_{hkl}) \exp(-i2\pi(hu_i + kv_i + lw_i)) \quad (11.100b)$$

$$= \sum_{i=1}^N F_i(\mathbf{Q}_{hkl}) [\cos(2\pi(hu_i + kv_i + lw_i)) - i \sin(2\pi(hu_i + kv_i + lw_i))] \quad (11.100c)$$

$$= \sqrt{A^2 + B^2} \exp(-i \arctan(A/B)) \quad (11.100d)$$

with

$$A = \sum_{i=1}^N F_i(\mathbf{Q}_{hkl}) \cos(2\pi(hu_i + kv_i + lw_i)) \quad (11.101a)$$

$$B = \sum_{i=1}^N F_i(\mathbf{Q}_{hkl}) \sin(2\pi(hu_i + kv_i + lw_i)) \quad (11.101b)$$

For a 2D and 1D lattice the scattering amplitude of the unit cell f_{hk} and f_h are calculated accordingly.

lattice	LAM	SQ (P4/mm)	HEX (P6/mm)	CREC (cmm)
n	1	1	1	2
v_d	a	a^2	$\sqrt{3}a^2/2$	ab
d	1	2	2	2
f_{hkl}	$f_h = 1$	$f_{hk} = 1$	$f_{hk} = 1$	$f_{hk} = 1$
m_{hkl}				
Ω_d	1	2π	2π	
\bar{a}	a	a	a	$\min \left\{ a, b, \frac{1}{2}\sqrt{a^2 + b^2} \right\}$
Q_{hkl}	$\frac{2\pi h}{a}$	$\frac{2\pi\sqrt{h^2+k^2}}{a}$	$\frac{4\pi\sqrt{h^2+hk+k^2}}{\sqrt{3}a}$	$2\pi\sqrt{\frac{h^2}{a^2} + \frac{k^2}{b^2}}$

lattice	BCT (I4/mmm)	FCC (Fm3m)	BCC (Im3m)	HCP (P6/mmc)	SC (Pm3m)
n	2	4	2	2	1
$\mathbf{R}_i = \begin{pmatrix} u_i \\ v_i \\ w_i \end{pmatrix}$	$\begin{pmatrix} 0 \\ 0 \\ 0 \end{pmatrix}, \begin{pmatrix} 1/2 \\ 1/2 \\ 1/2 \end{pmatrix}$	$\begin{pmatrix} 0 \\ 0 \\ 0 \end{pmatrix}, \begin{pmatrix} 1/2 \\ 1/2 \\ 0 \end{pmatrix}, \begin{pmatrix} 1/2 \\ 0 \\ 1/2 \end{pmatrix}, \begin{pmatrix} 0 \\ 1/2 \\ 1/2 \end{pmatrix}$	$\begin{pmatrix} 0 \\ 0 \\ 0 \end{pmatrix}, \begin{pmatrix} 1/2 \\ 1/2 \\ 1/2 \end{pmatrix}$	$\begin{pmatrix} 0 \\ 0 \\ 0 \end{pmatrix}, \begin{pmatrix} 2/3 \\ 1/3 \\ 1/2 \end{pmatrix}$	$\begin{pmatrix} 0 \\ 0 \\ 0 \end{pmatrix}$
v_d	$a^2 c$	a^3	a^3	$\sqrt{2}a^3$	a^3
d	3	3	3	3	3
$ f_{hkl} $	$ 1+\cos(\pi(h+k+l)) $	$\left \begin{array}{l} 1+\cos(\pi(h+k)) \\ +\cos(\pi(h+l)) \\ +\cos(\pi(k+l)) \end{array} \right $	$ 1+\cos(\pi(h+k+l)) $	$ 2\cos(\pi(\frac{h+2k}{3} + \frac{l}{2})) $	$f_{hkl}=1$
m_{hkl}					
Ω_d	4π	4π	4π	4π	4π
\bar{a}	$\sqrt{2}a/2$	$\sqrt{2}a/2$	$\sqrt{3}a/2$	a	a
Q_{hkl}	$2\pi\sqrt{\frac{h^2+k^2}{a^2} + \frac{l^2}{c^2}}$	$\frac{2\pi\sqrt{h^2+k^2+l^2}}{a}$	$\frac{2\pi\sqrt{\frac{4}{3}(h^2+hk+k^2) + \frac{3}{8}l^2}}{a}$	$\frac{2\pi\sqrt{h^2+k^2+l^2}}{a}$	$\frac{2\pi\sqrt{h^2+k^2+l^2}}{a}$

TABLE 1

11.5.2. Domains of ordered particle systems with preferred orientation.

$$\mathbf{k}_i = \begin{pmatrix} k_{i,x} \\ k_{i,y} \\ k_{i,z} \end{pmatrix} = \frac{2\pi}{\lambda} \begin{pmatrix} 0 \\ 0 \\ -1 \end{pmatrix} \quad (11.102)$$

$$\mathbf{k}_s = \begin{pmatrix} k_{i,x} \\ k_{i,y} \\ k_{i,z} \end{pmatrix} = \frac{2\pi}{\lambda} \begin{pmatrix} \cos(\psi) \sin(\theta) \\ \sin(\psi) \sin(\theta) \\ -\cos(\theta) \end{pmatrix} \quad (11.103)$$

$$\mathbf{Q} = \mathbf{k}_s - \mathbf{k}_i = \begin{pmatrix} Q_x \\ Q_y \\ Q_z \end{pmatrix} = \frac{2\pi}{\lambda} \begin{pmatrix} \cos(\psi) \sin(\theta) \\ \sin(\psi) \sin(\theta) \\ 1 - \cos(\theta) \end{pmatrix} \quad (11.104)$$

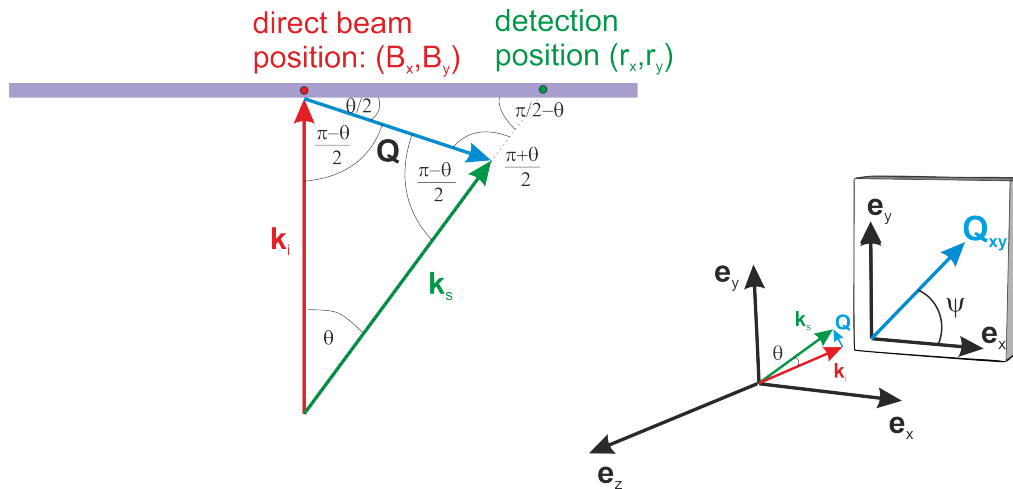


FIGURE 11.16. The scattering vector in polar coordinates coordination system with respect to a laboratory-fixed coordinate system based on the three orthogonal unit vectors $(\mathbf{e}_x, \mathbf{e}_y, \mathbf{e}_z)$. They are arranged such that the x-direction coincides with the x-direction of the detector, and the y-direction coincides with the y-direction of the detector. The direction of the incoming neutron beam is chosen to be $-\mathbf{e}_z$.

11.6. Multi Lamellar Structures

Multi-lamellar structures belong to the family of one dimensional structure factors. In practice the dimension of the structures in the direction of ordering is much smaller than perpendicular to it and it also has a random orientation, i.e. one can perform a powder average. For those structures the scattering function can be factorized [393, 222, 176, 542, 297, 371, 370, 141] in a cross-section term in the direction of the ordering and a shape factor for the long dimension.

11.6.1. Multi-Lamellar Structures, perfect finite stack.

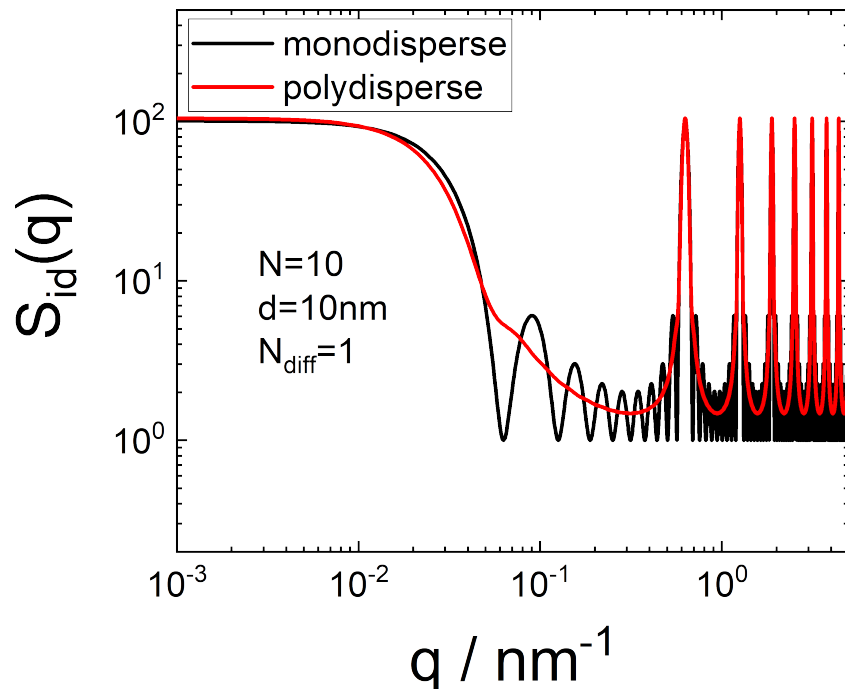


FIGURE 11.17. Perfectly ordered lamellar structures with and without a size distribution.

If the lamellar structures are perfectly arranged in a one-dimensional lattice with a lattice distance d its structure factor is given by

$$S_{N_k,\text{id}}(q) = N_k + 2 \sum_{k=1}^{N_k-1} (N_k - k) \cos(kqd) + N_{\text{diff}} \quad (11.105)$$

$$= \frac{\sin^2\left(\frac{1}{2}N_kqd\right)}{\sin^2\left(\frac{1}{2}qd\right)} + N_{\text{diff}} \quad (11.106)$$

The above formula is defined for integer values of N_k larger or equal 1. For non-integer values of N_k a mixture between $\lfloor N_k \rfloor$ and $\lfloor N_k \rfloor + 1$ is assumed where $\lfloor N_k \rfloor$ denotes the greatest integer less than or equal to N_k (`floor`-function). We finally get

$$S_{\text{id}}(q, N_k) = (1 - w)S_{\lfloor N_k \rfloor, \text{id}}(q) + wS_{\lfloor N_k \rfloor + 1, \text{id}}(q) \quad (11.107)$$

with $w = N_k - \lfloor N_k \rfloor$. This is a classical result for diffraction of perfect ordered limited sized domains. The Bragg peaks are centered around $q_h = 2\pi h/d$, where h denotes the diffraction order. The width of the peaks are only dependent on the domain size N_k .

The structure factors $S_{k,id}(q)$ with low, but fixed stacking numbers N_k show oscillations at low q (as can be seen in Fig. 11.17), but no such oscillations are found in experimental data. This can be understood as the consequence of polydispersity in the number of the different stacks. In order to eliminate these artifacts from strictly monodisperse systems, we use a ‘polydisperse’ structure factor, i.e. we use an average of a series of structure factors with varying numbers of bilayers [141]. The analytical form of the distribution is not known a priori. We use a Gaussian distribution approximated by a discrete series. The standard deviation σ for the Gaussian-weighted distribution is chosen as

$$\sigma = \begin{cases} \sqrt{N} & \text{for } N \geq 5, \\ 0.5(N-1) & \text{for } N < 5 \end{cases} \quad (11.108)$$

Therefore, N must be greater or equal to 2, which is a reasonable restriction for multilamellar stacks of bilayers. In the range of $N \pm 2\sigma$, structure factors are weighted by

$$x_k(N_k) = \frac{1}{\sigma\sqrt{2\pi}} \exp\left[-\frac{(N_k - N)^2}{2\sigma^2}\right] \quad (11.109)$$

where N is the mean number of stacks and N_k is one of the bilayers in the range $N \pm 2\sigma$. This polydispersity model does not introduce new free parameters and is symmetrical around the mean N . Due to the continuous definition in eq. 11.107 we therefore can write the polydispersity effect both as a sum or an integral.

$$S_{sd,id}(q) = \sum_{N_k=N-2\sigma}^{N+2\sigma} x_k(N_k) S_{id}(q, N_k) \quad (11.110)$$

$$= \int_{N-2\sigma}^{N+2\sigma} x_k(N_k) S_{id}(q, N_k) dN_k \quad (11.111)$$

SASfit supplies the original formula eq. 11.105 as `PerfectFiniteStack` and the smoothed version by introducing some polydispersity in the stacking number according to eq. 11.110 as `PerfectFiniteStack (polydisp.,sum)` and 11.111 as `PerfectFiniteStack (polydisp.,int)`.

Input Parameters for the models `PerfectFiniteStack`, `PerfectFiniteStack (polydisp.,sum)`, and `PerfectFiniteStack (polydisp.,int)`:

N: mean number of stacks N

d: stacking separation d

dummy: not used

Nu: number of uncorrelated scattering bilayers N_{diff}

Note:

- This structure factor is intended to be used with the `monodisperse` approximation.

11.6.2. Multi-Lamellar Structures, Thermal Disorder.

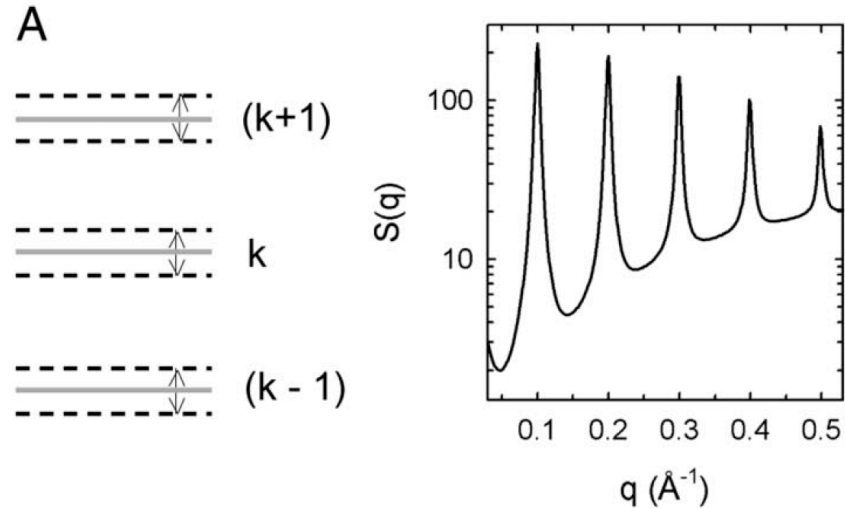


FIGURE 11.18. Thermal disorder, considering fluctuations of flat layers around well defined and evenly spaced equilibrium positions.

The first type describes thermal disorder (TD) caused by small fluctuations of the bilayers around well defined mean layer positions of equal separation (Fig. 11.18) [370, 141]. In such a crystal lattice the long-range order is preserved and the structure factor for a single domain of size $L = Nd$ is identical to that of a perfect finite crystal multiplied by the well known Debye-Waller temperature factor, where $\Delta = \langle (d_k - d)^2 \rangle$ denotes the mean square fluctuations of the bilayers. As shown in Fig. 11.18, $S_{\text{TD}}(Q)$ is characterized by a set of Bragg peaks of equal width, the diffraction order amplitudes of which decrease exponentially with the Debye-Waller factor. The lost intensity is found as a diffuse background scattering, which increases to the limit of N for large q . For this model and with a lattice distance d and fixed number N_k of layers per stack the structure factor is given by

$$S_{N_k, \text{TD}}(q) = \left(N_k + 2e^{-\frac{q^2 \Delta^2}{2}} \sum_{k=1}^{N_k-1} (N_k - k) \cos(kqd) \right) + N_{\text{diff}} \quad (11.112)$$

$$= N_k \left(1 - e^{-\frac{q^2 \Delta^2}{2}} \right) + e^{-\frac{q^2 \Delta^2}{2}} (S_{N_k, \text{id}}(q) - N_{\text{diff}}) + N_{\text{diff}} \quad (11.113)$$

N_{diff} accounts for an additional diffuse background, due to a number of uncorrelated scattering bilayers in $S_{\text{TD}}(q, N, d, \Delta, N_{\text{diff}})$, which is not included in the TD theory. Its origin is attributed to bilayers with strong lattice defects or unilamellar vesicles, which display neither short-range nor (quasi-) long-range order. The above formula is defined for integer values of N_k larger or equal 1. For non-integer values of N_k a mixture between $\lfloor N_k \rfloor$ and $\lfloor N_k \rfloor + 1$ is assumed where $\lfloor N_k \rfloor$ denotes the greatest integer less than or equal to N_k (**floor**-function). We finally get

$$S_{\text{TD}}(q, N_k) = (1 - w)S_{\lfloor N_k \rfloor, \text{TD}}(q) + wS_{\lfloor N_k \rfloor + 1, \text{TD}}(q) \quad (11.114)$$

with $w = N_k - \lfloor N_k \rfloor$. The Bragg peaks are centered around $q_h = 2\pi h/d$, where h denotes the diffraction order.

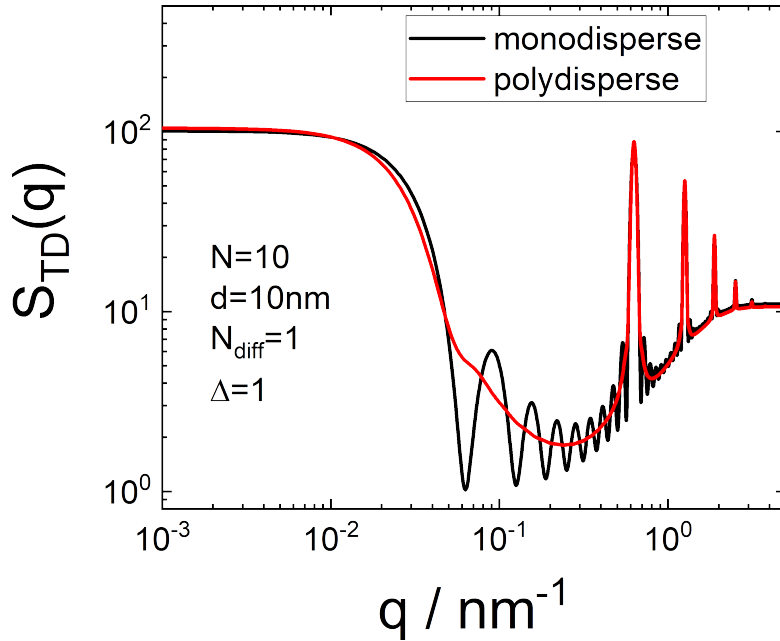


FIGURE 11.19. Structure factor of multi-lamellar structures with thermal disorder.

The structure factors $S_{N_k, \text{TD}}(q)$ with low, but fixed stacking numbers N_k show oscillations at low q (as can be seen in Fig. 11.18), but no such oscillations are found in experimental data. This can be understood as the consequence of polydispersity in the size of the different stacks. In order to eliminate these artifacts from strictly monodisperse systems, we use a ‘polydisperse’ structure factor, i.e. we use an average of a series of structure factors with varying numbers of bilayers [141]. The analytical form of the distribution is not known a priori. We use a Gaussian distribution approximated by a discrete series. The standard deviation σ for the Gaussian-weighted distribution is chosen as

$$\sigma = \begin{cases} \sqrt{N} & \text{for } N \geq 5, \\ 0.5(N-1) & \text{for } N < 5 \end{cases} \quad (11.115)$$

Therefore, N must be greater or equal to 2, which is a reasonable restriction for multilamellar stacks of bilayers. In the range of $N \pm 2\sigma$, structure factors weighted by

$$x_k = \frac{1}{\sigma\sqrt{2\pi}} \exp\left[-\frac{(N_k - N)^2}{2\sigma^2}\right] \quad (11.116)$$

are calculated, where N is the mean number of stacks and N_k is one of the bilayers in the range $N \pm 2\sigma$. This polydispersity model does not introduce new free parameters and is symmetrical around the mean N . Due to the continuous definition in eq. 11.114

we therefore can write the polydisperse effect both as a sum or an integral.

$$S_{\text{sd,TD}}(q) = \sum_{N_k=N-2\sigma}^{N+2\sigma} x_k(N_k) S_{\text{TD}}(q, N_k) \quad (11.117)$$

$$= \int_{N-2\sigma}^{N+2\sigma} x_k(N_k) S_{\text{TD}}(q, N_k) dN_k \quad (11.118)$$

SASfit supplies the original formula eq. 11.112 as `ThermalDisorder` and the smoothed version by introducing some polydispersity in the stacking number according to eq. 11.117 as `ThermalDisorder (polydisp.,sum)` and 11.118 as `ThermalDisorder (polydisp.,int)`.

Input Parameters for model ThermalDisorder, ThermalDisorder (polydisp.,sum), and ThermalDisorder (polydisp.,int):

N: mean number of stacks N

d: stacking separation d

Delta: Debye-Waller disorder parameter Δ

Nu: number of uncorrelated scattering bilayers N_{diff}

Note:

- This structure factor is intended to be used with the monodisperse approximation.

11.6.3. Multi-Lamellar Structures, Paracrystalline Theory.

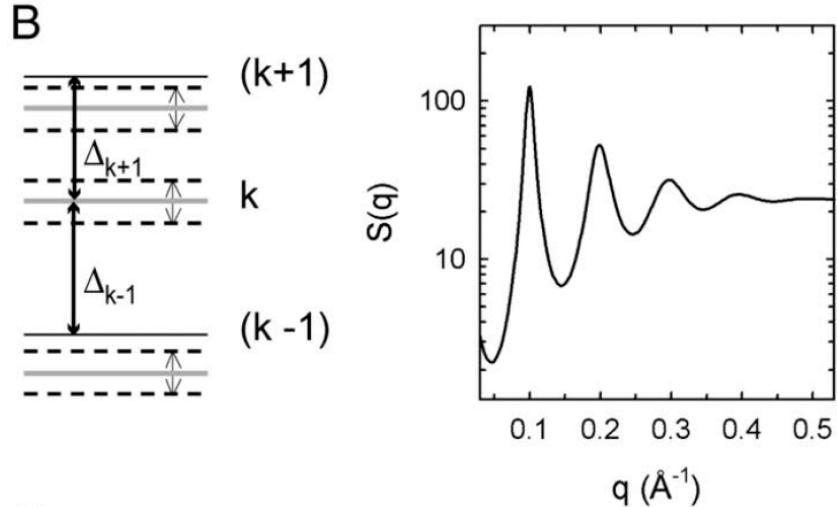


FIGURE 11.20. Stacking disorder as described within paracrystalline theory (PC) is due to displacements from the mean layer positions.

The second type of disorder accounts for the presence of small variations in the bilayer separations (Fig. 11.20), so-called stacking disorder, and is described within the paracrystalline theory (PC) [222, 176, 41, 370, 141]. As the position of an individual

fluctuating layer in a paracrystal is determined solely by its nearestneighbour membranes, the crystalline long-range order is lost. Still, we are able to observe Bragg-peak scattering due to the fact that there is quasi long-range order. However, these quasi-Bragg peaks will display a typical line shape. In the case of disorder of the second kind, the structure factor derived from paracrystalline theory is given by [176]

$$S_{N_k, \text{PC}}(q) = \left(N_k + 2 \sum_{k=1}^{N_k-1} (N_k - k) \cos(kqd) \exp\left(-\frac{kq^2\Delta^2}{2}\right) \right) + N_{\text{diff}} \quad (11.119)$$

N_{diff} accounts for an additional diffuse background, due to a number of uncorrelated scattering bilayers in $S_{\text{PC}}(q, N, d, \Delta, N_{\text{diff}})$, which is not included in the paracrystalline theory. Its origin is attributed to bilayers with strong lattice defects or unilamellar vesicles, which display neither short-range nor (quasi-) long-range order. The above formula is defined for integer values of N_k larger or equal 1. For non-integer values of N_k a mixture between $\lfloor N_k \rfloor$ and $\lfloor N_k \rfloor + 1$ is assumed where $\lfloor N_k \rfloor$ denotes the greatest integer less than or equal to N_k (`floor`-function). We finally get

$$S_{\text{PC}}(q, N_k) = (1 - w)S_{\lfloor N_k \rfloor, \text{PC}}(q) + wS_{\lfloor N_k \rfloor + 1, \text{PC}}(q) \quad (11.120)$$

with $w = N_k - \lfloor N_k \rfloor$. The Bragg peaks are centered around $q_h = 2\pi h/d$, where h denotes the diffraction order.

Fig. 11.20 shows that the quasi-Bragg peak intensity decreases for $S_{\text{PC}}(q)$, as in the previous case of thermal disorder. However, the decrease in peak height is also accompanied by a progressive broadening proportional to the square of the diffraction order h [446]. The line shape of the tails is essentially Lorentzian with

$$S_{k, \text{PC}}(q) \propto (q - q_h)^2,$$

where q_h is the position of the h^{th} diffraction order in q space. Again, the loss in intensity shows up as diffuse background scattering, which is stronger than from pure thermal disorder.

The structure factors $S_{k, \text{PT}}(q)$ with low, but fixed stacking numbers N show oscillations at low q (as can be seen in Fig. 11.20), but no such oscillations are found in experimental data. This can be understood as the consequence of polydispersity in the size of the different stacks. In order to eliminate these artifacts from strictly monodisperse systems, we use a ‘polydisperse’ structure factor, i.e. we use an average of a series of structure factors with varying numbers of bilayers [141]. The analytical form of the distribution is not known a priori. We use a Gaussian distribution approximated by a discrete series. The standard deviation σ for the Gaussian-weighted distribution is chosen as

$$\sigma = \begin{cases} \sqrt{N} & \text{for } N \geq 5, \\ 0.5(N-1) & \text{for } N < 5 \end{cases} \quad (11.121)$$

Therefore, N must be greater or equal to 2, which is a reasonable restriction for multilamellar stacks of bilayers. In the range of $N \pm 2\sigma$, structure factors weighted by

$$x_k = \frac{1}{\sigma\sqrt{2\pi}} \exp\left[-\frac{(N_k - N)^2}{2\sigma^2}\right] \quad (11.122)$$

are calculated, where N is the mean number of stacks and N_k is one of the bilayers in the range $N \pm 2\sigma$. This polydispersity model does not introduce new free parameters and is symmetrical around the mean N . Due to the continuous definition in eq. 11.120 we therefore can write the polydisperse effect both as a sum or an integral.

$$S_{sd,PC}(q) = \sum_{N_k=N-2\sigma}^{N+2\sigma} x_k(N_k) S_{PC}(q, N_k) \quad (11.123)$$

$$= \int_{N-2\sigma}^{N+2\sigma} x_k(N_k) S_{PC}(q, N_k) dN_k \quad (11.124)$$

SASfit supplies the original formula eq. 11.119 as **Paracrystalline** and the smoothed version by introducing some polydispersity in the stacking number according to eq. 11.123 as **Paracrystalline (polydisp.,sum)** and 11.124 as **Paracrystalline (polydisp.,int)**.

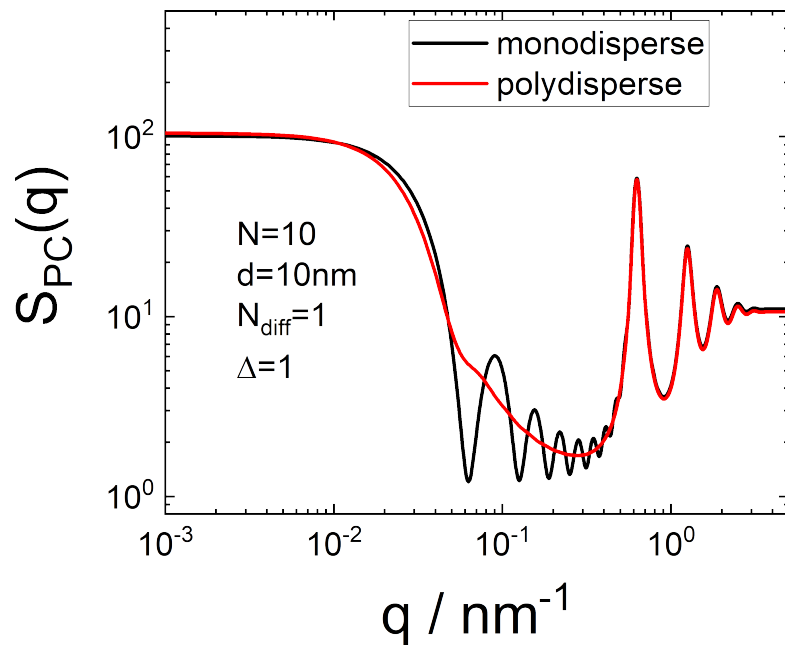


FIGURE 11.21. Structure factor of multi-lamellar structures with paracrystalline disorder.

Input Parameters for model Paracrystalline, Paracrystalline (polydisp.,sum), and Paracrystalline (polydisp.,int):

N: mean number of stacks N

d: stacking separation d

Delta: stacking disorder parameter Δ

Nu: number of uncorrelated scattering bilayers N_{diff}

Note:

- This structure factor is intended to be used with the monodisperse approximation.

11.6.4. Multi-Lamellar Structures, Modified Caillé Theory.

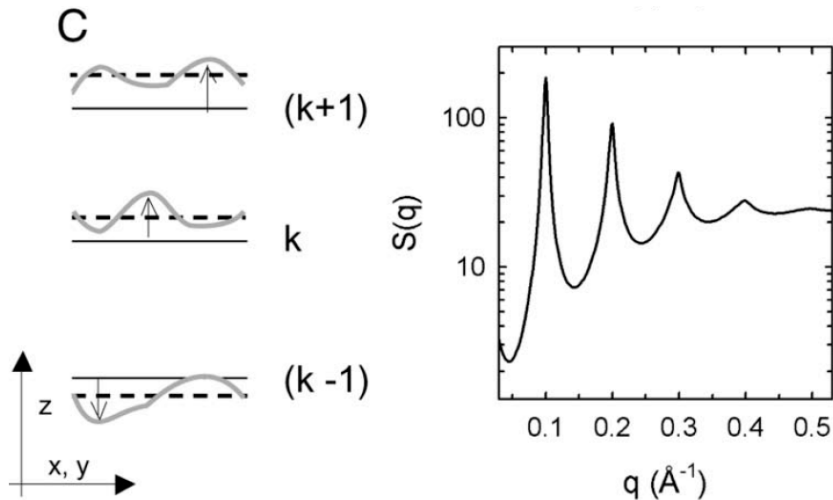


FIGURE 11.22. Bending fluctuation disorder is a particular feature of the L_α (smectic A) phase and is caused by bilayer undulations. The particular shape of the Bragg peaks is given by the modified Caillé theory (MC).

There is another type of disorder when bilayer bending fluctuations are considered (Fig. 11.22) [370, 141]. Such fluctuations are particularly pronounced in the fluid L_α phase (equivalent to smectic A). Caillé bending fluctuation disorder is a particular feature of the L_α (smectic A) phase and is caused by bilayer undulations. The particular shape of the Bragg peaks is given by the modified Caillé theory (MC). [75] realized the impact on the structure factor, which in a modified version [542] of the Caillé theory is

$$\begin{aligned} S_{N_k, \text{MC}}(q) = & N_{\text{diff}} + N_k \\ & + 2 \sum_{k=1}^{N_k-1} (N_k - k) \cos(kqd) e^{-\left(\frac{d}{2\pi}\right)^2 q^2 \eta_1 \gamma} (\pi k)^{-(d/2\pi)^2 Q^2 \eta_1} \end{aligned} \quad (11.125)$$

Here, γ is Euler's constant and

$$\eta_1 = \pi k_B T / 2d^2 (BK_c)^{1/2} \quad (11.126)$$

is the Caillé parameter, which is a measure for the bilayer fluctuations and is inversely proportional to the square root of the bilayer bending rigidity K_c times the bulk modulus of compression B (De Gennes & Prost, 1993). Therefore, a lineshape analysis of the quasi-Bragg peaks opens an important experimental window on interbilayer interactions. Further, K_c and B can be decoupled as demonstrated recently by hydration studies [386, 370], or more elegantly by measuring multibilayers aligned on a solid substrate [320]. N_{diff} accounts for an additional diffuse background, due to a number of uncorrelated scattering bilayers in $S_{N_k, \text{MC}}(q, d, \eta_1, \gamma, N_{\text{diff}})$, which is not included in the MCT. Its origin is attributed to bilayers with strong lattice defects or unilamellar vesicles, which

display neither short-range nor (quasi-) long-range order. The above formula is defined for integer values of N_k larger or equal 1. For non-integer values of N_k a mixture between $\lfloor N_k \rfloor$ and $\lfloor N_k \rfloor + 1$ is assumed where $\lfloor N_k \rfloor$ denotes the greatest integer less than or equal to N_k (**floor**-function). We finally get

$$S_{\text{MC}}(q, N_k) = (1 - w)S_{\lfloor N_k \rfloor, \text{MC}}(q) + wS_{\lfloor N_k \rfloor + 1, \text{MC}}(q) \quad (11.127)$$

with $w = N_k - \lfloor N_k \rfloor$.

Fig. 11.22 shows a typical example of $S_{\text{MC}}(q)$, which is similar to $S_{\text{PC}}(q)$ with respect to the progressive decrease in peak height and increase in peak width, but which differs significantly in line shape as

$$S_{\text{MC}}(q) \propto (q - q_h)^{-1+\eta_1 h^2} \quad (11.128)$$

for randomly oriented scattering domains [428, 542].

The structure factors $S_{\text{MC}}(q)$ with low, but fixed stacking numbers N_k show oscillations at low q (as can be seen in Fig. 11.22), but no such oscillations are found in experimental data. This can be understood as the consequence of polydispersity in the size of the different stacks. In order to eliminate these artifacts from strictly monodisperse systems, we use a ‘polydisperse’ structure factor, i.e. we use an average of a series of structure factors with varying numbers of bilayers [141]. The analytical form of the distribution is not known a priori. We use a Gaussian distribution approximated by a discrete series. The standard deviation σ for the Gaussian-weighted distribution is chosen as

$$\sigma = \begin{cases} \sqrt{N} & \text{for } N \geq 5, \\ 0.5(N-1) & \text{for } N < 5 \end{cases} \quad (11.129)$$

Therefore, N must be greater or equal to 2, which is a reasonable restriction for multilamellar stacks of bilayers. In the range of $N \pm 2\sigma$, structure factors weighted by

$$x_k = \frac{1}{\sigma\sqrt{2\pi}} \exp\left[-\frac{(N_k - N)^2}{2\sigma^2}\right] \quad (11.130)$$

are calculated, where N is the mean number of stacks and N_k is one of the bilayers in the range $N \pm 2\sigma$. This polydispersity model does not introduce new free parameters and is symmetrical around the mean N .

Due to the continuous definition in eq. 11.127 we therefore can write the polydisperse effect both as a sum or an integral.

$$S_{\text{sd,MC}}(q) = \sum_{N_k=N-2\sigma}^{N+2\sigma} x_k(N_k) S_{\text{MC}}(q, N_k) \quad (11.131)$$

$$= \int_{N-2\sigma}^{N+2\sigma} x_k(N_k) S_{\text{MC}}(q, N_k) dN_k \quad (11.132)$$

SASfit supplies the original formula eq. 11.125 as **ModifiedCaille** and the smoothed version by introducing some polydispersity in the stacking number according to eq. 11.131 as **ModifiedCaille** (**polydisp.,sum**) and 11.132 as **ModifiedCaille** (**polydisp.,int**).

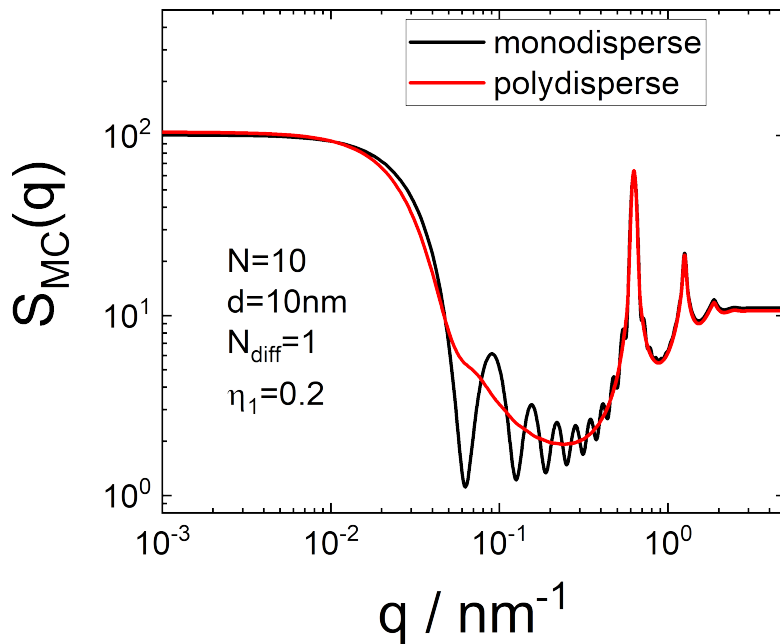


FIGURE 11.23. Structure factor of multi-lamellar structures according to the modified Caillé theory.

Input Parameters for model `ModifiedCaillé`, `ModifiedCaillé (polydisp.,sum)`, and `ModifiedCaillé (polydisp.,int)`:

N: mean number of stacks N

d: stacking separation d

eta: the Caillé parameter η_1 is a measure for the bilayer fluctuations and inversely proportional to the square root of the bilayer bending rigidity

Nu: number of uncorrelated scattering bilayers N_{diff}

Note:

- This structure factor is intended to be used with the `monodisperse` approximation.

11.7. Mass Fractal

For a fractal object, the structure factor $S(q)$ can be calculated [482, 481, 443, 459, 458, 227, 307, 308, 309, 310] via the pair correlation function $g(r)$, which describes the total number of particles within a sphere of radius r centered in a central particle and is given (for $\dim = 3$) by

$$N(r) = \Phi \int_0^r g(r) 4\pi r^2 dr \quad (11.133)$$

or

$$dN(r) = \Phi g(r) 4\pi r^2 dr \quad (11.134)$$

On the other hand, a fractal object is characterized by a spatial distribution of the individual scatterers given by

$$N(r) = \left(\frac{r}{r_0}\right)^D \quad (11.135)$$

where r_0 is the gauge of the measurement, which has the magnitude of the characteristic dimension of each individual scatterer. Differentiation of 11.135 and identification with 11.134 gives

$$\Phi g(r) = \frac{D}{4\pi r_0^D} r^{D-3} \quad (11.136)$$

Because D is smaller than 3, $g(r)$ goes to zero at large r . This is clearly unphysical. At some large scale, the sample will show a macroscopic density. A good knowledge of the sample allows in general a reasonable assumption for the large-scale behavior of $g(r)$. Therefore a cut-off function $h(r, \xi)$ has to be introduced, where ξ is a cut-off distance, to describe the behavior of the pair correlation function at large distances. To derive the analytical form of $S(q)$ within this assumption, one can use the general theory of liquids, where the uniform density is subtracted to avoid a divergence in the evaluation of $S(q)$. We then write [482]

$$4\pi\Phi[g(r) - 1] = \frac{D}{r_0^D} r^{D-3} h(r, \xi) \quad (11.137)$$

The meaning of ξ is only qualitative and has to be made precise in any particular situation. Generally speaking, it represents the characteristic distance above which the mass distribution in the sample is no longer described by the fractal law. In practice, it can represent the size of an aggregate or a correlation length in a disordered material. For isotropic systems

$$S(q) = 1 + 4\pi\Phi \int_0^\infty [g(r) - 1] \frac{\sin(qr)}{qr} r^2 dr \quad (11.138)$$

Combined with 11.137 one gets

$$S(q) = 1 + \frac{D}{r_0^D} \int_0^\infty r^{D-3} h(r, \xi) \frac{\sin(qr)}{qr} r^2 dr \quad (11.139)$$

Several cut-off functions $h(r, \xi)$ have been discussed in the literature and compared by Sorensen et al. [459, 458].

$$h_{\text{Exp}}(r, \xi) = \exp\left[-\frac{r}{\xi}\right] \quad (11.140)$$

$$h_{\text{Gauss}}(r, \xi) = \exp\left[-\left(\frac{r}{\xi}\right)^2\right] \quad (11.141)$$

$$h_{\text{Exp}(-x^a)}(r, \xi, \alpha, D) = \exp\left[-\left(\frac{r}{\xi}\right)^\alpha\right] \quad (11.142)$$

$$h_{\text{OverlapSph}}(r, \xi) = \begin{cases} \left(1 + \frac{r}{4\xi}\right) \left(1 - \frac{r}{2\xi}\right)^2 & \text{for } r \leq 2\xi \\ 0 & \text{for } r > 2\xi \end{cases} \quad (11.143)$$

For the cut-off functions 11.140 and 11.141 the integral 11.139 can be solved analytically and the corresponding structure factors are given by

$$S_{\text{Exp}}(q, \xi, D, r_0) = 1 + \frac{D\Gamma(D-1) \sin([D-1] \arctan(q\xi))}{(qr_0)^D \left[1 + \frac{1}{q^2\xi^2}\right]^{(D-1)/2}} \quad (11.144)$$

$$S_{\text{Gauss}}(q, \xi, D, r_0) = 1 + \Gamma\left[\frac{D}{2}\right] \frac{D}{2} \left(\frac{\xi}{r_0}\right)^D {}_1F_1\left[\frac{D}{2}, \frac{3}{2}, -\frac{q^2\xi^2}{4}\right] \quad (11.145)$$

where D is the fractal dimension, ξ is a cut-off length for the fractal correlations, $\Gamma(x)$ is the gamma function. ${}_1F_1$ is the Kummer or hypergeometric function. For the cut-off functions 11.142 and 11.143 the integral 11.139 is solved numerically.

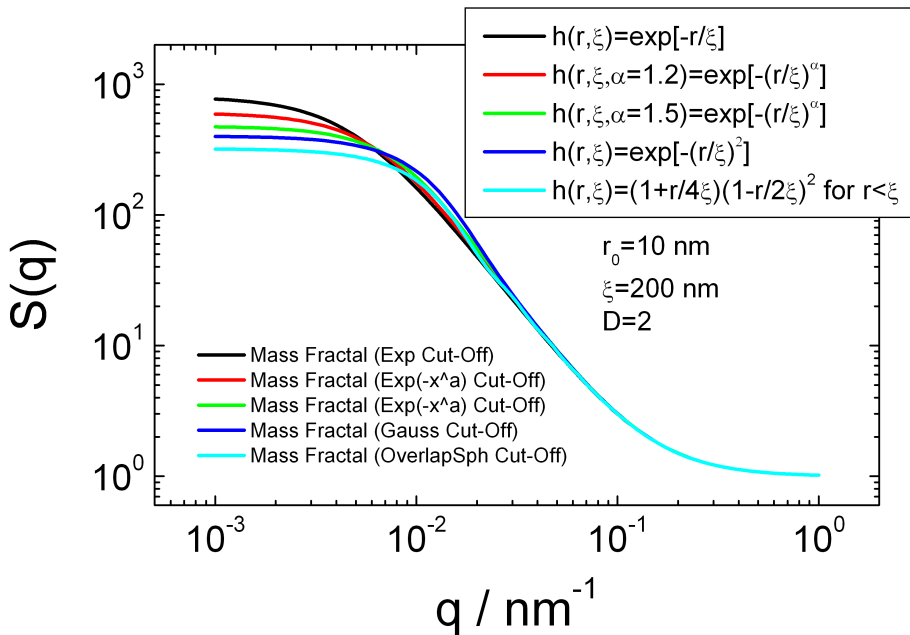


FIGURE 11.24. Comparison of the different structure factors for mass fractals.

11.7.1. Mass Fractal (Exp Cut-Off).

The cut-off function for this type of fractal is given by eq. 11.140 as $h_{\text{Exp}}(r, \xi) = \exp\left[-\frac{r}{\xi}\right]$. Its structure factor is given analytically by

$$S_{\text{Exp}}(q, \xi, D, r_0) = 1 + \frac{D\Gamma(D-1) \sin([D-1] \arctan(q\xi))}{(qr_0)^D \left[1 + \frac{1}{q^2\xi^2}\right]^{(D-1)/2}} \quad (11.146)$$

In the limit of $q \rightarrow 0$ the structure factor should be equal to the number N of particles in the aggregate. For this type of mass fractal structure factor this limit is given by

$$N - 1 = \lim_{q \rightarrow 0} S_{\text{Exp}}(q, \xi, D, r_0) - 1 = D\Gamma(D) \frac{\xi^D}{r_0^D} \quad (11.147)$$

This allows to rewrite the structure factor also as a function of N instead of r_0

$$S_{\text{Exp}}(q, \xi, D, N) = 1 + (N-1) \frac{\sin([D-1] \arctan(q\xi))}{(D-1)(q\xi)^D \left[1 + \frac{1}{q^2\xi^2}\right]^{(D-1)/2}} \quad (11.148)$$

Input Parameters for model Mass Fractal (Exp Cut-Off):

r0: characteristic dimension of individual scattering objects r_0

xi: cut-off length for the fractal correlations ξ

D: fractal dimension D

Note:

- D needs to be larger than 1 ($D > 1$). Physical values for D are between 1 and 3 ($1 < D < 3$).
- The fractal dimension needs to be larger than the size of the individual scattering objects ($r_0 < \xi$).
- The number of particles in the aggregate should be larger or equal to 1 ($N \geq 1$)

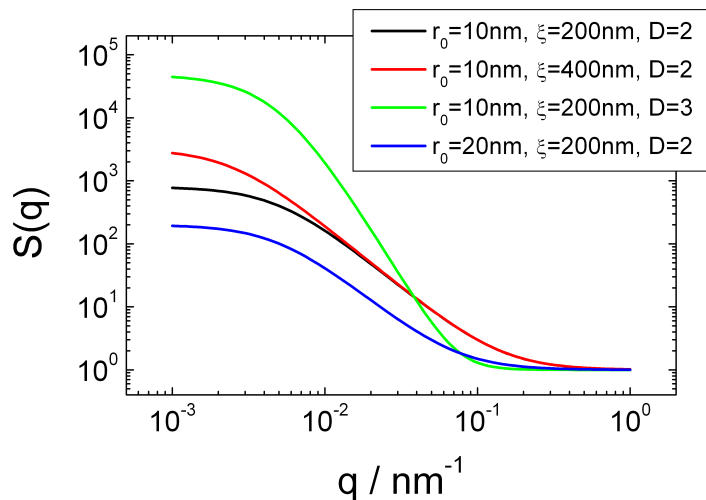


FIGURE 11.25. Structure factor of a mass fractal with an exponential cut-off function $h_{\text{Exp}}(r, \xi) = \exp\left[-\frac{r}{\xi}\right]$.

11.7.2. Mass Fractal ($\text{Exp}(-x^\alpha)$ Cut-Off).

Input Parameters for model Mass Fractal ($\text{Exp}(-x^\alpha)$ Cut-Off):

r0: characteristic dimension of individual scattering objects r_0

xi: cut-off length for the fractal correlations ξ

D: fractal dimension D

Note:

- D needs to be larger than 1 ($D > 1$). Physical values for D are between 1 and 3 ($1 < D < 3$).
- The fractal dimension needs to be large than the size of the individual scattering objects ($r_0 < \xi$).
- the exponents α should be larger than 1, as otherwise the integral 11.139 for $S(q)$ does not converges.

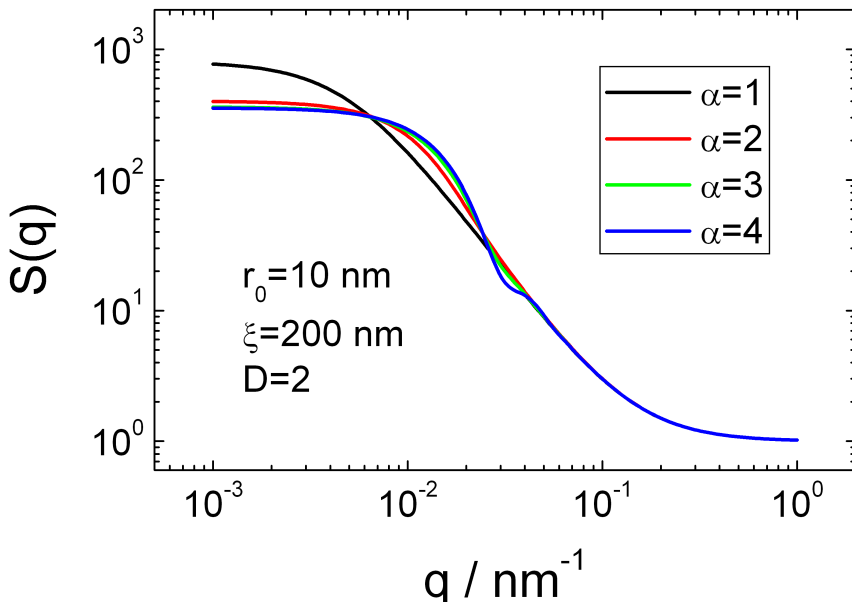


FIGURE 11.26. Structure factor of a mass fractal with a cut-off function $h_{\text{Exp}(-x^\alpha)}(r, \xi, \alpha) = \exp\left[-\left(\frac{r}{\xi}\right)^\alpha\right]$.

11.7.3. Mass Fractal (Gaussian Cut-Off).

The cut-off function for this type of fractal is given by eq. 11.141 as $h_{\text{Exp}}(r, \xi) = \exp\left[-\left(\frac{r}{\xi}\right)^2\right]$. Its structure factor is given analytically by

$$S_{\text{Gauss}}(q, \xi, D, r_0) = 1 + \Gamma\left[\frac{D}{2}\right] \frac{D}{2} \left(\frac{\xi}{r_0}\right)^D {}_1F_1\left[\frac{D}{2}, \frac{3}{2}, -\frac{q^2\xi^2}{4}\right] \quad (11.149)$$

In the limit of $q \rightarrow 0$ the structure factor should be equal to the number N of particles in the aggregate. For the mass fractal structure factor this limit is given by

$$N - 1 = \lim_{q \rightarrow 0} S_{\text{Gauss}}(q, \xi, D, r_0) - 1 = \frac{D}{2} \Gamma\left(\frac{D}{2}\right) \frac{\xi^D}{r_0^D} \quad (11.150)$$

This allows to rewrite the structure factor also as a function of N instead of r_0

$$S_{\text{Gauss}}(q, \xi, D, N) = 1 + (N - 1) {}_1F_1\left[\frac{D}{2}, \frac{3}{2}, -\frac{q^2\xi^2}{4}\right] \quad (11.151)$$

Input Parameters for model Mass Fractal (Gaussian Cut-Off):

r0: characteristic dimension of individual scattering objects r_0

xi: cut-off length for the fractal correlations ξ

D: fractal dimension D

Note:

- D needs to be larger than 1 ($D > 1$). Physical values for D are between 1 and 3 ($1 < D < 3$).
- The fractal dimension needs to be large than the size of the individual scattering objects ($r_0 < \xi$).
- The number of particles in the aggregate should be larger or equal to 1 ($N \geq 1$)

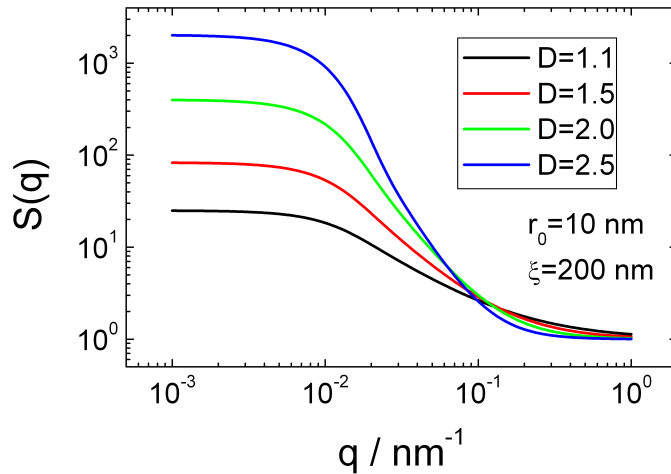


FIGURE 11.27. Structure factor of a mass fractal with an Gaussian cut-off function $h_{\text{Gauss}}(r, \xi) = \exp\left[-\left(\frac{r}{\xi}\right)^2\right]$.

11.7.4. Mass Fractal (OverlapSph Cut-Off).

In the limit of $q \rightarrow 0$ the structure factor should be equal to the number N of particles in the aggregate. For the mass fractal structure factor this limit is given by

$$N - 1 = \lim_{q \rightarrow 0} S_{\text{OverlapSph}}(q, \xi, D, r_0) - 1 = \frac{3D2^D}{D^3 + 4D^2 + 3D} e^{\frac{\xi^D}{r_0^D}} \quad (11.152)$$

Input Parameters for model Mass Fractal (OverlapSph Cut-Off):

r0: characteristic dimension of individual scattering objects r_0

xi: cut-off length for the fractal correlations ξ

D: fractal dimension D

Note:

- D needs to be between 1 and 3 ($1 < D < 3$).
- The fractal dimension needs to be large than the size of the individual scattering objects ($r_0 < \xi$).

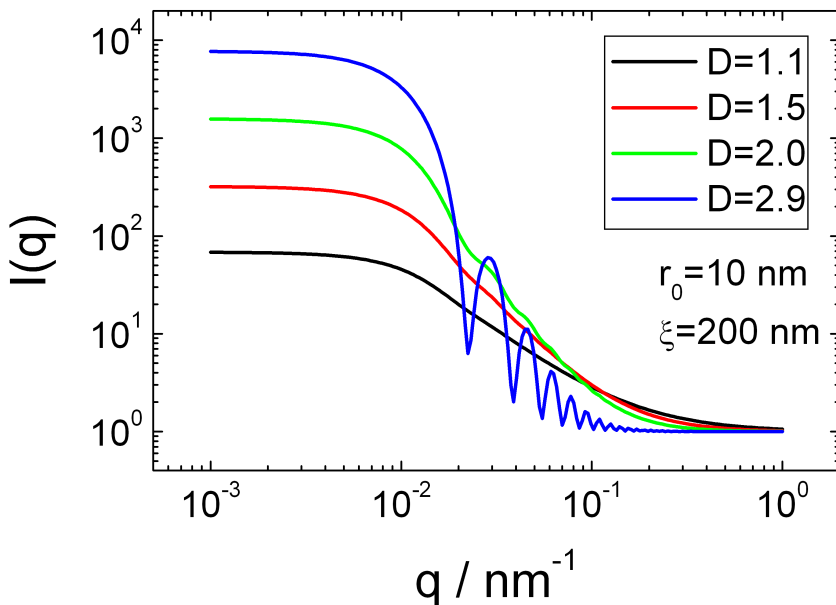


FIGURE 11.28. Structure factor of a mass fractal with a cut-off function $h_{\text{OverlapSph}}(r, \xi) = \left(1 + \frac{r}{4\xi}\right) \left(1 - \frac{r}{2\xi}\right)^2$ for $r \leq 2\xi$.

11.7.5. Structure factor of a random flight model.

The random flight model describes a discrete chain, where the positions of the N units forming the discrete chains follow a 3D random walk. The distance between neighbouring units is constant.

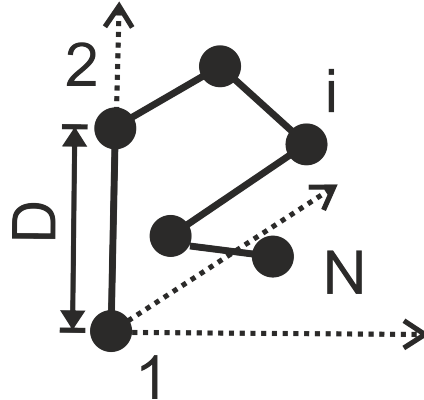


FIGURE 11.29. Random flight of N particles with constant distances D .

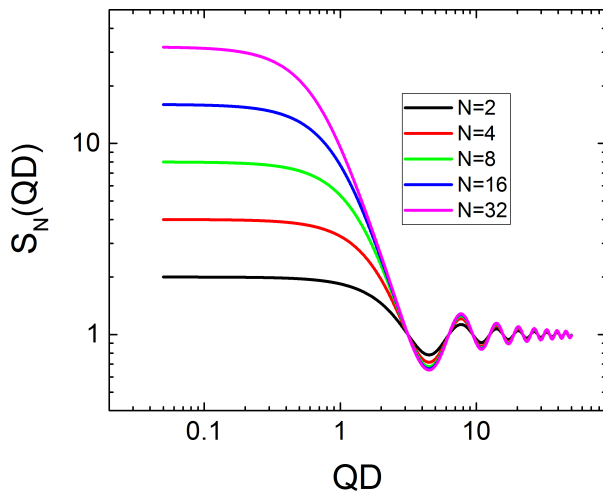


FIGURE 11.30. Random flight structure factor with N steps of length D .

The structure factor $S_N(QD)$ describing such an arrangement of N particles on a random flight with a constant step size D is given by [63] as

$$S_N(QD) = 1 + 2 \sum_{k=1}^{N-1} \left(1 - \frac{k}{N}\right) \left[\frac{\sin(QD)}{QD} \right]^k \quad (11.153)$$

$$\frac{2}{1 - \frac{\sin(QD)}{QD}} - 1 - \frac{2 \left[1 - \left[\frac{\sin(QD)}{QD} \right]^N \right]}{N \left[1 - \frac{\sin(QD)}{QD} \right]^2} \frac{\sin(QD)}{QD} \quad (11.154)$$

The formula above is only real for all values of QD for integer values of N . For non integer values N a linear interpolation between $[N]$ and $[N] + 1$ is taken [151], where

$[N]$ is the largest integer smaller or equal to N . With $w = N - [N]$ we get

$$S_N(QD) = (1 - w)S_{[N]}(QD) + wS_{[N]+1}(QD) \quad (11.155)$$

Input Parameters for model random flight:

D: step length D

n: number of steps N

Note:

- N needs to be larger or equal to 1. For non-integer values of N the curve is linear interpolated between the structure factor for N and $N + 1$.

11.7.6. Structure factor of a random flight model with a paracrystalline like disorder parameter.

$$S_N(Q, D, \Delta) = 1 + 2 \sum_{k=1}^{N-1} \left(1 - \frac{k}{N}\right) \left(\frac{\sin(DQ)}{DQ}\right)^k \exp\left(-\frac{1}{2}k\Delta^2 Q^2\right) \quad (11.156)$$

$$= \frac{Q^2 D^2 e^{\Delta^2 Q^2} - \sin^2(QD)}{\left(\sin(QD) - QDe^{\frac{\Delta^2 Q^2}{2}}\right)^2} + \frac{\sin(QD) \left(2QD \left(e^{-\frac{(N-1)\Delta^2 Q^2}{2}} \left(\frac{\sin(QD)}{QD}\right)^N - e^{\frac{\Delta^2 Q^2}{2}}\right)\right)}{N \left(\sin(QD) - QDe^{\frac{\Delta^2 Q^2}{2}}\right)^2} \quad (11.157)$$

Input Parameters for model PC:random flight:

D: step length D

n: number of steps N

n: paracrystalline-like disorder parameter Δ

Note:

- N needs to be larger or equal to 1. For non-integer values of N the curve is linear interpolated between the structure factor for N and $N + 1$.

11.7.7. Extended cluster structure factor with local hardsphere interactions.

This structure factor assume clusters of particles with a cluster size ξ , whereas the particle within a cluster interact via a hard sphere potential and a local volume fraction ϕ . In the original paper [286] the clusters are described by a spherical form factor and a Gaussian size distribution. It was also mentioned, that the polydisperse spherical form factor can be replaced by any other form factor better describing the shape of the clusters. In this implementation of the extended cluster model we use the extended Debye-Anderson-Brumberger model from section 9.14.5 describing the scattering of the

clusters.

$$S_{\text{ec}}(q) = S_{\text{PY}}(q) + (N - S_{\text{PY}}(q)) P_{\epsilon\text{DAB}}(q) \quad (11.158)$$

$$P_{\epsilon\text{DAB}}(q) = I_{\epsilon\text{DAB}}(q) / (8\pi\xi^3\epsilon) \quad (11.159)$$

$$N = \frac{8\pi\xi^3\epsilon}{\frac{4}{3}\pi R^3} \quad (11.160)$$

The structure factor $S_{\text{PY}}(q)$ is described in sec. 11.1.6 and the form factor $I_{\epsilon\text{DAB}}(q)$ is defined in equations 9.691 and 9.692. The volume of the DAB-particle can be obtained via the correlation function $\gamma_{0,\text{DAB}}(r) = \exp(-r/\xi)$ according to eq. 9.756 and is for the ϵDAB model given as $V_{\epsilon\text{DAB}} = 8\pi\xi^3\epsilon$.

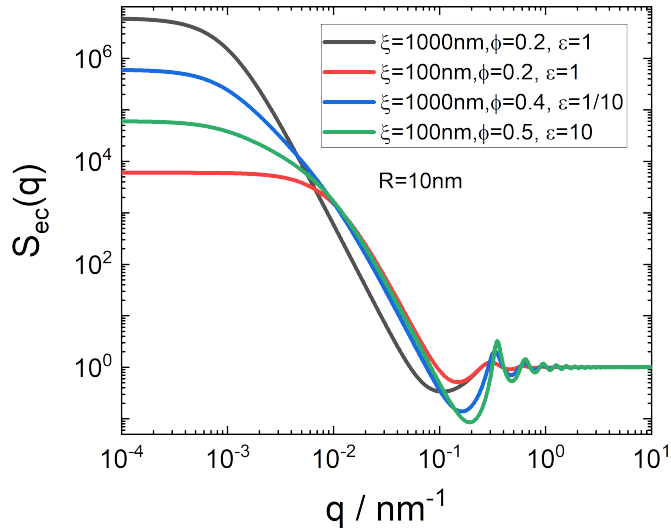


FIGURE 11.31. Examples for extended cluster structure factor.

Input Parameters for model extended cluster Sq:

R: radius of particles in cluster R

phi: local volume fraction inside cluster ϕ

xi: size (correlation length) of cluster ξ

epsilon: shape parameter of cluster (<1:disc; >1:rod) ϵ

Note:

- the volume fraction needs to be positive and smaller or equal 1: $\phi \in [0, 1]$.
- the correlation length should be significant larger than R to be physical meaningful

11.7.8. Mass fractal with nearest neighbor perturbations.

The fractal aggregate with nearest neighbor perturbations has been derived by [110].

The structure factor was tested against other models by [286] and reads as

$$S(q) = 1 + z_1 \operatorname{sinc}(2qR) + z_A \int_{2R}^{\infty} r^{D-1} \exp(-r/\xi) \operatorname{sinc}(qr) dr \quad (11.161)$$

$$z_A = \frac{N - z_1 - 1}{\int_{2R}^{\infty} \exp(-r/\xi) dr} \quad (11.162)$$

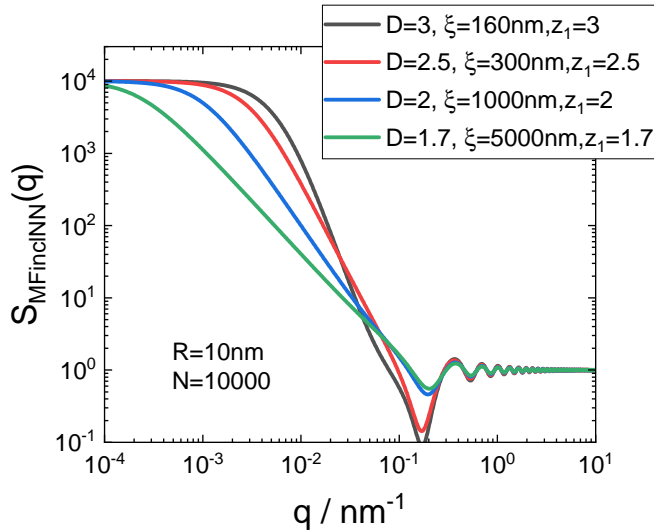


FIGURE 11.32. Examples for mass fractal aggregates with nearest neighbor perturbations.

Input Parameters for model `mass fractal incl nn perturbation`:

R: radius of particles in cluster R

z1: number of particles in first shell z_1

xi: size (correlation length) of cluster ξ

D: fractal dimension D

N: number of particles in the fractal aggregate N

Note:

- Certain combinations of parameters can lead to nonphysical negative values for the structure factor.
- The correlation length of the cluster ξ should scale with the fractal dimension D and the cluster mass, i.e. z_1 , N as well as D .
- Also the fractal dimension D should increase with the number of nearest neighbors z_1 .

11.7.9. aggregate with nearest neighbor perturbations.

The diffusion limited cluster (DLC) aggregates and reaction limited cluster (RLC) aggregates with nearest neighbor perturbations have been derived and compared with

Monte Carlo cluster–cluster aggregation simulations in [287]. The model only has two parameters, the particle radius R and the number of particles in the aggregate N . The particle–particle correlation function $g(r)$ has been parameterised as follows

$$g(r) = \begin{cases} 0, & \text{if } r < 2R \\ \frac{N_{nn}}{4\pi(2R)^2} \delta(r - 2R), & \text{if } r = 2R \\ \frac{a}{R^{b+3}} r^b, & \text{if } 2R < r < 4R \\ \frac{c}{R^D} r^{D-3} \exp\left(-\left(\frac{r}{\xi}\right)^\gamma\right), & \text{otherwise.} \end{cases} \quad (11.163)$$

D is the fractal dimension and is set to $D = 1.85$ or $D = 2.05$ for DLCA or RLCA. The parameters a , b , and γ as well as the number of nearest neighbor N_{nn} have been calculated using the approximation

$$F(N) = d \frac{(N - e)^m}{(N - e)^m + f} \quad (11.164)$$

and the values given in the table 2. The cut-off length or correlation length is obtained

$$\xi = \frac{h}{k_f^{1/D}} R N^{1/D} \quad (11.165)$$

with $h = 0.957$ and 0.91 and $k_f = 0.46$ and 0.33 for DLCA and RLCA, respectively. N is the number of particles in the cluster aggregate. The remaining parameter c is given by

$$c = \frac{N - 1 - N_{nn} - \frac{4\pi a}{b+3} (4^{b+3} - 2^{b+3})}{\frac{4\pi}{\gamma} \left(\frac{\xi}{R}\right)^D \Gamma\left(\frac{D}{\gamma}\right) \left(1 - \Gamma_{\text{inc}}\left(\left(\frac{4R}{\xi}\right)^\gamma, \frac{D}{\gamma}\right)\right)} \quad (11.166)$$

where $\Gamma()$ and $\Gamma_{\text{inc}}()$ are the gamma and the incomplete gamma function, respectively.

TABLE 2. Values of the parameters d , e , f , and m to be used in Eq. 11.164 to compute the parameters of the particle–particle correlation function: N_{nn} , a , b , and γ as a function of the number of particles per cluster N , for both DLCA and RLCA

parameter of the $g(r)$ function	Aggregation mechanism	d	e	f	m
N_{nn}	DLCA	2.0342	1.1477	0.9997	1
	RLCA	2.0415	1.1511	1.0086	1
a	DLCA	0.0095	4.1292	0.1997	2
	RLCA	0.0138	2.7544	4.1792	2
b^1	DLCA	0.6425	6.2352	5.1747	1
	RLCA	0.4857	9.6836	11.6665	1
γ	DLCA	2.1976	3.8377	-0.1784	1
	RLCA	2.16	0.1966	-3.5926	2

11.7.9.1. DLC aggregate with nearest neighbor perturbations.

This model assumes a fractal dimension of $D = 1.85$. All other parameters like z_1 and ξ have been obtained by fitting them according to MC simulation results. All other relations and parameters are available in [287].

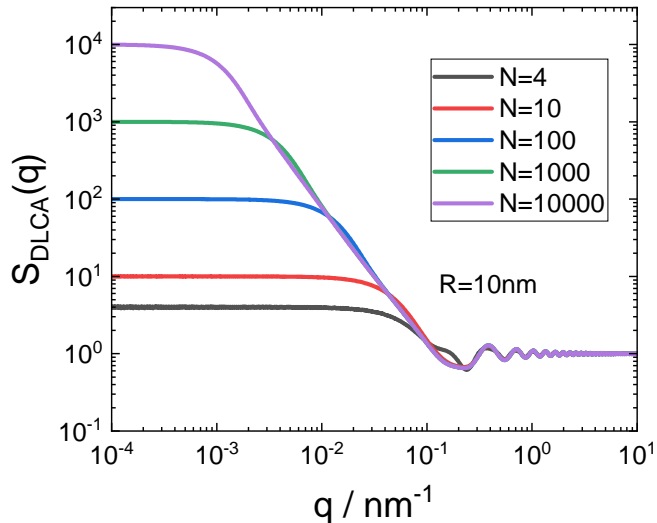


FIGURE 11.33. Examples for DLC aggregate with nearest neighbor perturbations.

Input Parameters for model DLCA incl nn perturbation:

R: radius of particles in cluster R

N: number of particles in the fractal aggregate N

11.7.9.2. RLC aggregate with nearest neighbor perturbations.

The reaction limited cluster (RLC) aggregates with nearest neighbor perturbations has been derived and compared with Monte Carlo cluster-cluster aggregation simulations by [287]. It only has two parameters, the particle radius R and the number of particles in the aggregate N . This model assumes a fractal dimension of $D = 2.05$. All other parameters like z_1 and ξ have been obtained by fitting them according to MC simulation results. All other relations and parameters are available in [287].

Input Parameters for model RLCA incl nn perturbation:

R: radius of particles in cluster R

N: number of particles in the fractal aggregate N

¹The parameter b is 0 for DLCA clusters with $N < 7$ and for RLCA clusters with $N < 10$.

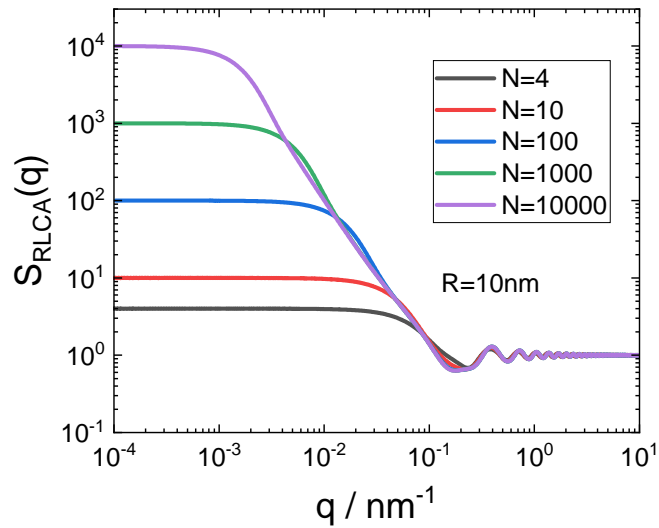


FIGURE 11.34. Examples for RLC aggregate with nearest neighbor perturbations.

11.8. Structure factors for Yukawa like potentials

For charged colloidal dispersions analytical structure factors have been found in the mean spherical approximation [204, 191, 312]. The hard core Yukawa potential (also called a screened Coulomb potential) is defined as

$$u^Y(r, K, Z) = k_B T \begin{cases} \infty, & \text{if } 0 \leq r < \sigma \\ -\frac{K}{r/\sigma} \exp(-Z(r/\sigma - 1)), & r \leq \sigma. \end{cases} \quad (11.167)$$

In the limit of no screening, i.e. $Z = 0$ the interaction is a purely Coloumb interaction proportional to $1/r$.

11.8.1. Hard core double Yukawa interaction.

To describe a short range attractive and long range repulsive interaction Liu et al. [312] calculated an analytical solution of Ornstein-Zernike equation in the mean spherical approximation. They assumed a potential of the form

$$\frac{u^{2Y}(r, \dots)}{k_B T} = \begin{cases} \infty, & \text{if } r < \sigma \\ -K_1 \frac{\exp(-Z_1(\frac{r}{\sigma}-1))}{r/\sigma} - K_2 \frac{\exp(-Z_2(\frac{r}{\sigma}-1))}{r/\sigma}, & r \leq \sigma. \end{cases} \quad (11.168)$$

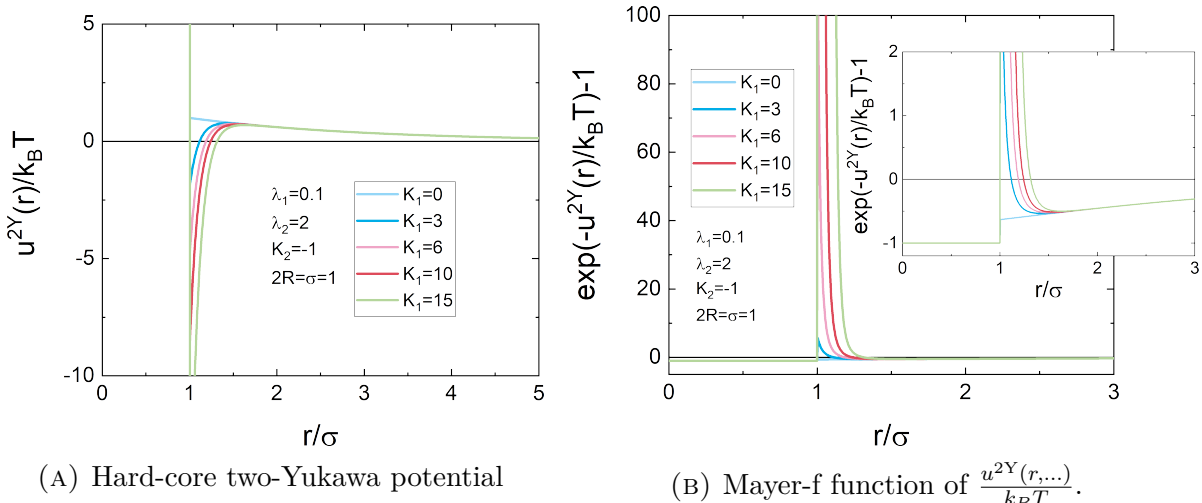
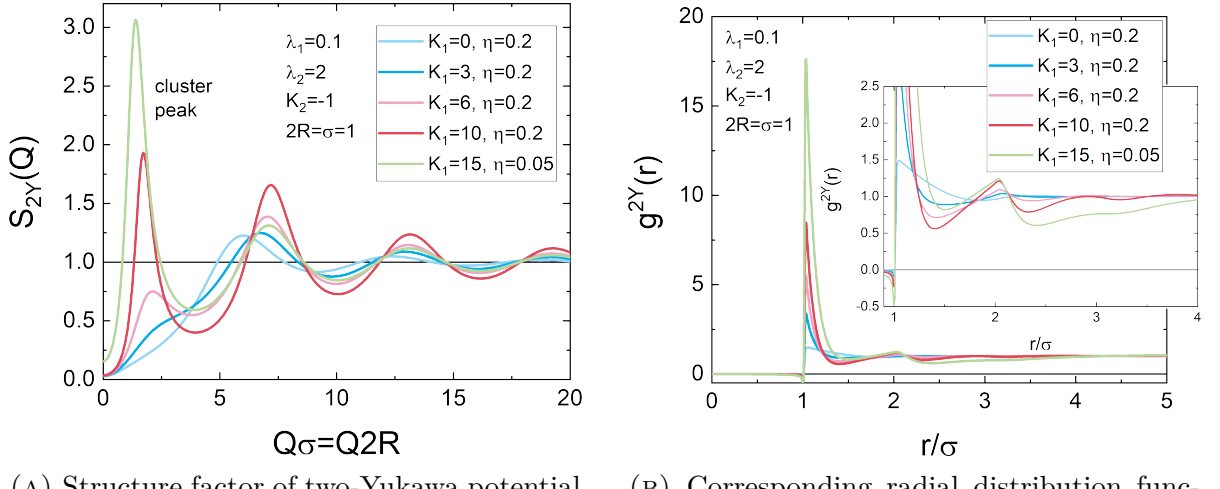


FIGURE 11.35. Potential and corresponding Mayer-f function

Note:

- The code in **SASfit** is based on Matlab code supplied by Yun Liu. The XOP version of this function is based in parts on c-code supplied by Marcus Henning and used for the implementation of this plugin.
- For nonphysical or no solution an error message is returned.
- For values close to $Z_1 = Z_2$ the separately implemented structure factor a single Yukawa interaction potential should be used.



(A) Structure factor of two-Yukawa potential in the mean spherical approximation showing a cluster peak.

(B) Corresponding radial distribution function $g(r)$ to the structure factor on the left.

FIGURE 11.36. Structure factor radial distribution function for a two-Yukawa potential with an attractive as well as repulsive term.

11.8.2. Hayter-Penfold structure factor for a screened coulomb interaction (single Yukawa, RMSA). This structure factor has been published in [204, 191]. The original Fortran code has been translates to C by f2c and is used for this plugin. The repulsive potential used is that one between two identical spherical macroions is given by

$$\frac{U_{HP}(x)}{k_B T} = \begin{cases} \gamma \frac{\exp(-kx)}{x}, & \text{if } x > 1 \\ \infty, & \text{otherwise.} \end{cases} \quad (11.169)$$

$$x = r/\sigma \quad (11.170)$$

$$\sigma = 2R \quad (11.171)$$

$$k = \kappa\sigma \quad (11.172)$$

$$K = q\sigma \quad (11.173)$$

$$k_b T : \text{ thermal energy} \quad (11.174)$$

$$\gamma = \frac{\pi\epsilon_0\epsilon\sigma}{k_B T} \Psi_0^2 \exp(k) \text{ dimensionless coupling constant} \quad (11.175)$$

$$\gamma \exp(-k) \text{ contact potential for macroion pair in unit of } k_B T \Psi_0 = ze/(\pi\epsilon_0 R(2 + \kappa)) \quad (11.176)$$

$$\kappa = 1/\lambda \text{ inverse screening length with } \kappa^2 = 4\pi\lambda_B \sum_i n_i z_i \quad (11.177)$$

$$\lambda_B = \frac{e^2}{4\pi\epsilon_0\epsilon_r k_B T} \text{ Bjerrum length} \quad (11.178)$$

with e being the elementary charge, ϵ_r relative dielectric constant of the medium, ϵ_0 is the vacuum permittivity, n_i number density of ion i with charge z_i in units of e .

CHAPTER 12

Special topics

12.1. Fitting absolute intensities

Absolute intensities in the simulation can be obtained by using proper units for the scattering vector \mathbf{Q} , the size dimensions of the scatterer, the scattering length densities etc. In the following a few example are discussed for absolute calibrated data sets. One question which is asked quite frequently is "What is the meaning of N in the size distribution and what are its units?". The answer is normally "That depends on the units of your data you are fitting and the units of your scattering length densities". In the following a few explanations will be given to clarify this in some more detail.

Let us consider first the scattering intensity of a single sphere. The form factor of a sphere is given by eq. 3.1a as

$$I_{\text{Sphere}}(Q, R, \Delta\eta) = \left[\frac{4}{3} \pi R^3 \Delta\eta 3 \frac{\sin QR - QR \cos QR}{(QR)^3} \right]^2 \quad (12.1)$$

The radius R and the scattering vector Q have reciprocal units, i.e. if Q is given in $1/\text{nm}$ the radius R has a unit of nm. The other variable in the form factor is the scattering length density contrast $\Delta\eta$ between sphere and surrounding matrix or solvent. The unit of the scattering length density is length/volume and has therefore a unit $1/\text{cm}^2$ or some other sites are using units of $1/\text{\AA}^2$. The difference is only a constant factor of

$$\Delta\eta \frac{1}{\text{cm}^2} = 10^{16} \Delta\eta \frac{1}{\text{\AA}^2}. \quad (12.2)$$

The overall unit of the scattering intensity (differential cross-section) of a single sphere is therefore

$$[I_{\text{Sphere}}(Q, R, \Delta\eta)] = [R]^6 [\Delta\eta]^2 = \frac{\text{nm}^6}{\text{cm}^4} = 10^{-42} \text{cm}^2 \quad (12.3)$$

for the case that $[R] = \text{nm}$ and $[\Delta\eta] = \text{cm}^{-2}$. The unit for the scattering cross-section of a single sphere with $[R] = \text{\AA}$ and $[\Delta\eta] = \text{\AA}^{-2}$ is then

$$[I_{\text{Sphere}}(Q, R, \Delta\eta)] = [R]^6 [\Delta\eta]^2 = \frac{\text{\AA}^6}{\text{\AA}^4} = \text{\AA}^2 = 10^{-16} \text{cm}^2, \quad (12.4)$$

respectively. The scattering cross-section of a single scatterer is calculated by **SASfit** if one chooses in the tab for distribution functions the probability functions **Monodisperse**.

Differential cross-section have a unit of an area

$$\left[\frac{d\Sigma}{d\Omega}(Q) \right] = \text{cm}^2. \quad (12.5)$$

Many instruments deliver with their data reduction software a cross-section normalized by the sample volume so that the unit is in reciprocal length:

$$\left[\frac{d\sigma}{d\Omega}(Q) \right] = \frac{1}{[V]} \left[\frac{d\Sigma}{d\Omega}(Q) \right] = \frac{1}{\text{cm}}. \quad (12.6)$$

For fitting a form factor to experimental data one needs next to the size parameter also a scaling parameter. For the simplest case this is done by choosing as a distribution function **Delta**. **Delta** simply multiplies a constant value N to the form factor. The meaning and the unit of N now depends on the unit of the cross-section, whether it is normalized or not normalized on the sample volume. **SASfit** calculates in the case of a form factor of **Sphere** with **Delta** as a distribution function

$$I_{\text{SASfit}} = N \times I_{\text{Sphere}}(Q, R, \Delta\eta). \quad (12.7)$$

Fitting N to a data set, which is given in units of $1/\text{cm}$ and where $[Q] = \text{nm}^{-1}$, $[R] = \text{nm}$ and $[\Delta\eta] = \text{cm}^{-2}$ would mean that N has the unit

$$[N] = \frac{\left[\frac{d\sigma}{d\Omega}(Q) \right]}{[I_{\text{Sphere}}(Q, R, \Delta\eta)(Q)]} = \frac{\frac{1}{\text{cm}}}{10^{-42} \text{cm}^2} = 10^{42} \text{cm}^{-3}. \quad (12.8)$$

One therefore needs to multiply the value N obtained by **SASfit** with 10^{42} to get the number density of scatterers in units of cm^{-3} .

Let us now consider the simplest case of spheres with a size distribution and no structure factor, which are fitted to experimental data. All the size distribution have a scaling parameter N . The units of the parameter N in the size distribution is the same than for **Delta**. The size distribution $n(x)$ are implemented as distribution function $n(x) = Np(x)$ with $p(x)$ being a probability function. In case of polydisperse spheres **SASfit** calculates the integral

$$I_{\text{SASfit}}(Q) = \int_0^\infty n(R) I_{\text{Sphere}}(Q, R, \Delta\eta) dR \quad (12.9)$$

$$= N \int_0^\infty p(R) I_{\text{Sphere}}(Q, R, \Delta\eta) dR \quad (12.10)$$

The probability function $p(x)$ is normalized to

$$\int_0^\infty p(x) dx = 1, \quad (12.11)$$

so that the parameter N has like for the **Delta**-distribution the unit $[N] = 10^{42} \text{cm}^{-3}$ if the data set is given in units of $1/\text{cm}$ and $[Q] = \text{nm}^{-1}$, $[R] = \text{nm}$ and $[\Delta\eta] = \text{cm}^{-2}$.

Most of the form factor are implemented in a way that they return the scattering cross-section of a single object like the example of a sphere above, but a few are not, like for example the standard form of a gaussian chain **Gauss**. In this particular case two other versions **Gauss2** and **Gauss3** with different parameterizations of the forward scattering of a single gaussian chain are available. However, there are some form factors, which have been implemented according to the literature but which are normalized

differently. This has to be checked before the parameter N in the size distribution is interpreted in terms of number density of scatterers.

12.2. Forward Scattering - Volume Fraction - Absolute Scale

A frequently asked question is if the scattering intensity is consistent with the concentration of material in the sample. Especially people working with micellar solution, star polymers, but also proteins, etc. want to cross-check the absolute intensity with the known concentration. In the dilute case the differential cross-section is simply N times the cross-section of an individual scatterer

$$\frac{d\sigma}{d\Omega}(Q) = \frac{N}{V_{\text{tot}}} P(Q) \quad (12.12)$$

N is number of particles/molecules/proteins in the illuminated volume, V_{tot} the illuminated sample volume, $n = N/V_{\text{tot}}$ the particle number density, and $P(Q)$ the scattering cross-section of a single particle. $P(Q)$ has the dimension cm^2 , N/V_{tot} the dimension cm^{-3} , and $\frac{d\sigma}{d\Omega}(Q)$ the dimension cm^{-1} . Eq. 12.12 can also be expressed in terms of concentration c in units of g/cm^3

$$c = n m_{\text{mol}} = n M_r u = n \frac{M_r M_u}{N_A} = \frac{N}{V_{\text{tot}}} \frac{M_r M_u}{N_A} \quad (12.13)$$

so that

$$\frac{d\sigma}{d\Omega}(Q) = c \frac{N_A}{M_r M_u} P(Q) \quad (12.14)$$

M_r is the relative molar mass of the particle ¹ (Molecular weight (M.W.) and formula weight (F.W.) are older terms) which is a dimensionless quantity (i.e., a pure number, without units). To get units in g/mol the relative molar mass needs to be multiplied by the molar mass constant M_u . The value of the molar mass constant M_u is defined to be 1 g/mol in SI units. The molar mass constant is important in writing dimensionally correct equations. It is common to see phrases such as "*The molar mass of an element is the atomic weight in grams per mole.*" However molecular or atomic weight are dimensionless quantities, and cannot take the units of grams per mole. Formally, the operation is the multiplication by a constant which has the value 1 g/mol , that is the molar mass constant². The molecule mass m_m in units of g is $m_m = M_r M_u / N_A$.

Now we need to look on the forward scattering $P(Q=0)$ of a single particle/protein/polymer chain. For a simple particle like a sphere, the forward scattering is given by

$$P(Q=0) = (\eta_{\text{sol}} - \eta_{\text{sp}})^2 V_{\text{sp}}^2 \quad (12.15)$$

¹Definition of relative atomic mass and relative molecular mass can be found on the url-address <http://physics.nist.gov/Pubs/SP811/sec08.html>

Relative atomic mass (formerly atomic weight): ratio of the average mass per atom of an element to 1/12 of the mass of the atom of the nuclide ¹²C.

Relative molecular mass (formerly molecular weight): ratio of the average mass per molecule or specified entity of a substance to 1/12 of the mass of an atom of the nuclide ¹²C.

²Definition of unified atomic mass unit: $1\text{u} = m_u = m(^{12}\text{C})/12 = 1M_u/N_A = 1(\text{g/mol}) / (6.02214129 \times 10^{23}\text{mol}^{-1}) = 1.660538921 \times 10^{-24}\text{g}$

where $(\eta_{\text{sol}} - \eta_{\text{sp}})$ is the scattering contrast between spherical particle and solvent and V_{sp} the volume of a single sphere. In case of a spherical particle the boundary between particle and solvent is well defined and therefore also the volume of the particle as it has a sharp interface. The scattering contrast of a spherical particle can also be written in terms of the overall scattering length of the sphere b_{sp} , i.e. the sum of the scattering length of all atoms forming the sphere, the volume of the sphere and the scattering length density of the solvent. The volume of the sphere can be calculated from its mass m_{sp} or relative molar mass $M_{r,\text{sp}}$ and its density ρ_{sp} .

$$(\eta_{\text{sol}} - \eta_{\text{sp}}) = \left(\eta_{\text{sol}} - \frac{b_{\text{sp}}}{V_{\text{sp}}} \right) = \left(\eta_{\text{sol}} - \frac{b_{\text{sp}}\rho_{\text{sp}}}{m_{\text{sp}}} \right) = \left(\eta_{\text{sol}} - \frac{b_{\text{sp}}\rho_{\text{sp}}N_A}{M_{r,\text{sp}}M_u} \right) \quad (12.16)$$

But what about the forward scattering of a gaussian polymer coil? A polymer does not have a sharp boundary to the solvent. Polymer and solvent can penetrate each other. To determine the polymer volume one would need a detailed model for the polymer molecule and its interaction with solvent molecules. As a first approximation the volume of a polymer molecule can be obtained by $V_{\text{polym}} = \frac{\rho_{\text{polym}}}{m_{\text{polym}}}$. For a polymer coil with a relative molar mass $M_{r,\text{polym}}$ the forward scattering in a solvent is given by

$$P(Q=0) = \left(\frac{M_{r,\text{polym}}M_u}{\rho_{\text{polym}}N_A} \right)^2 \left(\eta_{\text{sol}} - \frac{b_{\text{polym}}\rho_{\text{polym}}N_A}{M_{r,\text{polym}}M_u} \right)^2 \quad (12.17)$$

The volume of a polymer molecule

$$V_{\text{polym}} = \frac{M_{r,\text{polym}}M_u}{\rho_{\text{polym}}N_A}$$

is the volume occupied by single polymer chain in the solvent or in other word the amount of solvent volume displaced by one polymer chain. For the forward scattering it does not matter, if the coil is collapsed or swollen. As long as the scattering length density of the solvent inside the swollen polymer coil is the same than in the bulk and the molecular volume of the polymer chain does not change with the solvent quality the forward scattering does not depend on the conformation of the polymer. Sometimes the relative molar mass of a polymer is given in degree of polymerization p and relative molar mass of the monomer $M_{r,\text{m}}$. In this case and assuming that the mass densities of polymer and monomer are the same the forward scattering is given by

$$\begin{aligned} P(Q=0) &= \left(\frac{p M_{r,\text{m}}M_u}{\rho_{\text{m}}N_A} \right)^2 \left(\eta_{\text{sol}} - \frac{b_{\text{m}}\rho_{\text{m}}N_A}{M_{r,\text{m}}M_u} \right)^2 \\ &= \left(\frac{p M_{r,\text{m}}M_u}{\rho_{\text{m}}N_A} \right)^2 \left(\eta_{\text{sol}} - \frac{b_{\text{m}}\rho_{\text{m}}N_A}{M_{r,\text{m}}M_u} \right)^2 \end{aligned} \quad (12.18)$$

Let us now come back to the measured differential cross-section $\frac{d\sigma}{d\Omega}(Q)$. For $Q = 0$ we get

$$\frac{d\sigma}{d\Omega}(Q=0) = \frac{N}{V_{\text{tot}}} P(Q=0) = c \frac{N_A}{M_{r,\text{Gauss}} M_u} P(Q=0) \quad (12.19)$$

$$= c \frac{N_A}{p M_{r,\text{m}} M_u} \left(\frac{p M_{r,\text{m}} M_u}{\rho_{\text{m}} N_A} \right)^2 \left(\eta_{\text{sol}} - \frac{b_{\text{m}} \rho_{\text{m}} N_A}{M_{r,\text{m}} M_u} \right)^2 \quad (12.20)$$

$$= c \frac{p M_{r,\text{m}} M_u}{N_A \rho_{\text{m}}^2} \left(\eta_{\text{sol}} - \frac{b_{\text{m}} \rho_{\text{m}} N_A}{M_{r,\text{m}} M_u} \right)^2 \quad (12.21)$$

The last equation says, that the forward scattering of a solution of dilute non-interacting polymer molecules consisting of p monomer units depends linearly on the number of monomer units p in the polymer. Even though the scattering of a single polymer molecule depends quadratically on the number of monomer units. The reason is simply that the larger the degree of polymerization the lower the number density of molecules in the solution as we assume a constant concentration, i.e. $c \propto pn$ and therefore $\frac{d\sigma}{d\Omega}(Q=0) \propto p^2 n$.

12.3. Moments of scattering curves and size distribution

The relevance of moments both for scattering curves as well as size distributions has been discussed in several publications [94, 454, 93, 516, 342, 177].

Moments $\langle x^m \rangle$ of any order m of a function $f(x)$ are defined by integrating $f(x)$ with a suitable power of x over its domain $[a, b]$

$$\langle x^m \rangle = \int_a^b f(x) x^m dx \quad (12.22)$$

The different moments of the scattering curve together with the forward scattering $I(0)$ and the Porod constant can be used to calculate easily several structural parameters

of the scatterers.

$$\tilde{Q}_{\text{inv}} = \int_0^{\infty} Q^2 I(Q) dQ \text{ (scattering invariant)} \quad (12.23a)$$

$$\frac{S}{V} = \frac{\pi}{\tilde{Q}_{\text{inv}}} \lim_{Q \rightarrow \infty} \left\{ Q^4 I(Q) \right\} \text{ (specific surface)} \quad (12.23b)$$

$$\langle R_G \rangle^2 = 3 \left(- \lim_{Q \rightarrow 0} \left\{ \frac{d[\ln I(Q)]}{d(Q^2)} \right\} \right) \text{ (squared Guinier radius)} \quad (12.23c)$$

$$l_i = \langle d \rangle = \frac{4}{\pi} \frac{\int_0^{\infty} Q^2 I(Q) dQ}{\lim_{Q \rightarrow \infty} \left\{ Q^4 I(Q) \right\}} \text{ (average intersection length)} \quad (12.23d)$$

$$l_c = \langle l \rangle = \frac{\pi}{\tilde{Q}_{\text{inv}}} \int_0^{\infty} Q I(Q) dQ \text{ (correlation length)} \quad (12.23e)$$

$$A_c = \langle A \rangle = \frac{2\pi}{\tilde{Q}_{\text{inv}}} \int_0^{\infty} I(Q) dQ \text{ (correlation surface)} \quad (12.23f)$$

$$V_P = \langle V \rangle = \frac{2\pi^2}{\tilde{Q}_{\text{inv}}} I(0) \text{ (correlation volume, Porod volume)} \quad (12.23g)$$

These structural parameters are calculated by **SASfit** via the menu [Calc|integral parameters...].

On the other side the structural parameters from above can depend on specific moments of the size distribution in the case the scattering objects are spheres. The m -th moment $\langle R^m \rangle$ of a size distribution $n(R)$ is given by

$$\langle R^m \rangle = \frac{\int_0^{\infty} n(R) R^m dR}{\int_0^{\infty} n(R) dR} \quad (12.24)$$

From these moments the following integral structural parameters in case of polydisperse spheres can be calculated and are listed together with a hypothetical radius of monodisperse spheres having the same structural parameter.

intersection length l_i :

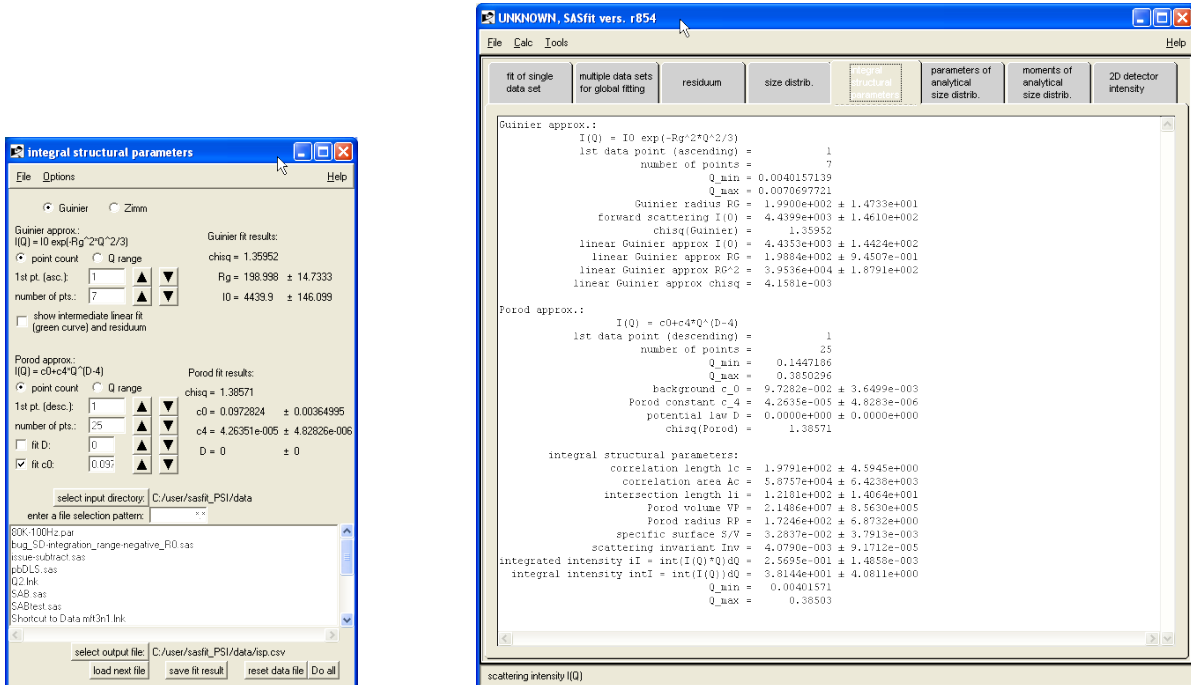
$$l_i = \frac{\langle R^3 \rangle}{\langle R^2 \rangle} \text{ and } R_{l_i} = \frac{3}{4} l_i$$

correlation length l_c :

$$l_c = \frac{\langle R^4 \rangle}{\langle R^3 \rangle} \text{ and } R_{l_c} = \frac{2}{3} l_c$$

Guinier radius R_G :

$$R_G = \sqrt{\frac{\langle R^8 \rangle}{\langle R^6 \rangle}} \text{ and } R_{R_G} = \sqrt{\frac{5}{3}} R_G$$



(A) GUI for defining fit ranges for Porod and Guinier approximations

(B) Tabbed menu displaying the integral structural parameters calculated via the different moments of the scattering curve the Porod and Guinier extrapolations to $Q \rightarrow 0$ and $Q \rightarrow \infty$.

FIGURE 12.1. Menu and tabbed window for integral structural parameters. SASfit also supports analysis of series of data, whereby the structural parameters are stored in CSV format readable by many software packages in a separate file for further analysis.

correlation cross section A_c :

$$A_c = \frac{4\pi}{5} \frac{\langle R^5 \rangle}{\langle R^3 \rangle} \text{ and } R_{A_c} = \sqrt{\frac{5}{4\pi} A_c}$$

Porod Radius R_{V_P} :

$$V_P = \frac{4\pi}{3} \frac{\langle R^6 \rangle}{\langle R^3 \rangle} \text{ and } R_{V_P} = \sqrt[3]{\frac{3}{4\pi} V_P}$$

Fig. 12.2 shows the SASfit menu displaying these values for each scattering contribution having a size distribution and also for the sum of all scattering contributions. Next to the integral structural parameters also the different moments of the size distribution up the 8th moment are supplied.

12.4. Volume fractions

Having measured SAS-data versus $[Q] = \text{nm}^{-1}$ in absolute scale (1/cm) and knowing the scattering contrast also in absolute scale (1/cm²) one can get the number density of particles. However, in general the volume fraction is known by other means but not

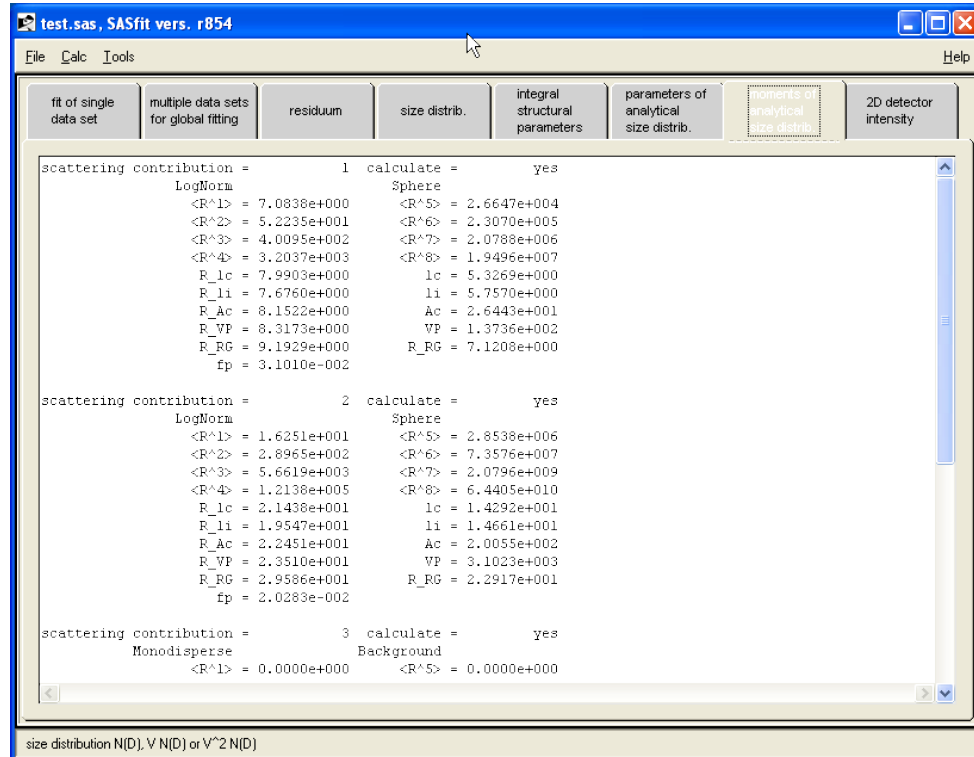


FIGURE 12.2. Menu displaying the different moments of a size distribution. At the moment these values are only calculated for single data sets but not yet for multiple data sets

the number density. The volume fraction can be calculated from the size distribution for some simple geometric shapes of the particles.

Let us first consider the case of simple spheres (**Sphere**) with a size distribution over their radii. The size distribution can be interpreted as a number density distribution function. The volume fraction f_p of the spheres can be easily calculated by

$$f_p = \int_0^\infty n(R) \frac{4}{3} \pi R^3 dR = \int_0^\infty N p(R) \frac{4}{3} \pi R^3 dR = N \frac{4}{3} \pi \langle R^3 \rangle \quad (12.25)$$

where $\langle R^3 \rangle$ is the third moment of the size distribution. The different moments of a size distribution can be calculated analytically for some special cases like the log-normal distribution. However, **SASfit** calculates the moments and displays them on the menu [**calc|single data single**]. Up to the 8th-moment of a distribution function is displayed in the menu tab **moments of analytical size distrib.** like in Fig. 12.2 together with some other parameters defined in section 12.3. To compute the volume fraction f_p , which is a dimensionless parameter, one has to use the proper units for N and $\langle R^3 \rangle$. $\langle R^3 \rangle$ has here units of $[\langle R^3 \rangle] = \text{nm}^3 = 10^{-21} \text{cm}^3$ and N is in units of $[N] = 10^{42} \text{cm}^{-3}$. The volume fraction f_p can as an example be computed for

$N = 8.55241 \times 10^{-28}$ and $\langle R^3 \rangle = 5.6619 \times 10^3$ as

$$f_p = 10^{42} \times 8.55241 \times 10^{-28} \frac{4}{3} \pi 5.6619 \times 10^3 10^{-21} = 0.020283. \quad (12.26)$$

The numbers for N and $\langle R^3 \rangle$ can be directly taken from the **SASfit** gui.

Let us now consider the case of cylinders with a circular cross-section with radius R and length L . We will have a look on the two cases of having either a distribution in the radius R or a distribution in the length L . The volume of a cylinder V_{cyl} is given by

$$V_{\text{cyl}}(R, L) = \pi R^2 L \quad (12.27)$$

To calculate the volume fraction from the size distribution we need to integrate over the particle volume. The integration is done either over the radius dR

$$f_p = \int_0^\infty n(R) V_{\text{cyl}}(R, L) dR = \int_0^\infty N p(R) \pi R^2 L dR = NL\pi \langle R^2 \rangle \quad (12.28)$$

or over the cylinder length dL

$$f_p = \int_0^\infty n(L) V_{\text{cyl}}(R, L) dL = \int_0^\infty N p(L) \pi R^2 L dL = NR^2 \pi \langle L \rangle \quad (12.29)$$

depending if we have a distribution over the radius R or the length L . In both cases the volume fraction can be expressed in terms of moments of the size distribution supplied by **SASfit**. In the first case it can be expressed by the second moment $\langle R^2 \rangle$ of the cylinder radius and in the second case by the first moment $\langle L \rangle$ of the cylinder length, i.e. the mean cylinder length. The required moments are displayed in **SASfit** in the menu shown in Fig. 12.2. Also here one has to take care using proper units, but this is done equivalently to the first example of a sphere in eq. 12.26.

The three examples above show that the volume fraction f_p of scatterers can be calculated in many cases via the moments of the size distribution and for simple cases all necessary parameters are supplied in the **SASfit** menu interface. The volume fraction **fp** in Fig. 12.2 is numerically calculated from the size distribution. For some specific other form factor and the special case of a **LogNorm** distribution a plugin size distribution named **LogNorm_fp** described in section 10.1.1 has been implemented. Calculating volume fractions for any size distribution and for any form factor is not easy to implement. It would require quite some knowledge about the form factor and how exactly the volume fraction is defined. The plugin **LogNorm_fp** distinguishes between volume fraction of a core only, a volume fraction of a core together with a shell and a volume fraction of a shell only. For the general case one also needs to know which size parameter of the form factor has a distribution. This already shows that the user has to supply additional information. For the calculation a volume function has to be associated to each form factor. If this is not the case the **SASfit** routine returns 0. For those functions a volume function is associated to the form factor **SASfit** calculates numerically the volume fraction for any size distribution by integration. The plugin function **LogNorm_fp** on the other side has a lognormal distribution implemented and the information about the form factor and the size parameter of the form factor having a distribution has to be given by the user via an input value called **shape**. Only a very limited number of form factors can be selected by this parameter. For other form factors the plugin needs to be

extended or an routine calculating the volume for the specific form factor needs to be implemented.

12.5. How to use quantile distribution function in SAS

The quantile distribution and quantile density distribution are typically named $Q(y)$ and $q(y)$. To not mix them with the scattering vector, the character for the scattering vector in this section will be named h .

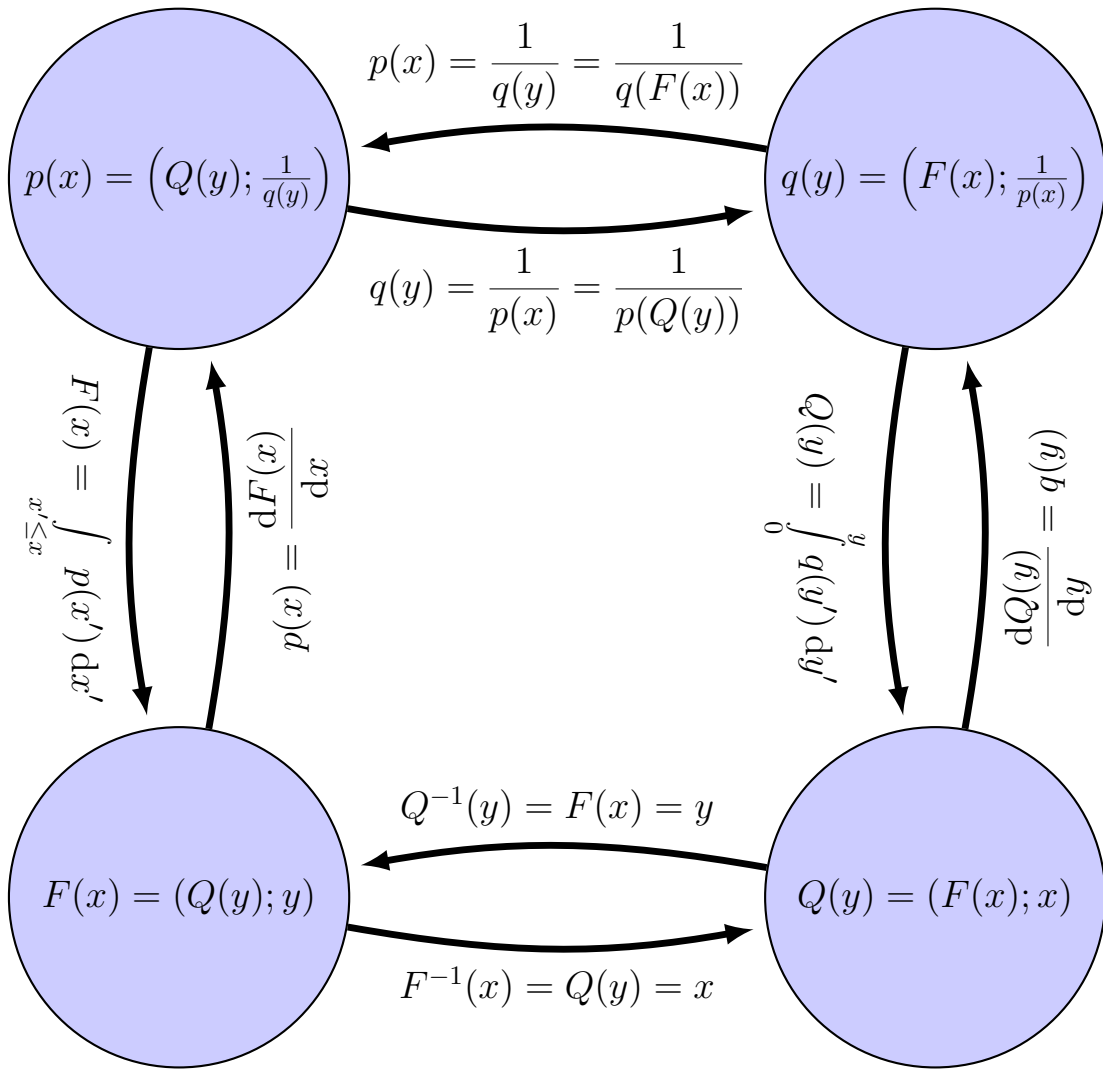


FIGURE 12.3. Transformation cycle between $p(x)$, $F(x)$, $Q(y)$ and $q(y)$.

In this chapter we discuss briefly how the concept of quantile distribution function can be used in small angle scattering. The quantile function $Q(y)$ is used in statistics and is directly related to the probability $p(x)$ and cumulative distribution $F(x)$. The probability distribution function is a non-negative Lebesgue-integrable function and its

integral over its entire domain \mathfrak{D} is 1.

$$p(x) \geq 0 \quad \forall x \in \mathfrak{D} \quad (12.30)$$

$$\int_{\mathfrak{D}} p(x) dx = 1 \quad (12.31)$$

where the domain \mathfrak{D} can be all real numbers or a half bounded or a two side bounded interval. The cumulative distribution function is defined as the integral below $p(x)$ until the value x , i.e.

$$F(x) = y = \int_{x' \leq x} p(x') dx' \quad \forall x \in \mathfrak{D} \quad (12.32)$$

The cumulative distribution function is strictly monotonic and in many practical cases relevant for small angle scattering also continuous as the practical relevant probability function do not have poles. The quantile distribution function is now simply the inverse of the cumulative distribution function, i.e.

$$Q(y) = F^{-1}(y) = x \quad (12.33)$$

and is as well strictly monotonic. Its derivation, the quantile density distribution function, is related to the probability distribution by

$$q(y) = \frac{dx}{dy} = \frac{dQ(y)}{dy} \quad (12.34)$$

$$p(x) = \frac{1}{q(y)} = \frac{1}{q(F(x))} \quad (12.35)$$

12.5.1. List of some selected quantile distribution function to describe size distributions.

Quantile distribution functions of a few standard distributions used in small angle scattering analysis belonging to a probability distribution decaying fast enough to serve as a number distribution function are listed in the following:

Normal

$$p_{\text{normal}}(x) = \frac{1}{\sigma\sqrt{2\pi}} e^{-\frac{1}{2}\left(\frac{x-\mu}{\sigma}\right)^2} \quad (12.36)$$

$$F_{\text{normal}}(x) = \Phi\left(\frac{x-\mu}{\sigma}\right) = \frac{1}{2} \left[1 + \operatorname{erf}\left(\frac{x-\mu}{\sigma\sqrt{2}}\right) \right] \quad (12.37)$$

$$Q_{\text{normal}}(y) = \mu + \sigma\sqrt{2} \operatorname{erf}^{-1}(2y - 1) \quad (12.38)$$

lognormal

$$p_{\text{lognormal}}(x) = \frac{1}{x\sigma\sqrt{2\pi}} \exp\left(-\frac{(\ln x - \mu)^2}{2\sigma^2}\right) \quad (12.39)$$

$$F_{\text{lognormal}}(x) = \frac{1}{2} \left[1 + \operatorname{erf}\left(\frac{\ln x - \mu}{\sigma\sqrt{2}}\right) \right] = \Phi\left(\frac{\ln(x) - \mu}{\sigma}\right) \quad (12.40)$$

$$Q_{\text{lognormal}}(y) = \exp\left(\mu + \sqrt{2\sigma^2} \operatorname{erf}^{-1}(2y - 1)\right) \quad (12.41)$$

Weibull

$$p_{\text{Weibull}}(x) = \begin{cases} \frac{k}{\lambda} \left(\frac{x}{\lambda}\right)^{k-1} e^{-(x/\lambda)^k}, & x \geq 0, \\ 0, & x < 0. \end{cases} \quad (12.42)$$

$$F_{\text{Weibull}}(x) = \begin{cases} 1 - e^{-(x/\lambda)^k}, & x \geq 0, \\ 0, & x < 0. \end{cases} \quad (12.43)$$

$$Q_{\text{Weibull}}(y) = \lambda(-\ln(1-y))^{\frac{1}{k}} \quad (12.44)$$

Gamma

$$p_{\text{Gamma}}(x) = \frac{1}{\Gamma(k)\theta^k} x^{k-1} e^{-x/\theta} \quad (12.45)$$

$$F_{\text{Gamma}}(x) = \frac{1}{\Gamma(k)} \gamma\left(k, \frac{x}{\theta}\right) \quad (12.46)$$

$$Q_{\text{Gamma}}(y) = \gamma^{-1}(k, y\Gamma(k)) \theta \quad (12.47)$$

where $\gamma^{-1}(s, y)$ is the inverse of the lower incomplete gamma function $\gamma(s, x)$

beta

$$p_{\text{beta}}(x) = \frac{x^{\alpha-1} (1-x)^{\beta-1}}{B(\alpha, \beta)} \quad (12.48)$$

where $B(\alpha, \beta) = \frac{\Gamma(\alpha)\Gamma(\beta)}{\Gamma(\alpha+\beta)}$ and Γ is the Gamma function.

$$F_{\text{beta}}(x) = I_x(\alpha, \beta) \quad (12.49)$$

where $I_x(\alpha, \beta)$ is the regularized incomplete beta function. The beta distribution is bounded for values $x \in [0; 1]$.

$$Q_{\text{beta}}(y) = I_y^{-1}(\alpha, \beta) \quad (12.50)$$

uniform

$$p_{\text{uniform}}(x) = \begin{cases} 0, & \text{if } x < a \\ 0, & \text{if } x > b \\ \frac{1}{b-a}, & \text{otherwise.} \end{cases} \quad (12.51)$$

$$F_{\text{uniform}}(x) = \begin{cases} 0, & \text{if } x < a \\ 1, & \text{if } x > b \\ \frac{x-a}{b-a}, & \text{otherwise.} \end{cases} \quad (12.52)$$

$$Q_{\text{uniform}}(y) = by + a(1-y) \quad (12.53)$$

triangular

$$p_{\text{triangular}}(x) = \begin{cases} \frac{2(x-a)}{(b-a)(c-a)}, & \text{if } a \leq x \leq c \\ \frac{2(b-x)}{(b-a)(b-c)}, & \text{if } c < x \leq b \\ 0, & \text{otherwise.} \end{cases} \quad (12.54)$$

$$F_{\text{triangular}}(x) = \begin{cases} \frac{(x-a)^2}{(b-a)(c-a)}, & \text{if } a \leq x \leq c \\ 1 - \frac{(b-x)^2}{(b-a)(b-c)}, & \text{if } c < x \leq b \\ 1, & \text{if } x > b \\ 0, & \text{otherwise.} \end{cases} \quad (12.55)$$

$$Q_{\text{triangular}}(y) = \begin{cases} a + \sqrt{(b-a)(c-a)y}, & \text{if } 0 \leq y \leq \frac{c-a}{b-a} \\ b - \sqrt{(b-a)(b-c)(1-y)}, & \text{if } 1 \geq y > \frac{c-a}{b-a} \end{cases} \quad (12.56)$$

12.5.2. MetaLog distribution.

A distribution function designed to be very flexible is the metalog distribution. The quantile function of the metalog distribution $Q(y) = M_k(y)$ is defined as [259, 257, 258]

$$M_k(y) = \begin{cases} a_1 + a_2 \ln \frac{y}{1-y}, & k = 2 \\ a_1 + a_2 \ln \frac{y}{1-y} + a_3(y - \frac{1}{2}) \ln \frac{y}{1-y}, & k = 3 \\ a_1 + a_2 \ln \frac{y}{1-y} + a_3(y - \frac{1}{2}) \ln \frac{y}{1-y} + a_4(y - \frac{1}{2}), & k = 4 \\ M_{k-1}(y) + a_k(y - \frac{1}{2})^{\frac{k-1}{2}}, & \text{odd } \wedge k \geq 5 \\ M_{k-1}(y) + a_k(y - \frac{1}{2})^{\frac{k}{2}-1} \ln \frac{y}{1-y}, & \text{even } \wedge k \geq 6 \end{cases} \quad (12.57)$$

and its quantile density distribution function $q(y) = m_k(y)$ which is related to the probability distribution function $p(x)$ by $p(x) = 1/q(y)$ with $x = M_k(y)$ reads as

$$m_k(y) = \begin{cases} \frac{y(1-y)}{a_2}, & k = 2 \\ \left(\frac{a_2}{y(1-y)} + a_3 \left(\frac{y-\frac{1}{2}}{y(1-y)} + \ln \frac{y}{1-y} \right) \right)^{-1}, & k = 3 \\ \left(\frac{a_2}{y(1-y)} + a_3 \left(\frac{y-\frac{1}{2}}{y(1-y)} + \ln \frac{y}{1-y} \right) + a_4 \right)^{-1}, & k = 4 \\ \left(\frac{1}{m_{k-1}(y)} + a_k \frac{k-1}{2} (y - \frac{1}{2})^{(k-3)/2} \right)^{-1}, & \text{odd } \wedge k \geq 5 \\ \left(\frac{1}{m_{k-1}(y)} + a_k \left(\frac{(y-\frac{1}{2})^{\frac{k}{2}-1}}{y(1-y)} + (\frac{k}{2} - 1)(y - \frac{1}{2})^{(\frac{k}{2}-2)} \ln \frac{y}{1-y} \right) \right)^{-1}, & \text{even } \wedge k \geq 6 \end{cases} \quad (12.58)$$

The metalog distribution as defined above is an unbounded distribution. In case of describing a size distribution it needs to be bounded (Logit metalog) or at least semi-bounded (bounded below, Log metalog). This can be easily done by a transformation of $z(x) = \ln(x - b_l)$ for a distribution with a lower bound b_l or $z(x) = \ln(\frac{x-b_l}{b_u-x})$ with a lower bound b_l and an upper bound b_u , where z is then metalog-distributed. The

corresponding quantile functions and quantile density functions read as

$$M_k^{\log}(y) = \begin{cases} b_l + e^{M_k(y)}, & 0 < y < 1 \\ b_l, & y = 0 \end{cases} \quad (12.59)$$

$$m_k^{\log}(y) = \begin{cases} m_k(y)e^{-M_k(y)}, & 0 < y < 1 \\ 0, & y = 0 \end{cases} \quad (12.60)$$

$$M_k^{\text{logit}}(y) = \begin{cases} \frac{b_l + b_u e^{M_k(y)}}{1 + e^{M_k(y)}}, & 0 < y < 1 \\ b_l, & y = 0 \\ b_u, & y = 1 \end{cases} \quad (12.61)$$

$$m_k^{\text{logit}}(y) = \begin{cases} m_k(y) \frac{(1 + e^{M_k(y)})^2}{(b_u - b_l)e^{M_k(y)}}, & 0 < y < 1 \\ 0, & y = 0 \\ 0, & y = 1 \end{cases} \quad (12.62)$$

12.5.3. use of quantile distribution function to describe size distributions.

A standard task in the modelling of small angle scattering data is to smear the scattering model due to a size distribution. If $A(h; \mathbf{a}_i, x)$ is the scattering amplitude of a model, \mathbf{a}_i its parameters and x the parameter with a distribution the typical size averages to perform are

$$\langle A(h; \mathbf{a}_i, x) \rangle = N \int_0^\infty p(x) A(h; \mathbf{a}_i, x) dx \quad (12.63)$$

$$\langle A^2(h; \mathbf{a}_i, x) \rangle = N \int_0^\infty p(x) A^2(h; \mathbf{a}_i, x) dx \quad (12.64)$$

N is the overall scaling factor and describes for standard form factor the overall number density of particles. At the moment **SASfit** is actually performing the integration over the probability distribution function. Initial test have shown an issues for cases with a very narrow size distribution. Numerical integrals over the semi-infinite interval (a, ∞) can be mapped onto the semi-open interval $(0, 1]$ using the transformation $x = a + (1 - t)/t$, so that

$$\int_a^\infty f(x) dx = \int_0^1 f(a + (1 - t)/t)/t^2 dt \quad (12.65)$$

which then can be solved efficiently with adaptive quadrature algorithms. However, if the probability distribution is very narrow the algorithms might miss the range for which the probability distribution $p(x)$ is significantly larger than 0. On the other side choosing a meaningful integration range requires both knowledge about the behaviour of the chosen probability function as well as of the form factor itself. The scattering intensity of spherical objects scales with their squared volume, i.e. with R^6 in case of solid spheres with radius R , or with R^4 for thin hollow spheres or even L^2 for long cylinders of length L . **SASfit** has internally a routine, which calculates the mode of $p(x)x^\alpha$, i.e. the most probable size x_{m_α} in the distribution $D_\alpha(x) = x^\alpha p(x)$ and then

calculates those size values $[a; b]$ below and above x_{x_α} , where the intensity distribution drops below 10^{-6} .

$$x_{m_\alpha} = \arg \max_{x \in \mathbb{R}^+} (x^\alpha p(x)) = \left\{ x \in \mathbb{R}^+ : s^\alpha p(s) \leq x^\alpha p(x) \text{ for all } s \in \mathbb{R}^+ \right\} \quad (12.66)$$

$$a = \max \left\{ \inf \left\{ x \in \mathbb{R}^+ : x_{m_\alpha}^\alpha p(x_{m_\alpha}) 10^{-6} = x^\alpha p(x) \wedge x < x_{m_\alpha} \right\}; 0 \right\} \quad (12.67)$$

$$b = \sup \left\{ x \in \mathbb{R}^+ : x_{m_\alpha}^\alpha p(x_{m_\alpha}) 10^{-6} = x^\alpha p(x) \right\} \quad (12.68)$$

As the scattering intensities of objects scale with up to the sixth power of its length $A^2(q; \mathbf{a}_i, x) \propto x^\alpha$ with $\alpha = 6$ all distribution functions $p(x)$ needs to decay faster than the $(\alpha + 1)^{\text{th}}$ power otherwise the integral in 12.64 becomes improper and diverges. Alternatively the size distribution needs to be artificially clipped by an upper bound.

A work-around to avoid the calculation of the lower and upper integration bound would be the use of quantile distribution function, if they are known analytically for the used probability distribution function. Using quantile distribution functions the integral can be rewritten as

$$N \int_0^\infty p(x) A^n(h; \mathbf{a}_i, x) dx = N \int_0^\infty p(Q(y)) A^n(h; \mathbf{a}_i, Q(y)) dx \quad (12.69)$$

$$= N \int_0^1 A^n(h; \mathbf{a}_i, Q(y)) dy \quad (12.70)$$

by a change of variables using $dx/dy = dQ(y)/dy = q(y) = 1/p(x)$ and $x = Q(y)$. $n = [1, 2]$ depending if the average scattering amplitude ($n = 1$) or the average scattering intensity ($n = 2$) needs to be calculated. The change of variable like above has the additional side effect that now the integration over semi-infinite interval for the size distribution becomes an integral with finite limits over the cumulative distribution y from 0 to 1. Furthermore, by doing this transformation the quadrature behaves numerically well for both very sharp and very broad distributions for all distribution functions decaying fast enough so that the integral in eq. 12.69 stays finite. In **SASfit** only those size distribution are supplied, which fulfill this condition for any form factor. The reason, that for some distribution functions the integral diverges is, that the form factor scale typically with the squared volume of the particle, i.e. with up to the 6-th power of its size parameter. Therefore, already in the past it was suggested to use instead of the number density distribution $p(x)$ the volume $D_v(x) = p(x)x^3$ ($\alpha = 3$) or intensity distribution $D_i(x) = p(x)x^6$ ($\alpha = 6$) [156]. The third and sixth power have been chosen due to the assumption, that the volume scales with the third power of its size parameter which, however, would need an adjustment in case of objects with different scaling behaviour. Applying this strategy using quantile distribution functions would in combination of a

distribution proportional to $p_\alpha(x) = c_\alpha x^\alpha p(x)$ result in

$$N \int_0^\infty p(x) A^n(h; \mathbf{a}_i, x) dx = N \int_0^\infty \underbrace{p(x)x^\alpha}_{=p_\alpha(x)/c_\alpha} x^{-\alpha} A^n(h; \mathbf{a}_i, x) dx = \quad (12.71)$$

$$= \frac{N}{c_\alpha} \int_0^\infty p_\alpha(Q_\alpha(y)) Q_\alpha^{-\alpha}(y) A^n(h; \mathbf{a}_i, Q_\alpha(y)) dy \quad (12.72)$$

$$= \frac{N}{c_\alpha} \int_0^1 Q_\alpha^{-\alpha}(y) A^n(h; \mathbf{a}_i, Q_\alpha(y)) dy \quad (12.73)$$

with $dx/dy = dQ_\alpha(y)/dy = q_\alpha$, $1/q_\alpha(y) = p_\alpha(Q_\alpha(y))$, and $x = Q_\alpha(y)$. c_α is needed so that $p_\alpha(x)$ is again a probability distribution function and normalized to 1, but on the other side the overall scaling factor N should keep its definition. For this one needs to define c_α as

$$p_\alpha(x) = c_\alpha x^\alpha p(x) \quad (12.74)$$

$$\Rightarrow \int_0^\infty p_\alpha(x) x^{-\alpha} dx = c_\alpha \int_0^\infty p(x) dx \quad (12.75)$$

$$\Leftrightarrow c_\alpha = \int_0^1 Q_\alpha^{-\alpha}(y) dy \quad (12.76)$$

The problem with convergence in eq. 12.73 seems to be easing, but it has only shifted to the calculation of c_α in eq. 12.76.

12.5.4. highly flexible quantile distribution function used as scattering length distribution profiles.

In 9.2.7.2 sigmoidal functions have been used to generate a smoothed interface between phase boundaries, in that case between water, head groups of lipids and tail groups of lipids. For that specific case the Laplace cumulative distribution function has been used. Actually new more flexible distribution functions are developed in terms of quantile distribution functions. Both presentation can be used to introduce smooth profiles as will be shown below.

As described in 9.2 the scattering intensity for very thin random orientated particles the form factor can be factorize according to Porod [393] in a cross section term $P_{cs}(h)$ for the shorter or thin dimension and a shape factor $P'(h)$ for the long dimension.

$$I(h) = P'(h)P_{cs}(h). \quad (12.77)$$

$P'(h)$ for 3D objects is 1, for local cylindrical (2D) objects several cases are listed in paragraph 9.2.4 and for local planar objects (1D) in paragraph 9.2.3. The cross-section form factors $P_{cs}(h)$ can be easily calculated if the scattering length density contrast profile $\Delta\eta_{cs}(x)$ is known. For structures with a local planar geometry and a symmetric

cross-section the form factor is given by

$$P_{\text{cs}}^{\text{1D}}(h) = \left| 2 \int_0^\infty \Delta\eta_{\text{cs}}(x) \cos(hx) dx \right|^2 \quad (12.78)$$

In case of local cylindrical particles with a centro-symmetric scattering length density distribution the form factor is given by

$$P_{\text{cs}}^{\text{2D}}(Q) = \left| 2\pi \int_0^\infty \Delta\eta_{\text{cs}}(x) J_0(hx) x dx \right|^2 \quad (12.79)$$

The form factor of spherical symmetric objects the scattering intensity reads as

$$P_{\text{cs}}^{\text{3D}}(h) = \left| \int_0^\infty \Delta\eta_{\text{cs}}(x) 4\pi x^2 \frac{\sin(hx)}{hx} dx \right|^2 \quad (12.80)$$

We assume now, that the scattering length density distribution of a typically multi-shell model with boundary between phase i and $i+1$ at position x_i is smoothed by a decreasing transition function from 1 to 0 in phase i and a raising transition function in phase $i+1$ from 0 to 1 multiplied by the corresponding scattering length density differences to the solvent, i.e.

$$\Delta\eta_{\text{cs}}(x) = \sum_i \Delta\eta_i (1 - F_i(x, \mu_i)) + \Delta\eta_{i+1} F_i(x, \mu_i) \quad (12.81)$$

where μ_i are the position of the i^{th} phase boundary as well as the mean values of the cumulative distribution functions $F_i(x = \mu_i, \mu_i) = \frac{1}{2}$. By choosing the same cumulative distribution function $(1 - F_i)$ for the falling phase i and F_i for the neighbouring raising phase $i+1$ the sum of both stays equal 1 everywhere, so that it could be interpreted as a local volume fraction of the corresponding phases. We then obtain for the scattering intensities of the 1D, 2D and 3D profiles

$$P_{\text{cs}}^{\text{1D}}(h) = \left| \sum_i \int_0^\infty [\Delta\eta_i (1 - F_i(x, \mu_i)) + \Delta\eta_{i+1} F_i(x, \mu_i)] 2 \cos(hx) dx \right|^2 \quad (12.82)$$

$$P_{\text{cs}}^{\text{2D}}(h) = \left| \sum_i \int_0^\infty [\Delta\eta_i (1 - F_i(x, \mu_i)) + \Delta\eta_{i+1} F_i(x, \mu_i)] 2\pi x J_0(hx) dx \right|^2 \quad (12.83)$$

$$P_{\text{cs}}^{\text{3D}}(h) = \left| \sum_i \int_0^\infty [\Delta\eta_i (1 - F_i(x, \mu_i)) + \Delta\eta_{i+1} F_i(x, \mu_i)] 4\pi x^2 \frac{\sin hx}{hx} dx \right|^2 \quad (12.84)$$

In those case where the cumulative distribution is not known analytically but the quantile distribution function the integrals can be rewritten by variable transformation using

$x = Q_i(y_i)$ and $\mathrm{d}x/\mathrm{d}y_i = \mathrm{d}Q(y_i)/\mathrm{d}y_i = q(y_i)$ and result in

$$P_{\text{cs}}^{\text{1D}}(h) = \left| \sum_i \int_0^1 [\Delta\eta_i(1 - y_i) + \Delta\eta_{i+1}y_i] 2 \cos(hQ_i(y_i))q_i(y_i) \mathrm{d}y_i \right|^2 \quad (12.85)$$

$$P_{\text{cs}}^{\text{2D}}(h) = \left| \sum_i \int_0^1 [\Delta\eta_i(1 - y_i) + \Delta\eta_{i+1}y_i] 2\pi Q_i(y_i) J_0(hQ_i(y_i))q_i(y_i) \mathrm{d}y_i \right|^2 \quad (12.86)$$

$$P_{\text{cs}}^{\text{3D}}(h) = \left| \sum_i \int_0^1 [\Delta\eta_i(1 - y_i) + \Delta\eta_{i+1}y_i] 4\pi Q_i^2(y_i) \frac{\sin hQ_i(y_i)}{hQ_i(y_i)} q_i(y_i) \mathrm{d}y_i \right|^2 \quad (12.87)$$

12.5.5. Test of some quantile distribution function describing SLD profiles.

CHAPTER 13

Basic Analysis of Dynamic Light Scattering Data

In a typical dynamic light scattering (DLS) or photo correlation scattering (PCS) experiment, the autocorrelation function $G^{(2)}(\tau)$ of the intensity scattered by dispersed particles is determined as a function of the delay τ . $G^{(2)}(\tau)$ is related to the modulus of the normalized field autocorrelation function $g_1(\tau)$ by a Siegert relationship

$$G^{(2)}(\tau) = Ag_1^2(\tau) + B. \quad (13.1)$$

Here B is a background term often designated as the baseline and A can be considered as another instrumental factor. The time dependence of $g_1(\tau)$ is related to the dynamics of the dispersed particles. For particles in Brownian motion, the time decay of $g_1(\tau)$ is determined by the diffusion coefficient of the dispersed particles. In particular, for monodisperse samples $g_1(\tau)$ is an exponentially decaying function:

$$g_1(\tau) = \exp(-\Gamma\tau) \quad (13.2)$$

or

$$G^{(2)}(\tau) = A \exp(-2\Gamma\tau) + B \quad (13.3)$$

where the decay rate Γ is linked to the particles' diffusion coefficient D by $\Gamma = DQ^2$, where Q is the modulus of the scattering vector

$$Q = \frac{4\pi m_1}{\lambda_0} \sin(\theta/2) \quad (13.4)$$

m_1 is the refraction index of the solution, λ_0 the wavelength in vacuo of the incident light and θ the scattering angle. At the end the Stokes-Einstein expression for the diffusion coefficient is used to get an average particle radius R_{DLS}

$$D = \frac{kT}{6\pi\eta R_{\text{DLS}}} \quad (13.5)$$

where k is Boltzmann's constant, T the absolute temperature, η the viscosity of the dispersion medium and R_{DLS} the particle radius (only valid for noninteracting particles).

13.1. Cumulant Analysis

The formulas in eq. 13.2 to 13.5 are valid for monodisperse dispersions only. For polydisperse dispersions the cumulants method of Koppel (1972) [271] is widely used, which assumes a multi-exponential behaviour so that $g_1(\tau)$ and $G^{(2)}(\tau)$ can be written in a series expansion as:

$$g_1(\tau) = \exp\left(-\Gamma_1\tau + \frac{\Gamma_2\tau^2}{2} - \frac{\Gamma_3\tau^3}{6} + \dots\right) \quad (13.6)$$

$$G^{(2)}(\tau) = A \exp\left(-2\Gamma_1\tau + \Gamma_2\tau^2 - \frac{\Gamma_3\tau^3}{3} + \dots\right) + B \quad (13.7)$$

SASfit assumes for the cumulant fit-routine that the function $G^{(2)}(\tau)$ is supplied. As normally no error bar is available from the correlator a robust least square procedure is implemented.

The formula given by Koppel has been obtained by a Taylor expansion of $\ln g_1(\tau)$ around $\tau = 0$. A more stable expansion can be obtained by a series expansion of $g_1(\tau)$ around the average relaxation time Γ_1 [404, 109, 140, 323].

$$g_1(\tau) = \exp(-\Gamma_1\tau)\left(1 + \frac{\Gamma_2\tau^2}{2} - \frac{\Gamma_3\tau^3}{6} + \dots\right) \quad (13.8)$$

$$G^{(2)}(\tau) = A \exp(-2\Gamma_1\tau)\left(1 + \frac{\Gamma_2\tau^2}{2} - \frac{\Gamma_3\tau^3}{6} + \dots\right)^2 + B \quad (13.9)$$

13.2. Double Decay Cumulant Analysis

$$G^{(2)}(\tau) = A \left[p e^{-2\Gamma_{a,1}\tau + \Gamma_{a,2}\tau^2} + (1-p) e^{-2\Gamma_{b,1}\tau + \Gamma_{b,2}\tau^2} \right] + B \quad (13.10)$$

13.3. Fit of Double Stretched Exponentials

$$G^{(2)}(t) = A \left\{ p \exp \left(\left[\frac{t}{\tau_1} \right]^{\gamma_1} \right) + (1-p) \exp \left(\left[\frac{t}{\tau_2} \right]^{\gamma_2} \right) \right\} + B \quad (13.11)$$

13.3.1. The least squares minimiser and the robust least squares procedure. The function to be minimised is

$$\chi^2 = \sum_i \left(\frac{r_i}{\Delta I_i} \right)^2$$

where the residual is defined as

$$r_i = I_i - I_{i,th}.$$

Here I_i is the intensity correlation function $G^{(2)}(t_i)$ at time t_i with already subtracted baseline as received from a correlator, $I_{i,th}$ is the value of the cumulant fit according to eq. 13.7 or a double exponential decay according to eq. 13.11. Normally no error values ΔI_i are supplied from the correlator so that all data points are weighted the same. A robust fitting with bisquare weights is implemented which uses an iteratively reweighted least squares algorithm, and follows the procedure:

- (1) Fit the model by an unweighted least squares (that is, χ).
- (2) Standardize the residuals via $u_i = r_i/(Ks)$. Here K is a tuning constant equal to 4.685, and s is the robust variance given by $MAD/0.6745$, where MAD is the median absolute deviation of the residuals

$$MAD = \sum_{i=1}^N \frac{1}{N} |I_{i,th} - I_i|$$

- (3) Compute the robust weights w_i as a function of the standardized residuals u_i . The bisquare weights are given by

$$w_i = \begin{cases} (1 - u_i^2)^2 & |u_i| < 1 \\ 0 & |u_i| \geq 1 \end{cases}$$

- (4) Re-do the fit using the weighted minimiser:

$$\chi^2 = \sum_i w_i \left(\frac{r_i}{\Delta I_i} \right)^2$$

- (5) The fit converges when the MAD changes by no more than the fraction set by `residual_tolerance` (which has been chosen to be 10^{-8}). Otherwise, perform the next iteration of the fitting procedure by returning to the first step.

CHAPTER 14

Scattering Theory

14.1. Scattering Cross-Section

In a scattering experiment one is interested in a detailed analysis of the scattering pattern as a function of the characteristics of the incident beam. Monochromator and collimator specify direction and energy of the incident radiation. The radiation interacts with the sample and receives thereby a momentum transfer $\hbar\mathbf{Q}$. By this process the radiation receives beside a direction change also an energy change. The result is described with the help of a cross-section.

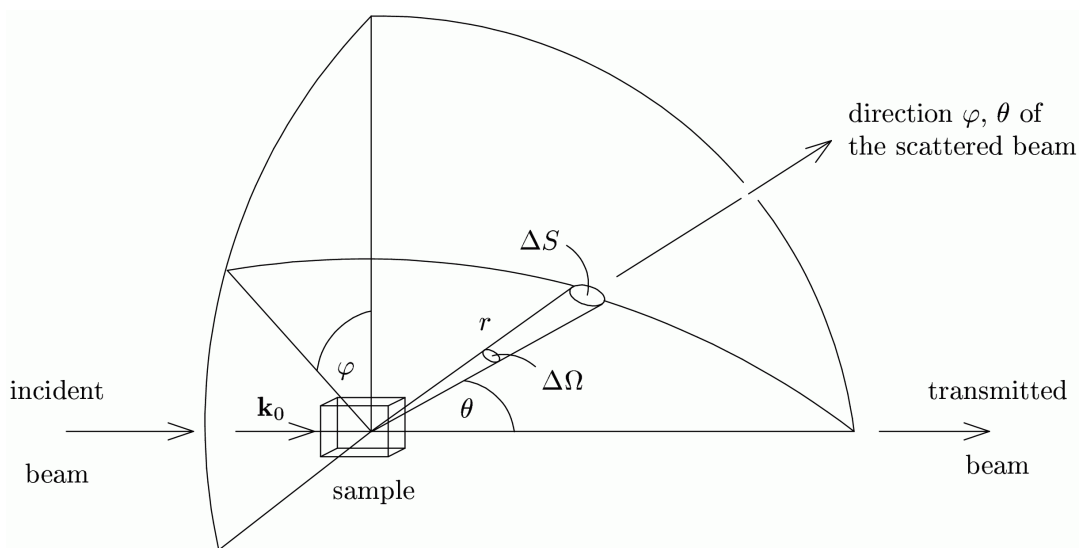


FIGURE 14.1. Schematic representation of a scattering process

A detector with an efficiency ϵ measures for this the number of the scattered neutrons or photons in a given direction $\mathbf{k}_0 + \mathbf{Q}$. The distance between detector and sample should be large in comparison to the linear dimension of the detector, so that the solid angle included by the detector element $\Delta\Omega$ is small.

If the incident beam has a homogeneous, continuous flow density Φ_0 ($[\Phi_0] = \text{neutron (photons -) per cm}^2 \text{ and second}$) and if the beam contain N identical particles, then the counting rate C of the detector is proportional to all these quantities. The proportionality constant is called differential scattering cross-section $\frac{d\sigma}{d\Omega} = \frac{C}{\Phi_0 \epsilon N \Delta\Omega}$. In the case of inelastic scattering the counting rate is in a certain interval δE of transferred energy in addition proportionally to δE . The appropriate proportionality constant is the partial

(or double) differential scattering cross-section

$$\frac{d^2\sigma}{d\Omega dE} = \frac{C}{\Phi_0 \epsilon N \Delta\Omega \Delta E} = \frac{\text{Number of neutrons (photons), which are scattered per second into the solid angle } d\Omega \text{ toward } \phi, \theta \text{ with an energy between } E \text{ and } E + dE}{N\Phi_0 d\Omega dE}$$

The total differential cross-section is defined as

$$\sigma_t = (\text{total number of scattered neutrons (photons) per sec})/\Phi_0. \quad (14.1)$$

The three different cross-section are related to each other by

$$\sigma_t = \int d\Omega \frac{d\sigma}{d\Omega} \quad \text{and} \quad \frac{d\sigma}{d\Omega} = \int_0^\infty dE \frac{d^2\sigma}{d\Omega dE}. \quad (14.2)$$

14.1.1. Scattering of neutrons on atoms. The scattering of neutrons can be explained by two types of interactions between neutrons and matter; once the strong spin dependent nuclear forces between nuclei and neutron (interaction range $\sim 10^{-15}\text{m}$) and secondly the dipole-dipole interaction between the magnetic moment of the neutron and that of an unpaired electron, or nuclei accordingly. Both interactions have in common that their interaction potential $V(\mathbf{r})$ for $r \rightarrow \infty$ decays faster than $1/r$. For this kind of interaction potential the quantum mechanical scattering theory [214] yields as an asymptotic approximation for the Schrödinger equation of the wave function

$$\psi_{\mathbf{k}_0}(\mathbf{r}) \xrightarrow[r \rightarrow \infty]{} \frac{1}{(2\pi)^{3/2}} \left[e^{i\mathbf{k}_0 \cdot \mathbf{r}} + f(\theta, \phi) \frac{e^{ik_0 r}}{r} \right]. \quad (14.3)$$

For low energy particles and short range potential the partial waves methods yields for the scattering amplitude $f(\theta, \phi) = -b$, whereby the so called scattering length b can be determined experimentally. Via another Ansatz, the Born approximation, one gets a series expansion for $f(\theta, \phi)$. The first term of this series expansion is give by

$$f^{(0)}(\theta, \phi) = -\frac{m_N}{2\pi\hbar^2} \int d\mathbf{r} e^{i\mathbf{Q} \cdot \mathbf{r}} V(\mathbf{r}), \quad (14.4)$$

with $\mathbf{Q} = \mathbf{k} - \mathbf{k}_0$. A comparison of this result with the partial wave method ($f(\theta, \phi) = -b$), shows that the pseudo potential $V(\mathbf{r}) = \frac{2\pi\hbar^2}{m_N} b \delta(\mathbf{r})$ (Fermi's pseudo potential) has an equivalent solution. For an ensemble of N atoms, e.g. a crystal, the total potential is in kinematic approximation the sum of the individual potentials

$$V(\mathbf{r}) = \frac{2\pi\hbar^2}{m_N} \sum_{j=1}^N b_j \delta(\mathbf{r} - \mathbf{r}_j), \quad (14.5)$$

whereby \mathbf{r}_j describes the position of nuclei j with scattering the length b_j and N the number of scattering atoms. The scattering length b_j depends on the element or isotope which is the scattering center. Furthermore it can depend on the spin state of the neutron and the nuclei and on unpaired electrons in non fully occupied atomic electron shells. In the kinematic approximation it is assumed that the intensity of the incoming beam is identical at each scattering center, i.e. that the scattered intensity does not attenuate the incoming beam. Furthermore it is assumed that the incoming beam is only scattered once and multiple scattered can be neglected.

In the static approximation, i.e. for a scattering process which does not change the state of the scattering center and therefore is an elastic scattering process, the differential scattering cross-section can be described in terms of a scattering amplitude $f^{(0)}(\theta, \phi)$ by

$$\frac{d\sigma}{d\Omega}(\mathbf{Q}) = \frac{1}{N} |f^{(0)}(\theta, \phi)|^2 = \frac{1}{N} \left(\frac{m_N}{2\pi\hbar^2} \right)^2 \left| \int d\mathbf{r} e^{i\mathbf{Q}\mathbf{r}} V(\mathbf{r}) \right|^2 . \quad (14.6)$$

Using Fermi's pseudo potentials (eq. 14.5) leads to the expression

$$\frac{d\sigma}{d\Omega}(\mathbf{Q}) = \frac{1}{N} \left| \sum_{j=1}^N b_j e^{i\mathbf{Q}\mathbf{r}_j} \right|^2 = \frac{1}{N} \sum_{i,j} b_i b_j e^{i\mathbf{Q}\mathbf{r}_i} e^{-i\mathbf{Q}\mathbf{r}_j} \quad (14.7)$$

Let us now consider a new system of scatterers, which are only different to those from eq. 14.7 that the scattering length of the nuclei are exchanged. Hereby both the position and fraction of the scattering length b_i are kept the same. For a large number of scattering centers the average over the cross-sections of all possible systems of scatterers which are identical to the one in 14.7 can be described by

$$\frac{d\sigma}{d\Omega}(\mathbf{Q}) = \frac{1}{N} \sum_{i,j} \overline{b_i b_j} e^{i\mathbf{Q}\mathbf{r}_i} e^{-i\mathbf{Q}\mathbf{r}_j} . \quad (14.8)$$

If the scattering length b_i occur in the same fraction x_i , whereby $\sum_i x_i = 1$, so that the averages \bar{b} and \bar{b}^2 can be written as

$$\bar{b} = \sum_i x_i b_i \quad \text{and} \quad \bar{b}^2 = \sum_i x_i b_i^2 . \quad (14.9)$$

Under the condition that there are no correlations between the scattering lengths of the individual nuclei one can write

$$\overline{b_i b_j} = \bar{b}^2 \quad \text{for } i \neq j \quad \text{and} \quad \overline{b_i b_j} = \bar{b}^2 \quad \text{for } i = j \quad (14.10)$$

From this it follows for the differential cross-section

$$\frac{d\sigma}{d\Omega}(\mathbf{Q}) = \frac{1}{N} \left(\bar{b}^2 + \bar{b}^2 \sum_{\substack{i,j \\ i \neq j}} e^{i\mathbf{Q}\mathbf{r}_i} e^{-i\mathbf{Q}\mathbf{r}_j} \right) = \underbrace{\frac{1}{N} (\bar{b}^2 - \bar{b}^2)}_{\frac{d\sigma_{\text{inc}}}{d\Omega}} + \underbrace{\frac{1}{N} \bar{b}^2 \left| \sum_i e^{i\mathbf{Q}\mathbf{r}_i} \right|^2}_{\frac{d\sigma_{\text{coh}}}{d\Omega}} \quad (14.11)$$

14.1.1.1. Nuclear scattering. The simplest system of scatterers consist of only one isotope with nuclear spin I . As the spin of the neutron is $s = \pm 1/2$ only two orientations are possible: parallel spins of neutron and nuclei, i.e. a total spin of $J_{(+)} = I + 1/2$ or antiparallel spins, i.e $J_{(-)} = I - 1/2$. The corresponding scattering length are named $b_{(+)}$ and $b_{(-)}$.¹

The number of possible states for the total spin $J_{(\pm)}$ are $2J_{(+)} + 1 = 2I + 2$ and $2J_{(-)} + 1 = 2I$. In case of unpolarized neutrons and/or random oriented nuclear spins

¹For coherent scattering the spin of the neutrons keep constant in contrast to incoherent scattering where a part come along with a spin-flip. This can e.g. be used to change the ration between coherent and incoherent scattering.

parallel and antiparallel spin states have the same probability. The fraction $x_{(\pm)}$ of the scattering lengths $b_{(\pm)}$ is therefore proportional to the corresponding number of states

$$x_{(+)} = \frac{2J_{(+)}}{(2J_{(+)}) + (2J_{(-)})} = \frac{I+1}{2I+1} \text{ and } x_{(-)} = \frac{I}{2I+1} . \quad (14.12)$$

For the average scattering length \bar{b} we therefore get

$$\bar{b} = \sum_{i=(+),(-)} x_i b_i = \frac{1}{2I+1} [(I+1)b_{(+)} + I b_{(-)}] . \quad (14.13)$$

For a mixture of different elements and isotopes of type l with nuclear spin I_l and the fraction x_l (with $\sum_l x_l = 1$) the averages can be written as

$$\bar{b} = \sum_l \frac{x_l}{2I_l+1} [(I_l+1)b_{l(+)} + I_l b_{l(-)}] \quad (14.14)$$

$$\bar{b}^2 = \sum_l \frac{x_l}{2I_l+1} [(I_l+1) (b_{l(+)}^2) + I_l (b_{l(-)}^2)] . \quad (14.15)$$

14.1.1.2. Magnetic Scattering. In magnetic materials the contribution of the interaction between neutrons and atomic magnetic dipole moments to the scattering length has the same order of magnitude than the nuclear scattering length. The magnetic scattering is based on the interaction of the magnetic moment of the neutron μ_n with the magnetic moment of the scattering atom μ_A . The magnetic interaction potential $V(\mathbf{r})$ is described by

$$V(\mathbf{r}) = -\mu_n \cdot \mathbf{B}(\mathbf{r}), \quad (14.16)$$

whereby $\mu_n = \gamma \frac{e\hbar}{2m_p} \boldsymbol{\sigma} = \gamma \mu_N$ is the magnetic dipole moment² of the neutron, $\boldsymbol{\sigma}$ Pauli's spin operator, γ the neutron magnetic moment to nuclear magneton ratio³ and $\mathbf{B}(\mathbf{r})$ the magnetic field of an atom at the position of the neutron. An atom generates a magnetic field due to the magnetic dipole moment μ_S of its electrons $\mathbf{B}_S(\mathbf{r})$

$$\mathbf{B}_S(\mathbf{r}) = \nabla \times \mathbf{A} \text{ with } \mathbf{A} = \frac{\mu_0}{4\pi} \frac{\mu_S \times \mathbf{r}}{r^3} \quad (14.17)$$

and due to the orbital angular momentum of the electrons $\mathbf{l} = -\mathbf{p} \times \mathbf{r}$ which generates a field of $\mathbf{B}_L(\mathbf{r})$

$$\mathbf{B}_L(\mathbf{r}) = -\frac{\mu_0}{4\pi} \frac{2\mu_B}{\hbar} \frac{\mathbf{p} \times \mathbf{r}}{r^3} . \quad (14.18)$$

The magnetic interaction potential $V(\mathbf{r}) = -\mu_n \cdot (\mathbf{B}_S(\mathbf{r}) + \mathbf{B}_L(\mathbf{r}))$ is a weak long range potential which also can be treated with Born's approximation. Compared to the nuclear

²neutron magnetic moment: $\mu_n = -0.96623645 \times 10^{-26} \text{ JT}^{-1}$, neutron magnetic moment to Bohr magneton ratio: $\mu_n/\mu_B = -1.04187563 \times 10^{-3}$, nuclear magneton: $\mu_n = 5.05078343 \times 10^{-27} \text{ JT}^{-1}$, Bohr magneton: $\mu_B = \frac{e\hbar}{2m_e} = 927.400949 \times 10^{-26} \text{ JT}^{-1}$, proton mass: $m_p = 1.6726171 \times 10^{-27} \text{ kg}$, neutron mass: $m_n = 1.67492728 \times 10^{-27} \text{ kg}$, electron mass: $m_e = 9.1093826 \times 10^{-31} \text{ kg}$, elementary charge: $e = 1.60217653 \times 10^{-19} \text{ C}$, Planck constant over 2π : $\hbar = h/2\pi = 1.05457168 \times 10^{-34} \text{ J s}$

³neutron magnetic moment to nuclear magneton ratio $\gamma = \mu_n/\mu_N = 1.91304273$

scattering amplitude the corresponding magnetic scattering amplitude b_M is given by the Fourier transformation of the magnetic interaction potential $\mathcal{F}[V(\mathbf{r})]$

$$b_M = -\frac{m_n}{2\pi\hbar^2} \boldsymbol{\mu}_n \cdot \int d^3r e^{i\mathbf{Q}\mathbf{r}} (\mathbf{B}_S(\mathbf{r}) + \mathbf{B}_L(\mathbf{r})). \quad (14.19)$$

The Fourier transformation of the magnetic field is related in case of a static magnetic field to the Fourier transformation of the local magnetization $\mathbf{M}(\mathbf{Q}) = \mathcal{F}[\mathbf{M}(\mathbf{r})]$ [461] by

$$\mathbf{B}(\mathbf{Q}) = \mu_0 \frac{\mathbf{Q} \times [\mathbf{M}(\mathbf{Q}) \times \mathbf{Q}]}{Q^2} = \mu_0 \mathbf{M}_\perp(\mathbf{Q}), \quad (14.20)$$

whereby $\mathbf{M}_\perp(\mathbf{Q})$ is the component of $\mathbf{M}(\mathbf{Q})$ perpendicular to \mathbf{Q} and $\mu_0 = 4\pi 10^{-7}$ Vs/Am the magnetic constant. For the magnetic scattering amplitude⁴ b_M we find than

$$b_M = D_M \mu_0 \boldsymbol{\sigma} \cdot \mathbf{M}_\perp(\mathbf{Q}) \text{ with } D_M = -\gamma \frac{m_n}{2\pi\hbar^2} \mu_N = 2.31605 \times 10^{14} \frac{1}{\text{m}^2 \text{Tesla}}. \quad (14.21)$$

For scattering on magnetic structures always two interactions have to be considered, nuclear scattering which is caused by fluctuations in the number density and composition and magnetic scattering caused by fluctuations in amplitude and/or orientation of the local magnetization. In case of a preferred orientation, e.g. the direction of an external applied magnetic field \mathbf{H} , the magnetic scattering depends on the spin state $\boldsymbol{\sigma}$ of the neutron. If \mathbf{e}_x describes the direction of the preferred axis and (+) and (-) the neutron spin polarisation antiparallel and parallel to \mathbf{e}_x than the scattering can be described by four scattering processes; these are two spin non-flip (++,--) and two spin flip (+,-+) processes. Moon, Riste und Koehler [343] have shown that for coherent scattering the four scattering length are given by

$$b_{\pm\pm} = b_N \mp D_M \mu_0 M_{\perp x} \quad (14.22)$$

$$b_{\pm\mp} = -D_M \mu_0 (M_{\perp z} \pm i M_{\perp y}). \quad (14.23)$$

whereby b_N is the nuclear scattering length. In case of unpolarized neutrons the differential scattering cross-section can be written as

$$\frac{d\sigma_{\text{unp}}}{d\Omega}(\mathbf{Q}) = \frac{d\sigma_{\text{nuc}}}{d\Omega}(\mathbf{Q}) + \frac{d\sigma_{\text{mag}}}{d\Omega}(\mathbf{Q}), \quad (14.24)$$

because $(b_{++}^2 + b_{--}^2 + b_{+-}^2 + b_{-+}^2)/2 = b_N^2 + D_M^2 \mu_0^2 M_\perp^2$. For unpolarized neutrons the interference contribution only has an influence on the degree of polarization of the scattered neutrons but not on the scattering intensity.

⁴Frequently the magnetization is given in units of Bohr magnetons ($\mu_B = \frac{e\hbar}{2m_e} = 927.400949 \times 10^{-26}$ J/T, 1[J/T]=1[Am²]) per atomic volume Ω so that the magnetic scattering length density can be written as $b_M = D_\mu \sum_i c_i M_i / \Omega_i$ with $D_\mu = 2.69914 \times 10^{-15} \text{ m}^2$. The two constants are related via $D_\mu = D_M \mu_0 \mu_B$.

14.1.2. Scattering of x-ray at atoms. The scattering of x-rays on matter practically exclusively depends on the interaction of the incoming radiation with electrons. The contribution on the nuclei is negligible small because the mass of the nuclei is more than 10^3 times larger than the mass of an electron and the energy of the nuclear scattering more than 10^6 smaller than the energy of the scattering on electrons.

The frequency $\nu_0 = c/\lambda$ of the incoming x-ray beam is in general large against the resonance frequency of the electrons. In this case the electrons can be considered to be free and the special properties of the chemical binding are of no importance. These are the conditions for Thomson-scattering. J.J. Thomson developed a simple classical model for this type of scattering. Under the influence of an electric field of x-rays electrons start to oscillate. For an incoming plane and monochromatic wave with an electric field $\mathbf{E} = \mathbf{E}_0 e^{i(\mathbf{k}_0 \mathbf{r} - \omega t)}$ the amplitude E_s of a wave scattered on a free electron is

$$E_s = -E_0 \frac{e^2}{m_e c^2} \frac{1}{r} \sin \psi. \quad (14.25)$$

Hereby e and m_e are the charge⁵ and mass⁶ of the electron, respectively. c is the speed of light⁷, r the distance between sample and detector and ψ the angle between the direction of the accelerated electrons by the incoming wave and the direction of the scattered wave.

Analogously to the neutron scattering length for an electron the x-ray scattering length (far field of a Hertz dipole) is defined as

$$b_{\text{x-ray}} = \frac{e^2}{m_e c^2} \sin \psi = r_0 \sin \psi \quad (14.26)$$

whereby $r_0 = e^2/(m_e c^2) = 2.82 \times 10^{-13}$ cm is the classical electron radius. For small angle scattering $\psi \simeq \pi/2$ whereby the angle dependent polarization factor is approximately 1.

For calculating the scattering amplitude of an atom with Z electrons one has to sum up the scattered waves from the different electrons with the correct phase. To do this an electron density distribution $\rho_e(\mathbf{r})$ can be introduced which describes the time average probability distribution of the electron in the atom. The scattering amplitude of an atom is than

$$f_a(\mathbf{Q}) = r_0 \underbrace{\sum_{\text{polarization factor}} L(Q)}_{\sim 1} \int d\mathbf{r} \rho_e(\mathbf{r}) e^{i\mathbf{Q}\mathbf{r}} \stackrel{Q \rightarrow 0}{=} r_0 Z. \quad (14.27)$$

The charge distribution in an atom can be described in good approximation by a radial symmetric function so that

$$f_a(Q) = r_0 \int_0^\infty \frac{\sin Qr}{Qr} \rho_e(r) 4\pi r^2 dr \stackrel{Q \rightarrow 0}{=} r_0 \int_0^\infty \rho_e(r) 4\pi r^2 dr = r_0 Z. \quad (14.28)$$

In small angle scattering the scattering length of an atom is therefore $f_a = r_0 Z$ or in units of "electron units [e.u.]" $f = f_a/r_0 = Z$.

⁵ $e = 1.60217653 \times 10^{-19}$ C

⁶ $m_e = 9.1093826 \times 10^{-31}$ kg

⁷ $c = 299792458$ m s⁻¹

14.1.2.1. Anomalous scattering of x-rays. The relation $f = Z$ for atomic scattering length is only valid as long as the energy of the incoming radiation is much larger than the energy of the K-, L-, etc. shells. In case that the absorption edge of an atom is close to the energy of the incoming beam the scattering length has to be corrected by a dispersion term. In general the scattering length of an atom depends on the energy of the x-rays and is a complex number

$$f(E) = Z + f'(E) + i f''(E) \quad . \quad (14.29)$$

The correction terms f' and f'' change the scattering length f near a K_α absorption edge typically up to 30%. Figure 14.2 shows the energy dependency of the scattering length of iron f'_{Fe} und f''_{Fe} . The dispersion terms are related via the Karamer-Kronig relation

$$f'(E) = \frac{2}{\pi} \int_0^\infty dE' \frac{E' f''(E')}{E'^2 - E^2}. \quad (14.30)$$

In general the imaginary part f'' can be determined experimentally by the mass ab-

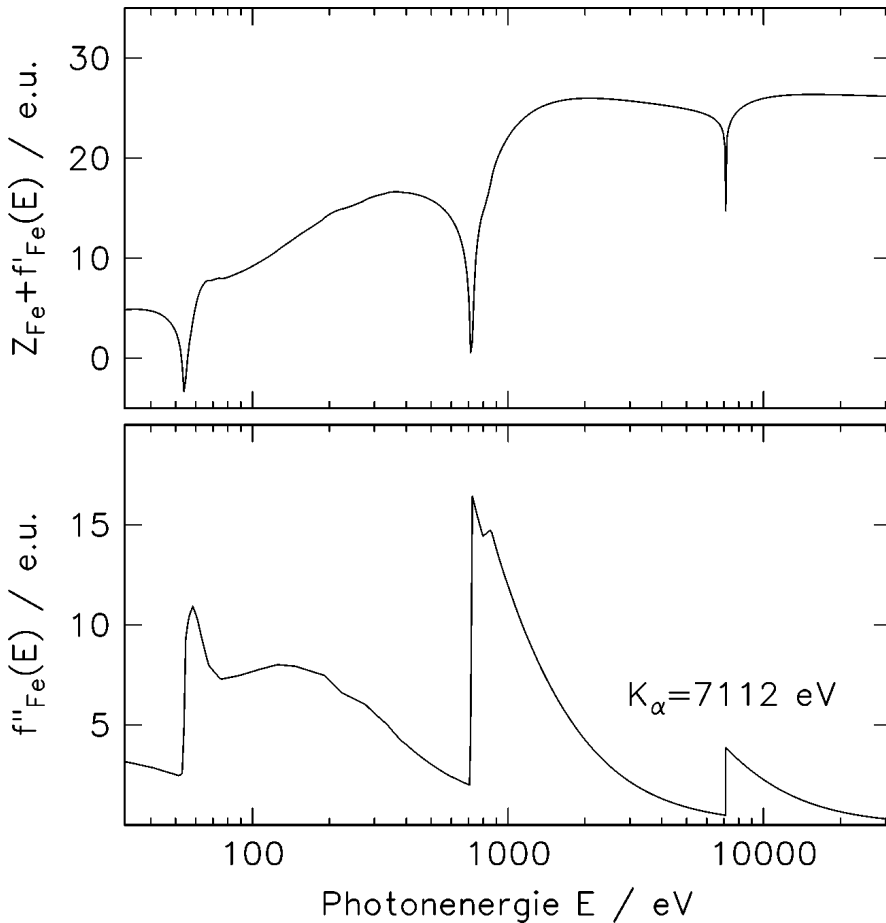


FIGURE 14.2. Energy dependence of the real and imaginary part of the scattering length of iron: $Z_{\text{Fe}} + f'_{\text{Fe}}(E)$ and $f''_{\text{Fe}}(E)$ ($Z_{\text{Fe}} = 26$)

sorption coefficient $\mu_m(E) = \frac{2N_A}{A} \lambda r_0 f''(E)$ (N_a Avogadro number, A mass of atom in

resonance) to calculate than with equation 14.30 the real part of the scattering length $f'(E)$.

14.2. Small angle scattering

In small angle scattering geometry the structural unit down to single atoms can not be resolved, only structures larger than several atomic layers can be seen by that method. Small angle scattering techniques measure the beam scattered close to forward direction whereby the beam divergence is in the order $\lambda/L \ll 1$. For a wavelength of $\lambda = 1 \text{ nm}$ and a characteristic dimension $L = V^{1/3}$ of the scatterer of about 10 nm the divergency of the beam is about $\lambda/L = 0.1 \text{ rad} \simeq 6.3^\circ$.

In principle with small angle scattering both information on size as well as shape of the scatterer and information on the relative arrangement of the scatterer can be obtained. In the following an overview of the theoretical basics to analyze small angle scattering data will be given.

In section 14.1 the scattering of an ensemble of atoms has been discussed. There interference terms between the waves scattered by the individual atoms were important for the differential scattering cross-section (eq. 14.7, 14.28).

$$\frac{d\sigma}{d\Omega}(\mathbf{Q}) = \frac{1}{N} \left| \sum_{j=1}^N b_j e^{i\mathbf{Q}\mathbf{r}_j} \right|^2 \quad \text{or} \quad \frac{d\sigma}{d\Omega}(\mathbf{Q}) = \frac{1}{N} \left| \sum_{j=1}^N f_{a,j}(\mathbf{Q}) e^{i\mathbf{Q}\mathbf{r}} \right|^2. \quad (14.31)$$

Small angle scattering normally does not resolve dimension down to atomic dimensions. Therefore the summation over the individual atoms can be replaced by an integration over the illuminated volume V :

$$\frac{d\sigma}{d\Omega}(\mathbf{Q}) = \frac{1}{N} \left| \int_V d\mathbf{r} \rho(\mathbf{r}) e^{i\mathbf{Q}\mathbf{r}} \right|^2 = \frac{1}{N} I(\mathbf{Q}), \quad (14.32)$$

whereby $\rho(\mathbf{r})$ is the local scattering length density and $I(\mathbf{Q})$ the scattering amplitude. The differential scattering cross-section is mathematically the square of the modulus of the Fourier transformation of the scattering length density. The scattering length density $\rho(\mathbf{r})$ is proportional to the locally averaged scattering potential $\bar{V}(\mathbf{r})$. Thats why equation 14.32 is except a constant identical to equation 14.6. The scattering intensity $I(\mathbf{Q}) = |z|^2 = z z^*$ can therefore be written as

$$I(\mathbf{Q}) = \iint d\mathbf{r}_1 d\mathbf{r}_2 \rho(\mathbf{r}_1) \rho^*(\mathbf{r}_2) e^{i\mathbf{Q}(\mathbf{r}_1 - \mathbf{r}_2)}. \quad (14.33)$$

By using the substitution $\mathbf{r} = \mathbf{r}_1 - \mathbf{r}_2$ one get

$$I(\mathbf{Q}) = \int d\mathbf{r} e^{i\mathbf{Q}\mathbf{r}} \underbrace{\int d\mathbf{r}_1 \rho(\mathbf{r}_1) \rho^*(\mathbf{r}_1 - \mathbf{r})}_{\Gamma(\mathbf{r}) = \rho(\mathbf{r}) \otimes \rho(\mathbf{r})} = \int d\mathbf{r} \Gamma(\mathbf{r}) e^{i\mathbf{Q}\mathbf{r}}. \quad (14.34)$$

$\Gamma(\mathbf{r})$ is the autocorrelation function⁸. In case of a real scattering length density eq. 14.34 is the convolution integral $\Gamma(\mathbf{r}) = \rho(\mathbf{r}) * \rho(\mathbf{r}) = \int d\mathbf{r}_1 \rho(\mathbf{r}_1) \rho(\mathbf{r}_1 - \mathbf{r})$ of the scattering length density and is called Patterson function⁹.

14.2.1. Autocorrelation function $\Gamma(\mathbf{r})$ and $\gamma(r)$. In the following we will make use of two simplifications. Firstly the scattering system is assumed to be isotropic. Hereby the isotropy can have its origin both in the shape of the scatterer or being a consequence of the temporal change of the particle orientation. The consequence is that $\Gamma(\mathbf{r})$ only depends on the modulus of r and $e^{i\mathbf{Q}\mathbf{r}}$ can be averaged over all orientations of \mathbf{r} . (The second simplification will follow further below)

14.2.1.1. *Isotropic averages.* If α is assigned to the angle between \mathbf{Q} and \mathbf{r} and if all orientations α are equal probable than the probability $p_\alpha d\alpha$ that \mathbf{Q} and \mathbf{r} include the angle α is equal to $\frac{1}{2} \sin \alpha d\alpha$.

$$p_\alpha d\alpha = \frac{2\pi R \sin \alpha}{4\pi R^2} R d\alpha = \frac{\sin \alpha}{2} d\alpha \quad (14.35)$$

The average of $e^{i\mathbf{Q}\mathbf{r}}$ over all orientations of \mathbf{r} is

$$\begin{aligned} \overline{e^{i\mathbf{Q}\mathbf{r}}}^{\mathbf{r}} &= \int_0^\pi d\alpha \frac{\sin \alpha}{2} e^{iQr \cos \alpha} = \frac{\sin Qr}{Qr} \\ &= \underbrace{\int_0^\pi d\alpha \frac{\sin \alpha}{2} \cos(Qr \cos \alpha)}_{\text{symmetric to } \alpha=\pi/2} + i \underbrace{\int_0^\pi d\alpha \frac{\sin \alpha}{2} \sin(Qr \cos \alpha)}_{\text{antisymmetric to } \alpha=\pi/2 \Rightarrow =0} \\ &= 2 \int_0^{\frac{\pi}{2}} d\alpha \frac{\sin \alpha}{2} \cos(Qr \cos \alpha) = \frac{1}{Qr} \int_0^{Qr} du \cos u = \frac{\sin Qr}{Qr} \end{aligned} \quad (14.36)$$

and equation 14.34 is simplified to

$$I(Q) = \int dr 4\pi r^2 \Gamma(r) \frac{\sin Qr}{Qr} . \quad (14.37)$$

14.2.1.2. *Absence of long range order.* As a second simplification it will be assumed that long range order is absent. The consequence is that the autocorrelation $\Gamma(r)$ becomes constant for large values of r . It converges to $\bar{\Gamma} = \bar{\rho}^2 V$. $\bar{\rho}$ is the average scattering

⁸Normally the autocorrelation function is defined as $\rho(\mathbf{r}) \otimes \rho(\mathbf{r}) = \int d\mathbf{r}_1 \rho(\mathbf{r}_1) \rho^*(\mathbf{r}_1 + \mathbf{r})$, so that in fact $\Gamma(\mathbf{r})$ should be $\Gamma(\mathbf{r}) = \rho(-\mathbf{r}) \otimes \rho(-\mathbf{r})$.

⁹Here the Patterson function is defined as the autocorrelation of the scattering length density $\rho(\mathbf{r})$. Instead of defining the cross-section via a scattering length density as in 14.34 in neutron scattering the differential cross-section is often defined as $d\sigma_{coh}(\mathbf{Q})/d\Omega = (\sigma_{coh}/4\pi N) \int d\mathbf{r} \rho(\mathbf{r}) \otimes \rho(\mathbf{r}) \exp(i\mathbf{Q}\mathbf{r})$, whereby $\sigma_{coh} = 4\pi \bar{b}^2$ is the coherent cross-section and $\rho(\mathbf{r})$ the particle number density. The Patterson function is than the autocorrelation of the particle number density. This function is independent of the scattering lengths and only dependent on the geometric arrangement of the scattering centers. The Fourier transformation of the Patterson function is therefore sometimes called Structure factor $S(\mathbf{Q})$ and is related in case of a static approximation to the differential cross-section by the equation $d\sigma_{coh}(\mathbf{Q})/d\Omega = (\sigma_{coh}/4\pi N) S(\mathbf{Q})$.

length density defined by

$$\int d\mathbf{r} (\rho(\mathbf{r}) - \bar{\rho}) = \int d\mathbf{r} \eta(\mathbf{r}) = 0 . \quad (14.38)$$

Structural information is therefore only contained in a finite range of $\Gamma(\mathbf{r})$ where it deviates from the average value $\bar{\Gamma}$. This is due to the fact that only a deviation of $\eta(\mathbf{r})$ from the average $\bar{\rho}$ leads to a scattering contribution for $Q \neq 0$. An additional constant value $\bar{\rho}$ only contributes to the scattering at $Q = 0$ and is therefore not accessible. Consequently the average scattering length density can be subtracted without loss of generality and only deviations $\eta(\mathbf{r}) = \rho(\mathbf{r}) - \bar{\rho}$ have to be considered. The autocorrelation function is therefore defined as

$$\gamma(r) = \frac{1}{V} \overline{\eta(\mathbf{r}) \otimes \eta(\mathbf{r})}^{\mathbf{r}} = \frac{1}{V} \overline{(\rho(\mathbf{r}) - \bar{\rho}) \otimes (\rho(\mathbf{r}) - \bar{\rho})}^{\mathbf{r}} \quad (14.39)$$

$$\Rightarrow I(Q) = V \int_0^\infty dr 4\pi r^2 \gamma(r) \frac{\sin Qr}{Qr} . \quad (14.40)$$

$V\gamma(\mathbf{r})$ is different from $\Gamma(\mathbf{r})$ due to the definition of $\bar{\rho}$ (eq. 14.38) only by a constant term $\bar{\rho}^2 V$, i.e. $V\gamma(\mathbf{r}) = \Gamma(\mathbf{r}) - \bar{\rho}^2 V$ because

$$\Gamma(\mathbf{r}) = \int d\mathbf{r}_1 \rho(\mathbf{r}_1) \rho^*(\mathbf{r}_1 - \mathbf{r}) = \int d\mathbf{r}_1 (\bar{\rho} + \eta(\mathbf{r}_1)) (\bar{\rho} + \eta(\mathbf{r}_1 - \mathbf{r}))^* \quad (14.41)$$

$$= \bar{\rho}^2 V + \underbrace{\int d\mathbf{r}_1 (\bar{\rho} \eta(\mathbf{r}_1) + \bar{\rho}^* \eta^*(\mathbf{r}_1 - \mathbf{r}))}_{= 0 \text{ due to def. of } \eta(\mathbf{r}) \text{ in eq. 14.38}} + \int d\mathbf{r}_1 \eta(\mathbf{r}_1) \eta^*(\mathbf{r}_1 - \mathbf{r}) \quad (14.42)$$

$$= \bar{\rho}^2 V + \gamma(\mathbf{r}) V . \quad (14.43)$$

14.2.1.3. *Limits $r = 0$ and $r = \infty$.* The limits $r = 0$ and $r \rightarrow \infty$ for the autocorrelation $\gamma(\mathbf{r})$ are $\gamma(0) = \bar{\eta}^2$ and $\gamma(\infty) = 0$. The limit $r \rightarrow \infty$ is zero because $\eta(\mathbf{r})$ is defined as the deviation of the average scattering length density $\bar{\rho}$. As long range correlation is assumed not to be present $\eta(\mathbf{r}) \otimes \eta(\mathbf{r}) \xrightarrow{r \rightarrow \infty} \bar{\eta}^2 = 0$. $\gamma(r)$ can be calculated by the inverse Fourier transformation of the scattering intensity $I(Q)$ (eq. 14.40)

$$V\gamma(r) = \frac{1}{2\pi^2} \int_0^\infty dQ Q^2 I(Q) \frac{\sin Qr}{Qr} . \quad (14.44)$$

An important special case is $r = 0$ for which equation 14.44 can be simplified to

$$V\gamma(0) = V\bar{\eta}^2 = \frac{1}{2\pi^2} \int_0^\infty dQ Q^2 I(Q) = \frac{\tilde{Q}}{2\pi^2} . \quad (14.45)$$

The integration of the intensity $I(Q)$ in reciprocal space is therefore directly related to the average quadratic deviation of the scattering length density $\bar{\eta}^2$ but independent to the shape of the scatterers. If for example the scattering particle undergoes deformation the scattering pattern may change drastically but the integral \tilde{Q} in eq. 14.45 keeps invariant against such a deformation.

14.2.2. Volume fraction. The average quadratic deviation of the scattering length density is directly related in a two-phase system to the scattering contrast $\Delta\eta$ and volume fraction f_p of one or the other $(1 - f_p)$ phase. The average quadratic deviation of the scattering length density is defined as

$$\overline{\eta^2} = \eta_1^2 f_p + \eta_2^2 (1 - f_p), \quad (14.46)$$

whereby η_1 and η_2 are the scattering length density differences of the two phases from the average value $\bar{\rho}$ and the scattering contrast is than defined as $\Delta\eta = \eta_1 + \eta_2$. The average value $\bar{\rho}$ is given by

$$\begin{aligned} \bar{\rho} = (\bar{\rho} - \eta_1) f_p + (\bar{\rho} + \eta_2)(1 - f_p) &\Leftrightarrow f_p (\eta_1 + \eta_2) = f_p \Delta\eta = \eta_2 \\ \text{or } (1 - f_p) \Delta\eta &= \eta_1 . \end{aligned} \quad (14.47)$$

Replacing η_1 and η_2 in eq. 14.46 leads to

$$\overline{\eta^2} = \Delta\eta^2 f_p (1 - f_p). \quad (14.48)$$

The second moment of the scattering intensity, the so-called scattering invariant \tilde{Q} from eq. 14.45, can therefore be related to the volume fractions of the two phases f_p and $(1 - f_p)$ by

$$\tilde{Q} = \int dQ Q^2 I(Q) = 2\pi^2 V \Delta\eta^2 f_p (1 - f_p) . \quad (14.49)$$

Due to the Babinet principle in a scattering experiment the volume fractions can not be uniquely assigned to one or the other phase. A system with exchanged phases would have the same invariant A unique solution of eq. 14.49 for the volume fraction can only be obtained if either one already knows from somewhere else that the volume fraction of one phase is much smaller than the volume fraction of the other (dilute case) or if time resolved experiments are performed during the formation of the structure and when it is known that one phase is growing on the cost of the other one (Ostwald ripening).

14.2.3. Interparticle interferences. The square of the Fourier transformation of the scattering length density of a sample with a volume V is equal to the scattering intensity $I(\mathbf{Q})$

$$I(\mathbf{Q}) = \left| \int_V d\mathbf{r} \rho(\mathbf{r}) e^{i\mathbf{Q}\mathbf{r}} \right|^2 . \quad (14.50)$$

The integration has to be carried out over the whole illuminated sample volume V . If the sample volume contains N particles embedded in a matrix with a constant scattering length density ρ_M and if \mathbf{R}_i defines the center of particle i with a constant scattering length density $\rho_{P,i} = \Delta\eta_i + \rho_M$ the scattering intensity can be written as

$$\begin{aligned} I(\mathbf{Q}) &= \left| \sum_{i=1}^N F_i(\mathbf{Q}) e^{i\mathbf{Q}\mathbf{R}_i} \right|^2 \\ \text{with } F_i(\mathbf{Q}) &= \int_{V_i(\mathbf{R}_i)} d\mathbf{r} \Delta\eta_i e^{i\mathbf{Q}(\mathbf{r}-\mathbf{R}_i)} = \Delta\eta_i \int_{V_i(\mathbf{0})} d\mathbf{r} e^{i\mathbf{Q}\mathbf{r}} = \Delta\eta_i V_i f_i(\mathbf{Q}). \end{aligned} \quad (14.51)$$

$V_i(\mathbf{R}_i)$ describes the integration volume of scatterer i located at \mathbf{R}_i and $V_i(\mathbf{0})$ describes the integration volume of the scatterer i moved to the origin of the coordinate system.

$\Delta\eta_i$ and V_i are the scattering contrast and particle volume, respectively. The square of the modulus in eq. 14.51 can be rewritten to

$$\begin{aligned} I(\mathbf{Q}) &= \sum_{i=1}^N \sum_{j=1}^N F_i(\mathbf{Q}) F_j^*(\mathbf{Q}) e^{i\mathbf{QR}_{ij}} \\ &= \sum_{i=1}^N |F_i(\mathbf{Q})|^2 + \\ &\quad \underbrace{2 \sum_{i=1}^N \sum_{j>i}^N [\Re(F_i(\mathbf{Q}) F_j^*(\mathbf{Q})) \cos \mathbf{QR}_{ij} - \Im(F_i(\mathbf{Q}) F_j^*(\mathbf{Q})) \sin \mathbf{QR}_{ij}]}_{\Psi(\mathbf{Q})} \end{aligned} \quad (14.52)$$

The first term for which $i = j$ the phase factor is identical to 1 and describes the sum of the scattering intensity of individual particles. The double sum in the second term describes interference effects of the scattering amplitudes scattered from different particles which depends on their relative arrangement $\mathbf{R}_{ij} = \mathbf{R}_i - \mathbf{R}_j$. The scattering amplitude $F_i(\mathbf{Q})$ is among other things dependent on the scattering contrast $\Delta\eta_i$ and on the normalized form factor $F_i(\mathbf{Q})/\Delta\eta_i V_i = f_i(\mathbf{Q})$, whereby $f_i(\mathbf{Q})$ is a real-valued function with $f_i(Q = 0) = 1$. Analytical expressions for scattering intensities $i_0(Q) = \overline{|f(Q)|^2}$ of simple geometric bodies are listed in the chapter 3. In case $\Delta\eta_i$ is complex valued, i.e. the scatterer has an absorption contrast $\Delta\eta''_i$, the scattering contrast can be written as $\Delta\eta_i = \Delta\eta'_i + i\Delta\eta''_i$ and for the interference term we get

$$\begin{aligned} \Psi(\mathbf{Q}) &= 2 \sum_{i=1}^N \sum_{j>i}^N f_i(\mathbf{Q}) f_j(\mathbf{Q}) V_i V_j \\ &\quad \times [(\Delta\eta'_i \Delta\eta'_j + \Delta\eta''_i \Delta\eta''_j) \cos \mathbf{QR}_{ij} - (\Delta\eta'_i \Delta\eta''_j - \Delta\eta''_i \Delta\eta'_j) \sin \mathbf{QR}_{ij}] \end{aligned} \quad (14.53)$$

If now all particle have an identical scattering contrast $\Delta\eta = \Delta\eta_i = \Delta\eta_j$ we get for the scattering intensity (eq. 14.51) the expression

$$\begin{aligned} I(\mathbf{Q}) &= \sum_{i=1}^N V_i^2 (\Delta\eta'^2 + \Delta\eta''^2) |f_i(\mathbf{Q})|^2 \\ &\quad + 2 \sum_{i=1}^N \sum_{j>i}^N f_i(\mathbf{Q}) f_j(\mathbf{Q}) V_i V_j (\Delta\eta'^2 + \Delta\eta''^2) \cos \mathbf{QR}_{ij} \end{aligned} \quad (14.54)$$

For identical scattering contrasts there is consequently no interference between the scattering amplitude of waves scattered at the real and at the imaginary (absorption) part of the scattering contrast.

14.2.3.1. Isotropic ensemble of particles. In the following we assume as another simplification an isotropic ensemble of particles. Such a system of scatterer is defined as follows: If \mathbf{R}_i defines the position of any particle i and \mathbf{R}_{ij} is the difference vector between the position of particle i and j than a system of particles is called isotropic if all vectors \mathbf{R}_{ij} of the same length will take with equal probability any direction. Under this simplification the interference term $\Psi(\mathbf{Q})$ in eq. 14.53 can be averaged over all directions \mathbf{R}_{ij} . This average yield for $\overline{\sin \mathbf{QR}_{ij}}^{\mathbf{R}_{ij}} = 0$ and for $\overline{\cos \mathbf{QR}_{ij}}^{\mathbf{R}_{ij}} = \frac{\sin Q R_{ij}}{Q R_{ij}}$ (compare

with eq. 14.37). The interference term can then be written as

$$\Psi(\mathbf{Q}) = 2 \sum_{i=1}^N \sum_{j>i}^N f_i(\mathbf{Q}) f_j(\mathbf{Q}) V_i V_j (\Delta\eta'_i \Delta\eta'_j + \Delta\eta''_i \Delta\eta''_j) \frac{\sin QR_{ij}}{QR_{ij}}. \quad (14.55)$$

Therefore also for an isotropic ensemble of scatterers no interferences between waves scatterer at the real and imaginary part of the scattering contrast disappears as already shown for systems of particles with identical scattering contrast.

14.2.4. Influence of the relative arrangement of scatterers on interparticle interferences. The expression for $\Psi(\mathbf{Q})$ can be further simplified if the scattering system consist of identical particles which fulfill the condition that for all of them each orientation be likewise probable and furthermore the relative position of two particles do not have an influence on their orientation. The second part of the assumption is for radial symmetric particle automatically fulfilled. However, in case of a system of close packed ellipsoidal particles with half axis R , R and νR with $\nu > 1$ distance of $2R$ between the centers of the ellipsoids are possible, but for such an arrangement not all orientations of the ellipsoids are allowed anymore. That means that the relative distance has an influence on allowed orientations of the particles. The general case without the restrictions made in this paragraph are discussed by Guinier and Fournet in [177]. For only slightly anisotropic and not to closely packed systems the assumptions made here are at least fulfilled in first approximation. Under the made assumptions the averaging over the particle orientations can be separated from the averaging of the particle positions. As a result from the average one gets for the scattering intensity

$$\overline{I(Q)} = N \overline{|F(Q)|^2} + 2 \left| \overline{F(Q)} \right|^2 \sum_{i=1}^N \sum_{j>i}^N \frac{\sin QR_{ij}}{QR_{ij}} \quad (14.56)$$

For low concentrations this averaging is in first approximation also valid for particles with a size distribution. The probability to find a particle at the position \mathbf{R}_i is in average $\frac{N}{V} d\mathbf{R}_i$ and the probability to find at the same time another particle at position \mathbf{R}_j is $\frac{N}{V} d\mathbf{R}_i \frac{N}{V} d\mathbf{R}_j$. A deviation from this is considered by $P(R_{ij})$ so that the double sum in eq. 14.56 can be written as

$$\sum_{i=1}^N \sum_{j>i}^N \frac{\sin QR_{ij}}{QR_{ij}} = \iint_{VV} \frac{\sin QR_{ij}}{QR_{ij}} P(R_{ij}) \frac{N^2}{V^2} d\mathbf{R}_i d\mathbf{R}_j. \quad (14.57)$$

For isotropic media the function $P(R_{ij})$ is independent of the indices i and j and only a function of the distance R . $P(R)$ has the property to converge for large distance against one. By the substitution $P(R) = 1 - (1 - P(R))$ one gets for the interference term

$$\Psi(Q) = \left| \overline{F(Q)} \right|^2 \frac{N^2}{V^2} \iint_{VV} \frac{\sin QR_{ij}}{QR_{ij}} d\mathbf{R}_i d\mathbf{R}_j \quad (14.58)$$

$$- \left| \overline{F(Q)} \right|^2 \frac{N^2}{V^2} \iint_{VV} \frac{\sin QR_{ij}}{QR_{ij}} (1 - P(R_{ij})) d\mathbf{R}_i d\mathbf{R}_j. \quad (14.59)$$

The first term can be interpreted as the scattering of a particle with the volume V and the average scattering contrast $\overline{F(Q)} \frac{N}{V}$. As the illuminated sample volume V is relatively large this contribution is practically zero for all experimental accessible scattering angles.

As for isotropic media the integration over $d\mathbf{R}_i$ is independent from the integration over $d\mathbf{R}_j$ and $(1 - P(R))$ quickly converges against zero the first integration in the second term (neglecting side effects) can be written as

$$\int_0^\infty dR \frac{\sin QR}{QR} (1 - P(R)) \frac{N^2}{V^2} 4\pi R^2. \quad (14.60)$$

The second integration only yields an additional multiplication factor V . Finally one gets for the scattering intensity the expression

$$\overline{I(Q)} = N \left\{ \overline{|F(Q)|^2} - \overline{|F(Q)|}^2 \underbrace{\frac{N}{V} \int dR 4\pi R^2 (1 - P(R)) \frac{\sin QR}{QR}}_{\Upsilon(Q)} \right\}. \quad (14.61)$$

14.2.4.1. Formula from Prins and Zernicke. For radial symmetric identical scatterer the square of the average form factor $\overline{|F(Q)|^2}$ and the average of the squared form factor $\overline{|F(Q)|^2}$ are the same so that one gets for the expression from Prins and Zernicke [541] and from Debye und Mencke [104]

$$\overline{I(Q)} = N F^2(Q) \underbrace{\left\{ 1 - \frac{N}{V} \int dR 4\pi R^2 (1 - P(R)) \frac{\sin QR}{QR} \right\}}_{S(Q)=1-\Upsilon(Q)}. \quad (14.62)$$

The problem of applying eq. 14.61 or 14.62 is the evaluation of $P(R)$. $P(R)$ depends on the geometric arrangement of the scatterer. For liquid emulsions the geometric arrangement can be related to thermodynamic quantities like concentration, temperature and interaction potential between the particles. In a theory of Raman [406] the geometric arrangement is associated to the interaction potential $U(r)$ in a simple way. According to his theory the potential is the sum of two-body interactions and he finds for $P(r)$ the relation $P(r) = \exp(-U(r)/kT)$. For larger concentrations many-body interactions have to be taken into account. In a more general theory of Born and Green [47] three-body interactions are at least considered in first approximation and they find for the scattering intensity the expression

$$\begin{aligned} \overline{I(Q)} &= N \left\{ \overline{|F(Q)|^2} + \overline{|F(Q)|}^2 \frac{\chi(Q)}{\frac{V}{N}(2\pi)^{-3/2} - \chi(Q)} \right\} \\ \text{with } \chi(Q) &= \sqrt{\frac{2}{\pi}} \int_0^\infty dr \left[e^{-U(r)/kT} - 1 \right] r^2 \frac{\sin Qr}{Qr}. \end{aligned} \quad (14.63)$$

For a simple hard sphere model with the interaction potential $U(r) = \begin{cases} 0 & \text{for } r > 2R \\ \infty & \text{for } r \leq 2R \end{cases}$ the scattering intensity can be calculated analytically. According to Raman's theory Debye calculates for the scattering intensity of spheres with a radius R and a volume V_P the expression

$$\overline{I(Q)} = N K^2(QR) \left\{ 1 - 8N \frac{V_P}{V} K(2QR) \right\}, \quad (14.64)$$

whereby $K(x)$ is the scattering function of a sphere given in section 3.1.1. Following the theory of Born and Green one gets a similar expression

$$\overline{I(Q)} = N K^2(QR) \left\{ 1 + 8N \frac{V_p}{V} K(2QR) \right\}^{-1}. \quad (14.65)$$

Nonetheless both theories are only valid for monodisperse systems of scatterer. In practice, however, most scattering systems have a more or less pronounced size distribution and frequently also an additional variety of shapes. For such systems the interaction potential can not be expressed in a closed form. One has to introduce for each pair of particle type a separate potential [10] which complicates the analytical treatment a lot.

14.2.4.2. Isolate particles. A system of isolate particles is characterized by its property that the positions of a particle is not influenced by the positions of any other particle. For this case the interaction potential $U(r)$ and consequently also $\chi(Q)$ is identical zero. Therefore the expression for the scattering intensity simplifies to

$$I(Q) = N \overline{|F(Q)|^2} \quad \text{or} \quad I(\mathbf{Q}) = \sum_{i=1}^N |F_i(\mathbf{Q})|^2. \quad (14.66)$$

The total scattering intensity is simply the sum of the intensity scattered by the individual particles. A system of non-interacting particles can be realized by diluting the system. Thereby the average distance between the particles is increased and the interaction potential becomes negligible small and does not influence anymore the arrangement of the scatterer.

14.2.4.3. Polydisperse System of isolated particles. The scattering function of a polydisperse system of isolated particles is determined by the shape and size of the particles. In a scattering experiment it is not possible to separate both quantities at the same time. In the data analysis one has to assume one of the quantities either the shape or the size distribution to get then the other quantity. Normally the shape is assumed whereby the size distribution is than obtained from the scattering curve [159, 511]. To get an information about the shape one normally need a system of identical particles, like for example a system of identical proteins. An additional but known size distribution would smear out the scattering too much to still allow to extract confidential information about the particle shape. The scattering intensity of a system of isolated particles of different shape and a size distribution is given by

$$I(\mathbf{Q}) = \sum_{\mu=1}^M \int N_{\mu}(R) \overline{|F_{\mu}(Q, R)|^2} dR, \quad (14.67)$$

whereby $N_{\mu}(R)$ is the size distribution of particles of type μ and $F_{\mu}(Q, R)$ its form factor. Form factor of simple objects are listed in chapter 3 and frequently used size distributions in chapter 7.

14.2.5. Influence of $N(R)$ and $F(Q, R)$ on interparticle interferences. Interparticle interferences in small angle scattering signals have been described in eq. 14.61 and 14.62 by

$$\overline{I(Q)} = N \overline{|F(Q)|^2} \left\{ 1 + \frac{\overline{|F(Q)|^2}}{\overline{|F(Q)|^2}} (S(Q) - 1) \right\} \quad (14.68)$$

Hereby $S(Q)$ describes the influence of the relative arrangement of the scatterers on $\overline{I(Q)}$ and can be calculated by the interaction potential between the scattering particles (eq. 14.63). Interparticle interferences depends next to the relative arrangement also on the square of the average form factor $|\overline{F(Q)}|^2$. Only for the case of identical and spherical symmetric scatterer the relation $|\overline{F(Q)}|^2 \equiv |\overline{F(Q)}|^2$ is valid. In this case the interparticle interferences only depends on $S(Q)$. For particles with an irregular shape, however, the two averages are different and depends both on the size distribution as well as on the particle shape and their orientation distribution. For such systems the condition for the derivation the relation from Prins and Zernicke 14.61 namely the independency of orientation and size for higher concentrations is not anymore fulfilled. This condition allowed in eq. 14.56 to separate the averaging of the particle positions from the averaging of the form factor. Nevertheless the principle influence of a irregular particle shape and a size distribution can be made clear by the means of eq. 14.68. For judging their influence the ratio $|\overline{F(Q)}|^2/|\overline{F(Q)}|^2$ is considered.

Taking for example a system of identical but random oriented rotational ellipsoids with the half axis $R, R, \nu R$ the ratio of the two averages is shown in figure 14.3 together with the scattering intensity $|\overline{F(Q)}|^2$ of the corresponding ideal dilutes system. The figure shows that the ratio decreases for larger scattering vectors Q the more the shaper of the rotational ellipsoid is different from the ideal spherical case ($\nu = 1$). An irregular particle shape already is sufficient to reduce the influence interparticle interferences.

Accordingly also the particle size distribution give rise to a difference in the averages $|\overline{F(Q)}|^2$ and $|\overline{F(Q)}|^2$. Figure 14.3b shows the ratio of the two averages of spherical scatterers with a lognormal size distribution of different width as a function of Q . For $Q = 0$ the ratio is given by $|\overline{F(Q)}|^2/|\overline{F(Q)}|^2 = \exp(-9\sigma^2)$. One can see that the width of the size distribution strongly reduces the interference effect [494].

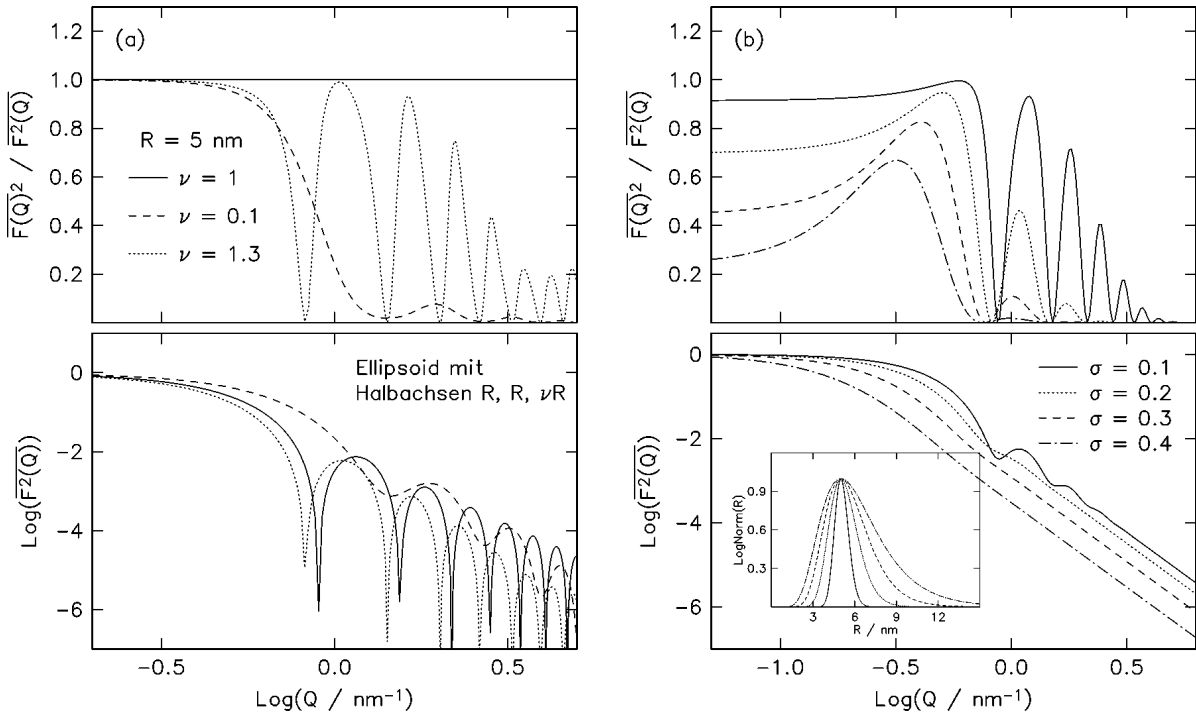
In general one can say that each kind of disorder reduces interferences. The disorder can have its origin in a random arrangement of particles (dilute systems), in an orientation distribution of irregular shaped particles, or also in a size distribution.

14.2.6. Scattering laws and structural parameter. In this section a series of useful scattering laws are presented, which are useful for a simple analysis of experimental data and which allow an easy determination of structural parameters. [177].

14.2.6.1. *Porod volume.* The ratio of the scattering intensity in forward direction $I(Q = 0) = N V_P^2 \Delta\eta^2$ and the scattering invariant $\tilde{Q} = 2\pi^2 \Delta\eta^2 V f_p (1 - f_p)$ can be used to determine the particle volume V_P (V describes the illuminated sample volume). $f_p V = N V_P$ corresponds to the total volume of all scatterers whereby the particle volume V_P can be calculated by

$$\frac{V_P}{1 - f_p} \stackrel{f_p \ll 1}{\approx} V_P = 2\pi^2 \frac{I(Q = 0)}{\tilde{Q}}. \quad (14.69)$$

The measurement of the scattering curve in relative units is therefore sufficient to determine the volume of a homogeneous scatterer. Sources of errors for this way of determination of particle sizes are the extrapolation into forward direction und more important the extrapolation to large scattering angles (Q^{-4} -extrapolation). Furthermore for large volume fractions f_p the particle volume has to be eventually corrected by a prefactor $1/(1 - f_p)$ which is not always known.



(A) The influence of irregular particle shapes on $|\overline{F(Q)}|^2 / |\overline{F(Q)}|^2$ is shown for an example of random orientated rotational ellipsoids with the half axis $R, R, \nu R$ for $\nu = 1, 0.1$, and 1.3.

(B) Influence of a particle size distribution $\text{LogNorm}(R) = \exp(-(\ln \mu - \ln R)^2 / (2\sigma^2))$ of the widths $\sigma = 0.1, 0.2, 0.3, 0.4$ for $\mu = 5 \text{ nm}$ on $|\overline{F(Q)}|^2 / |\overline{F(Q)}|^2$.

FIGURE 14.3. For identical and spherical symmetric scatterers the ratio $|\overline{F(Q)}|^2 / |\overline{F(Q)}|^2 \equiv 1$. Interparticle interferences depend then only on the relative positions of the scatterers. Size distribution and irregular shapes reduce these interference effects.

14.2.6.2. Radius of gyration and Guinier approximation. The scattering intensity for small angles can be approximated in a series expansion by replacing the expression $\frac{\sin Qr}{Qr}$ in eq. 14.40 by a McLaurin series which leads to

$$I(Q) = V \int 4\pi r^2 \gamma(r) \left[1 - \frac{Q^2 r^2}{3!} + \frac{Q^4 r^4}{5!} - \dots \right] dr , \quad (14.70)$$

i.e. $I(Q)$ is expanded by moments $\overline{r^n}$ of $\gamma(r)$. The first term corresponds to the scattering intensity of $Q = 0$. For the second term Guinier and Fournet [177] have shown, that it can be related to the gyration radius of the scattering length density R_G by

$$V \int 4\pi r^2 \frac{Q^2 r^2}{3!} \gamma(r) dr = I(0) \frac{Q^2 R_G^2}{3} \Rightarrow I(Q) = I(0) \left(1 - \frac{Q^2 R_G^2}{3} \right) \quad (14.71)$$

with $R_G^2 = \int \eta(r) r^2 dr / \int \eta(r) dr$. Up to the term of Q^4 this series expansion at the beginning of the scattering curve is identical to the series expansion of an exponential

function which then leads to the well known Guinier approximation

$$I(Q) = I(0) e^{-Q^2 R_G^2 / 3}. \quad (14.72)$$

The Guinier law is valid for any particle shape which is roughly isodiametric. For flat or elongated structures the Guinier law has to be corrected slightly [122, 177]. The radius of gyration for a sphere with radius R is given by $R_G = \sqrt{3/5} R$. The Guinier law is valid in the scattering vector interval $0 < Q < 1/R_G$.

14.2.6.3. Correlation length. Another characteristic quantity, which can be easily extracted from the scattering curve $I(Q)$ is the correlation length l_c . The correlation length is defined as the average width of the correlation function $\gamma(r)$:

$$l_c = \frac{2}{\gamma(0)} \int \gamma(r) dr. \quad (14.73)$$

Together with the definition of the scattering invariant \tilde{Q} in eq. 14.49 and the relation between $I(Q)$ and $\gamma(r)$ in eq. 14.44 this results to

$$\begin{aligned} l_c &= \frac{2}{\frac{1}{2\pi^2 V} \int_0^\infty Q^2 I(Q) dQ} \int \frac{1}{2\pi^2 V} \int_0^\infty Q^2 I(Q) \frac{\sin Qr}{Qr} dQ dr \\ &= \frac{2}{\int_0^\infty Q^2 I(Q) dQ} \int_0^\infty Q^2 I(Q) \int_0^\infty \frac{\sin Qr}{Qr} dr dQ \\ &= \frac{2}{\int_0^\infty Q^2 I(Q) dQ} \int_0^\infty Q^2 I(Q) \frac{\pi}{2Q} dQ \\ &= \pi \frac{\int Q I(Q) dQ}{\int Q^2 I(Q) dQ} . \end{aligned} \quad (14.74)$$

A sphere with radius R has therefore a correlation length of $l_c = \frac{3}{2} R$.

14.2.6.4. Porod law and specific surfaces. The Porod law describes the scattering behavior at large Q values. As the scattering intensity $I(Q)$ and the correlation function $\gamma(r)$ are related via the Fourier transformation the intensity $I(Q)$ is determined at large values of Q mainly by $\gamma(r)$ at small r . For small r the correlation function $\gamma(r)$ can be expanded in a Taylor series and one gets according to Guinier and Fournet [177]

$$\frac{\gamma(r)}{\gamma(0)} = 1 - \frac{1}{4} \frac{S}{V} + \dots , \quad (14.75)$$

whereby S is the total surface of all scatterer in the illuminated sample volume V . Eq. 14.75 together with 14.40 result for large Q values into the Porod law

$$I(Q) \longrightarrow \Delta\eta^2 \frac{2\pi S}{Q^4}. \quad (14.76)$$

In case of a system of N identical spheres with radii R a scattering contrast $\Delta\eta$ this law can be easily verified. The scattering intensity of N spherical particles is given by

$$I(Q) = N \left[\Delta\eta^2 \frac{4}{3} \pi R^3 \frac{\sin QR - QR \cos QR}{(QR)^3} \right]^2 \quad (14.77)$$

in the limit $Q \rightarrow \infty$ we get

$$\lim_{Q \rightarrow \infty} I(Q)(QR)^4 = N \left[\Delta\eta \frac{4}{3}\pi R^3 3 \frac{\sin QR - QR \cos QR}{(QR)^3} \right]^2 (QR)^4 \quad (14.78)$$

$$\rightarrow N [\Delta\eta 4\pi R^3]^2 \cos^2 QR \quad (14.79)$$

Due to resolution limits the oscillations normally smear out in average so that

$$I(Q) \rightarrow N \frac{[\Delta\eta 4\pi R^3]^2}{2(QR)^4} = N \Delta\eta^2 \frac{2\pi A_{sp}}{Q^4} = \Delta\eta^2 \frac{2\pi S}{Q^4} \quad (14.80)$$

where $A_{sp} = 4\pi R^2$ is the area of the sphere's surface and $NA_{sp} = S$ the total surface of all spheres in the beam. By scaling the scattering intensity on \tilde{Q} one obtains an expression for the specific surface S/V of

$$\lim_{Q \rightarrow \infty} \pi \frac{I(Q)}{\tilde{Q}} Q^4 f_p (1 - f_p) = \frac{S}{V}. \quad (14.81)$$

The Porod law can be applied to all systems having sharp interfaces.

CHAPTER 15

Experimental Setup of a Small Angle Scattering Instrument

15.1. SANS-Camera

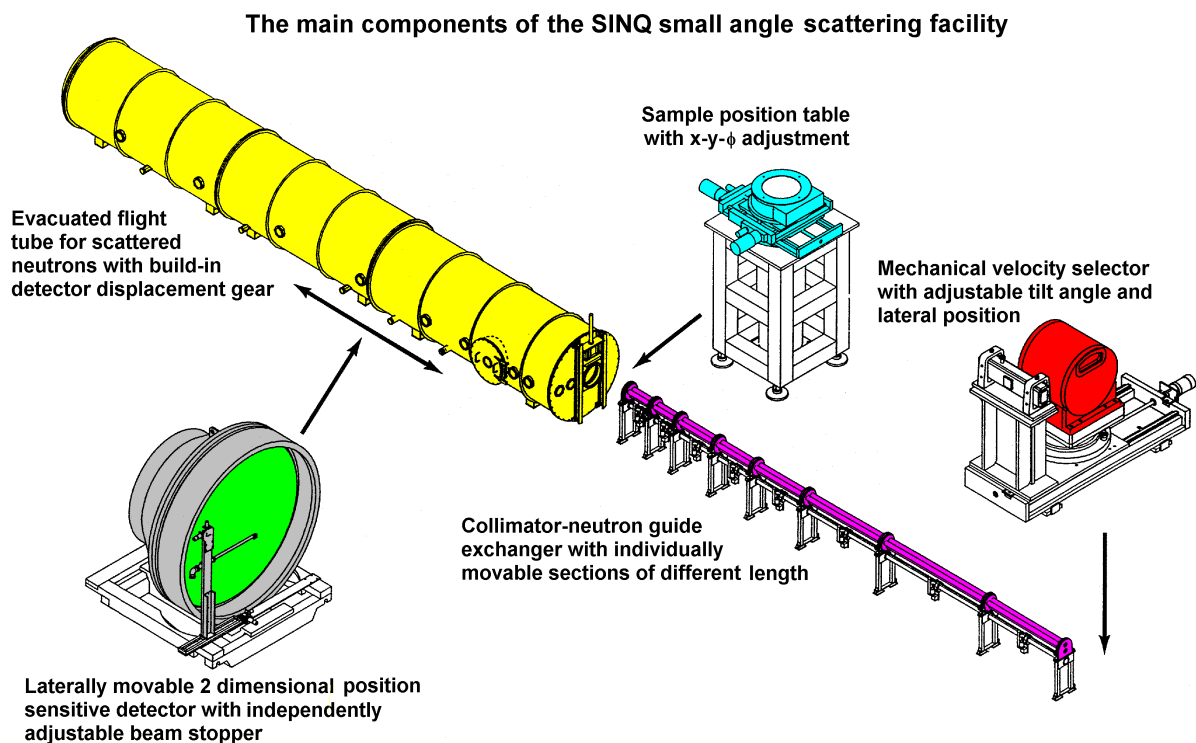


FIGURE 15.1. SANS-1 instrument at PSI, Switzerland

15.2. SAXS-Camera

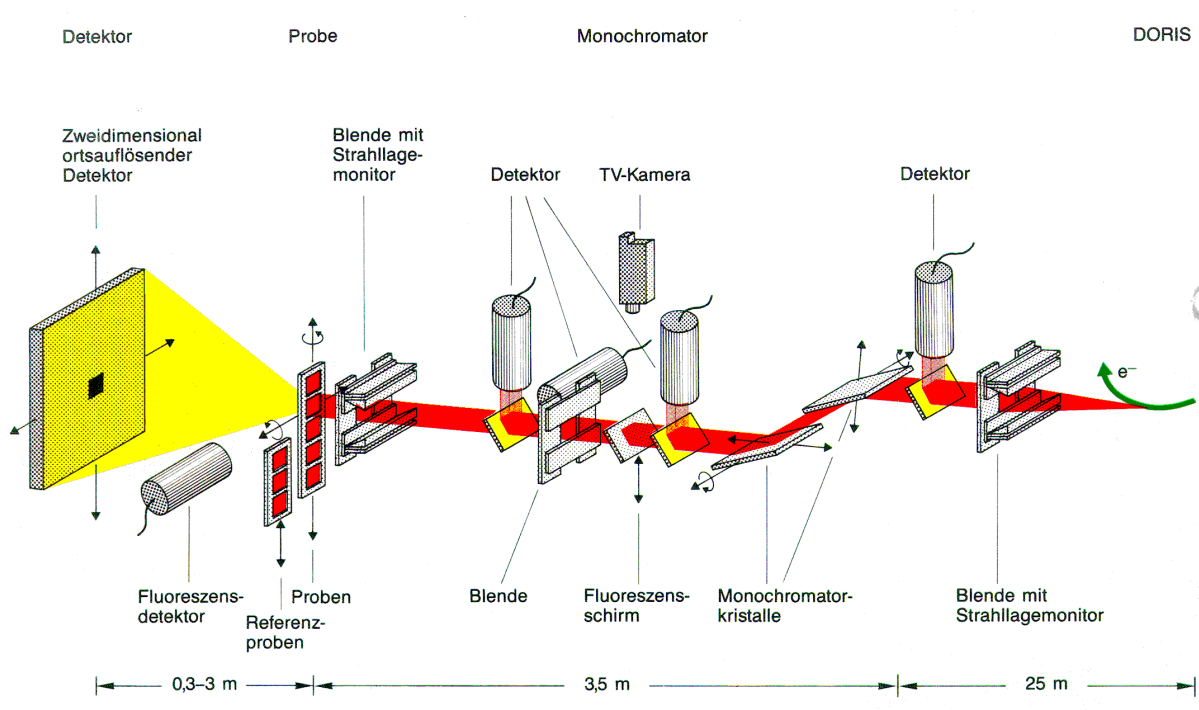


FIGURE 15.2. Small angle x-ray scattering instrument Jusifa at the synchrotron light source HASYLAB in Hamburg

CHAPTER 16

Data Reduction in SAS

16.1. Correction and Normalization of SANS-Raw data

A detector of a small angle scattering camera measures the superposition of intensities of different origin:

- (1) Background noise I_B
- (2) Scattering of the empty sample holder I_H
- (3) scattering of the isolated sample I_S

Furthermore the detector elements can have different efficiencies ϵ_i . To determine the differential cross-section of the sample all the different contribution to the total scattering intensity have to be considered and determined separately by different measurements. The quantity to be known is the scattering contribution of the isolated sample I_S , which in general can not be measured directly. Experimental accessible scattering contributions are the scattering of the sample in the sample holder I_{S+H} , the contribution of the empty sample holder I_H and the background noise I_B . From this experimental accessible data the wanted scattering contribution of the isolated sample has to be determined.

16.1.1. Contribution of the isolated sample. The intensity of the incident beam will be attenuated by absorption and scattering effects within the sample. Also the scattered neutrons will be further attenuated on their residual path through the sample. The measured intensity in a detector element i is given by

$$I_{S,i}^0 = \int_0^d dx \Phi_0 \Delta\Omega_i \epsilon_i e^{-\alpha x} A \rho e^{-\frac{\alpha(d-x)}{\cos\theta}} \left\{ \frac{d\sigma_{coh}}{d\Omega} + \frac{d\sigma_{inc}}{d\Omega} \right\}. \quad (16.1)$$

Hereby d describes the sample thickness in cm, Φ_0 the incident neutron flux in neutrons per $\text{cm}^2 \times \text{sec}$, $d\Omega_i$ is the solid angle of the detector element i in steradian, ϵ_i the detection efficiency of detector element i and α the extinction coefficient of the sample in cm^{-1} . A the illuminated sample area in cm^2 . θ describes the angle between the wave vector \mathbf{k}_0 of the incident neutrons and the wave vector \mathbf{k} of the scattered neutrons. $\frac{d\sigma_{coh}}{d\Omega}$ and $\frac{d\sigma_{inc}}{d\Omega}$ are the coherent and incoherent differential cross-sections, respectively. For small angle scattering $\cos\theta \simeq 1$ and one yields after integration

$$I_{S,i}^0 = \Phi_0 \Delta\Omega_i \epsilon_i \underbrace{A \rho d}_{N_S} \underbrace{e^{-\alpha d}}_{T_S} \left\{ \frac{d\sigma_{coh}}{d\Omega} + \frac{d\sigma_{inc}}{d\Omega} \right\}. \quad (16.2)$$

The quantity $N_S = A \rho d$ corresponds to the number of scattering atoms and $T_S = e^{-\alpha d} = \frac{I_{trans}}{I_0}$ to the transmissions coefficient, which can be determined from the ration of the intensity of the transmitted primary beam I_{trans} and the intensity of the incident

beam I_0 . The incoherent scattering is isotropically and equally distributed over the whole solid angle of 4π . Therefore one gets for $I_{S,i}^0$

$$I_{S,i}^0 = \Phi_0 \Delta\Omega_i \epsilon_i \left\{ N_S T_S \frac{d\sigma_{coh}}{d\Omega} + A \frac{1 - T_S}{4\pi} \right\}. \quad (16.3)$$

16.1.2. Correction for sample holder and background noise. The scattering intensity of an isolated sample can practically never measured directly. The scattering of the sample is always superposed by scattering from the sample holder and by background noise. Background noise is meant to be electronic noise, cosmic radiation, and detection of neutrons, which have not passed through the sample like scattered neutrons from neighboring experiments. Because of this reasons additional measurements have to be carried out, which are a measurement of the empty sample holder I_H and a measurement with a strong absorber like Cadmium in front of the sample to measure the background noise I_B . Together with the measurement of the sample in the sample holder $I_{S+H,i}$ the scattering of the isolated sample $I_{S,i}^0$ on the detector element i can be calculated by

$$I_{S,i}^0 = \left(\frac{I_{S+H,i}}{M_{S+H}} - \frac{I_{B,i}}{M_B} \right) - \frac{T_{S+H}}{T_H} \left(\frac{I_{H,i}}{M_H} - \frac{I_{B,i}}{M_B} \right). \quad (16.4)$$

The index B stands for background, H for the empty sample holder, $S+H$ for the sample in the sample holder and S for the scattering of the isolated sample. All intensities have to be normalized on the number of incident neutrons. This can be done for example by division of the measured intensity my a monitor count rate M . The factor $\frac{T_{S+H}}{T_H}$ takes account for the attenuation of the beam by the sample.

The differential cross-section in eq. 16.3 can now be calculated from the measurable intensities in eq. 16.4. Nevertheless the quantities Φ_0 , $\Delta\Omega_i$ and ϵ_i still have to be known. Furthermore I_S^0 is not given in physical standard units but in units per monitor count. All this can be overcome by a comparison with a standard substance St . Common standard materials are in general materials with a small coherent cross-section and a large incoherent cross-section like vanadium or water. For both of these materials the coherent cross-section is negligible small. The scattering intensities of the standard materials have to be corrected in the same way than the sample itself according to eq. 16.4. The ratio of both intensities $I_{S,i}^0/I_{St,i}^0$ leads to

$$\frac{I_{S,i}^0}{I_{St,i}^0} = \frac{T_S N_S \left(\frac{d\sigma_{coh}}{d\Omega} + \frac{d\sigma_{inc}}{d\Omega} \right)}{T_{St} N_{St} \frac{d\sigma_{inc}^{St}}{d\Omega}} \quad (16.5)$$

$$\Leftrightarrow \frac{d\sigma_{coh}}{d\Omega} + \frac{d\sigma_{inc}}{d\Omega} = \frac{I_{S,i}^0}{I_{St,i}^0} \frac{T_{St} N_{St}}{T_S N_S} \frac{d\sigma_{inc}^{St}}{d\Omega} \quad (16.6)$$

$$\text{or } \frac{d\sigma_{coh}}{d\Omega} + \frac{d\sigma_{inc}}{d\Omega} = \frac{I_{S,i}^0}{I_{St,i}^0} \frac{(1 - T_{St}) \frac{A_{St}}{4\pi}}{T_S N_S}. \quad (16.7)$$

If water is used as a standard the last formula has to be multiplied on the right side with an emical factor $f(\lambda, \sigma_t, T) \simeq 1$. This factor corrects for the different efficiencies

of the detector for different neutron energies. This correction can become important in case of water because of its inelastic scattering behavior.

16.2. Correction and normalization of SAXS raw data

History

2023-xx-xx: SASfit 0.94.13

- added a pySASfit source subdirectory containing several tools like io routines for some data formats used at PSI as well as a python library accessing all plugins directly in python without recompiling the SASfit source tree
- added a plugin form factor for a second reparameterized version of Porod-Cylinder
- implemented a form factor for fibres consisting of solid cylinders packed in a two-dimensional hexagonal paracrystalline order.
- implemented an approximation of a long thin ribbon and a second one with an additional gamma distribution for two of its shorter edge lengths. An approximation assuming C»B»A for the edge length is assumed
- implemented form factor of two more oriented primitive objects, one of a rhombic dodecahedron and a second one of an octahedron together with their random oriented variant.
- corrected scaling factor of parallelepiped plugins to get proper absolute scaled values.
- bugfix in Chawe and QWE algorithm to calculate Hankel transform
- added a routine for optimized Frolov sparse-grids to extend the algorithm for sasfit_cubature (<https://ins.uni-bonn.de/content/software-frolov>)
- keep memory of previous sparse grid and only renew it if necessary
- Supplied several spars-grid quadrature routines to sasfit_cubature
- Supplied (randomized) quasi Monte Carlo (R)QMC integration routines using the quasi number generators from gsl. (R)QMC integration might converge faster than MC integration.
- Scrambled quasi random numbers for RQMC has been implemented using routines from B. Burley <http://jcgt.org/published/0009/04/01/>
- reparametrized plugins "parallelepiped (OPO,random)" and "superellipsoid (OPO,random)"

2023-01-07: SASfit 0.94.12

- improved numerical stability of wormlike structure factor according to Koyama
- some older plugins are now using the new integration routines supplied in SASfit : ellcylshell, torus, ellipsoidal shell, superhelices, stacked discs, ring polymers, triaxial ellipsoidal shell, carved triaxial ellipsoidal shell, khodenko worm, ring and linear polymer under shearflow, sheared spheroids, sheared cylinders, koyama worm
- made a variable substitution for the integration in `sasfit_orient_avg` to get more homogeneously distributed points on a spherical surface
- added form factor of cylinder with globular end caps
- the 1-Yukawa and 2-Yukawa structure factor stores now some previously calculated coefficients, which make it a bit more efficient.
- bugfix in calculating integral structural parameter. In certain (nonphysical) cases the fit as well as the plot of the fit result crashed.
- bugfix for star polymer with rigid arms

- due to flexible integration routines some of them calculate the function to integrate at its integration limits. For mass fractals this caused an error using these integration routines. There might be more such cases. The mass fractal plugins have been debugged.
- corrected in "sq 2D hard disks Rosenfeld" bug: $J_1(2x)/x = 2 \text{jinc}(2x)$ instead $J_1(2x)/x = 1/2 \text{jinc}(2x)$
- changed lognorm_fp-size distribution as plugin and included now also the other cases as described in the manual. So far only the shape 1 was implemented.
- renaming dodecahedra into rhombic dodecahedra
- added size distribution plugin based on generalized beta distribution
- added skewed gaussian and exponentially modified gaussian size distribution
- added spherical-t design algorithm for integration over the surface of a sphere
- added a new form factor of PEGylated vesicle with smoothed interfaces
- added metalog size distribution as well as the Johnson's family of distributions (SN, SL, SB, SU) and its generalization
- update to FFTW 3.3.10
- supply of a piecewise constant potential for OZ solver
- moved sticky hard sphere and square well structure factors into the plugin menu folder. The order of parameters changed slightly to be a bit more consistent
- added RLCA and DLCA structure factors for aggregates, which include nearest neighbor correlations
- supply of internal multidimensional integration routines, which can be configured via GUI
- supply of internal orientation average integration routines, which can be configured via GUI
- added form factor of super-ellipsoid
- added form factor of super-egg
- update to gsl 2.7
- update to FFTW 3.3.9
- use under Widows systems a powershell script to copy a 2D image to the clipboard as the previous code does not work anymore under MSYS2. A similar solution might be available under Unix and MacOS
- added form factor for an octahedron
- added form factor for an tetrahedron
- added form factor for a cone with six-fold symmetry
- added form factor for a cone
- added form factor for a rectangular base pyramid
- added perl necklace model both with stiff rodlike connections as well as "freely connected rods"
- extended "random flight" structure model by introducing an uncertainty parameter for the step width identical to the paracrystalline model for lamellar structures

- for merging files a multiplier instead of divisor is used now
- added structure factor for a 2-Yukawa potential in MSA approximation
- added a parameter choosing for some of the wormlike micelle structure factors either a polydisperse or a monodisperse contour length
- added three more radial profiles of spherical symmetric objects showing a Porod-law different from q^{-4}
- added a trapezoidal peak function and its generalized as well as its symmetric variant
- added some cluster models from [286]
- implemented a modified DAB model assuming a deformation and subsequent random orientation average of the standard DAB model
- implemented structure factors for multilamellar structures as plug-in function and added the monodisperse stacking case. In earlier version only the more practically relevant case of polydisperse case was implemented.
- added structure factors for one and two dimensional hard sphere potentials both for aligned structures in a certain direction as well as for random oriented 1D structures.
- the model Pcs:Plate+Chains(RW) now assumes always a non-zero surface area to avoid division by zero for zero layer thickness
- fixed a memory leak, when resolution function for single data set was used
- added form factor for ring polymer under shear flow in the approximation of Rouse modes
- successfully updated from gsl2.5 to gsl2.6 library.
- added a plugin for randomly oriented ellipsoids with a gamma-size distribution, where the integration over the size distribution can be performed analytically.
- added a generalized and lesser generalised form factor according to Fedorova describing several shapes and geometries of objects depending on only one size parameter visible in the q-range of the SAS instrument
- added a form factor describing the scaling function of a phase separating system after a quench in the miscibility gap
- added form factor for cylinders with a fuzzy interface (Pcs:Boucher cyl., Pcs:Boucher2 cyl., Pcs:fuzzy cyl., Pcs:linear shell cyl.) and the corresponding profiles in real space ("profile:Boucher cyl.", "profile:Boucher2 cyl.", "profile:fuzzy cyl.", "profile:linear shell cyl.")
- added in integral structural parameters a command for developing model-free calculations of size distributions using EM algorithms as well as Maximum Entropy methods and traditional Tikhonov regularization methods. This part is still experimental and not well documented in the manual.
- bug fix for TetraheadronDoubleShell. The double sum over the number of spheres has been corrected.
- bug fix in Porod cylinder as by moving the form factor to the plugin area the length parameter was assigned to the wrong index of the parameter array.
- supplied those models available for SESANS analysis as multiple scattering models because the projected correlation function is directly related to the

intermediate function $s(r)$ as described in the reference paper from Schelten and Schmatz, J. Appl. Cryst. (1980). 13, 385-390

- bug fix in the SESANS model of $G_gDAB(z)$
- added form factors of clipped random waves for 5 different two-point correlation functions
- added form factor of a stochastic model of a boolean union model of spheres with LogNorm size distribution.
- added form factor of a stochastic model of a dead-leave model of spheres with LogNorm size distribution.
- added form factors of polymers under shear flow
- added anisotropic form factor for step deformed networks according to the tube models of Warner-Edwards and a second one from Heinrich-Straube-Helmis
- added some additional azimuthal intensity distributions valid for long objects with certain orientation distribution (Maier-Saupe, Onsager)
- added some azimuthal intensity distributions based on the model of sheared cylinders and spheroids following a Maier-Saupe, Onsager, Heaviside, Gauss, or a Boltzmann orientation distribution. These functions return $I(\psi)$ instead of $I(q)$
- extended the reading routine for SESANS data. A common file format has been established. These data files have in their header a version information (FileFormatVersion 1.0). At the moment some old formats from Delft, where the projected correlation function still has to be calculated from the polarisation and the new format 1.0 are supported.
- removed the old entries for mass fractal structure factors which have been moved to the plug-in sub-menu.
- Added some structure factors for worm-like micelles: one RPA approximation and three different PRISM approximations. For all of them an exponential length distribution is included.

2018-11-15: SASfit 0.94.11

- reduced the frequency of updating the progress bar as well as checking of pressing the interrupt button to maximal 10 times per second.
- added two additional form factors for ring polymers with excluded volume effects ("RingPolymerBZ", "RingPolymerBMB") and renamed the old one from "FlexibleRingPolymer" to "RingPolymerCasassa"
- bug fix in ring polymers, daisy-like ring and m-membered twisted ring.
- bug fix of "GzSphere", returns wrong value for $z > 2R$
- bug fix of "GzgDAB" for extrapolation to $z \rightarrow 0$
- added two more models for $P'(Q)$ of thin cylindrical objects describing wormlike structure: "Koyama worm" and "freely joined chain of rods"
- Some form factors for polymers like Gaussian chains, star polymers and ring polymers have been moved to the plug-in area.
- As all peak functions are now available as plug-ins the obsolete old code has been deleted

- The Lorenz-Mie form factors for static light scattering are now made available as plug-in form factors
- **SASfit** now tries to avoid starting a new fit or simulation before the previous one is finished
- Successfully updated from gsl2.4 to gsl2.5 library.
- The new 2D/3D hard sphere structure factors are now available in the structure factor plug-in folder named "Hard Sphere 2D/3D"
- update to FFTW 3.3.8 worked after disabling threads however on Windows McAfee had to be switched off during configure process.
- implemented some thermodynamic self-consistent hard sphere structure factors based on the rational function approximation method
- tried to avoid overflow of sinh-function in the model "Khodolenko-Worm"
- now between thin objects (local planar and local cylindrical approximation) and anisotropic shapes is distinguished.
- new plug-in folder for azimuthal data
- new plug-in folder for deformed or sheared objects
- new form factors for partly aligned cylinders and ellipsoids following a Maier-Saupe, Onsager, Heaviside, Gauss, or a Boltzmann orientation distribution
- new form factor of a reptating chain after a deformation step
- new plug-in structure factors for 2-dimensional fluids of monodisperse hard spheres, "2D hard disks (Rosenfeld)" and "2D hard disks (Guo)"

2018-03-20: SASfit 0.94.10

- The form factors "EllipsoidalCoreShell", "Ellipsoid i", "Ellipsoid ii", and "triaxEllShell1" have been disabled and replaced by a series of plug-in functions. Those replacements make use of a faster routine for multidimensional integrals (pcubature). Because of this an optional size distribution became part of the supplied plug-in form factors.
- bug fix of unit conversion via clipboard
- added a plug-in for a random flight structure factor
- bug fix in the algorithm for calculating the resolution parameter in case of averaging neighboring data points
- plug-in implementation of several variants of helices
- plug-in for rectangular parallelepipeds have been extended so that it can have a size distribution of one, two or all three axis. The multiple integration is done by using the pcubature code from Steven G. Johnson
- multi dimensional integration package "cubature" from Steven G. Johnson becomes generally available also in plug-ins ([cubature](#))

2017-08-16: SASfit 0.94.9

- changed scaling of SESANS correlation functions by factor $1/(2\pi)^2$
- unit conversion for reading ASCII files corrected and extended
- update to FFTW 3.3.6-pl2 did not work, went back to 3.3.5
- update to gsl 2.4
- bug fix: resolution bar was not plotted properly
- Uncertainties on x and y axis are now plotted symmetrically from $x \pm \Delta x$ and $y \pm \Delta y$. Before they were plotted from $x \pm 0.5\Delta x$ and $y \pm 0.5\Delta y$.

2016-12-16: SASfit 0.94.8

- Moved all peak functions into the plugin area.
- Added the possibility to apply after the summation of all scattering contributions a final operator. At the moment between three operator can be chosen:
 - (1) Unit operator which does not do anything with the data
 - (2) Taking the Hankel transform $2\pi^*H[I(Q)]$ for converting SAS model into a projected correlation function $G(\delta)$, which defines the SESANS signal
 - (3) Applying the operator from 2) and taking the exponential function of it $\exp(2\pi^*H[I(Q)])$ to get SESANS signal
- For the extension to SESANS also an option for reading SESANS data has been supplied. The format has been defined by TU Delft and has the default extension *.ses.
- added a model for of a self-fine random density distribution (gDAB) both under non-particular structures as well as under SESANS as a correlation function.
- added a SESANS correlation function for a generalized Gaussian chain for Flory exponents between nu in (0,1/2)
- updated to FFTW 3.3.5
- updated to sundials 2.7.0
- updated to gsl 2.3
- supplying some alternative integration routines for integrating over the size distribution
- bug fix of sasfit_integrate routine, which caused a crash when called from plugin functions
- first minimal routine for reading simple ascii data from ALV-5000 with single correlation function for DLS-analysis
- adding the PLHNC and RMSA closure to the OZ solver
- fixed a bug in the scaling parameter of the Teubner-Strey model
- bugfix in routine for reading data in BerSANS format

2016-04-25: SASfit 0.94.7

- implementation of another cumulant formula for DLS
- bug-fix in the unit conversion routine
- implementation of GMRES, Bi-CGStab, TFQMR and Andersen Acceleration for solving efficiently the Ornstein Zernicke fixpoint problem
- bug fix: since version 0.94.4 the new interrupt option suppressed a proper error reporting to the GUI for undefined input values
- removed some old structure factors, which were rarely used and theoretically not up to date
- a first version of a plugin for ordered mesoscopic and nano structures. The plugin is providing a part of the structure factors available in the software package "scatter" from S. Förster.
- plugin of a radial profile for a sphere resulting in a Porod law both below and above Q^{-4} (Boucher Sphere)

2014-12-14: SASfit 0.94.6

- improved analysis of confidence intervals of fit parameters:
- clickable correlation coefficients in the matrix highlight associated pair of fit parameters
- covariance matrix elements are highlighted according to their correlation coefficient
- highlighting and selection of correlated params improved

2014-10-03: SASfit 0.94.5

- storing intensity and size distribution in batch processing routine
- changed the width of the error bar, assuming that the supplied error is FWHM
- changed the internal procedure for plotting error bars
- resolution parameter can now also be plotted
- changed the order of plotting the fit results in "integral structural parameters"
- interruption of batch processing or series analysis implemented

2014-09-03: SASfit 0.94.4

- a new interrupt button can stop now the intensity evaluation of fitting procedure after each q-value. Before the whole scattering curve needed to be calculated.
- progress bar has been added to the GUI
- bug fix in plotting error bars of multiple data sets.
- implementation of another method for thinning out oversampled data sets. The new methods is performing an averaging of data points depending on a user-defined maximum allowed q-smearing and a user-defined maximum distance in intensity in units of the error bar of the data points, i.e. an averaging is only performed, if the intensities look similar with n-times the intensity error bars.
- bug fix in GUI if one wants to forget old data and load a new data sets.

2014-07-02: SASfit 0.94.3

- bug fix in the plugin for parallel epiped
- spelling errors in the menu interface
- in case of slow convergence the OZ solver can be interrupted now

2014-02-06: SASfit 0.94.2

- new binding for zoom option, which works better for a mouse with one button (plot zoom by ctrl+left-mouse btn)
- removed <delete> key binding for scattering contributions
- Added several iteration schemes for finding the fixpoint of the OZ equation.
- Added a tab for the total correlation function $h(r)$
- Added also some root finding algorithms for solving OZ equation.
- resolution parameter from file was not scaled during the change of units for Q
- bug fix in calculation of χ_i for sq for wormlike structures (PS1 model)
- wrong label for contrast in Teubner-Strey model
- bug fix in SPHERE+R=a_Nagg form factor in assignment of core volume
- data export format set to scientific notation in the form $x.yyyE?zz$ only

2014-02-05: SASfit 0.94.1

- added missing parameter label for Hamaker constant in DLVO potential
- Penetrable Sphere Model was not properly assigned.
- added all available plugins into the distribution binaries

2014-01-20: SASfit 0.94.0

- A new interface for solving the Ornstein Zernike equation for different closure relations and potentials (OZ-solver) has been added. The solutions of the OZ-solver can be used as a structure factor as a spline function without the possibility to fit a parameter of the potential at the moment.
- manual has been extended for the ferrofluid plugin scattering functions
- orientation of the 2D simulation was rotated by 90deg.
- correction of the manual for Porod's approximation of cylinders.
- minor bug fix for Porod's approximation of long cylinders.

2013-06-09: SASfit 0.93.5

- implementation of a plugin for a form factor and correlation function for spin misalignment
- bug fix for the scattering contribution of the individual chains in the form factors `WORM*`, `ROD*`, and `DISC*`
- bug fix in the form factor `MagneticShellCrossTerm`
- added some subfolders for form factor plugins
- bug fix in the calculation of the scattering length density SLD(E) of x-rays

2013-04-30: SASfit 0.93.4

- In the menu for confidence interval the non-diagonal elements of correlation matrix are shown together with the confidence interval for the fitted parameters as diagonal elements.
- added some additional parameters into the fit menu useful to evaluate the goodness of a fit
- new plugin for `Parallelepiped_abc` of dimension a^*b^*c to be found under [by `plugins|anisotropic obj`]
- new plugin for `generalized Guinier law` to be found under [by `plugins|non-particular structures`]
- Renamed HMI format into BerSANS format and did some debugging. Now also all masked data points (negative errors) are ignored.
- added key bindings `Home`, `End`, `PgUp`, `PgDn`, `Insert`, `Delete` for going to first-last-next-previous entry or to add and remove an entry
- adding plugin with a series of form factor for strongly anisotropic structures with local planar and local cylindrical shapes
- adding a new plugin form factor for spheres with fuzzy interfaces. The existing form factors `ExpShell`, `LinShell` and `LinShell2` have been moved to this plugin.
- New plugin of `FuzzySphere` and `CoreShellMicrogel`. Also the related functions for calculating the corresponding radial profiles have been added.
- new section in the manual about absolute scale, molecular weight, etc.
- for the form factors `flat cylinder` `long cylinder`, and `Porod cylinder` the limiting case $q \equiv 0$ is now treated properly
- small bug fix in the peak function `Gamma (Area)` for checking validity of parameter

- bug fix of the resolution parameter handling in case it will be read in from a data file
- included under peak function the Maxwell distribution and the generalized Maxwell distribution
- batch fitting

2011-05-04: SASfit 0.93.3

- bug fix in the model **Stacked Discs**. The structure factor describing the stacking order contained a bug.
- extended plugin for stroboscopic measurements, especially for TISANE
- plotting: ignore negative y values on log() and sqrt() scales
- included **Pcs_homogeneousCyl** form factor
- bug fix of **ferrofluid plugin**
- added radial averaged form factor in **ferrofluid plugin**
- extended the spline plugin to be used also as form factors. In case somebody wants to fit a spline function to e.g. a TEM size distribution, this function need to be available as a form factor and not only as a size distribution.
- added configuration file **config.ini** as replacement for deprecated **sasfit_init_public.tcl**
- added switch for disabling **About** popup at start time via config file
- added checkbox (ascii options) for ignoring zero(0) intensity at the beginning of data
- removed , as data column separator
- added substitution of ,⇒ . for data columns (german decimal format to english format)
- added interface function for covariance matrix output
- covar matrix visualisation with parameter highlighting
- added a chapter about particle number densities, volume fraction and absolute intensities in the manual.
- **LogNorm_fp** size distribution is now plugin function. The new plugin is not backwards compatible. The manual explains a bit the difficulties in describing the size distribution in terms of a volume fraction.
- added scrollbars for fit parameter window

2010-07-08: SASfit 0.93.2

- bug fix in ferrofluid plugin
- added radial averaged form factor. Included radial averaged form factors also for SAW model
- Extended the spline plugin to be used also as form factors. In case somebody wants to fit a spline function to a size distribution, this function needs to be available as a form factor and not only as a size distribution.
- forwarding intermediate linear Guinier approximation results to the plot window (green curve)
- display of linear Guinier approximation results in **ISP** text output window
- residuum window updated with linear Guinier approximation residuum
- by default disabled, see checkbox in **ISP** window
- fixed **SLDCalculator** in source package (missing data files)
- added **KNOWN_BUGS.txt** (not complete)

- optical (layout) GUI improvements:
 - removed thick margin around text boxes for ISP/analyt results
 - added resizable file list in ISP window
 - added resizable 'merge files' list when loading data files
- added menu->tools->toggle console to show the console, it is hidden by default now
- added `OPTIM` parameter to `src/CMakeLists.txt` for optimized binary generation on the underlying hardware, use: '`cmake -DOPTIM=TRUE`'
- added configuration file `config.ini` as (working) replacement for deprecated `sasfit_init_public.tcl`
- added switch for disabling 'about' popup at start time via config file
- added switch to set the default data directory
- added checkbox (ascii options) for ignoring zero(0) intensity at the beginning of data

2010-05-13: SASfit 0.93.1

removed obsolete print menu entries and fix of textual output bug

2010-05-05: SASfit 0.93.0

- copy&paste-able text output, as well as `csv` export (semicolon separated) for
 - integral structural parameters (ISP) data
 - parameters of contributions
 - moments of size distribution
- improved/rewritten file selection GUI for ISP series fitting
- new and improved plugins: `Kratky Sphere`, `JuelichCoreShell` (rewritten), `Langevin`
- data is always plotted first, below the calculated lines
- error bars are drawn behind data points
- fixed wrong plotting of very large error bars
- for log-plotting on the y-axis, negative data is ignored (not plotted, was `abs()` before)
- fix to prevent the user from loading a `SASfit` project file as data
- fix in Form-Factor `Background` (improved numerical stability)
- bug fix for saving parameter files on windows
- bug fix in gui when selecting form factor `TwoAttachedSpheres`
- bug fix for "Singular Matrix" error

2010-01-02: SASfit 0.92.3

- implemented three different versions for worm like chains as described in Macromolecules 1996, 29, 7602-7612. They have been implemented as structure factors [`anisotropic obj|P'(Q):local cylindrical geometry`], so that it can be combined with different cross-section form factors of local cylindrical objects [`anisotropic obj.|Pcs(Q) for cylindrical obj.`].
- new form factor plugin for a sphere with 3 shells
- new structure factor for a regular cluster up to maximal 5 particle (tetrahedron like)

- correction of menu entry order for magnetic shell and superparamagnetic shell
- new plugin for ferrofluid particles with a scheme similar to the one of J.S. Pedersen for Gaussian Chains attached to a spherical particle
- bug fix in `mMemberedTwistedRing`
- two more default plot: `Guinier (rods)` and `Guinier (sheets)`
- bug fix in `loglogistic` peak
- implementation of asymptotic limits for fractals, which require a numerical integration. The integration often fails for large q-values for which an asymptotic solution is available or has been constructed.
- reprogrammed `SquareWell11` structure factor for a squared well potential
- replaced `sasfit_qromb` function by `sasfit_integrate` function in the form factor for the torus. The `sasfit_qromb` routine did not work for some unknown reason. This needs to be checked.
- new structure factor for a thin square well potential
- bug fix in `BeaucageExpPowLaw2`
- Bug fix for setting plot option `Holtzer` in multiple data set tab
- public initialization file `sasfit_init_public.tcl` for setting the default working directory by the user to any path

2009-10-08: `SASfit` 0.92.2

- data reduction without data loss, after loading a project file the data reduction can be reversed
- info message about a guessed error bar is displayed only once when the ascii options are changed (not for every file)
- added tooltip for complete filenames in merge window
- color for selected fit region stays at dark grey after loading an old project file
- removed unused help buttons in file open dialogs
- fixed error loop when adding new data to previously loaded project file
- fix for a homedir being e.g. 'U:at startup on Windows
- minor correction in the routine to guess the error bar (normalization) when only two column are supplied
- fix of rare error "form factor param out of range: -1"

13th of September: `SASfit` 0.92.1

- fix for GUI problem with two plugin form factors (contribution updates). If there are two plugin model functions with a different number of parameters, you can't switch/cycle through the contributions anymore (Next, Previous).
- fix for saving a parameter file (file creation was disabled by accident in previous version)

8.7.2009: `SASfit` 0.91.1: Since the previous version of `SASfit` (0.90.1, January 2009) there were a lot of changes to primarily improve the quality and portability of the code. Here is only a short summary of the larger changes done:

- added detailed documentation on setup and installation of `SASfit`, as well as plugin development (how to add own model functions)
- fixed some bugs in plugin framework
- added automatic determination of available plugins at build time

- enabled static building for plugins
- increasing maximum number of model parameter in GUI
- verified build compatibility for MacOS
- Extended and improved Scattering Length Density (SLD) Calculator. Now the scattering length density for x-ray energies between 1keV and 24.9 keV can be calculated.
- a few new form factor have been included: `generalized Gaussian coil`, `generalized Gaussian coil 1`, `generalized Gaussian coil 2`, `ellCylShell1`, `ellCylShell2`

12.01.2009: SASfit 0.90.1 : bug-fix in plugin-GUI

5.01.2009: SASfit 0.90: new release including full source code and binaries for windows and linux. Since the previous version of v (0.87, March 2008) there were a lot of changes to primarily improve the quality and portability of the code. Here only a short summary of the 'big' changes done (as of Dec. 17th, 2008):

- (1) Structured the source code into the modules `sasfit_common`, `sasfit_sd`, `sasfit_sq`, `sasfit_ff`, `sasfit_core`.
- (2) Switched to CMake build environment for platform independence. Build and tested SASfit on Linux and Windows, 32bit as well as 64bit.
- (3) Replaced intensive string comparisons for model function selection in each iteration step by more reasonable selection of functions pointers at initialization time and direct call of the according function at iteration time.
- (4) Fixed a lot of bugs and typos in the GUI (but there are still some)
- (5) Added flexible plugin system for external model functions. This way, all model functions can be provided as plugins and though move out of the core algorithms. Also enables easy customization. In the future the modules `sasfit_sd`, `sasfit_sq`, `sasfit_ff` and `sasfit_peaks` will be converted to external plugins.
- (6) Added `sasfit_peaks`, a new class of model functions containing peaks.
- (7) Added capability to ship SASfit as standalone executable, allows running on system without the need of external libraries (e.g. Tcl, BLT, ...)

4.03.2008: (SASfit version 0.87) The last modification in the menu navigation still had bugs. Hopefully they are removed in this version.

28.02.2008: (SASfit version 0.86) The menu navigation has been debugged and optimized. Corrected a bug in calculating the polydispersity index (PDI) in DLS cumulant analysis ($PDI = \Gamma_{\text{Gamma}2}/\Gamma_{\text{Gamma}1^2}$)

25.01.2008: (SASfit version 0.85) A bug for the form factors $ROD+R^{-a}$ has been corrected. The implementation of the scaling approximation, partial structure factors and local monodisperse approach has been improved.

9.01.2008: (SASfit version 0.84) Form factor for worm-like micelles (`WORM+Chains(RW)`, `WORM+Chains(RW)_Rc`, `WORM+Chains(RW)_Nagg`) and for cluster aggregates (`Mass Fractal (Exp(-x) Cut-Off)`, `Fisher-Burford`, `MassFractExp`, `MassFractGauss`, `Mass Fractal (Exp(-x^a) Cut-Off)`, `DLCAggregation`, `RLCAggregation`, `MassFractOverlappingSph` have been implemented. Furthermore a simple scheme for importing data from the clipboard has been implemented, which e.g. allows to copy/paste data from

spread-sheets directly into **SASfit**. Corrected a bug for the form factors **ROD+R^{^-}a***

4.10.2007: (**SPHERE+Chains(RW)**, **SPHERE+Chains(RW)_Rc**, **SPHERE+Chains(RW)_NaggSASfit** version 0.80) Next to the correction of some bugs a simulation option for multiple data sets has been implemented. Furthermore an option has been implemented to subtract a theoretical scattering contribution from the experimental data set, like e.g. a constant background signal. The format of the project files have up to now never been tested for compatibility. An attempt has been started to change this for the future versions.

20.8.2007: A couple of form factors for spherical, elliptical, cylindrical and very long rod-like micelles consisting of a homogeneous core and which are either grafted with Gaussian chains ***(RW)***, or grafted with semi-flexible self-avoiding and interacting chains ***(SAW)*** or a corona with a power-law decaying profile $r^{-\alpha}$ ***(R^{^-}a)*** have been implemented: **SPHERE+Chains(RW)**, **SPHERE+Chains(RW)_Rc**, **SPHERE+Chains(RW)_Nagg**, **SPHERE+Chains(SAW)**, **SPHERE+Chains(SAW)_-Rc**, **SPHERE+Chains(SAW)_Nagg**, **SPHERE+R^{^-}a**, **SPHERE+R^{^-}a_-Rc**, **SPHERE+R^{^-}a_Nagg**, **ELL+Chains(RW)**, **ELL+Chains(RW)_-Rc**, **ELL+Chains(RW)_Nagg**, **CYL+Chains(RW)**, **CYL+Chains(RW)_-Rc**, **CYL+Chains(RW)_Nagg**, **ROD+Chains(RW)**, **ROD+Chains(RW)_Rc**, **ROD+Chains(RW)_nagg**, **ROD+R^{^-}a**, **ROD+R^{^-}a_Rc**, **ROD+R^{^-}a_nagg**

30.6.2007: Rudimental copy algorithm to copy plots or parameters into window-clipboard. Everything is copied in wmf-format and the option only works fine for information in non-scrolled widgets. Copy-option can be activated with right mouse button or double click of left mouse button. A triaxial ellipsoidal (**triaxEllShell**) shell with semiaxis **a**, **b**, **c** and shell thickness **t** is available.

4.6.2007: Implementation of form factors for cylindrical shells with circular cross-section and capped ends (**CylShell2**) and without capped ends (**CylShell1**) together with an approximation for very long cylindrical shells (**LongCylShell**)

27.3.2007: Implementation of form factors for bi-continuous systems (**TeubnerStrey** and **DAB**)

23.2.2007: Implementation of the structure factor for a system of charged, spheroidal objects in a dielectric medium according to the RMSA model of Hayter and Penfold

11.11.2006: Implementation of a semiflexible polymer according to Kholodenko, some form factors with plane geometry, which are intended to be used with lamellar structure factors (**homogenousXS**, **TwoInfinitelyThinPlates**, **LayeredCentroSymmetricXS**, **BiLayerGauss**), a sphere with Gaussian chains attached **SphereWithGaussChains** and a slightly different parametrised form factor named **BlockCopolymerMicelle**. An additional option for reading ASCII data files is now available, which allows to convert values for the scattering vector from nm⁻¹ into Å⁻¹ and vice versa.

23.10.2006: Implementation of a polydisperse star **PolydisperseStar** and of flexible ring polymers **FlexibleRingPolymer** and **mMemberedTwistedRing**.

22.10.2006: Implementation of the form factor of a flexible polymer with Gaussian statistics (in different parameterisations `Gauss`, `Gauss2`, `Gauss3`) for a polydisperse flexible polymer with Gaussian statistics (`GaussPoly`) and a flexible ring of polymer with Gaussian statistics (`FlexiblePolymerRing`)

12.10.2006: Under the menu option `Calc/DLS...` next to a cumulant fit also a double stretched exponential decay can be selected to fit dynamic light scattering data.

5.10.2006: Implementation of a spherical shell with a diffuse (exponential) scattering length density profile inside the shell caused by solvent penetration into the shell

13.9.2006: Implementation of a form factor for spheres with gaussian chains attached.

19.7.2006: First release (current version: 0.71) at the moment only a windows version is available. The installation files for tcl/tk and blt are included in the distribution file.

Bibliography

- [1] R. P. Agarwal, D. O'Regan, and D. R. Sahu. Iterative construction of fixed points of nearly asymptotically nonexpansive mappings. *Journal of Nonlinear and Convex Analysis*, 8(1):61–79, 2007. URL <http://www.ybook.co.jp/online2/jncav8-1.html>.
- [2] D. M. Agra-Kooijman, M. R. Fisch, and S. Kumar. The integrals determining orientational order in liquid crystals by x-ray diffraction revisited. *Liquid Crystals*, 45(5):680–686, sep 2017. doi: [10.1080/02678292.2017.1372526](https://doi.org/10.1080/02678292.2017.1372526).
- [3] S. Alexander, P. M. Chaikin, P. Grant, G. J. Morales, P. Pincus, and D. Hone. Charge renormalization, osmotic pressure, and bulk modulus of colloidal crystals: Theory. *The Journal of Chemical Physics*, 80(11):5776–5781, jun 1984. doi: [10.1063/1.446600](https://doi.org/10.1063/1.446600).
- [4] D. G. Anderson. Iterative procedures for nonlinear integral equations. *Journal of the ACM*, 12(4):547–560, oct 1965. doi: [10.1145/321296.321305](https://doi.org/10.1145/321296.321305).
- [5] W. L. Anderson. A hybrid fast hankel transform algorithm for electromagnetic modeling. 54(2):263–266. doi: [10.1190/1.1442650](https://doi.org/10.1190/1.1442650).
- [6] R. Andersson, L. F. van Heijkamp, I. M. de Schepper, and W. G. Bouwman. Analysis of spin-echo small-angle neutron scattering measurements. *Journal of Applied Crystallography*, 41(5):868–885, sep 2008. doi: [10.1107/s0021889808026770](https://doi.org/10.1107/s0021889808026770).
- [7] S. R. Aragón. Theory of dynamic light scattering from polydisperse systems. *The Journal of Chemical Physics*, 64(6):2395, 1976. doi: [10.1063/1.432528](https://doi.org/10.1063/1.432528).
- [8] L. Arleth and C. Vermehren. An analytical model for the small-angle scattering of polyethylene glycol-modified liposomes. 43(5):1084–1091. doi: [10.1107/s0021889810026257](https://doi.org/10.1107/s0021889810026257).
- [9] K. Arslan, B. Bulca, B. Bayram, G. Ozturk, and H. Ugail. On spherical product surfaces in e3. In *2009 International Conference on CyberWorlds*. IEEE, 2009. doi: [10.1109/cw.2009.64](https://doi.org/10.1109/cw.2009.64).
- [10] N. W. Ashcroft and J. Lekner. Structure and resistivity of liquid metals. *Physical Review*, 145(1):83–90, may 1966. doi: [10.1103/physrev.145.83](https://doi.org/10.1103/physrev.145.83).
- [11] M. V. Avdeev, V. L. Aksenov, Z. Gazová, L. Almásy, V. I. Petrenko, H. Gojzewski, A. V. Feoktystov, K. Siposova, A. Antosova, M. Timko, and P. Kopcansky. On the determination of the helical structure parameters of amyloid protofilaments by small-angle neutron scattering and atomic force microscopy. *Journal of Applied Crystallography*, 46(1):224–233, jan 2013. doi: [10.1107/s0021889812050042](https://doi.org/10.1107/s0021889812050042).
- [12] M. Bakry, H. Haddar, and O. Bunău. A robust expectation-maximization method for the interpretation of small-angle scattering data from dense nanoparticle samples. *Journal of Applied Crystallography*, 52(5), aug 2019. doi: [10.1107/s1600576719009373](https://doi.org/10.1107/s1600576719009373).
- [13] P. Ballone, G. Pastore, G. Galli, and D. Gazzillo. Additive and non-additive hard sphere mixtures. *Molecular Physics*, 59(2):275–290, oct 1986. doi: [10.1080/00268978600102071](https://doi.org/10.1080/00268978600102071).
- [14] B. Barboy. On a representation of the equation of state of fluids in terms of the adhesive hard-spheres model. *The Journal of Chemical Physics*, 61(8):3194–3196, oct 1974. doi: [10.1063/1.1682475](https://doi.org/10.1063/1.1682475).
- [15] Barr. Superquadrics and angle-preserving transformations. *IEEE Computer Graphics and Applications*, 1(1):11–23, jan 1981. doi: [10.1109/mcg.1981.1673799](https://doi.org/10.1109/mcg.1981.1673799).
- [16] P. Bartlett and R. H. Ottewill. A neutron scattering study of the structure of a bimodal colloidal crystal. *The Journal of Chemical Physics*, 96(4):3306–3318, feb 1992. doi: [10.1063/1.461926](https://doi.org/10.1063/1.461926).
- [17] F. Bauer and M. A. Lukas. Comparing parameter choice methods for regularization of ill-posed problems. 81(9):1795–1841. doi: [10.1016/j.matcom.2011.01.016](https://doi.org/10.1016/j.matcom.2011.01.016).

- [18] R. Baxter. Percus-yeck equation for hard spheres with surface adhesion. *J. Chem. Phys.*, 49(6):2770–2774, 1968. doi: [10.1063/1.1673684](https://doi.org/10.1063/1.1673684).
- [19] G. Beauchage. Approximations leading to a unified exponential/power-law approach to small-angle scattering. *Journal of Applied Crystallography*, 28(6):717–728, dec 1995. doi: [10.1107/s0021889895005292](https://doi.org/10.1107/s0021889895005292).
- [20] G. Beauchage. Small-angle scattering from polymeric mass fractals of arbitrary mass-fractal dimension. *Journal of Applied Crystallography*, 29(2):134–146, apr 1996. doi: [10.1107/s0021889895011605](https://doi.org/10.1107/s0021889895011605).
- [21] P. Beck, M. Liebi, J. Kohlbrecher, T. Ishikawa, H. Rüegger, P. Fischer, P. Walde, and E. Windhab. Novel type of bicellar disks from a mixture of dmpe and dmpe-dtpa with complexed lanthanides. 26(8):5382–5387. doi: [10.1021/la903806a](https://doi.org/10.1021/la903806a).
- [22] C. Benham, G. Brady, and D. Fein. X-ray scattering from randomly oriented superhelices. circular superhelical DNA. *Biophysical Journal*, 29(3):351–366, mar 1980. doi: [10.1016/S0006-3495\(80\)85139-3](https://doi.org/10.1016/S0006-3495(80)85139-3).
- [23] H. Benoit. On the effect of branching and polydispersity on the angular distribution of the light scattered by gaussian coils. *Journal of Polymer Science*, 11(5):507–510, nov 1953. doi: [10.1002/pol.1953.120110512](https://doi.org/10.1002/pol.1953.120110512).
- [24] A. Bensafi, U. Maschke, and M. Benmouna. Cyclic polymers in good solvents. *Polymer International*, 49(2):175–183, feb 2000. doi: [10.1002/\(sici\)1097-0126\(200002\)49:2<175::aid-pi323>3.0.co;2-m](https://doi.org/10.1002/(sici)1097-0126(200002)49:2<175::aid-pi323>3.0.co;2-m).
- [25] F. Benvenuto. A study on regularization for discrete inverse problems with model-dependent noise. *SIAM Journal on Numerical Analysis*, 55(5):2187–2203, jan 2017. doi: [10.1137/15m1049051](https://doi.org/10.1137/15m1049051).
- [26] F. Benvenuto, H. Haddar, and B. Lantz. A robust inversion method according to a new notion of regularization for poisson data with an application to nanoparticle volume determination. *SIAM Journal on Applied Mathematics*, 76(1):276–292, jan 2016. doi: [10.1137/15m1024354](https://doi.org/10.1137/15m1024354). cited By 0.
- [27] A. Bergmann, G. Fritz, and O. Glatter. Solving the generalized indirect Fourier transformation (GIFT) by Boltzmann simplex simulated annealing (BSSA). 33(5):1212–1216. doi: [10.1107/S0021889800008372](https://doi.org/10.1107/S0021889800008372).
- [28] N. F. Berk. Scattering properties of the leveled-wave model of random morphologies. *Physical Review A*, 44(8):5069–5079, oct 1991. doi: [10.1103/physreva.44.5069](https://doi.org/10.1103/physreva.44.5069).
- [29] I. Berndt, J. S. Pedersen, P. Lindner, and W. Richtering. Influence of shell thickness and cross-link density on the structure of temperature-sensitive poly-n-isopropylacrylamide-poly-n-isopropylmethacrylamide core-shell microgels investigated by small-angle neutron scattering. *Langmuir*, 22(1):459–468, jan 2006. doi: [10.1021/la052463u](https://doi.org/10.1021/la052463u).
- [30] I. Berndt, J. S. Pedersen, and W. Richtering. Structure of multiresponsive “intelligent” core-shell microgels. *Journal of the American Chemical Society*, 127(26):9372–9373, jul 2005. doi: [10.1021/ja051825h](https://doi.org/10.1021/ja051825h). PMID: 15984856.
- [31] I. Berndt, J. S. Pedersen, and W. Richtering. Temperature-sensitive core-shell microgel particles with dense shell. *Angewandte Chemie*, 118(11):1769–1773, mar 2006. doi: [10.1002/ange.200503888](https://doi.org/10.1002/ange.200503888).
- [32] J. Berntsen, T. O. Espelid, and A. Genz. An adaptive algorithm for the approximate calculation of multiple integrals. 17(4):437–451. doi: [10.1145/210232.210233](https://doi.org/10.1145/210232.210233).
- [33] P. Bevington and D. K. Robinson. *Data Reduction and Error Analysis for the Physical Sciences*. McGraw-Hill, 3rd edition, 23 July 2002. URL <http://catalogs.mhhe.com/mhhe/viewProductDetails.do?isbn=0072472278>. ISBN-10: 0072472278, ISBN-13: 978-0072472271.
- [34] R. Biehl. Jscatter, a program for evaluation and analysis of experimental data. *PLOS ONE*, 14(6):e0218789, jun 2019. doi: [10.1371/journal.pone.0218789](https://doi.org/10.1371/journal.pone.0218789).
- [35] D. S. Biggs. *Accelerated iterative blind deconvolution*. PhD thesis, 1998. URL <http://hdl.handle.net/2292/1760>.
- [36] D. S. C. Biggs and M. Andrews. Conjugate gradient acceleration of maximum-likelihood image restoration. *Electronics Letters*, 31(23):1985–1986, Nov 1995. doi: [10.1049/el:19951400](https://doi.org/10.1049/el:19951400).
- [37] D. S. C. Biggs and M. Andrews. Acceleration of iterative image restoration algorithms. *Applied Optics*, 36(8):1766, mar 1997. doi: [10.1364/ao.36.001766](https://doi.org/10.1364/ao.36.001766).

- [38] C. Blanc and C. Schlick. Ratioquadrics: an alternative model for superquadrics. *The Visual Computer*, 12(8):420–428, aug 1996. doi: [10.1007/bf01785874](https://doi.org/10.1007/bf01785874).
- [39] A. Blanchard. SANS study of the non-linear relaxation mechanisms in a step-strain elongated linear polymer melt, 2004.
- [40] C. E. Blanchet and D. I. Svergun. Small-angle x-ray scattering on biological macromolecules and nanocomposites in solution. 64(1):37–54. doi: [10.1146/annurev-physchem-040412-110132](https://doi.org/10.1146/annurev-physchem-040412-110132). PMID: 23216378.
- [41] A. E. Blaurock. Evidence of bilayer structure and of membrane interactions from x-ray diffraction analysis. *Biochimica et Biophysica Acta (BBA) - Reviews on Biomembranes*, 650(4):167–207, may 1982. doi: [10.1016/0304-4157\(82\)90016-8](https://doi.org/10.1016/0304-4157(82)90016-8).
- [42] V. Bloomfield and B. H. Zimm. Viscosity, sedimentation, et cetera, of ring- and straight-chain polymers in dilute solution. *The Journal of Chemical Physics*, 44(1):315–323, jan 1966. doi: [10.1063/1.1726463](https://doi.org/10.1063/1.1726463).
- [43] C. Bohren and D. Huffman. *Absorption and Scattering of Light by Small Particles*. Wiley-VCH Verlag GmbH, apr 1998. doi: [10.1002/9783527618156](https://doi.org/10.1002/9783527618156).
- [44] J.-M. Bomont. *Recent Advances in the Field of Integral Equation Theories: Bridge Functions and Applications to Classical Fluids*, chapter Chapter 1, pages 1–84. John Wiley & Sons, Inc., apr 2008. doi: [10.1002/9780470259498.ch1](https://doi.org/10.1002/9780470259498.ch1).
- [45] J. M. Bomont and J. L. Bretonnet. A self-consistent integral equation: Bridge function and thermodynamic properties for the lennard-jones fluid. *The Journal of Chemical Physics*, 119(4):2188–2191, jul 2003. doi: [10.1063/1.1583675](https://doi.org/10.1063/1.1583675).
- [46] J.-M. Bomont and J.-L. Bretonnet. A consistent integral equation theory for hard spheres. *The Journal of Chemical Physics*, 121(3):1548–1552, jul 2004. doi: [10.1063/1.1764772](https://doi.org/10.1063/1.1764772).
- [47] M. Born and H. S. Green. A general kinetic theory of liquids. i. the molecular distribution functions. *Proceedings of the Royal Society A: Mathematical, Physical and Engineering Sciences*, 188(1012):10–18, dec 1946. doi: [10.1098/rspa.1946.0093](https://doi.org/10.1098/rspa.1946.0093).
- [48] M. Borowko, S. Sokolowski, and D. Henderson. Integral equations in the theory of simple fluids. In *Surfactant Science*, chapter 3, pages 135–165. CRC Press, feb 2000. doi: [10.1201/9781420030037.ch3](https://doi.org/10.1201/9781420030037.ch3).
- [49] B. Boucher, P. Chieux, P. Convert, and M. Tournarie. Small-angle neutron scattering determination of medium and long range order in the amorphous metallic alloy TbCu3.54. *Journal of Physics F: Metal Physics*, 13(7):1339–1357, jul 1983. doi: [10.1088/0305-4608/13/7/006](https://doi.org/10.1088/0305-4608/13/7/006).
- [50] R. Bracewell. Strip integration in radio astronomy. *Australian Journal of Physics*, 9(2):198, 1956. doi: [10.1071/ph560198](https://doi.org/10.1071/ph560198).
- [51] R. Bracewell. *The Projection-Slice Theorem*, pages 493–504. Springer US, Boston, MA, 2003. doi: [10.1007/978-1-4419-8963-5_14](https://doi.org/10.1007/978-1-4419-8963-5_14).
- [52] I. Breßler, J. Kohlbrecher, and A. F. Thünemann. Sasfit: a tool for small-angle scattering data analysis using a library of analytical expressions. *Journal of Applied Crystallography*, 48(5):1587–1598, sep 2015. doi: [10.1107/s1600576715016544](https://doi.org/10.1107/s1600576715016544).
- [53] G. Bricogne. A Bayesian statistical theory of the phase problem. I. A multichannel maximum-entropy formalism for constructing generalized joint probability distributions of structure factors. 44(4):517–545. doi: [10.1107/S01087673800354X](https://doi.org/10.1107/S01087673800354X).
- [54] G. Bricogne. Maximum entropy and the foundations of direct methods. 40(4):410–445. doi: [10.1107/S0108767384000866](https://doi.org/10.1107/S0108767384000866).
- [55] P. L. Britten and D. M. Collins. Information theory as a basis for the maximum determinant. 38(1):129–132. doi: [10.1107/S0567739482000230](https://doi.org/10.1107/S0567739482000230).
- [56] J. Brunner-Popela and O. Glatter. Small-Angle Scattering of Interacting Particles. I. Basic Principles of a Global Evaluation Technique. 30(4):431–442. doi: [10.1107/S0021889896015749](https://doi.org/10.1107/S0021889896015749).
- [57] M. R. Brzustowicz and A. T. Brunger. X-ray scattering from unilamellar lipid vesicles. 38(1):126–131. doi: [10.1107/s0021889804029206](https://doi.org/10.1107/s0021889804029206).
- [58] J. Bull and T. Freeman. Parallel globally adaptive algorithms for multi-dimensional integration. 19(1-2):3–16. doi: [10.1016/0168-9274\(95\)00076-7](https://doi.org/10.1016/0168-9274(95)00076-7).

- [59] W. Burchard. Angular dependence of scattered light from hyperbranched structures in a good solvent. a fractal approach. 37(10):3841–3849. doi: [10.1021/ma0499501](https://doi.org/10.1021/ma0499501).
- [60] W. Burchard. Particle scattering factors of some branched polymers. 10(5):919–927. doi: [10.1021/ma60059a008](https://doi.org/10.1021/ma60059a008).
- [61] W. Burchard. *Static and dynamic light scattering from branched polymers and biopolymers*, pages 1–124. Springer Berlin Heidelberg. doi: [10.1007/3-540-12030-0_1](https://doi.org/10.1007/3-540-12030-0_1).
- [62] W. Burchard. Statistics of star-shaped molecules. i. stars with polydisperse side chains. *Macromolecules*, 7(6):835–841, nov 1974. doi: [10.1021/ma60042a027](https://doi.org/10.1021/ma60042a027).
- [63] W. Burchard and K. Kajiwara. The statistics of stiff chain molecules. i. the particle scattering factor. *Proceedings of the Royal Society A: Mathematical, Physical and Engineering Sciences*, 316(1525):185–199, apr 1970. doi: [10.1098/rspa.1970.0074](https://doi.org/10.1098/rspa.1970.0074).
- [64] W. Burchard, K. Kajiwara, and D. Nerger. Static and dynamic scattering behavior of regularly branched chains: A model of soft?sphere microgels. 20(2):157–171. doi: [10.1002/pol.1982.180200201](https://doi.org/10.1002/pol.1982.180200201).
- [65] W. Burchard, E. Michel, and V. Trappe. Conformational properties of multiply twisted ring systems and daisy-like structures. *Macromolecules*, 29(18):5934–5939, jan 1996. doi: [10.1021/ma9603286](https://doi.org/10.1021/ma9603286).
- [66] W. Burchard and R. Schweins. Branched conformational properties of macromolecules in close relation to chemical synthesis. i. unperturbed structures. 143(11):114906. doi: [10.1063/1.4928962](https://doi.org/10.1063/1.4928962).
- [67] W. Burchard, R. Schweins, and M. Werner. Branched conformational properties of macromolecules in close relation to chemical synthesis. ii. influence of excluded volume interactions. 143(11). doi: [10.1063/1.4928963](https://doi.org/10.1063/1.4928963).
- [68] C. Burger and W. Ruland. Evaluation of equatorial orientation distributions. *Journal of Applied Crystallography*, 39(6):889–891, nov 2006. doi: [10.1107/s0021889806038957](https://doi.org/10.1107/s0021889806038957).
- [69] J. Burkardt. C code which creates sparse grids based on gauss-legendre, gauss-hermite, gauss-patterson, or a nested variation of gauss-hermite rules. URL https://people.sc.fsu.edu/~jburkardt/c_src/sparse_grid_hw/sparse_grid_hw.html.
- [70] J. Burkardt. Filon quadrature for oscillatory integrands. URL https://people.math.sc.edu/Burkardt/c_src/filon/filon.html.
- [71] J. Burkardt. Smolpack multidimensional quadrature using sparse grids. URL https://people.sc.fsu.edu/~jburkardt/c_src/smolpack/smolpack.html.
- [72] B. Burley. Practical hash-based Owen scrambling. 10(4):1–20. URL <http://jcgt.org/published/0009/04/01/>.
- [73] C. Byrne and P. P. B. Eggermont. EM algorithms. In *Handbook of Mathematical Methods in Imaging*, pages 271–344. Springer New York, 2011. doi: [10.1007/978-0-387-92920-0_8](https://doi.org/10.1007/978-0-387-92920-0_8).
- [74] C. Caccamo. Integral equation theory description of phase equilibria in classical fluids. *Physics Reports*, 274(1-2):1–105, sep 1996. doi: [10.1016/0370-1573\(96\)00011-7](https://doi.org/10.1016/0370-1573(96)00011-7).
- [75] A. Caille. X-ray scattering in smectic a. *Comptes Rendus des Seances de l'Academie des Sciences, Serie B: Sciences Physiques*, 274:891–893, 1972.
- [76] L. Cannavacciulo, J. S. Pedersen, and P. Schurtenberger. Monte carlo simulation study of concentration effects and scattering functions for polyelectrolyte wormlike micelles. *Langmuir*, 18(7):2922–2932, apr 2002. doi: [10.1021/la010884f](https://doi.org/10.1021/la010884f).
- [77] L. Cannavacciulo, J. S. Pedersen, and P. Schurtenberger. Single-coil properties and concentration effects for polyelectrolyte-like wormlike micelles: a monte carlo study. *Journal of Physics: Condensed Matter*, 14(9):2283–2295, feb 2002. doi: [10.1088/0953-8984/14/9/317](https://doi.org/10.1088/0953-8984/14/9/317).
- [78] N. F. Carnahan and K. E. Starling. Equation of state for nonattracting rigid spheres. *The Journal of Chemical Physics*, 51(2):635–636, jul 1969. doi: [10.1063/1.1672048](https://doi.org/10.1063/1.1672048).
- [79] E. F. Casassa. Some statistical properties of flexible ring polymers. *Journal of Polymer Science Part A: General Papers*, 3(2):605–614, feb 1965. doi: [10.1002/pol.1965.100030217](https://doi.org/10.1002/pol.1965.100030217).
- [80] E. F. Casassa and G. C. Berry. Angular distribution of intensity of rayleigh scattering from comblike branched molecules. 4(6):881–897. doi: [10.1002/pol.1966.160040605](https://doi.org/10.1002/pol.1966.160040605).
- [81] J. Castellanos, S. Gómez, and V. Guerra. The triangle method for finding the corner of the l-curve. *Applied Numerical Mathematics*, 43(4):359–373, dec 2002. doi: [10.1016/s0168-9274\(01\)00179-9](https://doi.org/10.1016/s0168-9274(01)00179-9).

- [82] M. Chae, R. Martin, and S. G. Walker. On an algorithm for solving fredholm integrals of the first kind. *Statistics and Computing*, 29(4):645–654, aug 2018. doi: [10.1007/s11222-018-9829-z](https://doi.org/10.1007/s11222-018-9829-z).
- [83] I. Charpentier and N. Jakse. Exact numerical derivatives of the pair-correlation function of simple liquids using the tangent linear method. *The Journal of Chemical Physics*, 114(5):2284–2292, feb 2001. doi: [10.1063/1.1332808](https://doi.org/10.1063/1.1332808).
- [84] S. M. Chase and L. D. Fosdick. An algorithm for filon quadrature. 12(8):453–457. doi: [10.1145/363196.363209](https://doi.org/10.1145/363196.363209).
- [85] A. D. Chave. Numerical integration of related hankel transforms by quadrature and continued fraction expansion. 48(12):1671–1686. doi: [10.1190/1.1441448](https://doi.org/10.1190/1.1441448).
- [86] S.-H. Chen and S. Choi. Mesoscopic scale structures in self-organized surfactant solutions determined by small-angle neutron scattering. *Supramolecular Science*, 5(3-4):197–206, jul 1998. doi: [10.1016/s0968-5677\(98\)80001-1](https://doi.org/10.1016/s0968-5677(98)80001-1).
- [87] W.-R. Chen, P. D. Butler, and L. J. Magid. Incorporating intermicellar interactions in the fitting of SANS data from cationic wormlike micelles. *Langmuir*, 22(15):6539–6548, jul 2006. doi: [10.1021/la0530440](https://doi.org/10.1021/la0530440).
- [88] J. Chihara. Integral euqations for fluids with long-range and short-range potentials. *Progress of Theoretical Physics*, 50(2):409–423, aug 1973. doi: [10.1143/ptp.50.409](https://doi.org/10.1143/ptp.50.409).
- [89] N. Choudhury and S. K. Ghosh. Integral equation theory of lennard-jones fluids: A modified verlet bridge function approach. *The Journal of Chemical Physics*, 116(19):8517, 2002. doi: [10.1063/1.1467894](https://doi.org/10.1063/1.1467894).
- [90] R. Chugh, V. Kumar, and S. Kumar. Strong convergence of a new three step iterative scheme in banach spaces. *American Journal of Computational Mathematics*, 02(04):345–357, 2012. doi: [10.4236/ajcm.2012.24048](https://doi.org/10.4236/ajcm.2012.24048).
- [91] F. H. C. Crick. The fourier transform of a coiled-coil. *Acta Crystallographica*, 6(8):685–689, sep 1953. doi: [10.1107/s0365110x53001952](https://doi.org/10.1107/s0365110x53001952).
- [92] S. Cusack, A. Miller, P. Krijgsman, and J. Mellema. An investigation of the structure of alfalfa mosaic virus by small-angle neutron scattering. 145(3):525–543. doi: [10.1016/0022-2836\(81\)90543-x](https://doi.org/10.1016/0022-2836(81)90543-x).
- [93] G. Damaschun and H.-V. Pürschel. Röntgen-kleinwinkelstreuung von isotropen proben ohne ferndnung. i. allgemeine theorie. *Acta Crystallographica Section A*, 27(3):193–197, may 1971. doi: [10.1107/s0567739471000457](https://doi.org/10.1107/s0567739471000457).
- [94] G. Damaschun, H.-V. Pürschel, and G. Sommer. Bestimmung der Gestalt gelöster Makromoleküle aus Röntgen-Kleinwinkeldiagrammen mit Hilfe von Gleichungssystemen. *Acta Crystallographica Section A*, 25(6):708, nov 1969. doi: [10.1107/s0567739469001586](https://doi.org/10.1107/s0567739469001586).
- [95] H. E. Daniels. XXI.—the statistical theory of stiff chains. *Proceedings of the Royal Society of Edinburgh. Section A. Mathematical and Physical Sciences*, 63(03):290–311, 1952. doi: [10.1017/s0080454100007160](https://doi.org/10.1017/s0080454100007160).
- [96] M. Daoud and J. Cotton. Star shaped polymers : a model for the conformation and its concentration dependence. *Journal de Physique*, 43(3):531–538, 1982. doi: [10.1051/jphys:01982004303053100](https://doi.org/10.1051/jphys:01982004303053100).
- [97] J. Dave and IBM Palo Alto Scientific Center. *Subroutines for Computing the Parameters of the Electromagnetic Radiation Scattered by a Sphere*. IBM Scientific Center, 1968. URL <https://books.google.ch/books?id=LQp4NAAACAAJ>.
- [98] J. V. Dave. Scattering of electromagnetic radiation by a large, absorbing sphere. *IBM Journal of Research and Development*, 13(3):302–313, may 1969. doi: [10.1147/rd.133.0302](https://doi.org/10.1147/rd.133.0302).
- [99] J. V. Dave. Scattering of visible light by large water spheres. *Applied Optics*, 8(1):155, jan 1969. doi: [10.1364/ao.8.000155](https://doi.org/10.1364/ao.8.000155).
- [100] W. I. F. David. Powder diffraction peak shapes. parameterization of the pseudo-voigt as a voigt function. *Journal of Applied Crystallography*, 19(1):63–64, feb 1986. doi: [10.1107/s0021889886089999](https://doi.org/10.1107/s0021889886089999).
- [101] W. Dębski. Probabilistic inverse theory. In R. Dmowska, editor, *Advances in Geophysics*, volume 52 of *Advances in Geophysics*, pages 1–102. Elsevier, 2010. doi: [10.1016/s0065-2687\(10\)52001-6](https://doi.org/10.1016/s0065-2687(10)52001-6).

- [102] M. L. de Haro and M. Robles. The structure factor and equation of state of hard-sphere fluids. *Journal of Physics: Condensed Matter*, 16(22):S2089–S2096, may 2004. doi: [10.1088/0953-8984/16/22/007](https://doi.org/10.1088/0953-8984/16/22/007).
- [103] P. Debye. Zerstreuung von röntgenstrahlen. *Annalen der Physik*, 351(6):809–823, 1915. doi: [10.1002/andp.19153510606](https://doi.org/10.1002/andp.19153510606).
- [104] P. Debye. Über die Zerstreuung von Röntgenstrahlen an amorphen Körpern. *Physik. Z.*, 28:135–141, 1927.
- [105] P. Debye. Molecular-weight determination by light scattering. *Journal of Physical and Colloid Chemistry*, 51(1):18–32, jan 1947. doi: [10.1021/j150451a002](https://doi.org/10.1021/j150451a002).
- [106] P. Debye, H. R. Anderson, and H. Brumberger. Scattering by an inhomogeneous solid. ii. the correlation function and its application. *Journal of Applied Physics*, 28(6):679–683, jun 1957. doi: [10.1063/1.1722830](https://doi.org/10.1063/1.1722830).
- [107] P. Debye and A. M. Bueche. Scattering by an inhomogeneous solid. *Journal of Applied Physics*, 20(6):518–525, jun 1949. doi: [10.1063/1.1698419](https://doi.org/10.1063/1.1698419).
- [108] A. P. Dempster, N. M. Laird, and D. B. Rubin. Maximum likelihood from incomplete data via the em algorithm. *Journal of the Royal Statistical Society. Series B (Methodological)*, 39(1):1–38, 1977. URL <http://www.jstor.org/stable/2984875>.
- [109] J. Dhont. *An Introduction to Dynamics of Colloids*. Studies in Interface Science. Elsevier Science, 1996. URL <https://books.google.ch/books?id=mmArTF5SJ9oC>.
- [110] P. Dimon, S. K. Sinha, D. A. Weitz, C. R. Safinya, G. S. Smith, W. A. Varady, and H. M. Lindsay. Structure of aggregated gold colloids. 57(5):595–598. doi: [10.1103/physrevlett.57.595](https://doi.org/10.1103/physrevlett.57.595).
- [111] M. Donatelli and L. Reichel. Square smoothing regularization matrices with accurate boundary conditions. *Journal of Computational and Applied Mathematics*, 272:334–349, dec 2014. doi: [10.1016/j.cam.2013.08.015](https://doi.org/10.1016/j.cam.2013.08.015).
- [112] W. D. Dozier, J. S. Huang, and L. J. Fetter. Colloidal nature of star polymer dilute and semidilute solutions. *Macromolecules*, 24(10):2810–2814, may 1991. doi: [10.1021/ma00010a026](https://doi.org/10.1021/ma00010a026).
- [113] D.-M. Duh and A. D. J. Haymet. Integral equation theory for uncharged liquids: The lennard-jones fluid and the bridge function. *The Journal of Chemical Physics*, 103(7):2625–2633, aug 1995. doi: [10.1063/1.470724](https://doi.org/10.1063/1.470724).
- [114] H. Durchschlag and P. Zipper. Prediction of Hydrodynamic Parameters of Biopolymers from Small-Angle Scattering Data. 30(6):1112–1124. doi: [10.1107/S0021889897003336](https://doi.org/10.1107/S0021889897003336).
- [115] J. Dzubiella, A. Jusufi, C. N. Likos, C. von Ferber, H. Löwen, J. Stellbrink, J. Allgaier, D. Richter, A. B. Schofield, P. A. Smith, W. C. K. Poon, and P. N. Pusey. Phase separation in star-polymer–colloid mixtures. *Physical Review E*, 64(1):010401, jun 2001. doi: [10.1103/physreve.64.010401](https://doi.org/10.1103/physreve.64.010401).
- [116] P. P. B. Eggermont. Nonlinear smoothing and the EM algorithm for positive integral equations of the first kind. *Applied Mathematics and Optimization*, 39(1):75–91, jan 1999. doi: [10.1007/s002459900099](https://doi.org/10.1007/s002459900099).
- [117] P. P. B. Eggermont and V. N. LaRiccia. Maximum smoothed likelihood density estimation for inverse problems. *The Annals of Statistics*, 23(1):199–220, feb 1995. doi: [10.1214/aos/1176324463](https://doi.org/10.1214/aos/1176324463).
- [118] J. A. Elliott and S. Hanna. A model-independent maximum-entropy method for the inversion of small-angle X-ray diffraction patterns. 32(6):1069–1083. doi: [10.1107/S0021889899010560](https://doi.org/10.1107/S0021889899010560).
- [119] M. Engel, B. Stühn, J. J. Schneider, T. Cornelius, and M. Naumann. Small-angle x-ray scattering (SAXS) off parallel, cylindrical, well-defined nanopores: from random pore distribution to highly ordered samples. *Applied Physics A*, 97(1):99–108, jul 2009. doi: [10.1007/s00339-009-5346-4](https://doi.org/10.1007/s00339-009-5346-4).
- [120] S. M. Fan, G. R. Luckhurst, and S. J. Picken. A deuterium nuclear magnetic resonance investigation of orientational order and director kinetics in aramid solutions. *The Journal of Chemical Physics*, 101(4):3255–3267, aug 1994. doi: [10.1063/1.467573](https://doi.org/10.1063/1.467573).
- [121] I. S. Fedorova and P. W. Schmidt. A general analytical method for calculating particle-dimension distributions from scattering data. *Journal of Applied Crystallography*, 11(5):405–411, oct 1978. doi: [10.1107/s0021889878013503](https://doi.org/10.1107/s0021889878013503).
- [122] L. A. Feigin and D. I. Svergun. *Structure Analysis by Small-Angle X-ray and Neutron Scattering*. Plenum Press, 1987.

- [123] M. E. Fisher and R. J. Burford. Theory of critical-point scattering and correlations. i. the ising model. *Physical Review*, 156(2):583–622, apr 1967. doi: [10.1103/physrev.156.583](https://doi.org/10.1103/physrev.156.583).
- [124] S. Förster, L. Apostol, and W. Bras. Scatter: software for the analysis of nano- and mesoscale small-angle scattering. *Journal of Applied Crystallography*, 43(3):639–646, apr 2010. doi: [10.1107/s0021889810008289](https://doi.org/10.1107/s0021889810008289).
- [125] S. Förster, S. Fischer, K. Zielske, C. Schellbach, M. Sztucki, P. Lindner, and J. Perlich. Calculation of scattering-patterns of ordered nano- and mesoscale materials. *Advances in Colloid and Interface Science*, 163(1):53–83, mar 2011. doi: [10.1016/j.cis.2010.12.003](https://doi.org/10.1016/j.cis.2010.12.003).
- [126] S. Förster, N. Hermsdorf, C. Böttcher, and P. Lindner. Structure of polyelectrolyte block copolymer micelles. *Macromolecules*, 35(10):4096–4105, may 2002. doi: [10.1021/ma011565y](https://doi.org/10.1021/ma011565y).
- [127] S. Förster, N. Hermsdorf, W. Leube, H. Schnablegger, M. Regenbrecht, S. Akari, P. Lindner, and C. Böttcher. Fusion of charged block copolymer micelles into toroid networks. *The Journal of Physical Chemistry B*, 103(32):6657–6668, aug 1999. doi: [10.1021/jp9900761](https://doi.org/10.1021/jp9900761).
- [128] S. Förster, A. Timmann, M. Konrad, C. Schellbach, A. Meyer, S. S. Funari, P. Mulvaney, and R. Knott. Scattering curves of ordered mesoscopic materials. *The Journal of Physical Chemistry B*, 109(4):1347–1360, feb 2005. doi: [10.1021/jp0467494](https://doi.org/10.1021/jp0467494).
- [129] Y. Fougerolle, A. Gribok, S. Foufou, F. Truchetet, and M. Abidi. Boolean operations with implicit and parametric representation of primitives using r-functions. *IEEE Transactions on Visualization and Computer Graphics*, 11(5):529–539, sep 2005. doi: [10.1109/tvcg.2005.72](https://doi.org/10.1109/tvcg.2005.72).
- [130] Y. Fougerolle, A. Gribok, S. Foufou, F. Truchetet, and M. Abidi. Implicit surface modeling using supershapes and r-functions. In *In Proc. of Pacific Graphics*, pages 169–172, 2005.
- [131] Y. D. Fougerolle, A. Gribok, S. Foufou, F. Truchetet, and M. A. Abidi. Radial supershapes for solid modeling. *Journal of Computer Science and Technology*, 21(2):238–243, mar 2006. doi: [10.1007/s11390-006-0238-y](https://doi.org/10.1007/s11390-006-0238-y).
- [132] Y. D. Fougerolle, A. Gribok, S. Foufou, F. Truchetet, and M. A. Abidi. Rational supershapes for surface reconstruction. In D. Fofi and F. Meriaudeau, editors, *Eighth International Conference on Quality Control by Artificial Vision*. SPIE, jan 2007. doi: [10.1117/12.736916](https://doi.org/10.1117/12.736916).
- [133] R. E. Franklin and A. Klug. The nature of the helical groove on the tobacco mosaic virus particle x-ray diffraction studies. *Biochimica et Biophysica Acta*, 19(Supplement C):403–416, jan 1956. doi: [10.1016/0006-3002\(56\)90463-2](https://doi.org/10.1016/0006-3002(56)90463-2).
- [134] P. Fratzl. Statistical model of the habit and arrangement of mineral crystals in the collagen of bone. *Journal of Statistical Physics*, 77(1-2):125–143, 1994. doi: [10.1007/BF02186835](https://doi.org/10.1007/BF02186835).
- [135] P. Fratzl and J. Lebowitz. Universality of scaled structure functions in quenched systems undergoing phase separation. *Acta Metallurgica*, 37(12):3245–3248, dec 1989. doi: [10.1016/0001-6160\(89\)90196-x](https://doi.org/10.1016/0001-6160(89)90196-x).
- [136] R. W. Freund. A transpose-free quasi-minimal residual algorithm for non-hermitian linear systems. *SIAM Journal on Scientific Computing*, 14(2):470–482, mar 1993. doi: [10.1137/0914029](https://doi.org/10.1137/0914029).
- [137] H. Frielinghaus and W. Pyckhout-Hintzen. Neutron scattering on different states of polymer-clay compounds: From solution to dry states. In *Clay-Polymer Nanocomposites*, pages 327–361. Elsevier, 2017. doi: [10.1016/b978-0-323-46153-5.00010-0](https://doi.org/10.1016/b978-0-323-46153-5.00010-0).
- [138] M. Frigo and S. G. Johnson. The fastest Fourier transform in the west. Technical Report MIT-LCS-TR-728, Massachusetts Institute of Technology, September 1997. URL <http://www.fftw.org/fftw-paper.pdf>.
- [139] M. Frigo and S. G. Johnson. The design and implementation of FFTW3. *Proceedings of the IEEE*, 93(2):216–231, 2005. doi: [10.1109/JPROC.2004.840301](https://doi.org/10.1109/JPROC.2004.840301). Special issue on “Program Generation, Optimization, and Platform Adaptation”.
- [140] B. J. Friskin. Revisiting the method of cumulants for the analysis of dynamic light-scattering data. *Applied Optics*, 40(24):4087, aug 2001. doi: [10.1364/ao.40.004087](https://doi.org/10.1364/ao.40.004087).
- [141] T. Frühwirth, G. Fritz, N. Freiberger, and O. Glatter. Structure and order in lamellar phases determined by small-angle scattering. *Journal of Applied Crystallography*, 37(5):703–710, sep 2004. doi: [10.1107/s0021889804012956](https://doi.org/10.1107/s0021889804012956).

- [142] H. Fukuda, A. Goto, and T. Imae. Structure determination of helical fibers by numerical simulation for small-angle neutron scattering†. *Langmuir*, 18(19):7107–7114, sep 2002. doi: [10.1021/la025528r](https://doi.org/10.1021/la025528r).
- [143] H. Furukawa. Dynamics-scaling theory for phase-separating unmixing mixtures: Growth rates of droplets and scaling properties of autocorrelation functions. *Physica A*, 123:497, 1984. doi: [10.1016/0378-4371\(84\)90168-7](https://doi.org/10.1016/0378-4371(84)90168-7).
- [144] M. Galassi, J. Davies, J. Theiler, B. Gough, G. Jungman, P. Alken, M. Booth, F. Rossi, and R. Ulerich. *GNU Scientific Library - Release 2.7*.
- [145] W. Gao, K. Yu, and Y. Wu. A new method for optimal regularization parameter determination in the inverse problem of load identification. doi: [10.1155/2016/7328969](https://doi.org/10.1155/2016/7328969).
- [146] D. Gazzillo and A. Giacometti. Analytic solutions for baxter’s model of sticky hard sphere fluids within closures different from the percus–yevick approximation. 120(10):4742–4754. doi: [10.1063/1.1645781](https://doi.org/10.1063/1.1645781).
- [147] D. Gazzillo and A. Giacometti. Pathologies in the sticky limit of hard sphere yukawa models for colloidal fluids: a possible correction. 101(14):2171–2179. doi: [10.1080/0026897031000122379](https://doi.org/10.1080/0026897031000122379).
- [148] D. Gazzillo, A. Giacometti, R. G. D. Valle, E. Venuti, and F. Carsughi. A scaling approximation for structure factors in the integral equation theory of polydisperse nonionic colloidal fluids. *The Journal of Chemical Physics*, 111(16):7636–7645, oct 1999. doi: [10.1063/1.480089](https://doi.org/10.1063/1.480089).
- [149] S. Gazzola, P. C. Hansen, and J. G. Nagy. IR tools: a MATLAB package of iterative regularization methods and large-scale test problems. *Numerical Algorithms*, 81(3):773–811, aug 2018. doi: [10.1007/s11075-018-0570-7](https://doi.org/10.1007/s11075-018-0570-7).
- [150] A. Genz and A. Malik. Remarks on algorithm 006: An adaptive algorithm for numerical integration over an n-dimensional rectangular region. 6(4):295–302. doi: [10.1016/0771-050x\(80\)90039-x](https://doi.org/10.1016/0771-050x(80)90039-x).
- [151] L. Giehm, C. L. P. Oliveira, G. Christiansen, J. S. Pedersen, and D. E. Otzen. SDS-induced fibrillation of α -synuclein: An alternative fibrillation pathway. *Journal of Molecular Biology*, 401(1):115–133, aug 2010. doi: [10.1016/j.jmb.2010.05.060](https://doi.org/10.1016/j.jmb.2010.05.060).
- [152] J. Gielis. A generic geometric transformation that unifies a wide range of natural and abstract shapes. *American Journal of Botany*, 90(3):333–338, mar 2003. doi: [10.3732/ajb.90.3.333](https://doi.org/10.3732/ajb.90.3.333).
- [153] C. J. Gilmore. Maximum Entropy and Bayesian Statistics in Crystallography: a Review of Practical Applications. 52(4):561–589. doi: [10.1107/S0108767396001560](https://doi.org/10.1107/S0108767396001560).
- [154] O. Glatter. A new method for the evaluation of small-angle scattering data. 10(5):415–421. doi: [10.1107/S0021889877013879](https://doi.org/10.1107/S0021889877013879).
- [155] O. Glatter. Comparison of two different methods for direct structure analysis from small-angle scattering data. 21(6):886–890. doi: [10.1107/S002188988007381](https://doi.org/10.1107/S002188988007381).
- [156] O. Glatter. Determination of particle-size distribution functions from small-angle scattering data by means of the indirect transformation method. 13(1):7–11. doi: [10.1107/S0021889880011429](https://doi.org/10.1107/S0021889880011429).
- [157] O. Glatter. Evaluation of small-angle scattering data from lamellar and cylindrical particles by the indirect transformation method. 13(6):577–584. doi: [10.1107/S0021889880012794](https://doi.org/10.1107/S0021889880012794).
- [158] O. Glatter. The interpretation of real-space information from small-angle scattering experiments. 12(2):166–175. doi: [10.1107/S0021889879012139](https://doi.org/10.1107/S0021889879012139).
- [159] O. Glatter. Data evaluation in small angle scattering: Calculation of the radial electron density distribution by means of indirect Fourier transformation. *Acta Physica Austriaca*, 47:83–102, 1977.
- [160] O. Glatter. Convolution square root of band-limited symmetrical functions and its application to small-angle scattering data. *Journal of Applied Crystallography*, 14(2):101–108, Apr 1981. doi: [10.1107/S002188988100887X](https://doi.org/10.1107/S002188988100887X).
- [161] O. Glatter and K. Gruber. Indirect transformation in reciprocal space: desmearing of small-angle scattering data from partially ordered systems. 26(4):512–518. doi: [10.1107/S0021889893000561](https://doi.org/10.1107/S0021889893000561).
- [162] O. Glatter and B. Hainisch. Improvements in real-space deconvolution of small-angle scattering data. 17(6):435–441. doi: [10.1107/S0021889884011894](https://doi.org/10.1107/S0021889884011894).
- [163] O. Glatter and O. Kratky, editors. *Small Angle X-ray Scattering*. Academic Press, 1982. URL http://web.archive.org/web/20110824105733/http://physchem.kfunigraz.ac.at/sm/Service/Glatter_Kratky_SAXS_1982.zip.

- [164] O. Glatter, J. Sieberer, and H. Schnablegger. A comparative study on different scattering techniques and data evaluation methods for sizing of colloidal systems using light scattering. 8(1-4):274–281. doi: [10.1002/ppsc.19910080150](https://doi.org/10.1002/ppsc.19910080150).
- [165] A. Goldin. Processing of experimental data in photon correlation spectroscopy under homodyne measuring scheme. *Optika i Spectroskopija*, pages 485–489, 1991.
- [166] C. J. Gommes. Stochastic models of disordered mesoporous materials for small-angle scattering analysis and more. *Microporous and Mesoporous Materials*, 257:62–78, feb 2018. doi: [10.1016/j.micromeso.2017.08.009](https://doi.org/10.1016/j.micromeso.2017.08.009).
- [167] C. J. Gommes and A. P. Roberts. Structure development of resorcinol-formaldehyde gels: Microphase separation or colloid aggregation. *Physical Review E*, 77(4), apr 2008. doi: [10.1103/physreve.77.041409](https://doi.org/10.1103/physreve.77.041409).
- [168] S. Goofsen, A. R. Brás, W. Pyckhout-Hintzen, A. Wischnewski, D. Richter, M. Rubinstein, J. Roovers, P. J. Lutz, Y. Jeong, T. Chang, and D. Vlassopoulos. Influence of the solvent quality on ring polymer dimensions. *Macromolecules*, 48(5):1598–1605, feb 2015. doi: [10.1021/ma502518p](https://doi.org/10.1021/ma502518p).
- [169] M. Gräf and D. Potts. On the computation of spherical designs by a new optimization approach based on fast spherical fourier transforms. 119(4):699–724. doi: [10.1007/s00211-011-0399-7](https://doi.org/10.1007/s00211-011-0399-7).
- [170] G. S. Greschner. Mathematical properties of polydisperse systems, 2. application to light scattering. *Die Makromolekulare Chemie*, 170(1):203–229, 1973. doi: [10.1002/macp.1973.021700117](https://doi.org/10.1002/macp.1973.021700117).
- [171] GSL Team. qawf-adaptive-integration-for-fourier-integrals. URL <https://www.gnu.org/software/gsl/doc/html/integration.html#qawf-adaptive-integration-for-fourier-integrals>.
- [172] GSL Team. qawo-adaptive-integration-for-oscillatory-functions. URL <https://www.gnu.org/software/gsl/doc/html/integration.html#qawo-adaptive-integration-for-oscillatory-functions>.
- [173] X. Gu and D. F. R. Mildner. Ultra-small-angle neutron scattering with azimuthal asymmetry. *Journal of Applied Crystallography*, 49(3):934–943, may 2016. doi: [10.1107/S1600576716005586](https://doi.org/10.1107/S1600576716005586).
- [174] X. Gu and D. F. R. Mildner. Determination of porosity in anisotropic fractal systems by neutron scattering. *Journal of Applied Crystallography*, 51(1):175–184, feb 2018. doi: [10.1107/S1600576718000080](https://doi.org/10.1107/S1600576718000080).
- [175] A. Guinier. La diffraction des rayons x aux très petits angles : application à l'étude de phénomènes ultramicroscopiques. *Annales de Physique*, 11(12):161–237, 1939. doi: [10.1051/anphys/193911120161](https://doi.org/10.1051/anphys/193911120161).
- [176] A. Guinier. *X-ray Diffraction*. San Francisco: Freeman, 1963.
- [177] A. Guinier and G. Fournet. *Small-Angle Scattering of X-Rays*. John Wiley & Sons, Inc., 1955.
- [178] X. Guo and U. Riebel. Theoretical direct correlation function for two-dimensional fluids of monodisperse hard spheres. *The Journal of Chemical Physics*, 125(14):144504, oct 2006. doi: [10.1063/1.2358133](https://doi.org/10.1063/1.2358133).
- [179] D. Guptasarma and B. Singh. New digital linear filters for hankel j_0 and j_1 transforms. 45(5):745–762. doi: [10.1046/j.1365-2478.1997.500292.x](https://doi.org/10.1046/j.1365-2478.1997.500292.x).
- [180] F. Gürsoy and V. Karakaya. A Picard-S hybrid type iteration method for solving a differential equation with retarded argument. *ArXiv e-prints*, Mar. 2014, [1403.2546](https://arxiv.org/abs/1403.2546). URL <https://arxiv.org/abs/1403.2546>.
- [181] W. C. Hamilton. Significance tests on the crystallographic r factor. *Acta Crystallographica*, 18(3):502–510, may 1965. doi: [10.1107/s0365110x65001081](https://doi.org/10.1107/s0365110x65001081).
- [182] B. Hammouda. *SANS from homogeneous polymer mixtures: A unified overview*, pages 87–133. Springer-Verlag, Berlin, Heidelberg, 1993. doi: [10.1007/bfb0025862](https://doi.org/10.1007/bfb0025862).
- [183] B. Hammouda. A new guinier-porod model. *Journal of Applied Crystallography*, 43(4):716–719, may 2010. doi: [10.1107/s0021889810015773](https://doi.org/10.1107/s0021889810015773).
- [184] B. Hammouda. Small-angle scattering from branched polymers. *Macromolecular Theory and Simulations*, 21(6):372–381, mar 2012. doi: [10.1002/mats.201100111](https://doi.org/10.1002/mats.201100111).
- [185] B. Hammouda. Form factors for branched polymers with excluded volume. *Journal of Research of the National Institute of Standards and Technology*, 121:139, apr 2016. doi: [10.6028/jres.121.006](https://doi.org/10.6028/jres.121.006).

- [186] B. Hammouda. the sans toolbox. [.../the_SANS_toolbox.pdf](http://www.ncnr.nist.gov/staff/hammouda/the_SANS_toolbox.pdf), 2016. URL http://www.ncnr.nist.gov/staff/hammouda/the_SANS_toolbox.pdf.
- [187] B. Hammouda, R. A. Bubeck, and D. F. Mildner. Macromolecular orientation in hot stretched and injection moulded polystyrene. *Polymer*, 27(3):393–397, mar 1986. doi: [10.1016/0032-3861\(86\)90155-2](https://doi.org/10.1016/0032-3861(86)90155-2).
- [188] B. Hammouda, D. F. R. Mildner, R. A. Bubeck, and M. T. Malanga. The inclination angle of nonisotropic inhomogeneities determined by SANS. *Journal of Applied Crystallography*, 19(5):320–323, oct 1986. doi: [10.1107/S002188988608929X](https://doi.org/10.1107/S002188988608929X).
- [189] M. Hanke. Iterative regularization techniques in image reconstruction. In D. Colton, H. W. Engl, A. K. Louis, J. R. McLaughlin, and W. Rundell, editors, *Surveys on Solution Methods for Inverse Problems*, pages 35–52. Springer Vienna, Vienna, 2000. doi: [10.1007/978-3-7091-6296-5_3](https://doi.org/10.1007/978-3-7091-6296-5_3).
- [190] H. J. M. Hanley, C. D. Muzny, D. L. Ho, and C. J. Glinka. A small-angle neutron scattering study of a commercial organoclay dispersion. *Langmuir*, 19(14):5575–5580, jul 2003. doi: [10.1021/la026342v](https://doi.org/10.1021/la026342v).
- [191] J.-P. Hansen and J. B. Hayter. A rescaled MSA structure factor for dilute charged colloidal dispersions. *Molecular Physics*, 46(3):651–656, jun 1982. doi: [10.1080/00268978200101471](https://doi.org/10.1080/00268978200101471).
- [192] J.-P. Hansen and I. R. McDonald. *Theory of Simple Liquids with Applications to Soft Matter*. Academic Press, fourth edition, 2013. doi: [10.1016/B978-0-12-387032-2.00013-1](https://doi.org/10.1016/B978-0-12-387032-2.00013-1).
- [193] P. Hansen. The l-curve and its use in the numerical treatment of inverse problems. In *InviteComputational Inverse Problems in Electrocadiology*. WIT Press, 2000.
- [194] P. C. Hansen. *Rank Deficient and Discrete Ill-Posed Problems*. Society for Industrial and Applied Mathematics, jan 1998. doi: [10.1137/1.9780898719697](https://doi.org/10.1137/1.9780898719697).
- [195] S. Hansen. Bayesian estimation of hyperparameters for indirect Fourier transformation in small-angle scattering. 33(6):1415–1421. doi: [10.1107/S0021889800012930](https://doi.org/10.1107/S0021889800012930).
- [196] S. Hansen. Bayesian estimation of hyperparameters for indirect Fourier transformation in small-angle scattering. 33(6):1415–1421. doi: [10.1107/S0021889800012930](https://doi.org/10.1107/S0021889800012930).
- [197] S. Hansen. Estimation of chord length distributions from small-angle scattering using indirect Fourier transformation. 36(5):1190–1196. doi: [10.1107/S0021889803014262](https://doi.org/10.1107/S0021889803014262).
- [198] S. Hansen. Simultaneous estimation of the form factor and structure factor for globular particles in small-angle scattering. 41(2):436–445. doi: [10.1107/S0021889808004937](https://doi.org/10.1107/S0021889808004937).
- [199] S. Hansen. Estimation of the density distribution from small-angle scattering data. *Journal of Applied Crystallography*, 49(3), Jun 2016. doi: [10.1107/S1600576716004969](https://doi.org/10.1107/S1600576716004969).
- [200] S. Hansen and J. J. Müller. *The Maximum-Entropy Method in Small-Angle Scattering*, chapter The Maximum-Entropy Method in Small-Angle Scattering, pages 69–78. Springer Netherlands. doi: [10.1007/978-94-009-0107-0_8](https://doi.org/10.1007/978-94-009-0107-0_8).
- [201] S. Hansen and J. S. Pedersen. A comparison of three different methods for analysing small-angle scattering data. 24(5):541–548. doi: [10.1107/S0021889890013322](https://doi.org/10.1107/S0021889890013322).
- [202] R. H. Hardin and N. J. A. Sloane. McLaren’s improved snub cube and other new spherical designs in three dimensions. 15(4):429–441. doi: [10.1007/bf02711518](https://doi.org/10.1007/bf02711518).
- [203] T. Hashimoto, T. Kawamura, M. Harada, and H. Tanaka. Small-angle scattering from hexagonally packed cylindrical particles with paracrystalline distortion. 27(11):3063–3072, 1994. doi: [10.1021/ma00089a025](https://doi.org/10.1021/ma00089a025).
- [204] J. B. Hayter and J. Penfold. An analytic structure factor for macroion solutions. *Molecular Physics*, 42(1):109–118, jan 1981. doi: [10.1080/00268978100100091](https://doi.org/10.1080/00268978100100091).
- [205] J. B. Hayter and J. Penfold. Use of viscous shear alignment to study anisotropic micellar structure by small-angle neutron scattering. *The Journal of Physical Chemistry*, 88(20):4589–4593, sep 1984. doi: [10.1021/j150664a030](https://doi.org/10.1021/j150664a030).
- [206] A. Heinemann, H. Hermann, A. Wiedenmann, N. Mattern, and K. Wetzig. A small-angle neutron scattering model for polydisperse spherical particles with diffusion zones and application to soft magnetic metallic glass. *Journal of Applied Crystallography*, 33(6):1386–1392, dec 2000. doi: [10.1107/s0021889800013248](https://doi.org/10.1107/s0021889800013248).
- [207] G. Heinrich, E. Straube, and G. Helm. Rubber elasticity of polymer networks: Theories. In *Polymer Physics*, pages 33–87. Springer Berlin Heidelberg, 1988. doi: [10.1007/bfb0024050](https://doi.org/10.1007/bfb0024050).

- [208] F. Heiss and V. Winschel. Likelihood approximation by numerical integration on sparse grids. 144(1):62–80. doi: [10.1016/j.jeconom.2007.12.004](https://doi.org/10.1016/j.jeconom.2007.12.004).
- [209] F. Heiss and V. Winschel. Quadrature on sparse grids: code to generate and readily evaluated nodes and weights. URL <http://www.sparse-grids.de/>.
- [210] D. Henderson and E. W. Grundke. Direct correlation function: Hard sphere fluid. *The Journal of Chemical Physics*, 63(2):601–607, jul 1975. doi: [10.1063/1.431378](https://doi.org/10.1063/1.431378).
- [211] N. C. Henderson and R. Varadhan. Damped anderson acceleration with restarts and monotonicity control for accelerating EM and EM-like algorithms. *Journal of Computational and Graphical Statistics*, pages 1–13, may 2019. doi: [10.1080/10618600.2019.1594835](https://doi.org/10.1080/10618600.2019.1594835).
- [212] J. Hermans and J. J. Hermans. Light scattering by zig-zag and worm-like chains. *The Journal of Physical Chemistry*, 62(12):1543–1546, dec 1958. doi: [10.1021/j150570a018](https://doi.org/10.1021/j150570a018).
- [213] A. C. Hindmarsh, P. N. Brown, K. E. Grant, S. L. Lee, R. Serban, D. E. Shumaker, and C. S. Woodward. SUNDIALS. *ACM Transactions on Mathematical Software*, 31(3):363–396, sep 2005. doi: [10.1145/1089014.1089020](https://doi.org/10.1145/1089014.1089020).
- [214] O. Hittmair. *Lehrbuch der Quantentheorie*. Verlag Karl Thiemicig, 1972.
- [215] R. P. Hjelm, C. Schteingart, A. F. Hofmann, and D. S. Sivia. Form and structure of self-assembling particles in monoolein-bile salt mixtures. *The Journal of Physical Chemistry*, 99(44):16395–16406, nov 1995. doi: [10.1021/j100044a030](https://doi.org/10.1021/j100044a030).
- [216] R. P. Hjelm, C. D. Schteingart, A. F. Hofmann, and P. Thiyagarajan. Structure of conjugated bile salt-fatty acid-monoglyceride mixed colloids: Studies by small-angle neutron scattering. *The Journal of Physical Chemistry B*, 104:197–211, 2000. doi: [10.1021/jp992157n](https://doi.org/10.1021/jp992157n).
- [217] R. P. Hjelm, P. Thiyagarajan, and H. Alkan-Onyuksel. Organization of phosphatidylcholine and bile salt in rodlike mixed micelles. *The Journal of Physical Chemistry*, 96(21):8653–8661, oct 1992. doi: [10.1021/j100200a080](https://doi.org/10.1021/j100200a080).
- [218] R. Hofstadter. Electron scattering and nuclear structure. *Reviews of Modern Physics*, 28(3):214–254, jul 1956. doi: [10.1103/revmodphys.28.214](https://doi.org/10.1103/revmodphys.28.214).
- [219] H. H. Homeier, S. Rast, and H. Krienke. Iterative solution of the ornstein-zernike equation with various closures using vector extrapolation. *Computer Physics Communications*, 92(2-3):188 – 202, dec 1995. doi: [10.1016/0010-4655\(95\)00116-0](https://doi.org/10.1016/0010-4655(95)00116-0).
- [220] K. M. Hong and J. Noolandi. Non-equilibrium static form factor of a reptating chain. *Die Makromolekulare Chemie, Rapid Communications*, 4(9):617–621, sep 1983. doi: [10.1002/marc.1983.030040907](https://doi.org/10.1002/marc.1983.030040907).
- [221] K. Horne. Images of accretion discs - i. the eclipse mapping method. *Monthly Notices of the Royal Astronomical Society*, 213(2):129–141, mar 1985. doi: [10.1093/mnras/213.2.129](https://doi.org/10.1093/mnras/213.2.129).
- [222] R. Hosemann and S. Bagchi. *Direct Analysis of Diffraction by Matter*. Amsterdam: North-Holland., 1962.
- [223] H. Hsu, W. Paul, and K. Binder. One- and two- component bottle-brush polymers: Simulations compared to theoretical predictions. 16(7):660–689. doi: [10.1002/mats.200700031](https://doi.org/10.1002/mats.200700031).
- [224] H.-P. Hsu, W. Paul, and K. Binder. Structure of bottle-brush polymers in solution: A monte carlo test of models for the scattering function. 129(20). doi: [10.1063/1.3025893](https://doi.org/10.1063/1.3025893).
- [225] K. Huber and W. Burchard. Scattering behavior of wormlike star macromolecules. *Macromolecules*, 22(8):3332–3336, aug 1989. doi: [10.1021/ma00198a024](https://doi.org/10.1021/ma00198a024).
- [226] M. Hunter, V. Backman, G. Popescu, M. Kalashnikov, C. W. Boone, A. Wax, V. Gopal, K. Badizadegan, G. D. Stoner, and M. S. Feld. Tissue self-affinity and polarized light scattering in the born approximation: A new model for precancer detection. *Physical Review Letters*, 97(13):138102, sep 2006. doi: [10.1103/physrevlett.97.138102](https://doi.org/10.1103/physrevlett.97.138102).
- [227] A. J. Hurd and W. L. Flower. In situ growth and structure of fractal silica aggregates in a flame. *Journal of Colloid and Interface Science*, 122(1):178–192, mar 1988. doi: [10.1016/0021-9797\(88\)90301-3](https://doi.org/10.1016/0021-9797(88)90301-3).
- [228] M. Huš, M. Zalar, and T. Urbic. Correctness of certain integral equation theories for core-softened fluids. *The Journal of Chemical Physics*, 138(22):224508, jun 2013. doi: [10.1063/1.4809744](https://doi.org/10.1063/1.4809744).

- [229] T. Ida, M. Ando, and H. Toraya. Extended pseudo-voigt function for approximating the voigt profile. *Journal of Applied Crystallography*, 33(6):1311–1316, dec 2000. doi: [10.1107/s0021889800010219](https://doi.org/10.1107/s0021889800010219).
- [230] W. R. Inc. Mathematica, Version 12.1. URL <https://www.wolfram.com/wolfram-alpha-notebook-edition>. Champaign, IL, 2021.
- [231] B. Ingham, H. Li, E. L. Allen, and M. F. Toney. SAXSMorph: a program for generating representative morphologies for two-phase materials from small-angle x-ray and neutron scattering data. *Journal of Applied Crystallography*, 44(1):221–224, dec 2010. doi: [10.1107/s0021889810048557](https://doi.org/10.1107/s0021889810048557).
- [232] U. B. Institut für Numerische Simulation. Frolov cubature points in $[0, 1]^d$. URL <https://ins.uni-bonn.de/content/software-frolov>.
- [233] S. Ishikawa. Fixed points by a new iteration method. *Proceedings of the American Mathematical Society*, 44(1):147–150, jan 1974. doi: [10.1090/s0002-9939-1974-0336469-5](https://doi.org/10.1090/s0002-9939-1974-0336469-5).
- [234] J. Jakeš. Testing of the constrained regularization method of inverting laplace transform on simulated very wide quasielastic light scattering autocorrelation functions. *Czechoslovak Journal of Physics B*, 38(12):1305–1316, 1988. doi: [10.1007/BF01597611](https://doi.org/10.1007/BF01597611).
- [235] J. Jakeš and V. Saudek. Emical molecular weight distribution functions as determined from gel permeation chromatography data. *Die Makromolekulare Chemie*, 187(9):2223–2234, sep 1986. doi: [10.1002/macp.1986.021870919](https://doi.org/10.1002/macp.1986.021870919).
- [236] J. Jakeš and P. Štěpánek. Positive exponential sum method of inverting laplace transform applied to photon correlation spectroscopy. *Czechoslovak Journal of Physics*, 40(9):972–983, 1990. doi: [10.1007/BF01607285](https://doi.org/10.1007/BF01607285).
- [237] J. Jakeš. A simple method of estimation of the polydispersity index of narrow molecular weight distributions by using quasielastic light scattering data. *Collect. Czech. Chem. Commun.*, 56:1642–1652, 1991. doi: [10.1135/cccc19911642](https://doi.org/10.1135/cccc19911642).
- [238] J. Jakeš. Regularized positive exponential sum (repes) program - a way of inverting laplace transform data obtained by dynamic light scattering. *Collect. Czech. Chem. Commun.*, 60:1781–1797, 1995. doi: [10.1135/cccc19951781](https://doi.org/10.1135/cccc19951781).
- [239] P. R. Jemian and A. J. Allen. The effect of the shape function on small-angle scattering analysis by the maximum-entropy method. 27(5):693–702. doi: [10.1107/S0021889894000373](https://doi.org/10.1107/S0021889894000373).
- [240] G. V. Jensen and J. G. Barker. Effects of multiple scattering encountered for various small-angle scattering model functions. *Journal of Applied Crystallography*, 51(5):1455–1466, sep 2018. doi: [10.1107/s1600576718010816](https://doi.org/10.1107/s1600576718010816).
- [241] G. Jerke, J. S. Pedersen, S. U. Egelhaaf, and P. Schurtenberger. Static structure factor of polymerlike micelles: overall dimension, flexibility, and local properties of lecithin reverse micelles in deuterated isoctane. *Physical Review E*, 56(5):5772–5788, nov 1997. doi: [10.1103/physreve.56.5772](https://doi.org/10.1103/physreve.56.5772).
- [242] H. G. Jerrard. Theories of streaming double refraction. *Chemical Reviews*, 59(3):345–428, jun 1959. doi: [10.1021/cr50027a001](https://doi.org/10.1021/cr50027a001).
- [243] J. Jiang, J. Huang, and G. Zhang. An accelerated motion blurred star restoration based on single image. *IEEE Sensors Journal*, 17(5):1306–1315, mar 2017. doi: [10.1109/jsen.2016.2645861](https://doi.org/10.1109/jsen.2016.2645861).
- [244] H. Jinnai, Y. Nishikawa, S.-H. Chen, S. Koizumi, and T. Hashimoto. Morphological characterization of bicontinuous structures in polymer blends and microemulsions by the inverse-clipping method in the context of the clipped-random-wave model. *Physical Review E*, 61(6):6773–6780, jun 2000. doi: [10.1103/physreve.61.6773](https://doi.org/10.1103/physreve.61.6773).
- [245] S. G. Johnson. multi-dimensional adaptive integration (cubature) in C, 2017. URL <https://github.com/stevengj/cubature>.
- [246] J. E. Jones. On the determination of molecular fields. II. from the equation of state of a gas. *Proceedings of the Royal Society A: Mathematical, Physical and Engineering Sciences*, 106(738):463–477, oct 1924. doi: [10.1098/rspa.1924.0082](https://doi.org/10.1098/rspa.1924.0082).
- [247] M. R. Jones, R. J. Macfarlane, B. Lee, J. Zhang, K. L. Young, A. J. Senesi, and C. A. Mirkin. Dna-nanoparticle superlattices formed from anisotropic building blocks. 9(11):913–917. doi: [10.1038/nmat2870](https://doi.org/10.1038/nmat2870).

- [248] A. Jusufi, J. Dzubiella, C. N. Likos, C. von Ferber, and H. Löwen. Effective interactions between star polymers and colloidal particles. *Journal of Physics: Condensed Matter*, 13(28):6177, jun 2001. doi: [10.1088/0953-8984/13/28/303](https://doi.org/10.1088/0953-8984/13/28/303).
- [249] C. Kacwin, J. Oettershagen, M. Ullrich, and T. Ullrich. Numerical performance of optimized frolov lattices in tensor product reproducing kernel sobolev spaces. 21(3):849–889. doi: [10.1007/s10208-020-09463-y](https://doi.org/10.1007/s10208-020-09463-y).
- [250] K. Kajiwara, W. Burchard, and M. Gordon. Angular distribution of rayleigh scattering from randomly branched polycondensates. 2(2):110–115. doi: [10.1002/pi.4980020203](https://doi.org/10.1002/pi.4980020203).
- [251] Z.-B. Kang, A. Prokudin, N. Sato, and J. Terry. Efficient fourier transforms for transverse momentum dependent distributions. 258:107611. doi: [10.1016/j.cpc.2020.107611](https://doi.org/10.1016/j.cpc.2020.107611).
- [252] I. Karahan and M. Ozdemir. Fixed point problems of the picard-mann hybrid iterative process for continuous functions on an arbitrary interval. *Fixed Point Theory and Applications*, 2013(1):244, 2013. doi: [10.1186/1687-1812-2013-244](https://doi.org/10.1186/1687-1812-2013-244).
- [253] I. Karahan and M. Ozdemir. A general iterative method for approximation of fixed points and their applications. *Advances in Fixed Point Theory*, 3(3):510–526, 2013. URL <http://scik.org/index.php/afpt/article/view/1100/527>.
- [254] T. Kawaguchi. Radii of gyration and scattering functions of a torus and its derivatives. *Journal of Applied Crystallography*, 34(5):580–584, sep 2001. doi: [10.1107/s0021889801009517](https://doi.org/10.1107/s0021889801009517).
- [255] H. Kaya. Scattering from cylinders with globular end-caps. *Journal of Applied Crystallography*, 37(2):223–230, mar 2004. doi: [10.1107/s0021889804000020](https://doi.org/10.1107/s0021889804000020).
- [256] H. Kaya and N.-R. de Souza. Scattering from capped cylinders. addendum. *Journal of Applied Crystallography*, 37(3):508–509, may 2004. doi: [10.1107/s0021889804005709](https://doi.org/10.1107/s0021889804005709).
- [257] T. W. Keelin. The metalog distributions. 13(4):243–277. doi: [10.1287/deca.2016.0338](https://doi.org/10.1287/deca.2016.0338).
- [258] T. W. Keelin, L. Chrisman, and S. L. Savage. *The Metalog Distributions and Extremely Accurate Sums of Lognormals in Closed Form*, pages 3074–3085. IEEE Press.
- [259] T. W. Keelin and B. W. Powley. Quantile-parameterized distributions. 8(3):206–219. doi: [10.1287/deca.1110.0213](https://doi.org/10.1287/deca.1110.0213).
- [260] C. T. Kelley. *Solving Nonlinear Equations with Newton's Method*. Society for Industrial and Applied Mathematics, jan 2003. doi: [10.1137/1.9780898718898](https://doi.org/10.1137/1.9780898718898).
- [261] M. Kerker. *The Scattering of Light and Other Electromagnetic Radiation*. Elsevier, 1969. doi: [10.1016/c2013-0-06195-6](https://doi.org/10.1016/c2013-0-06195-6).
- [262] M. Kern. *Numerical Methods for Inverse Problems*. John Wiley & Sons, Inc., may 2016. doi: [10.1002/9781119136941](https://doi.org/10.1002/9781119136941).
- [263] K. Key. Is the fast hankel transform faster than quadrature? 77(3):F21–F30. doi: [10.1190/geo2011-0237.1](https://doi.org/10.1190/geo2011-0237.1).
- [264] S. Khan. A picard-mann hybrid iterative process. *Fixed Point Theory and Applications*, 2013(1):69, 2013. doi: [10.1186/1687-1812-2013-69](https://doi.org/10.1186/1687-1812-2013-69).
- [265] A. L. Kholodenko. Analytical calculation of the scattering function for polymers of arbitrary flexibility using the dirac propagator. *Macromolecules*, 26(16):4179–4183, aug 1993. doi: [10.1021/ma00068a017](https://doi.org/10.1021/ma00068a017).
- [266] L. Klimeš. Correlation functions of random media. *Pure and Applied Geophysics*, 159(7-8):1811–1831, jul 2002. doi: [10.1007/s00024-002-8710-2](https://doi.org/10.1007/s00024-002-8710-2).
- [267] S. R. Kline and E. W. Kaler. An Optimization Regularization Method for Determination of Partial Structure Factors from Small-Angle Scattering Experiments. 29(4):427–434. doi: [10.1107/S0021889896001616](https://doi.org/10.1107/S0021889896001616).
- [268] J. Kohlbrecher and A. Studer. Transformation cycle between the spherically symmetric correlation function, projected correlation function and differential cross section as implemented in *SASfit*. *Journal of Applied Crystallography*, 50(5):1395–1403, Oct 2017. doi: [10.1107/S1600576717011979](https://doi.org/10.1107/S1600576717011979).
- [269] J. Kohlbrecher, A. Wiedenmann, and H. Wollenberger. Magnetic coupling between the different phases in nanocrystalline fe-si-b studied by small angle neutron scattering. *Zeitschrift für Physik B Condensed Matter*, 104(1):1–4, jan 1997. doi: [10.1007/s002570050411](https://doi.org/10.1007/s002570050411).
- [270] F. Kong. Hankel transform filters for dipole antenna radiation in a conductive medium. 55(1):83–89. doi: [10.1111/j.1365-2478.2006.00585.x](https://doi.org/10.1111/j.1365-2478.2006.00585.x).

- [271] D. E. Koppel. Analysis of macromolecular polydispersity in intensity correlation spectroscopy: The method of cumulants. *The Journal of Chemical Physics*, 57(11):4814–4820, 1972. doi: [10.1063/1.1678153](https://doi.org/10.1063/1.1678153).
- [272] A. Korolkovas, S. Prévost, M. Kawecki, A. Devishvili, F. A. Adlmann, P. Gutfreund, and M. Wolff. The viscoelastic signature underpinning polymer deformation under shear flow. *Soft Matter*, 15(3):371–380, 2019. doi: [10.1039/c8sm02255k](https://doi.org/10.1039/c8sm02255k).
- [273] M. Kotlarchyk and S.-H. Chen. Analysis of small angle neutron scattering spectra from polydisperse interacting colloids. *The Journal of Chemical Physics*, 79(5):2461–2469, sep 1983. doi: [10.1063/1.446055](https://doi.org/10.1063/1.446055).
- [274] A. Kovalenko and F. Hirata. Self-consistent description of a metal–water interface by the kohn–sham density functional theory and the three-dimensional reference interaction site model. *The Journal of Chemical Physics*, 110(20):10095–10112, may 1999. doi: [10.1063/1.478883](https://doi.org/10.1063/1.478883).
- [275] R. Koyama. Light scattering of stiff chain polymers. *Journal of the Physical Society of Japan*, 34(4):1029–1038, apr 1973. doi: [10.1143/jpsj.34.1029](https://doi.org/10.1143/jpsj.34.1029).
- [276] R. Koyama. Light scattering of stiff chain polymers. II. *Journal of the Physical Society of Japan*, 36(5):1409–1417, may 1974. doi: [10.1143/jpsj.36.1409](https://doi.org/10.1143/jpsj.36.1409).
- [277] M. A. Krasnoselskij. Two remarks on the method of successive approximations, (russian). *Uspehi Mat. Nauk.* 10, 63(1):123–127, 1955. URL <http://mi.mathnet.ru/eng/umn7954>.
- [278] O. Kratky. Zum deformationsmechanismus der faserstoffe, i. *Kolloid-Zeitschrift*, 64(2):213–222, aug 1933. doi: [10.1007/bf01434162](https://doi.org/10.1007/bf01434162).
- [279] O. Kratky and O. Glatter. *Small angle x-ray scattering / edited by O. Glatter and O. Kratky*. Academic Press London ; New York, 1982.
- [280] O. Kratky and G. Porod. Diffuse small-angle scattering of x-rays in colloid systems. *Journal of Colloid Science*, 4(1):35–70, feb 1949. doi: [10.1016/0095-8522\(49\)90032-x](https://doi.org/10.1016/0095-8522(49)90032-x).
- [281] H. G. Krauthäuser, W. Lennartz, and G. Nimtz. Real-Space Distributions from Small-Angle Scattering Data: Structure Interference Method *versus* Indirect Transformation Method. 29(1):7–15. doi: [10.1107/S0021889895008338](https://doi.org/10.1107/S0021889895008338).
- [282] T. Krouglov, I. M. de Schepper, W. G. Bouwman, and M. T. Rekeldt. Real-space interpretation of spin-echo small-angle neutron scattering. 36(1):117–124. doi: [10.1107/s0021889802020368](https://doi.org/10.1107/s0021889802020368).
- [283] C. G. D. Kruif, P. W. Rouw, W. J. Briels, M. H. G. Duits, A. Vrij, and R. P. May. Adhesive hard-sphere colloidal dispersions. a small-angle neutron-scattering study of stickiness and the structure factor. *Langmuir*, 5(2):422–428, mar 1989. doi: [10.1021/la00086a023](https://doi.org/10.1021/la00086a023).
- [284] K. Kubota, Y. Tominaga, S. Fujime, J. Otomo, and A. Ikegami. Dynamic light scattering study of suspensions of purple membrane. *Biophysical Chemistry*, 23(1):15 – 29, 1985. doi: [10.1016/0301-4622\(85\)80060-0](https://doi.org/10.1016/0301-4622(85)80060-0).
- [285] A. H. Larsen, L. Arleth, and S. Hansen. Analysis of small-angle scattering data using model fitting and bayesian regularization. *Journal of Applied Crystallography*, 51(4):1151–1161, jul 2018. doi: [10.1107/s1600576718008956](https://doi.org/10.1107/s1600576718008956).
- [286] A. H. Larsen, J. S. Pedersen, and L. Arleth. Assessment of structure factors for analysis of small-angle scattering data from desired or undesired aggregates. *Journal of Applied Crystallography*, 53(4), jul 2020. doi: [10.1107/s1600576720006500](https://doi.org/10.1107/s1600576720006500).
- [287] M. Lattuada, H. Wu, and M. Morbidelli. A simple model for the structure of fractal aggregates. 268(1):106–120. doi: [10.1016/j.jcis.2003.07.027](https://doi.org/10.1016/j.jcis.2003.07.027).
- [288] C. L. Lawson and R. J. Hanson. 23. linear least squares with linear inequality constraints. In *Solving Least Squares Problems*, pages 158–173. Society for Industrial and Applied Mathematics, jan 1995. doi: [10.1137/1.9781611971217.ch23](https://doi.org/10.1137/1.9781611971217.ch23).
- [289] A. Leadbetter and E. Norris. Distribution functions in three liquid crystals from x-ray diffraction measurements. *Molecular Physics*, 38(3):669–686, sep 1979. doi: [10.1080/00268977900101961](https://doi.org/10.1080/00268977900101961).
- [290] D. Lebedev, D. Baitin, A. Islamov, A. Kuklin, V. Shalguev, V. Lanzov, and V. Isaev-Ivanov. Analytical model for determination of parameters of helical structures in solution by small angle scattering: comparison of RecA structures by SANS. *FEBS Letters*, 537(1-3):182–186, feb 2003. doi: [10.1016/s0014-5793\(03\)00107-8](https://doi.org/10.1016/s0014-5793(03)00107-8).

- [291] V. Lebedev. Values of the nodes and weights of ninth to seventeenth order gauss-markov quadrature formulae invariant under the octahedron group with inversion. *USSR Computational Mathematics and Mathematical Physics*, 15(1):44–51, jan 1975. doi: [10.1016/0041-5553\(75\)90133-0](https://doi.org/10.1016/0041-5553(75)90133-0).
- [292] V. Lebedev. Quadratures on a sphere. *USSR Computational Mathematics and Mathematical Physics*, 16(2):10–24, jan 1976. doi: [10.1016/0041-5553\(76\)90100-2](https://doi.org/10.1016/0041-5553(76)90100-2).
- [293] V. I. Lebedev. Spherical quadrature formulas exact to orders 25?29. *Siberian Mathematical Journal*, 18(1):99–107, 1977. doi: [10.1007/BF00966954](https://doi.org/10.1007/BF00966954).
- [294] J. L. Lebowitz and J. K. Percus. Mean spherical model for lattice gases with extended hard cores and continuum fluids. *Physical Review*, 144(1):251–258, apr 1966. doi: [10.1103/physrev.144.251](https://doi.org/10.1103/physrev.144.251).
- [295] L. L. Lee. An accurate integral equation theory for hard spheres: Role of the zero-separation theorems in the closure relation. *The Journal of Chemical Physics*, 103(21):9388–9396, dec 1995. doi: [10.1063/1.469998](https://doi.org/10.1063/1.469998).
- [296] H. N. Lekkerkerker and R. Tuinier. *Colloids and the Depletion Interaction*, volume 833 of *Lecture Notes in Physics*. Springer Netherlands, 2011. doi: [10.1007/978-94-007-1223-2](https://doi.org/10.1007/978-94-007-1223-2).
- [297] J. Lemmich, K. Mortensen, J. H. Ipsen, T. Hønger, R. Bauer, and O. G. Mouritsen. Small-angle neutron scattering from multilamellar lipid bilayers: Theory, model, and experiment. *Physical Review E*, 53(5):5169–5180, may 1996. doi: [10.1103/physreve.53.5169](https://doi.org/10.1103/physreve.53.5169).
- [298] E. Leutheusser. Exact solution of the percus-yevick equation for a hard-core fluid in odd dimensions. *Physica A: Statistical Mechanics and its Applications*, 127(3):667–676, oct 1984. doi: [10.1016/0378-4371\(84\)90050-5](https://doi.org/10.1016/0378-4371(84)90050-5).
- [299] P. Levitz. Off-lattice reconstruction of porous media: critical evaluation, geometrical confinement and molecular transport. *Advances in Colloid and Interface Science*, 76-77:71–106, jul 1998. doi: [10.1016/s0001-8686\(98\)00042-6](https://doi.org/10.1016/s0001-8686(98)00042-6).
- [300] R. M. Lewitt and G. Muehllehner. Accelerated iterative reconstruction for positron emission tomography based on the EM algorithm for maximum likelihood estimation. *IEEE Transactions on Medical Imaging*, 5(1):16–22, mar 1986. doi: [10.1109/tmi.1986.4307734](https://doi.org/10.1109/tmi.1986.4307734).
- [301] X. Li, C.-Y. Shew, L. He, F. Meilleur, D. A. A. Myles, E. Liu, Y. Zhang, G. S. Smith, K. W. Herwig, R. Pynn, and W.-R. Chen. Scattering functions of platonic solids. 44(3):545–557. doi: [10.1107/s0021889811011691](https://doi.org/10.1107/s0021889811011691).
- [302] C. N. Likos. Effective interactions in soft condensed matter physics. *Physics Reports*, 348(4-5):267–439, jul 2001. doi: [10.1016/s0370-1573\(00\)00141-1](https://doi.org/10.1016/s0370-1573(00)00141-1).
- [303] C. N. Likos. Soft matter with soft particles. *Soft Matter*, 2(6):478, 2006. doi: [10.1039/B601916C](https://doi.org/10.1039/B601916C).
- [304] C. N. Likos. Structure and thermodynamics of ionic microgels. In A. F.-N. H. M. Wyss, J. Mattsson, and D. A. Weitz, editors, *Microgel Suspensions*, chapter Chapter 7., pages 163–193. Wiley-VCH Verlag GmbH & Co. KGaA, feb 2011. doi: [10.1002/9783527632992.ch7](https://doi.org/10.1002/9783527632992.ch7).
- [305] C. N. Likos, H. Löwen, M. Watzlawek, B. Abbas, O. Jucknischke, J. Allgaier, and D. Richter. Star polymers viewed as ultrasoft colloidal particles. *Physical Review Letters*, 80(20):4450–4453, may 1998. doi: [10.1103/physrevlett.80.4450](https://doi.org/10.1103/physrevlett.80.4450).
- [306] M. Lin, R. Klein, H. Lindsay, D. Weitz, R. Ball, and P. Meakin. The structure of fractal colloidal aggregates of finite extent. *Journal of Colloid and Interface Science*, 137(1):263–280, jun 1990. doi: [10.1016/0021-9797\(90\)90061-r](https://doi.org/10.1016/0021-9797(90)90061-r).
- [307] M. Lin, H. Lindsay, D. Weitz, R. Ball, R. Klein, and P. Meakin. Universality of fractal aggregates as probed by light scattering. *Proc. R. Soc. Lond. A*, 423:71–87, 1989. doi: [10.1098/rspa.1989.0042](https://doi.org/10.1098/rspa.1989.0042).
- [308] M. Y. Lin, H. M. Lindsay, D. A. Weitz, R. C. Ball, R. Klein, and P. Meakin. Universal reaction-limited colloid aggregation. *Physical Review A*, 41(4):2005–2020, feb 1990. doi: [10.1103/physreva.41.2005](https://doi.org/10.1103/physreva.41.2005).
- [309] M. Y. Lin, H. M. Lindsay, D. A. Weitz, R. Klein, R. C. Ball, and P. Meakin. Universal diffusion-limited colloid aggregation. *Journal of Physics: Condensed Matter*, 2(13):3093–3113, apr 1990. doi: [10.1088/0953-8984/2/13/019](https://doi.org/10.1088/0953-8984/2/13/019).
- [310] M. Y. Lin, H. M. Lindsay, D. A. Weitz, R. Klein, R. C. Ball, and P. Meakin. Universal diffusion-limited colloid aggregation. *Journal of Physics: Condensed Matter*, 2(23):5283–5283, jun 1990. doi: [10.1088/0953-8984/2/23/521](https://doi.org/10.1088/0953-8984/2/23/521).

- [311] W. Liu, X. Sun, and J. Shen. A v-curve criterion for the parameter optimization of the tikhonov regularization inversion algorithm for particle sizing. *Optics & Laser Technology*, 44(1):1–5, feb 2012. doi: [10.1016/j.optlastec.2011.04.019](https://doi.org/10.1016/j.optlastec.2011.04.019).
- [312] Y. Liu, W.-R. Chen, and S.-H. Chen. Cluster formation in two-yukawa fluids. *The Journal of Chemical Physics*, 122(4):044507, jan 2005. doi: [10.1063/1.1830433](https://doi.org/10.1063/1.1830433).
- [313] Y. Liu, J. Lin, G. Huang, Y. Guo, and C. Duan. Simple empirical analytical approximation to the voigt profile. *Journal of the Optical Society of America B*, 18(5):666, may 2001. doi: [10.1364/josab.18.000666](https://doi.org/10.1364/josab.18.000666).
- [314] A. K. Livesey and J. Skilling. Maximum entropy theory. 41(2):113–122. doi: [10.1107/S0108767385000241](https://doi.org/10.1107/S0108767385000241).
- [315] E. Lomba and L. L. Lee. Consistency conditions for the integral equations of liquid structures. *International Journal of Thermophysics*, 17(3):663–672, may 1996. doi: [10.1007/bf01441512](https://doi.org/10.1007/bf01441512).
- [316] A. A. Louis, P. G. Bolhuis, and J. P. Hansen. Mean-field fluid behavior of the gaussian core model. *Physical Review E*, 62(6):7961–7972, dec 2000. doi: [10.1103/physreve.62.7961](https://doi.org/10.1103/physreve.62.7961).
- [317] L. B. Lucy. An iterative technique for the rectification of observed distributions. *The Astronomical Journal*, 79:745, jun 1974. doi: [10.1086/111605](https://doi.org/10.1086/111605).
- [318] L. B. Lucy. Optimum strategies for inverse problems in statistical astronomy. *Astronomy and Astrophysics*, 289:983–994, Sep 1994. URL <https://ui.adsabs.harvard.edu/abs/1994A&A...289..983L>.
- [319] V. Luzzati and D. Taupin. Information content and retrieval in solution scattering studies. II. Evaluation of accuracy and resolution. 19(1):39–50. doi: [10.1107/S0021889886090027](https://doi.org/10.1107/S0021889886090027).
- [320] Y. Lyatskaya, Y. Liu, S. Tristram-Nagle, J. Katsaras, and J. F. Nagle. Method for obtaining structure and interactions from oriented lipid bilayers. *Phys. Rev. E*, 63(1):011907, Dec 2000. doi: [10.1103/PhysRevE.63.011907](https://doi.org/10.1103/PhysRevE.63.011907).
- [321] W. G. Madden and S. A. Rice. The mean spherical approximation and effective pair potentials in liquids. *The Journal of Chemical Physics*, 72(7):4208–4215, apr 1980. doi: [10.1063/1.439651](https://doi.org/10.1063/1.439651).
- [322] M. Magnani, P. Puliti, and M. Stefanon. Numerical solution of the inverse problem in the analysis of neutron small angle scattering experiments. *Nuclear Instruments and Methods in Physics Research Section A: Accelerators, Spectrometers, Detectors and Associated Equipment*, 271(3):611–616, sep 1988. doi: [10.1016/0168-9002\(88\)90330-0](https://doi.org/10.1016/0168-9002(88)90330-0).
- [323] A. G. Mailer, P. S. Clegg, and P. N. Pusey. Particle sizing by dynamic light scattering: non-linear cumulant analysis. *Journal of Physics: Condensed Matter*, 27(14):145102, mar 2015. doi: [10.1088/0953-8984/27/14/145102](https://doi.org/10.1088/0953-8984/27/14/145102).
- [324] V. V. Makarova, M. Y. Tolstykh, S. J. Picken, E. Mendes, and V. G. Kulichikhin. Rheology–structure interrelationships of hydroxypropylcellulose liquid crystal solutions and their nanocomposites under flow. *Macromolecules*, 46(3):1144–1157, feb 2013. doi: [10.1021/ma301095t](https://doi.org/10.1021/ma301095t).
- [325] A. Malijevský and J. Veverka. New equations of state for pure and binary hard-sphere fluids. *Physical Chemistry Chemical Physics*, 1(18):4267–4270, 1999. doi: [10.1039/a902831e](https://doi.org/10.1039/a902831e).
- [326] W. R. Mann. Mean value methods in iteration. *Proceedings of the American Mathematical Society*, 4(3):506–510, mar 1953. doi: [10.1090/s0002-9939-1953-0054846-3](https://doi.org/10.1090/s0002-9939-1953-0054846-3).
- [327] M. L. Mansfield and W. H. Stockmayer. Unperturbed dimensions of wormlike stars. *Macromolecules*, 13(6):1713–1715, nov 1980. doi: [10.1021/ma60078a064](https://doi.org/10.1021/ma60078a064).
- [328] S. Maric, T. K. Lind, J. Lyngsø, M. Cárdenas, and J. S. Pedersen. Modeling small-angle x-ray scattering data for low-density lipoproteins: Insights into the fatty core packing and phase transition. *ACS Nano*, 11(1):1080–1090, jan 2017. doi: [10.1021/acsnano.6b08089](https://doi.org/10.1021/acsnano.6b08089).
- [329] R. Marques, C. Bouville, M. Ribardière, L. P. Santos, and K. Bouatouch. Spherical fibonacci point sets for illumination integrals. *Computer Graphics Forum*, 32(8):134–143, jul 2013. doi: [10.1111/cgf.12190](https://doi.org/10.1111/cgf.12190).
- [330] C. Marquest and T. Witten. Simple cubic structure in copolymer mesophases. *Journal de Physique*, 50(10):1267–1277, 1989. doi: [10.1051/jphys:0198900500100126700](https://doi.org/10.1051/jphys:0198900500100126700).
- [331] G. Martynov and G. Sarkisov. Exact equations and the theory of liquids. v. *Molecular Physics*, 49(6):1495–1504, aug 1983. doi: [10.1080/00268978300102111](https://doi.org/10.1080/00268978300102111).

- [332] G. A. Martynov and A. G. Vompe. Differential condition of thermodynamic consistency as a closure for the ornstein-zernike equation. *Physical Review E*, 47(2):1012–1017, feb 1993. doi: [10.1103/physreve.47.1012](https://doi.org/10.1103/physreve.47.1012).
- [333] S. V. G. Menon, V. K. Kelkar, and C. Manohar. Application of baxter’s model to the theory of cloud points of nonionic surfactant solutions. *Physical Review A*, 43(2):1130–1133, jan 1991. doi: [10.1103/physreva.43.1130](https://doi.org/10.1103/physreva.43.1130).
- [334] S. V. G. Menon, C. Manohar, and K. S. Rao. A new interpretation of the sticky hard sphere model. *J. Chem. Phys.*, 95(12):9186–9190, dec 1991. doi: [10.1063/1.461199](https://doi.org/10.1063/1.461199).
- [335] B. Mergell and R. Everaers. Tube models for rubber-elastic systems. *Macromolecules*, 34(16):5675–5686, jul 2001. doi: [10.1021/ma002228c](https://doi.org/10.1021/ma002228c).
- [336] A. Michels and J.-P. Bick. Autocorrelation function of the spin misalignment in magnetic small-angle neutron scattering: application to nanocrystalline metals. *Journal of Applied Crystallography*, 46(3):788–790, apr 2013. doi: [10.1107/s0021889813005402](https://doi.org/10.1107/s0021889813005402).
- [337] G. Mie. Beiträge zur optik trüber medien, speziell kolloidaler metallösungen. *Annalen der Physik*, 330(3):377–445, 1908. doi: [10.1002/andp.19083300302](https://doi.org/10.1002/andp.19083300302).
- [338] D. F. R. Mildner. Efficient use of two-dimensional detectors for small-angle neutron scattering contours from polymers under external constraint. *Macromolecules*, 16(11):1760–1763, nov 1983. doi: [10.1021/ma00245a014](https://doi.org/10.1021/ma00245a014).
- [339] T. T. Mills, G. E. Toombes, S. Tristram-Nagle, D.-M. Smilgies, G. W. Feigenson, and J. F. Nagle. Order parameters and areas in fluid-phase oriented lipid membranes using wide angle x-ray scattering. *Biophysical Journal*, 95(2):669–681, jul 2008. doi: [10.1529/biophysj.107.127845](https://doi.org/10.1529/biophysj.107.127845).
- [340] R. Mittelbach and O. Glatter. Direct Structure Analysis of Small-Angle Scattering Data from Polydisperse Colloidal Particles. 31(4):600–608. doi: [10.1107/S0021889898002209](https://doi.org/10.1107/S0021889898002209).
- [341] B. Mladek, M. Fernaud, G. Kahl, and M. Neumann. On the thermodynamic properties of the generalized gaussian core model. *Condensed Matter Physics*, 8(1):135–148, 2005. doi: [10.5488/cmp.8.1.135](https://doi.org/10.5488/cmp.8.1.135).
- [342] J. Möller, R. Kranold, J. Schmelzer, and U. Lembke. Small-angle x-ray scattering size parameters and higher moments of the particle-size distribution function in the asymptotic stage of ostwald ripening. *Journal of Applied Crystallography*, 28(5):553–560, oct 1995. doi: [10.1107/s0021889895003827](https://doi.org/10.1107/s0021889895003827).
- [343] R. M. Moon, T. Riste, and W. C. Koehler. Polarization analysis of thermal-neutron scattering. *Physical Review*, 181(2):920–931, may 1969. doi: [10.1103/physrev.181.920](https://doi.org/10.1103/physrev.181.920).
- [344] P. B. Moore. Small-angle scattering. Information content and error analysis. 13(2):168–175. doi: [10.1107/S00218898001179X](https://doi.org/10.1107/S00218898001179X).
- [345] M. Mori. Developments in the double exponential formulas for numerical integration. pages 1585–1594, 1990. URL <https://api.semanticscholar.org/CorpusID:14900392>.
- [346] M. Mori and M. Sugihara. The double-exponential transformation in numerical analysis. 127(1–2):287–296. doi: [10.1016/s0377-0427\(00\)00501-x](https://doi.org/10.1016/s0377-0427(00)00501-x).
- [347] J. D. Morrison, J. D. Corcoran, and K. E. Lewis. The determination of particle size distributions in small-angle scattering using the maximum-entropy method. 25(4):504–513. doi: [10.1107/S0021889892001729](https://doi.org/10.1107/S0021889892001729).
- [348] J. Mroczka and D. Szczuczy’nski. Improved technique of retrieving particle size distribution from angular scattering measurements. *Journal of Quantitative Spectroscopy and Radiative Transfer*, 129:48–59, nov 2013. doi: [10.1016/j.jqsrt.2013.05.030](https://doi.org/10.1016/j.jqsrt.2013.05.030).
- [349] M. Mulato and I. Chambouleyron. Small-Angle X-ray and Neutron Scattering of Polydisperse Systems: Determination of the Scattering-Particle-Size Distribution. 29(1):29–36. doi: [10.1107/S0021889895008776](https://doi.org/10.1107/S0021889895008776).
- [350] M. Mulato, D. Tygel, and I. Chambouleyron. On the Retrieval of Particle Size Distributions from Small-Angle Scattering Data: the Influence of Statistical Data Dispersion. 31(2):149–153. doi: [10.1107/S0021889897008789](https://doi.org/10.1107/S0021889897008789).
- [351] M. Mulato, D. Tygel, and I. Chambouleyron. The Influence of the Available Scattering Vector Range on the Retrieval of Particle-Size Distributions from Small-Angle Scattering Intensity Data. 30(5 Part 2):808–810. doi: [10.1107/S0021889897001726](https://doi.org/10.1107/S0021889897001726).

- [352] F. Muller, M. Delsanti, L. Auvray, J. Yang, Y. Chen, J. Mays, B. Demé, M. Tirrell, and P. Guenoun. Ordering of urchin-like charged copolymer micelles: Electrostatic, packing and polyelectrolyte correlations. *The European Physical Journal E*, 3(1):45–53, sep 2000. doi: [10.1007/s101890070040](https://doi.org/10.1007/s101890070040).
- [353] J. J. Müller, S. Hansen, and H.-V. Pürschel. The Use of Small-Angle Scattering and the Maximum-Entropy Method for Shape-Model Determination from Distance-Distribution Functions. 29(5):547–554. doi: [10.1107/S0021889896004840](https://doi.org/10.1107/S0021889896004840).
- [354] G. Nägele. On the dynamics and structure of charge-stabilized suspensions. *Physics Reports*, 272(5-6):215–372, jul 1996. doi: [10.1016/0370-1573\(95\)00078-x](https://doi.org/10.1016/0370-1573(95)00078-x).
- [355] G. Nägele. The physics of colloidal soft matter, 2004.
- [356] H. Niederreiter. Random number generation and quasi-monte carlo methods. jan 1992. doi: [10.1137/1.9781611970081](https://doi.org/10.1137/1.9781611970081).
- [357] J. E. Nielsen, V. A. Bjørnestad, and R. Lund. Resolving the structural interactions between antimicrobial peptides and lipid membranes using small-angle scattering methods: the case of indolicidin. 14(43):8750–8763. doi: [10.1039/c8sm01888j](https://doi.org/10.1039/c8sm01888j).
- [358] F. Nobile, R. Tempone, and C. G. Webster. A sparse grid stochastic collocation method for partial differential equations with random input data. 46(5):2309–2345. doi: [10.1137/060663660](https://doi.org/10.1137/060663660).
- [359] J. Noolandi and K. Hong. Non-equilibrium correlation function of a reptating chain. *Journal de Physique Lettres*, 45(3):149–157, 1984. doi: [10.1051/jphyslet:01984004503014900](https://doi.org/10.1051/jphyslet:01984004503014900).
- [360] M. A. Noor. New approximation schemes for general variational inequalities. *Journal of Mathematical Analysis and Applications*, 251(1):217–229, nov 2000. doi: [10.1006/jmaa.2000.7042](https://doi.org/10.1006/jmaa.2000.7042).
- [361] O. D. of crystallography. R factor. http://reference.iucr.org/dictionary/R_factor. URL http://reference.iucr.org/dictionary/R_factor.
- [362] H. Ogata. A numerical integration formula based on the bessel functions. 41(4):949–970. doi: [10.2977/prims/1145474602](https://doi.org/10.2977/prims/1145474602).
- [363] J. Olivero and R. Longbothum. Emical fits to the voigt line width: A brief review. *Journal of Quantitative Spectroscopy and Radiative Transfer*, 17(2):233–236, feb 1977. doi: [10.1016/0022-4073\(77\)90161-3](https://doi.org/10.1016/0022-4073(77)90161-3).
- [364] T. Ooura. DE-Quadrature. URL <https://www.kurims.kyoto-u.ac.jp/~ooura/intde.html>.
- [365] T. Ooura and M. Mori. The double exponential formula for oscillatory functions over the half infinite interval. *Journal of Computational and Applied Mathematics*, 38(1-3):353–360, dec 1991. doi: [10.1016/0377-0427\(91\)90181-i](https://doi.org/10.1016/0377-0427(91)90181-i).
- [366] L. Ornstein and F. Zernike. Accidental deviations of density and opalescence at the critical point of a single substance. *Koninklijke Nederlandse Akademie van Wetenschappen Proceedings*, 17:793–806, 1914. URL <http://www.dwc.knaw.nl/DL/publications/PU00012727.pdf>.
- [367] S. Oversteegen and H. Lekkerkerker. On the accuracy of the derjaguin approximation for depletion potentials. *Physica A: Statistical Mechanics and its Applications*, 341(1-4):23–39, oct 2004. doi: [10.1016/j.physa.2004.04.103](https://doi.org/10.1016/j.physa.2004.04.103).
- [368] A. B. Owen. Randomly permuted (t,m,s)-nets and (t, s)-sequences. In H. Niederreiter and P. J.-S. Shiue, editors, *Monte Carlo and Quasi-Monte Carlo Methods in Scientific Computing*, pages 299–317. Springer New York.
- [369] G. Pabst, J. Katsaras, V. A. Raghunathan, and M. Rappolt. Structure and interactions in the anomalous swelling regime of phospholipid bilayers. 19(5):1716–1722. doi: [10.1021/la026052e](https://doi.org/10.1021/la026052e).
- [370] G. Pabst, R. Koschuch, B. Pozo-Navas, M. Rappolt, K. Lohner, and P. Laggner. Structural analysis of weakly ordered membrane stacks. *Journal of Applied Crystallography*, 36(6):1378–1388, nov 2003. doi: [10.1107/s0021889803017527](https://doi.org/10.1107/s0021889803017527).
- [371] G. Pabst, M. Rappolt, H. Amenitsch, and P. Laggner. Structural information from multilamellar liposomes at full hydration: Fullq-range fitting with high quality x-ray data. *Physical Review E*, 62(3):4000–4009, sep 2000. doi: [10.1103/physreve.62.4000](https://doi.org/10.1103/physreve.62.4000).
- [372] S. Paul, A. M. Friedman, C. Bailey-Kellogg, and B. A. Craig. Bayesian reconstruction of $P(r)$ directly from two-dimensional detector images via a markov chain monte carlo method. *Journal of Applied Crystallography*, 46(2):404–414, mar 2013. doi: [10.1107/s002188981300109x](https://doi.org/10.1107/s002188981300109x).

- [373] J. S. Pedersen. Determination of size distribution from small-angle scattering data for systems with effective hard-sphere interactions. *Journal of Applied Crystallography*, 27(4):595–608, aug 1994. doi: [10.1107/s0021889893013810](https://doi.org/10.1107/s0021889893013810).
- [374] J. S. Pedersen. Analysis of small-angle scattering data from colloids and polymer solutions: modeling and least-squares fitting. *Advances in Colloid and Interface Science*, 70(0):171–210, jul 1997. doi: [10.1016/s0001-8686\(97\)00312-6](https://doi.org/10.1016/s0001-8686(97)00312-6).
- [375] J. S. Pedersen. Form factors of block copolymer micelles with spherical, ellipsoidal and cylindrical cores. *Journal of Applied Crystallography*, 33(3):637–640, jun 2000. doi: [10.1107/s0021889899012248](https://doi.org/10.1107/s0021889899012248).
- [376] J. S. Pedersen. *Modelling of Small-Angle Scattering Data from Colloids and Polymer Systems*, chapter 6, pages 391–420. Elsevier Science, 2002.
- [377] J. S. Pedersen. Small-angle scattering from surfactants and block copolymer micelles. In *Soft Matter Characterization*, pages 191–233. Springer Netherlands, 2008. doi: [10.1007/978-1-4020-4465-6_4](https://doi.org/10.1007/978-1-4020-4465-6_4).
- [378] J. S. Pedersen and M. C. Gerstenberg. Scattering form factor of block copolymer micelles. *Macromolecules*, 29(4):1363–1365, jan 1996. doi: [10.1021/ma9512115](https://doi.org/10.1021/ma9512115).
- [379] J. S. Pedersen, D. Posselt, and K. Mortensen. Analytical treatment of the resolution function for small-angle scattering. *Journal of Applied Crystallography*, 23(4):321–333, aug 1990. doi: [10.1107/s0021889890003946](https://doi.org/10.1107/s0021889890003946).
- [380] J. S. Pedersen and P. Schurtenberger. Scattering functions of semiflexible polymers with and without excluded volume effects. *Macromolecules*, 29(23):7602–7612, jan 1996. doi: [10.1021/ma9607630](https://doi.org/10.1021/ma9607630).
- [381] J. S. Pedersen and P. Schurtenberger. Static properties of polystyrene in semidilute solutions: A comparison of monte carlo simulation and small-angle neutron scattering results. *Europhysics Letters (EPL)*, 45(6):666–672, mar 1999. doi: [10.1209/epl/i1999-00219-7](https://doi.org/10.1209/epl/i1999-00219-7).
- [382] J. S. Pedersen and P. Schurtenberger. Scattering functions of semidilute solutions of polymers in a good solvent. *Journal of Polymer Science Part B: Polymer Physics*, 42(17):3081–3094, jul 2004. doi: [10.1002/polb.20173](https://doi.org/10.1002/polb.20173).
- [383] M. C. Pedersen, S. L. Hansen, B. Markussen, L. Arleth, and K. Mortensen. Quantification of the information in small-angle scattering data. *Journal of Applied Crystallography*, 47(6):2000–2010, nov 2014. doi: [10.1107/s1600576714024017](https://doi.org/10.1107/s1600576714024017).
- [384] P. A. Penttilä, L. Rautkari, M. Österberg, and R. Schweins. Small-angle scattering model for efficient characterization of wood nanostructure and moisture behaviour. 52(2):369–377. doi: [10.1107/s1600576719002012](https://doi.org/10.1107/s1600576719002012).
- [385] J. K. Percus and G. J. Yevick. Analysis of classical statistical mechanics by means of collective coordinates. *Physical Review*, 110(1):1–13, apr 1958. doi: [10.1103/physrev.110.1](https://doi.org/10.1103/physrev.110.1).
- [386] H. I. Petracche, N. Gouliaev, S. Tristram-Nagle, R. Zhang, R. M. Suter, and J. F. Nagle. Interbilayer interactions from high-resolution x-ray scattering. *Phys. Rev. E*, 57(6):7014–7024, Jun 1998. doi: [10.1103/PhysRevE.57.7014](https://doi.org/10.1103/PhysRevE.57.7014).
- [387] K. Petras. Smolyak cubature of given polynomial degree with few nodes for increasing dimension. 93(4):729–753. doi: [10.1007/s002110200401](https://doi.org/10.1007/s002110200401).
- [388] W. Phuengrattana and S. Suantai. On the rate of convergence of mann, ishikawa, noor and SP-iterations for continuous functions on an arbitrary interval. *Journal of Computational and Applied Mathematics*, 235(9):3006–3014, mar 2011. doi: [10.1016/j.cam.2010.12.022](https://doi.org/10.1016/j.cam.2010.12.022).
- [389] E. Picard. Mémoire sur la théorie des équations aux dérivées partielles et la méthode des approximations successives. *Journal de mathématiques pures et appliquées*, 6(4):145–210, 1890. URL http://portail.mathdoc.fr/JMPA/PDF/JMPA_1890_4_6_A3_0.pdf.
- [390] S. J. Picken, J. Aerts, R. Visser, and M. G. Northolt. Structure and rheology of aramid solutions: x-ray scattering measurements. *Macromolecules*, 23(16):3849–3854, aug 1990. doi: [10.1021/ma00218a021](https://doi.org/10.1021/ma00218a021).
- [391] P. Pieruschka and S. Marčelja. Statistical mechanics of random bicontinuous phases. *Journal de Physique II*, 2(2):235–247, feb 1992. doi: [10.1051/jp2:1992127](https://doi.org/10.1051/jp2:1992127).

- [392] R. Pike. Particle sizing by laser light scattering. In Sabatier, R. Pike, and Pierre, editors, *Scattering*, pages 895–919. Elsevier, London, 2002. doi: [10.1016/b978-012613760-6/50048-6](https://doi.org/10.1016/b978-012613760-6/50048-6).
- [393] G. Porod. Die Abhangigkeit der Roentgenkleinwinkelstreuung von Form und Grosse der Kolloiden Teilchen in verdunnten Systemen, IV. *Acta Physica Austriaca*, 2:255–292, 1948.
- [394] D. Potschke, P. Hickl, M. Ballauff, P.-O. Astrand, and J. S. Pedersen. Analysis of the conformation of worm-like chains by small-angle scattering: Monte-carlo simulations in comparison to analytical theory. *Macromolecular Theory and Simulations*, 9(6):345–353, jul 2000. doi: [10.1002/1521-3919\(20000701\)9:6<345::aid-mats345>3.0.co;2-9](https://doi.org/10.1002/1521-3919(20000701)9:6<345::aid-mats345>3.0.co;2-9).
- [395] J. A. Potton, G. J. Daniell, and B. D. Rainford. A new method for the determination of particle size distributions from small-angle neutron scattering measurements. 21(6):891–897. doi: [10.1107/S0021889888004595](https://doi.org/10.1107/S0021889888004595).
- [396] J. A. Potton, G. J. Daniell, and B. D. Rainford. Particle size distributions from SANS data using the maximum entropy method. 21(6):663–668. doi: [10.1107/S0021889888004819](https://doi.org/10.1107/S0021889888004819).
- [397] W. H. Press, S. A. Teukolsky, W. T. Vetterling, and B. P. Flannery. *Numerical Recipes. The Art of Scientific Computing*. Cambridge University Press, 3rd edition, 2007.
- [398] O. A. Pringle and P. W. Schmidt. Small-angle x-ray scattering from helical macromolecules. *Journal of Applied Crystallography*, 4(4):290–293, aug 1971. doi: [10.1107/s002188987100699x](https://doi.org/10.1107/s002188987100699x).
- [399] S. W. Provencher. A constrained regularization method for inverting data represented by linear algebraic or integral equations. *Computer Physics Communications*, 27(3):213–227, sep 1982. doi: [10.1016/0010-4655\(82\)90173-4](https://doi.org/10.1016/0010-4655(82)90173-4).
- [400] S. W. Provencher. Contin: A general purpose constrained regularization program for inverting noisy linear algebraic and integral equations. *Computer Physics Communications*, 27(3):229–242, sep 1982. doi: [10.1016/0010-4655\(82\)90174-6](https://doi.org/10.1016/0010-4655(82)90174-6).
- [401] S. W. Provencher. Contin: A general purpose constrained regularization program for inverting noisy linear algebraic and integral equations. *Computer Physics Communications*, 35:C–818–C–819, jan 1984. doi: [10.1016/s0010-4655\(84\)82935-5](https://doi.org/10.1016/s0010-4655(84)82935-5).
- [402] S. W. Provencher, J. Hendrix, L. De Maeyer, and N. Paulussen. Direct determination of molecular weight distributions of polystyrene in cyclohexane with photon correlation spectroscopy. 69(9):4273–4276. doi: [10.1063/1.437112](https://doi.org/10.1063/1.437112).
- [403] L. C. Puigjaner and J. A. Subirana. Low-angle x-ray scattering by disordered and partially ordered helical systems. *Journal of Applied Crystallography*, 7(2):169–173, apr 1974. doi: [10.1107/s002188987400906x](https://doi.org/10.1107/s002188987400906x).
- [404] P. N. Pusey, D. E. Koppel, D. E. Schaefer, R. D. Camerini-Otero, and S. H. Koenig. Intensity fluctuation spectroscopy of laser light scattered by solutions of spherical viruses. r17, q.beta., BSV, PM2, and t7. i. light-scattering technique. *Biochemistry*, 13(5):952–960, feb 1974. doi: [10.1021/bi00702a020](https://doi.org/10.1021/bi00702a020).
- [405] J. Quintanilla, R. F. Reidy, B. P. Gorman, and D. W. Mueller. Gaussian random field models of aerogels. *Journal of Applied Physics*, 93(8):4584–4589, apr 2003. doi: [10.1063/1.1563038](https://doi.org/10.1063/1.1563038).
- [406] C. Raman. LXI. on the mean distance between neighbouring molecules in a fluid. *The London, Edinburgh, and Dublin Philosophical Magazine and Journal of Science*, 47(280):671–679, may 1924. doi: [10.1080/14786442408634406](https://doi.org/10.1080/14786442408634406).
- [407] S. Rathgeber, M. Monkenbusch, M. Kreitschmann, V. Urban, and A. Brulet. Dynamics of starburst dendrimers in solution in relation to their structural properties. 117(8):4047–4062. doi: [10.1063/1.1493771](https://doi.org/10.1063/1.1493771).
- [408] S. Rathgeber, T. Pakula, A. Wilk, K. Matyjaszewski, and K. L. Beers. On the shape of bottle-brush macromolecules: Systematic variation of architectural parameters. 122(12). doi: [10.1063/1.1860531](https://doi.org/10.1063/1.1860531).
- [409] L. Rayleigh. On the theory of long waves and bores. *Proceedings of the Royal Society A: Mathematical, Physical and Engineering Sciences*, 90(619):324–328, jul 1914. doi: [10.1098/rspa.1914.0055](https://doi.org/10.1098/rspa.1914.0055).
- [410] D. J. Read. Calculation of scattering from stretched copolymers using the tube model: incorporation of the effect of elastic inhomogeneities. *Macromolecules*, 37(13):5065–5092, jun 2004. doi: [10.1021/ma030438u](https://doi.org/10.1021/ma030438u).

- [411] D. J. Read and T. C. B. McLeish. Microscopic theory for the “lozenge” contour plots in scattering from stretched polymer networks. *Macromolecules*, 30(20):6376–6384, oct 1997. doi: [10.1021/ma970571k](https://doi.org/10.1021/ma970571k).
- [412] C. Regnaut and J. C. Ravey. Application of the adhesive sphere model to the structure of colloidal suspensions. *The Journal of Chemical Physics*, 91(2):1211–1221, jul 1989. doi: [10.1063/1.457194](https://doi.org/10.1063/1.457194).
- [413] C. Regnaut and J. C. Ravey. Erratum: Application of the adhesive sphere model to the structure of colloidal suspensions [j. chem. phys. 91, 1211 (1989)]. *The Journal of Chemical Physics*, 92(5):3250–3250, mar 1990. doi: [10.1063/1.458616](https://doi.org/10.1063/1.458616).
- [414] J. M. Ren, T. G. McKenzie, Q. Fu, E. H. H. Wong, J. Xu, Z. An, S. Shanmugam, T. P. Davis, C. Boyer, and G. G. Qiao. Star polymers. *Chemical Reviews*, 116(12):6743–6836, jun 2016. doi: [10.1021/acs.chemrev.6b00008](https://doi.org/10.1021/acs.chemrev.6b00008).
- [415] G. Renaud, R. Lazzari, and F. Leroy. Probing surface and interface morphology with grazing incidence small angle x-ray scattering. 64(8):255–380. doi: [10.1016/j.surfrep.2009.07.002](https://doi.org/10.1016/j.surfrep.2009.07.002).
- [416] W. Research. EulerAngles. <https://reference.wolfram.com/language/ref/EulerAngles.html>, 2015. URL <https://reference.wolfram.com/language/ref/EulerAngles.html>. 18-April-2023.
- [417] L. E. Reynolds and D. F. R. Mildner. The elliptical average of small-angle scattering data. *Journal of Applied Crystallography*, 17(6):411–416, dec 1984. doi: [10.1107/S0021889884011857](https://doi.org/10.1107/S0021889884011857).
- [418] W. H. Richardson. Bayesian-based iterative method of image restoration. *Journal of the Optical Society of America*, 62(1):55, jan 1972. doi: [10.1364/josa.62.000055](https://doi.org/10.1364/josa.62.000055).
- [419] A. P. Roberts. Morphology and thermal conductivity of model organic aerogels. *Physical Review E*, 55(2):R1286–R1289, feb 1997. doi: [10.1103/physreve.55.r1286](https://doi.org/10.1103/physreve.55.r1286).
- [420] A. P. Roberts and M. Teubner. Transport properties of heterogeneous materials derived from gaussian random fields: Bounds and simulation. *Physical Review E*, 51(5):4141–4154, may 1995. doi: [10.1103/physreve.51.4141](https://doi.org/10.1103/physreve.51.4141).
- [421] C. Robertus, W. H. Philipse, J. G. H. Joosten, and Y. K. Levine. Solution of the percus-yevick approximation of the multicomponent adhesive sphere system to the small angle x-ray scattering from microemulsions. *The Journal of Chemical Physics*, 90(8):4482–4490, apr 1989. doi: [10.1063/1.456635](https://doi.org/10.1063/1.456635).
- [422] M. Robles and M. L. de Haro. On the contact values of the derivatives of the hard-sphere radial distribution function. *The Journal of Chemical Physics*, 107(12):4648–4657, sep 1997. doi: [10.1063/1.474826](https://doi.org/10.1063/1.474826).
- [423] M. Robles and M. L. de Haro. On the liquid-glass transition line in monatomic lennard-jones fluids. *Europhysics Letters (EPL)*, 62(1):56–62, apr 2003. doi: [10.1209/epl/i2003-00362-7](https://doi.org/10.1209/epl/i2003-00362-7).
- [424] F. J. Rogers and D. A. Young. New, thermodynamically consistent, integral equation for simple fluids. *Physical Review A*, 30(2):999–1007, Aug 1984. doi: [10.1103/physreva.30.999](https://doi.org/10.1103/physreva.30.999).
- [425] Y. Rosenfeld. Free-energy model for the inhomogeneous hard-sphere fluid inDdimensions: Structure factors for the hard-disk ($d=2$) mixtures in simple explicit form. *Physical Review A*, 42(10):5978–5989, nov 1990. doi: [10.1103/physreva.42.5978](https://doi.org/10.1103/physreva.42.5978).
- [426] Y. Rosenfeld and N. W. Ashcroft. Theory of simple classical fluids: Universality in the short-range structure. *Physical Review A*, 20(3):1208–1235, sep 1979. doi: [10.1103/physreva.20.1208](https://doi.org/10.1103/physreva.20.1208).
- [427] D. A. Ross, H. S. Dhadwal, and K. Suh. Regularized inversion of dynamic light scattering intensity data, jul 1994. doi: [10.1117/12.179736](https://doi.org/10.1117/12.179736).
- [428] D. Roux and C. Safinya. A synchrotron x-ray study of competing undulation and electrostatic interlayer interactions in fluid multimembrane lyotropic phases. *Journal de Physique*, 49(2):307–318, 1988. doi: [10.1051/jphys:01988004902030700](https://doi.org/10.1051/jphys:01988004902030700).
- [429] Y. Saad. A flexible inner-outer preconditioned GMRES algorithm. *SIAM Journal on Scientific Computing*, 14(2):461–469, mar 1993. doi: [10.1137/0914028](https://doi.org/10.1137/0914028).
- [430] Y. Saad and M. H. Schultz. GMRES: A generalized minimal residual algorithm for solving non-symmetric linear systems. *SIAM Journal on Scientific and Statistical Computing*, 7(3):856–869, jul 1986. doi: [10.1137/0907058](https://doi.org/10.1137/0907058).
- [431] I. C. Sanchez. Virial coefficients and close-packing of hard spheres and disks. *The Journal of Chemical Physics*, 101(8):7003–7006, oct 1994. doi: [10.1063/1.468456](https://doi.org/10.1063/1.468456).

- [432] R. Santer and M. Herman. Particle size distributions from forward scattered light using the chahine inversion scheme. *Applied Optics*, 22(15):2294, aug 1983. doi: [10.1364/ao.22.002294](https://doi.org/10.1364/ao.22.002294).
- [433] Santos, Yuste, and L. de Haro. Rational-function approximation for fluids interacting via piece-wise constant potentials. *Condensed Matter Physics*, 15(2):23602, jun 2012. doi: [10.5488/CMP.15.23602](https://doi.org/10.5488/CMP.15.23602).
- [434] A. Santos, S. B. Yuste, M. L. de Haro, M. Bárcenas, and P. Orea. Structural properties of fluids interacting via piece-wise constant potentials with a hard core. *The Journal of Chemical Physics*, 139(7):074505, aug 2013. doi: [10.1063/1.4818601](https://doi.org/10.1063/1.4818601).
- [435] E. Santos and A. Bassrei. L- and $\hat{\iota}$ -curve approaches for the selection of regularization parameter in geophysical diffraction tomography. 33(5):618–629. doi: [10.1016/j.cageo.2006.08.013](https://doi.org/10.1016/j.cageo.2006.08.013).
- [436] R. F. Saraf. Small-angle scattering from anisotropic systems in the guinier region. *Macromolecules*, 22(2):675–681, mar 1989. doi: [10.1021/ma00192a028](https://doi.org/10.1021/ma00192a028).
- [437] G. Savin and W. Burchard. Uncommon solution behavior of poly(n-vinylimidazole). angular dependence of scattered light from aggregates in ethanol. 37(8):3005–3017. doi: [10.1021/ma0353639](https://doi.org/10.1021/ma0353639).
- [438] J. Schelten and W. Schmatz. Multiple-scattering treatment for small-angle scattering problems. *Journal of Applied Crystallography*, 13(4):385–390, aug 1980. doi: [10.1107/s0021889880012356](https://doi.org/10.1107/s0021889880012356).
- [439] H. A. Scheraga, J. T. Edsall, and J. O. Gadd. Double refraction of flow: Numerical evaluation of extinction angle and birefringence as a function of velocity gradient. *The Journal of Chemical Physics*, 19(9):1101–1108, sep 1951. doi: [10.1063/1.1748483](https://doi.org/10.1063/1.1748483).
- [440] O. Scherzer, editor. *Handbook of Mathematical Methods in Imaging*. Springer New York, 2011. doi: [10.1007/978-0-387-92920-0](https://doi.org/10.1007/978-0-387-92920-0).
- [441] P. W. Schmidt. The small angle x-ray scattering from polydisperse solutions of ellipsoidal particles. *Acta Crystallographica*, 11(10):674–676, oct 1958. doi: [10.1107/s0365110x5800181x](https://doi.org/10.1107/s0365110x5800181x).
- [442] P. W. Schmidt. Small angle x-ray scattering from helical filaments. *Journal of Applied Crystallography*, 3(4):257–264, aug 1970. doi: [10.1107/s0021889870006155](https://doi.org/10.1107/s0021889870006155).
- [443] P. W. Schmidt. Small-angle scattering studies of disordered, porous and fractal systems. *Journal of Applied Crystallography*, 24(5):414–435, oct 1991. doi: [10.1107/s0021889891003400](https://doi.org/10.1107/s0021889891003400).
- [444] P. W. Schmidt and M. Kalliat. A simple approximation for calculating the small-angle x-ray and neutron scattering from polydisperse samples of independently scattering uniform spheres. *Journal of Applied Crystallography*, 17(1):27–32, feb 1984. doi: [10.1107/s002188984010955](https://doi.org/10.1107/s002188984010955).
- [445] K.-V. Schubert, R. Strey, S. R. Kline, and E. W. Kaler. Small angle neutron scattering near lifshitz lines: Transition from weakly structured mixtures to microemulsions. *J. Chem. Phys.*, 101:5343, 1994. doi: [10.1063/1.467387](https://doi.org/10.1063/1.467387).
- [446] S. Schwartz, J. Cain, E. Dratz, and J. Blasie. An analysis of lamellar x-ray diffraction from disordered membrane multilayers with application to data from retinal rod outer segments. *Biophysical Journal*, 15(12):1201–1233, dec 1975. doi: [10.1016/s0006-3495\(75\)85895-4](https://doi.org/10.1016/s0006-3495(75)85895-4).
- [447] A. V. Semenyuk and D. I. Svergun. GNOM – a program package for small-angle scattering data processing. *Journal of Applied Crystallography*, 24(5):537–540, 1991-10. doi: [10.1107/S002188989100081X](https://doi.org/10.1107/S002188989100081X).
- [448] D. Sen, A. Das, and S. Mazumder. An iterative method to extract the size distribution of non-interacting polydisperse spherical particles from small-angle scattering data. *Journal of Applied Crystallography*, 47(2):712–718, mar 2014. doi: [10.1107/s1600576714003835](https://doi.org/10.1107/s1600576714003835).
- [449] R. Serimaa, V. Eteläniemi, O. Serimaa, T. Laitalainen, and A. Bienenstock. An Improved Regularization Technique for Analysis of Anomalous X-ray Scattering Data; Platinum Uridine Blue Sulfate as an Example. 29(4):390–402. doi: [10.1107/S0021889895016979](https://doi.org/10.1107/S0021889895016979).
- [450] R. V. Sharma and K. C. Sharma. The structure factor and the transport properties of dense fluids having molecules with square well potential, a possible generalization. *Physica A: Statistical Mechanics and its Applications*, 89(1):213 – 218, oct 1977. doi: [10.1016/0378-4371\(77\)90151-0](https://doi.org/10.1016/0378-4371(77)90151-0).
- [451] P. Sharp and V. A. Bloomfield. Light scattering from wormlike chains with excluded volume effects. *Biopolymers*, 6(8):1201–1211, aug 1968. doi: [10.1002/bip.1968.360060814](https://doi.org/10.1002/bip.1968.360060814).
- [452] M. Shibayama, S. Nomura, T. Hashimoto, and E. L. Thomas. Asymptotic behavior and lorentz factor for small-angle elastic scattering profiles from preferentially oriented asymmetric bodies. 66(9):4188–4197, 1989. doi: [10.1063/1.344005](https://doi.org/10.1063/1.344005).

- [453] M. T. Sims, L. C. Abbott, R. M. Richardson, J. W. Goodby, and J. N. Moore. Considerations in the determination of orientational order parameters from x-ray scattering experiments. *Liquid Crystals*, 46(1):11–24, mar 2018. doi: [10.1080/02678292.2018.1455227](https://doi.org/10.1080/02678292.2018.1455227).
- [454] B. Sjöberg. Small-angle x-ray investigation of the equilibria between copper(II) and glycyl-l-histidylglycine in water solution. a method for analysing polydispersed systems. *Journal of Applied Crystallography*, 7(2):192–199, apr 1974. doi: [10.1107/s0021889874009241](https://doi.org/10.1107/s0021889874009241).
- [455] J. Skilling and R. K. Bryan. Maximum entropy image reconstruction: general algorithm. *Monthly Notices of the Royal Astronomical Society*, 211(1):111–124, 1984. doi: [10.1093/mnras/211.1.111](https://doi.org/10.1093/mnras/211.1.111).
- [456] W. R. Smith, D. Henderson, and Y. Tago. Mean spherical approximation and optimized cluster theory for the square-well fluid. *The Journal of Chemical Physics*, 67(11):5308–5316, dec 1977. doi: [10.1063/1.434709](https://doi.org/10.1063/1.434709).
- [457] C. M. Sorensen. Light scattering by fractal aggregates: A review. *Aerosol Science and Technology*, 35(2):648–687, jan 2001. doi: [10.1080/02786820117868](https://doi.org/10.1080/02786820117868).
- [458] C. M. Sorensen, J. Cai, and N. Lu. Test of static structure factors for describing light scattering from fractal soot aggregates. *Langmuir*, 8(8):2064–2069, aug 1992. doi: [10.1021/la00044a029](https://doi.org/10.1021/la00044a029).
- [459] C. M. Sorensen and G. M. Wang. Size distribution effect on the power law regime of the structure factor of fractal aggregates. *Physical Review E*, 60(6):7143–7148, dec 1999. doi: [10.1103/physreve.60.7143](https://doi.org/10.1103/physreve.60.7143).
- [460] T. Sottmann, R. Strey, and S.-H. Chen. A small-angle neutron scattering study of nonionic surfactant molecules at the water–oil interface: Area per molecule, microemulsion domain size, and rigidity. *The Journal of Chemical Physics*, 106(15):6483–6491, apr 1997. doi: [10.1063/1.473638](https://doi.org/10.1063/1.473638).
- [461] G. L. Squires. *Thermal Neutron Scattering*. Cambridge University Press, 1978. doi: [10.1017/CBO9781139107808](https://doi.org/10.1017/CBO9781139107808).
- [462] S. Steenstrup and S. Hansen. The maximum-entropy method without the positivity constraint – applications to the determination of the distance-distribution function in small-angle scattering. 27(4):574–580. doi: [10.1107/S0021889894000932](https://doi.org/10.1107/S0021889894000932).
- [463] P. S. Stephanou. static structure factor of ring polymers under shear flow based on Rouse-model. private communication, 2019.
- [464] M. Stieger, J. S. Pedersen, P. Lindner, and W. Richtering. Are thermoresponsive microgels model systems for concentrated colloidal suspensions? a rheology and small-angle neutron scattering study. *Langmuir*, 20(17):7283–7292, aug 2004. doi: [10.1021/la049518x](https://doi.org/10.1021/la049518x). PMID: 15301516.
- [465] E. Straube, V. Urban, W. Pyckhout-Hintzen, D. Richter, and C. J. Glinka. Small-angle neutron scattering investigation of topological constraints and tube deformation in networks. *Physical Review Letters*, 74(22):4464–4467, may 1995. doi: [10.1103/physrevlett.74.4464](https://doi.org/10.1103/physrevlett.74.4464).
- [466] R. Strey, J. Winkler, and L. Magid. Small-angle neutron scattering from diffuse interfaces. 1. mono- and bilayers in the water-octane-pentaoxyethylene monododecyl ether (c12es) system. *The Journal of Physical Chemistry*, 95(19):7502–7507, sep 1991. doi: [10.1021/j100172a070](https://doi.org/10.1021/j100172a070).
- [467] N. Stribeck. Analysis of scattering from polydisperse structure using Mellin convolution. 39(2):237–243. doi: [10.1107/S0021889806003979](https://doi.org/10.1107/S0021889806003979).
- [468] Y. Su, C. Burger, B. S. Hsiao, and B. Chu. Characterization of tempo-oxidized cellulose nanofibers in aqueous suspension by small-angle x-ray scattering. 47(2):788–798. doi: [10.1107/s1600576714005020](https://doi.org/10.1107/s1600576714005020).
- [469] G. C. Summerfield and D. F. R. Mildner. Small-angle scattering with azimuthal asymmetry. *Journal of Applied Crystallography*, 16(4):384–389, aug 1983. doi: [10.1107/S002188983010663](https://doi.org/10.1107/S002188983010663).
- [470] C. Svaneborg and J. S. Pedersen. Form factors of block copolymer micelles with excluded-volume interactions of the corona chains determined by monte carlo simulations. *Macromolecules*, 35(3):1028–1037, jan 2002. doi: [10.1021/ma011046v](https://doi.org/10.1021/ma011046v).
- [471] D. I. Svergun. Mathematical methods in small-angle scattering data analysis. *Journal of Applied Crystallography*, 24(5):485–492, 1991-10. doi: [10.1107/S0021889891001280](https://doi.org/10.1107/S0021889891001280).
- [472] D. I. Svergun. Determination of the regularization parameter in indirect-transform methods using perceptual criteria. *Journal of Applied Crystallography*, 25(4):495–503, 1992. doi: [10.1107/S0021889892001663](https://doi.org/10.1107/S0021889892001663).

- [473] D. I. Svergun. A direct indirect method of small-angle scattering data treatment. *Journal of Applied Crystallography*, 26(2):258–267, 1993. doi: [10.1107/S0021889892011828](https://doi.org/10.1107/S0021889892011828).
- [474] D. I. Svergun and J. S. Pedersen. Propagating errors in small-angle scattering data treatment. *Journal of Applied Crystallography*, 27(3):241–248, 1994. doi: [10.1107/S0021889893008337](https://doi.org/10.1107/S0021889893008337).
- [475] D. I. Svergun, A. V. Semenyuk, and L. A. Feigin. Small-angle-scattering-data treatment by the regularization method. *Acta Crystallographica Section A*, 44(3):244–250, 1988-05. doi: [10.1107/S0108767387011255](https://doi.org/10.1107/S0108767387011255).
- [476] D. A. Svetogorsky. The properties of anisotropic small-angle scattering. *Journal of Applied Crystallography*, 23(2):79–81, apr 1990. doi: [10.1107/S0021889889008253](https://doi.org/10.1107/S0021889889008253).
- [477] R. Swinbank and R. J. Purser. Fibonacci grids: A novel approach to global modelling. 132(619):1769–1793. doi: [10.1256/qj.05.227](https://doi.org/10.1256/qj.05.227).
- [478] D. Tatchev and R. Kranold. Maximum-entropy method as a routine tool for determination of particle size distributions by small-angle scattering. *Journal of Applied Crystallography*, 37(1):32–39, 2004. doi: [10.1107/S0021889803023069](https://doi.org/10.1107/S0021889803023069).
- [479] D. Taupin and V. Luzzati. Information content and retrieval in solution scattering studies. I. Degrees of freedom and data reduction. *Journal of Applied Crystallography*, 15(3):289–300, 1982-06. doi: [10.1107/S0021889882012011](https://doi.org/10.1107/S0021889882012011).
- [480] C. V. Teixeira, H. Amenitsch, T. Fukushima, J. P. Hill, W. Jin, T. Aida, M. Hotokka, and M. Lindén. Form factor of anN-layered helical tape and its application to nanotube formation of hexa-peri-hexabenzocoronene-based molecules. *Journal of Applied Crystallography*, 43(4):850–857, jun 2010. doi: [10.1107/s0021889810015736](https://doi.org/10.1107/s0021889810015736).
- [481] J. Teixeira. Experimental methods for studying fractal aggregates. In *On Growth and Form*, pages 145–162. Springer Netherlands, 1986. doi: [10.1007/978-94-009-5165-5_9](https://doi.org/10.1007/978-94-009-5165-5_9).
- [482] J. Teixeira. Small-angle scattering by fractal systems. *Journal of Applied Crystallography*, 21(6):781–785, dec 1988. doi: [10.1107/s002188988000263](https://doi.org/10.1107/s002188988000263).
- [483] M. Teubner. Level surfaces of gaussian random fields and microemulsions. *Europhysics Letters (EPL)*, 14(5):403–408, mar 1991. doi: [10.1209/0295-5075/14/5/003](https://doi.org/10.1209/0295-5075/14/5/003).
- [484] M. Teubner and R. Strey. Origin of the scattering peak in microemulsions. *J. Chem. Phys.*, 87:3195, 1987. doi: [10.1063/1.453006](https://doi.org/10.1063/1.453006).
- [485] J. C. Thomas. The determination of log normal particle size distributions by dynamic light scattering. *Journal of Colloid and Interface Science*, 117(1):187–192, may 1987. doi: [10.1016/0021-9797\(87\)90182-2](https://doi.org/10.1016/0021-9797(87)90182-2).
- [486] O. B. Toon and T. P. Ackerman. Algorithms for the calculation of scattering by stratified spheres. *Applied Optics*, 20(20):3657, oct 1981. doi: [10.1364/ao.20.003657](https://doi.org/10.1364/ao.20.003657).
- [487] A. Toth and C. T. Kelley. Convergence analysis for anderson acceleration. *SIAM Journal on Numerical Analysis*, 53(2):805–819, jan 2015. doi: [10.1137/130919398](https://doi.org/10.1137/130919398).
- [488] A. Trokhymchuk, I. Nezbeda, J. Jirsák, and D. Henderson. Hard-sphere radial distribution function again. *The Journal of Chemical Physics*, 123(2):024501, jul 2005. doi: [10.1063/1.1979488](https://doi.org/10.1063/1.1979488).
- [489] A. Trokhymchuk, I. Nezbeda, J. Jirsák, and D. Henderson. Erratum: “hard sphere radial distribution function again” [j. chem. phys. 123, 024501 (2005)]. *The Journal of Chemical Physics*, 124(14):149902, apr 2006. doi: [10.1063/1.2188941](https://doi.org/10.1063/1.2188941).
- [490] C. S. Tsao and T. L. Lin. Analysis of Small-Angle Scattering Data from Spherical Particles by both the Indirect Transform Method and the Maximum-Entropy Method. *Journal of Applied Crystallography*, 30(3):353–361, 1997. doi: [10.1107/S0021889896014574](https://doi.org/10.1107/S0021889896014574).
- [491] G. Tsolou, N. Stratikis, C. Baig, P. S. Stephanou, and V. G. Mavrntzas. Melt structure and dynamics of unentangled polyethylene rings: Rouse theory, atomistic molecular dynamics simulation, and comparison with the linear analogues. *Macromolecules*, 43(24):10692–10713, dec 2010. doi: [10.1021/ma1017555](https://doi.org/10.1021/ma1017555).
- [492] J. Ulander, H. Greberg, and R. Kjellander. Primary and secondary effective charges for electrical double layer systems with asymmetric electrolytes. *The Journal of Chemical Physics*, 115(15):7144–7160, oct 2001. doi: [10.1063/1.1398587](https://doi.org/10.1063/1.1398587).

- [493] R. A. Vaia and W. Liu. X-ray powder diffraction of polymer/layered silicate nanocomposites: Model and practice. *Journal of Polymer Science Part B: Polymer Physics*, 40(15):1590–1600, jun 2002. doi: [10.1002/polb.10214](https://doi.org/10.1002/polb.10214).
- [494] P. van Beurten and A. Vrij. Polydispersity effects in the small-angle scattering of concentrated solutions of colloidal spheres. *The Journal of Chemical Physics*, 74(5):2744–2748, mar 1981. doi: [10.1063/1.441443](https://doi.org/10.1063/1.441443).
- [495] H. van de Hulst. *Light Scattering by Small Particles*. Wiley, New York, 1957.
- [496] H. A. van der Vorst. Bi-CGSTAB: A fast and smoothly converging variant of bi-CG for the solution of nonsymmetric linear systems. *SIAM Journal on Scientific and Statistical Computing*, 13(2):631–644, mar 1992. doi: [10.1137/0913035](https://doi.org/10.1137/0913035).
- [497] J. R. van Dorp and S. Kotz. Generalized trapezoidal distributions. *Metrika*, 58(1):85–97, aug 2003. doi: [10.1007/s001840200230](https://doi.org/10.1007/s001840200230).
- [498] R. van Engelen. Improving the double exponential quadrature tanh-sinh, sinh-sinh and exp-sinh formulas. URL <https://www.genivia.com/qthsh.html>.
- [499] R. A. van Engelen. qthsh: Tanh-sinh quadrature formula. URL <https://hub.fastgit.org/Robert-van-Engelen/Tanh-Sinh/blob/main/qthsh.c>.
- [500] R. A. van Engelen. quad: Tanh-sinh, sinh-sinh and exp-sinh quadrature formula. URL <https://hub.fastgit.org/Robert-van-Engelen/Tanh-Sinh/blob/main/quad.c>.
- [501] E. J. J. van Rensburg. Virial coefficients for hard discs and hard spheres. *Journal of Physics A: Mathematical and General*, 26(19):4805–4818, oct 1993. doi: [10.1088/0305-4470/26/19/014](https://doi.org/10.1088/0305-4470/26/19/014).
- [502] Y. Vardi and D. Lee. From image deblurring to optimal investments: Maximum likelihood solutions for positive linear inverse problems. *Journal of the Royal Statistical Society: Series B (Methodological)*, 55(3):569–598, jul 1993. doi: [10.1111/j.2517-6161.1993.tb01925.x](https://doi.org/10.1111/j.2517-6161.1993.tb01925.x).
- [503] L. Verlet. Integral equations for classical fluids. *Molecular Physics*, 41(1):183–190, sep 1980. doi: [10.1080/00268978000102671](https://doi.org/10.1080/00268978000102671).
- [504] L. Verlet. Integral equations for classical fluids. *Molecular Physics*, 42(6):1291–1302, apr 1981. doi: [10.1080/00268978100100971](https://doi.org/10.1080/00268978100100971).
- [505] B. Vestergaard and S. Hansen. Application of Bayesian analysis to indirect Fourier transformation in small-angle scattering. *Journal of Applied Crystallography*, 39(6):797–804, 2006. doi: [10.1107/S0021889806035291](https://doi.org/10.1107/S0021889806035291).
- [506] L. Viererblová, J. Kolafa, S. Labík, and A. Malijevský. Virial coefficients and equation of state of the penetrable sphere model. *Phys. Chem. Chem. Phys.*, 12(1):254–262, 2010. doi: [10.1039/b917204a](https://doi.org/10.1039/b917204a).
- [507] K. Vilcinskas, B. Norder, K. Goubitz, F. M. Mulder, G. J. M. Koper, and S. J. Picken. Tunable order in alginate/graphene biopolymer nanocomposites. *Macromolecules*, 48(22):8323–8330, nov 2015. doi: [10.1021/acs.macromol.5b01380](https://doi.org/10.1021/acs.macromol.5b01380).
- [508] A. G. Vompe and G. A. Martynov. The bridge function expansion and the self-consistency problem of the ornstein-zernike equation solution. *The Journal of Chemical Physics*, 100(7):5249–5258, apr 1994. doi: [10.1063/1.467189](https://doi.org/10.1063/1.467189).
- [509] C. von Ferber, M. Bishop, T. Forzaglia, and C. Reid. Form factor of simple three and four junction comb polymers. *Macromolecules*, 46(6):2468–2473, 2013. doi: [10.1021/ma302385z](https://doi.org/10.1021/ma302385z).
- [510] C. G. Vonk. On two methods of determination of particle size distribution functions by means of small-angle X-ray scattering. *Journal of Applied Crystallography*, 9(6):433–440, 1976. doi: [10.1107/S0021889876011874](https://doi.org/10.1107/S0021889876011874).
- [511] C. G. Vonk. On two methods of determination of particle size distribution functions by means of small-angle x-ray scattering. *Journal of Applied Crystallography*, 9(6):433–440, dec 1976. doi: [10.1107/s0021889876011874](https://doi.org/10.1107/s0021889876011874).
- [512] A. Vrij. Mixtures of hard spheres in the percus-yevick approximation. light scattering at finite angles. *J. Chem. Phys.*, 71(8):3267–3270, oct 1979. doi: [10.1063/1.438756](https://doi.org/10.1063/1.438756).
- [513] J. Wagner. Small-angle scattering from spherical core-shell particles: an analytical scattering function for particles with schulz-flory size distribution. *Journal of Applied Crystallography*, 37(5):750–756, sep 2004. doi: [10.1107/s002188980401581x](https://doi.org/10.1107/s002188980401581x).

- [514] W. Wagner and J. Kohlbrecher. Small-angle neutron scattering. In Y. Zhu, editor, *Modern Techniques for Characterizing Magnetic Materials*, chapter Small-angle neutron scattering, pages 65–105. Springer-Verlag, 2005. doi: [10.1007/0-387-23395-4_2](https://doi.org/10.1007/0-387-23395-4_2).
- [515] H. F. Walker and P. Ni. Anderson acceleration for fixed-point iterations. *SIAM Journal on Numerical Analysis*, 49(4):1715–1735, jan 2011. doi: [10.1137/10078356X](https://doi.org/10.1137/10078356X).
- [516] G. Walter, R. Kranold, T. Gerber, J. Baldrian, and M. Steinhart. Particle size distribution from small-angle x-ray scattering data. *Journal of Applied Crystallography*, 18(4):205–213, aug 1985. doi: [10.1107/s0021889885010160](https://doi.org/10.1107/s0021889885010160).
- [517] H. Wang and P. C. Miller. Scaled heavy-ball acceleration of the richardson-lucy algorithm for 3d microscopy image restoration. *IEEE Transactions on Image Processing*, 23(2):848–854, feb 2014. doi: [10.1109/tip.2013.2291324](https://doi.org/10.1109/tip.2013.2291324).
- [518] Y. Wang, X. Li, Z. Nashed, F. Zhao, H. Yang, Y. Guan, and H. Zhang. Regularized kernel-based {BRDF} model inversion method for ill-posed land surface parameter retrieval. *Remote Sensing of Environment*, 111(1):36–50, nov 2007. doi: [10.1016/j.rse.2007.03.007](https://doi.org/10.1016/j.rse.2007.03.007).
- [519] M. Warner and S. F. Edwards. Neutron scattering from strained polymer networks. *Journal of Physics A: Mathematical and General*, 11(8):1649–1655, aug 1978. doi: [10.1088/0305-4470/11/8/024](https://doi.org/10.1088/0305-4470/11/8/024).
- [520] J. D. Weeks, D. Chandler, and H. C. Andersen. Role of repulsive forces in determining the equilibrium structure of simple liquids. *The Journal of Chemical Physics*, 54(12):5237–5247, jun 1971. doi: [10.1063/1.1674820](https://doi.org/10.1063/1.1674820).
- [521] E. W. Weisstein. Superegg. URL <http://mathworld.wolfram.com/Superegg.html>.
- [522] M. S. Wertheim. Exact solution of the percus-yevick integral equation for hard spheres. *Physical Review Letters*, 10(8):321–323, apr 1963. doi: [10.1103/physrevlett.10.321](https://doi.org/10.1103/physrevlett.10.321).
- [523] S. Westermann, M. Kreitschmann, W. Pyckhout-Hintzen, D. Richter, E. Straube, B. Farago, and G. Goerigk. Matrix chain deformation in reinforced networks: a SANS approach. *Macromolecules*, 32(18):5793–5802, sep 1999. doi: [10.1021/ma990112e](https://doi.org/10.1021/ma990112e).
- [524] S. Westermann, W. Pyckhout-Hintzen, D. Richter, E. Straube, S. Egelhaaf, and R. May. On the length scale dependence of microscopic strain by SANS. *Macromolecules*, 34(7):2186–2194, mar 2001. doi: [10.1021/ma0014259](https://doi.org/10.1021/ma0014259).
- [525] S. Westermann, V. Urban, W. Pyckhout-Hintzen, D. Richter, and E. Straube. SANS investigations of topological constraints in networks made from triblock copolymers. *Macromolecules*, 29(19):6165–6174, jan 1996. doi: [10.1021/ma9602381](https://doi.org/10.1021/ma9602381).
- [526] B. Weyerich, J. Brunner-Popela, and O. Glatter. Small-angle scattering of interacting particles. II. Generalized indirect Fourier transformation under consideration of the effective structure factor for polydisperse systems. *Journal of Applied Crystallography*, 32(2):197–209, 1999. doi: [10.1107/S0021889898011790](https://doi.org/10.1107/S0021889898011790).
- [527] A. Wiedenmann, R. Gähler, C. D. Dewhurst, U. Keiderling, S. Prévost, and J. Kohlbrecher. Relaxation mechanisms in magnetic colloids studied by stroboscopic spin-polarized small-angle neutron scattering. *Physical Review B*, 84(21):214303, dec 2011. doi: [10.1103/physrevb.84.214303](https://doi.org/10.1103/physrevb.84.214303).
- [528] C. M. Wijmans and E. B. Zhulina. Polymer brushes at curved surfaces. *Macromolecules*, 26(26):7214–7224, dec 1993. doi: [10.1021/ma00078a016](https://doi.org/10.1021/ma00078a016).
- [529] Wikipedia contributors. Lebedev quadrature — Wikipedia, the free encyclopedia. https://en.wikipedia.org/w/index.php?title=Lebedev_quadrature&oldid=1251349087. [Online; accessed 30-November-2024].
- [530] Wikipedia contributors. Spherical design — Wikipedia, the free encyclopedia. https://en.wikipedia.org/w/index.php?title=Spherical_design&oldid=1222304099. [Online; accessed 30-November-2024].
- [531] Wikipedia contributors. Star-shaped polymer — Wikipedia, the free encyclopedia, 2018. URL https://en.wikipedia.org/wiki/Star-shaped_polymer. [Online; accessed 22-August-2018].
- [532] L. Willner, A. Poppe, J. Allgaier, M. Monkenbusch, P. Lindner, and D. Richter. Micellization of amphiphilic diblock copolymers: Corona shape and mean-field to scaling crossover. *Europhysics Letters (EPL)*, 51(6):628–634, sep 2000. doi: [10.1209/epl/i2000-00384-1](https://doi.org/10.1209/epl/i2000-00384-1).

- [533] W. Wiscombe. Mie scattering calculations: Advances in technique and fast, vector-speed computer codes. Technical report, National Center For Atmospheric Research, Boulder, Colorado, 1979. doi: [10.5065/d6zp4414](https://doi.org/10.5065/d6zp4414).
- [534] W. J. Wiscombe. Improved mie scattering algorithms. *Applied Optics*, 19(9):1505–1509, may 1980. doi: [10.1364/AO.19.001505](https://doi.org/10.1364/AO.19.001505).
- [535] R. Xu and B. Chu. Dynamic light scattering of thin disks: Coupling of diffusive motions. *Journal of Colloid and Interface Science*, 117(1):22 – 30, 1987. doi: [10.1016/0021-9797\(87\)90164-0](https://doi.org/10.1016/0021-9797(87)90164-0).
- [536] F. Yang, A. Wang, L. Dong, and H. Ming. Determination of particle-size distributions from light-scattering measurement using lucy-richardson algorithm. *Optical Engineering*, 52(4):043605, apr 2013. doi: [10.1117/1.oe.52.4.043605](https://doi.org/10.1117/1.oe.52.4.043605).
- [537] T. Yoshizaki and H. Yamakawa. Scattering functions of wormlike and helical wormlike chains. *Macromolecules*, 13(6):1518–1525, nov 1980. doi: [10.1021/ma60078a030](https://doi.org/10.1021/ma60078a030).
- [538] S. B. Yuste, M. L. de Haro, and A. Santos. Structure of hard-sphere metastable fluids. *Physical Review E*, 53(5):4820–4826, may 1996. doi: [10.1103/physreve.53.4820](https://doi.org/10.1103/physreve.53.4820).
- [539] D. Zaslavsky. quasimontecarlo. URL <https://github.com/diazona/quasimontecarlo>.
- [540] G. Zerah and J.-P. Hansen. Self-consistent integral equations for fluid pair distribution functions: Another attempt. *The Journal of Chemical Physics*, 84(4):2336–2343, feb 1986. doi: [10.1063/1.450397](https://doi.org/10.1063/1.450397).
- [541] F. Zernike and J. A. Prins. Die beugung von röntgenstrahlen in flüssigkeiten als effekt der molekulanordnung. *Zeitschrift für Physik A Hadrons and nuclei*, 41(2-3):184–194, jun 1927. doi: [10.1007/bf01391926](https://doi.org/10.1007/bf01391926).
- [542] R. Zhang, R. M. Suter, and J. F. Nagle. Theory of the structure factor of lipid bilayers. *Phys. Rev. E*, 50(6):5047–5060, Dec 1994. doi: [10.1103/PhysRevE.50.5047](https://doi.org/10.1103/PhysRevE.50.5047).
- [543] D. Zhenhai and S. Lianyun. Application research of GMRES algorithm in dynamic light scattering particles size distribution inversion. *Physics Procedia*, 24:2089–2093, 2012. doi: [10.1016/j.phpro.2012.02.306](https://doi.org/10.1016/j.phpro.2012.02.306). International Conference on Applied Physics and Industrial Engineering 2012.
- [544] B. H. Zimm. Apparatus and methods for measurement and interpretation of the angular variation of light scattering; preliminary results on polystyrene solutions. *The Journal of Chemical Physics*, 16(12):1099–1116, dec 1948. doi: [10.1063/1.1746740](https://doi.org/10.1063/1.1746740).
- [545] B. H. Zimm. The scattering of light and the radial distribution function of high polymer solutions. *The Journal of Chemical Physics*, 16(12):1093–1099, dec 1948. doi: [10.1063/1.1746738](https://doi.org/10.1063/1.1746738).
- [546] J. Zlopasa, B. Norder, E. A. B. Koenders, and S. J. Picken. Origin of highly ordered sodium alginate/montmorillonite bionanocomposites. *Macromolecules*, 48(4):1204–1209, feb 2015. doi: [10.1021/ma502147m](https://doi.org/10.1021/ma502147m).